

Handbook of Environmental Degradation of Materials

Edited by

Myer Kutz

Myer Kutz Associates, Inc.

Delmar, New York



**William Andrew
Publishing**

Norwich, NY, U.S.A.

Copyright © 2005 by William Andrew, Inc.

No part of this book may be reproduced or utilized in any form or by any means, electronic or mechanical, including photocopying, recording, or by any information storage and retrieval system, without permission in writing from the Publisher.

Cover art © 2005 by Brent Beckley / William Andrew, Inc.

ISBN: 0-8155-1500-6 (William Andrew, Inc.)

Library or Congress Catalog Card Number: 2005005496

Library of Congress Cataloging-in-Publication Data

Handbook of environmental degradation of materials / edited by Myer Kutz.

p. cm.

Includes bibliographical references and index.

ISBN 0-8155-1500-6 (0-8155)

1. Materials—Effect of environment on—Handbooks, manuals, etc. I. Kutz, Myer.

TA418.7.H354 2005

620.1'122—dc22

2005005496

Printed in the United States of America

This book is printed on acid-free paper.

10 9 8 7 6 5 4 3 2 1

Published by:

William Andrew Publishing

13 Eaton Avenue

Norwich, NY 13815

1-800-932-7045

www.williamandrew.com

NOTICE

To the best of our knowledge the information in this publication is accurate; however the Publisher does not assume any responsibility or liability for the accuracy or completeness of, or consequences arising from, such information. This book is intended for informational purposes only. Mention of trade names or commercial products does not constitute endorsement or recommendation for their use by the Publisher. Final determination of the suitability of any information or product for any use, and the manner of that use, is the sole responsibility of the user. Anyone intending to rely upon any recommendation of materials or procedures mentioned in this publication should be independently satisfied as to such suitability, and must meet all applicable safety and health standards.

For my lifelong friendships, none the worse for wear

PREFACE

The idea for the *Handbook of Environmental Degradation of Materials* originated several years ago when Bill Woishnis, the founder of William Andrew Publishing, and I met at my upstate New York office to discuss materials information needs at the practitioner level, an area that Bill and I had been involved in for some time. Several handbooks that I had already published or was then working on dealt entirely with materials or had substantial numbers of chapters devoted to materials. Bill and his partner, Chris Forbes, were embarking on a new electronic publishing venture, Knovel Corporation, that would deliver technical information, much of it on materials, to engineers' desktops. We thought that a handbook that dealt with the harm that environmental factors could cause to a wide range of engineering materials would be useful to practitioners, and that my expertise at developing handbooks could be combined successfully with his companies' capabilities for delivering information in print and electronically.

The aim of this handbook is to present practical aspects of environmental degradation of materials (which I shall call "EDM" here): what causes EDM; how to detect and measure it; how to control it—what remediation strategies might be employed to retard damage caused by EDM; and how to possibly even prevent it. Because an engineer, no matter the industry he or she is employed in, may have to work with multiple materials, including metals, plastics, composites (such as reinforced concrete), even textiles and wood, it is useful to know how many different kinds of industrial materials degrade environmentally, what the principal environmental agents of degradation are for each class of materials, and the degradation control and prevention strategies and techniques that are most successful for each class of materials. The handbook deals with a broad range of degradation media and environmental conditions, including water and chemicals, weather, sunlight and other types of radiation, and extreme heat generated by explosion and fire.

The handbook has a design orientation. I want the handbook to be useful to people with questions such as these:

I'm designing a structure, which will have to operate under adverse environmental conditions. What materials should I specify?

How can I protect the surface of a product from degrading in the environment in which consumers will use the product?

What protective measures can I apply to structural materials if they are subjected to a potentially catastrophic attack by intense heat?

The handbook has a practical, not a theoretical, orientation. A substantial portion includes chapters on preventive and remedial aspects of industrial and commercial applications where EDM can have major and, in some cases, even catastrophic consequences. I want this handbook to serve as a source of practical advice to the reader. I would like the handbook to be the first information resource a practicing engineer reaches for when faced with a new problem or opportunity—a place to turn to even before turning to other print sources, including officially sanctioned ones, or to Internet search engines. So the handbook is more than a voluminous reference or collection of background readings. In each chapter, the reader should feel that he or she is in the hands of an experienced consultant who is providing sensible engineering-design-oriented advice that can lead to beneficial action and results.

But why develop such a handbook? The data in a single handbook of the scope outlined above can be indicative only, not comprehensive. After all, this handbook cannot purport to cover any of the subjects it addresses in anywhere near the detail that an information resource devoted to a single subject can. Moreover, no information resource—I mean no handbook, no shelf of books, not even a web site or an Internet portal or search engine (not yet, at least!)—can offer an engineer, designer, or materials scientist complete assurance that he or she will, by consulting such a resource, gain from it all the knowledge necessary to incorporate into the design of a part, component, product, machine, assembly, or structure measures that will prevent its constituent materials from degrading to the point of failure or collapse when confronted by adverse environmental conditions, whether anticipated, such as weathering, or unexpectedly severe, such as the heat generated by a fire resulting from an explosion.

Nevertheless, when a practitioner is considering how to deal with any aspect of EDM, whether in the design, control, prevention, inspection, or remedia-

tion phase, he or she has to start somewhere. The classic first step, which I have confirmed in surveys and focus groups of engineering professionals, was, in the pre-Internet era, either to ask a colleague (usually, the first choice), open a filing cabinet to look for reports or articles that might have been clipped and saved, scan the titles on one's own bookshelves or, when all else had failed, go to an engineering library, where one would hope to find more information sources than in one's own office, sometimes with the help of a good reference librarian.

To be sure, there are numerous references that deal with separate aspects of EDM. Corrosion, for example, is a topic that has been covered in great detail in voluminous references, from the points of view of materials themselves, of corroding media, and of testing and evaluation in various industries. Professional societies—NACE, ASM International, and ASTM—have devoted great energy to developing and disseminating information about corrosion. The topic of environmental degradation of plastics, to take another example, has been covered in other reference books, albeit to a lesser extent. So there are many print references where a practitioner can begin the study of many individual topics within the subject of EDM.

Of course, this is the Internet era. Many, if not most, practitioners now begin the search for EDM information by typing words or phrases into a search engine. Such activity, if the search has been done properly (a big if, just ask any reference librarian) will yield whatever the search engines have indexed, which, of course, may or may not be information useful to the particular situation. And a search engine will not connect practitioners and students to the content of valuable engineering references, unless one has access to web sites where such references are offered in full text.

Moreover, engineers, designers, and materials scientists also practice in an era of innovative materials selection and substitution that enable them to develop new versions of products, machines, or assemblies that are cheaper and more efficient than older versions made with more expensive, harder to form, and heavier materials. There can be competition for the attention of practitioners. For example, while steel may still account for slightly more than half of the material in an automobile, the rest is made from a wide variety of metallic and non-metallic materials, and the competition among suppliers of these non-ferrous materials for inclusion by automobile manufacturers is, to judge by the wars of words waged by materials trade associations, intense.

So here is the situation with regard to EDM knowledge and information that practitioners find themselves in: they must have access to information that covers numerous materials, as well as numerous degradation media and environments, but it has not been easy to find information of such broad scope in a single, easily accessible resource. What I have sought to do with this handbook is to deal with the EDM knowledge and information situation by including enough information about a broad range of subjects that deal with multiple aspects of EDM so that the handbook will be positioned at the hub of an information wheel, if you will, with the rim of the wheel divided into segments, each of which includes the wealth of information that exists for each of the topics within the subject of materials' environmental degradation. Each individual chapter in the handbook is intended to point readers to a web of information sources dealing with the subjects that the chapter addresses. Furthermore, each chapter, where appropriate, is intended to provide enough analytical techniques and data so that the reader can employ a preliminary approach to solving problems. The idea, then, is for the handbook to be the place for practitioners, as well as advanced students, to turn to when beginning to look for answers to questions in a way that may enable them to select a material, substitute one material or another, or employ a protection technique or mechanism that will save money, energy, or time.

I have asked contributors to write, to the extent their backgrounds and capabilities make possible, in a style that will reflect practical discussion informed by real-world experience. I would like readers to feel that they are in the presence of experienced teachers and consultants who know about the multiplicity of technical and societal issues that impinge on any topic within the subject of environmental degradation of materials. At the same time, the level is such that students and recent graduates can find the handbook as accessible as experienced engineers.

I have gathered together contributors from a wide range of locations and organizations. While most of the contributors are from North America, there are two from India, one from Hong Kong, two from Russia (who collaborated on a chapter), and one from Sweden. Personnel from the Royal Thai Navy contributed to the chapter on oil tankers. Sixteen chapters are by academic authors; 11 are by authors who work in industry, are at research organizations, or are consultants.

The handbook is divided into six parts. Part I, which deals with an assessment of the economic cost

of environmental degradation of materials, has just one chapter, a recapitulation of the work done by a team including Mike Brongers and Gerhardus Koch, both at CC Technologies, a corrosion consultancy in Dublin, Ohio. Part II contains three chapters on failure analysis and measurement, by K.E. Perumal, a consultant in Mumbai, India, Sean Brossia, who works on corrosion at the Southwest Research Institute in Can Antonio, Texas, and Jim Harvey, a plastics consultant in Corvallis, Oregon.

Part III deals with several different types of degradation. Professors Raymond Buchanan and E.E. Stansbury of the University of Tennessee and A.S. Khanna of the Indian Institute of Technology in Bombay cover metallic corrosion. Jim Harvey, in his second chapter in the handbook, treats polymer aging. Neal Berke, who works at WR Grace in Cambridge, Massachusetts, writes about the environmental degradation of reinforced concrete. Professor J.D. Gu of the University of Hong Kong deals with biodegradation. Part III concludes with a chapter on material flammability by Marc Janssens, also at Southwest Research Institute.

In Part IV, the handbook moves on to protective measures, starting with a chapter on cathodic protection by Prof Richard Evitts of the University of Saskatchewan in Saskatoon, Canada. In addition to metals, Part IV deals with polymers, textiles, and wood. Professors Gennadi Zaikov and S.M. Lomakin of the Institute of Biochemical Physics in Moscow cover polymeric flame retardants. Hechmi Hamouda, at North Carolina State University in Raleigh, North Carolina, writes about thermal protective clothing. The contributors of the two chapters on wood and measures that can be taken to protect it are from the Pacific Northwest—Phil Evans and his colleagues, Brian Matthews and Jahangir Chowdhury, are at the University of British Columbia in Vancouver and Jeff Morrell is at Oregon State in Corvallis.

Protection issues are also the subjects of Part V, which is called Surface Engineering and deals with coatings. Gary Halada and Clive Clayton, professors at SUNY in Stony Brook, set the stage for this section of the handbook with a chapter on the intersection of design, manufacturing, and surface engineering. Professor Tom Schuman at the University of Missouri—Rolla, continues with a discussion of protective coatings for aluminum alloys. Professor Rudy Buchheit, at the Ohio State University in Columbus,

writes about anti-corrosion paints, and Mark Nichols, at Ford Motor Company in Dearborn, Michigan, writes about paint weathering tests, a topic of great interest to auto makers. Mitch Dorfman, who works at Sulzer Metco in Westbury, Long Island, covers thermal spray coatings. Professor “Vipu” Vipulanandan, with his colleague, J. Liu, deals with concrete surface coatings issues. Ray Taylor of the University of Virginia closes Part V with a discussion of coatings defects.

The handbook concludes with five chapters that cover industrial applications with, collectively, a wide variety of materials. The chapters are meant to illustrate in a hands-on way points made more generally elsewhere in the handbook. The first of these chapters, on degradation of spacecraft materials, comes from a Goddard Research Center group, including Bruce Banks, Joyce Dever, Kim de Groh, and Sharon Miller. Branko Popov of the University of South Carolina in Columbia wrote the next chapter, which deals with metals, and is on cathodic protection for pipelines. The next chapter is also on metals. David Olson, a professor at the Colorado School of Mines in Golden headed a team, including George Wang of Mines, John Spencer of the American Bureau of Shipping, and Sittha Saidarammoot and Brajendra Mishra of the Royal Thai Navy, that provides practical insight into the real-world problem of tanker corrosion. Mikael Hedenqvist of Institutionen för Polymerteknologi, Kungliga Tekniska Högskolan in Stockholm deals with polymers in his chapter on barrier packaging materials used in consumer products. Steve Tait, an independent consultant in Madison, Wisconsin, closes the handbook with a chapter on preventing and controlling corrosion in chemical processing equipment.

My undying thanks to all of the contributors: I salute their professionalism and perseverance. I know how difficult it is to fit a writing project into a busy schedule. Chapters like those in this handbook do not get written in an evening or in a few hours snatched from a weekend afternoon. Thanks also to Millicent Treloar, the acquisitions editor at William Andrew Publishing. And, of course, many thanks to my wife Arlene, who successfully cushions each day, no matter how frustrating it's been.

Myer Kutz
Delmar, New York

CONTRIBUTORS

Stephen Ayer

Forintek Canada Corporation
Vancouver, Canada

Bruce Banks

NASA Glenn Research Center
Cleveland, Ohio

Neal Berke

WR Grace Construction Products
Cambridge, Massachusetts

Michiel Brongers

CC Technologies
Dublin, Ohio

Sean Brossia

Southwest Research Institute
San Antonio, Texas

Raymond A. Buchanan

University of Tennessee
Knoxville, Tennessee

Rudolph G. Buchheit

The Ohio State University
Columbus, Ohio

Jahangir Chowdhury

University of British Columbia
Vancouver, BC, Canada

Clive Clayton

State University of New York
Stony Brook, New York

Joyce Dever

NASA Glenn Research Center
Cleveland, Ohio

Mitchell R. Dorfman

Sulzer Metco, Inc.
Westbury, New York

Philip D. Evans

University of British Columbia
Vancouver, BC, Canada

Richard W. Evitts

University of Saskatchewan
Saskatoon, Canada

Kim de Groh

NASA Glenn Research Center
Cleveland, Ohio

J. D. Gu

The University of Hong Kong
Hong Kong, China

Gary Halada

State University of New York
Stony Brook, New York

Hechmi Hamouda

North Carolina State University
Raleigh, North Carolina

James A. Harvey

Under the Bridge Consulting
Corvallis, Oregon

Mikael S. Hedenqvist

Royal Institute of Technology
Stockholm, Sweden

Marc Janssens

Southwest Research Institute
San Antonio, Texas

Yutaka Kataoka

Tsukuba Norin
Ibaraki, Japan

Anand Sawroop Khanna

Indian Institute of Technology
Bombay, India

Makoto Kiguchi

Tsukuba Norin
Ibaraki, Japan

Gerhardus Koch

CC Technologies
Dublin, Ohio

Swaminatha P. Kumaraguru

University of South Carolina
Columbia, South Carolina

J. Liu

University of Houston
Houston, Texas

S. M. Lomakin

Institute of Biochemical Physics
Moscow, Russia

Brian Matthews

University of British Columbia
Vancouver, BC, Canada

Sharon Miller

NASA Glenn Research Center
Cleveland, Ohio

Brajendra Mishra

Colorado School of Mines
Golden, Colorado

Jeff Morrell

Oregon State University
Corvallis, Oregon

Mark Nichols

Ford Motor Company
Dearborn, Michigan

David L. Olson

Colorado School of Mines
Golden, Colorado

Joseph Payer

Case Western Reserve University
Cleveland, Ohio

K. E. Perumal

Corrosion and Metallurgical Consultancy Centre
Mumbai, India

Branko Popov

University of South Carolina
Columbia, South Carolina

Sittha Saidarasamoot

Royal Thai Navy

Karl Schmalzl

University of British Columbia
Vancouver, Canada

Thomas Schuman

University of Missouri—Rolla
Rolla, Missouri

John S. Spencer

American Bureau of Shipping
Houston, Texas

E. E. Stansbury

University of Tennessee
Knoxville, Tennessee

William Stephen Tait

Pair O Docs Professionals L.L.C.
Madison, Wisconsin

S. Ray Taylor

University of Mississippi Medical Center
Jackson, Mississippi

Neil Thompson

CC Technologies
Dublin, Ohio

Swieng Thuanboon

Royal Thai Navy

Cumaraswamy Vipulanandan

University of Houston
Houston, Texas

Paul Virmani

Turner-Fairbank Highway Research Center
McLean, Virginia

Ge Wang

American Bureau of Shipping
Houston, Texas

Gennadii E. Zaikov

Institute of Biochemical Physics
Moscow, Russia

TABLE OF CONTENTS

| | |
|---|------------|
| Preface | vii |
| Contributors | xi |
| PART 1 DEGRADATION ECONOMICS | 1 |
| 1. Cost of Corrosion in the United States | 3 |
| <i>Gerhardus H. Koch, Michiel P. H. Brongers, Neil G. Thompson, Y. Paul Virmani, and Joe H. Payer</i> | |
| PART 2 ANALYSIS | 25 |
| 2. Analysis of Failures of Metallic Materials Due to Environmental Factors | 27 |
| <i>K. E. Perumal</i> | |
| 3. Laboratory Assessment of Corrosion | 47 |
| <i>Sean Brossia</i> | |
| 4. Lifetime Predictions of Plastics | 65 |
| <i>James A. Harvey</i> | |
| PART 3 TYPES OF DEGRADATION | 79 |
| 5. Electrochemical Corrosion | 81 |
| <i>R. A. Buchanan and E. E. Stansbury</i> | |
| 6. High Temperature Oxidation | 105 |
| <i>A. S. Khanna</i> | |
| 7. Chemical and Physical Aging of Plastics | 153 |
| <i>James A. Harvey</i> | |
| 8. Environmental Degradation of Reinforced Concrete | 165 |
| <i>Neal Berke</i> | |
| 9. Biofouling and Prevention: Corrosion, Biodeterioration and Biodegradation of Materials .. | 179 |
| <i>Ji-Dong Gu</i> | |
| 10. Material Flammability | 207 |
| <i>Marc L. Janssens</i> | |
| PART 4 PROTECTIVE MEASURES | 227 |
| 11. Cathodic Protection | 229 |
| <i>Richard W. Evitts</i> | |
| 12. Polymeric Flame Retardants: Problems and Decisions | 243 |
| <i>G. E. Zaikov and S. M. Lomakin</i> | |
| 13. Thermal Protective Clothing | 261 |
| <i>Hechmi Hamouda</i> | |
| 14. Weathering and Surface Protection of Wood | 277 |

*Philip Evans, Mohammed Jahangir Chowdhury, Brian Mathews, Karl Schmalzl,
Stephen Ayer, Makoto Kiguchi, and Yutaka Kataoka*

15. Protection of Wood-Based Materials 299
Jeff Morrell

PART 5 SURFACE ENGINEERING 319

16. The Intersection of Design, Manufacturing, and Surface Engineering 321
Gary P. Halada and Clive R. Clayton
17. Protective Coatings for Aluminum Alloys 345
Thomas P. Schuman
18. Corrosion Resistant Coatings and Paints 367
Rudolph G. Buchheit
19. Paint Weathering Tests 387
Mark E. Nichols
20. Thermal Spray Coatings 405
Mitchell R. Dorfman
21. Coatings for Concrete Surfaces: Testing and Modeling 423
C. Vipulanandan and J. Liu
22. The Role of Intrinsic Defects in the Protective Behavior of Organic Coatings 449
S. Ray Taylor

PART 6 INDUSTRIAL APPLICATIONS 463

23. Degradation of Spacecraft Materials 465
Joyce Dever, Bruce Banks, Kim de Groh, and Sharon Miller
24. Cathodic Protection of Pipelines 503
Branko N. Popov and Swaminatha P. Kumaraguru
25. Tanker Corrosion 523
*Ge Wang, John S. Spencer, David L. Olson, Brajendra Mishra, Sittha Saidarasamoot,
and Swieng Thuanboon*
26. Barrier Packaging Materials 547
Mikael S. Hedenqvist
27. Corrosion Prevention and Control of Chemical Processing Equipment 565
William Stephen Tait

Index 583

P • A • R • T • 1

DEGRADATION ECONOMICS

CHAPTER 1 COST OF CORROSION IN THE UNITED STATES 3

CHAPTER 1

COST OF CORROSION IN THE UNITED STATES

Gerhardus H. Koch
Michiel P. H. Brongers
Neil G. Thompson

CC Technologies Laboratories, Inc., Dublin, Ohio

Y. Paul Virmani

Federal Highway Administration, Turner-Fairbank Highway Research Center, McLean, Virginia

Joe H. Payer

Case Western Reserve University, Cleveland, Ohio

| | |
|--------------------------|---|
| 1.1 INTRODUCTION | 3 |
| 1.2 OBJECTIVES AND SCOPE | 3 |
| 1.3 APPROACH | 3 |
| 1.4 RESULTS | 6 |

| | |
|---------------------------|----|
| 1.5 DISCUSSION | 20 |
| 1.6 PREVENTIVE STRATEGIES | 21 |
| 1.7 ACKNOWLEDGMENTS | 22 |
| 1.8 REFERENCES | 22 |

1.1 INTRODUCTION

The latest Cost of Corrosion Study⁽¹⁾ (2001) conducted by CC Technologies for the Federal Highway Administration (FHWA) focused on infrastructure, utilities, transportation, production and manufacturing, and government. It was determined that the total direct cost of corrosion in the United States is approximately \$276 billion per year, which is 3.1 percent of the nation's gross domestic product (GDP). This chapter presents the results of this recent study.

Corrosion costs result from equipment and structure replacement, loss of product, maintenance and repair, the need for excess capacity and redundant equipment, corrosion control, designated technical support, design, insurance, and parts and equipment inventories. Previous studies in the United States⁽²⁻⁴⁾ and abroad⁽⁵⁻⁸⁾ had already shown that corrosion is very costly and has a major impact on the economies of industrial nations. While all these studies emphasized the financial losses due to corrosion, no systematic study was conducted to investigate preventive strategies to reduce corrosion costs.

1.2 OBJECTIVES AND SCOPE

The primary objectives of this study were:

1. Develop an estimate of the total economic impact of metallic corrosion in the United States.

2. Identify national strategies to minimize the impact of corrosion.

The work to accomplish these objectives was conducted through the following main activities:

- Determination of the cost of corrosion, based on corrosion control methods and services.
- Determination of the cost of corrosion for specific industry sectors.
- Extrapolation of individual sector costs to a national total corrosion cost.
- Assessment of barriers to progress and effective implementation of optimized corrosion control practices.
- Development of implementation strategies and recommendations for the realization of cost savings.

1.3 APPROACH

A critical review of previous national studies was conducted. These studies have formed the basis for much of the current thinking regarding the cost of corrosion to the various national economies, and have led to a number of recent national studies.⁽⁹⁻¹¹⁾

The earliest study was reported in 1949 by Uhlig, who estimated the total cost to the economy by summing materials and procedures related to corrosion

control. The 1949 Uhlig report, which was the first to draw attention to the economic importance of corrosion, was followed in the 1970s by a number of studies in various countries, such as the United States, the United Kingdom, and Japan. The national study by Japan, conducted in 1977, followed the Uhlig methodology. In the United States, Battelle-NBS estimated the total direct cost of corrosion using an economic input/output framework. The input/output method was adopted later by studies in two other nations, namely, Australia in 1983 and Kuwait in 1995. In the United Kingdom, a committee chaired by T. P. Hoar conducted a national study in 1970 using a method where the total cost was estimated by collecting data through interviews and surveys of targeted economic sectors.

Although the efforts of the above-referenced studies ranged from formal and extensive to informal and modest, all studies arrived at estimates of the total annual cost of corrosion that ranged from 1 to 5 percent of each country's GNP.

In the current study, two different approaches were taken to estimate the cost of corrosion. The first approach followed a method where the cost is determined by summing the costs for corrosion control methods and contract services. The costs of materials were obtained from various sources, such as the U.S. Department of Commerce Census Bureau, existing industrial surveys, trade organizations, industry groups, and individual companies. Data on corrosion control services, such as engineering services, research and testing, and education and training, were obtained primarily from trade organizations, educational institutions, and individual experts. These services included only contract services and not service personnel within the owner/operator companies.

The second approach followed a method where the cost of corrosion was first determined for specific industry sectors and then extrapolated to calculate a national total corrosion cost. Data collection for the sector-specific analyses differed significantly from sector to sector, depending on the availability of data and the form in which the data were available. In order to determine the annual corrosion costs for the reference year of 1998, data were obtained for various years in the last decade, but mainly for the years 1996 to 1999.

The industry sectors for corrosion cost analyses represented approximately 27 percent of the U.S. economy gross domestic product (GDP), and were divided among five sector categories: infrastructure,

utilities, transportation, production and manufacturing, and government.

The total cost of corrosion was estimated by determining the percentage of the GDP of those industry sectors for which direct corrosion costs were estimated and extrapolating these numbers to the total U.S. GDP. The direct cost used in this analysis was defined as the cost incurred by owners or operators of the structures, manufacturers of products, and suppliers of services.

The following elements were included in these costs:

- Cost of additional or more expensive material used to prevent corrosion damage.
- Cost of labor attributed to corrosion management activities.
- Cost of the equipment required because of corrosion-related activities.
- Loss of revenue due to disruption in supply of product.
- Cost of loss of reliability.
- Cost of lost capital due to corrosion deterioration.

For all analyzed industry sectors, the direct corrosion costs were determined. Indirect costs are incurred by individuals other than the owner or operator of the structure. Measuring and valuing indirect costs are generally complex assessments, and several different methods can be used to evaluate potential indirect costs. Owners or operators can be made to assume the costs through taxation, penalties, litigation, or payment for cleanup of spills. In such cases, these expenses become direct costs. In other cases, costs are assumed by the end user or the overall economy. Once assigned a dollar value, the indirect costs are included in the cost of corrosion management of the structure and treated the same way as direct costs.

1.3.1 Data Collection

Data collection for the sector-specific analyses differed significantly from sector to sector depending on the availability of data and the form in which the data were available. For many of the public sectors, such as infrastructure and utilities, much of the information is public and could be obtained from government reports and other publicly available documents. The advice of experts in the specific sectors was sought in order to obtain further relevant information. Discussions with industry experts provided

the basis of the industry sector data collection. Corrosion-related cost information from the private industry sectors was more difficult to obtain directly, because either the information was not readily available or could not be released because of company policies. In those cases, information from publicly available industry records on operation and maintenance costs was obtained and, with the assistance of industry experts, corrosion-related costs could be estimated.

While a general approach for corrosion cost calculations was followed, it was recognized that each of the individual industry sectors had its own economic characteristics, specific corrosion problems, and methods to deal with these problems. For some sectors, a multitude of reports was found describing the mechanisms of corrosion in detail for that particular area. In some cases, formal cost data were not available and a “best estimate” had to be made based on experts’ opinions. In other cases, a convenient multiplier was determined, and a cost per unit was calculated. By multiplying the cost per unit by the number of units used or made in a sector, a total cost could be determined. It was found that by analyzing each sector individually, a corrosion cost could be determined using a calculation method appropriate for that specific industry sector. After the costs were calculated, the components of the cost determined which Bureau of Economic Analysis (BEA) industry category would be the best match for correlating that industry sector to a BEA subcategory.

1.3.2 Correlation Between BEA Categories and Industry Sectors

The basic method used for extrapolating the cost analysis performed in the current study to the entire GDP was to correlate categories defined by the BEA to the industry sectors that were analyzed in the current study. For clarification, BEA “categories” and “subcategories” were used to specify BEA classifications, and “industry sectors” was used to classify industries that were analyzed for the current study.

1.3.2.1 BEA Categories

Each BEA category represents a portion of the U.S. GDP. In 1998, the total GDP was \$8.79 trillion, divided into the major BEA categories as follows: Services (20.90 percent), Finance, Insurance, and Real Estate (19.22 percent), Manufacturing (16.34 percent), Retail Trade (9.06 percent), State and Local Government (8.48 percent), Transportation

and Utilities (8.28 percent), Wholesale Trade (6.95 percent), Construction (4.30 percent), Federal Government (4.10 percent), Agriculture (1.45 percent), and Mining (1.20 percent). These figures are summarized in Table 1.1 and graphically shown in Figure 1.1.

1.3.2.2 Analyzed Industry Sectors

Table 1.2 shows the list of 26 industry sectors that were analyzed in the current study, which were divided into five sector categories (not to be confused with the BEA categories).

The basis for selecting the industry sectors was done to represent those areas of industry for which corrosion is known to exist. This was accomplished by examining the Specific Technology Groups (STGs) within NACE International (The Corrosion Society). Table 1.3 shows the listing of current STGs. Each STG has various Task Groups and Technology Exchange Groups. It can be expected that these groups are formed around those industrial areas that have the largest corrosion impact, because the membership of NACE represents industry corrosion concerns.

A comparison of the industry sectors (Table 1.2) with the STGs (Table 1.3) shows that the industry sectors selected for analysis in the current study cover most industries and technologies represented in NACE’s STGs. One exception was noted—the absence of an industry sector that would represent the NACE STG of “Building Systems.” Some of the NACE STGs do not have a direct sector related to

TABLE 1.1 Distribution of 1998 U.S. Gross Domestic Product for BEA Industry Categories.

| | GDP | |
|-------------------------------------|--------------|------------|
| | \$ x billion | percentage |
| Services | 1,837.2 | 20.90 |
| Finance, Insurance, and Real Estate | 1,689.4 | 19.22 |
| Manufacturing | 1,435.9 | 16.34 |
| Retail Trade | 796.8 | 9.06 |
| State and Local Government | 745.1 | 8.48 |
| Transportation and Utilities | 727.9 | 8.28 |
| Wholesale Trade | 610.9 | 6.95 |
| Construction | 378.1 | 4.30 |
| Federal Government | 360.7 | 4.10 |
| Agriculture | 127.3 | 1.45 |
| Mining | 105.6 | 1.20 |
| Statistical Discrepancy | -24.8 | -0.28 |
| TOTAL GDP | \$8,790.1 | 100% |

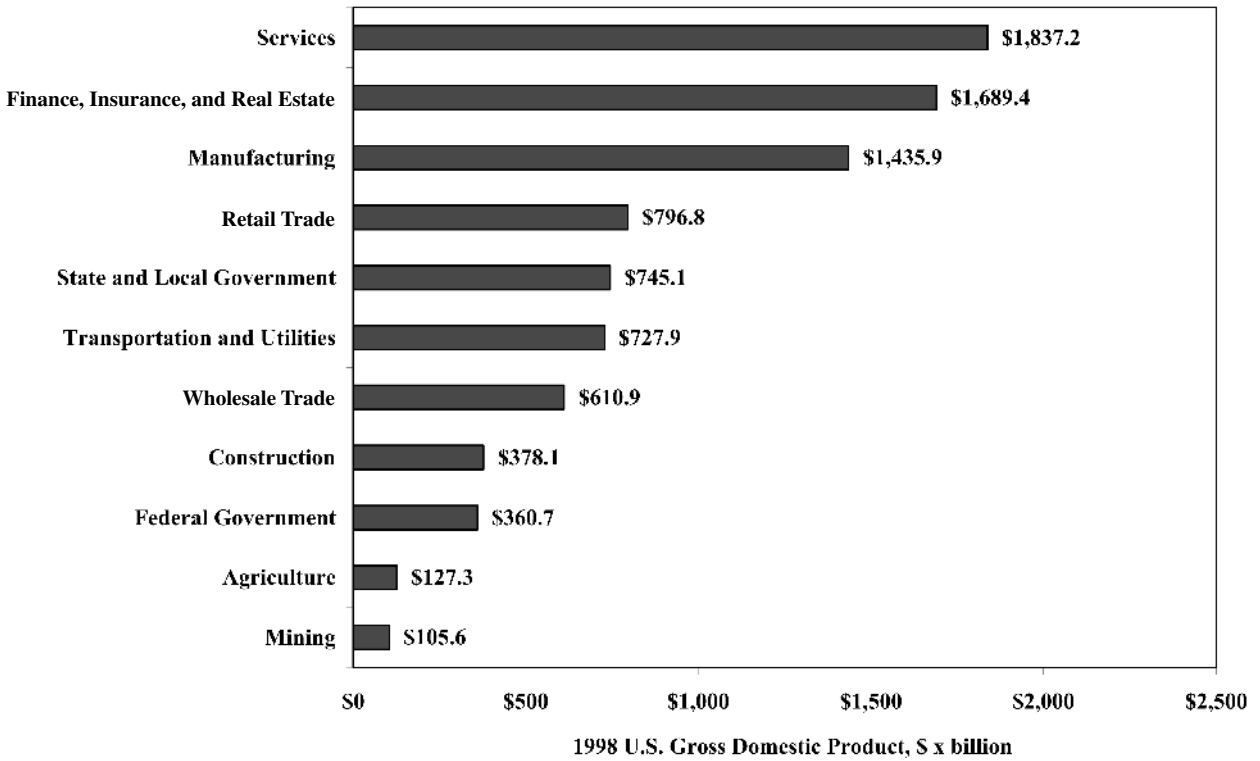


FIGURE 1.1 Distribution of 1998 U.S. gross domestic product for BEA industry categories.

them; however, those STGs were generally covered in the section on Corrosion Control Methods and Services of the study.

The method used for the extrapolation of corrosion cost per industry sector to total corrosion cost was based on the percentages of corrosion costs in the BEA categories. If a non-covered BEA category or subcategory was judged to have a significant corrosion impact, then an extrapolation was made for that non-covered BEA category or subcategory by multiplying its fraction of GDP by the percentage of corrosion costs for subcategories that were judged to have a similar corrosion impact. If a non-covered sector was judged to have no significant corrosion impact, then the direct corrosion cost for that non-covered sector was assumed to be zero.

For complete details on the correlation between BEA categories and industry sectors, the reader is referred to the full report by CC Technologies.⁽¹⁾

1.4 RESULTS

Two different methods are used in the current study to determine the total cost of corrosion to the United States. Method 1 is based on the Uhlig method⁽⁴⁾ where the costs of corrosion control materials, meth-

ods, and services are added up. Method 2 analyzes in detail the specific industry sectors that have a significant impact on the national economy. The percentage contribution to the nation's GDP is estimated, and the total cost of corrosion is then expressed as a percentage of the GDP by extrapolation to the whole U.S. economy. It is noted that this extrapolation is non-linear because most of the analyzed sectors have more corrosion impact than the non-analyzed industrial sectors.

1.4.1 Method 1—Corrosion Control Methods and Services

The corrosion control methods that were considered include organic and metallic protective coatings, corrosion-resistant alloys, corrosion inhibitors, polymers, anodic and cathodic protection, and corrosion control and monitoring equipment. Other contributors to the total cost that were reviewed include corrosion control services, corrosion research and development, and education and training.

1.4.1.1 Protective Coatings

Both organic and metallic coatings are used to provide protection against corrosion of metallic sub-

TABLE 1.2 Summary of the Industry Sectors Analyzed in the Current Study.

| SECTOR CATEGORY | 26 ANALYZED INDUSTRY SECTORS | |
|------------------------------|---|-----------------------|
| Infrastructure | Highway Bridges | |
| | Gas and Liquid Transmission Pipelines | |
| | Waterways and Ports | |
| | Hazardous Materials Storage | |
| | Airports | |
| | Railroads | |
| Utilities | Gas Distribution | |
| | Drinking Water and Sewer Systems | |
| | Electrical Utilities | |
| | Telecommunications | |
| Transportation | Motor Vehicles | |
| | Ships | |
| | Aircraft | |
| | Railroad Cars | |
| | Hazardous Materials Transport | |
| | Oil and Gas Exploration and Production | |
| Production and Manufacturing | Mining | |
| | Petroleum Refining | |
| | Chemical, Petrochemical, Pharmaceutical | |
| | Pulp and Paper | |
| | Agricultural | |
| | Food Processing | |
| | Electronics | |
| | Home Appliances | |
| | Government | Defense |
| | | Nuclear Waste Storage |

strates. These metallic substrates, mostly carbon steel, will corrode in the absence of the coating, resulting in the reduction of the service life of the steel part or component. The total annual cost for organic and metallic protective coatings is \$108.6 billion.

According to the U.S. Department of Commerce Census Bureau, the total amount of organic coating material sold in the United States in 1997 was 5.56 billion L (1.47 billion gal), at a cost of \$16.56 billion.⁽¹²⁾ The total sales can be broken down into architectural coatings, product Original Equipment Manufacturers (OEM) coatings, special-purpose coatings, and miscellaneous paint products. A portion of each of these was classified as corrosion coatings at a total estimate of \$6.7 billion. It is important to note that raw material cost is only a portion of a total coating application project, ranging from 4 to 20 percent of the total cost of application.⁽¹³⁻¹⁴⁾

TABLE 1.3 Summary of Specific Technology Groups in NACE International.

| NACE SPECIFIC TECHNOLOGY GROUP NUMBER | SPECIFIC TECHNOLOGY GROUP NAME |
|---------------------------------------|--|
| 01 | Concrete and Rebar |
| 02 | Protective Coatings and Linings—Atmospheric |
| 03 | Protective Coatings and Linings—Immersion/Buried |
| 05 | Cathodic/Anodic Protection |
| 06 | Chemical and Mechanical Cleaning |
| 09 | Measurement and Monitoring Techniques |
| 10 | Nonmetallic Materials of Construction |
| 11 | Water Treatment |
| 31 | Oil and Gas Production—Corrosion and Scale Inhibition |
| 32 | Oil and Gas Production—Metallurgy |
| 33 | Oil and Gas Production—Nonmetallics and Wear Coatings (Metallic) |
| 34 | Petroleum Refining and Gas Processing |
| 35 | Pipelines, Tanks, and Well Casings |
| 36 | Process Industry—Chemicals |
| 37 | Process Industry—High Temperature |
| 38 | Process Industry—Pulp and Paper |
| 39 | Process Industry—Materials Applications |
| 40 | Aerospace/Military |
| 41 | Energy Generation |
| 43 | Land Transportation |
| 44 | Marine Corrosion and Transportation |
| 45 | Pollution Control, Waste Incineration, and Process Waste |
| 46 | Building Systems |
| 60 | Corrosion Mechanisms |
| 61 | Corrosion and Scaling Inhibition |
| 80 | Intersociety Joint Coatings Activities |

When applying these percentages to the raw materials cost, the total annual cost of coating application ranges from \$33.5 billion to \$167.5 billion (an average of \$100.5 billion).

The most widely used metallic coating for corrosion protection is galvanizing, which involves the application of metallic zinc to carbon steel for corrosion control purposes. Hot-dip galvanizing is the most common process, and as the name implies, it consists of dipping the steel member into a bath of molten zinc. Information released by the U.S. Department of Commerce in 1998 stated that about 8.6 million metric tons of hot-dip galvanized steel and 2.8 million metric tons of electrolytic galvanized

steel were produced in 1997. The total market for metallizing and galvanizing in the United States is estimated at \$1.4 billion. This figure is the total material costs of the metal coating and the cost of processing, and does not include the cost of the carbon steel member being galvanized/metallized.

1.4.1.2 Corrosion-Resistant Metals and Alloys

Corrosion-resistant alloys (CRAs) are used where corrosive conditions prohibit the use of carbon steels and protective coatings provide insufficient protection or are economically not feasible. CRAs include stainless steels, nickel-base alloys, and titanium alloys.

According to U.S. Census Bureau statistics, a total of 2.5 million metric tons of raw stainless steel was sold in the United States in 1997.⁽¹⁵⁾ With an estimated cost of \$2.20 per kg (\$1 per lb) for raw stainless steel, a total annual production cost of \$5.5 billion (1997) was estimated. It is assumed that all production is for U.S. domestic consumption. The total consumption of stainless steel also includes imports, which account for more than 25 percent of the U.S. market. The total consumption of stainless steel can therefore be estimated at \$7.3 billion.

Where environments become particularly severe, nickel-base alloys and titanium alloys are used. Nickel-base alloys are used extensively in the oil production and refinery and chemical process industries, and other industries where high temperature and/or corrosive conditions exist. The annual average price of nickel has steadily increased from less than \$2.20 per kg in the 1960s to about \$4.40 per kg in 1998.⁽¹⁶⁾ Chromium and molybdenum are also common alloying elements for both corrosion-resistant nickel-base alloys and stainless steels. The price of chromium has increased steadily from \$2 per kg in the 1960s to nearly \$8 per kg in 1998, while the price of molybdenum has remained relatively constant at \$5 per kg.⁽¹⁷⁾ With the average price for nickel-base alloys (greater than 24 percent nickel) at \$13 per kg in 1998, the total sales value in the United States was estimated at \$285 million.

The primary use of titanium alloys is in the aerospace and military industries where the high strength-to-weight ratio and the resistance to high temperatures are properties of interest. Titanium and its alloys are, however, also corrosion resistant to many environments, and have therefore found application in oil production and refinery, chemical processes, and pulp and paper industries. In 1998, it

was estimated that 65 percent of the titanium alloy mill products were used for aerospace applications and 35 percent for non-aerospace applications.⁽¹⁸⁾ In 1998, the domestic consumption of titanium sponge (the most common titanium form) was 39,100 metric tons, which, at a price of approximately \$10 per kg, sets the total price at \$391 million. In addition, 28,600 metric tons of scrap were used for domestic consumption at a price of approximately \$1 per kg, setting the total price at \$420 million. As mentioned previously, only 35 percent of mill products were for non-aerospace applications, which leads to a titanium consumption price estimate of \$150 million for titanium and titanium alloys with corrosion control applications.

The total consumption cost of the corrosion-resistant stainless steels, nickel-base alloys, and titanium alloys in 1998 is estimated at \$7.7 billion (\$7.3 billion + \$0.285 billion + \$0.150 billion).

1.4.1.3 Corrosion Inhibitors

A “corrosion inhibitor” may be defined, in general terms, as a substance that when added in a small concentration to an environment effectively reduces the corrosion rate of a metal exposed to that environment. Inhibition is used internally with carbon steel pipes and vessels as an economic corrosion control alternative to stainless steels and alloys, coatings, or non-metallic composites. A particular advantage of corrosion inhibition is that it can be implemented or changed *in situ* without disrupting a process. The major industries using corrosion inhibitors are the oil and gas exploration and production industry, the petroleum refining industry, the chemical industry, heavy industrial manufacturing industry, water treatment facilities, and the product additive industries. The largest consumption of corrosion inhibitors is in the oil industry, particularly in the petroleum refining industry.⁽¹⁹⁾ The use of corrosion inhibitors has increased significantly since the early 1980s. The total consumption of corrosion inhibitors in the United States has doubled from approximately \$600 million in 1982 to nearly \$1.1 billion in 1998.

1.4.1.4 Engineering Plastics and Polymers

In 1996, the plastics industry accounted for \$274.5 billion in shipments.⁽²⁰⁾ It is difficult to estimate the fraction of plastics used for corrosion control, because in many cases, plastics and composites are used for a combination of reasons, including corro-

sion control, light weight, economics, strength-to-weight ratio, and other unique properties. Certain polymers are used mostly, if not exclusively, for corrosion control purposes. The significant markets for corrosion control by polymers include composites (primarily glass-reinforced thermosetting resins), PVC pipe, polyethylene pipe, and fluoropolymers. The fraction of polymers used for corrosion control in 1997 is estimated at \$1.8 billion.

1.4.1.5 Cathodic and Anodic Protection

The cost of cathodic and anodic protection of metallic buried structures or structures immersed in seawater that are subject to corrosion can be divided into the cost of materials and the cost of installation, operation, and maintenance. Industry data have provided estimates for the 1998 sales of various hardware components, including rectifiers, impressed current cathodic protection (CP) anodes, sacrificial anodes, cables, and other accessories, totaling \$146 million. The largest share of the CP market is taken up by sacrificial anodes at \$60 million, of which magnesium has the greatest market share. Major markets for sacrificial anodes are underground pipelines, the water heater market, and the underground storage tank market. The costs of installation of the various CP components for underground structures vary significantly depending on the location and the specific details of the construction. For 1998, the average total cost for installing CP systems was estimated at \$0.98 billion (range: \$0.73 billion to \$1.22 billion), including the cost of hardware components. The total cost for replacing sacrificial anodes in water heaters and the cost for corrosion-related replacement of water heaters was \$1.24 billion per year; therefore, the total estimated cost for cathodic and anodic protection is \$2.22 billion per year.

1.4.1.6 Corrosion Control Services

In the context of the 1998 Cost of Corrosion study, services were defined as companies, organizations, and individuals that are providing their services to control corrosion. By taking the NACE International membership as a basis for this section, a total number of engineers and scientists that provide corrosion control services was estimated. In 1998, the number of NACE members was 16,000, 25 percent of whom are providing consulting and engineering services as outside consultants or contractors. Assuming that the average revenue of each is \$300,000 (including

salary, overhead, benefits, and the cost to direct one or more non-NACE members in performing corrosion control activities), the total services cost can be calculated as \$1.2 billion. This number, however, is conservative since many professionals who follow a career in corrosion are not members of NACE International.

1.4.1.7 Research and Development

Over the past few decades, less funding has been made available for corrosion-related research and development, which is significant in light of the cost and inconvenience of dealing with leaking and exploding underground pipelines, bursting water mains, corroding storage tanks, aging aircraft, and deteriorating highway bridges. In fact, several government and corporate research laboratories have significantly reduced their corrosion research staff or even have closed down their research facilities.

Corrosion research can be divided into academic and corporate research. NACE International has listed 114 professors under the Corrosion heading. Assuming an average annual corrosion research budget of \$150,000, the total academic research budget is estimated at approximately \$20 million. No estimates were made for the cost of corporate or industry corrosion-related research, which is likely to be much greater than the annual academic budget.

1.4.1.8 Education and Training

Corrosion-related education and training in the United States includes degree programs, certification programs, company in-house training, and general education and training. A few national universities offer courses in corrosion and corrosion control as part of their engineering curricula. Professional organizations such as NACE International (The Corrosion Society)⁽²¹⁾ and SSPC (The Society for Protective Coatings)⁽²²⁾ offer courses and certification programs that range from basic corrosion to coating inspector to cathodic protection specialist. NACE International offers the broadest range of courses and manages an extensive certification program. In 1998, NACE held 172 courses with more than 3,000 students, conducted multiple seminars, and offered publications, at a total cost of \$8 million.

1.4.1.9 Summary

A total annual direct cost of corrosion was estimated by adding the individual cost estimates of corrosion

TABLE 1.4 Summary of Annual Costs of Corrosion Control Methods and Services.

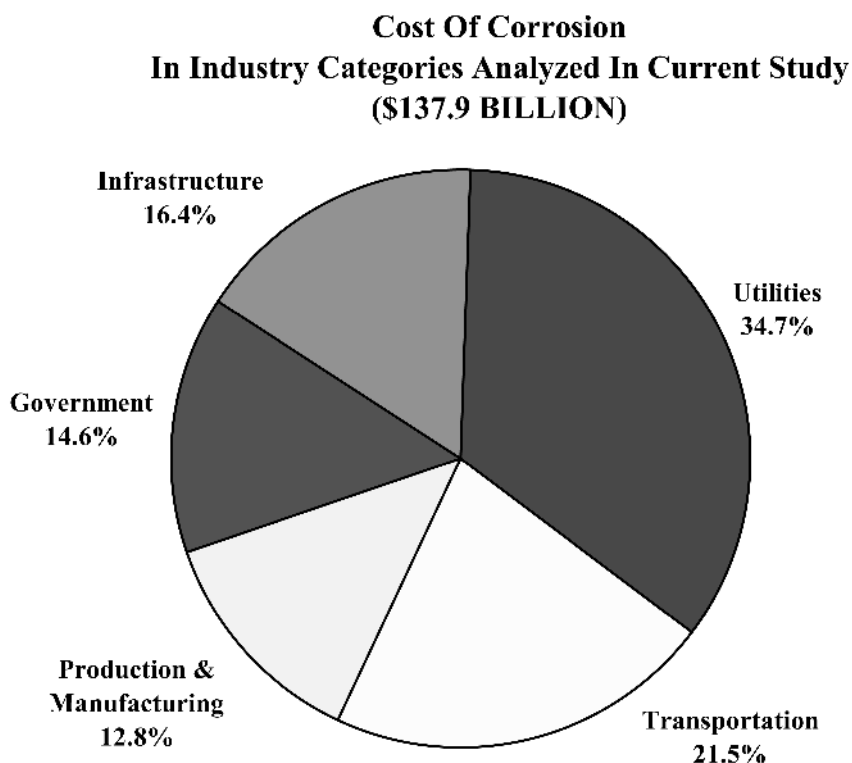
| MATERIAL AND SERVICES | RANGE | AVERAGE COST | |
|--------------------------------|-------------------------|-----------------|-------------|
| | (\$ x billion) | (\$ x billion) | (%) |
| Protective Coatings | | | |
| Organic Coatings | 40.2–174.2 | 107.2 | 88.3 |
| Metallic Coatings | 1.4 | 1.4 | 1.2 |
| Metals and Alloys | 7.7 | 7.7 | 6.3 |
| Corrosion Inhibitors | 1.1 | 1.1 | 0.9 |
| Polymers | 1.8 | 1.8 | 1.5 |
| Anodic and Cathodic Protection | 0.73–1.22 | 0.98 | 0.8 |
| Services | 1.2 | 1.2 | 1.0 |
| Research and Development | 0.020 | 0.02 | <0.1 |
| Education and Training | 0.01 | 0.01 | <0.1 |
| TOTAL | \$54.16–\$188.65 | \$121.41 | 100% |

control materials, methods, services, and education and training (see Table 1.4). The total cost was estimated at \$121 billion, or 1.381 percent of the \$8.79 trillion GDP in 1998. In some categories, such as organic coatings and cathodic protection, a wide range of costs was reported based on installation costs.

When taking these ranges into account, the total cost sum ranges from \$54.2 billion to \$188.7 billion. The table shows that the highest cost is for organic coatings at \$107.2 billion, which is approximately 88 percent of the total cost. Notably, the categories of Research and Development and Education and Training indicate unfavorably low numbers.

1.4.2 Method 2—Industry Sector Analysis

For the purpose of the 1998 Cost of Corrosion study, the U.S. economy was divided into five sector categories and 26 industrial sectors, selected according to the unique corrosion problems experienced within each of the groups. In this study, the sector categories were: (1) infrastructure, (2) utilities, (3) transportation, (4) production and manufacturing, and (5) government. The sum of the direct corrosion costs of the analyzed industrial sectors was estimated at \$137.9 billion. Since these sectors only represent a fraction of the total economy, this cost does not represent the total cost of corrosion to the U.S. economy, and therefore was extrapolated to calculate the total cost. Figure 1.2 shows the percentage contribution to the total cost of corrosion for the five sector categories analyzed in the current study.

**FIGURE 1.2** Percentage contribution to the total cost of corrosion for the five sector categories.

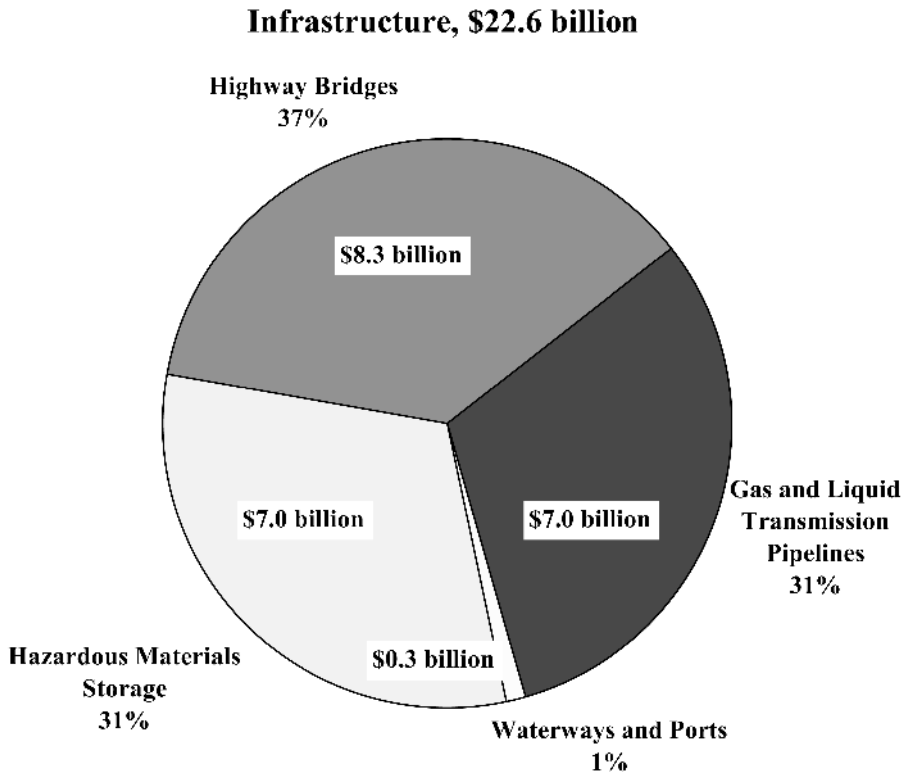


FIGURE 1.3 Annual cost of corrosion in the Infrastructure category.

1.4.2.1 Infrastructure

Figure 1.3 shows the annual cost of corrosion in the Infrastructure category to be \$22.6 billion, which is 16.4 percent of the total cost of the sector categories examined in the study. The U.S. infrastructure and transportation system allows for a high level of mobility and freight activity for the nearly 270 million residents and 7 million business establishments.⁽²³⁾ In 1997, more than 230 million motor vehicles, transit vehicles, ships, airplanes, and railroad cars using more than 6.4 million km (4 million mi) of highways, railroads, and waterways connecting all parts of the United States were used. The transportation infrastructure also includes more than 800,000 km (approximately 500,000 mi) of oil and gas transmission pipelines, and 18,000 public and private airports.

Highway Bridges. There are 583,000 bridges in the United States (1998). Of this total, 200,000 bridges are steel, 235,000 are conventional reinforced concrete, 108,000 are constructed using pre-stressed concrete, and the balance is made using

other materials of construction. Approximately 15 percent of the bridges are structurally deficient, primarily due to corrosion of steel and steel reinforcement. The annual direct cost of corrosion for highway bridges is estimated at \$8.3 billion, consisting of \$3.8 billion to replace structurally deficient bridges over the next 10 years, \$2.0 billion for maintenance and cost of capital for concrete bridge decks, \$2.0 billion for maintenance and cost of capital for concrete substructures (minus decks), and \$0.5 billion for maintenance painting of steel bridges. Life-cycle analysis estimates indirect costs to the user due to traffic delays and lost productivity at more than 10 times the direct cost of corrosion maintenance, repair, and rehabilitation.

Gas and Liquid Transmission Pipelines. There are more than 528,000 km (328,000 mi) of natural gas transmission and gathering pipelines, 119,000 km (74,000 mi) of crude oil transmission and gathering pipelines, and 132,000 km (82,000 mi) of hazardous liquid transmission pipelines.^{(24) (25)} For all natural gas pipeline companies, the total investment in 1998 was \$63.1 billion, from which a total

revenue of \$13.6 billion was generated. For liquid pipeline companies, the investment was \$30.2 billion, from which a revenue of \$6.9 billion was generated. At an estimated replacement cost of \$643,800 per km (\$1,117,000 per mi), the asset replacement value of the transmission pipeline system in the United States is \$541 billion; therefore, a significant investment is at risk, with corrosion being the primary factor in controlling the life of the asset. The average annual corrosion-related cost is estimated at \$7.0 billion, which can be divided into the cost of capital (38 percent), operation and maintenance (52 percent), and failures (10 percent).

Waterways and Ports. In the United States, 40,000 km (25,000 mi) of commercial navigable waterways serve 41 states, including all states east of the Mississippi River. Hundreds of locks facilitate travel along these waterways. In January 1999, 135 of the 276 locks had exceeded their 50-year design life. U.S. ports play an important role in connecting waterways, railroads, and highways. The nation's ports include 1,914 deepwater ports (seacoast and Great Lakes) and 1,812 ports along inland waterways. Corrosion is typically found on piers and docks, bulkheads and retaining walls, mooring structures, and navigational aids. There is no formal tracking of corrosion costs for these structures. Based on figures obtained from the U.S. Army Corps of Engineers and the U.S. Coast Guard, an annual corrosion cost of \$0.3 billion could be estimated. It should be noted that this is a low estimate since the corrosion costs of harbor and other marine structures are not included.

Hazardous Materials Storage. The United States has approximately 8.5 million regulated and non-regulated aboveground storage tanks (ASTs) and underground storage tanks (USTs) for hazardous materials (HAZMAT). While these tanks represent a significant investment and good maintenance practices would be in the best interest of the owners, federal and state environmental regulators are concerned with the environmental impact of spills from leaking tanks. In 1988, the U.S. Environmental Protection Agency set a December 1998 deadline for UST owners to comply with requirements for corrosion control on all tanks, as well as overfill and spill protection. In case of non-compliance, tank owners face considerable costs related to cleanup and penalties. As a result, the number of USTs has decreased from approximately 1.3 million to 0.75 million in

that 10-year period.⁽²⁶⁾ The total annual direct cost of corrosion for HAZMAT storage is \$7.0 billion, broken down into \$4.5 billion for ASTs and \$2.5 billion for USTs.

Airports. According to Bureau of Transportation statistics data, there were 5,324 public-use airports and 13,774 private-use airports in the United States in 1999. A typical airport infrastructure is complex, and components that might be subject to corrosion include the natural gas distribution system, jet fuel storage and distribution system, de-icing storage and distribution system, vehicle fueling system, natural gas feeders, dry fire lines, parking garages, and runway lighting. Generally, each of these systems is owned or operated by different organizations or companies; therefore, the impact of corrosion on an airport as a whole is not known or documented.

Railroads. In 1997, there were nine Class I freight railroads accounting for 71 percent of the industry's 274,399 km (170,508 mi) track operated. In addition, there were 35 regional railroads and 513 local railroads. The elements that are subject to corrosion include metal members, such as rail and steel spikes; however, corrosion damage to railroad components is either limited or goes unreported. Hence, an accurate estimate of the corrosion cost could not be determined.

1.4.2.2 Utilities

Figure 1.4 shows the annual cost of corrosion in the Utilities category to be \$47.9 billion. Utilities form an essential part of the U.S. economy by supplying end users with gas, water, electricity, and telecommunications. All utility companies combined spent \$42.3 billion on capital goods in 1998, an increase of 9.3 percent from 1997.⁽²⁷⁾ Of this total, \$22.4 billion was used for structures and \$19.9 billion was used for equipment.

Gas Distribution. The natural gas distribution system includes 2,785,000 km (1,730,000 mi) of relatively small-diameter, low-pressure piping, which is divided into 1,739,000 km (1,080,000 mi) of distribution main and 1,046,000 km (650,000 mi) of services.^(28,29) There are approximately 55 million services in the distribution system. A large percentage of the mains (57 percent) and services (46 percent) are made of steel, cast iron, or copper, which are subject to corrosion. The total annual direct cost

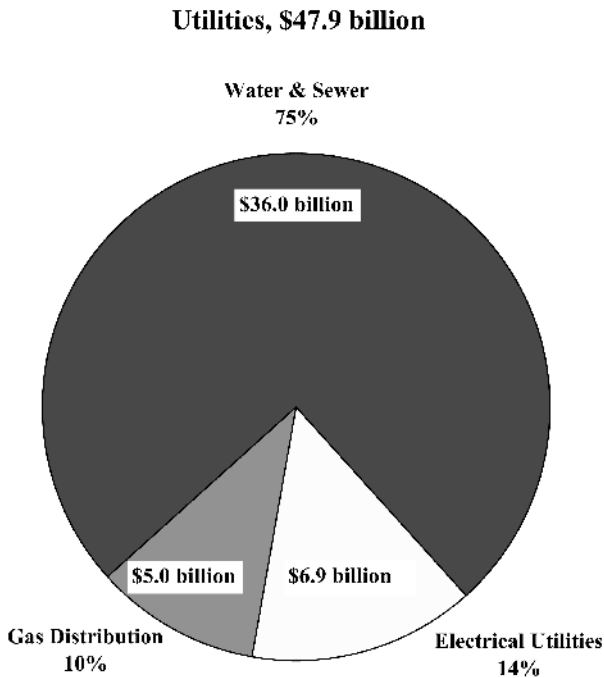


FIGURE 1.4 Annual cost of corrosion in the Utilities category.

of corrosion was estimated at approximately \$5.0 billion.

Drinking Water and Sewer Systems. According to the American Water Works Association (AWWA) industry database, there is approximately 1.483 million km (876,000 mi) of municipal water piping in the United States.⁽³⁰⁾ This number is not exact, since most water utilities do not have complete records of their piping system. The sewer system is similar in size to the drinking water system with approximately 16,400 publicly owned treatment facilities releasing some 155 million m³ (41 billion gal) of wastewater per day during 1995.⁽³¹⁾

In March 2000, the Water Infrastructure Network (WIN)⁽³²⁾ estimated the current annual cost for new investments, maintenance, operation, and financing of the national drinking water system at \$38.5 billion per year, and of the sewer system at \$27.5 billion per year. The WIN report was presented in response to a 1998 study⁽³³⁾ by AWWA and a 1997 study⁽³⁴⁾ by the U.S. Environmental Protection Agency (EPA). Those studies had already identified the need for major investments to maintain the aging water infrastructure.

The total annual direct cost of corrosion for the nation's drinking water and sewer systems was estimated at \$36.0 billion. This cost consists of the cost

of replacing aging infrastructure and the cost of unaccounted-for water through leaks, corrosion inhibitors, internal mortar linings, external coatings and cathodic protection.

Electrical Utilities. The electrical utilities industry is a major provider of energy in the United States. The total amount of electricity sold in the United States in 1998 was 3.24 trillion GWh at a cost to consumers of \$218 billion.⁽³⁵⁾ Electricity generation plants can be divided into seven generic types: fossil fuel, nuclear, hydroelectric, cogeneration, geothermal, solar, and wind. The majority of electric power in the United States is generated by fossil fuel and nuclear supply systems.⁽³⁶⁾ The total annual direct cost of corrosion in the electrical utilities industry in 1998 is estimated at \$6.9 billion, with the largest amounts for nuclear power at \$4.2 billion and fossil fuel at \$1.9 billion, and smaller amounts for hydraulic and other power at \$0.15 billion, and transmission and distribution at \$0.6 billion.

Telecommunications. According to the U.S. Census Bureau, the total value of shipments for communications equipment in 1999 was \$84 billion. Important corrosion cost factors are painting and galvanizing of communication towers and shelters, and underground corrosion of buried copper grounding beds and galvanic corrosion of the grounded steel structures. No corrosion cost was determined because of the lack of information on this rapidly changing industry.

1.4.2.3 Transportation

Figure 1.5 shows the annual cost of corrosion in the Transportation category at \$29.7 billion. The Transportation category includes vehicles and equipment used to transport people and products (i.e., automobiles, ships, aircraft).

Motor Vehicles. U.S. consumers, businesses, and government organizations own more than 200 million registered motor vehicles. Assuming the average value of an automobile is \$5,000, the total investment Americans have made in motor vehicles can be estimated at \$1 trillion. Since the 1980s, car manufacturers have increased the corrosion resistance of vehicles by using corrosion-resistant materials, employing better manufacturing processes, and designing corrosion-resistant vehicles. Although significant progress has been made, further improvement can be achieved in corrosion resis-

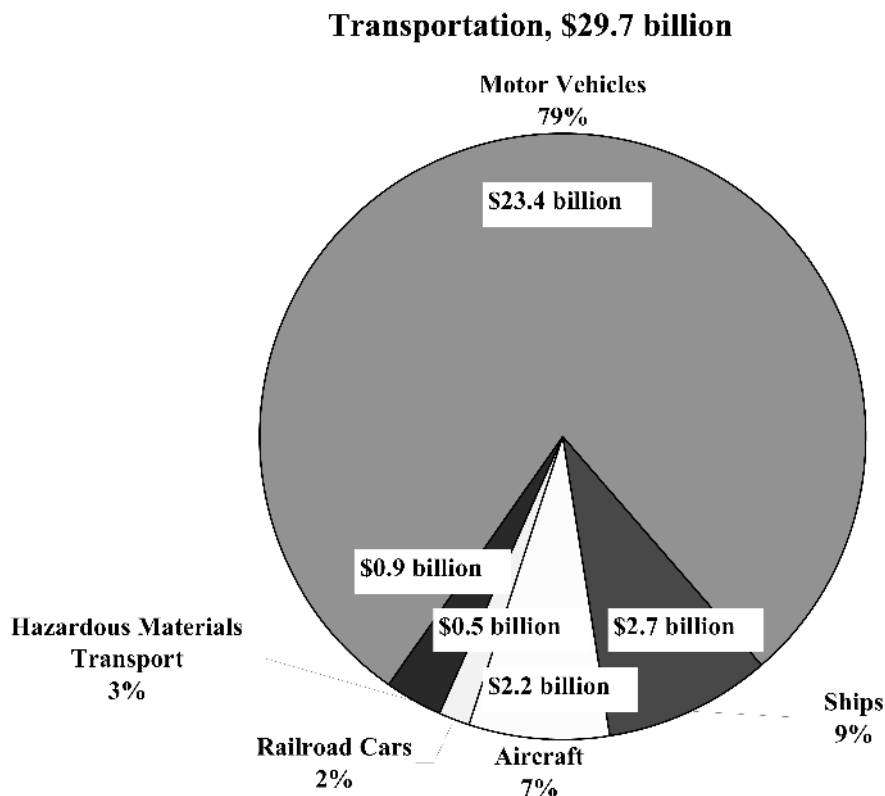


FIGURE 1.5 Annual cost of corrosion in the Transportation category.

tance of individual components. The total annual direct cost of corrosion is estimated at \$23.4 billion, which is broken down into the following three components: (1) increased manufacturing costs due to corrosion engineering and the use of corrosion-resistant materials (\$2.56 billion per year); (2) repairs and maintenance necessitated by corrosion (\$6.45 billion per year); and (3) corrosion-related depreciation of vehicles (\$14.46 billion per year).

Ships. The U.S. flag fleet consists of the Great Lakes with 737 vessels at 100 billion ton-km (62 billion ton-mi), inland with 33,668 vessels at 473 billion ton-km (294 billion ton-mi), ocean with 7,014 vessels at 563 billion ton-km (350 billion ton-mi), recreational with 12.3 million boats, and cruise ships with 122 boats serving North American ports (5.4 million passengers). The total annual direct cost of corrosion to the U.S. shipping industry is estimated at \$2.7 billion. This cost is broken down into costs associated with new ship construction (\$1.1 billion), maintenance and repairs (\$0.8 billion), and corrosion-related downtime (\$0.8 billion).

Aircraft. In 1998, the combined commercial aircraft fleet operated by U.S. airlines was more than 7,000 airplanes.⁽³⁷⁾ At the start of the jet age (1950s to 1960s), little or no attention was paid to corrosion and corrosion control. One of the concerns is the continued aging of the airplanes beyond the 20-year design life. Only the most recent designs (e.g., Boeing 777 and late-version 737) have incorporated significant improvements in corrosion prevention and control in design and manufacturing. The total annual direct cost of corrosion to the U.S. aircraft industry is estimated at \$2.2 billion, which includes the cost of design and manufacturing (\$0.2 billion), corrosion maintenance (\$1.7 billion), and downtime (\$0.3 billion).

Railroad Cars. In 1998, 1.3 million freight cars and 1,962 passenger cars were operated in the United States. Covered hoppers (28 percent) and tanker cars (18 percent) make up the largest segment of the freight car fleet. The type of commodities transported range from coal (largest volume) to chemicals, motor vehicles, farm products, food

products, and ores and minerals. Railroad cars suffer from both external and internal corrosion. The total annual direct cost of corrosion is estimated at \$0.5 billion, broken down into external coatings (\$0.25 billion) and internal coatings and linings (\$0.25 billion).

Hazardous Materials Transport. According to the U.S. Department of Transportation, there are approximately 300 million hazardous materials shipments of more than 3.1 billion metric tons annually in the United States.⁽³⁸⁾ Bulk transport over land includes shipping by tanker truck and rail car, and by special containers on vehicles. Over water, ships loaded with specialized containers, tanks, and drums are used. In small quantities, hazardous materials require specially designed packaging for truck and air shipment. The total annual direct cost of corrosion for hazardous materials transport is more than \$0.9 billion. The elements of the annual corrosion cost include the cost of transporting vehicles (\$0.4 billion per year), specialized packaging (\$0.5 billion per year), and the direct and indirect costs of accidental

releases and corrosion-related transportation incidents.

1.4.2.4 Production and Manufacturing

Figure 1.6 shows the annual cost of corrosion in the Production and Manufacturing category to be \$17.6 billion. This category includes industries that produce and manufacture products of crucial importance to the economy and the standard of living in the United States. These include gasoline products, mining, petroleum refining, various chemical and pharmaceutical products, paper, and agricultural and food products.

Oil and Gas Exploration and Production. Domestic oil and gas production can be considered to be a stagnant industry, because most of the significant available onshore oil and gas reserves have been exploited. Oil production in the United States in 1998 consisted of 3.04 billion barrels.⁽³⁹⁾ The significant recoverable reserves left to be discovered and produced are probably limited to less convenient lo-

Production and Manufacturing, \$17.6 billion

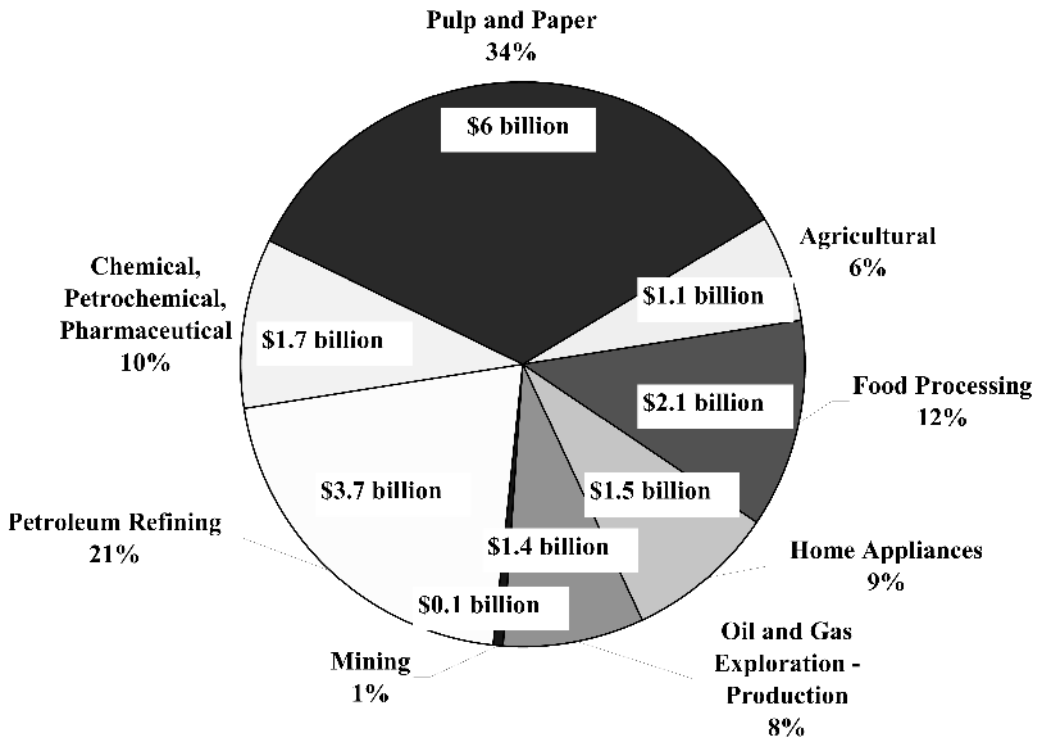


FIGURE 1.6 Annual cost of corrosion in the Production and Manufacturing category.

cations, such as in deep water offshore, remote arctic locations, and difficult-to-manage reservoirs with unconsolidated sands. The total annual direct cost of corrosion in the U.S. oil and gas production industry is estimated at \$1.4 billion, broken down into \$0.6 billion for surface piping and facility costs, \$0.5 billion in downhole tubing expenses, and \$0.3 billion in capital expenditures related to corrosion.

Mining. In the mining industry, corrosion is not considered to be a significant problem. There is a general consensus that the life-limiting factors for mining equipment are wear and mechanical damage rather than corrosion. Maintenance painting, however, is heavily relied upon to prevent corrosion, with an annual estimated expenditure for the coal mining industry of \$0.1 billion.

Petroleum Refining. The U.S. refineries represent approximately 23 percent of the world's petroleum production, and the United States has the largest refining capacity in the world, with 163 refineries.⁽⁴⁰⁾ In 1996, U.S. refineries supplied more than 18 million barrels per day of refined petroleum products. The total annual direct cost of corrosion is estimated at \$3.7 billion. Of this total, maintenance-related expenses are estimated at \$1.8 billion, vessel turnaround expenses at \$1.4 billion, and fouling costs are approximately \$0.5 billion annually.

Chemical, Petrochemical, and Pharmaceutical. The chemical industry includes those manufacturing facilities that produce bulk or specialty compounds by chemical reactions between organic and/or inorganic materials. The petrochemical industry includes those manufacturing facilities that create substances from raw hydrocarbon materials such as crude oil and natural gas. The pharmaceutical industry formulates, fabricates, and processes medicinal products from raw materials. The total annual direct cost of corrosion for this industry sector is estimated at \$1.7 billion per year (8 percent of total capital expenditures). No calculation was made for the indirect costs of production outages or indirect costs related to catastrophic failures. The costs of operation and maintenance related to corrosion were not readily available; estimating these costs would require detailed study of data from individual companies.

Pulp and Paper. The \$165 billion pulp, paper, and allied products industry supplies the United States with approximately 300 kg (661 lb) of paper per per-

son per year.⁽⁴¹⁾ More than 300 pulp mills and more than 550 paper mills support its production. The total annual direct cost of corrosion is estimated at \$6.0 billion, with the majority of this cost in the paper and paperboard industry, and calculated as a fraction of the maintenance costs. No information was found to estimate the corrosion costs related to the loss of capital.

Agricultural Production. Agricultural operations are producing livestock and crops. According to the National Agricultural Statistics Service, there are approximately 1.9 million farms in the United States.⁽⁴²⁾ Based on the 1997 Farm Census, the total value of farm machinery and equipment is approximately \$15 billion per year. The two main reasons for replacing machinery or equipment include upgrading old equipment and replacement because of wear and corrosion. Discussions with experts in this industrial sector resulted in an estimate of corrosion costs in the range of 5 percent to 10 percent of the value of all new equipment. Therefore, the total annual direct cost of corrosion in the agricultural production industry is estimated at \$1.1 billion.

Food Processing. The food processing industry is one of the largest manufacturing industries in the United States, accounting for approximately 14 percent of the total U.S. manufacturing output.⁽⁴³⁾ Sales for food processing companies totaled \$265.5 billion in 1999. Because of food quality requirements, stainless steel is widely used. Assuming that the stainless steel consumption and cost in this industry are entirely attributed to corrosion, a total annual direct cost of corrosion is estimated at \$2.1 billion. This cost includes stainless steel usage for beverage production, food machinery, cutlery and utensils, commercial and restaurant equipment, appliances, aluminum cans, and the use of corrosion inhibitors.

Electronics. Corrosion in electronic components manifests itself in several ways, and computers, integrated circuits, and microchips are being exposed to a variety of environmental conditions. Corrosion in electronic components is insidious and cannot be readily detected; therefore, when corrosion failure occurs, it is often dismissed as just a failure and the part or component is replaced. Particularly in the case of consumer electronics, devices would become technologically obsolete long before corrosion-induced failures would occur. Although it has been suggested that a significant part of all electric com-

ponent failures is caused by corrosion, no corrosion cost could be estimated.

Home Appliances. The appliance industry is one of the largest consumer products industries. For practical purposes, two categories of appliances are distinguished: “Major Home Appliances” and “Comfort Conditioning Appliances.” In 1999, 70.7 million major home appliances and 49.5 million comfort conditioning appliances were sold in the United States, for a total of 120.2 million appliances. The cost of corrosion in home appliances was estimated at \$1.5 billion per year.

1.4.2.5 Government

Federal, state, and local governments play increasingly important roles in the U.S. economy, with a 1998 GDP of approximately \$1.105 trillion. While the government owns and operates large assets under various departments, the U.S. Department of Defense (DoD) was selected because of its significant direct and indirect impact on the U.S. economy. A second government sector that was selected is nuclear waste storage under the U.S. Department of Energy (DoE). The cost of corrosion in these two sectors was used to estimate the cost of corrosion for the Government category. This cost was \$20.1 billion per year (see Figure 1.7).

Defense. Corrosion of military equipment and facilities has been, for many years, a significant and ongoing problem. The corrosion-related problems are becoming more prominent as the acquisition of new equipment is decreasing and the reliability required of aging systems is increasing. The data provided by the military services (Army, Air Force, Navy, and Marine Corps) indicate that corrosion is potentially the number one cost driver in life-cycle costs. The total annual direct cost of corrosion incurred by the military services for systems and infrastructure is approximately \$20 billion.⁽⁴⁴⁾

Nuclear Waste Storage. Nuclear wastes are generated from spent nuclear fuel, dismantled nuclear weapons, and products such as radio pharmaceuticals. The most important design item for the safe storage of nuclear waste is effective shielding of radiation. Corrosion is an important issue in the design of the casks used for permanent storage, which have a design life of several thousand years. A 1998 total life-cycle cost analysis⁽⁴⁵⁾ by the U.S. Department of

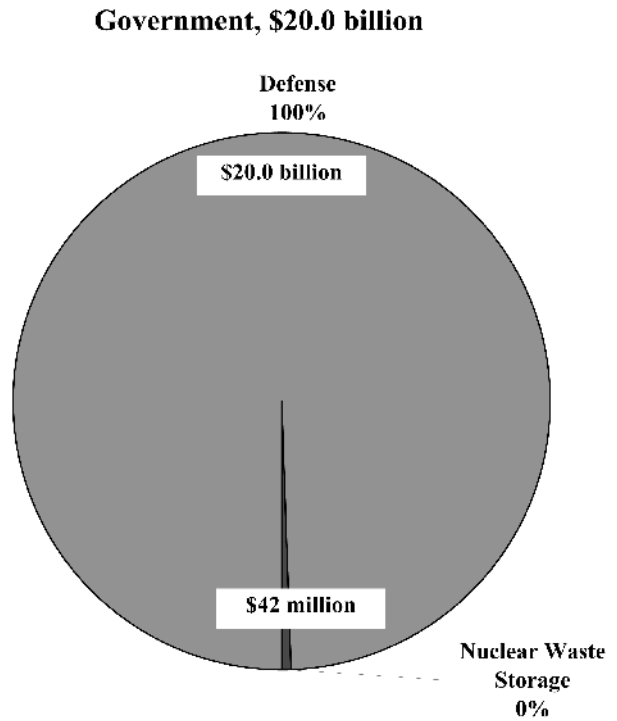


FIGURE 1.7 Annual cost of corrosion in the Government category.

Energy for the permanent disposal of nuclear waste in Yucca Mountain, Nevada, estimated the total repository cost by the construction phase (2002) at \$4.9 billion with an average annual cost (from 1999 to 2116) of \$205 million. Of this cost, \$42.2 million is corrosion-related.

Summary of Sector Studies. Table 1.5 shows the costs of corrosion for each industry sector analyzed in the current study. The dollar values are rounded to the nearest \$0.1 billion because of the uncertainty in the applied methods. The total cost of corrosion in the analyzed sectors was \$137.9 billion per year. Figure 1.8 shows the data in graphical form. The cost of \$137.9 billion was believed to be a very conservative estimate. In each sector, only the “major” corrosion costs were considered. In addition, even major costs were left out when no basis for an estimate was found. Most notable of these were the following: (1) no operation and maintenance costs were included for the Chemical, Petrochemical, and Pharmaceutical sectors; (2) no capital costs were included for the Pulp and Paper sector; (3) no capital costs were included for the Gas and Distribution sec-

TABLE 1.5 Summary of Estimated Direct Cost of Corrosion for Industry Sectors Analyzed in This Study.

| CATEGORY | INDUSTRY SECTORS | APPENDIX | ESTIMATED DIRECT COST OF CORROSION PER SECTOR | |
|---|---|----------|---|----------|
| | | | \$ x billion | percent* |
| Infrastructure (16.4% of total) | Highway Bridges | D | 8.3 | 37 |
| | Gas and Liquid Transmission Pipelines | E | 7.0 | 31 |
| | Waterways and Ports | F | 0.3 | 1 |
| | Hazardous Materials Storage | G | 7.0 | 31 |
| | Airports | H | ** | ** |
| | Railroads | I | ** | ** |
| SUBTOTAL | | | \$22.6 | 100% |
| Utilities (34.7% of total) | Gas Distribution | J | 5.0 | 10 |
| | Drinking Water and Sewer Systems | K | 36.0 | 75 |
| | Electrical Utilities | L | 6.9 | 14 |
| | Telecommunications | M | ** | ** |
| SUBTOTAL | | | \$47.9 | 100% |
| Transportation (21.5% of total) | Motor Vehicles | N | 23.4 | 79 |
| | Ships | O | 2.7 | 9 |
| | Aircraft | P | 2.2 | 7 |
| | Railroad Cars | Q | 0.5 | 2 |
| | Hazardous Materials Transport | R | 0.9 | 3 |
| SUBTOTAL | | | \$29.7 | 100% |
| Production and Manufacturing (12.8% of total) | Oil and Gas Exploration and Production | S | 1.4 | 8 |
| | Mining | T | 0.1 | 1 |
| | Petroleum Refining | U | 3.7 | 21 |
| | Chemical, Petrochemical, Pharmaceutical | V | 1.7 | 10 |
| | Pulp and Paper | W | 6.0 | 34 |
| | Agricultural | X | 1.1 | 6 |
| | Food Processing | Y | 2.1 | 12 |
| | Electronics | Z | ** | ** |
| Home Appliances | AA | 1.5 | 9 | |
| SUBTOTAL | | | \$17.6 | 100% |
| Government (14.6% of total) | Defense | BB | 20.0 | 99.5 |
| | Nuclear Waste Storage | CC | 0.1 | 0.5 |
| SUBTOTAL | | | \$20.1 | 100% |
| TOTAL | | | \$137.9 | |

*Individual values do not add up to 100% because of rounding.

**Corrosion costs not determined.

tor; and (4) replacement costs were considered only for water heaters in the Home Appliances sector. In most cases, conservative estimates were made when no basis was available. Most notable was that only 5 percent of water heaters are replaced due to corrosion. Therefore, the total cost of corrosion is a conservative value and is probably higher.

These data show that the highest corrosion costs are incurred by drinking water and sewer systems. The largest value of \$36.0 billion per year for both types of systems together is due to the extent of the water transmission and distribution network in the

United States. For the U.S. population of 265 million people, an average of 550 L (145 gal) per person per day is used for personal use and for use in production and manufacturing. The metal piping systems are aging and will require increased maintenance in the future. For the Drinking Water sector, large indirect costs are expected as well, but are not quantified in the current study.

The second largest corrosion cost (\$23.4 billion per year) was found in the Motor Vehicles sector. With more than 200 million registered vehicles, the corrosion impact consists of corrosion-related de-

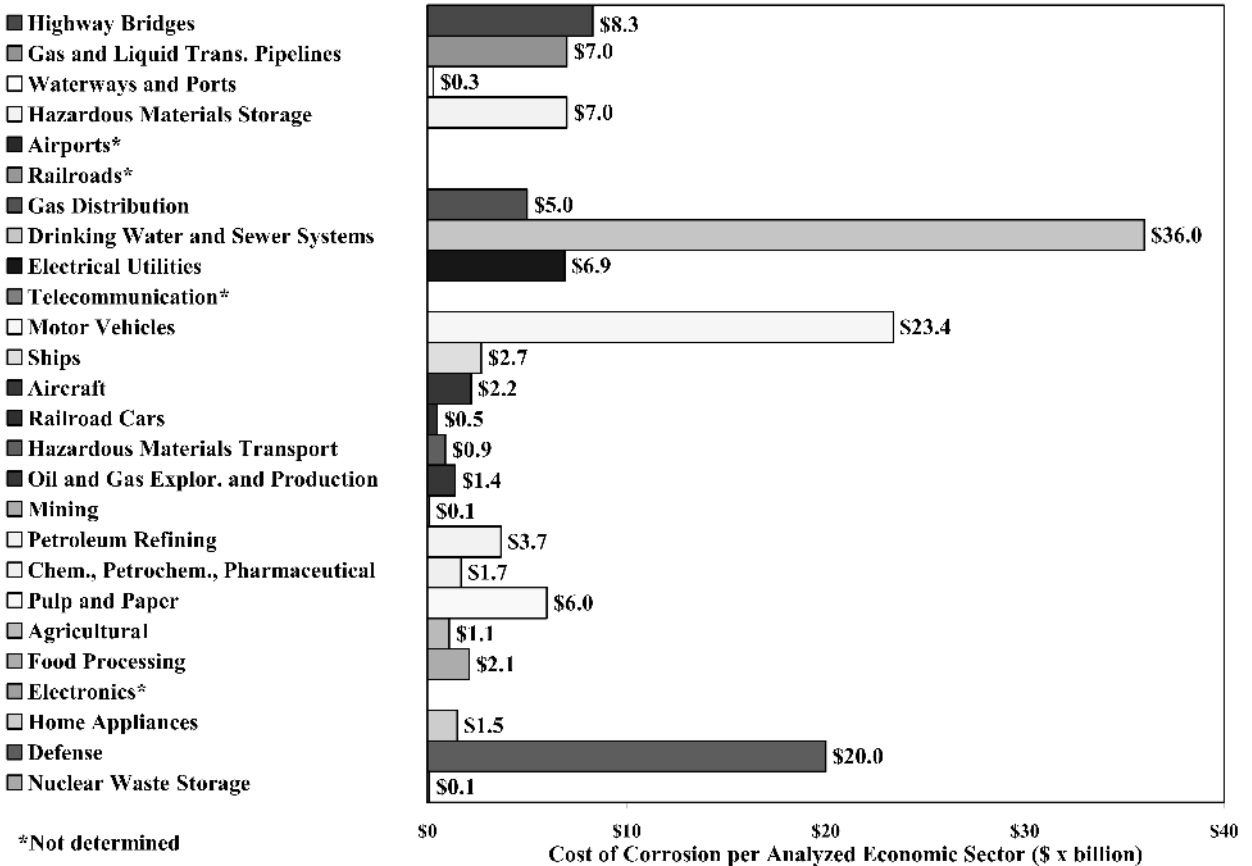


FIGURE 1.8 Summary of estimated direct cost of corrosion for industry sectors analyzed in this study.

preciation costs (62 percent), corrosion-resistant materials of construction (10 percent), and the cost of increased maintenance because of corrosion (28 percent). The indirect cost in this sector is expected to be large, especially because of the time users of motor vehicles lose when having to deal with car maintenance and repair.

The third largest corrosion cost (\$20 billion per year) was observed in defense systems. Reliability and readiness are of crucial importance, and thus military vehicles, aircraft, ships, weapons, and facilities must be continuously maintained. A determining factor in the Defense sector is the readiness for operation under any circumstance and in corrosive environments such as seawater, swamps or wetlands, and in rain and mud.

Large corrosion costs were also found in the sectors for highway bridges (\$8.3 billion per year), gas and liquid transmission pipelines (\$7.0 billion per year), electrical utilities (\$6.9 billion per year), pulp and paper (\$6.0 billion per year), and gas distribu-

tion (\$5.0 billion per year). There were two factors that were important for these sectors: (1) large number of units, and (2) severely corrosive environments. The following lists specific concerns regarding corrosion for some of the sectors that have large corrosion costs:

- The national system of highways requires many bridges to be maintained. With the commonly used approach that bridges are constructed to have a design life, rather than “being there forever,” the burden to maintain and repair this infrastructure will continue to grow because of aging components.
- The network of transmission pipelines is quite large [779,000 km (484,000 mi)] and transports potentially corrosive liquids and gas, which makes their operation sensitive to public opinion related to environmental spills and highly publicized ruptures. Although pipelines have proven to be the safest way to transport large quantities of

product over long distances, controlling corrosion comes at a significant cost.

- The same argument for potential spills (oil) holds for the hazardous materials storage sector. Corrosion protection is a significant cost per tank for both underground and aboveground tanks, and the total number of HAZMAT storage tanks is estimated at 8.5 million.
- Electrical utilities have large corrosion costs due to the affected operation and maintenance costs, depreciation costs, and the cost of forced outages. The greatest cost is found for nuclear power-generated plants, because of the higher inspection frequency in nuclear plants as opposed to fossil fuel plants.
- The pulp and paper industry uses corrosive media to make pulp from wood. Changes in processing conditions over the last decades have had a significant impact on the materials used for construction. Paper quality and processing reliability are driving spending in this sector.

In the following discussion, the individual sector analyses will be extrapolated to calculate total corrosion costs in the United States.

1.5 DISCUSSION

1.5.1 Extrapolation to Total Cost of Corrosion

The total cost of corrosion in the analyzed sectors was \$137.9 billion per year. This estimate was based on detailed analysis of industrial sectors that are known to have a significant corrosion impact. The sum of these sectors represented 27.55 percent of the GDP. Based on the procedure for extrapolation, which used the percentage of cost of corrosion for BEA subcategories, an estimated total direct cost of corrosion of \$275.7 billion per year was calculated. This is 3.1 percent of the 1998 U.S. GDP (see Figure 1.9).

Figure 1.10 illustrates the impact of corrosion on the nation's economy. The purpose of this figure is to show the relative corrosion impact (3.1 percent) with respect to the total GDP. In fact, corrosion costs are as great as or greater than some of the individual categories, such as agriculture and mining.

The non-linear extrapolation shows a stepwise, cumulative calculation for total corrosion cost. Figure 1.11 shows the non-linear extrapolation graphically.

Extrapolated Corrosion Costs: \$276 billion, 3.1% of GDP

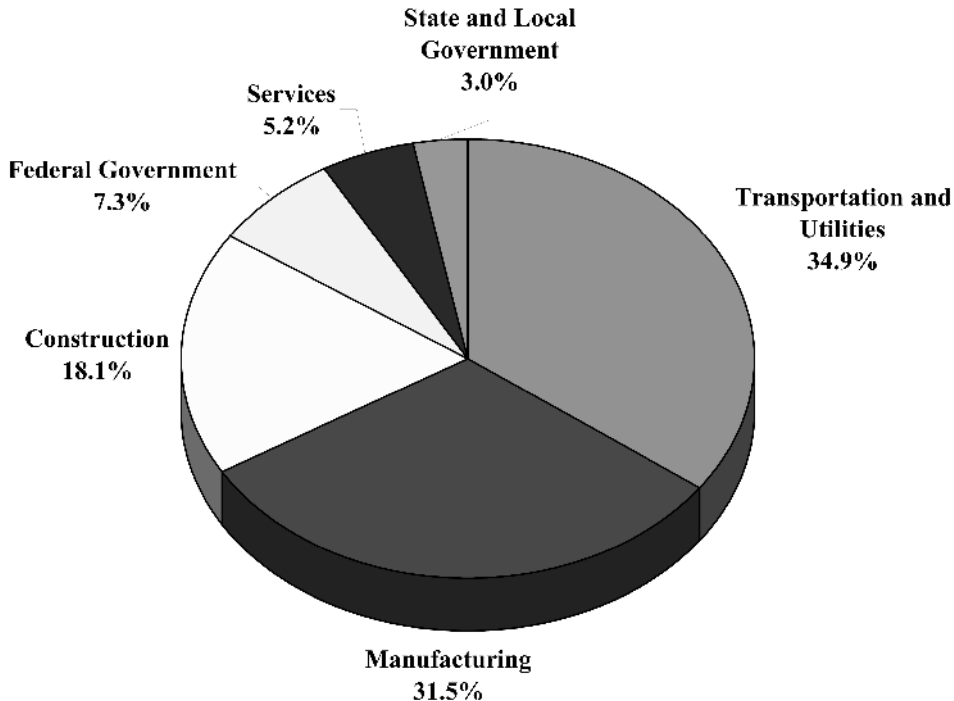
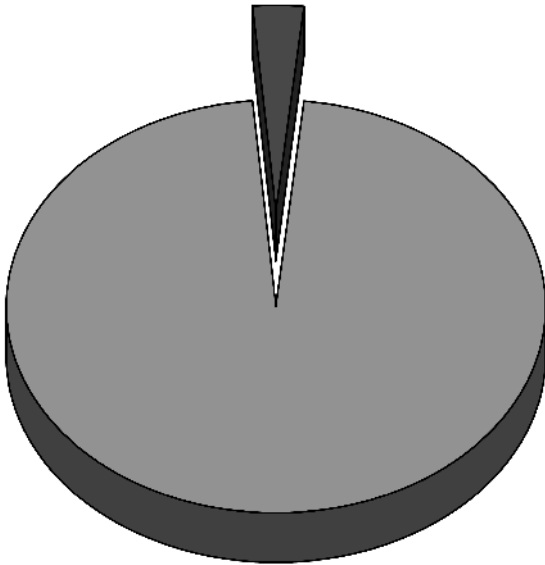


FIGURE 1.9 Total direct corrosion costs for BEA categories.

**Extrapolated
Corrosion Costs:
\$276 billion, 3.1%**



**1998 U.S. Gross
Domestic Product
(\$8.79 trillion)**

FIGURE 1.10 Diagram illustrating the impact of corrosion on the U.S. economy.

At 3.1 percent of the GDP, the cost of corrosion to the U.S. economy is already significant if only based on the direct cost of corrosion. However, the impact of corrosion can be significantly greater when indirect costs are included. The assumption can be made that the indirect costs over the entire industry can be equal to, if not greater than, the direct costs. This would result in a total direct and indirect impact of corrosion of approximately \$551.4 billion annually, or 6.3 percent of the GDP.

1.5.2 Summary of Total Cost of Corrosion Calculation

The research presented in this chapter showed that the direct cost of corrosion in the United States was approximately \$275.7 billion per year, which is 3.1 percent of the GDP. This percentage lies in the range that previous studies for various countries showed in the past. However, the 1998 CC Technologies Cost of Corrosion study was more detailed and specified corrosion costs using two methods: (1) cost of corrosion control methods and services, and (2) corro-

sion costs in individual industrial sectors. It is estimated that the indirect cost to the end user can double the economic impact, making the cost of corrosion, including indirect costs, \$551.4 billion or more.

1.6 PREVENTIVE STRATEGIES

The current study showed that technological changes have provided many new ways to prevent corrosion and the improved use of available corrosion management techniques. However, better corrosion management can be achieved using preventive strategies in non-technical and technical areas. These preventive strategies include: (1) increase awareness of significant corrosion costs and potential cost-savings; (2) change the misconception that nothing can be done about corrosion; (3) change policies, regulations, standards, and management practices to increase corrosion cost-savings through sound corrosion management; (4) improve education and training of staff in the recognition of corrosion control; (5) implement advanced design practices for better corrosion management; (6) develop advanced life prediction and performance assessment methods; and (7) improve corrosion technology through research, development, and implementation.

While corrosion management has improved over the past several decades, the United States is still far from implementing optimal corrosion control practices. There are significant barriers to both the development of advanced technologies for corrosion control and the implementation of those technological advances. In order to realize the savings from reduced costs of corrosion, changes are required in three areas: (1) the policy and management framework for effective corrosion control; (2) the science and technology of corrosion control; and (3) the technology transfer and implementation of effective corrosion control. The policy and management framework is crucial because it governs the identification of priorities, the allocation of resources for technology development, and the operation of the system.

Incorporating the latest corrosion strategies requires changes in industry management and government policies, as well as advances in science and technology. It is necessary to engage a larger constituency composed of the primary stakeholders, government and industry leaders, the general public, and consumers. A major challenge involves the dissemination of corrosion awareness and expertise

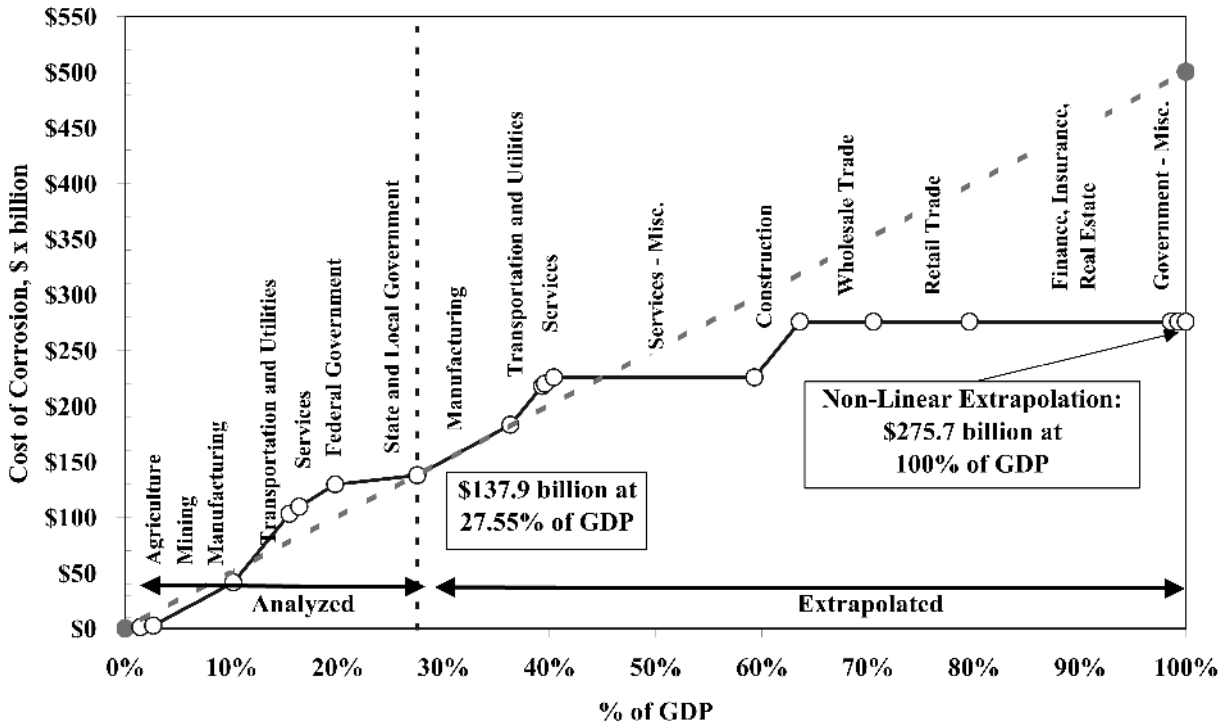


FIGURE 1.11 Illustration of non-linear extrapolation of cost of corrosion based on assumption that non-analyzed sectors have a different corrosion impact, depending on industry category

that are currently scattered throughout government and industry organizations. In fact, there is no focal point for the effective development, articulation, and delivery of corrosion cost-savings programs.

Therefore, the following recommendations are made:

1. Form a Committee on Corrosion Control and Prevention of the National Research Council.
2. Develop a national focus on corrosion control and prevention.
3. Improve policies and corrosion management.
4. Accomplish technological advances for corrosion savings.
5. Implement effective corrosion control.

1.7 ACKNOWLEDGMENTS

The authors acknowledge the support of the Federal Highway Administration (FHWA), under Cooperative Agreement Number DTFH61-99-X-00004. The cooperation of NACE International and their efforts

to make the contents of this important study known to their members and the general public are greatly appreciated. The authors of this report would further like to acknowledge the valuable input of the many experts who supplied information to this study from many different industries. Without the continuous feedback and thorough review of these people, the CC Technologies Cost of Corrosion Study would not contain such a large range of corrosion cost data.

1.8 REFERENCES

1. "Corrosion Costs and Preventive Strategies in the United States," G. H. Koch, M. P. H. Brongers, N.G. Thompson, Y. P. Virmani, and J. H. Payer, Study by CC Technologies, Report FHWA-RD-01-156, September 2001.
2. *Economic Effects of Metallic Corrosion in the United States*, NBS Special Publication 511-1, SD Stock No. SN-003-003-01926-7, 1978, and *Economic Effects of Metallic Corrosion in the United States, Appendix B*, NBS Special Publication 511-2, SD Stock No. SN-003-003-01926-5, 1978.
3. *Economic Effects on Metallic Corrosion in the United States—Update*, Battelle, 1995.

4. H. H. Uhlig, "The Cost of Corrosion in the United States," *Corrosion*, Vol. 6, 1952, p. 29.
5. *Report of the Committee on Corrosion Protection—A Survey of Corrosion Protection in the United Kingdom*, Chairman T. P. Hoar, 1971.
6. *Report of the Committee on Corrosion and Corrosion Protection—A Survey of the Cost of Corrosion in Japan*, Japan Society of Corrosion Engineering and Japan Association of Corrosion Control, Chairman G. Okamoto, 1977.
7. B. W. Cherry and B. S. Skerry, *Corrosion in Australia—The Report of the Australian National Centre for Corrosion Prevention and Control Feasibility Study*, 1983.
8. F. Al-Kharafi, A. Al-Hashem, and F. Martrouk, *Economic Effects of Metallic Corrosion in the State of Kuwait*, KISR Publications, Final Report No. 4761, December 1995.
9. H. Jotisschky and N. R. Whitehouse, *From Hoar to the Millennium: Continuity and Change in the U.K. Corrosion Scene. An Introduction to a Current DTI-Funded Project*, EuroCorr 2000, London, U.K., September 2000.
10. P. McIntyre, *Corrosion Costs in the U.K. Offshore and Chemical Industries*, EuroCorr 2000, London, U.K., September 2000.
11. T. Shibata, *JSCE Activity for Cost of Corrosion in Japan*, EuroCorr 2000, London, U.K., September 2000.
12. *Current Industrial Reports*, Paint and Allied Products, formerly Series No. MA28F, www.census.gov/ftp/pub/industry/1/ma28f99.pdf, U.S. Department of Commerce, Economics and Statistics Administration, U.S. Census Bureau, issued September 2000.
13. *A Survey of the United States Industrial Maintenance Coatings Market*, SSPC and WEH Corporation, October 1999.
14. L. M. Smith and G. R. Tinkelenberg, *Lead-Containing Paint Removal, Containment, and Disposal*, Report No. FHWA-RD-94-100, U.S. Federal Highway Administration, Turner-Fairbank Highway Research Center, McLean, VA, 1995.
15. *1997 Economic Census*, www.census.gov, October 2000.
16. *Mineral Industry Surveys*, <http://minerals.usgs.gov/minerals/nickel>, December 1999.
17. *Mineral Industry Surveys*, <http://minerals.usgs.gov/minerals/chromium>, December 1999.
18. *Mineral Industry Surveys*, <http://minerals.usgs.gov/minerals/titanium>, December 1999.
19. *Corrosion Inhibitors*, Publications Resource Group, Business Communications Company, July 1999.
20. *Contributions of Plastics to the U.S. Economy*, Society of Plastics Industry, 1997.
21. NACE International (The Corrosion Society), www.nace.org, September 2000.
22. SSPC (The Society for Protective Coatings), October 2000.
23. *Transportation Statistics Annual Report*, 1999.
24. P. J. Katchmar, *OPS Overview & Regulation Update*, Rocky Mountain Short Course, January 2000.
25. *Pipeline Safety—The Office of Pipeline Safety Is Changing How It Oversees the Pipeline Industry*, GAO/RCED-00-128, Report to Ranking Minority Member, Committee on Commerce, U.S. House of Representatives, May 2000.
26. *Code of Federal Regulations*, Vol. 40, Part 280, U.S. Government Printing Office, U.S. Environmental Protection Agency (EPA), Office of Underground Storage Tanks, July 1999.
27. *Annual Capital Expenditure Survey: 1998*, U.S. Department of Commerce, Economics and Statistics Administration, U.S. Census Bureau, April 2000.
28. *Pipeline Statistics, Distribution and Transmission Annual Mileage Totals*, www.ops.dot.gov/stats, December 2000.
29. *1998 Distribution Annuals Data*, FOIA On-Line Library, www.ops.dot.gov/DT98.htm
30. *Water Industry Data Base: Utility Profiles*, American Water Works Association (AWWA), Denver, CO, 1992.
31. W. B. Solley, R.R. Pierce, and H. A. Perlman, *Estimated Use of Water in the United States in 1995*, U.S. Geological Survey Circular 1200, U.S. Department of the Interior, 1998.
32. *Clean and Safe Water for the 21st Century—A Renewed National Commitment to Water and Waste Water Infrastructure*, Water Infrastructure Network (WIN), 2000.
33. *Infrastructure Needs for the Public Water Supply Sector Final Report*, by Stratus Consulting, Inc., Boulder, CO, for the American Water Works Association (AWWA), December 1998.
34. *Drinking Water Infrastructure Needs Survey, First Report to Congress*, Publication No. EPA-812-R-97-001, U.S. Environmental Protection Agency, Office of Water, Office of Ground Water and Drinking Water Implementation and Assistance Division, Washington, D.C., January 1997.
35. FERC Form No 1, reports for 1998, www.ferc.fed.us/sips, November 2000.
36. *Electric Power Industry Statistics for the United States, 1997 and 1998*, www.eia.doe.gov/cneaf/electricity/epav2/html_tables/epav2t1pl/html.
37. *The Aviation & Aerospace Almanac*, Aviation Week Newsletters (Source: GKMC Consulting Services, Inc., based on carrier Form 41 filings with U.S. Department of Transportation), 1999.
38. *Hazardous Materials Shipments*, Office of Hazardous Materials Safety, Research, and Special Programs Administration, U.S. Department of Transportation, Washington, D.C., October 1998.
39. *Oil and Gas Journal* 97, Vol. 1, 1999.
40. *Energy and Environmental Profile of the U.S. Petroleum Refining Industry*, Report by Energetics Inc. for U.S. Department of Energy, 1998.
41. *2000 Lockwood-Post's Directory of the Pulp, Paper, and Allied Trades*, Million Freeman, United News and Media Company, 1999.
42. USDA National Agricultural Statistics Service, www.usda.gov/nass/aggraphs, October 2000.
43. C. R. Handry and S. Neff, *Globalization of the Processed Foods Market*, Edited by D. R. Henderson, Food and Con-

sumer Economics Division, Economic Research Service, U.S. Department of Agriculture, Agriculture Economic Report No. 742.

44. *Science of Technology News*, Vol. 2, Headquarters, U.S. Army Materiel Command, November 1997.

45. *Analysis of the Total System Life-Cycle Cost of the Civilian Radioactive Waste Management Program*, DOE/RW-510, U.S. Department of Energy, Office of Civilian Radioactive Waste Management, Washington, D.C. 20586, December 1998.

ANALYSIS

| | |
|--|-----------|
| CHAPTER 2 ANALYSIS OF FAILURES OF METALLIC MATERIALS DUE TO ENVIRONMENTAL FACTORS | 27 |
| CHAPTER 3 LABORATORY ASSESSMENT OF CORROSION | 47 |
| CHAPTER 4 LIFETIME PREDICTIONS OF PLASTICS | 65 |

CHAPTER 2

ANALYSIS OF FAILURES OF METALLIC MATERIALS DUE TO ENVIRONMENTAL FACTORS

K. E. Perumal

Corrosion and Metallurgical Consultancy Centre, Mumbai, India

| | |
|--|----|
| 2.1 INTRODUCTION | 27 |
| 2.2 CLASSIFICATION OF FAILURES | 27 |
| 2.3 ANALYSIS OF FAILURES | 28 |
| 2.4 CASE HISTORIES OF ENVIRONMENT-RELATED FAILURES | 29 |

| | |
|-----------------|----|
| 2.5 CONCLUSIONS | 45 |
| 2.6 REFERENCES | 45 |

2.1 INTRODUCTION

In a *Handbook of Environmental Degradation of Materials*, inclusion of the chapter “Analysis of Failures Due to Environmental Factors” assumes great importance. This is because unless the failures are analyzed in a systematic, detailed manner, the main causative factor arising from the environment cannot be determined. If such determination is not made and appropriate remedial measures are not implemented, there is no guarantee that the failure would not repeat itself on the replaced structure, column, vessel, pipe, tube, and so forth. This chapter presents certain case studies of recent failures, analyzed by the author, attributable to environmental factors. All the case studies are concerned with process equipment used in chemical process industries and made of metallic materials, carbon steel, stainless steel or nickel base alloy.

2.2 CLASSIFICATION OF FAILURES

The word “failure” in chemical process equipment denotes unexpected unsatisfactory behavior of the equipment leading to non-functioning with respect to desired operation within the design life period of the equipment. Such behavior is often referred to as “premature failure.” The causative factors can be classified into two main categories:

1. Material/Manufacturing-related
2. Environment/Operation-related

2.2.1 Material/Manufacturing-Related Causes

These causes arise from defects in material of construction (MOC) of the equipment and the fabrication steps through which the material was shaped and processed to arrive at the desired equipment. This chapter will not discuss this category of causes.

2.2.2 Environment-Related Causes

These causes arise from the environment to which the equipment is exposed during service, both the internal chemical process medium and the external medium, such as the prevailing atmosphere, insulation, and so forth. The operation-related causes are closely linked to the environment in that failures arise if the actual operating conditions fall short of or exceed the specified limits.

2.2.3 Environment-Related Categories

The environmental factors can be further classified into five categories, as follows:

1. Deviations within the chemical composition of the fluid being handled in the chemical process, such as the following:

- Condensation occurring within the vapor phase
 - Concentration of aggressive species suddenly increasing
2. Unexpected impurities present within the fluid being handled, such as the following:
 - Chloride and oxygen in boiler feed water
 - Sulfur in petroleum crude
 3. Operating temperatures different from those designed and specified
 - Exceedingly high temperatures leading to creep, oxidation, sulfidation, etc.
 4. Operating pressures different from those designed and specified, such as high pressures in autoclaves and boilers
 5. The environment external to the process equipment becoming aggressive, such as marine and humid atmospheres attacking uninsulated external surfaces of the equipment
 - Insulations becoming wet and corrosive

2.2.4 Environmentally Induced Failures

The environmentally induced failures in process equipment can be also classified into the following, based on the final appearance or mode in which the failure presents itself:

1. High temperature failures (temperatures higher than the boiling point of the process medium to which the equipment is exposed)
 - a. Oxidation
 - b. Sulfidation
 - c. Carburization
 - d. Chlorination
 - e. Creep
 - f. Plastic deformation—yielding, warping, sagging, bowing, etc.
2. Ambient temperature failures (temperatures less than the above-mentioned boiling point)
 - a. Corrosion in its various forms
 - General uniform corrosion
 - Pitting
 - Crevice corrosion
 - Galvanic corrosion
 - Intergranular corrosion
 - Selective leaching
 - Stress corrosion cracking (including hydrogen-related cracking)
 - Corrosion fatigue

- Erosion corrosion by high velocity and by slurry movement
- b. Overload mechanical failure

3. Low temperature failures (temperatures lower than ambient, including sub-zero)
 - a. Brittle mechanical failures at temperatures lower than ductile brittle transition temperature (DBTT)

2.3 ANALYSIS OF FAILURES

This chapter presents a few case studies illustrating some of the above-listed environmental factors leading to premature failures of chemical process equipment. Each failure has been analyzed by the author to the extent the case merits, so as to arrive at the actual cause of the failure and to make appropriate recommendations to avoid the repetition of the same failure in the future.

The detailed failure analysis involves roughly the following steps.

2.3.1 SITE Visit

Site visits are for the following purposes:

- Inspect the failed equipment and also the nearby upstream and downstream equipment to the extent accessible.
- Closely examine the failed area and record relevant features.
- Obtain representative cut samples containing the failed spots and the failure features, and also samples from typical unfailed areas. Cutting of samples may not be possible and/or may not be necessary in many cases. Detailed records of the appearance of the failure must be relied upon in such cases, and at times such records are themselves sufficient. If necessary, non-destructive tests such as radiography, ultrasonic, or dye-penetrant tests need to be performed on the equipment in position at the failed locations.
- Obtain representative samples of scales, deposits, corrosion products, etc. in loose or adherent contact with the inside surface (process side) of the equipment.
- Thoroughly discuss with plant personnel the design, material of construction, specified and operating service conditions, and operational/inspection history of the failed equipment. The service conditions would include the chemical composi-

tions of the fluids being handled, and the equipment's design, operating temperatures, and pressures. Variations in these factors over a meaningful period of time prior to the failure should also be noted.

2.3.2 TESTING OF SAMPLES

Some of the more frequently used tests are listed below, but not all of these need to be performed. Depending upon the merit of each case, select from the following:

- Non-destructive tests like radiography, ultrasonic, dye-penetrant, etc.
- Chemical and/or X-ray diffraction analysis of both the metal and deposit samples
- Mechanical tests—strength, ductility, hardness, toughness, etc.
- Microscopic examination (optical and/or scanning)

The purpose of the tests is to trace the progress of the failure mode, to check the nature and purity of the metal and deposit samples, to determine whether any unusual impurity has been present in the medium, and to verify whether the equipment conforms to the stated specification under which it was designed, fabricated, and put to use.

2.3.3 Analysis, Interpretation, and Diagnosis of the Failure

The site observations and sample test results should be analyzed as a whole package. If necessary, support from published literature should be obtained. All these should be viewed together, with the aim of arriving at the right diagnosis and the root cause of the failure.

2.3.4 Submission of Failure Analysis Report

The report should contain the following:

- Statement of why the said failure analysis was necessary, verifying that the failure was premature
- Factual summary of the site observations and discussions
- Actual sample test results

- Interpretation, discussion and analysis of all the input information
- Diagnosis of the failure
- Explanation of all the observed symptoms using the stated diagnosis
- Easily implementable, practical recommendations to prevent similar failures in the particular site

2.4 CASE HISTORIES OF ENVIRONMENT-RELATED FAILURES

This section deals with the actual case studies conducted by the author. In the presentation of each case study, the environmental factor that was responsible for the failure is discussed in detail. In all the cases, the material and manufacturing quality of the equipment were checked during the failure analysis procedure, and were found to be not responsible for any failures. Hence, the material and manufacturing quality of the equipment are not discussed here.

2.4.1 Failure of A Natural Gas Feed Preheater in a Fertilizer Plant

A fertilizer plant producing ammonia and urea uses natural gas (NG) as the feedstock. The waste heat from the primary reformer is used to heat various streams for different purposes. One such purpose is to preheat the feedstock NG from ambient temperature to some elevated temperature prior to different processing steps. The preheating is done in a set of parallel coils. The coils are made of seamless pipes of low-alloy steel conforming to ASTM Specification A-335/P-11, a chromium-molybdenum alloy steel containing 1.0–1.5% Cr, 0.44–0.65% Mo and 0.05–0.15% C. The pipes are of size 4.5 in. outside diameter (OD) and 6.03 mm wall thickness (WT). The pipes failed by leaking at several places after about 23 months of operation, and this was considered a premature failure.

The pipe is finned on the outside surface with carbon steel strips. The source of heat, namely, the flue gas from the reformer, flows along the outside surface of the pipe. Its heat is dissipated through the wall to the NG feed gas flowing along the inside surface of the pipe. The preheater was designed for NG feed inlet and outlet temperatures of 30 °C and 370 °C, respectively.



FIGURE 2.1 The leaking pipes of the NG Feed Pre-heater Coil. Water-leaks during testing are seen.

The leakage spots were so wide that during water testing after the pipes were removed, the water profusely leaked out in thick streams (see Figure 2.1). The pipe was longitudinally cut and its inside surface examined. Formation of thick corrosion product scale, its breaking after a certain thickness followed by hole formation could be seen on the inside surface (see Figures 2.2 and 2.3). A close-up view of one of the leaking holes on the inside surface revealed that it initiated on the inside surface and propagated toward the outside surface (see Figure 2.4).

The outside surface of the pipe showed warping of the fins at many places. At a few places where leakage has occurred, heavy scales could be seen. The latter is considered a post-leakage occurrence.

The scale on the inside surface was collected, examined and analyzed. It was highly magnetic. Chemical analysis of the scale for certain elements gave the following results:



FIGURE 2.2 View of localized heavy scale with a leaky spot on the inside surface.



FIGURE 2.3 Close view of the inside thick scale showing areas of localized rupture leading to hole formation.



FIGURE 2.4 Close-up view of the leaky hole on the cut sample, as seen on the inside surface. Initiation of the hole on the inside surface and growth towards the outside surface can be seen.

| Elements | Wt. (%) |
|------------|---------|
| Carbon | 19.56 |
| Sulfur | 10.06 |
| Chromium | 0.32 |
| Molybdenum | 0.25 |
| Iron | 60.00 |

From the magnetic nature of the scale and predominance of iron and sulfur, it was inferred that the scale was mainly iron sulfide. There was entrapment of hydrocarbon from the NG and trace quantities of chromium and molybdenum from the pipe steel. Figure 2.5 shows penetration by some species of the NG gas into the metallic structure of the pipe



FIGURE 2.5 Microstructure of the wall of the coil pipe, near the inside surface showing penetration by some species (sulfur) from the NG. (100×).

through the inside surface; the species was apparently sulfur.

The sulfur content in the NG feed is not routinely measured, but was said to be about 0.3 ppm. This level is considered normal by the plant personnel and was taken into account during design of the pre-heater with respect to choosing the material of construction (MOC), sizing, and establishing operating parameters.

Figure 2.6 shows the microstructure of a longitudinal section of the wall of the pipe near a leaking hole. The pipe wall is seen in the bottom half, with thickness reducing from right to left. The fin is

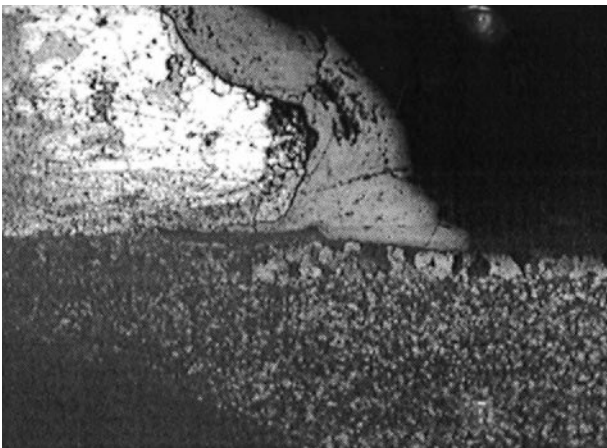


FIGURE 2.6 Microstructure of the wall of the coil pipe, longitudinally cut across a place close to the leaky hole. Gradual wall thinning of the coil, grain growth on the coil outside surface, the outside fin and the scale on the outside fin, all can be seen. (50×).

shown in the top half covered with heavy oxide scale. Heavy grain growth can be seen on the outside surface of the pipe close to the fin.

Figure 2.7, at a higher magnification, shows excessive grain growth on the outside surface of the pipe, at a place between the fins where there is direct flue gas contact.

This excessive grain growth indicates that there had been some continuous exposure to some elevated temperatures (much higher than the design value) for a long period of time. Scrutiny of the records of the operating parameters revealed actual temperatures much higher than the design values, as shown in the table below.

| Parameter | Design °C | Actual °C |
|------------------------------|-----------|-----------|
| NG outlet temperature | 370 | 490 |
| Flue gas inlet temperature. | 425 | 521 |
| Flue gas outlet temperature. | 350 | 428 |

The reader's attention is drawn to the following three observations:

1. The scale was mostly iron sulfide.
2. Finite quantity of sulfur was present in the NG feedstock.
3. Operating temperatures, and hence the pipe wall temperatures, were much higher than the design values.

From these three significant observations it was diagnosed that the leakage was due to excessive sulfidation on the inside surface of the pipe due to the

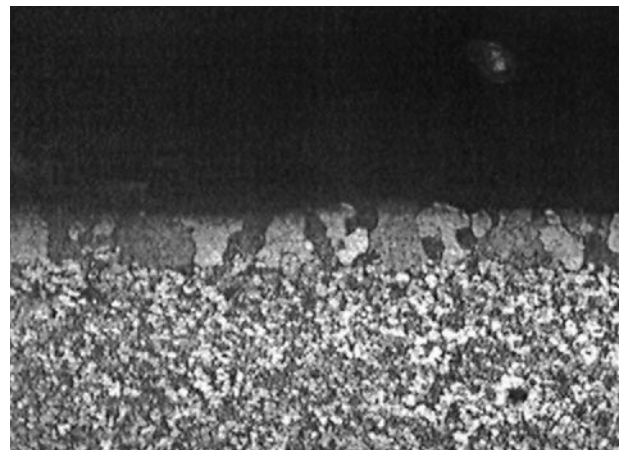


FIGURE 2.7 Microstructure of the wall of the coil pipe, near the outside surface showing excessive grain growth on areas between the fins. (100×).

actual operating temperatures being much higher than the design values. This was an environmental factor. Direct reaction of organic sulfur compounds, present in the petroleum crude with the metal surface was the predominant mechanism of high temperature sulfidation.

Figure 2.8, from Reference 1, shows the effect of temperature on the corrosion rate by sulfur on carbon and alloy steels. The figure is a summary of actual industrial experience. The strong effect of temperature on the corrosion rate can be seen. One can notice that 1–3% Cr steels corrode at an average rate of 2.54 mm/year at 400 °C, while the pipe under consideration has corroded at a much higher rate of 3.15 mm/year (6.03 mm in 23 months). This means that the tube wall temperatures must have gone to values much higher than 400 °C. This had actually happened, as shown in the table of comparison above.

Iron sulfide film on steel surfaces is initially protective. But after a certain thickness, particularly at elevated temperatures, film breaks up locally and exposes the base metal. More and more sulfidation takes place preferentially at these localized places. The film thus formed at these localized places breaks

up after a certain thickness. This cycle continues, leading to hole formation followed by leakage.

The following recommendations were made for remedial measures:

1. Sulfur in the feedstock NG must be checked on a routine basis. Any abnormally high value should be noted and corrective actions should be taken at the source of NG to reduce the level of sulfur to acceptable levels.
2. Operating temperatures must be kept well below the maximum design values.
3. As a long-term measure, alloy steels with higher alloy content should be considered for replacement with a better MOC.

2.4.2 Failure of a Reformer Tube in a Fertilizer Plant

Fertilizer plants that produce ammonia use reformer tubes to reform the feedstock gas into synthetic gas in the presence of steam for further processing to produce ammonia. These are a series of centrifugally-cast, thick-walled, high-alloy stainless steel tubes installed in a furnace. The inside of the tubes is packed with a catalyst through which the process gas travels, while the outside of the tubes is exposed to the furnace atmosphere. The process gas enters the tubes at the top at about 530 °C. It gets reformed within the tubes at a pressure of 38 kg/mm² while traveling downward, and exits at about 730 °C at the bottom.

Recently, in one such plant, a reformer tube suddenly cracked after about 10 years of service; its expected service life was about 20 years. Since the cracking was sudden and unexpected, a detailed failure analysis study was carried out.

The tubes were made of high-alloy austenitic stainless steel, 25/35CrNiNbTi, and were of size 152 mm OD, 12.0 mm WT and 11.0 m long. The cracked tube was inspected in position within the reformer. It had been split by two diagonally opposite longitudinal (vertical) cracks, one on the “east” side and the other on the “west” side. A close examination of the cracked tube in position within the reformer showed that the cracks initiated in the bottom-most segment and propagated to the next top segment above across a butt weld (see Figure 2.9).

The crack was first detected during a fire on the east side. During the process of shutting off the reformer and putting out the fire, the crack on the west side occurred. The entire cracked length with 6 in. above and below was cut from the 11-meter long

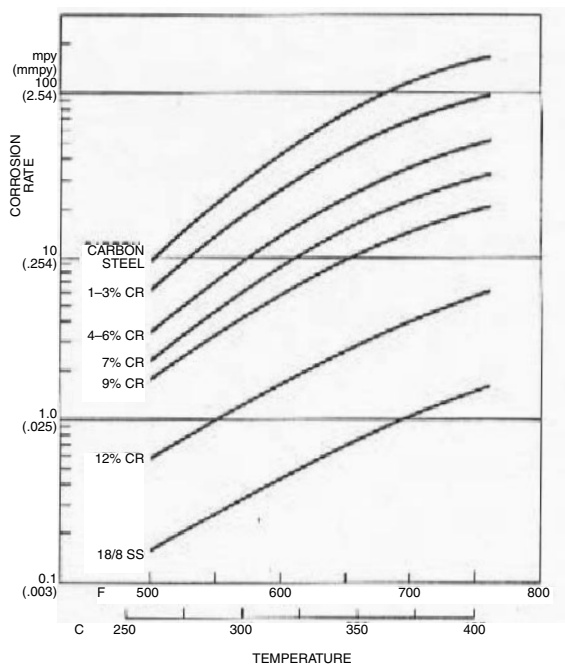


FIGURE 2.8 Average Corrosion rates of high temperature sulphur corrosion in a hydrogen-free environment as compiled from 1961 A.P.I questionnaire data from industry desulfurizing processes and published or reported data—nondesulfurizing processes (Ref. 1).



FIGURE 2.9 A close-up of the top portion of the reformer tube crack extending into the second segment from the bottom across a butt weld.

tube (see Figure 2.10). On this cut length, measurements of wall thickness and circumference on the east and west split portions were made at short intervals over the entire length. From the measured circumference, outer diameter values were computed. Thickness and OD values are given in Table 2.1.

One can notice the following in this table:

1. Wall thickness is consistently lower on the eastern crack tip (average 12.46 mm) and higher on the western crack tip (average 12.86 mm).
2. A maximum OD of 157.18 mm was measured. This corresponds to 2.7% circumferential elongation, considering 153 mm as the originally installed OD. This is quite a high amount of plastic deformation in the cracked portion.

Two samples were cut for detailed microscopic examination. Sample 1 is from the cracked bottom-most segment, while Sample 2 is from the next segment on the top, at a section well away from the crack. A close examination of the inside surface of Sample 1 showed a series of bubbles on the surface (see Figure 2.11). Such bubbles were present only on the east half of the cracked portion and not on the west half. Sample 1 was highly magnetic while Sample 2 was totally non-magnetic.

Transverse (radial) and longitudinal (along the length) cross sections were cut from both samples and microscopically examined. Figure 2.12 shows, in the as-polished condition, the transverse cross section near the inside surface across the bubble areas of Sample 1. One can notice localized carbur-



FIGURE 2.10 The length containing the cracks cut from the reformer tube.

TABLE 2.1 Outside Diameter, OD, and Wall Thickness at Various Locations Along the Cracked Portion of the Failed Reformer Tube

| Circumference (mm) | OD (mm) | Wall Thickness (mm) | |
|--------------------|---------|---------------------|------|
| | | East | West |
| 489 | 155.59 | 12.6 | 12.7 |
| 488 | 155.27 | 12.5 | 12.6 |
| 479 | 152.41 | 12.6 | 12.8 |
| 483 | 153.68 | 12.7 | 12.8 |
| 490 | 155.91 | 12.6 | 13.3 |
| 487 | 154.95 | 12.7 | 13 |
| 490 | 155.91 | 12.4 | 12.9 |
| 488 | 155.27 | 12.2 | 12.8 |
| 489 | 155.95 | 12.4 | 12.8 |
| 491 | 156.23 | 12.5 | 12.7 |
| 490 | 155.91 | 12.4 | 12.6 |
| 489 | 155.59 | 12.1 | 12.8 |

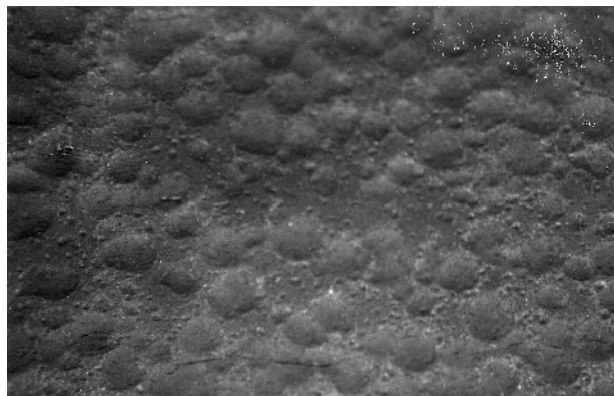


FIGURE 2.11 A close-up view of the bubbles on the inside surface of Sample 1 cut from the bottom segment of the reformer tube.

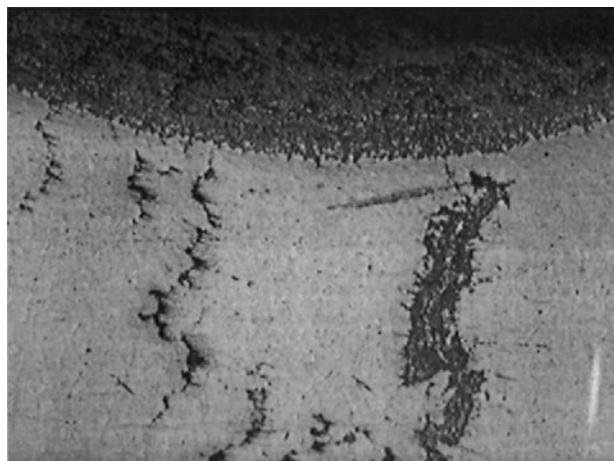


FIGURE 2.12 Photomicrograph, in the as polished condition, of the transverse cross section near the inside surface of Sample No. 1, from the cracked segment (50 \times).

ization and sections of longitudinal cracks. These cracks are within the wall of the tube, not necessarily starting from the inside or outside surface of the tube. Figure 2.13 shows two such cracks well within the interior of the wall of the tube. Figure 2.14 shows the transverse cross section, in the as-etched condition, well within the wall. Cracks could be seen along grain boundaries not connected to the inside or outside surface.

The longitudinal cross sections showed long cavities rather than sharp cracks. This indicates that the cracks observed in the transverse cross section run parallel to the central axis, not radially.

The microstructural features described above for Sample 1 (from the cracked portion on the bottom



FIGURE 2.13 Photomicrograph of cracks in the mid-wall of Sample No. 1. (50 \times).

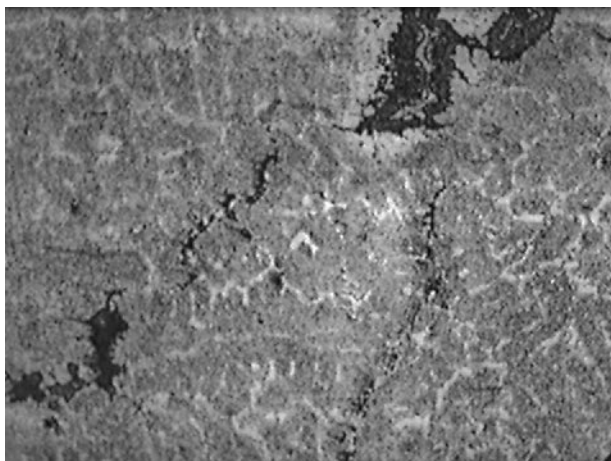


FIGURE 2.14 Photomicrograph, in the as etched condition, of the transverse cross section of Sample No. 1 from the cracked segment, within the mid-wall. (100 \times).

segment) were not observed in Sample 2 (from the uncracked next top segment). No unusual features were seen.

The following diagnosis was drawn from the above observations: The sudden cracking was the result of “*accumulated localized creep*” at the bottom-most segment of the tube, particularly on the east half. The presence of multiple longitudinal grain boundary cracks within the body of the wall, not connected to inside or outside surface, strongly points to this diagnosis.

The ASM Metals Handbook (Reference 2) defines “creep” as follows: “The flow or plastic deformation of metals held for long periods of time at stresses lower than the normal yield strength. The ef-

fect is particularly important if the temperature of stressing is in the vicinity of the recrystallization temperature of the metal.”

As is clear from the above definition, creep results in plastic deformation, and the partitioning of grains leads to cracks along the grain boundaries. The circumferential elongation of 2.7% measured at the maximum diameter position at the cracked bottom segment demonstrates the gross plastic deformation the tube had undergone. Consistent lower wall thickness along the east side, where crack initiated, was a result of such plastic deformation. Apparently the net creep was much higher on the east side than on the west side. Presence of bubbles on the internal surface of the tube on the east side also indicated localized plastic deformation (creep) within the wall close to the internal surface.

The observed cracks were all longitudinal, running along the length of the tube, not radially. This is also evidence of the creep phenomenon. The stress necessary for the creep was the hoop stress due to internal operating pressure of 38 kg/mm². Since the stress acted circumferentially, the cracks occurred in a perpendicular direction, namely, along the length of the tube.

Creep occurs at elevated temperatures—the higher the temperature, the faster the creep rate. The creep rate of centrifugally-cast, high-alloy austenitic stainless steel 25/35CrNiNbTi at the reformer operating temperature of 730 °C maximum is well within limits (well below 0.05% per year). Hence, it would not be expected to show excessive creep at operating conditions of 730 °C temperature and 38 kg/mm² pressure, since the latter introduces a stress well below the allowable stress. Therefore, the observed high creep must have occurred due to some localized undetected “very high temperatures,” an environmental factor. Localized carburization on the inside surface of the bottom-most segment, resulting in this segment becoming magnetic, suggests exposure to very high temperatures in this segment.

During routine periodic inspection (every two weeks in the service period of 10 years), hot spots had often been observed in this tube and corrective actions were taken immediately. Similarly, the tube had shown outside skin temperatures exceeding the normal maximum limit of 880 °C, quite often reaching 930 °C. Though these were considered normal and preventive steps were taken as soon as they were detected, the accumulated damage (creep) could not be removed. Creep is very sensitive to slight increases in temperatures.

The following recommendation was made as a preventive measure: For tubes which show accumulated creep of 1.5% and above, monitor hot spots and outside skin temperatures more frequently than the current schedule and take corrective actions immediately.

2.4.3 Failure of a Furnace Tube in a Petrochemical Plant

In a petrochemical plant, one of the processes involves thermal cracking of organic chloride in the vapor phase at temperatures well above 250°C in a furnace, producing the organic monomer chloride and hydrogen chloride gas. The feedstock is preheated in a preheater coil from 35 °C to 160 °C, vaporized in a vapor coil at about 240 °C, and then cracked in the radiant coil. The cracked products leave the furnace at about 510 °C. A schematic sketch of this process is shown in Figure 2.15. The NiCrFe alloy (Alloy 800HT, as per UNS N08811) is the normally accepted material of construction for the radiant coil. The coil in this case was made of seamless pipes of this material, of size 152.4 mm OD by 12.5 mm WT.

In this case of failure, several portions of the bottom three turns of the radiant coil started leaking within nine to 10 months of service. In several other places on the same coil, wall thickness was reduced to less than 5.00 mm (from the original 12.5 mm). Observations on cut samples established that wall thickness reduction, followed by leakage, was the result of general corrosion. This was followed by hole formation on the inside surface of the pipes (the process side), and not on the outside surface of the pipe (the furnace side). A wall of 12.5 mm thickness which leaks in 10 months due to thickness reduction corresponds to a corrosion rate of 15.00 mm/year. This was an abnormally high corrosion rate, never expected of any material of construction (not even carbon steels). A high-nickel alloy such as UNS N08811 exhibiting such a high corrosion rate was quite unusual and demanded a detailed study.

Representative samples of the pipe containing the leaking area were cut and split open, and the inside surface examined. The latter showed heavy coke deposition, brownish corrosion product and gradual reduction in the wall thickness near the leaking hole (see Figure 2.16). Such features were not present on the outside (furnace side) surface of the coil. Figure 2.17 shows the sample of a coke lump collected from the inside surface of the coil. Coke formation is a part of the process. A decoking operation using

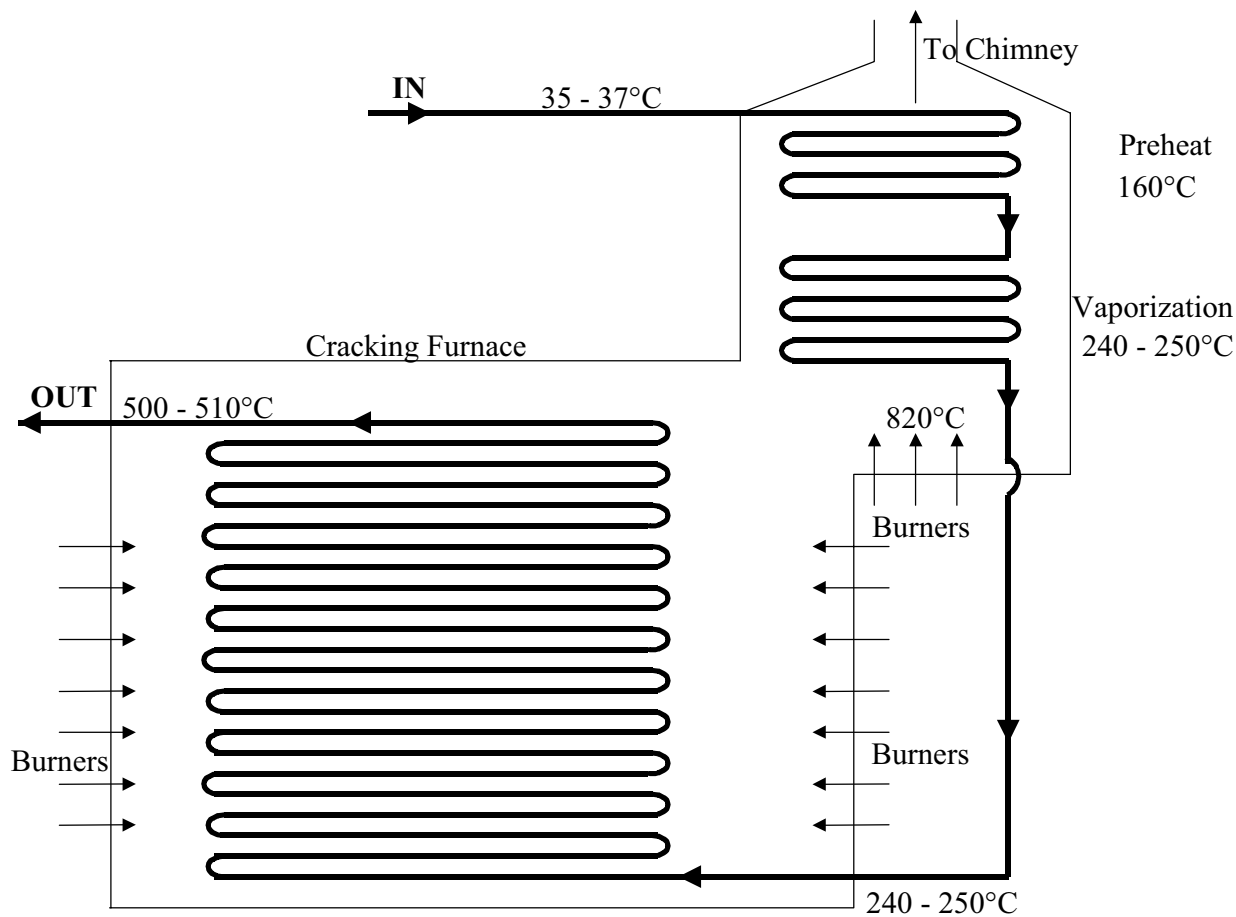


FIGURE 2.15 Furnace coil for cracking organic chloride.

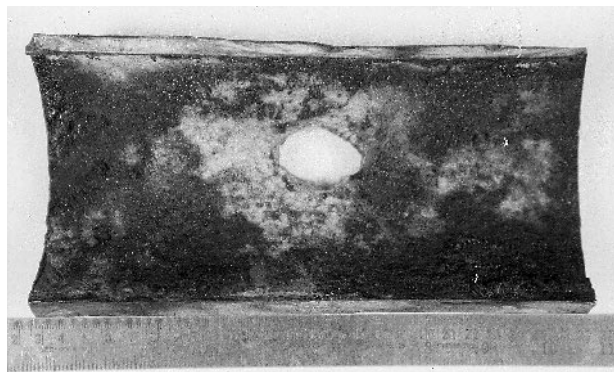


FIGURE 2.16 The inside surface of the radiant coil near the leaked area.



FIGURE 2.17 A sample of a coke lump collected from the inside surface of the radiant coil.

steam is often carried out. Interconnecting network of cracks and heavy porosity could be seen in the coke lump.

While affected pipe samples and the coke lump were being handled, droplets of some liquid oozed out from the pipe inside surface, from the cross section of the wall, and from the coke lump. The liquid actually produced a burning sensation on one's hands, and was chemically determined to be very highly acidic. It also responded positively to tests for acidity and chlorides. The parameters given in the following table were obtained through chemical analysis of the deposit collected from the inside surface:

| | |
|-------------------|------------|
| pH of 1% solution | 3.7 |
| Cr | 0.035 wt.% |
| Ni | 0.042 wt.% |
| Fe | 0.058 wt.% |
| Chloride | 0.048 wt.% |

These observations indicate that liquid hydrochloric acid had been present, in contact with the tube's internal surface. This led to corrosion of the tube material, contributing to the metallic constituents in the deposit. Apparently liquid hydrochloric acid had been entrained into the coke deposits.

Figure 2.18 shows a typical metallographic cross section of the pipe, cut across the leaking hole in the wall near the inside surface of the coil. Three layers can be seen. The bottom-most layer is that of the par-

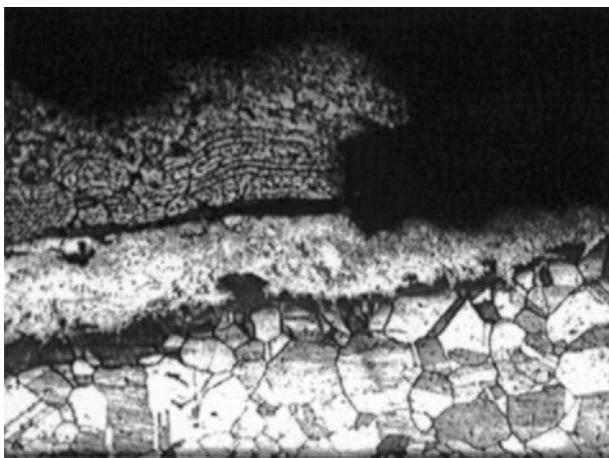


FIGURE 2.18 Photomicrograph of a cross section across a leaked hole near the inside surface of the radiant coil. (50×).

ent metal. Next is a carbide layer with porosity of significant size. The next layer is that of the adherent coke deposit, also porous. Corrosive attack can be seen on the parent metal just below the carbide layer. The attack is general, uniform, and not localized. Liquid hydrochloric acid from the process environment had trickled through the pores in the coke deposit and attacked the base metal, a typical case of corrosion by an environmental factor.

The nickel base alloy UNS N08811 is *not resistant* to corrosion by liquid hydrochloric acid. It is resistant to dry HCl gas, but not to wet HCl acid. As per the data sheet on "INCOLOY 800/800HT" (Reference 3), these alloys have "only limited usefulness for applications involving exposure to sulfuric and hydrochloric acids."

The liquid hydrochloric acid developed in the following way: For some reason, the auxiliary burners for the upstream vaporizer coils had not been in operation. This caused incomplete vaporization, resulting in liquid organic chloride carryover to the radiant sections of the furnace. A look at the operational history of the furnace showed that the extent of vaporization in the feedstock to the radiant section was varying from only 30–58%, while 100% is the satisfactory and expected value.

The moisture in the feedstock was about 50 ppm. In addition, as mentioned earlier, steam is frequently used for removing coke deposit, the latter invariably forming during cracking operations. Some of the steam was entrapped as moisture in the porosity of the adherent coke deposit.

In the radiant section, HCl gas is generated as a byproduct as soon as cracking starts. This HCl gas dissolves in the moisture and forms liquid hydrochloric acid in the first few turns of the radiant coil, where the temperatures are in the lower cracking range. This liquid hydrochloric acid attacks the coil wall from inside. As mentioned above, UNS N08811 is not a suitable material of construction for liquid HCl.

In the farther turns of the radiant coil, the generated HCl gas and the moisture are both in vapor form because of increasing temperatures. The alloy UNS N08811 is resistant to this vapor, being a material basically developed for high temperature service. Hence, there was no attack on the upper turns of the coil.

This was an unusual occurrence because this particular alloy has been a proven material for the said service under design conditions. Unfortunately, during operation, the environmental conditions deviated from those of design, resulting in the failure.

As a remedial measure, it was recommended that the upstream vaporizer should be always on line so that the feedstock organic chloride does not enter the radiant section of the coil in liquid form.

2.4.4 Failure of Plate Elements in a Plate Type Heat Exchanger in a Sulfuric Acid Plant

In plants producing sulfuric acid, the final product (the concentrated acid) is cooled either through a shell and tube cooler or through a plate-type heat exchanger (PHE). Alloy C-276, a nickel-base alloy containing Mo, Cr, Fe, W and Co as major alloying elements corresponding to UNS N10276, is a common acceptable material of construction for such PHEs in sulfuric acid plants. This alloy has extremely good corrosion resistance to both concentrated sulfuric acid and cooling water. In this case study, plate elements of Alloy C-276, 0.63 mm thick, developed pinhole leaks within one year of operation, a very premature failure.

On one side of the plate elements of the PHE, concentrated sulfuric acid (92–99%) enters at 90 °C and gets cooled to 70 °C. On the other side of the element, cooling water enters at 32 °C, extracts heat from the acid through the element and leaves at 43 °C.

Within a year of operation, pinholes developed in the elements, allowing water to enter the acid (see Figure 2.19). On the acid side, sharp holes and corrosive attack downstream of the holes could be seen. On the acid side, immediately downstream of the leaking hole, mixing of water with acid made the

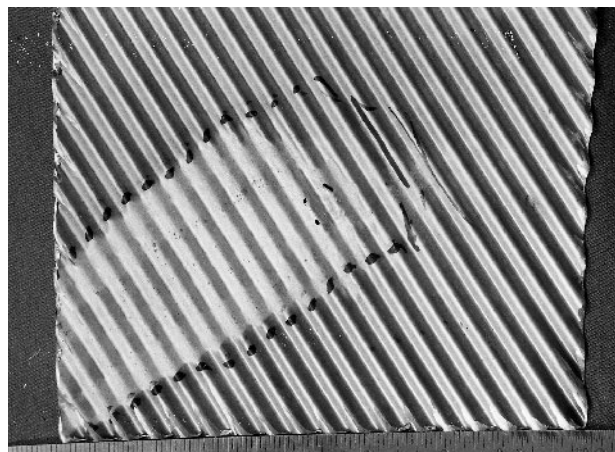


FIGURE 2.19 The leaky pin holes along with the corroded area on the acid side.

acid dilute and increased the local temperature. Hot dilute sulfuric acid corrodes Alloy C-276. Other than this corroded region, the rest of the element area (which was also in contact with the acid) was corrosion-free. A close examination of the affected area near the leaking holes on the acid side showed general uniform acid corrosion (see Figure 2.20).

Interesting observations were made when the cooling water side of the affected plate elements near the leaking holes was closely examined. Thin deposit-like material interspersed with white circles was the main observation (see Figures 2.21 and 2.22). Within each of the white circles, shiny central spots could be seen.

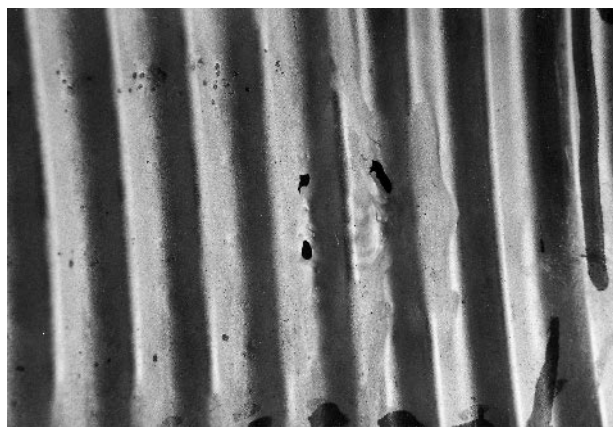


FIGURE 2.20 A closer view of the leaky pinholes and the nearby affected area on the acid side.

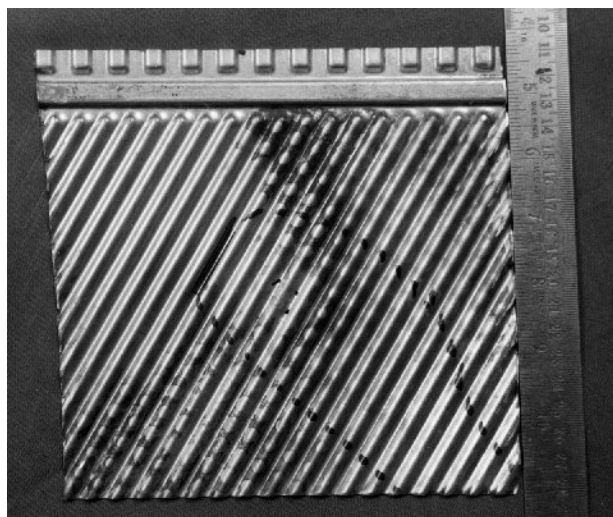


FIGURE 2.21 Appearance of the waterside surface near the leaky pinholes.

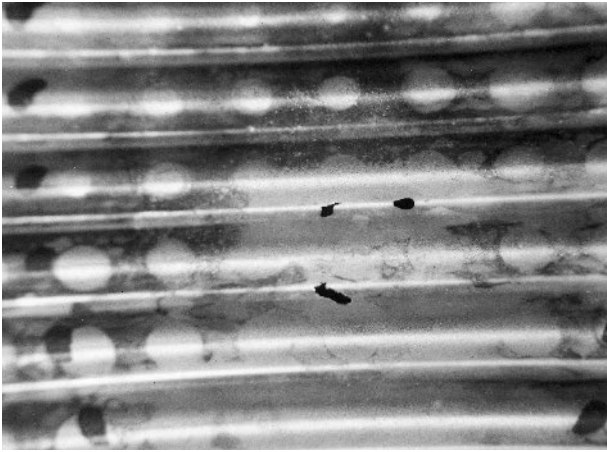


FIGURE 2.22 A closer view of the pinholes and the nearby affected area on the waterside.

These shiny white areas were bacterial colonies on the cooling water side. Microscopic bacteria thrive in such colonies, generating highly acidic secretions. Since bacteria strongly cling to the metal surface, such acidic secretions remain stagnant, initiating and propagating pitting corrosion of the underlying metal, and very quickly lead to pinhole leaks. In this case, these pinholes were the starting points of the leakage problem, undoubtedly an environmentally-induced failure.

The cooling water used for industrial purposes is a good medium for fostering microbacterial organisms. As these organisms thrive, they grow large and cause fouling as well as localized pitting corrosion, as described above.

The usual preventive action against this phenomenon is to kill these microbial organisms by adding biocides, either gaseous chlorination or proprietary chemical biocides.

Apparently the cooling water used in the plant under consideration had not been treated properly against microbial organisms. Proper chlorination with specially studied and formulated biocide treatment would have prevented the plate failures. Such actions were recommended as remedial measures.

2.4.5 Failure of Tubes in an Alcohol Superheater in a Petrochemical Plant

In petrochemical plants where alcohol is used as a raw material, it is preheated, vaporized and also superheated in shell and tube heat exchangers. The equipment in this case was a vertical heat exchanger

used for superheating alcohol vapor. The equipment was in operation for only seven months when leakage occurred in almost 30% of the tubes. Since this is a highly premature failure, a detailed failure analysis study was conducted.

The seamless tubes were made of Type 304 stainless steel (304SS) (UNS S30400), manufactured per ASTM Specification A-213/304. They were of size 19.05 mm OD, 2.77 mm WT, and 2,500 mm length. There were 195 of them in this case. The shell was made of carbon steel and the top and bottom tube-sheets were also made of Type 304SS. Alcohol vapor enters the inside of the tubes at the bottom at about 115°C and leaves at the top at about 185°C. The necessary heat was supplied through high-pressure steam flowing on the shell side (outside of the tubes) from top to bottom.

The positions of the leaking tubes were random, as shown in Figure 2.23, without any pattern or preference to locations. Every leaking tube that was pulled out was found to have a completely penetrating circumferential crack at a distance of about 5 mm from the top side of the bottom tube-sheet, as shown in Figure 2.24.

The cracked tubes could be easily separated into two pieces along the cracked section. Examination of the fracture surface at the crack of one of the failed tubes showed the following: (1) there was no thickness reduction on the wall of the tubes at the fractured section; (2) the fracture did not conform to

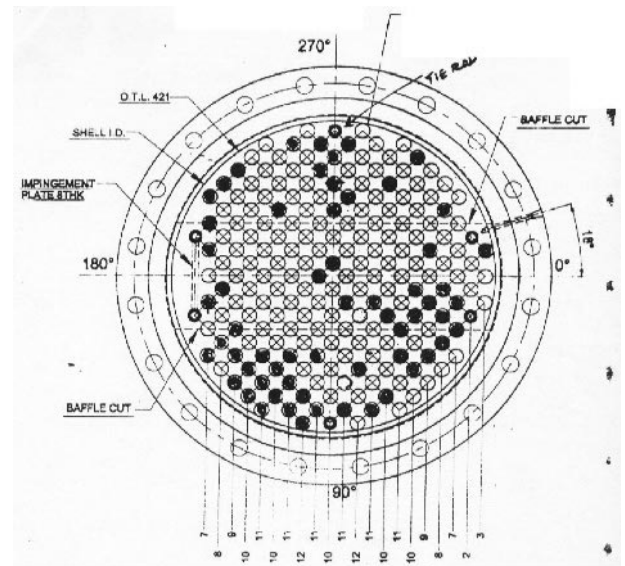


FIGURE 2.23 Random location of the leaky tubes in the alcohol vapor superheater.

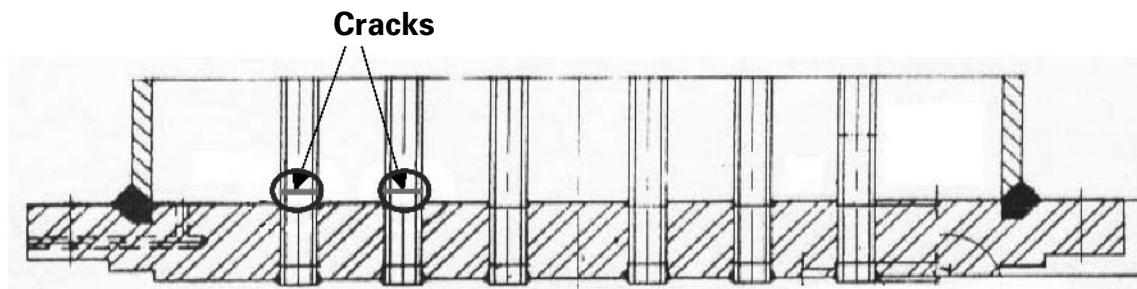


FIGURE 2.24 Longitudinal sketch of the bottom portion of tubes and bottom tube-sheet showing the location of the circumferential cracks in the alcohol vapor superheater.

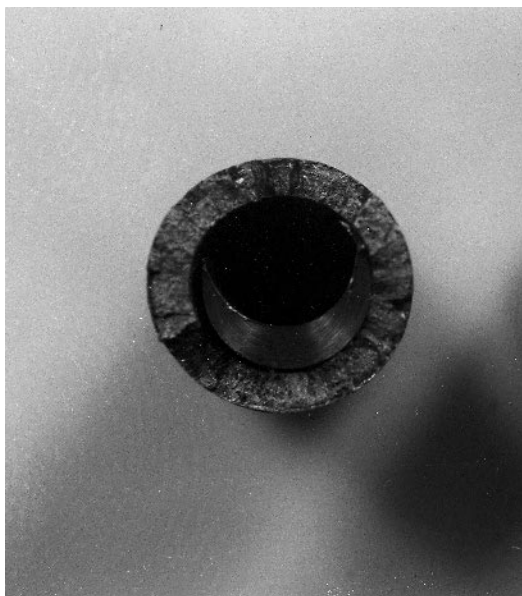


FIGURE 2.25 Fracture surface at the crack of a failed tube of the alcohol vapor superheater.

any mechanical overload ductile/brittle failure; and (3) the crack was not clean shear—it was step-wise grain breakage (see Figure 2.25).

One of the cracked tubes was sectioned longitudinally and examined inside. There was heavy brownish rust deposit on the inside surface for a short distance on either side of the crack (see Figure 2.26). When the rust was removed by light rubbing, localized deep pits and circumferential cracks could be seen on the inside surface. These features were not present on the outside (steam side) surface of the tubes. This means the cracks initiated on the inside surface.

The process-side input was said to consist of roughly 80% alcohol vapor and 20% steam. There

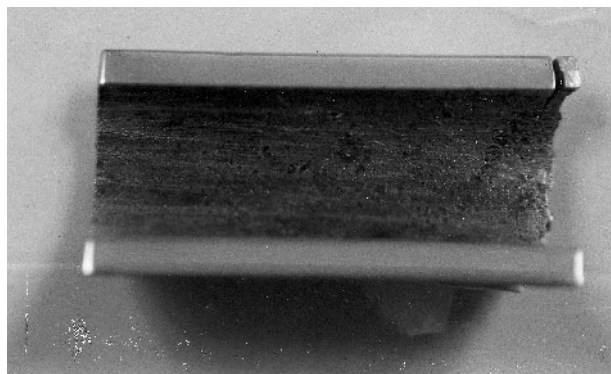


FIGURE 2.26 Inside surface of a failed tube of the alcohol vapor superheater longitudinally cut across the main crack.

was some carryover of liquid alcohol and moisture droplets from the equipment upstream, namely, the alcohol vaporizer. The raw alcohol obtained from distilleries is routinely checked for purity and moisture content among other factors. The following table gives typical specifications for purity and moisture, and the actual test results in this case study:

| Test | Result | Specification |
|------------------------|--------|---------------|
| Purity (% by weight) | 91.30 | 91.96 minimum |
| Purity (% by volume) | 94.06 | 94.68 minimum |
| Moisture (% by weight) | 07.64 | Trace |

One can notice that this particular batch of alcohol did not meet the required specification with respect to both purity and moisture content. Similar quantities of moisture, 7–11%, were reported for certain months within the completed operating period prior to the failure.

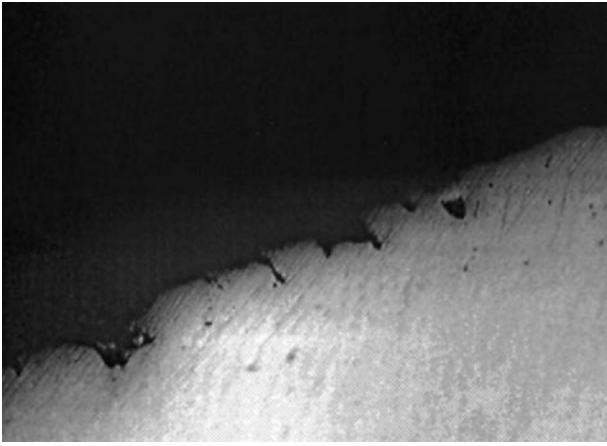


FIGURE 2.27 Microstructure of the longitudinal cross section of the inside surface of a failed tube of the alcohol vapor superheater showing localized deep pits, (200 \times).

A sample of the tube cut longitudinally across the leak location was examined under a metallurgical microscope. Figure 2.27 shows a section of the inside surface, a short distance from the main leaking crack. Localized deep pits can be seen, starting from the inside surface and growing in depth and width. These are corrosion pits typical of chloride attack on austenitic stainless steels.

Figures 2.28 and 2.29 show, in the as-polished condition, many cracks starting from several locations on the inside surface. Cracks initiate both on smooth portions and on the bottom of corrosion pits on the inside surface, and propagate toward the out-

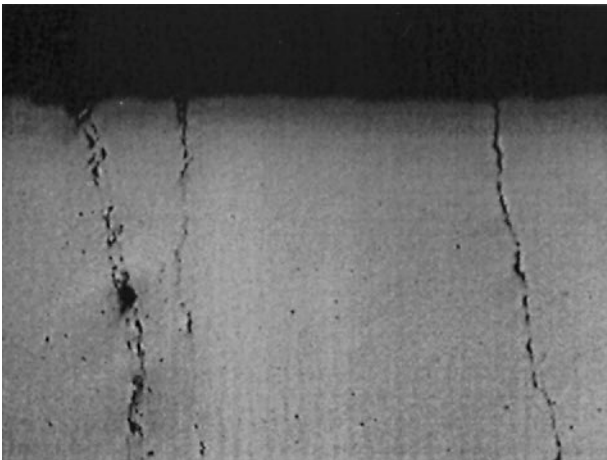


FIGURE 2.28 Microstructure of the longitudinal cross section of the inside surface of a failed tube of the alcohol vapor superheater showing multiple cracks initiating on localized pits, (50 \times).

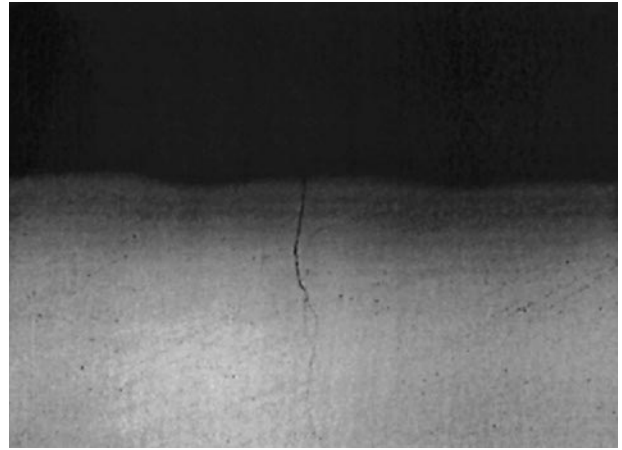


FIGURE 2.29 Microstructure of the longitudinal cross section of the inside surface of a failed tube of the alcohol vapor superheater showing crack initiation on a smooth portion of the surface free from pits, (100 \times).

side surface. The locations where these cracks initiate are about 10–15 mm above the main leaking crack. Figure 2.30 is a composite photomicrograph of two neighboring cracks in the as-etched condition showing the initiation on the inside surface and propagation toward the outside surface. One can notice multiple initiation sites, transgranular path, and branching during propagation of the cracks. These features are typical of chloride stress corrosion cracking (CSCC) of austenitic stainless steels of which Type 304 is one.

The occurrence of CSCC in stainless steels requires the simultaneous presence of the following factors:

- An operating skin temperature above approximately 60 °C
- Dissolved chloride ion in an aqueous phase, even in a small quantity
- Tensile stress, applied or residual, even at low values

In the present case, the skin temperature on the inside surface just above the bottom tube-sheet was well above 60 °C.

Due to carryover of liquid alcohol with the associated water, along with the vapor and steam, there was an aqueous phase present in the areas where cracks occurred. As the process fluid moved vertically up on the tube-side (inside), the water evaporated and there was no further problem in the remaining length of the tubes. The chemical analysis

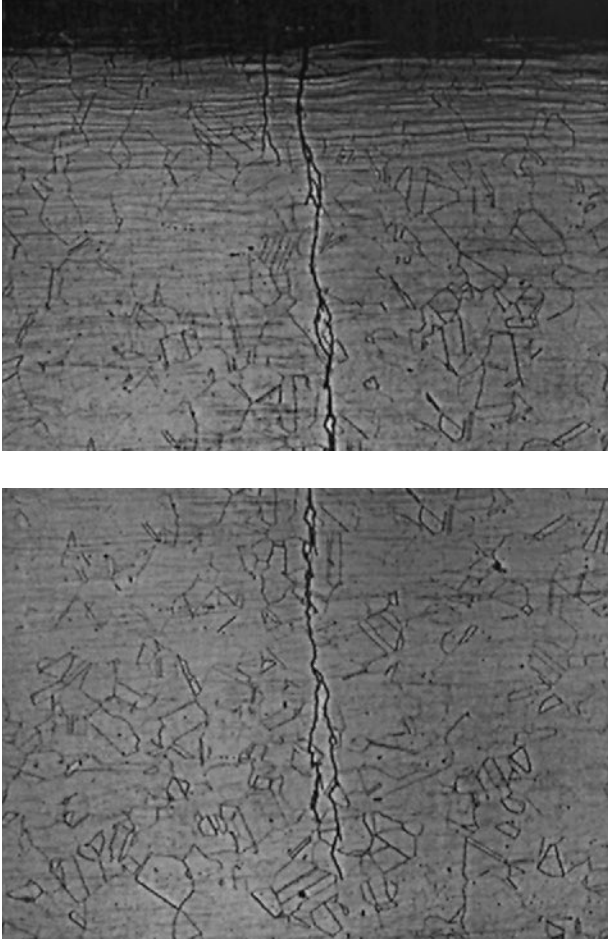


FIGURE 2.30 Composite photomicrograph of two neighboring cracks on the longitudinal cross section of the inside surface of a failed tube of the alcohol vapor superheater, (100 \times).

was performed for the extent of chloride present both in the as-received alcohol and in the process condensate somewhere downstream from the subject superheater, along with pH measurements of the corresponding liquids. The following are the results:

| Sample | pH | Chloride (ppm) |
|-------------------------------|-----|----------------|
| As-received alcohol from tank | 4.8 | 43.0 |
| Downstream condensate | 3.5 | 9.0 |

One can notice that the water associated with the inlet to the superheater under study is acidic in nature and contains an appreciable amount of chloride. As soon as the evaporation within the superheater

starts, the remaining liquid in contact with the hot tube surface at the lower portions becomes much higher in chloride.

Regarding the presence of tensile stress, even a small level of stress (much lower than the mechanical code allowable level) is sufficient to initiate CSCC. Austenitic stainless steels crack by CSCC even at stress levels of about 0.1–0.2 times their ultimate tensile strength. In the present case, a small amount of residual stress was present in the tubes at positions close to the tube-sheet, where the tubes are expanded to the tube-sheet. Stress also arose due to differential expansion of carbon steel and stainless steel. Although these were within the mechanical design limits, they were sufficient to initiate stress corrosion cracks.

Thus, it was diagnosed that the problem was that of stress corrosion cracking due to chloride, an environmental factor.

These were the suggested remedial measures:

- Avoid liquid (alcohol and the associated water) carryover to the evaporator.
- Change the source of alcohol to one free from chloride.
- If the above two measures are not feasible, then change the material of construction to a cost-effective “duplex stainless steel” which has much higher resistance to CSCC than austenitic stainless steels.

2.4.6 Failure of Package Boiler Tubes in an Alcohol Distillery

In distilleries manufacturing alcohol, package boilers are used for meeting steam requirements. The steam condensate from the plant is recycled to the boiler as part of the boiler feed water. In this case, the subject boiler was a fire tube boiler in which the fuel gas flows within the tube while water flows along the outside (shell side) of the tubes. The tubes are made of boiler-quality carbon steel.

After regular commissioning of the boiler, first major inspection of the outside surface (water side) of the accessible boiler tubes was made after about 11 months. Heavy localized rust trees (tubercles) were found to be present at several places. These were mechanically brushed off to the extent they were accessible and the boiler was put back into operation. Tubes showed leakage after an additional operation of about two months, followed by further

leakages after about two and six more months of operation. At that time it was decided to replace the tubes with fresh ones and subject the leaking tubes to a detailed failure analysis study.

The outside surface of the affected tubes showed localized pitting corrosion, with loose brownish rust (corrosion product) within the pits along with grayish black metal (the steel of the tube) underneath (see Figures 2.31 and 2.32). These localized pits had grown in depth and resulted in leakage. Figure 2.33 is the microstructure of a longitudinal section of an affected tube cut across a pit. Localization of pitting corrosion can be seen very clearly. Corrosion was occurring not uniformly throughout the surface, but randomly at localized spots. The depth of the pit seen in this micrograph is about 0.15 mm. Localization of corrosion resulting in deep pitting is typical of attack by chloride, an environmental factor.

The brownish rust collected from the pits was chemically analyzed. The following are the results:

| | |
|---------------------|-------------------|
| pH of 1.0% solution | 3.5 |
| Iron | 67.62% |
| Calcium | 0.14% (1,400 ppm) |
| Sodium | 0.074% (740 ppm) |
| Chloride | 0.030% (300 ppm) |

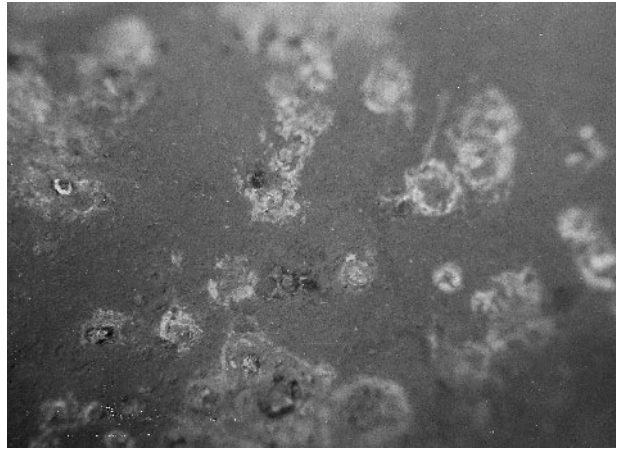


FIGURE 2.32 Close-up view of the pits on the outside surface of one of the affected package boiler tubes.

These results indicate that the deposit was highly acidic and consisted of corrosion product (iron oxide) along with appreciable quantities of calcium, sodium and chloride. Acidity and chlorides are not expected to be present in boiler tube deposits and are not acceptable. Their presence indicated that there had been some ingress of acidic chloride salts into the boiler water circuit. These salts dissolved in water and their solubility limits were exceeded on the hot surface of the boiler tubes, resulting in local-

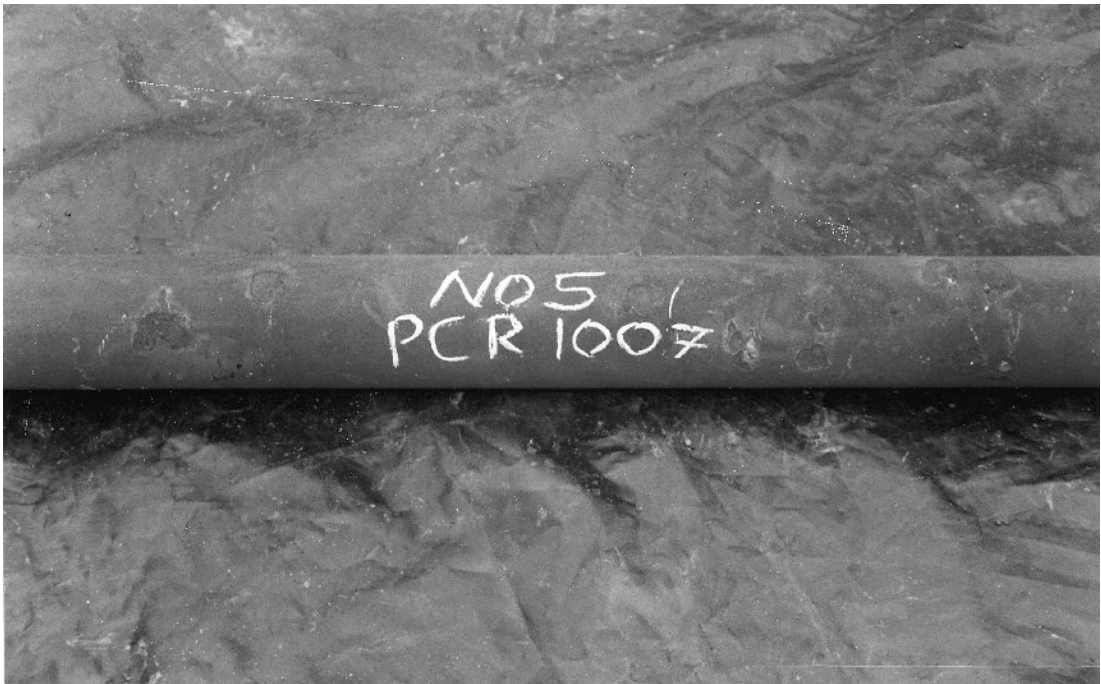


FIGURE 2.31 The outside surface of one of the affected package boiler tubes showing localized pitting.

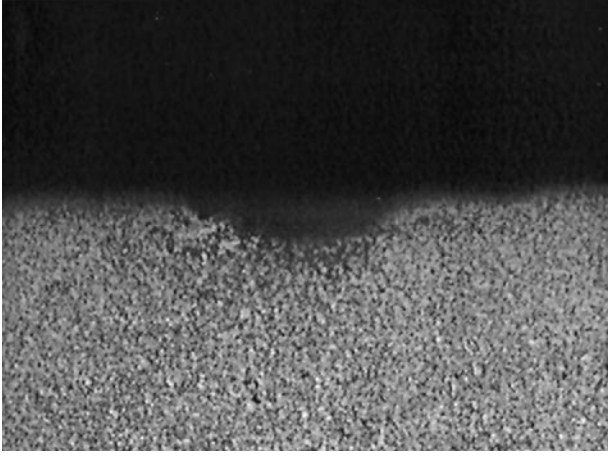


FIGURE 2.33 Microstructure of the longitudinal cross section of a pit on the outside surface of one of the affected package boiler tubes, (50 \times).

ized deposition of salts. The water trapped under these deposits remained stagnant instead of flowing with the bulk water. The deposits were acid-forming and the trapped water became acidic and corroded the tubes locally, leading to leakage over a period of time. This is called “under deposit corrosion.” This would have continued to occur until the deposits

were chemically cleaned and the water chemistry was controlled to avoid entry of acid-forming salts, the chlorides.

The formation of acidic deposits in the boiler under consideration occurred for a long period, some time prior to the first inspection at 11 months after commissioning. Figure 2.34 shows the variation of daily average chloride level in the blow-down water in a month when leakage occurred. One can notice that the chloride increased slowly from about 50 ppm in the beginning (first day of the month) to as high as 180 ppm on the eleventh day of the month. Leakage occurred on fifteenth day, forcing boiler shutdown. Attempts seem to have been made to reduce the chloride level. The boiler was commissioned again on the twenty-sixth day of the month, with about 30 ppm chloride in the blow-down water. This again slowly rose and then fell to a low value of about 20 ppm at the end of the month. One can draw the following inferences from this figure:

- There was a source of chloride contributing to the boiler water. The entire boiler feed water chemical treatment prior to the addition of condensate was found to be satisfactory without contributing chloride. Hence, the chloride came from leakage of distillery process chemicals into the condensate.

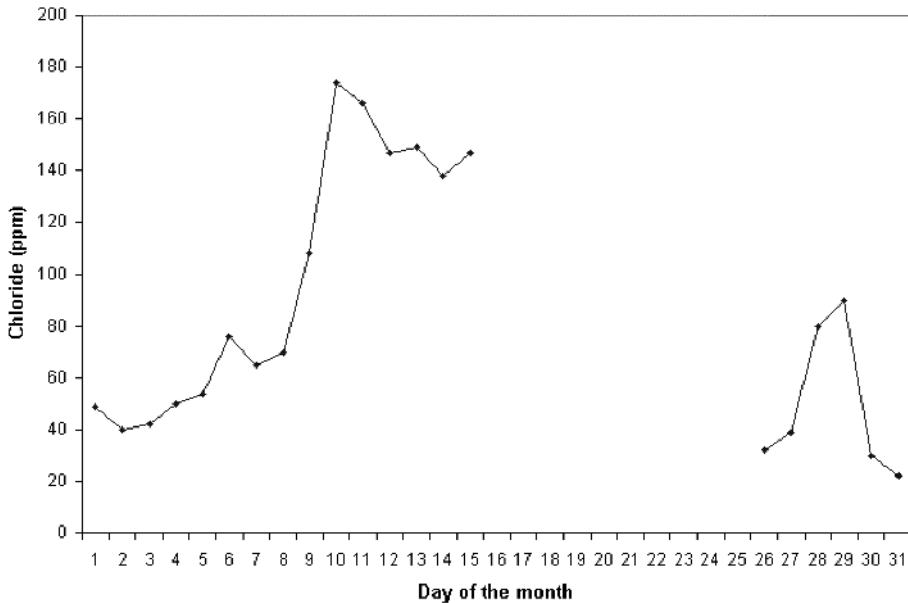


FIGURE 2.34 Variation of chloride in the blow down water over a period of one month in which leakage has occurred in the package boiler tube

- High content of chloride in the boiler water led to leakage in a short time.
- The plant personnel were capable of identifying the source of chloride and controlling it, but not to a desired low value (nil).

It was concluded that the leakage of boiler tubes was due to ingress of chlorides to the boiler water through distillery process chemicals via the steam condensate, which is recycled to the boiler feed water circuit.

It was recommended that this source of leakage within the distillery processes be identified and plugged.

2.5 CONCLUSIONS

This chapter has given some case histories of failure analysis investigations of chemical process equipment made of metallic materials due to certain environmental factors. These environmental factors include:

1. Operating temperatures higher than the design values, either intentional or unnoticed, leading to the high temperature problems of sulfidation and creep

2. Presence of aqueous phase (condensed moisture) in high temperature process gases such as organic chloride gas and alcohol vapor
3. Presence of external acidic chloride salts in boiler water
4. Presence of micro-organisms in cooling water.

These contributory elements cropped up unexpectedly in the operating environment, and therefore were not incorporated in the original design of the equipment. In this respect, the control and maintenance of environmental factors deserve more careful attention than they are presently being given.

2.6 REFERENCES

1. White, R. A, *Materials of Construction for Refineries and Associated Facilities*, NACE, Houston, 1991, Figure 1.11, p.21.
2. *Metals Handbook*, ASM., 1948, p.4.
3. "Incoloy Alloys 800 and 800HT," Data Sheet of Inco Alloys International, 1986.

CHAPTER 3

LABORATORY ASSESSMENT OF CORROSION

Sean Brossia

*Environmental Performance of Materials Section
Southwest Research Institute, San Antonio, Texas*

| | |
|---------------------------|----|
| 3.1 INTRODUCTION | 47 |
| 3.2 IMMERSION TESTS | 48 |
| 3.3 CABINET TESTS | 53 |
| 3.4 ELECTROCHEMICAL TESTS | 55 |

| | |
|------------------|----|
| 3.5 CONCLUSIONS | 62 |
| 3.6 REFERENCES | 63 |
| 3.7 BIBLIOGRAPHY | 63 |

3.1 INTRODUCTION

Corrosion is normally defined as the interaction of a material with its environment through which a chemical or electrochemical reaction takes place, thereby degrading the material. Although there are several alternative (and in many cases similar) definitions, the overall effect of corrosion is that material properties are degraded from interactions with the environment, or the structure itself becomes compromised due to a breach or hole induced by corrosion. Because of the destructive nature of corrosion, there is a considerable economic cost associated with it. A recent study has estimated the annual cost of corrosion in the United States to be at least \$270 billion (1). To minimize long-term costs and other consequences, selection of appropriate materials for construction is particularly vital. To accomplish this, laboratory (as well as field) corrosion tests are often performed to aid in the selection.

In addition to aiding in material selection, laboratory corrosion tests are often utilized to better understand observed failures. In such situations, exposure to the nominal service environment may not be sufficient to induce the in-service corrosion failures observed. This arises because in many cases failure occurs due to upset conditions in which a deviation from the nominal service conditions are encountered. Under these circumstances, a clear understanding of the nominal and upset (or possible upset)

conditions is critical to conducting a laboratory test that is viable and provides the required information.

Selection of appropriate testing conditions, however, can be difficult and is dependent on the anticipated corrosion modes that the structure may encounter while in service. There are many forms (modes, mechanisms) of corrosion that may be encountered. These include the following:

- General corrosion
- Localized corrosion (typically referring to pitting or crevice corrosion, but has also been applied to exfoliation and intergranular corrosion)
- Environmentally assisted cracking (including stress corrosion cracking, hydrogen embrittlement, hydrogen-induced cracking)

General corrosion refers to the overall thinning of the material when it is exposed to the environment of interest (Fig. 3.1). In many respects, general corrosion can be “engineered” around because often times the corrosion rate can be measured in suitable laboratory tests and the subsequent life expectancy calculated. If a longer life is desired, the gage thickness can be increased. For localized corrosion, the corrosion attack is confined to particular locations on the metal and tends to propagate significantly faster than what is observed in general uniform corrosion. An example of pitting corrosion is shown in Fig. 3.2. Consequently, perforation and potential

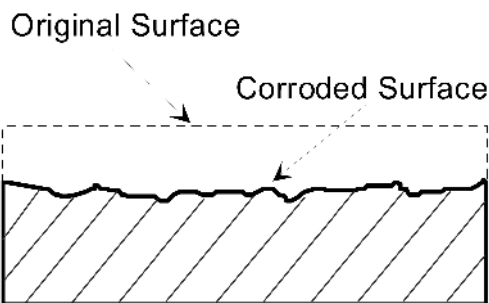


FIGURE 3.1 Schematic illustration of general, uniform corrosion.

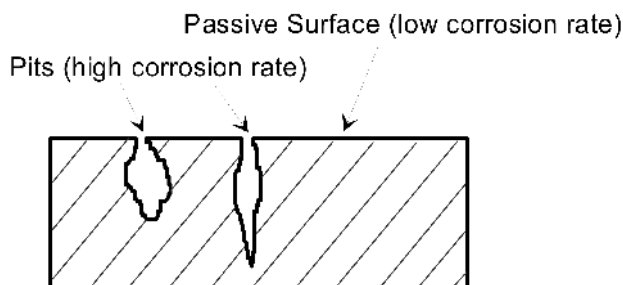


FIGURE 3.2 Schematic illustration of pitting corrosion.

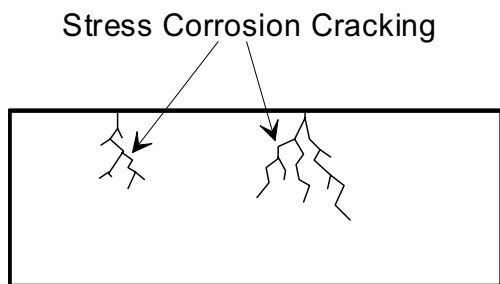


FIGURE 3.3 Schematic illustration of stress corrosion cracking.

loss of adequate strength tends to occur very rapidly. Similarly, environmentally assisted cracking (Fig. 3.3) tends to result in the formation of cracks in the material that propagate much more rapidly than the corrosion rates typically encountered in general corrosion. What makes localized corrosion and environmentally assisted cracking particularly insidious is the fact that they often occur under conditions where the material chosen is expected to perform well and the attack (or at least its extent) can be hidden. Thus, the failures encountered tend to be unanticipated and in many cases catastrophic.

Because corrosion can occur under a variety of conditions, there is a wide array of laboratory tests

that can be performed. These include tests intended to study atmospheric corrosion, corrosion during episodic wet/dry conditions, corrosion under fully immersed conditions, corrosion in soil, corrosion in aqueous solutions, corrosion in non-aqueous solutions (e.g., organic solvents), and molten salts. Because of the wide range in types of corrosion tests available, it is important to consider the in-service environment and the objectives of the tests being performed. If the main objective of the test is to establish anticipated performance or to select a suitable material, then the test environment should closely mimic the expected environment. Care should also be taken to ensure that the expected in-service corrosion failure mechanism is reflected in the laboratory test (e.g., if crevice corrosion is expected in service then the laboratory test should also be conducted with crevices present). Because of the wide range of possible test environments and conditions that may be encountered and used in conducting laboratory corrosion tests, the discussion of various test methods is not all-inclusive. The following sections are intended to provide a general overview of the types of methods that may be used, to illustrate the effects of some test variables on the observed results, and to highlight caveats and potential pitfalls in interpreting the results. As the body of corrosion literature on any given method tends to be vast, a comprehensive review of each method and its various nuances is beyond the scope of this chapter. A bibliography has been provided to offer other suggested reading material on the subject. What is noted are the specific standards that have been developed concerning most of these tests and it is recommended that the standards be consulted prior to conducting the tests. The test methods have been broadly grouped into three main classifications in the following sections:

- Immersion tests
- Cabinet tests
- Electrochemical tests

3.2 IMMERSION TESTS

Immersion tests tend to be the most straightforward and easiest to accomplish. They involve the exposure of a material to an environment of interest in an immersed condition. The simplest manifestation of this test is the placement of a specimen in a beaker or other container filled with a solution or the environment of interest. From this simplest form, more complex variations have been designed, including

those that intentionally include the presence of a crevice and those that include a stress component to examine environmentally assisted cracking. These tests are often used to aid in materials selection for applications in various processing plants for piping and other equipment. The main advantage of immersion tests is that with minimal effort and equipment, a wide range of conditions and materials can be evaluated simultaneously. This offers the advantage of establishing “safe operating” conditions where a particular material can be used. For example, the corrosion rate of Type 303 stainless steel in 65% nitric acid has been reported to be <0.5 mm/y at temperatures less than 120 °C. If the temperature, however, is increased to 135 °C the measured corrosion rate increased to 5 mm/y with further temperature increases leading to accelerated corrosion (2). The implication from these results then is that Type 303 stainless steel may be acceptable for use if the temperature is closely controlled and known to be less than 120 °C. If the operating temperature is known or expected to exceed this value, then Type 303 stainless steel may not be an acceptable material choice and another material must be selected for construction. Similar tests exploring a range of expected environmental variables can be conducted to aid in the material selection/suitability process. Some commonly examined variables include:

- Temperature
- pH
- Halide concentration (chloride, fluoride, bromide, etc.)
- Acidic gases (e.g., CO_2 , H_2S)
- Pressure
- Flow rate and type (e.g., single phase, multi-phase)

In many cases, conducting such tests can lead to surprising results. Recent tests of an as-fabricated material in a relatively benign environment revealed the presence of significant residual stresses. These stresses, when combined with the environment, led to unexpected stress corrosion cracking (Fig. 3.4) and possible disqualification of this material for its intended purpose.

Immersion tests, in addition to their utility in conducting material selection and environmental screening tests, are often specified in acceptance criteria for use of various chemicals. For example, to accept new fire retardant chemicals used in airdrop fire fighting equipment (e.g., fixed wing and rotary aircraft) the U.S. Forest Service (part of the U.S. Department of Agriculture) specifies no significant cor-

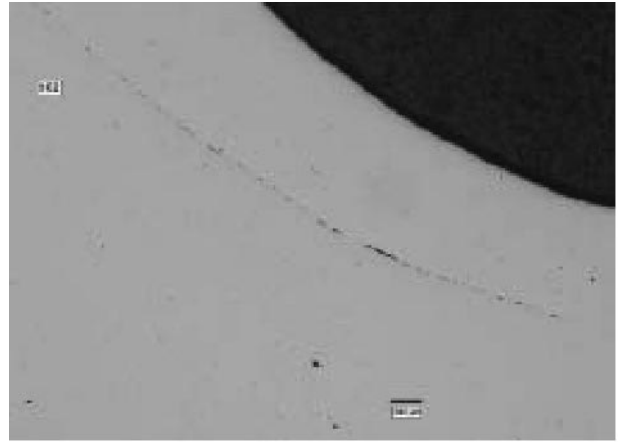


FIGURE 3.4 Stress corrosion cracking resulting from residual stresses encountered during immersion testing.

rosion after 90-day partial and full immersion testing (3). Because immersion tests are so prevalent, there are a large number of standardized procedures that have been developed and published, as summarized in Table 3.1.

For immersion testing, there are a number of evaluation criteria that are often used to quantify the effect of corrosion. The most commonly used criteria are appearance (simply, what the specimen looks like after testing) and weight change. For the most part, the standard method used to conduct the test also includes information regarding evaluation and pass/fail criteria. In addition, there are a number of relevant standard evaluation procedures, including:

- ASTM G1
- ASTM G46

Some evaluation procedures tend to be specific to a form of corrosion. For example, ASTM G31 (weight change or weight loss) can be applicable to any mode or form of corrosion, and converted to a corrosion rate via Eq. (3.1):

$$CR(\text{mm/y}) = \frac{8.76 \times 10^4 W}{At\rho} \quad (3.1)$$

where CR = corrosion rate
 W = mass loss in g
 A = exposed area in cm^2
 t = time in hours
 ρ = material density in g/cm^3

However, measurement of a weight loss will generally lead to an underestimation of the true corro-

TABLE 3.1 Partial List of Standardized Immersion Tests

| Designation | Title |
|----------------|--|
| ASTM G31 | Standard Practice for Laboratory Immersion Corrosion Testing of Metals |
| ASTM G48 | Standard Test Methods for Pitting and Crevice Corrosion Resistance of Stainless Steels and Related Alloys by Use of Ferric Chloride Solution |
| ASTM G36 | Standard Practice for Evaluating Stress-Corrosion-Cracking Resistance of Metals and Alloys in a Boiling Magnesium Chloride Solution |
| ASTM G49 | Standard Practice for Preparation and Use of Direct Tension Stress-Corrosion Test Specimens |
| ASTM G30 | Standard Practice for Making and Using U-Bend Stress-Corrosion Test Specimens |
| ASTM G38 | Standard Practice for Making and Using C-Ring Stress-Corrosion Test Specimens |
| ASTM G41 | Standard Practice for Determining Cracking Susceptibility of Metals Exposed Under Stress to a Hot Salt Environment |
| ASTM G44 | Standard Practice for Exposure of Metals and Alloys by Alternate Immersion in Neutral 3.5% Sodium Chloride Solution |
| ASTM G78 | Standard Guide for Crevice Corrosion Testing of Iron-Base and Nickel-Base Stainless Alloys in Seawater and Other Chloride-Containing Aqueous Environments |
| ASTM G35 | Standard Practice for Determining the Susceptibility of Stainless Steels and Related Nickel-Chromium-Iron Alloys to Stress-Corrosion Cracking in Polythionic Acids |
| NACE MR0174-95 | Recommendations for Selecting Inhibitors for Use as Sucker-Rod Thread Lubricants |
| NACE TM0198-98 | Slow strain rate test method for screening corrosion-resistant alloys for stress corrosion cracking in sour oil-field service |
| NACE TM0169 | Laboratory Corrosion Testing of Metals |
| NACE TM0171 | Autoclave corrosion testing in high-temperature water |
| USFS 5100 | Standard Test Procedures For the Evaluation of Wildland Fire Chemical Products |
| NACE TM0177 | Standard Practice for Determining the Susceptibility of Stainless Steels and Related Nickel-Chromium-Iron Alloys to Stress-Corrosion Cracking in Polythionic Acids |

sion rate if localized corrosion is the dominant corrosion mechanism. This arises because the corrosion rate of the localized corrosion sites tends to be several orders of magnitude greater than the rest of the material surface. Another difficulty with weight change methods is establishing quantitative information on corrosion resistant materials in relatively benign environments. Such situations result in negligible changes in specimen weight, making interpretation and extrapolation of performance difficult. To help overcome this, ASTM G31 recommends a minimum test duration given by the following expression:

$$\text{Test Time (h)} \approx \frac{787.4}{\text{CR}(\text{mm/yr})}$$

Thus, if a corrosion rate of 1 mm/y is measured, the recommended minimum test time is 787 hours, or approximately 32 days. Very small corrosion rates, therefore, require longer test times to verify their accuracy. Because of this, any minor fluctuation may disproportionately alter the measured corrosion rate. Such fluctuations may arise from the effects of post-

test cleaning procedures and possible deposition of environmental species (e.g., scale or deposits). For example, if a passive material (e.g., a Ni-Cr-Mo alloy) exhibits a very low corrosion rate of 10^{-5} mm/y in a given natural environment, the weight loss experienced by a 40 cm² specimen after a one-year exposure was only 0.35 mg. To offset this weight loss, the Cr-oxide film on the material would have to grow only 17 nm thicker or, alternatively, deposition of a silica layer (found in many natural environments) would only need to be 37 nm (4). As these changes in thickness are quite small, it is obvious that care must be taken when utilizing gravimetric or weight change methods to determine the corrosion rate. In addition, special care must be taken when establishing the corrosion rate in environments in which deposition is possible, and in verifying that the post-test cleaning procedure (i.e., ASTM G1) does not remove the underlying substrate material.

Classification of corrosion mode is nearly always determined (or at least confirmed) using some sort of visual examination. In this context, visual examination includes all magnifications of optical as well as electron microscopy (e.g., scanning electron microscopy). Though this form of evaluation is used

with all laboratory corrosion test methods, it is included here for discussion because in many cases this is a primary means of noting the effects of corrosion during immersion testing. Beyond the mere classification of the form of corrosion, there are some specifications to quantify the corrosion observed. For example, ASTM G46 describes a method to quantify localized corrosion based on a visual observation of the depth and density of corrosion pits that are present. This is illustrated in Fig. 3.5. Using this classification process, the pit nucleation kinetics of Type 316L stainless steel compared to Alloy 600 as a function of time were determined for a variety of environments (Fig. 3.6). This information was then used to establish how different environmental variables (e.g., temperature, chloride concentration, pH) influenced the observed pit nucleation rate as measured by pit density.

Because localized corrosion tends to be a stochastic process, statistical information pertaining to its initiation is also important. One of the aims of ASTM G48 is to provide that information by forming multiple crevice locations simultaneously, using a multiple crevice assembly (Fig. 3.7). After testing, relative ranking of materials (or, alternatively, a ranking of the environmental severity) can be accomplished by comparing the fraction of crevice sites that initiated. For example, the results in Fig. 3.8 clearly show that Alloy 625 is more resistant to localized corrosion (in this case, crevice corrosion) in that, at any given time, the fraction of sites initiated is lower than the other two materials.

Environmentally assisted cracking tests are also often conducted under nominally immersed (or sometimes alternate immersion) conditions. The only principle difference between cracking tests and the other types of tests is the requirement for an induced stress. There exist several methods to induce the stress component, including the use of jigs (e.g., 3-point bend, 4-point bend, static tensile) that are immersed with the sample. In such cases, care must be taken so as to not induce galvanic corrosion influences between the jigs and the sample. Furthermore, the jig itself must be resistant to the environment of the test so it can reliably induce the stress without itself becoming compromised over time. In addition, significant corrosion of the test jig changes the chemical composition of the test environment, thereby potentially influencing the performance of the test material. Other methods, such as C-ring and wedge-open loaded specimens that rely on a bolt and nut and wedges, respectively, have similar concerns regarding possible galvanic corrosion and integrity

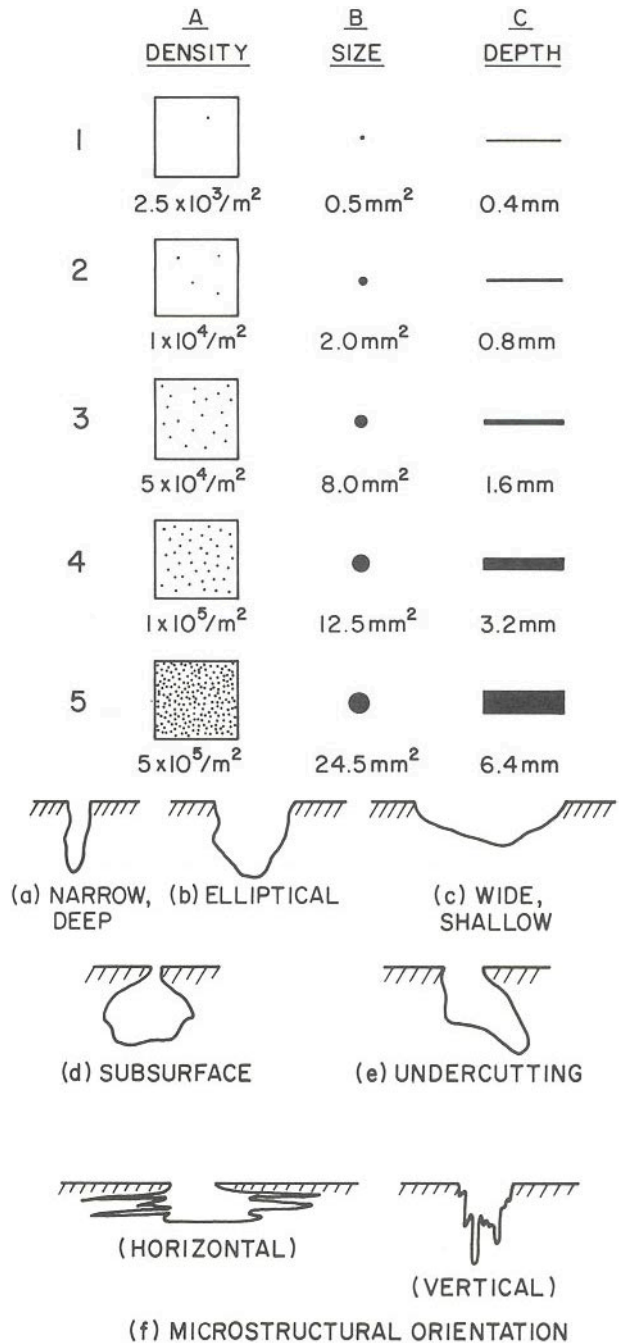


FIGURE 3.5 Pit classification index from ASTM G46.

of the stressing member. Slow strain rate and fracture mechanics methods can also be employed and, in many cases, the connections to the specimen can be made outside the test environment, thereby eliminating any such influences.

There is a wide range of specimen geometries that have been employed in conducting environmentally

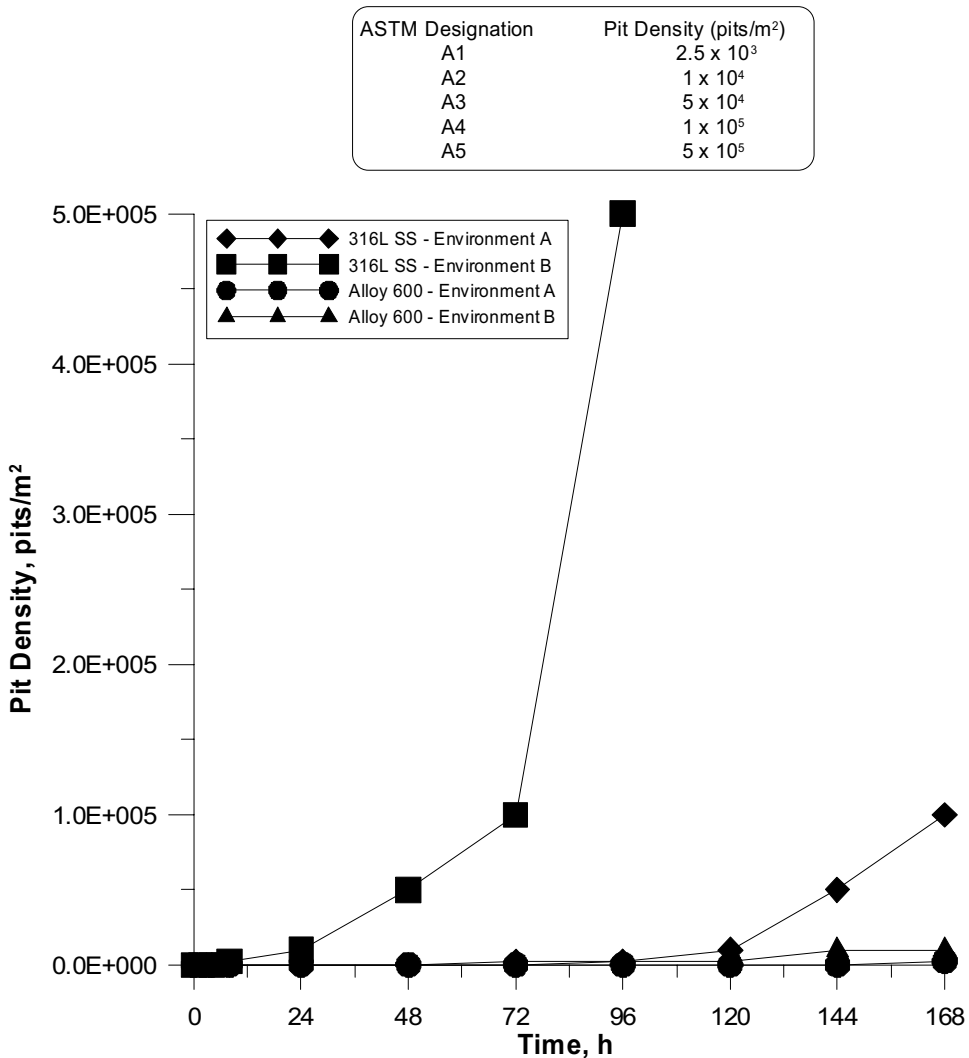


FIGURE 3.6 Pit density determined using ASTM G46 for Type 316L stainless steel and Alloy 600 exposed to two environments.

assisted cracking tests, ranging from bolts to traditional dog-bone tensile samples, ring-shaped specimens, and well-defined fracture mechanics-based geometries. Each geometry has advantages and limitations and should be chosen according to the desired intent and objective of the test. In many cases, it is often preferred to fabricate a test specimen in such a way that closely mimics the actual in-service situation. An example of this is evaluation of tubular products by fabricating C-ring specimens and inducing a stress to mimic either internal or external pressures. In most cases, the test method standard will have specific information regarding acceptable specimen geometries. For example, NACE TM0177 contains four different test methods using four different specimen geometries (tensile, bent beam, C-ring,

double cantilever beam) along with specific instructions on how to conduct tests using each geometry.

There are additional variations on the overall theme of immersion testing which include alternate immersion and high pressure/high temperature testing. The real motivation behind such variations is to conduct tests under conditions more representative of the actual in-service environment. The principle differences between these types of tests and the more simple tests previously discussed are that the equipment needed to conduct them tends to be more expensive, and the test complexity tends to be greater. Otherwise, the same evaluation criteria are often used. For alternate immersion, there is a prescribed residence time in the solution and the remainder of the time is outside the environment. Sometimes the

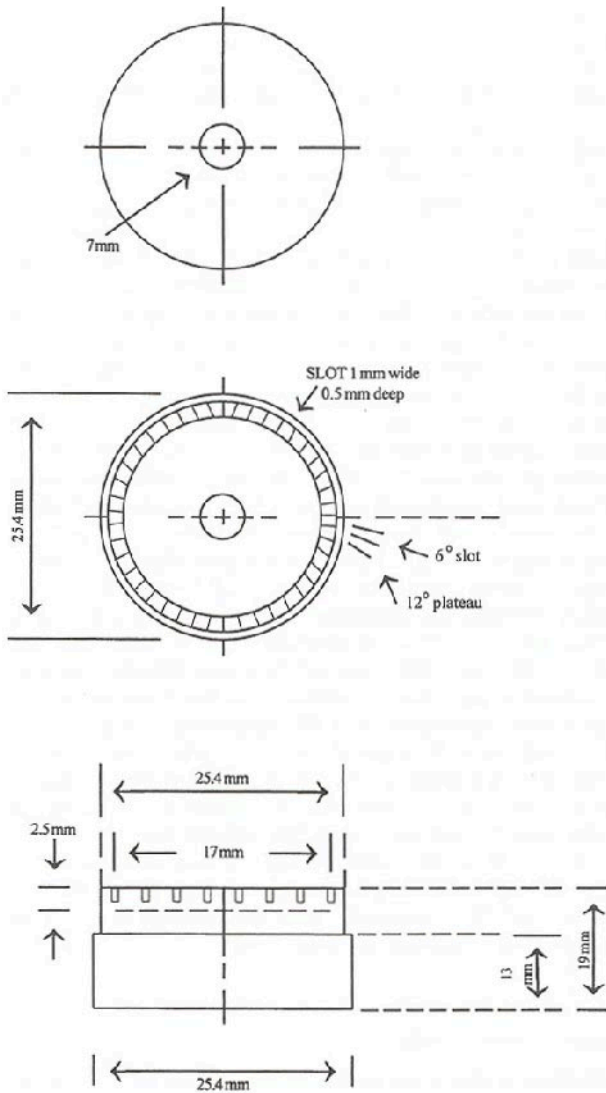


FIGURE 3.7 Illustration of a multicrevices assembly (5).

conditions for the outside solution time period are also defined in terms of temperature, relative humidity, and so forth. For high pressure and high temperature testing, autoclaves are typically used. For such tests, there are specific safety considerations as well as steps needed to ensure that the autoclave will be suitable under the temperatures and pressures of interest for the environment under consideration.

The influence of microorganisms on corrosion and materials performance is receiving ever-increasing attention. Microorganisms in the form of bacteria and fungi have been shown to both increase and decrease corrosion, depending on the environment, organism, and material. Conducting tests to study microbially influenced corrosion (MIC) is essen-

tially no different than any of the previous test methods described. The only significant differences arise from particular requirements associated with culturing specific bacteria (e.g., some bacteria cannot live in the presence of oxygen) and the need to foster sessile bacteria (those that attach to the metal surface) over planktonic (free floating) bacteria. Evaluation procedures are similar, as well, in that if general corrosion results, then weight loss can be used to quantify the effects. Alternatively, if localized corrosion occurs, then the standard evaluation procedures for pitting can be used.

3.3 CABINET TESTS

Cabinet tests generally refer to tests in which specimens are placed in a testing apparatus where the exposure conditions can be controlled. These tests are usually aimed at examining the performance of materials to corrosive atmospheres that may be encountered in various locations, including coastal and industrial areas. Thus, these tests can include the effects of moisture (RH), salt, corrosive gases (e.g., SO_2 , H_2S , CO_2), temperature, and UV radiation. A partial list of standardized test methods can be found in Table 3.2. The main objective of cabinet tests is often to accelerate material degradation in order to eliminate the long time period needed to induce significant corrosion during in-service exposure. In practice, however, the objective of accelerated duplication of in-service corrosion damage in cabinet tests is rarely achieved. That being said, cabinet tests have proven to be a useful indication of possible corrosion performance in natural environments and, in many cases, can be used to provide a relative comparison of material performance.

The level of complexity of the tests extends over a wide range, as does the complexity of the test chambers. In its simplest form, a cabinet can be constructed to maintain a constant temperature and humidity. More complicated cabinets introduce various controls and instrumentation to facilitate sprays of different solutions (e.g., salt solutions), introduction of different gases, and the possibility of controlling these variables independently and in a cyclic fashion. Because of the widespread use of cabinet tests, there are a number of commercial vendors that produce different cabinets to conduct such tests.

The post-test evaluation methods and criteria are similar to those employed for immersion tests and include weight loss, appearance, metallographic examination, and changes in electrical and mechanical properties. Often the evaluation criteria are de-

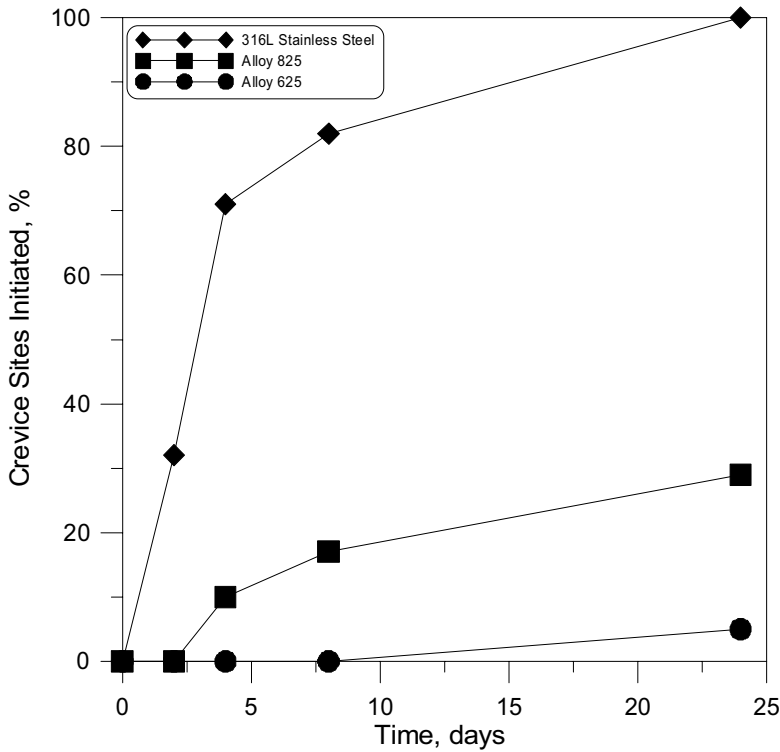


FIGURE 3.8 Fraction of multicreviced assembly locations that experience crevice corrosion for different alloys as a function of time.

TABLE 3.2 Partial List of Standard Cabinet Test Methods

| Designation | Title |
|-------------|--|
| ASTM B117 | Standard Practice for Operating Salt Spray (Fog) Apparatus |
| ASTM G60 | Standard Test Method for Conducting Cyclic Humidity Tests |
| ASTM G85 | Standard Practice for Modified Salt Spray (Fog) Testing |
| ASTM G87 | Standard Practice for Conducting Moist SO ₂ Tests |
| SAE J2334 | Cosmetic Corrosion Lab Test |
| GM9540P | Accelerated Corrosion Test |

scribed in the test specification and are dependent on the purpose of the test. For example, if the purpose of the test is to evaluate coating integrity and adherence during exposure, then delamination, blister formation, and scribe creep back are key parameters of interest, as illustrated in Fig. 3.9. Any localized corrosion that develops can again be classified and evaluated using standards such as ASTM G46. Evaluation based on appearance in many cases tends to be subjective. There are methods that can be used in an attempt to quantify the corrosion damage. One ex-

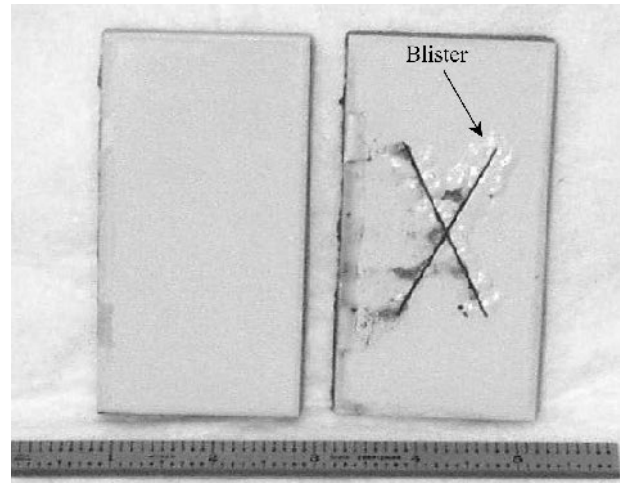


FIGURE 3.9 Appearance of damaged (x-scribe) and undamaged carbon steel coupons after exposure to salt spray testing.

ample of such an approach is the use of image analysis to quantify the fractional surface rust coverage for different materials subjected to different environments (Fig. 3.10). Such methods minimize the subjective nature of the analysis and tend to mitigate

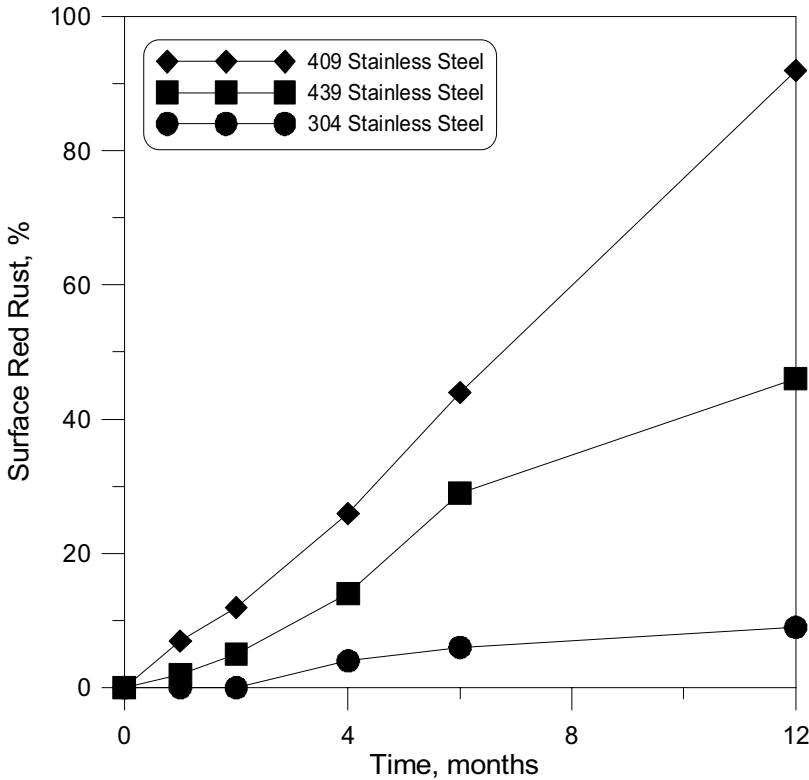


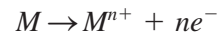
FIGURE 3.10 Fractional surface coverage of red rust on several stainless steel alloys after outdoor oceanfront exposure.

any inherent bias introduced by utilizing different personnel to conduct the analysis. They can also provide a finer differentiation and ranking between similar performing materials. The main focus of post-test evaluation should be to ensure that the evaluation is relevant to the intended purpose of the material and its in-service use.

Another example of results obtained using cabinet testing is shown in Fig. 3.11. Two different ferritic stainless steels, one with 11% Cr and the other with 18% Cr, were exposed to a test regimen designed to mimic and yet accelerate the anticipated in-service conditions. For this test, each test cycle consisted of periods of salt spray, high temperature-high relative humidity exposure, and a weekly high temperature thermal treatment. In this case, the most important parameter of interest was pit depth leading to perforation of the material. Comparison of the performance of the two materials clearly shows that the 18% Cr stainless steel performed much better than the 11% Cr material in this test and would be expected to do so again in-service (which was subsequently found to be the case).

3.4 ELECTROCHEMICAL TESTS

Because metallic corrosion is usually electrochemical in nature and involves the transfer of electrons during the process, many test methods have been developed to capitalize on this phenomenon. In many cases, this enables very sensitive measures of corrosion rates and reactions to be conducted. This is illustrated in the following equation representing the corrosion of a metal M:



The dissolution of the metal following the above reaction sequence can then be translated into an electrical current density by the expression:

$$i = nFJ$$

where i = current density in A/cm²
 n = number of electrons transferred in equivalents/mol

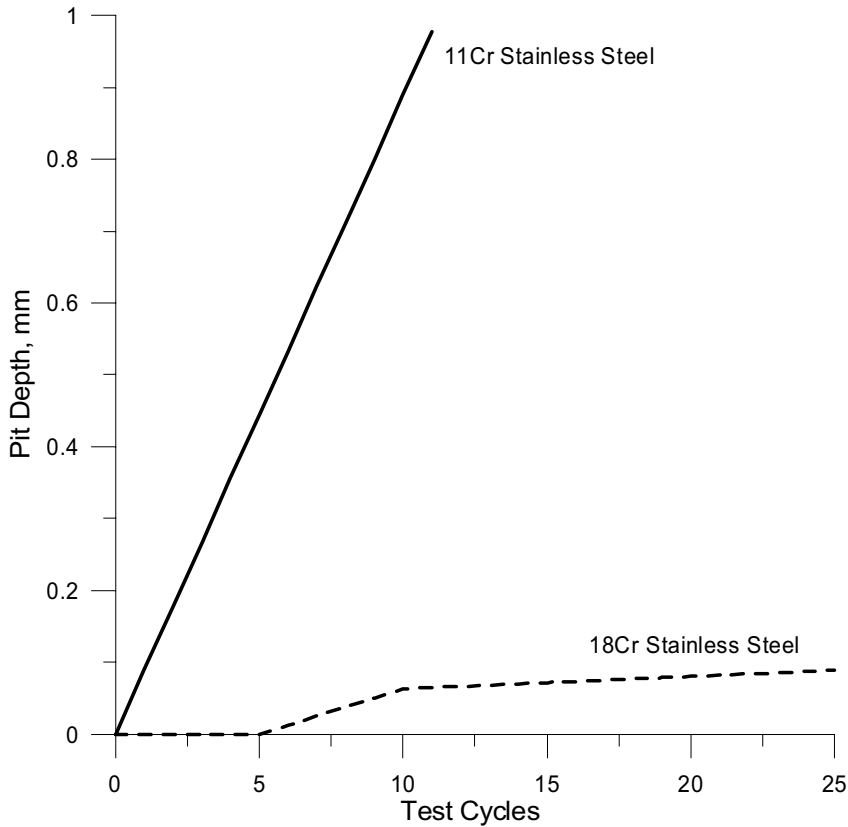


FIGURE 3.11 Pit penetration depth for two ferritic stainless steels subjected to a cyclic cabinet test designed to mimic and yet accelerate corrosion induced during in-service operations.

J = reaction rate in mol/cm²-s

F = Faraday's constant (96,484 C/equivalent)

To facilitate measurement of this electrical current resulting from metal dissolution (or any electrochemical reaction, including the oxidation or reduction of any electroactive species), specialized instrumentation has been developed. The most common is the potentiostat that controls and measures the potential and current supplied to a material. When the potentiostat is coupled with specialized software, standardized electrochemical corrosion tests can be conducted relatively easily.

Most electrochemical tests are conducted in a test vessel utilizing three main electrodes: reference, counter, and working. A schematic illustration of a typical configuration is shown in Fig. 3.12. The working electrode (WE) is the specimen that undergoes corrosion and is made from the material of interest. In general, there is no standardized specimen geometry for all tests, though some specific test methods do

specify sample shape and dimensions. As a result, there is a wide range of geometries that have been examined, including square blocks, cylinders, disks, wire loops, and flat sheets, to name a few. The reference electrode (RE) is designed to provide a stable reference potential against which other potential measurements are conducted. Several reference electrodes are commercially available, but the most commonly used electrodes in laboratory tests are the saturated calomel electrode (SCE) and the silver-silver chloride electrode (SSE). For most tests, the selection of a reference electrode is arbitrary since reference electrodes can be likened to thermometers reading on different temperature scales. The potential that is being measured is the same but the scale is different. In cases where high temperatures will be examined, the SCE system tends to be unstable and should be avoided. The reference electrode does not pass any significant current in the arrangement; otherwise, it would no longer provide a stable reference point. As a result, the counter electrode (CE) is present to provide the current to the working electrode, thereby in-

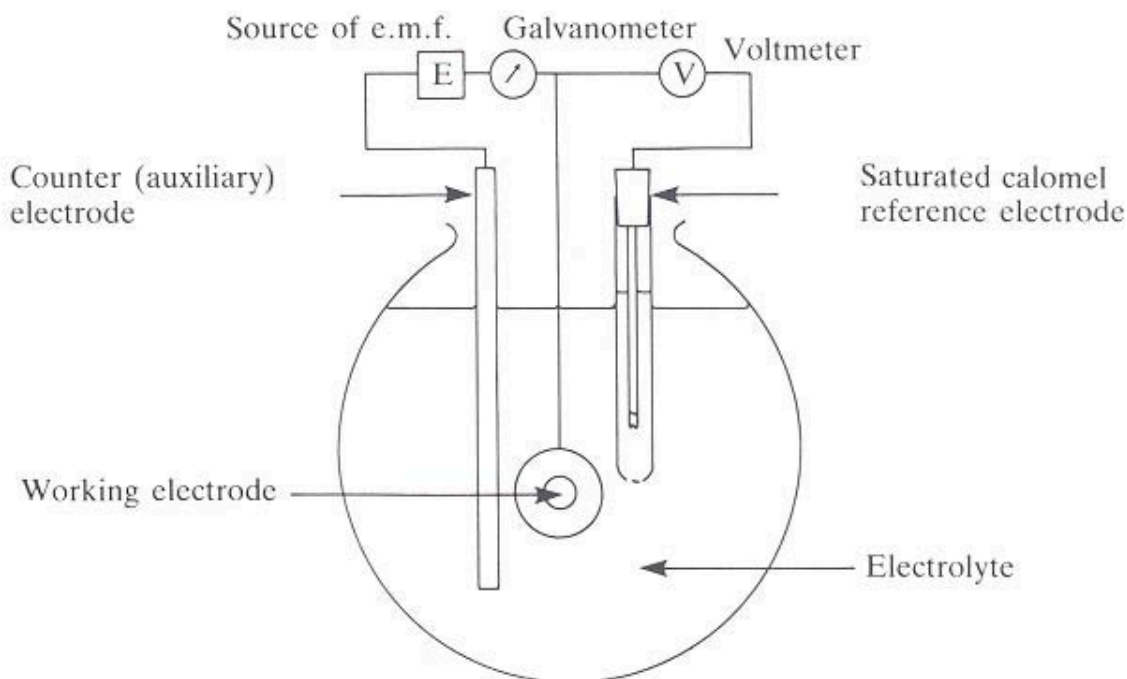


FIGURE 3.12 Typical electrochemical test cell configuration.

ducing through the instrument the corrosion (or any other electrochemical) reactions under investigation. Because the counter electrode itself may undergo corrosion (since it is providing all the current in the system), inert materials are generally used. The most common materials used for counter electrodes are graphite rods, platinum or gold (as foil, mesh, or wire), and platinized niobium or titanium. Graphite rods are the least expensive but, since they are porous, can occlude the test solution, resulting in contamination of subsequent tests if not carefully cleaned (e.g., ultrasonic agitation in deionized water). Platinum and

gold are the most expensive, but are easily cleaned and can provide higher currents than graphite and can therefore be physically smaller. Platinized niobium and titanium are less expensive than pure platinum, provide comparable current capability, and are easier to utilize because of the stiffness offered by the niobium or titanium substrate.

There are a number of standard electrochemical laboratory corrosion tests that have been developed. A partial list is shown in Table 3.3. The overall premise of these methods is described in the following paragraphs.

TABLE 3.3 Partial Listing of Standard Electrochemical Corrosion Tests

| Test Designation | Title |
|------------------|---|
| ASTM G3 | Standard Practice for Conventions Applicable to Electrochemical Measurements in Corrosion Testing |
| ASTM G5 | Standard Reference Test Method for Making Potentiostatic and Potentiodynamic Anodic Polarization Measurements |
| ASTM G61 | Standard Test Method for Conducting Cyclic Potentiodynamic Polarization Measurements for Localized Corrosion Susceptibility of Iron-, Nickel-, or Cobalt-Based Alloys |
| ASTM G102 | Standard Practice for Calculation of Corrosion Rates and Related Information from Electrochemical Measurements |
| ASTM G106 | Standard Practice for Verification of Algorithm and Equipment for Electrochemical Impedance Measurements |
| ASTM G108 | Standard Test Method for Electrochemical Reactivation (EPR) for Detecting Sensitization of AISI Type 304 and 304L Stainless Steels |
| ASTM G150 | Standard Test Method for Electrochemical Critical Pitting Temperature Testing of Stainless Steels |

Linear polarization resistance (LPR) is a method in which the electrochemical response of a corroding metal is investigated near its open circuit, or corrosion, potential. Typically, this involves polarization of the material of interest 15–30 mV below the corrosion potential and a slow increase (or scan) of the potential to the comparable potential above the corrosion potential. Within this potential region, it is assumed that the relationship between potential and log-current is linear, thereby allowing the calculation of the corrosion rate via:

$$CR = C_1 \frac{i_{corr} EW}{\rho}$$

and

$$i_{corr} = 10^6 \frac{B}{R_p}$$

where CR = corrosion rate

C_1 = a constant depending on the units of measure used

i_{corr} = corrosion current density

EW = equivalent weight (g/equivalent)

ρ = metal density

B = Stern-Geary coefficient

R_p = polarization resistance obtained from the LPR test

Example LPR test results are shown in Fig. 3.13 in comparisons to weight loss measurements. Under

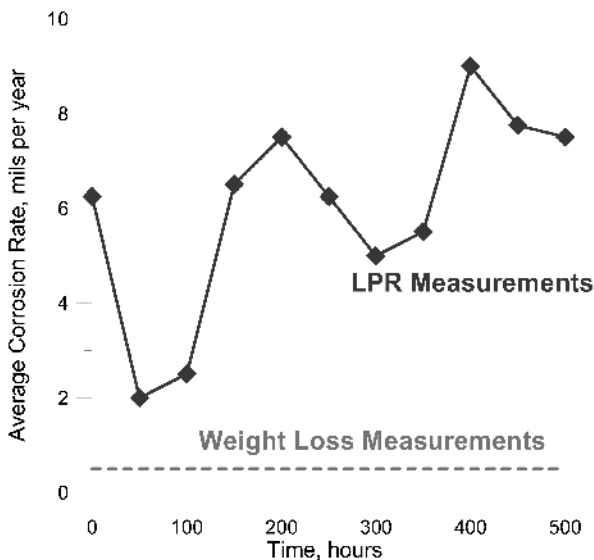


FIGURE 3.13 Effect of environment on the initiation of crevice corrosion of 304 stainless steel using potentiostatic testing.

identical conditions, the LPR results indicate significantly higher corrosion rates than those noted using gravimetric methods. This arises in many cases because of the complications discussed previously with respect to immersion tests.

One of the potential complications with LPR (and any scanning electrochemical tests) is the effect of scan rate. Scan rates (the rate of change of the applied potential) tend to be on the order of 0.167 mV/sec (or 0.6 V/h). A slow scan rate is usually used to ensure that the test closely mimics steady state conditions.* LPR can be a valuable method to determine the corrosion rate of a material because it provides an instantaneous measurement without having to conduct long experiments to achieve significant weight loss, and can be conducted at high temperatures and pressures. The main assumption in conducting LPR tests is the corrosion occurring is not localized in nature. Additionally, if the material is highly passive (e.g., stainless steels, Ti-, Al-, and Ni-based alloys) and the passive corrosion rate is desired, LPR can provide misleading results. In such cases, other methods such as potentiostatic polarization should be examined.

Potentiostatic polarization involves adjusting the potential of the metal in the environment away from its corrosion potential and holding it constant for some specified period of time. When polarized and maintained for extended periods of time, the true steady state condition of the material at that potential can be obtained. This can be done to examine the long-term passive corrosion rate, but also can be used to determine long-term susceptibility to localized corrosion or stress corrosion cracking (in the case of a stressed sample). Localized corrosion would be manifested by an eventual increase in the measured current that is then maintained over an extended period of time. By comparison of the time needed to observe the current increase, the relative resistance of different materials to localized corrosion can be obtained. Furthermore, the effects of corrosion inhibitors and possible corrosion accelerants on localized corrosion can be examined.

*If faster scan rates are utilized in any potentiodynamic related test, the results will tend to be skewed toward higher than actual currents. This occurs because the metal-solution interface in its simplest form is composed of a resistor in parallel with a capacitor (the current through which is directly dependent on the voltage change with time) and the total current flowing through the circuit is the sum of the current in the resistor and the current in the capacitor.

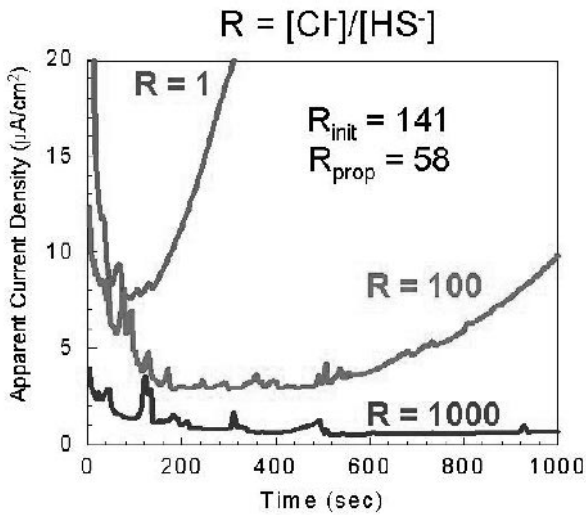


FIGURE 3.14 Effect of $[Cl^-]/[HS^-]$ ratio on crevice corrosion initiation determined using potentiostatic tests (6).

For example, Fig. 3.14 illustrates the effects of solution chemistry in the form of the chloride/sulfide ratio on the initiation of crevice corrosion of Type 304 stainless steel (6). Potentiostatic tests, although useful, can also prove to be problematic. First, it is unclear *a priori* how long such tests need to be run. Cases have shown that polarization for periods of up to several years may be necessary to achieve the desired answers. In other cases, polarization for periods as brief as a few minutes were needed. Secondly, when using potentiostatic polarization to make sensitive measures of very low currents, it is critical to eliminate as best as possible any sources of parasitic current. For making measurements of the passive corrosion rate, extreme care must be taken to remove all traces of oxygen in the system, since any cathodic reduction of oxygen will result in an underestimation of the passive corrosion rate.

Potentiodynamic, or cyclic, polarization as the name implies, involves a continuous sweeping or changing of the potential. This method is similar to the LPR method, except the range of potentials examined goes far beyond the limited range near the open circuit potential of the LPR approach. Potentiodynamic polarization can provide information on the overall electrochemical behavior of a material in a given environment. Because of this, the general corrosion performance and rate can be estimated by examining the behavior near the open circuit potential; the reaction kinetics of any cathodic species can be explored through cathodic polarization; the passive corrosion rate (if the material is passive) can be

examined; and, finally, the localized corrosion behavior can also be determined.

A schematic of a typical potentiodynamic polarization curve for a passive material that undergoes localized corrosion is shown in Fig. 3.15. Again, the same concerns regarding the effects of scan rate on measurements raised previously apply here. The results from conducting a series of potentiodynamic tests can be utilized to compare the relative performance of different materials as well as define “safe” environmental operating regions. Fig. 3.16 illustrates this by comparing the repassivation potential (the potential above which localized corrosion is possible) of different materials as a function of chloride concentration. If the system in question is constructed of Alloy 825 and the environment contains 10^{-2} M chloride at 95 °C, no localized corrosion would be expected if the corrosion potential in that process stream did not exceed approximately 0 V on the saturated calomel scale (SCE). If, on the other hand, either the corrosion potential or the chloride concentration was higher, Alloy 825 would be expected to suffer from localized corrosion and, thus, selection of another material such as Alloys 625 or 22 would be warranted.

Galvanostatic and galvanodynamic polarization are identical to potentiostatic and potentiodynamic polarization except instead of controlling the potential, the current is controlled. Although much less

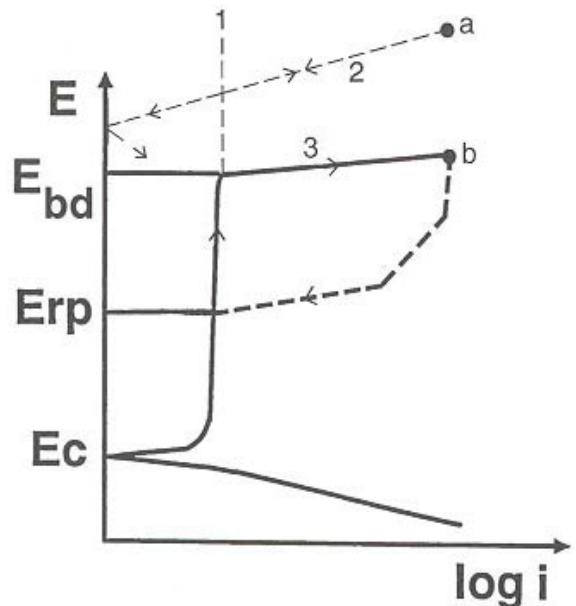


FIGURE 3.15 Schematic illustration of a potentiodynamic polarization test result (5).

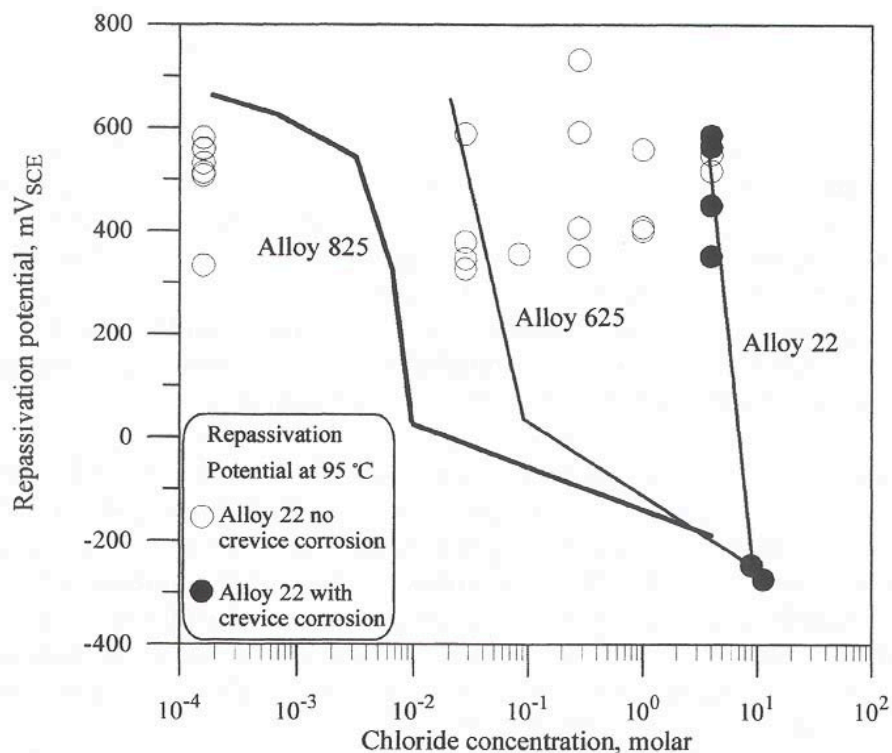


FIGURE 3.16 Relationship between the repassivation potential for different materials and chloride concentration defining regions where localized corrosion will and will not occur.

frequently used than potential-controlled methods, control of the current enables the precise control of the total amount of charge that is passed during the experiment. This level of control is useful in minimizing the overall damage that is done to a given specimen, thereby facilitating post-test analyses.

Electrochemical Impedance Spectroscopy (EIS) is a method that utilizes an alternating voltage or current (AC) source as the input to the system rather than the purely direct current (DC) source used in the methods previously discussed. The simplest manifestation of the metal-solution interface is a resistor and capacitor in parallel, as illustrated in Fig. 3.17, known as Randle's circuit. Because electrical components (e.g., resistors, capacitors, inductors, etc.) have certain characteristics, and because electrochemical (and thus corrosion) processes can be mimicked as electrical components, EIS offers a valuable tool to study these reactions (Fig. 3.18). EIS is particularly adept at examining corrosion in low conductivity environments (such as organic liquids) because the measurement of corrosion rate (as R_p) is relatively unaffected since the individual components can, in many cases, be separated out. In con-

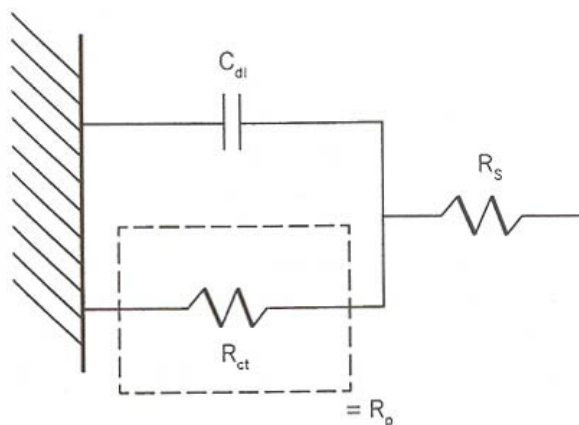


FIGURE 3.17 Circuit diagram of Randle's Circuit (5).

trast, accurate measurements of the corrosion rate using the DC methods described above can be compromised in high resistivity media. EIS is also effective at examining the integrity of coatings and films, including organic coatings and paints, on metal surfaces. Though EIS has proven to be a powerful method to study corrosion under a wide range of

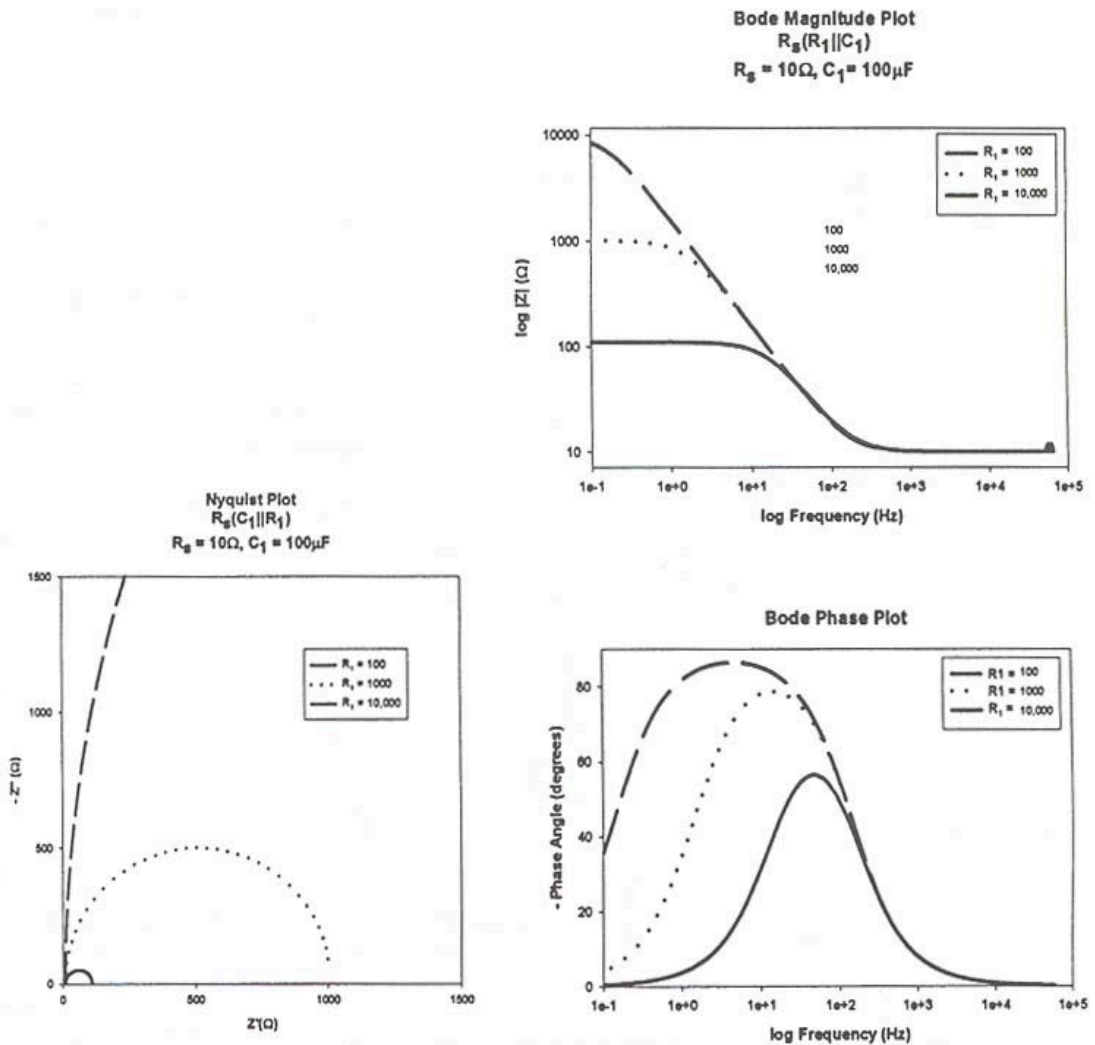


FIGURE 3.18 Typical results obtained using EIS (for Randle's Circuit) (5).

conditions, it has also been found to be highly difficult to interpret in many cases, and often requires highly specialized and expensive equipment to conduct.

For example, because the EIS response of the actual metal-environment under study is compared to a circuit model, any number of circuit models can be designed that generate identical or highly similar responses. Thus, to develop a suitable model, some knowledge of the corrosion and other reactions taking place is needed. Furthermore, just because the model compares well with the system under study does not mean that the model is correct, since the physical meaning of the model may not be accurate. Despite its limitations, EIS is gaining in acceptance and is now widely used.

Electrochemical noise (EN) measurements consist of spontaneous fluctuations in the current and potential during various corrosion processes. These fluctuations, depending on their frequency and magnitude, have been linked with many corrosion processes including:

- Propagation of stress corrosion cracks via dissolution of freshly exposed metal at the crack tip
- Pit initiation and eventual growth
- Crevice corrosion
- Particulate impingement (erosion)
- Microbial corrosion
- Uniform corrosion
- Inhibitor efficacy screening

Though typically used in in-service monitoring for corrosion, EN has been utilized in laboratory testing. EN is often utilized in an attempt to determine underlying electrochemical mechanisms associated with corrosion. That being said, however, EN has been used for more routine testing. For example, EN has been used to rapidly screen corrosion inhibitors for efficacy as well as to evaluate the performance of many organic coatings as a function of time. The primary limitations associated with EN testing are: (1) the requirements for rather specialized testing equipment; (2) there is no existing standardized method currently available; and (3) interpretation of the results obtained can be complicated. Of these, the fact that there is no existing standardized method to conduct and interpret EN tests is the greatest limitations to its widespread use. It should be noted, however, that efforts are underway to develop standardized EN methods and, in time, these should make conducting these tests easier.

In addition to the methods described above, there also is a considerable amount of ancillary equipment and variations that can be explored. For example, the effect of fluid flow on corrosion is often studied using rotating specimens as cylinders, disks, and rings in conjunction with nearly all electrochemical test methods. New methods to study flow, including jet impingement, are also used in conjunction with these methods. Furthermore, other conditions such as high temperature and pressure can also be explored utilizing many electrochemical corrosion test methods, provided that adequate steps are taken to ensure proper functionality of various components (especially the reference electrode).

3.5 CONCLUSIONS

In summary, the selection of a suitable laboratory corrosion test and the conditions under which it is run depends on many factors, including:

- Expected in-service environment
- Type of information desired
- Life expectancy of the component
- How sensitively the corrosion can be measured
- Whether quantitative information is needed, or if qualitative comparison is sufficient

In many cases, there exist standardized methods and procedures for conducting such tests. It should be noted, however, that just because a method is standardized does not mean it is the best or most appro-

priate test to conduct in a given situation. Standardized test methods generally cannot capture the wide range of environments, materials, and conditions that are encountered in service. Thus, care should be taken when selecting which tests will be conducted and how they will be carried out. In some cases, using a standard method and making modifications to suit the particular needs of the application is often quite effective. Furthermore, use of test methods in combination has also proven to be highly valuable. For example, Fig. 3.19 shows the results from utilizing a sensor system based on EIS. The condition of different paint coatings was evaluated during cyclic environmental exposure (similar to SAE J2334). In this case, the sensor provided a quantitative measure of coating performance that was more accurate than traditional visual inspection, even detecting degradation that was not evident visually. Due to the inherent complexity of many in-service systems, it can be difficult to properly design a test and interpret the results effectively, and it is suggested that trained corrosion professionals be consulted.

In addition, it may be necessary to develop test methods and parameters to suit specific needs and desires. A good example of this was shown in Fig. 3.11, in which a new test methodology was developed over time that fairly accurately reproduced in a short period of time the corrosion damage observed

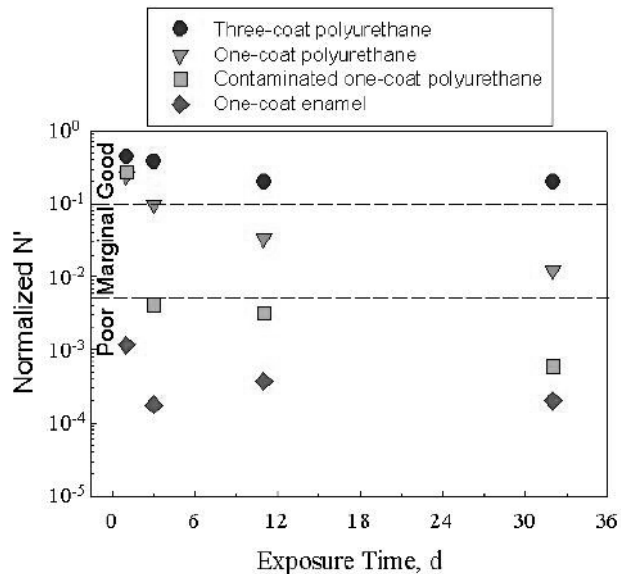


FIGURE 3.19 Coating integrity as a function of exposure time measured using a sensor based on EIS illustrating the utility of using multiple test methods in combination [1].

in-service over much longer time frames. By putting forth this effort, the new test method that was developed allowed rapid screening of different processing steps, alloy modifications, and other treatments for improved corrosion performance without going through the expense of conducting full fabrication runs and placing components in service for several years. In this case, no standard test method would have provided the same information in terms of a reliable estimate of in-service life—the accelerated testing produced the same corrosion modes at the same locations as those seen from failed components.

3.6 REFERENCES

1. *Corrosion Costs and Preventive Strategies in the United States*, FHWA-RD-01-156, U.S. Federal Highway Administration, 2002.
2. *NACE Corrosion Standards*, TM0169 “Laboratory Corrosion Testing of Materials,” Houston, TX, NACE International, 2002.
3. *Standard Test Procedures For the Evaluation of Wildland Fire Chemical Products*, U.S. Department of Agriculture, 2001.
4. O. Pensado, D. S. Dunn, G. A. Cragnolino, and V. Jain, *Passive Dissolution of Container Materials—Modeling and Experiments*, CNWRA 2003-01, San Antonio, TX, Center for Nuclear Waste Regulatory Analyses, 2002.
5. R. G. Kelly, J. R. Scully, D. W. Shoesmith, and R. G. Buchheit, *Electrochemical Techniques in Corrosion Science and Engineering*, New York, NY, Marcel Dekker, 2003.
6. C. S. Brossia and R. G. Kelly, *Corrosion Science*, Vol. 40, No. 11, pp. 1851–1871, 1998.

3.7 BIBLIOGRAPHY

- ASTM Annual Book of Standards*, Vol. 03.02, “Wear and Erosion, Metal Corrosion,” West Conshohocken, PA, ASTM International, 2003.
- NACE Corrosion Standards*, Houston, TX, NACE International, 2003.
- Corrosion Tests and Standards, Application and Interpretation*, ASTM Manual 20, R. Baboian, Editor, West Conshohocken, PA, ASTM International, 1995.
- ASTM Special Technical Publications on various corrosion and testing topics.

CHAPTER 4

LIFETIME PREDICTIONS OF PLASTICS

James A. Harvey

Under the Bridge Consulting, Inc., Corvallis, Oregon

| | |
|---------------------------------------|----|
| 4.1 INTRODUCTION | 65 |
| 4.2 MASTER CURVES | 66 |
| 4.3 CHEMICAL KINETICS | 69 |
| 4.4 THERMAL DECOMPOSITION EXPERIMENTS | 71 |

| | |
|-----------------------------------|----|
| 4.5 MECHANICAL EXPERIMENTS | 73 |
| 4.6 MISCELLANEOUS EXPERIMENTATION | 75 |
| 4.7 SUMMARY | 76 |
| 4.8 REFERENCES | 76 |

4.1 INTRODUCTION

When one puts a product into service, the ability to predict its lifetime or failure rate would be highly beneficial. The plastic part should be tested in real time and in environments similar to those in which the part will be exposed. However, this is not always possible. Complicating factors include development times, time to market considerations, and the service life. We will discuss some methods in which lifetime predictions “may” be predictable. Accurate predictions are highly dependent on the testing methodology, the type and form of the plastic used, and the plastic’s processing history.

Plastics are defined as polymers with additives. The behavior of the material changes as the additive package changes. The material from company A might perform totally differently in comparison with a material from company B, even though they belong to the same polymer family with similar properties, such as molecular weights and distributions and thermal behavior. Thus, whenever we look at lifetime predictions, we must have the same material throughout the plastics testing protocol. Also, we must have testing methods that are amenable to the end use of the product. The handbooks are full of tensile and compression types of test data; however, in actuality very few products are pulled apart or pushed together. We may not have the luxury of making a part, subjecting it to normal usage, and

monitoring the time to failure. We need tests for performing some sort of accelerating testing.

Another unusual twist in knowing the lifetime or failure rates of plastics involves solid waste materials. Each year, tons of plastics are disposed of in landfills. A lot of work is being done to controllably degrade the waste plastic materials to conserve landfill space. The two principle mechanisms for accomplishing this are photodegradation and photothermodegradation.

As we follow the performance of a product, its data may take different forms. The data may be linear, semi-logarithmic, logarithmic, or cyclic. Metals offer simpler solutions because S/N (signal to the number of cycles to failure) curves can be generated. In the case of polymers, we do not have that luxury. As previously mentioned, a plastic is highly dependent upon the manufacturer, the additive package, and its thermal history. Slight composition and manufacturing changes can cause drastic changes in performance and results. Metals are more forgiving in predicting lifetimes.

Metals also have the advantage over plastics in that they are stable over a wider temperature range. Plastics have a useful temperature range of less than 200 °C. Thus, the testing of plastic parts must be performed within the useful temperature of the material. A simple explanation of what could happen can be illustrated with a chicken and an egg. Place an egg under its mother; in a few days we have a baby

chick. Place the egg in boiling water; in a few minutes we have a hardboiled egg. Place the egg in an isolated spot; in a few weeks we have a smelly, rotten egg. The same starting material with three different thermal histories produces three different results. The traditional accelerated testing protocol (1) may not be an option for the chemical and physical aging of plastics.

Some of the criteria for failure or lifetime predictions can be quite arbitrary. For example, PMR-15, a thermosetting polyimide used in advanced composite applications, has a requirement of a less than 10 percent weight loss at elevated temperatures, independent of time of exposure.

In this chapter we have selectively chosen published aging studies with testing data and have transformed the results into meaningful lifetime predictions.

4.2 MASTER CURVES

One of the most useful analytical techniques for determining lifetime predictions is the generation of master curves utilizing the dynamic mechanical analyzer (DMA). This technique involves time-temperature superimposition (TTS).

In polymer literature, a set of experimental curves can frequently be translated along a given direction to form a master curve. One of the most famous examples is the time-temperature superimposition, where the translation is generally performed along the horizontal axis. The superimposition of the different experimental curves is normally made graphically, leading to some ambiguities in the construction of the master curve and in the determination of the translation paths. Starting from the analytical conditions to be satisfied by a set of curves that were related by a translation along a given direction, a computer program can be developed to obtain the master curve from a set of experimental data. Finally, some examples can be obtained of the applicability of the computer program developed for simulated storage, shear compliance, viscosity against shear rate, and stress relaxation data (2).

Dynamic mechanical testing involves subjecting the plastic specimen to an alternating strain, and simultaneously measuring the stress. For linear viscoelastic behavior, at equilibrium, stress and strain vary sinusoidally, but the strain lags behind the stress. Thus we write

$$\text{strain } e = e_0 \sin \omega t \quad (4.1)$$

and

$$\text{stress } \sigma = \sigma_0 \sin(\omega t + \delta), \quad (4.2)$$

where ω is the angular frequency and the δ the phase lag.

Thus, we can we can rewrite stress to be equal to

$$\sigma = \sigma_0 \sin \omega t \cos \delta + \sigma_0 \cos \omega t \sin \delta. \quad (4.3)$$

Stress has two components: (1) magnitude ($\sigma_0 \cos \delta$) in phase with the strain; and (2) magnitude ($\sigma_0 \sin \delta$) out of phase with the strain.

Now we may define two new quantities: G_1 is in phase with the strain, and the quantity G_2 is 90 degrees out of phase with the strain. We may rewrite strain as

$$\sigma = e_0 G_1 \sin \omega t + e_0 G_2 \cos \omega t, \quad (4.4)$$

where

$$G_1 = (\sigma_0/e_0) \cos \delta \text{ and } G_2 = (\sigma_0/e_0) \sin \delta.$$

If we construct a phasor diagram (see Fig. 4.1) with G_1 and G_2 , we may define a new quantity G^* , complex modulus.

If $e = e_0 \exp(i\omega t)$, then $\sigma = \sigma_0 \exp[i(\omega t + \delta)]$, so that

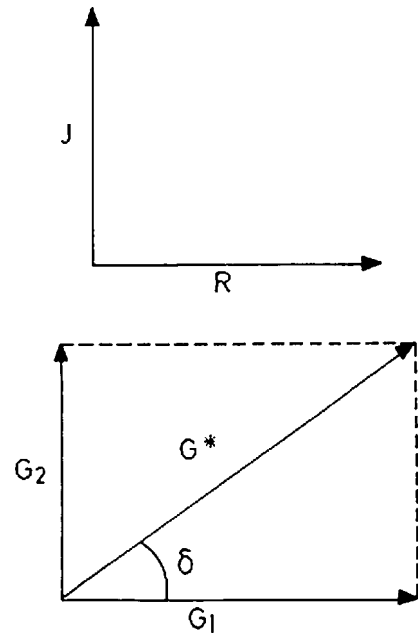


FIGURE 4.1 Phasor diagram for complex modulus $G^* = G_1 + iG_2$ and phase lag, $\tan \delta = G_2/G_1$.

$$G^* = \sigma/e = (\sigma_0/e_0) \exp(i\delta) \quad (4.5)$$

$$= \sigma_0/e_0 (\cos\delta + i\sin\delta) \quad (4.6)$$

$$= G_1 + G_2, \quad (4.7)$$

where G_1 , which is in phase with the strain, is called the storage modulus because it defines the energy stored in the specimen due to the applied strain, and G_2 , which is $\pi/2$ out of phase with the strain, defines the dissipation of energy and is referred to as the loss modulus. The energy (ΔE) dissipated per cycle can be defined as

$$\Delta E = \int (\sigma de) = \int_0^{2\pi\omega} (\sigma(de/dt)dt). \quad (4.8)$$

Substituting for stress and strain, solving the integration, and evaluating ΔE over a quarter cycle rather than the entire period, we can reduce the variables to

$$E = 1/2 (G_1 e_0^2), \quad (4.9)$$

which is independent of frequency.

G_1 and G_2 can be rewritten as

$$G_1 = (2E/e_0^2).$$

and

$$G_2 = (\Delta E/\pi e_0^2).$$

Hence,

$$G_2/G_1 = \tan\delta = \Delta E/(2\pi E). \quad (4.10)$$

The ratio $\Delta E/E$ is called the specific loss

$$\Delta E/E = 2\pi \tan\delta. \quad (4.11)$$

Typical values of G_1 , G_2 and $\tan\delta$ for a polymer are 10^9 Pa, 10^7 Pa, and 0.01, respectively. In such cases, $|G^*|$ is approximately equal to G_1 . It is customary to define the dynamic mechanical behavior in terms of the "modulus," G_1 , and the phase angle, δ , or $\tan\delta = G_2/G_1$.

A complementary treatment can be developed to define a complex compliance, $J^* = J_1 - iJ_2$, which is directly related to the complex modulus, as $G^* = 1/J^*$. Consider the variation of G_1 , G_2 , and $\tan\delta$ with frequency for a viscoelastic solid that shows no flow

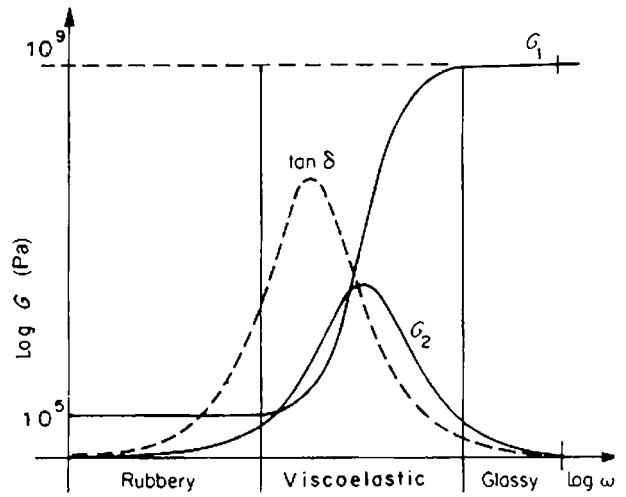


FIGURE 4.2 The complex modulus $G^* = G_1 + iG_2$ as a function of frequency (3).

(Fig. 4.2). At very low frequencies, the polymer is rubber-like and has a low modulus (G_1 is probably about 10^5 Pa), which is independent of frequency. At the highest frequencies, the rubber is glassy, with a modulus around 10^9 Pa, which is again independent of frequency. In the intermediate region, where the material behaves viscoelastically, the modulus will increase with increasing frequency. The loss modulus will be zero at low and high frequencies, where stress and strain are in phase for the rubbery and glassy states. In the intermediate viscoelastic region, G_2 rises to a maximum value, close to the frequency at which G_1 is changing most rapidly with frequency. The loss factor, $\tan\delta$, also has a maximum in the viscoelastic region, but this occurs at a slightly lower frequency than that in G_2 , since $\tan\delta = G_2/G_1$, and G_1 is also changing rapidly in that frequency region. An analogous diagram shows the variation of the compliances J_1 and J_2 with frequency (3).

Professors Miyano and Kimpara and their groups at Kanazawa Institute of Technology have proposed an accelerating testing methodology for assessing long-term mechanical performance of carbon fiber reinforced polymer (CFRP) composites. The methodology was composed of constructing the master curve for several deformation modes based on four hypotheses:

1. Same failure mechanisms of CFRP composites under constant strain rate (CSR), creep and cyclic loading over the same time and temperature,

which is controlled by the viscoelastic instability of polymer resins

2. Same time-temperature superimposition principle for all the failure modes
3. Linear cumulative damage law for monotonic loading
4. Linear dependence of fatigue strength under various stress ratios ($R_s = \sigma_{\min}/\sigma_{\max}$)

The master curves for CSR, creep (constant loading), and fatigue tests were constructed by applying the time-temperature superimposition principle. The variations of the CSR strength (σ_s), creep strength (σ_c) and fatigue strength (σ_f) to the time to failure (t_s , t_c and t_f) is shifted by the time-temperature shift factor [$a_{T_0}(T)$] given in Eq. (4.12), which is independent of the loading modes.

$$a_{T_0}(T) \exp[\Delta H/2.3R(1/T(1/T_0))], \quad (4.12)$$

where R is the gas constant and T_0 is the reference temperature. The value of ΔH for the CFRP failure and storage modulus of the polymer resin are found to be identical due to the failure mechanism of CFRP composites controlled by the viscoelastic flow of polymer resins. To determine the master curves [$\sigma_s(t_s': T_0)$, $\sigma_c(t_c': T_0)$ and $\sigma_f(t_f': R_s, f, T_0)$], the reduced failure time (t_s' , t_c' and t_f') is defined by

$$t_s' = t_s/a_{T_0}(T) \text{ for CSR}, \quad (4.13a)$$

$$t_c' = t_c/a_{T_0}(T) \text{ for creep}, \quad (4.13b)$$

$$\text{and } t_f' = t_f/a_{T_0}(T) = N_f/f a_{T_0}(T) = N_f/f', \text{ for fatigue}, \quad (4.13c)$$

where N_f is the number of cycles to failure and f is the frequency of cyclic loading. The master curve can be applied in a wide temperature range above and below the glass transition temperature, although ΔH becomes different, depending on the polymer structure.

For the CSR tests, the variations of σ_s to t_s are measured under various loading rates and temperatures. For the creep test, t_c is determined as a function of constant σ_c at various temperatures. Different cumulative damage proceeds in CFRP composites subjected to rising (CSR) and constant (creep) loading. In order to estimate t_c from the CSR tests, linear cumulative damage for monotonic loading (approximated stepwise) is defined by

$$\int_0^{t^*} dt/t_c[\sigma(t)] = \sum_i^{2n-1} \Delta t/t_c[\sigma_i(t)] = [t_s(\sigma_{2n})/n] [1/t_c(\sigma_1) + \dots + 1/t_c(\sigma_{2n-1})] - 1, \quad (4.14)$$

where t^* [= $t_s(\sigma_{2n})$] is the failure time under stress history, Δt ($= t^*/n$) is the time interval for stepwise loading, and $t_c[\sigma_i(t)]$ is the creep failure time under $\sigma_i(t)$. Thus, $t_c(\sigma_{2n-1})$ can be determined from $t_s(\sigma_{2n-2})$ and $t_s(\sigma_{2n})$ using Eq. (4.15) derived from Eq. (4.14):

$$t_c(\sigma_{2n-1}) = t_s(\sigma_{2n}) t_s(\sigma_{2n-2}) / [n t_s(\sigma_{2n-2}) - (n-1) t_s(\sigma_{2n})]. \quad (4.15)$$

The linear cumulative damage law for the loading history [hypothesis (c)] has been proven by good agreement of the master curves for the CRS and creep observed in many CFRP systems.

In order to construct the fatigue master curve, the value of t_f is converted from N_f using f , and t_f' is defined by the shifted frequency (f') (Eq. 4.13c). Moreover, changing f and R_s , as well as temperatures, affects the relationships of σ_f to t_f' . By applying a linear dependence of the fatigue strength on R_s [hypothesis (d)], the fatigue master curve [$\sigma_f(t_f'; R_s, f, T)$] for the various R_s is estimated by

$$\sigma_f(t_f'; R_s, f, T) = \sigma_{f:1}(t_f'; f, T) R_s + \sigma_{f:0}(t_f'; f, T)(1 - R_s), \quad (4.16)$$

where $\sigma_{f:1}$ is the fatigue strength for $R_s = 1$ and $\sigma_{f:0}$ is the CSR strength ($R_s = 0$, $N_f = 1/2$ or $t_f = 1/2f$). As N_f is increased, σ_f drastically decreases when t_f' is relatively short.

The hypothesis (d) is verified by series of fatigue experiments performed under various R_s . The applicability of the hypotheses (a–d) for several CFRP composite systems is summarized in Table 4.1. In various GFRP/metal joining systems (conical shaped joints, brittle and ductile adhesive joints, and bolted joints), it is possible to construct the master curves as well. Based on the study performed, it is unequivocal that the accelerating testing methodology is applicable when polymer resins fracture in a brittle manner and the deformation behavior in carbon fibers is time independent. Moreover, the environmental degradation of CFRP composites can be assessed using the time-temperature-water adsorption superimposition principle.

Polymer-modified asphalt is a highly temperature sensitive material. To obtain the master curves, the material was tested over a temperature interval from -30°C to at least 90°C . Since the polymer-modified asphalt undergoes the transition from a glass-like to a Newtonian-like material in this temperature range, three testing geometries were studied. The geome-

TABLE 4.1 Applicability of Master Curve for Various CFRP Composites Subjected to Various Loading Modes (4).

| Fiber | Matrix | Type | Fiber/matrix | Loading Mode | Hypothesis | | | | | |
|--------|--------|------------|--------------|--------------------|------------|---|---|---|---|---|
| | | | | | a | b | c | d | | |
| Carbon | PAN | Epoxy | UD | T400/828 | LT | O | O | O | O | |
| | | | | T300/2500 | LB | O | O | O | O | |
| | | | | TB | O | O | O | O | | |
| | | PEEK | SW | T400/3601 | LB | O | O | O | O | |
| | | | UD | T300/PEEK | LB | O | x | x | Δ | |
| | | | | TB | Δ | x | x | x | | |
| Glass | Pitch | Epoxy | UD | XN40/25C | LB | O | Δ | x | O | |
| | | | | E-glass/epoxy | LB | O | Δ | O | x | |
| | | Vinylester | PW | E-glass/vinylester | LB | O | O | O | O | x |

Type of fibers: UD: Unidirectional, SW: Strain woven, PW: Plain woven

Loading modes: LT: Longitudinal tension, LB: Longitudinal bending, TB: transverse bending

tries used were as follows: plate-plate (PP) for the mid-range temperatures; torsion bar (TB) for the low temperatures; and bob and cup (BC) for the high temperatures. The shift from one fixture to another must be done at a temperature that depends on the viscoelastic properties of the material. In the case of asphalt, it is theoretically possible to measure rheological properties using PP for the whole range of temperatures. However, when close to the glass transition temperature, slippage and breakage can occur, thus leading to very scattered and noisy data. Such problems were eliminated with TB. On the other hand, close to room temperature asphalt started to become soft so it was unable to support its own weight and keep the bar shape; whereas slipping and breaking were no longer a problem for PP. Plate-plate and BC geometries remained the best until the material approached the liquid state. In this case, the problems were the tendency to flow out from the space between the plates and the low torque values (due to the limited PP surface). Both problems were solved with a BC fixture. In conclusion, this paper showed examples of how isotherms obtained with three sample geometries and two rheometers followed the time-temperature-superimposition principle. This gave a solid confirmation of how data from different sources was combined to build reliable master curves covering a very wide range of reduced frequency. Master curves obtained from these geometries covered up to 20 decades of reduced frequencies (5).

4.3 CHEMICAL KINETICS

Another means of predicting lifetimes involves chemical kinetics and the use of the Arrhenius rela-

tionship, which shows that the chemical rate constant varies as a negative exponential of the reciprocal absolute temperature. In this procedure, we are monitoring the change in concentration of one or more of the reactants with respect to time. There are some fundamental rules for being able to apply chemical kinetics. One is that the reaction or the aging process involved must be chemical in nature. Many times individuals will apply the same rules and procedures to nonchemical events. And, with luck, they (and this author) were able to obtain meaningful lifetime predictions or failure rates.

Another principle involves the establishment of reaction order. We will define zero-, first-, second- and n^{th} - order reactions. With zero-order, the rate can be written as follows:

$$R = -kd[A]/dt = k[A]^0 = k, \quad (4.17)$$

where k is a proportionality constant; A is equal to reactant A .

Zero-order reactions are mainly homogeneous reactions on surfaces. The rate of reaction for a zero-order is independent of concentration.

We can rewrite the above equation as

$$d[A] = -kdt. \quad (4.18)$$

If we integrate over t_1 and t_2 and assume the concentration for $A_{t_1} = 0$ and $A_{t_2} = t$, then

$$[A]_t = [A]_0 = -k(t-0). \quad (4.19)$$

Rewriting the above we have

$$[A]_t = [A]_0 - kt. \quad (4.20)$$

A plot of $[A]$ versus time should yield a straight line with an intercept of $[A]_0$ and slope k .

A first-order reaction is the case in which the rate of reaction is dependent upon one reactant. We may write the rate of change of A as

$$R = -(1/a)(d[A]/dt) = d[A]^1. \quad (4.21)$$

Since A equals 1, the equation becomes

$$-d[A]/dt = k[A]. \quad (4.22)$$

Now if we integrate that equation we end up with

$$-(\ln[A]_t - \ln[A]_0) = kt. \quad (4.23)$$

Manipulation of the equations will result in

$$\ln([A]_t/[A]_0) = -kt \quad (4.24)$$

or

$$[A]_t/[A]_0 = e^{-kt}, \quad (4.25)$$

where e is the base of the natural log, which is equal to 2.718. Again, with manipulation of the equations we end up with

$$\log_{10}[A]_t = \log_{10}[A]_0 - kt/2.303. \quad (4.26)$$

Now, a semi-log plot of $[A]_t$ versus t will give us a straight line with a slope of $-k/2.303$ and an intercept of $[A]_0$.

There are two special cases for second-order reactions. The first case involves $A + A$, yielding the product, and the second case involves $A + B$. The rates in the first case may be written as

$$R = -(1/2)(k[A]^2/dt) = k[A]^2. \quad (4.27)$$

In the second case, the rate expression may be written as

$$R = -(d[A]/dt) = k[A][B]. \quad (4.28)$$

By performing the appropriate mathematical treatments, in the first case we end up with

$$1/[A]_t = 1/[A]_0 + 2kt. \quad (4.29)$$

A plot of the inverse concentration of A ($[A]^{-1}$) versus time will give us a straight line with a slope equal to $2k$ and an intercept of $1/[A]_0$.

And in the second case, we end up with

$$1/([A]_0 - [B]_0) \ln \left(\frac{[B]_0[A]_t}{[A]_0[B]_t} \right) = kt. \quad (4.30)$$

The left-hand side of the equation is plotted against t , the slope being equal to k .

For the n^{th} -order, the rate expression may be written as

$$R = -(1/n)d[A]/dt = k[A]^n. \quad (4.31)$$

Now, if we conduct experiments at different temperatures, preferably using three different temperatures, we will end up with a family of rates at different times and temperatures. This can be translated into lifetimes or survival rates. This author has employed this technique on numerous occasions, in particular in the absorption of water in plastics. The kinetics obtained were very useful in designing plastic parts based upon the observations (6).

An extremely useful extension of kinetic data can be illustrated in Fig. 4.3. After the rate was determined at one temperature, a series of rates was determined at different temperatures. The result of this was translated into a lifetime prediction. By plotting the difference in yellowing index versus $1/\text{Temperature}$

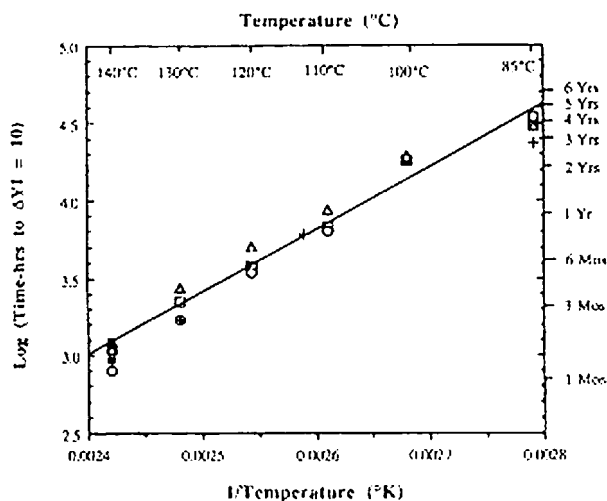


FIGURE 4.3 The effect of temperature on the thermal oxidative yellowing of BPA-PC. The different symbols represent data points obtained from four different studies. [Reprinted with permission from A. Factor, Ch 5 in *Polymer Durability, Degradation, Stabilization and Lifetime Prediction*, edited by R. L. Clough, N. C. Billingham and K. T. Gillen, *Advances in Chemistry Series 249*, American Chemical Society, Wash, D.C., pp. 59–76 (1993). (c) American Chemical Society.]

ture, an effective life of the BPA-PC over time was determined (7).

This extremely useful work of the thermal and photodegradation of bisphenol A-polycarbonate was performed by the manufacturer. The data generated were the result of four different studies at six different temperatures. A graph of this nature gave a high degree of confidence of lifetime performance of BPA-PC over a wide range of conditions with a minimum of experimentation.

The Arrhenius methodology has been used for many years to predict polymer lifetimes in various applications. However, it should be pointed out that there are numerous potential limitations associated with this technique. Many of the results indicated non-Arrhenius behavior. A publication reported on the limitations of the Arrhenius methodology. The report included a mention of diffusion-limited oxidation effects and a discussion of the implication of changes in the effective Arrhenius activation energy, or in the dominant reactions as temperature changes. Changes in the activation energies or in the dominant reactions with temperature can happen for any material, making extrapolations beyond the experimental temperature range challenging. However, when mechanistic changes occur, they invariably result in a reduction in effective Arrhenius activation energy, leading to lower than expected material lifetimes. Thus, it is critically important to derive methods for testing the Arrhenius extrapolation assumption. One approach that the authors have developed involves ultrasensitive oxygen consumption measurements. Results from the application of this approach were reviewed (8).

Accelerated heat aging tests were carried out to predict the useful lifetimes of ethylene-propylene-diene monomer (EPDM) vibration-isolating rubber components of ventilation fan motors used in clean rooms. The Arrhenius plot was derived from the reciprocal absolute temperature to predict the lifetimes of the rubbers, and the compression set of 20 percent was used as a threshold. The useful lifetimes at variable temperatures and activation energy were obtained from the Arrhenius relationship. An accelerated test program to predict useful lifetimes was designed to reduce time. The effect of antioxidant agents on the lifetimes of the rubbers was also studied (9).

Conventional high temperature compression stress-relaxation (CSR) experiments, using a Shawbury-Wallace relaxometer, can measure the force periodically at room temperature. An experiment describing modifications that allow the force measurements to be made isothermally and showing that the

measurements lead to more exact estimates of sealing force decay was performed. Using conventional Arrhenius analysis and linear extrapolation of the high temperature (80–100 °C) CSR results for two butyl o-ring elastomers showed that the second butyl was predicted to have a lifetime of approximately three times longer at room temperature. Testing the linear extrapolation assumed by the Arrhenius approach, a test was conducted for ultrasensitive oxygen consumption measurements from 110 °C to room temperature for the two butyl elastomers. The results demonstrate that linear extrapolation of the high temperature CSR results for the first butyl elastomer was acceptable; whereas a considerable curvature to a lower activation energy was observed for the second butyl below 80 °C. Using the oxygen consumption to extrapolate the CSR from 80 °C to 23 °C resulted in the conclusion that the second butyl degraded faster than the first butyl at 23 °C; which is opposite the earlier result based solely on extrapolation of the high temperature CSR results. Since samples of both materials that had aged in the field for approximately 20 years at 23 °C were available, it was possible to verify the prediction using compression set measurements (10).

One of the most critical aspects of this type of analysis is the ability to draw a straight line through the various data points. However, a discontinuation in the linear line also gives us a great amount of information. Once the discontinuation is realized, this can be translated into a change of mechanism within the chemical kinetics phenomena. We may have one or more events or mechanisms occurring; and if we have a discontinuation, we have two or more events or mechanisms occurring.

4.4 THERMAL DECOMPOSITION EXPERIMENTS

Attempts were made to use kinetics parameters from thermal decomposition experiments at high temperatures to predict service lifetimes of polymeric materials at lower temperatures. However, besides the obvious measurement and extrapolation errors (which can be considerable), there were two fundamental reasons why quantitative long-range extrapolations cannot be made for complex softening temperatures. They are as follows: (a) Arrhenius kinetics parameters cannot be extrapolated through phase transitions or softening temperatures; and (b) Arrhenius kinetics parameters cannot be extrapolated through the ceiling temperature region. Satisfactory lifetime prediction methods can be developed only

after a thorough analysis of the causes of service failure. A real method was taken from the literature to illustrate the correct procedures (11).

The lifetime of carbon fiber-reinforced plastics was estimated using thermogravimetric analytical kinetics. However, weight-loss kinetics was initially assumed as evidence. However, weight loss occurred without degradation, and degradation occurred without weight loss. Also, the degradation of composites by thermoxidative means was very complex, with ≥ 2 volatilization reactions taking place. Additionally, the method assumed that thermal oxidative degradations of composites were not autocatalytic reactions (12).

An approximation was developed of an integral method for analysis of thermogravimetric data, similar to but simpler than that of Doyle. The equations incorporated the heating rate A , giving the expressions $-\log A1 - 0.4567 \Delta E/RT_1 = -\log A2 - 0.4567 \Delta E/RT_2$ for equivalent weight losses at different heating rates. $\log A$ plotted versus $1/T$ for a given value of fractional residual weight gave a straight line, the slope of which gave the activation energy. Plotting fractional residual weight versus $1/T$ for various heating rates provided a series of identical curves with lateral displacement proportional to $\log A$. Superimposition of such curves provided a master thermogravimetric curve, which is a standard and is more accurate than individual curves. The procedure was applied to pyrolysis of CaC_2O_4 and nylon 6. Results were in good agreement with reported values (13).

A method for determining the activation energy from thermogravimetric analysis plots involved only the reading of the temperature at a constant weight loss from several integral thermograms at different heating rates. From the slope of $\log \beta$ versus $1/T$, the activation energy may be closely approximated by the equation equal or nearly to $-4.35 d \log \beta/d 1/T$. (14).

Based on the works of Ozawa, d Flynn, and Wall, their efforts were combined into what is now known as the Ozawa-Flynn-Wall method.

By thermogravimetric analysis, the decomposition processes and reaction mechanisms of the thermal degradation of nylon 1212 in N_2 were studied. The thermogravimetric analysis plot of nylon 1212 indicated that the thermal degradation process of nylon 1212 was a one-step reaction. The activation energy of this solid state process was determined by means of Kissinger and Ozawa-Flynn-Wall methods (which did not require knowledge of the reaction mechanism); it was 227.5–228.2 kJ/mol. Different

integral methods and reaction mechanisms reported in the literature were used and compared with these values (15).

The thermal stability of polypropylene was investigated by thermogravimetry and differential scanning calorimetry. Two different forms of polypropylene, as well as a polypropylene-glass composite material, made from pellets and commingled fibers were evaluated. Compression molded plates were made and tested. The determination of the apparent activation energy of each system, using the Ozawa-Flynn-Wall method, delivered information about the effect of polymer processing on the thermal degradation behavior (16).

Another study using thermogravimetric analysis and the Ozawa-Flynn-Wall method was conducted on cellulose. Mass decrease of cellulose powders and cotton fabrics was investigated at different heating rates and other different flow rates of air and nitrogen. The relationships between the lifetime of cotton, holding temperature and mass decrease were obtained. The lifetime of 10 percent mass decrease varied from several hundred years to several seconds in temperatures ranging from room temperature to 300 °C. The effect of the atmosphere was significant in a high temperature range (17).

Nonisothermal kinetic experiments of polymeric wastes, such as polyethylene (PE), polypropylene (PP), polystyrene (PS), and polyethylene terephthalate (PET), were studied in a nitrogen atmosphere, and kinetic parameters were analyzed using the Ozawa-Flynn-Wall method. The mixture containing polymeric wastes, which were combined to the ratio of 2:2:2:1 for PE, PP, PET, and PS from weight fraction, was also studied and analyzed in the same way. Theoretical activation energies of mixtures were calculated and compared with experimental activation energy obtained by the Ozawa-Flynn-Wall method. The nonisothermal kinetic results of polymeric wastes showed that most of the polymeric wastes had single-step reactions and similar activation energies for observed conversion ranges, respectively. In kinetic parameter analysis of the mixtures, the activation energy showed lower values than values of activation energies for all observed conversion ranges. This meant that lower activation energies were the result of interaction among polymeric wastes during thermal decomposition of mixtures (18).

Using differential scanning calorimetry under isothermal and dynamic conditions, the kinetics of curing of bisphenol A diglycidyl ether containing various amounts of poly(ether imide) (PEI) with 1,3-bis(aminomethyl)cyclohexane at 80–105 °C were

studied. Kinetic analysis was performed using three kinetic models: Kissinger, Ozawa-Flynn-Wall, and Kamal. Diffusion control was incorporated to describe the cure in the latter stages, predicting the cure kinetics over the whole range of conversion. The values of the activation energies for all the PEI/epoxy blends were higher than the values for the neat system. The autocatalytic mechanism was observed in the neat system as in the blends. The reaction rates were higher with PEI; however, the conversions decreased with the PEI content (19).

Thermogravimetric analysis was used to predict the respective lifetimes of two three-component systems of diglycidyl ether of bisphenol A ($n=0/1,2$ -diamine cyclohexane [DGEBA ($n=0/1,2$ -DCH)] modified with different concentrations of an epoxy reactive diluent, vinylcyclohexene dioxide (VCHD). Experimental results were treated using two methods. The first method was independent of the degradation mechanism, and the second was based on the thermodegradation kinetic mechanism. The activation energies of the reaction were determined using the Ozawa-Flynn-Wall method. These values were compared with those obtained using Kissinger's method. From experimental results, it was found that the optimum temperatures of service for these materials were different, so one or the other must be selected, depending on the application temperature considered (20).

The kinetics of thermal decomposition of poly(phenylene sulfide) (PPS) were studied by thermogravimetry of two different manufactured polymers. The kinetic parameters, such as activation energy and Arrhenius pre-exponential factor, were calculated using three methods: the Kissinger, the Ozawa-Flynn-Wall, and the Day methods. All methods indicated first-order reaction kinetics. Half-time estimation of the materials indicated that one was more stable than the other (21).

Four kinetic techniques were evaluated for predicting service lifetime of polymers from weight loss data: (a) factor-jump thermogravimetry, (b) iso-conversional diagnostic plots, (c) varied heating rate analysis, and (d) analysis at low conversion. The methods were illustrated by examples of polystyrene and polyurethane degradation. The factor-jump method gave high precision and values for the activation and values for the activation energy, which were independent of one another and of sample history (22).

The thermostability of carbon-fiber/epoxy-cyanate composites prepared from an autoadhesive and autoextinguish prepreg were tested. Dynamic

and isothermal aging tests were carried out to evaluate the composite thermal stability. Thermal degradation products were identified by chromatography and mass spectrometry analysis, and the results obtained were compared with data known on the material network structure. The physico-chemical network structure changes and the thermal aging data were correlated with the interlaminar shear strength (ILSS) mechanical results. For epoxy-cyanate composites, cracking appeared at longer times of aging in comparison to epoxy composites. This new epoxy-cyanate material isothermal stability seemed to be more thermally stable, particularly after it was post-cured. The comparison of chemical, mechanical, and crack formation results obtained by accelerated aging tests allowed us to determine models to predict long-term behavior (23).

4.5 MECHANICAL EXPERIMENTS

The long-term durability of polymeric composites was associated with the gradual change in physical properties, which occurs with the passage of time and with loading. The many mechanisms that effect composite long-term durability were grouped into three categories: (1) nonlinear constitutive behavior (such as viscoelastic or viscoplastic behavior); (2) mechanical degradation (such as matrix cracking, fiber failures, and delaminations); and (3) aging effects. The latter was further divided into physical and chemical aging phenomena. Analytical and/or empirical models were developed, which accounted for each of these factors separately. The challenge before the composites community was to develop predictive methodologies that would account for all factors acting simultaneously (24).

A method for predicting the time to brittle failure of polyethylenes was proposed. The method included modeling slow crack-growth in polyethylenes and the experimental determination of material parameters for the model. The model was based on the concept of the crack layer, such as a system consisting of the strongly interacting crack and process zone and the kinetic equations that govern the crack layer growth. The process zone in polyethylenes usually appeared to be a thin strip of drawn material extending along the crack line. This permitted a characterization of the crack layer by two parameters: the crack and process-zone lengths. The two-parameter crack layer kinetic model allowed description of slow crack growth as the discontinuous (stepwise) process, which is commonly observed in

the brittle fracture of polyethylenes. The model also predicted a relationship between time to failure and applied stress, identical to the established experimental stress. The material parameters of the kinetic model can be determined by experiments on smooth specimens relating to slow crack growth, requiring relatively short-term observations. Thus, the combination of the material testing and the mathematical modeling of the crack layer evolution were proposed as a method for lifetime prediction in the brittle fracture of polyethylenes (25).

The aim of a published study was to analyze the creeping process of polysulfone and its composites reinforced with carbon fibers in vitro conditions. All samples were observed as load-bearing implants. The investigations were carried out at room temperature in air and in vitro in Ringer's solution. Mechanical testing was carried out on a Zwick 1435 machine, with the force between 300–1,800 Newtons. The nominal strain and the time of failure were observed. As a result, long-term behavior was observed for the samples under mechanical tension and in biological environments. On the basis of the completed experimental data, the critical force was determined, under which the material could work for extended times without failure, and the lifetime for remote load and acceptable deformation were estimated (26).

To evaluate the degradation in stiffness for determining a damage function, flexural fatigue tests with different stress levels were first conducted on the carbon fiber reinforced plastics cross-ply laminates. Then, based on the damage function, a cumulative fatigue damage rule for predicting the lifetime for the composites subjected to a multi-stress level fatigue loading was proposed. Finally, the two-stress level fatigue tests were performed to verify the proposed rule. From the present study, the damage function was found to increase cubically with an increasing number of cycles for each stress level. It was also found that the lifetime obtained from the two-stress level fatigue tests was longer than the predicted one for the stress increasing case, while it was shorter for the stress-decreasing case (27).

A study was conducted based upon creep of composites used in implant applications during in vitro conditions. Samples were prepared from polysulfone and its carbon-reinforced composites and applied to load-bearing implant applications. Testing was conducted at room temperature in air and in vitro Ringer's solutions. Mechanical property testing was conducted on a Zwick 1465 machine with forces between 300 and 1,800 Newtons. Both nomi-

nal strains and the time to failure were measured. The results of the testing indicated that the data enabled estimation for long-term sample behavior under mechanical tension and the biological environment's influence on it. Critical forces were determined under which the material can work for extended time without failure, and the lifetime for remote load and acceptable deformation of investigated samples was estimated (28).

A comprehensive analytical model for predicting long-term durability of resins and of fiber-reinforced plastics was presented. It took into account viscoelastic/viscoplastic creep, hydrothermal effects and the effects of physical and chemical aging on polymer response. An analytical tool consisting of a specialized test-bed finite element code, NOCA-3D, was used for the solution of complex stress analytical problems, including interactions between non-linear material constitutive behavior and environmental effects. Computer simulations of the hydrothermal cycling of a woven graphite/epoxy laminate and transverse creep response of a unidirectional IM7/5260 (graphite/epoxy) composite were presented as benchmark problems to demonstrate some of the predictive capabilities of the proposed durability prediction model. Good agreement was obtained between the proposed model predictions, the exact solutions, and the published results for cases where physical aging was not considered.

When physical aging was included in the proposed model using an effective-time parameter, the predicted increase in the rate of stiffening was found to be small when compared with actual test data. It was therefore likely that in addition to physical aging, there were other aging processes that may have caused the IM7/5260 specimen to become increasingly "stiff" with continued thermomechanical cycling. However, the accuracy of the aging predictions could be completely verified only after the momentary creep properties for the IM7/5260 composite were determined from short time tests (29).

The creep behavior of a longitudinal polymer liquid crystal (PLC) was examined in the region of nonlinear viscoelasticity. The creep compliance D curves at nine different stress σ levels, from 10–50 $\text{J}\cdot\text{cm}^{-3}$ at a constant temperature were determined and shifted along the log time axis for $\sigma_{\text{ref}} = 20 \text{ J}\cdot\text{cm}^{-3}$ to produce the D versus t/a_σ master curve. A fairly general formula for stress shift factor a_σ based on free volume v^f and the chain relaxation capability (CRC) derived by one of the authors was applied. The formula predicted values that agreed with the experimental ones within the limits of the experi-

mental accuracy. Thus, experiments at several stress levels could serve for prediction of long-term behavior from short-term tests. The same value of the Doolittle constant B was obtained separately from temperature shift and stress experiments for the PLC (30).

An excellent study based upon the prediction of adhesive fatigue vulnerability using dynamic mechanical analysis (DMA) has recently been reported in the literature. The vulnerability of an adhesively-bonded joint to fatigue effects is difficult to assess. Many physical tests were performed to determine or predict the useful lifetime of an adhesive bond. Most of these tests are destructive and are based on multiple samples and a statistical analysis of results. It is impossible to test all conditions and loads.

Adhesive failure under fatigue was traced to many compounding factors. DeGennes has shown that the T_g at the adhesive interface differs from the bulk T_g by as much as 50 °C lower than the bulk material (31). Further, adhesive failure under fatigue was linked to frequency effects, with low-frequency fatigue being more detrimental than higher strain rates, and the attendant creep was the principal contributor to failure (32).

Since creep is more prevalent in lower modulus materials, the low surface T_g , low-frequency fatigue rates, and creep-dominant failure support the notion that adhesive failure is time dependent (creep dominant) rather than cycle dependent, as is the case for metals or other materials (33–35).

Creep is difficult to measure and is usually measured with a static load test (for example, per ASTM D1780). One manifestation of creep is a reduction in the T_g of a material. As creep exerts its influence, the apparent T_g of a material will decrease due to the “stretched” polymer chains or the reduction of bulk steric interactions resulting from creep. The resistance to creep flow was particularly evident at low strain rates, where the creep-affected polymer chains exhibited their poorest response to stress, having become more “plastic.” After a “creep-inducing fatigue event,” measurement of the shift in apparent T_g of the adhesive, or a miniature bonded joint, at low strain rate can provide an indication of the relative susceptibility of the material or the joint to fatigue effects.

For several years, dynamic mechanical analysis tests on bulk adhesive samples and small test joints were studied to determine their relative susceptibility to fatigue effects. This involved a series of T_g measurements and a comparison of the shift in T_g after a fatigue event. The general practice was to

measure the T_g of the adhesive or joint at 1 Hz initially, then at 0.1 Hz, using a standard temperature sweep program. A fatigue cycle was then performed at some predetermined series of load cycles. The T_g was then re-measured at 0.1 Hz. Shifts in T_g at 0.1 Hz before and after the fatigue cycle were used to evaluate the relative tendency of the adhesive or joint system to fatigue effects (36).

4.6 MISCELLANEOUS EXPERIMENTATION

Nonisothermal crystallization kinetic data obtained from differential scanning calorimetry (DSC) for a poly(ethylene terephthalate) were corrected for the effects of temperature lag between the DSC sample and furnace, using the method of Eder and Janeshitz-Kriegl. This method was based on experimental data alone, without resorting to any kinetic model. The method was presented for shifting the corrected nonisothermal crystallization kinetic data with respect to an arbitrarily chosen reference temperature to obtain a master curve (37).

Vickers micro-indentation was utilized to follow the changes in microhardness and to evaluate the chemical aging and oxidation phenomena in high-performance carbon fiber-reinforced thermoplastic-toughened thermoset composite (a modified cyanate ester resin) and a semicrystalline thermoplastic composite. Oxidation profiles with aging were obtained on [00°]8 (unidirectional) composite specimens by indenting across the thickness of the samples in the fiber direction. Samples were aged up to six months in environmental chambers at 150 °C in three different environments: an inert nitrogen environment, a reduced air pressure of 13.8 KPa (2 psi air), and ambient air pressure. The experimental results showed a considerable drop in overall hardness of both thermoset and thermoplastic composites after a week of aging in all of the three environments. This was attributable to a thermal stress-relieving effect. Very little additional change was observed after six weeks' aging. Thereafter, the hardness profiles showed drops in hardness starting at the specimen edges initially, and then gradually spreading to the specimens' interiors with time. These observations were indicative of diffusion-controlled oxidation in the samples. Also, the hardness drops in the composites appeared to be sensitive to oxygen partial pressure in the aging environment. Samples aged in ambient air were the most affected, while those in nitrogen were least affected. A similar diffusion-

controlled oxidative process was also developed from Vickers indentation results on aged thermoset (bismaleimide) composites (38).

A simple mathematical equation based on a diffusion model was utilized to estimate migration of both acrylonitrile and styrene from polymers produced from these monomers, which were used under a wide variety of food-contact applications. These calculated migration values have subsequently been used to estimate U.S. consumers' exposure to acrylonitrile and styrene from food stored in these materials. The basic assumptions integral to the model were discussed in relation to potential errors in migration estimates that could be experienced if the assumptions were not true. In addition to the discussion of the basic assumptions, factors affecting the migration predictions were evaluated in this study, including polymer "aging"; temperature changes during the lifetime of the polymeric item; the effects of polymer-modifying materials, such as plasticizers; impact modifiers; and the physical form of the article or test sample (39).

An area of medical applications related to denture lining materials was studied. Soft denture lining materials are an important treatment option for patients who have chronic soreness associated with dental prostheses. Three distinctly different types of materials are generally used. These are plasticized polymers or copolymers, silicones, or polyphosphazene fluoroelastomers. The acceptance of these materials by patients and dentists is variable. The objective of this study was to compare the tensile strength, percent elongation, hardness, tear strength, and tear energy of eight plasticized polymers or copolymers, two silicones, and one polyphosphazene fluoroelastomer. Tests were run at 24 hours after specimen preparation and repeated after 900 hours of accelerated aging in a Weather-Ometer device. The data indicated a wide range of physical properties for soft denture lining materials and showed that accelerated aging dramatically affects the physical and mechanical properties of many of the elastomers. No soft denture liner proved to be superior to all others. The data obtained provided clinicians with useful information for selecting soft denture lining materials (40).

4.7 SUMMARY

In the preparation of this chapter on lifetime predictions of plastics, many different sources were used. The author wishes to point out several for the

reader's perusal. One includes a chapter on lifetime predictions that contains a review with 16 references on plastic degradation testing with emphasis on standardized procedures, models for change of parameters with time, time-dependent mechanical properties, environmental degradation tests, test limitations and simulated design life by accelerated exposure of products (41).

Another set of references was found by searching the Internet. It was located in a Google search of a professional society—the Society For the Advancement of Materials and Processes (SAMPE). This useful and informative site includes lifetime predictions of fiber reinforced plastics, especially those used in advanced composite applications.

A good reference for lifetime predictions can be found in a treatise on the subject. This treatise covers various aspects of the types of testing involved in performing lifetime predictions. It covers the following subjects: (a) standardized procedures; (b) models for change of parameters with time; (c) time-dependent mechanical properties which include creep and stress relaxation, fatigue, and abrasion; (d) environmental degradation tests which include models for effect of level of degradation agents, Arrhenius relationships, time/temperature shifts based upon the Williams-Landel-Ferry equation, artificial weathering, ionizing radiation, effect of liquids, and dynamic conditions; (e) limitations; and (f) simulated design life exposure of products. This treatise gives the reader a good general overview of all the mathematical techniques available to determine lifetimes (41).

In the determination of lifetime predictions, key factors must be observed. One includes the ability to draw a straight line through the data points, depending on how they are plotted. A slight deviation in the drawn line can reflect major changes in the time of life of a product. This becomes more evident in the determination of lifetime by chemical kinetics methods. In some cases, attempts have been made to force data to fit into a particular pattern that may be incorrect. Chemical kinetics techniques should be reserved only for chemical-caused events. This author finds the generation of master curves the best overall technique, if it can be employed.

4.8 REFERENCES

1. Wayne Nelson, *Accelerated Testing—Statistical Models, Test Plans, and Data Analyses*, Hobbs Engineering, Westminster, CO, 1990.
2. F. Povolò, *Polymer Journal*, Vol. 26(9), pp. 981–992, 1994.

3. I. M. Ward and D. L. Hadley, *An Introduction to the Mechanical Properties*, John Wiley & Sons, New York, pp. 62–64, 2000.
 4. Y. Miyano, *Proceedings of the 5th International Conference on Durability Analysis of Composite Systems*, Tokyo University of Science, November 6–9, 2001.
 5. G. Polacco, O. J. Vacin, D. Biondi, J. Stastna and L. Zanzotto, *Applied Rheology*, Vol. 13(3), pp. 118–124, 2003.
 6. J. A. Harvey, unpublished results, 1998.
 7. A. Factor, *Polymer Durability, Degradation, Stabilization and Lifetime Prediction*, R. L. Clough, N. C. Billingham, and K. T. Gillen, Eds., *Advances in Chemistry Series 249*, American Chemical Society, Washington, DC, Chapter 5, pp. 59–76, 1993.
 8. K. T. Gillen, M. Celina, and R. L. Clough, *Proceedings of the 26th Water Reactor Safety Information Meeting*, Vol. 3, pp. 303–313, 1998.
 9. W. D. Kim, W. S. Kim, C. S. Woo, and S. J. Cho, *Eyasutoma*, Vol. 37(2), pp. 107–114, 2002.
 10. K. T. Gillen, M. Celina, and R. Bernstein, *Polymer Degradation and Stability*, Vol. 82(1), pp. 25–35, 2003.
 11. J. H. Flynn, *Journal of Thermal Analysis*, Vol. 44(2), pp. 499–512, 1995.
 12. A. B. Hunter and C. H. Sheppard, *Polymer Preprints*, Vol. 28(2), pp. 411–412, 1987.
 13. T. Ozawa, *Bulletin of the Chemical Society of Japan*, Vol. 38(11), pp. 1881–1886, 1965.
 14. J. H. Flynn and L. A. Wall, *Journal of Polymer Science*, “Part B: Polymer Letters,” Vol. 4(5), pp. 323–328, 1966.
 15. C. Zhang, M. Liu, Q. Zhao, Y. Wang, and S. Cao, *Suliao Gongye*, Vol. 30(6), pp. 38–40, 53, 2002.
 16. S. Wiedmer, G. Bechtold, and K. Friedrich, “Composite Systems: Macrocomposites, Microcomposites, Nanocomposites,” *Proceedings of the ACUN-4 International Composites Conference*, 4th, Sydney, Australia, July 21–25, 2002.
 17. T. Hatakeyama, J. Nakazawa, M. Iijima, and H. Hatakeyama, *Sen’i Gakkaishi*, Vol. 58(11), pp. 405–408, 2002.
 18. Y. S. Kim, Y. S. Kim, K. M. Kim, S. U. Jeong, and S. H. Kim, *Journal of Industrial and Engineering Chemistry*, Vol. 9(3), pp. 219–224, 2003.
 19. L. Barral, J. Cano, J. Lopez, I. Lopez-Bueno, P. Nogueira, M. J. Abad, and C. Ramirez, *Polymer*, Vol. 41(7), pp. 2657–2666, 2000.
 20. L. Nunez, M. Villanueva, M.R. Nunez, and B. Rial, *Journal of Applied Polymer Science*, Vol. 89(14), pp. 3835–3839, 2003.
 21. L. G. Lage and Y. Kawano, *Polimeros: Ciencia e Tecnologia*, Vol. 9(4), pp. 82–85, 1999.
 22. J. H. Flynn and B. Dickens, *American Chemical Society Symposium Series*, Vol. 95 (“Durability Macromolecular Materials”), pp. 97–115, 1979.
 23. B. Mortaigne and N. Regnier, *Journal of Applied Polymer Science*, Vol. 77(14), pp. 3142–3153, 2000.
 24. M. E. Tuttle, “Progress in Durability Analysis of Composite Systems,” *Proceedings of the International Conference on Durability Analysis of Composites Systems*, Brussels, July 16–21, 1996.
 25. A. Chudnovsky, Y. Shulkin, D. Baron, and K. P. Lin, *Journal of Applied Polymer Science*, Vol. 56(11), pp. 1465–1478, 1995.
 26. P. Rosol and J. Chlopek, *Kompozyty*, Vol. 3(7), pp. 291–295, 2003.
 27. H. Kasano, O. Hasegawa and G. Takagi, “Durability Analysis of Composite Systems 2001,” *Proceedings of the International Conference on Durability Analysis of Composite Systems*, 5th, Tokyo, Japan, Nov. 6–9, 2001.
 28. P. Rosol, J. Chlopek, and K. Ceramiki, *Pol. Kompozyty*, Vol. 3(7), pp. 291–295, 2003.
 29. R. Samit, *Reinforced Plastics Durability*, pp. 349–368, 1999.
 30. A. E. Akinay, W. Brostow and R. Maksimov, *Polymer Engineering and Science*, Vol. 41(6), pp. 977–981, 2001.
 31. P. G. deGennes, *Plenary Address*, 23rd Annual Meeting of the Adhesion Society, Myrtle Beach, SC, 2000.
 32. J. A. Harris and P. A. Fay, *International Journal of Adhesion and Adhesives*, Vol. 12(1), pp. 9–18, 1992.
 33. S. Mall and G. Ramamurthy, *International Journal of Adhesion and Adhesives*, Vol. 9(1), pp. 33–37, 1989.
- AU: “Journal” correct?
34. W. K. Chiu and R. Jones, *International Journal of Adhesion and Adhesives*, Vol. 15(3), pp. 131–136, 1995.
 35. R. Jones, W. K. Chiu, and J. Paul, *Composite Structures*, Vol. 25, pp. 201–207, 1993.
 36. G. W. Ritter, *Proceedings of the Annual Technical Conference of the Society Plastics Engineers*, Nashville, TN, May 4–8, 2003, pp. 77–79.
 37. T. V. Chan, G. D. Shyu, and A. I. Isayev, *Polymer Engineering and Science*, Vol. 35(9), pp. 733–740, 1995.
 38. H. Parvtareddy, J. Z. Wang, J. J. Lesko, D. A. Dillard, and K. L. Reifsnider, *Journal of Composites Materials*, Vol. 30(2), pp. 210–230, 1996.
 39. T. D. Lickly, M. L. Rainey, L. C. Burgert, C. V. Breder, and L. Borodinsky, *Food Additives and Contaminants*, Vol. 14(1), pp. 65–74, 1997.
 40. E. R. Dootz, A. Koran, and R. G. Craig, *Journal of Prosthetic Dentistry*, Vol. 69(1), pp. 114–119, 1993.
 41. *The Handbook of Polymer Testing*, Chapter 29, R. Brown, Ed., Marcel Dekker, New York, 1999.

TYPES OF DEGRADATION

| | |
|---|-----|
| CHAPTER 5 ELECTROCHEMICAL CORROSION | 81 |
| CHAPTER 6 HIGH TEMPERATURE OXIDATION | 105 |
| CHAPTER 7 CHEMICAL AND PHYSICAL AGING OF PLASTICS | 153 |
| CHAPTER 8 ENVIRONMENTAL DEGRADATION OF REINFORCED CONCRETE | 165 |
| CHAPTER 9 BIOFOULING AND PREVENTION: BIODETERIORATION AND BIODEGRADATION OF MATERIALS | 179 |
| CHAPTER 10 MATERIAL FLAMMABILITY | 207 |

CHAPTER 5

ELECTROCHEMICAL CORROSION

R. A. Buchanan

E. E. Stansbury

Department of Materials Science and Engineering, University of Tennessee, Knoxville, Tennessee

| | |
|--|----|
| 5.1 INTRODUCTION | 81 |
| 5.2 ELECTROCHEMICAL THERMODYNAMICS | 81 |
| 5.3 ELECTROCHEMICAL KINETICS AND CORROSION PROCESSES | 92 |
| 5.4 EXPERIMENTAL POLARIZATION CURVES | 96 |

| | |
|--|-----|
| 5.5 EXAMPLES OF ELECTROCHEMICAL CORROSION MEASUREMENTS AND CHARACTERIZATIONS | 98 |
| 5.6 SUMMARY | 102 |
| 5.7 REFERENCES | 103 |

5.1 INTRODUCTION

The term *corrosion* for a metallic material in a liquid environment normally refers to the loss-of-mass of the material as a function of time through interaction with the environment. The loss of mass may be uniform over the material surface or highly localized, as in crevice and pitting corrosion. Furthermore, the loss of mass may result in simple or complex metal ions dissolved in the solution, or as solid corrosion products formed at the metal/solution interface, often as metal hydroxides or oxides. If solid corrosion products are formed, and if they are adherent to the metal surface, nonporous, and have good resistance to electron and/or ion transport, a “passive film” will be developed that can drastically reduce the corrosion rate of the metal.

The fundamental mechanisms that control the metallic aqueous-corrosion processes (corrosion in acids, bases, salt solutions, etc.) are electrochemical in nature. To understand the electrochemical mechanisms, one must understand the underlying sciences of electrochemical thermodynamics and electrochemical kinetics. Electrochemical thermodynamics allows the prediction of whether corrosion will occur for a given metal in a given solution at a given temperature. If corrosion does occur, thermodynamics allows prediction of the form of the corrosion products (ionic or solid) and whether passive film formation is possible. Electrochemical kinetics (in combination with thermodynamics) is the basis

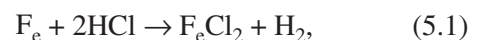
for rapid electrochemical corrosion measurements, including characterizations of corrosion rates, uniform versus localized corrosion, and passivation behaviors.

Most of the following information is presented in more detail in *Fundamentals of Electrochemical Corrosion* by E. E. Stansbury and R. A. Buchanan.¹

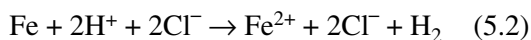
5.2 ELECTROCHEMICAL THERMODYNAMICS

5.2.1 Electrochemical Reactions, the Electrochemical Cell, and the Gibb’s Free-Energy Change

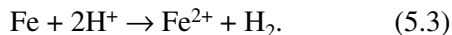
Electrochemical reactions may be divided into at least two half-reactions, with each half-reaction involving loss or gain of electrons by chemical species that, as a result, undergo valence changes. The half-reactions involve metal surfaces at which (1) metal ions either pass into or are deposited from solution, or (2) the valence state of another species is changed. If the half-reactions occur on physically separated metals in an appropriately conducting medium (usually an aqueous solution), a difference in electrical potential is generally observed to exist between them. For example, consider the following corrosion reaction:



or, if the ionized states of the HCl and FeCl₂ are taken into account, the equivalent reactions of



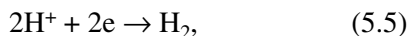
and



Reaction 5.3 is the sum of the following half-reactions:



and



in which the iron, having lost electrons to form ferrous ions, is oxidized, and the hydrogen ions are reduced to hydrogen gas. Conceptually, these two half-reactions may be caused to occur at physically distinct surfaces by placing iron into a solution of ferrous ions and platinum, which is normally chemically inert, in a solution of hydrogen ions into which hydrogen gas is bubbled. The arrangement is shown in Figure 5.1. A porous barrier is indicated between the two electrodes, across which ionic electrical conduction can occur (but with minimum mixing of solutions). There is a potential difference at this liquid/liquid junction, but it is generally small compared to other potential differences and will not be considered in the present discussion.

The electrochemical cell (or battery) that results will have a difference in electrical potential between the metal electrodes.²⁻³ This potential difference is a function of the concentrations of Fe²⁺ and H⁺ ions

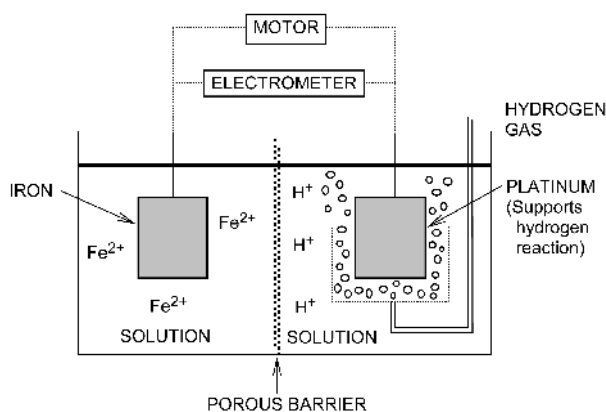


FIGURE 5.1 Electrochemical cell.

and the pressure of the hydrogen gas, at a given temperature. If these variables are adjusted to unit activity (essentially unit molality for the ions in dilute solution, and one atmosphere pressure for the hydrogen), the potential difference in the limiting idealized case at 25 °C, with the electrodes not electrically connected, is 440 mV, with the platinum on which the hydrogen reaction occurs being positive. It is noted that when the two electrodes are not electrically connected, each half-cell reaction is at equilibrium ($\text{Fe} = \text{Fe}^{2+} + 2e$ and $2\text{H}^+ + 2e = \text{H}_2$). It is important to note that measurement of the potential difference with an electrometer does not constitute electrical connection, since the internal resistance is extremely high ($>10^{14}$ ohms) and essentially no current is allowed to flow. Also, the assumption is made here that the spontaneous hydrogen reaction on Fe is negligible compared to that on Pt. The overall reaction (Reaction 5.3) will not occur until the two electrodes are connected externally, either directly or through some device utilizing the current to perform work.

For example, upon connection of an electrical motor (Figure 5.1), electrons will flow from the iron electrode (at which net oxidation occurs, $\text{Fe} \rightarrow \text{Fe}^{2+} + 2e$), through the motor, to the platinum electrode (at which net reduction occurs, $2\text{H}^+ + 2e \rightarrow \text{H}_2$). (Unfortunately, we are accustomed to considering electrical current as a flow of positive charge from the positive to the negative terminal—just the opposite of the electron flow direction.) If the motor is mechanically and electrically perfect, then the electrochemical energy released by the cell reaction results in an equivalent amount of work; otherwise, part or all of this energy may be dissipated as heat.

The maximum amount of work that can be obtained per unit of reaction (i.e., per unit overall reaction—here, per mole of iron) is that of the reversible transfer of the electrons (electrical charge) through the potential difference between the electrodes. It can be shown that this maximum work, w'_r , is equal to the decrease in Gibb's free energy, ΔG_{react} , for the overall reaction at constant pressure and temperature, as follows:⁴

$$w'_r = -\Delta G_{\text{react}} \quad (5.6)$$

Conventional electrical circuit analysis considers that positive electricity (positive charge) flows as a consequence of the difference in potential. If unit positive charge (with magnitude equal to that of the electron charge) is designated as e^+ and c charges are transferred per unit of reaction, then the reversible electrical work is given by

$$w'_r = ce^+E_{\text{cell}}, \quad (5.7)$$

where E_{cell} is defined such as to be positive when w'_r work is done as a consequence of the spontaneous reaction (i.e., work done by the system). If each symbol for a chemical species in a reaction is interpreted to represent a mole of the species, then in the present example the unit of reaction involves one mole, or Avogadro's number (N_0) of iron atoms, which produces $2N_0$ charges upon reaction. In general then, $c = nN_0$, where n is the number of moles of unit charges (electrons) transferred per unit of reaction. The reversible electrical work, therefore, is

$$w'_r = nN_0e^+E_{\text{cell}} \quad (5.8)$$

$$w'_r = nFE_{\text{cell}}, \quad (5.9)$$

where $N_0e^+ = F$ is Faraday's constant or the absolute value of the charge of N_0 electrons. Substitution of Equation 5.9 into Equation 5.6 gives

$$\Delta G_{\text{react}} = -nFE_{\text{cell}}. \quad (5.10)$$

Since E_{cell} is defined to be positive for a spontaneous reaction, this equation correctly expresses a decrease in Gibb's free energy (negative value of ΔG_{react}), which is the thermodynamic criterion for a spontaneous reaction at constant temperature and pressure.

An electrochemical cell, such as that represented in Figure 5.1, will have a difference in potential, E_{cell} , between the metallic conductors extending out of the solution (i.e., Fe and Pt). This difference in potential is a consequence of the electrochemical reaction at each metal/solution interface and the accompanying potential difference established across each interface. If these individual interface potential differences could be measured, then the cell potential for any combination of electrochemical reactions could be calculated.

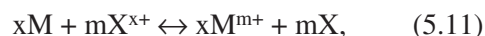
Unfortunately, a single metal/solution interface potential difference cannot be measured directly, since the metal probe from an electrometer used to measure the potential difference will, on contacting the solution, introduce another metal/solution interface. Hence, the electrometer will indicate only the difference in potential between the metal under investigation and the metal probe in contact with the same solution. A practical solution to this dilemma is provided by selecting one of several specific metal/aqueous-environment combinations that will give a highly reproducible interface potential differ-

ence, and therefore function as a standard reference electrode. More specifically, these combinations are referred to as standard reference half-cells, since they must be used in conjunction with the metal under investigation to produce a complete electrochemical cell, with metal contacts between which a difference in potential can be determined.

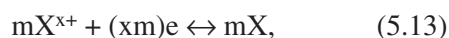
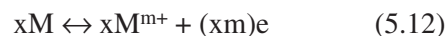
The accepted primary reference electrode is the hydrogen half-cell described in association with Figure 5.1.⁵ It consists of platinum (which serves as an inert conductor) in contact with a solution at 25 °C, saturated with hydrogen gas at one atmosphere pressure, and containing hydrogen ions at pH = 0 (hydrogen-ion activity, $a_{\text{H}^+} = 1$). In practice, the major use of the standard hydrogen electrode (SHE) is for calibration of secondary reference electrodes that are more convenient to use. Two common reference electrodes are the saturated calomel electrode (SCE) or mercury/saturated-mercurous-chloride half-cell with a potential of +241 mV relative to the SHE, and the silver/saturated-silver-chloride half-cell with a relative potential of +196 mV. Both of these electrodes are saturated with potassium chloride to maintain a constant chloride and hence metal-ion concentration.

5.2.2 The Generalized Cell Reaction

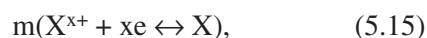
It is useful to establish a more generalized representation for the electrochemical cell reaction, as follows:



which is the sum of the following two half-cell reactions:



or



where the parentheses above contain the usual representations of the half-cell reactions (except for the \leftrightarrow symbol) that are tabulated in reference tables for the equilibrium condition (i.e., for example, $M = M^{m+} + me$).⁶⁻⁸ The standard equilibrium half-cell potentials for several reactions are given in Table 5.1. The \leftrightarrow

TABLE 5.1 Standard Equilibrium Half-Cell Potentials

| | Standard Equilibrium Half-Cell Potentials, E^0 , mV(SHE) |
|---|--|
| $\text{Zn} = \text{Zn}^{2+} + 2e$ | -763 |
| $\text{Fe} = \text{Fe}^{2+} + 2e$ | -440 |
| $\text{Pb} = \text{Pb}^{2+} + 2e$ | -126 |
| $\text{Cu} = \text{Cu}^{2+} + 2e$ | +342 |
| $\text{Ag} = \text{Ag}^+ + e$ | +799 |
| $\text{H}^+ + e = 1/2 \text{H}_2$ | 0 |
| $\text{H}_2\text{O} + e = 1/2 \text{H}_2 + \text{OH}^-$ | -820 |
| $\text{O}_2 + 4\text{H}^+ + 4e = 2\text{H}_2\text{O}$ | +1,229 |
| $\text{O}_2 + 2\text{H}_2\text{O} + 4e = 4\text{OH}^-$ | +401 |

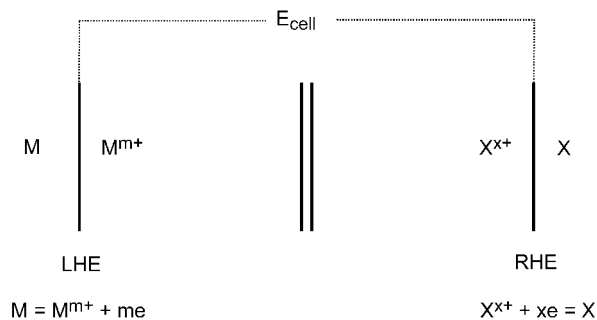
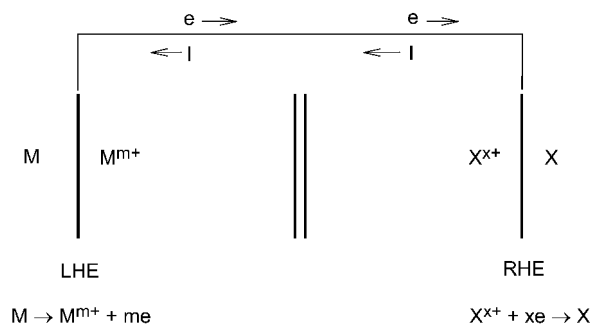
symbol is used in this text to denote the stoichiometric relationship between reactive species. It is specifically employed to indicate that no assumption is being made regarding the spontaneous direction of the overall reaction—Reaction 5.11 (i.e., it could be either left-to-right or right-to-left). If, for example, the spontaneous direction for Reaction 5.11 is left-to-right, the spontaneous direction for the half reactions, 5.12–5.15, also will be left-to-right.

It is convenient to use an abbreviated cell representation for the generalized reaction, as shown in Figure 5.2. The reduced species on the left side of the overall reaction (M) and its associated ion (M^{m+}) are identified as the left-hand-electrode (LHE); the reduced species on the right side (X) and its associated ion (X^{x+}) are identified as the right-hand-electrode (RHE).

If Reaction 5.11 occurs spontaneously from left-to-right, then

$$\Delta G_{\text{react}} < 0, \quad (5.16)$$

where ΔG_{react} always applies to the left-to-right direction of Reaction 5.11. For this condition, if the

**FIGURE 5.2** Abbreviated cell representation showing E_{cell} and half-cell reactions.**FIGURE 5.3** Abbreviated cell representation showing current flow when the half-cell reactions are coupled.

electrochemical cell reaction is allowed to occur, the electron flow and conventional-current flow directions will be as shown in Figure 5.3. According to electrical circuit convention, X (in this case) is at a higher potential than M, and the flow of current from X to M provides electrical energy capable of doing work. As discussed previously, this work is related to the change in Gibbs's free energy through Equation 5.10, namely:

$$\Delta G_{\text{react}} = -nFE_{\text{cell}} \quad (n = xm) \quad (5.17)$$

In this relationship, n is the number of moles of electrons transferred per unit of the reaction (i.e., per x moles of M, etc).

Care must be exercised in assigning a sign to E_{cell} such that the cell potential and the change in the Gibbs's free energy for the reaction are consistent with Equation 5.17. This is one of the most critical points with respect to notation in electrochemistry. If Reaction 5.11 occurs spontaneously from left-to-right, ΔG_{react} must be negative (Equation 5.16). Then, in order to be consistent with Equation 5.17, E_{cell} must be positive. For these conditions, as shown in Figure 5.3, the half-cell potential of the RHE is greater than that of the LHE. Therefore, a positive E_{cell} value is accomplished by defining $E_{\text{cell}} = E'_{\text{RHE}} - E'_{\text{LHE}}$, where E'_{RHE} and E'_{LHE} are the equilibrium half-cell potentials of the right-hand and left-hand electrodes, respectively. Indeed, for all conditions, E_{cell} will have the proper sign if the following convention is adopted:

$$E_{\text{cell}} = E'_{\text{RHE}} - E'_{\text{LHE}} \quad (5.18)$$

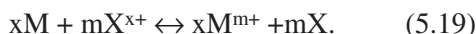
It follows from the above discussion that if calculations result in $E'_{\text{RHE}} < E'_{\text{LHE}}$, E_{cell} will be negative. A negative value of E_{cell} results in $\Delta G_{\text{react}} > 0$ and,

hence, the conclusion is that the reaction will not proceed from left-to-right, but rather that the spontaneous direction is from right-to-left. Similarly, if calculations result in $E'_{\text{RHE}} = E'_{\text{LHE}}$, E_{cell} will be zero. Therefore, $\Delta G_{\text{react}} = 0$, and the overall reaction will be at equilibrium.

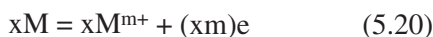
During the corrosion process, it is important to realize that both the anodic reaction (oxidation, e.g., $M \rightarrow M^{m+} + me$) and the cathodic reaction (reduction, e.g., $2H^+ + 2e \rightarrow H_2$) occur on the same metal. In this case, therefore, the electron-conducting phase for both the LHE and the RHE would be the metal, M.

5.2.3 The Nernst Equation: Effect of Concentration on Equilibrium Half-Cell Potential^{2,9}

Again consider the generalized overall electrochemical reaction



To determine whether the reaction proceeds from left-to-right, from right-to-left, or is at equilibrium, one must determine the equilibrium potentials (E' values) for the two half-reactions:



One of the most significant equations derived from chemical thermodynamics permits calculation of the change in the Gibb's free energy for the overall reaction at constant total pressure and temperature as a function of change in Gibb's free energy of the reactant and product species in their standard states, and the concentrations of those species whose concentration can be varied. The equation is:

$$\Delta G_{\text{react}} = \Delta G_{\text{react}}^{\circ} + RT \ln \frac{a_M^m \cdot a_{M^{m+}}^x}{a_M^x \cdot a_{X^{x+}}^m}. \quad (5.22)$$

In this equation, $\Delta G_{\text{react}}^{\circ}$ is the change in the Gibb's free energy for the overall reaction as written for reactants and products in their standard states. The a 's are the activities of the species indicated by the subscripts—each activity is raised to a power equal to the stoichiometric coefficient of the species as it appears in the reaction. The activity is frequently called the effective concentration of the

species since it naturally arises as a function of the concentration that is necessary to satisfy the changes in the thermodynamic functions (here, the Gibb's free energy). In electrochemical systems, the activity is usually related to the molality of the species (moles per 1,000 grams of solvent) by the following equation:

$$a = \gamma m, \quad (5.23)$$

where γ is the activity coefficient and m the molality.

The standard state for reactants and products in Reaction 5.19 is pure solid for solid species, one atmosphere pressure for gas species, and unit activity (approximately unit molality) for ionic species. The activity is unity in each of these standard states. If one or more species are solids under the actual conditions of the reaction, or a gas exists at one atmosphere pressure, then unit activity for each of these species is substituted in Equation 5.22, which effectively removes these activities from the log term. Also, the activity of water can usually be set equal to unity, since its concentration changes insignificantly in most reactions in aqueous solution. Thus, taking M and X as solids, Equation 5.22 reduces to

$$\Delta G_{\text{react}} = \Delta G_{\text{react}}^{\circ} + RT \ln \frac{a_{M^{m+}}^x}{a_{X^{x+}}^m}. \quad (5.24)$$

Another significant equation, previously derived in this section, permits calculation of the change in Gibb's free energy for the overall reaction from the electrochemical cell potential, E_{cell}

$$\Delta G_{\text{react}} = -nFE_{\text{cell}}, \quad (5.25)$$

where $n = xm$ in the present case.

Therefore, relative to the generalized overall reaction of Equation 5.19,

$$\Delta G_{\text{react}} = -(xm)FE_{\text{cell}} \quad (5.26)$$

$$\Delta G_{\text{react}}^{\circ} = -(xm)FE_{\text{cell}}^{\circ}. \quad (5.27)$$

On substituting into Equation 5.24,

$$E_{\text{cell}} = E_{\text{cell}}^{\circ} - \frac{RT}{xmF} \ln \frac{a_{M^{m+}}^x}{a_{X^{x+}}^m}. \quad (5.28)$$

Also,

$$E_{\text{cell}} = E'_{\text{RHE}} - E'_{\text{LHE}} = E'_{X, X^{x+}} - E'_{M, M^{m+}} \quad (5.29)$$

$$E_{\text{cell}}^{\circ} = E_{\text{RHE}}^{\circ} - E_{\text{LHE}}^{\circ} = E_{\text{X},\text{X}^{x+}}^{\circ} - E_{\text{M},\text{M}^{m+}}^{\circ} \quad (5.30)$$

Substitution into Equation 5.28 yields

$$\begin{aligned} & E'_{\text{X},\text{X}^{x+}} - E'_{\text{M},\text{M}^{m+}} \\ &= \left(E_{\text{X},\text{X}^{x+}}^{\circ} + \frac{RT}{xF} \ln a_{\text{X}^{x+}} \right) \\ & \quad - \left(E_{\text{M},\text{M}^{m+}}^{\circ} + \frac{RT}{mF} \ln a_{\text{M}^{m+}} \right), \quad (5.31) \end{aligned}$$

or

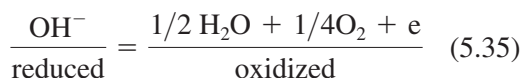
$$E'_{\text{X},\text{X}^{x+}} = E_{\text{X},\text{X}^{x+}}^{\circ} + \frac{RT}{xF} \ln a_{\text{X}^{x+}} \quad (5.32)$$

$$E'_{\text{M},\text{M}^{m+}} = E_{\text{M},\text{M}^{m+}}^{\circ} + \frac{RT}{mF} \ln a_{\text{M}^{m+}}. \quad (5.33)$$

Equations 5.32 and 5.33 are Nernst half-cell equations. For example, with Equation 5.33, when $a_{\text{M}^{m+}} = 1$, $E'_{\text{M},\text{M}^{m+}} = E_{\text{M},\text{M}^{m+}}^{\circ}$. Hence, $E_{\text{M},\text{M}^{m+}}^{\circ}$ is the half-cell potential at unit activity of the ions (i.e., the standard equilibrium half-cell potential). Values of the standard potentials of many electrode reactions are available in the literature, some of which are given in Table 5.1.⁶⁻⁸ All values are given in sign and magnitude relative to the standard hydrogen electrode (SHE). Many half-cell reactions involve species on both sides of the reaction that have variable concentrations in solution. These circumstances are handled by using the Nernst half-cell equation in the following more general form:

$$E'_{\text{X},\text{Y},\text{Z}} = E_{\text{X},\text{Y},\text{Z}}^{\circ} + \frac{RT}{nF} \ln \frac{\Pi[\text{Ox}_i]^{v_i}}{\Pi[\text{Red}_i]^{v_i}} \quad (5.34)$$

In this equation, X, Y, and Z are symbolic representatives of the species involved in the reaction; $\Pi[\text{Ox}_i]^{v_i}$ is the product of the activities of the species on the "oxidized side" of the reaction (the side showing electrons produced), each raised to its stoichiometric coefficient (v_i); $\Pi[\text{Red}_i]^{v_i}$ has similar meaning for the "reduced side" of the reaction; and n is the number of moles of electrons produced (or consumed) per unit of the half reaction. Application of Equation 5.34 is illustrated in the following examples:

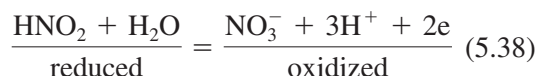


$$E'_{\text{OH}^-, \text{O}_2} = E_{\text{OH}^-, \text{O}_2}^{\circ} + \frac{RT}{1F} \ln \frac{P_{\text{O}_2}^{1/4}}{a_{\text{OH}^-}} \quad (5.36)$$

When the values of the constants R and F are inserted, the natural logarithm converted to base-ten logarithm, and the temperature assumed to be 298 °K (25 °C, essentially room temperature), Equation 5.36 becomes

$$E'_{\text{OH}^-, \text{O}_2} [\text{mV}(\text{SHE})] = E_{\text{OH}^-, \text{O}_2}^{\circ} + \frac{59}{1} \log \frac{P_{\text{O}_2}^{1/4}}{a_{\text{OH}^-}}. \quad (5.37)$$

Similarly, for



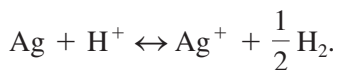
$$\begin{aligned} & E'_{\text{HNO}_2, \text{NO}_3^-, \text{H}^+} [\text{mV}(\text{SHE})] \\ &= E_{\text{HNO}_2, \text{NO}_3^-, \text{H}^+}^{\circ} + \frac{59}{2} \log \frac{a_{\text{NO}_3^-} a_{\text{H}^+}^3}{a_{\text{HNO}_2}}. \quad (5.39) \end{aligned}$$

5.2.4 Examples of Electrochemical Cell Calculations in Relationship to Corrosion

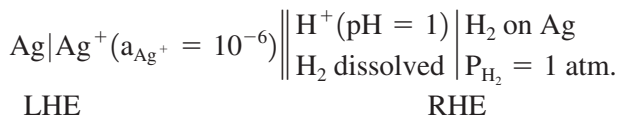
In most corrosion calculations, the metal-ion concentration in the environment is usually unknown. In the absence of specific values of activity, a reasonably low activity of 10^{-6} is usually assumed. This corresponds to less than one ppm (parts per million) by weight. Also, most environments will not contain hydrogen and the question arises as to the value of P_{H_2} to use in calculations on cathodic reactions involving hydrogen evolution. Since hydrogen bubbles cannot form unless the hydrogen pressure is about one atmosphere (the usual approximate pressure of the surroundings), it is common practice to assume $P_{\text{H}_2} = 1$ atm. Assuming zero for either the metal-ion concentration or the pressure of the hydrogen leads to an infinite potential because the activity appears in the log term of the Nernst half-cell equation. This implies that some corrosion should always occur initially, since E_{cell} would be infinite corresponding to an infinite decrease in ΔG . Therefore, it is reasonable to assume that activities of the above magnitude are quickly established on contact of a metal with an aqueous environment if corrosion is thermodynamically possible at all.

5.2.4.1 Example 1

Determine the thermodynamic tendency for silver to corrode in a deaerated acid solution of pH = 1.0. Assume $a_{\text{Ag}^+} = 10^{-6}$ and $P_{\text{H}_2} = 1.0$ atm. Cell reaction:



Cell representation and calculations:



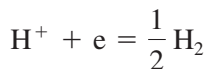
At LHE:



$$E'_{\text{LHE}} = E'_{\text{Ag,Ag}^+} = 799 + \frac{59}{1} \log 10^{-6}$$

$$E'_{\text{LHE}} = 445 \text{ mV(SHE).}$$

At RHE:



$$E'_{\text{RHE}} = E'_{\text{H}_2, \text{H}^+} = 0 + \frac{59}{1} \log \left(\frac{a_{\text{H}^+}}{1} \right)$$

$$\text{pH} = -\log a_{\text{H}^+}$$

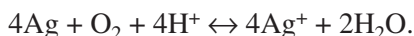
$$E'_{\text{RHE}} = -59 \text{ pH} = -59 \text{ mV(SHE)}$$

$$E_{\text{cell}} = E'_{\text{RHE}} - E'_{\text{LHE}} = -59 - (445) = -504 \text{ mV.}$$

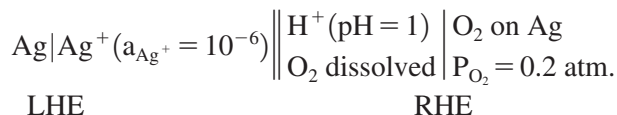
E_{cell} is found to be negative, which means that $\Delta G = -nFE_{\text{cell}}$ is positive. Therefore, the spontaneous direction for the cell reaction is right-to-left; consequently, silver will not corrode due to the acidity represented by pH = 1.0.

5.2.4.2 Example 2

Determine the thermodynamic tendency for silver to corrode in an aerated acid solution at pH = 1.0. Assume $a_{\text{Ag}^+} = 10^{-6}$, $P_{\text{H}_2} = 1.0$ atm., and $P_{\text{O}_2} = 0.2$ atm. Compare the result to that of Example 1 (deaerated solution). Cell reaction:



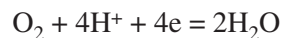
Cell representation and calculations:



At LHE, same as Example 1:

$$E'_{\text{LHE}} = 445 \text{ mV(SHE).}$$

At RHE:



$$E'_{\text{RHE}} = E'_{\text{O}_2, \text{H}^+}$$

$$E'_{\text{RHE}} = 1,229 + \frac{59}{4} \log P_{\text{O}_2} a_{\text{H}^+}^4$$

$$E'_{\text{RHE}} = 1,229 - 59 \text{ pH} + 15 \log 0.2$$

$$E'_{\text{RHE}} = 1,160 \text{ mV(SHE)}$$

$$E_{\text{cell}} = E'_{\text{RHE}} - E'_{\text{LHE}} = 1,160 - (445)$$

$$E_{\text{cell}} = 715 \text{ mV.}$$

E_{cell} is found to be positive, which means that ΔG is negative. Therefore, the spontaneous direction for the cell reaction is left-to-right; consequently, silver will corrode in this aerated acid solution (pH = 1.0) due to the dissolved oxygen.

5.2.4.3 Example 3

Determine the pH at which silver will not corrode in an aerated aqueous solution. Refer to Example 2 and set $E_{\text{cell}} = 0$, with the pH as the unknown variable.

$$E_{\text{cell}} = E'_{\text{RHE}} - E'_{\text{LHE}}$$

$$0 = (1,229 - 59 \text{ pH} + 15 \log 0.2) - 445$$

$$\text{pH} = 13.1.$$

5.2.5 Graphical Representation of Electrochemical Equilibrium: Pourbaix Diagrams

The equilibrium electrochemistry of an element in aqueous solution can be represented graphically utilizing coordinates of equilibrium half-cell potential, E' , and pH. These graphical representations, known as Pourbaix diagrams in honor of Marcel Pour-

baix,¹⁰ are essentially phase diagrams from which the conditions for thermodynamic stability of a single aqueous phase, or equilibrium of this phase with one or more solid phases, may be determined. The objective of these diagrams is to provide a large amount of information in a convenient form for quick reference.

A somewhat simplified Pourbaix diagram for the iron/water system is shown in Figure 5.4. In this case, the possible solid phases are restricted to metallic iron, Fe_3O_4 , and Fe_2O_3 .

Interpretation of the Pourbaix diagram in Figure 5.4 requires discussion of the experimental conditions under which, at least in principle, it would be determined. The coordinates are pH and electrode potential, and it is implied that each of these may be established experimentally. Their values will locate a point on the diagram and from this point the equilibrium state of the system is determined. It is assumed that the pH may be established by appropriate additions of an acid or base.

To establish any predetermined electrode potential, the experimental arrangement shown in Figure

5.5 is used. The components and their functions include the following:

- a. The aqueous solution of controlled pH. This solution may contain dissolved oxygen (aerated), or the container may be closed and an inert gas such as N_2 or He bubbled through the solution to remove the oxygen present from contact with air (deaerated).
- b. The working electrode which is the electrode under study. It may be an active metal such as iron, with iron ions being exchanged between the electrode and the solution. This electrode may also be an inert metal such as platinum, which supplies a conducting surface through which electrons pass to oxidize or reduce species in solution.
- c. The auxiliary or counter electrode, usually platinum, against which the potential of the working electrode is established.
- d. The reference electrode, against whose known half-cell potential the electrode potential of the working electrode is measured.

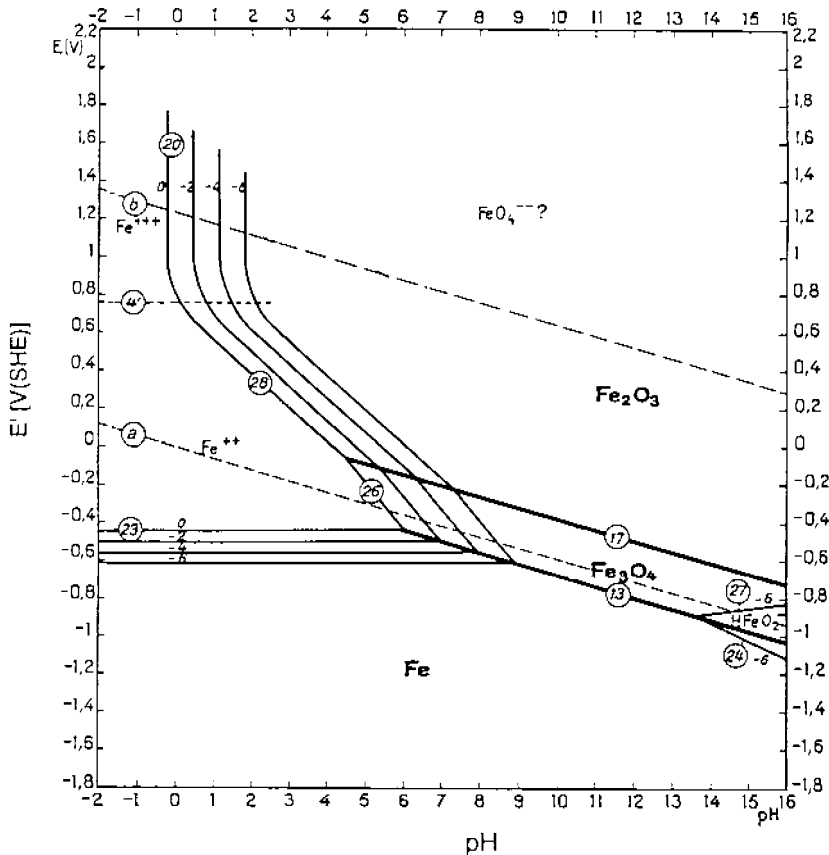


FIGURE 5.4 Pourbaix diagram for the iron/water system.

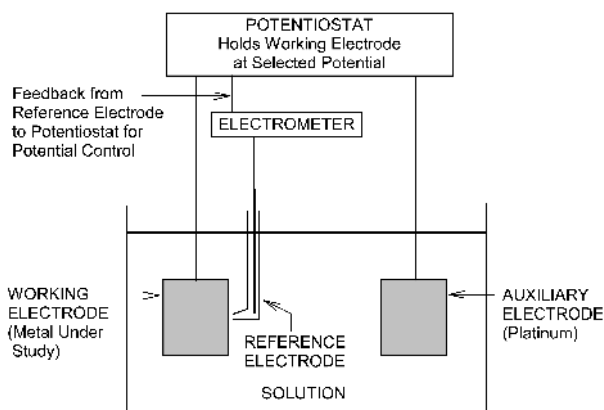


FIGURE 5.5 The potentiostatic-circuit/polarization-cell arrangement.

- e. The electrometer or high-impedance voltmeter that is used to measure the potential of the working electrode relative to the reference electrode. The impedance of these instruments should be approximately 10^{14} ohms or greater, such that the current required to allow measurement will have a negligible effect on the working electrode.
- f. The potentiostat that establishes the potential of the working electrode. The potential between the working and auxiliary electrodes is changed until the electrometer indicates the desired potential for the working electrode relative to the reference electrode. Potentiostats are usually electronic instruments that may be set to the desired potential; and this potential is maintained by feedback control from the reference electrode.

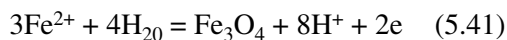
In the following discussion of the Pourbaix diagram for the system iron/water (Figure 5.4), it is convenient to consider that the potentials represented along the ordinate axis have been established by a potentiostat. Thus, if the potential is established at -0.44 V(SHE) on an iron working electrode in contact with an aqueous solution at $\text{pH} < 6.0$, then the equilibrium condition is that of Line 23(0) on the diagram with the “0” representing a Fe^{2+} activity of 10^0 . Further interpretations of this line, and other lines and areas (all labeled in accordance with Pourbaix’s published diagrams¹⁰), are as follows:

1. Lines 23 (i.e., 23(0), 23(-2), etc.) represent the equilibrium half-cell or electrode potential of iron as a function of Fe^{2+} activity ($\text{Fe} = \text{Fe}^{2+} + 2e$) (i.e., by application of the Nernst equation):

$$E'_{\text{Fe},\text{Fe}^{2+}} = -440 + \frac{59}{2} \log a_{\text{Fe}^{2+}} \quad (5.40)$$

The parallel lines are identified by the exponent of 10 of the activity of Fe^{2+} ions in solution (i.e., $= 10^0, 10^{-2}, 10^{-4}, 10^{-6}$, and others, which are not shown, at greater dilution). The lines are horizontal, since the half-cell potential is independent of the pH at lower values of pH. If the potential that is applied to the iron is below the equilibrium potential corresponding to the iron in contact with iron, the iron will be stable and will not corrode. Rather, iron will tend to be deposited from solution (i.e., ferrous ions will be reduced to metallic iron). If E_{applied} is above E' for a given ion concentration, then iron will tend to pass into solution, increasing the concentration of iron ions up to the equilibrium value corresponding to the applied potential. Indeed, if $E_{\text{applied}} > E_{-}$, net oxidation will occur. If $E_{\text{applied}} < E'$, net reduction will occur.

2. At a given $a_{\text{Fe}^{2+}}$, increasing the pH eventually results in the reaction:



$$E' = +980 - 236\text{pH} - 89 \log a_{\text{Fe}^{2+}} \quad (5.42)$$

Lines 26 therefore represent the equilibrium of Fe^{2+} ions with Fe_3O_4 , at various Fe^{2+} activities (i.e., $10^0, 10^{-2}$, etc.).

3. Conditions along Line 13 correspond to a film of Fe_3O_4 on Fe. That is, Fe and Fe_3O_4 coexist at equilibrium with water containing Fe^{2+} ions at an activity given by the appropriate Line 23. Actually, Line 13 is the locus of intersections of Lines 23 and 26.
4. Above Lines 23, the stable state of the system is virtually all iron in solution (i.e., $a_{\text{Fe}^{2+}} > 10^0$), with $a_{\text{Fe}^{2+}} > a_{\text{Fe}^{3+}}$.
5. Line 4' corresponds to $a_{\text{Fe}^{2+}} = a_{\text{Fe}^{3+}}$ and is located at the equilibrium half-cell potential for the $\text{Fe}^{2+} = \text{Fe}^{3+} + e$ reaction.

$$E_{\text{Fe}^{2+},\text{Fe}^{3+}}^0 = 770 \text{ mV(SHE)} \quad (5.43)$$

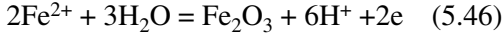
6. Below Line 4',

$$a_{\text{Fe}^{2+}} > a_{\text{Fe}^{3+}} \quad (5.44)$$

Above Line 4',

$$a_{\text{Fe}^{2+}} < a_{\text{Fe}^{3+}} \quad (5.45)$$

7. Lines 28 correspond to the reaction



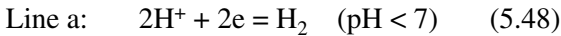
$$E' = -728 - 177\text{pH} - 59 \log a_{\text{Fe}^{2+}} \quad (5.47)$$

These lines give the conditions for precipitation of Fe_2O_3 from solution. Again, the lines are identified by the exponent of 10 for the $a_{\text{Fe}^{2+}}$.

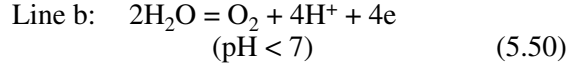
8. Lines 20 correspond to the formation of Fe_2O_3 from solutions of $a_{\text{Fe}^{3+}} > a_{\text{Fe}^{2+}}$. Here, the curves identified as 0, -2, -4, and -6 correspond to $a_{\text{Fe}^{3+}} = 10^0, 10^{-2}, 10^{-4},$ and 10^{-6} .

9. Line 17 corresponds to the equilibrium of $\text{Fe}_3\text{O}_4, \text{Fe}_2\text{O}_3,$ and solutions of indicated $a_{\text{Fe}^{2+}}$ as a function of potential and pH. With increasing potential, Fe_3O_4 is oxidized to Fe_2O_3 .

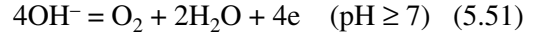
10. Lines a and b correspond to the following equilibrium reactions:



or

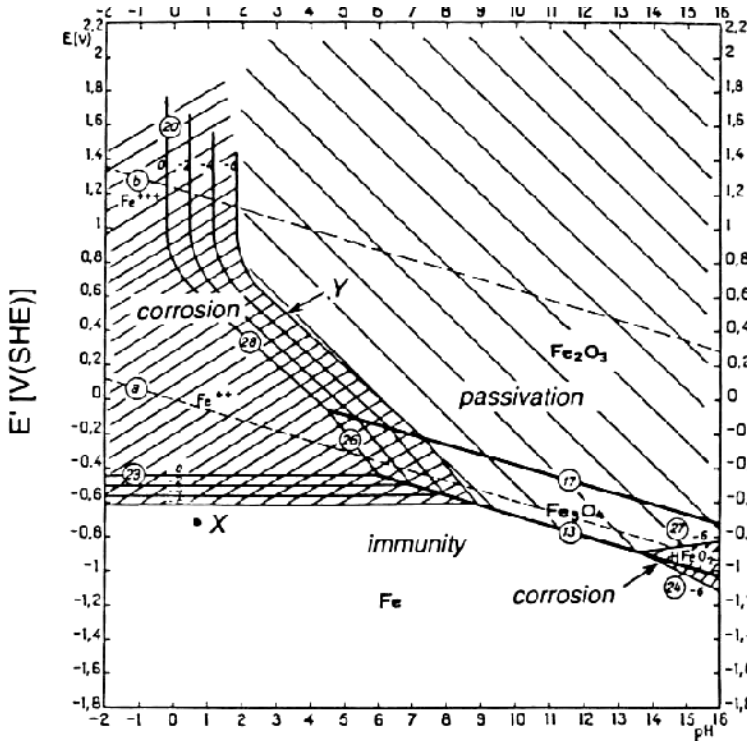


or

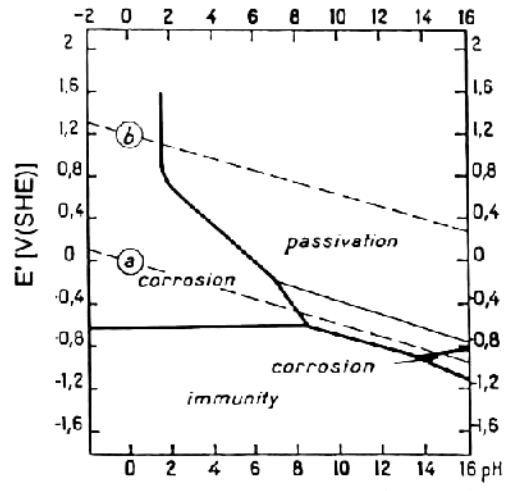


Therefore, below Line a, H_2 is produced by reduction of H^+ or H_2O , and above Line b, O_2 is produced by oxidation of H_2O or OH^- . Between Lines a and b, water is stable (i.e., it is neither reduced to H_2 nor oxidized to O_2).

The Pourbaix diagram can be used to make preliminary predictions of the corrosion of metals as a function of electrode potential and pH. It is emphasized that the predictions are very general and the method has been criticized in leading to incorrect conclusions, since reference only to the diagram does not recognize other often-controlling factors such as rate and non-equilibrium conditions. Figure 5.4 is reproduced in Figure 5.6a with Pourbaix's areas of corrosion, immunity and passivation indicated.¹⁰ Figure 5.6b shows the form frequently used



(a)



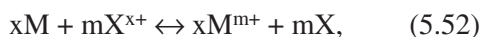
(b)

FIGURE 5.6 Pourbaix diagrams for the iron/water system showing regions of corrosion, immunity, and possible passivation.

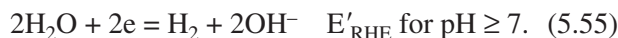
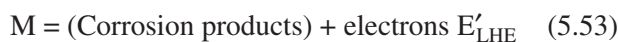
to represent these areas, assuming that the activity of reacting ions is 10^{-6} . The terms are defined as follows:

- *Immunity*: If the potential and pH are in this region, the iron is thermodynamically immune from corrosion. At a point such as “X” in Figure 5.6a, it is estimated that the Fe^{2+} activity should adjust to about 10^{-10} and no corrosion should occur. H_2 would be evolved.
- *Corrosion*: In these regions of potential and pH, the system should ultimately become virtually all ions in solution, and therefore iron existing at these conditions should corrode.
- *Passivation*: In this region, the equilibrium state is one of oxide plus solution. If iron is placed in this potential-pH environment, oxide will form on the surface. If this oxide is adequately adherent, non-porous, and has high resistance to ion and/or electron transport, it will significantly decrease the rate of corrosion. Under these conditions, the iron is said to have undergone passivation. These regions in Pourbaix diagrams would be more accurately identified as regions of “possible passivation.”

Based on previous discussions, one can determine from analysis of the Pourbaix diagram whether a given metal will corrode in aerated (oxygenated) solutions or deaerated (de-oxygenated) solutions at a given pH. For deaerated solutions, with reference to the generalized overall reaction,

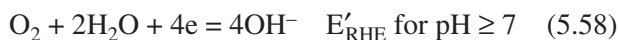
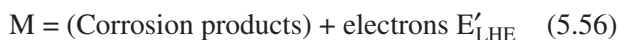


the specific equilibrium half reactions are



Line *a* in the Pourbaix diagram represents E'_{RHE} for half-reactions 5.54 and 5.55 as a function of pH, for $P_{\text{O}_2} = 1$ atm. The criterion for corrosion is that $E_{\text{cell}} = (E'_{\text{RHE}} - E'_{\text{LHE}}) > 0$ ($\Delta G_{\text{react}} < 0$). Therefore, for corrosion to occur in deaerated solutions, Line *a* must be above the metal equilibrium half-cell potential, E'_{LHE} . It is reasonable to use the upper metallic boundary for E'_{LHE} [i.e., Lines 23(-6), 13, and 24(-6) in the case of iron]. Consequently, iron is predicted to corrode in deaerated solutions at all pH values.

For aerated solutions, the specific equilibrium half-cell reactions are



Line *b* in the Pourbaix diagram represents E'_{RHE} for half-reactions 5.57 and 5.58 as a function of pH, for $P_{\text{O}_2} = 1$ atm. Again, the criterion for corrosion is that $E_{\text{cell}} = (E'_{\text{RHE}} - E'_{\text{LHE}}) > 0$. Therefore, for corrosion to occur in aerated solutions, Line *b* must be above the metal equilibrium half-cell potential, E'_{LHE} , which again is taken to be the upper boundary of the metal region in the Pourbaix diagram. Consequently, iron is predicted to corrode in aerated solutions at all pH values.

If corrosion is predicted to occur, one can determine from analysis of the Pourbaix diagram the nature of the corrosion products. First, however, one must be aware that the potential of the metal while it is freely corroding, E_{corr} (i.e., in this condition, the potential of the metal is not being externally influenced by, for example, a potentiostat) must be between the two equilibrium half-cell potentials:

$$E'_{\text{LHE}} < E_{\text{corr}} < E'_{\text{RHE}} \quad (5.59)$$

On labeling E'_{LHE} as E'_M (since it refers to the metal equilibrium half-cell potential), and recognizing that E'_{RHE} refers to Line *a* for the deaerated condition and Line *b* for the aerated condition, Equation 5.59 can be rewritten as

$$E'_M < E_{\text{corr}} < E'_{\text{Line a}} \quad \text{Deaerated} \quad (5.60)$$

or

$$E'_M < E_{\text{corr}} < E'_{\text{Line b}} \quad \text{Aerated.} \quad (5.61)$$

E_{corr} is known as the corrosion potential, the open-cell potential, or the open-circuit potential. Its exact location between E'_M and $E'_{\text{Line a}}$, or between E'_M and $E'_{\text{Line b}}$, is determined by thermodynamics and kinetics factors, and will be further discussed in a subsequent section.

Nevertheless, with regard to prediction of corrosion products under freely-corroding conditions, for iron in a deaerated solution at $\text{pH} = 2$, as an example (refer to Figure 5.4), the corrosion products are ferrous ions (Fe^{2+}) since E_{corr} must lie between Line

23(-6) and Line *a*. Under these conditions, passivation is impossible, since passivation requires the formation of solid corrosion products, not ions in solution. As another example, consider the corrosion of iron in an aerated solution at pH = 12. In this case, the corrosion product is either solid Fe₃O₄ or solid Fe₂O₃, since E_{corr} must lie somewhere between Line 13 and Line *b*. Therefore, passivation is possible, depending on the characteristics of Fe₃O₄ and Fe₂O₃. Obviously, these principles can be applied in the analyses of Pourbaix diagrams for all metals of interest.

5.3 ELECTROCHEMICAL KINETICS AND CORROSION PROCESSES

5.3.1 The Elementary Electrochemical Corrosion Circuit

The elementary electrochemical corrosion circuit is schematically represented in Figure 5.7. At the anodic site, the *net* oxidation reaction is $M \rightarrow M^{m+} + me$. At the cathodic site, the generalized *net* reduction reaction is $X^{x+} + xe \rightarrow X$. Actually, at the anodic and cathodic sites, both oxidation and reduction reactions are occurring, as indicated below with respective currents:

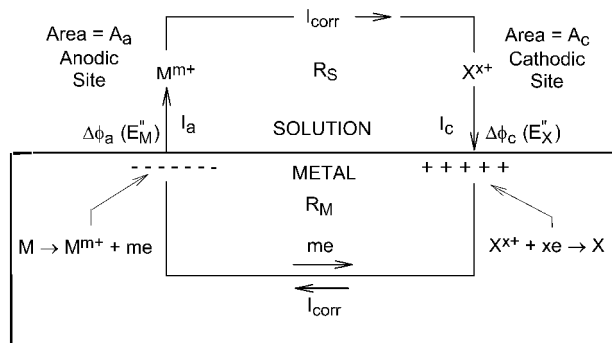
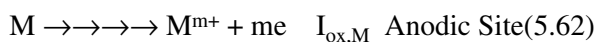


FIGURE 5.7 The elementary electrochemical corrosion circuit.

The net anodic and cathodic currents (or reaction rates) are

$$I_a = I_{\text{ox},M} - I_{\text{red},M} \quad (5.66)$$

$$I_c = I_{\text{red},X} - I_{\text{ox},X} \quad (5.67)$$

However, at the anodic site, the metal-ion reduction rate is normally quite small compared to the metal-atom oxidation rate, as indicated by the arrows in Reactions 5.62 and 5.63. Similarly, at the cathodic site, the oxidation rate of X is normally quite small compared to the reduction rate of X^{x+}. Therefore, the net anodic and cathodic currents are given approximately by

$$I_a \cong I_{\text{ox},M} \quad (5.68)$$

$$I_c \cong I_{\text{red},X} \quad (5.69)$$

As a consequence of the transfer of ions and electrons at each interface, differences in electrical potential, $\Delta\phi_a$ and $\Delta\phi_c$, develop between the metal and the solution at the anodic and cathodic sites, respectively, where

$$\Delta\phi_a = \phi_{M,a} - \phi_{S,a} \quad (5.70)$$

$$\Delta\phi_c = \phi_{M,c} - \phi_{S,c} \quad (5.71)$$

The subscripts *a* and *c* designate the anodic and cathodic sites, and the subscripts *M* and *S* designate the metal and solution phases. These differences in potential, coupled as shown, constitute the electrochemical cell in which electrons are caused to flow from the anodic to the cathodic site in the metal; conventional electrical current (positive charge) flows in the opposite direction. In the solution, current flows from the anodic to the cathodic site as a consequence of the potential in the solution being higher above the anodic site than above the cathodic site (i.e., $\phi_{S,a} > \phi_{S,c}$). This current is defined as a positive quantity for the spontaneous corrosion process represented in Figure 5.7. In practice, individual interfacial differences in potential, $\Delta\phi$, are assigned values relative to the standard hydrogen electrode (SHE). In this chapter, these values are designated by *E* for the general case, by *E'* for the case of no current passing (equilibrium), and by *E'* for the case of a corrosion current passing the interface. If the potential of the standard reference electrode is taken as zero (as is true for the SHE), then for the general case, $\Delta\phi_a = E_M$ and $\Delta\phi_c = E_X$.

The driving potential for the current in the solution, $\Delta\phi_S$, is

$$\Delta\phi_S = \phi_{S,a} - \phi_{S,c} = (\phi_{M,a} - \Delta\phi_a) - (\phi_{M,c} - \Delta\phi_c) \quad (5.72)$$

If it is assumed that the metal path is a good electrical conductor (as is the general case), the potential difference in the metal will be small and $\phi_{M,a} \approx \phi_{M,c}$. The driving potential for the current in the solution is then

$$\Delta\phi_S = \Delta\phi_c - \Delta\phi_a = E''_X - E''_M \quad (5.73)$$

where the E s are now double superscripted to emphasize that their values are associated with the corrosion current. Recognizing that Ohm's law must apply, the corrosion current is given by

$$I_{\text{corr}} = (E''_X - E''_M)/(R_S + R_M + R_{\text{interface}}), \quad (5.74)$$

where R_S and R_M are the resistances of the solution and metal paths of the current, and $R_{\text{interface}}$ is the resistance of any interface film that may form. The current is called the corrosion current, I_{corr} . When the area of the anode through which the current flows is taken into consideration, the corrosion penetration rate (CPR) can be calculated, for example in micrometers per year or mils (0.001 inch) per year. The total path resistance, $R_{\text{total}} = R_S + R_M + R_{\text{interface}}$, is obviously an important variable in determining the corrosion rate. Generally, however, the solution resistance dominates the total path resistance.

The relative sizes and locations of anodic and cathodic areas are important variables affecting corrosion rates. These areas may vary from atomic dimensions to macroscopically large areas. In Figure 5.7, areas have been depicted over which the anodic and cathodic reactions occur, designated as A_a and A_c . If the current is uniformly distributed over these areas, then the current densities, $i_a = I_a/A_a$ and $i_c = I_c/A_c$, may be calculated. The current density is fundamentally more important than the current for two reasons. First, through Faraday's law, the anodic current density, i_a , relates directly to corrosion intensity (CI) as mass loss per unit time per unit area, or to corrosion penetration rate (CPR) as a linear dimension loss per unit time. Second, it is observed that interface potentials (E) are functions of current density of the form (assuming charge-transfer polarization or Tafel behavior):

$$E_M = E'_M + \beta_{\text{ox},M} \log \frac{I_a/A_a}{i_{o,M}}$$

$$= E'_M + \beta_{\text{ox},M} \log \frac{i_a}{i_{o,M}} \quad (5.75)$$

$$\begin{aligned} E_X &= E'_X - \beta_{\text{red},X} \log \frac{I_c/A_c}{i_{o,X}} \\ &= E'_X - \beta_{\text{red},X} \log \frac{i_c}{i_{o,X}}. \end{aligned} \quad (5.76)$$

In these expressions, E_X and E_M become the potentials and if the current is zero and therefore relate to the potential differences across the individual interfaces at equilibrium (i.e., no net transport of ions or electrons). The β and i_o values are Tafel constants and exchange current densities, respectively—all constants for a given system. Equations 5.75 and 5.76, therefore, indicate that the existing potential with current flow is the equilibrium value plus or minus a term representing the shift in potential, or polarization, resulting from the current density. In other words, the corrosion process polarizes the potentials from the equilibrium E' values to the E'' values. During corrosion, the anodic current must equal the cathodic current, $I_a = I_c$, and this current is the corrosion current, I_{corr} (see Figure 5.7). Thus, Ohm's law can be written as (assuming that the solution resistance is the dominant resistance term)

$$\begin{aligned} I_{\text{corr}} &= \frac{E''_X - E''_M}{R_{\text{total}}} \\ &= \frac{\left[E'_X - \beta_{\text{red},X} \log \frac{I_{\text{corr}}/A_c}{i_{o,X}} \right] - \left[E'_M + \beta_{\text{ox},M} \log \frac{I_{\text{corr}}/A_a}{i_{o,M}} \right]}{R_S} \end{aligned} \quad (5.77)$$

If theoretically- or experimentally-based expressions for the polarized potentials (Equations 5.75 and 5.76) are available, the Ohm's law equation can be solved for the corrosion current, I_{corr} . I_{corr} is a measure of the *total* loss of metal from the anode surface during corrosion. The anodic current density during corrosion, $i_{\text{corr}} = I_{\text{corr}}/A_a$, is a measure of the corrosion intensity from which the corrosion penetration rate can be calculated.

Equation 5.77 can be interpreted in relationship to the conventional plotting of linear or Tafel polarization behavior of the anodic and cathodic reactions. For this purpose, the individual anodic and cathodic curves (Equations 5.75 and 5.76) are plotted in Figure 5.8 as functions of the current rather than current density. At the anode interface, the current is $I_a =$

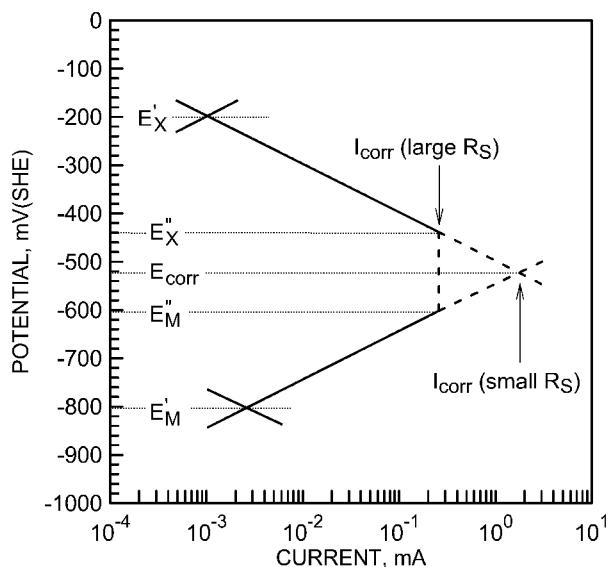


FIGURE 5.8 Tafel polarization curves for anodic and cathodic reactions illustrating the dependence of the corrosion current, I_{corr} , on the solution resistance, R_S .

$i_a A_a$, where A_a is the area at the anode/solution interface. Similarly, for the cathode interface, the current is $I_c = i_c A_c$. The polarization curves are plotted using exchange currents, I_o , obtained by multiplying the exchange current densities by the respective areas, and the Tafel slopes. Any vertical separation between the anodic and cathodic polarization curves is a potential difference driving the current in the solution from the anodic to the cathodic surface. This difference in potential must be such that Equation 5.77 is satisfied. The difference is determined graphically by determining $(E_X'' - E_M')$ at selected values of the current until a potential difference is found such that when divided by $R_{\text{total}} \approx R_S$, the resulting current has the same value as given along the log I axis. This current will be I_{corr} and, on division by A_a , will give the corrosion current density, i_{corr} . The corrosion rate can be calculated from this corrosion current density through Faraday's law.

As the solution resistance decreases, the above analysis indicates that the conditions satisfying Equation 5.77 move toward the intersection of the two polarization curves in Figure 5.8. A decrease in resistance between the anodes and cathodes results when the specific resistivity of the solution is decreased, and will occur even for higher resistivity environments if the anodic and cathodic areas are very small and separated by small distances. Under these conditions, corrosion will appear to be uniform

on a macroscopic scale. Movement of a reference electrode in the solution will measure a single corrosion potential, E_{corr} , independent of position with a value approaching the potential at which the anodic and cathodic polarization curves intersect in Figure 5.8. To appreciate how small this driving potential difference may be, consider an anodic area of 1 cm^2 (10^{-4} m^2) in a large cathodic area exposed to a relatively low resistivity environment such that $R_S = 10 \text{ ohms}$, and that the conditions are such as to cause the practically small current of 10^{-2} mA . The anodic current density is then 100 mA/m^2 , which for iron would be a corrosion penetration rate of about $125 \mu\text{m/y}$ (5 mpy). The driving potential supporting this corrosion would have the very small value of $(10^{-2} \text{ mA})(10 \text{ ohm}) = 0.1 \text{ mV}$, a difference so small that it cannot be represented graphically in Figure 5.8.

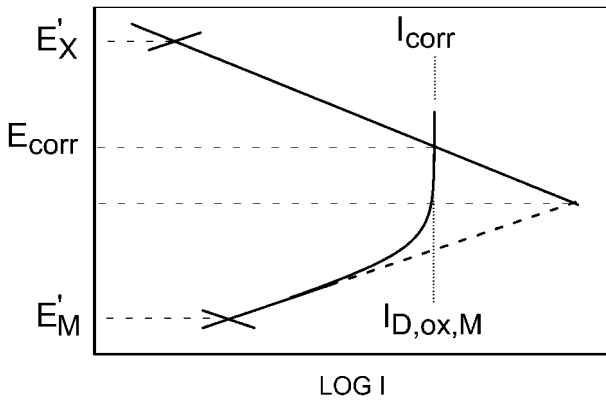
5.3.2 Types of Polarization Behavior

Not all half-cell reactions obey the charge-transfer type of polarization behavior (Tafel behavior) represented in Figure 5.8. At higher reaction rates (currents or current densities), the polarization behavior is often controlled by diffusion or concentration effects, as indicated schematically in Figure 5.9, where limiting diffusion currents ($I_{D,\text{ox},M}$ and $I_{D,\text{red},X}$) for the individual anodic and cathodic polarization curves are shown.^{2,11} Furthermore, many metals and alloys can undergo active-passive type anodic polarization behavior, as indicated in Figure 5.10. In this case, at lower potentials, Tafel behavior is demonstrated, but at a critical anodic current density (i_{crit}), the anodic current density (and corrosion rate) decreases drastically due to the formation of a passive film. The passive film may break down at a higher potential, resulting in high anodic current densities, either uniformly (transpassive behavior) or non-uniformly (localized pitting or crevice corrosion).

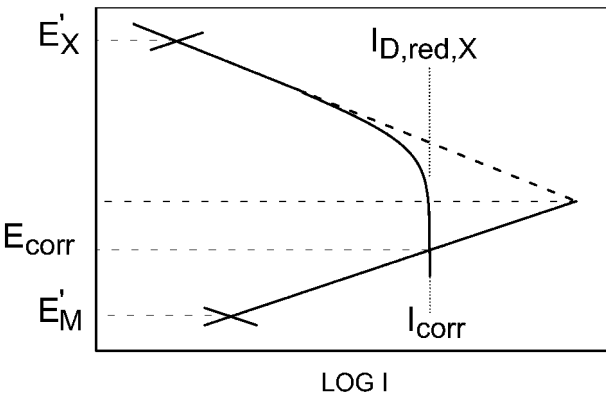
5.3.3 Faraday's Law

Faraday's law is the connecting relationship between the corrosion current density, $i_{\text{corr}} = I_{\text{corr}}/A_a$, and other expressions of "corrosion rate" such as corrosion intensity (CI), in units of mass-loss per unit area per unit time, and corrosion penetration rate (CPR) in units of loss-in-dimension perpendicular to the corroding surface per unit time.

To retain emphasis on corrosion processes, Faraday's law will be derived with reference to the gen-



(a)



(b)

FIGURE 5.9 Influence of relative positions and shapes of anodic and cathodic polarization curves on the corrosion current, I_{corr} : (a) anodic diffusion control, (b) cathodic diffusion control.

eralized metal oxidation reaction, $M \rightarrow M^{m+} + me$. In Figure 5.11, an anodic area, A_a , is shown over which $I_a = I_{ox,M} - I_{red,M} = I_{corr} \approx I_{ox,M}$. The current flows to the surface counter to the electrons and enters the solution as positive ions (cations), M^{m+} .

Consider that the corrosion current, I_{corr} , is expressed in amperes (A) or coulombs (C) per second. The unit of positive electricity (equivalent to the magnitude of the charge on the electron but with opposite sign) has a charge of 1.60×10^{-19} coulombs and will be designated e^+ . Each ion formed by detachment from the surface contributes me^+ coulombs to the current. W grams of metal entering the solution in t seconds contributes W/Mt moles per second, where M (g/mol) is the atomic mass. Multiplying by Avogadro's number, N_o , gives $(W/Mt)N_o$ ions per

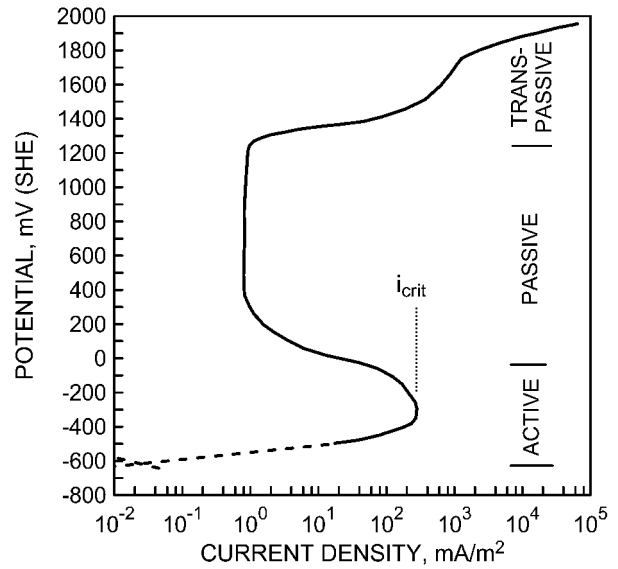


FIGURE 5.10 Active-passive type anodic polarization behavior.

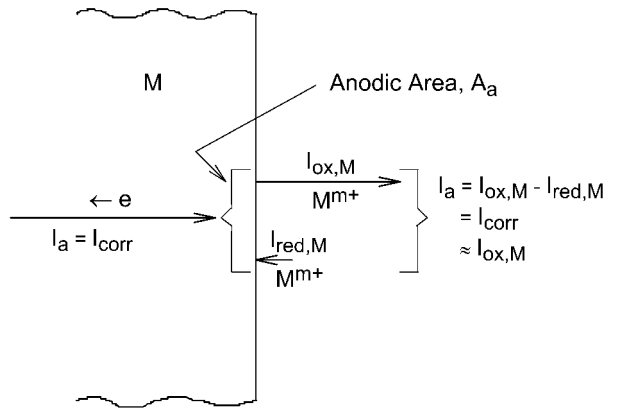


FIGURE 5.11 Components of ionic and electron flow at an area of metal surface referenced in the derivation of Faraday's law.

second. The product of the ions per second and the charge per ion gives the current. Thus,

$$I_{corr} = (WN_o/Mt)(me^+) \quad (5.78)$$

$$I_{corr} = (Wm/M)(N_o e^+)(1/t) = (Wm/M)(F)(1/t), \quad (5.79)$$

where $F = N_o e^+$ is Faraday's constant (the charge of one mole of electrons, $F = 96,490$ C/mole of electrons).

If Equation 5.79 is solved for W/t and then divided by the anode area, A_a (cm^2), an expression for the corrosion intensity (CI) is obtained, as follows:

$$CI(\text{g/cm}^2 \cdot \text{s}) = \frac{M(I_{\text{corr}}/A_a)}{mF} \quad (5.80)$$

$$CI(\text{g/cm}^2 \cdot \text{s}) = \frac{Mi_{\text{corr}}}{mF}, \quad (5.81)$$

where i_{corr} is the corrosion current density in A/cm^2 .

If Equation 5.81 is divided by the density of the material, ρ (g/cm^3), an expression for the corrosion penetration rate (CPR) is determined, as follows:

$$\text{CPR} (\text{cm/s}) = \frac{Mi_{\text{corr}}}{mF\rho}. \quad (5.82)$$

The expressions for CI and CPR (Equations 5.81 and 5.82) can be easily converted to more convenient and traditional sets of units. Other expressions for CI and CPR in various sets of units are given in Table 5.2.

5.4 EXPERIMENTAL POLARIZATION CURVES

Experimental electrochemical corrosion studies to determine both corrosion rates and behaviors frequently employ a potentiostatic circuit, which includes a polarization cell, as schematically shown in Figure 5.12. The working electrode (WE) is the corrosion sample (i.e., the material under evaluation). The auxiliary electrode (AE), or counter electrode, is ideally made of a material that will support electrochemical oxidation or reduction reactions with reactants in the electrolyte, but will not itself undergo corrosion and thereby contaminate the electrolyte. The AE is usually made of platinum or high-density

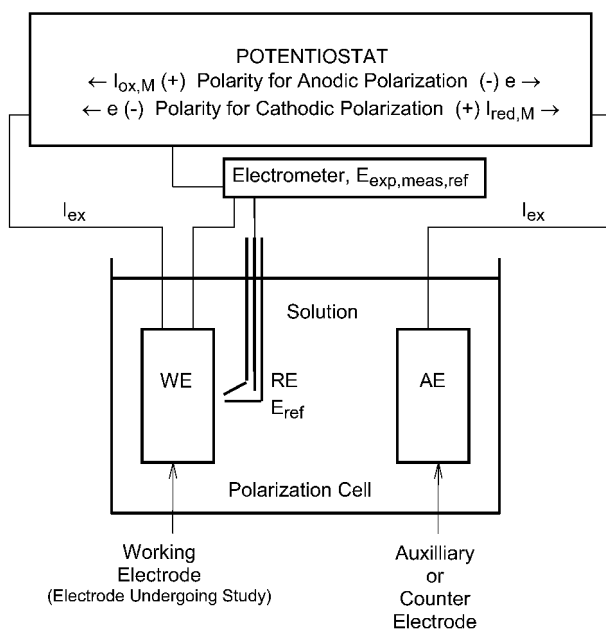


FIGURE 5.12 The potentiostatic circuit.

graphite. The reference electrode (RE) maintains a constant potential relative to which the potential of the WE is measured with an electrometer, a high-impedance ($>10^{14}$ ohms) voltmeter that limits the current through the electrometer to extremely small values that negligibly influence either the RE or WE potential. The potentiostat is a rapid response direct current (DC) power supply that will maintain the potential of the WE relative to the RE at a constant (preset or set point) value, even though the external circuit current, I_{ex} , may change by several orders of magnitude. When the potentiostat is disconnected from the corrosion sample (WE), the open-circuit or open-cell condition exists, the WE is freely corroding, the potential measured is the open-circuit corrosion potential, E_{corr} , and, of course, $I_{\text{ex}} = 0$.

The potentiostat can be set to polarize the WE either anodically, in which case the net reaction at the WE surface is oxidation (electrons removed from the WE), or cathodically, in which case the net reaction at the WE surface is reduction (electrons consumed at the WE). With reference to the potentiostatic circuit in Figure 5.12, determination of a polarization curve is usually initiated by first measuring the open-circuit corrosion potential, E_{corr} , until a steady-state value is achieved (e.g., less than 1.0 mV change over a five-minute period). Next, the potentiostat is set to control at E_{corr} and connected to

TABLE 5.2 Faraday's Law Expressions

Corrosion Intensity (CI)

$$CI(\text{g/m}^2 \cdot \text{y}) = 0.327 \frac{Mi_{\text{corr}}}{m}$$

$$CI(\text{mg/cm}^2 \cdot \text{y}) = 0.0327 \frac{Mi_{\text{corr}}}{m}$$

Corrosion Penetration Rate (CPR)

$$\text{CPR}(\mu\text{m/y}) = 0.327 \frac{Mi_{\text{corr}}}{m\rho}$$

$$\text{CPR}(\text{mm/y}) = 0.327 \times 10^{-3} \frac{Mi_{\text{corr}}}{m\rho}$$

$$\text{CPR}(\text{mpy}) = 0.0129 \frac{Mi_{\text{corr}}}{m\rho}$$

Units: M (g/mol), m (oxidation state or valence), ρ (g/cm^3), i_{corr} (mA/m^2), mpy = mils (0.001 inch) per year.

the polarization cell. Then, the setpoint potential is reset continuously or stepwise to control the potential-time history of the WE while I_{ex} is measured. If the setpoint potential is continuously increased (above E_{corr}), an anodic polarization curve is generated. Conversely, if the potential is continuously decreased (below E_{corr}), a cathodic polarization curve is produced.

Interpretation of an experimentally-determined polarization curve, including an understanding of the information derivable therefrom, is based on the form of the polarization curve that results from the polarization curves for the individual anodic and cathodic half-cell reactions occurring on the metal surface. These individual polarization curves, assuming Tafel behavior in all cases, are shown in Figure 5.13 (dashed curves) with E_{corr} and I_{corr} identified. It is assumed that over the potential range of concern, the $I_{ox,X}$ and $I_{red,M}$ contributions to the net anodic and cathodic curves are negligible. Consequently, $I_a = I_{ox,M}$ and $I_c = I_{red,X}$. At any potential of the WE established by the potentiostat, the experimentally-measured external current, I_{ex} , is the difference between $I_{ox,M}$ and

$I_{red,X}$. This difference, in terms of the Tafel expressions for the individual reactions, is

$$I_{ex} = I_{ox,M} - I_{red,X} = I_{o,M} e^{\frac{2.3(E-E'_M)}{\beta_{ox,M}}} - I_{o,X} e^{\frac{-2.3(E-E'_X)}{\beta_{red,X}}} \quad (5.83)$$

It is evident that I_{ex} changes from positive to negative when $I_{red,X}$ becomes greater than $I_{ox,M}$. This change in sign occurs as I_{ex} passes through $I_{ex} = 0$, at which point $E = E_{corr}$ and $I_{ox,M} = I_{red,X} = I_{corr}$. Thus, two current ranges can be identified: $I_{ex} > 0$ (over which the anodic or oxidation reaction is dominant) and $I_{ex} < 0$ (over which the cathodic or reduction reaction is dominant). The properties of these two ranges are summarized below.

In the current range, $I_{ex} > 0$, the WE potential set by the potentiostat is greater than E_{corr} . The electrons produced per unit time by the $M \rightarrow M^{m+} + me$ reaction exceed those consumed per unit time by the $X^{x+} + xe \rightarrow X$ reaction, and net oxidation occurs at the WE. A positive current is consistent with the sign convention that assigns a positive value to the external circuit current when net oxidation occurs at the WE. For $I_{ex} > 0$, a plot of E versus $\log I_{ex}$ takes the form of the upper solid curve in Figure 5.13, the anodic branch of the experimental polarization curve. When E is increased sufficiently above E_{corr} to cause $I_{red,X}$ to become negligible with respect to $I_{ox,M}$ (normally 50–100 mV),

$$I_{ex} = I_{ox,M} \quad (5.84)$$

and I_{ex} becomes a direct measure of the oxidation rate, $I_{ox,M}$, of the metal in this potential range. This linear portion of an experimental curve reveals the Tafel curve of the anodic metal reaction, and extrapolation of the Tafel curve to E'_M provides an estimate from experiment of the metal exchange current density, $I_{o,M}/A_a$, where A_a is the area of the WE.

In the current range, $I_{ex} < 0$, the WE potential set by the potentiostat is less than E_{corr} . At the metal surface, electrons consumed per unit time by the $X^{x+} + xe \rightarrow X$ reaction exceed those produced per unit time by the $M \rightarrow M^{m+} + me$ reaction. Net reduction is occurring and electrons must be supplied to the WE by the external circuit; the external circuit current (I_{ex}) will be negative. A plot of E versus $\log |I_{ex}|$ takes the form of the lower solid curve in Figure 5.13. When E is decreased sufficiently below E_{corr} to cause $I_{ox,M}$ to become negligible (normally 50–100 mV),

$$I_{ex} = -I_{red,X} \quad (5.85)$$

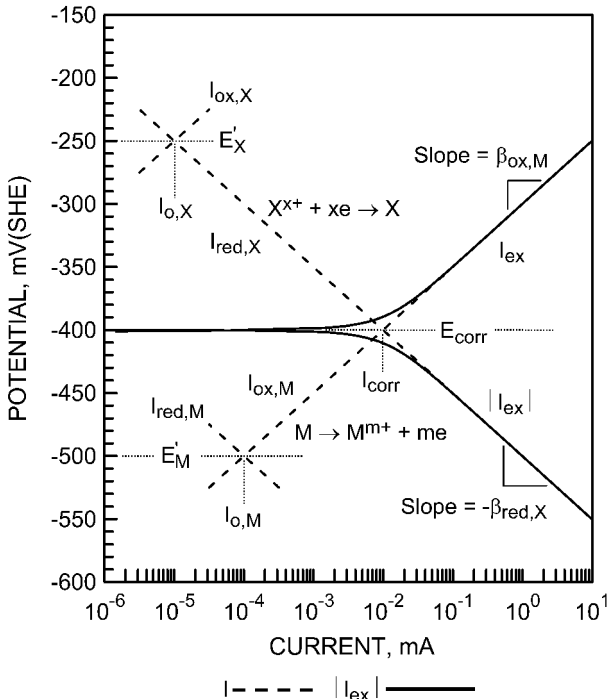


FIGURE 5.13 Schematic experimental polarization curves (solid curves) assuming Tafel behavior for the individual oxidation, and cathodic-reactant reduction polarization curves (dashed curves).

or

$$|I_{\text{ex}}| = I_{\text{red},X} \quad (5.86)$$

and I_{ex} becomes a direct measure of the rate of the cathodic reaction, $I_{\text{red},X}$, on the metal. This linear portion of an experimental curve reveals the Tafel curve of the cathodic reaction, and extrapolation of the Tafel curve to E'_X provides an estimate from experiment of the cathodic reaction exchange current density, $I_{0,X}/A_c$, where A_c is the area of the WE.

It is emphasized that, more generally, I_{ex} is the experimentally-measured current representing the net difference between the sum of all oxidation-reaction currents and the sum of all reduction-reaction currents at the interface:

$$I_{\text{ex}} = \Sigma I_{\text{ox}} - \Sigma I_{\text{red}} \quad (5.87)$$

For the two half-cell reactions under consideration,

$$I_{\text{ex}} = (I_{\text{ox},M} + I_{\text{ox},X}) - (I_{\text{red},X} + I_{\text{red},M}) \quad (5.88)$$

Under the condition that $I_{\text{ox},X}$ and $I_{\text{red},M}$ are negligible,

$$I_{\text{ex}} = I_{\text{ox},M} - I_{\text{red},X} \quad (5.89)$$

The above relationship is equally applicable if either the metal oxidation-rate curve or the reduction-rate curve for the cathodic reactant does not obey Tafel behavior. To illustrate this point, three additional schematic pairs of individual anodic and cathodic polarization curves are examined. In Figure 5.14, the metal undergoes active-passive oxidation

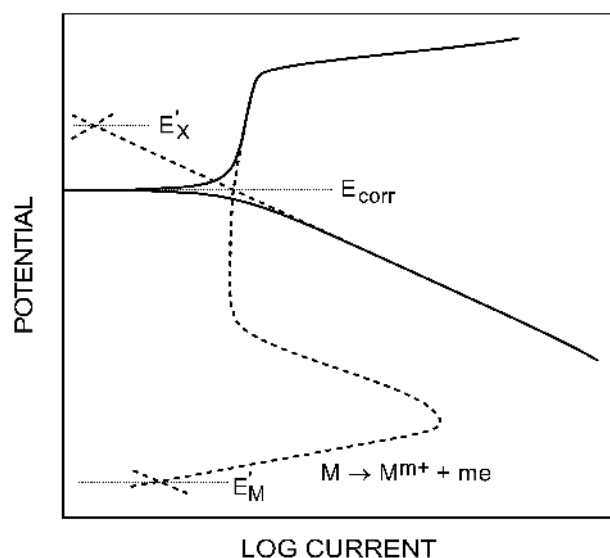


FIGURE 5.14 Schematic experimental polarization curves.

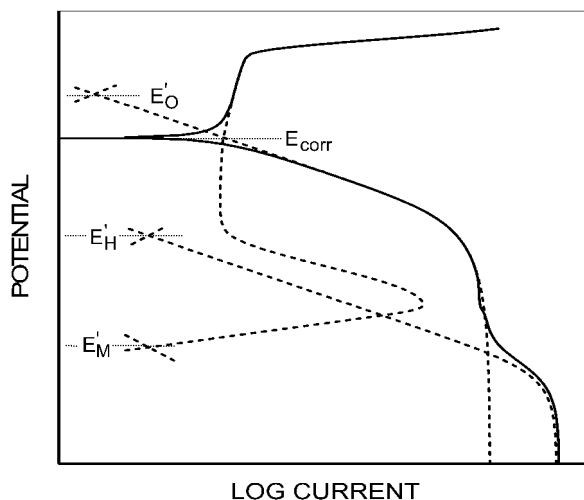


FIGURE 5.15 Schematic experimental polarization curves.

behavior and E_{corr} is in the passive region. In Figure 5.15, where the total reduction-rate curve involves reduction of both dissolved oxygen ($\text{O}_2 + 4\text{H}^+ + 4e \rightarrow 2\text{H}_2\text{O}$) and hydrogen ions ($2\text{H}^+ + 2e \rightarrow \text{H}_2$), and their respective limiting diffusion currents, the metal shown undergoes active-passive oxidation behavior and E_{corr} is in the passive region. It is to be noted for the example in Figure 5.15 that if the dissolved oxygen were removed from the electrolyte, E_{corr} would be in the active region, I_{corr} would be considerably larger, and the experimental polarization curves would appear as in Figure 5.16.

5.5 EXAMPLES OF ELECTROCHEMICAL CORROSION MEASUREMENTS AND CHARACTERIZATIONS

The thermodynamic and kinetic principles along with measurement techniques described in previous sections provide the basis for both predicting and measuring rates of corrosion. All electrochemical techniques for corrosion-rate determinations are directed to measurement of the corrosion current, I_{corr} , from which the corrosion current density ($i_{\text{corr}} = I_{\text{corr}}/A_a$), the corrosion intensity, and the corrosion penetration rate are calculated, providing the area of the anodic sites (A_a) also can be determined. In the limit, these sites are assumed to be uniformly distributed on a scale approaching atomic dimensions and indistinguishable from sites of the cathodic reaction supporting the corrosion. In this limit, the corrosion is uniform and the area of the anodic sites

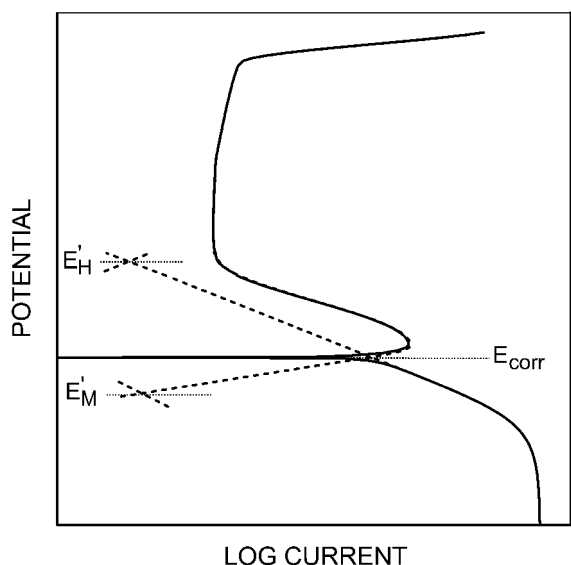


FIGURE 5.16 Schematic experimental polarization curves.

(A_a) is taken to be the total specimen area (A). From this limit, anodic sites can vary from microscopic to macroscopic dimensions, thus leading to localized corrosion. Hence, polarization measurements leading to a value for the corrosion current density [by dividing the corrosion current by the total specimen area ($i_{\text{corr}} = I_{\text{corr}}/A$)] must be accompanied by a surface examination to determine the actual anodic areas.

Furthermore, if there is a distribution over both anodic and cathodic sites with respect to the current density of these respective reactions, the calculations are obviously more difficult. Frequently, the heterogeneity of these reactions over the surface must be evaluated qualitatively, recognizing that the calculated corrosion current density, $i_{\text{corr}} = I_{\text{corr}}/A$, gives only a lower limit to the actual current density and, hence, that local corrosion intensities and penetration rates can be much higher. Assuming that a specimen surface undergoing measurement contains at least a statistical distribution of anodic and cathodic sites, and that the intersite electrical resistance is small, previous discussions have shown that the intersection of the extrapolated Tafel regions of the anodic and cathodic polarization curves gives I_{corr} . To establish this intersection experimentally requires determination of the anodic and cathodic polarization curves in the vicinity of the intersection. Since the data analysis techniques involve extrapolations and measurements of slopes of these curves,

the accuracy of their experimental determination is important. Thus, the experimental methods must be critically evaluated with respect to their sensitivity to the polarization variables and how various conditions established at the interface by the variables contribute to an electrochemical measurement. These variables include exchange current densities, Tafel slopes, diffusion of species to and from the interface, corrosion-product formation, and the potential scan rate.

5.5.1 Tafel Extrapolation

The most fundamental procedure for experimentally evaluating I_{corr} is by Tafel extrapolation. This method requires the presence of a linear or Tafel section in the E versus $\log I_{\text{ex}}$ curve. A potential scan of approximately ± 300 mV about E_{corr} is generally required to determine if a linear section of at least one decade of current is present, such that a reasonably accurate extrapolation can be made to the E_{corr} potential. Such linear sections are illustrated for the experimental cathodic polarization curves in Figures 5.13, 5.14, 5.15, and 5.16. The current value at the E_{corr} intersection is the corrosion current, I_{corr} , as shown in Figure 5.17. Assuming uniform corrosion, the corrosion current density is obtained by dividing I_{corr} by the specimen area (i.e., $i_{\text{corr}} = I_{\text{corr}}/A$). Anodic polarization curves are not often used in this method because of the absence of linear regions over at least one decade of current for many metals and alloys exhibiting active-passive behavior.

For example, inspection of Figure 5.16 shows that extrapolation of the linear portion of the cathodic curve would yield more accurate results than at-

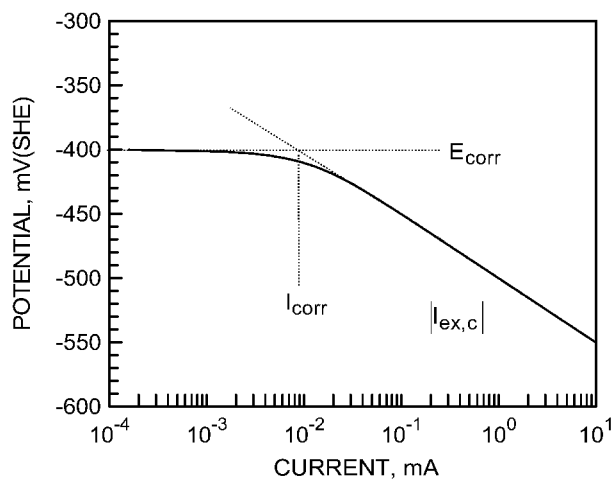


FIGURE 5.17 The Tafel extrapolation method.

tempted extrapolation of the anodic curve. In many cases, a linear region may not be observed even in the cathodic curve. This can be a result of the corrosion being under diffusion control or, on decreasing the potential, entering into the diffusion-control region, or even that the nature of the interface changes with changing potential.

The time required to determine I_{corr} by Tafel extrapolation is approximately three hours, which corresponds to the approximate time required for experimental setup and generation of a cathodic polarization curve at a commonly employed, slow scan rate of 600 mV/h. In comparison, a comparable gravimetric evaluation (mass-loss measurement) on a corrosion-resistant metal or alloy could take months, or longer. A limitation of the Tafel extrapolation method is the rather large potential excursion away from E_{corr} , which tends to modify the WE surface such that if the measurement is to be repeated, the sample should be re-prepared following initial procedures and again allowed to stabilize in the electrolyte until a steady-state E_{corr} is reached. Consequently, the Tafel extrapolation method is not amenable to studies requiring faster, or even continuous, measurements of I_{corr} .

5.5.2 Polarization Resistance¹²⁻¹⁸

The polarization resistance or Stern-Geary method allows faster corrosion rate measurements. The theoretical justification for this method will be briefly outlined. Recall that the external current is given by Equation 5.83. At the corrosion potential, $E = E_{\text{corr}}$, $i_{\text{ex}} = 0$, and $I_{\text{corr}} = I_{\text{ox},M} = I_{\text{red},X}$. Therefore,

$$I_{\text{corr}} = I_{\text{o},M} e^{\frac{+2.3(E_{\text{corr}} - E'_M)}{\beta_{\text{ox},M}}} = I_{\text{o},X} e^{\frac{-2.3(E_{\text{corr}} - E'_X)}{\beta_{\text{red},X}}}. \quad (5.90)$$

On dividing Equation 5.90 into Equation 5.83,

$$i_{\text{ex}} = I_{\text{corr}} \left[e^{\frac{2.3(E - E_{\text{corr}})}{\beta_{\text{ox},M}}} - e^{\frac{-2.3(E - E_{\text{corr}})}{\beta_{\text{red},X}}} \right]. \quad (5.91)$$

On dividing by the specimen area to convert to current density,

$$i_{\text{ex}} = i_{\text{corr}} \left[e^{\frac{+2.3(E - E_{\text{corr}})}{\beta_{\text{ox},M}}} - e^{\frac{-2.3(E - E_{\text{corr}})}{\beta_{\text{red},X}}} \right]. \quad (5.92)$$

This equation has the form of the solid curve in Figure 5.18 when plotted near E_{corr} (usually within ± 25 mV of E_{corr}).

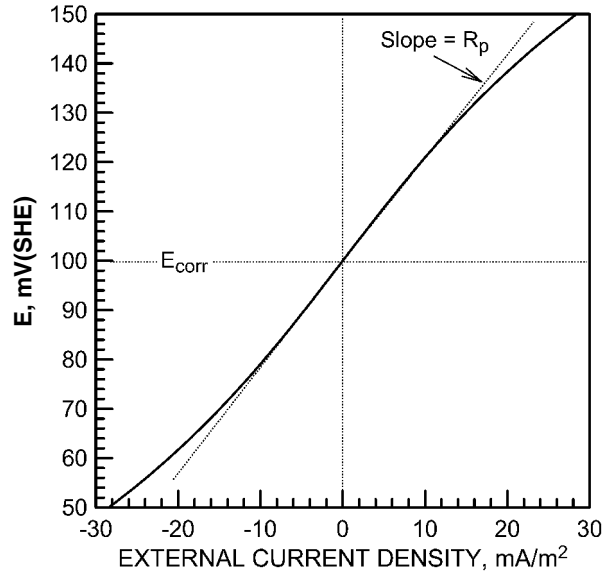


FIGURE 5.18 The polarization resistance method.

Differentiation of Equation 5.92, with respect to E yields

$$\frac{di_{\text{ex}}}{dE} = i_{\text{corr}} \left[\frac{2.3}{\beta_{\text{ox},M}} e^{\frac{+2.3(E - E_{\text{corr}})}{\beta_{\text{ox},M}}} + \frac{2.3}{\beta_{\text{red},X}} e^{\frac{-2.3(E - E_{\text{corr}})}{\beta_{\text{red},X}}} \right]. \quad (5.93)$$

At $E = E_{\text{corr}}$, the exponential terms are unity and upon rearrangement, Equation 5.93 reduces to

$$\left(\frac{dE}{di_{\text{ex}}} \right)_{E_{\text{corr}}} = R_p = \frac{\beta_{\text{ox},M} \beta_{\text{red},X}}{2.3 i_{\text{corr}} (\beta_{\text{ox},M} + \beta_{\text{red},X})}, \quad (5.94)$$

where $(dE/di_{\text{ex}})_{E_{\text{corr}}}$ is known as the polarization resistance, R_p . It has dimensions of resistance \times area (total specimen area, as in ohms-m²). As seen by Equation 5.94 and indicated in Figure 5.18, R_p is the slope of the experimental E versus i_{ex} curve at E_{corr} . The curve tends to be linear near E_{corr} , which facilitates determination of the slope.

Equation 5.94 may be rewritten in the following form, since the desired quantity in the polarization resistance analysis is the corrosion current density:

$$i_{\text{corr}} = \frac{\beta_{\text{ox},M} \beta_{\text{red},X}}{2.3 R_p (\beta_{\text{ox},M} + \beta_{\text{red},X})} = \frac{B}{R_p}. \quad (5.95)$$

This equation is used directly to determine i_{corr} . The analysis procedure involves evaluating the slope of the E versus i_{ex} curve at E_{corr} , as shown in Figure

5.18, to determine R_p . From R_p and known or experimentally-determined Tafel constants (β values), i_{corr} is calculated.

As previously stated, once R_p is determined, calculation of i_{corr} requires knowledge of the Tafel constants. In the absence of these values, an approximation is often used.

In terms of rationalizing an approximation for B in Equation 5.95, it is convenient to express B as

$$B = \frac{1}{2.3 \left(\frac{1}{\beta_{\text{ox},M}} + \frac{1}{\beta_{\text{red},X}} \right)}. \quad (5.96)$$

It has been observed that experimental values of $\beta_{\text{ox},M}$ normally range between 60 and 120 mV; whereas, values of $\beta_{\text{red},X}$ normally range between 60 mV and infinity (the latter corresponding to diffusion control for the cathodic reaction).^{17,19} Given the ranges in β values, the extreme values of B are 13 and 52 mV, corresponding to $\beta_{\text{ox},M} = \beta_{\text{red},X} = 60$ mV and $\beta_{\text{ox},M} = 120$ mV, $\beta_{\text{red},X} = \text{infinity}$, respectively. If one uses as an approximation, $\beta_{\text{ox},M} = \beta_{\text{red},X} = 120$ mV, then $B = 26$ mV. The expected error in the calculated value of i_{corr} (Equation 5.95) when using $B = 26$ mV as an approximation (as compared to extreme values of 13 and 52 mV) should be less than a factor of two. Therefore, the following approximation provides a reasonably good estimate of i_{corr} from polarization resistance measurements:

$$i_{\text{corr}} \cong \frac{26 \text{ mV}}{R_p}. \quad (5.97)$$

In generating an E versus i_{ex} curve for polarization resistance analysis, only very small potential excursions about E_{corr} are employed, normally on the order of ± 10 mV. The general assumption is that on scanning through this small potential range, the material surface remains unchanged. Consequently, repeat measurements may be made as a function of time without removing the sample and re-preparing the surface.

5.5.3 Cyclic-Anodic-Polarization Behavior Relative to Localized Corrosion

By analyzing cyclic-anodic-polarization behavior, information on localized corrosion susceptibility can be obtained rather rapidly for a given metal or alloy in a given electrolyte.²⁰ In this regard, certain parameters are identified in the schematic cyclic-anodic-polarization curves of Figure 5.19, which illustrate typical behaviors with regard to localized corrosion susceptibilities. It is noted that Figure 5.19 has the general form of Figure 5.14, where passive corrosion is taking place at E_{corr} . The plots in Figure 5.19 are potential (relative to the saturated calomel reference electrode [SCE]) versus the logarithm of the external-circuit current density, where the cur-

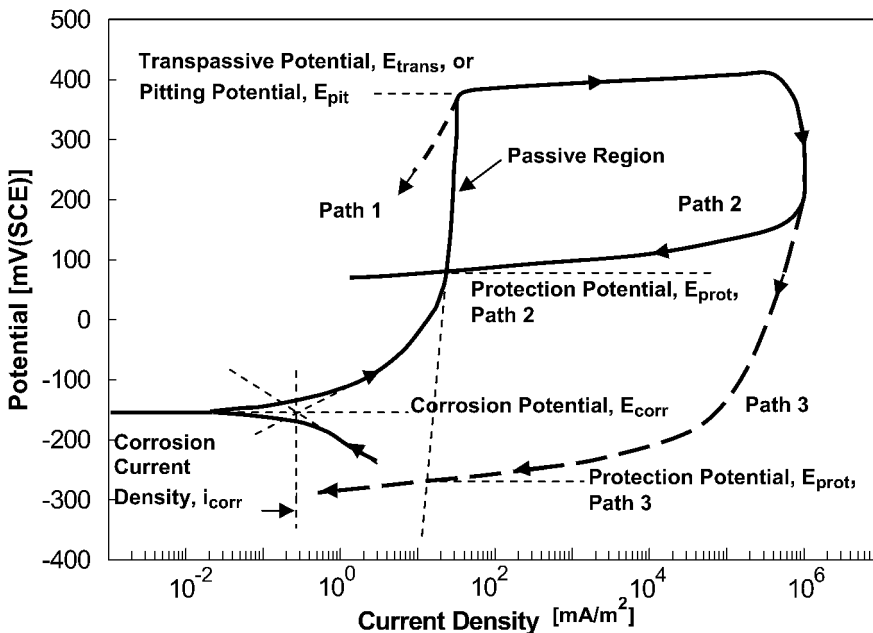


FIGURE 5.19 Cyclic anodic polarization curves illustrating localized corrosion behaviors.

rent density is the measured external-circuit current divided by the specimen area. The controlled specimen potential can be regarded as the “driving force” for corrosion, and the anodic current density is directly related to the specimen corrosion rate.

In Figure 5.19, the potential scan is started below the corrosion potential, E_{corr} . At E_{corr} , the external current density goes to zero, and then increases to a low and approximately constant anodic value ($\sim 10 \text{ mA/m}^2$) in the passive range. In this range, a thin oxide/hydroxide film, a passive film, protects the material from high corrosion rates. At higher potentials, the passive film may undergo uniform dissolution (transpassive behavior) or localized dissolution (pitting or crevice corrosion), which results in higher corrosion rates and higher external current densities. The passive film breakdown potential in Figure 5.19 is labeled either as the transpassive potential, E_{trans} , or the critical pitting potential, E_{pit} . It is noted that the breakdown potential also could correspond to a critical crevice corrosion potential, but such tests would involve specimen geometries with carefully designed synthetic crevices. The pitting form of localized corrosion will be emphasized in the present discussion.

In the cyclic-anodic-polarization test, the potential scan direction is reversed at a pre-selected anodic current density above the breakdown potential (often 10^4 mA/m^2). If, on potential-scan reversal, the current density decreases as in path 1, the material is shown to be immune to pitting corrosion. In this case, the breakdown potential corresponds to E_{trans} and, above E_{trans} , the passive film undergoes uniform dissolution because it is no longer thermodynamically stable at these potentials. Moreover, on the downscan, the passive film immediately reforms and is again stable below E_{trans} .

Alternatively, if, on the potential downscan, the current density remains high until finally decreasing to the passive-region value, as in path 2, the material is shown to undergo a form of localized corrosion (pitting corrosion in this discussion).

The breakdown potential in this case corresponds to the pitting potential, E_{pit} (i.e., the potential at which pits initiate locally on the surface—localized passive film dissolution). The potential at which the current density returns to the passive value is known as the repassivation potential or the protection potential, E_{prot} . Between E_{pit} and E_{prot} , existing pits are propagating and new pits may initiate with time. In the case of path 2, pits will neither initiate nor propagate at E_{corr} , the natural corrosion potential. Therefore, the material will not undergo pitting corrosion under natural corrosion conditions. If, on the other

hand, path 3 is exhibited, where E_{prot} is below E_{corr} , the material may undergo pitting corrosion at surface flaws or after incubation time periods at E_{corr} . In terms of overall resistance to pitting corrosion, two parameters are important: $(E_{\text{pit}} - E_{\text{corr}})$ and $(E_{\text{prot}} - E_{\text{corr}})$. Higher values of both are desirable to reflect high values of E_{pit} and E_{prot} relative to E_{corr} .

5.6 SUMMARY

Some of the important electrochemical principles and mechanisms controlling the aqueous corrosion of metals and alloys have been summarized. It was shown how to use principles in electrochemical thermodynamics to predict whether or not corrosion will occur for a given metal in a given electrolyte (with pH and oxygen content as principal variables) at a given temperature. Sufficient detail was provided to allow these calculations. The thermodynamics calculations also were related to Pourbaix (or potential-pH) diagrams in order to provide an understanding of the source of these useful, summary diagrams. It also was shown that, if corrosion is predicted to occur, the electrochemical thermodynamics (as represented in Pourbaix diagrams) allow prediction of the form of the corrosion product, either ions dissolved in the electrolyte or solids precipitated at the surface. Because many metals rely on passivation to maintain low corrosion rates, and because passivation can occur only with solid corrosion products, this analysis allows prediction of whether passivation is possible for a given metal/electrolyte system.

In moving to the analyses of corrosion rates and corrosion behaviors, the basic electrochemical corrosion circuit was described in terms of anodic sites and reactions, cathodic sites and reactions, interface potentials, resistances to current flow in the circuit, and the corrosion current. Simple Tafel or charge-transfer polarization behavior was defined for anodic and cathodic half-reactions, and appropriate equations were given. This simple behavior was expanded to include diffusion effects and active-passive behavior. Analyses of individual polarization curves, and experimentally determined polarization curves, were discussed relative to determining the open-circuit corrosion potential, E_{corr} , and the corrosion current density, i_{corr} . Faraday's law was derived, which allows calculation of the corrosion intensity or corrosion penetration rate from i_{corr} under the assumption of uniform corrosion.

And finally, several examples of specific types of electrochemical corrosion measurements and characterizations were described: Tafel extrapolation to

determine i_{corr} ; polarization resistance to determine i_{corr} more rapidly; and cyclic-anodic-polarization tests to examine for localized corrosion susceptibilities. It is suggested that sufficient background is given in this chapter for the reader to understand many additional types of electrochemical corrosion tests.

5.7 REFERENCES

1. Stansbury, E. E. and Buchanan, R. A. *Fundamentals of Electrochemical Corrosion*. Materials Park, OH: ASM International, 2000.
2. Bockris, J. O. and Reddy, A. K. N. *Modern Electrochemistry*. New York, NY: Plenum Press, 1973.
3. West, J. M. *Electrodeposition and Corrosion Processes*. New York: D. Van Nostrand Co., 1965.
4. Gaskell, D. R. *Introduction to Metallurgical Thermodynamic*. Taylor and Francis, 1981.
5. Ives, D. J. G. and Janz, G. J. *Reference Electrodes*. Houston: NACE International, reprinted 1996.
6. Lide, D. R., Ed. *CRC Handbook of Physics and Chemistry*, Cleveland, OH: CRC Press, 1997.
7. Bard, A. J., Parsons, R., and Jordan, J. *Standard Potentials in Aqueous Solutions*. New York: Marcel Dekker, 1985.
8. de Bethune, A. J. and Loud, N. A. S. *Standard Aqueous Electrode Potentials and Temperature Coefficients at 25°C*. Skokie, IL: Hampel, 1964.
9. West, J. M. *Basic Corrosion and Oxidation*. New York, NY: Halsted Press, 1980.
10. Pourbaix, M. *Atlas of Electrochemical Equilibria in Aqueous Solutions*. Houston: National Association of Corrosion Engineers, 1974.
11. Vetter, K. J. *Electrochemical Kinetics*. New York: Academic Press, 1967.
12. EG&G Princeton Applied Research. *Basics of Corrosion Measurements*. Application Note Corr. 1. Princeton, NJ, 1980.
13. Standard Practice for Conducting Potentiodynamic Polarization Resistance Measurements. ASTM Standard G 59-91. *Annual Book of ASTM Standards*, Vol. 03.02. Philadelphia: American Society for Testing and Materials, 1995.
14. Stern, M. and Roth, R. M. *Journal of the Electrochemical Society*. Vol. 104, p. 390, 1957.
15. Stern, M. *Corrosion*. Vol. 14, p. 440t, 1958.
16. Mansfeld, F. The Polarization Resistance Technique for Measuring Corrosion Currents. *Corrosion Science and Technology*. New York: Plenum Press, Vol. VI, p. 163, 1976.
17. Jones, Denny A. *Principles and Prevention of Corrosion*, New York: Macmillan Publishing Company, 1992.
18. Stern, M. and Geary, A. L. Electrochemical Polarization I: A Theoretical Analysis of the Shape of Polarization Curves. *Journal of the Electrochemical Society*. Vol. 104, pp. 56-63, 1957.
19. Stern, M. and Weisert, E. D. Proceedings ASTM. Philadelphia; ASTM, Vol 32, p. 1280, 1959.
20. Wilde, B. E. On Pitting and Protection Potentials: Their Use and Possible Misuses for Predicting Localized Corrosion Resistance of Stainless Alloys in Halide Media. In *Localized Corrosion NACE 3*. B. F. Brown, K. Kruger, and R. W. Staehle, Eds. Houston: National Association of Corrosion Engineers, pp. 342-352, 1974.

CHAPTER 6

HIGH TEMPERATURE OXIDATION

A. S. Khanna

Corrosion Science and Engineering, Indian Institute of Technology, Bombay, India

- 6.1 INTRODUCTION 105
- 6.2 CRITERIA OF METAL OXIDATION 106
- 6.3 KINETICS OF OXIDATION 106
- 6.4 TECHNIQUES INVOLVED IN MEASURING OXIDATION BEHAVIOR 108
- 6.5 MEASUREMENT OF OXIDATION KINETICS 109
- 6.6 IDENTIFICATION AND CHARACTERIZATION OF SCALES 110
- 6.7 WAGNER HAUFFE RULES 112
- 6.8 MARKER TECHNIQUE 113
- 6.9 OXYGEN TRACER TECHNIQUE 113
- 6.10 INITIAL OXIDATION OR THIN LAYER OXIDATION 115
- 6.11 OXIDATION OF PURE METALS 118
- 6.12 OXIDATION OF ALLOYS 122
- 6.13 INFLUENCE OF ALLOY ADDITIONS ON OXIDATION BEHAVIOR 122
- 6.14 OXIDATION BEHAVIOR OF SOME COMMERCIAL ALLOYS 128
- 6.15 OXIDATION IN MIXED GAS ENVIRONMENTS 132
- 6.16 PHASE STABILITY DIAGRAMS 137
- 6.17 SCALING OF ALLOYS IN SO₂-CONTAINING ATMOSPHERES 138
- 6.18 OXIDATION OF FE-CR-AL AND NI-CR-AL ALLOYS IN SO₂ AND O₂ ENVIRONMENTS 141
- 6.19 HOT CORROSION 142
- 6.20 OXIDE SPALLATION 145
- 6.21 PILLING BEDWORTH RATIO 145
- 6.22 STRESSES DEVELOPED DURING THERMAL CYCLING CONDITIONS 145
- 6.23 EXAMPLES OF HIGH TEMPERATURE CORROSION IN VARIOUS INDUSTRIES 148
- 6.24 PETROLEUM REFINING AND PETROCHEMICAL PROCESSES 151
- 6.25 REFERENCES 152

6.1 INTRODUCTION

Oxidation is a special form of corrosion degradation of metals and alloys that occurs when the metals or alloys are exposed to air or oxygen. Oxidation can also take place in other environments, such as sulfur dioxide and carbon dioxide, which have relatively low oxidation potentials. The degradation is generally in the form of scale formation. Sometimes, along with scale formation on the surface, there is oxide formation within the substrate next to the external scale.

Oxidation, in real sense, is the formation of the oxide scale. If the formed oxide scale is thin, slow-growing, and adherent, it protects the substrate from further oxidation. However, if the scale spalls frequently, the metal is consumed continuously and the material ultimately fails. The other form of degradation at high temperatures is sulfidation, in which either a thick sulfide scale is formed and/or sulfur penetrates deeper into the matrix through grain boundaries. Certain metals, such as titanium, zirconium, chromium, and so forth, form protective ni-

tride scales when exposed to nitrogen-containing environments. Carbon dioxide and carbon monoxide environments sometimes cause carburization and decarburization problems, leading to either embrittlement or loss in strength of the component. Another form of degradation that is known to occur at high temperatures is hot corrosion, where oxidation or sulfidation occurs beneath a salt melt deposit on the surface of the substrate.

What should one know about high temperature oxidation? A beginner needs to know why oxidation occurs. What is the life of a metal and alloy in a particular environment at a particular temperature? What type of products form due to oxidation? And, finally, what is the mechanism of the oxidation process?

In addition, it is important to know what causes the scale growth. What is the role of defect structure of an oxide, diffusion through oxide scales, and stress generation during the oxide growth process. Reasons for scale spallation and methods to improve oxidation behavior by active element effects are equally important. All these topics will be covered in

this chapter, with a few examples from important industries on the degradation of metals at high temperatures.

6.2 CRITERIA OF METAL OXIDATION

An oxidation reaction between a metal (M) and the oxygen gas (O₂) can be written as



Thermodynamically, an oxide will form on the surface of a metal when the oxygen potential in the environment is greater than the oxygen partial pressure in equilibrium with the oxide. This equilibrium oxygen pressure, also called the dissociation pressure of the oxide in equilibrium with the metal, is determined from the standard free energy of formation of the oxide. The standard free energy of the oxidation Reaction 6.1 can be written as

$$\Delta G^\circ = -RT \ln p(a_{MO_2} / a_M p(O_2)), \quad (6.2)$$

where a_{MO_2} and a_M are the activities of the oxide and the metal, respectively, and $p(O_2)$ is the partial pressure of the oxygen gas. In general, element activity in alloy is given by $a_M = \gamma_M X_M$, where γ_M and X_M are the activity coefficient and mole fraction, respectively, of M in the alloy. If the value of coefficient γ_M is not available, ideal behavior is assumed, and γ_M is assigned the value of unity. Assuming unit activity of the solid constituents (i.e., the metal and oxide), Equation 6.2 becomes

$$\Delta G^\circ = RT \ln p(O_2) \quad (6.3)$$

or

$$p(O_2) = \exp(\Delta G^\circ / RT). \quad (6.4)$$

Equation 6.4 permits the determination of the partial pressure of oxygen in equilibrium with the oxide from the standard free energy of formation. Plots of the standard free energies for the formation of oxides as a function of temperature are known as Ellingham/Richardson diagrams, which are used to obtain information about the partial pressure of oxygen required for any metal to form oxide at any temperature (Fig. 6.1). A linear behavior is expected for all the metals. The strong oxide former is shown at the bottom of the plot, while the weakest oxide forming metal is shown on the upper part of the

curve. The partial pressure of oxygen required for oxidation at various temperatures can be read from the nomographic scale given on the right side of the plot.

6.3 KINETICS OF OXIDATION

One of the limitations of Ellingham diagrams is that they do not take into account the kinetics of reaction. These equilibrium diagrams only tell us whether oxide formation is possible under certain conditions of temperature and partial pressure of oxygen. Sometimes it is possible that the kinetics of the process are so slow that even if there is a possibility of the reaction to occur thermodynamically, it will take very long to form. Thus, it appears that the oxidation reaction has not occurred. Therefore, it is imperative to know about the kinetics of oxidation reactions. Furthermore, if formation of more than one oxide is possible, the diagrams cannot *a priori* tell us which oxide will form in the given environment. The reaction kinetics of formation of different oxides need to be considered. A combination of thermodynamic and kinetic information can give a better understanding about the behavior of the oxide. Moreover, knowledge of reaction rates is an important basis for elucidation of the reaction mechanism. Rates of the reactions and the corresponding rate equations for the oxidation of a metal depend upon a number of factors. The most important are temperature, oxygen pressure, surface preparation, and pretreatment of the metal. For engineering design, kinetics of the oxidation is very important, as it gives an estimate of the design life of the metal to be used as a particular component at a specific temperature and environment. The following different rate laws are commonly encountered: linear, parabolic, logarithmic and combinations of them, such as parabolic (combination of linear and parabolic), etc.

6.3.1 Logarithmic Law

Logarithmic law usually represents oxidation in thin layer regime. In the case of most of metals heated at low temperatures, the kinetics usually obey logarithmic behavior. The rate of reaction rises very fast in the beginning and then slows down, either following a direct or inverse logarithmic law:

$$\text{Direct logarithmic law} \quad x = K \log t + A \quad (6.5)$$

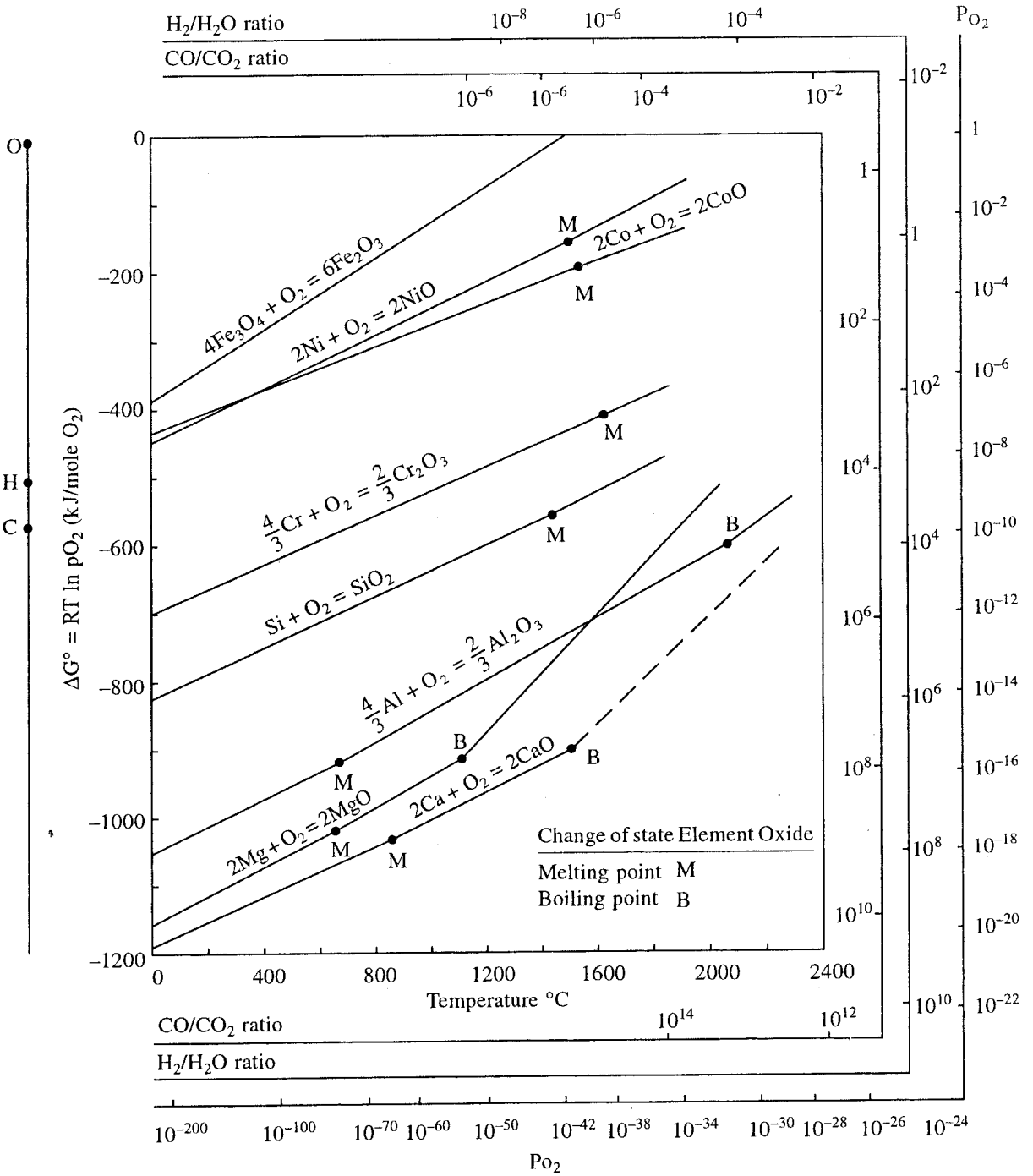


FIGURE 6.1 Ellingham diagram, showing the variation of free energy with temperature for various oxides.

and

$$\text{Inverse logarithmic law } 1/x = B + K_1 \log t, \quad (6.6)$$

where x can be the change in weight as a result of oxidation, thickness of the oxide formed, the amount of oxygen consumed per unit surface area of the

metal, or the amount of metal transformed to oxide. Time is denoted by t , and K and K_1 are the rate constants for logarithmic and inverse logarithmic process. A and B are the integration constants. The variation of x with time is shown in Fig. 6.2. There are a number of theories to explain the two logarithmic

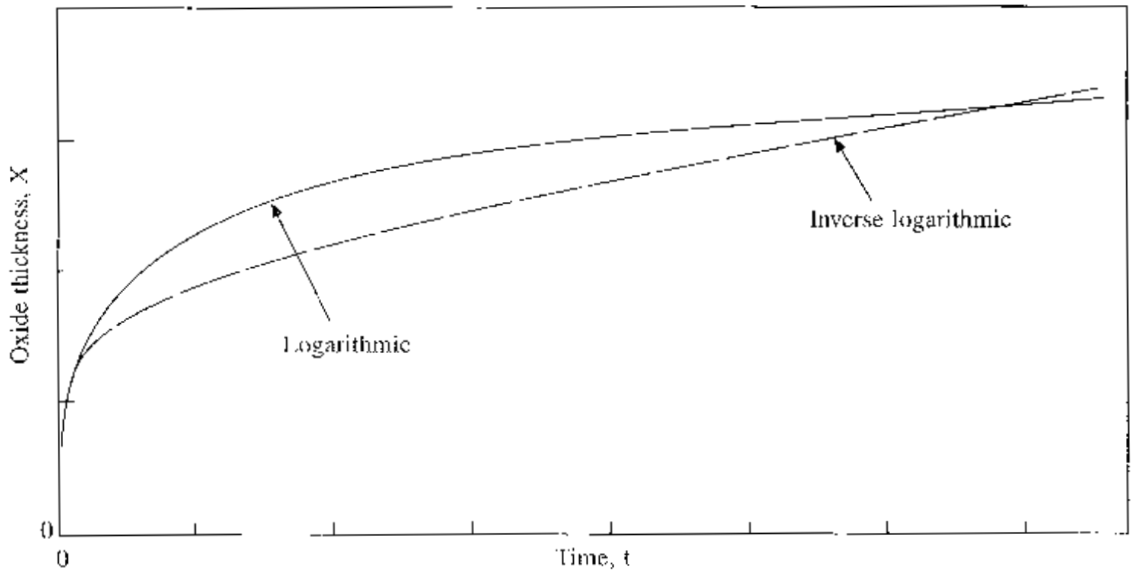


FIGURE 6.2 The kinetics of logarithmic oxidation.

mic laws. These are based on the transport of either ions or electrons. These are discussed in a subsequent chapter dealing with the oxidation in thin layer regime.

6.3.2 Parabolic Oxidation

From the standpoint of oxidation of engineering alloys, the parabolic law is of great importance. As per this law, the oxide growth occurs with a continuing decreasing oxidation rate. The rate of the reaction, therefore, is inversely proportional to the scale thickness or the weight of oxide formed. This is represented as

$$dx/dt = K_p / x \quad (6.7)$$

or, after integrating,

$$x^2 = 2K_p t + C, \quad (6.8)$$

where K_p is called the parabolic rate constant, and the variation of x versus t is given in Fig. 6.3. Most metals and engineering alloys follow parabolic kinetics at elevated temperatures. The oxide growth process is usually governed by the diffusion of ions or electrons through the initially formed oxide scale. The parabolic law was first derived by Wagner, assuming diffusion of charged species through the oxide layer. This will be discussed in detail in a subsequent section.

6.3.3 Linear Equation

There are certain metals where the rate of oxidation remains constant with time and is independent of the amount of gas or metal previously consumed in the reaction. In such cases, the rate of reaction is directly proportional to the time:

$$dx/dt = K' t \quad (6.9)$$

or

$$x = K' t + D, \quad (6.10)$$

where K' is the linear rate constant of the reaction. Such reactions usually take place by surface or phase boundary reactions. These may involve, for example: a steady state reaction limited by the supply (adsorption) of reactant at the surface; a reaction governed by a steady state formation of oxide at the metal/oxide interface; or diffusion through a protective layer with constant thickness. In addition to a few metals, such as alkali metals and alkaline earth metals, the linear rate law is usually followed when a protective scale cracks or spalls, leading to direct access of gas to metal. This results in very fast oxidation rates, invariably following linear kinetics.

6.4 TECHNIQUES INVOLVED IN MEASURING OXIDATION BEHAVIOR

Oxidation studies involve a combination of both theoretical and experimental knowledge. Topics such as

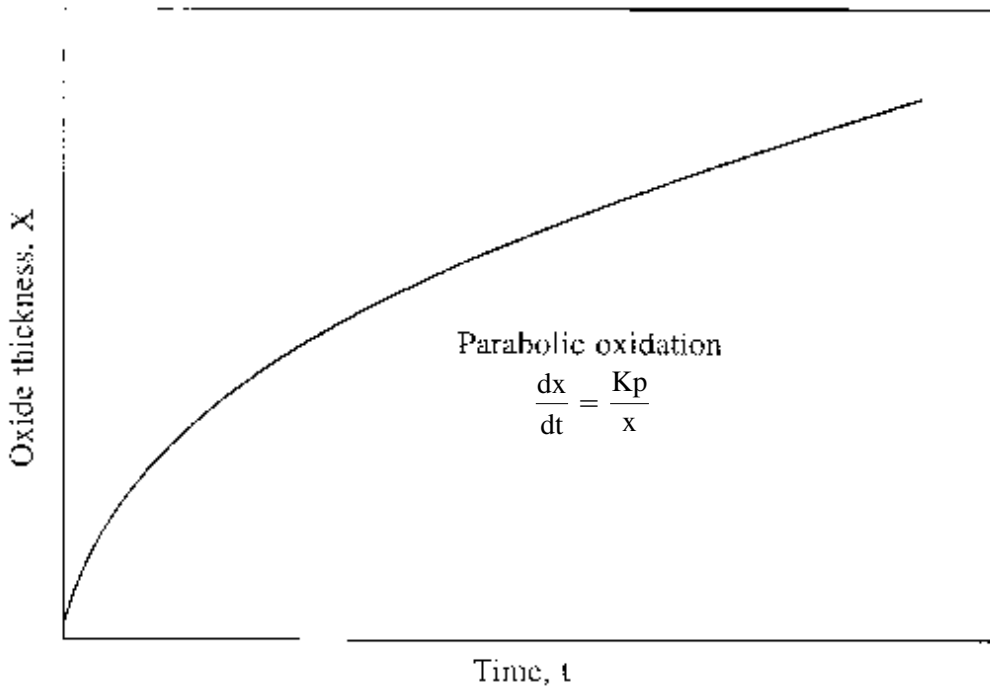


FIGURE 6.3 The kinetics of parabolic oxidation.

defect structure and diffusion need a sound mathematical background. An in-depth study of transporting species through oxide layers requires a sound knowledge of modeling a process and computer expertise to solve differential equations. But to obtain a viable model of the process, experiments are needed to generate data on the kinetics of the oxidation reactions, characterization of the corrosion products formed during oxidation, and information on the structure of the interface between oxide and the substrate metal or alloy. The most important oxidation data needed are the kinetics or rate laws for the oxidation process. Experimental techniques to determine oxidation kinetics are discussed first. This is followed by a brief discussion on the techniques utilized for scale characterization.

6.5 MEASUREMENT OF OXIDATION KINETICS

The most important method of measuring oxidation kinetics is the gravimetric method. The principle of the gravimetric method is to measure weight change due to oxidation as a function of time. A simple gravimetric technique involves the exposure of a known area of the sample in a furnace, followed by measuring the weight change at definite intervals of

time, using a sensitive balance. In this technique, the experiment is interrupted each time the weight change is measured. As a result, the sample experiences various thermal cycles each time it is cooled and heated again. This causes some changes in the scale behavior, such as formation of cracks, spallation of scale, etc. However, the advantage is that many samples can be exposed at one time and their weight changes can be measured simultaneously during each interruption. Hence, a number of alloys with various compositions, or a single alloy with different treatments, can be studied very quickly. One of the main limitations of this technique is that a significant change in the scale growth process can occur as a result of intermediate interruptions. This is due to the thermal stresses arising during cooling and heating at each interruption. The scale formed during the initial period may spall or crack due to thermal cycling. Therefore, an alternative way is to measure the weight change continuously during oxidation. This is conducted using a special type of thermobalances which continuously record the change in weight while the sample is heated.

Thermogravimetry is the measurement of mass change as a function of temperature or mass change as a function of time at a constant temperature. The former is known as a dynamic mode of thermogravimetry, where from a single curve of mass

change as function of temperature, one can get information about the activation energy of the reaction. This technique is more common for chemical or decomposition reactions and is usually not employed for oxidation studies. Oxidation studies are usually carried out by exposing the specimen in a furnace at a fixed temperature and measuring the weight change as function of time. This is called isothermal oxidation. Many such isothermal oxidation curves are generated at various temperatures and then utilized to determine the activation energy of the oxidation reaction.

In addition to isothermal tests, sometimes oxidation tests are carried out under cyclic conditions of temperature. In these tests, the sample is exposed to a cyclic program (i.e., exposure for a fixed duration of time at a high temperature, followed by cooling with a specific cooling rate; holding it for a certain time period; reheating and holding it at high temperature under similar conditions). Such tests are carried out for a number of cycles ranging from 10–20 to 100–200. Weight changes are measured after each cycle. Such tests are known as cyclic oxidation tests, and they give the information about the stability of the oxide scale under severe oxidation conditions (not only of heating at a particular temperature but also under the effect of thermal stresses), such as those generated during thermal cycles.

A *thermobalance* consists of a sensitive balance through which a sample is hung in a reaction chamber that is exposed to a furnace. In addition to these essential components, a sophisticated balance can have a vacuum system, so that oxidation is carried out in a vacuum or at various pressures, and a gas inlet and outlet system to carry out the tests in different atmospheres. It is also possible to have special modifications of the balance to carry out tests even in corrosive atmospheres, such as water vapor, steam, sulfur dioxide, chlorine, etc. A schematic of a bottom-loading balance is shown in Fig. 6.4.

Among the other methods of measuring oxidation kinetics are oxygen consumption rate measurement, the ellipsometric technique, solid state oxygen sensors, metallographic techniques of measuring scale thickness, the interference color technique, etc.

6.6 IDENTIFICATION AND CHARACTERIZATION OF SCALES

Reaction kinetics gives information regarding how fast the oxidation will occur or how long a metal will

survive in an atmosphere at a particular temperature. If the aim is to understand the mechanism of oxidation so that the oxidation behavior of the metal or alloy can be improved, then detailed information about the scale constituents, scale structure, and composition must be known. There are now a number of techniques that can be used to obtain this information.

The simplest techniques are visual and stereo-microscopic analysis, which give information about the scale cracks, spallation, exfoliation, etc. The scale is then subjected to either X-ray diffraction analysis to identify the various oxides formed during oxidation, or subjected to Secondary Ion Electron Microscopy (SIMS) coupled with Energy Dispersive X-ray Analysis (EDAX) for surface topography, surface morphology, and surface composition. Information such as nodule formation, convoluted layers, and type of oxide (whether it is crystalline or amorphous) can be obtained from SEM. Analysis of scale cross-section using optical microscopy, SEM/EDAX gives information about the number of oxide layers, scale adherence, interlayer scale adherence, and distribution of various elements in the scale.

Electron Spectroscopy (AES)/Electron Spectroscopy for Chemical Analysis (ESCA), and Scanning Ion Mass Spectrometry (SIMS) are used to gather information about the first few layers of the scale formed. Oxide structure and its concentration, along with depth profiles, can be obtained using these techniques. Another technique that is quite important is the Acoustic Emission Technique (AET), which is used to gain information on scale spallation, scale adherence or, in general, about the integrity of scale and coatings. It is based totally on the acoustics of the process during oxide growth and, therefore, the information obtained is complementary to the information obtained from kinetics and the other analyzing techniques [1].

6.6.1 Role of Defect Structure and Diffusion in Oxide Scales

When a metal is exposed to an oxidizing environment, an initial thin film of oxide is formed first, which covers the whole surface. As the oxide layer continues to grow, either the metal ions from the substrate or oxygen ions from the atmosphere must pass through the initial thin film. Transport of the ions through the oxide film usually occurs via solid state diffusion, which, in turn, depends upon the imperfections in the solid or its defect structure.

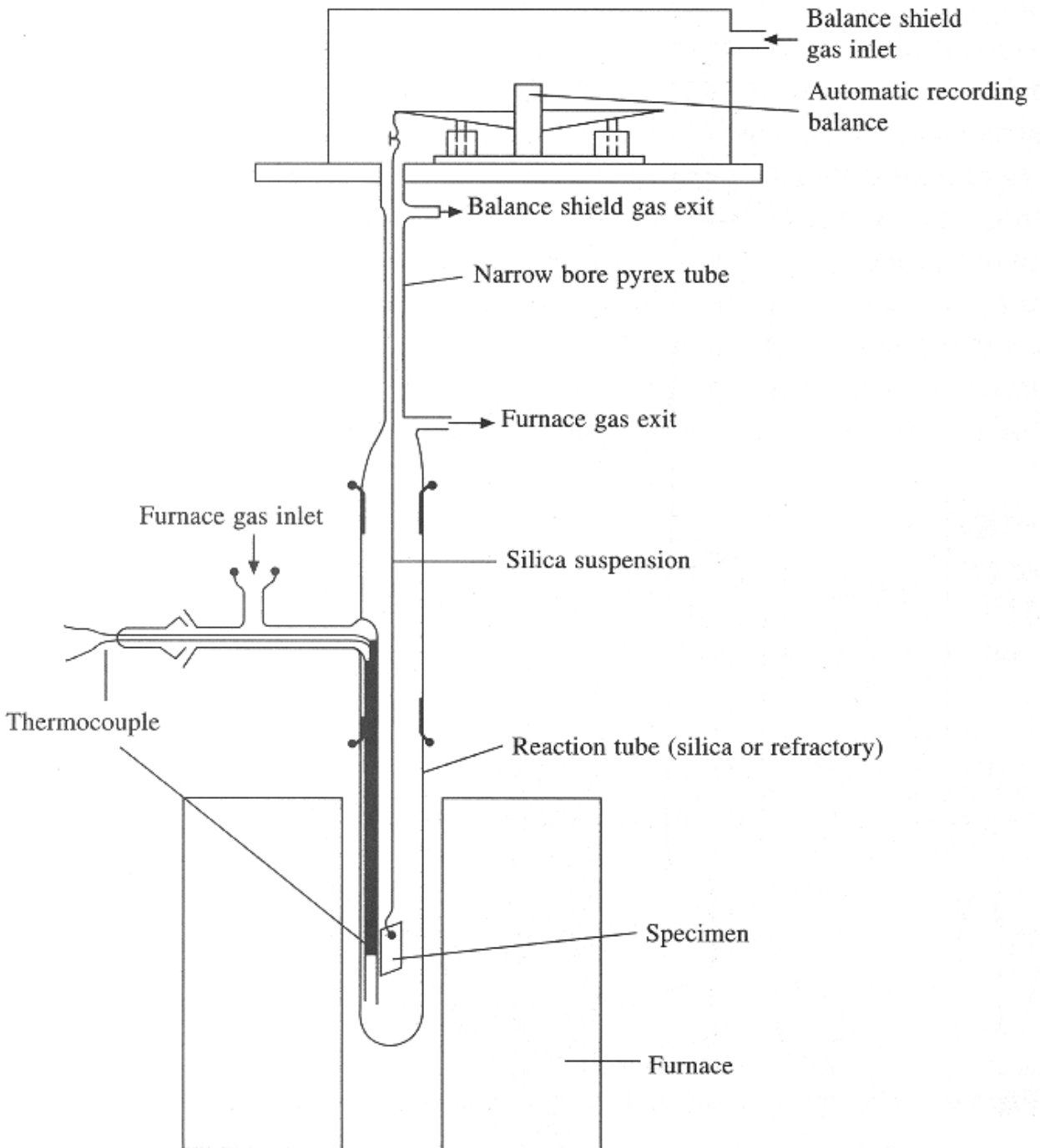


FIGURE 6.4 Schematic of a bottom loading balance.

Knowledge of the defect structure is important, therefore, to understand the growth of the oxide scales.

The most common imperfections in oxides are vacancies, interstitials, and impurities. Diffusion of

ions through oxide is generally favored by these defects. Fig. 6.5 shows various diffusion mechanisms generally found in solids, viz.: (a) exchange, (b) ring, (c) interstitialcy, (d) interstitials, and (e) vacancy mechanisms. These defects are termed as vol-

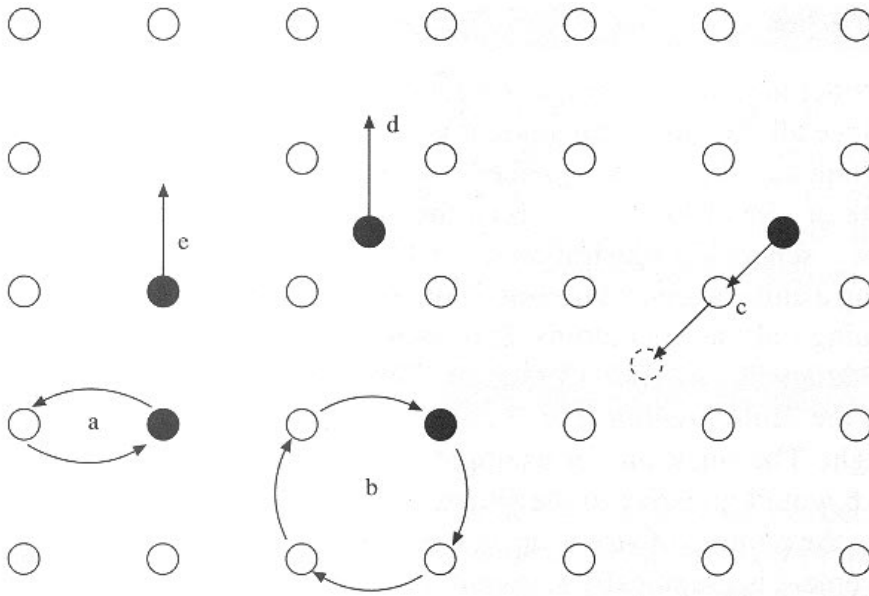


FIGURE 6.5 The various displacement mechanisms of diffusion: (a) place exchange; (b) ring mechanism; (c) interstitial mechanism; (d) interstitial atom movement; and (e) vacancy mechanism.

ume defects or lattice defects; they require high activation energy and usually occur at relatively higher temperatures. The other more common defects are grain boundaries, cracks, or surface diffusion. These are relatively easy paths, called short circuit diffusion paths, and are generally favored at lower temperatures.

The diffusion coefficient D_v (the subscript v represents volume diffusion) of silver is about five orders of magnitude lower than that of grain boundary diffusion (D_{gb}). Similarly, the activation energy for the latter is about half that of the former. The lower value of activation energy explains why short circuit diffusion plays an important role only at temperatures below three-quarters of the absolute melting point. Since the total grain boundary area is much smaller than the overall area of a polycrystalline alloy, the material transported by grain boundaries will also be much less than that transported by volume diffusion. A rough estimate shows the ratio of the grain boundary area to the overall area as 10^{-5} . Thus, if a comparable amount of material is to be transported by grain boundaries and bulk diffusion, then the ratio of D_{gb}/D_v should be about 10^5 . At high temperatures, this ratio is less than this value, but with a decrease in temperature, D_{gb} decreases much less than D_v , because of a much lower value of activation energy for the grain boundary diffusion.

6.7 WAGNER HAUFFE RULES

Depending upon the defects in an oxide, they can be classified into n or p type oxides :

6.7.1 n -Type Oxides

Addition of foreign cations of a valence higher than the cations of the parent oxide, a nonstoichiometric n -type oxide ($M_{1+x}O$ or MO_{1-x}) will decrease the concentration of oxygen vacancies in MO_{1-x} , or the concentration of interstitial metal ions in an oxide $M_{1+x}O$. This will then result in decrease in the conductivity in the oxide, leading to lower oxidation rates. Conversely, additions of cations of a lower valency would increase the corresponding defects and, hence, the conductivity, leading to higher oxidation rates.

Examples. Addition of Cr^{+3} to ZnO will reduce the number of Zn interstitials and, hence, lower its oxidation rate, while addition of Li^{+1} will increase the oxidation rate due to an increase in Zn interstitials.

6.7.2 p -Type Oxides

For p -type oxides ($M_{1-x}O$ or MO_{1+x}), addition of cations of higher valence increases the concentration

of vacancies in $M_{1-x}O$, or the concentration of interstitials in MO_{1+x} . In the same way, cations of a lower valence would decrease the corresponding defect concentrations.

Example. Addition of trivalent Cr ions in FeO would increase the concentration of iron vacancies and would, therefore, cause an increase in the conductivity and, hence, the oxidation rate. It is seen that the addition of small amounts of Cr always increases the oxidation rate of iron at first. Only when a higher level of Cr (beyond the doping limit) is present, does it help in reducing its oxidation rate.

Corresponding rules for the addition of foreign anions have also been set up. A good example is the change in the oxidation rate of zirconium when the environment is shifted from pure oxygen to air. Air contains nitrogen, which replaces some of the oxygen anions. ZrO_2 is *n*-type oxide, having oxygen vacancies. Replacement of higher valent N^{3-} with divalent O^{2-} would increase the oxygen vacancies and, hence, the oxidation rate. It is observed that oxidation of Zr is higher in air than in pure oxygen. Table 6.1 classifies the various oxides, sulfides, and nitrides into *p*-type, *n*-type, or amphoteric semiconductors.

To know the mechanism of oxidation, it is necessary to find the dominating transporting species. Two methods, based upon the diffusion of ionic species, are marker studies and oxygen tracer studies described below.

6.8 MARKER TECHNIQUE

In this technique, inert metal in the form of either a small wire or as metal deposited by plating or other deposition methods is placed at the original metal surface prior to the start of the oxidation test. After oxidation, the position of the marker is used to ascertain the mechanism of diffusion. In case the mechanism is dominated by inward diffusion, the marker

after oxidation will be located at the oxide/gas interface. If the scale grows by outward movement of metal ions, it will be located at the metal/oxide interface. If the marker is found in the scale, the growth mechanism involves both inward diffusion of oxygen ions and outward diffusion of metal ions. The reliability of this method can be influenced by the marker element, which is an outside body and can interfere with the growth process. In addition, sometimes the marker thickness is more than the scale thickness, and the location of markers after an oxidation test may not be accurate.

Currently, methods based on tracer diffusion are more reliable and provide reliable information, although interpretation is generally difficult. Tracers involving metal ions are also employed and may be easier to use. But not all metals have stable radioisotopes. Thus, an exchange during gaseous oxidation has become more practical and easy. The technique involves a two-stage oxidation involving ^{18}O tracers.

6.9 OXYGEN TRACER TECHNIQUE

The use of ^{18}O tracers to ascertain the mechanism of diffusion of an ionic species during the oxide growth process has become a successful method. The double oxidation technique is used to identify the diffusion processes involved. The alloy is sequentially oxidized, first in natural oxygen and then in oxygen gas containing ^{18}O as tracers. The oxide growth during the natural oxygen oxidation is referred to as the old oxide, while the oxide grown during tracer oxidation is referred to as the new oxide.

The position of the new oxide growth is determined from the concentration profile of the tracer across the oxide scale, which is determined either by Secondary Ion Mass Spectroscopy (SIMS) or by proton activation techniques. The oxide growth process could be either inward diffusion of oxygen ions or outward diffusion of metal ions. In several oxides, the mechanism involves diffusion of both

TABLE 6.1 Classification of Electrical Conductors: Oxides, Sulfides, and Nitrides

| | |
|--|---|
| Metal-excess semiconductors (<i>n</i> -type) | BeO, MgO, CaO, SrO, BaO, BaS, ScN, CeO ₂ , ThO ₂ , UO ₃ , TiO ₂ , TiS ₂ , TiN, ZrO ₂ , V ₂ O ₅ , VN, Mo ₂ O ₅ , Ta ₂ O ₅ , MoO ₃ , WO ₃ , WS ₂ , MnO ₂ , Fe ₂ O ₃ , ZnO, CdO, CdS, Al ₂ O ₃ , Tl ₂ O ₃ , In ₂ O ₃ , SiO ₂ , SnO ₂ , PbO ₂ |
| Metal-deficit semiconductors (<i>p</i> -type) | UO ₂ , Cr ₂ O ₃ , MgCr ₂ O ₄ , FeCr ₂ O ₄ , CoCr ₂ O ₄ , ZnCr ₂ O ₄ , WO ₂ , MoS ₂ , MnO ₂ , Mn ₃ O ₄ , Mn ₂ O ₃ , FeO, FeS, NiO, NiS, CoO, Co ₃ O ₄ , PdO, Cu ₂ O, Cu ₂ S, Ag ₂ O, CoAl ₂ O ₄ , NiAl ₂ O ₄ , GeO, SnS, Sb ₂ S ₃ |
| Amphoteric conductors | TiO, Ti ₂ O ₃ , VO, Cr ₂ O ₃ (>1,250°C), MoO ₂ , FeS ₂ , RuO ₂ , PbS |

ions. Such identification is not that difficult by the tracer method. However, as the tracer diffuses down the grain boundaries, it exchanges with ^{16}O , already existing in the grains. To get any quantitative information from the tracer concentration profiles, it is necessary to model the process of inward diffusion of tracer along grain boundary with exchange. The advantage of a quantitative model is that the grain boundary and the lattice diffusion coefficients are obtained from the shape of the tracer concentration profiles. The effect of structural parameters such as oxide grain size on tracer profiles can also be evaluated. The most important information obtained is regarding inward or outward growth.

In case the scale growth is a combination of both mechanisms, a simple mass balance test can be used to separate the two processes. In the model, the shape of the tracer concentration profile depends upon three parameters: grain size, grain boundary diffusion coefficient D_{gb} , and lattice diffusion coefficient D_{v} . By choosing appropriate values for the three parameters, a family of curves can be generated, which define a range of ^{18}O concentration pro-

files, which are quantitatively compatible with the mechanism of inward diffusion of oxygen. Conversely, if an experimental tracer profile is given, it should be possible to determine the values of the three parameters. Fig. 6.6 shows a schematic of ^{18}O profiles for several transport mechanisms. The new oxide is shown by the dotted area, and the old oxide by a region without shading. In an outward growth mechanism, the new oxide will appear next to the oxide/gas interface, without disturbing the old oxide formed under natural oxygen (Fig. 6.6a). In case the mechanism is dominated by inward transport of oxygen ions, the new oxide will appear next to the metal/oxide interface, while the old oxide at the gas/oxide interface appears as shown in Fig. 6.6b. In these ideal cases, no exchange of tracers occurs with natural oxygen. When exchange occurs, the inward diffusion profile is slightly modified to account for this exchange process and is shown in Fig. 6.6c. Finally, if the diffusion mechanism is a combination of the outward movement of metal ions and the inward movement of oxygen ion the profile appears as shown in Fig. 6.6d.

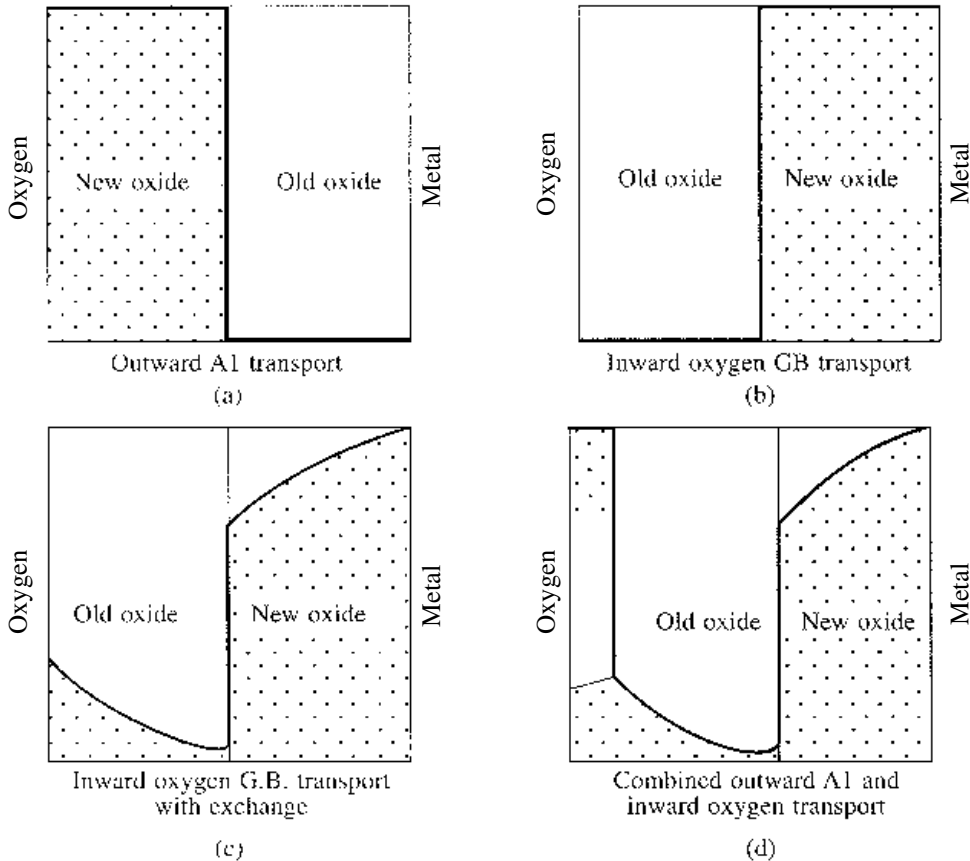


FIGURE 6.6 Oxygen tracer profiles of oxides formed.

6.10 INITIAL OXIDATION OR THIN LAYER OXIDATION

The study of initial oxidation is the most important, as it is the first step of metal reaction when the metal is exposed to an aggressive environment. At high temperatures, the reaction is so fast that it is difficult to estimate the gas/metal interactions in the initial stages. Thus, in order to know the mechanism of oxidation at the initial stages, experiments are conducted at either low temperatures or low pressures at high temperatures. In both these cases, the high temperature oxidation process is viewed at a slow speed in a manner similar to observing a movie in slow motion. The rate of reaction and, hence, the kinetics are quite different under these conditions and sometimes match the kinetics of noble metals, which usually exhibit very low oxidation rates.

The nature of the oxygen species adsorbed on a metal has been studied extensively using different analytical techniques, such as infrared (IR), electron spin resonance (ESR), XPS, LEED, and AES. Oxygen adsorbed on a metal or on a stable oxide surface at room temperature converts it to several subspecies. On the metal, a charged species exists, as indicated by surface potential charges. On the oxide surface, both neutral O_2 and O as well as ionic species O^{-1} , O^{2-} , and O^{3-} may exist alone or in equi-

librium with each other. Molecular oxygen has been found on Pt(111) at 120 °K. Molecules dissociate into atoms at higher temperatures, illustrating the activated nature of chemisorption. On copper (100) and (111) surfaces, chemisorbed molecular oxygen and weakly bonded atomic oxygen were detected between 100 °K and room temperature, while strongly chemisorbed atomic oxygen was identified at room temperature.

Most of the theories put forward by several researchers describe low temperature oxidation in terms of logarithmic kinetics. The kinetic law is either of the direct logarithmic or inverse logarithmic type. The first theory of low temperature oxidation was put forward by Cabrera in 1949. Since then, this theory has been elaborated by others, and several models have been proposed. A comprehensive list of these theories, compiled by Kofstad, is reproduced in Table 6.2. We will first explain the most simplified theory proposed by Cabrera and Mott. Most of these theories start after the oxygen has been adsorbed on the clean metal and a monolayer or a few layers of oxide have formed. As discussed previously, this step follows a linear behavior and will be treated separately afterwards.

In the Cabrera and Mott Theory of Inverse Logarithmic Kinetics, the following assumptions were made:

TABLE 6.2 Summary of Theories for Initial Oxidation and Oxide Scale Formation [2]

| | |
|-----------------------------|---|
| Kinetics, rate equation | Rate-determining processes, etc. |
| Linear | Adsorption on clean metal surfaces with constant sticking efficiency |
| Increasing reaction rate | Adsorption on clean metal surfaces with increasing sticking coefficient. Simultaneous adsorption and oxide growth |
| Logarithmic | Adsorption. Elovich equation. Increasing activation energy with gas uptake |
| Inverse Logarithmic | Electric field-induced transport of ions through thin oxide films |
| Logarithmic | Electric field-induced transport of ions through thin oxide films; rate determining transport of electrons |
| Logarithmic linear, etc. | Electric field-induced transport of ions through thin oxide film |
| Parabolic | Electric field-induced transport of metal ions through thin oxide films |
| Cubic | Electric field-induced transport of metal ions through thin <i>p</i> -conducting oxide films |
| Logarithmic | Electron flow controlled by space charge in oxide film |
| Logarithmic, x^n _ t | Coupled diffusion homogenous field approximations |
| Logarithmic | Adsorption/chemisorption model |
| Logarithmic | Diffusion along pores, mutual blockage of pores |
| Asymptotic | Diffusion along pores, self blockage of pores |
| Logarithmic, Asymptotic | Diffusion along pores, simultaneous self blockage and mutual blockage of pores |
| Logarithmic | Cavity formation |
| Logarithmic, etc. | Nonisothermal process |
| Logarithmic | Nucleation and growth increasing activation energy |
| Sigmoid, pseudo-logarithmic | Lateral growth of oxide crystal coupled with linear, parabolic growth normal to surface |
| Quasi-cubic | Dissolution of oxygen in metal with a concentration-dependent diffusion coefficient |

- Oxide growth is by cation movement
- Oxygen molecules dissociate on the oxide surface, giving rise to traps with an energy eV below the fermi level of the metal.
- The density of such traps is sufficient to provide enough electron levels to give a potential drop V across the film and, thus, a field F , such that $F = V/x$. It is known from changes in surface potential that a field often exists across an oxide film growing at low temperature.

The activation energy W for the movement of a cation in the oxide drops to $W - 1/2 qaF$, where q is the charge of the ion, a is the jump distance, and F is the field. An alternative assumption is that W is the energy needed for accommodating a metal atom into oxide. The growth rate can be written as

$$dx/dt = Na^4n \exp [-(W-1/2 qaV/x)/kT], \quad (6.11)$$

where N is the number of mobile ions per unit volume in the oxide and n is a phonon frequency. On integration, this leads to an inverse logarithmic law:

$$1/x = (A + C \log t),$$

where A and C are constants.

According to Ely and Wilkinsin, irrespective of the mechanism of movement of ions, activation energy will be of form

$$W_A = W_0 + \mu x, \quad (6.12)$$

where μ is a constant that depends upon the film structure.

As a matter of fact, many oxides formed at low temperature are of amorphous and glassy structures. Depending upon their bond strength, there have been two main categories in which these oxides can be divided: network formers and network modifiers. Network formers have higher bond strength than network modifiers. An example of a network former is SiO_2 , which has a three-dimensional network structure having a five- or six-member ring structure (Fig. 6.7).

An example of a network modifier is Na_2O when added to SiO_2 . This is shown in Fig. 6.8. The non-bridging oxygen atoms (due to the presence of Na_2O) tend to weaken the network structure of SiO_2 . In such a structure, no large channels are likely to form for anion transport and, since the cations are weakly bound, their transport is expected in the network modifiers. Thus, it is amply proved by the

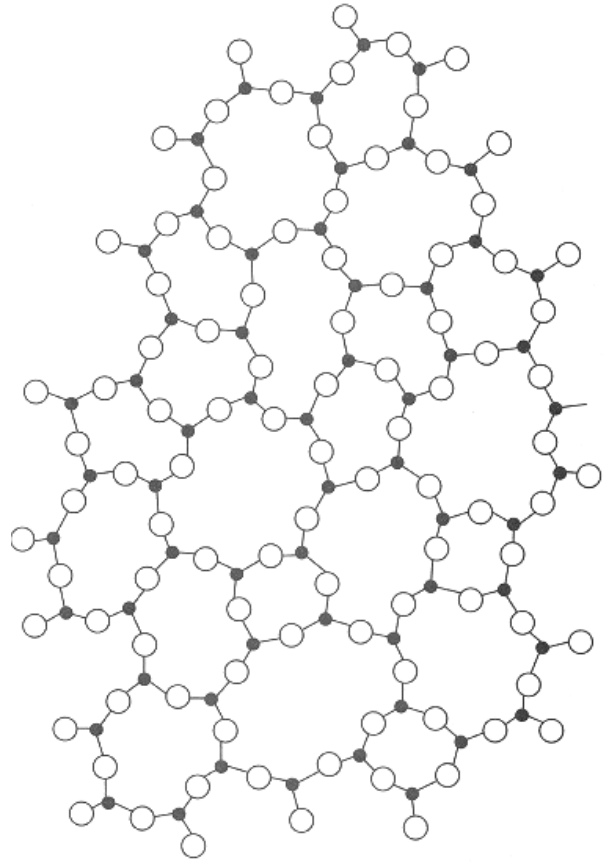


FIGURE 6.7 Schematic of SiO_2 network structure.

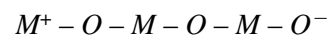
above discussion that the oxide structure plays an important role in ionic movement. Now, if one uses the expression of activation energy to determine the rate of oxidation:

$$dx/dt = C_2 \exp [-(W_0 + \mu x)/kT], \quad (6.13)$$

which, on integration, gives a direct logarithmic law,

$$x = A \log t + B.$$

Ely and Wilkinsin described low temperature oxidation in terms of the movement of a single ion, cation, or anion by a process known as *place exchange mechanism*. This simply involves the interchange of two ions over a spacing of a few angstroms, particularly in non-crystalline structures. It is possible that the rearrangement of the whole chain of atoms can occur simultaneously:



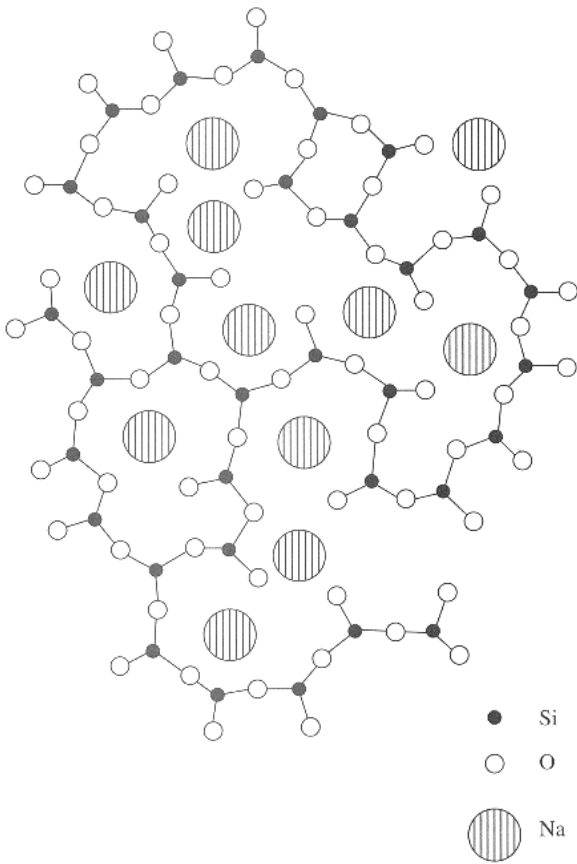


FIGURE 6.8 Schematic of network modifier structure.

A small activation energy is required for place exchange. However, this increases with an increase in the thickness of the oxide, thus resulting in a decrease in the rate, leading to logarithmic kinetics. Unlike the case of the Cabrera-Mott model, this activation energy is not limited to movement of any specific ion.

6.10.1 Mott Theory of Direct Logarithmic Law

The direct logarithmic law during the initial oxide growth process has also been explained by tunneling of electrons from the metal to the oxide as the rate-determining step. In principle, growth at low temperatures could be limited by electron or ion penetration. In the former case, Mott suggested the following equation for the rate of electron tunneling:

$$dx/dt = C_3 \exp[-2x(2mU)^{1/2}/h], \quad (6.14)$$

where C_3 is 10^7 cm/sec and U is the barrier height.

There is however, no evidence of growth limited by electron tunneling. Initially, it was thought that at very thin oxide scales, perhaps the migration of cations (as explained by the Cabrera and Mott theory) appears fine, but as the oxide scale gets thicker, this migration could be difficult. Hence, at a limiting thickness it is possible that the ion migration shifts to the electron tunneling process. Mott calculated the limiting thickness and found it to be approximately 30 \AA .

6.10.2 Thick Layer Oxidation—Wagner's Theory

When a metal is exposed to a high temperature, the first monolayer of the oxide is formed instantly. However, after the formation of the initial oxide layer, further growth process requires transport of either metal ions from the substrate or oxygen ions from the gaseous side. The former move from the metal/oxide interface to the oxide/gas interface, while the latter move from the gas/oxide interface to the metal/oxide interface. The transport of these species is controlled by the diffusion laws, and the diffusion is facilitated by the defect structure of the oxide. For a thicker scale, the ionic species have to travel a longer distance; whereas, the transport distance is shorter for thinner scales. Kinetics are generally parabolic in nature. Wagner's model for thick oxide layers begins with following assumptions:

1. The oxide scale is compact and adherent.
2. Migration of charged species, ions (cations or anions), electron, or electron holes is the rate-controlling process.
3. Thermodynamic equilibrium is established at both the metal/scale and scale/gas interface.
4. The oxide is more or less stoichiometric—there is very little deviation from stoichiometry.
5. Oxygen solubility in the metal may be neglected.

Because the thermodynamic equilibrium condition is established at both interfaces (metal/scale and scale/gas), the activity gradients of both metal and oxygen result across the scale (Fig. 6.9). Consequently, metal ions and oxygen ions will tend to migrate across the scale in opposite directions. Because the ions are charged, this migration will cause an electric field to be set up across the scale, moving from the metal side to atmosphere. The net result of the migration of ions (+ve or -ve) and electrons or electron holes, therefore, is to be balanced for an electroneutrality condition. As charged particles,

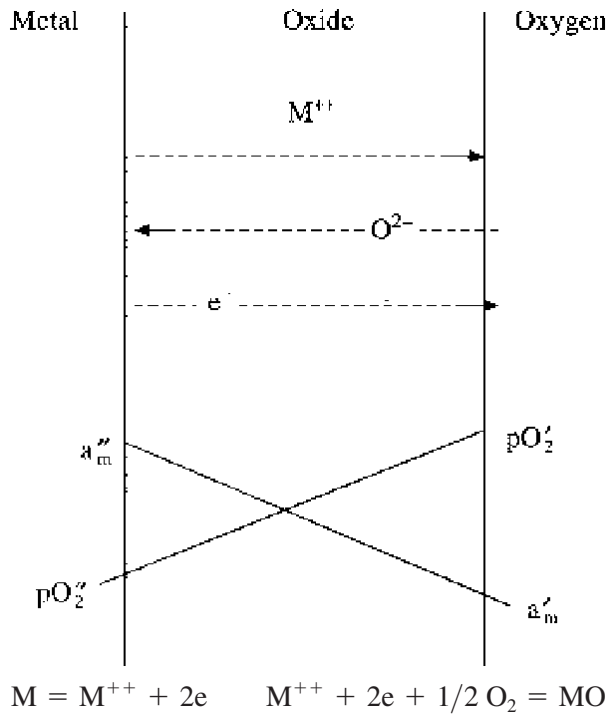


FIGURE 6.9 Schematic of scale formation according to Wagner's model.

ions will respond to both chemical and electrical potential gradients that, together, provide the net driving force for ionic migration. Based upon these considerations, the parabolic rate constant of a thick oxide scale controlled by cation movement can be given as

$$Kp = 1/Z^2 a F^2 C_A \int \sigma_a \sigma_e / \sigma_a + \sigma_e d\mu_m, \quad (6.15)$$

where Kp is the parabolic rate constant, Za is the charge on cations, σ_a and σ_e are the conductivities of cations and electrons, respectively, F is Faraday constant and μ_m is the chemical potential across the oxide scale. This can further be simplified by relating conductivities with diffusion coefficients and expressing chemical potential in terms of oxygen partial pressures as given below:

$$Kp = 1/RT \int D_M \ln p(O_2). \quad (6.16)$$

6.11 OXIDATION OF PURE METALS

It is well known that most metals, with exception of the noble metals, form tarnishing layers of oxides, even at room temperature. Their reaction with oxy-

gen is expected to be very rapid at high temperatures. It is very difficult to classify metals into various groups on the basis of their interaction in oxidizing environments, due to vast differences in terms of their mechanisms of oxidation, type of scale formed, etc. Perhaps the simplest classification would be in terms of their oxidation resistance. Noble metals, such as platinum, gold, palladium, etc., can be grouped into one class. They are the most resistant to oxidation.

Another group consists of transition elements, such as iron, nickel, cobalt, etc., which have moderate oxidation resistance but are the base elements for important alloys for high temperature applications. Alkali and alkaline-earth elements are the most reactive elements and, therefore, are not important for discussion in terms of their oxidation resistance.

Another method used to classify metals is in terms of the temperature of application: those used at low temperatures, such as copper, aluminum, zinc, etc.; those used at intermediate temperatures, such as iron, nickel, and cobalt; and those used at high temperatures, such as the refractory metals tungsten, molybdenum, etc., as well as a few noble metals, such as platinum and palladium. However, except at low temperatures, the use of pure metals is very limited at higher temperatures (except for platinum and palladium used as heating elements or thermocouples). Many refractory elements are used at high temperatures, but their use is limited to only reducing environments or in a vacuum.

Metals can also be classified in terms of their tendency to dissolve oxygen. In this classification, elements such as titanium, tantalum, zirconium, and hafnium can be considered. They dissolve considerable amounts of oxygen and, hence, make the oxidation process more complicated. Another way of classification may be in terms of the type of scale formed, whether single or multiple. Nickel is the best example to illustrate a single oxide-forming metal.

The oxidation behavior of the metals is highly dependent upon the physical properties of the metal, such as the melting point, structure, and the molar volume. For high temperature service, the melting point of the metal dictates the limits of practical use and structural changes that occur during heating and cooling, which affect the oxide adherence.

Among various metals, oxidation of nickel is perhaps the simplest. It forms a single oxide, NiO, when oxidized at high temperature. Oxidation behavior is governed by the defect structure of NiO, which is *p*-type and, hence, scale growth occurs by outward diffusion of nickel ions. If there are some impurities

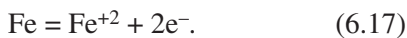
in nickel (e.g., carbon), a two-layered NiO scale is formed—an inner compact NiO formed by inward diffusion of oxygen and an outer loose layer formed by outward diffusion of nickel ions.

Many other important metals, such as iron and cobalt, form multilayer oxides. Iron oxidation forms a scale, which is a mixture of three oxides—wustite/FeO; magnetite/Fe₃O₄, and haematite/Fe₂O₃. The composition of the scale varies with temperature and with the oxygen partial pressure. Wustite does not form below 570 °C, and the scale consists of magnetite and hematite below this temperature. Above 570 °C, the scale consists of all three oxides in the following sequence: FeO next to the metal; Fe₃O₄ next to FeO, and Fe₂O₃ as the outermost layer. This gradation arises because FeO is metal-rich and requires the lowest oxygen partial pressure, while Fe₂O₃ is oxygen-rich and requires a higher partial pressure of oxygen to form.

Wustite/FeO is a *p*-type of semiconductor, with metal vacancies. It exists over a wide range of stoichiometry, from Fe_{0.95}O to Fe_{0.88}O at 1,000 °C. With such high cation vacancies, the mobility of cations and electrons via metal vacancies and electron holes is extremely high. The magnetite/Fe₃O₄ has inverse spinel structure (i.e., all the Fe⁺² ions and half of the trivalent Fe⁺³ ions are occupied by octahedral sites, and the other half of the trivalent ions Fe⁺³ occupy tetrahedral sites). Defects occur on both sites and, consequently, iron ions may diffuse over both tetrahedral and octahedral sites. The oxide has very little deviation from stoichiometry, especially at high temperatures. It however, behaves as a *p*-type semiconductor, with metal ions moving outwards.

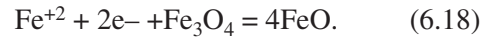
Haematite/Fe₂O₃ exists in the α and β forms, which are rhombohedral and cubic in structure respectively. Generally, at $T > 400$ °C, Fe₃O₄ is oxidized to α -Fe₂O₃. In the rhombohedral form, the oxygen ions exist in a close-packed hexagonal arrangement with iron ions in the interstices. With such a structure, it may be expected that iron ions would be mobile. However, experimental results have shown disorder on an anion sublattice only, from which only the oxygen ions are expected to be mobile. In general, Fe₂O₃ behaves as an *n*-type semiconductor, but there is some evidence of the possible migration of cations, also.

At the iron/wustite interface, iron ionizes in the following way:



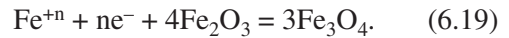
The iron ions and electrons migrate outwards through the FeO layer over iron vacancies and electron holes, respectively. At the wustite/magnetite in-

terface, magnetite is reduced by iron and electrons according to the following reaction:

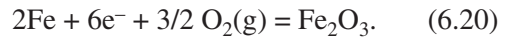


Iron ions and electrons surplus to this reaction proceed outward through the magnetite layer, over iron vacancies on the tetrahedral and octahedral sites and over electron holes and excess electrons, respectively.

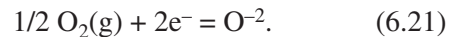
At the magnetite/haematite interface, magnetite is formed according to the reaction



The value of *n* is two and three for Fe⁺² or Fe⁺³ ions, respectively. If the iron ions are mobile in the haematite, they will migrate through this phase over iron ion vacancies V_{Fe} together with electrons, and new haematite will form at the Fe₂O₃/gas interface according to the following reaction:



At this interface, oxygen also ionizes according to the reaction



If the oxygen ions are mobile in the haematite layer, the iron ions and electrons in excess of the number required for the reduction of haematite to magnetite, will react with oxygen ions, diffusing inwards through the Fe₂O₃ layer over oxygen vacancies forming new Fe₂O₃ according to reaction $2\text{Fe}^{+3} + 3\text{O}^{2-} = \text{Fe}_2\text{O}_3$. The mechanism of three-layer oxide on pure iron above 570 °C is shown in Fig. 6.10.

Chromium is an important metal that is used as an alloying element in all stainless steels and superalloys. It is responsible for creating a passive layer at low temperature and a protective chromia scale at high temperatures. The chromium oxide (Cr₂O₃) scale, so formed, protects most of the high temperature alloys from further oxidation and sulfidation. However, this protection is viable only up to a temperature of 900 °C, above which the chromia scale starts destabilizing due to the conversion of Cr₂O₃ into CrO₃. CrO₃ is volatile and, hence, is unable to protect the substrate. Therefore, at and above 900 °C it is advisable to not use stainless steels or other Cr-based superalloys, especially in high partial pressure of oxygen.

Another class of important metals comprises titanium, zirconium, hafnium, tantalum, and niobium.

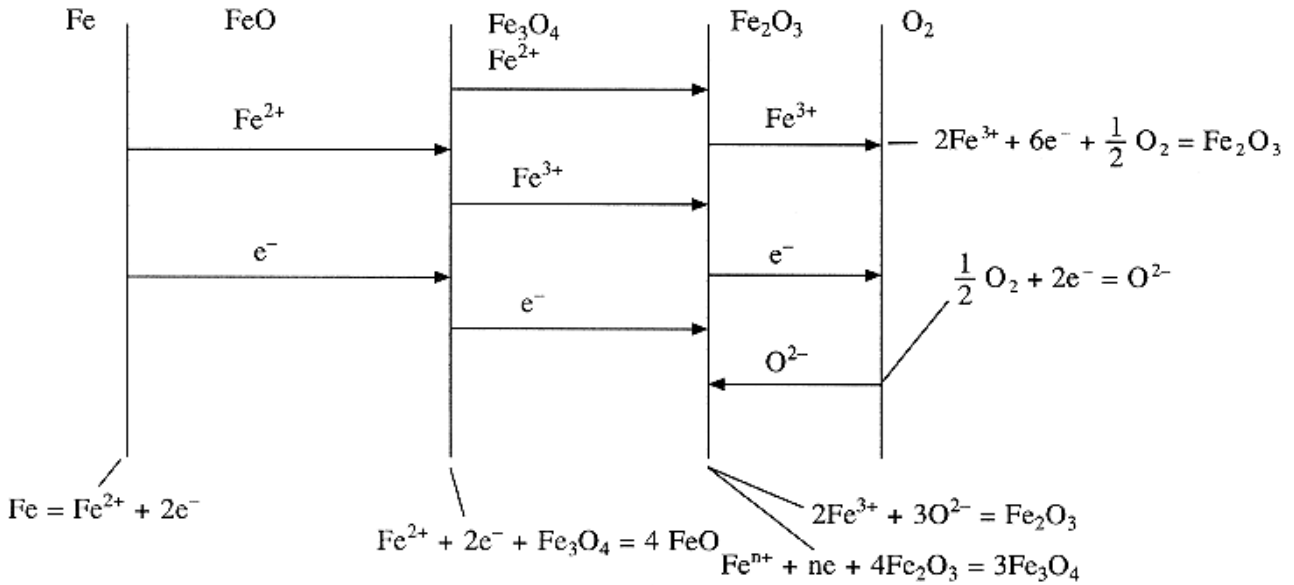


FIGURE 6.10 Mechanism of oxidation of iron showing the diffusion of various ionic species.

These metals differ from those described in the preceding paragraphs in that upon oxidation they not only form an outer oxide scale but also absorb a lot of oxygen. Thus, while calculating the oxidation rate, one should measure the weight change due to scale formation, as well oxygen diffused into the metal. The dissolution of oxygen in the metal is deleterious, as it can result in internal oxide formation and sometimes ordering of the structure.

Oxidation of titanium is quite complex. As per the phase diagram shown in Fig. 6.11, there are several stable oxides, such as Ti₂O, TiO, Ti₃O₃, Ti₃O₅ and TiO₂. Thermodynamically, one would expect the oxide scale to consist of several layers of different titanium oxides; however, oxidation in oxygen at near-atmospheric pressure and below about 1,000 °C, only TiO₂ is formed. But at higher temperatures, particularly at reduced oxygen pressures, lower oxides are expected to be formed.

Titanium exists in two allotropic modifications. The low temperature α form has an *hcp* structure, and the high temperature β form has a *bcc* structure. The transition between the two phases occurs at 882 °C. The solubility of oxygen in the α phase amounts to about 30 at.% and varies little with temperature. The solubility of oxygen in the β phase increases with temperature and is about 8 at.% at 1,700 °C. The α phase is stabilized by oxygen dissolution. Oxidation kinetics of titanium vary with temperature and time. Fig. 6.12 summarizes the various rate laws followed by titanium at various temperatures. Oxidation ki-

netics follow logarithmic rate law below 400 °C, during which a thin oxide layer of TiO₂ is formed. Between 400–600 °C, kinetics are found to follow cubic rate law. In fact, this cubic law can be described as a transition from logarithmic to parabolic behavior. Oxygen dissolution becomes quite important in this temperature range. It has been suggested that oxygen dissolution and diffusion of oxygen, the rate of which is a function of oxygen concentration, may give rise to cubic oxidation kinetics.

Between 600–1,000 °C, the kinetics are described by parabolic behavior. However, long exposure may lead to transition to linear behavior; and, above this temperature, the rate of oxidation is so fast that it can best be described by linear kinetics. Parabolic oxidation involves both oxygen dissolution and scale formation. Oxide formed during parabolic range is mainly rutile, TiO₂. The initially-formed oxide is compact, but after extended exposures, when a certain critical thickness is reached, the scale cracks. Therefore, the scale consists of a number of layers corresponding to the number of times the scale cracked after reaching critical thickness. A number of researchers have found a value of weight gain, corresponding to critical thickness at 750 °C, as 3 mg/cm².

The defect structure of rutile suggests there are two types of defects in TiO₂: oxygen anions and interstitial titanium ions. In terms of non-stoichiometry, rutile can be expressed as Ti_{1+y}O_{2-x}. In general, it is concluded that the interstitial titanium ions predominate at low oxygen pressures and high temper-

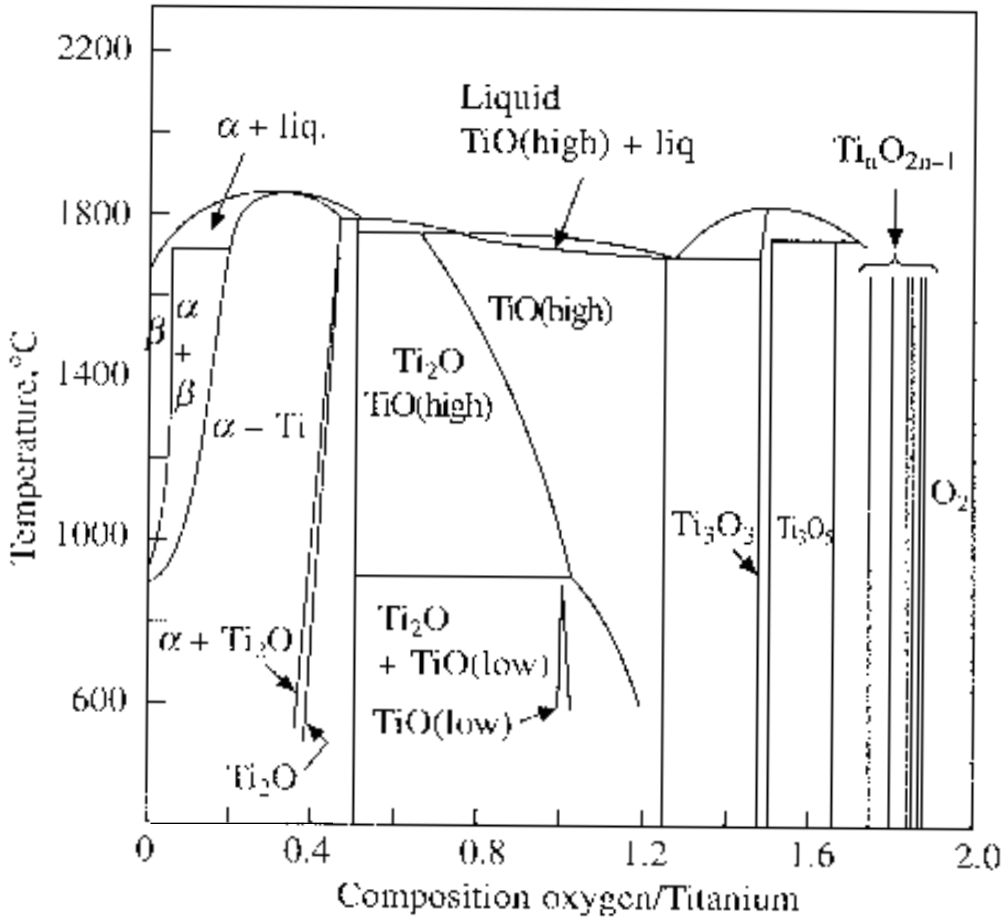


FIGURE 6.11 Phase diagram of titanium oxidation at various temperatures.

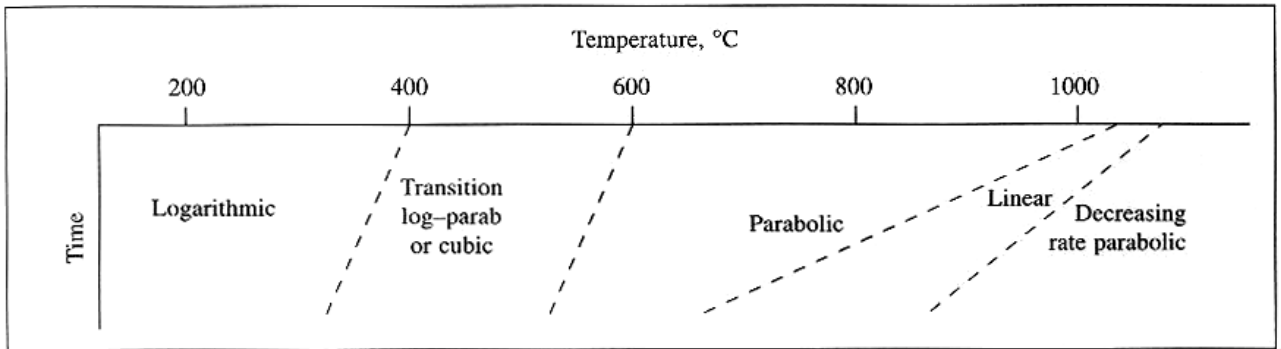


FIGURE 6.12 The various rate laws followed by titanium at different temperatures.

atures, and oxygen vacancies become important at high oxygen pressures and low temperatures. The mechanism of oxidation, therefore, appears to be the formation of rutile by outward diffusion of titanium ions in an inner layer and inward diffusion of oxygen ions in an outer part of the scale. This has also been confirmed by marker studies. The parabolic rate fi-

nally turns into linear rate after the critical thickness is reached. This critical thickness value may decrease with increase in temperature. Therefore, above 1,000 °C, one sees linear oxidation from the very beginning of oxidation. The linear rate reflects mainly an increased rate of oxide formation, while the dissolution continues at a rate determined by the

oxygen gradient and diffusion coefficient of oxygen in metal.

6.12 OXIDATION OF ALLOYS

In actual practice, alloys, rather than pure metals, are used in various high temperature applications. The oxidation behavior of metals is generally modified by the alloying addition, which renders them suitable for a particular high temperature application. Although oxidation of alloys follows the same general phenomenon as that presented earlier for pure metals, the presence of more than one element in the alloy necessitates consideration of a number of additional factors to describe the alloy oxidation behavior. This renders the mechanism of oxidation of alloys relatively complex compared to that of a pure metal. Several factors determine the effect of alloying additions on the oxidation process:

1. the nature of the alloying addition (i.e., whether it is more or less noble than the parent metal);
2. solubility in the parent metal;
3. affinity for oxygen and thermodynamic stability of its oxide;
4. mobility or diffusion of the metal in the oxide phase.

Depending upon these, the scale formed in an alloy may be as follows:

1. a mixture of oxides formed from various alloying elements;
2. a single oxide formed of a specific alloying element;
3. a single or mixed external oxide scale with internal oxides of certain elements.

The first case would be that of general oxidation, in which oxides of all the elements may form in the initial stage (transient oxidation), followed by the growth of the most stable oxide. In the second case, conditions for selective oxidation of a particular constituent of the alloy would result. Although this would protect the alloy from further oxidation, the selective oxidation can result in the depletion of this element from the underlying matrix, which, in the event of any scale damage, cracking, or spalling, may result in excessive scale growth rate, resulting in breakaway oxidation. In the third case, due to very high activity of certain elements, inward diffusion of oxygen can cause precipitation of oxides within the matrix, well below the external scale in the alloy. This type of internal oxide can be beneficial in some

cases. For example, they can strengthen the base alloy and, if formed at grain boundaries in the alloy, restrict grain boundary sliding. But a large amount of internal oxide is deleterious to the alloy because the grains, completely surrounded by oxidized matter, may be loosened and finally dislodged. Many other possibilities that arise during oxidation of binary alloys are given in Fig. 6.13.

Another phenomenon of interest in some alloys is the formation of low melting oxides of certain alloying elements (e.g., Mo and V). This may result in catastrophic oxidation. The second constituent in the metallic phase can also influence the oxidation in two ways. It can enter the primary oxide film, either increasing or decreasing the concentration of lattice defects, thereby enhancing or retarding the oxidation rate. Here, Hauffe's valency rule has been found helpful in many cases. Alternatively, the second constituent may accumulate as a new phase at the base of the primary oxide phase. Under favorable conditions, this may obstruct the passage between metal and film substance and, consequently, retard oxidation. Parabolic kinetics cease to apply under these conditions and may change to logarithmic kinetics.

6.13 INFLUENCE OF ALLOY ADDITION ON OXIDATION BEHAVIOR

Let us take the case of iron as the base metal with various alloying elements added to it. Nickel and chromium are the two major alloying elements in various heat resistant alloys, whose beneficial effect on oxidation resistance is well known. Silicon and aluminum are also quite effective, but they can have a harmful effect on the mechanical properties if not alloyed judiciously. In addition, small amounts of several other alloying elements are added to FeCrNi alloys to achieve specific properties.

6.13.1 Effect of Chromium Addition

Oxidation of pure iron leads to a three-layered scale with wustite as the major oxide at temperatures above 570 °C. Thus, oxidation of iron can be reduced if addition of some alloying element can eliminate the formation of wustite. This can be achieved when chromium is added as an alloying element to iron. Figure 6.14 shows the effect on the oxidation behavior of pure iron or mild steel when chromium is added to it. Addition of a small percentage of chromium results in the formation of a chromium-rich oxide, along with iron oxides. With an increase in concentration of chromium, iron chromium spinels are formed and the FeO layer correspond-

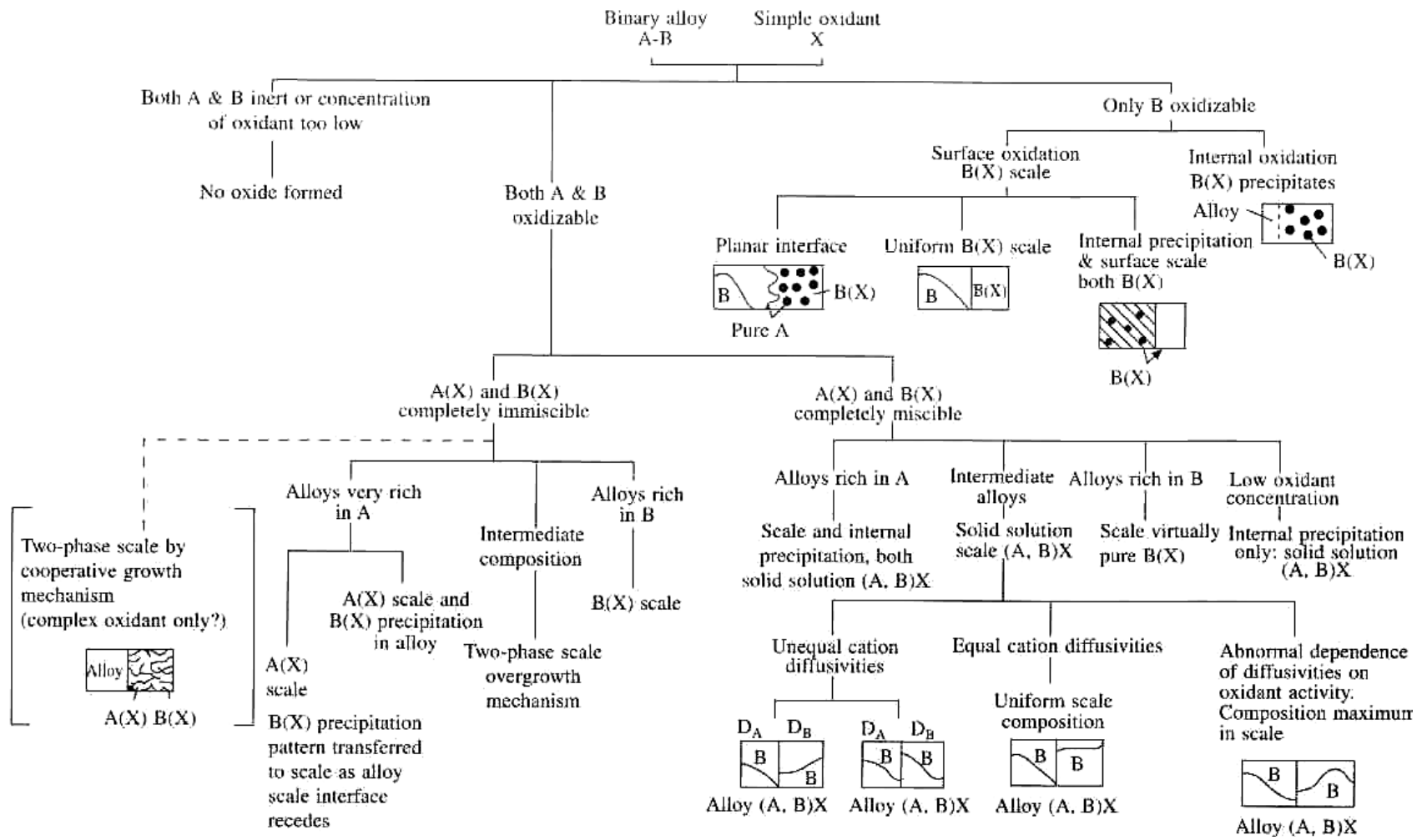


FIGURE 6.13 The formation of scales in case of partially miscible oxides.

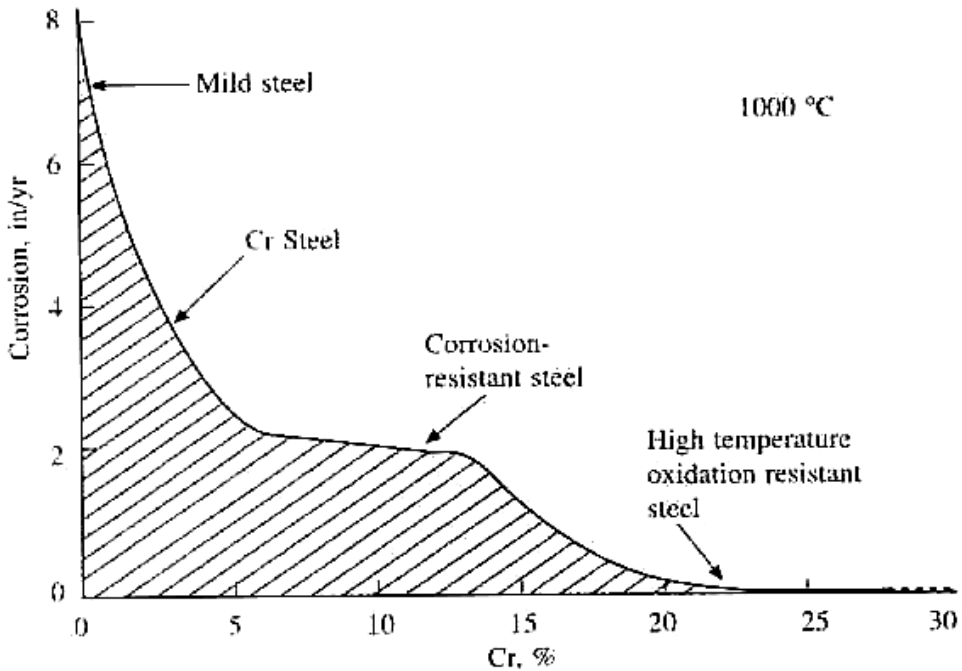


FIGURE 6.14 Effect of Cr addition on the corrosion rate of steel at 1,000 °C.

ingly becomes thinner relative to Fe_3O_4 , as Fe^{2+} ions are blocked by the spinel oxide. With the further increases in Cr, a mixed spinel of type $\text{Fe}(\text{Fe},\text{Cr})_2\text{O}_4$ is produced, which decreases the oxidation rate significantly and leads to a parabolic kinetics. Since the Fe ions are more mobile through this layer than the Cr^{3+} ions, the outer layer can still consist of the iron oxide, especially after long oxidation times. When chromium concentration exceeds the critical concentration, a selective oxide of outer layer of pure chromia is initially formed. But to sustain the chromia layer over a long exposure time, a substantially larger amount of chromium is required—about 20 wt% at 900 °C and 25 wt% 1,000 °C. Phases that form on an Fe-Cr alloy at 1,200 °C are given in a Fe-Cr-O phase diagram, shown in Fig. 6.15. Such isothermal diagrams can be plotted at various temperatures to establish the stability regions of oxide phases as a function of alloy composition.

6.13.2 Effect of Nickel Addition

Nickel is generally not alloyed with Fe for the purpose of improving high temperature properties of Fe. The main purpose of alloying Ni to Fe-Cr alloys is to transform the Fe from a ferritic to an austenitic phase, which has a FCC structure and is more stable at high temperatures. Nevertheless, it can be seen in Fig. 6.16 that addition of Ni to an Fe-11% Cr steel

results in a significant reduction in the oxidation rate at several temperatures. Thus, from the corrosion standpoint, ~20 wt% nickel is effective at 870 °C, 30% at 980 °C and ~50 wt% at 1,200 °C.

At higher chromium levels, the optimum nickel concentration for maximum air oxidation resistance decreases. This effect is depicted as isocorrosion lines (compositions with same weight loss) on a ternary diagram (Fig. 6.17). This indicates the relative amounts of Ni and Cr that need to be added to Fe to reduce its oxidation rate. It can be noted that at 1,200 °C, in air, an addition of ~28 wt% Cr is equivalent to a combined addition of ~50 wt% Ni plus 10 wt% Cr, since all compositions on a given isocorrosion line exhibit the same corrosion rate.

6.13.3 Effect of Aluminum

The beneficial effect of Al additions to Fe in suppressing its oxidation in air is very strong. For example, ~10 wt% Al added to Fe decreases the corrosion loss in Fe from more than six inches to less than two inches per year (see Fig. 6.18). However, mechanical properties of such binary alloys are degraded, making this approach less practical. The marked beneficial effect of Al addition to Fe-Cr alloys is clearly shown in Fig. 6.18. It is seen that ~5 wt% Al addition to a Fe-10Cr alloy reduces the oxidation rate from four to five inches per year to less

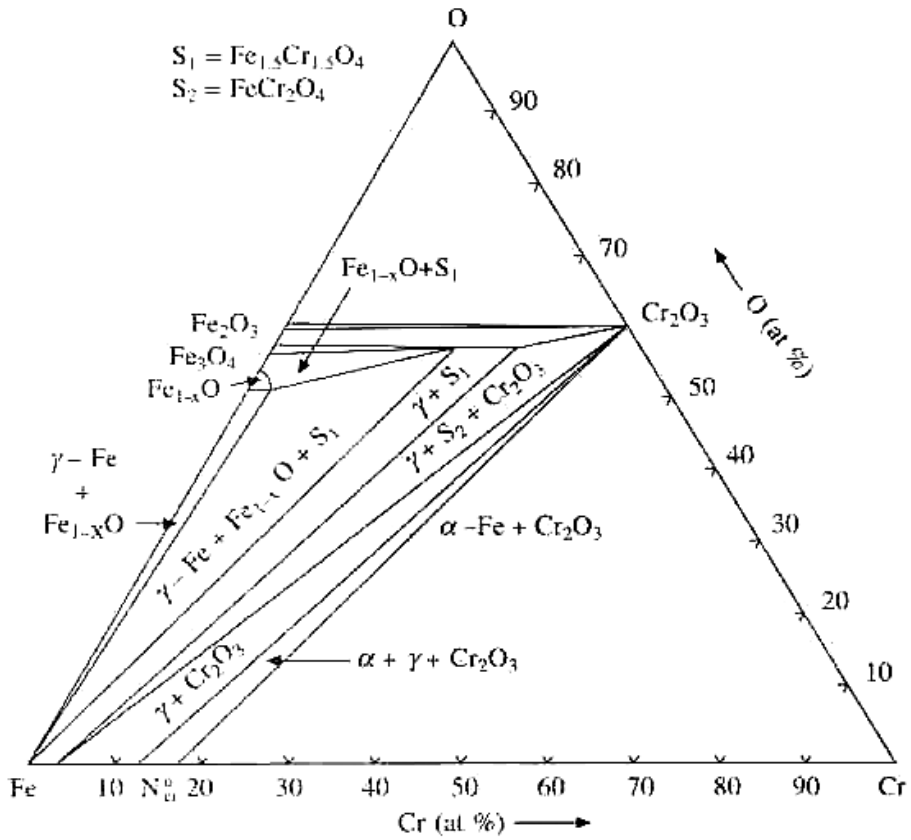


FIGURE 6.15 Isothermal section of Fe-Cr-O phase diagram at 1,200 °C.

than one inch per year. Under these conditions, a selective alumina scale is formed on the outer surface, somewhat protecting the base alloy from further oxidation.

6.13.4 Effect of Silicon

Silicon additions are beneficial in restricting the oxidation rate. However, when the amount exceeds 2–3%, marked embrittlement of the alloy has been noticed. When used in combination with other beneficial alloying elements, silicon can be quite effective. As shown in Fig. 6.19, addition of about 1% Si to a 5 Cr-0.5 Mo alloy reduces the oxidation rate substantially.

6.13.5 Oxidation of Multi-Component Alloys

As the number of alloying elements is increased, it becomes fairly difficult to predict the type of scale that will form, as well as the role of different alloying additions in the scaling process. Let us take the example of a ternary Ni-Cr-Al alloy. Several possi-

bilities exist for the formation of scale, depending upon the composition of the alloy at a given temperature and the partial pressure of oxygen in the exposed environment. One of the methods to predict the oxide scales that will form on an alloy is to draw a ternary phase diagram, if sufficient thermodynamic and kinetic data are available. Such a diagram will delineate the composition ranges for the formation of different types of oxide scales and enable one to predict the oxide phases present on an alloy. Such diagrams are called oxide maps.

One such oxide map for a ternary NiCrAl system is shown in Fig. 6.20 at 1,000 °C. Three different regimes of oxidation and reaction behavior can be delineated, as follows:

1. In dilute alloys, where the concentration of Cr and Al are insufficient to form a continuous scale of either chromia or alumina. The scale on such alloys consists of NiO and spinels of Ni-Al, as well as internal oxides of Cr and Ni. This is shown by the region in the Ni corner of the ternary diagram. Here, the oxidation process is dictated by the outward diffusion of Ni ions.

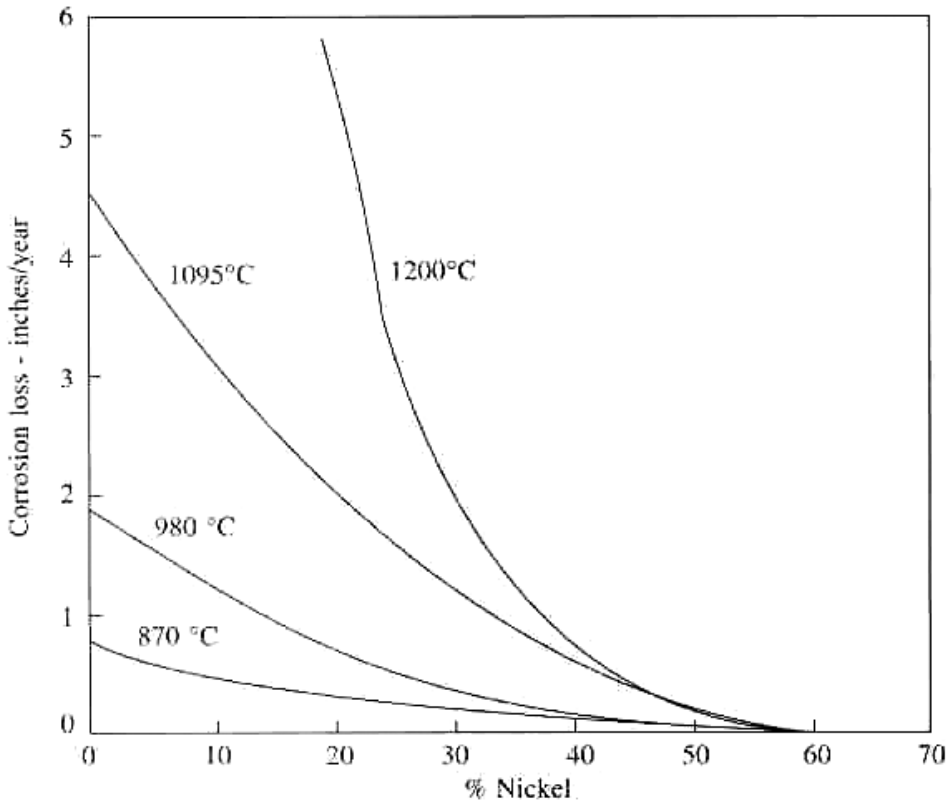


FIGURE 6.16 The effect of Ni addition on the oxidation of a Fe-11 Cr alloy in air at 870, 980, 1,095 and 1,200 °C.

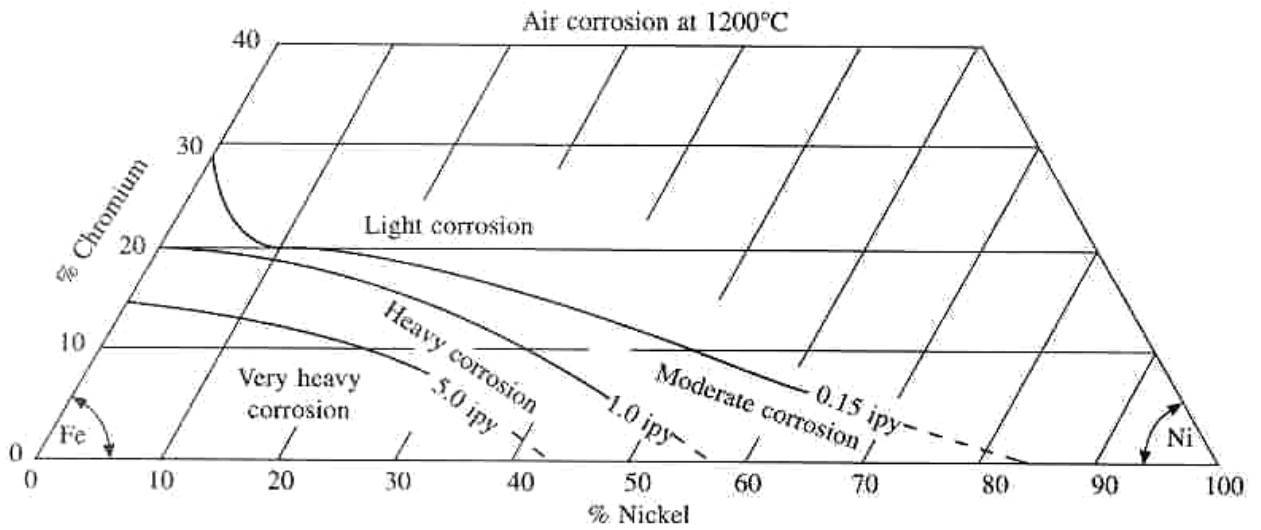


FIGURE 6.17 Ternary diagram showing alloy composition areas of relatively heavy and light corrosion in air at 1,200 °C.

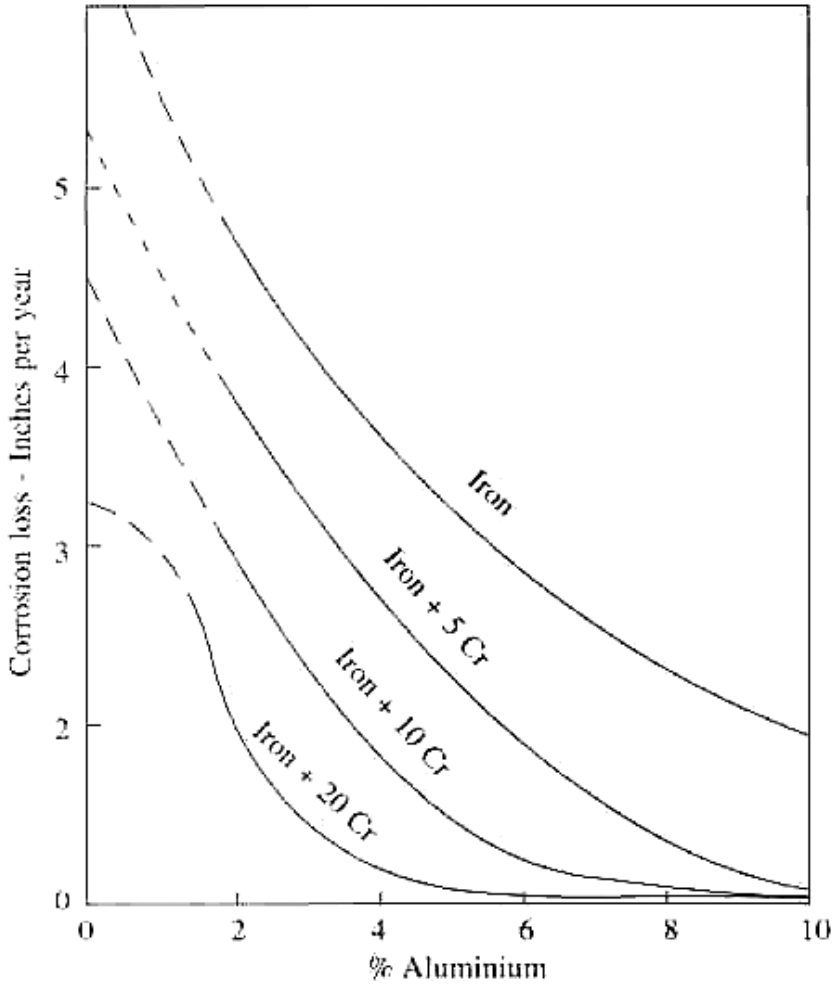


FIGURE 6.18 Effect of aluminum addition on the two Fe and Fe-Cr alloys oxidation in air at 1,095 °C.

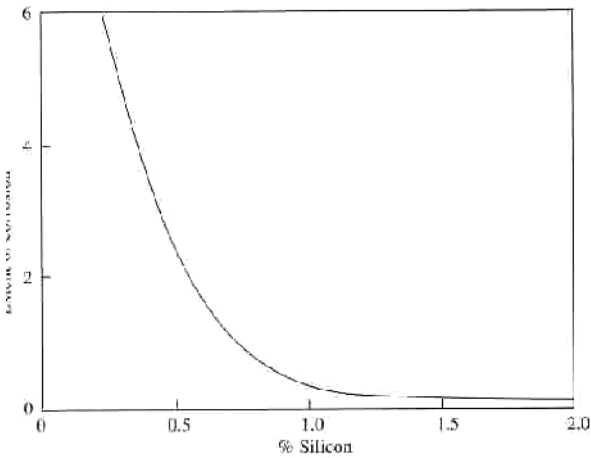


FIGURE 6.19 Effect of Si addition on the oxidation of 5Cr/0.5Mo alloy in air at 815 °C.

2. In alloys containing a high concentration of Cr and a low concentration of Al, a selective layer of chromia oxide forms. In these alloys, Al is internally oxidized. The oxidation process is primarily determined by the diffusional growth of chromia scale. This behavior is indicated by the region in the triangle, extending quite deep into the left corner.
3. In alloys containing a sufficiently high concentration of Al or a reasonable combination of Cr+Al level, a continuous alumina scale forms. As can be seen in Fig. 6.20, a large area of the diagram encompasses the conditions under which a continuous alumina scale can form. In this region, the oxidation process is controlled by diffusion of Al. Similar maps can be constructed for other alloy systems. In general, the ease of formation of pro-

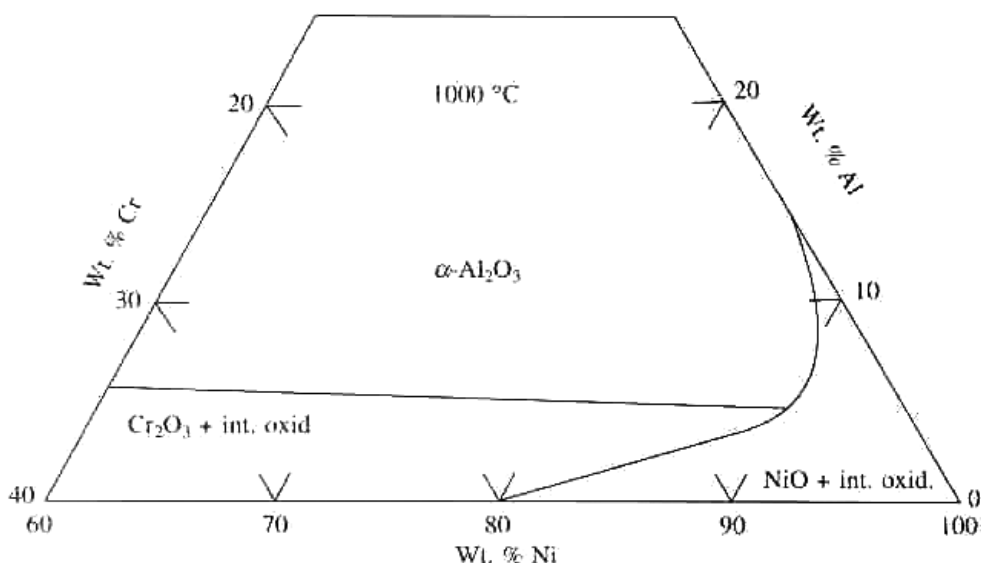


FIGURE 6.20 Oxide map for alloys in the NiCrAl system delineating the composition ranges for formation of different types of oxide scales.

tective (-alumina scale is of the order of Fe-Cr-Al > Ni-Cr-Al > Co-Cr-Al.

The delineation between the three regions should not be considered as absolute and can be influenced by temperature and other alloying additions. In addition, as discussed previously, the transition to selective oxidation will depend upon various other parameters, such as pretreatments, grain size, and specimen geometry.

6.13.6 Effect of Other Alloying Elements

High temperature alloys, in general, contain several other elements which are either added intentionally to reduce oxidation or are present for several other reasons. It is not our aim here to summarize the effect of each individual element on the oxidation process. However, it is worth mentioning here that the deliberate addition of rare earth and other oxygen-active elements improves oxidation behavior. Addition of rare earth elements in small concentrations improves not only the oxidation resistance but also enhances the scale adherence and reduces scale spallation.

There are certain other elements, such as *Mn*, *Mo*, *V*, *Ta*, etc., that are present in several high temperature alloys to improve their mechanical properties. However, they can have a deleterious effect from the standpoint of the oxidation resistance of the alloy. Manganese, which is generally present in most of the Fe-base alloys, has no pronounced effect on the

oxidation rate. In fact, a mild detrimental effect on oxidation has been reported for the 200- and 300-series stainless steels. *Mo* and *V*, if present in large quantities, have a deleterious effect, as they can form low-melting oxides (MoO_2 and V_2O_5) and can lead to catastrophic oxidation. The effect of certain tramp elements, such as sulfur, phosphorus, boron, etc., has also been found to be detrimental to the scale adherence and its spallation resistance. Hence, where good scale adherence is required, these impurities have to be reduced to very low (part per million) levels. Boron, however, is added to many superalloys for grain boundary strengthening.

6.14 OXIDATION BEHAVIOR OF SOME COMMERCIAL ALLOYS

6.14.1 Carbon Steels and Low-Alloy Ferritic Steels

Carbon steel is probably the most widely used engineering material. It is extensively used for high temperature applications in power plants, chemical and petrochemical processing, oil refining, and in many other industries. Boiler tubes in power plants, reactor vessels in process industries, heat-treating fixtures, and exhaust train piping are a few examples of components made of mild steel.

The oxidation behavior of mild steels is very similar to that of iron, as discussed in the previous section. Carbon steels have negligible oxidation in air

up to temperatures of about 250–300 °C. Oxidation attack is less than about 20 mg/cm² up to 450 °C. Above this temperature, the oxidation rate increases rapidly, following linear kinetics, especially above 600 °C. High Strength Low Alloy (HSLA) steels, which contain minor additions of alloying elements (such as manganese, silicon, chromium and nickel), have a lower oxidation rate. Chromium-molybdenum steels are considered to be a better choice for moderate temperature applications. The presence of *Mo* enhances creep strength at these temperatures, while *Cr* helps in forming a chromium-rich scale that protects the steels from further oxidation. Ferritic steels of the type 21/4Cr-1Mo and 9Cr-1Mo are important materials for evaporator and superheater tubes, respectively, in power plants; whereas, other low-alloy steels (such as 1Cr-0.5 Mo, etc.) are used for other components where the temperature is not very high. Adding Si generally helps in further reducing the oxidation rate.

6.14.2 Oxidation Resistance of Stainless Steels

By definition, steels containing more than 12% Cr are called stainless. They can be martensitic, ferritic, or austenitic, depending upon the microstructure of the stainless steel. For high temperature applications, austenitic stainless steels are more suitable because of their inherent high strength and good ductility. Martensitic steels are suitable only for those applications where very high strength is the main requirement; whereas, ferritic stainless steels exhibit good oxidation resistance for relatively low temperature applications. These are suitable for temperatures below 640 °C, because these steels drastically lose strength above this temperature.

In general, corrosion resistance is imparted to all stainless steels by the formation of a protective chromia layer on the surface, which requires a minimum of ~18 wt% Cr. In austenitic stainless steels, the face-centered cubic structure is retained by addition of Ni. The 300-series stainless steels, therefore, are used in many high temperature applications up to 900–950 °C. Above this temperature, the chromia layer begins decomposing into volatile CrO₃ and the protective properties of the steels are no longer retained. Among various 300-series stainless steels, a superior corrosion resistance is exhibited by high-chromium stainless steels such as Type 310 (25Cr-20Ni) and Type 309 (25Cr-12Ni). These steels also possess good cyclic oxidation resistance (Fig. 6.21).

Among ferritic stainless steels, Type 446 has the maximum resistance to oxidation, followed by

Types 430, 416, and 410. Cyclic oxidation tests that were performed in air at 1,000 °C for 400 cycles (30 minutes in a furnace and 30 minutes outside) showed that oxidation resistance was poor for Types 409 (12Cr), 420 (13Cr), and 304 (18Cr-10Ni). Type 420 was completely oxidized in 100 cycles. Types 405 (14Cr), 430 (17Cr), 446 (27Cr), 310 (25Cr-20Ni), and DIN 4828 (19Cr-12Ni-2Si steel) exhibited good oxidation resistance, as shown in Fig. 6.22. Above 1,200 °C, all except Fe-15Cr-4Al suffered a severe attack within 400 cycles, indicating that alumina-forming steels are superior to the chromia-forming alloys. In a combustion environment with regular gasoline containing 0.01 wt% sulfur, considerable attack on stainless steels containing less than 17% Cr has been reported. Steels such as Types 310, 309, and 446 showed good corrosion resistance in these environments. Combustion products such as CO, CO₂, and hydrocarbons are expected to influence the oxidation behavior. Water vapor, for example, affects the oxidation behavior of even Type 310 stainless steels, as shown in Fig. 6.23.

6.14.3 Nickel-Based Alloys and Superalloy Oxidation

As the nickel content in the Fe-Ni-Cr system increases from austenitic stainless steels to Alloy 800 and other Ni-Cr alloys, the materials become more stable in terms of metallurgical structure, and also exhibit better resistance to creep deformation. The scaling resistance also increases significantly. As shown in Fig. 6.24, the cyclic oxidation resistance of an IN 601 alloy is considerably superior as compared to those of IN 600 (18 wt% Ni) and Alloy 800.

Nickel-based alloys can be classified into those that form chromia or alumina as protective scale on oxidation. Alumina-forming Ni-based alloys exhibit better high temperature oxidation resistance and possess sufficient strength and creep resistance properties. Aluminum present in the alloy forms gamma prime (Ni₃Al) precipitates that impart high strength to these alloys. Also, alumina-based alloys can be used at relatively higher temperatures compared to chromia-based alloys, because the latter decompose into volatile CrO₃ above 900–950 °C, thereby rendering the scale nonprotective.

Fe-Cr, Ni-Cr and Co-Cr alloys exhibit low oxidation rates when the Cr concentration is ~15–30 wt %. Therefore, most iron-, nickel- and cobalt-based commercial austenitic alloys typically contain about 16–25% Cr. Table 6.3 lists some of the common chromia-forming alloys. High-chromium alloys

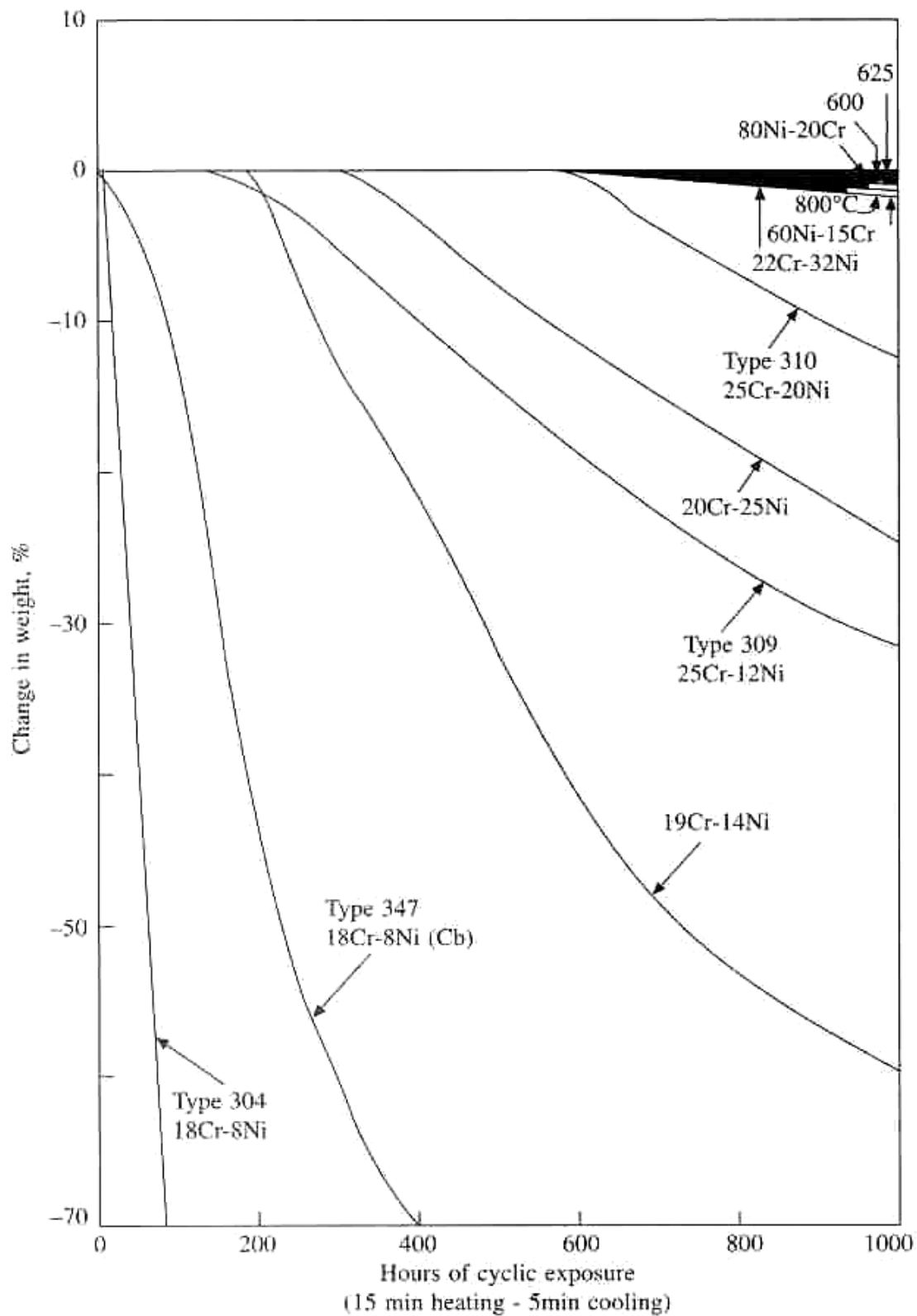


FIGURE 6.21 Cyclic oxidation resistance of several stainless steels and Ni-base alloys in air at 980 °C.

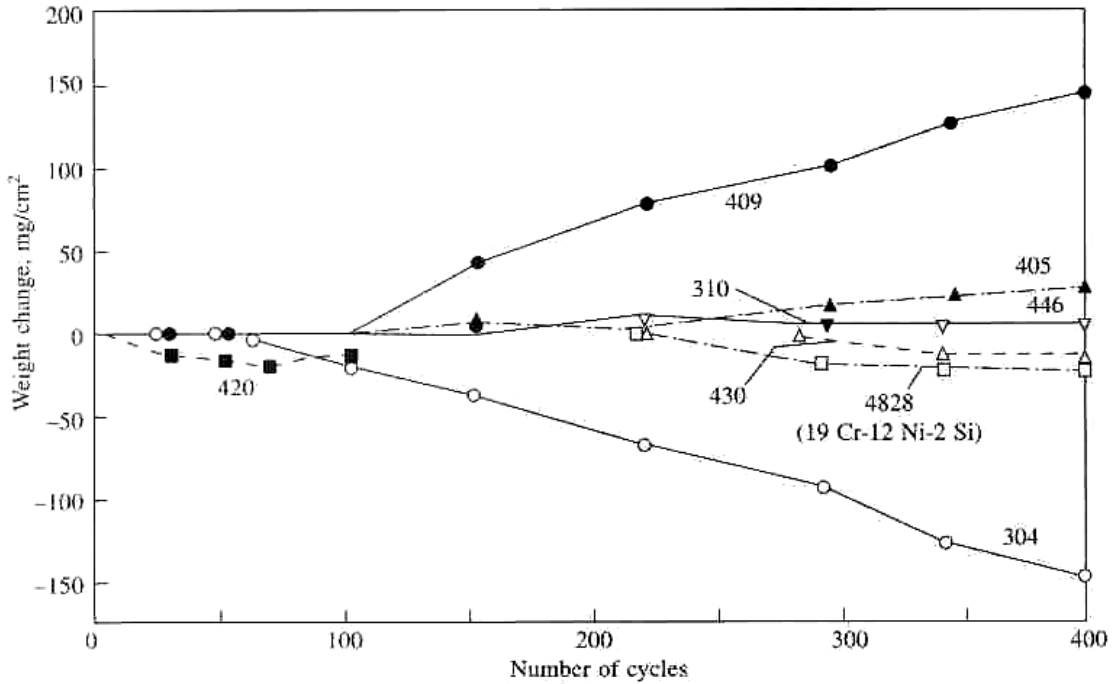


FIGURE 6.22 Cyclic oxidation resistance of several ferritic and austenitic stainless steels in air at 1,000 °C.

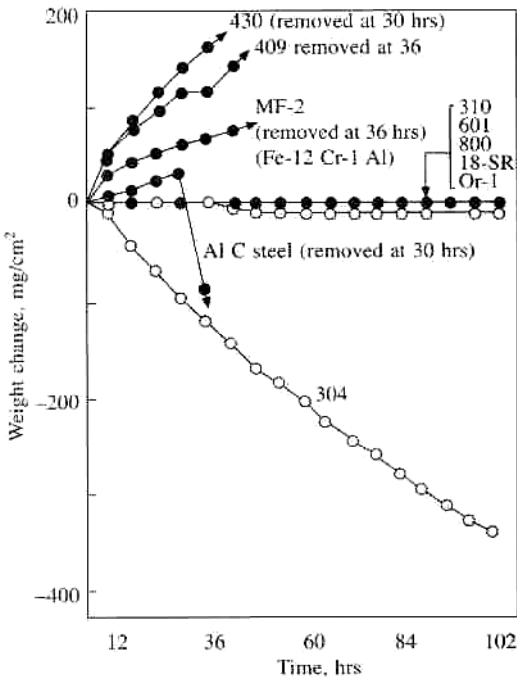


FIGURE 6.23 Cyclic oxidation resistance of several ferritic and austenitic stainless steels in (a) air + 10% water vapor at 980 °C.

have the drawback of forming an intermetallic sigma phase, especially after exposure for a long duration above 800 °C, which renders the alloy brittle. Nominal chemical compositions of several alumina-forming superalloys are listed in Table 6.4. They usually contain 5–7 wt% Al and greater than 10 wt% Cr. The alumina layer forms due to the gettering effect of Cr, as discussed previously. The oxidation rate in these alloys is generally low, and the oxide scales are thin. Scale spallation resistance is usually improved by addition of a small concentration of active elements such as Y, Ce, etc., the details of which will be presented in a subsequent section.

Superalloys have been developed for gas turbine engines, which require both superior high temperature strength and strong oxidation resistance. Many alumina-forming superalloys are being used for different parts of gas turbines. Applications of some of these alloys have now been extended to other industries, such as heat treating, chemical processing, petrochemicals, oil refining, and power generation.

For highly-stressed turbine blades and vanes, cast nickel- and cobalt-based alloys are used. For cast nickel-based alloys, substantial amounts of Al and Ti are used to produce a large volume fraction of

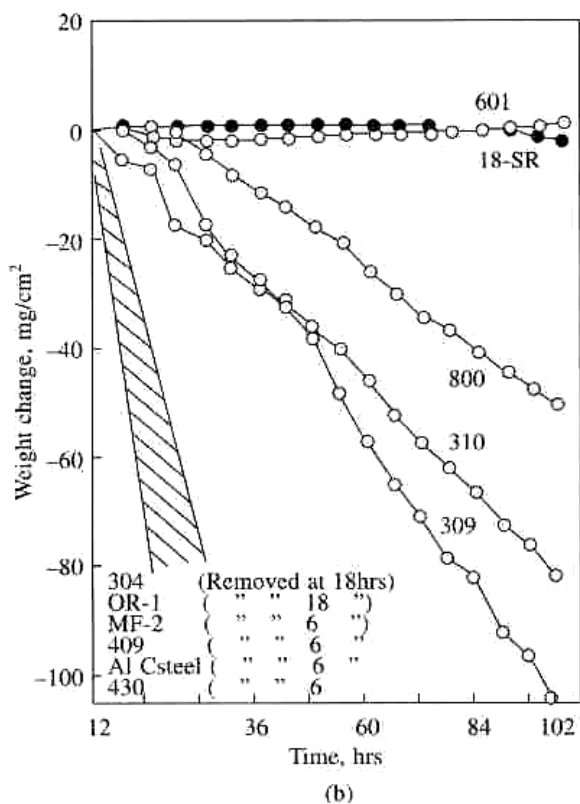


FIGURE 6.24 Cyclic oxidation resistance of several ferritic and austenitic stainless steels in (b) gasoline exhaust at 980 °C.

gamma prime precipitates. These alloys also contain substantial amounts of refractory elements, such as *Mo* and *W* for solid solution strengthening, and *B* and *Zr* for grain boundary strengthening.

In recent years, another group of commercial superalloys has been developed for gas turbines, generally classified as Oxide Dispersion-Strengthened (ODS) alloys. They are produced by mechanical alloying. Nominal chemical compositions of several of the alloys such as MA956, MA754, MA6000 are listed in Table 6.5. These ODS materials are superior to superalloys with gamma prime precipitates, as they contain a fine dispersion of inert oxide particles in the austenite matrix that do not coarsen with time and, therefore, retain high strength for a longer time period at relatively higher temperatures. Their environmental performance is also better than that of conventional superalloys from the standpoint of resistance to cyclic oxidation and scale spallation resistance.

6.15 OXIDATION IN MIXED GAS ENVIRONMENTS

Corrosion of materials at elevated temperatures is a potential problem in many systems within the chemical, petroleum, process, and power generating industries, but the environment in actual plants is far from a simple, single oxidant. So far, we have dealt with the reaction of metals and alloys in a purely oxidizing atmosphere (i.e., air or oxygen). Even in a single gas environment, we saw that the identification of oxides and the mechanism of their formation often become complex, especially when we deal with metals forming multi-layer oxides. Furthermore, if the gaseous environment is made more complex by the addition of one or more gaseous species, the scaling process will be even more complex. The mechanism of oxidation/corrosion would depend not only on the thermodynamic stability of the oxides of the metallic constituents but also the partial pressures of the two gaseous reactants in the exposure environment. Therefore, material selection for high temperature applications is based not only on a material's strength properties but also on its resistance to the complex environments prevalent in the anticipated exposure environment.

Considerable research on the causes, effects, and prevention of different types of corrosion has been underway for many years. However, when one studies reaction kinetics that involve only one reaction equilibrium (e.g., H_2O/H_2 or CO_2/CO for oxidation, H_2S/H_2 for sulfidation, CH_4/H_2 for carburization or NH_3/H_2 for nitridation), the reaction potential of the participating species can be uniquely established by the standard free energy of formation for the reaction, as discussed above.

Even though corrosion of materials in single-oxidant environments is fairly simple to examine and provides a basis for formulation of alloys and their development over the years, the selection and application of alloys solely on the basis of their oxidation resistance is very limited in practical systems in view of the complex nature of the environments in these systems.

6.15.1 Importance of Mixed Gas Environments

In a power plant, heat is generated by burning oil, gas, or coal. If complete combustion occurs, the resultant environment will consist of oxygen and carbon dioxide. In practice, however, complete com-

TABLE 6.3 Composition of Various Chromia-Forming Alloys

| Type | UNS No | C | Cr | Ni | Co | Fe | Mo | W | Others |
|--------------|---------|------|------|------|------|------|-----|-----|-------------------------------------|
| Incoloy 800 | NO8800 | 0.05 | 21 | 32.5 | — | Bal | — | — | 0.3Al, 0.3Ti |
| Incoloy 800H | NO8810 | 0.08 | 21 | 32.5 | — | Bal | — | — | 0.4Al, 0.4Ti |
| Incoloy802 | NO8802 | 0.4 | 21 | 32.5 | — | Bal | — | — | |
| Incoloy903 | N19903 | — | — | 38 | 15 | Bal | — | — | 1.4Ti, 0.9Al, 3Cb |
| Incoloy DS | — | 0.06 | 17 | 35 | — | Bal | — | — | 2.3Si |
| Kanthal AI | K92500 | — | 22 | — | — | Bal | — | — | 5.8Al |
| Inconel 600 | NO6600 | 0.08 | 15.5 | Bal | — | 8.0 | — | — | |
| Inconel 601 | NO6601 | 0.1 | 23.0 | Bal | — | 14.4 | — | — | 1.4Al |
| Inconel 625 | NO6625 | 0.1 | 21.5 | Bal | — | 2.5 | 9.0 | — | 3.6Cb |
| Inconel 706 | NO9706 | 0.03 | 16 | Bal | — | 37 | — | — | 1.8Ti,0.2Al,2.9Cb |
| Incone1718 | NO77 18 | 0.04 | 18 | Bal | — | 18.5 | — | — | 5.1Cb |
| Hastelloy X | N06002 | 0.1 | 22 | Bal | 1.5 | 18.5 | — | 0.6 | |
| Nimonic 70 | — | — | 20 | Bal | — | 25 | — | — | 1Al, 1.25Ti, 1.5Cb |
| Nimonic 75 | — | 0.1 | 19.5 | Bal | — | — | — | — | |
| Nimonic 81 | — | 0.03 | 30 | Bal | — | — | — | — | 0.9Al, 1.4Ti |
| Nimonic 90 | NO7090 | 0.07 | 19.5 | Bal | 16.5 | — | — | — | 1.5Al,2.5Ti |
| Nimonic 115 | — | 0.15 | 15 | Bal | 15 | — | 4.0 | — | 5Al, 4Ti |
| Waspaloy | NO7001 | 0.08 | 19 | Bal | 14 | — | 4.3 | — | 1.5Al,3Ti,0.05Zr,0.006B |
| Udimet 500 | — | 0.08 | 18 | Bal | 18.5 | — | 4.0 | — | 2.9Al,2.9Ti,0.05Zr, 0.006B |
| Udimet 520 | — | 0.05 | 19 | Bal | 12 | — | 6.0 | 1.0 | 2Al, 3Ti,0.005B |
| Udimet 700 | — | 0.03 | 15 | Bal | 18.5 | — | 5.2 | — | 5.3Al,3.5Ti,0.03B |
| Rene 77 | — | 0.07 | 15 | Bal | 15 | — | 4.2 | — | 4.3Al,3.3Ti,0.04Zr, 0.015B |
| Rene 80 | — | 0.17 | 14 | Bal | 9.5 | — | 4.0 | 4.0 | 3Al, 0.015B 5Ti,0.03Zr, |
| IN-738 | — | 0.17 | 16 | Bal | 8.5 | — | 1.7 | 2.6 | 3.4Al,3.4Ti,0.1Zr,1.7Ta,0.9Cb,0.01E |
| IN-792 | — | 0.12 | 12.4 | Bal | 9 | — | 1.9 | 3.8 | 3.1Al,4.5Ti, 1.7Ta,0.1Zr,0.02B |

TABLE 6.4 Composition of a Few Alumina-Forming Alloys

| Type | C | Al | Cr | Ni | Co | Fe | Mo | W | Others |
|------------|------|-----|------|------|------|-----|-----|------|----------------------------|
| IN713 C | 0.12 | 6 | 12.5 | Bal | — | — | 4.2 | — | 2 Nb, 0.8Ti 0.012B, 0.1Zr |
| IN 713LC | 0.05 | 6 | 12.0 | Bal | — | — | 4.5 | — | 2 Nb, 0.6Ti 0.01B, 0.1Zr |
| B 1900 | 0.1 | 6 | 8.0 | Bal | 10 | — | 6.0 | — | 4 Ta, 1.0Ti 0.015B, 0.10Zr |
| IN 100 | 0.18 | 6 | 10 | Bal | 15 | — | 3.0 | — | 4 Ta, 1.0Ti 0.015B, 0.10Zr |
| IN 731 | 0.18 | 5.5 | 9.5 | Bal | 10 | — | 2.5 | — | 4.6 Ti, 0.06Zr. 0.015B, 1V |
| MAR-M 200 | 0.15 | 5 | 9.0 | Bal | 10.0 | 1.0 | — | 12.5 | 2Ti, 0.05Zr,0.015B, 1.0Nb |
| Udimet 520 | 0.05 | 19 | Bal | 12 | — | 6.0 | 1.0 | — | 2Al, 3Ti,0.005B |
| Udimet 700 | 0.03 | 15 | Bal | 18.5 | — | 5.2 | — | — | 5.3Al,3.5Ti,0.03B |

TABLE 6.5 Composition of a Few Alumina-Forming Alloys

| Type | Cr | Ni | Fe | Ti | Al | Co | Mo | W | Others |
|----------|-------|-----|------|------|------|------|-----|------|---|
| MA956 | 20 | — | Bal | 0.5 | 4.5 | — | — | — | 0.5Y ₂ O ₃ |
| MA754 | 20 | Bal | 1.0 | 0.5 | 0.3 | — | 4.5 | — | 0.6Y ₂ O ₃ |
| MA 6000 | 15 | Bal | 0.75 | 2.88 | 4.38 | 16.0 | 2.0 | 4 | 2 Ta, 1.13Y ₂ O ₃ |
| NiCr8020 | 19–21 | Bal | 2.0 | — | — | — | — | — | 1Mn, 2Si |
| TDS-Ni | — | Bal | — | — | — | — | — | — | 2ThO ₂ |
| TMO-2 | 6.0 | Bal | — | 0.8 | 4.2 | 9.7 | 2.0 | 12.4 | 4.7 Ta, 0.01B, 0.05Zr, 0.05C, 1.13Y ₂ O ₃ |

bustion is often not possible, and the burning of coal or oil results in partial combustion, which generates gases such as CO and H₂. Secondly, all the fuels (whether coal, gas, or oil) are rarely pure. They generally contain sulfur in the form of an impurity. A part per million (ppm) level of sulfur impurity can create a sufficient partial pressure of sulfur vapor, either as sulfur dioxide or as hydrogen sulfide (by combining with water vapor—a usual impurity). Similarly, in petrochemical plants incomplete combustion of crude generates not only carbon monoxide but also several low molecular weight hydrocarbons, which can make the environment really complex and the prediction of reaction products more difficult. In gas turbines, it has been found that a ppm level of sulfur impurity may create ~1 vol.% of sulfur dioxide at about 1,000 °C, which is sufficient to cause severe deterioration of even a very stable superalloy. It is essential, therefore, to know how metals and alloys interact in mixed gas environments to predict the chemistry of the scale formed and, hence, the mechanism of scale formation.

There are several mixed gas environments of interest in many practical applications. They include oxygen plus water, oxygen plus sulfur dioxide or hydrogen sulfide, and oxygen plus carbon dioxide/carbon monoxide. Moisture is present in many industrial environments and is known to aggravate the corrosion reaction in many instances. Oxidizing environments that contain sulfur dioxide are prevalent in chemical processes used to manufacture sulfuric acid. In these processes, combustion of sulfur with excess of air at ~1150–1200 °C can result in 10–15 vol.% SO₂ and 5–10 vol.% O₂, with the balance being N₂. SO₂ is then converted to sulfuric acid. Such an environment is very oxidizing to structural alloys, which may form scales comprising mixtures of oxides and sulfides. On the other hand, the environment, in general, is very reducing in some of the cracking units of many petrochemical plants, coal gasification atmosphere, low NO_x boilers, etc. Here, sulfur is usually present as hydrogen sulfide, and the oxygen content is extremely low. In addition, other gases (such as CO, CO₂, H₂, and H₂O) are also present. Such an environment is considered a “reducing” atmosphere, and the exposure of metals and alloys usually leads to a severe sulfidation attack. As an example, a coal gasification atmosphere typically has a pS₂ of 10⁻⁵ to 10⁻¹⁰ atm and pO₂ of 10⁻¹⁵ to 10⁻²⁰ atm.

6.15.2 Oxidation versus Sulfidation

Let us first discuss how sulfidation differs from oxidation. The reactions of metals and alloys with sul-

fur are governed by the same principles as we have discussed for metal-oxygen reactions. For many metals, however, sulfur behaves much more aggressively than oxygen. The stability of various metal sulfides as a function of temperature is given by the Ellingham diagram for the sulfides. Fig. 6.25 shows the plot of free energy versus temperature for various metal sulfide reactions. There is very little difference in the stability of sulfides formed by iron, nickel, and cobalt. Chromium, however, forms a relatively stable sulfide compared to iron, cobalt, and nickel. The corresponding sulfur vapor pressure (defined by pS₂ or by the pH₂/pH₂S ratio) that is required for the formation of a sulfide at a given temperature is determined from the nomographic scale on the right-hand side of the figure. Here, pS₂ is obtained by drawing a straight line through the point ‘S’ (on the left of the figure) through the free energy line of the sulfide at the temperature of interest and extending the line to the pS₂ scale, giving the sulfur partial pressure in equilibrium with the sulfide. Similarly, the pH₂/pH₂S ratio can be deduced by drawing a line from the point ‘H’ (on the left) through the free energy of a sulfide at a given temperature and extending it to the pH₂/pH₂S scale (on the right).

Why are reactions of sulfur with several metals more aggressive than the corresponding reactions with oxygen? For example, silver, which is noble in oxygen, reacts violently with sulfur. Copper also undergoes an extremely rapid reaction with sulfur. The most common metals—iron, cobalt, nickel, and their alloys—have reaction rates with sulfur that are several orders of magnitude greater than those in oxygen. Table 6.6 compares the reaction rates for Ni, Cr, Co, and Fe in oxidizing and sulfidizing atmospheres. The reasons for the high oxidation rates for metal sulfur reactions are as follows:

1. Higher diffusion rates in sulfides, compared to those in oxides, due to a large concentration of lattice defects. For example, the defect concentration in cuprous sulfide, Cu_{2-y}O, is as high as 17 at.% (Cu_{0.65}S) at elevated temperatures; whereas, the deviation from stoichiometry in cuprous oxide, y in Cu_{2-y}O, is only 2×10^{-3} at 1,025 °C and 0.1 atm. oxygen. Similarly, for chromium sesquisulfide, Cr₂S₃, the stoichiometry ranges from CrS_{1.30} to CrS_{1.54} and the predominant defects are reported to be chromium interstitials. On the other hand, deviation from stoichiometry for chromium trioxide (Cr₂O₃), is reported to be negligible.
2. Many sulfides have tendency to form low-melting eutectics. The most common metals (iron, cobalt and nickel) form low-melting sulfides. Nickel, for

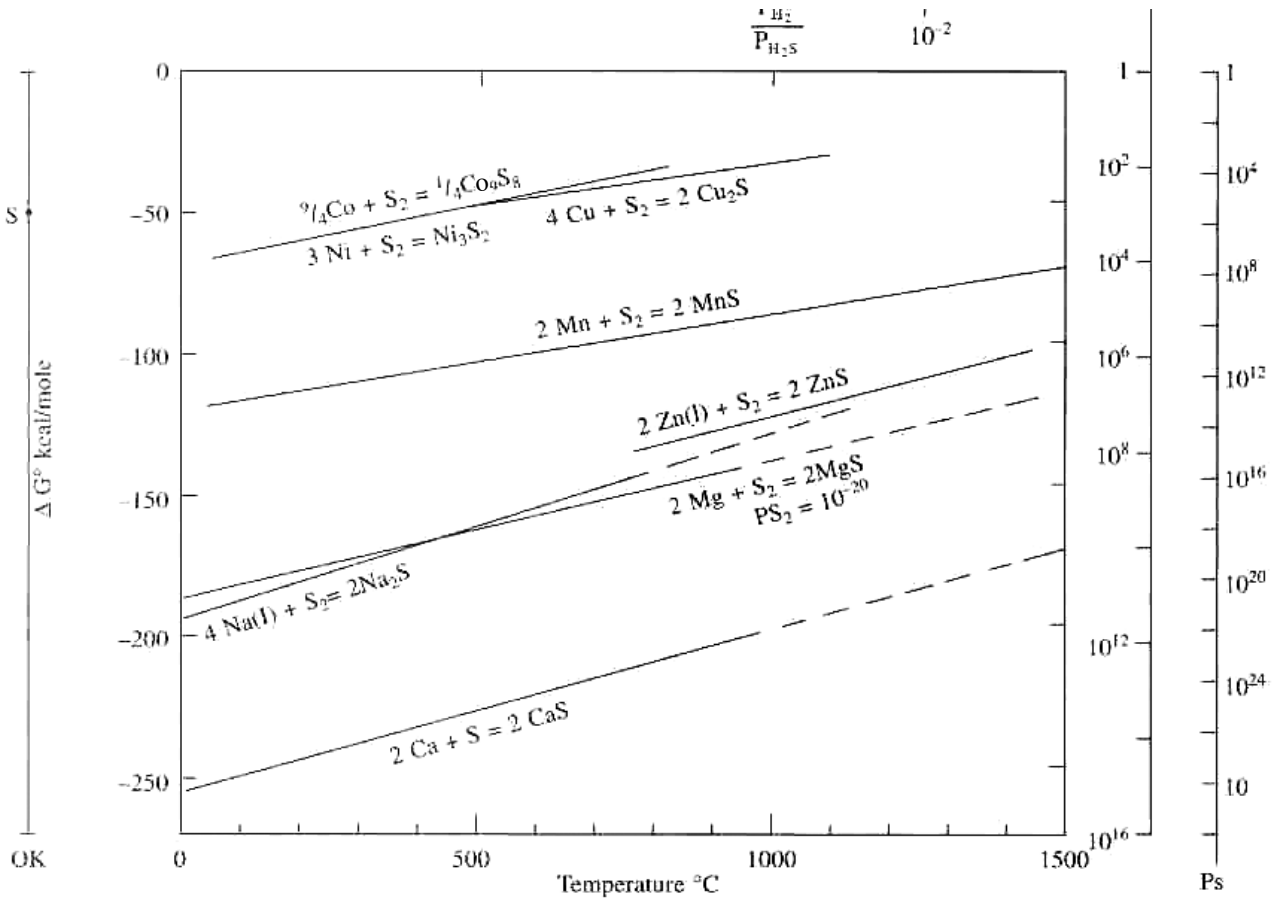


FIGURE 6.25 Ellingham diagram for the sulfidation of various metals.

TABLE 6.6 Parabolic Rate Constants for Oxidation and Sulfidation of Various Metals

| Environment | Parabolic Rate Constant (Kp) gm ² cm ⁻⁴ s ⁻¹ / Temperature | | | |
|-------------|---|-------------------------------|-------------------------------|---------------------------------|
| | Ni | Co | Fe | Cr |
| Oxidation | 9.1 × 10 ⁻¹¹ 1000 °C | 1.6 × 10 ⁻⁹ 950 °C | 5.5 × 10 ⁻⁸ 800 °C | 4.5 × 10 ⁻¹² 1000 °C |
| Sulfidation | 8.5 × 10 ⁻⁴ 650 °C | 6.7 × 10 ⁻⁶ 800 °C | 8.1 × 10 ⁻⁶ 800 °C | 8.1 × 10 ⁻⁷ 1000 °C |

example, forms Ni₃S₂, which melts at 635 °C; cobalt forms Co₄S₃, which melts at 880 °C; while iron forms FeS, which melts at 985 °C. The lowest temperature at which this happens is for nickel or nickel-based alloys. This is why nickel-based alloys suffer rapid degradation in sulfur-containing atmospheres.

3. As listed in Table 6.7, there is relatively little difference in the free energy of formation of the sulfides of various metals (such as iron, cobalt, nickel, and chromium) compared to that of their

corresponding oxides. Because of this, the requirement of the alloying element (e.g., Cr in Fe-Cr or Ni-Cr or Co-Cr alloys) for selective sulfide formation is relatively higher than the corresponding oxides.

4. Finally, the dissociation pressure of sulfides is much greater than those of the corresponding oxides. Consequently, in spite of forming compact scales, a high sulfur partial pressure is obtained at the scale/metal interface, which favors rapid intergranular corrosion of the alloy substrate.

TABLE 6.7 Standard Free Energy of Formation of Several Metal Sulfides and Oxides at 1,000 °C

| Sulfides | (G (kJ / mole) | Oxides | (G (kJ / mole) |
|------------------------------------|----------------|------------------------------------|----------------|
| 1/3 Al ₂ S ₃ | -219 | 1/3 Al ₂ O ₃ | -429 |
| 1/3 Cr ₂ S ₃ | -135 | 1/3 Cr ₂ O ₃ | -269 |
| FeS | -86 | FeO | -176 |
| CoS | -80 | CoO | -136 |
| NiS | -88 | NiO | -127 |
| MnS | -190 | MnO | -294 |

6.15.3 Sulfidation of Fe-Cr, Ni-Cr, and Co-Cr Alloys

As in the case of oxidation, alloying of chromium with iron, nickel, and cobalt considerably improves sulfidation resistance. The rate usually follows parabolic behavior and, for all the three classes of alloys, the parabolic rate constant decreases with an increase in the chromium content of the binary alloy. Above about 15 at.% Cr, there is no significant difference between the rate constants of binary alloys, as shown in Fig. 6.26.

The scale formed on binary alloys changes with a change in the chromium concentration. At low levels of chromium, a two-layer sulfide scale is formed—sulfide of the base metal as the outer layer and an

inner layer consisting of a solid solution of the sulfides of the base metal and chromium. For Fe-Cr alloys, the improved protection is attributed to the presence of an inner sulfide layer of type Fe(Fe_{2-y},Cr_x)S₄. Similarly, mixed sulfides are formed on Ni- and Co-based alloys. At high concentrations of chromium (~40%), the scale is a single layer of chromium sulfide, which offers complete protection against further corrosion.

In ternary alloys, the addition of aluminum has been found to be beneficial as an alloying element for corrosion resistance in both sulfur vapor and H₂/H₂S environments. The improved sulfidation resistance of Fe-Cr-Al alloys is due to the formation of an inner layer of Fe(Fe_xAl_yCr_{z-x-y})S₄. Similar reduction in the sulfidation rates occurs for the addition of aluminum to Co-Cr alloys; however, the effect is not as strong as it is for Fe-Cr-Al alloys.

On the other hand, Ni-Cr-Al alloys behave differently. Addition of Al to Ni-25Cr (up to 10%) showed very erratic behavior when tested in sulfur vapor from 600 to 950°C. The kinetics were found to vary from parabolic to linear. This might be due to the formation of low-melting nickel sulfide, as discussed previously.

Sulfidation of alloys in an H₂/H₂S mixture has been described by isocorrosion rate curves for various steels and stainless steels as a function of H₂S concentration and temperature. These are given in

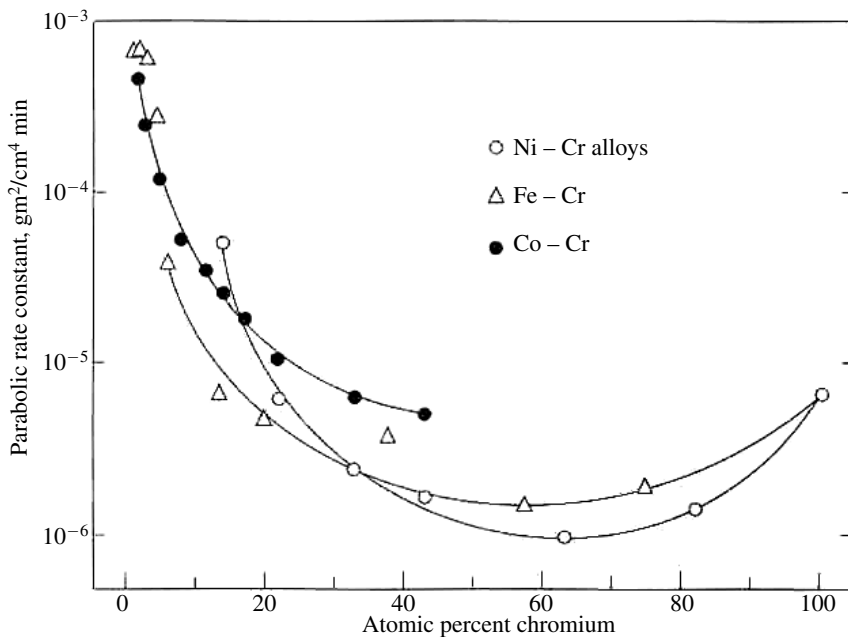


FIGURE 6.26 Parabolic rate constants for the sulfidation of Ni-Cr, Fe-Cr and Co-Cr alloys as a function of chromium concentration in the alloy.

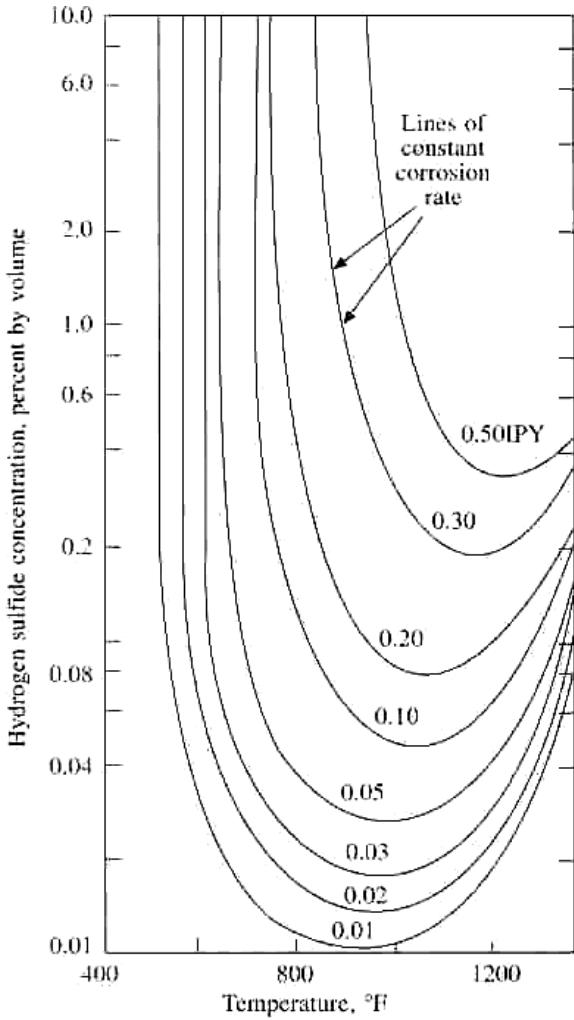


FIGURE 6.27 Isocorrosion rate curves for steels at various temperatures and partial pressures of H_2S .

Figs. 6.27 and 6.28 for steels and stainless steels, respectively.

6.16 PHASE STABILITY DIAGRAMS

When materials are exposed to multi-component gas environments or mixed oxidants, several of the fundamental processes mentioned above can occur simultaneously. Furthermore, the second reactant may either modify or degrade the corrosion-product layers that form by reaction of the first reactant and the substrate elements. In these situations, reactions will occur not only at the gas/scale interface, but also within the scales that develop on the surface and in the base metal beneath the reaction products. As a result, the development of suitable and meaningful

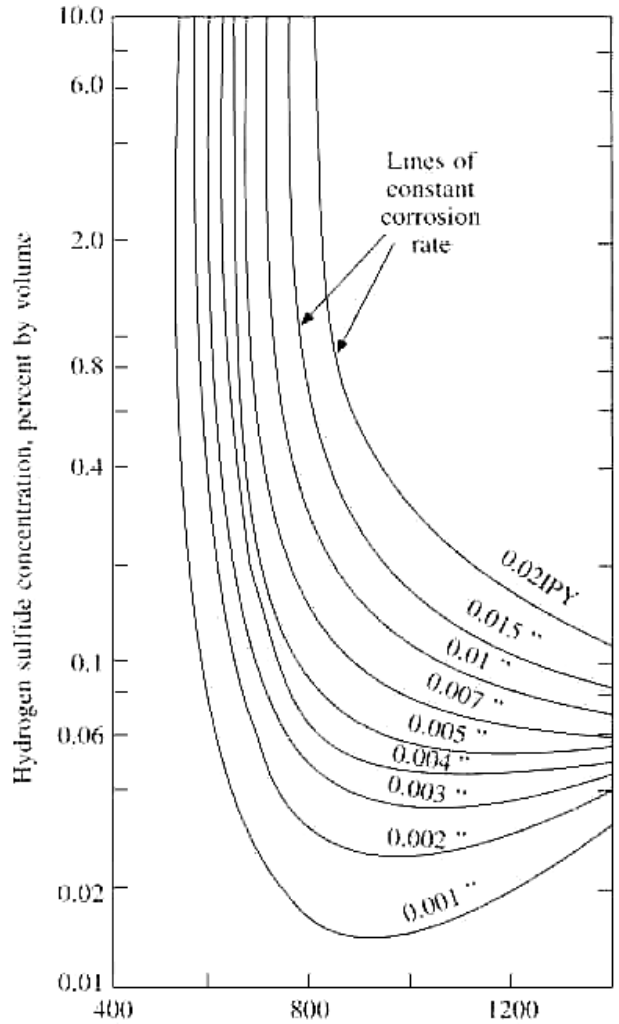


FIGURE 6.28 Isocorrosion rate curves for stainless steels at various temperatures and partial pressures of H_2S .

thermodynamic and kinetic frameworks for both nucleation and growth of scale layers on materials exposed to mixed-oxidant atmospheres is quite complex.

When studying reactions between metallic alloys and complex gas environments, the chemical activities of several reactive species in the gas phase must be considered simultaneously, and these activities are generally established by gas-phase equilibria, especially at elevated temperatures. In binary and ternary gas mixtures, the chemical potentials of the reactive species can be readily established, as a function of temperature, from the room-temperature gas composition and free-energy data for reactions. For a gas system that consists of CO , CO_2 , H_2 , H_2O , CH_4 , H_2S , and N_2 or NH_3 , several gas equilibria

have been used to formulate a set of nonlinear algebraic equations. One can use iterative procedures to determine gas compositions at elevated temperatures that yield minimum free energy for the system and satisfy the conservation of different reactive elements (i.e., C, H, S, O, and N) and the total pressure of the gas mixture. Results of such analyses have been used to establish the elevated temperature gas compositions; the partial pressures of oxygen, sulfur and nitrogen; and carbon activity in the gas mixture. In the analysis of gas/metal interactions in mixed-gas atmospheres, it is inherently assumed that equilibria among various molecular gas species prevail, and chemical activities are calculated by using the above approach or some similar method.

A convenient way of representing the possible corrosion products as a function of gas chemistry is to construct thermochemical diagrams that depict the stability ranges of various condensed phases as functions of the thermodynamic activities of the two components of the reactive gas. A schematic of the phase stability diagram for Fe, Cr, Ni, and Mn and their oxides and sulfides at 875 °C is shown in Fig. 6.29 as a function of the oxygen and sulfur partial pressures. The diagram shows that at oxygen and sulfur pressures below the metal/oxide and metal/

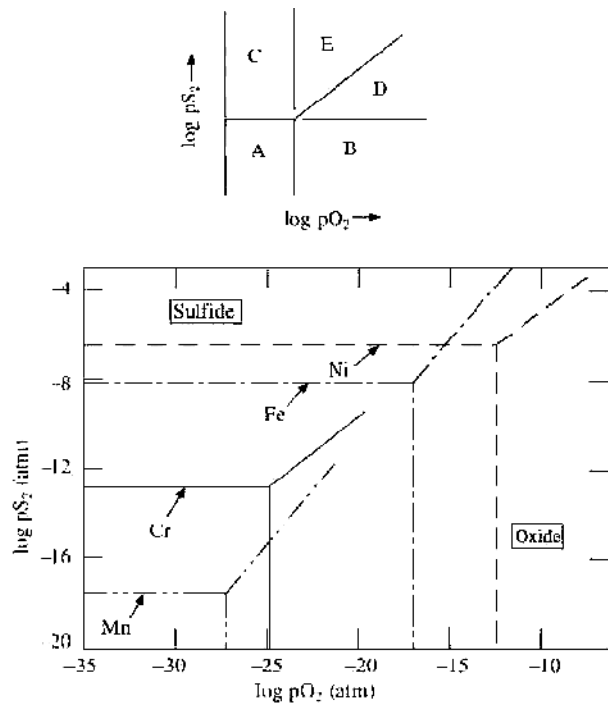


FIGURE 6.29 Thermochemical diagrams for M-S-O systems (where M = Cr, Fe, Ni, and Mn) at 875 °C.

sulfide boundaries, respectively, (region A of upper diagram), the metal will be stable and undergo neither an oxidation nor sulfidation reaction. In regions B and C, the oxygen or sulfur partial pressures are sufficient to form oxide and sulfide phases, respectively. In region D, the oxide is the thermodynamically stable phase; however, the sulfur partial pressure is sufficient to form sulfides in the subscale. The reverse is true in region E.

In the construction of these diagrams, the thermodynamic activities of the metal and corrosion-product phases are assigned a value of unity. Fig. 6.30 shows a phase stability diagram for the chromium-carbon-oxygen system developed for a temperature of 982 °C. In multi-component alloys, the activities of constituent elements will be less than unity and should be accounted for in the analysis. Furthermore, in gas/solid reactions that involve multi-component alloys, a more complex corrosion product (i.e., more complex than a binary compound) can result and will also decrease the thermodynamic activities of the specific phase in the mixture. This is especially true in cases where the corrosion reactions lead to a liquid phase.

6.17 SCALING OF ALLOYS IN SO₂ CONTAINING ATMOSPHERES

A mixed environment such as SO₂ and O₂ exhibits both sulfur and oxygen activities. Thus, to characterize the corrosion behavior in such an atmosphere,

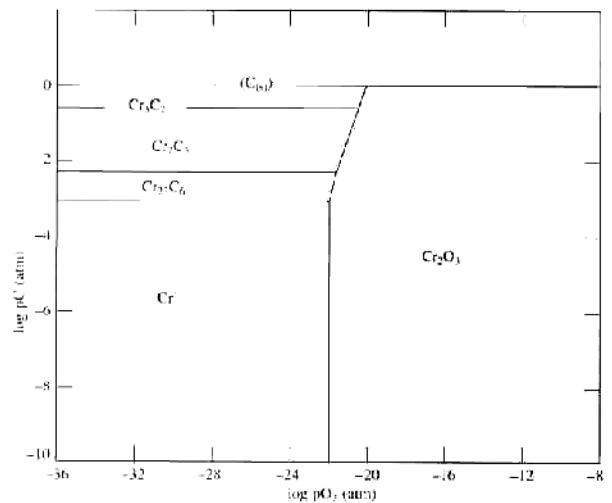
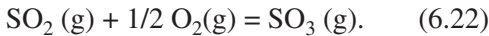


FIGURE 6.30 Thermochemical stability diagram for the chromium-carbon-oxygen system developed for a temperature of 982 °C.

it is necessary to construct the so-called stability diagrams described previously. There is hardly any application where the environment consists of 100% SO_2 . Even in the manufacture of sulfuric acid, where sulfur is oxidized to SO_2 , the partial pressure of SO_2 is 15%—the rest is oxygen (5–10%) and N_2 . However, several studies have been conducted in pure SO_2 atmosphere. This is mainly to understand the corrosion reaction. Sulfur dioxide, with oxygen, is perhaps the more common atmosphere and the reaction is a bit different in this atmosphere than in pure SO_2 , because under these conditions the following reaction may occur:



The presence of SO_3 changes the reaction. Since the formation of SO_3 is temperature dependent, the extent of the reaction with metal also varies with pressure. Let us look at the reaction in pure SO_2 with nickel—the most-studied metal. The reaction of nickel with SO_2 occurs in the following manner:



The scale is a duplex scale, and the reaction exhibits a significant temperature and pressure dependence. At 1 atm. SO_2 pressure and at 500–600 °C, per the stability diagram, NiSO_4 is a stable phase and exists in equilibrium at the outer surface of the scale. The growth of a duplex layer may also occur via the following reaction:



As the pressure is decreased below 0.1 atm. at 600 °C, the scale is no longer in equilibrium with NiSO_4 and, therefore, there is no possibility of the reaction shown in Equation 6.24. Hence, the reaction rate decreases, and there is a strong pressure dependence. The rate of reaction is linear from 1 atm. to about 0.01 atm. in the temperature range 500–1,000 °C; however, at 600 °C (due to stability of the NiSO_4 phase at high pressures), the rate is much higher from 0.1 atm. to 1 atm. and falls below 0.1 atm.

The strong temperature dependence can be explained as follows: Above 600 °C, the rate starts decreasing. This occurs, mainly, for two reasons:

1. NiSO_4 is stable up to 600 °C, above which it begins destabilizing. This reduces the possibility of the reaction in Equation 6.24.

2. At about 635 °C, the Ni-S liquid begins stabilizing. The reactions at 700–900 °C are linear, and the rates are proportional to SO_2 pressure. The rate decreases further as temperature increases above 800 °C, because Ni_3S_2 is unstable above this temperature. Thus, sulfide formation becomes thermodynamically impossible at sufficiently high temperatures and/or at low SO_2 pressures. Under these conditions, NiO is the only reaction product, which is why at 1,000 °C, the rate of reaction in SO_2 is same as the rate of reaction of Ni in 1 atm. O_2 .

The initial reaction in $\text{SO}_2 + \text{O}_2$ between 600 and 900 °C occurs in the same way as in an SO_2 environment, with the formation of a duplex scale of NiO and Ni_3S_2 , as per the reaction (Eq. 6.23). However, the subsequent reaction



depends very much on the reaction (Eq. 6.21). The rate of the reaction increases, depending upon the availability of SO_3 , as per the reaction (Eq. 6.21). The reaction of Ni and $\text{O}_2 + 4\% \text{SO}_2$ at 700 °C occurs very slowly in the beginning, as shown in Fig. 6.31. This shows the extent of the reaction with the total pressure of SO_2 and O_2 , until a time when SO_3 starts forming. At this point, the SO_3 pressure in the mix-

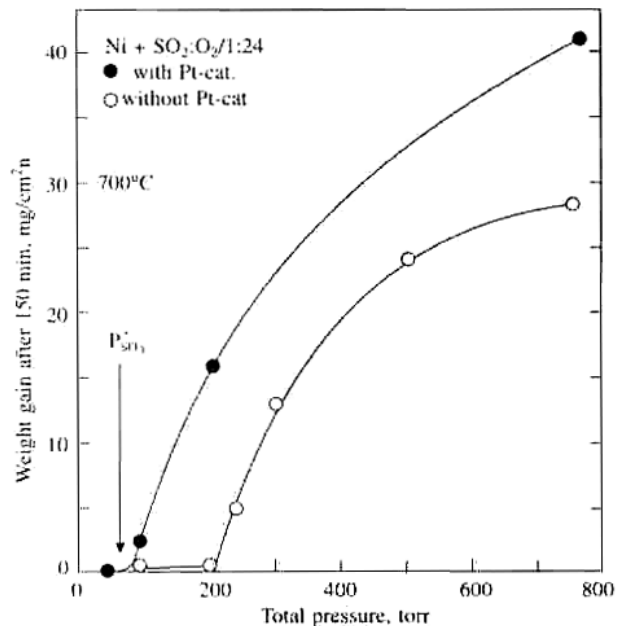


FIGURE 6.31 Oxidation of pure Ni in SO_2 and O_2 with and without the presence of Pt catalyst.

ture is higher than the equilibrium SO_3 pressure $p^*\text{SO}_3$ of the reaction (Eq. 6.25). Furthermore, it can be shown that the reaction of Ni in SO_2 and O_2 is highest when the ratio of $\text{SO}_2:\text{O}_2$ is 2:1.

The reaction of cobalt is very similar to that of nickel. In an SO_2 atmosphere, the linear rate increases with an increase in temperature up to 920°C , above which it decreases sharply, as shown in Fig. 6.32. The scale consists of CoO and cobalt sulfide. When oxygen is also present along with SO_2 , the scale is in equilibrium with cobalt sulfate. The rapid reaction rate for the $\text{Co}+\text{SO}_2$ reaction is displaced to higher temperatures, compared to that of the $\text{Ni}+\text{SO}_2$ reaction. Fig. 6.33 illustrates how the weight change at various temperatures for cobalt has been shifted toward the higher temperature side (shifting the temperature of maximum reaction from 600°C for Ni to 920°C for cobalt). This shift is due to two reasons: a higher stabilization temperature of cobalt sulfide Co_9S_8 ($780\text{--}930^\circ\text{C}$); and the higher stability of Co-S liquid solution (about 880°C).

The reaction of iron with SO_2 is slightly different from that of Co and Ni. Reaction of iron measured at 700°C mainly formed FeO as the outer scale. The sulfide FeS was found enriched in the inner part of the scale next to oxide metal interface. The rate of reaction in SO_2 was not very different from the rate in air, as shown in Fig. 6.34. The reason for this was

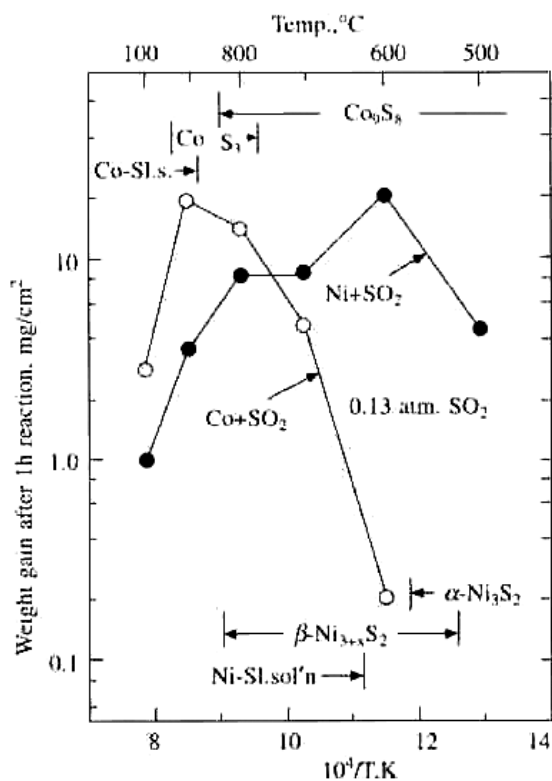


FIGURE 6.33 Comparison of oxidation of Ni and Co in SO_2 at various temperatures.

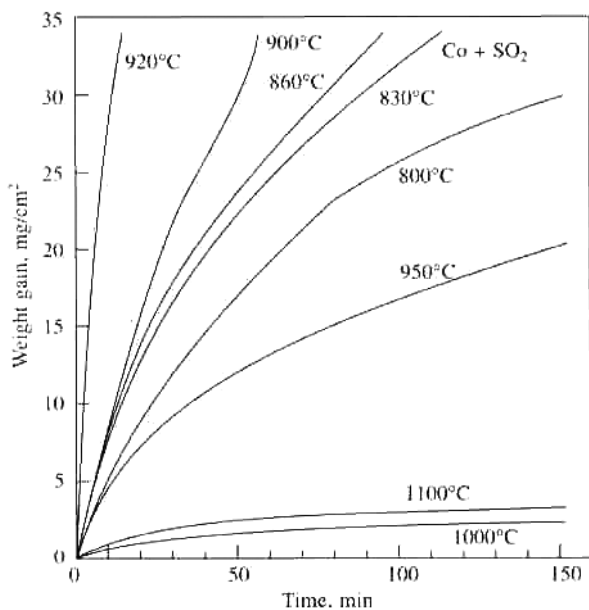


FIGURE 6.32 Oxidation kinetics of Co in SO_2 at various temperatures.

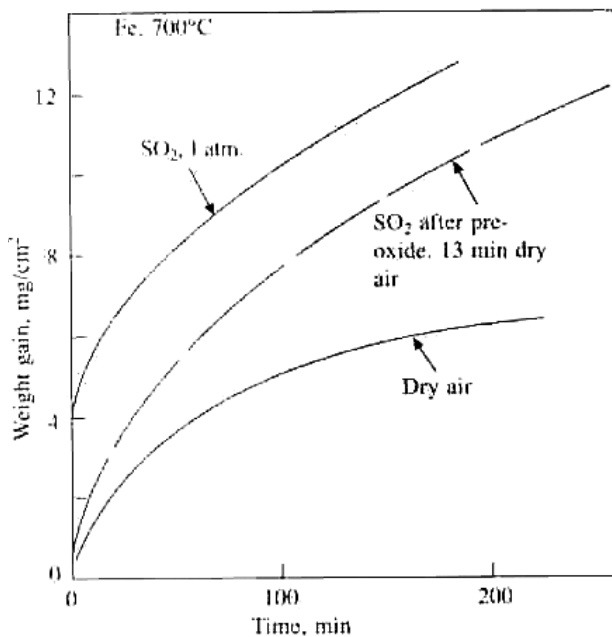


FIGURE 6.34 Effect of pre-oxidation on the sulfidation of iron at 700°C .

that both FeO and FeS are equally highly-defective oxides. Hence, the diffusion of metal ions does not differ significantly. The reaction of Fe in SO₂ becomes explosive after a temperature of 940 °C, as this is the temperature at which a eutectic mixture of FeO+FeS is formed. Chromium, when reacted with SO₂ at temperatures 700–1,000 °C, resulted in the formation of chromia scales. No sulfide was detected. However, extensive blistering of the surface was detected in a manner similar to that in oxygen.

Reaction of nickel chromium alloys in SO₂-bearing environments is dependent upon temperature and the partial pressure of SO₂. In 1 atm. pressure of SO₂, the reaction is very similar to that of pure nickel, with the rate of corrosion increasing with temperature from 600 °C to 800 °C; above this, the rate of reaction is much lower. This is because of the formation of a duplex NiO and Ni₃S₂ scale at these temperatures. However, the nickel sulfide melts after 635 °C and the rate increases up to 800 °C. Above 800 °C, the nickel sulfide is unstable. Also at these temperatures, a protective chromia scale starts forming. The reaction in an SO₂ and O₂ atmosphere also has a similar trend. For an SO₂:O₂ ratio of 2:1, the effect of the addition of chromium to nickel is shown in Fig. 6.35.

6.18 OXIDATION OF Fe-Cr-Al AND Ni-Cr-Al ALLOYS IN SO₂ AND O₂ ENVIRONMENTS

Ternary alloys of Fe and Ni with Cr and Al are the most important materials for many high temperature applications, especially for gas turbines. Superalloys and oxide-dispersed strengthened alloys are either Ni-based or Fe-Ni-based alloys with Cr and Al as the main alloying elements. Some of these alloys form protective chromia or alumina scale. Many of these alloys have good corrosion resistance in SO₂ and SO₂+O₂ environments, but no definite rule can be framed to generalize their behavior in these environments. However, it can be clearly stated that if the environment at the beginning of exposure is oxidizing (i.e., the environment has enough oxygen to form a protective alumina or chromia scale), the alloys will behave quite well, provided there is no scale cracking or spallation. In case of scale spallation, further oxidation may be fast and even catastrophic. Since many alumina-forming alloys have a strong tendency for spallation, chromia-based alloys are more suitable in such environments. If an alu-

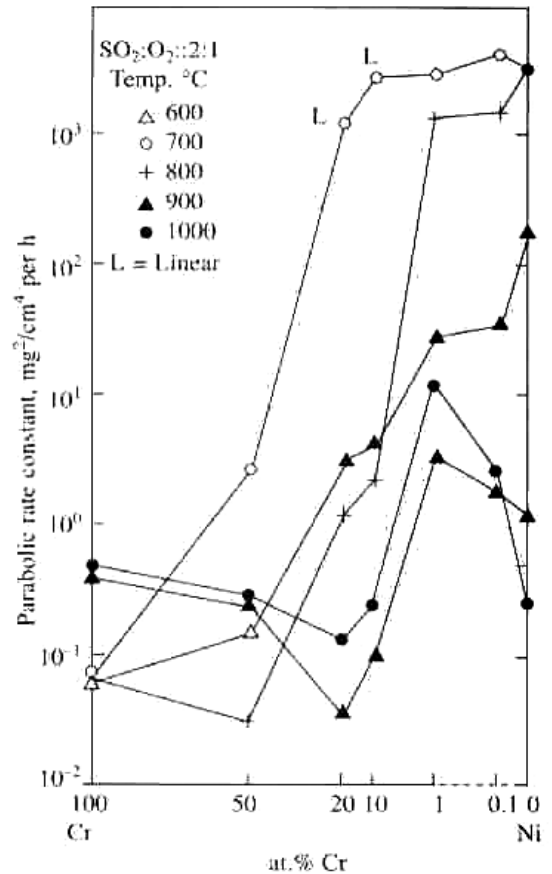


FIGURE 6.35 Effect of Cr concentration on the oxidation of Ni in SO₂ and O₂ at various temperatures.

mina-forming alloy is used, it must have enough chromium so that during scale spallation or cracking a fast-healing layer of either chromia or alumina is formed, without exposing the SO₂ environment to nickel.

It was shown that Ni-10Cr-9Al alloy, which behaved very well in oxygen at 1,000 °C, catastrophically oxidized in a 1% SO₂ (balance O₂) environment. But when the Cr level in the alloy was increased (e.g., alloy Ni-20Cr-6Al), it showed a similar behavior in a 1% SO₂ environment, as in oxygen or air. Furthermore, it was found that on the spalled regions there was a growth of either alumina or a spinel of NiCrAl. The iron-based alloys are expected to behave better than the corresponding nickel-based alloys because of less damage due to formation of FeS, compared to nickel-sulfide formation. This is why iron-based ODS alloys MA 956 and PM 2000 behave much better than the nickel-based alloys MA 6000 and MA 760.

6.19 HOT CORROSION

Sulfur impurity in coal produces an environment of sulfur dioxide at the temperature of operation. In fact, coal and certain oils also have other impurities: coals have salts of sodium and potassium, and oils have vanadium. These impurities are retained in the ash, which usually deposits on the hot spots of the outer parts of heat-exchanger tubes. At the temperature of operation, some of these salts are in the liquid state, or they get converted into complex salt mixtures in the presence of sulfur-bearing gases. Such complex mixtures melt at much lower temperatures, creating a liquid melt on the surface of the metal or alloy.

Corrosion in the presence of such liquid melts of salts is known as *hot corrosion*. It is also called deposit corrosion, as the salts first deposit on the surface and then change to liquid melt, either on their own or by forming complex mixtures of salts. Coal or oil impurities are not solely responsible for salt formation. Another source, for example, is ingress of salt in the air of marine environments. That is why gas turbines operating in marine environments have a severe hot corrosion problem. In this section, we will discuss the principle of hot corrosion, its types, methods of testing, and the way in which it deteriorates the protective oxide scale on the metal or alloy. Some of the examples of hot corrosion, especially in power plants and gas turbines, will also be discussed.

6.19.1 Types of Hot Corrosion

Hot corrosion is of two types:

Type I. Type I hot corrosion usually occurs at higher temperatures—when the salt deposit on the metal or alloy is in a liquid state. Under these conditions, the corrosion rate is very high, right from the beginning of the corrosion process, and the kinetics are mainly linear (as shown in Fig. 6.36) for the corrosion of Ni in the presence of Na_2SO_4 at 900°C . Since the melting point of Na_2SO_4 is 880°C , faster corrosion takes place from the initial stage and can be compared with the oxidation of Ni without the presence of salt, where the corrosion rate is negligible.

Type II. In Type II hot corrosion, the reaction in the beginning is very slow, until the rate increases suddenly, at a certain point, and follows linear kinetics. This is depicted in Fig. 6.37. In other words, there is an incubation period before the corrosion

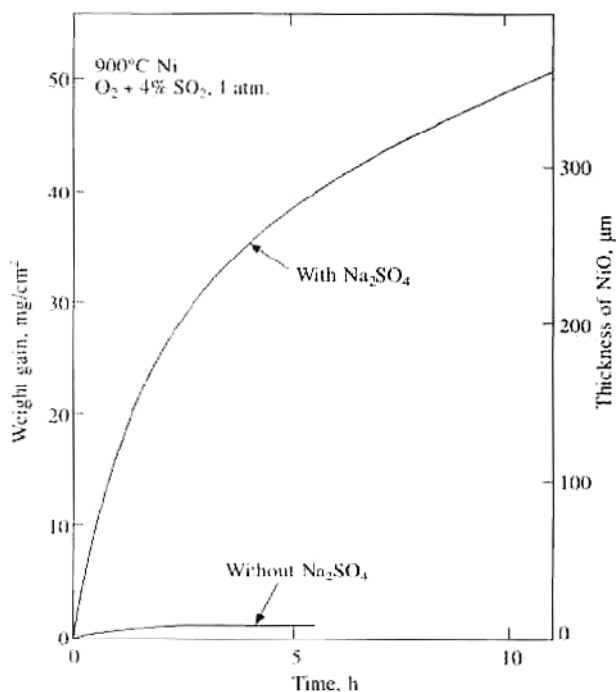


FIGURE 6.36 Corrosion of nickel, with and without the presence of the salt Na_2SO_4 in 1 atm. $\text{O}_2 + 4\% \text{SO}_2$ at 900°C .

rate rises with fast linear kinetics. This type of hot corrosion usually occurs at low temperatures (i.e., the temperature is lower than the melting temperature of the deposited salt). During the initial stages of oxidation, kinetics are just the oxidation of the base metal. As the oxidation progresses, the oxidation products react with the salt deposits and form a complex mixture of salts, which has a lower melting point than the original salt. At this stage, the corrosion reaction suddenly rises. Fig. 6.37, for example, shows the corrosion of nickel at 700°C with Na_2SO_4 as a deposit. In the initial stages, Na_2SO_4 is solid, and the corrosion reaction involves the oxidation of nickel to form NiO , which in the presence of SO_2 forms NiSO_4 . It is the mixture of Na_2SO_4 and NiSO_4 that melts at 671°C and, at this stage, the reaction rate increases.

In coal-based power plants, fireside corrosion involves Type II hot corrosion. Na_2SO_4 or K_2SO_4 , formed from the reaction of SO_2 with NaCl or KCl present in the coal, are the principle salt deposits in the ash. As the maximum outer wall temperature of steam generating tubes ranges from 550 – 650°C , the hot corrosion does not take place until the sulfate deposits react with SO_3 to form pyrosulfates. For the reaction

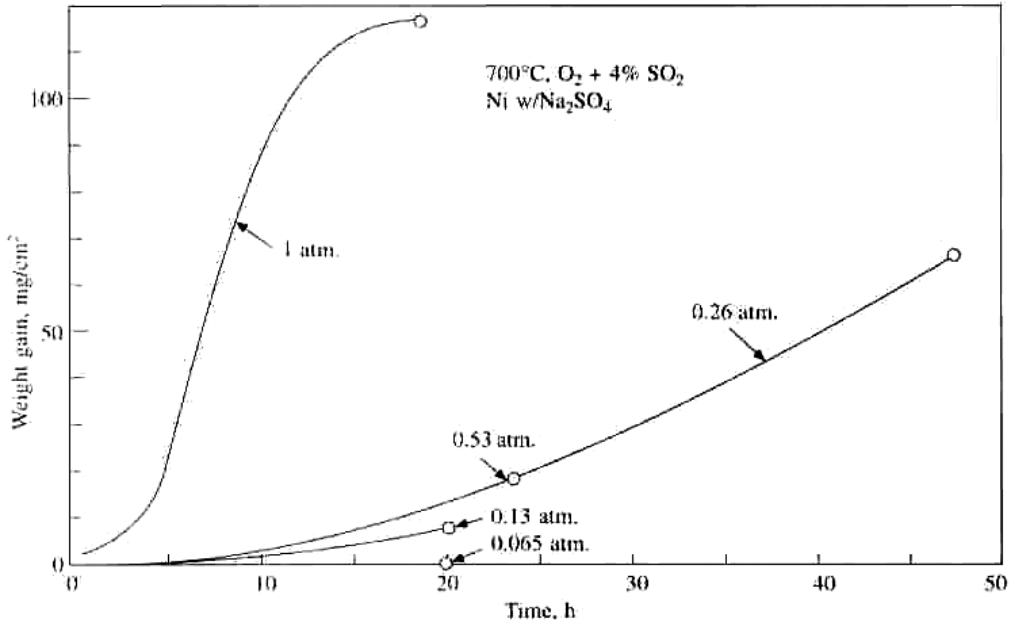
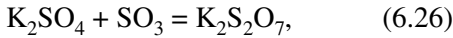


FIGURE 6.37 Corrosion of nickel at 700 °C, covered with Na₂SO₄ deposit (2.5 gm/cm²) in 1 atm. O₂ + 4% SO₂ at different total gas pressures.



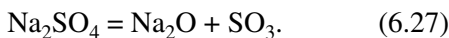
$$a_{Na_2O} a_{SO_3} = \text{constant } a_{Na_2SO_4}, \quad (6.28)$$

about 150 ppm of SO₃ is required. For a similar reaction with Na₂SO₄, the requirement of SO₃ is about 2,500 ppm. Once the pyrosulfates are formed, a complex mixture of two melts at about 451 °C for the potassium salt, and 551 °C for the sodium salt. Severe hot corrosion takes place.

6.19.2 How Hot Corrosion Affects the Corrosion Rate

The main purpose of salt deposits is to destroy the protective oxide films. Once a liquid salt deposit is formed, it dissolves the protective oxide and, hence, the corrosion rate increases. Dissolution of the oxide takes place by the fluxing of salts. This mechanism has been discussed in detail for sulfate melts.

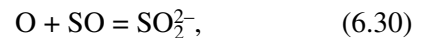
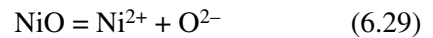
Pure Na₂SO₄ melts at 884 °C, but when other salts (such as NaCl, NiSO₄, etc.) are dissolved in it, its melting point is lowered. Na₂SO₄ can be broken into acidic and basic parts as



If one expresses the above equilibrium equation in terms of the activity of various components as

with the assumption that for pure a, Na₂SO₄ = 1, one finds that the activity of Na₂O (the basic component) is inversely related to the activity of SO₃. At sufficiently low sulfur activities, Na₂O is the only stable phase, and SO₃ has sufficiently low oxygen activity. The acid and basic fluxing models depend upon whether the oxide is being dissolved by Na₂O (the basic component of Na₂SO₄) or by SO₃ (the acidic component).

When NiO dissolves by the acidic process, the corresponding equation can be written as



meaning that under this condition, the nickel oxide changes to NiSO₄. Other oxides also exhibit similar behavior.

Thus, the concept of basic or acidic fluxing of oxide scale has provided the first interpretation of hot corrosion. A simple fluxing model is shown in Fig. 6.38, where it is assumed that the metal is covered by a thin, protective oxide scale that is continually dissolved in the salt melt. The linear reaction rate implies that the protective scale is reformed at

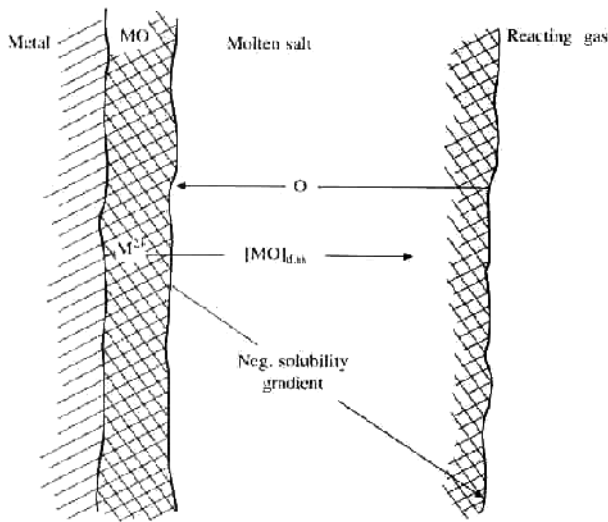


FIGURE 6.38 Simple model for fluxing of a continuous, protective oxide scale MO in a film of molten salt. The solubility of MO is assumed to have a negative gradient across the salt layer, which leads to the precipitation of MO at the film surface.

the same time it dissolves (i.e., the scale then has a stationary thickness).

In fact, the fluxing model, illustrated above, is valid for very initial stages of the reaction. But as the reaction proceeds, depending upon the $\text{SO}_2 + \text{O}_2$ concentration, a sulfate-induced hot corrosion process is sustained. This results in the formation of thick layers of reaction products, which primarily consist of NiO and nickel sulfides. Depending upon the reaction conditions, the sulfate phase is distributed throughout the layer of the reaction products or is concentrated in an outer layer, near the gas/scale interface.

6.19.3 Testing Methods for Hot Corrosion

Tests on hot corrosion of metals and alloys are relatively more difficult than the corresponding simple oxidation or sulfidation tests. The main problem here is the mode and the frequency of salt deposition on the test samples. Actual simulation is very difficult. Moreover, the deposit of salt spalls off quite often during the test. However, testing is being carried out using following methods:

1. The most common method applied in hot corrosion testing is by deposition of a calculated amount of salt from its saturated solution on the surface of the specimen, followed by measure-

ment of weight changes. The main limitation of this method is the spallation of salt during the test, and subsequent exposure of the oxide surface.

2. A second test, known as the bead test, more closely resembles practical situations. In this test, the salt vapors are continuously supplied to the sample by evaporating the salt at a higher temperature in a thermal gradient furnace and keeping the specimen on the lower temperature side of the furnace. This way, a continuous supply of salt vapor is maintained throughout the test (Fig. 6.39).
3. Another test is carried out by completely immersing the specimen in the salt melt for a fixed duration of time, followed by examination by optical or electron optical techniques. This permits analysis in terms of the depth of penetration and type of attack (whether uniform, localized, intergranular, etc.). This technique, although good, is far from simulating the exact conditions, but it is a nice technique to compare the relative performance of several materials (Fig. 6.40).
4. One of the most utilized methods to test hot corrosion is by burner rigs. The main advantages of such tests are that it is possible to simulate several conditions of salt supply, gas flow rates, and proper atmospheric control. Considerable data collected in hot corrosion is from burner rig tests (Fig. 6.41).

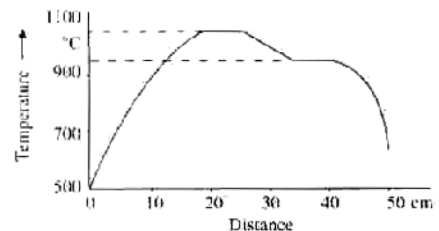
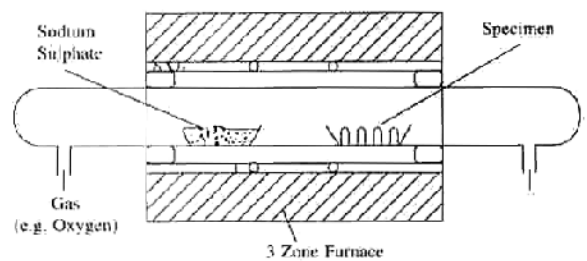


FIGURE 6.39 Schematic of bead test.

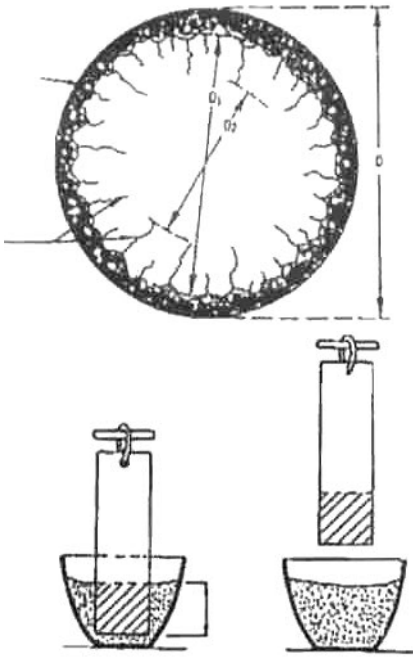


FIGURE 6.40 Schematic of the crucible test.

6.20 OXIDE SPALLATION

The study of high temperature oxidation is incomplete without a discussion of the problem of oxide scale spallation, its methods of detection, and prevention. The process of oxidation involves nucleation, growth and, finally, the formation of a protective oxide scale on the surface. In many cases, the scale formed is very smooth and adherent and does not spall at all. In other cases, the spallation starts at the very early stages of oxidation and continues with intermediate rebuilding of the scale. The main reason for scale spallation is the stress generation in the oxide during its growth. There are various reasons for stress generation during the scale growth process, and any one of them or a combination of these can lead to scale spallation.

When a scale grows, the stresses start accumulating. A plot of stress accumulation with time versus the corresponding weight gain during oxidation is shown in Fig. 6.42. The stresses start accumulating with the oxide growth process as the weight increases due to oxidation. However, at a certain point, T_c , the scale thickness is unable to bear the increased stress and releases it. This release can either be due to cracking in the scale or creep of the substrate metal. Both of these factors will lead to scale

spallation. There will be no scale damage only in those cases where there is a perfect match or only a little mismatch between the thermal expansion coefficients of oxide and the substrate. The various factors responsible for the accumulation of stress are as follows:

- difference in the molar volumes of metal and the oxide scale formed on it [the Pilling Bedworth Ratio (PBR)],
- epitaxial stresses,
- mode of diffusing species,
- geometry of the sample,
- composition of the scale,
- differences in the thermal expansion coefficients of oxide and the metal.

6.21 THE PILLING BEDWORTH RATIO

The Pilling Bedworth ratio (PBR) is defined as the ratio of the molar volume of metal to the molar volume of the oxide formed on it. If there is a large difference between the two, then the oxide has a tendency to spall. However, if the ratio is equal or close to 1, the oxide does not spall, and the scale remains adherent to the substrate metal. If the ratio is more than 1, the stress accumulated is compressive; whereas, if the PBR is less than 1, the scale has tensile stress. Alkali metals, which usually have very low values of PBR, have tensile stresses. These metals have a violent reaction when exposed to air. Here, since the metal volume is always more than that of the oxide, the metal is available for the oxidation reaction. Many metals (such as Zr) have a PBR value equal to 2.5 and have high compressive stresses. For example, Ni with a PBR value of 1.5 has very adherent and stable oxides.

There are several exceptions to the PBR rule. This is because the PBR is not the only factor responsible for scale spallation. Many other factors also act simultaneously. Hence, the PBR rule is merely an indication of the direction of stress, rather than an indication of spallation.

6.22 STRESSES DEVELOPED DURING THERMAL CYCLING CONDITIONS

Most industrial applications of high temperature materials involve temperature fluctuation. Complete cooling of a component to ambient temperature may occur frequently in practice, and the relative coefficients of expansion of the metal and oxide, there-

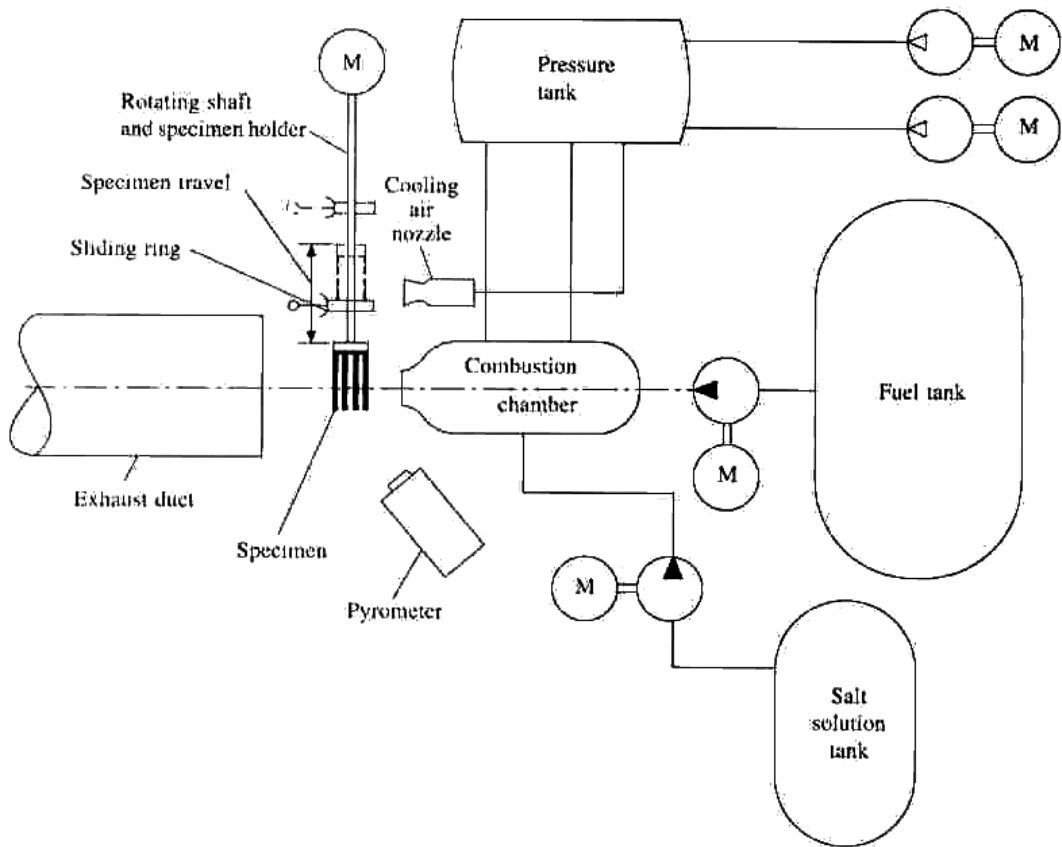


FIGURE 6.41 Schematic of the burner rig test.

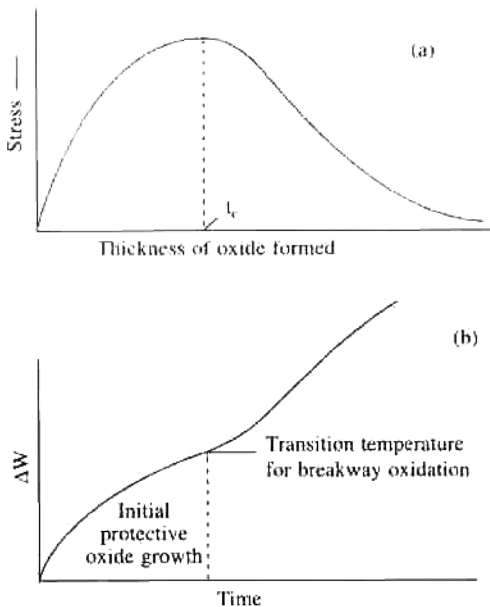


FIGURE 6.42 Stress accumulation in the growing oxide scale with time.

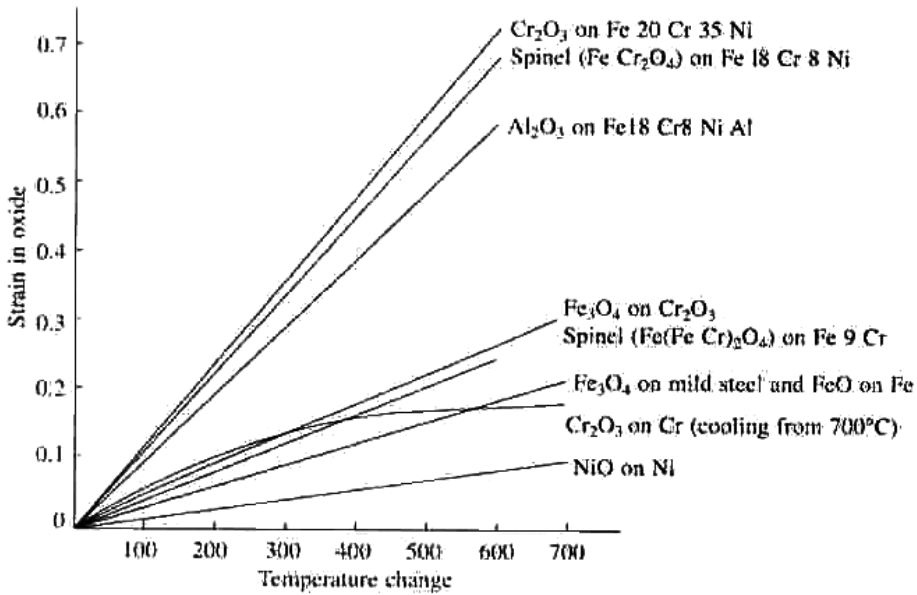
fore, are likely to be important in determining the stresses that are generated. The expansion coefficients of some metal-oxide systems are given in Table 6.8. The oxides on nickel and cobalt are known to be extremely tenacious and rarely spall during temperature cycling. This characteristic is undoubtedly due to the similarity of expansion coefficients of the metals and oxides, although the irregular nature of the interface (observed on oxidized nickel, for example) may also contribute to good adherence. The surface oxide strains developed on oxidized metals and alloys as a result of a change in temperature have been estimated for several systems, and the results are shown in Fig. 6.43.

The metal usually has a higher coefficient of expansion than the oxide; and, on cooling, it induces a compressive stress in the oxide with a magnitude given by

$$\sigma_{\text{oxide (compressive)}} = \frac{E_o \Delta T (\alpha_o - \alpha_m)}{1 + 2(E_o/E_m)(t_o/t_m)}, \quad (6.31)$$

TABLE 6.8 Linear Expansion Coefficients of Metals and Oxides [3]

| System | Oxide Coefficient ($10^{-6} \alpha_o$) | Temperature Range °C | Metal Coefficient ($10^{-6} \alpha_m$) | Temperature Range °C | Ratio α_o/α_m |
|------------------------------------|---|-------------------------|---|-------------------------|---------------------------|
| Fe / FeO | 12.1 | 100–1000 | 15.3 | 0–900 | 1.25 |
| Fe /Fe ₂ O ₃ | 14.9 | 20–900 | 15.3 | 0–900 | 1.03 |
| Ni/NiO | 17.1 | 20–1000 | 17.6 | 0–1000 | 1.03 |
| Co/CoO | 15.0 | 20–1000 | 14.0 | 25–350 | 0.93 |
| Cr/Cr ₂ O ₃ | 7.3 | 100–1000 | 9.5 | 0–1000 | 1.30 |
| Cu/Cu ₂ O | 4.3 | 20–750 | 18.6 | 0–800 | 4.32 |

**FIGURE 6.43** Strains generated at the interface between various oxides and substrates by differential thermal expansion.

where E_o and E_m are the Young's moduli of the oxide and metal, respectively; α_o and α_m are the coefficients of thermal expansion of the oxide and metal; t_o and t_m are the thicknesses of the oxide and metal; and T is the temperature drop. The compressive thermal stress in surface oxides on niobium was over 410 MN/m^2 , which, although considerably less than the fracture strength of 790 MN/m^2 , could cause failure of the oxide when taken in conjunction with growth stresses and other isothermally-induced stresses.

The greater the disparity between expansion coefficients, the less adherent the oxide becomes during cooling. Consequently, the system Cu/Cu₂O/CuO has received considerable attention; for, as shown in Table 6.8, the coefficients of expansion of the metal and oxides are very different. Cooling from temperatures below $700 \text{ }^\circ\text{C}$ causes the oxide on

copper to spall extensively. This is thought to be due to the fact that the oxide is less ductile, and a combination of growth and thermal stresses result in exfoliation. High plasticity of the oxide above this temperature prevents spalling by relieving growth stresses and leaving only the thermal stresses on cooling.

Since the disparity of thermal expansion coefficients in this system is extremely large, it could be inferred that the plasticity of the oxide is more important in a metal-metal-oxide system than any disparity in the thermal expansion coefficients. The imposition of thermal cycling during oxidation leads to enhanced oxidation due to oxide failure, either by decohesion or cracking, and the consequent exposure of the metal to the oxidant. However, it may be inferred from the above discussion that long soaking times at a high temperature between cooling sched-

ules should improve the adhesion of the scale by allowing stress relief at the high temperatures and, thus, increase its protective potential.

6.23 EXAMPLES OF HIGH TEMPERATURE CORROSION IN VARIOUS INDUSTRIES

6.23.1 Metal Dusting

In many high temperature processes in chemical and petrochemical industries that involve hydrocarbons as reactants and products, the carburization of metallic reaction tubes is a serious problem. A famous example involves the pyrolysis reactor tubes for ethylene production, where carburization of reactor tubes and that of the filament takes place. Several types of carburization processes exist. Some occur in straight carburization in the absence of any oxygen, while others focus on phenomena in environments containing a mixture of oxygen and carbon. Methane-hydrogen mixtures generally have been used to fix carbon activities in the former types of environments; whereas, in the latter type of environment a mixture of $\text{CO-H}_2\text{-H}_2\text{O}$ will fix the chemical potential of carbon and oxygen.

Carbon is rather unique in its interaction with metals compared to those of oxygen and sulfur. While in oxidizing and sulfadizing environments the metal generally forms an external oxide or sulfide scale, part of which can spall and, under certain circumstances, internal oxides and sulfides are formed within the metal. However, in the case of carbon interaction, carburization is almost always internal, even at very high concentrations of the easily carburized element. Perhaps extremely rapid diffusivity of carbon in the metal is the main cause of this phenomenon.

The combination of high carbon activity, close to unity, and relatively low oxygen partial pressure, is characteristic of many industrial process environments. Where a pure iron or an iron-rich alloy is exposed to a carbon-supersaturated environment ($a_c > 1$), a metastable Fe_3C surface carbide forms, generally a prelude to metal dusting.

Metal dusting is a specific form of carbon-induct corrosion, which leads to the disintegration of a bulk metal or alloy into a powder or dust. The metal dusting of iron and iron-rich alloys is indeed triggered by the initial formation of a surface carbide layer. Metal dusting generally occurs in a temperature range of 400–600 °C in environments that are supersaturated with respect to carbon. In other words, the carbon

activity of the environment exceeds unity. The carbon-containing molecule is generally a hydrocarbon or carbon monoxide.

A schematic of metal dusting corrosion of iron is given in Fig. 6.44 Three distinct stages indicated are as follows:

1. In the first stage, carbon from the gas phase is transferred to the surface iron, followed by its dissolution and diffusion into the alloy. Iron gets supersaturated with C up to a certain thickness, which depends upon temperature and the chemistry of the carbon-saturated gaseous environment. The dotted line represents a carbon activity of unity and the solid line—the actual carbon activity profile—indicates the super-saturation.
2. In the next step, a surface carbide of Fe_3C (M_3C) forms, which is generally stable only in carbon-supersaturated environments, requiring a carbon activity in excess of unity to form.
3. In the next stage, carbon (principally graphite) deposits on the Fe_3C surface, whereby the carbon activity at the carbide/graphite interface drops to unity. The carbon activity profile is thus altered. This destabilizes the Fe_3C and leads to its dissociation into iron particles and graphite. At this stage, metal dusting is in progress (Fig. 6.45).

One critical question relates to how the particles are carried away from the reaction interface in order to sustain corrosion. The studies by Schneider [4] and Grabke [5] conclude that iron atoms can indeed migrate via intergraphitic planes away from the dissociation interface. This is further confirmed by recent investigations by Ramanarayana et al., [6] who showed that in metal dusting corrosion of iron in CO-H_2 mixtures, the carbon deposit on Fe_3C is essentially a mixture of amorphous carbon and graphitic carbon. The proportion of graphitic carbon increases with temperature, accounting for nearly 80% of carbon next to the Fe_3C . Moreover, graphite planes are oriented more or less perpendicular to the dissociating Fe_3C facilitating the interaction of iron atoms into graphite. At the outer surface of the graphite deposit, filamentous carbon, which is catalyzed by iron particles, is evident. Thus, metal atoms from dissociation of Fe_3C intercalate and diffuse outward through intergraphitic planes and, ultimately, are carried away by filamentous carbon whose formation they catalyze (Fig. 6.46).

What, then, is the method to prevent metal dusting? There have been two approaches. The first is to decrease the sites on the surface for carbon transfer,

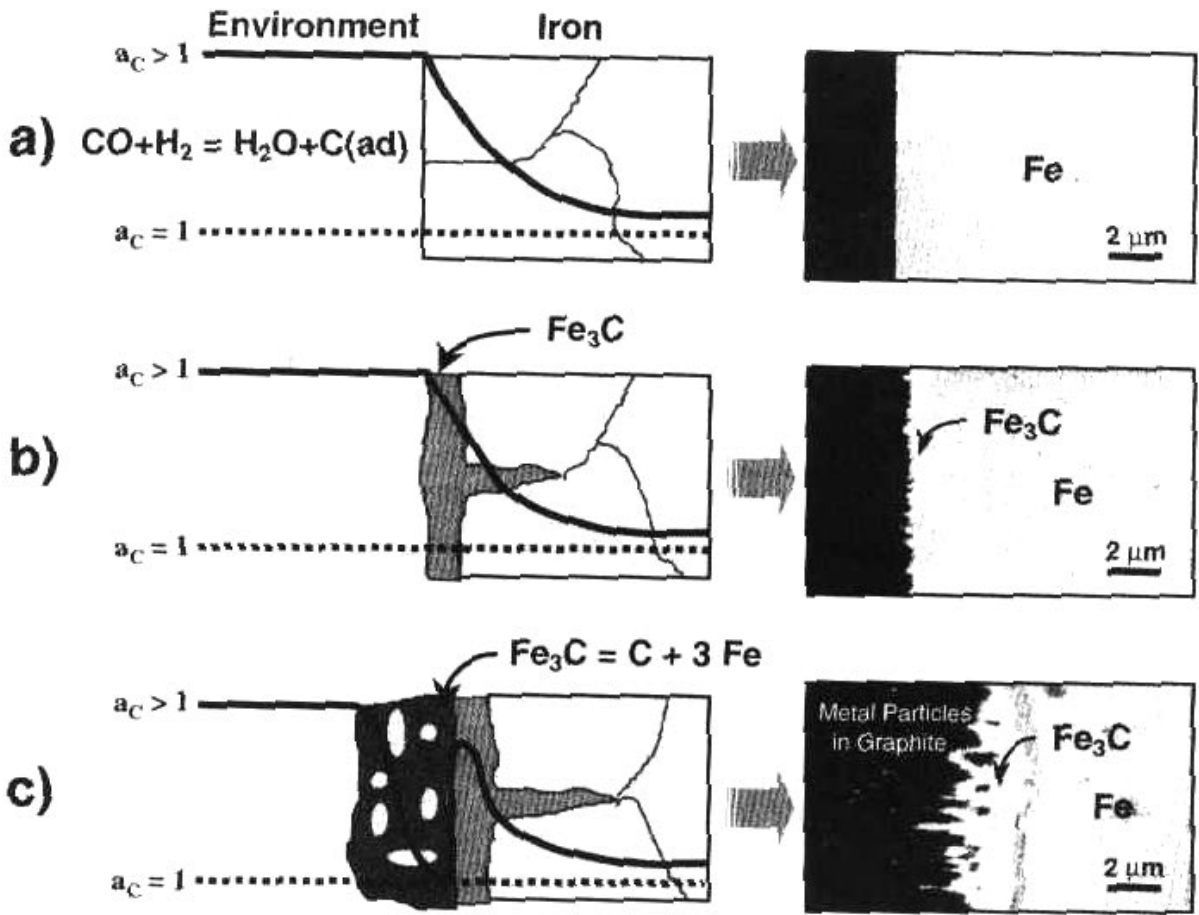


FIGURE 6.44 Thermodynamics of the metal dusting process.

thereby impeding the carburization. The second method is based upon creating a suitable barrier on the surface—one that does not allow carbon to diffuse and, hence, interact with it.

6.23.2 Inhibition by Sulfur

In the first method, metal dusting is inhibited or even prevented by the presence of sulfur. Additions of sulfur-bearing compounds to the atmosphere lead to the adsorption of sulfur on free metal surfaces. The adsorbed sulfur blocks the sites necessary for carbon transfer; thus, carburization is strongly impeded. The presence of adsorbed sulfur even interrupts the nucleation of graphite. Thus, the cementite formed on the surface of iron and steels is stabilized and will continue to grow, but relatively slowly since carbon transfer is retarded. The sulfur is not built into the cementite lattice; rather, it acts in its adsorbed state. At low temperatures, relatively low sulfur activities

are sufficient to suppress the attack (e.g., $\text{H}_2\text{S} / \text{H}_2 \sim 10^{-6}$ at 600°C). Therefore, H_2S is an effective agent against metal dusting of steels at low temperatures, and it appears that many processes in the petrochemical industry do not cause metal dusting, since small concentrations of H_2S in the process gas act as inhibitor.

6.23.3 Coal-Based Power Plants

The high temperature corrosion problem in a coal-based power plant has been a matter of great concern since the very early days of using the combustion of coal to produce steam to generate electricity. Superheaters and reheaters suffer from steam oxidation on their inner surfaces and hot corrosion on their fire sides. Steam oxidation occurs due to the superheated steam, which acts in a similar manner to oxygen at the same temperatures. The oxidation is a matter of concern above 540°C for low alloy steels due to

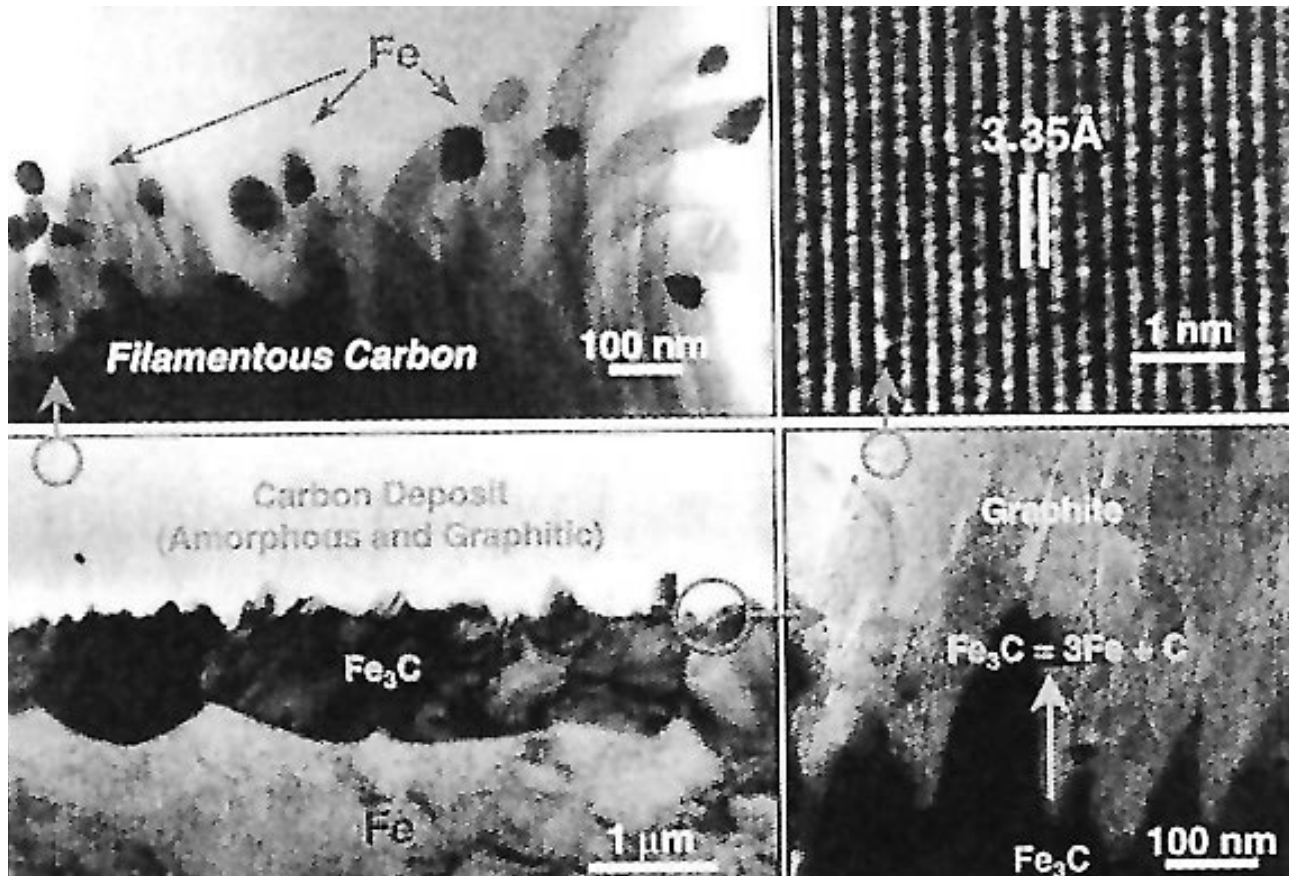


FIGURE 6.45 Scanning electron micrographs showing the metal dusting process.

their limited creep strength around this temperature. Alloys with a higher chromium content should be used for higher allowable stress and better steam oxidation resistance.

The fire-side corrosion of superheaters and reheaters in coal-fired utility boilers is one of the main problems that have limited main steam temperatures to 540 °C for the past 40 years. It exhibits its maximum rate of attack at 700–750 °C, where the corrodent is liquid, and decreases to a minimum at higher temperatures, where the corrodent does not condense. At higher temperatures, corrosion is predominantly the oxidation of uncooled parts, such as hangers.

6.23.4 High Temperature Corrosion of Combustion Turbines

Combustion turbine components are susceptible to oxidation-sulfidation corrosion at elevated temperatures, in addition to the aqueous corrosion problems encountered in the compressor blades and disks.

6.23.5 High Temperature Corrosion of Aircraft Power Plants

Aircraft power plants have the important function of providing thrust, or propulsion, to enable aircraft to take off and remain in flight. However, various components of an aircraft power plant system suffer from problems of high temperature corrosion. There are three predominant types of high temperature corrosion that have caused mechanical failures of aircraft power plant components: sulfidation, hot-salt SCC, and fires.

6.23.6 High Temperature Corrosion in Municipal Incinerators

The corrosion problems in boilers fueled with municipal refuse are different from those encountered with fossil fuels, as chlorine rather than sulfur is primarily responsible for the attack. The average chlorine content of the municipal solid waste is 0.5%, of which about one half is present as polyvinylchloride

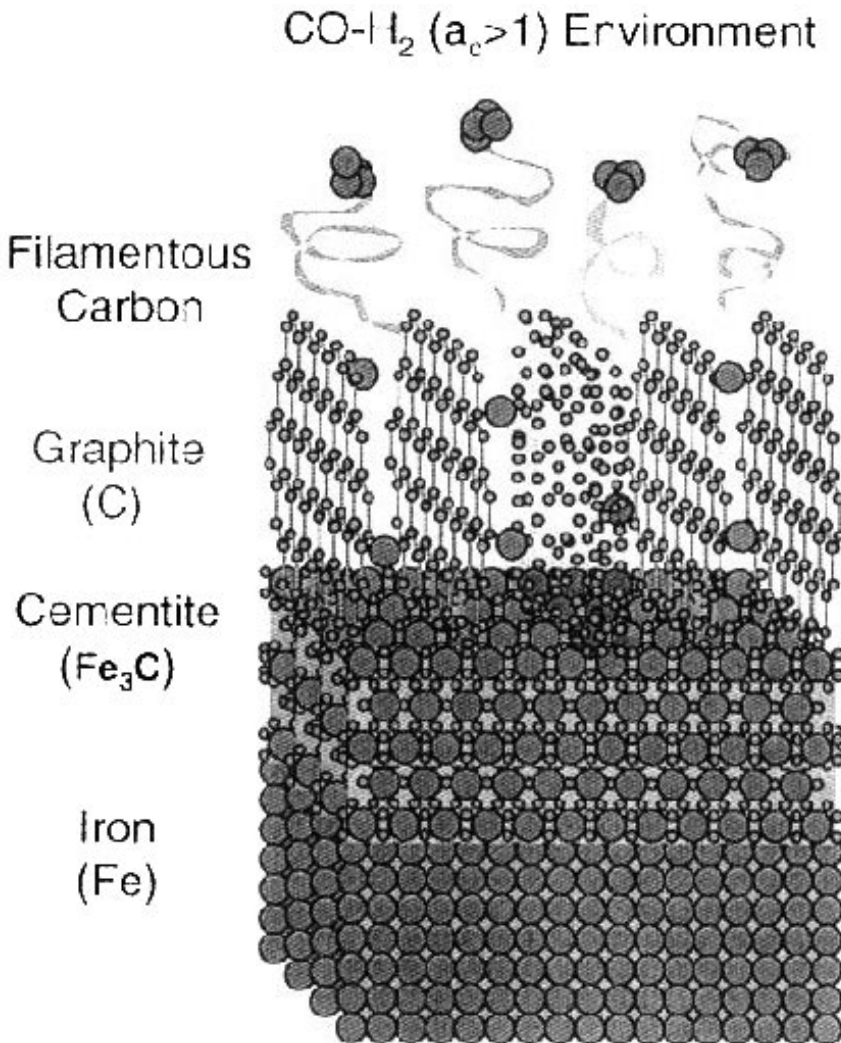


FIGURE 6.46 Mechanism of metal dusting showing how carbon is coming out from intergraphitic planes.

(PVC) plastic. The other half is inorganic NaCl. The chlorine in the PVC is converted to HCl in the combustion process. The inorganic chlorides are vaporized in the flame and, ultimately, condense in the boiler deposits or pass through the boiler with the flue gases. Zinc (Zn), lead (Pb), and tin (Sn) in the refuse also play a role in the corrosion process by reacting with the HCl to form metal chlorides and/or eutectic mixtures with melting points low enough to cause molten salt attack at water wall tube metal temperatures.

6.23.7 Gas Phase Corrosion

HCl alone has little effect on carbon steel at temperatures below 260 °C. However, in the presence of

excess air in the boiler, FeCl_2 is readily formed on the steel surface, which is stable at water wall tube temperatures. However, at a metal temperature of about 400 °C, which may occur in the superheater, the FeCl_2 is further chlorinated to the volatile FeCl_3 . If the gas temperature in the area exceeds 815 °C, the FeCl_3 will evaporate readily, and breakaway corrosion can then occur.

6.24 PETROLEUM REFINING AND PETROCHEMICAL PROCESSES

Most petroleum refining and petrochemical plant operations involve flammable hydrocarbon streams,

highly toxic or explosive gases, and strong acids or caustics that are often at elevated temperatures and pressures. Corrosion has always been an unavoidable part of petroleum refining and petrochemical operations. For practical purposes, corrosion in these applications can be classified into low temperature corrosion and high temperature corrosion. Low temperature corrosion is considered to occur below approximately 260 °C in the presence of water. On the other hand, high temperature corrosion occurs above 260 °C. The presence of water is not necessary, because corrosion occurs by the direct reaction of metal and environment. In the present context, we have confined ourselves to only some examples of high-temperature corrosion problems.

6.25 REFERENCES

1. A. S.Khanna, High Temperature Oxidation and Corrosion, ASM International, Materials Park, OH, April 2002.
2. Per Kofstad, High Temperature Oxidation of Metal, Elsevier Applied Science Publishers, Ltd. NY, 1988.
3. P. Hancock and R. C. Hurst, in *Advances in Corrosion Science and Technology*, Vol. 4, Plenum Press, NY, pp. 1–79, 1974.
4. E. Pippel, J. Woltersdorf and R. Schneide, *Materials and Corrosion*, Vol. 49, p. 309, 1998.
5. Q. Wei, E. Pippel, J. Woltersdorf and H. J.Grabke, *Materials and Corrosion*, Wiley-VCH, Weinheim, Vol. 50, p. 628, 1999.
6. T. A. Ramanarayan et.al., *Materials Forum*, The Institute of Materials Engineering, Australasia, North Melbourne, Vol. 55, pp. 369–372, 2001.

CHAPTER 7

CHEMICAL AND PHYSICAL AGING OF PLASTICS

James A. Harvey

Under the Bridge Consulting, Inc., Corvallis, Oregon

| | |
|-----------------------------------|-----|
| 7.1 INTRODUCTION | 153 |
| 7.2 CHEMICAL AGING | 153 |
| 7.3 ENVIRONMENTAL STRESS CRACKING | 154 |

| | |
|--------------------|-----|
| 7.4 PHYSICAL AGING | 154 |
| 7.5 SUMMARY | 162 |
| 7.6 REFERENCES | 162 |

7.1 INTRODUCTION

In the design of polymers, plastics and parts based on these materials it would be beneficial to have a firm understanding of how their performance is affected by their environments. These effects on the materials may be in the form of chemical, physical or a combination of the two. Physical effects can have many forms; they can be thermal, mechanical, radiation, and/or electrical.

7.2 CHEMICAL AGING

The first step of this chapter is to distinguish between chemical aging and physical aging. Chemical aging is simply the effects of chemicals on the plastic. A better way of explaining chemical aging is to use the term “chemical resistance.” There are some special cases of chemical aging that may be beyond the scope of this chapter. They include such topics as oxidation (reaction of the plastic with either oxygen or ozone). In chefouriermical aging, the dominating result is usually a decrease in molecular weight through chemical reactions, such as chain scission. This also implies that chemical aging is an irreversible process.

Chemical aging or chemical resistance of plastics can simply be related to the basic chemical principle of “like dissolves like.” In other words, aliphatic polymers (polyolefins) are affected by hydrocarbon

materials, while polymers containing oxygen, nitrogen, sulfur, and other non-carbon and hydrogen atoms within their backbones are affected by chemicals containing similar materials. This is a good first approximation in selecting the proper polymer for a plastic application.

Water represents a special case of aging. Water can either cause a reaction (hydrolysis) of the plastic or be absorbed by the plastic as either free or bound (hydrogen bonding) water. Depending upon the conditions, a plastic may undergo chemical aging, physical aging, or a combination of the two. Water does not truly affect polyolefins. It is stored in polyethylene containers. Water affects the properties of such polymers as nylons, polyesters, and epoxies in one of two different ways. Water is absorbed by these polymers, thus reducing their Tg. Drying of the polymer will cause it to return to its original Tg. If these polymers undergo chemical hydrolysis, their Tg is reduced through breaking of bonds.

One of the classic examples of chemical aging involves an aromatic nylon, Kelvar[®], poly (p-phenylene terephthalamide). Chemical resistance is good in Kelvar[®] fibers, except for a few strong acids and alkalis. The amide function, however, is susceptible to hydrolytic degradation. The amide linkage is split into a carboxylic acid fragment and an amine fragment. This degradation can be accelerated by impurities. When Kelvar[®] is subjected to sulfuric acid and sodium hydroxide solutions, and strengths are monitored, it was found that the rate of hydrolysis is 10⁵

and 10^3 times faster in H_2SO_4 and NaOH, respectively (1).

Chemical aging of polyimides in sodium hydroxide solutions causes the imide ring to open and form the sodium salt of the amic acid. When polyimides are digested in caustic, they totally unzip into their components. The dianhydride is identified from the salt of the tetracarboxylic acid formed and the diamine isolated from the digestion mixture. This technique was used by synthetic polymer chemists to determine the composition of the polyimides and to prepare new versions (2).

Another example of depolymerization by chemical aging is the basic catalytic reaction of polyethylene terephthalate. At first, a decrease in molecular weight is observed. The reaction continues until all fragments are broken down into ethylene glycol and the disodium salt of terephthalic acid.

7.3 ENVIRONMENTAL STRESS CRACKING

Another type of chemical aging is environmental stress cracking and crazing. Environmental stress cracking is a type of failure that occurs through surface interactions of polyolefins (such as high density polyethylene) with surfactants or detergents. It has been demonstrated that molded polyolefin plastic parts held under constant stress in an environment of either a surfactant or detergent change their failure behavior from a ductile failure at high stresses to a brittle failure at low stresses (3,4).

Igepal, a nonionic surfactant, assisted environmental stress cracking (ESC) of low density polyethylene (LDPE), by producing three characteristic regions with increasing crack driving force. These regions were: (I) where crack speed and craze length increased; (II) where crack speed and duplex plastic zone length were constant; and (III) where crack speed decreased while the deformation zone length increased. The activation energies for the three regions were 100, 23, and 20 kJ/mole, respectively. The proposed rate-controlling processes of ESC for the LDPE/Igepal system were as follows: Region I, controlled by α_1 -relaxations, and Regions II and III, controlled by lamellar orientation. The Igepal plasticizes the amorphous phase and facilitates the stress-induced orientation of the lamellar (5).

Fracture mechanics was used to investigate ESC of LDPE. Annealed and quenched samples were prepared by notching a single edge on each one and then fracturing the samples under constant load in a liquid methanol environment. The relation between

the stress intensity factor (K) and the crack speed (α) were investigated. There is a great difference between annealed and quenched samples in the variation of this relation with temperature and applied load. The cause of this difference is discussed in detail. It is proposed that thermally-activated molecular motion is essential to ESC of the annealed LDPE, while stress concentration contributes markedly to ESC of the quenched LDPE (6).

Another study based upon fracture mechanics was used to investigate ESC of LDPE with a 4.0 melt flow index. Annealed samples with a single edge notch were prepared and fractured under constant load in four different liquid alcohols. The log α (crack speed) versus log K (stress intensity factor) was influenced by temperature as well as the alcohol environment. The conclusions were as follows: the crack speed at high K was determined by the diffusion mechanism, and this mechanism was explained in terms of thermally-activated molecular motion. On the other hand, the crack speed at low K was strongly related to the plasticization and the stress relaxation of the crack tip material (7).

In addition to these well-known studies, other studies were performed using LDPE. These included different molecular weights, surfactants, bending the samples prior to immersion, and increasing temperatures (8,9).

Another example of environmental stress cracking pertains to rigid thermoplastic polyurethane (RTPU) materials. Two different RTPUs were studied for medical device applications. Significant differences in ESCR behavior was observed in the RTPUs, in spite of their similar chemical composition. One had better chemical resistance than the other under the same stress level and cracking agents. The second RTPU was sensitive to molding conditions. For the first RTPU, the assembling process control was very critical and may have had significant impact on the integrity of the devices made. Heat aging effect combined with chemical attacking should be taken into consideration to ensure long-term quality of medical devices (10).

7.4 PHYSICAL AGING

The effects of physical aging on the failure behavior of a typical brittle polymer, polystyrene, were studied. Properties examined were creep rupture lifetimes, fatigue lifetimes, and environmental stress cracking in ethanol. Fractured samples were examined optically and by scanning electron microscopy to determine the degree of crazing. It was found that

a longer physical aging time produced shorter life-times in all cases. The main reason for this was the reduction in craze strength caused by a reduced toughness due to physical aging. A long aging time was found to delay craze formation; but, once formed, these crazes were much less stable than those formed with a short aging time. The effects of aging were important in failure prediction criteria and testing methodologies (11).

Glassy plastics fail through the action of certain organic liquids that behave as crazing or cracking reagents. This is another form of environmental stress cracking. Failure occurs at stress and strain levels below those levels required for the unexposed condition. The mechanisms of failure may be multifaceted and differ from one glassy plastic to another.

The phenomenon of crazing was dramatically demonstrated with the application of alcohol on the surfaces of polycarbonate supermarket scanners and, also, in the failure of high performance fighter jet canopies through the action of aftershave lotion vapors on polycarbonate.

To evaluate the competition between shear and crazing, polycarbonate, acrylonitrile-styrene random copolymer, methyl methacrylate-styrene random copolymer and polystyrene-poly(2,6-dimethyl-1,4-phenylene oxide) were strained and examined using transmission electron microscopy (TEM). In these polymers, many crazes had tips blunted by shear deformation. This process led to stress relaxation at the craze tip, preventing further tip advance. In this way, short but broad cigar-shaped crazes were formed. Examination of the deformation at crack tips showed more complex structures—the initial high stress levels led to chain scission and fibrillation; but as the stress dropped, shear became the dominant mechanism of deformation, and the stress was further relieved. Finally, at long times under stress, chain disentanglement was more important, leading to fibrillation and craze formation again. The nature of the competition was thus both stress and time dependent. Physical aging of the polymers, via annealing below the glass transition temperature, suppressed shear leading to generation of simpler craze structures (12).

Using the criteria set forth in Struik's classic treatment of physical aging (13), our definition will be the following. Based on the earlier works of Simon and others, Struik stated that amorphous solids are considered not to be in thermodynamic equilibrium below their glass transition temperatures (T_g). These materials are said to be solidified supercooled liquids, with volume, enthalpy, and entropy greater than they would be at the equilibrium state.

The non-equilibrium state is unstable. Volume-relaxation studies of glassy materials have also shown that they undergo slow processes when attempting to establish equilibrium, thus indicating that molecular mobility is not zero below T_g .

This gradual approach to equilibrium changes many properties of the material. The properties change with time, and the material is physically aged. Physical aging is a gradual continuation of the glass formation. As the material is physically aged it becomes stiffer and more brittle; its damping decreases; and its creep- and stress-relaxation rate changes, as well as its dielectric constant and dielectric loss. The process of physical aging is irreversible.

Low density polyethylene (LDPE) was subjected to accelerated physical aging in a Weathering Tester (QUV) and weatherometer (WOM) chamber, and its surface mechanical properties were determined and monitored with a nano-indentation technique. It was determined that the surface hardness was three times greater than the bulk after 1,600 hours of exposure in the WOM chamber and with a similar increase after 800 hours of exposure in the QUV chamber. The elastic modulus at the tip of penetration (with a depth of 500 nm) showed a significant increase from 400 Mpa to 2,000 MPa for samples aged in the QUV chamber. Aging times of 200 hours and less showed variations of surface mechanical properties were small and restricted to a thin layer with a thickness less than one micron (14).

The application properties of plastic products were significantly influenced by the structural changes after conversion, resulting from a combination of post-crystallization and physical aging for semicrystalline materials. This was observed in a series of polypropylenes, including a homopolymer, ethylene-propylene (random and heterophasic copolymers), and two types of processed polymers (conversion-injection molding and cast film extrusion). The temperature level of the aging process played a decisive role in determining the effects—At least two important transitions were identified with increasing temperature. The cumulative effects of crystalline behavior of the polymer and cooling history determined the crystallinity and superstructure of the formed article, which, in turn, determined the aging behavior (15).

Poly(vinyl chloride) (PVC) is one of the major commodity polymers in the world, in spite of environmental concerns due to the presence of chlorine within its backbone. An enormous number of products are formed from the polymerization of vinyl chloride, from elastomeric to hard items. Independent of the mode of degradation (thermal, thermo-ox-

idative, or light), the major factor in degradation of PVC was the elimination of HCl from the polymer backbone and the simultaneous formation of conjugated double-bond moieties within the polymer chain. During the degradation of PVC, the highly corrosive gas HCl is formed, as well as the reactive double-bond moieties, which are capable of absorbing light in both the UV and visible regions. The color of aged PVC may range from yellow to black, depending on time of aging and stabilizers added (16).

Physical aging (thermal history) and large deformations (mechanical history) strongly affect the low-frequency mechanical and electrical properties of PVC. These include such properties as their dielectric loss factor. These properties cannot be neglected. Results for rigid polyvinyl chloride (PVC) were explained in terms of the free volume theory (17).

Polyvinylidene fluoride (PVDF) is a very useful polymer because of its unique properties, such as resistance to hostile environments, its pyro and piezoelectric properties, and its capability to lower friction. This polymer family sees wide applications in electronic and medical fields. Polyvinylidene fluoride has been used in the manufacture of sutures. An experiment utilizing creep measurements has been performed and service performance predictions from short-term testing have been made. Using the time-temperature superposition principle it was possible to predict long-term deformation from these reported tests. The kinetics of the molecular mobility was also studied and adjusted to the temperature shift factor, which was based on a free volume concept.

Dynamic mechanical analysis revealed two main relaxations. These were due to the B process (segmental mobility in the amorphous phase) and α_c -relaxation (which was a major consequence of conformational motions within the crystalline fraction). The α_c -relaxation was the main source for energy dissipation that is input to the system during constant mechanical loading. The general methodologies were applied to other suture PVDF formulations. It should be noted that PP exhibited similar relaxations as PVDF, even though it had to be shifted to a higher temperature with the B and α_c processes (18).

In addition to PVDF application as a suture material, it has undergone a lot of testing as a coating. Polyvinylidene fluoride exhibits excellent chemical resistance, gloss retention, flexibility, as well as renowned ability to resist chalking and cracking during weathering. It has been reported that PVDF has a 35-year history of outstanding performance in outdoor applications. Weathering tests in Florida have revealed that the gloss of PVDF coatings increased

by 15%, whereas a traditional acrylic coating exhibited a 65% decrease over the same time period (19).

As the use of PVDF grows, blending PVDF with other polymer systems becomes quite attractive. A recent PVDF blend with acrylic copolymers was evaluated before and after UV exposure. The copolymer used was a poly(methylmethacrylate) and poly(ethylacrylate). The system was PVDF-PMMA-co-PEA. Blends of the following ratios were studied: 70/30, 50/50, and 30/70. Film samples were characterized before and after UV exposure at 500 °C and 9% relative humidity for seven months. The surface of the blends having greater than 50% mass fraction of PVDF exhibit little change in the morphology after UV exposure. At the low concentration, (30%), a much rougher surface was observed due to the significant erosion of the acrylic copolymer under the same exposure. Additionally, substantial change in the microstructure of the spherulites of the PVDF was observed after UV exposure. That change may be attributed to the microstructural modification of the crystallites in the PVDF spherulites, as well as the aforementioned erosion of the PMMA-co-PEA.(19)

The anode and cathode of lithium ion batteries were cast onto metal current collectors as a formulated coating containing the electrochemical active ingredients, with polyvinylidene fluoride (PVDF) as the binder. In addition, PVDF was used in the production of gel electrolytes for the polymer lithium batteries. Anodes for lithium ion batteries were fabricated by mixing graphite in a solution of PVDF in *N*-methylpyrrolidone in a ball mill. A clean copper foil was coated with the dispersion and placed in an oven to dry at 150 °C for 30 minutes. The adhesion of PVDF coating on copper was measured by peel strength tests, and optimum graphite concentration was determined to be 1:2 for PVDF:graphite. The coated electrodes were subjected to pressing/lamination prior to final assembly into batteries to minimize voids. Gel separators were fabricated using microporous PVDF films with di-butyl phthalate as the plasticizer. The gel electrolyte was enclosed in a button-cell with stainless steel electrodes and the complex impedance and resistance of the electrolyte were measured. The swelling and aging of the gel electrolyte were determined (20).

In addition to the major polymer families and the plastics compositions formed from their incorporation with various additives, there is a wealth of materials based upon blends of two or more polymers mixed together. An example of one blend is the copolymer of PVDF/acrylic resin. Polyvinylidene fluoride coatings are being used as protective out-

door structures. Due to the structure of PVDF, these coatings exhibit excellent chemical resistance, outstanding gloss retention, good flexibility, and excellent chalking resistance. However, due to the chemical inertness of PVDF, it lacks good adhesion to various structures and has a high melt viscosity. In addition to these negative features, it has inferior scratching and marring resistance and has a high cost associated with it. Thus, it becomes commercially viable to blend PVDF with other materials.

Polyvinylidene fluoride has been blended with the acrylic resins, such as poly(methylmethacrylate) (PMMA) and its copolymers. By doing so, the resulting blend has good heat resistance, mechanical properties, weatherability, and optical clarity. These surface and interface properties have shown a strong influence on its service life and its adhesion to various substrates. Various studies have indicated that the service life of the material is greatly enhanced by the blending of the two polymers (19).

Poly(ethyl acrylates) and poly(ethyl methacrylates), chlorinated in the side groups, are known to release chlorine and experience intermolecular cross-linking when heated. Of poly(mono-, di-, and trichloroethyl methacrylates), the dichloroethyl esters showed the most significant change. This trend was observed at temperatures below 227 °C. At temperatures above 227 °C both poly(ethyl acrylates) and poly(ethyl methacrylates) decomposed into low molecular fragments, with the chlorinated poly(ethyl methacrylates) depolymerizing. The chlorinated polymers showed a lower thermal stability than their corresponding nonchlorinated counterparts (21).

An "interrupted creep" test has been used to determine the physical aging of low molecular weight polystyrene with a T_g of 69 °C. The results of this newly developed technique were comparable to the results obtained from traditional "periodic creep" testing. The "interrupted creep" test provided data pertaining to viscosity as well as to both recoverable creep and steady-state compliances during physical aging. The rationale for choosing low molecular weight polystyrene was due to its strong influence of temperature on steady-state compliance. Aging was performed at three temperatures at intervals of 7.2 °C below its glass transition temperature. The advantage of this new protocol is that it provides short-time recoverable creep compliance and long-time viscous flow data. Through simple mathematic functions, a more complete picture of glassy behavior during aging is obtained (22,23).

The buildup of a polarized state and its isothermal and nonisothermal relaxation behavior in an NLO

guest-host system obtained by doping of polystyrene (PS) with the disperse red 1 (DR1) dye molecules was studied by the isothermal absorption currents measurements. The thermally stimulated polarization (TSP) and depolarization (TSD), the AC dielectric spectroscopy, as well as the Hamon method were used in order to cover wide ranges of temperatures and frequencies. The 20- μm thick samples were pulsed by the "sandwich" method. Using isothermal polarization, depolarization, and depolarization currents, the validity of the superimposition principle was established. The Williams-Watts model, supplemented with a concept of intrinsic time, was employed to interpret the TSP curves, but it appeared that the isothermal behavior did not fully determine the TSP results. The "a" peak was observed in dielectric loss curves, with its position changing from 10 Hz at 100 °C to 3×10^4 Hz at 130 °C, and narrowing with temperature. Temperature dependence of the relaxation time above T_g agreed with the Williams-Landel-Ferry model, while the Arrhenius dependence was more appropriate at sub- T_g temperatures. It was shown that the PS/DR1 system was not thermorheologically simple. The temperature-time superposition was not entirely valid (24).

Enthalpy relaxation experiments on the miscible blends of poly(vinyl methyl ether)/polystyrene at various aging temperatures showed that the poly(vinyl methyl ether) component aged independently of the polystyrene component and was responsible for essentially all of the aging effects. The enthalpic aging data were analyzed in terms of two models for describing physical aging in polymer systems (25).

The yellowing of cellulose materials plays a very important role in the aging of documents. Due to the fast-growing number of different types of papers, this is a very important area of research within the technical community. Ultraviolet radiation from sunlight, moisture, and chemical pollutants all play a role in this aging phenomenon.

A systematic study of physical aging in cellulose acetate polymers that have been plasticized by the addition of dyes and polymeric plasticizers was undertaken using the heat capacity as the structural probe. The dyes were dye sets and mixtures of various dyes with slight differences, each with a different glass transition temperature (T_g). The polymeric plasticizers were low molecular weight polyesters that had low values of T_g . From experimental results and analysis, it was shown that aging occurred under ambient temperature conditions most rapidly for the polymer dye samples that had their T_g value at 20°C

above ambient temperature. The results for these thermorheological complex blends also indicated that the incorporation of the polymeric plasticizers substantially reduced the T_g of the blends. In addition, the distribution of relaxation times was broadened. Kinetics of aging for the blends was determined using the Tool-Narayanaswamy model for structural relaxation (26).

The effect of isothermal physical aging on creep behavior of stainless steel fiber/polyphenylene ether (PPE) composites was investigated. The PPE in metal fiber/PPE composites is a non-crystalline thermoplastic; the composites are often used in engineering plastics, which have been developed for electro-magnetic-interference (EMI) shielding. The results showed creep compliance curves to shift toward both the longer times and lower compliance with an increase in pre-aging treatment time. It was established that creep deformation was arrested due to the progression of physical aging. Thus, it was validated that pre-aged composites can withstand higher temperatures and longer time. The time-aging time superposition was established in creep of stainless steel fiber/PPE composites. It was also observed that within the aging-time range, the shift rate was constant at all temperatures. The results showed that the shift rate was less at lower temperatures and greater at higher temperatures; the shift rate reached its maximum value at a wide range of temperatures (27).

Compressive strength and the nature of the open pores (shape and number) of rigid polyurethane and polyisocyanurate foams were monitored during long-term aging. Changes in the physical and mechanical characteristics of foams as aging progressed were attributed to thermal and thermoxidative degradation of the polymer matrix (28).

The condensation polymer bisphenol A polycarbonate (BPA-PC) is a widely used engineering thermoplastic. It also has a magnitude of conditions that affect its properties upon aging. Bisphenol A polycarbonate may undergo hydrolytic, thermal, thermal oxidative, or photochemical aging.

Bisphenol A polycarbonate, being a hydrophilic polymer, is very susceptible to water attack. The carbonate linkage is split into an alcohol with the release of carbon dioxide. It is highly recommended to use polycarbonate free of acidic or basic catalytic residues. These catalysts are required to initially form the polymer, and any residues can hasten its degradation. It is also recommended to dry the resin prior to processing. A suggested moisture level of $\tau 0.05$ wt% can be achieved by drying at 120 °C for 2–4 hours. Stabilizers, such as hindered phosphites

(which are neutral and hydrolytically stable) are used (29).

Bisphenol A polycarbonate contains only two types of hydrogen, methyl and aromatic, which leads to its high thermal stability. Thermogravimetric analyses in nitrogen revealed a weight loss beginning at 550 °C. Heating the polymer in air above 340 °C showed a decrease in molecular weights. The use of model compounds indicated thermal rearrangements of the carbonate moiety. It should be pointed out that studies show that temperatures as low as 250 °C in either air or nitrogen have afforded the presence of fluorescence-emitting byproducts (30).

Glass fiber-reinforced nylon 66 composites are currently finding greater use as automotive under-the-hood components and, therefore, are submitted to aggressive environments. This study evaluated composites for radiator caps. The composite materials were in contact with antifreeze (50/50 vol/vol water/ethylene glycol) at 135 °C, resulting in a significant decrease in mechanical properties with time. Two main mechanisms of degradation were observed: (1) a reversible physical aging due to the plasticization of the nylon 66 matrix; and (2) an irreversible chemical aging due to hydrolysis (and, to some degree, due to glycolysis). Significant improvements were obtained by adding a new component in the sizing formulation of the fibers (31).

A study in an accelerated environment of the mechanical properties of glass fiber-reinforced thermoplastic composites based on nylon 66, poly(ethylene terephthalate) and poly(butylene terephthalate) was reported. Results showed a decrease of 50–90% in ultimate stress-to-failure and impact strength with aging according to the nature of the matrix. Increasing the aging temperature resulted in a faster degradation rate. Depending on the nature of the matrix, the mechanisms of aging seemed to be different. Nylon 66 and poly(butylene terephthalate) composites showed effects of both physical aging through plasticization and chemical degradation through chain scission. Poly(ethylene terephthalate) composites did not give evidence of any plasticization. The extent of hydrolysis was quantified through end-group analysis and gel permeation chromatography measurements. Scanning electron microscopy observations showed that hygrothermal aging reduced the effectiveness of the interfacial bonds (32).

Accelerated aging was performed on nylon 11 (polyamide 11) in 115–135 °C distilled water. The samples were characterized by mechanical testing, viscosity measurements, and differential scanning calorimetry (DSC). Viscosity, which is a measure of

molecular weight, decayed exponentially with times of exposure. The final level of the viscosity curve was dependent on temperature. The melt enthalpy, which is an indication of crystallinity, increased with exposure time. The viscosity and crystallinity both correlated with the observed changes in elongation at break, thus indicating both chemical and physical aging processes played a role in aging (33).

The physical aging of poly(vinylpyrrolidone) (PVP) was studied under different storage conditions by positron lifetime spectroscopy and SEM. The transition from the glassy state [at RT and 55% relative humidity (RH)] to the completely plasticized wet rubbery state (at RT and 75% RH) is not continuous in PVP. It was found that not only the actual water content of the material but also its storage history determines the size distribution of free volume holes in it. At 65% RH, a slow anomalous structure formation was observed. By the means of *ab initio* calculations on simplified molecular models, it was determined that polymer chains and water molecules were able to form a hydrogen-bound "network" under certain humidity conditions (34).

The application of membranes in gas separation and preevaporation requires materials that are resistant to plasticizing feed streams. The relationship between CO₂ sorption, permeability, and film swelling of a polyimide gas separation membrane and how these properties were affected by systematic changes to the polymer structure induced by thermal annealing and covalent cross-linking was demonstrated. Dilation of polyimide thin films (approximately 120 nm) exposed to high-pressure CO₂ (up to 100 atm. at 35 °C) was measured by *in situ* spectroscopic ellipsometry to decouple the effects of thermal and chemical treatments on the film swelling. The refractive index of the CO₂-swollen polymer was also used to estimate the CO₂ sorption for comparison against that measured on thick films (approximately 50 μm) by the pressure-decay method. Differences in sorption levels in thin and thick films appeared to be related to accelerated physical aging of the thin films. Both thermal annealing and covalent cross-linking of the polyimide films reduce polymer swelling to prevent large increases in the CO₂ diffusion coefficient at high feed pressures. The CO₂ permeability and polymer-free volume were strongly dependent on the annealing temperature. Different effects were observed for the cross-linked and uncross-linked membranes. The so-called "plasticization pressure" in permeation experiments, such as upturn in the permeation isotherm, appeared to correlate with a sorbed CO₂ partial molar volume of $29 \pm 2 \text{ cm}^3/\text{mol}$

in the polymer. Cross-linking of high glass transition polyimides produced a much greater reduction of the CO₂-induced dilation than does cross-linking of rubbery polymers, such as polydimethyl siloxane (PDMS), for swelling up to 25% (35).

The use of ambient cured E-glass/vinyl ester composites was considered for infrastructure applications both along the shore and offshore, thereby exposing the composite to a marine aqueous environment. The use of ambient cure potentially results in incomplete polymerization and susceptibility for degradation early in life. This study characterized the mechanical response of E-glass/vinyl ester quadriaxial composites immersed in deionized water, seawater, and synthetic seawater. It was shown that there were substantial differences based on the solution type, with deionized water immersion causing the maximum drop in interlaminar shear performance and with seawater causing the maximum reduction in tensile performance. The effect of cycling, simulating the tidal zone or the splash zone, was more pronounced in the resin-dominated responses. Drying of specimens, even over prolonged periods of time, was not shown to result in complete regain of performance. A clear competition was observed between the phenomena of moisture-induced residual cure/postcure and physical (fiber-matrix debonding, microcracking, plasticization) and chemical (hydrolysis) aging (36).

Upon curing, epoxy formulations based upon the epoxy resin of N,N,N',N'-tetraglycidyl-4,4'-diaminodiphenylmethane (TGDDM) co-reacted with two cross-linking agents—4,4'-diaminodiphenylsulfone (DDS) and dicyanodiamide (DDA); and thermal aging at high temperatures revealed a migration of the cross-linking agents from the epoxy at the surface. This separation has an effect on the quality of the cure and the thermal stability of the reacting moieties, thus affecting its overall performance. This was verified by monitoring the nitrogen, oxygen, and sulfur contents at the surface and comparing those results to the bulk (37).

The electrical and mechanical properties were determined for an epoxy resin, hardened with maleic anhydride and containing various amounts of a plasticizer and powdered quartz or talc fillers. The addition of the plasticizer caused the glass transition temperature to decrease while causing an increase in the dielectric loss and mechanical loss maxima. A shift resulted in the mechanical loss maximum to lower temperatures. The addition of the fillers raised the glass transition temperature. In addition, the filler-containing resin had improved heat resistance

compared to unfilled resins. The dielectric strength of the filled resins did not decrease during approximately eight months at ≤ 85 °C, but the dielectric strength of the unfilled resin decreased (38).

The degradation of epoxy composites due to humidity, physical aging, and chemical aging was examined. When stored under cover, the moisture absorption proved to be the most dominant effect. The absorbed moisture weakened the matrix and reduced its modulus of elasticity and its resistance. In serious cases, an irreversible aging was observed in the form of microcracks in the matrix and in the border phase. Carbon fibers were less sensitive to moisture than glass and aramid fibers. In glass fiber composites, the border phase between fiber and matrix appeared to be vulnerable to moisture. In aramid-reinforced composites, even the fibers absorbed moisture, so that the fiber burst lengthwise when crosswise charged. For polyester resins with glass fibers, no general conclusion was made (39).

The creep and creep-rupture of unidirectional composite laminates were characterized and modeled. Individual and interactive effects of stress, temperature, moisture, and physical aging on creep and creep-rupture of a polymer composite (epoxy reinforced with 54% by volume of carbon fibers) were studied. The composite exhibited linear creep at constant stresses ≥ 7 MPa in the temperature range 22–230 °C. Moisture accelerated creep through plasticization, such as lowering the T_g, of the epoxy matrix, and moisture-induced creep acceleration was found to be equal to creep acceleration in a dry sample by an equivalent temperature increase. Physical aging retarded creep and accelerated creep-rupture. In addition to reducing the moisture diffusivity and saturation moisture, physical aging caused a reduction in the magnitude of creep and creep-rupture acceleration by moisture when compared to non-aged material at the same moisture level. A similar interactive influence was observed at various stress and/or temperature levels (40).

Isothermal physical aging of glass fiber epoxy composites was examined at different aging temperatures and degrees of conversion as indicated by changes in glass temperatures and measured by torsional braid analysis (TBA). The range of temperatures of aging was from 10 to 130 °C. The conversion was progressively changed from T_g = 76 °C to T_g = 177 °C (fully cured). The effect of isothermal physical aging was enhanced as perturbations of the modulus and mechanical loss versus increasing aging temperatures. The data indicated a superposition in aging rate versus T_g aging temperature. This would imply that the physical aging process is inde-

pendent of the change in chemical structure as the conversion proceeds (41).

An earlier study of fully cured diglycidyl ether of bisphenol A epoxy reacted with a tetrafunctional aromatic amine showed that its relative rigidity increased with log time of aging, and the logarithmic decrement decreased with aging. This was the consequence of the spontaneous densification of the material in the glassy state. The rate of isothermal aging of a material fast-cooled from an equilibrium state was higher in the early stages of aging in comparison with a slow-cooled material. This was due to a higher initial free volume content for the former. With increasing time of isothermal aging (decreasing free volume), the rate of both fast-cooled and slow-cooled materials becomes indistinguishable. The analysis of this study was also performed by TBA (42,43).

Mechanical property deterioration of composites based on bismaleimides (BMI) was predicted. The cure-induced T_g increased in associated matrix in real service environments. Predictions were obtained through network structure interrelations with mechanical and thermal properties as a function of composition (initial monomer ratio) and time-temperature cure cycles. Tensile and flexural properties of four BMI compositions at six different cure cycles (or degree of cure) were determined at three temperatures (23, 177, and 250 °C) and correlated to T_g and density of the systems. Systematic studies on hygrothermal durability of BMI and various polyimide (PI)-carbon fiber composites and neat resins were conducted. The combined effects of moisture and thermal exposures [such as hygrothermal spikes up to 250 °C and hygrothermal aging under various time-temperature-moisture conditions, including accelerated aging at saturated steam environment (160 °C and 110 psi)] on microscopic damage, polymer-matrix physical structural state, and residual properties of those composites and neat resins were presented. The onset of blistering in moist PI-carbon fiber composites occurred at 229 °C during the thermal spiking. It was evident that the hygrothermal performance stability was one of the prime guidelines in future aerospace applications (44).

A fundamental problem of advanced airplane composite systems is often the lack of understanding of the aging process and how it affects the material properties associated with degradation. A cyanate ester resin/carbon fiber composite system was subjected to an accelerated aging environment to investigate the deterioration and degradation process. The change in viscoelastic properties of cured laminates in the range of the T_g was studied. Thermomechanical property changes were evaluated by dynamic me-

chanical analysis (DMA) through time-temperature equivalence. Master curves were constructed to compare the aging effect between specimens, and a model was developed that described the degradation phenomena. During the aging process, a swelling phenomenon of cured laminates was detected as a result of matrix degradation. Collectively, a modeling methodology was developed that quantitatively provided an understanding of the aging process of fiber reinforced composites in isothermal environments (45).

High temperature composite materials used in aerospace applications are subjected to extremely harsh conditions during operation. The surface of an aircraft flying at Mach 2.4 has been estimated to reach 177 °C. A study was conducted to verify the effect of isothermal aging on two high temperature composite materials, both based on two different bismaleimide systems. Changes in mechanical properties and resin chemistry at two different temperatures were measured in order to assess the merits of accelerated aging tests. One composite material was based on a developmental bismaleimide matrix resin system, while the other was based on a commercially available bismaleimide system.

Delamination was a major cause of failure in two composites. Mode I interlaminar fracture toughness (GIC) of both composites was measured using the double cantilever beam (DCB) test. After aging at 250 °C, the developmental bismaleimide composite exhibited a better retention of GIC than the commercially available bismaleimide composites. After six weeks of aging at this temperature, the developmental composite retained 100% of its initial interlaminar fracture toughness; however, the commercially available material retained only 64% of its initial GIC. This trend was reversed at the lower aging temperature, when after 30 weeks of aging at 2,040 °C, GIC was measured at 13% of its original value for the developed composites, whereas it was measured at 64% for the commercial bismaleimide system. When the fracture surfaces of these specimens were examined using scanning electron microscopy (SEM), the commercial material was observed to show an increasing degree of porosity with aging at 2,040 °C. It was concluded that the good property retention at that temperature, despite this observed porosity, was a result of the excellent fiber/matrix adhesion exhibited by this material.

Chemical degradation of the matrix of the composites was monitored by Fourier Transform Infrared (FTIR) and Raman spectroscopy. Chemical changes at the core of both of these bismaleimide composite materials were found to occur concur-

rently with the observed changes in interlaminar fracture toughness. Fourier Transform Infrared analysis of both matrix materials revealed the predominant degradation mechanism to be oxidation, specifically the oxidation of the methylene group bridging two aromatic rings common to the structure of both resins. This was substantiated by the growth of a broad peak centered at 1600 cm^{-1} . In addition to this, the pyromellitic anhydride unit present only in the developmental composites was found to be highly resistant to the effects of aging, whereas the saturated imide, common to the cured structures of both materials, was observed to degrade.

As a result of increased reaction of the allylic carbon-carbon double bond, Raman spectroscopy showed an increase in the intensity of the peak at 1646 cm^{-1} towards the center of the sample in the composites, based upon the commercial bismaleimide aged at 2500C. At 204 °C, the degree of reaction increased toward the surface of the material, possibly as a result of a reverse Diels-Alder reaction. The glass transition temperatures of both materials were found to decrease with aging, with the exception of the composites based upon the developmental material aged at 204 °C, which initially increased due to continued cross-linking of the resin. It was concluded that the degradation mechanisms at the two aging temperatures were very different (46).

This observation lends support to the original written statement. That is, to conduct aging studies properly, one must use the same material throughout the study. The previously mentioned illustration shows that even though the primary polymer family (bismaleimide) was the same, the two composites aged differently. Upon further examination of the data, one could speculate that these two materials were grossly different and may have been mislabeled.

In addition to the work that has been done with bismaleimides (BMI), dicyanate esters, and thermosetting polyimides, the benzocyclobutenes (BCB) have gained in popularity within the research community. The mechanisms of long-term isothermal aging of diketone-bis-benzocyclobutene (DK-bis-BCB) or methanone, 1,3-phenylene bis[bicyclo(4.2.0)octa-1,3,5-trien-3-yl], and the effects of aging on the mechanical properties of this polymer were determined. It was observed that when DK-bis-BCB polymer was exposed to a temperature of 275 °C in an air environment, it formed a dark skin on the surface, which increased in thickness as a function of exposure time. The skin thicknesses of samples, aged from 0 to 2,000 hours, were measured using optical techniques, which led to the calculation of the diffusivity of oxygen into the polymer at 275 °C. Photoacoustic

and infrared spectroscopy showed the chemical changes caused by oxidation, which included the loss of hydrogen atoms and the formation of aromatic anhydride structures. Scanning electron micrographs of the surfaces of the aged polymers revealed that the DK-bis-BCB aged predominantly by pitting. The mechanical property results showed that after 2,000 hours at 275 °C, 91% of the unaged flexural modulus and 34% of the unaged flexural strength were retained. The polymer weight loss after 2,000 hours at 275 °C was 8.24% (47).

An interesting example of aging pertains to the behavior of rubbers and elastomers. In the manufacturing of these polymeric materials, various chemicals are added to enhance their curing or vulcanization. With time, these additives migrate to the surface of the part, thus changing its physical properties. This migration is referred to as “bloom” for solid materials migrating, and “bleeds” for liquid materials.

Rubbers and elastomers may undergo similar forms of aging, as do thermosetting and thermoplastic materials with water; that is, chemicals can be absorbed into the lightly cross-linked network of the rubbers or elastomers. They may act in several different ways. One way is the lowering of the glass transition temperature. Another way is when chemicals are absorbed into the structure of the network and cause swelling.

Nanotechnology offers a new type of material as reinforcing elements. A study of the physical aging of carbon nanotubes made of reinforced epoxies illustrates that behavior. An epoxy resin was reinforced with three different varieties of nanotubes. These were SWNTs (single-walled nanotubes), MWNTs (multi-walled nanotubes), and nanotube bundles (NTs). These reinforcement elements were roughly on the order of 1 nm, 30 nm, and 100 nm, respectively. Sizes of this order are smaller than the diameters of typical microscale fibers traditionally used in polymer composites, which are on the order of 10 μm .

Because nanotubes are approximately the same length as the polymer chains, the polymer segments in the vicinity of the nanotubes may have local mobility different from the bulk polymer, and thus distinct mechanical properties. Due to their outstanding physical properties, nanotubes are gaining interest as a filler material in polymer systems. With the potential of strength- and modulus-to-weight ratios, nanotube-reinforced composites have the potential of being an order of magnitude greater than traditional polymer composites. The major drawback in using nanotubes is cost (48).

Another key feature in the topics of chemical and physical aging should be the inclusion of time in the

discussion. The role of rates and kinetics is discussed separately, in the companion chapter on “Lifetime Predictions.”

7.5 SUMMARY

In summary, this author wishes to advise the reader about the vast amount of literature available in the fields of chemical and physical aging of plastics. All of the major government laboratories have projects dealing with this subject. This is also true for the independent testing labs and the university labs. Some of the university labs have established consortiums where they work with industries to defray the cost of aging studies. This author does not want to single out a particular lab, but would like to advise the reader to search the Internet for these subject matters. This author firmly believes in the philosophy and recommendation of Jack Welch (the former C.E.O. of General Electric) to his scientists and engineers that they spend at least one hour per day searching the Internet.

This author also hopes to have given the reader a general idea regarding the type of information that is available for chemical and physical aging of polymers and plastics. Examples were given here to demonstrate the behavior of homopolymers, copolymers, plastics, blends, and composites with various reinforcements. In this author’s opinion, one should be able to find the material system of interest through searching the literature. However, precautions must be employed to ensure that the correct material system is referenced. The database for polymers and plastics has over 14,000 entries. And, whenever someone is discussing a particular polymer such as polyethylene, the first questions should always be “Which one?” “What were the additives and/or reinforcements?” and “How was it processed?”

7.6 REFERENCES

1. Roger J. Morgan, in *Thermal Characterization of Materials*, 2nd Ed., Edith A. Turi, Ed., New York, Academic Press, 1997. Also articles by R. J. M. cited in bibliography.
2. A. L. Landis, private communication, 1983.
3. R. J. Young and P. A. Povell, *Introduction to Polymers*, 2nd Ed., London, Chapman and Hall, 1991.
4. J. A. Harvey, unpublished work, 1997.
5. P. Chang and J. A. Donovan, *Polymer Engineering and Science*, Vol. 30(22), pp. 1,431–1,441, 1990.
6. N. Ogata, T. Yanagawa and K. Yoshida, *Journal of Polymer Science*, Part B (Polymer Physics), Vol. 24(9), pp. 1,917–1,929, 1986.

7. N. Ogata, T. Yanagwa and K. Yoshida, *Journal of Polymer Science*, Part B (Polymer Physics), Vol. 24(1), pp. 89–97, 1986.
8. S. Bandyopadhyay, *Journal of Polymer Science*, Part B (Polymer Physics), Vol. 10(5), pp. 749–761, 1981.
9. Y. Ohde and H. Okamoto, *Journal of Material Science*, Vol. 15(6), pp. 1,539–1,546, 1980.
10. Q. Chuan, S. Ding, K. Z. Hong, H. Dhyani and V. Zepchi, *Proceedings of the Annual Technical Conference*, Society of Plastics Engineers, Vol. 54(3), pp. 3,690–3,694, 1996.
11. J. C. Arnold, *Polymer Engineering and Science*, Vol. 35(2), pp. 165–169, 1995.
12. A. M. Donald and E. J. Kramer, *Journal of Materials Science*, Vol. 17(7), pp. 1,871–1,879, 1982.
13. L. C. E. Struik, *Physical Aging in Amorphous Polymers and Other Materials*, Amsterdam, Elsevier Scientific Publishing Co., 1978.
14. A. C. Tavares, J. V. Gulmine, C. M. Lepienski and L. Akcelrud, *Polymer Degradation and Stability*, Vol. 81, pp. 367–373, 2003.
15. J. Gahleitner, J. Fiebig, J. Wolfschwenger, H. Dreiling, and C. Paulik, *Journal of Macromolecular Science (Physics)*, Vol. B41(4-6), pp. 833–849, 2002.
16. B. Ivan, Chapter 2 in *Polymer Durability*, R. L. Clough, N. C. Billingham, and K. T. Gillen, Eds., Advances in Chemistry Series 249, Washington, D.C., American Chemical Society, pp. 19–32, 1993.
17. L. C. E. Struik, P. T. A. Klaase, P. H. Ong, D. T. F. Pals and J. Van Turnhout, *Annual Report—Conference on Electrical Insulation and Dielectric Phenomena*, pp. 443–452, 1978.
18. J. F. Mano, J. L. Lopes, R. A. Silva, W. Brostow, *Polymer*, Vol. 44, pp. 4,293–4,300, 2003.
19. X. Gu, L. P. Sung, D. L. Ho, C. A. Michaels, T. Nguyen, D. Nguyen, Y. C. Jean, “Global Connectivity,” *Proceedings of the FSCT 80th Annual Meeting Technical Program*, October 30–November 1, 2002, New Orleans, Federation of Societies for Coatings Technology, Blue Bell, PA, 2002.
20. M. Despotopoulou and M. T. Burchill, *Progress in Organic Coatings*, Vol. 45(2–3), pp. 119–126, 2002.
21. W. Schnabel, Chapter 3 in *Polymer Durability*, R. L. Clough, N. C. Billingham, and K. T. Gillen, Eds., Advances in Chemistry Series 249, Washington, D.C., American Chemical Society, pp. 33–46, 1993.
22. K. M. Bernatz, L. Girl, S. L. Simon, and D. J. Plazek, *Journal of Chemical Physics*, Vol. 111(5), pp. 2,235–2,241, 1999.
23. S. L. Simon, D. J. Plazek, and K. M. Bernatz, in *Proceedings of the AIChE Annual Technical Conference*, Paper 174f, New York, November 4, 1999.
24. S. N. Fedosov, A. Jose, M. M. Costa, and G. F. L. Ferreira, *Proceedings of SPIE—The International Society for Optical Engineering*, Vol. 4014 (Polymers and Liquid Crystals), pp. 59–66, 1999.
25. J. M. Cowie and R. Ferguson, *Macromolecules*, Vol. 22(5), pp. 2,312–2,317, 1989.
26. C. J. T. Landry, K. K. Lum and J. M. O’Reilly, *Polymer*, Vol. 42(13), pp. 5,781–5,792, 2001.
27. K. K. Biswas and S. Satoshi, *Materials Science Research International*, Vol. 7(3), pp. 172–177, 2002.
28. A. G. Dementyev, *Aging of Polymers, Polymer Blends and Polymer Composites*, Vol. 2, pp. 213–217, 2002.
29. A. Factor, Chapter 5 in *Polymer Durability*, R. L. Clough, N. C. Billingham, and K. T. Gillen, Eds., Advances in Chemistry Series 249, Washington, D.C., American Chemical Society, pp. 59–76, 1996.
30. I. B. Rufus, H. Shah, and C. E. Hoyle, *Journal of Applied Polymer Science*, Vol. 51, p. 1,549, 1994.
31. A. Bergeret, I. Pires, and A. Crespy, *Annales des Composites*, Vol. (1), pp. 9–18, 2001.
32. A. Bergeret, I. Pires, M. P. Foulc, B. Abadie, L. Ferry and A. Crespy, *Polymer Testing*, Vol. 20(7), pp. 753–763, 2001.
33. H. Fell and O. M. H. Jorg, *Proceedings of the Oilfield Engineering with Polymers Conference*, London, November 28–29, 2001, pp. 41–49.
34. K. Sueveghe and R. Zelko, *Macromolecules*, Vol. 35(3), pp. 795–800, 2002.
35. J. D. Wind, S. M. Sirard, D. R. Paul, P. F. Green, K. P. Johnston and W. J. Koros, *Macromolecules*, Vol. 36(17), pp. 6,433–6,441, 2003.
36. W. Lixin, K. Murphy, V. M. Karbhari and J. S. Zhang, *Journal of Applied Polymer Science*, Vol. 84(14), pp. 2,760–2,767, 2002.
37. X. Buch and M. E. R. Shanahan, *International Journal of Adhesion & Adhesives*, Vol. 23, pp. 261–267, 2003.
38. A. S. Akhriev, K. S. Isaev, V. S. Karasev and Y. V. Zelenev, *Plaste und Kautschuk*, Vol. 27(9), pp. 492–494, 1980.
39. M. Danilsons, *Journal of Applied Electrochemistry*, Vol. 26(22), Abstract N88-28102, 1988.
40. C. V. Iyer and M. A. Balachandar, *Proceedings of the 46th International SAMPE Symposium and Exhibition*, pp. 704–717, 2001.
41. J. K. Lee and S. H. Yoon, *Polymer (Korea)*, Vol. 25(3), pp. 359–366, 2001.
42. K. P. Pang and J. K. Gillham, *Journal of Applied Polymer Science*, Vol. 38, pp. 2,115–2,139, 1989.
43. G. Wisanrakkit and J. K. Gillham, *Journal of Applied Polymer Science*, Vol. 42, pp. 2,465–2,481, 1991.
44. E. E. Shin, R. J. Morgan, J. Zhou, J. Lincoln, R. Jurek and D. B. Curliss, *Journal of Thermoplastic Composite Materials*, Vol. 13(1), pp. 40–57, 2000.
45. K. Chung and J. C. Seferis, *Polymer Degradation and Stability*, Vol. 71(3), pp. 425–434, 2001.
46. “The Manufacture, Characterization and Aging of Novel High Temperature Carbon Fibre,” arc.cs.odu.edu:8080/dp9/getrecord/oai_dc/oai:anu:00000528.
47. S. A. Laman, S. Yalvac and R. L. McGee, *Proceedings of the 36th International SAMPE Symposium and Exhibition*, pp. 469–481, 1991.
48. F. T. Fisher and L. C. Brinson, *SEM Annual Conference on Experimental Mechanics*, Milwaukee, June 10–12, 2002.

CHAPTER 8

ENVIRONMENTAL DEGRADATION OF REINFORCED CONCRETE

Neal Berke

WR Grace Construction Products, Cambridge, Massachusetts

| | | | |
|---|-----|-------------------------------|-----|
| 8.1 INTRODUCTION | 165 | 8.6 CORROSION INHIBITORS | 170 |
| 8.2 CONCRETE PROPERTIES AFFECTING CHLORIDE INGRESS AND THRESHOLD VALUES | 166 | 8.7 REBAR COATINGS | 171 |
| 8.3 CORROSION MECHANISMS OF STEEL IN CONCRETE | 167 | 8.8 STAINLESS STEEL | 171 |
| 8.4 MECHANISMS OF CORROSION PROTECTION SYSTEMS | 169 | 8.9 CATHODIC PROTECTION | 171 |
| 8.5 REDUCING CHLORIDE INGRESS | 169 | 8.10 LIFE-CYCLE MODELING | 171 |
| | | 8.11 ENVIRONMENT AND GEOMETRY | 172 |
| | | 8.12 SUMMARY | 173 |
| | | 8.13 REFERENCES | 174 |

8.1 INTRODUCTION

Concrete is the most widely used construction material, with over six billion tons produced worldwide per year. While concrete has sufficient strength in compression for most engineering applications, it is a brittle material with relatively low tensile strength (approximately one-tenth of its compressive strength). Therefore, in order to utilize concrete in its numerous applications, it needs to be reinforced with a more ductile and higher tensile strength material. This is usually steel in the form of reinforcing bars. In some cases, a compressive load is placed on concrete to offset anticipated tensile loads by the use of high strength steel wire. In these cases, the concrete is either post-tensioned or prestressed.

Fortunately, for steel reinforcement, concrete provides an alkaline environment, typically between pH 12.5 and 13.5. This provides a naturally protective environment for steel under most exposure conditions. Furthermore, steel and concrete have almost identical coefficients of temperature expansion, providing good composite performance over a wide temperature range. These properties, coupled with the good mechanical properties and low costs of steel, have made steel reinforced concrete the building material of choice in numerous structures where strength and durability are needed.

Metals other than steel are occasionally used in concrete. However, due to the good performance of steel, they are usually not used in structural applica-

tions. If more than one type of metal is used they should be electrically isolated to prevent galvanic corrosion. Galvanized and epoxy-coated steel, as well as stainless steels, will be discussed in detail in the following corrosion protection and modeling sections. Copper is usually used with grounding rods and copper tubing. Aluminum is usually not recommended, since it corrodes rapidly at high pH and has a high coefficient of temperature expansion. Aluminum can be protected with calcium nitrite corrosion inhibitor [Berke et al 1990].

The corrosion protection provided to steel by concrete has led to the use of steel-reinforced concrete in severe exposures to chlorides. Typical applications include concrete piles, girders, decks, and walls in marine environments, and bridge and parking decks in de-icing salt environments. The ingress of chloride into the concrete eventually leads to de-passivation of the steel and subsequent cracking and spalling of the concrete, since the corrosion products have higher volume than the initial steel, and the concrete cannot withstand the high tensile forces from the volume expansion. A recent study has estimated that the annual cost of corrosion of steel in concrete in the United States is at least \$15 billion [Koch et al].

Another cause of corrosion of steel in concrete is the carbonation of the concrete. This occurs as carbon dioxide in the air reacts with calcium hydroxide and other calcium bearing phases in the cement paste portion of the concrete, lowering the pH to 10

or lower. This is usually not a major problem in higher strength concretes used in engineering structures, as the carbonation front rarely reaches the reinforcing steel over the design life of the structure due to the low permeability and higher cement contents of these concretes, as will be discussed in detail later. The rest of this section will primarily address corrosion of embedded steel due to the ingress of chloride. More information on carbonation corrosion can be found in the books referenced in the bibliography at the end of this chapter.

To fully understand the corrosion of steel in concrete, one needs to address several areas. These include the following:

1. concrete properties affecting the ingress of chloride and the chloride threshold value for corrosion initiation
2. corrosion mechanisms of steel in concrete or in an alkaline environment with chloride
3. corrosion protection systems, including combinations of several systems
4. life-cycle modeling

The above will be discussed in detail in the following sections, along with the appropriate test methods utilized to determine the key properties and mechanisms.

8.2 CONCRETE PROPERTIES AFFECTING CHLORIDE INGRESS AND THRESHOLD VALUES

Concrete is essentially the combination of cement, coarse and fine aggregates, and water. Chemical admixtures are usually added to improve handling of the fresh concrete or enhance performance of the hardened concrete. Supplementary cementitious materials include pozzolans such as fly ash, silica fume, or metakaoline, or ground blast furnace slag. These materials are typically added to enhance hardened properties of the concrete. The properties of concrete are a function of the types and proportions of the materials listed above, as well as placing and curing procedures in the field. The properties of concrete are explained in detail by Mindess, Young, Darwin [Mindess and Young].

For chloride-induced corrosion, the two key properties of the concrete are permeability and the chloride threshold value. Permeability is primarily controlled by the water-to-cementitious ratio (w/cm) [Mindess et al.]. Permeability to water ingress de-

creases significantly with a reduction in w/cm . A similar reduction is noted in the apparent diffusion coefficient for chloride as shown for mortars [Page et al.] and for concrete, [Berke and Hicks 1994.] Bentz et al. Note that fly ash and silica fume additions result in an even lower apparent diffusion coefficient than just adding additional cement. Figure 8.1 shows the effect of reducing diffusion coefficients on the estimated chloride levels after 75 years, for a case of a surface concentration of chloride increasing at the surface for 25 years and the assumption of one-dimensional Fickian diffusion. Thus, a reduction in w/cm can result in a significant reduction in chloride ingress in time. Reducing w/cm is accomplished by raising the cement and supplementary cementitious additive content, or by reducing the water content. Raising the cementitious content is beneficial to a point, but could cause an increase in cracking, or excessive heat development if it is too high. Reducing water results in a loss of workability, leading to poor consolidation and placement difficulties. Superplasticizing (or high range water reducing) chemical admixtures can be added to provide enhanced workability at lower water contents. Typically, concrete mixtures used in durable concrete will use both an increase in the cementitious content as well as a superplasticizer to reduce water. Several documents and books go into significant detail on the design of concrete properties for corrosion performance [ACI 222; Tuutti; Bentur, Berke, and Diamond; Broomfield; CANMET/ACI Symposia].

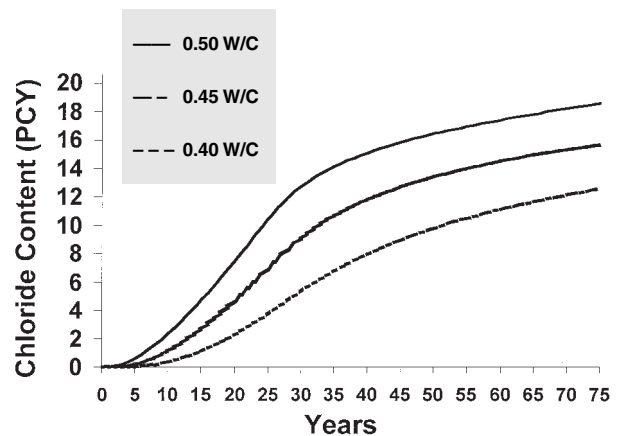


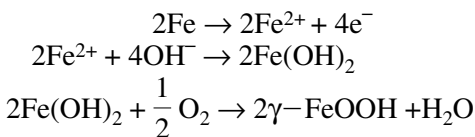
FIGURE 8.1 Diffusion profiles up to 75 years as a function of w/c . Note that chloride at the surface increases at 1 pcy (0.6 kg/m^3)

In addition to affecting the ingress of chloride, the concrete materials affect the chloride threshold value for corrosion initiation. In this case, the cement type and content are of primary importance and the supplementary cementitious materials also play a role. Several authors note that the tricalcium aluminate (C_3A) content of cement plays a key role in binding of chloride [Mehta]. Lower C_3A contents let more chloride in as the binding efficiency is lowered, and also lead to corrosion at lower values as more chloride is in the pore solution of the concrete. Lower C_3A values are usually desirable for enhanced resistance to sulfate attack of the concrete but, as pointed out by several researchers [Mehta], low w/cm is more important and there should be a 5 to 8% C_3A content.

Another cementitious factor affecting chloride threshold is the pH of the concrete pore water. Gouda et al., showed that there was a linear relationship between hydroxide content and the amount of chloride needed to initiate corrosion [Gouda]. Thus, concretes with a higher pore water pH can be expected to have higher threshold values for chloride initiation. However, too high pH content can lead to alkali attack of some aggregates; the concrete alkali content as K_2O equivalent is often limited to 3 kg/m³ [ACI 201]. Hansson has shown that cations associated with the chloride can change the internal pH and apparent threshold values [Hansson].

8.3 CORROSION MECHANISMS OF STEEL IN CONCRETE

The normally occurring oxides on steel are either ferrous (Fe^{+2}) or ferric (Fe^{+3}) in nature. Both are chemically stable in concrete in the absence of carbonation or chloride. However, the ferric oxide is more stable, especially in the presence of chloride. Over time, the ferrous oxide is converted to the more stable hydrated ferric oxide that is chemically referred to as $-FeOOH$. This process is never totally completed and is measured as a continuing very small passive corrosion rate, as will be discussed later. The development of the ferric oxide film proceeds according to the following anodic reactions:



Neither oxide is protective at pHs below approximately 11. Thus, corrosion will occur if carbonation is present at the reinforcing bars.

As noted above, the ferric oxide is more resistant to chloride than the ferrous oxide. If chloride ions are present, they will induce corrosion if they come into contact with the reinforcing bar at a location where the ferrous oxide has not been converted. This results in pitting corrosion. This competes with the normal passivation process and will only proceed when the chloride content is sufficiently high compared to the oxygen and hydroxide content. This is the underlying theory as to why chloride-to-hydroxide ratios are related to the onset of pitting corrosion. In concrete, this corrosion threshold is approximately 0.9 kg/m³ (1.5 lb/yd³) of concrete.

This passivation process can also be described in electrochemical terms [Rechberger; Berke; Bentur et al.]. Figure 8.2 shows the anodic and cathodic reaction curves for passive steel in an alkaline environment such as concrete. Curve A in Figure 8.2 schematically shows the relationship between the anodic reaction rate and the potential of steel relative to a reference electrode in a concrete-type environment. The anodic reaction rate is represented as a current density and describes the corrosion rate of the steel, with lower current densities indicating lower corrosion rates. At very high negative potentials, the corrosion rate increases rapidly as the potential becomes less negative, then suddenly drops by several orders of magnitude. The potential at which this occurs is known as the *primary passivation potential* (E_{pp}) and is related to the development of the ferric oxide. Then, over a large range of potentials (typically from approximately -800 to $+600$ mV versus saturated calomel electrode, in the absence of chloride), the steel is corroding at a negligible rate, and this is the passive region. At more positive potentials, the breakdown of water to pro-

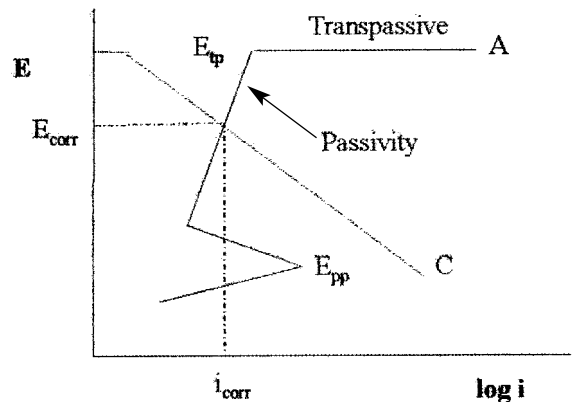
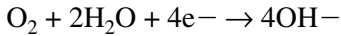


FIGURE 8.2 Steel in an alkaline environment.

duce oxygen occurs and severe corrosion can once again occur, and passivity is lost. The potential at which this occurs is the *transpassive potential* (E_{tp}).

Curve A in Figure 8.2 describes the anodic behavior of steel; that is, it only looks at the oxidation reactions that are occurring. The actual corrosion potential will also depend upon the oxygen content, which affects the cathodic reaction rate. For steel in concrete, the cathodic reaction is primarily the reduction of oxygen:



The cathodic behavior as a function of potential is schematically shown in Figure 8.2 as Curve C.

As in other chemical processes, the anodic reaction and the cathodic reaction have to be in balance. Thus, the point of intersection of the two curves portrays the only corrosion situation which can exist for these conditions. This is shown in Figure 8.2, in which the anodic and cathodic curves have been superimposed and the rates have been shown as currents. Since this figure is representative of steel in non-carbonated chloride-free concrete, the intersection of the two reactions is in the passive zone, and only the low passive corrosion currents are reached. The potential at which the anodic and cathodic currents are of equal magnitude is the *corrosion potential*, E_{corr} . The *corrosion current*, I_{corr} , is equal in magnitude to the anodic current and absolute value of the cathodic current. It is most useful to divide the corrosion current, I_{corr} , by the area to obtain the *corrosion current density*, i_{corr} .

The anodic behavior of steel in concrete is changed in the presence of chloride as shown in Figure 8.3, with chloride causing pitting to initiate. When pitting is present, the corrosion current density in the pit is high and is limited only by the amount of cathode present. This is schematically

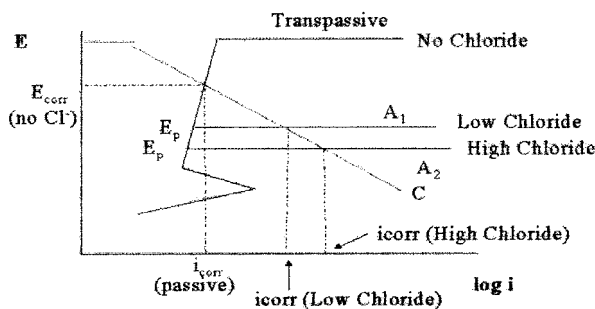


FIGURE 8.3 Effect of chloride on the corrosion of steel.

shown in Figure 8.3, which shows that the anodic curve, A_1 , is almost horizontal at the *pitting protection potential*, E_p . At potentials negative to E_p pits are not stable and pitting stops. Above E_p , the corrosion rate is orders of magnitude higher than the passive rate and severe local metal loss can occur.

Increasing the chloride content has the effect of facilitating the pitting process and results in a further lowering of the pitting protection potential, as shown with Curve A_2 in Figure 8.3. For the same amount of available cathode (i.e., for identical curve C), the corrosion rate increases further, as shown. This is where the rule of thumb about more negative corrosion potentials being associated with higher corrosion rates came from. However, even when chloride is present, and especially when it is not, corrosion potential values versus a saturated calomel reference electrode below $\times 280$ mV are not necessarily indicative of corrosion, as shown in Figure 8.3 and discussed below.

The role of oxygen on the corrosion rate when pitting is present is illustrated in Figure 8.4. Variations in oxygen availability change the location of the cathodic reaction curve. Thus, even if sufficient chloride is present for pitting, corrosion rates can be low if the oxygen content is low or cathodic area is small. Points W and X are the possible conditions when oxygen levels are low (the intersection at point Y represents an unstable situation which will convert to point W). If the steel has already been passivated due to higher oxygen conditions, at some time point W will be the potential. If passivation has not occurred, then point X will be the intersection point, and corrosion rates will be higher (active corrosion, but at a low rate). In both cases, corrosion rates are

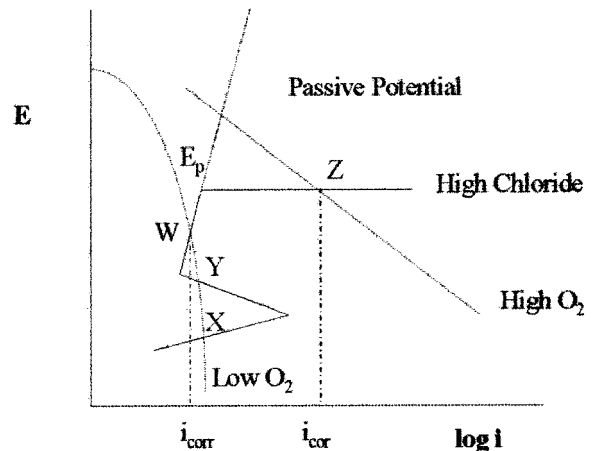


FIGURE 8.4 Role of oxygen in steel corrosion.

negligible. This is commonly observed for concrete piles far below the water line in marine environments, where oxygen levels are low.

At higher oxygen levels, pitting corrosion occurs because the oxygen reduction reaction intersects the anodic reaction above the protection potential, as shown in Figure 8.4. This is illustrated as the intersection that occurs at point Z. Because current density is on a log scale, the corrosion current density is orders of magnitude higher than in the low oxygen case.

8.4 MECHANISMS OF CORROSION PROTECTION SYSTEMS

Protection systems for corrosion act in one or more of the following ways:

- reduce the ingress of chloride into the concrete (low permeability concrete)
- keep chloride from the surface of the concrete (sealers and membranes)
- reduce corrosion in the presence of chloride next to the steel (corrosion inhibitors)
- provide a protective coating to the bar (epoxy-coated and galvanized steel)
- use more corrosion resistant steel (stainless steels)
- suppress the corrosion cell electrically (cathodic protection)

Each of these systems will essentially have one or more of the following three effects:

1. reduce the ingress of chloride
2. increase the chloride level at which corrosion initiates
3. reduce the corrosion rate of the active corrosion

Accelerated and long-term field and laboratory tests are needed to estimate the performance of a protection system as related to these three effects. The evaluation of the performance of these systems is not trivial and requires an understanding of corrosion and protection mechanisms. In addition, the same accelerated testing techniques cannot be used for all methods.

Once the performance of a corrosion protection system can be quantified, it is possible to perform a life-cycle cost analysis to select the most cost effective system. Since there is usually an upfront cost associated with corrosion protection, a net present value analysis looking at repair costs and loss of use

need to be considered. An example of this analysis is presented below.

8.5 REDUCING CHLORIDE INGRESS

Reduction of chloride ingress into concrete can be accomplished by reducing the porosity of the concrete or by the use of membranes or sealers. This section examines these approaches.

8.5.1 Low Permeability Concrete

Traditionally, the first steps in improving the durability of reinforced steel involved improving concrete quality. For example, ACI 318 and ACI 357 recommend water-to-cementitious [w/(cm)] ratios of 0.4 or under, and minimum covers of 50 mm for non-marine and 68 mm in marine exposures [ACI 318, ACI 357]. Other codes, such as Eurocode 2 and Norwegian Code N5 3474, are less stringent [Eurocode 2, Norwegian Code N5 3474].

Additional means of reducing the ingress of chloride into concrete involves the addition of pozzolans or ground blast furnace slag. These materials are often added as cement substitutes; they react with calcium hydroxide to reduce the coarse porosity of the concrete and to decrease the porosity at the paste-aggregate interfaces. Several conference proceedings document the positive benefits of these materials [CANMET/ACI Durability, CANMET/ACI Fly Ash].

Numerous references show that even if concrete is produced to the most stringent of the codes, chloride will ingress into the concrete and corrosion of the steel reinforcement will initiate [Browne, Pfeifer and Landgren, Tuutti, Berke, Scali, Regan, Shen 1991, Berke et al 1992].

Even for very low permeability concretes, chloride will eventually ingress into the concrete and initiate corrosion [Berke and Hicks 1994]. When chloride ingress is modeled as a function of w/c+p and pozzolan contents for various geometries and environmental exposures, times to corrosion in excess of 25 years are difficult to achieve for low permeability concretes [Berke and Hicks 1994, Berke, Hicks, Dallaire 1996]. Thus, additional protection systems are necessary to meet extended design lives that are becoming increasingly specified.

8.5.2 Sealers and Membranes

Sealers and membranes work by either reducing the ingress of chloride into the concrete, or by reducing

the movement of moisture. They either produce a continuous film on the surface (creating a hydrophobic layer lining the pores and surfaces of the concrete), or they produce reaction products that block the concrete pores. Surface preparation and application techniques must be carefully followed to have good results. Several references discuss these protection systems in great detail [Keer; CIRIA; Weyers et al.; C103; Pfeiffer and Scali; Bentur; Diamond and Berke].

Products that provide a continuous film or coating on the surface include acrylics, butadiene copolymer, chlorinated rubber, epoxy resin, oleoresinous, polyester resin, polyethylene copolymer, polyurethane, and vinyl. Rubberized asphalt is a popular sheet membrane material. Membranes exposed to wear typically have protective surface coatings. Hydrophobic pore liners include the silanes, siloxanes, and silicones. The pore blockers include silicate, silicofluoride, and crystal growth materials in a cementitious slurry.

An extensive review of sealer and membrane field performance was conducted as part of the Strategic Highway Research Program [Weyers et al., 1992]. It concluded that these systems had a useful effectiveness between 5 and 20 years. The importance of longer-term testing in evaluating these products was shown by Robinson [Robinson]. His accelerated laboratory testing showed an early 100% reduction in chloride ingress, which did not hold up over time. However, most products did offer an improvement.

8.6 CORROSION INHIBITORS

Corrosion inhibitors are chemical substances that reduce the corrosion of embedded metal without reducing the concentration of the corrosive agents. This definition, paraphrased from ISO 8044-89, makes the distinction between a corrosion inhibitor and other additions to concrete that improve corrosion resistance by reducing chloride ingress into the concrete.

Corrosion inhibitors can influence the anodic, cathodic, or both reactions. Since the anodic and cathodic reactions must balance, a reduction in either one will result in a lowering of the corrosion rate. Figure 8.5 illustrates the effects of both types of inhibitors, acting alone or in combination, when the chloride concentration has not been changed. When no inhibitors are present, the anodic (A_1) and cathodic curves (C_1) intersect at point W. Severe pit-

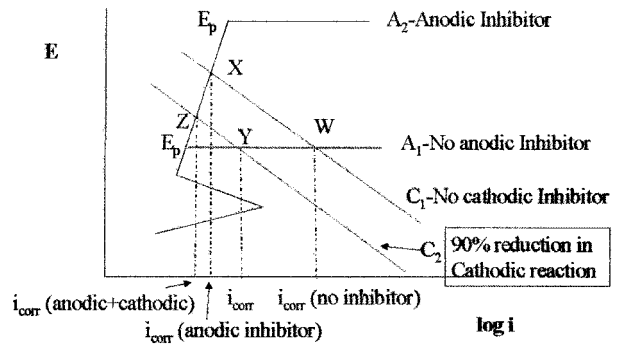


FIGURE 8.5 Comparison of anodic and cathodic inhibitors.

ting corrosion is occurring. The addition of an anodic inhibitor (curve A_2) promotes the formation of ($-\text{FeOOH}$ (passive oxide), which raises the protection potential E_p , so that the anodic and cathodic curves now intersect at point X. The corresponding corrosion rate, i_{corr} , is reduced by several orders of magnitude and the steel is passive. Increasing quantities of anodic inhibitor will move curve A_2 to more positive E_p values.

The addition of a cathodic inhibitor in the absence of an anodic inhibitor results in a new cathodic curve (C_2) as shown in Figure 8.5. The new intersection with the anodic curve (A_1) is at point Y. Though the corrosion rate is reduced, pitting corrosion still occurs because the potential remains more positive than E_p . Therefore, a cathodic inhibitor would have to reduce cathodic reaction rates by several orders of magnitude to be effective by itself.

The case of combined anodic and cathodic inhibition is illustrated in Figure 8.5 as the intersection of the anodic (A_2) and cathodic (C_2) curves at point Z. The steel is passive as in the case of the anodic inhibitor alone (point X), but the passive corrosion rate is reduced further.

Commercially available inhibitors include calcium nitrite, sodium nitrite and morphelene derivatives, amine and esters, dimethyl ethanol amine, amines and phosphates. Several reviews and other papers discuss the performance of inhibitors in concrete [Aldykiewicz, Berke, and Li; Elsener; Berke and Weil; Kessler et al.]. With the exception of calcium nitrite, little to no long-term data beyond 5–10 years is available on the other products.

The long-term performance benefits of calcium nitrite are well documented [Berke et al. 1992, 1994, 1997, 2003; Elsener; Berke and Weil]. Based upon these results, Table 8.1 was developed to indicate the

TABLE 8.1 Calcium Nitrite Dosage Rates versus Chloride Protection

| Calcium Nitrite (30% sol.) L/m ³ | Chloride Ion kg/m ³ |
|---|--------------------------------|
| 10 | 3.6 |
| 15 | 5.9 |
| 20 | 7.7 |
| 25 | 8.9 |
| 30 | 9.5 |

level of chloride that a given addition of 30% calcium nitrite protects against.

Furthermore, as noted in these papers, the use of calcium nitrite or any other inhibitor is not a substitute for good quality concrete, and guidelines for reducing chloride ingress must be followed.

Performance criteria for an amine and ester commercially available inhibitor were published [Johnson et al.]. This inhibitor at a dosage of 5 L/m³ was stated to protect to 2.4 kg/m³ of chloride. A reduction in the chloride diffusion coefficient of 22–43%, depending on concrete quality, was determined using accelerated test methods.

8.7 REBAR COATINGS

Rebar coatings now in large-scale commercial use are epoxy and zinc. Epoxy acts as a barrier to chlorides, and zinc (galvanized rebars) provides both a barrier and a sacrificial anode.

Epoxy-coated steel is extensively used in the United States. ASTM Standards [ASTM A 775/A 775M and D 3963/D 3963M] are available to ensure good performance. These standards set requirements for the number of holidays (small non-visible defects), repair area allowed, handling, and coating performance. Numerous studies have been conducted that show improved performance versus black steel controls [TRB]. However, several of these studies show that corrosion can occur over time, and that the coating can be damaged during the placing and consolidation of the concrete. The damaged portions of the coating can be initiation sites for corrosion. The best performance is obtained when all of the steel is epoxy-coated, which avoids large cathode-to-anode ratios.

Galvanized rebars are used more extensively outside of the United States. There is an applicable ASTM Standard [ASTM A 776/A 776M]. Several

papers exist documenting performance in tests (Yeomans 1993; Yeomans 1987; Treadaway, Brown and Cox;]. In general, the coating thickness determines overall life, with thicker coatings having better performance.

8.8 STAINLESS STEEL

A few studies exist on the performance of stainless steel alloys in concrete [McDonald, Sherman, Pfeifer and Virmani; Flint and Cox; Sorensen, Jensen and Maahn]. Though performance is improved significantly, depending upon the alloy used, initial costs are quite high [Sorensen, Jensen and Maahn]. Therefore, its use is limited. Furthermore, as will be shown later, there is an appreciable economic benefit (compared to stainless steel) to achieving desired service lives using combinations of the protection methods discussed above. A martensitic iron-chromium alloy without carbon phases has been introduced [Trejo, Darwin]. Performance is between that of stainless steels and black bars.

8.9 CATHODIC PROTECTION

Cathodic protection, if applied properly, can prevent and stop corrosion of steel in concrete. It works by making the reinforcing steel a cathode by the use of an external anode. This anode can be either inert or sacrificial, depending upon the exposure.

For cathodic protection to be effective, the reinforcement must be electrically continuous, the concrete conductivity between the anode and steel needs to be low, and alkali-reactive aggregates should not be used as the area next to the steel becomes more alkaline over time. More information is available in the references [Broomfield 1992; Broomfield 1993; Bennet] and in the NACE Recommended Practice [CEA 54286].

Due to the expense, relative to other corrosion protection systems, cathodic protection is most often used in repair. The reasons for this are quite evident once a life-cycle cost analysis is performed.

8.10 LIFE-CYCLE MODELING

In order to select among the corrosion protection systems noted above, and future ones, a rational approach is needed to select the optimal system or

combination of systems to provide the desired design life for the structure in question. This includes minimizing the life-cycle costs.

To perform a life-cycle analysis, several pieces of information are needed. These include the following:

1. environmental exposure and member geometry
2. estimate of the chloride diffusion coefficient (and sorptivity)
3. effect of the protection system on chloride ingress, chloride threshold value for corrosion initiation, and corrosion rate after corrosion initiates
4. initial costs of the protection system
5. repair costs
6. time between repairs

In many cases, one does not have a complete irrefutable set of information to fill-in the information required above. However, one can make reasonable estimates based upon the information available, and considerable work is underway to define the parameters needed. An example of predicting life-cycle costs will be given below. For more details, there are several models available with various degrees of complexity, and a few of them are in the references (Berke et al., Thomas et al., Marchand et al.).

8.11 ENVIRONMENT AND GEOMETRY

The exposure environment needs to be assessed to estimate the chloride exposure. Important parameters are temperature and degree of salt exposure. The salt exposure is different for submerged marine, splash-tidal zones, airborne chlorides, and de-icing salt applications. Submerged marine and tidal zone exposures quickly come to a fixed high surface concentration of chloride. In the case of de-icing salts and airborne chlorides, the surface concentration increases more slowly over time. Geometry plays a key role as a pile in the ocean represents a two-dimensional case of chloride ingress, whereas a deck or wall is a one-dimensional exposure.

8.11.1 Chloride Diffusion Coefficient

The ingress of chloride can be predicted from the diffusion coefficient for chloride in the concrete of interest. Due to the heterogeneous nature of concrete, the exact rate of chloride diffusion cannot be calculated, and it will vary with differences in concreting materials. However, approximate values can be ob-

tained with sufficient accuracy for estimating the ingress of chloride into concrete structures as a function of exposure conditions. Note that more advanced models address the degree of concrete saturation and the movement and chemical reactions of several ions in addition to chloride (Marchand et al.).

The diffusion of chloride in concrete follows Fick's second law of diffusion (Bamforth and Price; Browne; Tuutti; Berke, Hicks and Tourney; Bentur et al.; Hansson and Berke; Short and Page; Hobbs; Bentz, Evans, and Thomas; Goto and Roy; Garbozi; Dhir; Weyers and Cady; Pereira and Hegedus; Thomas and Mathews). This correlation can be used to calculate an *effective diffusion coefficient*, D_{eff} , if the chloride concentration at any time is known as a function of depth. A more rigorous approach would account for chloride binding and sorption effects (Pereira and Hegedus; Thomas and Mathews). If chloride profiles are used after longer exposure times of one to two years, then the effective diffusion coefficient calculated is a good approximation of future chloride ingress. D_{eff} can be adjusted for temperature using an Arrhenius equation [Berke and Hicks].

The one-dimensional solution to Fick's second law with a constant surface chloride and semi-infinite slab is given by the following:

$$C(x,t) = C_o[1 - \text{erf}(x/2(D_{\text{eff}}t)^{.5})], \quad (8.1)$$

where $C(x,t)$ is the chloride concentration at depth x and time t ,

C_o is the surface concentration
 D_{eff} is the effective diffusion coefficient,
 and
 erf is the error function.

The solution for a square pile under similar constant surface chloride conditions is

$$C(x,y,t) = C_o[1 - \text{erf}(x/2(D_{\text{eff}}t)^{.5}) \cdot \text{erf}(y/2(D_{\text{eff}}t)^{.5})], \quad (8.2)$$

where $C(x,y,t)$ is the chloride concentration at a distance x and y from the perpendicular sides at time t . Numerical methods can also be used and are necessary when C_o or D_{eff} change as a function of time.

One concern in modeling is the role of cracking. If cracking is severe, the above diffusion models will not be applicable in the crack regions. Work in this area is in progress. Shrinkage-reducing admixtures and structural synthetic fibers can significantly reduce drying shrinkage and resist crack opening

[Berke, Hicks, Li, Rieder] and, thus, make the models more applicable.

8.11.2 Cost Analysis

In order to perform a life-cycle cost analysis one needs to know the costs of initial corrosion protection as well as the Net Present Value (NPV) costs associated with repairs. The NPV is defined as

$$\text{NPV} = \text{Cost} \cdot (1 - D)^{-n}, \quad (8.3)$$

where Cost is the price for the repair if performed today,

- D is the discount rate or the interest rate less the inflation rate, and
- n is the number of years to repair.

A typical value for the discount rate is 4% ($D = 0.04$). Thus, the cost of a given protection system is the initial cost plus the NPV of the repairs.

8.11.3 Example of Life-Cycle Cost Analysis for a Bridge Deck

A bridge deck in the northern United States is exposed to de-icing salts over time. For this example, a typical average yearly temperature of 10 °C is chosen. The surface chloride concentration will increase over time at a rate of 0.6 kg/m³/yr, until a constant maximum value of 15 kg/m³ is reached. The rate of increase is less than that in a northern parking deck due to the effects of rain. Since the surface chloride concentration is a function of time, a numerical solution to Fick's Second Law is used.

Figure 8.6 shows the chloride concentration at a depth of 65 mm for several types of concretes at 75 years. One with an effective diffusion coefficient of 1.3×10^{-12} m²/s represents a concrete with a water-to-cement ration of 0.4. The lower curves represent

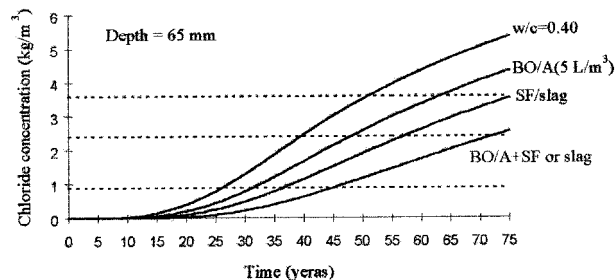


FIGURE 8.6 Estimated chloride concentration for a bridge deck (Chloride buildup = 0.6 kg/m³/year).

concretes produced with 40% ground blast furnace slag or 7.5% silica fume (0.78×10^{-12} m²/s) and the effects of a damp-proofing inhibitor in the concrete (0.98×10^{-12} and 0.58×10^{-12} m²/s).

Protection systems considered in Figure 8.6, in addition to the use of lower permeability concrete, are a 30% calcium nitrite solution at 10 and 15 L/m³, a butyl oleate and amine at 5 L/m³, and epoxy-coated reinforcing bars alone and in combination with calcium nitrite or butyl oleate. Repairs were considered to occur at five years after corrosion initiation and at 20-year intervals after that. The repairs were set at \$350/m² of surface, and it was estimated that only 10% of the surface would need to be repaired. These numbers are fairly representative, but should be adjusted for specific locations. Traffic delay costs (which can be considerable) were not included. Table 8.2 summarizes the initial cost, repair cost, and total NPV of the various combinations. Clearly, low permeability concrete alone is not the best life-cycle option. Figure 8.7 ranks the nine lowest cost systems against the base case, and further supports the benefits for corrosion protection systems even though initial costs are higher.

Membranes, stainless steel bars and cathodic protection were not included in the above analysis. At an initial cost of \$43–\$130/m² cathodic protection is not cost effective for a new bridge deck. Membranes have a service life of about 20 years and, at an initial cost of about \$30/m², they are also not cost effective for corrosion protection (although they could have other benefits where leaks to a lower level need to be avoided). Finally, Type 304 stainless steel comes in at about \$39/m² in new construction, which is much more costly than alternative protection mechanisms.

8.12 SUMMARY

Understanding and reducing the corrosion of steel in concrete is of major importance to reducing the life-cycle costs of bridges, marine structures, parking structures, and other concrete structures in severe environments. Numerous protection methods have been developed and models are coming into use to aid in the decision as to which method or methods to employ in a corrosion protection system. At this time, one of the most cost effective approaches is the use of good quality, low permeability concrete containing corrosion inhibitors. In addition to improving corrosion performance, the overall performance of the concrete is improved with this approach.

Future work, in addition to developing improved protection methods, will focus on improved model-

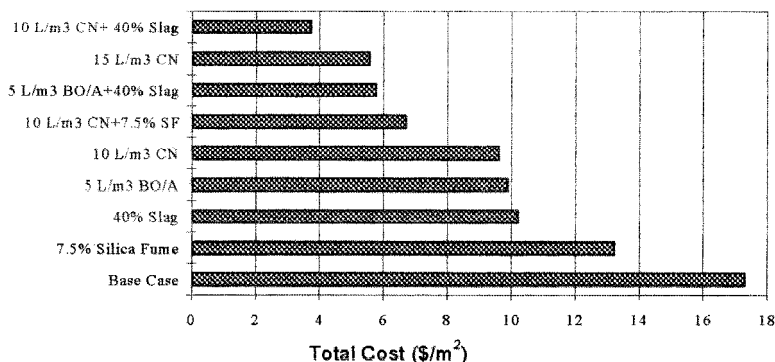
TABLE 8.2 75-Year Analysis for a Bridge Deck

| Case Design | Initial cost (\$/m ²) | Initiation (Years) | First Repair (Years) | Number of Repairs | NPV Repair (\$/m ²) | NPV Total (\$/m ²) |
|---|-----------------------------------|--------------------|----------------------|-------------------|---------------------------------|--------------------------------|
| Base Case | 0 | 26 | 31 | 3 | 17.28 | 17.28 |
| 10 L/m ³ CN | 3.70 | 50 | 55 | 2 | 5.90 | 9.60 |
| 15 L/m ³ CN | 5.55 | 76 | 81 | 0 | 0 | 5.55 |
| 40% Slag | 0 | 36 | 41 | 2 | 10.21 | 10.21 |
| 7.5% Silica Fume (SF) | 3 | 36 | 41 | 2 | 10.21 | 13.21 |
| 5 L/m ³ BO/A | 3.50 | 48 | 53 | 2 | 6.38 | 9.88 |
| ECR | 19.47 | 26 | 46 | 2 | 8.39 | 27.86 |
| 10 L/m ³ CN + 40% Slag | 3.70 | 74 | 79 | 0 | 0 | 3.70 |
| 10 L/m ³ CN + 7.5% Silica Fume | 6.70 | 74 | 79 | 0 | 0 | 6.70 |
| 5 L/m ³ BO/A + 40% Slag | 3.50 | 65 | 70 | 1 | 2.25 | 5.75 |
| 5 L/m ³ BO/A + ECR | 22.97 | 48 | 68 | 1 | 2.43 | 25.40 |
| 10 L/m ³ CN + ECR | 23.17 | 50 | 70 | 1 | 2.25 | 25.42 |
| 10 L/m ³ CN+ECR + 40% Slag | 23.17 | 74 | 94 | 0 | 0 | 23.17 |
| 5 L/m ³ BO/A + ECR + 40% Slag | 22.97 | 65 | 85 | 0 | 0 | 22.97 |

CN = 30 % solution of calcium nitrite

BO/A = Butyl Oleate/Amine

ECR = Epoxy-coated reinforcing steel (top and bottom mats)

**FIGURE 8.7** Total costs (\$/m²), for a 75-year design bridge deck.

ing of the processes and life-prediction. The new models will address corrosion and other deterioration processes of concrete, as well as quantify the role of cracking.

8.13 REFERENCES

- ACI 201.2R 2003 Guide to Durable Concrete, In *Manual of Concrete Practice, Part I—Materials and General Properties of Concrete*. Farmington Hills, MI: ACI International.
- ACI 222. 2003. Corrosion of Metals in Concrete. In *Manual of Concrete Practice, Part I—Materials and General Properties of Concrete*. Farmington Hills, MI: ACI International.
- ACI 318. 2003. Building Code Requirements for Reinforced Concrete. *Manual of Concrete Practice, Part I—Materials and General Properties of Concrete*. Farmington Hills, MI: ACI International.
- ACI 357.R 2003. Guide for the Design and Construction of Fixed Offshore Concrete Structures. In *Manual of Concrete Practice, Part 5*. Farmington Hills, MI: ACI International.
- Bennet, J. E. 1993. "Cathodic Protection Criteria under SHRP Contract." Paper 323 in *Corrosion '93*. Houston: NACE International.
- Bentur, A., Diamond, S., and Berke, N. S. 1998. *Steel Corrosion in Concrete—Fundamental and Civil Engineering Practice*. London: E & FN Spon.
- Bentz, E. C., Evans, C. M., and Thomas, M. D. A. 1996. Chloride Diffusion Modeling for Marine Exposed Concretes. In *Proceedings of the 4th International Symposium on Corrosion of Reinforcement in Concrete Construction*. C. L. Page,

- P. Bamforth and J. W. Figg, Eds. Cambridge July 1–4, 1996. 136–145.
- Berke, N. S. 1986. The Use of Anodic Polarization to Determine the Effectiveness of Calcium Nitrite as an Anodic Corrosion Inhibitor. In *Corrosion Effects of Stray Currents and the Techniques for Evaluating Corrosion of Rebars in Concrete*. V. Chaker, Ed., ASTM STP 906, Philadelphia: ASTM. 78–91.
- Berke, N. S., Shen, D. F. and Sundberg, K. M. 1990. Comparison of Polarization Resistance Technique to the Macrocell Corrosion Technique, In *Corrosion Rates of Steel in Concrete*. ASTM STP 1065. N. S. Berke, V. Chaker and D. Whiting, Eds. Philadelphia: ASTM International.
- Berke, N. S. and Weil, T. G. 1994. World Wide Review of Corrosion Inhibitors in Concrete. In *Advances in Concrete Technology*. Ottawa, Canada: CANMET. 891–914.
- Berke, N. S., Hicks, M. C. and Tourney, P. G. 1997. 100-Year Service Lives in Marine Environments Using Belts and Braces Approach with Calcium Nitrite. In *Proceedings of the International Conference on Repair of Concrete Structures— from Theory to Practice in a Marine Environment*, Svølvær, Norway, May 28–30, 1997.
- Berke, N. S., Dallaire, M. P. M., Hicks, C. et al., 1996. Holistic Approach to Durability of Steel Reinforced Concrete. Concrete in the Service of Mankind. Radical Concrete Technology. In *Proceedings of the International Conference*. Scotland: University of Dundee. June, 1996. 25–45.
- Berke, N. S. and Hicks, M. C. 1994. Predicting Chloride Profiles in Concrete. *Corrosion*. March. 234–239.
- Berke, N. S. 1991. Corrosion Inhibitors in Concrete. *Concrete International*. Vol. 13(7), July. 24–27.
- Berke, N. S., Aldykiewicz, A. J., Jr., and Li, L. 2003. What's New in Corrosion Inhibitors. *Structure*. July/August. 10–12.
- Berke, N. S., Dallaire, M. P. and Hicks, M. C. 1992. Plastic, Mechanical, Corrosion, and Chemical Resistance Properties of Silica Fume (Microsilica) Concretes. In *Proceedings of the 4th International Conference: Fly Ash, Silica Fume, Slag, and Natural Pozzolans in Concrete*. Istanbul, Turkey. V. M. Malhotra, Ed. SP-132 Detroit: American Concrete Institute. 1,125–1,149.
- Berke, N. S., Scali, M. J., Regan J. C., and Shen, D. F. 1991. Long-Term Corrosion Resistance of Steel in Silica Fume and/or Fly Ash Concretes. In *Proceedings of the 2nd CANMET/ACI Conference on Durability of Concretes*. V. M. Malhotra, Ed. Canada: CANMET. 899–924.
- Berke, N. S., Hicks, M. C., Li, L. and Rieder, K. A. 2003. Holistic Approach to Durable High Performance Concrete. In *Advances in Concrete and Structures, Proceedings of the International Conference ICACS 2003*. Y. Yuan, S. Shah and H. Lu, Ed. RILEM Publications S.A.R.L. 727–738. Bagneux, France.
- Broomfield, J. P. 1993. *Five Years' Research on Corrosion of Steel in Concrete: A Summary of the Strategic Highway Research Program Structures*. Research. Paper 318 in *Corrosion '93*. Houston: NACE International.
- Broomfield, J. P. 1992. *Results of a Field Survey of Cathodic Protection Systems in North American Bridges*. Paper 203 in *Corrosion '92*. Houston: NACE International.
- Broomfield, John 1997. *Corrosion of Steel in Concrete: Understanding, Investigation and Repair*. London: Routledge mot E & FN Spon.
- Browne, D. 1982. *Durability of Building Materials*. Vol. 1. 113–125.
- First CANMET/ACI Conference on Durability of Concrete 1988. V. M. Malhotra, Ed. Detroit: American Concrete Institute
- Second CANMET/ACI Conference on Durability of Concrete 1991. V. M. Malhotra, Ed. Detroit: American Concrete Institute.
- Third CANMET/ACI Conference on Durability of Concrete 1994. V. M. Malhotra, Ed. Detroit: American Concrete Institute
- Fourth CANMET/ACI Conference on Durability of Concrete 1997. V. M. Malhotra, Ed. Detroit: American Concrete Institute
- Fifth CANMET/ACI Conference on Durability of Concrete 2000. V. M. Malhotra, Ed. Farmington Hills, MI: ACI International.
- Sixth CANMET/ACI Conference on Durability of Concrete 2000. V. M. Malhotra, Ed. Farmington Hills, MI: ACI International.
- Proceedings of the 1st International Conference: Fly Ash, Silica Fume, Slag and Natural Pozzolans in Concrete*. 1983. V. M. Malhotra, Ed. SP 79. Detroit: American Concrete Institute.
- Proceedings of the 2nd International Conference: Fly Ash, Silica Fume, Slag and Natural Pozzolans in Concrete*. 1986. V. M. Malhotra, Ed. SP 91. Detroit: American Concrete Institute.
- Proceedings of the 3rd International Conference: Fly Ash, Silica Fume, Slag and Natural Pozzolans in Concrete*. 1989. V. M. Malhotra, Ed. SP 114. Detroit: American Concrete Institute.
- Proceedings of the 4th International Conference: Fly Ash, Silica Fume, Slag and Natural Pozzolans in Concrete*. 1992. V. M. Malhotra, Ed. SP 132. Detroit: American Concrete Institute.
- CEA 54286 “Cathodic Protection of Reinforced Concrete” developed jointly by NACE International and the Institute of Corrosion, UK Houston: NACE International.
- CIRIA. 1987. *Technical Note 130*. London: Construction Industry Research and Information Association.
- Dhir, R. K. et.al. 1990. Rapid Estimation of Chloride Diffusion Coefficients in Concrete. *Magazine of Concrete Research*. Vol. 42. 177–185.
- Elsener, B. 2001. Corrosion Inhibitors for Steel in Concrete. Publication 35. European Federation of Corrosion Publications: W.S. Manney and Son, Ltd. .
- Eurocode 2 . 1992 *Design of Concrete Structures*. European Pre-Standard ENV.
- Flint, G. N. and Cox, R. N. 1988. The Resistance of Stainless Steel Partly Embedded in Concrete to Corrosion in Seawater. *Magazine of Concrete Research*. Vol. 40(142), March. 13–27.
- Fushuang, C., Sagues, A. A. and Powers, R. G. 2001. *Corrosion Behavior of Stainless Steel Clad Rebar*. Paper 1645 in *Corrosion 2001*. Houston: NACE International.

- Garbozi, E. J. 1990. Permeability, Diffusivity, and Microstructural Parameters: A Critical Review. *Cement and Concrete Research*. Vol. 20. 591–601.
- Goto, S. and Roy, D. M. 1981. Diffusion of Ions Through Hardened Cement Pastes. *Cement and Concrete Research*. Vol. 11(5/6). 751–757.
- Gouda, V. K. 1970. Corrosion and Corrosion Inhibition of Reinforcing Steel: 1. Immersed in Alkaline Solution. *British Corrosion Journal*. Vol. 5. 198–203.
- Hansson, C. M. and Berke, N. S. November, 1988. Chlorides in Concrete. In *MRS Symposium Proceedings: Pore Structure and Permeability of Cementitious Materials*. L. R. Roberts and J. P. Skalny, Eds. Vol. 137. 253–270.
- Hansson, C. M. and Sorensen, B. 1988. Threshold Concentration of Chloride in Concrete for Initiation of Reinforcement Corrosion. In *Corrosion Rates of Steel in Concrete*, ASTM STP 1065. N. S. Berke, V. Chaker, and D. Whiting, Eds. West Conshohocken, PA: American Society for Testing and Materials. 3–16.
- Hausmann, D. A. 1967. Steel Corrosion in Concrete. *Materials Protection*. Vol. 6, November. 19–23.
- Hobbs, D. W. 1996. Chloride Ingress and Chloride-Induced Corrosion in Reinforced Concrete Members. In *Proceedings of the 4th International Symposium on Corrosion of Reinforcement in Concrete Construction*. C. L. Page, P. Bamforth and J. W. Figg, Eds. Cambridge, UK: July 1–4, 1996. 124–135.
- Hurley, M. F., Scully, J. R. and Clemena, G. G. 2001. *Selected Issues in Corrosion Resistance of Stainless Steel Clad Rebar*. Paper 1645 in *Corrosion 2001*. Houston: NACE International.
- Johnson, D. A., Miltenberger, M. A. and Almy, S. I. 1966. Determining Chloride Diffusion Coefficients for Concrete Using Accelerated Test Methods. In Third CANMET/ACI International Conference on Concrete in Marine Environment. Supplemental Papers. V. M. Malhotra, Ed. Ottawa, Canada: CANMET. 95–114.
- Keer, G. 1992. Surface Treatments. In *Durability of Concrete Structures*. G. Mays, Ed. London: E & FN Spon, 46–65.
- Kessler, R. J., Powers, R., Cerlanek, W. D. and Sagüés, A. A. 2003. *Corrosion Inhibitors in Concrete*. Paper 288. Corrosion 2003. Houston: NACE International.
- Koch, G. H., Brongers, M. P. H., Thompson, N. G., Virmani, Y. P., Payer, J. H. 2001. *Corrosion Cost and Prevention Strategies in the United States*. FHWA-RD-01-156. McLean, VA: Federal Highway Administration.
- Marchand, J., Maltais, Y., Ouellet, E., Samson, E. and Burke, D. 2003. Prediction of the Long-Term Durability of Lightweight Aggregate Concrete Mixtures Under Severe Marine Environment. In *Advances in Cement and Concrete Proceedings of the Copper Mountain, CO Conference*. D. A. Lange, K. I. Scrivener and J. Marchand, Eds. Urbana, IL: University of Illinois at Urbana-Champaign. 329–338.
- McDonald, D. B., Sherman, M. R., Pfeifer D. W., and Virmani, Y. P. 1995. Stainless Steel Reinforcing as Corrosion Protection. *Concrete International*. May. 65–70.
- Mehta, P. K. 1997. Effect of Cement Composition on Corrosion of Reinforcing Steel in Concrete. Chloride Corrosion of Steel in Concrete. *ASTM STP 629*. D. E. Toni and S. W. Dean, Jr., Eds. West Conshohocken, PA: American Society for Testing and Materials. 12–19.
- Mindess, S., Young, F. and Darwin, D. 2002. *Concrete*. Englewood Cliffs, New Jersey: Prentice-Hall, Inc.
- Morgan, D. R., Heere, R., McAskill, N., and Chan, C. 1999. Comparative Evaluation of System Ductility of Mesh and Fiber Reinforced Shotcretes. In *Proceedings of the 8th International Conference on Shotcrete for Underground Support VIII*. Sao Paulo, Brazil. April, 1999. 216–239.
- Norwegian Code N5 3474.
- Page, C. L., Short, N. R. and El Tarras, A. 1981. Diffusion of Chloride Ions in Hardened Cement Pastes. *Cement and Concrete Research*. Vol. 11. 395–406.
- Page, C. L., Short, N. R. and Holden, W. R. 1986. The Influence of Different Cements on Chloride-Induced Corrosion of Reinforcing Steel. *Cement and Concrete Research*. Vol. 16. 79–86.
- Pereira, C. J. and Hegedus, L. L. 1981. Diffusion and Reaction of Chloride Ions in Porous Concrete. In *Proceedings of the 8th International Symposium on Chemical Reaction Engineering*, Edinburgh, Scotland. September 10–13, 1981.
- Pfeifer, D. W. and Landgren, J. R. 1987. *Protective Systems for New Prestressed and Substructure Concrete*. Report No. FHWA/RP-86/193. Washington, D.C: Federal Highway Administration. April. 113.
- Pfeifer, D. W., and Scali, M. J. 1981. *Concrete Sealers for Protection of Bridge Structures*. NCHRP Report 244, Washington, DC: Transportation Research Board, National Research Council.
- Rasheduzzafar, M., Al-Sandoun, S. S., Al Gahtani, A. S. and Dakhil, F. H. 1990. Effects of Tricalcium Aluminate Content of Cement on Corrosion of Reinforcing Steel in Concrete. *Cement and Concrete Research*. Vol. 20. 723.
- Rechberger, P. 1983. *Zement-Kalk-Gips*. Vol. 36. 582.
- Robinson, H. L. 1987. “An Evaluation of Silane Treated Concrete.” *Journal of Oil Color Chemists Assoc*. Vol. 70.163–72.
- Short, N. R. and Page, C. L. 1982. The Diffusion of Chloride Ions Through Portland and Blended Cement Pastes. *Silicates Industriels*. Vol. 10. 237–240.
- Sorensen, P., Jensen, B., and Maahn, E. 1990. The Corrosion Properties of Stainless Steel Reinforcement. In *Corrosion of Reinforcement in Concrete*. C. L. Page, K. W. J. Treadaway, and P. B. Bamforth, Eds. London: Elsevier Applied Science. 601–610.
- Suryavanshi, A. K., Scantlebury, J. D. and Lyon, S. B. 1995. The Binding of Chloride Ions by Sulphate Resistant Portland Cement. *Cement and Concrete Research*. Vol. 25. 581–592.
- Thomas, M. D. A. and Mathews, J. D. 1996. Chloride Penetration and Reinforcement Corrosion in Fly Ash Concrete Exposed to a Marine Environment. In *Proceedings of the 3rd CANMET/ACI International Conference on Concrete in Marine Environments*. ACI SP-163-15. Canada. 317–338.

- Durability of Concrete*. Transportation Research Circular No. 494. December 1999. Washington D.C: Transportation Research Board, National Research Council.
- TRB. 1993. Epoxy-Coated Reinforcement in Highway Structures. *Transportation Research Circular No. 403*. Washington, DC: Transportation Research Board
- Treadaway, K. W. J., Brown, B.L., and Cox, R. N. 1980. Durability of Galvanized Steel in Concrete. *ASTM STP 713*. Philadelphia: American Society for Testing and Materials. 102–131.
- Tuutti, K., 1982. *Corrosion of Steel in Concrete*. Stockholm: Swedish Cement and Concrete Research Institute. 469.
- Weyers, R. E., Al-Qadi, I. L., Prowell, B. D., Dutta, T., Gou, H., and Berke, N. 1992. *Corrosion Protection Systems*. Report to the Strategic Highway Research Program, SHRP Contract C103. Washington, D.C.: National Research Council.
- Yeomans, S. R. 1987. Galvanized Steel Reinforcement in Concrete. In *Proceedings of the 1st National Structural Engineering Conference*, Australia: Barton, ACT Institution of Engineers. 662–667.
- Yeomans, S. R. 1993. *Aspects of the Characteristics and Use of Coated Steel Reinforcement in Concrete*. Paper 329 in *Corrosion '93*. New Orleans: NACE. March, 1993.

CHAPTER 9

BIOFOULING AND PREVENTION: CORROSION, BIODETERIORATION AND BIODEGRADATION OF MATERIALS

Ji-Dong Gu

*Laboratory of Environmental Toxicology, Department of Ecology & Biodiversity, The University of Hong Kong, China;
and The Swire Institute of Marine Science, The University of Hong Kong, China*

| | | | |
|--|-----|---|-----|
| 9.1 INTRODUCTION | 179 | 9.6 BIODETERIORATION OF POLYMERIC MATERIALS | 192 |
| 9.2 BACTERIAL ADHESION ON SURFACES | 180 | 9.7 SUMMARY | 195 |
| 9.3 MEDIATORS OF INVERTEBRATE SETTLEMENT | 181 | 9.8 ACKNOWLEDGEMENTS | 196 |
| 9.4 AN EXAMPLE WITH ZEBRA MUSSELS | 184 | 9.9 REFERENCES | 196 |
| 9.5 CORROSION OF METALS | 185 | | |

9.1 INTRODUCTION

Biofouling is an interesting natural phenomenon that often appears in the forms of microfouling and macrofouling visible on surfaces. Microfouling refers to microorganisms; whereas, macrofouling refers to larger organisms (e.g., invertebrates). At the same time, microfouling may also influence the initiation of macrofouling in several ways—positively, negatively, or neutrally. It is known that both natural and artificial surfaces are susceptible to the colonization of microorganisms forming a thin layer of microbial biofilms consisting of large quantities of microbial metabolites with some bacterial cells embedded inside. Seashore rocks often have a slippery feeling because of microbial biofilms and the presence of ample amounts of metabolites.

Biofilms of microorganisms are ubiquitous in marine waters of polar (Ford et al., 1989; Maki et al., 1990a), temperate (Berk et al., 1981), tropical ecosystems (Hofmann et al., 1978); they develop similarly in freshwater environments (Lock, 1993). Bacterial adhesion on surfaces is a result of complex communication between bacteria in the environment and the physical, chemical, and biological characteristics of the substratum surfaces, as well as the microbial cells. Multiplication and production of copolymeric materials by the already attached microorganisms can develop into a thin layer coating on surfaces, affecting the subsequent biological

processes taking place on the surface (van Loosdrecht et al., 1990).

Biofilms are interesting research areas for a number of reasons. They play an important role in corrosion of metals and the degradation of a wide range of inorganic and polymeric materials. They also mediate settlement and metamorphosis of invertebrate larvae (Kirchman and Mitchell, 1981 and 1983; Kirchman et al., 1982a–b; Maki and Mitchell, 1985 and 1986; Maki et al., 1988, 1989, 1990a, 1992, and 1994; Mitchell, 1984; Mitchell and Kirchman, 1984; Mitchell and Maki, 1988; Rodriguez et al., 1995). The role of bacterial biofilms can be either repulsion against settlement of invertebrate larvae (Maki et al., 1989, 1990a, and 1992) or induction for settlement (Lau and Qian, 2001; Lau et al., 2001). Since biofouling is commonly thought of as the attachment of visible animals (mostly invertebrates) on surfaces of natural and artificial materials, the role of biofilm mediating larval attachment on surfaces may provide important information on the mechanisms of biofouling and development of new biotechnologies utilizing microbial biofilms against macrofouling processes. Furthermore, corrosion of underwater structures, such as industrial heat exchangers, cooling towers, and water ducts and pipelines may be protected from biofouling using new innovative methods involving bacteria and their metabolites. Because the economic losses associated with biofouling are enormous, environmentally acceptable

means have been rigorously investigated to prevent both biofilm formation and/or biofouling.

9.2 BACTERIAL ADHESION ON SURFACES

9.2.1 Formation of Biofilms

Bacteria are very small; microscopes are usually needed to observe them. Their metabolic characteristics and genetic structures (nucleotide sequences) are the primary information used for their classification (Madigan et al., 2000). What is amazing about these small creatures is that they multiply very quickly ($m2^n$; where m is the starting population number and n is the numbers of generation) under a wide range of environmental conditions.

Certain microorganisms have specialized their adaptation to a narrow range of environmental conditions. It is a fact that they have been serving a vital role to *Homo sapiens* by digesting our food and also to our society as a whole by providing a variety of products from beverages, wines, cheese, etc., to waste water treatment and bioremediation. Of course, some of them are also known pathogens.

Ever since their initial appearance on this planet, microorganisms have tended to attach and aggregate on surfaces of minerals, and this attachment property has improved their success in the natural environment (Wächtershäuser, 1988). Because of their survival strategy, they evolved over time into distinctly different species, and provided an important basis for the evolution of large organisms. In addition, adhered bacteria also show increased metabolic activity in comparison with non-attached ones (van Loosdrecht et al., 1990), gaining further advantage to over number the planktonic cells.

The initial steps of microbial adhesion on surfaces of materials has been an interesting research topic for several generations of microbiologists. Marshall et al., reported both reversible and irreversible attachments of the bacteria using a marine *Pseudomonas* sp. on glass slides (Marshall, 1985; Marshall et al., 1971). Adhesion of bacteria to a surface can be completed in as little as several seconds to a few minutes (Wiencek and Fletcher, 1995). Material surfaces with different physical and chemical properties result in drastically different results of bacterial attachment (Fletcher and Leob, 1979). For example, it might be hard for most bacteria to attach firmly to Teflon, but modifying a Teflon surface with a little oil or grease will allow bacteria to attach on

the surface more readily. Polyethylene film in coastal marine water can be colonized by a diverse population of bacteria after short exposure to a subtropical environment (Figure 9.1). In contrast, they may attach very well on primary and secondary minerals of the environment. After adhesion on surfaces, bacteria not only reproduce by generating a three-dimensional structure of biofilms consisting of gelatinous materials with bacteria embedded in them but also affect the substratum surfaces, resulting in corrosion, deterioration of materials, or even infection when animal tissues become the colonized surfaces.

Although most early research focused on biofilm formation in marine ecosystems, recent developments allow medical and environmental microbiologists to more comprehensively understand lung infection in cystic fibrosis patients (Davies et al., 1998; Singh et al., 2000), and antibiotic resistance (Levy, 1992; Marshall et al., 1990). Bacteria form diverse microbial communities in both freshwater and marine environments; these microorganisms are an important driving force for carbon cycling in the natural ecosystems (Ford and Lock, 1987). However, the role of microorganisms in larval settlement or repulsion of invertebrates as a whole has not been clearly elucidated.

9.2.2 Chemotaxis of Bacteria

The existence of biofilms on submerged surfaces has gained wide understanding (Costerton et al., 1978; 1994), and knowledge of biofilm formation on a whole range of material surfaces has been advanced in recent years (Gu, 2003a; Gu et al., 2000a–d). The initial attachment of bacterial cells on any surface and the mechanisms governing those processes are still not clearly understood, however; and this lack of fundamental comprehension of adhesion processes prevents us from developing effective preventive strategies in control of bacterial biofilms. Biomolecules have been implicated in the processes (Gu et al., 2001b). Unfortunately, large quantities of biocides and antibiotics are used in industrial and medical areas; therefore, selective microorganisms may develop mechanisms resisting toxic chemicals.

Selective chemicals are capable of repelling marine bacteria under experimental conditions, as illustrated by Chet and Mitchell (1976a; 1976b). Strong repulsion was observed with α -amino-*n*-butyric acid, *N*, *N*-dimethylphenylene diamine, hydroquinone, and acrylamide, and, to a lesser extent,

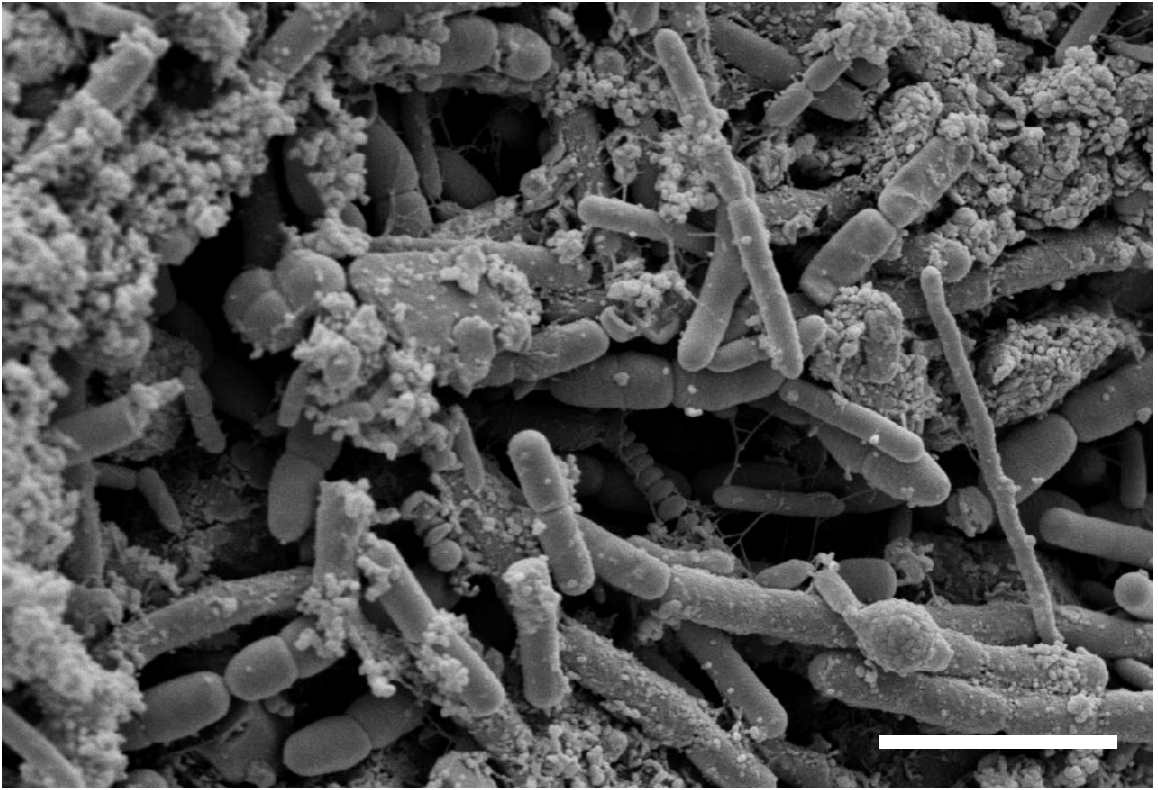


FIGURE 9.1 A scanning electron micrograph showing a natural bacterial biofilm on surface of a polyethylene film after 30 days of exposure to marine water in Victoria Harbor (Hong Kong). The sample was treated by fixing in glutaraldehyde and critical point dried and coated with palladium-gold before viewing (scale bar, 2 μ m).

with *n*-amyl acetate, benzene, benzoic acid, 2, 4-dichlorophenoxy acetic acid, indole, 3-methylindole (skatole), tannic acid, *N, N, N', N'*-tetramethylethylene diamine, thioacetic acid, phenylthiourea, and thiosalicylic acid (Chet and Mitchell, 1976a–b; Chet et al., 1975). The threshold concentration showing effective repulsion of bacteria from surfaces was between 0.1–1.0 mM (Chet et al., 1975). It is interesting that when tannin and tannic acid were tested for antifouling activity (Lau and Qian, 2000), the difficulty was in retaining these potentially effective chemicals in a formulated coating for slow release over an extended period of time.

Active movement of bacteria away from a particular chemical substance is called negative chemotaxis. Any chemical agent causing this phenomenon can prevent adhesion and then the early-stage growth of the targeted microorganisms. Toxic chemicals such as chloroform, toluene, ethanol benzene, CuSO_4 , and $\text{Pb}(\text{NO}_3)_2$ have been found to induce negative chemotaxis in marine microorganisms

(Young and Mitchell, 1973a–b). Obviously, selective chemicals can also serve as cues to attract certain bacteria; nutrients like acetate and glucose are effective attractants.

9.3 MEDIATORS OF INVERTEBRATE SETTLEMENT

9.3.1 Lectins as Chemical Cues

Lectins are biomolecules consisting of glycoproteins with multiple binding sites specific for carbohydrate sugars. They are widely found in a large number of organisms ranging from prokaryotes to mammals (McLean and Brown, 1974; Meints and Pardy, 1980; Mirelman and Ofek, 1986; Müller et al., 1979 and 1981). Because lectins are not ionized, binding mechanisms include only hydrophobic interactions and hydrogen bonds. The size of oligomeric proteins of a lectin ranges between

11,000 Dalton (kDa) and 335 kDa molecular weights, and the carbohydrate contents in lectins may vary from as little as almost zero in Concanavalin A (Con-A) to more than 50% in potato lectin. At present, more than 100 lectins have been purified and characterized (Mirelman and Ofek, 1986), and they are available for research use (Neu et al., 2001; Böckelmann et al., 2002).

The role of lectins and bacterial biofilms in the initial stage of larval settlement was investigated in 1980s at the Microbial Ecology Laboratory of Harvard University (Kirchman and Mitchell, 1981 and 1983; Kirchman et al., 1982a–b; Maki and Mitchell, 1985; Mitchell, 1984; Mitchell and Kirchman, 1984; Mitchell and Maki, 1988). The importance of microbial lectins in induction of invertebrate settlement has been recognized for many years. Guyot discovered microbial lectins in 1908 and Zobell reported their role in larval settlement in 1935 (reviewed by Kirchman and Mitchell, 1983). At the same time, other theories based on physical properties of substratum materials, such as texture, surface tension, or wettability (Maki et al., 1989 and 1994), were also tested but were found unsatisfactory to fully explain the relationship between the settlement by invertebrates and the preference for a certain material types. However, the lectin model was proposed to explain the settlement of larvae on bacterial biofilms, the modified surfaces. It was thought that invertebrate larvae bind to a specific carbohydrate molecule of the microbial biofilm to induce settlement of larvae. The exopolysaccharides of bacteria are also known to contain variable amounts of proteins, as well as sugar residues (Gu and Mitchell, 2001 and 2002). It should be pointed out here that while biofilm bacteria may also produce chemicals that inhibit settlement of invertebrates (Maki et al., 1989 and 1990b), most past research primarily focused on the chemical agents of bacterial biofilm origin that prevent the settlement of larvae (Maki and Mitchell, 1985).

The validity of the lectin model has been tested using several different simulation systems (Kirchman and Mitchell, 1981, 1982a–b, 1983, and 1984; Mitchell and Kirchman, 1984). An initial experiment utilized a natural sugar to block the interaction between invertebrate larvae and surface biofilms (Kirchman and Mitchell, 1983). It showed that glucose is an effective blocking agent for the initial settlement of the polychaete, *Janua (D.) brasiliensis* larvae; whereas, mannose, galactose, fucose, α -methyl-D-glucoside, ribose, α -methyl-D-mannose, and *N*-acetyl-D-glucosamine are ineffective. During

the assay, toxicity of glucose to larvae was not observed. Subsequent experiments found that formalin-killed biofilms are also capable of inducing settlement, indicating that settlement cues are probably chemical in nature, possibly resulting from the polysaccharides produced by the bacteria in the biofilm (Kirchman and Mitchell, 1981 and 1983).

Further experiments established that the alteration of chemical bonds in carbohydrate structure prohibited the settlement of larvae when periodate was used to cleave the 1,2-dihydroxyl units of carbohydrates in a biofilm specifically. As a result, settlement of *Janua* larvae was prevented. In addition, larvae do not settle on surfaces previously treated with the lectin Concanavalin A (Con-A), but will settle on lectins purified from peanuts (AHA). These results collectively suggest that the binding site is chemical-specific, because Con-A forms a glucoside bond with glucose and mannose, while AHA binds only galactose. These results show that the fundamental mechanisms of larval settlement may be understood on the basis of chemistry. Unfortunately, no major significant advance has been made in recent years. With the application of molecular techniques in various fields, it is hoped that further in-depth understanding may be realized soon.

9.3.2 Bacterial Films as Cues or Repellents

9.3.2.1 Biofilms as Settlement Cues

Microbial biofilms have generally been examined as a stimulus for the settlement of macrofouling organisms (Crisp, 1974). Examples from the earlier literature include studies comparing the settlement of *Ophelia bicornia* and *Protodrilus* sp. larvae on sands pre-colonized by microorganisms versus sterile (clean) sand. In those investigations, no settlement was observed on the clean sands in the pre-sterilized treatments. *Vibrio* species of bacteria were found to be effective in inducing settlement and metamorphosis of the coelenterates *Cassiopea andromeda* and *Hydractina echinata* (Hofmann et al., 1978; Neumann, 1979). The spirorbid worm, *Janua (D.) brasiliensis*, is often found on a wide range of surfaces, including other invertebrates *Mytilus edulis* (Shisko, 1975) and algae *Ulva lobata* (Shisko, 1975) and *Zostera marina* (Nelson, 1979). It should be pointed out that research on bacterial biofilms and their effects on settlement of larval invertebrates has been performed mostly by zoologists. Only fairly recently have researchers from other fields begun

to focus on the molecular understanding of the interactions between different species of bacteria and larvae.

Maki et al. (1990a) used the bacteria species *Deleya marina* and *Vibrio vulnificus* to test the settlement of cypris larvae *Balanus amphitrite* on three types of substratum surfaces including glass, polystyrene and Falcon® tissue-culture polystyrene. Results suggested that the relationship between the substratum, the biofilm, and the larvae is much more complex than previously reported in the lectin model. They found both stimulatory and inhibitory effects when different bacterial strains were used. Thus, species composition within the biofilm may play a critical role in settlement selection. This complex system in nature makes laboratory investigation more difficult and less realistic. In a recent investigation, 38 bacterial isolates belonging to three phylogenetic branches (i.e., γ -Proteobacteria, Gram positive, and *Cytophaga-Flexibacter-Bacteroides*) were tested, and approximately 42% of them were non-inductive to the settlement of marine polychaete *Hydroides elegans* (Lau et al., 2002). Interestingly, isolates inducing the highest settlement were affiliated with the *Cytophaga* group. In addition, bacterial isolates from the same genus may have significant different effects in induction of larval settlement. Adhesion of bacteria may be linked to changes of surface molecules and cause different domains of the copolymer to be exposed so that either inhibition or stimulation of larval settlement can be produced.

9.3.2.2 Biofilms As Settlement Inhibitors

Bacteria from cultures or concentrated suspensions can readily colonize surfaces of a wide range of materials within about eight hours to form a biofilm with density between 10^7 and 10^8 cells/cm². *Deleya marina* was used to compare settlement induction and inhibition with other bacterial species in a study. The results showed that biofilms of this species inhibit settlement of *Balanus amphitrite* (Maki et al., 1988 and 1992). In another study (Maki et al., 1988), three strains of *D. marina* were tested and showed inhibitory effects on the settlement of bryozoan *Bugula neritina*. Two unrelated species, *Vibrio vulnificus* and an estuarine isolate DLS1, did not show any inhibition on settlement. However, the age of bacterial biofilms has important impact on the induction or inhibition of settlement. Older (>12 days) natural biofilms induce settlement of *B. amphitrite* while younger ones have inhibitory effects (Wieczorek et al., 1995).

Other studies have examined the role of chemoreceptors in invertebrates. In the larvae of *Balanus amphitrite*, chemoreceptors were suspected of playing a major role in inhibition of larval settlement (Maki et al., 1994). In a study on the settlement induction of abalone, a neurotransmitter, γ -aminobutyric acid, was found to be involved and responsible for inhibiting the velar cilia movement of the planktonic larvae (Morse et al., 1979). Later studies, however, discarded this theory on the basis that concentration levels of this neurotransmitter molecule were not detectable, and that microbial degradation of γ -aminobutyric acid was likely to prevent significant accumulation (Kaspar and Mountfort, 1995). The low concentration of these neurotransmitting chemicals in the environment and their effect on larval settlement induction are important issues challenging research in this area because results showed that a wide range of environmental contaminants can serve as endocrine-disrupting chemicals responsible for the abnormality of animal development (Gray et al., 1999; Jobling et al., 1995). Accepting the fact, real ecosystem may harbour a vast variety of bioactive chemicals at concentration relatively low to our knowledge.

A number of factors may be involved in the inhibition of invertebrate settlement on surfaces. They include the species composition of the biofilm; inhibition of lectins action within the bacterial biofilms or surface of invertebrate; negative response via chemoreceptors in the larvae; and the possible existence of yet unrevealed neurotransmitters and mechanisms. The most promising research area involves the understanding of species composition of biofilms and the resultant larval settlement, because monoculture of bacteria and biofilm are almost impossible to find in natural environments. With better understanding, manipulation of biofilms and participating species might allow industry to deter macrofouling invertebrates from settling on surfaces. Other promising applications include the incorporation of environmentally acceptable chemicals into coatings to inhibit both bacteria and invertebrates (Rittschof et al., 2003).

9.3.2.3 Chemical Repellents

Chemicals initially found to inhibit the development of bacterial biofilms on surfaces are now being tested on other invertebrates, (e.g., zebra mussels [*Dreissena polymorpha*]). This freshwater fouling animal has caused enormous economic loss, particularly in North America, since the mid-1980s (Ross,

1994). Five chemicals tested are diphenylamine, benzoate, acrylamide, 3-methylindole (skatole), and *N,N,N',N'*-tetramethyl-*p*-phenylenediamine dihydrochloride. Diphenylamine seems to be the most effective repellent for *D. polymorpha* among those examined (Gu et al., 1997c). However, these chemicals are highly toxic and use of them poses environmental concerns regarding their fate and effect on natural ecosystems.

When bacteria were studied for their effect on inhibition of settlement of the barnacle *Balanus amphitrite* Darwin, biofilms of the 12 bacterial isolates were either inhibitory (3–41%) or did not have any effect on the cyprid settlement (Lau and Qian, 2000). In addition, the settlement of larvae on natural mixed populations of microorganisms was very similar to the biofilms prepared from pure isolated species of bacteria. It is apparent that non-toxic, natural antifoulants are ideal solutions to this long-evolved natural phenomenon. Feasible strategies might include the application of crude microbial products showing inhibitory properties and/or immobilized bacteria to the surface coating layer. In addition, biodegradable polymers have also been proposed to be used as coatings. Layers of such polymers could peel off many times over the service time period in the aquatic environment.

9.4 AN EXAMPLE WITH ZEBRA MUSSELS

Invertebrates of marine and freshwater are problematic organisms in a range of industries, including utilities, water distribution systems, and cooling systems. The zebra mussel, *Dreissena polymorpha*, a newly introduced species in North America, had an estimated cost of over \$5 billion in the year 2000 in the Great Lakes alone (Ross, 1994). Due to the slightly higher temperature in North America, compared to their native Caspian Sea, the animals grow rapidly and have spread extensively from the Great Lakes outward. Because of this, coupled with the fact that no natural predator has been encountered, zebra mussels have had such a significant impact on the environment that water of the Great Lakes became clearer by the filter feeding of these animals. However, damage by these mussels is mostly a direct result of fouling on surfaces, especially engineering surfaces. Industries suffer significant down time from these mussels fouling on surfaces. No effective measure is currently available to prevent the fouling by this organism, and the rapid spread of this organism all over the waterways (particularly in the

United States) has resulted in not only the potential of further fouling problems but also ecological damage (Carlton and Geller, 1993; Hebert et al., 1989; Mackie et al., 1989).

In the reproductive process, veligers of fouling invertebrates look for surfaces (“home”) within a small window of time. The settled surfaces are most likely the permanent places for their life spans. If suitable surfaces cannot be found within the short period of time, the veligers will die. Through evolution, invertebrates have adapted to this mode of survival over millions of years. When invertebrate larvae search for surfaces to settle on, specific chemicals in microbial biofilms might serve as chemical cues that attract the planktonic larvae to attach on a surface through chemical-chemical interaction, as previously illustrated in the lectin model. Research in this area, however, has been generally limited to the marine invertebrates, such as the barnacle *Balanus amphitrite* (Kon-ya, et al., 1995), the bryozoan *Bugula neritina* (Kirchman and Mitchell, 1984; Maki et al., 1989), the polychaete *Janua (Dexiospira) brasiliensis* (Kirchman and Mitchell, 1981; Kirchman et al., 1982a–b; Kirchman and Mitchell 1983 and 1984; Maki and Mitchell, 1985 and 1986; Maki et al., 1988, 1990a, 1992, and 1994; Kaspar and Mountfort, 1995; Morse et al., 1979), soft coral *Dendronephthya* sp. (Harder and Qian, 1999 and 2000), and the sponge (Müller et al., 1979 and 1981). Unfortunately, little research has focused on similar issues in freshwater ecosystems. The onslaught of the zebra mussel into North American lakes and waterways has drawn attention to the need for basic knowledge about the settlement mechanisms so that proper strategies can be formulated.

9.4.1 Microbial Community of the Mussels

Initial efforts to study zebra mussels were limited by the availability of larval stage specimens. Culturing techniques have largely been unsuccessful in obtaining viable larvae in large quantities on a routine basis in laboratory. However, juvenile zebra mussels from natural environments can be used for investigation, and animals collected from the field can be maintained in aquaria housed in temperature-controlled rooms at 10 °C for at least a year. The juvenile animals, after detaching from surfaces, are capable of forming new byssal threads within 24 hours.

The microbial community associated with *D. polymorpha* might provide insight to the potential pathogenicity of selective microorganisms against

the mussels. Using cultivation techniques, a large number of microorganisms were successfully isolated from live, moribund and dying mussel tissues to form a collection of bacterial culture. Selected bacterial isolates were found to be lethal to the mussels (Gu and Mitchell, 1995). Interestingly, mortality of juvenile mussels reached close to 100% in five days after exposure to selected bacterial species. In addition, bacteria were also isolated from natural surfaces where zebra mussels did not show any colonization. Further experiments comparing the resettlement of zebra mussels on biofilm-modified and clean surfaces, showed that biofilm-modified surfaces of the selected bacteria inhibit the resettlement by the mussels (Gu et al., 1995a). Between 95 and 100% of the zebra mussels reattached to cleaned surfaces of polystyrene Petri dishes, while less than 50% reattached to biofilm-modified surfaces, suggesting bacterial involvement in the inhibition of reattachment.

Zebra mussels selectively colonize surfaces in both natural habitats and sterile aquaria (initially) in the laboratory. Swabs of aquarium surfaces were cultured for isolation of pure bacterial strains to study their repulsion of zebra mussels. More than 60% of the isolated bacteria belong to environmental common pseudomonads, including *Pseudomonas corrugata*, *P. mucidolens*, *P. fluorescens* E, and *P. fluorescens* F, *P. cichorii*, and *P. vesicularis*. Four bacteria were chosen to substantiate the hypothesis that bacterial biofilms of selected species might repel zebra mussels. Early stationary phase cells of *Deleya aestiva*, *D. aquamarina*, *D. marina*, and *Acinetobacter lowfii* were harvested and used to form a thin layer of biofilm on surfaces of tissue-culture polystyrene Petri dishes. The bacterial biofilms had a cell density between 10^5 – 10^6 cells/cm². After placing randomly selected juvenile mussels on the biofilmed surfaces, only 20–40% reattachment was recorded, compared to 100% on clean surfaces as controls. It is likely that biochemicals produced by microorganisms in the biofilms act as repellents for the mussels, as speculated earlier by Maki et al. (1988, 1989, 1994). Further investigation of microbial metabolites indicated that exopolymers of bacteria are responsible for the killing, and the lethal metabolites may have a molecular weight of greater than 10 kDa (Gu and Mitchell, 1995, 2001, and 2002; Gu et al., 2001a).

Significant progress has been made in the developmental biology, physiology, ecology, and biological control of zebra mussels (Haag and Garton, 1992; Ram and Walker, 1993; Ramcharan et al., 1992; Schneider, 1992; Wu and Culver, 1991). How-

ever, laboratory rearing of zebra mussel larvae remains a challenge to many researchers. Until the larvae can be readily obtained for experiments, fundamental research on the interactions between invertebrate and microorganisms, and settlement behavior of the mussel larvae, can hardly be conducted. Furthermore, effective strategies (including antifouling chemicals and biochemicals [metabolites] and repelling microorganisms) based on research using larvae will facilitate our understanding of antifouling mechanisms. Environmentally acceptable antifouling chemicals may be found through further investigating the interactions between larvae and surfaces.

9.5 CORROSION OF METALS

Corrosion of metals is driven by either or both electrochemical and microbiological processes in the environment. When microorganisms are involved, the corrosion process is called microbiological-induced or -influenced corrosion (MIC). Significant economic loss has resulted from undesirable processes caused by the growth of microorganisms and subsequent accumulation of fouling organisms (Jensen, 1992; Ross, 1994). Corrosion results in severe economic consequences and 70% of the corrosion in gas transmission lines are due to problems caused by microorganisms (Pope et al., 1989). The American oil refining industry loses \$1.4 billion annually from microbial corrosion (Knudsen, 1981). A report illustrated the corrosion problems associated with various industrial sectors in the United States, where the direct corrosion costs were 3.1% of the U.S. gross domestic product, based on 1988 data (Koch et al., 2002). This process affects a wide range of industrial materials, including those used in oil fields, offshore drilling platforms, pipelines, pulp and paper factories, armaments, nuclear and fossil fuel power plants, chemical manufacturing facilities, and food processing plants (Corbett et al., 1987; Evans, 1948; Gu et al., 2000a; Hill et al., 1987; Kobrin, 1993; Pope et al., 1989; Sequeira and Tiller, 1988; Widdel, 1992; Zachary et al., 1980). The terminology of microbiological corrosion and the term “microfouling” have frequently been used interchangeably. The term “MIC” is not clearly defined and is commonly misused.

Biocorrosion of metals was first reported by von Wolzogen Kuhr and van der Vlugt in 1934. Current knowledge indicates that many microorganisms are capable of corroding metal alloys; the responsible

microorganisms include both aerobic and anaerobic bacteria. In the early investigations on corrosion, attention was primarily given to the strictly anaerobic sulfate-reducing bacteria (SRBs). See reviews by Dexter, 1993; Dowling and Guezennec, 1997; Dowling et al., 1992; Eashwar et al., 1995; Evans, 1948; Ford and Mitchell, 1990a–b; Gu et al., 2000a; Hamilton, 1985; and Lee et al., 1995. In addition to SRBs, thermophilic bacteria, iron-oxidizing bacteria, exopolymer- and acid-producing bacteria have also been shown to participate actively in corrosion processes. New mechanisms have been identified in which metal ions are either transformed by or complexed with functional groups of the exopolymers, resulting in release of metallic species into solution and form precipitation (Chen et al., 1995; Chen et al., 1996; Clayton et al., 1994; Ford and Mitchell, 1990b; Little et al., 1986b; Paradies, 1995; Schmidt, 1986; Siedlarek et al., 1994).

After exposure of surfaces to ambient environments, surface-attached microorganisms are capable of altering chemical and biological environments on the substratum by forming differential aeration zones under aerobic conditions, because dissolved oxygen is consumed beneath microbial colonies (Uhlig and Revie, 1985). The difference in oxygen concentrations between the two adjacent areas generates an electrochemical potential and electron flow. The area with the higher oxygen concentration serves as a cathode; whereas, the area with the lower oxygen concentration serves as an anode, resulting in dissolution of metallic matrices, crevice corrosion, and pitting (Ford and Mitchell, 1990b; Gu et al., 2000a; Vaidya et al., 1997; Videla, 1996; Walch et al., 1989; Wang, 1996). Subsequently, a decrease in oxygen levels provides an opportunity for anaerobic microorganisms to be established within a biofilm structure. Activity of sulfate-reducing bacteria corrode the underlying metals by a process of cathodic depolarization. In addition, methanogenic microorganisms may also participate in the corrosion (Daniels et al., 1987). Overall, the interactions between chemistry and biology create a unique niche for the propagation of corrosion.

9.5.1 Microorganisms Involved in Corrosion

9.5.1.1 Aerobic Microorganisms

Aerobic microorganisms, playing an important role in corrosion, include the sulfur bacteria, the iron(Fe)- and manganese(Mn)-depositing and exopolymer-producing bacteria, and fungi and algae. The “iron

bacteria” include *Gallionella*, *Leptothrix*, *Siderocapsa* and *Sphaerotilus* (Ehrlich, 1996). Two *Pedomicrobium*-like budding bacteria deposit Fe and Mn ions on the outside of cell walls (Ghiorse and Hirsch, 1978, 1979). Most of these bacteria have not been successfully cultured in laboratory (Hanert, 1981); elucidation of their involvement in corrosion is still limited by availability of proper culturing techniques. At neutral pH, Fe^{2+} is not stable in the presence of O_2 and is rapidly oxidized to the insoluble Fe^{3+} . In fully aerated fresh water at pH 7, the half-life of Fe^{2+} oxidation is less than 15 minutes (Ghiorse, 1989; Stumm and Morgan, 1996). Because of the rapidity of this reaction, the only neutral pH environments where Fe^{2+} is present are interfaces between anoxic and oxic conditions.

Improvement of microbiological techniques permit the isolation of new Fe^{2+} -oxidizing bacteria under micro-aerophilic conditions at neutral pH (Emerson and Moyer, 1997). Ferric oxides may be enzymatically deposited by *Gallionella ferruginea*, and non-enzymatically by *Acinetobacter*, *Archangium*, *Herpetosyphon*, *Leptothrix*, *Naumanniella*, *Ochrobium*, *Pedomicrobium*, *Seliberia*, *Siderocapsa*, *Siderococcus*, and *Toxothrix* (Ehrlich, 1996; Ghiorse and Hirsch, 1978). Fe-depositing bacteria include *Acholeplasma*, *Actinomyces*, *Arthrobacter*, *Caulococcus*, *Clonothrix*, *Crenothrix*, *Ferrobacillus*, *Gallionella*, *Hypomicrobium*, *Leptospirillum*, *Leptothrix*, *Lieskeela*, *Metallogenium*, *Naumanniella*, *Ochrobium*, *Pedomicrobium*, *Peloploca*, *Planctomyces*, *Seliberia*, *Siderococcus*, *Sphaerotilus*, *Sulfobolus*, *Thiobacillus*, *Thiopedia*, and *Toxothrix* (Ford and Mitchell, 1990b). However, it is still unclear as to the extent of microbial involvement in specific processes of corrosion involving iron oxidation.

Thiobacillus spp. are participants of active oxidative corrosion. They oxidize a range of sulfur compounds to sulfuric acid, and the acid released from the cells may attack alloys. Similarly, organic acid-producing bacteria and fungi may also carry out similar mechanisms. Acid-tolerant bacteria are capable of Fe^0 oxidation, with *Thiobacillus* sp. the most common. *Thiobacillus ferrooxidans* oxidizes Fe^{2+} to Fe^{3+} . However, the growth of the organisms is very slow (Ehrlich, 1996; Kuenen and Tuovinen, 1981). Sulfate (SO_4^{2-}) is required by the Fe-oxidizing system of *T. ferrooxidans*, and sulfur is probably required to stabilize the hexa-aquated complex of Fe^{2+} near the surface of the bacterium as a substrate for the Fe-oxidizing enzyme system. The electrons removed from Fe^{2+} are passed to periplasmic cy-

tochrome *c*. The reduced cytochrome *c* binds to the outer plasma membrane of the cell, allowing transport of electrons across the membrane to cytochrome oxidase located in the inner membrane.

Microorganisms accumulate Fe^{3+} on their outer surfaces by reacting with acidic polymeric materials. This mechanism has very important implications not only for corrosion of metals, but also for the accumulation of metals from natural habitats. For example, *Aquaspirillum magnetotacticum* is capable of taking up complexed Fe^{3+} and transforming it into magnetite (Fe_3O_4) by reduction and partial oxidation (Blakemore, 1982; Schüler and Frankel, 1999). The magnetite crystals are single-domain magnets aligned inside the bacteria. They play an important role in bacterial orientation to the two magnetic poles of the Earth in natural environments. However, magnetite can also be formed extracellularly by some non-magnetotactic bacteria (Lovley et al., 1987). However, the role of these bacteria in metal corrosion is still unknown.

Manganese deposition carried out by microorganisms also affects the corrosion behavior of alloys. Growth of *Leptothrix discophora* has resulted in ennoblement of stainless steel by elevating the open circuit potential to +375 mV (Dickinson et al., 1996 and 1997). Detailed examination of the deposits on surfaces of coupons using X-ray Photoelectron Spectroscopy (XPS) has confirmed that the product was MnO_2 . MnO_2 can also be reduced to Mn^{2+} by accepting two electrons generated by metal dissolution and the intermediate product is MnOOH (Olesen et al., 1998). Manganese-depositing bacteria include *Aeromonas*, *Bacillus*, *Caulobacter*, *Caulococcus*, *Citrobacter*, *Clonothrix*, *Cytophaga*, *Enterobacter*, *Flavobacterium*, *Hypomicrobium*, *Kuznetsovia*, *Lepothrix*, *Metallogenium*, *Micrococcus*, *Nocardia*, *Oceanspirillum*, *Pedomicrobium*, *Pseudomonas*, *Siderocapsa*, *Streptomyces*, and *Vibrio* spp.

9.5.1.2 Anaerobic Microorganisms

Sulfate-reducing bacteria are mostly responsible for corrosion under anaerobic conditions, as described earlier. Currently, 18 genera of dissimilatory sulfate-reducing bacteria have been recognized (Balow et al., 1992; Campaignolle and Crolet, 1997; Clapp, 1948; Enos and Taylor, 1996; Holland et al., 1986; Krieg and Holt, 1984). They are further divided into two physiological groups (Madigan et al., 2000; Odom, 1993; Odom and Singleton, 1993; Postgate, 1984). One group utilizes lactate, pyruvate, or

ethanol as carbon and energy sources and reduces sulfate to sulfide. Examples are *Desulfovibrio*, *Desulfomonas*, *Desulfotomaculum*, and *Desulfobulbus*. The other group oxidizes fatty acids, particularly acetate, and reduces sulfate to sulfide. This group includes *Desulfobacter*, *Desulfococcus*, *Desulfosarcina*, and *Desulfonema*. Some species of *Desulfovibrio* lack hydrogenase. For example, *D. desulfuricans* is hydrogenase-negative and *D. salexigens* is positive (Booth and Tiller, 1960). Booth et al. (1962 and 1968) observed that the rate of corrosion by these bacteria correlated with their hydrogenase activity. Hydrogenase-negative SRBs were completely inactive in corrosion. Apparently, hydrogenase-positive organisms utilize cathodic hydrogen, depolarizing the cathodic reaction that controls the kinetics.

In contrast to this theory, it has been suggested that ferrous sulfide (FeS) is the primary catalyst (Lee et al., 1995; Sanders and Hamilton, 1986; Weimer et al., 1988; Westlake, 1986; White et al., 1986). Other microorganisms should be noted for their role in anaerobic corrosion. They include methanogens (Daniels et al., 1987; Ferry, 1995), acetogens (Drake, 1994; Nozhevnikova et al., 1994), thermophilic bacteria (Ghassem and Adibi, 1995; Little et al., 1986a), and obligate proton reducers (Tomei et al., 1985). More work is needed to elucidate the role of their contributions to corrosion.

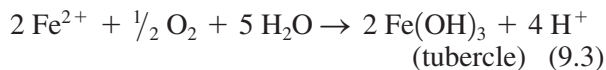
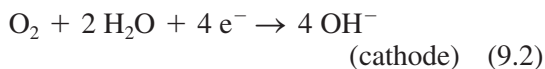
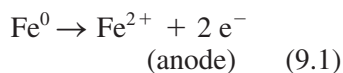
9.5.2 Mechanisms of Microbial Corrosion

9.5.2.1 Aerobic Conditions

Iron is the most abundant element in the Earth's crust, and has two oxidative states, ferrous (Fe^{2+}) and ferric (Fe^{3+}). When molecular oxygen (O_2) is available, serving as an electron acceptor for oxidation metallic iron (Fe), the area of the metal beneath the microbial colonies acts as an anode, whereas the area farther away from the colonies, where oxygen concentrations are relatively higher, serves as a cathodic site. Electrons flow from anode to cathode and corrosion is initiated, resulting in the dissolution of iron. Dissociated metal ions form ferrous hydroxides, ferric hydroxide and a series of Fe-containing minerals in the solution phase depending on the species of bacteria and the chemical conditions. Oxidation, reduction, and electron flow must all occur for corrosion to proceed. However, the electrochemical reactions never proceed at the theoretical rates because the rate of oxygen supply to cathodes and removal of products from the anodes limit the over-

all reaction (Dowling and Guezennec, 1997; Lee et al., 1993a–b; Little et al., 1990; Uhlig and Revie, 1985), even though the corrosion reaction is thermodynamically favorable. Atmospheric electrolytes affect the distance between the anode and cathode, being shorter at low-salt and longer at high-salt concentrations. Furthermore, impurities and contaminants of the metal matrices also stimulate corrosion by initiating the formation of differential cells and accelerated electrochemical reactions.

Corrosion products usually form a typical structure consisting of three layers called “tubercles” under aerobic conditions. The most aggressive form of corrosion is tuberculation caused by the formation of differential oxygen-concentration cells on material surfaces. The inner green layer is almost entirely ferrous hydroxide ($\text{Fe}(\text{OH})_2$), and the outer one consists of orange ferric hydroxide ($\text{Fe}(\text{OH})_3$). In between these two, magnetite (Fe_3O_4) forms a black layer (Lee et al., 1995). The overall reactions are summarized as follows:

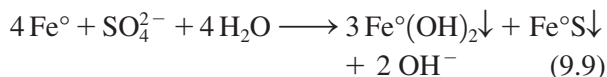
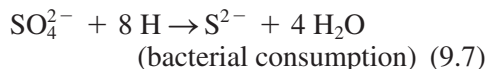
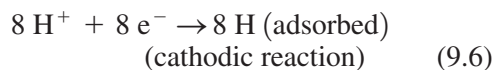
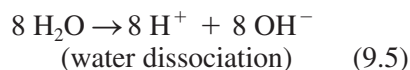
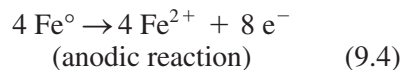


Initial oxidation of Fe^0 of mild steel at near neutral pH is driven by dissolved O_2 (Uhlig, 1971). Subsequent oxidation of Fe^{2+} to Fe^{3+} is an energy producing process carried out by a few bacterial species, including *Gallionella*, *Leptothrix*, and *Thiobacillus* spp. Since the amount of free energy extracted from this reaction is quite small for these microorganisms, approximately -31 kJ, large quantities of Fe^{2+} have to be oxidized to generate a sizable biomass indicating microbial growth. Because oxidation of Fe^{2+} is rapid under natural conditions, microorganisms in the environment must compete with chemical processes for Fe^{2+} . Because of this, biological oxidation of Fe may be underestimated under aerobic conditions (Ford and Mitchell, 1990a–b).

9.5.2.2 Anaerobic Conditions

Microorganisms tend to adhere to surfaces for survival and multiplication (Marshall, 1992). This provides opportunity for corrosion. Physical surfaces are

covered with microorganisms and their exopolymeric layers in all submerged environments, including freshwater and marine. Within this gelatinous matrix of a biofilm, there are oxic and anoxic zones, which permit aerobic and anaerobic processes to take place simultaneously within the biofilm layer. Since aerobic processes consume oxygen, which is toxic to the anaerobic microflora, anaerobes benefit from the decrease in oxygen tension. In the absence of oxygen, anaerobic bacteria (including methanogens, sulfate-reducing bacteria, acetogens, and fermentative bacteria) can actively participate in corrosion. Interactions between microbial species allows them to coexist under conditions where nutrients are limited. Sulfate-reducing bacteria (SRBs) are the single group of microorganisms widely recognized for their involvement in biological corrosion (Angell et al., 1995; Audouard et al., 1995; Gu et al., 2000a; Hadley, 1948; Iverson 1984; Little et al., 1994; Pope et al., 1989; Starkey, 1986; Walch and Mitchell, 1986; Widdel, 1988). Corrosion by SRBs results in pitting on metal surfaces. Since molecular oxygen is not available to accept electrons under anaerobic conditions, SO_4^{2-} or other compounds (CO_2 , H_2 and organic acids) are used as alternative electron acceptors for metabolic processes by anaerobic microorganisms. Each type of electron acceptor is unique in the pathway of microbial metabolism. A general summary of corrosion reactions may include the following:



Von Wolzogen Kuhr and van der Vlugt (1934) first suggested the above set of reactions by SRBs. After inoculation of a corrosion testing cell with SRBs, the electrochemical potential decreases from

the initial value of -470 mV to approximately -538 mV during bacterial growth phase (Figure 9.2). Further increase of potential may be observed that the process is a transition period before reaching the iron-sulfide potential, the maximum level. Apparently, several changes take place in the electrochemical potential of steel after inoculation with the SRBs. Before inoculation, the value is determined by the concentration of hydrogen ions in the medium. A film of hydrogen forms on surfaces of Fe^0 and steel, inducing polarization. Immediately after inoculation, SRBs begin growing and depolarization occurs, resulting in a drop in the anodic direction. The SRBs, by means of their hydrogenase system, remove the adsorbed hydrogen, depolarizing the system. The overall process has been described as depolarization, based on the theory that these bacteria remove hydrogen that accumulates on the surfaces of iron. The electron removal from hydrogen utilization results in cathodic depolarization and forces more iron to be dissolved at the anode.

Removal of hydrogen directly from the surface is equivalent to lowering the activation energy for hydrogen removal by providing a depolarization reaction. The enzyme hydrogenase, synthesized by many bacterial species of *Desulfovibrio* spp., is in-

involved in this specific depolarization process (Starkey, 1986). Under aerobic conditions, the presence of molecular oxygen serves as an electron sink; under anaerobic conditions, particularly in the presence of SRBs, SO_4^{2-} in the aqueous phase can be reduced to S^{2-} by the action of the microflora. The biogenically produced S^{2-} reacts with Fe^{2+} to form a precipitate of FeS . Controversy surrounding the mechanisms of corrosion includes more complex mechanisms involving both sulfide and phosphide (Iverson, 1981, 1984; Iverson and Olson, 1983; Iverson et al., 1986) and processes related to hydrogenase activity (Li and Lü, 1990; Starkey, 1986). The addition of chemically prepared Fe_2S and fumarate as electron acceptors also depolarizes the system. However, higher rates are always observed in the presence of SRBs.

As a result of the electrochemical reactions, the cathode always tends to be alkaline with an excess of OH^- . These hydroxyl groups also react with ferrous irons to form precipitates of hydroxy iron. Precipitated iron sulfites are frequently transformed into minerals, such as mackinawite, greigite, pyrrhotite, marcasite, and pyrite. Lee et al. (1993a; 1995) suggests that biogenic iron sulfides are identical to those produced by purely inorganic processes under the same conditions. Little et al. (1994) showed evi-

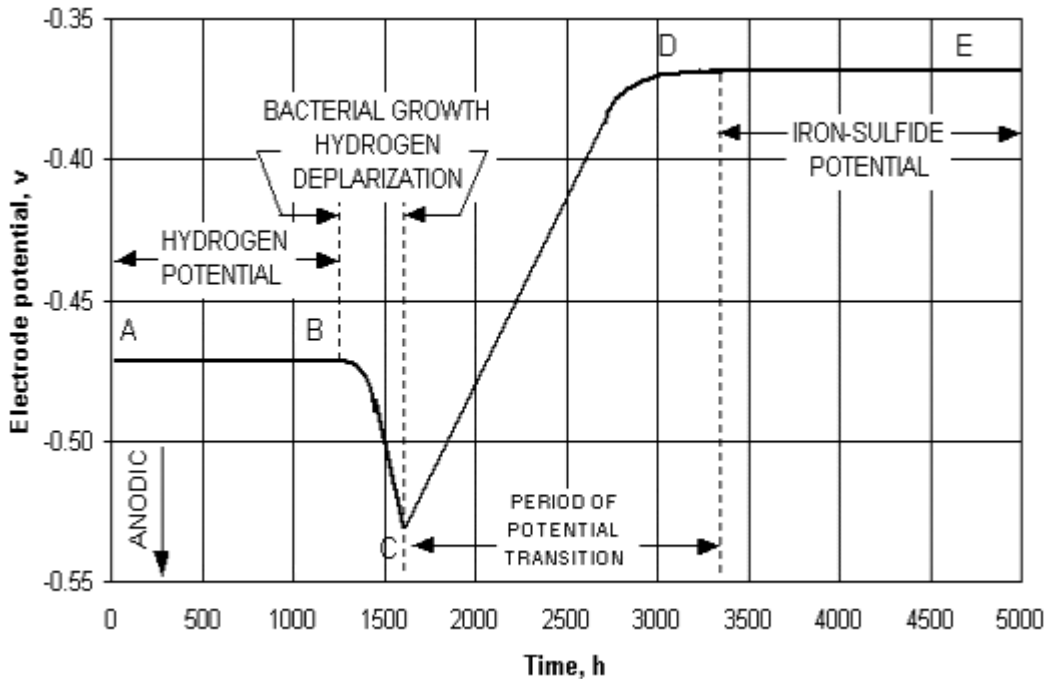


FIGURE 9.2 Cathodic depolarization potential after inoculation of a sulfate-reducing bacterium (redrawn from Hadley, 1948).

dence that biogenic minerals are microbiological signature markers.

9.5.2.3 Alternation Between Aerobic and Anaerobic Conditions

Constant oxic or anoxic conditions are rare in natural or industrial environments. It is more common that the two alternate, depending on oxygen gradient and diffusivity in a specific environment. Microbial corrosion under such conditions is quite complex, involving two different groups of microorganisms and an interface that serves as a transition boundary between the two conditions. Resultant corrosion rates are often higher than those observed under either oxic or anoxic conditions. Microbial activity reduces the oxygen level at interfaces, facilitating anaerobic metabolism. The corrosion products (such as FeS, FeS₂ and S⁰) resulting from anaerobic processes can be oxidized when free oxygen is available (Nielsen et al., 1993).

During oxidation of reduced sulfur compounds, more corrosive sulfides are produced under anoxic conditions, causing cathodic reactions. The corrosion rate increases as the reduced and oxidized FeS concentrations increase (Lee et al., 1993a–b). Cathodic depolarization processes also can yield free O₂, which reacts with polarized hydrogen on metal surfaces.

9.5.2.4 Other Processes Contributing to Corrosion

Bacteria produce copious quantities of exopolymers that appear to be implicated in corrosion (Ford et al., 1986, 1987b, 1988, 1990c–d, 1991; Little and Depalma, 1988; Paradies, 1995; Roe et al., 1996; Whitfield, 1988). These exopolymers are acidic and contain functional groups capable of binding to metal ions. Paradies (1995) recently reviewed this subject. The exopolymers facilitate adhesion of bacteria to surfaces. They are involved in severe corrosion of copper pipes and water supplies in large buildings and hospitals (Paradies et al., 1990). Some materials also play an important role in cueing the settlement of invertebrate larvae and others in repelling larvae from surfaces (Gu et al., 1997b; Holmström et al., 1992; Maki et al., 1989, 1990a–b; Mitchell and Maki, 1989; Rittschof et al., 1986). They primarily consist of polysaccharides and proteins, and influence the electrochemical potential of metals (Chen et al., 1995 and 1996). Surface analysis using XPS showed that these functionality-rich materials can complex metal ions from the surface, releasing them

into aqueous solution. As a result, corrosion is initiated. Proteins in polymeric materials use their disulfide-rich bonds to induce corrosion.

Bacterial polymers were recently found to promote corrosion of copper pipes in water supplies (Mittelman and Geesey, 1985; Paradies et al., 1990), owing to the high affinity of the polymeric materials for copper ions (Mittelman and Geesey, 1985; Ford et al., 1988). The corrosion processes are accelerated when the pipes are filled with stagnant soft water. Cations influence the production of bacterial exopolymers. Polysaccharide production by *Enterobacter aerogenes* is stimulated by the presence of Mg, K, and Ca ions (Wilkinson and Stark, 1956). Toxic metal ions (e.g., Cr⁶⁺) also enhance polysaccharide production. Synthesis is positively correlated with Cr concentration. These bacteria also can be used in the mining and recovery of precious metals, a process called “bioleaching” (Clark and Ehrlich, 1992; Davidson et al., 1996; Dunn et al., 1995).

The role of bacteria in embrittlement of metallic materials by hydrogen is not fully understood. During the growth of bacteria, fermentation processes produce organic acids and molecular hydrogen. This hydrogen can be adsorbed to material surfaces, causing polarization. Some bacteria (particularly the methanogens, sulfidogens, and acetogens) can also utilize hydrogen (Gottschalk, 1986). Walch and Mitchell (1986) proposed a possible role for microbial hydrogen in hydrogen embrittlement. They measured permeation of microbial hydrogen into metal, using a modified Devanathan cell (Devanathan and Stachurski, 1962). In a mixed microbial community commonly found in natural conditions, hydrogen production and consumption occur simultaneously. Competition for hydrogen between microbial species determines the ability of hydrogen to permeate metal matrices, causing crack initiation.

Microbial hydrogen involved in material failure may be explained by two distinct hypotheses—pressure and surface energy change (Borenstein, 1994; Gangloff and Kelly, 1994). The kinetic nature of hydrogen embrittlement of cathodically charged mild steel is determined by the competition between diffusion and plasticity. The greater the strength of the alloy, the more susceptible it is to embrittlement. However, microstructures were also proposed to be the more critical determinant of material susceptibility. Hydrogen permeation may increase the mobility of screw dislocations, but not the mobility of edge dislocations (Wang, 1996). On the other hand, corrosion may also be inhibited by the presence of

biofilms on surfaces (Hernandez et al., 1994; Jayaraman et al., 1997 and 1999; Mattila et al., 1997; Potekhina et al., 1999).

9.5.2.5 Inhibition of Corrosion by Microorganisms

The mechanisms involved during microbial corrosion of metals are as follows:

1. stimulation of an anodic or cathodic process by bacterial metabolites,
2. breakdown of the protective layers,
3. enhanced conductivity near the surface liquid environment.

However, bacteria may also inhibit corrosion processes by electrochemical processes (Hernandez et al., 1994; Jayaraman et al., 1997 and 1999; Mattila et al., 1997; Potekhina et al., 1999). Bacteria may also

1. neutralize the corrosive substances,
2. form protective layers on materials, or
3. decrease the corrosiveness of the aqueous environment.

9.5.2.6 Non-Ferrous Metals

Metals other than Fe are commonly used in alloys to inhibit corrosion and enhance mechanical properties. They include Mo, Cr, Ni, Cu, Zn and Cd. The selection of metal species and the quantities in the iron matrices are based on the engineering properties of the materials. Pure metals in common use are limited to Fe, Al, Cu and Ti. We know very little about biocorrosion of Al and Ti (Gu et al., 2000a). Aluminium (Al) reacts with molecular oxygen (O_2) under ambient conditions, forming an oxidized layer of protective aluminum oxide on the outer surface of the material matrix. When Al ions are released, the free Al^{3+} is toxic to both the microflora (Illmer and Schinner, 1999), and animals (Nieboer et al., 1995). Because of their corrosion resistance, titanium (Ti) alloys are used in water cooling systems on ships and in water recycling systems in space. Biofilm formation on these materials has been documented (Gu et al., 1998b). However, the extent of attack by microorganisms is unknown.

Recent research on microbial interactions with metals has focused on the precipitation (Fortin et al., 1994), mineral formation (Douglas and Beveridge, 1998), and oxidation/reduction processes (Santini et al., 2000; Stoltz and Oremland, 1999; Sugio et al.,

1992; Tebo and Obraztsova, 1998; Wang et al., 1989). Surprisingly, information on Zn, one of the most widely used metals, is very limited.

Microorganisms may affect transitional metals in several ways, including precipitation by metabolic products (Fortin et al., 1994), cellular complexation (Schembri et al., 1999; Schultzen-Lam et al., 1992), and concentration and mineral formation of internal cellular structures. Sulfate-reducing bacteria can effectively immobilize a wide range of soluble metals by forming sulfide precipitates (Sakaguchi et al., 1993). Recently, bacterial exopolymers have been found to be capable of complexing metals, leading to accumulation at the cell surface. This ability is not restricted to a specific group of microorganisms and has been documented in both the aerobic bacterium *Deleya marina* and an anaerobe, *Desulfovibrio desulfuricans* (Chen, 1996). Since many transitional metals exist in several oxidation/reduction states, both bacterial oxidation and reduction are possible.

Chromium (Cr) can exist in either the hexavalent or trivalent form. Reduction of Cr^{6+} to Cr^{3+} is mediated by both aerobic and anaerobic microorganisms. A change of phenotypic expression in *Pseudomonas indigoferas* (*Vogesella indigofera*) has been observed in the presence of Cr^{6+} (Gu and Cheung, 2001a; Cheung and Gu, 2002 and 2003). Bacterial reduction of Cr^{6+} to Cr^{3+} was reported in sulfate-reducing bacteria isolated from the marine environment (Cheung and Gu, 2003). Intracellular partition of Cr was reported using bacteria from a subsurface environment. Reduction of Cr^{6+} is a process in which the toxicity of the metal is greatly reduced. Bacteria possessing this ability include *Achromobacter eurydice*, *Aeromonas dechromatica*, *Agrobacterium radiobacter*, *Arthrobacter* spp., *Bacillus subtilis*, *B. cereus*, *Desulfovibrio vulgaris*, *Escherichia coli*, *Enterobacter cloacae*, *Flavobacterium devorans*, *Sarcina flava*, *Micrococcus roseus*, and *Pseudomonas* spp. (Ehrlich, 1996).

Similarly, Mo exists in a number of oxidation states, with Mo^{4+} and Mo^{6+} being most common. *Thiobacillus ferrooxidans* is capable of oxidizing Mo^{5+} to Mo^{6+} ; whereas, *Enterobacter cloacae*, *Sulfolobus* sp., and *Thiobacillus ferrooxidans* can reduce Mo^{6+} to Mo^{5+} (Sugio et al., 1992). Microbiological oxidation or reduction of other metals, including Cd, Ni and Zn, has not been fully established. Microbial exopolymers have a significant effect on the solubilization of metals from material matrices through complexation and chelation. Because of this property, wastewater containing these metals ions can be purified through biomass adsorp-

tion, a process in which metal ions are concentrated on a biosorbent (Gelmi et al., 1994).

Our knowledge of microbial transformation of metals is very limited. Recent developments in isolation of bacteria and archaea may provide new tools to investigate metal transformations in natural habitats (Amann et al., 1995). Molecular techniques, including DNA probes and *in situ* hybridization, permit the identification of physiologically unique bacteria without the need to culture the organisms. Microbial resistance to metals is widespread in nature (Lin and Olsen, 1995). Elucidation of the genetic structure of these bacteria should provide new insights into the processes involved in resistance.

9.6 BIODETERIORATION OF POLYMERIC MATERIALS

Polymers are widely used in various industries and daily applications. Thermosetting polyimides are chemically synthesized with high strength and resistance to degradation (Brown, 1982). Polyimides are used in load-bearing applications (e.g., struts, chassis, and brackets in automotive and aircraft structures), due to their flexibility and compressive strength. They are also used in appliance construction, cookware, and food packaging because of their chemical resistance to oils, greases, and fats and their microwave transparency and thermal resistance. Their electrical insulation properties are ideally suited for use in the electrical and electronics markets, especially as high temperature insulation materials and passivation layers in the fabrication of integrated circuits and flexible circuitry. In addition, the flame resistance of this class of polymers may provide a halogen-free, flame-retardant material for aircraft interiors, furnishings, and wire insulation. Other possible uses include fibers for protective clothing, advanced composite structures, adhesives, insulation tapes, foam, and optics operating at high temperatures (Verbiest et al., 1995).

Wide acceptance of polyimides in the electronics industry (Brown, 1982; Jensen, 1987; Lai, 1989; Verbicky, 1988; Verbiest et al., 1995) has drawn attention to the stability issues of these materials. The National Research Council (NRC, 1987) emphasized the need to apply these polymers in the electronic industries because data acquisition, information processing, and communication are critically dependent upon materials performance. The interlayering of polyimides and electronics in integrated circuits prompted several studies on the interactions

between these two materials (Hahn et al., 1985; Kelley et al., 1987).

9.6.1 Electronic Insulating Materials

Electronic packaging polyimides are particularly useful because of their outstanding performance and engineering properties. It is only recently that the biodeterioration problem of these polymers was investigated using pyromellitic dianhydride and 4,4'-diaminodiphenyl ether with molecular weight (M_w) of 2.5×10^5 (Gu et al., 1994a, 1995b, 1996a, 1996c, 1998a–b; Mitton et al., 1993, 1996, 1998). They are susceptible to deterioration by fungi (Gu et al., 1994a, 1995b, 1996a; Mitton et al., 1993, 1998). Though bacteria were isolated from cultures containing the deteriorated polyimides, further tests did not show comparable degradation rate by bacteria. Our studies showed that the dielectric properties of polyimides could be altered drastically following growth of a microbial biofilm (Gu et al., 1995b, 1996a; Mitton et al., 1993, 1998). This form of deterioration may be slow under ambient conditions. However, the deterioration processes can be accelerated in humid conditions or in enclosed environments (e.g., submarines, space vehicles, aircraft, and other closed facilities). Very small changes of material insulation properties may result in serious and catastrophic consequences in communications and control systems.

Initial isolation of microorganisms associated with deterioration of polyimides indicated the presence of both fungi and bacteria. Bacteria include *Acinetobacter johnsonii*, *Agrobacterium radiobacter*, *Alcaligenes denitrificans*, *Comamonas acidovorans*, *Pseudomonas* spp., and *Vibrio anguillarum*. These bacteria were not capable of degrading the polymer after inoculation, while fungi were more effective in degrading the polyimides.

Polyimide deterioration occurs through biofilm formation and subsequent physical changes in the polymer. Using electrochemical impedance spectroscopy (EIS) (Mansfeld, 1995, van Westing et al., 1994), a very sensitive technique for monitoring dielectric constants of polymers, fungal growth on polyimides has been shown to yield distinctive EIS spectra, indicative of failing resistivity. Two steps are involved during the degradation process. First, an initial decline in coating resistance is related to the partial ingress of water and ionic species into the polymer matrices. This is followed by further deterioration of the polymer by activity of the fungi, resulting in a significant decrease in resistivity. Fungi involved include *Aspergillus versicolor*, *Cladospo-*

rium cladosporioides, and *Chaetomium* sp. (Gu et al., 1995b, 1996b–c, 1997a–b, 1998a–b). The data support the hypothesis that polyimides are susceptible to microbial deterioration and also confirm the versatility of EIS as a method in evaluation of the biosusceptibility of polymers.

9.6.2 Packaging Polyethylenes

Polyethylenes (PEs) of high and low density are primarily used in product packaging as sheets and thin films. Their degradability in natural environments poses serious environmental concerns due to their slow degradation rates under natural conditions, and the hazard they present to freshwater and marine animals. Prior exposure of PEs to UV promotes polymer degradation. It is believed that polymer additives (such as starch, antioxidants, coloring agents, sensitizers, and plasticizers) may significantly alter the biodegradability of the parent polymers (Karlsson et al., 1988). Degradation rates may be increased by 2–4% following photosensitizer addition. However, degradation is very slow, estimated to take decades. Crystallinity, surface treatment, additives, molecular weight, and surfactants are all factors affecting the fate and rate of PE degradation, and may accelerate the process.

Biodegradation of PEs has been studied extensively (Albertsson, 1980; Albertsson et al., 1994; Breslin, 1993; Breslin and Swanson, 1993; Iman and Gould, 1990), but the results were based on PE blended with starch. For example, extracellular concentrates of three *Streptomyces* species cultures were inoculated to starch containing PE films (Pometto et al., 1992, 1993). Subsequently, PE was claimed to be degraded. Realizing that degradation may occur and the extent could be extremely insignificant, conclusions on PE degradation should be treated with caution. Other data describing degradation of PE containing starch is also questionable, and microbial metabolites may contaminate the PE surfaces, which could be interpreted as degradation products of the parent PE.

Abiotic degradation of PE is evident by the appearance of carbonyl functional groups in abiotic environments. In contrast, an increase of double bonds was observed when polymers showed weight loss resulting from biodegradation (Albertsson et al., 1994). It was proposed that microbial PE degradation is a two-step process involving an initial abiotic photo-oxidation, followed by a cleavage of the polymer carbon backbone. However, the mechanism of the second step needs extensive analysis before plausible conclusions can be confidently drawn.

Lower molecular weight PEs, including paraffin, can be biodegraded. Paraffin undergoes hydroxylation oxidatively to form an alcohol group, followed by formation of carboxylic acid. At higher temperatures, ketones, alcohols, aldehydes, lactones, and carboxylic acids are formed abiotically in six weeks (Albertsson et al., 1994). PE pipes used in gas distribution systems may fail due to cracking. It is unlikely that biological processes are involved (Zhou and Brown, 1995).

Polypropylenes (PPs) are also widely utilized in engineering pipes and containers. Degradation of PPs results in a decrease of their tensile strength and molecular weight. The mechanism may involve the formation of hydroperoxides, which destabilize the polymeric carbon chain to form a carbonyl group (Cacciari et al., 1993; Severini et al., 1988).

9.6.3 Structural Polymeric Composites

Fiber-reinforced polymeric composite materials (FRPCMs) are newly developed materials important to aerospace and aviation industries (Gu, 2003a–c; Gu et al., 1994a, 1995b–c, 1996a–c, 1997a, 1997b, 2000a–d; Wagner, 1995; Wagner et al., 1996). The increasing usage of FRPCMs as structural components in public structures, particularly in aerospace applications, has generated an urgent need to evaluate the biodegradability of this class of new materials. FRPCMs are also susceptible to attack by microorganisms (Gu et al., 1997a–b). It was suggested that impurities and additives that can promote microbial growth are implicated as potential sources of carbon and energy for the environmental microorganisms.

In this area of research, two research groups reported microbial degradation of FRPCMs (Gu et al., 1995b–c, 1996a–c, 1997a–b; Wagner et al., 1996). A mixed culture of bacteria including a sulfate-reducing bacterium was used to show the material deterioration (Wagner et al., 1996). In contrast, Gu et al. (1994a, 1996a–c, 1997a–b, 1998a–b) used a fungal consortium originally isolated from degraded polymers and a range of material composition including fluorinated polyimide/glass fibers, bismaleimide/graphite fibers, poly(ether-ether-ketone) (PEEK)/graphite fibers, and epoxy/graphite fibers (Gu et al., 1995c). The fungal consortium consisted of *Aspergillus versicolor*, *Cladosporium cladosporioides*, and a *Chaetomium* sp. Both bacteria and fungi are capable of growing on the graphite fibers of FRPCMs, but only fungi have been shown to cause deterioration detectable over more than 350 days (Gu et al., 1995b; 1997a–b). Physical and mechanical

tests were not sufficiently sensitive to detect any significant physical changes in the materials after the duration of exposure (Gu et al., 1997b; Thorp et al., 1994). However, the resins were actively degraded, indicating that the materials were at risk of failure. It is clear that both fiber surface treatment and resin processing supply enough carbon for microbial growth (Gu et al., 1995c). It has become clear that FRPCMs are not immune to adhesion and attack by microorganisms (Ezeonu et al., 1994a–b; Gu et al., 1998b; Mitchell et al., 1996).

Natural populations of microorganisms are capable of growth on surfaces of FRCPM coupons at both relatively high (65–70%) and lower humidity conditions (55–65%) (Gu et al., 1998b). The accumulation of fungi on surfaces of composites develops into a thick biofilm layer and decreases the resistance to further environmental changes. However, the resistivity of FRPCMs was found to decline significantly after the initial three months during a year of monitoring using EIS (Gu et al., 1996c, 1997b). Clear differences resulting from biofilm development were detected on FRPCMs used in aerospace applications (Gu et al., 1997b). Further study indicated that many fungi are capable of utilizing chemicals (e.g., plasticizers, surface treatment chemicals, and impurities) introduced during composite manufacture as carbon and energy sources (Gu et al., 1996a). Similarly, lignopolystyrene graft copolymers were also susceptible to attack by fungi (Milstein et al., 1992).

A critical question remains about the effect of FRPCM deterioration on mechanical properties of the composite materials. Thorp et al. (1994) attempted to determine mechanical changes in composite coupons after exposure to a fungal culture. No significant mechanical changes could be measured after 120 days of exposure. They suggested that methodologies sufficiently sensitive to detect surface changes need to be utilized. Acoustic techniques have also been proposed as a means of detecting changes in the physical properties of the FRPCMs (Wagner et al., 1996).

Many bacteria are capable of growth on surfaces of FRPCMs and resins (Gu et al., 1996b). The bacteria are believed to be introduced onto the polymers during production. Similar to the microorganisms isolated from polyimides, bacteria are less effective in degrading the composites than fungi (Gu, 2003a; Gu et al., 2000d). Degradation of composites was detected using electrochemical impedance spectroscopy, and similar spectra to polyimides were obtained.

9.6.4 Corrosion Protective Coatings

Corrosion protective coatings also have wide application due to the development of metallic materials and their susceptibility to both environmental and microbiological corrosion (Mitchell et al., 1996). Polymeric coatings are designed to prevent contact of the underlying materials with corrosive media and microorganisms. However, microbial degradation of coatings may accelerate and severely damage the underlying metals. A typical example is the corrosion of underground storage tanks.

Natural bacterial populations were found to readily form microbial biofilms on surfaces of coating materials, including epoxy and polyamide primers and aliphatic polyurethanes (Blake et al., 1998; Filip, 1978; Gu and Mitchell, 2004; Gu et al., 1998b; Stern and Howard, 2000; Thorp et al., 1997). Surprisingly, the addition of biocide diiodomethyl-*p*-tolylsulfone into polyurethane coatings did not inhibit bacterial attachment or growth of bacteria effectively, due to development of biofilm and bacterial resistance (Gu et al., 1998b; Mitchell et al., 1996).

Using EIS, both primers and aliphatic polyurethane top-coatings were monitored for their response to biodegradation by bacteria and fungi. Results indicated that primers are more susceptible to degradation than polyurethane (Gu et al., 1998b). The degradation process has mechanisms similar to polyimides and FRPCMs, as described previously. Aliphatic polyurethane-degrading bacteria have been isolated; one of them is *Rhodococcus globerulus* P1 base on 16S rRNA sequence (Gu, unpublished data).

Polyurethane-degrading microorganisms, including *Fusarium solani*, *Curvularia senegalensis*, *Aureobasidium pullulans*, and *Cladosporidium* sp. were isolated (Crabbe et al., 1994), and esterase activity was detected with *C. senegalensis*. A number of bacteria were also claimed to be capable of degrading polyurethane. They are as follows: four stains of *Acinetobacter calcoaceticus*, *Arthrobacter globiformis*, *Pseudomonas aeruginosa*, *Pseudomonas cepacia*, *Pseudomonas putida*, and two other *Pseudomonas*-like species (El-Sayed et al., 1996). A *Comamonas acidovorans* TB-35 was also reported (Akutsu et al., 1998; Nakajima-Kambe et al., 1995; 1997). In addition, *Pseudomonas chlororaphis* was isolated and included a lipase responsible for the degradation (Stern and Howard, 2000). We isolated a *Rhodococcus* species H07 from soil using water soluble polyurethane as the sole source of carbon

and energy, and the microorganisms also showed esterase activity.

9.6.5 Plasticizers

A large collection of chemical compounds are used as additives in the manufacture of plastic products. The plasticizer is not bound covalently to the plastic resin and, therefore is able to migrate into the environment (Jobling et al., 1995). In addition, plasticizers are widely used in building materials, home furnishings, transportation, clothing, and, to a limited extent, in food and medical products (Niazi et al., 2001). Due to the global utilization of large quantities of plasticized polymers, phthalate esters have been detected in almost all environments where they have been sought (Giam et al., 1978). Certain phthalate acids, phthalate esters, and their degradation intermediates are suspected of causing cancer and kidney damage. As a result, the U.S. Environmental Protection Agency has added this class of chemicals to its list of priority pollutants. (U.S. EPA, 1992).

Degradation of *ortho*-methyl phthalate ester (DMPE) was investigated using activated sludge and mangrove sediment for enrichment culture of aerobic bacteria. Morphologically distinctive microorganisms have been isolated and identified, and tested for their capability of degrading *o*-DMPE (Wang et al., 2003a–b). *Comamonas acidovorans* strain Fy-1 showed the greatest ability to degrade high concentrations of phthalate (PA), as high as 2,600 mg/L within two days (Fan et al., 2003; Wang et al., 2003a–c). Surprisingly, none of the bacteria from the enrichment culture were capable of degrading *o*-DMPE. When the isolates were reconstituted into consortia of culture, two consortia of microorganisms (one composed of *Pseudomonas fluorescens*, *Pseudomonas aureofaciens* and *Sphingomonas paucimobilis*, and the other of *Xanthomonas maltophilia* and *Sphingomonas paucimobilis*) showed ability to completely degrade *o*-DMPE in two to four days (Wang et al., 2003b). The three-species consortium

appeared to be more effective in degradation of *o*-DMPE. Both consortia proceeded through formation of mono-methyl phthalate (MMP) and then PA before mineralization (Figure 9.3).

While degradation of *o*-DMPE has also been observed using bacteria enriched from mangrove and deep-ocean sediment, in all cases the degradation of *o*-DMPE requires at least two different microorganisms to achieve the complete degradation of the chemical. In addition, degradation of dimethyl isophthalate also requires at least two microorganisms. The biochemical degradative pathway involves the two bacteria at different stages of hydrolysis of the substrate (unpublished data of this laboratory). Furthermore, the active degradative culture has also been immobilized on surfaces of membrane fibers, and high activity of the microorganisms was detected, further indicating the feasibility of utilizing the bacterial consortium in mineralizing *o*-DMPE. It is possible that high concentrations of endocrine-disrupting chemicals PA and DMPE can be mineralized in wastewater treatment systems by indigenous microorganisms.

9.7 SUMMARY

Biofouling is a natural phenomenon affecting a wide range of industries of our society. Conventional preventive strategies are chemical-based, but recent new understanding of biofouling mechanisms has shown that biotechnological approaches involving the utilization of microorganisms or their metabolites might provide effective alternatives to using chemicals. One current drawback is the dominance of chemical approaches to biofouling control. On the other hand, corrosion of metals and deterioration of polymeric materials have become economically significant in our society. New techniques have enabled the early detection of polymer failure, providing strong evidence that the control of such deterioration might be complicated due to the complexity of poly-

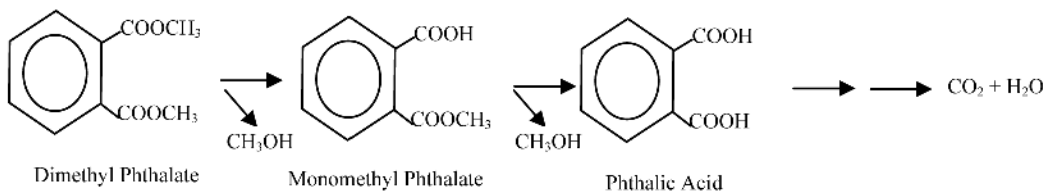


FIGURE 9.3 Proposed metabolic pathway of *ortho*-dimethyl phthalate (DMP) degradation by a bacterial consortium consisting *Xanthomonas maltophilia* and *Sphingomonas paucimobilis* isolated from an activated sludge of wastewater treatment plant.

mer processing. Plasticizers have been found to be significant chemicals that affect the environment as endocrine-disrupting chemicals, and also as nutrients promoting the growth of microorganisms that form biofilms on surfaces.

9.8 ACKNOWLEDGEMENTS

Research currently carried out in my laboratory is supported by the Innovative Technology Fund (ITS/265/00) and the Agriculture, Fisheries and Conservation Department (AFCD) of the Hong Kong government. Additional support is provided by Kou Hing Hou Scientific Supplies Co. I thank Jessie Lai for technical support of my research projects and the EM Unit of Queen Mary Hospital at the University of Hong Kong for SEM sample preparation and observation.

9.9 REFERENCES

- Akutsu, Y., Nakajima-Kambe, T., Nomura, N., and Nakahara, T. 1998. Purification and properties of a polyester polyurethane-degrading enzyme from *Comamonas acidovorans* TB-35. *Applied and Environmental Microbiology*. Vol. 64. 62–67.
- Albertsson, A. C. 1980. The shape of the biodegradation curve for low and high density polyethylenes in prolonged series of experiments. *European Polymer Journal*. Vol.16. 623–630.
- Albertsson, A. C., Barenstedt, C., and Karlsson, S. 1994. Abiotic degradation products from enhanced environmentally degradable polyethylene. *Acta Polymers*. Vol. 45. 97–103.
- Amann, R. I., Ludwig, W., and Schleifer, K. H. 1995. Phylogenetic identification and in situ detection of individual microbial cells without cultivation. *Microbiological Reviews*. Vol. 59. 143–169.
- Angell, P., Luo, J. S., and White, D. C. 1995. Studies of the reproducible pitting of 304 stainless steel by a consortium containing sulphate-reducing bacteria. In *Proceedings of the International Conference on Microbial Induced Corrosion*. P. Agell, S. W. Borenstein, R. A. Buchanan, S. C. Dexter, N. J. E. Dowling, B. J. Little, C. D. Lundin, M. B. McNeil, D. H. Pope, R. E. Tatnall, D. C. White, and H. G. Ziegenfuss, Eds. Houston: NACE International. 1–10.
- Audouard, J. P., Compère, C., Dowling, N. J. E., Feron, D., Festy, D., Mollica, A., Rogne, T., Scotto, V., Steinsmo, U., Taxen, K., and Thierry, D. 1995. Effect of marine biofilms on high performance stainless steel exposed in European coastal waters. In *Microbial Corrosion: Proceedings of the 3rd International European Federation of Corrosion (EFC) Workshop*. Lisbon, Portugal: European Federation of Corrosion. Publication 15. 198–210.
- Balow, A., Trüper, H. G., Dworkin, M., Harder, W., and Schleifer, K. H. 1992. *The Prokaryotes*. Vol. I–IV. New York: Springer-Verlag.
- Berk, S., Mitchell, R., Bobbie, R. J., Nickels, J. S., and White, D. C. 1981. Microfouling on metal surfaces exposed to seawater. *International Biodeterioration Bulletin*. Vol.17. 29–37.
- Blake II, R.C., Norton, W. N., and Howard, G. T. 1998. Adherence and growth of a *Bacillus* species on an insoluble polyester polyurethane. *International Biodeterioration and Biodegradation*. Vol. 42. 63–73.
- Blakemore, R. P. 1982. Magnetotactic bacteria. *Annual Reviews of Microbiology*. Vol. 36. 217–238.
- Böckelmann, U., Manz, W., Neu, T. R., and Szewzyk, U. 2002. Investigation of lotic microbial aggregates by a combined technique of fluorescent in situ hybridization and lectin-binding-analysis. *Journal of Microbiological Methods*. Vol. 49. 75–87.
- Booth, G. H. and Tiller, A. K. 1960. Polarization studies of mild steel in cultures of sulphate-reducing bacteria. *Transactions of the Faraday Society*. Vol. 56. 1,689–1,696.
- Booth, G. H. and Tiller, A. K. 1962a. Polarization studies of mild steel in cultures of sulphate-reducing bacteria. Part 2: Thermophilic organisms. *Transactions of the Faraday Society*. Vol. 58. 110–115.
- Booth, G. H., Tiller, A. K., and Wormwell, F. 1962b. Ancient iron nails well preserved from apparently corrosive soils. *Nature (London)*. Vol. 195. 376–377.
- Booth, G. H., Elford, L., and Wakerly, D. J. 1968. Corrosion of mild steel by sulfate-reducing bacteria: An alternative mechanism. *British Corrosion Journal*. Vol. 3. 242–245.
- Borenstein, S. 1994. *Microbiologically Influenced Corrosion Handbook*. Cambridge, MA: Woodhead Publishing., 56.
- Breslin, V. T. 1993a. Degradation of starch-plastic composites in a municipal solid waste landfill. *Journal of Environmental Polymer Degradation*. Vol. 1. 127–141.
- Breslin, V. T. and Swanson, R. L. 1993b. Deterioration of starch-plastic composite in the environment. *Journal of Air and Waste Management Association*. Vol. 43: 325–335.
- Brown, G. A. 1982. Implications of electronic and ionic conductivities of polyimide films in integrated circuit fabrication. In *Polymer Materials for Electronic Applications*. E. D. Feit and C. W. Wilkins, Eds. Washington DC: American Chemical Society., vol. ACS Symposium Series. 184, 151–169.
- Cacciari, I., Quatrini, P., Zirletta, G., Mincione, E., Vinciguerra, V., Lupattelli, P. and Sermanni, G. G. 1993. Isotactic polypropylene biodegradation by a microbial community: Physico-chemical characterization of metabolites produced. *Applied and Environmental Microbiology*. Vol. 59 3,695–3,700.
- Callow, M. E. 1993. A review of fouling in freshwaters. *Biofouling*. Vol. 7. 313–327.
- Callow, M. E. and Fletcher, R. L. 1994. The influence of low surface energy materials on bioadhesion—A review. *International Biodeterioration & Biodegradation*. Vol. 34. 333–348.

- Campaignolle, X. and Crolet, J. L. 1997. Method for studying stabilization of localized corrosion on carbon steel by sulfate-reducing bacteria. *Corrosion*. Vol. 53. 440–447.
- Carlton, J. T. and Geller, J. B. 1993. Ecological roulette: The global transport of nonindigenous marine organisms. *Science*. Vol. 261. 78–82.
- Chen, G. 1996a. *An XPS Study of the Passivity of Stainless Steels Influenced by Sulfate-reducing Bacteria*. Ph.D. dissertation. Stony Brook, NY: State University of New York at Stony Brook. 279.
- Chen, X., and Stewart, P. S. 1996. Chlorine penetration into artificial biofilm is limited by a reaction-diffusion interaction. *Environmental Science and Technology*. Vol. 30. 2,078–2,083.
- Chen, G., Clayton, C. R., Sadowski, R. A., Gillow, J. B., and Francis, A. J. 1995. Influence of sulfate-reducing bacteria on the passive film formed on austenitic stainless steel, AISI 304. *Corrosion/95*. Paper 217. Houston: NACE International.
- Chen, G., Kagwade, S. V., French, G. E., Ford, T. E., Mitchell, R., and Clayton, C. R. 1996b. Metal ion and expolymer interaction: A surface analytical study. *Corrosion*. Vol. 52. 891–899.
- Chet, I., and Mitchell, R. 1976a. The relationship between chemical structure of attractants and chemotaxis by a marine bacterium. *Canadian Journal of Microbiology*. Vol. 22. 1,206–1,208.
- Chet, I., and Mitchell, R. 1976b. Control of marine fouling by chemical repellents. In *International Biodegradation Symposium*. S.M. Sharpley and A.M. Kaplan, Eds. Applied Science Publication, Barking, England: Elsevier. 515–521.
- Chet, I., Asketh, P., and Mitchell, R. 1975. Repulsion of bacteria from marine surfaces. *Applied Microbiology*. Vol. 30. 1,043–1,045.
- Cheung, K. H. and Gu, J. D. 2002. Bacterial color response to hexavalent Chromium, Cr⁶⁺. *The Journal of Microbiology*. Vol 40. 234–236.
- Cheung, K. H., and Gu, J. D. 2003. Reduction of chromate (CrO₄²⁻) by an enrichment consortium and an isolate of marine sulfate-reducing bacteria. *Chemosphere*. Vol. 52. 1,523–1,529.
- Clapp, W. P. 1948. Macro-organisms in sea water and their effect on corrosion In: *The Corrosion Handbook*. H. H. Uhlig, Ed. New York: John Wiley & Sons, Inc. 433–441.
- Clark, T. R. and Ehrlich, H. L. 1992. Copper removal from an industrial waste by bioleaching. *Journal of Industrial Microbiology*. Vol. 9. 213–218.
- Clayton, C. R., Halada, G. P., Kearns, J. R., Gillow, J. B., and Francis, A. J. 1994. Spectroscopic study of sulfate reducing bacteria-metal ion interactions related to microbiologically influenced corrosion (MIC). In *Microbiologically Influenced Corrosion Testing*. J.R. Kearns and B.J. Little, Eds. Philadelphia: American Society for Testing and Materials. ASTM STP 1232. 141–152.
- Corbett, R. A., Morrison, W. S., and Bickford, D. F. 1987. Corrosion evaluation of alloys for nuclear waste processing. *Materials Performance*. Vol. 2. 40–45.
- Costerton, J. W., Geesey, G. G., and Cheng, K. J. 1978. How bacteria stick. *Scientific American*. Vol. 238. 86–95.
- Costerton, J. W., Lewandowski, Z., DeBeer, D., Caldwell, D., Korber, D., and James, G. 1994. Biofilms, the customized micro-niche. *Journal of Bacteriology*. Vol. 176. 2,137–2,142.
- Crabbe, J. R., Campbell, J. R., Thompson, L., Walz, S. L., and Scultz, W. W. 1994. Biodegradation of a colloidal ester-based polyurethane by soil fungi. *International Biodeterioration and Biodegradation*. Vol. 33. 103–113.
- Crisp, D. J. 1974. Factors influencing the settlement of marine invertebrate larvae. In *Chemoreception in Marine Organisms*. P.T. Grant and A.M. Mackie, Eds. London: Academic Press. 177–265.
- Daniels, L., Belay, N., Rajagopal, B., and Weimer, P. 1987. Bacterial methanogenesis and growth from CO₂ with elemental iron as the sole source of electrons. *Science*. Vol. 237. 509–511.
- Davidson, D., Beheshti, B., and Mittelman, M. W. 1996. Effects of *Arthrobacter* sp., *Acidovorax delafieldii*, and *Bacillus megaterium* colonisation on copper solvency in a laboratory reactor. *Biofouling*. Vol. 9. 279–292.
- Davies, D. G., Parsek, M. R., Pearson, P., Iglewski, B. H., Costerton, J. W., and Greenberg, E. P. 1998. The involvement of cell-to-cell signals in the development of a bacterial biofilm. *Science*. Vol. 280. 295–298.
- Devanathan, M. A. V., and Stachurski, Z. 1962. Adsorption and diffusion of electrolytic hydrogen in palladium. *Proceedings of the Royal Society of London. Series A*. Vol. 270. 90–110.
- Dexter, S. C. 1993. Role of microfouling organisms in marine corrosion. *Biofouling*. Vol. 7. 97–127.
- Dickinson, W. H., Caccavo, Jr., F., and Lewandowski, Z. 1996. The ennoblement of stainless steel by manganic oxide biofouling. *Corrosion Science*. Vol. 38. 1,407–1,422.
- Dickinson, W. H., Caccavo, Jr., F., Olesen, B., and Lewandowski, Z. 1997. Ennoblement of stainless steel by the manganese-depositing bacterium *Leptothrix discophora*. *Applied and Environmental Microbiology*. Vol. 63. 2,502–2,506.
- Douglas, S., and Beveridge, T. J. 1998. Mineral formation by bacteria in natural microbial communities. *FEMS Microbiology Ecology*. Vol. 26. 79–88.
- Dowling, N. J. E., Brooks, S. A., Phelps, T. J., and White, D. C. 1992. Effects of selection and fate of substrate supplied to anaerobic bacteria involved in the corrosion of pipeline steel. *Journal of Industrial Microbiology*. Vol. 10. 207–215.
- Dowling, N. J. E. and Guezenc, J. 1997. Microbially influenced corrosion In *Manual of Environmental Microbiology*. C. J. Hurst, G. R. Knudsen, M. J. McInerney, L. D. Stetzenbach, and M. V. Walter, Eds. Washington DC: ASM Press, 842–855.
- Drake, H. 1994. Acetogenesis, acetogenic bacteria, and the acetyl-CoA “Wood/Ljungdahl” pathway: Past and current

- perspectives. *Acetogenesis*. New York: Chapman and Hall. 1–60.
- Dunn, D. S., Sridhar, N., and Cragnolino, G. A. 1995. Effects of surface chromium depletion on localized corrosion of alloy 825 as a high-level nuclear waste container material. *Corrosion*. Vol. 51. 618–624.
- Eashwar, M., Martrhamuthu, S., Palanichamy, S., and Balakrishnan, K. 1995. Sunlight irradiation of seawater eliminates ennoblement-causation by biofilms. *Biofouling*. Vol. 8. 215–221.
- Ehrlich, H. L. 1996. Geomicrobial processes: A physiological and biochemical overview. In *Geomicrobiology*, 3rd ed. New York: Marcel Dekker. 108–142
- El-Sayed, A. H. M. M., Mohmoud, W. M., Davis, E. M., and Coughlin, R. W. 1996. Biodegradation of polyurethane coatings by hydrocarbon-degrading bacteria. *International Biodeterioration and Biodegradation*. Vol. 37. 69–79.
- Emerson, A. and Moyer, C. 1997. Isolation and characterization of novel iron-oxidizing bacteria that grow at circumneutral pH. *Applied and Environmental Microbiology*. Vol. 63. 4,784–4,792.
- Enos, D. G. and Taylor, S. R. 1996. Influence of sulfate-reducing bacteria on alloy 625 and austenitic stainless steel weldments. *Corrosion*. Vol. 52. 831–842.
- Evans, U. R. 1948. An outline of corrosion mechanisms, including the electrochemical theory. In *The Corrosion Handbook*. H. H. Uhlig, Ed. New York: John Wiley & Sons, Inc. 3–11.
- Ezeonu, I. M., Noble, J. A., Simmons, R. B., Price, D. L., Crow, S. A., and Ahearn, D. G. 1994a. Effect of relative humidity on fungal colonization of fiberglass insulation. *Applied and Environmental Microbiology*. Vol. 60. 2,149–2,151.
- Ezeonu, I. M., Price, D. L., Simmons, R. B., Crow, S. A., and Ahearn, D. G. 1994b. Fungal production of volatiles during growth on fiberglass. *Applied and Environmental Microbiology*. Vol. 60. 4,172–4,173.
- Ferry, J. G. 1995. Physiological ecology of methanogens. In *Methanogenesis: Ecology, Physiology, Biochemistry and Genetics*. J.G. Ferry, Ed. New York: Chapman and Hall. 128–206.
- Filip, Z. 1978. Decomposition of polyurethane in a garbage landfill leakage water and by soil microorganisms. *European Journal of Applied Microbiology*. Vol. 5. 225–231.
- Fletcher, M. and Loeb, G. I. 1979. Influence of substratum characteristics on the attachment of a marine Pseudomonad to solid surfaces. *Applied and Environmental Microbiology*. Vol. 37. 67–72.
- Ford, T.E. and Lock, M. A. 1987. Epilithic metabolism of dissolved organic carbon in boreal forest rivers. *FEMS Microbiology Ecology*. Vol. 45. 89–97.
- Ford, T. and Mitchell, R. 1990a. Metal embrittlement by bacterial hydrogen—An overview. *Marine Technological Society Journal*. Vol. 24. 29–35.
- Ford, T. and Mitchell, R. 1990b. The ecology of microbial corrosion. In *Advances in Microbial Ecology*, Vol. 11. 1K.C. Marshall, Ed. New York: Plenum Press. 231–262.
- Ford, T., Black, J. P., and Mitchell, R. 1986. Relationship between bacterial exopolymers and corroding metal surfaces. Paper 100 in *Corrosion/90*. Paper 110. Houston: NACE International.
- Ford, T.E., Walch, M., and Mitchell, R. 1987b. Corrosion of metals by thermophilic microorganisms. *Materials Performance*. Vol. 26. 35–39.
- Ford, T.E., Walch, M., Mitchell, R., Kaufman, M. J., Vestal, J. R., Dittner, S. A., and Lock, M. A. 1989. Microbial film formation on metals in an enriched arctic river. *Biofouling*. Vol. 1. 301–311.
- Ford, T., Maki, J., and Mitchell, R. 1988. Involvement of bacterial exopolymers in biodeterioration of metals. In *Biodeterioration*. D. R. Houghton, R. N. Smith, and H. O. W. Egginis, Eds. New York: Elsevier Science Publishing. 378–384.
- Ford, T. E., Season, P. C., Harris, T., and Mitchell, R. 1990c. Investigation of microbiologically produced hydrogen permeation through palladium. *Journal of Electrochemical Society*. Vol. 137. 1,175–1,179.
- Ford, T. E., Black, J. P., and Mitchell, R. 1990d. Relationship between bacterial exopolymers and corroding metal surfaces. *Corrosion/90*. Houston: NACE International.
- Ford, T., Sacco, E., Black, J., Kelley, T., Goodacre, R., Berkley, R. C. W., and Mitchell, R. 1991. Characterization of exopolymers of aquatic bacteria by pyrolysis-mass spectroscopy. *Applied and Environmental Microbiology*. Vol. 57. 1,595–1,601.
- Fortin, D., Southam, G., and Beveridge, T. J. 1994. Nickel sulfide, iron-nickel silfide and iron sulfide precipitation by a newly isolated Desulfotomaculum species and its relation to nickel resistance. *FEMS Microbiology Ecology*. Vol. 14. 121–132.
- Gangloff, R. P. and Kelly, R. G. 1994. Microbe-enhanced environmental fatigue crack propagation in HY130 steel. *Corrosion*. Vol. 50. 345–354.
- Gelmi, M., Apostoli, P., Cabibbo, E., Porru, S., Alessio, L., and Turano, A. 1994. Resistance to cadmium salts and metal absorption by different microbial species. *Current Microbiology*. Vol. 29. 335–341.
- Ghassem, H. and Adibi, N. 1995. Bacterial corrosion of reformer heater tubes. *Materials Performance*. Vol. 34. 47–48.
- Ghiorse, W. C. and Hirsch, P. 1978. Iron and manganese deposition by budding bacteria. In *Environmental Biogeochemistry and Geomicrobiology*, Vol. 3: *Methods, Metals and Assessment*. W.E. Krumbein, Ed. Ann Arbor: Ann Arbor Science Publishers. 897–909.
- Ghiorse, W. C. and Hirsch, P. 1979. An ultrastructural study of iron and manganese deposition associated with extracellular polymers of *Pedomicrobium*-like budding bacteria. *Archives of Microbiology*. Vol. 123. 213–226.
- Ghiorse, W. C. 1989. Manganese and iron as physiological electron donors and acceptors in aerobic-anaerobic transition zones. In *Microbial Mats: Physiological Ecology of Benthic Microbial Communities*. Y. Cohen and E. Rosenberg, Eds. Washington DC: American Society for Microbiology. 163–169.

- Giam, C. S., Chah, H. S., and Neff, G. S. 1978. Phthalate ester plasticizers: A new class of marine pollutants. *Science*. Vol. 199. 419–421.
- Gottschalk, G. 1986. *Bacterial Metabolism*, 2nd ed. New York: Springer-Verlag. 178–282.
- Gray L. E., Wolf, C. and Lambright, C. 1999. Administration of potentially antiandrogenic pesticides (procymidone, linuron, iprodione, chlozolinate, *p, p'*-DDE, and ketonazole) and toxic substances (dibutyl- and diethylhexyl phthalate, PCB 169, and ethane dimethane sulphonate) during sexual differentiation produces diverse profiles of reproductive malformations in the male rat. *Toxicology and Industrial Health*. Vol. 15. 94–118.
- Gu, J.-D. 2003a. Microbiological deterioration and degradation of synthetic polymeric materials: recent research advances. *International Biodeterioration and Biodegradation*. Vol. 52. 69–91.
- Gu, J.-D. 2003b. Microbial deterioration of synthetic and biological polymers used in engineering and construction. In *Biopolymers. Vol. 10: Special Applications and General Aspects*. A. Steinbüchel, Ed. Weinheim: Wiley-VCH Verlag GmbH. 97–138.
- Gu, J.-D. 2003c. Microorganisms and microbial biofilms in the degradation of polymeric materials. Paper 3570 in *Corrosion/2003*. paper 3570. Houston: NACE International.
- Gu, J.-D. and Cheung, K. H. 2001. Phenotypic expression of *Vogesella indigofura* upon exposure to hexavalent chromium, Cr⁶⁺. *World Journal of Microbiology and Biotechnology*. Vol. 17. 475–480.
- Gu, J.-D. and Mitchell, R. 1995. Use of indigenous bacteria and their metabolites for zebra mussel (*Dreissena polymorpha*) control. *Dreissena*. Vol. 6. 5–8.
- Gu, J.-D. and Mitchell, R. 2001. Antagonism of bacterial extracellular metabolites to the freshwater fouling zebra mussels, *Dreissena polymorpha*. *The Journal of Microbiology*. Vol. 39. 133–138.
- Gu, J.-D. and Mitchell, R. 2002. Indigenous microflora and opportunistic pathogens of the freshwater zebra mussels, *Dreissena polymorpha*. *Hydrobiologia*. Vol. 474. 81–90.
- Gu, J.-D. and Mitchell, R. 2004. Degradation of water-soluble polyester polyurethane by *Rhodococcus* species h07 isolated from soil. *Corrosion/2004*, Paper No. 4584, Houston: NACE International.
- Gu, J.-D., Fan, Y., and Mitchell, R. 2001a. Biological control of zebra mussels, *Dreissena polymorpha* by indigenous pathogenic bacteria and their extracellular metabolites. *Chinese Journal of Applied and Environmental Biology*. Vol. 7. 572–576.
- Gu, J.-D., Maki, J. S., and Mitchell, R. 1994. Biological control of zebra mussel *Dreissena polymorpha* by indigenous bacteria and their products. In *The 4th International Zebra Mussel Conference Proceedings*. Madison, Wisconsin. 219–229.
- Gu, J.-D., Ford, T. E., Thorp, K. E. G., and Mitchell, R. 1994a. Microbial degradation of polymeric materials. In *Proceedings of the Tri-Service Conference on Corrosion*. June 21–23, Orlando, FL. T. Naguy, Ed. Washington DC: U.S. Government Printing House. 291–302.
- Gu, J.-D., Ford, T. E., Mitton, B., and Mitchell, R. 1995b. Microbial degradation of complex polymeric materials used as insulation in electronic packaging materials. Paper 202 in *Corrosion/95*. Paper 202. Houston: NACE International.
- Gu, J.-D., Ford, T. E., Thorp, K. E. G., and Mitchell, R. 1995c. Microbial biodeterioration of fiber reinforced composite materials. In *1995 International Conference on Microbial Influenced Corrosion*. P. Angell, S. W. Borenstein, R. A. Buchanan, S. C. Dexter, N. J. E. Dowling, B. J. Little, C. D. Lundin, M. B. McNeil, D. H. Pope, R. E. Tatnall, D. C. White, and H. G. Zigenfuss, Eds., Houston: NACE International. 25/1–7.
- Gu, J.-D., Ford, T. E., and Mitchell, R. 1996a. Susceptibility of electronic insulating polyimides to microbial degradation. *Journal of Applied Polymer Science*. Vol. 62. 1,029–1,034.
- Gu, J.-D., Ford, T., Thorp, K., and Mitchell, R. 1996b. Microbial growth on fiber reinforced composite materials. *International Biodeterioration and Degradation*. Vol. 39: 197–204.
- Gu, J.-D., Lu, C., Thorp, K., Crasto, A., and Mitchell, R. 1996c. Susceptibility of polymeric coatings to microbial degradation. Paper 275 in *Corrosion/96*. Paper 275. Houston: NACE International.
- Gu, J.-D., Lu, C., Thorp, K., Crasto, A., and Mitchell, R. 1997a. Fiber-reinforced polymeric composite materials are susceptible to microbial degradation. *Journal of Industrial Microbiology and Biotechnology*. Vol. 18. 364–369.
- Gu, J.-D., Lu, C., Thorp, K., Crasto, A., and Mitchell, R. 1997b. Fungal degradation of fiber-reinforced composite materials. *Materials Performance*. Vol. 36. 37–42.
- Gu, J.-D., Maki, J. S., and Mitchell, R. 1997c. Microbial biofilms and their role in the induction and inhibition of invertebrate settlement. In *Zebra Mussels and Aquatic Nuisance Species*. F. M. D'Itri, Ed. Chelsea, Michigan: Ann Arbor Press. 343–357.
- Gu, J.-D., Mitton, D. B., Ford, T. E., and Mitchell, R. 1998a. Microbial degradation of polymeric coatings measured by electrochemical impedance spectroscopy. *Biodegradation*. Vol. 9. 35–39.
- Gu, J.-D., Roman, M., Esselman, T., and Mitchell, R. 1998b. The role of microbial biofilms in deterioration of space station candidate materials. *International Biodeterioration and Biodegradation*. Vol. 41, 25–33.
- Gu, J.-D., Ford, T. E., and Mitchell, R. 2000a. Microbial corrosion of metals. In *The H. H. Uhlig Corrosion Handbook*, 2nd ed. W. Revie, Ed. New York: John Wiley & Sons, Inc. 915–927.
- Gu, J.-D., Ford, T. E., and Mitchell, R. 2000b. Microbial corrosion of concrete. In *The H. H. Uhlig Corrosion Handbook*, 2nd ed. W. Revie, Ed. New York: John Wiley & Sons, Inc. 477–491.
- Gu, J.-D., Ford, T. E., and Mitchell, R. 2000c. Microbial degradation of materials: General processes In *The H. H. Uhlig Corrosion Handbook*, 2nd ed. W. Revie, Ed. New York: John Wiley & sons, Inc. 349–365.

- Gu, J.-D., Ford, T. E., Mitton, D. B., and Mitchell, R. 2000d. Microbial degradation and deterioration of polymeric materials. In *The H. H. Uhlig Corrosion Handbook*, 2nd ed. W. Revie, Ed. New York: John Wiley & Sons, Inc. 439–460.
- Gu, J.-D., Belay, B., and Mitchell, R. 2001b. Protection of catheter surfaces from adhesion of *Pseudomonas aeruginosa* by a combination of silver ions and lectins. *World Journal of Microbiology and Biotechnology*. Vol. 17. 173–179.
- Guezennec, J., Ortega-Morales, O., Ragueneas, G., and Geesey, G. 1998. Bacterial colonization of artificial substrate in the vicinity of deep-sea hydrothermal vents. *FEMS Microbiology Ecology*. Vol. 26. 89–99.
- Haag, W. R. and Garton, D. W. 1992. Synchronous spawning in a recently established population of the zebra mussel, *Dreissena polymorpha*, in western Lake Erie, USA. *Hydrobiology*. Vol. 234. 103–110.
- Hadley, R. F. 1948. Corrosion by micro-organisms in aqueous and soil environments. In *The Corrosion Handbook*. H. H. Uhlig, Ed. New York: John Wiley & Sons, Inc. 466–481.
- Hahn, P. O., Rubloff, G. W., Bartha, J. W., Legoues, F., Tromp, R., and Ho, P. S. 1985. Chemical interactions at metal-polymer interfaces. *Materials Research Society Symposium Proceedings*. Vol. 40. 251–263.
- Hamilton, W. A. 1985. Sulphate-reducing bacteria and anaerobic corrosion. *Annual Reviews of Microbiology*. Vol. 39. 195–217.
- Hanert, H. H. 1981. The genus *Siderocapsa* and other iron- or manganese-oxidizing eubacteria. In: *The Prokaryotes*. M. P. Starr, H. Stolp, H. G. Trüper, A. Balow, and H.G. Schlegel, Eds. New York: Springer-Verlag. 1,049–1,060.
- Harder, T. and Qian, P. Y. 1999. Amino acids as conspecific chemical signals for larval attachment and metamorphosis in the serpulid polychaete *Hydroides elegans* (Haswell). *Marine Ecology Progress Series*. Vol. 179. 259–271.
- Harder, T. and Qian, P. Y. 2000. Waterborne compounds from the green seaweed *Ulva reticulata* as inhibitive cues for larval attachment and metamorphosis in the polychaete *Hydroides elegans*. *Biofouling*. Vol. 16. 205–214.
- Hebert, P. D., Muncaster, B. W., and Mackie, G. L. 1989. Ecological and genetic studies on *Dreissena polymorpha* (Pallas): a new mussel in the Great Lakes. *Canadian Journal of Fish and Aquatic Sciences*. Vol. 46. 1,587–1,591.
- Hernandez, G., Kucera, V., Thierry, D., Pedersen, A., and Hermansson, M. 1994. Corrosion inhibition of steel by bacteria. *Corrosion*. Vol. 50. 603–608.
- Hespell, R. B. and O'Bryan-Shah, P. J. 1988. Esterase activities in *Butyrivibrio fibrisolvens* strains. *Applied and Environmental Microbiology*. Vol. 54. 1,917–1,922.
- Hill, E. C. 1987. *Microbial Problems in the Off-Shore Oil Industry*. London: Institute of Petroleum. 25–28.
- Hofmann, D. K., Neumann, R., and Henne, K. 1978. Strobilation, budding, and initiation of scyphistoma morphogenesis in the rhizostome *Cassiopea andromeda* (Cnidaria: Scyphozoa). *Marine Biology*. Vol. 47. 161–176.
- Holland, K. T., Knapp, J. S., and Shoesmith, J. G. 1986. Industrial Applications of Anaerobes. In *Anaerobic Bacteria*, K. T. Holland, J.S. Knapp, and J. G. Shoesmith, Eds. New York: Chapman and Hall. 165–188.
- Holmström, C., Rittschof, D., and Kjelleberg, S. 1992. Inhibition of settlement by larvae of *Balanus amphitrite* and *Ciona intestinalis* by a surface-colonizing marine bacterium. *Applied and Environmental Microbiology*. Vol. 58. 2,111–2,115.
- Illmer, P. and Schinner, F. 1999. Influence of nutrient solution on Al-tolerance of *Pseudomonas* sp. *FEMS Microbiology Letters*. Vol. 170. 187–190.
- Iman, S. H. and Gould, J. M. 1990. Adhesion of an amylolytic *Arthrobacter* sp. to starch-containing plastic films. *Applied and Environmental Microbiology*. Vol. 56. 872–876.
- Iverson, W. P. 1981. An overview of the anaerobic corrosion of underground metallic structures, evidence for a new mechanism. In *Technical Publication 741: Underground Corrosion*. E. Escalante, Ed. Philadelphia: American Society for Testing and Materials. Technical Publication No. 741. 33–52.
- Iverson, W. P. 1984. Mechanism of anaerobic corrosion of steel by sulfate reducing bacteria. *Materials Performance*. Vol. 23. 28–30.
- Iverson, W. P. and Olsen, G. J. 1983. *Microbial Corrosion*. London: The Metal Society. 46–53.
- Iverson, W. P., Olsen, G. J., and Heverly, L. F. 1986. The role of phosphorus and hydrogen sulfide in the anaerobic corrosion of iron and the possible detection of this corrosion by an electrochemical noise technique. In *Biological Influenced Corrosion*. S.C. Dexter, Ed. Houston: National Association of Corrosion Engineers. 154–161.
- Jayaraman, A., Earthman, J. C., and Wood, T. K. 1997. Corrosion inhibition by aerobic biofilms on SAE 1018 steel. *Applied Microbiology and Biotechnology*. Vol. 47. 62–68.
- Jayaraman, A., Ornek, D., Duarte, D. A., Lee, C. C., and Wood, T. K. 1999. Axenic aerobic biofilms inhibit corrosion of copper and aluminum. *Applied Microbiology and Biotechnology*. Vol. 52. 787–790.
- Jensen, R. J. 1987. Polyimides as interlayer dielectrics for high-performance interconnections of integrated circuits. In *Polymers for High Technology: Electronics and Photonics*. M.J. Bouwden and S. R. Turner, Eds. Washington DC: American Chemical Society., vol. ACS Symposium Series 346, 466–483.
- Jensen, R. A. 1992. Marine bioadhesive: Role for chemosensory recognition in a marine invertebrate. *Biofouling*. Vol. 5. 177–193.
- Jobling S., Reynolds, T., and White, R. 1995. A variety of environmentally persistent chemicals, including some phthalate plasticizers, are weakly estrogenic. *Environmental Health Perspectives*. Vol. 103 (Supplement 7). 582–587.
- Karlsson, S., Ljungquist, O., and Albertsson, A. C. 1988. Biodegradation of polyethylene and the influence of surfactants. *Polymer Degradation and Stability*. Vol. 21. 237–250.
- Kaspar, H. F. and Mountfort, D. O. 1995. Microbial production and degradation of γ -aminobutyric acid (GABA) in the abalone larval settlement habitat. *FEMS Microbiology Ecology*. Vol. 17. 205–212.

- Kirchmann, D. and Mitchell, R. 1981. A biochemical mechanism for marine biofouling. *Ocean*. September. 537–541.
- Kirchman, D., Graham, S. Reish, D., and Mitchell, R. 1982a. Bacteria induce settlement and metamorphosis of *Janua (dextiospira) brasiliensis* Grube (Polychaeta: Spirorbidae). *Journal of Experimental Biology and Ecology*. Vol. 56. 153–163.
- Kirchman, D., Graham, S., Reish, D., and Mitchell, R. 1982b. Lectins may mediate in the settlement and metamorphosis of *Janua (dextiospira) brasiliensis* Grube (Polychaeta: Spirorbidae). *Marine Biology Letters*. Vol. 3. 131–142.
- Kirchman, D. and Mitchell, R. 1983. Biochemical interactions between microorganisms and marine fouling invertebrates. In *Biodeterioration* 5. T. A. Oxley and S. Barry, Eds. New York: John Wiley & Sons, Inc. 281–290.
- Kirchman, D. and Mitchell, R. 1984. Possible role of lectins in the settlement and metamorphosis of marine invertebrate larvae on surfaces coated with bacteria. In *Bacteriologie Marine No. 331, Proceedings of the Colloques Internationaux du Centre National de la Recherche Scientifique*. Marseille, 1982. 173–177.
- Kon-ya, K., Shimidzu, N., Otaki, N., Yokoyama, A., Adachi, K., and Miki, W. 1995. Inhibitory effect of bacterial ubiquinones on the settling of barnacle, *Balanus amphitrite*. *Experientia*. Vol. 51. 153–155.
- Kelley, K., Ishino, Y., and Ishida, H. 1987. Fourier transform IR reflection techniques for characterization of polyimide films on copper substrates. *Thin Solid Films*. Vol. 154. 271–279.
- Knudsen, J. G. 1981. Fouling of heat transfer surfaces. In *Power Condenser Heat Transfer Technology*. New York: Hemisphere Publishing. 57–82.
- Kobrin, G. 1993. *A Practical Manual on Microbiological Influenced Corrosion*. Houston: NACE International. 68–72.
- Koch, G. H., Brouger, M. P. H., Thompson, N. G., Virmani, Y. P., and Payer, J. H. 2002. *Corrosion Costs and Preventive Strategies in the United States*. Publication FHWA-RD-01–156. Kanham, MD: Federal Highway Administration.
- Krieg, N. R. and Holt, J. G. 1984. *Bergey's Manual of Systematic Bacteriology, Vol. 1*. Baltimore: Williams and Wilkins.
- Kuenen, J. G. and Tuovinen, O. H. 1981. The genera *Thiobacillus* and *Thiomicrospira*. In *The Prokaryotes*. M. P. Starr, H. Stolp, H. G. Trüper, A. Balow, and H. G. Schlegel, Eds. New York: Springer-Verlag. 1,023–1,036.
- Lai, J. H. 1989. *Polymers for Electronic Applications*. Boca Ration, FL: CRC Press. 23–24.
- Lau, K. K. and Qian, P. Y. 2000. Inhibitory effect of phenolic compounds and marine bacteria on larval settlement of the barnacle *Balanus amphitrite* Darwin. *Biofouling*. Vol. 16. 47–58.
- Lau, S. C. K. and Qian, P. Y. 2001. Larval settlement in the serpulid polychaete *Hydroides elegans* (Haswell) in response to bacterial film: An investigation of the nature of putative larval settlement cue. *Marine Biology*. Vol. 138. 321–328.
- Lau, S. C. K., Chen, F., and Qian, P. Y. 2001. The identities and larval settlement induction activities of bacteria isolated from natural biofilms. *Marine Ecology Progress Series*. (in press).
- Lau, C. K. L., Mak, K. K. W., Chen, F., and Qian, P. Y. 2002. Bioactivity of bacterial strains isolated from marine biofilms in Hong Kong waters from the induction of larval settlement in the marine polychaete *Hydroides elegans*. *Marine Ecology Progress Series*. Vol. 226. 301–310.
- Lee, W., Lewandowski, Z., Okabe, S., Characklis, W. G., and Avci, R. 1993a. Corrosion of mild steel underneath aerobic biofilms containing sulfate-reducing bacteria, Part I: At low dissolved oxygen concentration. *Biofouling*. Vol. 7. 197–216.
- Lee, W., Lewandowski, Z., Morrison, M., Characklis, W. G., Avci, R., and Nielsen, P. H. 1993b. Corrosion of mild steel underneath aerobic biofilms containing sulfate-reducing bacteria, part II: At high dissolved oxygen concentration. *Biofouling*. Vol. 7. 217–239.
- Lee, W., Lewandowski, Z., Nielsen, P. H., and Hamilton, W. A. 1995. Role of sulfate-reducing bacteria in corrosion of mild steel: A review. *Biofouling*. Vol. 8. 165–194.
- Levy, S. B. 1992. *The Antibiocti Paradox: How Miracle Drugs are Destroying the Miracle*. New York: Plenum Press. 279.
- Li, D. and Lü, R. 1990. Purification and properties of periplasmic hydrogenase from *Desulfovibrio vulgaris* D-2. *Acta Microbiologia Sinica*. Vol. 30. 267–272.
- Lin, C. and Olson, B. H. 1995. Occurrence of *cop*-like copper resistance genes among bacteria isolated from a water distribution system. *Canadian Journal of Microbiology*. Vol. 41. 642–646.
- Little, B., Wagner, P., Gerchakov, S. M., Walch, M., and Mitchell, R. 1986a. The involvement of a thermophilic bacterium in corrosion processes. *Corrosion*. Vol. 42. 533–536.
- Little, B. J., Wagner, P., Maki, J. S., and Mitchell, R. 1986b. Factors influencing the adhesion of microorganisms to surfaces. *Journal of Adhesion*. Vol. 20. 187–210.
- Little, B. J. and Depalma, J. R. 1988. Marine biofouling. *Treatise on Material Science and Technology*. Vol. 28. 89–119.
- Little, B., Wagner, P., Characklis, W. G., and Lee, W. 1990. Microbial corrosion. In *Biofilms*. W. G. Characklis and K. C. Marshall, Eds. New York: John Wiley & Sons, Inc. 635–670.
- Little, B. J., Wagner, P., and Jones-Meehan, J. 1994. Sulfur isotopic fractionation in sulfite corrosion products as an indicator for microbiologically influenced corrosion (MIC). In: *Microbiologically Influenced Corrosion Testing, Vol. ASTM STP 1232*. J. R. Kearns and B. J. Little, Eds. Philadelphia: American Society for Testing and Materials. 180–187.
- Lock, M. A. 1993. Attached microbial communities in rivers. In: *Aquatic Microbiology: An Ecological Approach*. T. E. Ford, Ed. Boston: Blackwell Scientific Publications. 113–138.
- Lovley, D. R., Stolz, J. F., Nord, G. L., and Philips, E. J. P. 1987. Anaerobic production of magnetite by a dissimilatory iron-reducing microorganism. *Nature (London)*. Vol. 330. 252–254.
- Mackie, G., Gibbons, W. N., Muncaster, B. W., and Gray, I. M. 1989. *The Zebra Mussel, Dreissena Polymorpha: A Synthesis of European Experiences and A Preview for North America*. Ontario: Ontario Ministry of the Environment, Water Resources Section, Great Lakes Branch.

- Madigan, M. T., Martinko, J. M., and Parker, J. 2000. *Brock Biology of Microorganisms*, 9th Ed. Upper Saddle River, NJ: Prentice-Hall.
- Maki, J. S., Rittschof, D., Schmidt, A. R., Snyder, A. S., and Mitchell, R. 1989. Factors controlling attachment of bryozoan larvae: A comparison of bacterial films and unfiled surfaces. *Biological Bulletin*. Vol. 177. 295–302.
- Maki, J. S., Little, B. J., Wagner, P., and Mitchell, R. 1990a. Biofilm formation on metal surfaces in Antarctic waters. *Biofouling*. Vol. 2. 27–38.
- Maki, J. S., Rittschof, D., Samuelson, M. –O., Szewzyk, U., Yule, A. B., Kjelleberg, S., Costlow, J. D., and Mitchell, R. 1990b. Effect of marine bacteria and their exopolymers on attachment of barnacle cypris larvae. *Bulletin of Marine Science*. Vol. 46. 499–511.
- Maki, J. S. and Mitchell, R. 1985. Involvement of lectins in the settlement and metamorphosis of marine invertebrate larvae. *Bulletin of Marine Science*. Vol. 37. 675–683.
- Maki, J. S. and Mitchell, R. 1986. The function of lectins in interactions among marine bacteria, invertebrates, and algae. In *Microbial Lectins and Agglutinins: Properties and Biological Activity*. D. Mirelman, Ed. New York: John Wiley & Sons, Inc. 409–425.
- Maki, J. S., Rittschof, D., Costlow, J. D., and Mitchell, R. 1988. Inhibition of attachment of larval barnacles, *Balanus amphitrite*, by bacterial surface films. *Marine Biology* Vol. 97. 199–206.
- Maki, J. S., Rittschof, D., and Mitchell, R. 1992. Inhibition of larval barnacle attachment to bacterial films: an investigation of physical properties. *Microbial Ecology*. Vol. 23. 97–106.
- Maki, J. S., Rittschof, D., Schmidt, A. R., Snyder, A. G., and Mitchell, R. 1990a. Factors controlling attachment of bryozoan larvae: A comparison of bacterial films and unfiled surfaces. *Biological Bulletin*. Vol. 177. 295–302.
- Maki, J. S., Yule, A. B., Rittschof, D., and Mitchell, R. 1994. The effect of bacterial films on the temporary adhesion and permanent fixation of cypris larvae, *Balanus amphitrite* Darwin. *Biofouling*. Vol. 8. 121–131.
- Mansfeld, F. 1995. Use of electrochemical impedance spectroscopy for the study of corrosion by polymer coatings. *Journal of Applied Electrochemistry*. Vol. 25. 187–202.
- Marshall, K. C., Stout, R., and Mitchell, R. 1971. Mechanism of the initial events in the sorption of marine bacteria to surfaces. *Journal of General Microbiology*. Vol. 68. 337–348.
- Marshall, K. C. 1992. Biofilms: An overview of bacterial adhesion, activity, and control at surfaces. *ASM News*. Vol. 58. 202–207.
- Marshall, K. C. 1985. Mechanisms of bacterial adhesion at solid-water interfaces. In *Bacterial Adhesion*. D. C. Savage and M. Fletcher, Eds. New York: Plenum Press. 133–161.
- Marshall, B. M., Petrowski, D., and Levy, S. B. 1990. Inter- and intraspecies spread of *E. coli* in a farm environment in the absence of antibiotic usage. *Proceedings of National Academy of Sciences (U.S.A.)*. Vol. 87. 6,609–6,613.
- Mattila, K., Carpen, L., Hakkarainen, T., and Salkinoja-Salonen, M. S. 1997. Biofilm development during ennoblement of stainless steel in Baltic Sea water: A microscopic study. *International Biodeterioration and Biodegradation*. Vol. 40. 1–10.
- McLean, R. J. and Brown, R. M. 1974. Cell surface differentiation of *Chlamydomonas* during gametogenesis. *Developmental Biology*. Vol. 36. 279–285.
- Meints, R. H. and Pardy, R. L. 1980. Quantitative demonstration of cell surface involvement in a plant-animal symbiosis: Lectin inhibition of reassociation. *Journal of Cell Science*. Vol. 43. 239–251.
- Milstein, O., Gersonde, R., Huttermann, A., Chen, M. –J., and Meister, J. J. 1992. Fungal biodegradation of lignopolystyrene graft copolymers. *Applied and Environmental Microbiology*. Vol. 58. 3,225–3,232.
- Mirelman, D. and Ofek, I. 1986. Introduction of microbial lectins and agglutinins. In *Microbial Lectins and Agglutinins: Properties and Biological Activity*. D. Mirelman, Ed. New York: John Wiley & Sons, Inc. 1–19.
- Mitchell, R. and Maki, J. S. 1989. Microbial surface films and their influence on larval settlement and metamorphosis in the marine environment. In *Marine Biodeterioration: Advanced Techniques Applicable to the Indian Ocean*. M. F. Thompson, R. Sarojini, and R. Nagabhushanam, Eds. New Delhi: Oxford & IBH Publishing, PVT Ltd. 489–497.
- Mitchell, R., Gu, J. –D, Roman, M., and Soukup, S. 1996. Hazards to space missions from microbial biofilms. In *Biodeterioration and Biodegradation*. W. Sand, Ed. Frankfurt: VCH Verlagsgesellschaft. DECHEMA Monographs, Vol. 133. 3–16.
- Mitchell, R. 1984a. Colonization by higher organisms. In *Microbial Adhesion and Aggregation*. K. C. Marshall, Ed. Berlin: Springer-Verlag. 189–200.
- Mitchell, R. and Kirchman, d. 1984b. The Microbial ecology of marine surfaces. In *Marine Biodeterioration: An Interdisciplinary Study*. J. D. Costlow and R. C. Tipper, Eds. Annapolis, Maryland: Naval Institute Press. 49–56.
- Mitchell, R. and Maki, J. S. 1988. Microbial surface films and their influence on larval settlement and metamorphosis in the marine environment. In *Marine Biodeterioration: Advanced Techniques Applicable to the Indian Ocean*. M. Thompson, R. Sarojini, and R. Nagabhushanam, Eds. New Delhi: Oxford & IBH Publishing Co. 489–497.
- Mittelman, M. W. and Geesey, G. 1985. Copper-binding characteristics of exopolymers from a freshwater-sediment bacterium. *Applied and Environmental Microbiology*. Vol. 49. 846–851.
- Mittelman, M. W. 1995a. Biofilm development in purified water systems. In *Microbial Biofilms*. H. M. Lappin-Scott, and J. W. Costerton, Eds. Cambridge, UK: Cambridge University Press. 133–147.
- Mitton, B., Ford, T. E., LaPointe, E., and Mitchell, R. 1993. Biodegradation of complex polymeric materials. Paper 296 in *Corrosion/93*. Paper 296. Houston: NACE International.

- Mitton, D. B., Latanison, R. M., and Bellucci, F. 1996. The effects of post-cure annealing on the protective properties of polyimides on chromium substrates. *Journal of Electrochemical Society*. Vol. 143. 3,307–3,316.
- Mitton, D. B., Toshima, S., Latanison, R. M., Bellucci, F., Ford, T. E., Gu, J. D., and Mitchell, R. 1998. Biodegradation of polymer-coated metallic substrates. In *Organic Coatings for Corrosion Control*. G. P. Bierwagen, Ed. Washington DC: American Chemistry Society. ACS Symposium Series. 689, 211–222.
- Morse, D. E., Hooker, N., Duncan, H., and Jensen, L. 1979. γ -aminobutyric acid, a neurotransmitter, induces planktonic abalone larvae to settle and begin metamorphosis. *Science*. Vol. 204. 407–410.
- Müller, W. E. G., Kurelec, B., Zahn, R. K., Müller, I., Vaith, P., and Uhlenbruck, G. 1979. Aggregation of sponge cells: Function of a lectin in its homologous biological system. *Journal of Biochemistry*. Vol. 254. 7,479–7,481.
- Müller, W. E. G., Zahn, R. K., Kurelec, B., Lucu, C., Müller, I., and Uhlenbruck, G. 1981. Lectin, a possible basis for symbiosis between bacteria and sponges. *Journal of Bacteriology*. Vol. 145. 548–558.
- Nakajima-Kambe, T., Onuma, F., Kimpara, N., and Nakahara, T. 1995. Isolation and characterization of a bacterium which utilizes polyester polyurethane as a sole carbon and energy source. *FEMS Microbiology Letters*. Vol. 129. 39–42.
- Nelson, W. G. 1979. Observations on the settlement patterns of *Janua (Dexiospira) brasiliensis* (Polychaeta: Serpulidae). *Estuaries*. Vol. 2, 213–217.
- Neu, T. R., Swerhone, G. D. W., and Lawrence, J. R. 2001. Assessment of lectin-binding analysis for *in situ* detection of glycoconjugates in biofilm system. *Microbiology*. Vol. 147. 299–313.
- Neumann, R. 1979. Bacterial induction of settlement and metamorphosis in the planula larvae of *Cassiopea andromeda* (Cnidaria: Scyphozoa, Rhizostomeae). *Marine Ecology Progress Series*. Vol. 1. 21–28.
- Nieboer, E., Gibson, B. L., Oxman, A. D., and Kramer, J. R. 1995. Health effects of aluminum: A critical review with emphasis on aluminum in drinking water. *Environmental Reviews*. Vol. 3. 29–81.
- Nielsen, P. H., Lee, W., Lewandowski, Z., Morison, M., and Characklis, W. G. 1993. Corrosion of mild steel in an alternating oxic and anoxic biofilm system. *Biofouling*. Vol. 7. 267–284.
- Niazi, J. H., Prasad, D. T., and Karegoudar, T. B. 2001. Initial degradation of dimethylphthalate by esterases from *Bacillus* species. *FEMS Microbiology Letters*. Vol. 196. 201–205.
- Nozhevnikova, A. N., Kotsyurbenko, O. R., and Simankova, M. V. 1994. Acetogenesis. In *Acetogenesis at Low Temperature*. H. L. Drake, Ed. New York: Chapman and Hall. 416–431.
- NRC (National Research Council). 1987. *Agenda for Advancing Electrochemical Corrosion Science and Technology*. Publication NMAB438–2. Washington DC: National Academy Press. 87–96.
- Odian, G. 1991. *Principles of Polymerization*, 3rd Ed. New York: John Wiley & Sons, Inc. 691–745.
- Odom, J. M. 1993. Industrial and environmental activities of sulfate-reducing bacteria. In *The Sulfate-Reducing Bacteria: Contemporary Perspectives*. J. M. Odom and R. Singleton, Jr., Eds. New York: Springer-Verlag. 189–210.
- Odom, J. M. and Singleton, Jr., R. 1993. *The Sulfate-Reducing Bacteria: Contemporary Perspectives*. New York: Springer-Verlag. 289.
- Olesen, B.H., Avci, R., and Lewandowski, Z. 1998. Ennoblement of stainless steel studied by x-ray photoelectron spectroscopy. *Corrosion/98*. Paper 275. Houston: NACE International.
- Paradies, H. H., Haenbel, I., Fisher, W., and Wagner, D. 1990. *Microbial Induced Corrosion of Copper Pipes*. Report 444. New York: INCRA. 16.
- Paradies, H. H. 1995. Chemical and physical aspects of metal biofilms. In *Biorecovery and Biodegradation*. C. C. Gaylarde and H. A. Videla, Eds. Cambridge, UK: Cambridge University Press. 197–269.
- Pometto, III, A. L., Lee, B., and Johnson, K. E. 1992. Production of an extracellular polyethylene-degrading enzyme(s) by *Streptomyces* species. *Applied and Environmental Microbiology*. Vol. 58. 731–733.
- Pometto, III, A. L., Johnson, K. E., and Kim, M. 1993. Pure-culture and enzymatic assay for starch-polyethylene degradable plastic biodegradation with *Streptomyces* species. *Journal of Environmental Polymer Degradation*. Vol. 1. 213–221.
- Pope, D. H., Duquette, D., Wayner, Jr., P. C., and Johannes, A. H. 1989. In *Microbiologically Influenced Corrosion: A State-of-the-Art Review*, 2nd Ed. MTI Publication 13. Houston: National Association of Corrosion Engineers. Vol. 4. 1–3.
- Postgate, J. R. 1984. *The Sulfate-Reducing Bacteria* 2nd Ed. New York: Cambridge University Press. 132–152.
- Potekhina, J. S., Sherisheva, N. G., Povetkina, L. P., Pospelov, A. P., Rakitina, T. A., Warnecke, F., and Gottschalk, G. 1999. Role of microorganisms in corrosion inhibition of metals in aquatic habitats. *Applied Microbiology and Biotechnology*. Vol. 52. 639–646.
- Qian, P.Y., Rittschof, D., and Sreedhar, B. 2000. Macrofouling in unidirectional flow: Miniature pipes as experimental models for studying the interaction of flow and surface characteristics on the attachment of barnacle, bryozoan and polychaete larvae. *Marine Ecology Progress Series*. Vol. 207. 109–121.
- Qian, P.Y., Rittschof, D., Sreedhar, B., and Chia, F. S. 1999. Macrofouling in unidirectional flow: miniature pipes as experimental models for studying the effects of hydrodynamics on invertebrate larval settlement. *Marine Ecology Progress Series*. Vol. 191. 141–151.
- Qiu, J. W. and Qian, P. Y. 1999. Effects of salinity and temperature on the life-history of *Balanus amphitrite*: Effects of past experience. *Marine Ecology Progress Series*. Vol. 188. 123–132.
- Ram, J. L. and Walker, J. U. 1993. Effects of deionized water on viability of the zebra mussel, *Dreissena polymorpha*. *Comparative Biochemistry and Physiology*. Vol. 105C. 409–414.

- Ramcharan, C. W., Padilla, D. K., and Dodson, S. I. 1992. A multivariate model for predicting population fluctuations of *Dreissena polymorpha* in North American Lakes. *Canadian Journal of Fisheries and Aquatic Sciences*. Vol. 49. 150–158.
- Roe, F. L., Lewandowski, Z., and Funk, T. 1996. Simulation of microbiologically influenced corrosion by depositing extracellular biopolymers on mild steel surfaces. *Corrosion*. Vol. 52. 744–752.
- Ross, J. 1994. An aquatic invader is running amok in U.S. waterways. *Smithsonian*. Vol. 24. 40–51.
- Rittschof, D., Lai, C. H., Kok, L. M., and Teo, S. L. M. 2003. Pharmaceuticals as antifoulants: Concept and principles. *Biofouling*. Vol. 19. 207–212.
- Rittschof, D., Maki, J., Mitchell, R., and Costlow, J. D. 1986. Ion and neuropharmacological studies of barnacle settlement. *Netherlands Journal of Sea Research*. Vol. 20. 269–275.
- Rodriguez, S. R., Riquelme, C., Campos, E. O., Chavez, P., Brandan, E., and Inestrosa, N. C. 1995. Behavioral responses of *Concholepas concholepas* (Bruquière, 1789) larvae to natural and artificial settlement cues and microbial films. *Biological Bulletin*. Vol. 189. 272–279.
- Sakaguchi, T., Burgess, J. G., and Matsunaga, T. 1993. Magnetite formation by a sulphate-reducing bacterium. *Nature (London)*. Vol. 253. 47–49.
- Sanders, P. F. and Hamilton, W. A. 1986. Biological and corrosion activities of sulphate-reducing bacteria in an industrial process plant. In *Biologically Induced Corrosion: Proceedings of the International Conference on Biologically Induced Corrosion*. S.C. Dexter, Ed. Houston: National Association of Corrosion Engineers. 47–68.
- Santini, J. M., Sly, L. I., Schnagi, R. D., and Macy, J. M. 2000. A new chemolithoautotrophic arsenite-oxidizing bacterium isolated from a gold mine: Phylogenetic, physiological, and preliminary biochemical studies. *Applied and Environmental Microbiology*. Vol. 66. 92–97.
- Schembri, M. A., Kjærgaard, K., and Klemm, P. 1999. Bioaccumulation of heavy metals by fimbrial designer adhesions. *FEMS Microbiology Letters*. Vol. 170. 363–371.
- Schmidtt, C. R. 1986. Anomalous microbiological tuberculation and aluminum pitting corrosion—Case histories. In *Biologically Induced Corrosion: Proceedings of the International Conference on Biologically Induced Corrosion*. S.C. Dexter, Ed. Houston: National Association of Corrosion Engineers. 69–75.
- Schneider, D. W. 1992. A bioenergetics model of zebra mussel, *Dreissena polymorpha*, growth in the Great Lakes. *Canadian Journal of Fisheries and Aquatic Sciences*. Vol. 49. 1,406–1,416.
- Schüler, D. and Frankel, R. B. 1999. Bacterial magnetosomes: Microbiology, biomineralization and biotechnological applications. *Applied Microbiology and Biotechnology*. Vol. 52. 464–473.
- Schultzen-Lam, S., Harauz, G., and Beveridge, T. J. 1992. Participation of a cyanobacterial S layer in fine-grain mineral formation. *Journal of Bacteriology*. Vol. 174. 7,971–7,981.
- Sequeira, C. A. C. and Tiller, A. K. 1988. *Microbial Corrosion* Elsevier Science. London, New York, Vol. 1. 34–36.
- Severini, F., Gallo, R., and Ipsale, S. 1988. Environmental degradation of polypropylene. *Polymer Degradation Stability*. Vol. 22. 185–194.
- Shisko, J. F. 1975. *The life history of the annelid (Polychaeta: Serpulidae) Janus (Dexiospira) brasiliensis (Grube)*. Master's Thesis. Long Beach, California: California State University.
- Siedlarek, H., Wagner, D., Fischer, W. R., and Paradies, H. H. 1994. Microbiologically influenced corrosion of copper: The ionic transport properties of biopolymers. *Corrosion Science*. Vol. 36. 1,751–1,763.
- Singh, P. K., Schaefer, A. L., Parsek, M. R., Moninger, T. O., Welsh, M. J., and Greenberg, E. P. 2000. Quorum-sensing signals indicate that cystic fibrosis lungs are infected with bacterial biofilms. *Nature (London)*. Vol. 407. 762–764.
- Sneider, R. P., Chadwick, B. R., Pembrey, R., Jankowski, J., and Acworth, I. 1994. Retention of the gram-negative bacterium SW8 on surfaces under conditions relevant to the subsurface environment: Effects of conditioning films and substratum nature. *FEMS Microbiology Ecology*. Vol. 14. 243–254.
- Starkey, R. L. 1986. Anaerobic corrosion—Perspectives about causes. In *Biologically Induced Corrosion: Proceedings of the International Conference on Biologically Induced Corrosion*. S.C. Dexter, Ed. Houston: National Association of Corrosion Engineers. 3–7.
- Stern, R. V. and Howard, G. T. 2000. The polyester polyurethanase gene (pue A) from *Pseudomonas chlororaphis* encodes a lipase. *FEMS Microbiology Letters*. Vol. 185. 163–168.
- Stolz, J. F. and Oremland, R. S. 1999. Bacterial respiration of arsenic and selenium. *FEMS Microbiological Reviews*. Vol. 23. 615–627.
- Stumm, W. and Morgan, J. J. 1996. *Aquatic Chemistry: Chemical Equilibria and Rates in Natural Waters*, 3rd Ed. New York: John Wiley & Sons, Inc. 425–515.
- Sugio, T., Hirayama, K., Inagaki, K., Tanaka, H., and Tano, T. 1992. Molybdenum oxidation by *Thiobacillus ferrooxidans*. *Applied and Environmental Microbiology*. Vol. 58. 1,768–1,771.
- Tebo, B.M. and Obraztsova, A. Y. 1998. Sulfate-reducing bacterium grows with Cr(VI), U(VI), Mn(IV) and Fe(III) as electron acceptors. *FEMS Microbiology Letters*. Vol. 162. 193–198.
- Thorp, K. E. G., Crasto, A. S., Gu, J. -D., and Mitchell, R. 1994. Biodegradation of composite materials. In *Proceedings of the Tri-Service Conference on Corrosion*. T. Naguy, Ed. Washington DC: U.S. Government Printing House. 303–314.
- Thorp, K. E. G., Crasto, A. S., Gu, J. -D., and Mitchell, R. 1997. Contribution of Microorganisms to Corrosion. *Corrosion/97*. Paper 279. Houston: NACE International.
- Tomei, F. A., Maki, J. S., and Mitchell, R. 1985. Interactions in syntrophic associations of endospore-forming, butyrate-de-

- grading bacteria and H₂-consuming bacteria. *Applied and Environmental Microbiology*. Vol. 50. 1,244–1,250.
- Uhlig, H. H. 1971. *Corrosion and Corrosion Control*. New York: John Wiley & Sons, Inc.
- Uhlig, H. H. and Revie, R. W. 1985. *Corrosion and Corrosion Control: An Introduction to Corrosion Science and Engineering*, 3rd Ed. New York: John Wiley & Sons, Inc.
- U.S. Environmental Protection Agency. 1992. *Code of Federal Regulations*. 40CFR, Part 136. Washington, DC.
- Vaidya, R. U., Butt, D. P., Hersman, L. E., and Zurek, A. K. 1997. Effect of microbiological influenced corrosion on the tensile stress-stain response of aluminum and aluminum-particle reinforced aluminum composite. *Corrosion*. Vol. 53. 136–141.
- van Loosdrecht, M. C. M., Lyklema, J., Norde, W., and Zehnder, A. J. B. 1990. Influence of interfaces on microbial activity. *Microbiological Reviews*. Vol. 54. 75–87.
- van Westing, E. P. M., Ferrari, G. M., and De Witt, J. H., W. 1994. The determination of coating performance with impedance measurements. II: Water uptake of coatings. *Corrosion Science*. Vol. 36. 957–977.
- Verbicky, J. W. 1988. Polyimides. In *Encyclopedia of Polymer Science and Engineering*. New York: John Wiley & Sons, Inc. Vol. 12. 364–383.
- Verbiest, T., Burland, D. M., Jurich, M. C., Lee, V. Y., Miller, R. D., and Volksen, W. 1995. Exceptionally thermally stable polyimides for second-order nonlinear optical applications. *Science*. Vol. 268. 1,604–1,606.
- Videla, H. A. 1996. Corrosion inhibition by bacteria. In *Manual of Biocorrosion*. Boca Raton, Florida: CRC Press. 121–136.
- Wächtershäuser, G. 1988. Before enzymes and templates: Theory of surface metabolism. *Microbiological Reviews*. Vol. 52. 452–484.
- Wagner, P. 1995. Microbial degradation of stressed fiber reinforced polymeric composites. Paper 200 in *Corrosion/95*. Houston: NACE International.
- Wagner, P., Ray, R., Hart, K., and Little, B. 1996. Microbiological degradation of stressed fiber-reinforced polymeric composites. *Materials Performance*. Vol. 35. 79–82.
- Walch, M. and Mitchell, R. 1986. Microbial influence on hydrogen uptake by metals. In *Biologically Induced Corrosion: Proceedings of the International Conference on Biologically Induced Corrosion*. S.C. Dexter, Ed. Houston: National Association of Corrosion Engineers. 201–209.
- Walch, M., Ford, T. E., and Mitchell, R. 1989. Influence of hydrogen-producing bacteria on hydrogen uptake by steel. *Corrosion*. Vol. 45. 705–709.
- Wan, C. K., Sun, H., and Gu, J. -D. 2003. Surface properties of galvanized metals and attachment by the bacterium *Janthinobacterium lividum*. *Corrosion/2003*. Paper 3567. Houston: NACE International.
- Wang, J.-S. 1996. Hydrogen induced embrittlement and the effect of the mobility of hydrogen atoms. In *Hydrogen Effects in Materials*. A.W. Thompson and N.R. Moody, Eds. Warrendale, Pennsylvania: The Minerals, Metals and Materials Society. 61–75.
- Wang, P.-C., Mori, T., Komori, K., Sasatsu, M., Toda, K., and Ohtake, H. 1989. Isolation and characterization of an *Enterobacter cloacae* strain that reduces hexavalent chromium under anaerobic conditions. *Applied and Environmental Microbiology*. Vol. 55. 1,665–1,669.
- Wang, Y., Fan, Y., and Gu, J. -D. 2003a. Degradation of phthalic acid and dimethyl phthalate by aerobic microorganisms. *Chinese Journal of Applied and Environmental Biology*. Vol. 9. 63–66.
- Wang, Y., Fan, Y., and Gu, J. -D. 2003b. Microbial degradation of the endocrine-disrupting chemicals phthalic acid and dimethyl phthalate ester under aerobic conditions. *Bulletin of Environmental Contamination and Toxicology*. Vol. 71. 810–818.
- Wang, Y., Fan, Y., and Gu, J. -D. 2003c. Aerobic degradation of phthalic acid by *Comamonas acidovorans* Fy-1 and dimethyl phthalate ester by two reconstituted consortia from sewage sludge at high concentrations. *World Journal of Microbiology and Biotechnology*. Vol. 19. 811–815.
- Weimer, P. L., van Kavelaar, M. J., Michel, C. B., and Ng, T. K. 1988. Effect of phosphate on the corrosion of carbon steel and on the composition of corrosion products in two-stage continuous cultures of *Desulfovibrio desulfuricans*. *Applied and Environmental Microbiology*. Vol. 54. 386–396.
- Westlake, D. W. S., Semple, K. M., and Obuekwe, C. O. 1986. Corrosion by ferric iron-reducing bacteria isolated from oil production systems. In *Biologically Induced Corrosion: Proceedings of the International Conference on Biologically Induced Corrosion*. S.C. Dexter, Ed. Houston: National Association of Corrosion Engineers. 193–200.
- White, D. C., Nivens, D. E., Geesey, G. G., and Clarke, C. K. 1986. Role of aerobic bacteria and their extracellular polymers in the facilitation of corrosion: Use of Fourier Transforming Infrared Spectroscopy and “signature” phospholipid fatty acid analysis. In *Biologically Induced Corrosion. Proceedings of the International Conference on Biologically Induced Corrosion*. S.C. Dexter, Ed. Houston: National Association of Corrosion Engineers. 233–243.
- Whitfield, C. 1988. Bacterial extracellular polysaccharides. *Canadian Journal of Microbiology*. Vol. 34. 415–420.
- Widdel, F. 1988. Microbiology and ecology of sulfate- and sulfite-reducing bacteria. In *Biology of Anaerobic Microorganisms*. A. J. B. Zehnder, Ed. New York: John Wiley & Sons, Inc. 469–585.
- Widdel, F. 1992. Microbial corrosion In *Biotechnology Focus*. R. F. Finn, P. Prave, M. Schlingmann, W. Crueger, K. Esser, R. Thauer, and F. Wagner, Eds. Munich: Hanser Publishers. Vol. 3. 261–300.
- Wieczorek, S. K., Clare, A. S., and Todd, C. D. 1995. Inhibitory and facilitatory effects of microbial films on settlement of *Balanus amphitrite* larvae. *Marine Ecology Progress Series*. Vol. 119. 221–228.

- Wienczek, K. M. and Fletcher, M. 1995. Bacterial adhesion to hydroxyl- and methyl-terminated alkanethiol self-assembled monolayers. *Journal of Bacteriology*. Vol. 177. 1,959–1,966.
- Wilkinson, J. F. and Stark, G. H. 1956. The synthesis of polysaccharide by washed suspensions of *Klebsiella aerogenes*. *Proceedings of the Royal Physical Society of Edinburgh*. Vol. 25. 35–39.
- Wu, L. and Culver, D. A. 1991. Zooplankton grazing and phytoplankton abundance: An assessment before and after invasion of *Dreissena polymorpha*. *Journal of Great Lakes Research*. Vol. 17. 425–436.
- Young, L. Y. and Mitchell, R. 1973a. Negative chemotaxis of marine bacteria to toxic chemicals. *Applied Microbiology*. Vol. 25. 972–975.
- Young, L. Y. and Mitchell, R. 1973b. The role of microorganisms in marine fouling. *International Biodeterioration Bulletin*. Vol. 9. 105–109.
- Zachary, A., Taylor, M. E., Scott, F. E., and Colwell, R. R. 1980. Marine microbial colonization on material surfaces. In *Biodeterioration: Proceedings of the 4th International Biodeterioration Symposium*. T. A. Oxley, G. Becker, and D. Allsopp, Eds. London: Pitman Publishing. 171–177.
- Zhou, Z. and Brown, N. 1995. Slow crack growth in polyethylene gas pipes and resins. *Chinese Journal of Materials Research*. Vol. 9 (Supplement) 463–472. (in English).

CHAPTER 10

MATERIAL FLAMMABILITY

Marc L. Janssens

Department of Fire Technology, Southwest Research Institute, San Antonio, Texas

| | | | |
|---|-----|---|-----|
| 10.1 INTRODUCTION | 207 | 10.6 MATERIAL PROPERTY DATA | 219 |
| 10.2 THERMAL DEGRADATION OF MATERIALS | 208 | 10.7 COMPUTER MODELING OF MATERIAL DEGRADATION IN FIRES | 223 |
| 10.3 ELEMENTS OF MATERIAL FLAMMABILITY | 208 | 10.8 REFERENCES | 224 |
| 10.4 TESTS TO ASSESS MATERIAL FLAMMABILITY | 210 | | |
| 10.5 METHODS TO IMPROVE MATERIAL FLAMMABILITY | 217 | | |

10.1 INTRODUCTION

The subject of this chapter is the thermal degradation of synthetic and natural polymers under flaming fire conditions. In the United States, this is commonly referred to as “Material Flammability.” The more descriptive term, “Reaction to Fire,” is used in other parts of the world. To put this in perspective, it is useful to briefly describe the sequence of events in an uncontrolled compartment fire. The compartment could be a room in a building, a cabin on a cruise ship or commercial passenger aircraft, a passenger railcar, etc. A flaming fire in a compartment with adequate ventilation and no automatic or manual suppression typically consists of four stages.

1. *Initiation.* A compartment fire usually starts with the ignition of a small amount of combustible contents or finishes, for example due to an electrical fault or a smoldering cigarette.
2. *Pre-Flashover Stage.* Following initiation, the fire remains limited in size for some time and only one item or a small area is involved. As the fire grows, a hot smoke layer accumulates beneath the ceiling and temperatures gradually increase.
3. *Flashover.* Heat fluxes from the flame and hot smoke layer to the lower part of the compartment may become high enough to ignite common combustible materials. At this point, a rapid transition

occurs to a fully developed fire. This transition usually takes less than a minute and is referred to as flashover. When flashover occurs, it is no longer possible to survive in the fire compartment. Commonly-used criteria for the onset of flashover are a hot smoke layer temperature of 600 °C (1100 °F) and an incident heat flux at floor level of 20 kW/m² (1.8 Btu/s-ft²).

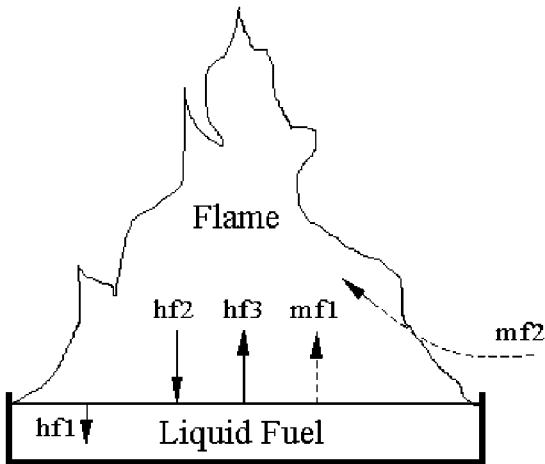
4. *Post-Flashover Stage.* Flashover leads to the fully developed stage of a fire in which all exposed combustibles in the compartment are involved. Typical temperatures in a fully developed fire are 800–1000 °C (1500–1800 °F), and corresponding incident heat fluxes range from 75–150 kW/m² (6.6–13.2 Btu/s-ft²). Once a fire reaches the post-flashover stage, it becomes a threat to the entire building and neighboring structures. Without intervention, the fire will eventually decay and burn out when all combustibles in the compartment are consumed.

Material flammability pertains to the first three stages of a fire (i.e., its ignition and contribution to fire growth toward flashover). Material flammability also includes characteristics that do not directly affect ignition and fire growth, but that are pertinent to the fire hazard to humans, such as the generation of vision-impairing smoke and toxic products of combustion.

10.2 THERMAL DEGRADATION OF MATERIALS

Combustion of liquid fuels takes place in the gas phase (see Figure 10.1). Fuel vapors mix with air and react with the oxygen. The reaction zone is usually luminous and is referred to as the flame. The liquid evaporates due to the heat feedback from the flame to the fuel surface. The temperature at the fuel surface is nearly equal to the boiling point of the liquid at atmospheric pressure. The burning rate of the fuel is determined by a heat balance at the fuel surface. The heat transferred by convection and radiation from the flame must be equal to the energy required to vaporize the fuel and the heat losses from the surface (conduction and convection into the liquid and radiation to the environment).

As with liquid fuels, polymers also produce volatiles that burn in the gas phase. However, the generation of these volatiles is much more complex because it involves thermal decomposition of the solid, also referred to as pyrolysis. Some polymers form a porous char layer at the exposed surface, which slows the pyrolysis rate down as burning progresses. Thermoplastics do not form a char and have a surface temperature that is nearly constant, similar to burning liquids.



hf1: conduction and convection into the liquid

hf2: flame radiation and convection

hf3: surface re-radiation

mf1: mass flow rate of fuel vapors

mf2: entrained air flow rate

FIGURE 10.1 Heat and mass flow in a liquid pool fire.

Four mechanisms contribute to the thermal decomposition of a polymer. Two of these reactions involve atoms in the main polymer chain. The remaining two reactions involve side chains or groups.

1. *Random Scission.* The most common reaction mechanism leading to the decomposition of simple thermoplastics involves the breaking of bonds in the polymer chain. These scissions can occur at random locations in the chain or at the ends. End-chain scissions result in the production of monomers, and this process is often referred to as unzipping. Random-chain scissions result in the generation of both monomers and oligomers (groups of 10 or less monomer units), and a variety of other compounds.
2. *Cross-Linking.* This is another reaction involving the main chain. The process consists of the formation of bonds between adjacent polymer chains and is very important in the creation of char.
3. *Elimination.* The main reactions involving side chains are referred to as elimination reactions. The bond between the side group and the main chain is broken. The resulting side group often reacts with other side groups that are cut off by elimination reactions. The resulting compounds are still relatively light and small enough to be volatile.
4. *Cyclization.* Two adjacent side groups form a bond that results in the formation of a cyclic structure. This process is also very important in the formation of a char matrix.

A more detailed discussion of polymer degradation in fires can be found in the literature [1].

10.3 ELEMENTS OF MATERIAL FLAMMABILITY

10.3.1 Ignition

When a combustible material is exposed to a constant external heat flux (radiative, convective, or a combination), its surface temperature starts to rise. The temperature inside the solid also increases with time, but at a slower rate. Provided the net flux into the material is sufficiently high, the surface temperature eventually reaches a level at which pyrolysis begins. The fuel vapors generated emerge through the exposed surface and mix with air in the gas

phase. Under certain conditions, this mixture exceeds the lower flammability limit and ignites.

The initiation of flaming combustion as described above is termed flaming ignition. Piloted ignition is initiated by a small pilot, such as a small gas flame (premixed or diffusion), an electric spark, or a glowing wire. Piloted ignition has been studied extensively over the past 40–50 years. These studies usually involved laboratory-scale experiments to measure the time to ignition at different levels of incident heat flux from a radiant panel. Autoignition occurs when no pilot is present and the hot surface of the solid triggers ignition of the flammable mixture of volatiles and air in the gas phase.

For some materials, or under certain conditions, combustion is not in the gas phase but in the solid phase. In such cases, no flame can be observed and the surface is glowing. This very different phenomenon is termed glowing ignition. Flaming combustion can be preceded by glowing ignition for char-forming materials exposed to low heat fluxes.

Spontaneous ignition or self-heating occurs when the heat generated by slow oxidation in a fuel exposed to air exceeds the heat losses to the surroundings. This leads to an increase in temperature, which in turn accelerates the chemical reaction and eventually leads to thermal runaway and glowing or flaming ignition. This process usually takes a long time (hours, days, or even longer). Whether spontaneous ignition occurs depends on the type, size, and porosity of the fuel array and the temperature of the surrounding air [2].

An exhaustive review of the theory and experimental data for different types of ignition phenomena was recently published by Babrauskas [3].

10.3.2 Surface Spread of Flame

Flames can spread over a solid surface in two modes (see Figure 10.2). The first mode is referred to as wind-aided flame spread. In this mode, flames spread in the same direction as the surrounding airflow. The second mode is referred to as opposed-flow flame spread, which occurs when flames spread in the opposite direction of the surrounding airflow. Flame spread in the upward direction is concurrent with the surrounding airflow and is therefore wind-aided. Flame spread in the downward direction is against the entrained airflow and is of the opposed-flow type. Upward or wind-aided flame spread is much faster and of greater concern than downward or opposed-flow flame spread because the flame heating extends over a much greater area.

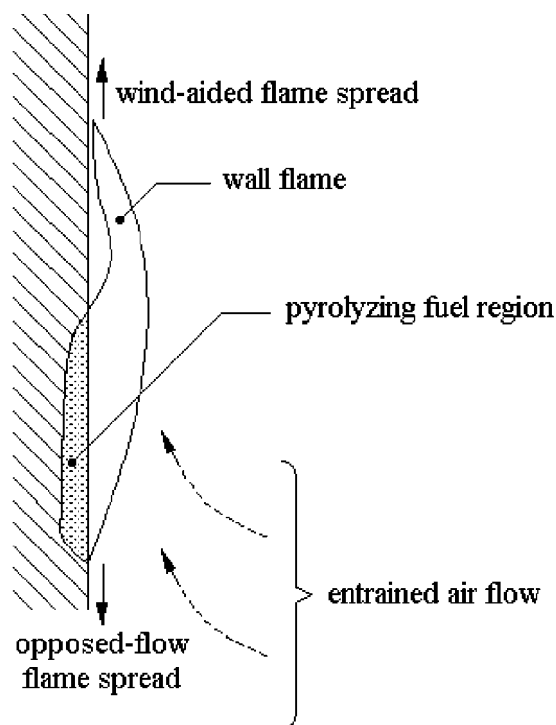


FIGURE 10.2 Modes of surface spread of flame.

10.3.3 Heat Release Rate

Heat release rate is the single most important variable in fire hazard [4]. Heat release rate at different heat fluxes can be measured in a bench-scale calorimeter. The most common devices used for this purpose rely on the oxygen consumption principle (i.e., the fact that for a wide range of materials undergoing complete combustion, a nearly constant amount of heat is released per unit mass of oxygen consumed) [5]. The average value is 13.1 kJ/g of O_2 consumed. Large-scale oxygen consumption calorimeters can be used to measure the heat release rate from room fires and burning objects such as furniture and various commodities.

10.3.4 Products of Combustion

Fires generate particulate matter, which reduces the intensity of light transmitted through smoke. The distance at which an exit sign can be seen through a smoke layer is a direct function of the concentration of particulates in the smoke [6].

Fires also generate toxic products of combustion, primarily in gaseous form. There are two types of toxic gases: narcotic gases such as carbon monoxide (CO) and hydrogen cyanide (HCN), and irritant gases such as hydrochloric acid (HCl) and hydrogen

bromide (HBr). Narcotic gases are absorbed into the blood stream and reduce the intake of oxygen, which can lead to loss of consciousness and death. Irritant gases cause respiratory distress and indirectly contribute to incapacitation and lethality during exposure to fire gases. Inflammation of the respiratory tract may result in death within days or even weeks after the fire. Acid gases can also cause corrosion damage to electronic and computer equipment.

10.4 TESTS TO ASSESS MATERIAL FLAMMABILITY

10.4.1 Testing for Compliance with Fire Safety Codes and Regulations

This section provides a discussion of test procedures that are specified in fire safety codes and regulations. The emphasis is on building and fire prevention codes in the United States [7, 8]. Building codes specify fire safety requirements for a newly constructed or renovated building. Fire prevention codes ensure that the same level of safety is maintained during the lifespan of the building. Diamantes published an excellent overview of the U.S. code system for fire prevention [9].

Although test details and acceptance criteria are different, the approach of building codes and regulations in other countries is very similar. Fire safety regulations for commercial passenger aircraft, cruise ships, ferries, passenger rail and road transportation vehicles, etc., are also based on the same concepts.

Building code provisions that pertain to material flammability have traditionally been prescriptive, meaning that they consist of specific requirements for building materials and products that are based on performance in a test. Fire safety objectives are not explicitly stated in traditional building codes, and it is assumed that an acceptable level of fire safety is obtained if the prescriptive code requirements are fulfilled. A brief discussion follows of the test procedures that are specified in U.S. building codes.

10.4.1.1 Non-Combustible and Limited Combustible Materials

One approach to accomplish a high level of fire safety is by the exclusive use of materials that produce a negligible amount of heat when exposed to a thermal environment representative of a post-flashover fire. These materials are referred to as non-combustible and obviously do not provide a signifi-

cant contribution to fire growth prior to flashover. It is not practical to apply such an approach to an entire building, but it may be appropriate to require the exclusive use of non-combustible materials for some high-hazard areas or components of a building.

Materials that are not explicitly recognized as non-combustible must be tested and must meet specific criteria. ASTM E 136, *Standard Test Method for Behavior of Materials in a Vertical Tube Furnace at 750 °C*, is the small-scale test procedure that is used in the United States to determine whether a material is non-combustible. A similar furnace method described in ISO 1182, *Reaction to fire tests for building products—Non-combustibility test*, is used in most other parts of the world (see Figure 10.3). Acceptance criteria in both tests are based on maximum temperature rise, specimen mass loss, and limited flaming.

Some building codes in the United States make a distinction between non-combustible and limited combustible materials. A maximum potential heat of 8.2 MJ/kg (3500 Btu/lb) is specified for limited combustible materials as determined by NFPA 259, *Standard Test Method for Potential Heat of Building Materials*. According to NFPA 259, the potential heat of a material is determined as the difference between the gross heat of combustion of the material measured with an oxygen bomb calorimeter, and the gross heat of combustion of its residue after heating in a muffle furnace at 750 °C (1382 °F) for two hours.

Furnace and oxygen bomb methods to assess combustibility have serious limitations. The most significant limitations are that materials cannot be evaluated in their end-use configuration, that test conditions are not representative of real fire exposure conditions, and that the test results do not provide a realistic measure of the expected heat release rate.

10.4.1.2 Small-Flame Ignition Tests

A large variety of combustible materials are typically used throughout a building. A major concern is that these materials might easily ignite when exposed to a small heat source (such as an electrical arc or a candle flame) and, thus, support flame propagation that quickly leads to a catastrophic fire. This concern can be addressed by requiring that materials used in significant quantities do not ignite and/or support flame propagation when exposed to a small flame. A large number of small-flame ignition tests have been developed for this purpose [3]. One of the

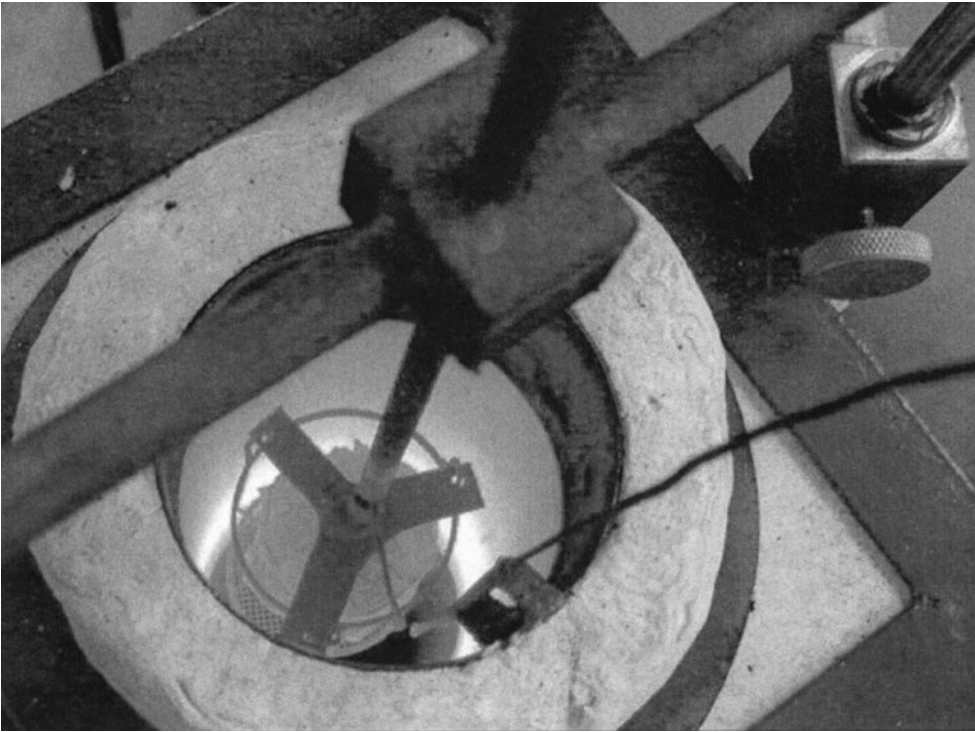


FIGURE 10.3 Test specimen inside ISO 1182 furnace.

most common tests of this type is briefly described below.

UL 94, *Test for Flammability of Plastic Materials for Parts in Devices and Appliances*, provides procedures for bench-scale tests to determine the acceptability of plastic materials for use in appliances or other devices with respect to flammability under controlled laboratory conditions. The standard includes several test methods that are employed depending upon the intended end-use of the material and its orientation in the device. The standard outlines a horizontal burning test, two classes of vertical burning tests, and a radiant panel flame spread test.

The most commonly used test in the UL 94 set is the vertical burning test referred to as the *20-mm Vertical Burning Test; V-0, V-1, or V-2* (see Figure 10.4). In this test, specimens measuring 125 mm (5 in.) in length by 13 mm (0.5 in.) wide are suspended vertically and clamped at the top end. A thin layer of cotton is positioned 300 mm (14 in.) below the test specimen to catch any molten material that may drop from the specimen. A 20-mm- (0.75-in.) long flame from a methane burner is applied to the center point on the bottom end of the specimen. The burner is positioned such that the burner barrel is located 10 mm (0.375 in.) below the bottom end of

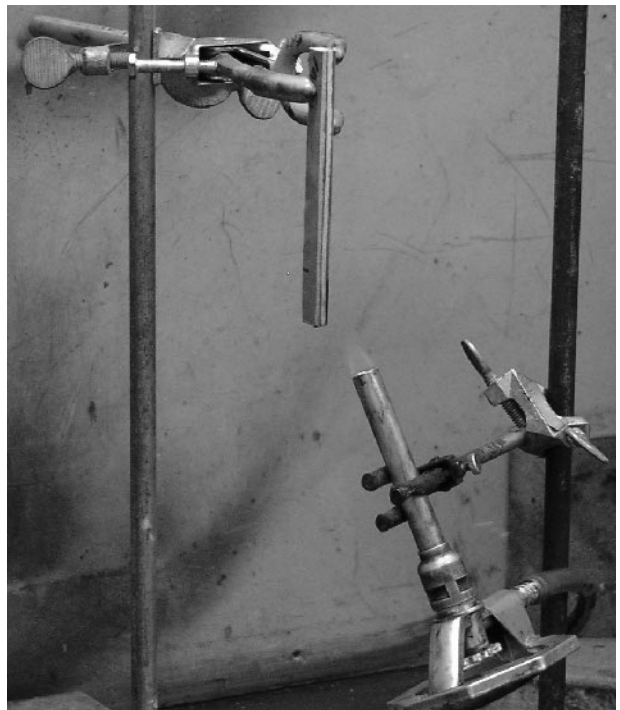


FIGURE 10.4 UL 94 20-mm vertical burning test.

the material specimen. The flame is maintained for 10 sec, and then removed to a distance of at least 150 mm (6 in.). Upon flame removal, the specimen is observed for afterflaming and its duration time recorded. As soon as the afterflame ceases, the burner flame is reapplied for an additional 10 sec, then removed again. The duration of afterflaming and/or afterglowing is again noted. The V-0 (best), V-1, or V-2 (worst) classification is based on the duration of afterflaming or afterglowing following the removal of the burner flame, as well as the ignition of cotton by dripping particles from the test specimen for a series of five tests.

10.4.1.3 Surface Finishes and Contents

Small-flame ignition tests serve a useful purpose. For example, it has been demonstrated that the lower number of fatalities in fires involving TV sets in the U.S. versus Europe can be attributed to the UL 94 V-0 requirement for the plastic TV housing in the U.S. [10]. However, these tests might give a false sense of safety. Materials that pass a small-flame ignition test often perform poorly when exposed to more severe conditions in a real fire. Therefore, to obtain a minimum level of fire safety, building codes specify that materials used in significant quantities meet more stringent flammability test requirements. These requirements are largely restricted to interior finishes, that is, wall and ceiling linings and floor coverings. Contents such as upholstered furniture, mattresses, and so on, are not regulated by the building codes because they are not a fixed part of the structure. However, the fire hazard associated with the contents is controlled by requirements for automatic fire suppression and alarm systems and provisions in the fire prevention codes.

Interior finishes cover large surfaces, and linings that are easily ignitable and release heat at a high rate will support rapid flame spread when exposed to a small or moderate size ignition source. It is therefore essential to control the flame spread characteristics of interior finishes so that flashover can be delayed and sufficient time can be made available for evacuation. The Steiner tunnel test is the most common material flammability test method prescribed by building codes in the United States to limit flame spread over wall and ceiling finishes. The test measures primarily wind-aided flame spread characteristics of surface finishes and is described in ASTM E 84, *Standard Test Method for Surface Burning Characteristics of Building Materials* (see Figure 10.5). The test specimen is 7.6 m (24 ft) long and is mounted in the ceiling position of a long tunnel-like

enclosure. It is exposed at one end to a 79-kW (5000-Btu/min) gas burner. There is a forced draft through the tunnel from the burner end. The measurements consist of flame spread over the surface and light obscuration by the smoke in the exhaust duct of the tunnel. Test duration is 10 min. A flame-spread index (FSI) is calculated on the basis of the area under the curve of flame tip location versus time. The FSI is zero for an inert board, and is normalized to approximately 100 for red oak flooring. The smoke developed index (SDI) is equal to 100 times the ratio of the area under the curve of light absorption versus time to the area under the curve for red oak flooring. Thus, the SDI of red oak flooring is 100, by definition.

The classification of linings in the model building codes is based on the FSI. There are three classifications: Class A, or I, for products with $FSI \leq 25$; Class B, or II, for products with $25 < FSI \leq 75$; and Class C, or III, for products with $75 < FSI \leq 200$. Class A, or I, products are generally permitted in enclosed vertical exits. Class B, or II, products can be used in exit access corridors, and Class C, or III, products are allowed in other rooms and areas.

Significant inconsistencies have been found between the FSI classification and real fire performance of certain products, such as plastic foams and textile wall coverings. To address these inconsistencies, the model building codes now require that plastic foams and textile wall coverings for use in unsprinklered spaces pass a room/corner test such as UBC 26-3, *Room Fire Test Standard for Interior of Foam Plastic Systems*, or NFPA 265, *Standard Methods of Fire Tests for Evaluating Room Fire Growth Contribution of Textile Wall Coverings*. The room/corner test apparatus consists of a room measuring 3.6 m (12 ft) deep by 2.4 m (8 ft) wide by 2.4 m (8 ft) high, with a single ventilation opening (doorway) measuring approximately 0.8 m (30 in.) wide by 2 m (80 in.) high in the front wall. The back wall, both side walls, and the ceiling are lined for tests according to UBC 26-3. For tests according to NFPA 265, the interior surfaces of all walls (except the front wall) are covered with the test product. The product is exposed to a wood crib (UBC 26-3) or propane burner (NFPA 265) ignition source, located on the floor in one of the rear corners of the room opposite the doorway. Pass/fail criteria are based primarily on the extent of fire growth. NFPA 286, *Standard Methods of Fire Test for Evaluation Contribution of Wall and Ceiling Interior Finish to Room Fire Growth*, provides a more recent room/corner test that is very similar to NFPA 265, and that is used to evaluate vinyl and other non-textile wall coverings. ISO 9705, *Reaction to fire tests*

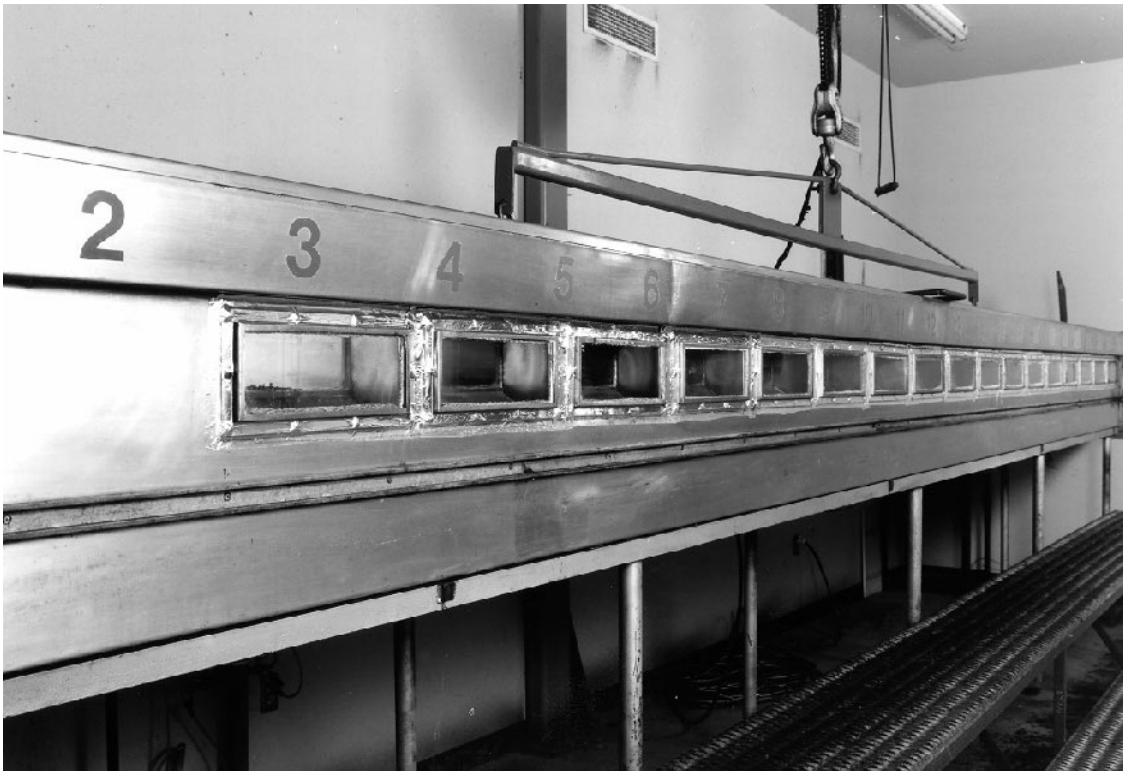


FIGURE 10.5 ASTM E 84 tunnel test apparatus.

for building products-Full scale room test for surface products, describes a room test apparatus and procedure that is used internationally (see Figure 10.6). Room and door dimensions are similar to those specified in the NFPA room test standards, but walls and ceiling are typically lined with the test material and a much more severe ignition source (100 kW for 10 min, followed by 300 kW for 10 min) is used.

Although wind-aided flame spread is the dominant mode in most fire scenarios involving interior finishes, opposed-flow flame spread needs to be considered in some cases. Research at the National Bureau of Standards (NBS), currently the National Institute of Standards and Technology (NIST), resulted in the development of the radiant flooring panel test for floor coverings. This test is described in ASTM E 648, *Standard Test Method for Critical Radiant Flux of Floor Covering Systems Using a Radiant Heat Energy Source*. The apparatus consists of an air-gas-fueled radiant heat panel inclined at 30 degrees to and directed at a horizontally mounted floor covering system specimen. The radiant panel generates a heat flux distribution along the 1-m (40-in.) length of the test specimen from a nominal maximum of 10 kW/m² (1 W/cm²) to a minimum of 1 kW/m² (0.1 W/cm²). The test is initiated by open-

flame ignition from a pilot burner. The heat flux at the location of maximum flame propagation is reported as critical radiant flux.

The test method described in ASTM E 162 also evaluates opposed-flow flame spread characteristics of a product, and is referred to in regulations that pertain to various modes of transportation.

10.4.1.4 Smoke and Toxicity

The model building codes do not permit interior finishes that produce excessive amounts of light-obscuring smoke. Products that have to be tested according to the tunnel test must have an SDI of 450 or less. UBC 26-3 also specifies limitations to smoke, but the acceptance criteria are qualitative and based on visual observations. The more recent room/corner test procedures NFPA 286 and ISO 9705 include quantitative measurements of the smoke production rate.

Test methods have been developed specifically to measure smoke obscuration. The prime example is the NBS smoke chamber. This method is described in ASTM E 662, *Standard Test Method for Specific Optical Density of Smoke Generated by Solid Materials* (see Figure 10.7). The apparatus consists of a



FIGURE 10.6 ISO 9705 room/corner test in progress.

0.5 m³ (18 ft³) enclosure. A 75 × 75-mm (3 × 3-in.) specimen is exposed in the vertical orientation to an electric heater. Tests can be conducted with or without small pilot flames impinging at the bottom of the specimen. A white light source is located at the bottom of the enclosure, and a photomultiplier tube is mounted at the top to measure obscuration and optical density of the smoke as it accumulates inside the enclosure. The procedure specifies that tests be conducted in triplicate at a heat flux of 25 kW/m² under each of the following conditions: with the pilot flames, and without the pilot flames. These conditions are referred to as the flaming and non-flaming modes, respectively. The latter is misleading because specimens often ignite spontaneously, leading to flaming combustion without the pilot flames. The model building codes do not specify requirements based on performance in the NBS smoke chamber, but fire safety regulations for various modes of transportation do. The test has been subjected to criticism because the smoke generated by the specimen accumulates inside the chamber and eventually affects combustion. The test conditions, therefore, are not well controlled and partly depend on the burning behavior of the product itself.

The University of Pittsburgh, or UPitt, method is used to demonstrate compliance with the requirement in the New York City building code that no product shall be more toxic than wood. A small sample of the product is heated in a muffle furnace, and four mice are exposed to the products of combustion diluted with air. The furnace temperature is ramped at a rate of 5 °C/min. The test is terminated after 30 min. The objective is to find the quantity of the product in grams that results in 50% mortality of the test animals. A product meets the requirements if this quantity, referred to as the LC50, is equal to or greater than 19.5 grams (the value generically assigned to wood).

A wide range of techniques is used to measure toxic gas concentrations in fire tests, ranging from simple qualitative sorption tube methods to sophisticated spectroscopy techniques. ASTM E 800, *Standard Guide for Measurement of Gases Present or Generated During Fires*, describes the most common analytical methods and sampling considerations for many gases. Fourier Transform InfraRed (FTIR) spectroscopy has emerged in recent years as the method of choice for real-time continuous analysis of fire gases (see Figure 10.7).

10.4.2 Testing for Research and Product Development

Prescriptive fire safety codes and regulations rely on flammability tests, which measure one or several parameters that are believed to be an indication of real fire performance. However, these tests do not provide a complete and quantitative assessment of real fire performance. For example, it is logical to assume that the propagation rate of a flame over the surface of a surface finish material in a real fire would be comparable to that in the ASTM E 84 test if the real ignition source is similar to that in the test. But what would happen if the real ignition source is twice as severe or persists for more than 600 sec, or if the surface of the material is in the vertical orientation instead of horizontal, facing down? The results could be dramatically different (i.e., the flame might propagate at a much faster rate and quickly result in a catastrophic fire). There are numerous examples of materials that pass the test with flying colors but perform miserably under slightly more stringent real fire conditions.

Advances in fire dynamics and computer modeling have led to the development of a more sophisticated approach. This modern approach involves a hazard assessment. Real fire scenarios are defined based on one or several statistical surveys. For each



FIGURE 10.7 NBS smoke chamber with FTIR spectrometer for gas analysis.

scenario, it is determined how materials and products contribute to the fire based on accident reports and full-scale fire test data. A model is developed to predict real fire performance on the basis of fire properties for the materials that are involved. The model can range in complexity from a relatively simple statistical correlation to a detailed computer simulation. A test methodology is developed to provide the properties that are needed for model input. As a minimum, the input data typically describe the ignition behavior and heat and smoke release rate characteristics of the material over a range of thermal exposure conditions. The corresponding properties can be measured in a heat release rate calorimeter.

The Cone Calorimeter is a small-scale fire test apparatus used primarily to measure the heat release rate of materials on the basis of the oxygen consumption method (see Figure 10.8). The Cone Calorimeter is standardized in North America as ASTM E 1354, *Standard Test Method for Heat and*

Visible Smoke Release Rates for Materials and Products Using an Oxygen Consumption Calorimeter. The equivalent international Cone Calorimeter standard is ISO 5660, *Fire tests—Reaction to fire—Part 1: Heat release (cone calorimeter method).* A square sample of 100×100 mm (4×4 in.) is exposed to the radiant flux of an electric heater. The heater has the shape of a truncated cone (hence the name of the instrument) and is capable of providing heat fluxes to the specimen in the range of 10–110 kW/m². Prior to testing, the exhaust flow is set at the desired rate (normally 24 L/sec) and the heater temperature is set at the appropriate value resulting in the desired heat flux. At the start of a test, the specimen in the appropriate holder is placed on the load cell, which is located below the heater. An electric spark is used to ignite the pyrolysis products released by the specimen. As soon as sustained flaming is observed, the electric spark igniter is removed. All combustion products and entrained air are col-

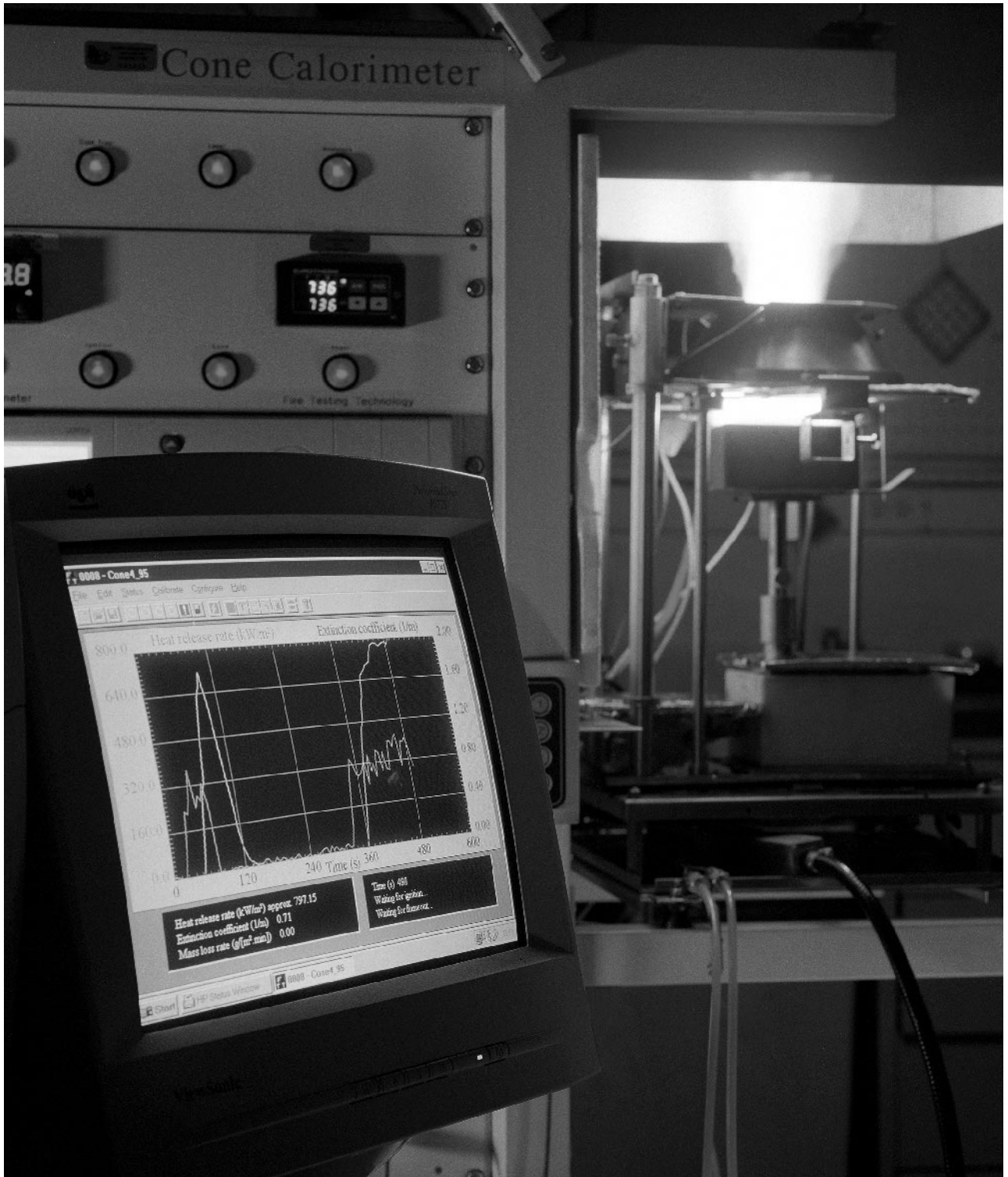


FIGURE 10.8 Cone calorimeter.

lected by an exhaust hood. At a sufficient distance downstream from a mixing orifice, a gas sample is taken and analyzed for oxygen concentration. A laser photometer is located close to the gas sampling point to measure light extinction by the smoke. Downstream of the fan is an orifice plate. Measurements of the gas temperature and differential pressure across the orifice plate are used for calculating the mass flow of the exhaust gases.

Similar data can be obtained with the Fire Propagation Apparatus described in ASTM E 2058, *Standard Test Method for Measurement of Synthetic Polymer Material Flammability Using a Fire Propagation Apparatus (FPA)*. Instead of a conventional electrical heater element as used in the Cone Calorimeter, heat flux to the specimen in the Fire Propagation Apparatus is generated by high-temperature tungsten filament lamps. The advantage of this approach is that a quartz tube can be placed around the specimen, which results in a better-defined flow environment at the specimen surface and facilitates performing tests in an oxygen-enriched or reduced environment. The disadvantage is that the specimen surface must be blackened to compensate for the fact that the spectral characteristics of high temperature lamps are different from those of typical sources of thermal radiation in fires.

To determine the heat release and smoke production rate of objects with complex shape and composition, it is more practical to perform measurements for the entire object as opposed to the individual components. For example, it is much easier to test an entire upholstered sofa instead of trying to estimate its burning behavior on the basis of the shape, dimensions, and ignition and heat release rate properties of the foam, fabric, and framing materials measured in the Cone Calorimeter. Based on the initial application, the test apparatus that is used to obtain heat release and smoke production rate data for an entire object is referred to as a Furniture Calorimeter. However, a wide variety of objects has been tested in Furniture Calorimeters over the past 10–15 years. A Furniture Calorimeter is essentially a large-scale version of a Cone Calorimeter without a scaled-up version of the heater. The object is placed on a load cell beneath the hood of a large-scale oxygen consumption calorimeter. The hood, exhaust duct and instrumentation are similar to those used for the room fire tests described in the previous section. A typical example of a Furniture Calorimeter standard is ASTM E 1537, *Test Method for Fire Testing of Upholstered Furniture*.

The Intermediate Scale Calorimeter (ICAL) is a special type of Furniture Calorimeter because it includes a large radiant gas panel that can be used to expose the test specimen to a heat flux 0–60 kW/m². The incident heat flux is uniform across the entire exposed surface for specimens up to 1 × 1 m (40 × 40 in.) in size. The ICAL apparatus and test protocol are described in ASTM E 1623, *Standard Test Method for Determination of Fire and Thermal Parameters of Materials, Products, and Systems Using an Intermediate Scale Calorimeter (ICAL)*.

The capacity of furniture calorimeters is typically around 1 MW continuous. To test objects and commodities that release heat at a higher rate, a larger scale calorimeter is needed (see Figure 10.9). The first industrial-size calorimeter for fires into the multiple MW range was built at Factory Mutual (currently FM Global) around 1980 [11]. This calorimeter, also referred to as the FM Fire Products Collector, was designed to measure heat and other fire products from test fires up to a size associated with sprinkler activation in commodity warehouse storage and other representative occupancies. Approximately 10 years later, a similar industrial-size calorimeter for heat release rate measurements up to 10 MW was constructed at the National Testing Laboratory (SP) in Sweden [12]. Since then, several other laboratories, such as the National Research Council of Canada, the Fire Research Station in the United Kingdom, and Underwriters Laboratories and Southwest Research Institute in the United States, have developed the capability of measuring heat release rate from large fires up to 40 MW.

10.5 METHODS TO IMPROVE MATERIAL FLAMMABILITY

The flammability of a material can be improved by adding flame-retardant chemicals to it, or by protecting its surface with a coating that contains flame retardants. This section provides a brief overview of flame retardancy. For detailed information, the reader is referred to one of the many excellent reviews that can be found in the literature [13, 14].

10.5.1 Polymer Formulation

A common approach to develop polymers with improved flammability involves the use of multiple monomers that are cross-linked in the polymer matrix. Thermal decomposition of these co-polymers tends to favor char formation, which results in better ignition and/or heat release rate characteristics.



FIGURE 10.9 Industrial-scale oxygen consumption calorimeter.

10.5.2 Flame-Retardant Treatments

Chemicals are often added to improve the flammability characteristics of a polymer to meet specific fire performance requirements. The three most commonly used groups of flame retardants are briefly described below.

10.5.2.1 Phosphorous-Containing Fire Retardants

Phosphorous-containing flame retardants can be effective in the condensed (polymer) phase as well as the gas phase. For example, phosphorous is known to promote char formation. The char insulates the polymer from the heat transfer from the flame. Phosphorous also traps some of the radicals in the flame, similar to halogens (see below).

10.5.2.2 Halogen-Containing Flame Retardant Compounds

Halogen-containing flame-retardant chemicals are one of the largest groups of additives in the plastics industry. Bromine and chlorine compounds are the most generally used halogen-containing fire retardants, because iodine compounds are not sufficiently stable and fluorine compounds are too stable to be useful. Halogen-containing fire retardants act primarily in the gas phase as hydrogen halides inhibit the radical-chain oxidation reactions in the flame. Various metals (antimony, bismuth, or tin) are used as synergistic agents in combination with halogen-containing fire retardants because metal halides are more efficient flame inhibitors than hydrogen halides. Environmental concerns have significantly affected the use of some brominated fire retardants in recent years.

10.5.2.3 Inorganic Hydroxides

Inorganic hydroxides account for more than 50% of the flame retardants sold on a global basis. Aluminum trihydroxide, or ATH ($\text{Al}(\text{OH})_3$), is by far the most widely used inorganic hydroxide fire retardant in the world, followed by magnesium trihydroxide ($\text{Mg}(\text{OH})_2$) as a distant second. Organic hydroxides act primarily in the condensed phase. A significant amount of energy is needed to decompose inorganic hydroxides (1.5–1.6 kJ/g). Large quantities of water are generated in the process, which dilutes the concentration of other gaseous decomposition products and reduces the flame temperature. Although not

thoroughly understood, organic hydroxides also significantly reduce the amount of smoke generated during combustion. Hydroxide loading levels in excess of 50% by mass are not uncommon.

10.5.3 Surface Coatings

Coatings that contain flame retardants can be used to protect wood products that cannot be pressure treated, or they can be used to improve the flammability of existing installations of untreated products. Intumescent coatings contain a blowing agent that forms vapor bubbles when heated. The bubbles are trapped inside an inert matrix and form a porous layer that significantly reduces the heat transfer to the protected substrate. Some truly amazing results have been obtained with intumescent coating systems.

10.6 MATERIAL PROPERTY DATA

It is important to know that within a single generic class of materials, flammability characteristics may vary greatly depending on the exact composition, presence of additives (in particular, flame retardants), and physical properties such as density and surface emissivity. Therefore, data reported in the literature have to be treated with great caution. The data presented in this section are intended to give the reader a feel for typical properties of commonly used natural and synthetic polymers. To obtain accurate property values for a specific material, a series of tests will have to be performed. ASTM E 1591, *Data for Deterministic Fire Models* provides guidelines for obtaining flammability properties.

10.6.1 Ignition Properties

10.6.1.1 Ignition of Materials Exposed to a Small Flame

Pure synthetic polymers generally do not meet the requirements for a UL 94 V-2 classification. However, polymers can be treated with flame-retardant chemicals to meet the requirements for a V-2, a V-1, and even a V-0 classification. This is true for many other small flame ignition tests.

10.6.1.2 Piloted Ignition of Materials Exposed to a Radiant Heat Source

Three properties are commonly used to describe the piloted ignition behavior of a material exposed to a radiant heat source.

1. The first property quantifies a critical condition for ignition. The most common criterion is based on the assumption that ignition occurs when a critical temperature at the surface, T_{ig} , is reached. T_{ig} can be measured with fine thermocouples attached to the exposed surface of ignition test specimens, or by using an optical pyrometer. However, it is very difficult to make accurate surface temperature measurements. A more practical approach involves analysis of piloted ignition data based on a simplified model to extract material properties. The data consist of the time to ignition measured at different heat flux levels, which can be obtained in a device such as the Cone Calorimeter or the Fire Propagation Apparatus.
2. The second property is the critical heat flux for ignition, CHF . Piloted ignition will not occur at heat fluxes below the CHF , even for very long exposure times. The CHF can be estimated by bracketing, i.e., by conducting ignition experiments at incrementally decreasing heat flux levels until ignition does not occur within a specified period (usually 10 or 20 min).
3. The third property is the thermal inertia, $k\rho c$. It is equal to the product of the average thermal conductivity (k), density (ρ), and specific heat (c) over the temperature range from ambient to T_{ig} . The thermal inertia is a measure of how fast the surface temperature of a material rises when exposed to heat. A material with lower $k\rho c$ will ignite faster than a material with higher $k\rho c$ and the same T_{ig} exposed to the same heat flux. The $k\rho c$ can be determined from the analysis of piloted ignition data to calculate T_{ig} described above.

Table 10.1 gives typical ignition property values for some common materials.

10.6.2 Flame Spread Propensity

As explained above, wind-aided flame spread is of much greater concern than opposed-flow flame spread. The FSI measured in the Steiner tunnel test is a measure of the wind-aided flame spread propensity of a material. Most untreated wood products have a FSI between 75 and 200. Some have a FSI between 25 and 75, and a few have a FSI that exceeds 200. An extensive list of FSI values for different wood products is published by the American Forest & Paper Association [22]. Pressure treatment with flame-retardant chemicals or protection with flame-retardant coatings can reduce the FSI below 25. Untreated synthetic polymers typically have a FSI in excess of 200. Polymers that contain halogens such as PVC and PTFE are an exception to this rule. Synthetic polymers can be treated or coated to dramatically improve performance in the tunnel test.

Fire growth in standard room fire tests is controlled primarily by upward spread to the ceiling and flame propagation over the ceiling and upper parts of the walls. The time to flashover is therefore a good indicator of the wind-aided flame spread propensity of a material. Untreated wood products tested according to NFPA 286 typically result in flashover times between 6 and 7 min (i.e., 1 to 2 min after increasing the burner output to 160 kW) [23]. Some untreated wood products and most synthetic polymers result in flashover during the first 5 min when the burner output is 40 kW. Natural and synthetic polymers can be treated or coated so that flashover does not occur during the 15-min test.

10.6.3 Heat Release Rate

Figures 10.10 and 10.11 show typical heat release rates measured in the Cone Calorimeter at different

TABLE 10.1 Typical Ignition Data of Common Solids

| Material | T_{ig} (°C) | CHF (kW/m ²) | $k\rho c$ (kJ/m ⁴ · K ² ·s) | Reference |
|-------------------------|------------------|----------------------------|---|-----------|
| Oven Dry Douglas Fir | 350 ^m | 13 | 0.16 | [15] |
| Oven Dry Oak | 301 ^c | 11 | 0.45 | [16] |
| Polyethylene | 323 ^m | 13 | 1.83 | [17] |
| Polymethylmethacrylate | 305 ^m | 12 | 2.12 | [18] |
| Polypropylene | 305 ^m | 12 | 2.15 | [15] |
| Polystyrene | 410 ^m | 16 | 1.17 | [19] |
| Polystyrene Foam | 376 ^c | 15 | 0.58 | [20] |
| Polyvinylchloride | 415 ^c | 16 | 1.31 | [21] |
| Rigid Polyurethane Foam | 370 ^c | 15 | 0.04 | [20] |

^m = Measured ^c = Calculated

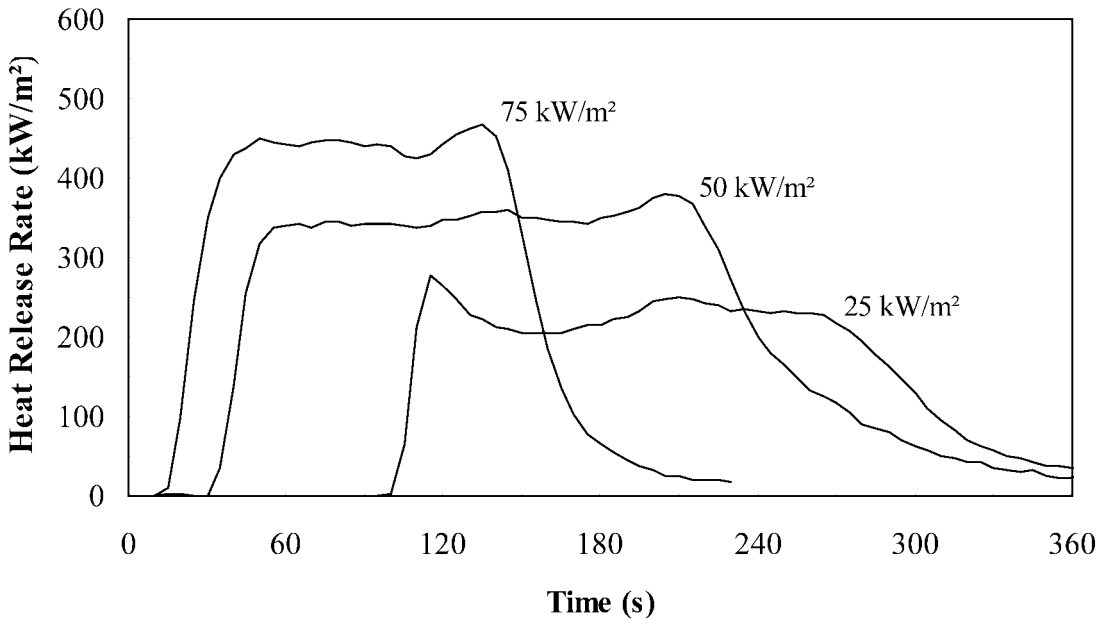


FIGURE 10.10 Cone calorimeter heat release rate data for GR polyester.

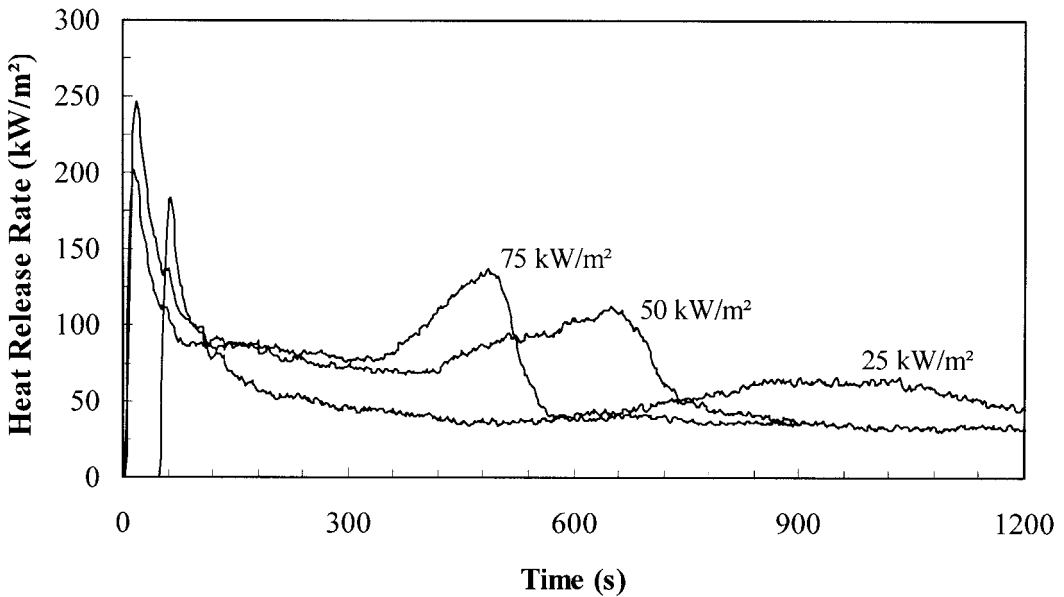


FIGURE 10.11 Cone calorimeter heat release rate data for western red cedar.

heat fluxes for glass fiber-reinforced polyester (GRP) and western red cedar, respectively. The heat release rate varies with time and incident heat flux for both materials. The heat release rate for GRP is approximately steady shortly after ignition and remains relatively constant during the entire test. This behavior is typical for plastics. The heat release rate of western red cedar reaches a peak shortly after ignition and then quickly decreases as a protective

char layer is formed at the surface. The heat release rate increases again at the end of the test due to the fact that the specimen is backed by thermal insulation. This bimodal behavior is typical for wood products and other char-forming materials.

Figures 10.10 and 10.11 illustrate why it is not very useful to tabulate “typical” heat release rates for different materials. Should peak or average values be presented? What are appropriate heat fluxes?

This problem can be addressed by tabulating fundamental heat release rate properties that are independent of exposure conditions and do not vary greatly with time. The two properties that are related to heat release rate are the effective heat of combustion, ΔH_c (MJ/kg), and the heat of gasification, L (MJ/kg). These properties are described below.

The effective heat of combustion is the ratio of heat release rate to mass loss rate measured in a small-scale calorimeter:

$$\Delta H_c \equiv \frac{\dot{Q}''}{\dot{m}''} \quad (10.1)$$

where \dot{Q}'' = heat release rate per unit exposed area (kW/m²)

\dot{m}'' = mass loss rate per unit exposed area (g/m²·s)

ΔH_c is different from the lower calorific value measured in an oxygen bomb calorimeter. The latter is measured in a small container under high pressure and in pure oxygen, conditions that are not representative of real fires. The conditions in bench-scale calorimeters such as the Cone Calorimeter resemble those in real fires much more closely. For some fuels, in particular gases, both values are nearly identical. However, for charring solids such as wood, ΔH_c is significantly lower and equal to the heat of combustion of the volatiles during flaming combustion.

The second material property is heat of gasification, L , defined as the net heat flow into the material required to convert one unit mass of solid material to volatiles. The net heat flux into the material can be obtained from an energy balance at the surface of the specimen. Typically, a sample exposed in a bench-scale calorimeter is heated by external heaters and by its own flame. Heat is lost from the surface in the form of radiation. Due to the small sample size, the flame flux is primarily convective, and flame absorption of external heater and specimen surface radiation can be neglected. Hence, L can be defined as

$$L \equiv \frac{\dot{q}_{net}''}{\dot{m}''} = \frac{\dot{q}_e'' + \dot{q}_f'' - \dot{q}_l''}{\dot{m}''} \quad (10.2)$$

where L = heat of gasification (MJ/kg)

\dot{q}_e'' = heat flux from external sources (kW/m²)

\dot{q}_f'' = heat flux from the flame (kW/m²)

TABLE 10.2 Typical Heat Release Rate Data of Common Solids

| Material | ΔH_c (kJ/g) | L (kJ/g) | Reference |
|-------------------------|---------------------|------------|-----------|
| Douglas Fir | 11.0 | 4.6–8.4 | [24] |
| Red Oak | 12.3 | 5.1–9.5 | [24] |
| Polyethylene | 38.4 | 1.9–2.3 | [25] |
| Polymethylmethacrylate | 24.2 | 1.4–1.6 | [25] |
| Polypropylene | 38.6 | 1.4–2.0 | [25] |
| Polystyrene | 27.0 | 1.7–2.2 | [25] |
| Polystyrene Foam | 25.5 | 1.3–1.9 | [25] |
| Polyvinylchloride | 7.3 | 3.1 | [25] |
| Rigid Polyurethane Foam | 16.4 | 1.2–5.6 | [25] |

\dot{q}_l'' = heat losses from the exposed surface (kW/m²)

Table 10.2 gives typical heat release property values for some common materials.

10.6.4 Smoke and Toxicity

The same problem exists with reporting typical generation rates of smoke and toxic products of combustion as with heat release rate because they also vary as a function of time and incident heat flux. The problem can be addressed by reporting yields of smoke (soot) and different toxic gases. The yield of a particular compound is equal to the mass of that compound that is generated per mass unit of fuel burnt. Table 10.3 gives typical yields for some common materials. The values in Table 10.3 are valid for overventilated conditions, i.e., when much more air is supplied to the fire than required for complete stoichiometric combustion of the fuel and the equivalence ratio is much smaller than one ($\Phi \ll 1$). The yields of most species are relatively insensitive to

TABLE 10.3 Typical Yields of Soot and Toxic Gases for Common Solids (g/g) [25, 26]

| Material | Soot | CO | HCN | NO _x | HCl |
|-------------------------|-------|-------|--------|-----------------|-------|
| Douglas Fir | 0.015 | 0.004 | — | — | — |
| Red Oak | 0.015 | 0.004 | — | — | — |
| Polyethylene | 0.060 | 0.024 | — | — | — |
| Polymethylmethacrylate | 0.022 | 0.010 | — | — | — |
| Polypropylene | 0.059 | 0.024 | — | — | — |
| Polystyrene | 0.164 | 0.060 | — | — | — |
| Polystyrene Foam | 0.194 | 0.061 | — | — | — |
| Polyvinylchloride | 0.172 | 0.063 | — | — | 0.480 |
| Rigid Polyurethane Foam | 0.118 | 0.036 | 0.0018 | 0.090 | — |

the ventilation rate, but CO yields increase dramatically as the equivalence ratio approaches and exceeds one [27].

10.6.5 Application of the Heat Release Rate Properties and Yield Data

This section illustrates how the data in Tables 10.1 through 10.3 can be used to estimate the release rate of heat, smoke, and toxic products of combustion for a material exposed under specified conditions. The first step is to determine the net heat flux to the material. The net heat flux is equal to the incident radiation from remote sources, plus the heat flux from the material's own flame minus re-radiation losses from the surface. The flame flux is typically between 20 and 40 kW/m² depending on the size of the flame (larger burning surface ⇒ higher heat flux) and the type of material (higher soot yield ⇒ higher heat flux). The *CHF* is a reasonable estimate for the re-radiation losses. The second step is to calculate the mass loss rate of the fuel. This can be done via Eq. (10.2), based on the heat of gasification for the material and the net heat flux estimated in the first step. The resulting mass flux is multiplied by the exposed area to obtain the mass loss rate. The final step is to calculate the heat release rate and generation rate of different products of combustion by multiplying the mass loss rate from step two with the effective heat of combustion and appropriate yields, respectively.

This approach can best be illustrated with an example. Consider a burning slab of Douglas fir exposed to radiation from the flame of a burning object and a hot layer of gases accumulated below the ceiling of the room. The exposed area of the burning slab is approximately 1 m², and the average incident heat flux from remote sources is 40 kW/m². The heat release rate and generation rate of soot and CO can be calculated as follows:

Step 1: Calculate net heat flux

| | |
|---|----------------------------|
| Heat flux from remote radiation sources | 40 kW/m ² |
| Assumed flame flux | + 30 kW/m ² |
| Critical heat flux | - 13 kW/m ² |
| Net heat flux | <u>57 kW/m²</u> |

Step 2: Calculate mass loss rate (use average heat of gasification from Table 10.2)

$$\dot{m} = \dot{m}'' \times A = \frac{\dot{q}_{net}''}{L} \times A = \frac{57}{6.5} \times 1 = 8.77 \frac{\text{g}}{\text{s}}$$

Step 3: Calculate heat release rate and generation rate of soot and CO

$$\dot{Q} = \dot{m} \times \Delta H_c = 8.77 \times 12.3 = 108 \text{ kW}$$

$$\dot{m}_s = \dot{m} \times Y_s = 8.77 \times 0.015 = 0.13 \frac{\text{g}}{\text{s}}$$

$$\dot{m}_{CO} = \dot{m} \times Y_{CO} = 8.77 \times 0.004 = 0.035 \frac{\text{g}}{\text{s}}$$

The estimated generation rate of CO is only valid for overventilated conditions ($\Phi \ll 1$). According to correlations developed by Tewarson, the generation rate of CO would increase to 0.042 g/s if $\Phi = 0.8$, 0.16 g/s if $\Phi = 1.0$, and 1.27 g/s if $\Phi = 2.0$ [25]. Obviously, the concentrations of CO and the toxic hazard to occupants would increase accordingly.

10.7 COMPUTER MODELING OF MATERIAL DEGRADATION IN FIRES

Evolutions in fire science and technology and computing have resulted in a growing number of powerful mathematical models that are used in support of fire safety engineering design and analysis. The most commonly used computer fire models simulate the consequences of a fire in an enclosure. Zone models as well as field, or Computational Fluid Dynamics (CFD), models are used for this purpose. Zone models are based on the observation that gases inside a fire room generally accumulate in two distinct layers: a hot smoke layer beneath the ceiling, and a layer of relatively cool air above the floor. The temperature and composition of both layers are assumed to be uniform, which greatly simplifies the equations to be solved. CFD models subdivide the room into thousands of small elements and solve the conservation equations of mass, momentum, and energy for each element. CFD models are therefore much more detailed than zone models, but require powerful computational resources. Enclosure fire models have been extended to simulate the spread of fire and smoke through multi-room structures.

A second category of computer fire models predicts how materials, systems, or people respond when exposed to specific fire conditions. This includes models that predict how solids thermally degrade when exposed in a fire. The most extensive work in this area has been done on the development of models that predict the rate of pyrolysis and charring of wood exposed to fire. Janssens et al., recently reported that more than 50 models of this type have been described in the literature since WW II [28].

Models that simulate how a product performs in a fire test also fall in the second category. Several correlations and mathematical models have been developed to calculate performance in the tunnel test [29–33]. However, these predictions are restricted to specific classes of products and have limited accuracy. Extensive research has been conducted over the past two decades to explore the use of small-scale fire test data in conjunction with correlations and models to predict room/corner test performance [34]. The primary application of calculation methods that predict tunnel or room/corner test performance is for product development. Such calculations may also be used to demonstrate code equivalency and in support of performance-based design.

10.8 REFERENCES

1. C. Beyler and M. Hirschler. Chapter 7: Thermal Decomposition of Polymers. In *SFPE Handbook of Fire Protection Engineering*, 3rd Ed. P. DiNenno, Ed. Quincy, MA: NFPA, 2002, pp. 110–131.
2. T. Ohlemiller. Section 2, Chapter 9: Smoldering Combustion. In *SFPE Handbook of Fire Protection Engineering*, 3rd Ed., P. DiNenno, Ed. Quincy, MA: NFPA, 2002, pp. 200–210.
3. V. Babrauskas. *Ignition Handbook*. Issaquah, WA: Fire Science Publishers, 2003.
4. V. Babrauskas and R. Peacock. Heat Release Rate: The Single Most Important Variable in Fire Hazard. *Fire Safety Journal*, 1992, Vol. 18, pp. 255–272.
5. C. Huggett. Estimation of the Rate of Heat Release by Oxygen Consumption. *Journal of Fire and Materials*, 1980, Vol. 12, pp. 61–65.
6. T. Jin. Visibility Through Fire Smoke. *Journal of Fire & Flammability*, 1978, Vol. 9, pp. 135–157.
7. NFPA. NFPA 5000: Building Construction and Safety Code. Quincy, MA: National Fire Protection Association, 2003.
8. ICC. International Building Code. Fairfax, VA: International Code Council, 2003.
9. D. Diamantes. *Fire Prevention: Inspection and Code Enforcement*, 2nd Ed. Albany, NY: Delmar, 2002.
10. J. Roed. *Low Voltage Directive*. Presented at FIRESEL 2003, SP, Borås, Sweden, 2003.
11. G. Heskestad. *A Fire Products Collector for Calorimetry into the MW Range*. Technical Report FMRC.J.I0C2E1.RA. Norwood, MA: Factory Mutual Research Corporation, 1981.
12. M. Dahlberg. *The SP Industry Calorimeter—For Rate of Heat Release Measurements up to 10 MW*. SP Report 1992:43. Borås, Sweden: Swedish National Testing and Research Institute, 1992.
13. D. Horrocks and D. Price. *Fire Retardant Materials*. Boca Raton, FL: CRC Press, 2001.
14. A. Grand and C. Wilkie. *Fire Retardancy of Polymeric Materials*. New York: Marcel Dekker, 2000.
15. M. Janssens. *Thermophysical Properties of Wood and Their Role in Enclosure Fire Growth*. Ghent, Belgium: The University of Ghent, 1991.
16. H. Tran and R. White. Burning Rate of Solid Wood Measured in an Oxygen Consumption Calorimeter. *Fire and Materials*, 1992, Vol. 16, pp. 197–206.
17. D. Hopkins and J. Quintiere. Material Fire Properties and Predictions for Thermoplastics. *Fire Safety Journal*, 1996, Vol. 26, pp. 241–268.
18. J. Quintiere and M. Harkleroad, *New Concepts for Measuring Flame Spread Properties*. NBSIR 84-2943. Gaithersburg, MD: National Bureau of Standards, 1984.
19. B. Dlugogorski, D. Pope, B. Moghtaderi, E. Kennedy, and J. Lucas. *Fire Properties of Australian Eucalyptus*. Presented at Wood & Fire Safety—4th International Scientific Conference, The High Tatras, Slovak Republic, 2000.
20. T. Cleary and J. Quintiere. *Flammability Characteristics of Foam Plastics*. NISTIR 4664. Gaithersburg, MD: National Institute of Standards and Technology, 1991.
21. S. Dillon. *Analysis of ISO 9705 Room/Corner Test: Simulations, Correlations and Heat Flux Measurements*. College Park, MD: University of Maryland, 1998.
22. AF&PA. *DCA 1: Flame Spread Performance of Wood Products*. Washington DC: American Forest & Paper Association, American Wood Council, 2002.
23. H. Tran and M. Janssens. Wall and Corner Fire Tests on Selected Wood Products. *Journal of Fire Sciences*, 1991, Vol. 9, pp. 106–124.
24. M. Spearpoint and J. Quintiere. Predicting the Piloted Ignition of Wood in the Cone Calorimeter Using an Integral Model: Effect of Species, Grain Orientation, and Heat Flux. *Fire Safety Journal*, 2001, Vol. 36, pp. 391–415.
25. A. Tewarson. Generation of Heat and Chemical Compounds in Fire. In *SFPE Handbook of Fire Protection Engineering*, 3rd Ed. P. DiNenno, Ed. Quincy, MA: NFPA, 2002, Section 3, Chapter 4, pp. 82–161.
26. B. Persson and M. Simonson. Fire Emissions into the Atmosphere. *Fire Technology*, 1998, Vol. 34.
27. D. Gottuk and B. Lattimer. Effect of Combustion Conditions on Species Production. In *SFPE Handbook of Fire Protection Engineering*, 3rd Ed. P. DiNenno, Ed. Quincy, MA: NFPA, 2002, pp. 54–82.
28. M. Janssens and B. Douglas. Chapter 7: Wood and Wood Products. In *Handbook of Materials in Fire Protection*. New York: McGraw-Hill, 2003.
29. D. Sheppard and P. Gandhi. Estimating Smoke Hazard from Steiner Tunnel Smoke Data. *Fire Technology*, 1996, Vol. 32, pp. 65–75.
30. M. Janssens. *Modeling the E 84 Tunnel Test for Wood Products*. Presented at Fire and Materials, 1st International Conference, Arlington, VA, 1992.

31. J. Quintiere. Some Factors Influencing Fire Spread over Room Linings and in the ASTM E 84 Tunnel Test. *Fire and Materials*, 1985, Vol. 9, pp. 65–74.
32. M. Stevens, V. Voruganti, and R. Rose. *Correlation of Small-Scale Fire Tests to ASTM E 84 Tunnel Performance for Thermoset Resin Systems*. Presented at Fire and Materials, 4th International Conference and Exhibition, Crystal City, VA, 1995.
33. M. Stevens. *Cone Calorimeter as a Screening Test for ASTM E 84 Tunnel Test*. Presented at Fire and Materials, 5th International Conference and Exhibition, San Antonio, TX, 1998.
34. M. Janssens. *A Survey of Methods to Predict Performance of Wall Linings in the Room/Corner Test*. Presented at 3rd International Symposium on Computer Applications in Fire Safety Engineering, Baltimore, MD, 2001.

PROTECTIVE MEASURES

| | | |
|------------|--|-----|
| CHAPTER 11 | CATHODIC PROTECTION | 229 |
| CHAPTER 12 | POLYMERIC FLAME RETARDANTS: PROBLEMS AND DECISIONS | 243 |
| CHAPTER 13 | THERMAL PROTECTIVE CLOTHING | 261 |
| CHAPTER 14 | WEATHERING AND SURFACE PROTECTION OF WOOD | 277 |
| CHAPTER 15 | PROTECTION OF WOOD-BASED MATERIALS | 299 |

CHAPTER 11

CATHODIC PROTECTION

Richard W. Evitts

Department of Chemical Engineering, University of Saskatchewan, Saskatoon, Canada

11.1 INTRODUCTION 229
11.2 CORROSION FUNDAMENTALS 229
11.3 GALVANIC CATHODIC PROTECTION SYSTEMS 230

11.4 IMPRESSED CATHODIC PROTECTION SYSTEMS 237
11.5 GROUND BED SPACING 238
11.6 REFERENCES 241

11.1 INTRODUCTION

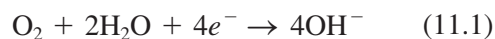
This chapter presents a discussion of cathodic protection systems and their design. It is divided into four sections. The first section presents an introduction to corrosion fundamentals and cathodic protection (CP) principles. The second section presents the design of galvanic systems and includes ground bed design and the algorithm for overall galvanic CP system design. In the third part, the design procedure for the more commonly used impressed systems is described. The final section presents the equations describing the attenuation of electrical potential along long buried structures, such as pipelines, and current demand equations for impressed CP systems. The application of these equations is presented as a methodology to determine the numbers of ground beds and their placement for CP of pipeline systems. The major problem associated with CP systems, stray current corrosion, is also discussed.

11.2 CORROSION FUNDAMENTALS

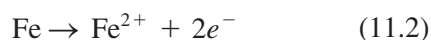
It has been estimated by the U.S. Federal Highway Administration that the cost of corrosion in the United States in 2000 was approximately \$276 billion, or 3.1% of the Gross Domestic Product.¹ It can be safely assumed that the costs to other industrialized nations would constitute the same fraction of their GDPs. This is the direct cost of corrosion, in

other words, the cost of replacing or fixing damaged equipment. The indirect cost of corrosion, such as reduction of equipment efficiency, leakage and contamination, and over-design, is estimated to be about the same as the direct costs. In addition, safety is also a significant concern. A major portion of the cost of corrosion can be reduced if economical corrosion reduction measures are undertaken. The focus of this chapter is one of the most widely used of those measures, cathodic protection.

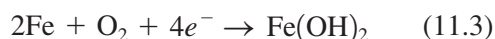
First, it is important to explain the basic process of metallic corrosion. This will provide the background to understand how CP works. Corrosion can be defined as an electrochemical reaction where metal dissolution occurs at anodic sites, and one or more reduction reactions occur at cathodic sites. At the cathodic sites the reduction of oxygen typically occurs



Carbon steel and cast irons are the most important and commonly used industrial alloys in use today. The anodic reaction for these metals is:



These two so-called half-cell reactions are combined to form the overall corrosion reaction



with further chemical oxidation to brown-colored iron (III) hydroxide. Corrosion prevention measures frequently focus upon the electrochemical nature of the corrosion reaction. If the corrosion circuit can be altered or broken, corrosion rates can be eliminated or at least reduced to insignificant levels. The simplest way to break the corrosion circuit is to apply one or more electrically resistant coatings, such as paint, which can successfully mitigate the corrosion problem when applied correctly. However, holes in coatings may occur and therefore cathodic protection is frequently used in conjunction with coatings.

Cathodic protection is a thermodynamic means of controlling the rate of corrosion, and there are two methods to apply it:

1. by electrically coupling the metal to more reacted metal that corrodes, or
2. through the application of an impressed or rectified direct current.

From a thermodynamic point of view, the cathodic protection process can be illustrated in a Pourbaix diagram for iron. It can be seen that there are two effects. The first effect (1→2) is the thermodynamic effect whereby the potential of the metal is shifted into the immune section of the diagram. It can be considered a thermodynamic effect because the Gibb's Free Energy for electrochemical reactions can be represented by electrical potential

$$\Delta G = -nFE \quad (11.4)$$

where ΔG is the free energy of the reaction, n is the number of electrons transferred, F is the Faraday and E is the electrical potential. The second effect (2→3) is an increase in the pH of the solution at the surface of the metal. It is a result of the imbalance caused by shifting the anodic reaction to remotely located anodes; in other words, the protected metal is cathodic. However, the increase in pH at the protected structure is highly localized, and the effect on the surrounding soil or water is miniscule. The application of cathodic protection is not restricted to carbon steel and iron. It can be used on many other materials (such as stainless steel, magnesium, and bronze) as long as the protection potential (the potential of the metal when it is immune from corrosion) is known or calculated for that material.

11.2.1 Protection Potential, E_{prot}

As illustrated in Figure 11.1, the potential of the metal must be brought into the immune zone. This potential, which is called the protection potential

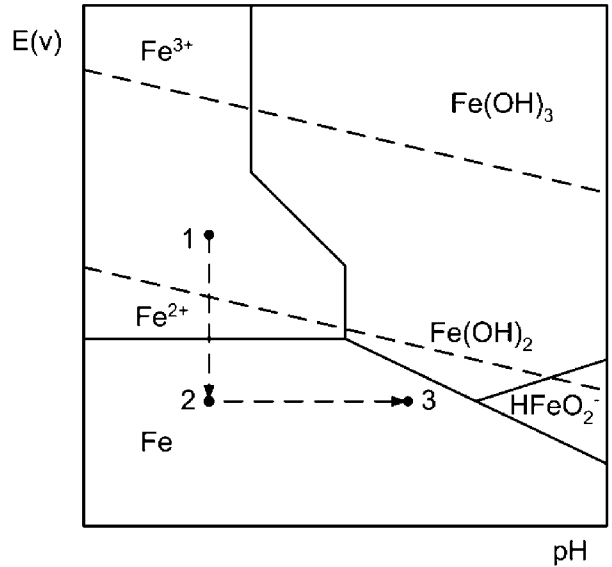


FIGURE 11.1 Pourbaix diagram for iron showing the effect of cathodic protection. Protection is afforded by the thermodynamic effect (1→2) but there is also a localized increase in pH on the surface of the metal (2→3).

(E_{prot}), can be determined from the application of the Nernst equation to the dissolution reaction. For iron

$$E = E^0 + \frac{RT}{nF} 2.303 \log[\text{Fe}^{2+}] \quad (11.5)$$

at a temperature of 298 K, and with a concentration of ferric ions selected to be 1×10^{-4} M, the protection potential is -0.532 V on the standard hydrogen scale.

As it is impractical to use a standard hydrogen electrode in the field, the much more robust copper/copper sulphate electrode is frequently used. This electrode is easy and inexpensive to construct; it is illustrated in Figure 11.2. The protection potential is generally taken as -0.85 V_{Cu/CuSO₄} for carbon steel. The protection potential for other metals is readily determined from the Nernst equation applied to the respective dissolution reaction.

11.3 GALVANIC CATHODIC PROTECTION SYSTEMS

There are two fundamental designs of cathodic protection systems, galvanic systems, and impressed systems. In a galvanic system, one or more metals are protected at the expense of a sacrificial metal that

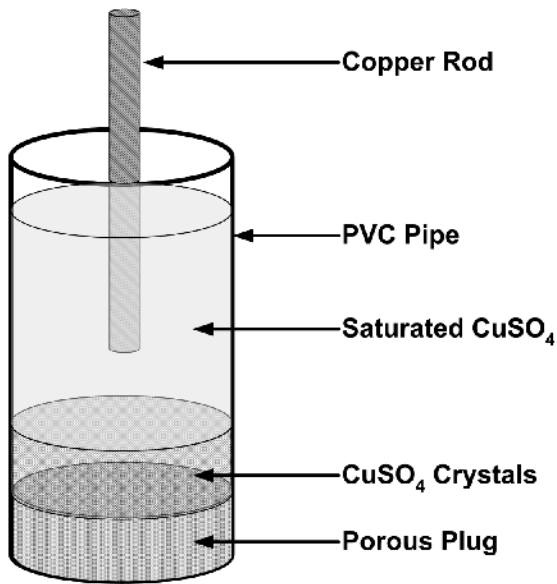


FIGURE 11.2 Construction of a copper/copper sulfate reference electrode.

corrodes preferentially. These sacrificial anodes are typically made of a metal that has low thermodynamic nobility, such as magnesium or zinc. Table 11.1 lists some common alloys, in decreasing order of thermodynamic nobility. Note the difference in nobility of the active-passive metals such as stainless steel.

When a less noble metal is electrically coupled to a more noble metal, the less noble metal will corrode and protect the more noble metal, if the more noble

TABLE 11.1 Partial Galvanic Series of Metals in Water, in Order of Decreasing Thermodynamic Nobility

| Most Noble |
|-----------------------------|
| Graphite |
| Platinum |
| Passive Titanium |
| Passive Hastelloy C276 |
| Passive Inconel 625 |
| Passive 316 Stainless Steel |
| Copper |
| Active Titanium |
| Active Hastelloy C276 |
| Active Inconel 625 |
| Active 316 Stainless Steel |
| 1018 Carbon Steel |
| Aluminum Alloys |
| Zinc |
| Magnesium |

metal is a good cathode and can support the cathodic reaction. Hence, coupling magnesium or zinc to common industrial alloys (such as carbon steel, stainless steels, or copper and nickel alloys) will result in the protection of the more noble metal, and the magnesium or zinc will preferentially corrode.

Figure 11.3 shows the layout of a galvanic cathodic protection system. It consists of the buried structure that is to be protected (in this case, a pipeline, but any buried metallic object could be externally protected by this system), one or more sacrificial anodes, a reference electrode, and basic instrumentation (such as an ammeter and a voltmeter). Galvanic systems are typically used for the protection of smaller-scale systems or when an external power source is unavailable. Some applications of galvanic CP systems are as follows:

- protection of storage tanks (e.g., in tank farms)
- in-plant buried piping systems
- condenser boxes
- marine applications, such as oil rigs, ship hulls, and piers
- local corrosion hot spots (e.g., drainage areas where water collects)
- hot water tanks in homes
- community water storage tanks

Galvanic CP can also be used to protect the inside of externally coated water lines. However, a special ribbon-like anode must be used to ensure that the pipeline is completely protected, due to the inability of a CP system to protect internal structures over long distances.

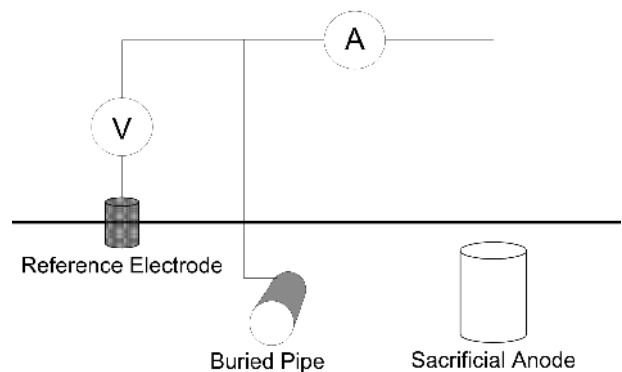


FIGURE 11.3 Schematic of a galvanic CP System. In this system, the buried pipe is protected at the expense of corroding the sacrificial anode.

11.3.1 Kinetics of Galvanic Systems

The kinetics of galvanic CP systems can be illustrated by plotting a kinetic corrosion diagram, which is a graph of potential versus the logarithm of the current. Figure 11.4 shows the following interesting features:

- E_a : This is the potential of the sacrificial anode, and it is often referred to as the solution potential. $E_a(\text{Mg}) \sim -1.5 \text{ V}_{\text{Cu}/\text{CuSO}_4}$; $E_a(\text{Zn}) \sim -1.1 \text{ V}_{\text{Cu}/\text{CuSO}_4}$. These values depend upon the composition of the alloy.
- E_c : This is the potential of the buried structure; $-0.85 \text{ V}_{\text{Cu}/\text{CuSO}_4}$
- The protection current, I_{prot}
- The corrosion rates for the uncoupled iron and zinc, $I_{\text{corr,Fe}}$ and $I_{\text{corr,Zn}}$
- The total corrosion rate of zinc when it is coupled to the iron is the corrosion rate of the zinc plus the

corrosion rate of the iron if it were unprotected and at a potential of E_a . Thus, the zinc will corrode much faster when coupled to the iron than when it is buried alone. However, the iron is cathodically protected and will not corrode.

I_{prot} is generally equal to the cathodic current density on the protected metal due to the reduction of oxygen. However, in acidic systems, hydrogen evolution also must be taken into account.

$$I_{\text{prot}} = I_{\text{H}_2} + I_{\text{O}_2} \quad (11.6)$$

In order to achieve protection, the difference in potential between the anode and cathode (the protection potential and the solution potential) must be greater than the product of the protection current and the total electrical resistance flow of current. In other words, for a galvanic system

$$E_c - E_a \geq I_{\text{prot}} R \quad (11.7)$$

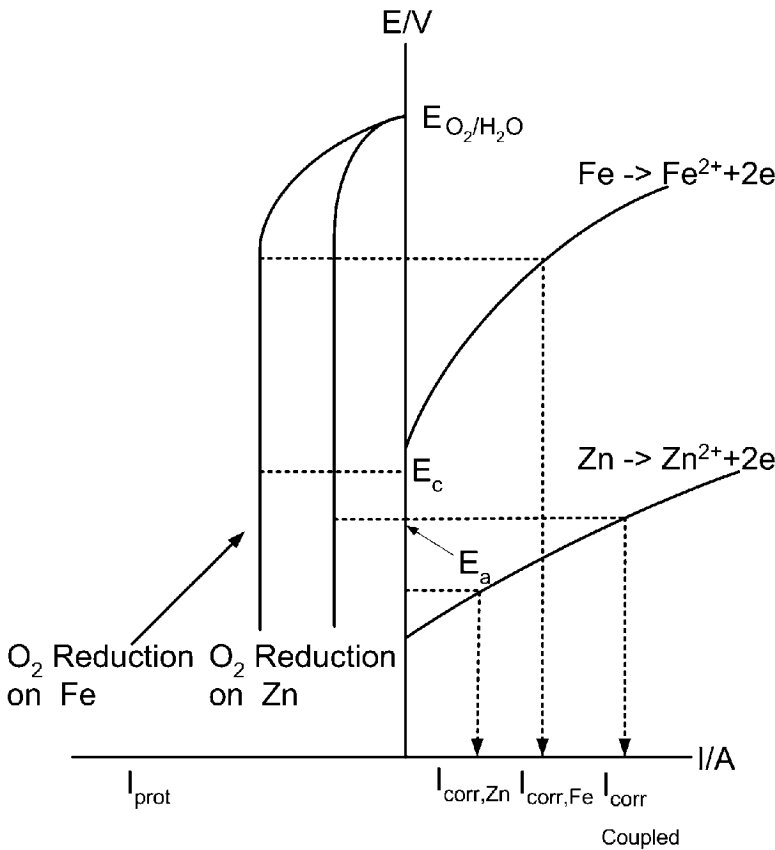


FIGURE 11.4 Kinetic corrosion diagram illustrating the galvanic cathodic protection process. The diagram shows the corrosion rates of uncoupled iron and zinc, the corrosion rate of zinc when the iron and zinc are coupled, and the protection current, I_{prot} .

Unless there is a significant length of wire used in the installation, the major portion of the resistance occurs in the anode ground bed; this resistance calculation is provided below. A schematic of the variation in electrical resistance from the protected structure to the anode ground bed is provided as Figure 11.5. It shows that the majority of the resistance occurs in the ground bed, and that there is a much smaller electrical resistance at the protected structure. The resistance of the medium between the ground bed and the protected structure is not obvious from the diagram, as the current is distributed through a large area. It is important, however, and must be determined in CP design. The cathodic and anodic overpotentials, η_c and η_a , which are deviations from the equilibrium potentials of the cathodic and anodic reactions, respectively, are of the order of a few millivolts. As the protected structure is the cathode of the system, it is very important to control the cathodic overpotential, which is generally several orders of magnitude lower than the total voltage loss. This is the major design problem with galvanic CP systems, because protection may be lost if this is not controlled. As maintenance of the voltage of the structure below a critical value is the objective of cathodic protection, the reference electrode should be placed as close as possible to the structure. This

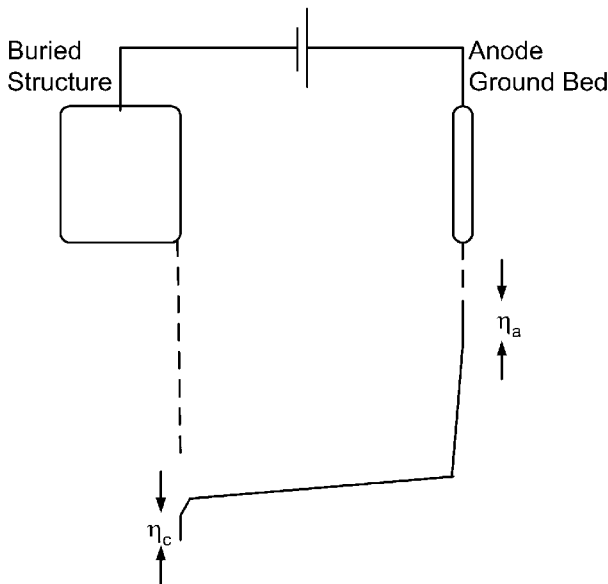


FIGURE 11.5 The voltage losses in a CP system. The majority of the loss occurs in the ground bed, but losses in the soil/water must be accounted for, too. Adapted from Shrier.²

will minimize the iR drop, which is the electrical potential that is used up moving ions through the soil. If the iR drop is large, there will be discrepancies between the voltage reading with respect to the reference electrode and the actual voltage of the structure.

The electrical current needed to achieve the protection potential and the solid resistivity are both obtained by on-site measurements. Numerous devices are available for measuring the soil resistivity, and some of these are shown below. Figure 11.6 shows a Wenner four-pin soil resistivity system in which the pins are placed in the ground, potential is applied between the two outer pins, and the current flowing in the system is measured. Pins 2 and 3 are the reference electrodes used to measure the potential difference between pins 1 and 4. The soil resistivity can be determined by the following equation³:

$$\rho = 2\pi a \frac{\Delta E}{I}, \quad (11.8)$$

where the pins are spaced “ a ” units apart.

If it is inconvenient to measure the soil resistivity in the field, samples can be taken into the laboratory and the resistivity determined. However, this is generally not advisable, as changes to the moisture content during transport will occur, affecting the soil resistivity. If it is necessary to determine the soil resistance in the laboratory, several devices are available, including the soil box presented as Figure 11.7, where the resistivity is determined by⁴

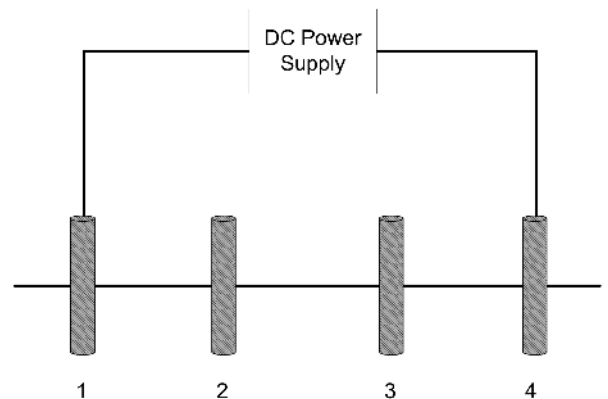


FIGURE 11.6 A Wenner four-pin soil resistivity apparatus.

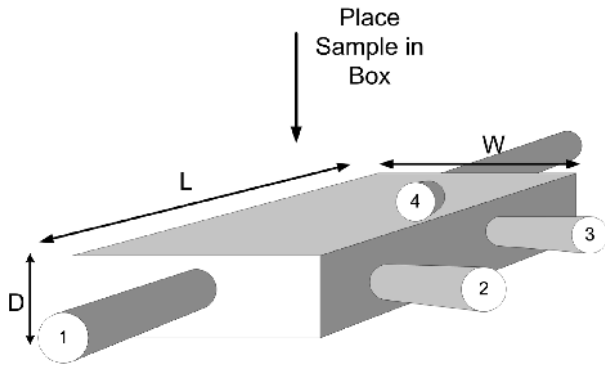


FIGURE 11.7 Soil box method for determining soil resistivity.

$$\rho = R \frac{WDR}{L}, \quad (11.9)$$

where the W , D , and L are the dimensions of the soil box (between the electrodes) and R is the measured resistance when current is passed between pins 1 and 4 and the potential gradient is measured between pins 2 and 3.

Finally, a Wenner 8-pin circular system is presented in Figure 11.8. In this method, eight separate measurements are made using adjacent sets of four pins. The outer set supplies the current; the inner set supplies the voltage reading. The average sample resistance, R_{avg} , is calculated, and the resistivity is determined via³

$$\rho = f(R_{avg}K_1 + K_2), \quad (11.10)$$



FIGURE 11.8 A photograph of a Wenner eight-pin electrical resistivity measurement cell.

where f is a temperature correction factor, and K_1 and K_2 are cell constants that depend upon the cell design and are determined from the measurement of a specimen of known resistivity.

The values of the protection current depend upon the integrity of the protective coating on the structure, the velocity and salinity of the water, and the presence of sulphate-reducing bacteria. Typically, i_{prot} varies from one to two microamps per square foot of protected structure, in less corrosive conditions at the metal surface, to 50 or 60 $\mu A/ft^2$ in severe service conditions.

11.3.2 Resistance Calculations

The resistance of the medium between the anodes and the cathodically protected structure plays an important role in determining the number of anodes and, for impressed systems, the rectifier voltage, as discussed below. When a ground bed is designed, the anodes are placed in augured holes and surrounded by a backfill that is comprised of coke or some other conductive carbonaceous material. This backfill effectively increases the surface area of each anode, which reduces the electrical resistance of the ground bed. If the overlying soil surface is very shallow, the anodes can be laid horizontally in a trench. Figure 11.9 gives some typical ground bed layouts. For a typical vertical arrangement, the anodes are placed in holes 8–12 in. in diameter with a 6 in. to 1 ft allowance for backfill at the top and bottom of the hole. If multiple anodes are used, they can be placed linearly with a separation distance of 15–20 ft.

For a single anode, the following empirical design equation is used in the resistance calculation:

$$R = \frac{\rho}{2\pi L} \left[\ln\left(\frac{8L}{D}\right) - 1 \right], \quad (11.11)$$

- Where ρ = resistivity of the backfill or soil
- D = anode backfill diameter or anode diameter
- L = length of the backfill or soil

If multiple vertical anodes are required, with linear spacing S , in a single ground bed, the anodes will interfere with one another, and the result obtained by Eq. (11.8) should not simply be divided by the number of anodes, N . Instead, an interference factor is incorporated into the equation, which yields the multi-anode ground bed resistance equation

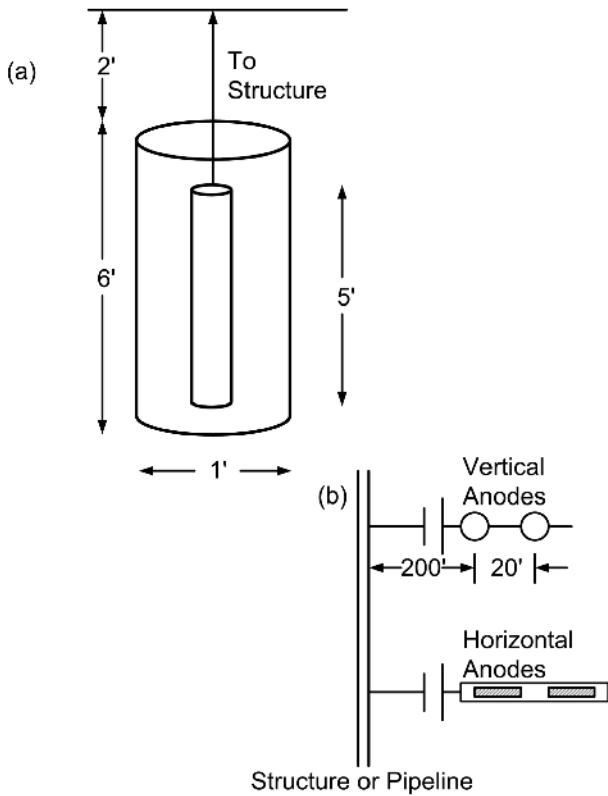


FIGURE 11.9 (a) Typical anode and backfill dimensions. (b) Spacing of vertical and horizontal anodes.

$$R = \frac{\rho}{2\pi LN} \left[\ln\left(\frac{8L}{D}\right) - 1 + \frac{2L}{S} \ln(0.656N) \right]. \quad (11.12)$$

For horizontal anodes, a single equation is used for both single and multiple anodes. This is possible because multiple anodes are surrounded by the same electrically conductive backfill as shown in Figure 11.10. The design equation in this case is

$$R = \frac{\rho}{2\pi L} \left[\ln\left(\frac{4L}{D}\right) + \ln\left(\frac{L}{X}\right) - 2 + \frac{2X}{L} \right], \quad (11.13)$$

where X is the anode depth and the other symbols have the usual meanings. Equations (11.8), (11.9), and (11.10) are used for both galvanic and impressed ground bed resistance calculations.

11.3.3 Resistance Calculation Procedure

Both the ground bed resistance, which is often called the internal resistance, and the soil resistance have to

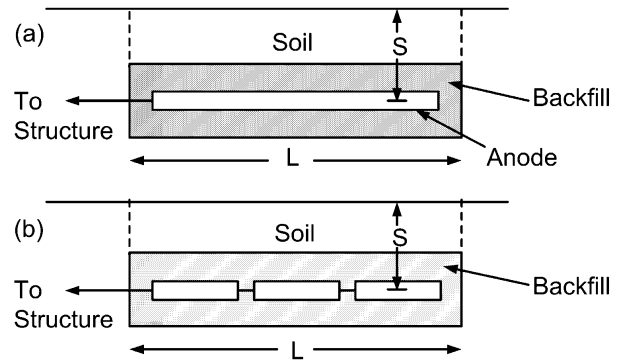


FIGURE 11.10 Arrangement of horizontal anodes with calculation nomenclature. (a) Single Anode. (b) Multiple anodes in a single ground bed.

be added to give the total resistance between the ground bed and the buried structure. The following procedure is recommended to determine the total resistance:

1. Calculate the resistance between the anode and the protected structure, using the anode dimensions, the resistivity of the backfill, and the appropriate equation for the number of anodes and geometry.
2. Calculate the resistance between the backfill and the protected structure, using the backfill dimensions, the resistivity of the backfill, and the appropriate equation for the number of anodes and geometry.
3. Subtract the value calculated in Step 2 from that calculated in Step 1. This will give the internal resistance.
4. Calculate the soil resistance, using the backfill dimensions and the soil resistivity.
5. Add the results of Step 3 and Step 4 to provide the total resistance.

11.3.4 Comparison of Magnesium and Zinc Anodes

Magnesium anodes are more frequently used in galvanic systems because magnesium has a greater driving force, since it is a less noble metal than zinc. Also, magnesium anodes generally produce more theoretical amp-hours per pound of magnesium, and the number of theoretical pounds that are used per year is less than that of zinc anodes. However, these advantages are somewhat offset by the low density of magnesium, which can result in large, bulky anodes and a current efficiency that is approximately half

that of zinc anodes. This changes these theoretical values and makes zinc anodes more competitive. However, zinc anodes are only used when the soil or water resistivity is low. In all other situations, magnesium anodes should be used. Figure 11.11 schematically illustrates the differences between magnesium and zinc anodes. As the corrosion current density, i_{corr} , on magnesium anodes is greater, these anodes will be consumed faster than zinc anodes.

The consumption rate of anodes can be estimated using Dwight's equation, which determines the output current of an anode:

$$I = \frac{2\pi VL}{\rho \ln(8L/D - 1)} \quad (11.14)$$

The size of bare anodes varies with application and vendor, but typical anodes weigh from a few pounds to 60 or so, with dimensions of a few inches to several feet. Anodes are also available pre-packed with a surrounding of electrically conductive back-fill. This adds considerably to the size and weight of the anodes, sometimes even doubling the weight.

11.3.5 Design Procedure for a Galvanic CP System

The design procedure for galvanic systems is iterative, as the engineer does not know at the start whether the resistance of the ground bed and soil will be so high as to prevent current from flowing between the anodes and the protected structure, as in

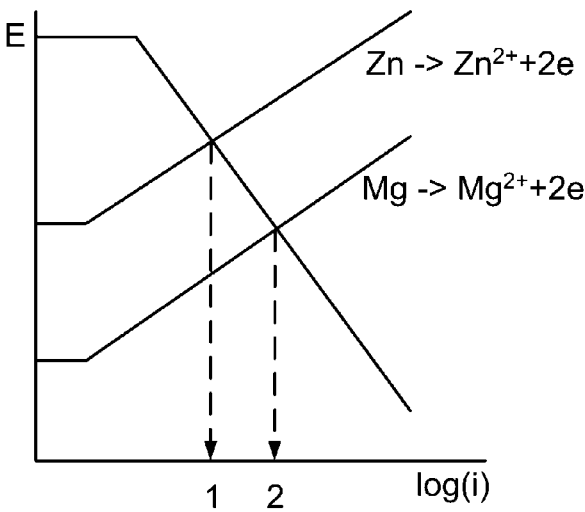


FIGURE 11.11 Schematic of the kinetics of zinc and magnesium anodes showing the lesser corrosion rate of zinc (1) than magnesium.

$$E_c - E_a < I_{prot}R. \quad (11.15)$$

This is due to the fact that the protection potential (E_c) is fixed and determined by the construction material of the object to be protected. The solution potential (E_a) is also fixed and depends upon the anode composition. Therefore, unlike impressed system, these potentials cannot be adjusted to accommodate a particularly high ground bed and/or soil resistance. The design procedure is as follows:

1. Determine the current requirements from field current demand tests. Measures the electrical density of the soil during a field survey of the amount of current required to achieve the protection potential.
2. Calculate the total weight of anodes required to last for a given anode life. To take into account the fact that the anodes will break apart after a period of time, a utilization factor is incorporated into the equation that is used to calculate the weight:

$$W = \frac{I_{prot}tM}{zF\varepsilon U} \quad (11.16)$$

where W = total weight of anode required
 t = time
 M = molar mass
 z = charge transferred in the electrode reaction
 F = Faraday's constant
 ε = current efficiency
 U = utilization factor

This equation can also be written as

$$W = \frac{\Theta I_{prot}}{\eta U}, \quad (11.17)$$

where Θ is the theoretical pounds of anode used per year per ampere.

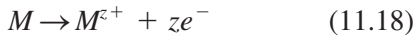
1. Select the number of anodes that are needed to make up the total weight of anodes required.
2. Determine the total resistance between the anodes and the buried structure.
3. Check to see if $E_c - E_a \geq I_{prot}R$. If this condition is true, then the calculation is finished. If this is not true, a different ground bed configuration is specified and the calculation repeated. In this case, it

is usual to increase the number of anodes, but keep the same total weight.

11.4 IMPRESSED CATHODIC PROTECTION SYSTEMS

Impressed CP systems are much more widely used than galvanic systems, and they are used to protect larger systems, such as pipelines. In these systems, a rectifier that converts alternating to direct current replaces the sacrificial anode. Thus, a source of alternating current must be available close to the structure, which may be problematic in areas that are remote or difficult to access. In these cases, sacrificial anodes should be employed as the source of current. A schematic of the equipment used in a typical impressed CP system is shown in Figure 11.12, which consists of single or multiple anodes in a ground bed, a rectifier, plus monitoring equipment, such as a voltmeter and reference electrode.

In an impressed CP system the metal wastage anodic reactions, such as



should be avoided by controlling the potential. Instead, reactions involving oxygen or chlorine liberation are preferred, with oxygen evolution first occurring, followed by chlorine liberation at higher potentials if chloride ions are present, as follows:

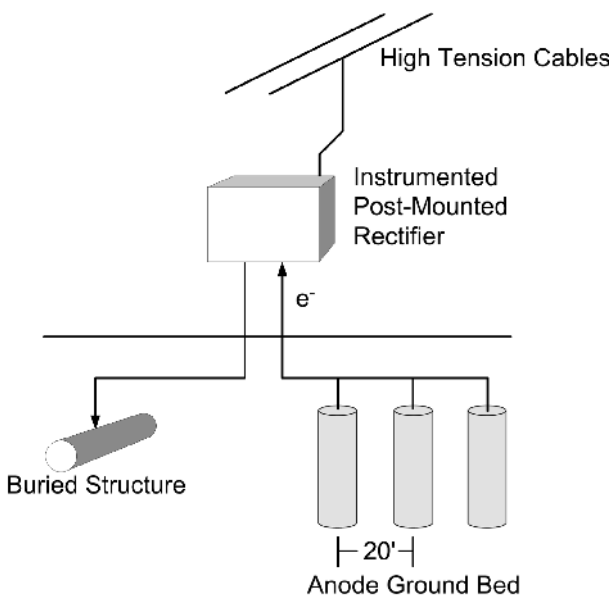
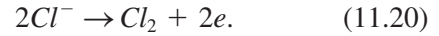
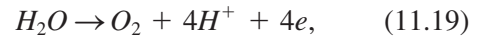


FIGURE 11.12 A schematic of an impressed CP system.



Because these reactions liberate gases, the ground bed ideally should be vented.

11.4.1 Anode Materials

The ideal anode material should be inexpensive, have low consumption rates, and be able to easily evolve the oxygen and/or chlorine gas. There are numerous anode materials available for use in a ground bed, as described below.

11.4.1.1 Graphite

This material is commonly used in compacted form, and it easily evolves both oxygen and chlorine. However, it is brittle and can easily be damaged. It is inert but care has to be taken to ensure that high current densities are not passed through the ground bed, as this will result in the oxidation of the anodes to carbon dioxide. Graphite anodes are typically used in soil systems. Figure 11.13 shows the kinetics of oxygen evolution on graphite anodes that are used to protect a carbon steel structure. The difference in potential between the oxygen evolution reaction at the anode and the reversible potential of iron ($E_c - E_a$) is 2 volts.

11.4.1.2 Cast Iron and Scrap Steel

These materials should be avoided because of the anodic reaction described in Eq. (11.2), and the fact that

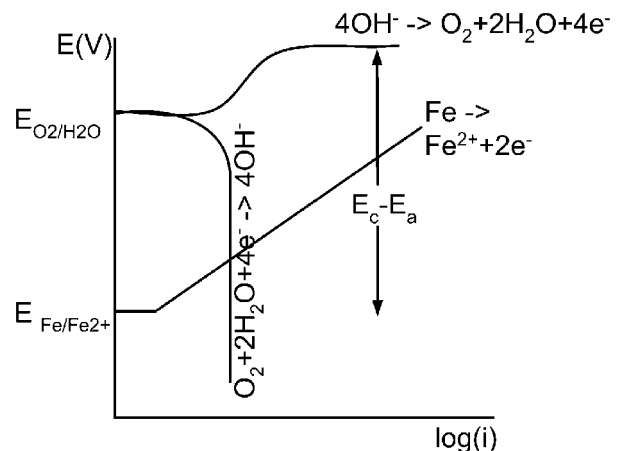


FIGURE 11.13 The kinetics of oxygen evolution on graphite anodes.

there may be high consumption rates of the anodes. This leads to contamination of the surrounding area. This type of anode should be avoided unless protection is required for a short duration only. The primary advantage of these electrodes is their low cost.

11.4.1.3 Chromium-Bearing High Silicon Cast Iron

This low-cost passive alloy is suitable for soil applications but it should not be used where significant levels of chloride ions are present, as pitting corrosion may occur. There is slight anodic dissolution (but the consumption rate of the anode is very slow), and oxygen evolution is the predominant anodic reaction. These electrodes are suitable for use in soils, freshwater, and saltwater. Stainless steels should not be used as anodes, as they are expensive and the protective passive film, which is responsible for corrosion resistance, breaks down near the oxygen evolution potential.

11.4.1.4 Other Anode Materials

There are numerous other materials that can be used as anodes, including lead alloys, conductive oxides, polymers, and platinized electrodes, such as expensive platinized titanium. However, these exotic anodes are used infrequently.

11.4.2 Design Procedure for an Impressed CP System

Since the source of electrons is rectified alternating current, there is no limitation on the amount of current that can be supplied to the system, unlike galvanic systems. Thus, the engineer can choose a ground bed design and set the voltage required to protect the buried structure on the rectifier controls. Hence, the calculation is not iterative. There are four steps in the design process.

1. Determine the current requirements from field current demand tests. This provides the protection current, I_{prot} . A soil survey should also be conducted to determine the soil resistivity.
2. Using 1 ampere per anode as a guide, specify the number of anodes in the ground bed.
3. Choose the anode arrangement (horizontal or vertical) and calculate the resistance between the structure to be protected and the ground bed. Use equations (11.11) to (11.13) and the calculation procedure presented in Section 11.3.3.

4. Calculate the rectifier voltage:

$$E = E_c - E_a + I_{\text{prot}}(R + R_l), \quad (11.21)$$

where R_l is the resistance of the wiring used in the installation. For oxygen evolution on graphite anodes protecting a carbon steel structure, $E_c - E_a$ is 2 volts (as illustrated in Figure 11.13), but this will, of course, be different for other combinations of anodes, anodic reactions, and protected metals.

11.5 GROUND BED SPACING

For most structures, it is difficult to theoretically determine the electrical potential over the surface of the structure. It is generally easier to perform experiments to determine potential attenuation characteristics. When a large structure is to be protected, a single ground bed may not be sufficient to protect the whole structure. As discussed earlier, the potential of a steel structure must have a maximum potential of $-0.85 \text{ V}_{\text{Cu/CuSO}_4}$ for protection. If this potential is applied at a pipe wall, for example, the potential will increase along the pipe length and the protection will be attenuated until no protection is afforded to the structure. This decrease in potential is schematically illustrated in Figure 11.14 for a pipeline, for which analytical equations have been developed that describe the potential attenuation. This section first derives these equations for this special case and, second, shows how these can be used to determine the

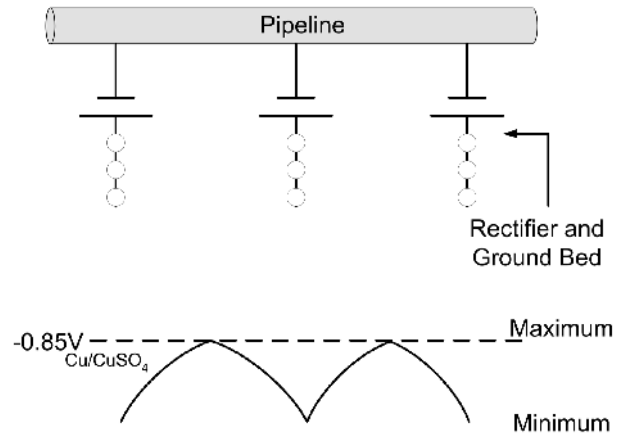


FIGURE 11.14 Potential attenuation along a pipeline. If the maximum potential of $-0.85 \text{ V}_{\text{Cu/CuSO}_4}$ is exceeded, the pipeline will not be protected in those areas.

spacing of multiple anode ground bed installations for the protection of large linear buried structures such as pipelines.

The following derivation (Figure 11.15) is after Uhlig.⁷ Consider a section of well-coated pipeline, to which a single ground bed is attached, where

- E = the difference between the actual potential at the pipe and E_{corr} ,
- E_a = the difference between the potential of the pipe and E_{corr} at the bonding point,
- E_x = the difference between the potential of the pipe and E_{corr} at a distance of x from the bonding point,
- i_x = the current density at the pipe surface at x ,
- I_x = the total current in the pipewall at x ,
- r = the pipe radius,
- R_L = electrical resistance of the pipe per unit length,
- x = the distance from the ground bed to a point on the pipe,
- z = electrical resistance of the pipe coating per unit area.

The objective is to mathematically determine the rate of attenuation of potential along the structure. The total current flowing in the pipe is the integral of the current density along the pipe multiplied by the cross sectional area. Or, in terms of a fractional length of pipe, dx :

$$\frac{dI_x}{dx} = -2\pi r i_x \tag{11.22}$$

Applying Ohm's law over the fractional length of pipeline

$$dE_x = -R_L dx I_x \tag{11.23}$$

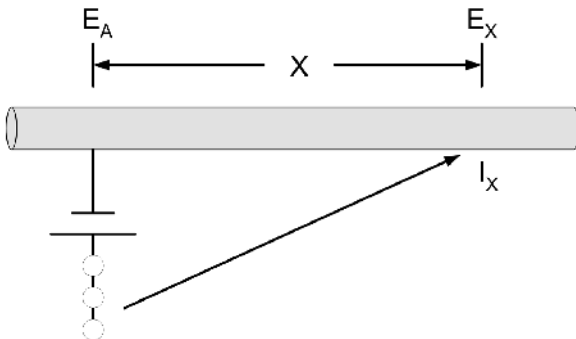


FIGURE 11.15 A segment of a pipeline with a single ground bed. Adapted from Uhlig.⁷

Equations (11.22) and (11.23) yield

$$\frac{d^2 E_x}{dx^2} = R_L (2\pi r i_x) \tag{11.24}$$

This equation has two dependent variables. Therefore, another equation is needed for closure. Assuming that the potential is proportional to the product of the resistivity of the porous coating and the current density at the pipe surface, then,

$$E_x = k z i_x \tag{11.25}$$

where k is a proportionality constant. Eq. (11.21) provides closure; thus,

$$\frac{d^2 E_x}{dx^2} = \left(\frac{R_L 2\pi}{kz} \right) E_x \tag{11.26}$$

Eq. (11.26) describes the potential attenuation along a buried structure.

11.5.1 Determination of the Number of Ground beds

To ensure that the potential of the protected structure does not rise above E_{prot} , the appropriate spacing of CP stations can be determined from Eq. (11.26). If insufficient numbers of (and, consequently, large separations between) stations occur, then the potential will be located in the active region in Figure 11.1; corrosion will occur in those zones that fall in this region. However, the procedure to determine a sufficient number of stations is relatively simple.

First, the parameter product kz is determined. The solution of Eq. (11.26) for a single station on an infinitely long pipeline can be obtained by applying the following boundary conditions:

$$E_x|_{x=0} = E_a \tag{11.27}$$

$$E_x|_{x=\infty} = 0, \tag{11.28}$$

with result

$$E_x = E_a \exp \left[\left(- \frac{R_L 2\pi r}{kz} \right)^{0.5} x \right], \tag{11.29}$$

or

$$\ln \frac{E_x}{E_a} = \left(- \frac{R_L 2\pi r}{kz} \right)^{0.5} x. \tag{11.30}$$

By applying a current on the pipeline, the attenuation along it can be measured at various locations along the pipe and a plot $\ln(E_x/E_a)$ versus distance, x , will have a slope of $(-R_L 2\pi r/kz)^{0.5}$. The product kz can be determined from the slope since all other parameters are known.

To determine the actual spacing of stations, Eq. (11.26) is solved for the case of two identical stations separated by a distance, P . At the midpoint between the stations, $P/2$, no current will flow, yielding the following boundary condition:

$$\left. \frac{dE_x}{dx} \right|_{x=P/2} = 0. \quad (11.31)$$

This yields the a potential distribution between stations as

$$E_a = E_{P/2} \cosh \left[\left(-\frac{R_L 2\pi r}{kz} \right)^{0.5} \frac{P}{2} \right]. \quad (11.32)$$

Since E_a is specified by the corrosion engineer and dialed into the rectifier, $E_{P/2}$ is the maximum potential in the pipeline, which is E_{prot} . Thus, E_{prot} , R_L , r and kz are known, and the spacing between stations can be determined. It would seem from this equation that a single station or ground bed could protect an extremely large structure by decreasing the potential at the station to a very low value. However, this is not the case, as too low of a potential would debond the anticorrosive coating on the metal and values of E_a of restricted to a few volts.

11.5.2 Current Requirements for Impressed Systems

To determine the drainage current at the bonding point, consider a single station on a pipeline as shown in Figure 11.16.

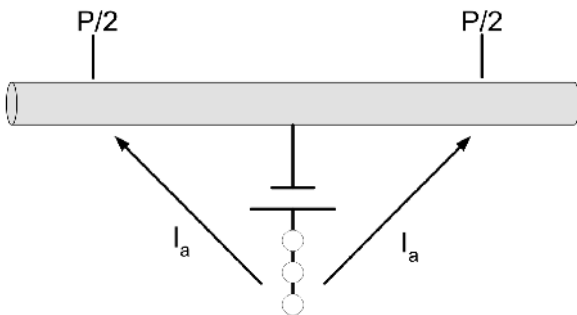


FIGURE 11.16 Current from a single ground bed installation.

The current distribution along the pipeline can be obtained from Eqs. (11.23) and (11.29), yielding Eq. (11.30).⁷

$$I_a = \left(\frac{2\pi r R_L}{kz} \right)^{0.5} \frac{E_a}{R_L} \exp \left[-\left(\frac{2\pi r R_L}{kz} \right)^{0.5} x \right]. \quad (11.33)$$

At the station, the drainage current is two times that calculated via this equation. In other words,

$$I_x = 2 \left(\frac{2\pi r R_L}{kz} \right)^{0.5} \frac{E_a}{R_L}. \quad (11.34)$$

For several stations spaced a distance a apart, a similar argument produces the design equation

$$I_x = 2 \left(\frac{2\pi r R_L}{kz} \right)^{0.5} \frac{E_{P/2}}{R_L} \sinh \left[\left(\frac{2\pi r R_L}{kz} \right)^{0.5} \frac{a}{2} \right]. \quad (11.35)$$

11.5.3 Cathodic Protection of Internal Surfaces

Cathodic protection is not generally used for the protection of enclosed equipment, except for tanks or other pieces of equipment that have a low surface area of metal-to-volume ratio and an open structure. This is because the CP equipment cannot usually pass current easily in equipment due to the low electrical resistance of the solution. This ability to pass current is called *throwing power*. The throwing power of a CP system that is protecting the outside of a structure is limited by the electrical resistance of structure, which is made of an alloy or metal; thus, the throwing power is much greater.

For the case of a CP system protecting internal surfaces, the most prudent way of designing is to perform pilot scale tests. A second option would be to determine the potential of the surfaces by mathematical modeling. This option is difficult and computationally intensive, but it can be used for determining the potential of both internal and external surfaces. The mathematical procedure involves solving Poisson's Equation with the appropriate potential and geometric boundary conditions. In this procedure, the rectifier potential would be set in the model, and the potential calculated and checked to see if protection was afforded over the structure by measuring the potential at numerous equations. Poisson's Equation is

$$\nabla^2 \phi = 0, \quad (11.36)$$

where ϕ is the potential. However, one way of estimating the throwing power in simple systems, such as heat exchanger tubes or pipes connecting tanks to chemical process equipment is to apply Eq. (11.37):

$$TP = \left(r \frac{E_c - E_a}{\rho_s i} \right)^{0.5} \quad (11.37)$$

In this equation, the difference between the cathodic (E_c) and (E_a) anodic potentials is taken as 2 V, and i and ρ_s are the current density in and the resistivity of the solution in the vessel or pipe.

11.5.4 Stray Current Corrosion

When a CP system is installed, care should be taken to electrically bond the protected structure to other buried metal objects. If structures are not bonded, a cathode-anode couple may be formed between the protected structure and other structure. The resulting current flow may cause local areas of corrosion on the unprotected structure. Consider the two crossing pipelines in Figure 11.17. If the lower pipeline is protected, the upper pipeline will corrode at the closest crossing points. This problem can be resolved by electrically bonding the two pipelines which, in essence, causes both pipelines to be cathodically protected. To minimize the risk of stray current corrosion, the potential difference between the two pipelines should be checked and an electrical resistor placed at one of the bonding points to eliminate any differences. Figure 11.18 presents a protected structure that is close to a buried or semi-buried

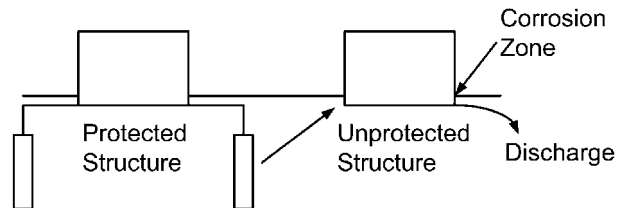


FIGURE 11.18 Stray current corrosion with two closely situated structures. Current is discharged on the unprotected structure, causing localized corrosion.

structure. In this situation, the structure would corrode as the stray currents pass in at one side and are discharged at a corrosion zone on the opposite side of the structure. Electrical bonding of the structure to the pipeline would minimize damage.

11.5.5 Overprotection

To ensure completeness of protection, engineers may overprotect a system by reducing the potential lower than that determined by the Nernst Equation. There is generally no harm in overprotecting a system except increased power consumption and an increased rate of anode consumption. However, if the overprotection is excessive, coatings may be damaged, and hydrogen embrittlement and blistering may occur.⁸

11.6 REFERENCES

1. Report No. FHWA-RD-01-156. Washington, DC: Federal Highway Administration, 2001.
2. Shrier, L. L and Jarman, R. A. *Corrosion, 3rd Ed., Vol. 2*. Oxford: Butterworth-Heinemann, Ltd., 1994, pp. 10–19.
3. Uhlig, H. H. and Revie, W. *Corrosion and Corrosion Control—An Introduction to Corrosion Science and Engineering*. New York: John Wiley and Sons, Inc., 1985, p. 425.
4. Kailinski, R. J. and Kelly, W. E. Estimating Water Content of Soils from Electrical Resistivity. *Geotechnical Testing Journal*, 16(3), 1993, p. 324.
5. Kailinski, R. J. and Kelly, W. E. Electrical-Resistivity Measurements for Evaluating Compacted-Soil Liners. *Journal of Geotechnical Testing*, Vol. 120(2), 1994, p. 455.
6. Roberge, P. *Handbook of Corrosion Engineering*. New York: McGraw-Hill, 2000, p. 873.
7. Uhlig, H. H. and Revie, W. *Corrosion and Corrosion Control—An Introduction to Corrosion Science and Engineering*. New York: John Wiley and Sons, Inc., 1985, pp. 421–422.
8. Schweitzer, P. A. Cathodic Protection. In *Corrosion Engineering Handbook*. P. A. Schweitzer, Ed. New York: Marcel Dekker, 1996, p. 553.

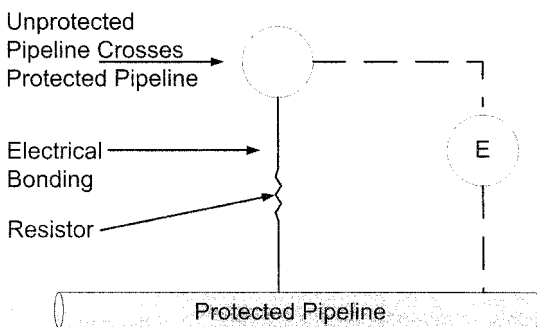


FIGURE 11.17 Stray current corrosion and crossing pipelines. Without the electrical bonding in place, there would be a difference in potentials of the two pipelines and the unprotected pipeline would corrode. With the bonding in place, both structures are protected, although more current will be needed to be supplied by the rectifier to account for the increased surface area to be protected.

CHAPTER 12

POLYMERIC FLAME RETARDANTS: PROBLEMS AND DECISIONS

G. E. Zaikov
S. M. Lomakin

Institute of Biochemical Physics of Russian Academy of Sciences, Moscow, Russia

| | |
|--|-----|
| 12.1 INTRODUCTION: HOW FLAME RETARDANTS WORK | 243 |
| 12.2 TOXICOLOGY OF DBDPO, OBDPO, PeBDPO, AND HBCD | 246 |
| 12.3 DIOXINS | 249 |
| 12.4 EXPOSURE LEVELS | 255 |
| 12.5 REGULATORY CONTROLS | 256 |
| 12.6 REFERENCES | 257 |

12.1 INTRODUCTION: HOW FLAME RETARDANTS WORK

Flame retardants are chemicals added to polymeric materials, both natural and synthetic, to enhance flame-retardant properties and to prevent fire. The term “flame retardant” represents a class of use, not a class of chemical structure. Preventive flame protection, including the use of flame retardants, has been practiced since ancient times—Romans used a mixture of alum and vinegar on wood in about 200 BC.

Flame retardant systems for synthetic or organic polymers act in five basic ways: (1) gas dilution, (2) thermal quenching, (3) protective coating, (4) physical dilution, (5) chemical interaction; or through a combination of these mechanisms.

1. *Inert gas dilution* involves using additives that produce large volumes of non-combustible gases on decomposition. These gases dilute the oxygen supply to the flame or dilute the fuel concentration below the flammability limit. Metal hydroxides, metal salts, and some nitrogen compounds function in this way.
2. *Thermal quenching* is the result of endothermic decomposition of the flame retardant. Metal hydroxides, metal salts, and nitrogen compounds act to decrease surface temperature and the rate of burning.

3. Some flame retardants form a *protective liquid or char barrier*. This limits the amount of polymer available to the flame front and/or acts as an insulating layer to reduce the heat transfer from the flame to the polymer. Phosphorus compounds and intumescent systems based on melamine and other nitrogen compounds are examples of this category.
4. Inert fillers (glass fibres and microspheres) and minerals (talc) act as thermal sinks to increase the heat capacity of the polymer or reduce its fuel content (*physical dilution*).
5. Halogens and some phosphorus flame retardants act by *chemical interaction*. The flame retardant dissociates into radical species that compete with chain-propagating steps in the combustion process.

Chemicals that are used as flame retardants can be inorganic, organic, mineral, halogen-containing, or phosphorus-containing. Halogenated products are based primarily on chlorine and bromine. This group represents a large volume of the worldwide production. Halogenated flame retardants can be divided into three classes: aromatic, aliphatic, and cycloaliphatic. Bromine and chlorine compounds are the only halogen compounds having commercial significance as flame-retardant chemicals. Fluorine compounds are expensive and, except in special cases, are ineffective because the C-F bond is too strong. Iodine

compounds, although effective, are expensive and too unstable to be useful [1]. The brominated flame retardants are much more numerous than the chlorinated types because of their higher efficacy [2].

With respect to processability, halogenated flame retardants vary in their thermal stability. In general, aromatic brominated flame retardants are more thermally stable than chlorinated aliphatics, which are more thermally stable than brominated aliphatics. Brominated aromatic compounds can be used in thermoplastics at fairly high temperatures without the use of stabilizers, and at very high temperatures with stabilizers. The thermal stability of the chlorinated and brominated aliphatics is such that, with few exceptions, they must be used with thermal stabilizers, such as a tin compound.

Halogenated flame retardants are either added to or reacted with the base polymer. Additive flame retardants are those that do not react in the application designated. There are a few compounds that can be used as an additive in one application and as a reactive in another; tetrabromobisphenol A is the most notable example. Reactive flame retardants become a part of the polymer either by becoming a part of the backbone or by grafting onto the backbone. The choice of a reactive flame retardant is more complex than the choice of an additive type. Synergists, such as antimony oxides, are frequently used with halogenated flame retardants.

Natural or synthetic material that burns produces potentially toxic products. There has been considerable debate on whether addition of organic flame retardants results in the generation of smoke that is more toxic and may result in adverse health effects on those exposed. There has been concern, in particular, about the emission of polybrominated dibenzofurans (PBDFs) and polybrominated dibenzodioxins (PBDDs) during manufacture, use and combustion of brominated flame retardants. Combustion of any organic chemical may generate carbon monoxide (CO), which is a highly toxic non-irritating gas, and a variety of other potentially toxic chemicals. Some of the major toxic products that can be produced by pyrolysis of flame retardants are: CO, CO₂, HCl, P_xO_y, ammonia, bromofurans, HBr, HCN, NO_x, and phosphoric acid. In general, the acute toxicity of fire atmospheres is determined mainly by the amount of CO, the source of which is the amount of generally available flammable material. Most fire victims die in post-flashover fires where the emission of CO is maximized and the emission of HCN and other gases is less. The acute toxic potency of smoke from most materials is lower than that of CO [3].

Flame retardants significantly decrease the burning rate of the product, reducing heat yields and quantities of toxic gas. In most cases, smoke was not significantly different in room fire tests between flame-retarded and non-flame-retarded products [4]. Morikawa et al. [5] reported toxicity studies on gases from full-scale room fires involving fire retardant materials (a variety, but not specified). HCN and CO were the two major toxicants. There was no evidence that the smoke from flame-retarded materials was more toxic to rabbits than the smoke from non-flame-retarded materials.

Regarding brominated flame retardants, Cullis [2] stated that unless suitable metal oxides or metal carbonates are also present, virtually all the bromine is eventually converted to gaseous hydrogen bromide (HBr). This is a corrosive and powerful sensory irritant. In a fire situation, however, it is always carbon monoxide (CO) or hydrogen cyanide (HCN), rather than an irritant, that causes rapid incapacitation. Owing to its high reactivity, hydrogen bromide is unlikely to reach dangerously high concentrations [2].

Halogenated dibenzofurans and dibenzodioxins (PBDFs and PBDDs) can be formed from polybrominated diphenyl ethers (PBDEs), polybrominated phenols, polybrominated biphenyls (PBBs), and other brominated flame retardants under various laboratory conditions, including heating. Because chlorinated derivatives are preferably formed during pyrolysis, mixed halogen compounds will be predominantly produced if a chlorine source is also available [6]. As in the case of PCDD/PCDF, it is the 2,3,7,8-substituted isomers that are toxic.

In the late 1980s, many pyrolysis experiments (at temperatures of 400–900 °C) on brominated flame retardants and flame retardant systems were performed, and the breakdown products measured. Flame retardants or intermediates tested included PBBs, PBDEs, 2,4,6-tribromophenol, pentabromophenol, tetrabromobisphenol A, and tetrabromophthalic anhydride [7–11]. Pyrolysis of the flame retardants alone, as well as with polymer mixtures, was investigated [12–14]. Although they indicate which flame retardants are likely to form PBDF (and, to a lesser extent, PBDD), pyrolysis experiments are not generally comparable to actual fire situations.

Exposure of the general population to flame retardants can occur via inhalation, dermal contact, and ingestion. Potential sources of exposure are consumer products, manufacturing or disposal facilities, and environmental media (including food intake). The same routes are possible for occupational exposure, mainly during production, processing, trans-

portation and disposal or recycling of the flame retardants or the treated products.

Occupational exposure to the breakdown products may also occur during fire fighting. As several of the compounds used are lipophilic and persistent, they may bioaccumulate. Some of the compounds have been shown to cause organ damage, genotoxic effects and cancer. There is also concern for occupational health and environmental effects from combustion/pyrolysis products, especially the polyhalogenated dibenzofurans and dibenzo-*p*-dioxins, from some organic flame retardants. Other breakdown products also need to be taken into account.

The properties of a number of flame retardants make them persistent and/or bioaccumulative, and they may therefore pose hazards to the environment. Some of the compounds that have been evaluated so far (polybrominated biphenyls, polybrominated diphenyl ethers and chlorinated paraffins) have been found to belong to this group. Some of these have therefore been recommended to not be used.

The availability of relevant data on flame retardants in the open literature is limited, especially for some existing chemicals produced before regulations for commercialization were strengthened in several countries. A recent study on the risk reduction of halogenated flame retardants (polyhalogenated biphenyls, precursors of dioxins and furans), commissioned by the Organization for Economic Cooperation and Development (OECD), has led to a voluntary industry commitment from the brominated flame retardant manufacturers [15]. The key points of this commitment are as follows:

1. There will be no manufacture of polybrominated biphenyls (PBBs), except deca-BB, which is manufactured by a single company in Europe. (This will be reviewed in five years.)
2. There will be no manufacture of the non-commercial polybrominated biphenyl ethers (PBBEs).
3. The impurities in deca- and octabromodiphenyl ethers will be minimized.
4. The release of pentabromodiphenyl ether during manufacturing, processing, and handling will be minimized.
5. Producers will cooperate with use and end-use industries on the safe disposal of polymers and textiles containing the selected brominated flame retardants.
6. Additional environmental fate studies will be initiated, as identified in the World Health Organiza-

tion's (WHO) International Program on Chemical Safety (IPCS) assessment and the European Union's Existing Chemicals program.

7. Producers will issue and update product literature to ensure safe handling of these flame retardants at customers and equipment manufacturers.
8. Producers will regularly evaluate the risk of these flame retardants on the basis of the latest information available.

However, there is no scientific justification for phasing out all brominated flame retardants (BFRs). BFRs, which are part of the halogenated flame retardants group, represent a category of 75 flame retardants, each with differing structures and properties. The only thing each has in common is the presence of bromine. Only one out of 75 BFRs is widely found in the environment, and this at declining levels. This is penta-BDE for which an E.U. risk assessment has been completed, leading to a proposal for phase-out in 2003. The industry fully accepts the proposed phase-out of penta-BDE, as it is based on a comprehensive risk assessment.

In 1991, a directive was proposed in the E.U. to limit PBDPO use in articles to 0.1%. The proposed directive was blocked from proceeding by the E.U. Environment Committee until such time as fire protection safety standards could be formulated and adopted in the E.U., due to the Committee's concern that adequate alternatives for these products did not exist. In 1994, the European Commission withdrew the directive from the E.U. regulatory process on the grounds that it was out of date. In doing so, the Commission noted that neither Germany nor the Netherlands had proceeded to introduce national rules on the PBDPO, and that the "international scientific community is now much less convinced that the PBDPO pose an unacceptable danger to human health and the environment" [8].

In May, 2001 the European Committee on the Environment, Public Health and Consumer Policy issued the proposal for a European Parliament and Council directive amending for the twenty-fourth time Council Directive 76/769/EEC, which relates to restrictions on the marketing and use of certain dangerous substances and preparations (pentabromodiphenyl ether). The last proposal is amended as follows: By way of derogation these provisions do not apply to technical grade octabromodiphenyl ether provided it contains less than 2% diphenylether, pentabromo derivative (pentaBDE) by mass. This proposal was justified by the contradiction

to prohibit the use of pentaBDE as a substance while permitting its residues to be present in significant quantities in other substances. The proposed maximum of 2% pentaBDE as a residue in technical grade octabromodiphenyl ether corresponds to the lowest percentage which allows the production of octabromodiphenyl ether to continue, pending completion of the risk assessment for this substance. [Council Directive 76/769/EEC, OJ No. L262, 27.9.76, p. 201.]

This chapter describes some basic features of dioxins and related compounds, and their influence on the environment. The word “dioxin” stands for a group of chemicals that occurs rarely, if ever, in nature. A very large proportion of dioxin comes from human sources. Dioxin began accumulating in the environment around 1900, when the founder of Dow Chemical (in Midland, Michigan) invented a way to split table salt into sodium atoms and chlorine atoms, thus making large quantities of “free chlorine” available for the first time [16]. Initially, Dow considered free chlorine a useless and dangerous waste. Soon, however, a way was found to turn this waste into a useful product by attaching chlorine atoms onto petroleum hydrocarbons, thus creating, during the 1930s and 1940s, a vast array of “chlorinated hydrocarbons.” These new chemicals, in turn, gave rise to many of today’s pesticides, solvents, plastics, and so forth.

Unfortunately, when these chlorinated hydrocarbons are processed in a chemical plant, or are burned in an incinerator, they release an unwanted byproduct—dioxin—the most toxic family of chemicals ever studied.

12.2 TOXICOLOGY OF DBDPO, OBDPO, PeBDPO, AND HBCD

The three commercial PBDPO flame retardants are DBDPO, OBDPO, and PeBDPO. The potential toxicologic effects of these three products vary with their degree of bromination. That is, in general, the greater the degree of bromination on the diphenyl oxide molecule, the lesser the toxicity of the PBDPO. (This also appears to hold true with the PBB.) Minimal effects are observed with DBDPO, in which both aromatic rings are fully brominated. Because of this variation in toxicology associated with the degree of bromination, generalized statements regarding the potential health and environmental effects of the entire class of PBDPO brominated flame retardants are inappropriate.

12.2.1 Decabromodiphenyl Oxide (DBDPO)

The DBDPO commercial product is composed of $\geq 97\%$ DBDPO. DBDPO is a very large molecule with a molecular weight of 959 g/m. DBDPO has undergone a wide range of toxicology tests in mammalian and aquatic species, and its toxicology is well characterized (Table 12.1) [17]. DBDPO is not acutely toxic to mammalian or aquatic species. DBDPO is not irritating to the skin or eye, is not a sensitizer, and does not induce chloracne or hepatic enzymes. The soot and char combustion products from HIPS/DBDPO/Sb₂O₃ are also not acutely toxic and are not chloracnegenic. DBDPO is not a reproductive toxicant and is not teratogenic. DBDPO has a low degree of long-term toxicity that can be attributed to its poor absorption, rapid elimination, and capacity to be metabolized. Doses of 10% and 5% of the diet were tolerated with no adverse effects by rats and mice for 14 and 90 days, respectively. Doses of 5% of the diet were tolerated for two years by rats and mice with no effect on body weight or mortality and only minimal evidence of organ effects. Two two-year carcinogenicity bioassays have been conducted. The first, at a top dose level of 1 mg/kg in rats, produced no evidence of carcinogenicity. The second one, conducted at 2.5 and 5% of the diet in rats and mice, produced some evidence of carcinogenicity depending on genus and sex [17].

DBDPO does not bioconcentrate in fish and can undergo photodegradation (at a very slow rate). DBDPO aqueous photodegradation products are not lower brominated diphenyl oxides. Leaching from polymers is insignificant. DBDPO is not widely distributed in the environment and, where found, is largely confined to sediments near point sources. DBDPO is likely to be highly bound to sediment, which will limit its bioavailability and is unlikely to be toxic or accumulated in sediment-dwelling species. DBDPO is not being detected in fish and water samples. DBDPO is not likely to present a toxicologic risk to wildlife, based on its low degree of toxicity in multiple studies in mammals. DBDPO does not present a bioaccumulation risk, based on its physical/chemical properties, and results of laboratory studies and environmental monitoring.

12.2.2 DBDPO Compared to PBB and PCB

DBDPO has been assumed by some to have similar properties and to pose the same potential environ-

TABLE 12.1 DBDPO Toxicology Summary, Composed of Existing Data [17]

| Test | Results |
|------------------------------------|---|
| Oral LD50 | > 2,000 mg/kg |
| Dermal LD50 | > 2,000 mg/kg |
| Inhalation LC50 | > 48.2 mg/L |
| Eye Irritation | Not an irritant |
| Skin Irritation | Not an irritant |
| Human Skin Sensitization | Not a skin sensitizer |
| Ames | Not mutagenic |
| Mouse Lymphoma | Not mutagenic |
| Sister Chromatid Exchange | Not mutagenic |
| Chromosome Aberration | Did not induce aberrations |
| 14-Day Rat and Mice Oral (Diet) | NOEL > 100,000 ppm (10%) |
| 90-Day Rat and Mice Oral (Diet) | NOEL > 50,000 ppm (5%) |
| Rat 1 Generation Reproduction | NOEL = 100 mg/kg (highest dose tested) |
| Rat Teratogenicity | NOEL > 1,000 mg/kg |
| Rat & Mouse Carcinogenicity (Diet) | 25,000 (2.5%) or 50,000 (5%) ppm Negative or equivocal evidence of carcinogenicity No effect body weight or mortality Minimal evidence of chronic toxicity |
| Rat Carcinogenicity (Diet) | NOEL > 1 mg/kg (highest dose tested) |
| Rat Hepatic Enzyme Induction | Did not induce hepatic enzymes |
| Rabbit Skin Acnegenicity | Not acnegenic; Soot and char not acnegenic |
| Rat Pharmacokinetics (Oral and IV) | Low bioavailability Poorly absorbed (<1%) from GI tract Rapidly Eliminated with short half-life (< 24 hours) |
| Ready Biodegradation | Not readily biodegradable |
| Fish LC50 | > 500 mg/L |
| Algae EC50 | > 1 mg/L |
| Fish Bioaccumulation | Not bioaccumulative; BCF<5 (60 µg/L) and <50 (6 µg/L) 6wk |
| Aqueous Photodegradation | Half-life >> 90 days; Products not lower BrDPOs |
| Polymer Extraction | Negligible |

mental threats as the polychlorinated biphenyls (PCBs) and the polybrominated biphenyls (PBBs). This assumption is apparently based on their seemingly similar chemical structures. However, these chemicals are very different from one another.

The first difference among the PCBs, PBBs, and DBDPOs are found in their physical/chemical properties. The PCBs are liquids. PBBs and DBDPOs are solids. The lower chlorinated PCBs are volatile. The PBBs and DBDPOs have extremely low vapor pressures and are not volatile. Their molecular weights vary greatly between the different classes. Hexachlorobiphenyl (HxCB) weighs 358 g/m; hexabromobiphenyl (HxBB) weighs 622 g/m; and DBDPO 959 g/m. The great difference in the molecular weights of HxCB and HxBB is due to the difference in weight of chlorine and bromine. Chlorine's atomic weight is 35; whereas, bromine's atomic weight is 79. The molecular volumes of the PCBs,

PBBs, and DBDPOs are also very different, again due to the influences of chlorine and bromine. Bromine atoms occupy a considerably larger volume than do chlorine atoms.

The above properties greatly influence the bioavailability, absorption, and bioaccumulation of the PCBs, PBBs, and DBDPOs in biotic systems. Pharmacokinetic studies show DBDPO has a half-life in rats of less than 24 hours [17]; whereas, less than 10% of the total HxBB dose would ever be excreted by rats [17]. In a study directly comparing the fish bioconcentration of DBDPO, octabromobiphenyl and tetrachlorobiphenyl, DBDPO and octabromobiphenyl were not taken up by the fish; whereas, the tetrachlorobiphenyl bioconcentrated at least 50 times over the exposure level within 4 hours [18]. In addition, the PCB and PBB effect levels in mammals are considerably lower than those of DBDPO and present a different toxicological picture.

The toxicology of the PCB/PBB/dioxins are generally accepted to be a receptor-mediated event. The lack of coplanarity and the orthogonal relationship of the diphenyl rings will not allow DBDPO to induce PCB/PBB/dioxin-like toxicity. There is an additional difference between these molecules, resulting from the presence of the ether linkage. The ether linkage causes a 120° bend in the alignment of the phenyl rings in the diphenyl oxide molecule. PCB and PBB, having no oxygen link between the two aromatic rings, lack this bend. Thus, the phenyl rings in the PBDPO cannot adopt a coplanar conformation similar to the toxic PCB and PBB congeners, 2,3,7,8-TCDD, and 2,3,7,8-TBDF. The PBDPO and 2,3,7,8-TCDD/F have distinctly different molecular geometries. The PBDPO are electronically and geometrically dissimilar to 2,2',4,4',5,5'-HxBB, due to the presence of the ether linkage.

Another major difference between these chemicals is in their use. PCBs were used in applications with a high potential for environmental release (as liquids in large volume transformers and capacitors and in paperless copiers). As a result of their physical properties and uses, PCB residues are found in many diverse locations around the world [19]. The production, distribution, and use of PBBs was not as widespread as PCBs; and PBBs, unlike PCBs, were not used in applications with significant potential for release to the environment. A main use of HxBB was in thermoplastics used as housings for typewriters and business machines; in these applications there has been little tendency to migrate from the thermoplastic [19].

As a result of these differences in properties and uses, environmental contamination with PCB, PBB and DBDPO commercial chemicals is vastly different in magnitude. PCBs were steadily released into the environment in many countries, presumably over decades, and were found to be pervasive, worldwide contaminants as early as 1978 [19]. In addition, the number of PCBs reaching the environment is probably nearly 100 different compounds. PBBs, encompassing a small number of chemical structures to begin with, are of concern due to a single contamination incident in 1973 in which a hexabromobiphenyl (HxBB) product was accidentally mixed in animal feed (this was apparently limited to the state of Michigan) [19]. Today, only one PBB, decabromobiphenyl, remains in commercial production. This PBB does not share the properties of HxBB. Finally, DBDPO is not a widespread or diffuse environmental contaminant; its primary use in

thermoplastics limits its environmental release and, thus, environmental exposure [17].

12.2.3 Octabromodiphenyl Oxide (OBDPO)

The molecular weight of the OBDPO molecule is 801 g/m. The commercial OBDPO product is a mixture of PBDPO congeners ranging from penta- to nonabromodiphenyl oxide. Existing data on OBDPO toxicology is summarized in Table 12.2. [17]. Like DBDPO, OBDPO is not acutely toxic, is not irritating, is not mutagenic, and is not bioconcentrating. OBDPO's toxicology data demonstrate that its properties on repeated exposure are different from that of DBDPO. OBDPO induced liver effects in 14-, 28-, and 90-day studies (12 mg/kg for 14 days or 100 mg/kg for 28 days), whereas DBDPO did not at significantly higher levels (10% diet for 14 days). OBDPO was also effective in inducing hepatic enzymes, whereas DBDPO was not. OBDPO produced teratogenic effects in the rat, but not the rabbit.

12.2.4 Pentabromodiphenyl Oxide (PeBDPO)

The molecular weight of the PeDPO molecule is 564 g/m. The commercial PeBDPO product is a mixture of PBDPO congeners consisting primarily of tetra- and pentabromodiphenyl oxide. Existing data on PeBDPO toxicology is summarized in Table 12.3 [17]. Like DBDPO and OBDPO, the PeBDPO commercial product is not acutely toxic, is not irritating, and is not mutagenic. Like OBDPO, PeBDPO's toxicology data demonstrates that its properties on repeated exposure are different from those of DBDPO. Liver effects were induced at 100 mg/kg in a 28-day study, and the No-Observable-Effect-Level (NOEL) in a 90-day study in rats was 2 mg/kg. PeBDPO was effective in inducing hepatic enzymes and, while the commercial mixture was found to bioconcentrate in fish, the major constituent of the product, the pentabromodiphenyl oxide molecule, showed no significant accumulation. Furthermore, the solvent dimethylsulfoxide (DMSO) was used in the fish bioconcentration study, which may have enhanced the uptake of the tetrabromodiphenyl oxide congener. DMSO is known for its ability to enhance the absorption of chemicals (including drugs) through the skin.

TABLE 12.2 OBDPO Toxicology Summary [17]

| Test | Results |
|------------------------------|---|
| Oral LD50 | > 28,000 mg/kg |
| Dermal LD50 | > 2,000 mg/kg |
| Inhalation LC50 | > 50 mg/L |
| Eye Irritation | Not an irritant |
| Skin Irritation | Not an irritant |
| Ames | Not mutagenic |
| Sister Chromatid Exchange | Not mutagenic |
| Unscheduled DNA Synthesis | Did not induce |
| 28-Day Rat Oral (Diet) | Liver effects @ 100, 1,000, 10,000 mg/kg diet |
| 90-Day Rat Oral (Diet) | Liver effects @ 100, 1,000, 10,000 mg/kg diet |
| 14-Day Rat Inhalation | NOEL = 1.2 mg/m ³ |
| Rat Teratogenicity | Teratogenic; NOEL = 2.5 mg/kg |
| Rabbit Teratogenicity | Not teratogenic |
| | NOEL = 5 mg/kg (fetotoxicity @ maternally toxic dose) |
| Rat Hepatic Enzyme Induction | Induced hepatic enzymes |
| Fish Bioaccumulation | BCF < 4 after 8-week exposure period |

TABLE 12.3 PeBDPO Toxicology Summary [17]

| Test | Results |
|------------------------------|--|
| Oral LD50 | > 500 mg/kg in CD rats 7,400 or 5,800 mg/kg in male or female Wistar rats, respectively |
| Dermal LD50 | > 2,000 mg/kg |
| Inhalation LD50 | > 200 mg/L |
| Eye Irritation | Slight irritation |
| Skin Irritation | Not an irritant |
| Ames | Not mutagenic |
| 28-Day Rat Oral (Gavage) | Liver effects at 100 and 1,000 mg/kg |
| 90-Day at Oral (Diet) | NOEL = 2 mg/kg |
| Rat Teratogenicity | Not teratogenic; NOEL maternal toxicity = 100 mg/kg |
| Rat Hepatic Enzyme Induction | Induced hepatic enzymes |
| Fish Bioaccumulation | BCF not significant (PeBDPO) BCF > 10,000 (TeBDPO); DMSO interaction |

12.2.5 Hexabromocyclododecane (HBCD)

HBCD is a cyclic aliphatic and is structurally distinct from the PBDPO flame retardants. HBCD's molecular weight is 641 g/m. The existing toxicology data on HBCD is summarized in Table 12.4. [17]. HBCD is not acutely toxic, is not irritating, and is not mutagenic. HBCD is not teratogenic in the rat at a top dose of 1% of the diet. Pharmacokinetics show that HBCD is rapidly absorbed from the gastrointestinal tract of rats and is rapidly metabolized and excreted. Over 86% of the dose was eliminated within 72 hours. HBCD's LC/EC50 in fish, daphnia, and algae are greater than HBCD's recently determined water solubility. Negligible migration from

foam insulation boards, HBCD's major use, was found.

Toxicology testing is ongoing on DBDPO, OBDPO, PeBDPO and HBCD, per industry's commitments under the E.U. risk assessment programs.

12.3 DIOXINS

Halogenated dibenzo-*p*-dioxins and related compounds (commonly known simply as dioxins) are contaminants present in a variety of environmental media. This class of compounds has caused great concern in the general public as well as intense interest in the scientific community. Much of the public concern revolves around the characterization of

TABLE 12.4 HBCD Toxicology Summary [17]

| Test | Results |
|----------------------------------|---|
| Oral LD50 | > 10,000 mg/kg |
| Dermal LD50 | > 8,000 mg/kg |
| Inhalation LC50 | > 200 mg/L |
| Eye Irritation | Not an irritant |
| Skin Irritation | Not an irritant |
| Ames | Not mutagenic |
| Rat Teratogenicity (Diet) | NOEL > 10,000 ppm (1%) |
| Rat Pharmacokinetics (Oral) | Rapidly absorbed from GI tract Rapidly metabolized Eliminated 86% of dose within 72 hr |
| Chicken Cataractogenicity (Diet) | NOEL > 10,500 ppm (1.5%) |
| Fish LC50 | L. macrochirus >100 mg/L L. idus > 10,000 mg/L |
| Daphnia EC50 | >1000 mg/L (24 hr) and = 146 mg/L (48 hr) |
| Bacterial EC50 | > 10,000 mg/L |
| Algae EC50 | EC50 > water solubility: S. subspicatus > 500 mg/L Chlorella sp. > 1.5 mg/l S. costatum, T. Pseudonana = 9.3 µg/L to 0.37 mg/L |
| Foam Migration | Negligible |

these compounds as among the most potent synthetic toxicants ever studied. Indeed, these compounds are extremely potent in producing a variety of effects in experimental animals, based on traditional toxicology studies at levels hundreds or thousands of times lower than most chemicals of environmental interest. In addition, human studies demonstrate that exposure to dioxin and dioxin-related compounds is associated with subtle biochemical and biological changes whose clinical significance is yet unknown and with chloracne, a serious skin condition associated with these and similar organic chemicals.

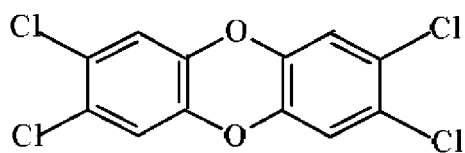
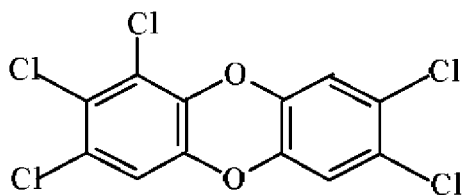
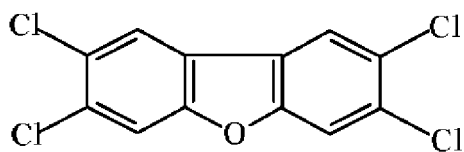
Laboratory studies suggest the probability that exposure to dioxin-like compounds may be associated with other serious health effects, including cancer. Recent laboratory studies have provided new insights into the mechanisms involved in the impact of dioxins on various cells and tissues and, ultimately, on toxicity. Dioxins have been demonstrated to be potent modulators of cellular growth and differentiation, particularly in epithelial tissues.

12.3.1 Chemical Structure and Properties of Dioxins

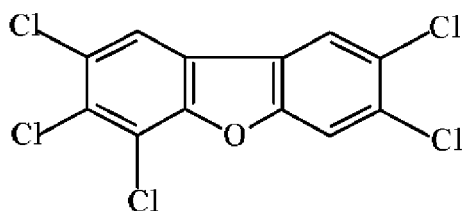
Polychlorinated dibenzodioxins (PCDDs), polychlorinated dibenzofurans (PCDFs), and polychlorinated biphenyls (PCBs) are chemically classified as halo-

genated aromatic hydrocarbons. The chlorinated and brominated dibenzodioxins and dibenzofurans are tricyclic aromatic compounds with similar physical and chemical properties, and both classes are similar structurally. Certain of the PCBs (the so-called coplanar or mono-ortho coplanar congeners) are also structurally and conformationally similar. The most widely studied of these compounds is 2,3,7,8-tetrachlorodibenzo-*p*-dioxin (TCDD). This compound, often called simply dioxin, represents the reference compound for this class of compounds. The structure of TCDD and several related compounds is shown in Figure 12.1.

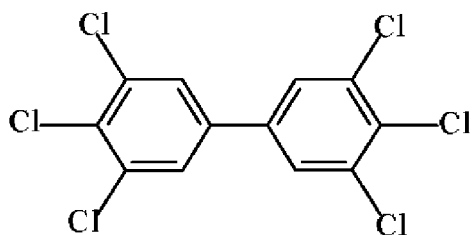
Dioxin-like compounds are defined to include the subset of this class of compounds, which are generally agreed to produce dioxin-like toxicity. These compounds are assigned individual toxicity equivalence factor (TEF) values as defined by international convention [20]. Results of *in vitro* and *in vivo* laboratory studies contribute to the assignment of a relative toxicity value. TEFs are estimates of the toxicity of dioxin-like compounds relative to the toxicity of TCDD, which is assigned a TEF of 1.0. All chlorinated dibenzodioxins (CDDs) and chlorinated dibenzofurans (CDFs) with chlorines substituted in the 2,3,7, and 8 positions are assigned TEF values. Additionally, the analogous brominated dioxins and furans (BDDs and BDFs) and certain polychlorinated biphenyls have recently been identified as hav-

2,3,7,8-Tetrachlorodibenzo-*p*-dioxin1,2,3,7,8-Pentachlorodibenzo-*p*-dioxin

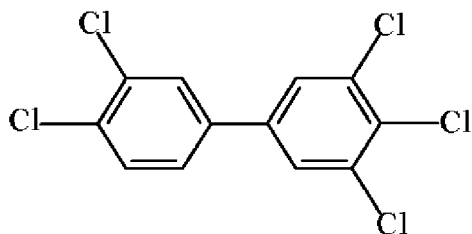
2,3,7,8-Tetrachlorodibenzofuran



2,3,4,7,8-Pentachlorodibenzofuran



3,3',4,4',5,5'-Hexachlorobiphenyl



3,3',4,4',5,5'-Pentachlorobiphenyl

FIGURE 12.1 The structures of dioxin and similar compounds.

ing dioxin-like toxicity and, thus, are also included in the definition of dioxin-like compounds. Generally accepted TEF values for chlorinated dibenzodioxins and dibenzofurans are shown in Table 12.5.

A World Health Organization International Program on Chemical Safety meeting, held in The Netherlands in December, 1993, considered the need to derive internationally acceptable interim TEFs for the dioxin-like PCBs. Recommendations arising from that meeting of experts [21] suggest that, in general, only a few of the dioxin-like PCBs are likely to be significant contributors to general population exposures to dioxin-like compounds. Dioxin-like PCBs may be responsible for approximately one-fourth to one-half of the total toxicity equivalence associated with environmental exposures to this class of related compounds. These findings are supported by the refinement of the toxicity equivalence factors for dioxin-like PCB congeners [22], as well as a compilation and analysis of all available data on relative toxicities of dioxin-like PCBs with respect to a number of end points [21]. Although these findings have been published recently, additional review and data collection will be needed.

In addition, this panel urged investigation of companion TEFs for ecotoxicological use, based on data from ecotoxicological studies. The concentrations of

dioxin and related compounds will be presented as TCDD equivalents (TEQs). TEQs are determined by summing the products of multiplying concentrations of individual dioxin-like compounds and the corresponding TEF for that compound (where TCDD is 2,3,7,8-tetrachlorodibenzo-*p*-dioxin). At times, levels will be presented as concentration of CDDD because many past studies monitored this congener alone. There are 75 individual compounds comprising the CDDs, depending on the positioning of the chlorine(s), and 135 different CDFs. These are called individual congeners. Likewise, there are 75 different positional congeners of BDDs and 135 different congeners of BDFs. Only seven of the 75 congeners of CDDs or of BDDs are thought to have dioxin-like toxicity; these are ones with chlorine/bromine substitutions in, at least, the 2, 3, 7, and 8 positions. Only 10 of the 135 possible congeners of CDFs or of BDFs are thought to have dioxin-like toxicity—those with substitutions in the 2, 3, 7, and 8 positions. While this suggests 34 individual CDDs, CDFs, BDDs, or BDFs with dioxin-like toxicity, inclusion of the mixed chloro/bromo congeners substantially increases the number of possible congeners with dioxin-like activity.

There are 209 PCB congeners. Only 13 are believed to have dioxin-like toxicity; these are PCBs with four or more chlorines with just one or no substitution in the *ortho* position. These compounds are sometimes referred to as coplanar, meaning that they can assume a flat configuration with rings in the same plane. Similarly configured polybrominated biphenyls are likely to have similar properties; however, the data based on these compounds with regard to dioxin-like activity have been less extensively evaluated. Mixed chlorinated and brominated congeners also exist, increasing the number of compounds considered dioxin-like. The physical/chemical properties of each congener vary according to the degree and position of chlorine and/or bromine substitution. Very little is known about occurrence and toxicity of the mixed (chlorinated and brominated) dioxin, furan, and biphenyl congeners. In general, these compounds have very low water solubility, high octanol-water partition coefficients, low vapor pressure, and they tend to bioaccumulate.

TABLE 12.5 Toxicity Equivalence Factors (TEFs) for CDDs and CDFs [21]

| Compound | Toxicity Equivalence Factor (TEF) |
|--------------------------|-----------------------------------|
| Mono-, Di-, and Tri-CDDs | 0 |
| 2,3,7,8-TCDD | 1 |
| Other TCDDs | 0 |
| 1,2,3,7,8-PeCDD | 0.5 |
| Other PeCDDs | 0 |
| 1,2,3,4,7,8-HxCDD | 0.1 |
| Other HxCDDs | 0 |
| 1,2,3,4,7,8,9-HpCDD | 0.01 |
| Other HpCDDs | 0 |
| Mono-, Di-, and Tri-CDFs | 0 |
| 2,3,7,8-TCDF | 0.1 |
| Other TCDFs | 0 |
| 1,2,3,7,8-PeCDF | 0.05 |
| 2,3,4,7,8-PeCDF | 0.5 |
| Other PeCDFs | 0 |
| 1,2,3,4,7,8-HxCDF | 0.1 |
| Other HxCDFs | 0 |
| 1,2,3,4,7,8,9-HpCDF | 0.01 |
| Other HpCDFs | 0 |
| OCDF | 0.001 |

12.3.2 Environmental Impact of Dioxin-like Compounds

In soil, sediment, the water column, and (probably) air, CDDs and CDFs are primarily associated with particulate and organic matter because of their high lipophilicity and low water solubility. They exhibit

little potential for significant leaching or volatilization once sorbed to particulate matter. The available evidence indicates that CDDs and CDFs, particularly the tetra- and higher chlorinated congeners, are extremely stable compounds under most environmental conditions, with environmental persistence measured in decades. The only environmentally significant transformation process for these congeners is believed to be photodegradation of chemicals not bound to particles in the gaseous phase or at the soil- or water-air interface. Brominated congeners are significantly more readily transformed by photodegradation. CDDs and CDFs entering the atmosphere are removed either by photodegradation or by dry or wet deposition. Although some volatilization of dioxin-like compounds on soil does occur, the predominant fate of CDDs and CDFs sorbed to soil is to remain in place near the surface of undisturbed soil or to move to water bodies with erosion of soil. CDDs and CDFs entering the water column primarily undergo sedimentation and burial. The ultimate environmental sink of these CDDs and CDFs is believed to be aquatic sediments.

Little information exists on the environmental transport and fate of the dioxin-like PCBs. However, the available information on the physical and chemical properties of dioxin-like PCBs, coupled with the body of information available on the widespread occurrence and persistence of PCBs in the environment, indicates that these PCBs are likely to be associated primarily with soils and sediments and are thermally and chemically stable. The dominant transport mechanisms responsible for the widespread environmental occurrence of PCBs are believed to be soil erosion and sediment transport in water bodies and emissions to the air (via volatilization, dust resuspension, or point source emissions), followed by atmospheric transport and deposition. Photodegradation to less chlorinated congeners, followed by slow anaerobic and/or aerobic biodegradation, is believed to be the principal path for destruction of PCBs. Similar situations exist for the polybrominated biphenyls (PBBs).

12.3.3 Sources of Dioxin-like Compounds

PCBs are produced in relatively large quantities for use in such commercial products as dielectrics, hydraulic fluids, plastics, and flame retardants. A similar situation exists for the commercially produced PBBs, which are produced for a number of uses like flame retardants. Dioxin-like compounds are released to the environment in a variety of ways and in varying quantities, depending on the source. This

trend suggests that the presence of dioxin-like compounds in the environment has occurred primarily as a result of industrial practices and is likely to reflect changes in release over time.

Although these compounds are released from a variety of sources, the congener profiles of CDDs and CDFs found in sediments have been linked to combustion sources [23]. Three theories have been suggested to explain formation of CDDs and CDFs during combustion [24]: (1) CDDs and CDFs are present in the fuels or feed materials and pass through the combustion intact; (2) precursor chemicals are present in the fuels or feed materials and undergo reactions catalyzed by particles and other chemicals to form CDDs and CDFs; and (3) the CDDs and CDFs are formed *de novo* from organic and inorganic substrates bearing little resemblance in molecular structure.

The principal identified sources of environmental release of CDDs and CDFs may be grouped into four major types, as discussed in the following sections.

12.3.3.1 Combustion and Incineration Sources

Dioxin-like compounds, such as CDDs and CDFs, can be generated and released to the environment from various combustion processes when chlorine donor compounds are present. These sources can include: (1) incineration of wastes (such as municipal solid waste, sewage sludge, hospital and hazardous wastes); (2) metallurgical processes (such as high-temperature steel production, smelting operations, and scrap metal recovery furnace); and (3) the burning of coal, wood, petroleum products, and used tires for power or energy generation and polymers-FR combustion. There are three primary mechanisms for CDD/CDF emissions from combustion sources [25].

MECHANISM 1 This refers to CDDs and CDFs contained in the feed that passes through the combustor intact and are subsequently released to the environment. For most systems, this is not thought to be a major contributor to CDD and CDF emissions for two reasons. First, for commercial systems with good combustion controls, the temperatures and residence times should result in the destruction of most CDDs and CDFs in the feed. Second, mass balance studies of a number of combustion systems show that more CDDs and CDFs can be detected downstream from the furnace than in the feed. Consequently, synthesis appears to be a more important mechanism than pass-through.

MECHANISM 2 This is the formation of CDDs and CDFs from the thermal breakdown and molecular rearrangement of aromatic precursors, either originating in the feed or forming as a product of incomplete combustion. Actual synthesis of CDDs and CDFs occurs in the postcombustor environment. The CDDs and CDFs form when the precursors sorb onto binding sites on the surface of fly ash particles. This reaction has been observed to be catalyzed by the presence of a transition metal sorbed to the particulate. The most potent catalyst is copper chloride. Heat in a range of 200–450 °C has been identified as a necessary condition for these reactions to occur, with either lower or higher temperatures inhibiting the process. Since these reactions involve heterogeneous chemistry, the rate of emissions is less dependent on reactant concentration than on conditions that promote formation, such as temperature, retention time, and availability of catalytic surfaces. For this mechanism to be significant, two broad conditions are needed.

MECHANISM 3 This is the formation of CDDs and CDFs in the post-combustion environment in the absence of aromatic precursors. This *de novo* synthesis involves the oxidative breakdown of macromolecular carbon structures (e.g., graphite) leading to the formation of aromatic CDD and CDF precursors. These precursors then undergo the transformations associated with Mechanism 2 to form CDDs and CDFs. As with Mechanism 2 (since this mechanism involves heterogeneous chemistry), the rate of emissions is dominated by the same physical conditions as discussed in Mechanism 2.

Mechanisms 2 and 3 can occur simultaneously, share a number of common reaction pathways, occur in the same physical environment, and are controlled by many of the same physical conditions. In well-designed and well-operated combustion systems, the precursor species needed for Mechanism 2 are not in abundant supply; consequently, *de novo* synthesis can become the dominant pathway for formation. In systems with incomplete combustion, it is difficult to sort out the relative contribution of these two mechanisms to total emissions. Both mechanisms, however, can be curtailed if steps are taken to minimize the physical conditions needed to support formation (i.e., time, temperature, and reactive surface). The combustion formation chemistry of PCBs is less well-studied than for CDDs and CDFs, but it is reasonable to assume that these same three

mechanisms would apply. For waste incineration, PCBs can exist in significantly higher concentrations in the feed than CDDs and CDFs. Consequently, Mechanism 1 may play a more prominent role in PCB emissions from some forms of waste combustion.

12.3.3.2 Chemical Manufacturing/Processing Sources

Dioxin-like compounds can be formed as byproducts from the manufacture of chlorine and such chlorinated compounds as chlorinated phenols (e.g. pentachlorophenol), PCBs, phenoxy herbicides (e.g. 2,4,5-T), chlorinated benzenes, chlorinated aliphatic compounds, chlorinated catalysts, and halogenated diphenyl ethers and other flame retardants.

12.3.3.3 Industrial/Municipal Processes

Dioxin-like compounds can be formed through the chlorination of naturally occurring phenolic compounds, such as those present in wood pulp. The formation of CDDs and CDFs resulting from the use of chlorine bleaching processes in the manufacture of bleached pulp and paper has resulted in the presence of CDDs and CDFs in paper products, as well as in liquid and solid wastes from this industry. Municipal sewage sludge has been found to occasionally contain CDDs and CDFs.

12.3.3.4 Reservoir Sources

The persistent and hydrophobic nature of these compounds causes them to accumulate in soils, sediments, and organic matter, and to persist in waste disposal sites. The dioxin-like compounds in these “reservoirs” can be redistributed by various processes, such as dust or sediment resuspension and transport. Such releases are not original sources in a global sense, but can be on a local scale. For example, releases may occur naturally from sediments through volatilization or from operations that disturb them, such as dredging. Aerial deposition and accumulation on leaves can lead to releases during forest fires or leaf composting operations.

These studies assume that emissions to air make up the major portion of dioxins released to the environment. Estimates of total release in European countries range from approximately 100–1,000 g TEQ/year in West Germany and 100–200 g TEQ/year in Sweden, to approximately 1,000 and 4,000 g TEQ/year maximum emissions in The Netherlands and the United Kingdom, respectively. Similar na-

tionwide estimates for the United States have not been compiled prior to this reassessment effort. The Exposure Document estimates U.S. emissions to be in the range of 3,300–26,000 g TEQ/year, with a central estimate of 9,300 g TEQ/year. These estimates were derived from data from emission tests at relatively few facilities in each combustion class. These data were used to develop emission factors and then extrapolated to a nationwide basis using the total amount of waste feed material in each class. Because of the limited number of measurements and the large number of potential sources for each of these emissions, total estimated emissions from these sources are considered highly uncertain. Diesel-fueled vehicles, hazardous waste burning, forest fires, and metal smelting are more moderate contributors of dioxin-like compounds, but the magnitude of their contribution is also highly uncertain. Sewage waste incineration and residential wood burning, as well as a few minor processes, round out the current analysis and provide lower range estimates of medium to low certainty.

12.4 EXPOSURE LEVELS

While all of the above emission and deposition values are given in the form of TEQs, it should be noted that neither emission nor deposition is equivalent to exposure or intake. Significant changes in composition can occur to complex mixtures of CDDs, CDFs, and PCBs as they move through the environment. Measurements at or near the point of human contact provide the best estimates of human exposure. TEQs are most relevant to potential for hazard and risk when they represent intake values. CDDs, CDFs, and PCBs have been found throughout the world in practically all media. This assessment proposes the hypothesis that the primary mechanism by which dioxin-like compounds enter the terrestrial food chain is by atmospheric deposition. Dioxin and related compounds enter the atmosphere directly through air emissions, or indirectly, for example, through volatilization from land or water or from resuspension of particles. Deposition can occur directly onto soil or onto plant surfaces. Soil deposits can enter the food chain by direct ingestion (e.g. grazing animals, earthworms, fur preening by burrowing animals). Dioxin-like compounds in soil can become available to plants by volatilization and vapor absorption or by particle resuspension and adherence to plant surfaces. In addition, dioxin-like compounds in soil can adsorb directly to underground portions of plants.

Support for this air-to-food hypothesis is provided by Hites [26], who concluded that “background environmental levels of dioxin-like compounds are caused by dioxin-like compounds entering the environment through the atmospheric pathway” [26]. His conclusion was based on demonstrations that the congener profiles in lake sediments could be linked to congener profiles of combustion sources. Further arguments supporting this hypothesis include the following: (1) numerous measurements show that emissions occur from multiple sources and deposition occurs in most areas, including remote locations; (2) atmospheric transport and deposition are the only mechanisms that could explain the widespread distribution of these compounds in soil; and (3) other mechanisms of uptake into food, for instance, from direct contamination or through packaging, are much less plausible. Direct uptake into food from soil or sediments is possible and could be important for “local” exposures. These routes are less likely to explain the general background level of dioxin and related compounds found in the diet of the general population.

The term *background exposure* has been used throughout this reassessment to describe exposure of the general population—which is not exposed to readily identifiable point sources of dioxin-like compounds—to widespread, low-level circulation of dioxin-like compounds in the environment. The primary route of this exposure is thought to be the food supply, and most of the dioxin-like compounds are thought to come from non-natural sources. A background exposure level of 120 pg TEQ/day for the United States has been estimated [21]. These estimates are comparable to estimates for European countries: Estimates for Germany range from 79 pg TEQ/day, based on Furst et al., [27] to 158 pg TEQ/day [28]; 118–126 pg TEQ/day exposure through numerous routes in The Netherlands [29], and 140–290 pg TEQ/day for the typical Canadian exposed mainly through food ingestion [30]. It is generally concluded by these researchers that dietary intake is the primary pathway of human exposure to CDDs and CDFs. These investigators, among others, suggest that greater than 90% of human exposure occurs through diet, with foods from animal origins being the predominant pathway. Use of one-half of the detection level for nondetects is a reasonable but conservative approach to estimating low levels in samples. For some data sets, use of zero values for nondetects would result in significantly lower estimates. Setting nondetects equal to zero, however, does not significantly change the average

TEQ levels estimated for most categories. In the current assessment, similar estimates of TEQs derived from different data sets, developed by different investigators in several countries, strengthen the probability that this inference represents the exposure of the general population in industrialized countries to dioxin and related compounds [31].

Levels of dioxin-like compounds found in human tissue and blood appear similar in Europe and North America. Schechter [32] compared levels of dioxin-like compounds found in blood among people from the United States (pooled samples from 100 subjects) and Germany (pooled samples from 85 subjects). Although mean levels of individual congeners differed by as much as a factor of two between the two populations, the total TEQ averaged 42 pg TEQ/g (42 ppt) in the German subjects and was 41 pg TEQ/g (41 ppt) in the pooled U.S. samples. These values do not include TEQs for PCBs.

New information on levels of dioxin-like compounds in human adipose tissue and blood has been published [33]. These measurements show that concentrations of dioxin-like PCBs can be more than an order of magnitude higher than concentrations of TCDD. Comparison with other published information suggests much higher levels of nondioxin-like congeners of PCBs and the possibility that concentrations of both types of congeners will depend heavily on previous human activities such as fish consumption. These data are consistent with the previous statement that dioxin-like PCBs may account for approximately one-third of the total TEQ in the general population.

The potential for formation of polychlorinated dibenzofurans (PCDFs) and dibenzo-*p*-dioxins (PCDDs) during thermal destruction of PCBs can be examined by thermochemical equilibrium calculations. The calculations predict that, under oxidizing conditions, formation of PCDFs and PCDDs is not thermodynamically favored. However, under pyrolytic conditions (absence or near absence of oxygen), as may arise in an inadequately designed or operated incinerator, thermochemical equilibrium calculations indicate that trace amounts of possible precursors to PCDFs and PCDDs can form [34].

12.5 REGULATORY CONTROLS

The flame retardant chemicals industry has historically been driven by regulations and standards. The normal fire-, smoke-, and toxicity-related standards have been augmented by environmental standards prompted by the alleged environmental impact of

halogens and the alleged toxicity of antimony. Although suitable replacements have not been found for these materials in all cases, the environmental concern has served to depress their growth levels from what it would otherwise have been, and/or to channel the growth of alternative chemical products.

In connection with the amendment of Germany's Ordinance on Dangerous Substances, the German federal government passed a new ordinance on the ban and restriction of certain chemicals, compounds, and products (Chemikalien-Verbots-Verordnung at www.sidiblume.de/info-rom/gefstoff/chemverbotsv.htm), which became effective on November 1, 1993 (BGB I I, 1720). It was amended the first time on July 6, 1994 (BGB I I, 1493). The new ordinance has replaced the following ordinances:

1. 1989 ordinance on the ban of PCB and PCT
2. 1989 ordinance on the ban of pentachlorophenol
3. first ordinance (1991) on chloroaliphates
4. ordinance on dioxins and furans

In addition to tetra- up to hexachlorodibenzo-*p*-dioxins/furans with chlorine atoms at positions 2, 3, 7, and 8 (eight substances transferred from the Ordinance on Dangerous Substances, App. V, 3), the amendment of July 6, 1994 extends the number of congeners of this type by some additional penta- up to octachlorodibenzo-*p*-dioxins/furans. Now the total number of restricted chlorinated PCDD/PCDF-congeners amounts to 17 substances. The threshold concentrations for these chemicals in substances, preparations, and products were decreased considerably, depending on their toxic potentials. However, plant treatment agents, intermediates, and a few more products were excluded from this regulation. For the first time, 2, 3, 7, 8-brominated dioxins and furans are restricted now as well; eight PBDC/PBCF-congeners were added to the list of the regulation. This was the result of an approximation process relating to the scientific progress concerning the appearance, environmental fate, toxicity, and analytical methodology of these substances.

In December 1992, the European Commission granted Germany an exception under Article 100 (A) (4) of the treaty from E.U. legislation issued in 1991, restricting the marketing and use of substances and preparations containing PCP and its compounds (Council Directive 91/173 EEC, amending for the ninth time Directive 76/769 EEC). This consent was necessary because the German legislation imposed wider restrictions and lower concentrations limits of PCP, which differed from the E.U. directive. After an action by France against the consent, in May 1994

the European Court of Justice annulled the decision by the Commission on the grounds that no adequate reasons had been given for it and, thereby, Article 190 of the treaty had been violated. In September 1994, the Commission pronounced a new decision and confirmed the German legislation again.

The Commission has verified that is now considering the possibility of proposing a total ban on PCP for the E.U. In this connection, there could be some new, unexpected steps in this direction. Several national regulatory bodies have implemented regulations on specific substances associated with flame-retardant applications.

In the E.U., the use of tris(2,3-dibromopropyl) phosphate (EC Directive 76/769/EEC) and tris(1-aziridinyl)phosphine oxide (EC Directive 83/264/EEC) in textiles has been banned. In 1977, the U.S. Consumer Product Safety Commission banned the use of tris(2,3-dibromopropyl)phosphate in children's clothing [35]. The EU has also banned the use of PBBs in textiles (EC Directive 83/264/EEC). Several countries have either taken or proposed regulatory actions on PBBs, as outlined in Table 12.6 [36].

Controls on the emissions of dioxins and furans from municipal solid waste incinerators have been implemented in the United Kingdom under the Environmental Protection Act (1990). In Germany, a second modification of the Chemicals Prohibition Ordinance, which was adopted in 1994, imposes limits on 2,3,7,8-substituted chlorinated dioxins and furans and, for the first time, on some 2,3,7,8-substituted brominated dioxins and furans [36].

There are no regulations proposed or in effect anywhere around the world banning the use of brominated flame retardants. The proposed E.U. directive on the brominated diphenyl oxides has been withdrawn. Deca- and tetrabromo bis-phenol A, as well as other brominated flame retardants, meet the requirements of the German Ordinance regulating dioxin and furan content of products sold in Germany. The European search for a replacement for decabromo diphenyl oxide in HIPS has led to consideration of other bromoaromatics, such as Saytex 8010 from Albemarle and a heat-stable chlorinated paraffin from ATOCH EM. The former product is more costly, and the latter, if sufficiently heat stable, lowers the heat distortion under the load (HDUL) significantly.

This does not necessarily mean there will be a total ban of halogenated flame retardants in the next five to 10 years. But it actually suggests a complete reconsideration of polymer flame retardancy development. Obviously, new efforts will be directed toward ecologically-friendly flame retardant systems.

12.6 REFERENCES

1. Pettigrew, A. Halogenated flame retardants. In *Kirk-Othmer Encyclopedia of Chemical Technology*, 4th Ed. New York: John Wiley & Sons, Inc., Vol. 10, pp. 954–976. 1993.
2. Cullis, C. F. Bromine compounds as flame retardants. In *Proceedings of the International Conference on Fire Safety*, Vol. 12, pp. 307–323. 1987.

TABLE 12.6 Country-Specific Actions on PBBs, Either Taken or Proposed [36]

| Country | Actions |
|-------------|---|
| Austria | Prohibits the manufacture, placing on the market, import and use of PBBs and products containing these substances. |
| Canada | Prohibits the manufacture, use, processing, offer for sale, selling or importation of PBBs for commercial, manufacturing or processing purposes. |
| Denmark | Implements EC Directive 89/677 banning the use of PBBs in textiles. |
| Finland | PBB may not be used in textile articles intended to come into contact with the skin (in accordance with EC Directive 83/264). |
| France | Implements EC Directive concerning PBBs and their use on textiles. |
| Netherlands | Proposed resolution would prohibit the storage of PBBs or products or preparations containing these substances or making them available to third parties. (Exports are excluded from the resolution). |
| Norway | Ban on PBBs in textiles intended to come into contact with skin, implementation of EC Directives 76/769/EEC, 83/264 and 89/677. |
| Sweden | Ban on PBBs in textiles intended to come into contact with skin by implementation of EC Directive 76/769. |
| Switzerland | Prohibits manufacture, supply, import and use of PBBs and products containing these substances. Supply and import of capacitors and transformers containing PBBs is forbidden. |
| USA | No current production or use. Companies intending to resume manufacture must notify U.S. EPA 90 days in advance for approval. |

3. Nelson, G. L. Carbon monoxide and fire toxicity. In *Recent Advances in Flame Retardancy of Polymeric Materials*, handout at the 6th Annual BCC Conference on Flame Retardancy. Stamford, CT, May, 1995, p. 16.
4. Babrauskas, V., Harris, R. H., Jr., Gann, R. G., Levin, B. C., Lee, B. T., Peacock, R. D., Paabo, M., Twilley, W., Yoklavich, M. F., and Clark, H. M. *Fire Hazard Comparison of Fire-Retarded and Non-Fire-Retarded Products*. Washington, DC: U.S. Department of Commerce, National Bureau of Standards NBS Special Publication 749. 1988.
5. Morikawa, T., Okada, T., Kajiwara, M., Sato, Y., and Tsuda, Y. Toxicity of gases from full-scale room fires involving fire retardant contents. *Journal of Fire Science*, Vol.13(1), pp. 23–42. 1995.
6. Buser, H. R. Brominated and brominated/chlorinated dibenzodioxins and dibenzofurans: Potential environmental contaminants. *Chemosphere*, Vol. 16(8–), pp. 1,873–1,876. 1987.
7. IPCS. *Environmental Health Criteria 140: Polychlorinated Biphenyls and Terphenyls, 2nd Ed.* Geneva: World Health Organization, International Programme on Chemical Safety. 1992.
8. IPCS. *Environmental Health Criteria 152: Polybrominated Biphenyls*. Geneva: World Health Organization, International Programme on Chemical Safety. 1994.
9. IPCS. *Environmental Health Criteria 172: Tetrabromobisphenol-A and Derivatives*. Geneva: World Health Organization, International Programme on Chemical Safety. 1995.
10. IPCS. *Environmental Health Criteria 185: Polybrominated Dibenzo-p-dioxins and Dibenzofurans*. Geneva: World Health Organization, International Programme on Chemical Safety. 1996.
11. Addink, R. and Olie, K. Mechanisms of formation and destruction of polychlorinated dibenzo-p-dioxins and dibenzofurans in heterogeneous systems. *Environmental Science and Technology*, Vol. 29, pp. 1,425–1,435. 1995.
12. Ahling, B. and Lindskog, A. Emission of chlorinated organic substances from combustion. In *Chlorinated Dioxins and Related Compounds, Impact on the Environment*. O. Hutzinger, and S. Safe, Eds. New York: Pergamon Press. 1982.
13. Behrooz, G. S. and Altwicker, E. R. Rapid formation of polychlorinated dioxins/furans during the heterogeneous combustion of 1,2-dichlorobenzene and 2,4-dichlorophenol. *Chemosphere*, Vol. 32 (1), pp. 133–144. 1996.
14. Blumenstock, M., Zimmermann, R., Schraumm, L-W, Kaune, A., Henkelmann, B., and Kettrup, A. Presence of polychlorinated dibenzo-p-dioxins (PCDD), dibenzofurans (PCDFs), biphenyls (PCB), chlorinated benzenes (PCBz) and polycyclic aromatic hydrocarbons (PAH) under various combustion conditions in a post combustion chamber. *Organohalogen Compounds*, Vol. 36, pp. 59–63. 1998.
15. Brominated FR Producers Make Universal Commitment. In *Fire and Flammability Bulletin*, p.2, November, 1995.
16. Weinberg, J., Ed. *Dow Brand Dioxin*. Washington, DC: Greenpeace, September, 1995.
17. Hardy, M. L. *Regulatory Status and Environmental Properties of Brominated Flame Retardants Undergoing Risk Assessment in the EU: DBDPO, OBDPO, PeBDPO and HBCCD*. 6th European Meeting on Fire Retardancy of Polymeric Materials, Lille, France, September 24–26, 1997, p. 15.
18. Norris, R. et al. *Applied Polymer Symposium*, Vol. 22, p. 195–219. 1973.
19. Pomerantz, I. et al. *Health Perspectives*, Vol. 24, pp. 133–146. 1978.
20. Ahlborg, U. G., Becking, G. C., Birnbaum L. S., et al. *Chemosphere*, Vol. 28 (6), pp. 1,049–1,067. 1994.
21. U.S. Environmental Protection Agency. *Estimating Exposure to Dioxin-Like Compounds*. EPA/600/6-88/005 Ca, Cb, Cc. Washington DC: U.S. Environmental Protection Agency. 1994.
22. DeVito, M. J., Maier, W. E., Diliberto, J. J., and Birnbaum, L. S., *Fundamentals of Applied Toxicology*, Vol. 20, pp. 125–130. 1993.
23. U.S. Environmental Protection Agency. EPA/600, Vol. 3. 1994.
24. Stehl, R. H. et al. The stability of chlorinated dioxins to sunlight, heat and combustion. In *Chlorodioxins—Origin and Fate*. E. C. Blair, Ed. Washington, DC: American Chemical Society, Vol. 120, p. 119. 1973.
25. Huang, H. and Buekens, A. On the mechanisms of dioxin formation in combustion processes. *Chemosphere*, Vol. 31 (9), pp. 4,099–4,117. 1995.
26. Hites, R. A. *Atmospheric transport and deposition of polychlorinated dibenzo-p-dioxins and dibenzofurans*. Prepared for the U.S. Environmental Protection Agency, Methods Research Branch, Atmospheric Research and Assessment Laboratory, Office of Research and Development, Research Triangle Park, NC., EPA/600/3-91/002. 1991.
27. Furst, P., Furst, C., and Groebel, W. *Chemosphere*, Vol. 20, pp. 7–9, 787–792. 1990.
28. Beck, H., Dross, A., and Ende, M. et al. Ergebnisse von Ruckstandsuntersuchungen auf polychlorierte Dibenzofurane und Dibenzodioxine in Frauenmilch aus der Bundesrepublik Deutschland. V01.34, Bundesgesundheitsblatt, pp. 564–568. 1991.
29. Theelen, R. M. C. Modeling of human exposure to TCDD and I-TEQ in The Netherlands: background and occupational. In *Biological Basis for Risk Assessment of Dioxin and Related Compounds*. M. Gallo, R. Scheuplein, and K. Van der Heijden, Eds. Banbury Report 35. Plainview, NY: Cold Springs Harbor Laboratory Press. 1991.
30. Gilman, A. and Newhook, R. *Chemosphere*, Vol. 23, pp. 1,661–1,667. 1991.
31. Furst, P., Furst, L., and Widmers, K. Body burdens with PCDD and PCDF from food. In *Biological Basis for Risk Assessment of Dioxin and Related Compounds*. M. Gallo, R. Scheuplein, and K. Van der Heijden, Eds. Banbury Report 35. Plainview, NY: Cold Springs Harbor Laboratory Press. 1991.

32. Schecter, A. Dioxins and related compounds in humans and the environment. In *Biological Basis for Risk Assessment of Dioxin and Related Compounds*. M. Gallo, R. Scheuplein, and K. Van der Heijden, Eds. Banbury Report 35. Plainview, NY: Cold Springs Harbor Laboratory Press. 1991.
33. Dewailly, E., Ryan, J. J., Laliberte, C. et al. *Environmental Health Perspectives* Vol. 102, pp. 205–209. 1994.
34. Abbot, B. D. and Birnbaum, T. S. *Teratology*, Vol. 43, pp. 119–32. 1991.
35. IPCS. *Environmental Health Criteria 162: Brominated diphenyl ethers*. Geneva: World Health Organization, International Programme on Chemical Safety, 1994b. IPCS. *Environmental Health Criteria 172: Tetrabromobisphenol-A and derivatives*. Geneva: World Health Organization, International Programme on Chemical Safety. 1995a.
36. OECD. *Selected brominated flame retardants*. Risk Reduction Monograph 3. Paris: Organisation for Economic Cooperation and Development, Environment Directorate. 1994.

CHAPTER 13

THERMAL PROTECTIVE CLOTHING

Hechmi Hamouda

*Department of Textile Engineering, Chemistry, and Science
North Carolina State University, Raleigh, North Carolina*

| | | | |
|-----------------------------|-----|----------------------------------|-----|
| 13.1 INTRODUCTION | 261 | 13.6 SENSING DEVICES | 268 |
| 13.2 GENERAL CONCEPTS | 261 | 13.7 SKIN BURN DAMAGE EVALUATION | 271 |
| 13.3 TPC MATERIALS | 262 | 13.8 OTHER MODELING COMPONENTS | 272 |
| 13.4 TPC EXPOSURE PROCESS | 263 | 13.9 CONCLUSION | 274 |
| 13.5 TESTING AND EVALUATION | 265 | 13.10 REFERENCES | 274 |

13.1 INTRODUCTION

Clothing will burn when exposed to intense heat or flames. However, the characteristics of these combustions are vastly different, depending on the fabric fiber, cloth structure, moisture trapped within the garment, and the nature of the applied finish. It is well known that wool burns much less promptly than other natural fibers such as cotton, linen, or silk. The relatively unimpaired motion of gases within a loosely woven or knitted light fabric promotes fire propagation within those materials more rapidly than in a tight, heavy fabric structure. Garment flammability is also affected by the surface morphology of the fabric, as well as by the moisture trapped within the structure or absorbed by the fiber materials. A large amount of free fiber ends extending beyond the plane of the fabric would also enable prompt transmission of fire throughout the cloth. Fire retardant chemical additives are usually applied to natural fibers to essentially delay the onset of the fabric combustion, thereby providing additional time to control or attenuate the flames.

On the other hand, man-made (synthetic) fibers such as polyester or nylon, usually do not burn as easily as natural fibers. Once these fibers reach their melting temperature, they became a mixture of viscous burning material combined with hot fumes and flaming gases. As the combustion temperature increases, additives and additional chemicals within the fabric might also provide additional fuel. Fortu-

nately, some fibers made of glass, and few recently developed synthetic fibers such as Nomex[®], Kevlar[®], PBI blends and others, are flame-resistant. The pertinent protection is provided via a charred carbon shield that forms as a result of combustion, between the heat source and the garment wearer, slowing the burning rate. Combustion fumes turn into nonflammable gases as a result of the ensuing release of carbon dioxide and water vapor as byproducts of the reaction.

13.2 GENERAL CONCEPTS

Textile products are constantly improving to meet human needs. Thermal Protective Clothing (TPC) is among the products that have changed a lot in the past few years. Research and development have found ways to alter fiber materials or to apply chemical finishes to certain textile fabrics, enabling them to delay or even resist flammability. Generally, at a given stage of fabric manufacturing, flame retardant finishes are applied to fabrics made of cotton, polyester, wool, or various blends of these fibers. The main purpose of flame retardant finishes is to reduce clothing flammability, so that the fabric material does not melt or ignite when exposed to intense heat. This added value is accomplished by either of two chemical processes. The first process interrupts radical combustion during the vapor phase to prevent the fabric from igniting. The chemical finish applied

to the fabric acts as a protective barrier by shielding the fire from the molecules within the fiber. In the second process, fire retardants promote charring on the surface of the fiber, which in turn slows the burning rate. In this case, chemicals reacting with combustible gases and tars generated by the fabric turn the tar into carbon char that forms a shield on the surface of the fabric. Flame retardant additives, when applied to cellulosic fabrics, function via the second process; the two main chemicals used are ammonium sulfate and boric acid.

In past times, flame retardant finishes applied to fabric surfaces resulted in stiffer cloth with a harsh feel—a fabric with a poor “hand.” A solution to this disadvantage was provided by a nondurable (i.e., not machine washable) finish that is adequate for cellulosic fabrics. For example, tetrakis(hydroxymethyl)phosphonium hydroxide finish, when applied to these fabrics, provides a very soft hand.

Polyester fabric reacts differently than cotton to fire or intense heat, by shrinking away from the flame and melting. Therefore, the flame retardant finish, decabromodiphenyl oxide, stiffens rather than softens such fabrics. Other chemicals exist for various fabrics made of synthetic, natural, or any other traditional blend of these fibers. These finishes behave as flame retardants, each acting in much the same way as the ones used on cellulosic and polyester fabrics.

This chapter reviews some of the major concepts and mechanisms used to investigate, characterize, assess, and enhance the performance of TPC in extremely hot or fire-prone environments. First, the major fabric materials used as outer shells for TPC are reviewed, and then the various stages of the exposure process are described. The major testing methods, evaluation tools, and computing models are also discussed, including the associated thermal sensors and burn damage evaluation schemes.

13.3 TPC MATERIALS

There are several fibers available that provide thermal protection. Glass is inherently fire resistant, due to its inert oxidized silicone structure (SiO_2). This material, in spite of its low cost and good strength, often results in poor hand when made into textile fabrics. It is also known that very small glass fibers, when in contact with human skin, may result in allergic reactions. Carbon fiber is composed almost entirely of a very stable conjugated carbon matrix, shown in Figure 13.1, and can result in a material

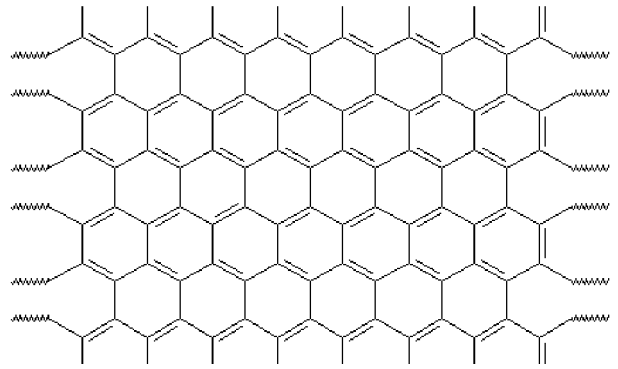


FIGURE 13.1 Conjugated carbon matrix.

that is inherently heat resistant. However, the poor hand and the high cost of carbon fibers negates their selection as a textile fabric for TPC applications, regardless of their exceptional strength and very high modulus* and good electrical conductivity.

Aramids fibers [1] are a subset of nylon fibers. Renowned fibers such as Nomex® and Kevlar® are a major part this family. Blends of these fibers are used to make the outer layer of textiles that face the heat source (the outer face of fire protective garments). Other layers, usually a moisture barrier film and a fabric liner, are part of the composite forming a thermal protective garment material. Each of these materials plays an important role in this fireproof combination.

Aramids fibers are spun as a multifilament by a proprietary process developed by DuPont. Additionally, these fibers are known to have no melting point, low flammability, and good fabric integrity at elevated temperatures. Para-aramid fibers, which have a slightly different molecular structure, provide similar high strength-to-weight properties, high tenacity, and high modulus.

Kevlar is a polyamide in which all the amide groups are joined by para-phenylene groups at carbons 1 and 4 of the aromatic group. This class of fibers achieves its fire resistance property through high crystallinity and an inherent stability of conjugation. Figure 13.2 depicts the para-linkage through the 1 and 4 positions for Kevlar, and meta-linkage through the 1 and 3 positions for Nomex.

*The ratio of change in stress to change in strain following the removal of crimp from the material being tested. Stress is expressed in either force per unit of linear density or force per unit area of the original specimen, and strain is expressed as either a fraction of the original length or percentage elongation.

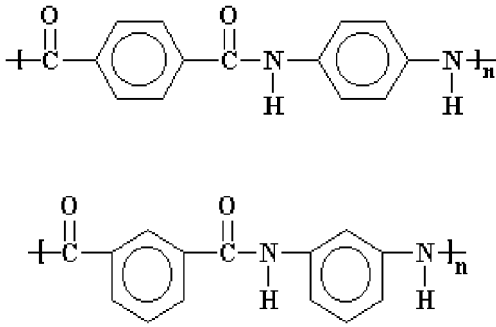


FIGURE 13.2 Para-linkage for Kevlar® and meta-linkage for Nomex

In 1965, two scientists from DuPont, Stephanie Kwolek and Herbert Blades, developed a fiber called Kevlar that had strength, weight, and flexibility properties much better than existing fibers. Since Kevlar is a very crystalline polymer, for a long time no useful application could be found for it, since this material would not dissolve in anything. However, when this polymer was spun into a fiber, it became even a better fiber than the non-aromatic polyamides, such as nylon 6.6.

This fiber quickly became a known technology of choice for bullet-resistant vests. In addition to its excellent mechanical properties, the thermal properties of Kevlar made this fiber a good candidate for becoming a TPC material. This para-aramid fiber possesses a low thermal shrinkage and is described as self-extinguishing and flame resistant. Kevlar® fibers are long-molecular, highly-oriented chains produced from poly-paraphenylene terephthalamide. Kevlar®'s enhanced mechanical and thermal properties are due to the strong interchain bonding of its molecules. Kevlar retains its properties from very low temperatures up to 400 °C.

A fiber manufacturer, TEIJIN Limited, developed Technora®, a similar para-aramid textile fiber that has been commercially available since 1987. Technora® is advertised as a material that exhibits high tensile strength, high modulus, and excellent resistance to heat and chemicals, especially acids, alkalis, and organic solvents. It is also resistant to sea water and steam. Additionally, the material has a decomposition temperature of 500 °C; this fiber can be used at 200°C and even at 250 °C for long exposure periods with good consistent tensile strength. TEIJIN's web page [2] provides instructive diagrams showing both the thermal properties changes of the Technora® fiber when exposed to heat, as well as its level of strength retention when exposed to high temperature for long

periods of time. Polytetrafluoroethylene, also known as PTFE or Teflon®, can be spun as a fiber composed of only stable carbon and fluorine. This slippery product, which has high chemical resistance, medium cost, and average strength, is better known for making non-stick cooking utensils and anything else that needs to be slippery or non-stick. PTFE is also used to treat yarns and fibers to make them stain and heat resistant. This treatment has resulted in some applications as a TPC fabric blend material, for it resists fairly high temperatures.

Sulfur, polyphenylene sulfide (PPS), usually used in a resin form, is a high performance plastic that can resist very high temperatures and is very strong. It melts around 300 °C. This flame resistant component has high chemical and thermal resistance and high fire stability due to its conjugated nature and heavy sulfur content, as shown in Figure 13.3. This material is relatively expensive, has a high chemical resistance, and a high dimensional integrity. PPS is used for certain applications requiring good heat resistance.

Polybenzimidazole (PBI), as shown in Figure 13.4, poly(phenylene-benzobisoxazole) (PBO), and poly(imide) (PI) are all highly conjugated and crystalline polymers. These components have high fire and heat stability.

13.4 TPC EXPOSURE PROCESS

The main purpose of TPC is to prevent or minimize burns and damages to skin tissues. Understanding

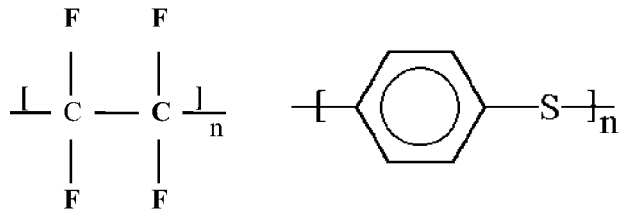


FIGURE 13.3 Polytetrafluoroethylene and polyphenylene sulfide.

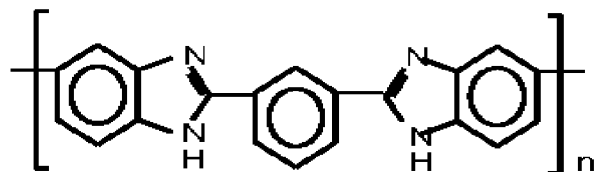


FIGURE 13.4 Polybenzimidazole (PBI).

the exposure process of TPC and its associated performance requires a review and analysis of the heat transfer from the source of exposure (e.g., a flash fire), through the protective clothing, through interfacial air gaps, and, finally, through the skin. Long or intense exposures of TPC also involve additional mass transfer due to off-gassing and other byproducts resulting from subsequent reaction of the TPC material with heat. Mathematical and/or numerical models of these phenomena and their residual issues are complex and are being addressed. The most significant modeling challenges are associated with understanding the behavior of fabric systems under intense heat exposure.

When a TPC-skin system is exposed to intense heat, an initial warmup phase takes place. During this phase, the temperature of both the fibers forming the fabric, and the moisture retained between and within these fibers, increases at a rate dictated by the system's thermal properties and the level of the incident heat. Consequently, the amount of retained moisture and its thermal properties vary. However, this phase is notable for the fact that, in most fabric systems, the fiber contents and their thermal properties will remain constant.

The second phase during fabric systems exposure to intense heat is marked by the onset of changes in the thermal properties of the fiber contents. Changes in the amount of retained moisture and its thermal properties continue to occur during this phase. Most of these changes are initially due to surface chemical treatments and finishes reacting to the effect of heat, or are due to slight degradation of the surface fibers. The bulk of these variations will start at the exposed (outer) side of the fabric system and propagate inward, toward the inner fabric layers.

During both of these phases, the fabric system structural integrity is maintained due to the fact that none of the fiber melting or transition temperatures are reached. From a design point of view, the end of the second phase represents the temperature criteria below which a thermally protective fabric system is supposed to function. A protective fabric system that is exposed beyond the second phase would lose its protective property and, in some instances, would become a source of harm to the wearer.

The third and terminal phase of a fabric system exposure is marked by the chemical and structural degradation of the fabric system. At this point, all moisture content is exhausted from the fabric system. This phase, spontaneous for some fabric systems, is followed by combustion of the fibers. The protective properties of the fabric system are therefore reversed

and the fabric system becomes a source of damage due to the additional intense off-gassing heat and fiber combustion. Instead of protecting, the TPC becomes in this terminal phase an additional source of harm by fueling the occurring exposure. In practice, the occurrence of the third phase is unintentional and takes place only when the fabric system is pushed beyond its intended limits of application.

Figure 13.5 shows the response [3] at the inner side of the fabric (the skin side), of three different thermally protective fabric systems. The Nomex blend and the FR cotton were single-layer fabrics. The third system was a typical firefighter coat with a three-layer composite. The outer layer (facing the heat source) is made of a Kevlar/PBI blend placed on top of a moisture barrier film and a fabric liner. All three thermally protective fabric systems were exposed to a heat source rated at $2 \text{ cal/cm}^2/\text{sec}$. After a 10-second exposure, both the firefighter coat three-layer composite and the Nomex materials experienced only the first and the second phase of exposure. They provided, respectively, a 93% and 63% protection level against the incident heat. On the other hand, the FR cotton fabric system experienced all three phases of exposure, with the third phase starting after approximately four seconds of exposure, followed by flaming combustion. The combined heat supplied by the flame source and the fiber combustion reached approximately $4.3 \text{ cal/cm}^2/\text{sec}$, more than twice the heat level supplied by the source. Photographs of the exposed samples are shown on Figure 13.6.

Since phases I and II are the intended phases of application of TPC, it is imperative that mathematical models initially focus on these two phases, where no major chemical reactions or spontaneous combustion are occurring. Once these models are established and validated, the third phase can be modeled, based on modification of the initial model by including the appropriate equations depicting the chemical reactions and spontaneous combustion that are typical of this final phase.

Mathematical modeling for all three phases of exposure would rely on the thermal and physical properties of the fabric system(s) under consideration. These properties are known to vary with time, temperature, moisture contents, and ambient conditions. Pure mathematical analysis would be very difficult, if not impossible, in this case. Therefore, it is necessary that during the development, validation, and application of a mathematical model, experimental data based on bench-top testing of appropriate fabric samples is made available as an input to the model.

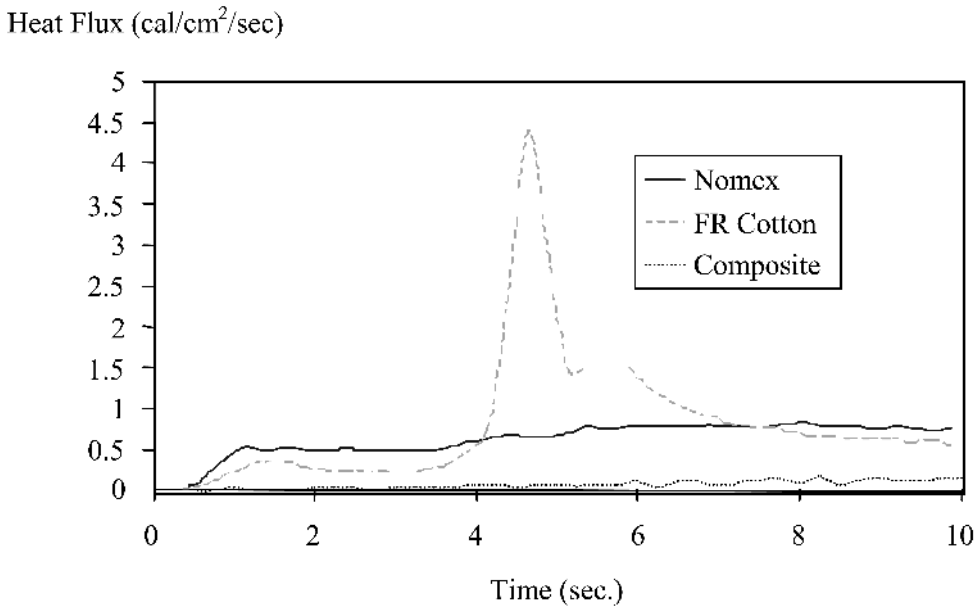


FIGURE 13.5 Heat through three fabric systems exposed to at 2 cal/cm²/sec source.

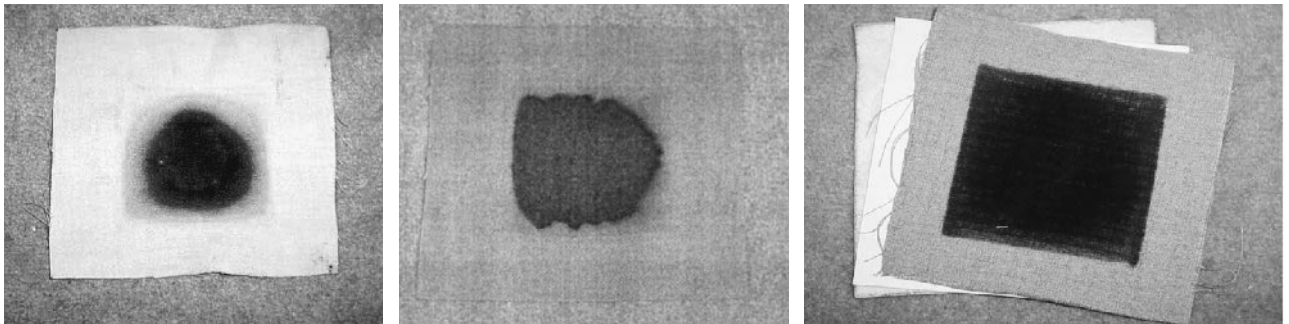


FIGURE 13.6 (a) Exposed Nomex sample; (b) Exposed FR cotton sample; (c) Exposed composite sample.

13.5 TESTING AND EVALUATION

TPC is evaluated based on either bench-top testing of a swatch sample of the garment material, or with the help of full-size exposure testing of the whole garment (i.e., instrumented manikin fire testing systems). During both exposures, heat measurement can be made either indirectly by deriving the sensed temperature of an exposed material, or via direct heat flux sensing by using calorimeter sensors. The intermediary step of deriving heat flux from temperature versus time data can be a cumbersome operation, depending on the material(s) and the heat flux path between the heat and the sensing device.

The Center for Research on Textile Protection and Comfort (TPACC) at North Carolina State Uni-

versity (NCSU) [4] utilizes most of the conventional bench-top testing setups, including the Thermal Protective Performance (TPP) system, the Radiant Protective Performance (RPP) system, the Stored Energy Test (SET) system, and the Radiant Panel System. In the same line of testing, Pyroman, a fully instrumented, life-size manikin is also housed and used by the Center. These systems are briefly described in the following paragraphs. New sensors are being developed at this time.

13.5.1 The TPP System

The Thermal Protective Performance (TPP) system accommodates the exposure of test specimens, 15 × 15 cm in size, to specific thermal heat flux lev-

els and exposure duration times. This is part of a standard ASTM test, as described by the ASTM TPP Test for Clothing by an Open Flame Method (D 4108-82). The TPP sensor assesses the heat flux via a copper disk. The exposure is adjusted and generated by the control of the gas flow feeding two burners. Additional heat to the sample is also generated by a bank of nine electrically heated quartz tubes, as shown on the diagram in Figure 13.7. The sample holder allows exposure of up to 100 cm² of the test sample. A mechanical shutter controls the onset of the exposure as well as its duration. A photographic view of the TPP exposure/sensing hardware is shown on Figure 13.8, with the shutter closed. The gas burners and the quartz tubes can be calibrated to generate an exposure heat flux ranging approximately from 0.05–3.0 cal/cm²/sec.

A desktop computer that interfaces with the sensor via a dedicated data acquisition card and associated software, controls the hardware of the TPP testing system. Data generated by the calibrated copper calorimeter sensor is used in conjunction with the calorimeter constants to compute the heat flux through the fabric sample. Subsequent computations and data analysis are also part the software that determine, based on the Stoll criterion [5], tolerance times to second-degree burns.

13.5.2 The RPP System

A vertical exposure configuration of the TPP system would drastically reduce the convective component of the heat reaching the test sample. The thermal resistance of the tested material is measured using the

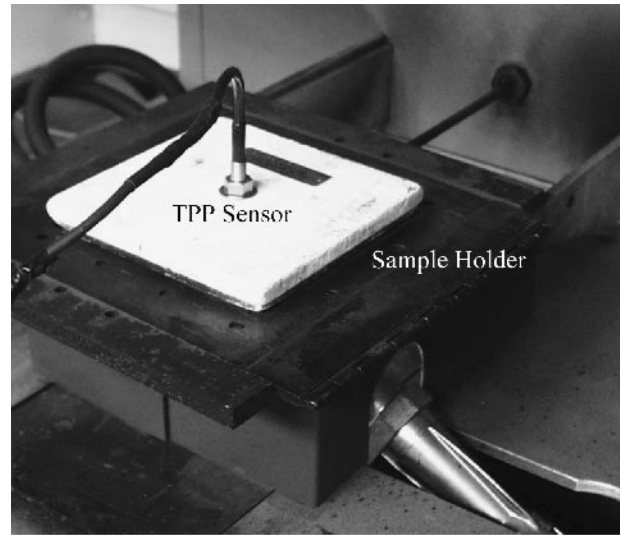


FIGURE 13.8 Sensor and exposure components of the TPP system

Indacore Radiant Protective Performance (RPP) test apparatus. The test protocol is performed according to the ASTM F1939 standard test method for radiant protective performance of flame resistant clothing materials. The radiant exposure is generated by a bank of five 500 W infrared tubular translucent quartz tubes, as shown on the diagram in Figure 13.9. A routine exposure level is accomplished via the application of 80 volts to the quartz lamps in order to radiate the sample with a heat flux of 2.0 cal/cm²/sec (8.4 watts/cm²). A calibration procedure is required for the instrument to ensure the delivery of an accurate,

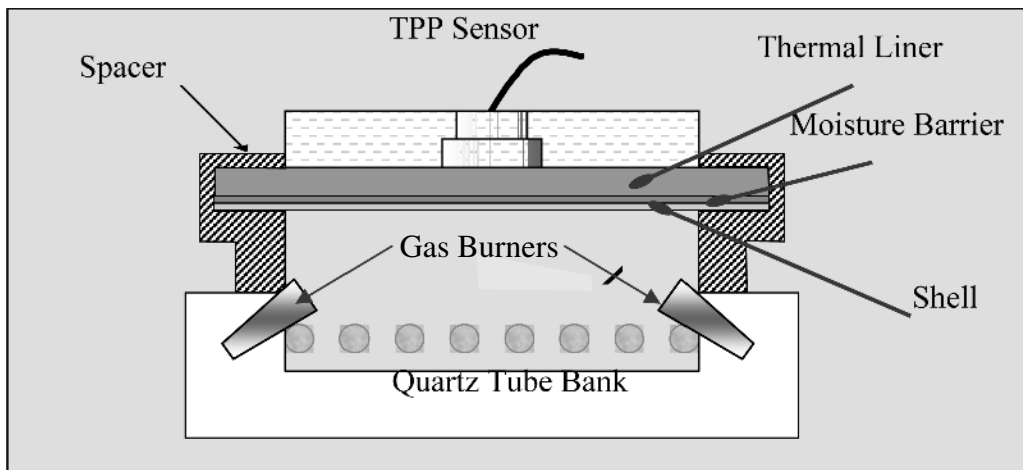


FIGURE 13.7 Thermal Protective Performance (TPP) system.

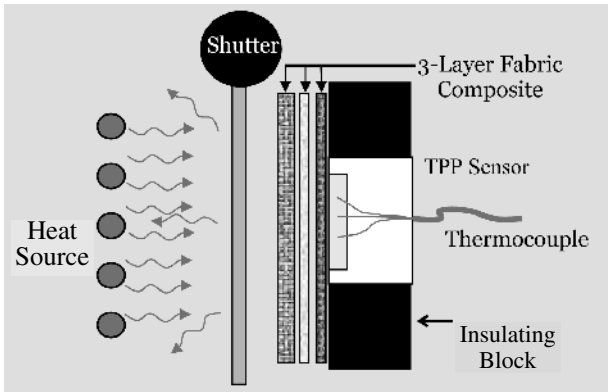


FIGURE 13.9 Radiant Protective Performance (RPP) system.

steady heat flux. The fabric sample is vertically mounted in a holder facing the heat source. A manual shutter controls the onset of the exposure as well as its duration. A photographic view of the RPP exposure hardware is shown on Figure 13.10, without the shutter. The sensor, computer hardware, and software used with the RPP system are similar to that of the TPP previously described.

The RPP testing apparatus is limited to short exposures, whereas the TPP system exposure duration times can extend up to 10 minutes and longer for lower heat flux exposure levels.

13.5.3 The SET System

The Stored Energy Test (SET) system utilizes exposure hardware similar to that of the RPP setup. The major differences are the horizontal configuration, instead of a vertical sample exposure setup, and a

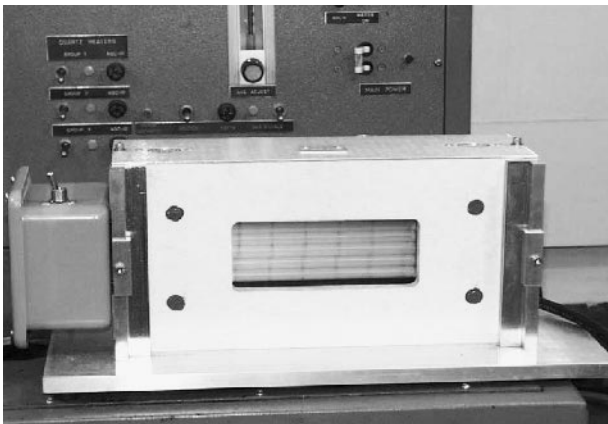


FIGURE 13.10 Exposure Components of the RPP system.

bank of nine quartz tubes that can be adjusted to higher heat flux levels. Additionally, a water cooling arrangement interfaces with the exposure hardware, allowing prolonged exposures at heat flux levels relatively higher than the RPP. The exposure hardware of the apparatus is shown in Figure 13.11. A manual shutter controls the onset of the exposure as well as its duration. Heat sensing, data gathering, and analysis are conducted similarly to the RPP system.

13.5.4 The Radiant Panel System

The Radiant Panel System, as described by the ASTM E162 standard method, is organized around a gas-fired radiant panel as a source of exposure to assess the performance of TPC material to prolonged radiant heat exposures. The sample holder for the material is set at adjustable positions from the heat source. The heat exposures achieved by this setup vary between 1.0 to more than 50 kW/m². A shutter controls the onset of the exposure as well as its duration. Exposure duration can extend up to 30 minutes. Thermocouples are used to measure the temperature of the fabrics during the test.

13.5.5 The Pyroman System

The Pyroman System is an instrumented manikin, size 40* regular male, normally used for assessing and evaluating the performance of TPC against exposures to a realistic simulation of a flash fire condi-

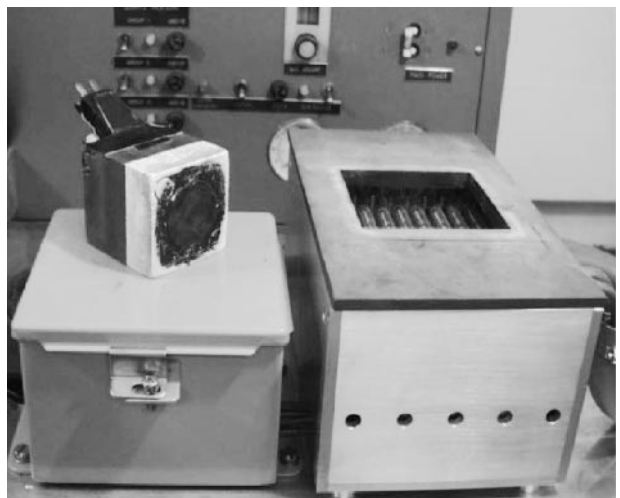


FIGURE 13.11 Exposure Components of the SET system.

*U.S. clothing size system.

tion. The system is an upgrade of Thermoman, which is a similarly instrumented manikin developed by DuPont for the same purpose; it is housed in a 11 × 18-ft fire resistant room that has been constructed by TPACC. Eight industrial burners are appropriately positioned around the manikin to generate the flash fire, as shown on Figure 13.12(a), that fully engulfs the chamber. Pyroman is one of few such manikins in the world, and the only one housed in a university research setting in the United States. The evaluation of the performance of TPC is conducted with aid of 122 specially designed slug calorimeter sensors, known as Pyrocal sensors, distributed throughout the manikin body, as shown on Figure 13.12(b). This TPC analysis system also includes a computer system that monitors safety conditions, controls the exposure procedure, acquires the data from the Pyrocal sensors, and calculates the results. The data acquired by the system is used to calculate the incident heat flux and predict the potential tissue burn damage to a wearer, for each sensor region, during and after the exposure. Figure 13.13 shows one of the reporting forms, depicting the borders of each sensor region.

The primary criterion for protective performance is a material's ability to reduce heat transfer to the manikin, which is reported as predicted burn injury. The calculated incident heat flux is used to determine the temperature of human tissue at two depths below the surface of the skin, one representing second-degree and the other representing third-degree burn injury.



FIGURE 13.12 (a) Pyroman fully engulfed in flames; (b) Bare pyroman.

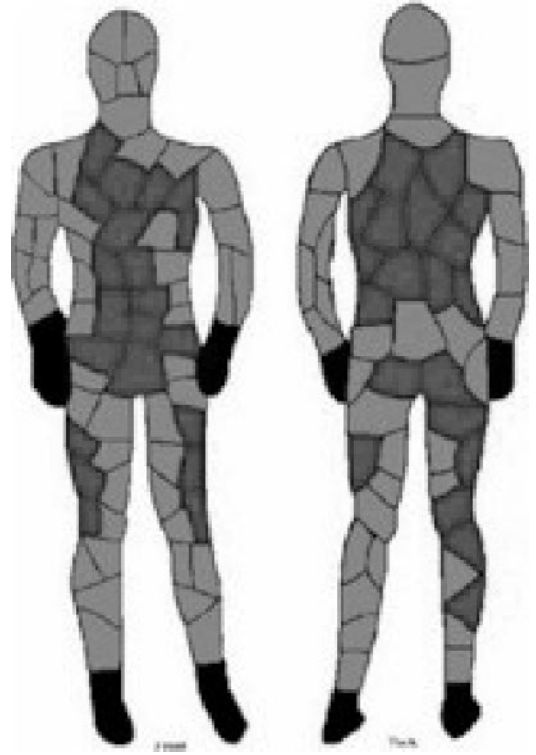


FIGURE 13.13 Burn injury report by sensor region.

Relevance of the results from the evaluation and analysis of the wealth of data generated by all these testing systems is governed by the accuracy of the sensing devices as well as the precision and stability of the numerical calculation programs used in association with these systems.

13.6 SENSING DEVICES

When skin burn damage assessment, based on skin surface temperature, is the purpose of a measurement exercise, a skin simulant sensor should be used. Materials that have been dubbed “skin simulants” are epoxies that have thermal inertia close to that of human skin. This approach would replicate the heat transfer through the skin due to contact with heated fabric, thereby replicating the subsequent skin surface temperature. In such exposures, the skin thermal conductivity, k , and the blood perfusion rate govern the heat transfer around the exposed area. To truly match human skin, a skin simulant should mimic these two parameters rather than the skin thermal inertia (which is a lumped product of k , the skin density ρ and the dermal thermal capacity C ,

which happens to be close to that of some epoxy resins).

On the other hand, when skin burn damage assessment is based on heat exposure, direct heat flux measurement is the method of choice. It is known that a calorimeter-type sensor such as the TPP sensor, which tracks the heat flux through the fabric, has a copper disk of a considerable size that would disturb the thermal balance during heat flux measurement. This variation occurs through heat loss and heat absorption by the copper disk. These two shortcomings have been corrected with the recently developed Pyrocal sensor. Its design incorporates a guard ring to limit heat losses and a small size copper disk (1.3g versus a TPP disk's 17.9g) to minimize the heat sink effect.

Based on the response and behavior that have been observed through the multiple usages of both Pyrocal and TPP sensors, the Pyrocal sensor will probably soon replace the TPP sensor for routine TPP testing. These sensors, which play an important role in TPC testing and evaluation, are described in greater detail in the following paragraphs.

13.6.1 TPP Sensor

The TPP sensor, shown in Figure 13.14, is a slug-type sensor widely used for bench-top testing of thermally protective clothing materials. The sensor consists of a copper disk, 4 cm in diameter and 0.16 cm thick. Four J-type (iron-constantan) thermocouples are secured to the disk, positioned at 120-degree intervals and at the center. Heat flux is calculated

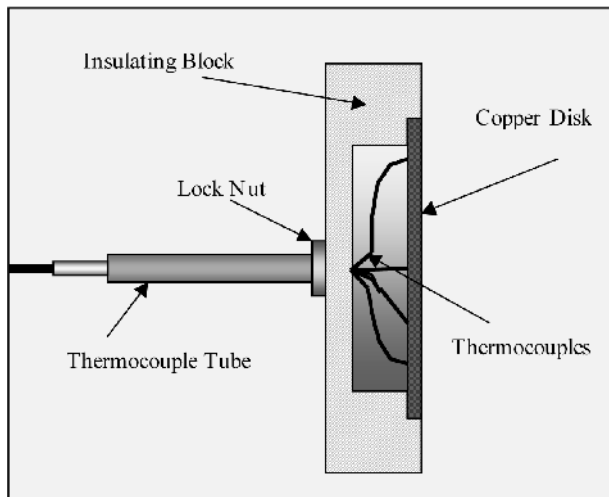


FIGURE 13.14 Thermal Protection Performance (TPP) sensor.

from the temperature rise, indicated by the thermocouple output, and from the mass and specific heat capacity of the copper disk. Compared to other sensors, the TPP sensor does not require any calibration or heat loss management. It is highly reliable and rugged. A direct measurement of heat flux using temperature differencing can be achieved, based on the following basic differential equation:

$$q = \frac{MC_p}{\varepsilon A} \frac{dT}{dt}, \quad (13.1)$$

where q is the incident heat flux, M the mass of the calorimeter slug, C_p the heat capacity of copper, ε the surface emissivity, and A the disk area.

Generally associated with this sensor, a square wave exposure sequence is used so that results can be related to the values obtained by Stoll [5]. A human tissue tolerance overlay, obtained by integration of the Stoll curve with respect to time, is used to determine tolerance times to second-degree burns. The TPP values are the product of the incident heat flux and the recorded tolerance time to second-degree burn, expressed in cal/cm².

13.6.2 Pyrocal Sensor

The insulated copper sensor, Pyrocal, shown in Figure 13.15, is a slug type sensor developed at NCSU for use with Pyroman, an instrumented manikin fire testing system. This insulated copper sensor consists of a thin copper disk, 1.27 cm in diameter and 0.15 cm thick, radially surrounded by a thin copper ring as a thermal guard. Both the disk and the ring are supported by an insulating holder to minimize heat transfer to and from the body of the calorimeter, thus approximating one-dimensional heat flow [6]. Beneath the surface of the copper disk, an insulating cavity is maintained and a T-type (copper-constantan)

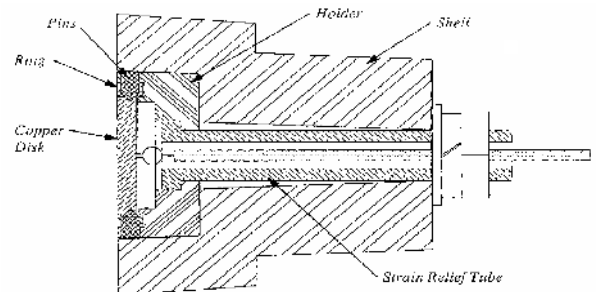


FIGURE 13.15 Insulated copper sensor, Pyrocal.

tan) thermocouple is attached to the lower side of the disk. The entire assembly is encapsulated within a protective shell. Heat flux is calculated from temperature rise and the known properties of the copper slug, using a procedure that increases the accuracy of the heat flux estimate by compensating for heat losses, compared with the TPP sensor.

Direct measurement of heat flux using temperature differentiations for this sensor is computed by modifying the previous TPP equation as:

$$q = \frac{MC_p C_l}{A} \frac{dT}{dt} + K_l(T_d - T_i), \quad (13.2)$$

where C_l is the thickness factor, K_l the heat loss coefficient, T_d the surface temperature of disk at time t , and T_i the initial or ambient temperature. Both C_l and K_l are experimentally determined. This highly reliable and rugged sensor requires a calibration and has a heat loss management scheme.

The physical constants used in the heat flux computation for the TPP and the Pyrocal sensors are shown in Table 13.1.

13.6.3 Embedded Thermocouple Sensor

The embedded thermocouple sensor shown in Figure 13.16, known as a polymeric skin simulant sensor, has been developed by DuPont for use with the Thermoman fire test manikin. This sensor employs a thin-skin calorimeter that incorporates a Type-T thermocouple buried below the exposed surface of a cast resin plug. The resin plug is made of a thermoset polymer that reportedly exhibits a thermal inertia similar to undamaged human skin. Heat transfer is evaluated using an inverse heat transfer calculation that relies on an accurate location of the thermocouple bead [7].

Heat flux calculation procedures used for the embedded thermocouple sensor require a cumbersome numerical computation based on an inverse heat transfer method to calculate the incident heat flux. This moderately reliable and rugged sensor requires an extensive calibration to compensate for the error

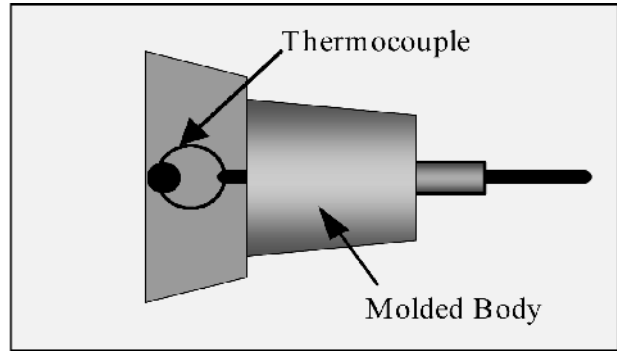


FIGURE 13.16 Embedded thermocouple sensor.

associated with the varying position of the thermocouple bead (tip) in reference to the outer surface of the sensor.

13.6.4 Additional Sensor Types and their Limitations

Calorimeter-type and thermocouple-type sensors, those that were previously described and others not covered here, are limited to relatively short exposure durations, mainly a few seconds. All of these sensors contain material with low thermal conductivity that emancipates retention of heat during the exposure time. Subsequently, the sensor internal temperature rises to levels that would make the sensor unable to accurately assess the incident heat flux. To a certain extent, the sensor becomes heat restrained by being unable to discern between its own temperature and that of the fabric.

Optical sensors are not good candidates for heat or temperature assessment behind exposed fabrics, because a good portion of the heat transmitted would be unseen by these sensors (this portion is the conductive and convective components of the heat flux being sensed).

Two water-cooled thermal sensors are commercially available for users. ThermogageTM is a water-cooled transducer that measures the absorbed heat flux through a thin circular constantan foil [8]. A second water-cooled sensor, made by Hy-Cal Engineering [9], is based on the same principle of ab-

TABLE 13.1 Copper Slug Sensor Constants

| Sensor | Mass (g) | Area (cm ²) | ϵ | C_l | K_l (cal/cm ² · sec · °C) | C_p (cal/g °C) |
|---------|----------|-------------------------|------------|-------|--|------------------|
| TPP | 17.89 | 12.56 | 0.95 | | | 0.0927 |
| Pyrocal | 1.31 | 0.99 | 0.95 | 1.04 | 0.00358 | 0.0927 |

sorbed heat flux measurement. Both sensors have a built-in cooling system that removes the heat absorbed during exposure. This heat removal process prevents the sensors' temperature from rising and allows these sensors to function much longer than the non-cooled sensors. However, because of the thermal inertia of their cooling systems and their relatively slow response time, these sensors are not suitable for measurement of transient heat transfers [10]. The capability and accuracy of these sensors are limited to only those exposure types, levels, and duration that are indicated by the sensor's manufacturers. An experimental liquid cooled heat flux sensor was developed at NCSU for usage in association with the evaluation of fire protective clothing in extended-time, low heat flux exposures [11]. This thermal sensing system, shown in Figure 13.17, is basically a water-cooled TPP sensor. Not shown in the figure are the water cooling auxiliaries. The sensor assesses incident heat flux via measurements of the temperature of the coolant flowing through the system, as well as the temperature of the copper disk. The temperature rise in the coolant is calibrated to known levels of incident heat flux.

13.7 SKIN BURN DAMAGE EVALUATION

Burn damage to the skin is evaluated based on the cumulative heat energy transferred to and absorbed by the dermal layer during and beyond the exposure duration. Second-degree burn estimates are usually calculated based on readings from different types of thermal sensors, such as the ones previously cited.

13.7.1 Simple Approach

Burn predictions have been based solely on temperature registered by a thermocouple attached to the

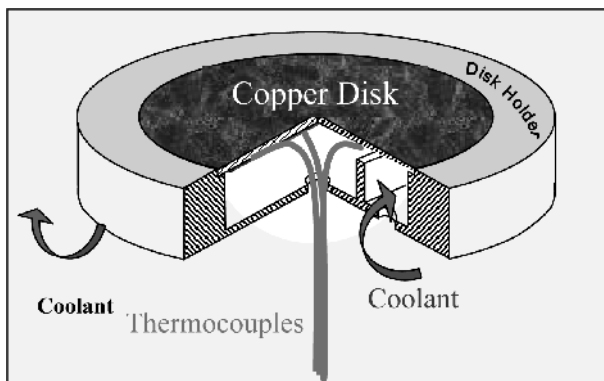


FIGURE 13.17 Liquid cooled heat flux sensor.

innermost thermal liner fabric of a TPC. In this case, a criterion used by researchers at NIST and the 3M Company [12] is based on the time for the innermost fabric surface to achieve a temperature of 55 °C. This time is used as an indication of the potential for second-degree burn. According to Neal [13], the amount of protection time that a fabric system would provide prior to achieving a second-degree burn is usually higher when using a skin burn model approach versus using the surface temperature of the innermost fabric layer.

13.7.2 Stoll Curve

The Stoll criterion [14] is used to predict time to second-degree burn by a simple graphical approach based on comparing the heat flux response of the sensor to a given exposure with the "Stoll Curve." With the traditional TPP operating system, however, the burn time to second-degree burn can be determined, in real time, based on the position of the intersection point between the temperature profile generated by the TPP sensor and a Stoll temperature curve obtained via a numerical integration of the original heat flux "Stoll Curve." A typical exposure resulting in a burn time of approximately 2.9 seconds is shown on Figure 13.18.

13.7.3 Henriques Damage Integral

A more evolved burn model is based on criteria suggested by Henriques [15]. The Henriques burn integral utilizes a specific equation to estimate time to second- and third-degree burn. A few numerical models were developed based on this integral and the heat flux measured at the surface of different

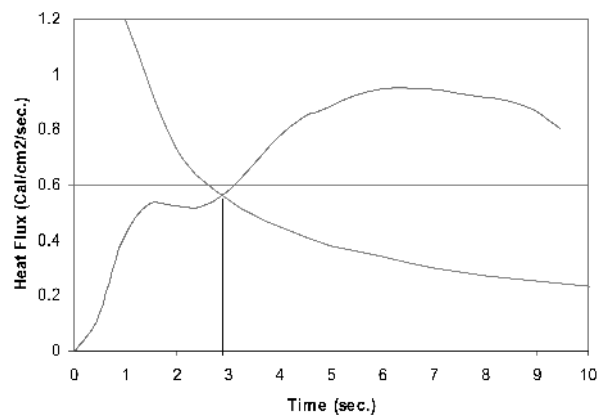


FIGURE 13.18 Second-degree burn assessment based on the Stoll criterion.

thermal sensors (embedded thermocouple, TPP and Pyrocal) to estimate skin burn injury. Associated with this model is a finite difference subroutine used to estimate the skin temperature, and resulting skin burn damage, at different depths in the skin. The program assumes that blood thermal circulatory effects and radiative heat transfer within the skin are negligible. Conduction is the only means of energy transfer. The skin is modeled as a series of contiguous isothermal layers, each with an assigned thickness, thermal conductivity, and specific heat, as shown in Table 13.2. The surface boundary condition is determined by the heat flux measured at the surface of the sensor. Thermal energy transfer is assumed to be adiabatic deep within the skin itself [3].

A numerical model based on the Crank-Nicolson implicit computational method can be used to estimate skin temperatures. From the skin temperature distribution, an Arrhenius relationship is applied to estimate burn injury as

$$\frac{d\Omega}{d\vartheta} = Ce^{\frac{-\Delta E}{RT}}, \quad (13.3)$$

where C is the rate constant (sec^{-1}), ΔE the activation energy for tissue destruction (cal/mole), R the universal gas constant (cal/mole/°K), and T the absolute temperature at the basal layer at time t (°K). Values of the resulting integral, Ω , known as the "Henriques Damage Integral," are assessed based on the following criteria: $\Omega > 1.0$, at a given skin depth, is equated with irreversible skin damage [15]. Once Ω is calculated, time to second- and third-degree burn can be estimated. The node spacing in the model is set at 0.01 cm. Burn damage is calculated at 0.01 cm and 0.1250 cm, based on average human skin thickness.

13.7.4 Pennes Model

TABLE 13.2 Thermal Properties of Human Skin [3]

| Properties | Skin Layer | |
|---|-----------------------|------------------------|
| | Epidermis | Dermis |
| Node depth (cm) | 100×10^{-4} | $1,250 \times 10^{-4}$ |
| k (cal/cm · sec · °C) | 8.0×10^{-4} | 8.0×10^{-4} |
| ρ (g/cm ³) | 1.2 | 1.2 |
| C (cal/g · °C) | 0.77 | 0.77 |
| α (cm ² /sec) | 8.66×10^{-4} | 8.66×10^{-4} |
| $k\rho C$ (cal ² /cm ⁴ · °C ² · sec) | 7.39×10^{-4} | 7.39×10^{-4} |

The first model that addressed heat transfer in living tissues is known as the Pennes model [16]. This relatively advanced model was based on the assumption that energy exchange between blood vessels and surrounding tissues occurs mainly across the wall of capillaries, where blood velocity is very low. The model assumes that blood enters the capillary bed at the temperature of major supply vessels, T_a , and immediately thermally equilibrates with surrounding tissues. Therefore, when the blood exits the capillary bed and enters the venous circulation, it has the tissue temperature, T . As a result, the total energy exchange by the flowing blood can be modeled as a heat source, whose magnitude is proportional to the volumetric heat flow and to the differential between the blood temperature in the major supply arteries and the local tissue temperature. These assumptions resulted in the following form of the bio-heat transfer equation:

$$\rho c \frac{\partial T}{\partial t} = \nabla \cdot (k \nabla T) + (\rho c)_b \omega_b (T_a - T) + q_m. \quad (13.4)$$

In this equation, ρ is the density, c the specific heat, T the temperature of the tissue, t the time, k the thermal conductivity, ω_b the blood perfusion, T_a the arterial temperature, and q_m the metabolic volumetric heat.

Subsequent investigators questioned the assumptions made by Pennes for the previous model. First, Wulff [17] claimed that the blood flow contribution to heat transfer in tissue must be modeled as a directional term of the form $(\rho c)_b \bar{u} \cdot \nabla T$ rather than the scalar perfusion term as previously suggested.

Other investigators, such as Klinger [18], reproached the lack of accurately assessing the heat transfer in the vicinity of large blood vessels by Pennes equations, due to the fact that the modeled process did not consider the main thermal equilibrium that takes place in capillaries, but rather in pre- and post-capillary vessels. Additionally, Pennes's model accounts for neither the directional convective mechanism of heat transfer due to the blood flow, nor the possible heat exchange between the small and closely-spaced, thermally significant, countercurrent vessels.

13.8 OTHER MODELING COMPONENTS

The additional components that are playing an important role in the transfer of heat and transport of

moisture across and within the TPC are the fabric layers and their composition, the air surrounding the garment, and the air gaps trapped inside the fabric material. Constitutive equations for such heat transfer process can be simply modeled as purely heat conduction within a semi-infinite slab exposed to a constant heat flux boundary condition. This problem has a known solution, based on the complementary error function $erfc(\eta)$. The solution equation for this process has been derived as [19]

$$T(x,t) - T_i = 2 \frac{q''}{k} \left(\frac{\alpha t}{\pi} \right)^{1/2} \exp\left(-\frac{x^2}{4\alpha t}\right) - \frac{q''}{k} x erfc\left[\frac{x}{2(\alpha t)^{1/2}}\right], \quad (13.5)$$

where $T(x,t)$ is the temperature distribution in the system, T_i the initial temperature, q'' the incident heat flux, k the thermal conductivity and α is thermal diffusivity.

This formulation would be very acceptable if the material under consideration was isotropic, but textile fabrics are highly anisotropic with thermal properties dependant upon temperature and moisture contents.

To solve for the heat transfer through a TPC, a multiple eigenvalue conduction problem consisting of separate eigenvalue problems for each fabric layer, linked through interfacial boundary conditions, would be a better formulation of the process. Additionally, since the moisture introduced into the fabric systems will undergo a phase change, the heat transfer problem would most correctly have to be solved using a moving boundary layer method.

An initial simplified approach to such a complex problem would be to consider the thermal properties of the dry material thermal forming the TPC, lumped as if they were thermal properties of homogeneous and isentropic material. The effects of adding moisture to TPC systems can be adjusted by combining the dry material properties for the systems with the physical and thermal properties of water, using a weighting method.

For typical firefighter garments, (three layers of TPC), the dry system material properties can be approximately modified, using the rule of mixture, by weight, to account for the gradual addition of water into the systems. A complete listing of material values used in typical analysis is shown in Table 13.3. The first row, corresponding to 0% moisture, represents the properties of the dry system material. Prop-

TABLE 13.3 Effect of Moisture Contents on TPC Material Thermal Properties

| Moisture | k w/(m C) | ρ kg/m ³ | C _p w s/(kg C) | α m ² /s | α (cm ² /s) |
|----------|--------------|------------------------|------------------------------|------------------------|---------------------------|
| 0% | 0.050 | 250.00 | 1150.00 | 1.74E-07 | 1.74E-03 |
| 5% | 0.077 | 285.47 | 1294.01 | 2.09E-07 | 2.09E-03 |
| 10% | 0.102 | 317.72 | 1424.93 | 2.26E-07 | 2.26E-03 |
| 20% | 0.146 | 374.15 | 1654.04 | 2.35E-07 | 2.35E-03 |
| 30% | 0.182 | 421.89 | 1847.90 | 2.34E-07 | 2.34E-03 |
| 50% | 0.241 | 498.29 | 2158.08 | 2.24E-07 | 2.24E-03 |
| 70% | 0.286 | 556.71 | 2395.28 | 2.14E-07 | 2.14E-03 |
| 100% | 0.337 | 622.44 | 2662.12 | 2.03E-07 | 2.03E-03 |

erties of water are shown in the last row of the table, corresponding to 100% moisture contents.

An approximation of the previous lengthy equation has been used to estimate transient incident heat conduction into a semi-infinite slab based on surface temperature, T_s , as follows [20]:

$$q = \frac{\sqrt{\pi k \rho C_p}}{2\sqrt{t}} (T_s - T_\infty), \quad (13.6)$$

where k is the thermal conductivity, ρ the density, T_s the surface temperature at time t , and T_∞ the initial or ambient temperature.

The same author, Torvi [20] accounts for convection and radiation on the outside of the TPC material, which is exposed to the flames, and conduction/convection and radiation in the air gap contacting the skin. The radiation heat flux on the outside is expressed as the sum of blackbody components from hot gases, from the fabric to ambient air, and from the burner head to the fabric,

$$q_{rad} = \sigma \epsilon_g T_g^4 - \sigma \epsilon_f F_a (1 - \epsilon_g)(T_f^4 - T_a^4) + \frac{\sigma F_b (1 - \epsilon_g)(T_b^4 - T_f^4)}{1 + F_b (1 - \epsilon_g) \left(\frac{1 - \epsilon_f}{\epsilon_f} + \frac{A_f}{A_b} \frac{1 - \epsilon_b}{\epsilon_b} \right)}, \quad (13.7)$$

where σ is the Stefan-Boltzmann constant; ϵ_g , ϵ_f and ϵ_b are emissivities of the hot gases, the fabric, and the burner head, respectively; T_g , T_f , T_a , and T_b are the temperatures of the hot gases, the outside of the fabric, the ambient air, and the burner head, respectively; F_a and F_b are view factors accounting for the geometry of the fabric with respect to the ambient air and to the burner, respectively; and A_f and A_b are the surface areas of the fabric and the burner head, re-

spectively. The radiation heat flux on the inside of the TPC is expressed as:

$$q_{rad} = \frac{\sigma(T_f^4 - T_s^4)}{\frac{1 - \varepsilon_s}{\varepsilon_s} + \frac{A_s}{A_f} \left(\frac{1}{F_s} + \frac{1 - \varepsilon_f}{\varepsilon_f} \right)}, \quad (13.8)$$

where T_s , ε_s , and A_s are the temperature, emissivity, and surface area, respectively, of a test sensor taking the place of skin, and F_s accounts for the geometry of the fabric with respect to the sensor.

Other researchers have investigated the heat transfer through fabric systems. The Mell and Lawson model [21] extend Torvi's approach to a multi-layer composite of fabrics. Conduction is modeled throughout the system, and convection is modeled on both the outside and the inside of the composite. The treatment of radiation is extended to the multi-layer system, accounting not only for incident heat flux from the heat source, but also for heat flux due to internally reflected energy radiation between layers and within the garments' air pockets, voids and cavities. The model is a reasonable treatment of heat transfer to and from the fabric and in between the fabric layers, and, like the Torvi model, can be extended to treat heat transfer in three dimensions, and accounts for conduction or convection by water vapor.

Finally, the most complex issue to model is the combustion and thermal degradation of polymers during intense heat exposures. The complex processes involve physical and chemical phenomena that are only partially understood. A number of different approaches for modeling this problem have been suggested in the literature. Ricci [22], Whiting et al. [23], Delichatsios and Chen [24], and Staggs [25] suggested modeling of thermal degradation of polymers in terms of a Stefan problem, where the degradation of the solid is assumed to occur infinitely rapidly at a critical temperature. Other authors have attempted to model solid-phase degradation using limited global in-depth reactions [26, 27, 28].

13.9 CONCLUSION

Heat effects on the dermal layers of the skin have been thoroughly investigated and the modeling of human skin burn injuries is very adequate. However, there is no extensive numerical/empirical modeling of thermal mechanisms in TPC when exposed to intense heat sources, mainly due to its complexity. Most of the existing models are based on simplified,

steady state, one-dimensional heat transfer processes that can be assessed in a bench-top Thermal Protective Performance (TPP) evaluation environment. When it comes to a generalized model for heat transfer and fabric thermal degradation processes (off-gassing, material morphology transformations, and phase changes) of TPC in realistic configurations interfacing with a human body, there are no known existing extensive models.

When burn damage is assessed based on skin surface temperature, a skin simulant sensor should be used. This approach would replicate the heat transfer through human skin due to contact with heated fabric, and thereby replicate the subsequent skin surface temperature. However, for such exposures, the skin thermal conductivity, k , and the blood perfusion rate govern the heat transfer around the exposed area. To truly match human skin, a skin simulant should mimic these two parameters and not the skin thermal inertia (a lumped product of k , ρ and C), which happens to be close to that of some resins.

On the other hand, it is admitted that a calorimeter-type sensor such as the TPP sensor, which tracks the heat flux through the TPC fabric, has a copper disk of a considerable size that would disturb the thermal balance during heat flux measurement. This variation occurs through heat loss and heat absorption by the copper disk. These two shortcomings have been corrected with the Pyrocal sensor by adopting a design that incorporates a guard ring to limit heat losses, and a small size copper disk (1.3g versus 17.9g) to minimize the heat sink effect.

13.10 REFERENCES

1. <http://www.pleo.com/dupont/nomex/>
2. http://www.teijin-aramid.com/ENG/tech_frame.ht
3. Barker, R., Pawar, M., Shalev, I., Hamouda, H., and Johnson, J. W. *Review and Evaluation of Thermal Sensors for Use in Testing Firefighters Protective Clothings*, NIST GCR 99-772, 1999.
4. <http://www.tx.ncsu.edu/tpacc/protection/protection.htm#thermal>
5. Stoll, A. M., and Chianta, M.A. Heat Transfer Through Fabrics as Related to Thermal Injury. *Transactions—New York Academy of Sciences*, Vol. 33 (7), 1971.
6. Grimes, R., Mulligan, J. C., Hamouda, H., and Barker, R. The Design of a Surface Heat Flux Transducer for Use in Fabric Thermal Protection Testing. *Performance of Protective Clothing: 5th Volume*. James S. Johnson and S. Z. Mansdorf, Eds. ASTM STP 1237. West Conshohocken, PA: American Society for Testing and Materials., pp. 607–624, 1966.

7. Grimes, R. *Design of a Heat Flux Transducer for Evaluating Fire Resistant Fabrics*. M. S. Thesis, North Carolina State University, Raleigh, NC, 1995.
8. Watell Corporation, 2001 South Main Street, Blacksburg, VA 24060. (540) 961-2001.
9. Hy-Cal Sensing Products, Honeywell Inc., 9650 Telstar Avenue, El Monte, CA 91731. (800) 932-2702.
10. Clayton, W. A. Heat-Flow Transducers. *Handbook of Applied Thermal Design*. New York: McGraw-Hill, pp. 12-78 to 12-84. AU: What year, please
11. Heath, D. *A Liquid Cooled Heat Flux Transducer for Use in Evaluating the Thermal Protective Performance of Fire-fighter Clothing*. M. S. Thesis, North Carolina State University, Raleigh, NC, 2000.
12. Jensen, R. L., Jr., *Thermal Performance of Firefighters' Protective Clothing*. Safety and Security Systems Division, 3M Center, Building 225-4N-14, St. Paul, MN 55144-1000.
13. Neal, T. E. *Prediction of Fire Fighter Burn Injury Using Skin Model Sensors at Low Level Heat Flux Exposures—Preliminary Results*. NFPA 1971 Technical Committee. November 5, 1998.
14. Stoll, A. M. and Chianta, M. A. Heat Transfer Through Fabrics as Related to Thermal Injury. *Transactions—New York Academy of Sciences*, Vol. 33 (7), 1971.
15. Henriques, F. C. Studies of Thermal Energy: V. The Predictability and the Significance of Thermally Induced Rate Process Leading to Irreversible Epidermal Injury. *Archives of Pathology*, Vol. 43, p.489, 1947.
16. Pennes, H. Analysis of Tissue and Arterial Blood Temperatures in the Resting Human Forearm. *Journal of Applied Physiology*, Vol. 1, pp. 93–122, 1948.
17. Wulff, W. The Energy Conservation Equation for Living Tissue. *IEEE Transactions of Biomedical Engineering*, Vol. BME-21, pp. 494–495, 1974.
18. Klinger, H. G., Heat Transfer in Perfused Biological Tissue: I: General Theory. *Bulletin of Mathematical Biology*, Vol. 36, pp. 403–415, 1974.
19. Incropera, F. P. and Dewitt, D. P. *Fundamentals of Heat and Mass Transfer, 5th Ed.* New York: John Wiley & Sons, Inc., 2002.
20. Torvi, D. A. Ph.D. Thesis. University of Alberta, Canada, 1997.
21. Mell, W. and Lawson R. *A Heat Transfer Model for Fire Fighter's Protective Clothing*. NISTIR 6299, NIST, January, 1999.
22. Ricci, R. Traveling Wave Solutions of the Stefan and the Ablation Problems. *SIAM Journal of Mathematical Analysis*, Vol. 21, pp. 1,386–1,393, 1990.
23. Whiting, P., Dowden, J. M., Kapadia, P. D., and Davis, M. P. A One-Dimensional Mathematical Model of Laser Induced Thermal Ablation of Biological Tissue. *Lasers in Med. Sci.*, Vol. 7, pp. 357-368, 1992.
24. Delichatsios, M. A. and Chen, Y. Asymptotic, Approximate and Numerical Solutions for the Heatup and Pyrolysis of Materials Including Reradiation Losses. *Combustion and Flame*, Vol. 92, pp. 292–307, 1993.
25. Staggs, J. E. J. A Discussion of Modeling Idealized Ablative Materials with Particular Reference to Fire Testing. *Fire Safety Journal*, Vol. 28, pp. 47–66, 1997.
26. Vovelle, C., Delfau, J., and Reuillon, M. Experimental and Numerical Study of Thermal Degradation of PMMA. *Combustion Science and Technology*, Vol. 53, pp. 187–201, 1987.
27. Wichman, I. S. and Atreya, A. A Simplified Model for the Pyrolysis of Charring Materials, *Combustion and Flame*, Vol. 68, pp. 231–247, 1987.
28. Di Blasi, C. and Wichman, I. S. Effects of Solid-Phase Properties on Flames Spreading over Composite Materials. *Combustion and Flame*, Vol. 102, pp. 229–240, 1995.

CHAPTER 14

WEATHERING AND SURFACE PROTECTION OF WOOD

Philip Evans
Mohammed Jahangir Chowdhury
Brian Mathews
Karl Schmalzl

Centre for Advanced Wood Processing, University of British Columbia, Vancouver, Canada

Stephen Ayer

Forintek Canada Corporation, Vancouver, Canada

Makoto Kiguchi
Yutaka Kataoka

Forestry and Forest Products Research Institute, Tsukuba Norin, Ibaraki, Japan

| | |
|--|------------|
| 14.1 INTRODUCTION | 277 |
| 14.2 MECHANISMS AND ENVIRONMENTAL FACTORS | 277 |
| 14.3 EFFECTS OF WEATHERING | 281 |

| | |
|-------------------------------|------------|
| 14.4 PROTECTION | 287 |
| 14.5 FUTURE DIRECTIONS | 293 |
| 14.6 REFERENCES | 293 |

14.1 INTRODUCTION

The surface degradation that occurs when wood is used outdoors and above ground is termed weathering. Weathering should not be confused with decay caused by basidiomycete fungi, microorganisms capable of significantly reducing the strength of structural timber (Feist 1990). Because weathering is a superficial phenomenon, its effects on the mechanical properties of wood are small and, accordingly, there are examples of wooden buildings such as the stave (pole) churches in Norway that remain structurally sound despite having been exposed to weathering for over 1,000 years (Borgin 1969). The most obvious features of weathered wood are its gray coloration and rough surface texture (Figure 14.1). While microorganisms do colonize weathered wood, conditions at exposed wood surfaces generally do not favor decay. Hence, the defining features of weathering are its superficial nature and the minor role of microorganisms compared to environmental factors in degradative processes. This paper reviews the weathering of wood, with emphasis on the causal agents of weathering, the effects of weathering on wood properties and performance and, finally, the protection of wood from weathering.

The first scientific article on the weathering of wood appeared in the 19th century [Berzelius (1827), cited in Feist and Hon (1984)], and a number of comprehensive reviews have been published [Kal-

nins (1966), Feist and Hon (1984), and Feist (1990)]. This paper seeks to update these reviews in some areas.

14.2 MECHANISMS AND ENVIRONMENTAL FACTORS

The main environmental factors involved in the weathering of wood are solar electromagnetic radiation (ultraviolet and visible light), molecular oxygen (O₂), water, heat, particulate matter, and environmental pollutants. This section outlines the factors and mechanisms involved in wood surface deterioration.

14.2.1 Absorption and Penetration of Light into Wood

The maximum amount of solar radiation available at the earth's surface on a clear day is normally 1,000 W/m². The composition of such radiation is approximately 5% ultraviolet (286–380 nm), 45% visible (380–780 nm) and 50% infrared (780–3,000 nm). Light of shorter wavelength is more energetic, in accord with Eq. (14.1). The critical wavelengths to cleave carbon-carbon, carbon-oxygen, and carbon-hydrogen single bonds are 346, 334, and 289 nm, respectively. These bonds connect the basic structural units of the polymeric materials in wood (i.e. cellulose, hemicelluloses, and lignin).

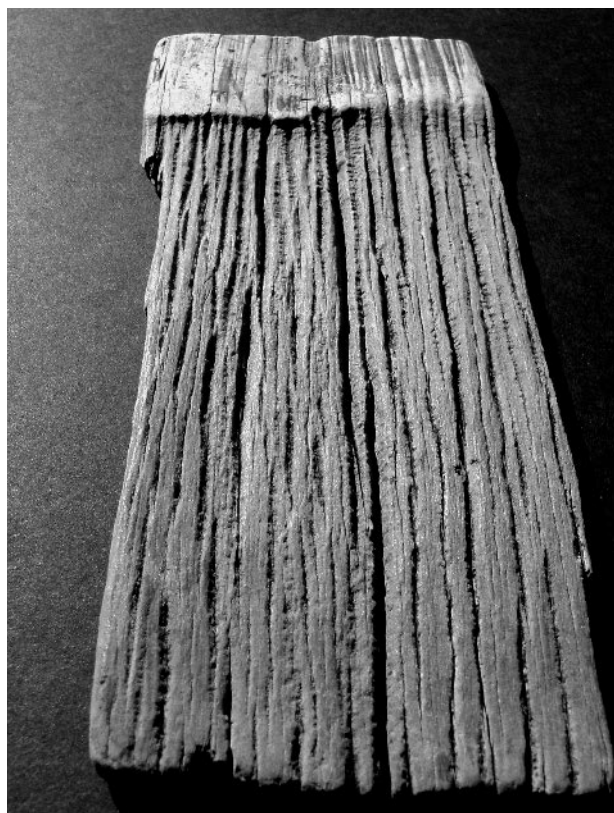


FIGURE 14.1 Weathered Norfolk Island pine (*Araucaria heterophylla* [Salisb.] Franco) roofing shingle, measuring 160×70 mm, from a 19th century building in Norfolk Island, Australia. Note the severe erosion and checking of the exposed surface.

$$E = \frac{2.86 \times 10^4}{\lambda}, \quad (14.1)$$

where E = energy of a photon (kcal/mol), and
 λ = wavelength (nm).

In order to act upon wood, solar radiation must be absorbed by one of wood's chemical constituents. Experimentation has shown that the aromatic lignin component of wood strongly absorbs ultraviolet (UV) light with a distinct maximum at 280 nm, and decreasing absorption extending beyond 380 nm into the visible region of the spectrum (Kalnins 1966). Discoloration of wood occurs at wavelengths in the range of 305–335 nm (Sandermann and Schlumbom 1962; Kitamura et al. 1989). The chromophoric centers in lignin that absorb UV light are phenolic groups, double bonds, carbonyl groups, quinones, quinonemethides and biphenyls (Hon 1979b). Acetal (Hon 1975) and ketonic carbonyl (Bos 1972) groups are responsible for the absorption of UV light by cel-

lulose. Cellulose also absorbs light between 200 and 300 nm (Feist and Hon 1984), but little UV light at these wavelengths reaches the earth's surface (Wallace and Hobbs 1977). The absorption of UV light by hemicelluloses is thought to be identical to that of cellulose. The heartwood of many wood species also absorbs light beyond 500 nm because of the presence of low molecular weight extractives such as flavonoids, tannins, stilbenes and quinones.

As all of the chemical constituents of wood absorb UV light to some extent, UV light is reported to only penetrate the surface of wood. For example, Browne and Simonson (1957) found that the penetration of ultraviolet light into wood was negligible. Subsequent experimentation has confirmed that the penetration of UV light into wood is small, approximately 75 μm (Hon and Ifju 1978). There are some discrepancies in the literature, however, regarding the extent to which visible light penetrates into wood. Hon and Ifju (1978) suggested, on the basis of electron spin resonance (ESR) measurements, that visible light penetrates wood only to a depth of 200 μm . Recently, however, Kataoka et al. (2004) demonstrated that the penetration of UV-visible light extended into wood well beyond 200 μm (Figure 14.2). They observed that the first 75- μm thick layer of wood absorbed 90% of 350-nm UV light, and the first 220- μm thick layer absorbed 90% of 420-nm visible light. One percent of the UV and visible light was, however, capable of penetrating wood to depths of 150 and 440 μm , respectively. According to Browne and Simonson (1957), the penetration of visible and infrared light into wood roughly follows Beer's law, Eq. (14.2):

$$\text{Log}_{10}(I_0/I) = \epsilon^* \beta^* \chi, \quad (14.2)$$

where I_0 is the initial light intensity; I is the intensity of transmitted light; ϵ is the wavelength dependent absorptivity coefficient; β is the path length (or wood thickness); χ is the concentration of the material (or wood density).

14.2.2 Ultraviolet and Visible Light

In accord with energetic considerations, the UV portion of the solar spectrum is most effective in causing degradation of wood, but visible light is also involved in weathering. Thus, Derbyshire and Miller (1981) noted that "wood exposed only to wavelengths greater than 400 nm will degrade at about half the rate of material exposed to the full solar spectrum." Norrstrom (1969) suggested that 80–95% of the degradation of wood by light was due to the photo-oxidation of lignin. When wood absorbs UV light,

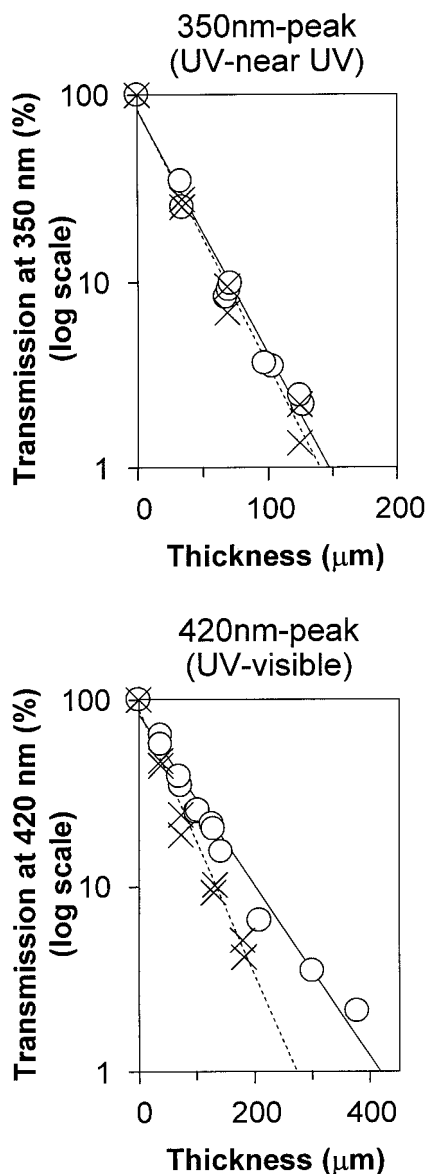


FIGURE 14.2 Percentage transmission of 350-nm UV (left) and 420-nm visible (right) light through Japanese cedar sections of varying thickness. Circles indicate unexposed sections. Crosses indicate that sections were irradiated for 1,000 hours before light transmission measurements (Kataoka et al. 2003).

the chemical changes that follow include dehydrogenation, dehydroxylation, dehydroxymethylation and demethoxylation of lignin (Hon 1991). Lignin has various reactive groups and sites such as primary and secondary hydroxyl groups, carbonyl groups, carboxyl groups, aromatic and phenolic groups that interact with light to form free radicals. Oxidation of phenolic hydroxyl groups in lignin is thought to be an

important source of free radicals in wood (Hon 1991). The phenolic radicals thus formed are converted to *o*- and *p*-quinonoid structures by demethylation or by cleavage of the side chain. Free radicals generated in wood are thought to react with molecular oxygen to form peroxides, hydroperoxides, as well as peroxy and alkoxy radicals (Kalnins 1966; Hon and Chang 1984). Lignin breakdown probably also involves cleavage of the α - β bond in a typical β -aryl ether lignin subunit (Figure 14.3) (Schmalzl 1986). When $R_2 = \text{H}$ (Figure 14.3), the aldehyde fragmentation product is vanillin. Vanillin is readily detected during UV irradiation of wood (Sandermann and Schlumbom 1962). Fragmentation of the α - β bond is also important in lignin breakdown by chemical oxidation (Schultz and Templeton 1986) or fungal decay (Schoemaker et al. 1985).

The rate of photodegradation of *cellulose* in wood is reported to be dependent on the wavelength of the incident light. Wavelengths less than 280 nm increase the rate of degradation of cellulose, whereas the rate is very slow on exposure to light of wavelengths longer than 340 nm (Hon 1991). Free radicals can be formed in cellulose at the C-1 and C-4 positions through the cleavage of glycosidic bonds when the cellulose is exposed to light with wavelengths longer than 340 nm in the presence of oxygen (Hon 1976a). After cellulose is exposed to light of wavelengths greater than 280 or 254 nm, dehydrogenation at the C_2 , C_3 , and C_4 and C_6 positions or dehydroxymethylation by cleavage of the C_5 - C_6 bond, respectively, can be detected by ESR (Hon 1976b). Hon and Chang (1984) suggested that UV light absorbed by lignin helped to degrade cellulose by energy transfer. There is also a suggestion that the reverse might occur, that is, photon energy absorbed by cellulose might be transferred to lignin (due to its phenolic structure) and that this energy transfer

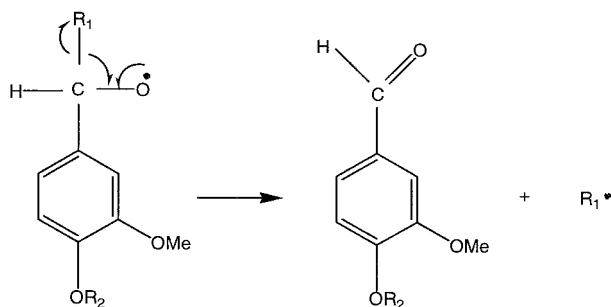


FIGURE 14.3 Proposed key fragmentation mechanism for lignin photolysis (Schmalzl 1986).

could reduce the degradation of cellulose to some extent (Hon 1975).

For illustration purposes, photodegradation of synthetic homopolymers such as polyethylene can be represented in a simplified manner as follows. Energy absorbed from radiation (*) can be dissipated in the polymer through the cleavage of molecular bonds (photolysis), resulting in the formation of a free radical ($R^* \rightarrow R\bullet$), a molecular species that is highly reactive because it has an unpaired valence electron. Once a free radical has formed it can readily react with atmospheric oxygen to form a peroxy radical ($R\bullet + O_2 \rightarrow ROO\bullet$). The peroxy radical is capable of attacking the polymer backbone (RH) via hydrogen abstraction, forming a hydroperoxide and another free radical ($ROO\bullet + RH \rightarrow ROOH + R\bullet$). The hydroperoxide is very unstable to UV radiation and undergoes photolysis, forming additional free radicals ($ROOH \rightarrow RO\bullet + \bullet OH$). The bond dissociation energies of RO-OH, R-OOH, and ROO-H bonds are 42, 70, and 90 kcal/mol, respectively (Benson 1965). Therefore, photolysis of RO-OH bonds is easier than that of R-OOH and ROO-H bonds. Light of wavelength <320 nm has sufficient energy to break the RO-OH and R-OOH bonds, whereas light of wavelength <223 nm can break the ROO-H bond (Hon and Feist 1992).

The literature indicates that free radical formation and the degradation of wood fits some, but not all, of the aspects of the general scheme for the photodegradation of synthetic polymers outlined above. The photodegradation of wood is undoubtedly more complicated than that of synthetic homopolymers because it consists of a blend of polymers (lignin, cellulose, and hemicellulose) and low molecular weight extractives that differ in their susceptibility to solar radiation. Furthermore, it is clear that the precise mechanisms and reaction pathways involved in the photodegradation of each of these components have not been fully elucidated. However, the key step involved in the photodegradation of wood appears to be photolysis and fragmentation of lignin, resulting in the formation of aromatic radicals (Feist and Hon 1984). These free radicals may then cause further degradation of lignin and photo-oxidation of cellulose and hemicelluloses. Free radical reactions may be terminated by reaction of radicals with photodegraded lignin fragments, forming colored unsaturated carbonyl compounds, which explains why wood initially yellows when exposed to light.

An ESR study of Douglas fir (*Pseudotsuga menziesii* (Mirb.) Franco.) wood sections after exposure to fluorescent light for 24 hours showed a radical signal at 2.003 g-value, which was thought to be due to

formation of aromatic radicals (phenoxy radicals) from lignin and polyphenols [Hon and Feist (1980), cited in Hon and Feist (1981)]. Schmid et al. (2000) also detected the formation of aromatic radicals in UV irradiated Scots pine (*Pinus sylvestris* L) sapwood using ESR. Hon et al. (1980) observed an increase in the concentration of free radicals detected by ESR when Douglas fir wood was exposed to sunlight, and Hon and Chang (1984) reported that a large proportion of the free radicals generated in the wood were short-lived. Infrared spectroscopy of UV-irradiated wood surfaces showed an increase in carbonyl and carboxylic groups (Hon 1979a). This was thought to be due to the reaction of carbon-centered radicals with oxygen molecules, leading to the formation of unstable peroxides that were subsequently transformed into carbonyl and carboxylic groups (Hon 1979). The increasing accumulation of free radicals in wood following exposure to sunlight results in extensive cleavage of molecular bonds and consequent loss of the physical properties of wood fibers.

14.2.3 Water

Water has an important role in the weathering of wood. The leaching of photodegraded lignin and hemicellulose fragments from weathered wood surfaces by rain (Evans et al. 1993) is in part responsible for the characteristic gray color of weathered wood. Dimensional change caused by the wetting and drying of wood generates surface stresses that cause checking and warping of timber (Feist 1990). The photodegradation of wood also proceeds more rapidly in the presence of moisture, possibly because water molecules swell wood, thereby opening up inaccessible regions of the cell wall and facilitating their degradation by light (Feist and Hon 1984). Prolonged exposure of wood to water at mild temperatures (50–65 °C) results in degradation of hemicelluloses and lignin with little degradation of cellulose (Evans and Banks 1988, 1990). Moisture in the presence of superficial solar heating (see below) may thus result in hydrolytic degradation of the non-cellulosic components of wood. In the absence of solar heating, slow hydrolytic degradation of the middle lamella may occur due to water. Wood that is water saturated is often resistant to fungal or insect attack due to oxygen depletion, but may undergo hydrolysis and mild degradation from the effects of anaerobic bacteria or soft-rot fungi (Zabel and Morrell 1992).

14.2.4 Heat/Freezing

Heat accelerates the chemical reactions involved in the weathering of wood, including photo-oxidation

and hydrolysis. The softening temperature (glass transition temperature) of lignin is approximately 130–150 °C, and structural degradation of wood's chemical components is observed at temperatures at or above 200 °C. The maximum surface temperature that has been recorded on wood surfaces exposed outdoors in the United States is 52 °C (Wengert 1966). Therefore, it is unlikely that heat directly causes degradation of wood during weathering. Exposure of wood to low temperatures and repeated freezing and thawing, however, has been shown to cause physical deterioration of wood (Borgin 1969).

An additional factor involved in the weathering of wood in cold climates is abrasion by wind-blown particles of ice. For example, the Australian Antarctic explorer Mawson (1915) wrote: “[T]he abrasion-effects produced by the impact of the snow particles were astonishing. . . . A deal (*Pinus* sp.) box, facing the wind, lost all its painted bands and in a fortnight was handsomely marked; the hard knotty fibres being only slightly attacked, whilst the softer, pithy laminae were corroded to a depth of one-eighth of an inch [approximately 3 mm].” Windblown sand and salt can also cause similar, if less spectacular, abrasion of wood (Feist 1990).

14.2.5 Airborne Pollutants

The main pollutants in the atmosphere are dust and smoke particles, and volatile pollutants including sulfur compounds, ammonia, nitrogen oxides, carbon monoxide, and saturated/unsaturated aliphatic and aromatic hydrocarbons and their derivatives. Wood absorbs atmospheric sulfur dioxide (SO₂) (Spedding 1970), which, when converted into sulfuric acid, may degrade wood fibers. Observations in the field and laboratory experiments have all tended to suggest that the weathering of wood is more rapid in polluted than in unpolluted atmospheres (Williams 1987). Raczkowski (1980) observed significant losses in tensile strength of Norway spruce (*Picea abies* (L) Karsten) wood veneers exposed in the winter in Poland, which were attributed to high levels of airborne sulfur dioxide arising from the burning of coal. Hinoki (*Chamaecyparis obtusa* [Siebold & Zucc] Endl.) irradiated with UV light following a daily 20-minute soak in sulfuric acid solution (pH 2) degraded faster than control specimens. Degradation initially occurred in the middle lamella, followed by degradation on both sides of the secondary wall, leading to complete destruction of the cell wall (Park et al. 1996). This pattern of degradation closely matched the concentration of lignin in the cell wall. The erosion of earlywood during artificial

weathering is accelerated if the samples are pre-soaked in dilute (pH 3.0–4.0) sulfuric or nitric acid (Williams 1987). Hon and Feist (1993) observed color changes in southern pine (*Pinus* sp.) exposed to sulfur dioxide and nitrogen dioxide, and noted that the rate of discoloration was influenced by UV light. The combination of UV light and SO₂ brought about the greatest color change.

14.2.6 Microorganisms

The frequent wetting and drying, high temperatures, and levels of solar radiation at exposed wood surfaces are often unfavorable to microbial activity. Nevertheless, bacteria and certain microfungi are frequently observed colonizing weathered wood, where they contribute to its gray coloration. The dimorphic black yeast *Aureobasidium pullulans* (de Bary) Arnaud, in particular, is frequently isolated from weathered wood. *A. pullulans* is capable of withstanding temperatures of 80 °C, growing over a pH range of 1.9–10.1, and surviving for long periods without moisture. Hence, it is particularly well suited to the micro-environment of weathered wood (Schmidt and French 1976). *A. pullulans* metabolizes photodegraded lignocellulose (Schoeman and Dickenson 1997), but organisms capable of enzymatically degrading wood also colonize weathered timber. However, their ability to cause significant degradation is, as mentioned in the introduction, limited by conditions at weathered wood surfaces.

14.3 EFFECTS OF WEATHERING

The effects of weathering are superficial in nature and are to the upper 2–3 mm of wood, except for checks which can extend more deeply into wood. Weathering significantly alters the appearance of wood and its surface properties.

14.3.1 Physical Properties

Wood exposed to the weather changes color very rapidly. Light colored woods, including most coniferous species, darken in color and become yellow or brown due to the accumulation of photodegraded lignin constituents in the wood. Dark colored woods that are rich in phenolic extractives may fade initially before becoming yellow or brown. Irrespective of these initial color changes, wood exposed outdoors for six to 12 months (depending on climatic conditions) becomes gray as photodegraded lignin fragments are leached from the wood, resulting in surface layers that are rich in cellulose. Wood ex-

posed outdoors in coastal (exposed to salt) or very dry environments is often silvery-gray in color, but in other environments weathered wood has a dark gray, blotchy appearance due to the presence of fungal spores, hyphae and pigments within surface wood layers. The lustre of wood may decrease during weathering as the surface becomes rougher and the scattering of light becomes more diffuse (Hon and Minemura 1991). Stresses develop due to differential swelling/shrinkage of the surface layers, leading to fiber separation and the formation of checks (Panshin and DeZeeuw 1980). The rapid erosion of low-density earlywood often gives weathered wood a corrugated appearance (Figure 14.1).

The rate of erosion of wood during exterior exposure largely depends on its density. Accelerated weathering studies have shown an inverse, but not linear relationship, within the density range 0.25–1.0 g/cm³, between wood density and erosion (Figure 14.4). Accordingly, low density species such as western red cedar (*Thuja plicata* D. Don) erode at a rate of 12 mm per century when exposed vertically, facing south, in the Northern Hemisphere. Comparable figures for higher density softwoods such as Douglas fir and high density hardwoods are 6 mm and 3 mm, respectively (Feist 1990). Photodegradation and erosion is more pronounced in thin-walled earlywood tissue (Borgin 1971), but within-ring differences in the density of earlywood and latewood influence the erosion occurring in individual

species. In species with distinct earlywood and latewood, erosion is more rapid in the first formed earlywood, which subsequently exposes the denser latewood tissue to photodegradation (Williams et al. 2001a). Where growth rings show a gradual change from earlywood to latewood, erosion appears to be more rapid in the central portion of the earlywood (Williams et al. 2001b).

In addition to erosion, the surface texture of weathered wood is further degraded by the formation of checks. Photodegradation of wood and stresses generated by wetting and drying result in the formation of macroscopic checks where adjacent cells or tissues differ in cell wall thickness or strength. For example, checks often develop at growth ring boundaries (Figure 14.5) (Evans 1989), and at the interfaces between rays and tracheids (Yata and Tamaru 1995). In photodegraded sugi (*Cryptomeria japonica* [L.f.] D. Don) earlywood degradation was exacerbated by collapse of cells during drying (Yata and Tamaru 1995).

14.3.2 Anatomy

Microscopic changes to the structure of wood usually precede any evidence of macroscopic damage during weathering. Microchecking usually develops in exposed cell walls, and checks commonly follow the microfibril angle of the secondary wall (S₂). Tracheids may also separate as a result of erosion and

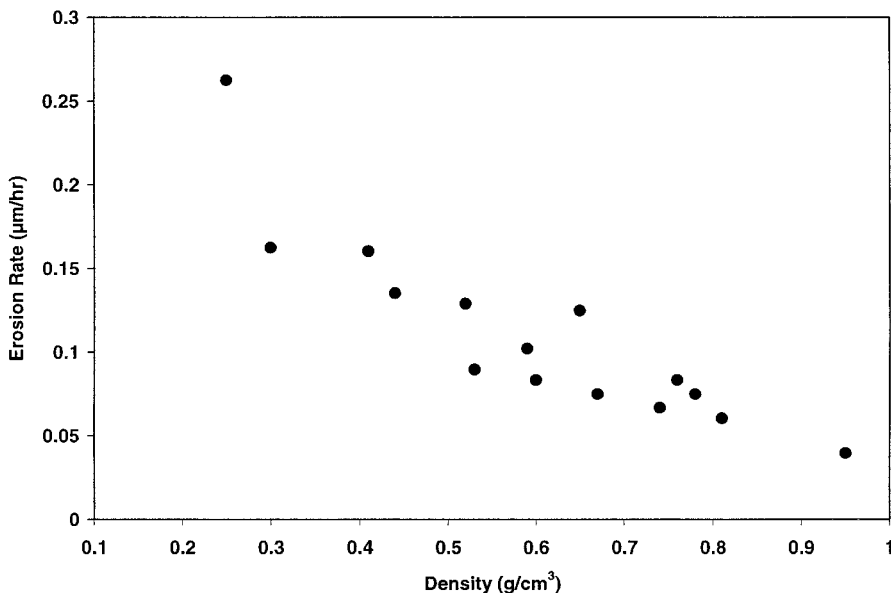


FIGURE 14.4 Erosion rate versus air dry wood density in a range of wood species subjected to artificial accelerated weathering (Sell and Feist 1986).

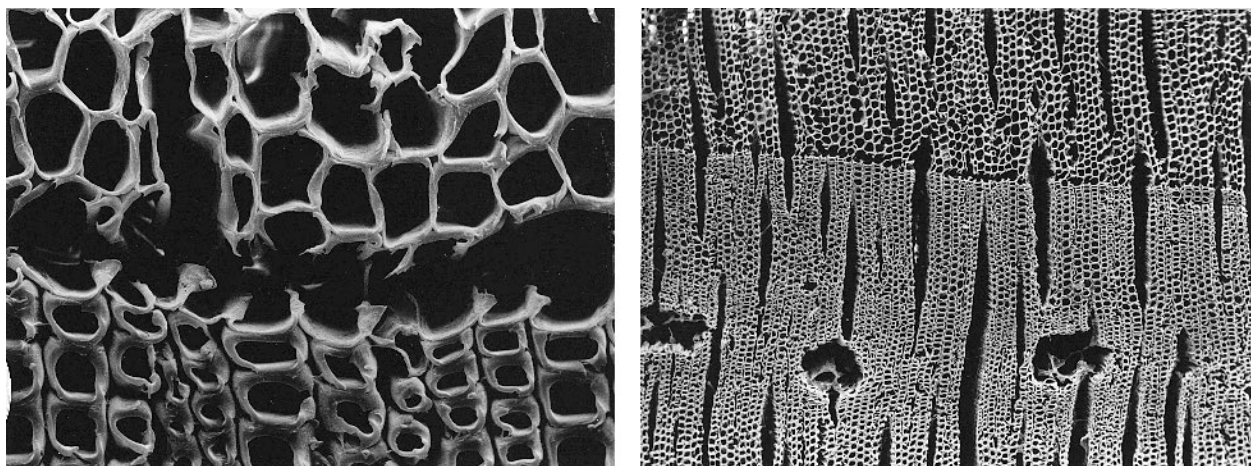


FIGURE 14.5 Check development at a growth ring boundary in radiata pine (Evans 1989).

checking of the middle lamella (Miniutti 1964, 1967). Miniutti (1964) found that longitudinally-oriented microchecks developed in tangential wood cell walls of southern pine and redwood (*Sequoia sempervirens* [D. Don] Endl) exposed to artificial UV light, but these microchecks were more aligned with the cell axis rather than the microfibril angle of the S₂ layer. Derbyshire and Miller (1981) reported microchecking of Scots pine exposed to natural weathering. Checks oriented at 30–60 degrees to the cell axis developed after 35 days of natural exposure, and in the case of specimens protected from rain, after 85 days. In addition, they reported that pronounced ridges developed in the latewood tracheids and fibres of lime wood (*Tilia vulgaris* L) exposed to natural weathering.

The lignin-rich middle lamella that bonds adjacent tracheids and fibres together is rapidly eroded during weathering, and adjacent primary and secondary cell wall layers show progressive thinning with increasing exposure (Evans 1989; Evans et al. 2002) (Figure 14.6a–d). At longitudinal surfaces, where the lumen, and hence double cell walls may be exposed, degradation also occurs rapidly. The exposed edges of cell walls are rapidly eroded, resulting in subsequent delamination of secondary wall layers (Miniutti 1967; Borgin 1971). Fissures develop in the wall and parts of the cell wall detach and flake off (Borgin 1971). Additionally, complete breakdown of the middle lamella during the weathering of wood results in fibres being washed off through the action of rain (Borgin 1969).

The most obvious change that occurs to the microscopic structure of cell walls during weathering is the formation of microchecks originating in bor-

dered and half-bordered pits. These develop first in earlywood and later in the latewood (Miniutti 1964, 1967) (Figure 14.6e–f). The margo microfibrils in bordered pits are fragile and are easily degraded and lost during the early stages of weathering (Borgin 1971; Imamura 1993). Miniutti (1967) first described the formation of pit microchecks in Californian redwood exposed to artificial UV light. Diagonal hairline checks first developed in one half of a border, and subsequently on the adjacent side of the pit surface. Significant enlargement of these checks occurred with increasing exposure until the border was destroyed, leaving an intact annulus. In species such as Californian redwood, where bordered pits are frequently paired, pit annuli would coalesce, leaving crassulae which appeared to be resistant to further degradation. Where pitting was uniseriate, the annulus would eventually be lost with increasing exposure.

A similar pattern of degradation was reported for half-bordered pits, but it occurred at a slower rate than for bordered pits (Miniutti 1967). Conversely, Chang et al. (1982) found that half-bordered pits degraded at a faster rate than bordered pits in southern pine exposed to artificial UV light. On tangential surfaces where an earlywood tracheid was superimposed on a latewood tracheid, pit checking occurred first in the underlying latewood pit (Miniutti 1967). When both tracheids forming a pit pair were within the latewood, checking was observed in both pits. Coupe and Watson (1967) observed that checking of bordered pits did not develop in a range of hardwoods including beech (*Fagus sylvatica* L), opepe (*Nauclea diderrichii* Merrill) and oak (*Quercus robur* L.) exposed to artificial weathering. They also

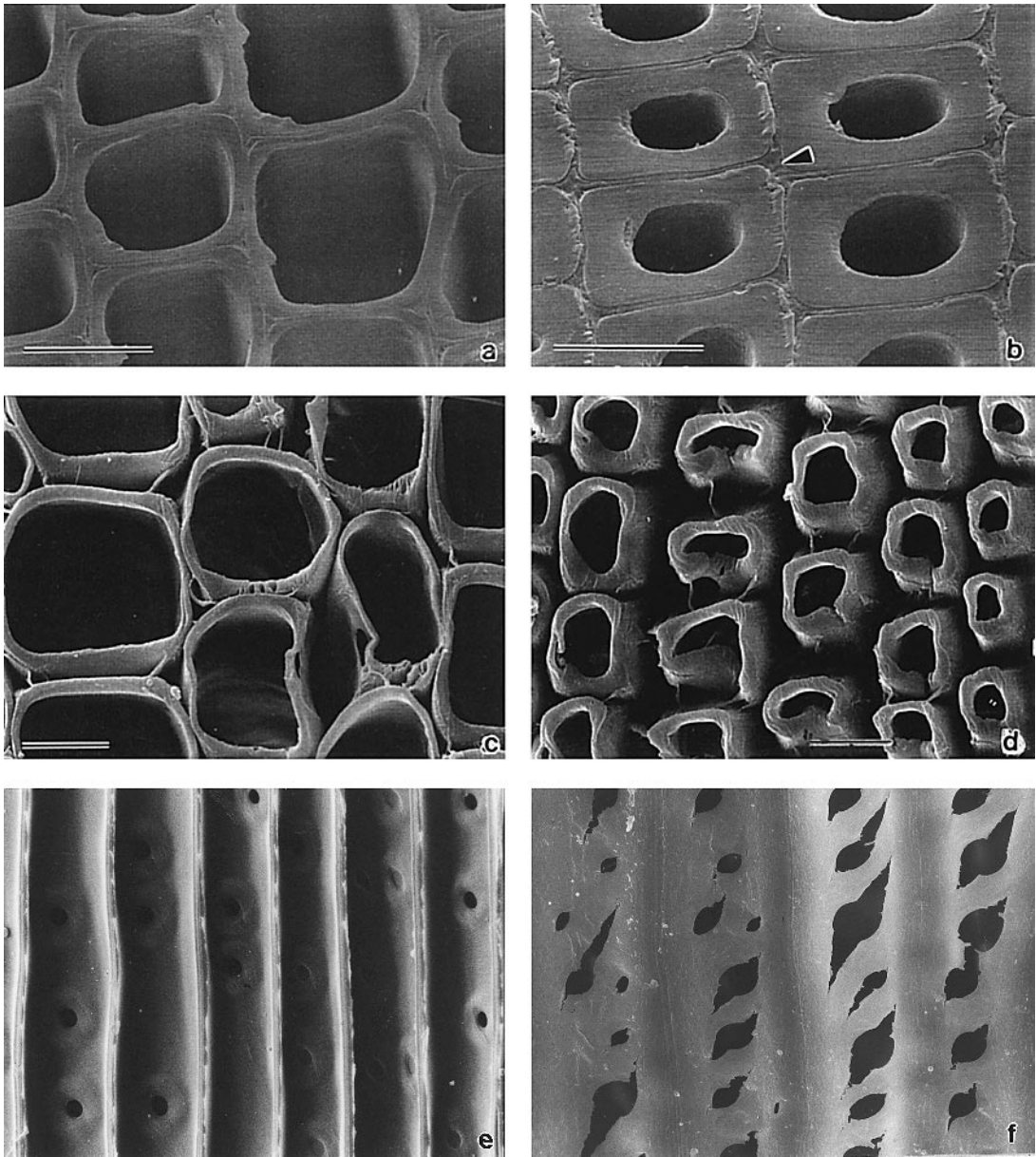


FIGURE 14.6 Effects of weathering on the microscopic structure of Scots pine wood. (a) Unexposed earlywood tracheids with thin undamaged cell walls and large cell lumens; (b) Unexposed latewood tracheids with thick cell walls and small lumens (note the middle lamellae that cements tracheids together, arrowed); (c) Earlywood tracheids exposed to the weather for 30 days (note erosion of middle lamellae, particularly at cell corners and thinning of cell walls); (d) Latewood tracheids exposed to the weather for 30 days (note erosion of middle lamellae and delamination of cell walls); (e) Unexposed earlywood tracheids showing the apertures of bordered pits that allow water in conifer trees to flow from one cell to another; (f) Earlywood tracheids exposed to the weather for 30 days (note microchecking originating in bordered pit apertures).

tested a range of softwoods (Scots pine, radiata pine, Douglas fir and western red cedar) and only noted checking of half bordered pits in western red cedar.

Significant structural changes occur in ray tissue during the weathering of wood. Softwood rays are readily degraded, but extractives within the ray ap-

pear to be resistant to degradation (Miniutti 1967). In hardwoods such as beech, large multiseriate rays have been reported to be more resistant to weathering than the surrounding ground tissue (Kučera and Sell 1987). Axial and transverse checking, due to cyclical wetting and drying, results in longitudinal

separation of ray tissue and hence intact rays are readily detached from weathered wood surfaces (Kucera and Sell 1987). Microchecking in sugi and hinoki was reported to develop in the ray tissue after 100 days of outdoor exposure, while in similarly exposed hemlock (*Tsuga heterophylla* [Raf.] Sarg.) small checks developed first in the first formed earlywood (Yata and Tamaru 1995).

The extent to which chemical treatments alter the pattern of degradation of wood surfaces exposed to weathering has received little attention. Paajanen (1994) compared the weathering of untreated Scots pine and Norway spruce specimens to that of specimens treated with an unpigmented primer. The treated specimens showed a similar pattern of degradation to that observed in the untreated controls. Microchecking occurred first in the latewood and was aligned both parallel to the microfibril angle and to the cell axis (Paajanen 1994). Large tangentially-oriented checks or shakes first appeared at growth ring boundaries in thin-walled earlywood tracheids near those of the thick-walled latewood. Delamination of the secondary wall was reported, but there was little separation of individual cells after 24 weeks' exposure (Paajanen 1994).

14.3.3 Chemistry

All of the major chemical constituents of wood are degraded during weathering. Lignin is depolymerized and low molecular weight lignin fragments are leached from wood by rain. One hundred and forty years ago it was reported that weathered wood surfaces (the gray layer at the surface) consisted of pure or nearly pure cellulose and had a very low lignin content (Wiesner 1864, cited in Kalnins 1966). The degradation of wood by UV light results in a reduction in the methoxyl and lignin content of wood, and an increase in its acidity and carbonyl content (Leary 1967, 1968). Kalnins (1966) identified CO, CO₂, hydrogen, water, methanol, formaldehyde, and organic acids as degradation products of wood during weathering.

The use of spectroscopic techniques that can probe the chemical composition of surfaces (e.g., Fourier transform infrared spectroscopy (FTIR), X-ray photoelectron spectroscopy (XPS), and nuclear magnetic resonance (NMR) spectroscopy) has shown that the degradation of lignin at exposed wood surfaces is extremely rapid. Infrared spectroscopic characterization of UV-exposed wood surfaces has shown an increase in carbonyl and carboxylic functional groups, and a decrease in aromatic functional groups due to degradation of

lignin (Hon and Chang 1984). A CP/MAS ¹³C NMR spectroscopic study of photodegraded newsprint showed demethoxylation and destruction of lignin aromaticity, formation of carboxylic acids and production of soluble carbohydrate and lignin fragments (Hemmingson and Morgan 1990). FTIR spectroscopy of naturally weathered radiata pine veneers showed a remarkably rapid decrease in the peak at 1,505 cm⁻¹, which corresponds to aromatic C=C bond stretching in lignin. Spectra suggested perceptible surface (1–2 μm) delignification after four hours of exposure, substantial delignification after three days, and almost complete surface delignification after six days (Figure 14.7) (Evans et al. 1996). Changes in peaks at 1,601 cm⁻¹ (C=C bond stretching), 1,263 cm⁻¹ (C-O bond stretching vibration in lignin and hemicelluloses), and 870 cm⁻¹ (CH out-

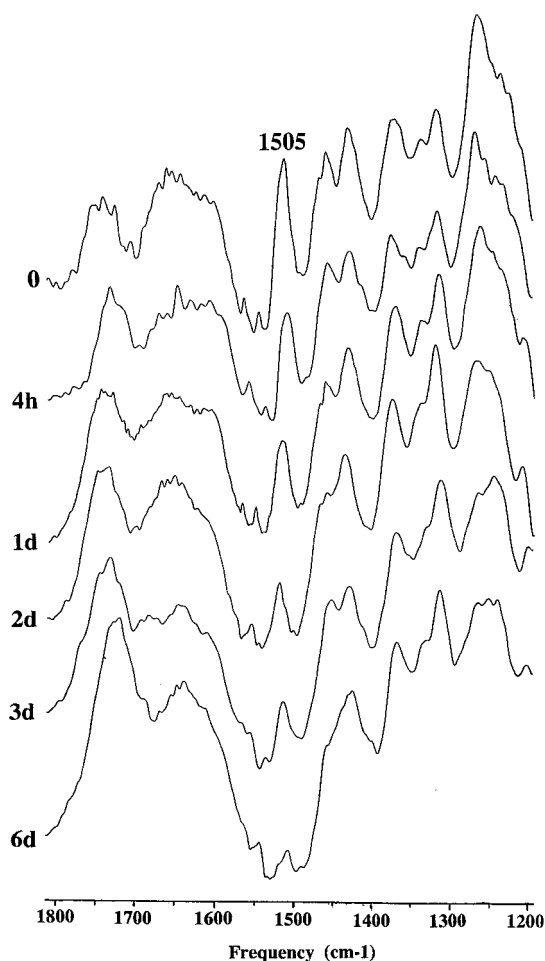


FIGURE 14.7 Fourier transform infrared internal reflectance spectra of radiata pine veneers exposed to the weather for periods ranging from four hours (4h) to six days (6d) compared to the spectrum for an unexposed control (0) (Evans et al. 1996).

of-plane bending vibration in lignin) also suggested substantial and rapid degradation of lignin. Reduction of the peak at $1,728\text{ cm}^{-1}$ ($\text{C}=\text{O}$ stretching vibration in acetyl and carboxyl in hemicelluloses) and 809 cm^{-1} (mainly vibration of mannan in hemicelluloses and CH out-of-plane bending vibration in lignin) indicate the degradation of hemicelluloses (Evans et al. 1992). XPS of weathered and UV-irradiated wood surfaces have shown increases in the intensities of carbon-oxygen and oxygen-carbon-oxygen bond signals, and decreases in the intensities of carbon-carbon and carbon-hydrogen bond signals, suggesting oxidation of the wood surface (Hon 1984). The increase in XPS signal intensity due to the higher oxygen-to-carbon ratio indicates degradation of lignin at the wood surface and enrichment of the surface with cellulose.

Hemicelluloses, particularly those containing xylose and arabinose, are also degraded during weathering and are leached from weathered wood surfaces (Evans et al. 1992), and hence, as mentioned above, weathered wood surfaces are rich in cellulose. It was assumed for many years that cellulose was less affected by weathering than the other chemical constituents of wood (Rowell 1983). Derbyshire and Miller (1981), however, showed that glycosidic linkages in cellulose could be cleaved by sunlight, leading to a reduction in the degree of polymerization of cellulose. Viscometry studies of holocellulose isolated from weathered wood have shown that cellulose in wood is also rapidly depolymerized when exposed to the weather (Evans et al. 1996).

The effects of weathering on the structure and chemical composition of wood are superficial in nature, but there are discrepancies regarding the depth to which weathering occurs in wood. Estimates of the depth to which such degradation extends into wood varies greatly from $200\text{ }\mu\text{m}$ to as much as $2,540\text{ }\mu\text{m}$ (Hon and Ifju 1978; Brown and Simonson 1957). These discrepancies appear to be due, in part, to differences in the methods and duration of exposure of wood prior to depth profile analysis, and the techniques used to assess the photodegradation of wood. Schramm (1906) reported that light acted on wood to a depth of $100\text{--}250\text{ }\mu\text{m}$ during natural exposure, but did not specify the duration of exposure of wood to the weather or how photodegradation was assessed. Browne and Simonson (1957) measured the depth of "brown discoloration" in well-weathered wood and concluded that weathering "sometimes extended more than $2,540\text{ }\mu\text{m}$." The maximum depth at which histochemical changes in lignin were detected in wood exposed outdoors in Australia for four and a half years was reported to be

only $400\text{ }\mu\text{m}$ (Bamber and Summerville 1981). Yata and Tamura (1995) also used histochemical techniques to assess the depth of photodegradation in wood, and observed that lignin was degraded to a depth of $700\text{ }\mu\text{m}$ in wood naturally weathered in Japan for two years. Horn et al. (1994) found that the infrared spectrum of wood exposed to 300 hours of accelerated weathering was essentially unchanged beyond a depth of $200\text{ }\mu\text{m}$. Kataoka et al. (2004) detected photochemical changes in sugi earlywood at a depth of $700\text{ }\mu\text{m}$ after 1,500 hours of exposure to artificial sunlight (Figure 14.8). They also suggested that the depth of photodegradation of wood depends on the spectral characteristics of the light source and the length of exposure.

14.3.4 Properties

Processing technologies and applications of wood that depend on its surface properties are severely affected by weathering. Notable in this regard is the painting and finishing of wood. Weathering of wood for two to four weeks prior to painting has been shown to significantly reduce the adhesion and performance of finishes applied to wood (Ashton 1967; Desai 1967; Boxall 1977; Underhaug et al. 1983; Williams and Feist 1993a; Williams et al. 1987, 1990). Evans et al. (1996) found that the adhesion of exterior acrylic primers on radiata pine was reduced if the wood was exposed to the weather for only five to 10 days prior to painting. They also found that "primer adhesion was lower on weathered radial surfaces than on similarly exposed tangential surfaces." There are reports of imperfect hardening of cement in contact with weathered form-ply (Yoshimoto et al. 1967) due to the presence of sugars, mainly arabinose and polysaccharides (produced by the photodegradation of holocellulose), interfering with the curing of the cement. Weathering also reduces the natural durability of western red cedar roofing shakes by leaching fungitoxic thujaplicins from wood (Johnson and Cserjesi 1980). Because weathering is confined to wood surface layers, the mechanical properties of wood, assuming decay to be absent, are largely unaffected by prolonged exposure of wood to the weather. The mechanical properties of wood composites, however, which depend in part on the strength of wood-adhesive bonds, can be significantly reduced by moisture-induced dimensional changes when they are used outdoors. Despite the deleterious effects of weathering on the use of wood, in certain specialized applications weathered wood is preferred to fresh wood. A good example of this is the use of weatherboards for the

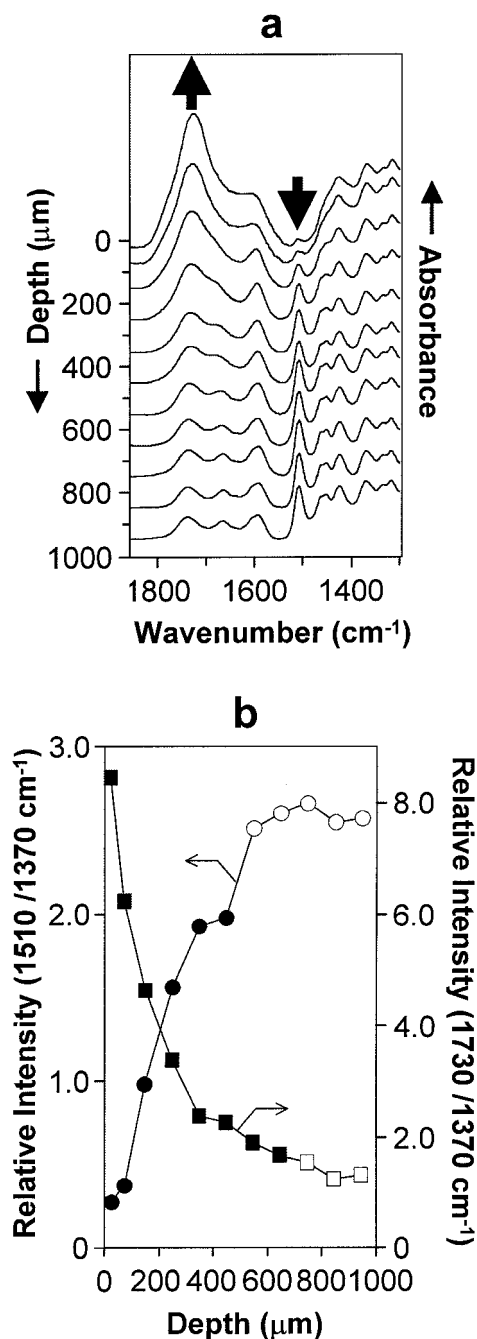


FIGURE 14.8 (a) FTIR depth profile spectra in the range 1,800–1,400 cm^{-1} of Japanese cedar earlywood after 1,500 h of exposure. (b) Changes in absorption peaks at 1,510 (circles) and at 1,730 (squares) cm^{-1} as a function of depth obtained from (a). Filled circles and squares in (b) indicate that significant changes in peaks occurred as a result of exposure of wood to light ($n = 35$, difference between unexposed controls and exposed specimens assessed using Smirnov–Grubbs test at the 5% significance level) (Kataoka et al. 2004). Changes in the absorption peaks at 1,510 and 1,730 cm^{-1} are expressed relative to that of a standard reference peak at 1,370 cm^{-1} .

construction of “New England type” barns, where the wood may be artificially weathered prior to building construction in order to give the building an aged appearance in keeping with its rural surroundings (Anon 1976).

14.4 PROTECTION

The most common method of protecting wood from weathering is through the use of a wide range of coatings such as paints, varnishes, stains, or water repellents.

14.4.1 Photoprotection of Wood with Finishes

Wood coatings are generally classed as either film-forming or penetrating, and the latter can be used as a pretreatment or as a final finish. Film-forming finishes such as paints contain pigments that screen wood from solar radiation and, because they form a barrier over the wood surface, they also prevent surface wetting and erosion. Feist (1990) points out that a correctly applied and maintained paint system including a primer and at least two topcoats can greatly reduce the deleterious effects of weathering on wood. However, a major problem with *clear* film forming finishes on wood is their loss of adhesion during weathering (Borgin 1968), which is due to failure of the underlying wood (Singh and Dawson 2003). The inability of opaque finishes to bond to weathered wood has been documented in several studies (Ashton 1967; Desai 1967; Boxall 1977; Underhaug et al. 1983; Williams and Feist 1993a; Williams et al. 1987, 1990). Paints perform better on wood that has been pre-treated with a water-repellent preservative, but the high maintenance requirements of paints and their tendency (when used on non-durable timber) to trap water and encourage decay has led to increased use of penetrating water repellent stains as a means of protecting wood used outdoors.

Penetrating finishes typically contain a hydrophobe such as wax, pigments, as well as an oil- or resin-based binder. The binder fixes any pigments and seals the wood surface. Fungicides and mildewcides are often added (to water repellent preservatives) to retard the growth of micro-organisms on finished wood surfaces (Williams and Feist 1993b). Unlike paints, which create a physical barrier, water repellents rely on the formation of hydrophobic external and internal wood surfaces which raise the

contact angle of the treated wood and applied water droplets to over 90 degrees, preventing water from being taken up by surface or sub-surface capillaries. Water repellents reduce moisture absorption so they impart a certain degree of dimensional stability to the wood. Effective penetration of end-grain by water repellents is essential in order to obtain good performance from finished joinery (Voulgaridis and Banks 1983). In practice, however, the hydrophobic system eventually breaks down due to the presence of impurities and imperfections in the external and internal coatings (Borgin 1968).

Penetrating stains are water repellent preservatives that contain a variety of additives to reduce the weathering of wood, including pigments and UV stabilizers to screen wood from solar radiation. Penetrating stains on wood tend to fail during exterior exposure through cracking of the wood substrate and erosion of pigments from wood surfaces (Kiguchi et al. 1996, 1997b). This leads to discoloration of the finish through loss of pigmentation and accumulation of atmospheric pollutants (Kiguchi et al. 1997a). Semi-transparent stains contain pigments that partially obscure the wood surface and hence they reduce the amount of light reaching the wood. At pigment concentrations of 8.4%, stains reduce wood erosion caused by weathering by 65%. The use of water repellents in the formulation provides added protection, but photodegradation cannot be prevented completely (Feist 1988). High-build stains applied as successive coats may create films similar to paints and may be semi-transparent to opaque, thus obscuring the wood surface. Their behavior and mechanism of failure then becomes more similar to that of paints (Hilditch and Crookes 1981). Stains provide protection against weathering for three to six years, depending on wood species and surface texture, type and quantity of stain applied to the wood and degree of exposure to the weather.

Paints, and to a lesser extent, stains, modify the appearance of wood. For end uses where it is important to retain natural color, the wood can be finished with a clear coating. Clear film-forming finishes, although they often contain UV stabilizers and a biocide, are limited in their ability to protect wood from weathering because they transmit visible light, which can degrade the underlying wood surface (Figure 14.9). Hence, they perform poorly on wood used outdoors and invariably fail by peeling and cracking within one to three years of application.

One means of increasing the performance of clear finishes on wood is to photostabilize the underlying wood surface with simple inorganic compounds, for

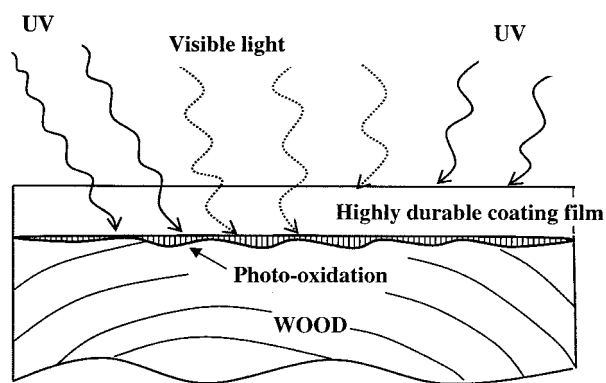


FIGURE 14.9 Photo-oxidation of a wood surface under a transparent film-forming finish (Kiguchi 1997).

example, chromium trioxide prior to application of the clear finish. Coating additives, such as UV absorbers and hindered amine light stabilizers that achieve similar photoprotective effects, also improve the performance of clear finishes on wood (Rogez 2001).

14.4.2 Photoprotection of Wood with Inorganic Chemicals

Pretreatment of wood surfaces with aqueous inorganic chemicals improves the weathering durability of wood and also increases the service life of natural finishes used outdoors (Black and Mraz 1974). Black and Mraz (1974) investigated the ability of acid copper chromate, acid cobalt chromate, acid zinc chromate, lead chromate, ammonium chromate, sodium dichromate, acid copper-chrome-arsenate, ammoniacal copper-chrome-arsenate, ammoniacal copper chromate, ammoniacal cupric oxide and copper, chromium, and iron molybdate to protect wood from the effects of weathering, and improve the performance of finishes. Among the different chromates investigated, the copper, lead and ammonium salts performed better than the cobalt, zinc and sodium salts. Ammonium chromate and ammoniacal copper chromate were the most effective treatments. Treatment of wood surfaces with chloride solutions of iron, aluminum, chromium, zinc, copper, tin, barium, magnesium and calcium were ineffective at protecting wood surfaces from photodegradation.

Chromium trioxide (i.e., chromic acid treatment) has been shown to be highly effective at protecting wood surfaces from weathering (Feist 1979; Feist and Ellis 1978; Chang et al. 1982; Evans and

Schmalzl 1989). Chromic acid treatment reduces the checking of simple and bordered pits during exposure of wood to UV light (Chang et al. 1982) and natural weathering (Evans et al. 1994), and the surface erosion of wood during artificial accelerated weathering (Feist 1977). Chromic acid treatment also imparts dimensional stability to wood, reduces its hygroscopicity and improves the finishing properties of wood (Williams and Feist 1988). Chromium trioxide treated radiata pine veneers exhibited dramatically reduced weight losses in a natural weathering trial. After 35 days exposure, treated thin wood veneers lost only 5% of weight compared to 27% for untreated controls (Evans and Schmalzl 1989). However, the strength losses of the veneers were similar to those of untreated weathered veneers, which indicates that the treatment was ineffective at reducing cellulose degradation. Several studies have been carried out to understand the chemical basis for wood surface stabilization with chromium trioxide. Pizzi (1980) used a dilute solution of guaiacol as a model to study the reaction of chromium (VI) with wood. He suggested that chromium (VI) forms an insoluble complex with lignin. He also suggested that chromium (VI) was not reduced to chromium (III) during its reaction with lignin. Schmalzl et al. (1995) reinvestigated the reaction of the lignin model guaiacol with excess aqueous chromium trioxide. They concluded that guaiacol oligomers, which are tightly held in polymeric complexes, are bound or cross-linked by hydroxylated trivalent (presumably octahedral) chromium species to form complicated three-dimensional high molecular weight polymers. They postulated that similar complexes, formed when phenolic lignin units react with chromium trioxide, were responsible for the weather resistance of chromium trioxide treated wood surfaces. Recently, Schmalzl et al. (2003) used the reaction of guaiacol and 2,6-dimethoxyphenol with metal oxidants as a model to further clarify the chromium mediated reaction and photostabilization of lignin on wood surfaces. Oxidation of 2,6-dimethoxyphenol with chromic acid resulted in the formation of an amorphous chromium III coerulignone complex, which they characterized using solid-state ^{13}C NMR and IR spectroscopy. They postulated that chromic acid oxidizes lignin phenols in wood, resulting in the formation of chromium III quinone complexes that confer weathering durability to the treated wood surface.

Pretreatment of wood with hexavalent chromium compounds results in a green coloration (initially brown) which is undesirable when the aim of finish-

ing is to preserve the natural appearance of wood. Hexavalent chromium compounds are also carcinogenic, a fact that has prevented their widespread commercial use as photostabilizing treatments. Chromium trioxide was used in the 1980s in Japan, however, as a pretreatment for wooden doors to enhance the weathering resistance of acrylic-urethane finishes (Ohtani 1987).

Trivalent chromium compounds (e.g. chromium nitrate), which are not as toxic as hexavalent chromium components, were found to be less effective at protecting wood from photodegradation than chromic acid (Williams and Feist 1988). Treatment of wood surfaces with iron (III) chloride or nitrate was found to be ineffective at protecting wood from natural weathering (Evans and Schmalzl 1989; Evans et al. 1992), although Chang et al. (1982) found that treatment with iron (III) chloride reduced the microchecking of pits during the exposure of wood to artificial UV light. Treatment of wood surfaces with oxidative manganese compounds such as manganese (III) acetate dihydrate and potassium permanganate has recently been shown to protect wood from photodegradation. The treatments were not, however, as effective as chromium trioxide (Schmalzl and Evans 2003). Schmalzl and Evans (2003) also tested the effectiveness of some non-oxidative titanates and zirconates as photoprotective treatments for wood. Tetrabutyl, tetraisopropyl, and a range of other titanates enhanced the tensile strength of wood both before and after weathering, possibly due to the formation of complexes between the titanates and cellulose in wood. The titanates, however, were unable to substantially restrict veneer weight losses during natural weathering, indicating that they did not form stable complexes with lignin. Tetrapropyl and tetrabutyl zirconate were not as effective at protecting wood from weathering as the titanates that were tested (Schmalzl and Evans 2003).

14.4.3 Photoprotection of Wood with Wood Preservatives

Inorganic compounds used as components of wood preservatives can also provide some photoprotection to wood. Feist and Williams (1991) examined the ability of a chromated copper arsenate (CCA) wood preservative and chromium trioxide to reduce the weathering degradation of unfinished wood and improve the durability of semitransparent and solid-color stains applied to wood. CCA provided long-term protection against weathering-induced erosion and greatly extended the lifetime and durability of a

partially UV-transparent stain. Feist and Williams (1991) also observed that a CCA pressure treatment provided better penetration and higher deposition of chromium at the surfaces of wood than a brush treatment of chromium trioxide.

Jin et al. (1991) investigated the weathering degradation of alkylammonium compound (AAC) and ammoniacal copper quat (ACQ) treated wood samples. They found that ACQ retarded the weathering degradation of wood, whereas AACs accelerated photodegradation. Thus, AAC-treated samples showed considerable latewood delignification and severe earlywood erosion during exposure. FTIR spectroscopy indicated that ACQ reduced the formation of carbonyl groups and delignification of wood during weathering (Liu et al. 1994). They also found that the rate of carbonyl formation was higher in CCA-treated wood than in ACQ-treated wood. Recently, Zhang (2003) observed that a range of alkylammonium compounds (AACs) did not greatly retard the photodegradation of treated wood samples exposed to UV light. However, wood treated with AACs together with copper as a co-biocide were more resistant to degradation.

Cornfield et al. (1994) found that copper azole preservatives enhanced the weathering resistance of wood, and Zhang and Kamden (2000) found that copper monoethanolamine (Cu-MEA), which is a component of some of the newer copper-based wood preservatives, increased the hydrophobicity of wood and reduced the susceptibility of the wood to photodegradation. Water repellent emulsion additives are commonly added to water-borne preservatives

(CCA, ACQ) to increase the water repellency of the treated wood and reduce the physical deterioration of the wood exposed outdoors (Zahora 1992).

14.4.4 Photoprotection of Wood by Chemical Modification

The weathering durability of wood can be improved by chemical modification. Chemical modification usually involves covalently bonding chemicals to hydroxyl groups on lignin and holocellulose (Figure 14.10), and, in certain cases, bulking the cell wall (Figure 14.11). Chemical modification usually improves the dimensional stability of wood by reducing its hygroscopicity and keeping the wood cell wall in a swollen (bulked) state. Chemical modification of wood by methylation, acetylation, or alkylation improves the color stability of wood during weathering because the “blocking” of phenolic hydroxyl groups retards the formation of quinones (Kalnins 1984; Kiguchi 1997).

Acetylation of wood to weight gains (WGs) of 10–20% has been shown to reduce the photoyellowing (Tarkow et al. 1946; Plackett et al. 1992), checking (Dunningham et al. 1992), and erosion (Feist et al. 1991) of wood exposed to natural or artificial weathering. The ability of chemical modification to prevent checking and erosion of wood during weathering may be explained by the increased dimensional stability and hydrophobicity of the modified wood. Evans et al. (2000), however, observed that acetylation of Scots pine to low WGs (5–10%) reduced the photostability of modified

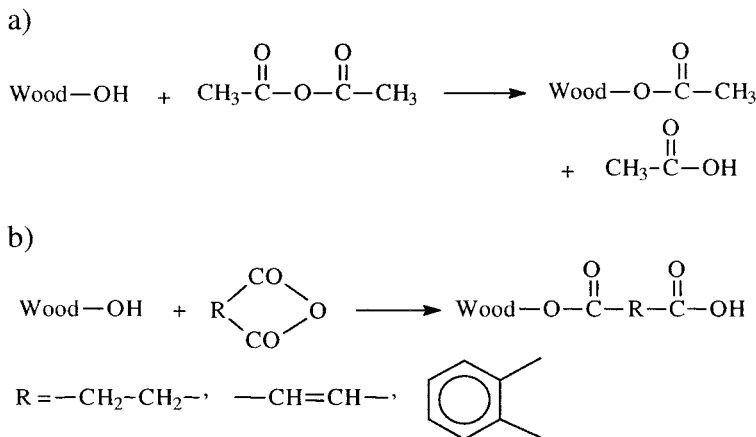


FIGURE 14.10 Chemical modification of wood with (a) acetic anhydride and (b) dicarboxylic acid anhydride.

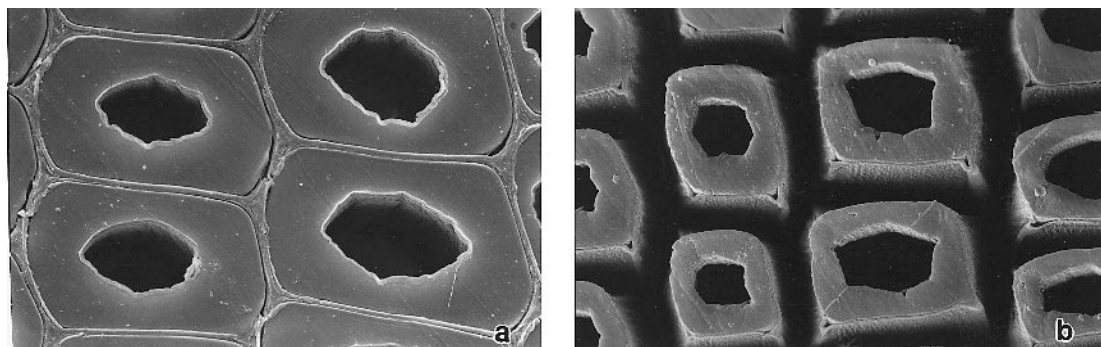


FIGURE 14.11 SEM photographs of (a) acetylated wood showing swelling (bulking) of the S_3 layer of the secondary wall, and (b) weathered acetylated wood (Evans et al. 2000).

wood. They also observed that the photostability of cellulose in acetylated wood increased at higher WGs (around 20%). At higher WGs, a higher degree of substitution of cellulosic hydroxyl groups is likely. Cellulose derivatives are generally less susceptible to photodegradation than unmodified cellulose (Usmanov 1978). Thus, it appears that acetylation can protect cellulose to some degree (Feist et al. 1991; Evans et al. 2000), but it is unable to photostabilize lignin (Kalnins 1984; Kiguchi 1997; Torr et al. 1996; Evans et al. 2000). Similar findings have been reported for wood modified with dicarboxylic acid anhydrides (Evans 1998).

Chang and Chang (2001) observed that acetylation or succinic anhydride treatment of wood surfaces reduced the formation of chromophores at the surface of UV-irradiated China fir (*Cunninghamia lanceolata* (Lamb.) Hook. F.) wood. Conversely, phthalic anhydride treatment of wood surfaces accelerated photo-discoloration. Modification of wood with butylene oxide, methyl isocyanate, or butyl isocyanate at higher WGs (around 25% or more) did not enhance the photostability of wood (Rowell et al. 1981; Feist and Rowell 1982). In contrast, chemical modification of wood with a maleic acid-glycerol mixture has been found to enhance the resistance of wood to weathering (Fujimoto 1992).

Recently, Evans et al. (2002) found that benzoylation of wood with benzoyl chloride (to high weight gains) was effective at photostabilizing wood, including its lignin component. They observed an inverse relationship between WGs (due to benzoylation) and mass losses of benzoylated wood during weathering. In order to explain their findings, they suggested that the benzoyl groups in benzoylated wood absorbed UV light or scavenged free radicals. Benzoylation of wood to higher WGs, however,

caused pronounced swelling of the wood cell wall, which reduced the strength of treated wood veneers.

14.4.5 Photoprotection of Wood by Monomer/Polymer Wood Lumen Fill Treatments

Filling wood cell lumens with polymerizable monomers (i.e., impregnation and subsequent curing/polymerization of the monomers in the lumens) improves the weathering durability of wood (Desai 1972; Rowell et al. 1981; Feist and Rowell 1982; Feist et al. 1991). Methyl methacrylate (MMA) monomer impregnation and subsequent polymerization in cell lumens reduces the rate of moisture sorption and increases the hardness of wood (Rowell et al. 1981). Filling wood cell lumens with MMA reduced the erosion of wood by 40% or more during accelerated weathering (Rowell et al. 1981; Feist et al. 1991). The combination of acetylation followed by MMA cell lumen filling further increased the weathering durability of wood (Feist et al. 1991), and reduced surface erosion by about 85%. Butylene oxide (BO), methyl-isocyanate (MI), or butyl-isocyanate (BI) treatment of wood followed by MMA impregnation and polymerization *in situ* was also found to enhance the resistance of wood to UV light and accelerated weathering (Feist and Rowell 1982; Rowell et al. 1981), despite earlier findings that modification of wood with BO, MI and BI was ineffective at enhancing photostability (Rowell et al. 1981; Feist and Rowell 1982). Stamm (1959) found that treatment of wood with polyethylene glycol (PEG) reduced the face checking of wood during seasoning. PEG also dimensionally stabilizes wood by bulking the fibers. Kiguchi et al. (1997c) found that pretreatment of Douglas fir plywood with a 10%

solution of PEG reduced film failure of clear finishes exposed outdoors for two years. Recently, Ohkoshi (2002) used FTIR-PAS to examine the chemical changes occurring at the surfaces of wood specimens impregnated with PEG and irradiated with UV light. PEG impregnation decreased the generation of carbonyl groups and degradation of lignin in wood during exposure, but the PEG was itself degraded by UV light, and it was suggested that this would limit its ability in the long term to photostabilize wood.

14.4.6 Wood-Plastic Composites

Extruded/molded wood-plastic composites (WPCs) contain wood fibres or flours which act as reinforcing fillers in a thermoplastic matrix. Both the thermoplastic and wood are susceptible to photodegradation. Matuana et al. (2001) investigated the UV resistance of unpigmented and rutile-titanium-dioxide-pigmented rigid polyvinyl chloride (PVC) wood fibre composites. They observed that incorporation of wood fiber into a PVC matrix accelerated the UV degradation of the thermoplastic polymer. Addition of a photoactive pigment (rutile titanium dioxide) to the composite enhanced its UV-light stability. This is in accord with Blackburn et al.'s (1991) observation that "[F]ine particle titanium dioxide offered significant improvements over conventional UVAs and HALS in stabilizing alkyd based wood finishes." Grafting of an epoxy functionalized benzophenone-type UV absorber (2-hydroxy-4-(2,3-epoxypropoxy)-benzophenone, HEPBP) to wood fibres used in WPCs also improved the color stability of the composite material during accelerated weathering (Kiguchi et al. 2000).

14.4.7 Photoprotection of Wood with UV Absorbers and Hindered Amine Light Stabilizers

Additives such as UV absorbers (UVAs), hindered amine light stabilizers (HALS), and hindered phenolic antioxidants (AOs) have also been used to protect wood from photodegradation and improve the performance of clear finishes (Kalnins 1966; Williams 1983; Rogez 2001). UVAs act to prevent the formation of free radicals via preferential absorption of incident UV light and dissipation of the incident energy as non-radiative heat. In comparison, HALS prevent the formation of high concentrations of free radicals. The precise mechanism by which this is achieved in wood has not been fully elucidated, but is thought to include energy transfer, free radical ter-

mination, or peroxide decomposition. UVAs and HALS are widely incorporated into coatings to reduce photodegradation of the polymeric binder. Their effectiveness for this application is dependant upon the type of UVA or HALS and their concentrations in the coating. Increased film thickness will reduce the concentration of UVA required to retard degradation of wood beneath clear coatings, but may result in problems associated with the lack of flexibility of thick coatings on wood. Hindered phenolic antioxidants (AOs) are traditionally used to terminate free radicals originating from heat-induced degradation of coatings. They are similar in function to HALS, so they can be used to retard the degradative effects of UV light on wood. Unlike HALS, however, they are non-regenerative and decrease in concentration during the photostabilization process.

Kalnins (1966) found that treatment of Douglas fir veneers with a UVA (dibenzoylresorcinol) reduced the production of gaseous and volatile photodegradation products produced during irradiation of wood with artificial UV light. In contrast, Hon et al. (1985) found that the addition of a HALS or AO to a clear acrylic film-forming finish containing an internal UVA did not prevent the photo-oxidative discolouration of the underlying pine wood surface. Wood coated with UV-curable clear coatings was also reported to turn yellow following exposure to UV light (Chang and Chou 1999) and, although some discoloration occurred in the coating, the majority was found in the substrate. Chang and Chou (1999) found, however, that incorporating UVAs into clear coatings significantly reduced the yellowing of both the coating and substrate, whereas HALS were ineffective. The authors did report that HALS reduced the photo-yellowing of wood coated with an aliphatic urethane-modified acrylate finish containing a UVA. They speculated that this might have been due to a synergy between the HALS and the UVA. Recently Rogez and coworkers (Rogez 2001; Hayoz et al. 2002) described the synergistic effects of combinations of UVA/HALS on the performance of clear coatings on wood, and the progress that has been made in developing more effective UVA/HALS systems for the photoprotection of wood and clear finishes. HALS have also been shown to be useful inhibitors of iron oxidation and water degradation of wood (Hussey and Nicholas 1985).

14.4.8 Photoprotection of Wood by Grafting of UV Absorbers

Grafting or chemically bonding of UVAs to synthetic polymers is a highly effective method of protecting

polymers from photodegradation. Williams (1983) first reported the grafting of a reactive UVA, 2-hydroxy-4-(2,3-epoxypropoxy)-benzophenone (HEPBP) to the surface of wood (western red cedar) and demonstrated that the grafted UVA reduced the erosion of unfinished wood, and, as pretreatment, enhanced the performance of clear finishes during artificial accelerated weathering. Kiguchi and Evans (1998) investigated the reaction conditions required to graft HEPBP to wood. They found that in the presence of an amine catalyst (dimethylbenzylamine) and at temperatures in excess of 80 °C, HEPBP could be grafted to wood resulting in permanent WGs. Grafting of HEPBP was found to be as effective as chromium trioxide at restricting mass losses of veneers during natural weathering, and better than chromium trioxide at restricting veneer tensile strength losses. XPS spectra indicated that the photoprotective effect of grafting on mass losses was due to the protection of lignin at exposed surfaces. Grafting of reactive UVAs such as HEPBP and some epoxy-functionalized triazine-type UVAs to wood has also been found to reduce photochemical changes at UV irradiated wood surfaces, and greatly improve the performance of clear coatings on modified veneer surfaces (Kiguchi et al. 2001). Grafting of a benzotriazole UV absorber containing an isocyanate group to wood supplemented by other additives (such as polyethylene glycol or a HALS) to grand fir (*Abies grandis* Lindl.), and European oak, was found to be effective at preventing photoyellowing of the wood (Grelier et al. 1997). Commercialization of such treatments awaits the development of less costly UV absorbers that can be more easily bonded to wood.

14.5 FUTURE DIRECTIONS

Architects and engineers are increasingly insisting on materials that offer longer service life and lower repair and maintenance costs. In addition, there is pressure to use materials that can be recycled and produced on a sustainable basis. Wood is a renewable material that can be easily repaired and in most cases recycled. However, weathering reduces the service life of wood and increases its maintenance costs. For example, premature failure and replacement of preservative-treated pine poles and decking are often caused by checking, and the higher maintenance costs of exterior wooden joinery compared to substitutes made from unplasticized polyvinyl chloride or aluminum are caused in part by weathering-induced failure of surface coatings. Hence, there is likely to

be continuing interest in the development of additives and treatments to reduce the weathering of wood. A deeper understanding of the mechanisms involved in photodegradation of wood could lead to more economical and effective methods of photostabilizing wood, which could significantly improve the durability of clear finishes for timber. Wood is increasingly being converted into a wide range of composites using a diverse range of matrix materials, including thermoplastic and thermosetting polymers and ceramics. The evaluation of the weathering resistance of such composites and the development of appropriate treatments to enhance their durability will become increasingly important in the future.

14.6 REFERENCES

- Anon. 1976. New wood with an old look. *Wood & Wood Prod.* Vol. 81, pp. 33–35.
- Ashton, H. E. 1967. Clear finishes for exterior wood. Field exposure tests. *J. Paint Technol.* Vol. 39(507), pp. 212–224.
- Bamber, R. K. and Summerville, R. 1981. Microscopic studies of the weathering of radiata pine sapwood. *J. Inst. Wood Sci.* Vol. 9(2), pp. 84–88.
- Benson, S. W. 1965. Bond energies. *J. Chem. Educ.* Vol. 42(9), pp. 502–518.
- Black, J. M. and Mraz, E. A. 1974. *Inorganic Surface Treatments for Weather-resistant Natural Finishes.* Research Paper FPL 232. Madison, WI: U.S.D.A. Forest Service.
- Blackburn, S. R., Meldrum, B. J. and Clayton, J. 1991. The use of fine particle titanium dioxide for UV protection in wood finishes. *Faerg och Lack Scandinavia.* Vol. 37(9), pp. 192–196.
- Borgin, K. 1968. The protection of wood against dimensional instability. *Forestry in South Africa.* Vol. 9, pp. 81–94.
- Borgin, K. 1969. The stability, durability, and weather resistance of wooden houses under cold climatic conditions. *Architect Builder.* June–July.
- Borgin, K. 1971. The mechanism of the breakdown of the structure of wood due to environmental factors. *J. Inst. Wood Sci.* Vol. 5(4), pp. 26–30.
- Bos, A. 1972. Ultraviolet spectra of cellulose and some model compounds. *J. Appl. Polym. Sci.* Vol. 16(10), pp. 2,567–2,576.
- Boxall, J. 1977. Painting weathered timber. *Buildg. Res. Est. (UK) Information Sheet.* Vol. 20/77, pp. 1–2.
- Browne, F. L. and Simonson, H. C. 1957. The penetration of light into wood. *Forest Prod. J.* Vol. 7(10), pp. 308–314.
- Chang, S.-T. and Chang, H.-T. 2001. Comparisons of the photostability of esterified wood. *Polym. Deg. Stab.* Vol. 71(2), pp. 261–266.
- Chang, S.-T. and Chou, P. -L. 1999. Photo-discoloration of UV-curable acrylic coatings and the underlying wood. *Polym. Deg. Stab.* Vol. 63(3), pp. 435–439.

- Chang, S-T, Hon, D. N. S., and Feist, W. C. 1982. Photodegradation and photoprotection of wood surfaces. *Wood Fiber Sci.* Vol. 14(2), pp. 104–117.
- Cornfield, J. A., Hale, M. and Fellis, G. 1994. A comparison of analytical and visual techniques used for assessment of weathering properties of chromium and copper azole treated timber. Int. Res. Group on Wood Pres. Doc. No. IRG/WP/20023.
- Coupe, C. and Watson, R. W. 1967. Fundamental aspects of weathering. In *Record of the 17th Annual Convention*. British Wood Preservers Association. Vol. 2, pp. 37–49.
- Desai, R. L. 1967. Coating adhesion to weathered wood. Can. Dept. Fisheries and Forestry. Bi-monthly Res. Notes 23, pp. 36–37.
- Desai, R. L. and Juneja, S. C. 1972. Weather-O-Meter studies on wood-plastic composites. *Forest Prod. J.* Vol. 22(9), pp. 100–103.
- Derbyshire, H. and Miller, E. R. 1981. The photodegradation of wood during solar irradiation. Part 1. Effects on the structural integrity of thin wood strips. *Holz Roh-Werkst.* Vol. 39(8), pp. 341–350.
- Dunningham, E. A., Plackett, D. V., and Singh, A. P. 1992. Weathering of chemically modified wood. Natural weathering of acetylated radiata pine: Preliminary results. *Holz Roh-Werkst.* Vol. 50(11), pp. 429–432.
- Evans, P. D. 1989. Structural changes in *Pinus radiata* during weathering. *J. Inst. Wood Sci.* Vol. 11(5), pp. 172–181.
- Evans, P. D. 1998. Weather resistance of wood esterified with dicarboxylic acid anhydrides. *Holz Roh-Werkst.* Vol. 56(5), p. 294.
- Evans, P. D. and Banks, W. B. 1988. Degradation of wood surfaces by water. Changes in mechanical properties of thin wood strips. *Holz Roh-Werkst.* Vol. 46(11), pp. 427–435.
- Evans, P. D. and Banks, W. B. 1990. Degradation of wood surfaces by water: Weight losses and changes in ultrastructure and chemical composition. *Holz Roh-Werkst.* Vol. 48(4), pp. 159–163.
- Evans, P. D., Michell, A. J., and Schmalzl, K. J. 1992. Studies of the degradation and protection of wood surfaces. *Wood Sci. Tech.* Vol. 26(2), pp. 151–163.
- Evans, P. D., Owen, N. L., Schmid, S., and Webster, R. D. 2002. Weathering and photostability of benzoylated wood. *Polym. Deg. Stab.* Vol. 76(2), pp. 291–303.
- Evans, P. D., Pirie, J. D. R., Cunningham, R. B., Donnelly, C. F., and Schmalzl, K. J. 1994. A quantitative weathering study of wood surfaces modified by chromium VI and iron III compounds. Part 2. Image analysis of cell wall pit micro-checking. *Holzforchung.* Vol. 48(4), pp. 331–336.
- Evans, P. D. and Schmalzl, K. J. 1989. A quantitative weathering study of wood surfaces modified by chromium VI and iron III compounds. Part 1. Loss in zero-span tensile strength and weight of thin wood veneers. *Holzforchung.* Vol. 43(5), pp. 289–299.
- Evans P. D., Schmalzl, K. J., and Michell, A. F. 1993. Rapid loss of lignin at wood surfaces during natural weathering. In *Cel-lulosics: Pulp, Fibre and Environmental Aspects*. J. F. Kennedy, G. O. Phillips, and P. A. Williams, Eds. Chichester: Ellis Horwood, pp. 335–340.
- Evans, P. D., Thay, P. D., and Schmalzl, K. J. 1996. Degradation of wood surfaces during natural weathering. Effects on lignin and cellulose and on the adhesion of acrylic latex primers. *Wood Sci. Tech.* Vol. 30(6), pp. 411–422.
- Evans, P. D., Wallis, A. F. A., and Owen, N. L. 2000. Weathering of chemically modified wood surfaces. Natural weathering of Scots pine acetylated to different weight gains. *Wood Sci. Tech.* Vol. 34(2), pp. 151–165.
- Feist, W. C. 1990. Outdoor Wood Weathering and Protection. In *Archaeological Wood: Properties, Chemistry, and Preservation*. R. M. Rowell and R. J. Barbour, Eds. Washington, DC: American Chemistry Society.
- Feist, W. C. 1988. Role of pigment concentration in the weathering of semitransparent stains. *Forest Prod. J.* Vol. 38(2), pp. 41–44.
- Feist, W. C. 1979. *Protection of Wood Surfaces with Chromium Trioxide*. Research Paper FPL-339. Madison, WI: U.S.D.A. Forest Service, Forest Products Laboratory.
- Feist, W. C. 1977. Finishing wood for exterior application—Paints, stains, and pretreatments. In *Wood Technology, Chemical Aspects*. I. S. Goldstein, Ed. Washington, DC: American Chemistry Society Series 43, Chapter 19.
- Feist, W. C. and Ellis, W. D. 1978. Fixation of hexavalent chromium on wood surfaces. *Wood Sci.* Vol. 11(2), pp. 76–81.
- Feist, W. C. and D. N. -S. Hon. 1984. Chemistry of Weathering and Protection. In *Chemistry of Solid Wood*. R. M. Rowell, Ed. Washington, DC: American Chemistry Society, pp. 401–454.
- Feist, W. C. and Rowell, R. M. 1982. Ultraviolet degradation and accelerated weathering of chemically modified wood. In *Graft Copolymerization of Lignocellulosic Fibres*. D. N. -S. Hon, Ed. Washington, DC: American Chemistry Society Symposium Series 187, pp. 349–370.
- Feist, W. C., Rowell, R. M., and Ellis, W. D. 1991. Moisture sorption and accelerated weathering of acetylated and methacrylated aspen. *Wood Fiber Sci.* Vol. 23(1), pp. 128–136.
- Feist, W. C. and Williams, R. S. 1991. Weathering durability of chromium-treated southern pine. *Forest Prod. J.* Vol. 41(1), pp. 8–14.
- Fujimoto, H. 1992. Weathering behaviour of chemically modified wood with a maleic acid-glycerol (MG) mixture. In *Chemical Modification of Lignocellulosics*. D. V. Plackett and E. A. Dunningham, Eds. FRI Bulletin 176. Rotorua, New Zealand: New Zealand Forest Research Institute, pp. 87–96.
- Grelier, S., Castellan, A., Desrousseaux, S., Nourmamode, A., and Podgorski, L. 1997. Attempt to protect wood colour against UV/Visible light by using antioxidants bearing isocyanate groups and grafted to the materials with microwave. *Holzforchung.* Vol. 51(6), pp. 511–518.
- Hemmingson J. A. and Morgan, K. R. 1990. A CP/MAS carbon-13 NMR study of photodegraded newsprint. *Holzforchung.* Vol. 44(2), pp. 127–131.

- Hilditch, E. A. and Crookes, J. V. 1981. Exterior wood stains, varieties, performance and appearance. *Record of the Annual Convention*. British Wood Preservers Association, pp. 59–66.
- Hoyoz, P., Wolfgang, P., and Rogez, D. 2002. A new innovative stabilization method for the protection of natural wood. In *Proceedings of the 28th Conference on Coatings Science and Technology*, Athens, Greece, July 1–5, pp. 67–86.
- Hon, D. N.-S. 1991. Photochemistry of wood. In *Wood and Cellulosic Chemistry*. D. N. -S. Hon and N. Shiraiishi, Eds. New York: Marcel Dekker, pp. 525–555.
- Hon, D. N.-S. 1984. ESCA study of oxidized wood surfaces. *J. Appl. Polym. Sci.* Vol. 29(9), pp. 2,777–2,784.
- Hon, D. N.-S. 1979a. Photo-oxidative degradation of cellulose: Reactions of the cellulosic free radicals with oxygen. *J. Polym. Sci. Polym. Chem. Ed.* Vol. 17(2), pp. 441–454.
- Hon, D. N.-S. 1979b. On possible chromophoric structures in wood and pulps—A survey of the present state of knowledge. *Polym.—Plast. Technol. Eng.* Vol. 12(2), pp. 159–179.
- Hon, D. N.-S. 1976a. Fundamental degradation processes relevant to solar irradiation of cellulose: ESR studies. *J. Macromol. Sci.-Chem.* Vol. A10, pp. 1,175.
- Hon, N.-S. 1976b. Formation of free radicals in photoirradiated cellulose. VIII. Mechanisms. *J. Polym. Sci. Polym. Chem. Ed.* Vol. 14(10), pp. 2,497–2,512.
- Hon, N.-S. 1975. Formation of free radicals in photoirradiated cellulose. 1. Effect of wavelength. *J. Polymer. Sci. Polym. Chem. Ed.* Vol. 13(6), pp. 1,347–1,361.
- Hon, D. N.-S. and Chang, S.-T. 1984. Surface degradation of wood by ultraviolet light. *J. Polym. Sci.* Vol. 22(9), pp. 2,227–2,235.
- Hon, D. N.-S., Chang, S.-T., and Feist, W. C. 1985. Protection of wood surfaces against photo-oxidation. *J. Appl. Polym. Sci.* Vol. 30(4), pp. 1,429–1,448.
- Hon, D. N.-S. and Feist, W. C. 1993. Interaction of sulfur dioxide and nitric oxide with photoirradiated wood surfaces. *Wood Fiber Sci.* Vol. 25(2), pp.136–141.
- Hon, D. N.-S. and Feist, W. C. 1992. Hydroperoxidation in photoirradiated wood surfaces. *Wood Fiber Sci.* Vol. 24(4), pp. 448–455.
- Hon, D. N.-S. and Feist, W. C. 1981. Free radical formation in wood: The role of water. *Wood Sci.* Vol. 14(1), pp. 41–47.
- Hon, D. N.-S. and Feist, W. C. 1980. Role of Free Radicals in Weathering of Wood. Paper presented at the 34th FPRS Annual Meeting, Boston, MA, June 6–10.
- Hon, D. N.-S. and Ifju, G. 1978. Measuring penetration of light into wood by detection of photo-induced free radicals. *Wood Sci.* Vol. 11(2), pp.118–127.
- Hon, D. N.-S., Ifju, G., and Feist, W. C. 1980. Characteristics of free radicals in wood. *Wood and Fiber Sci.* Vol. 12(2), pp. 121–130.
- Hon, D. N.-S. and Minemura, N. 1991. Colour and Discoloration in Wood and Cellulose Chemistry. D. N. -S. Hon and N. Shiraiishi, Eds. New York: Marcel Dekker, pp. 395–454.
- Horn, B. A., Qui, J., Owen, N. L., and Feist, W. C. 1994. FT-IR studies of weathering effects in western red cedar and southern pine. *Appl. Spectrosc.* Vol. 48(6), pp. 662–668.
- Hussey, B. E. and Nicholas, D. D. 1985. The effect of light stabilizers on the iron and water degradation of wood. In *Proceedings of American Wood-Preservers Association*. Vol. 81, pp. 169–173.
- Imamura, Y. 1993. Morphological changes in acetylated wood exposed to weathering. *Wood Res. Bull. Wood Res. Inst. Kyoto Univ.* Vol. 79, pp. 54–61.
- Johnson, E. L. and Cserjesi, A. J. 1980. Weathering effect on thujaplicin concentration in western redcedar shakes. *Forest Prod. J.* Vol. 30(6), pp. 52–53.
- Jin, L., Archer, K., and Preston, A. 1991. Surface characteristic of wood treated with various AAC, ACQ and CCA formulations after weathering. *Int. Res. Group on Wood Pres.*, Document IRG/WP/2369.
- Kalnins, M. A. 1966. *Surface Characteristics of Wood as They Affect the Durability of Finishes. Part 2: Photochemical Degradation of Wood*. U.S. Forest Products Laboratory Report. Vol. 57, pp. 23–60.
- Kalnins, M. A. 1984. Photochemical degradation of acetylated, methylated, phenylhydrazine-modified and ACC-treated wood. *J. Appl. Polym. Sci.* Vol. 29(1), pp. 105–115.
- Kataoka, Y., Kiguchi, M., and Evans P. D. 2004. Photodegradation depth profile and penetration of light in sugi exposed to artificial solar radiation. Vol. 87(B3) pp. 187–193. *Surface Coatings International Part B: Coating Transactions*.
- Kiguchi, M. 1997. Photo-deterioration of chemically modified wood surfaces: Acetylated wood and alkylated wood. *JARQ (Japan Agricultural Research Quarterly)*. Vol. 31(2), pp. 147–154.
- Kiguchi, M., Evans, P. D., Ekstedt, J., Williams, R. S., and Kataoka, Y. 2001. Improvement of the durability of clear coatings by grafting of UV-absorbers on to wood. *Surface Coating International Part B: Coating Transactions*. Vol. 84(B4), pp. 263–270.
- Kiguchi, M., Kataoka, Y., Doi, S., Mori, M., Hasegawa, M., Morita, S., Kadegaru, Y., and Imamura, Y. 1997c. Improvement of weather resistance of film-forming type clear finishes by pre-treatment with PEG and influence of exposure test sites. *Mokuzai Gakkaishi*. Vol. 23(4), pp. 168–175.
- Kiguchi, M., Kataoka, Y., Doi, S., Mori, M., Hasegawa, M., Morita, S., Kinjo, M., Kadegaru, Y., and Imamura, Y. 1996. Evaluation of weathering resistance of the commercial pigmented stains by outdoor exposure tests in Japan. *Mokuzai Gakkaishi*. Vol. 22(3), pp. 150–159.
- Kiguchi, M., Kataoka, Y., Kaneiwa, H., Akita, K., and Evans, P. D. 2000. Photostabilisation of woodfibre-plastic composites by chemical modification of woodfibre. In *Proceedings of the 5th Pacific Rim Bio-Based Composites Symposium*. Canberra, Australia, December 10–13., pp 145–150.
- Kiguchi, M., Suzuki, M., Kinoshita, T., and Kawamura, J. 1997a. Evaluation of exterior pigmented stains by a new criterion of refinishing. *Mokuzai Gakkaishi*. Vol. 52(12), pp. 612–617.

- Kiguchi, M., Suzuki, M., Kinoshita, T., and Kawamura, J. 1997b. Estimation of weather resistance of wooden sashes finished with exterior stains. *Materials Life*. Vol. 9(4), pp. 188–195.
- Kiguchi, M. and Evans, P. D. 1998. Photostabilisation of wood surfaces using a grafted benzophenone UV absorber. *Polym. Deg. Stab.* Vol. 61(1), pp. 33–45.
- Kitamura, Y., Setoyama, K., and Kurosu, H. 1989. Wavelength dependency of light-induced discoloration in wood and dyed wood. In *Wood Processing and Utilization*. J. F. Kennedy, G. O. Phillips, and P. A. Williams, Eds. Chichester: Ellis Horwood, Vol. 51, pp. 387–392.
- Kucera, L. J. and Sell, J. 1987. Weathering behaviour of beech around the ray tissue region. *Holz Roh-Werkst.* Vol. 45(3), pp. 89–93.
- Leary, G. J. 1967. Yellowing of wood by light. *Tappi*. Vol. 50(1), pp. 17–19.
- Leary, G. J. 1968. The yellowing of wood by light. II. *Tappi*. Vol. 51(6), pp. 257–260.
- Liu, R., Ruddick, J. N. R., and Jin, L. 1994. The influence of copper (II) chemicals on the weathering of treated wood. Part I: ACQ treatment of wood on weathering. *Int. Res. Group on Wood Pres.* Document IRG/WP/30040.
- Matuana, L. M., Kamdem, D. P., and Zhang, J. 2001. Photoaging and stabilization of rigid PVC/woodfiber composites. *J. Appl. Polym. Sci.* 80(11), pp. 1943–1950.
- Mawson, D. 1915. *The Home of the Blizzard. Being the Story of the Australasian Antarctic Expedition, 1911–1914*. London: William Heinemann, pp. 123–124.
- Miniutti, V. P. 1964. Preliminary observations. Microscale changes in cell structure at softwood surfaces during weathering. *Forest Prod. J.* Vol. 14(12), pp. 571–576.
- Miniutti, V. P. 1967. *Microscopic Observations of Ultraviolet Irradiated and Weathered Softwood Surfaces and Clear Coatings*. U.S.D.A. Forest Service Research Paper FPL 74, pp. 1–32.
- Norrstrom, H. 1969. Color of unbleached sulfate pulp. *Svensk Papperstidn.* Vol. 72(19), pp. 605–614.
- Ohkoshi, M. 2002. FTIR-PAS study of light-induced changes in the surface of acetylated or polyethylene glycol-impregnated wood. *J. Wood Sci.* Vol. 48(5), pp. 394–401.
- Ohtani, K. 1987. Chromium trioxide enhances the durability of wooden doors. *Chromium Rev.* Vol. 8, pp. 4–7.
- Paajanen, L. M. 1994. Structural changes in primed Scots pine and Norway spruce during weathering. *Materials and Structures*. Vol. 27(168), pp. 237–244.
- Panshin, A. J. and DeZeeuw, C. 1980. *Textbook of Wood Technology*, 4th Ed. New York: McGraw-Hill.
- Park, B. S., Furuno, T., and Uehara, T. 1996. Histochemical changes of wood surfaces irradiated with ultraviolet light. *Mokuzai Gakkaishi*. Vol. 42(1), pp. 1–9.
- Pizzi, A. 1980. Wood waterproofing and lignin crosslinking by means of chromium trioxide/guaiacyl units complexes. *J. Appl. Polym. Sci.* Vol. 25(11), pp. 2,547–2,553.
- Plackett, D. V., Dunningham, E. A., and Singh, A. P. 1992. Weathering of chemically modified wood. Accelerated weathering of acetylated radiata pine. *Holz Roh-Werkst.* Vol. 50(4), pp. 135–140.
- Raczkowski, J. 1980. Seasonal effects on the atmospheric corrosion of spruce micro-sections. *Holz Roh-Werkst.* Vol. 38(6), pp. 231–234.
- Rogez, D. 2001. Wood photoprotection. *Polymers Paint Colour Journal*. Vol. 191(4,446), pp. 33–35.
- Rowell, R. M. 1983. Chemical modification of wood. *Forest Prod. Abstracts*. Vol. 6, pp. 363–382.
- Rowell, R. M., Feist, W. C., and Ellis, W. D. 1981. Weathering of chemically modified southern pine. *Wood Sci.* Vol. 13(4), pp. 202–208.
- Sandermann, W. and Schlumbom, F. 1962. Über die Wirkung gefilterten ultravioletten Lichtes auf Holz. Erste Mitteilung. Photometrische und chromatographische Untersuchungen an Holzmehlen. (On the effect of filtered ultraviolet light on wood. Part 1. Photometric and chromatographic investigations on wood powders). *Holz Roh-Werkst.* Vol. 20(7), pp. 245–252.
- Schmalzl, K. J. 1986. The chemical modification of wood surfaces for protection against weathering. A presentation delivered at CSIRO Division of Chemical & Wood Technology, Clayton, Australia, November 27, 1986.
- Schmalzl, K. J. and P. D. Evans. 2003. Wood surface protection with some titanium, zirconium and manganese compounds. *Polym. Deg. Stab.* Vol. 82(3), pp. 409–419.
- Schmalzl, K. J., Forsyth, C. M., and Evans, P. D. 1995. The reaction of guaiacol with iron III and chromium VI compounds as a model for wood surface modification. *Wood Sci. Tech.* Vol. 29(4), pp. 307–319.
- Schmalzl, K. J., Forsyth, C. M., and Evans, P. D. 2003. Evidence for the formation of chromium III diphenanthroquinone complexes during oxidation of guaiacol and 2,6-dimethoxyphenol with chromic acid. *Polym. Deg. Stab.* Vol. 82(3), pp. 399–407.
- Schmid, S., Webster, R. D., and Evans, P. D. 2000. The use of ESR spectroscopy to assess the photostabilising effects of wood preservatives. *Int. Res. Group on Wood Pres.* Document IRG/WP 00-20186.
- Schmidt, E. L. and French, D. W. 1976. Aureobasidium pulullans on wood shingles. *Forest Prod. J.* Vol. 26(7), pp. 34–37.
- Schoemaker, H. E., Harvey, P. J., Bowen, R. M., and Palmer, J. M. 1985. On the mechanism of enzymatic lignin breakdown. *FEBS Letters*. Vol. 183(1), pp. 7–12.
- Shoeman, M., and Dickenson, D. J. 1997. Growth of Aureobasidium pulullans on lignin breakdown products at weathered wood surfaces. *Mycologist*. Vol. 11(4), pp. 168–172.
- Schramm, W. H. 1906. *Jahresber. Vereinigung Angew. Bot.* Vol. 3, pp. 116–53.
- Schultz, T. P. and Templeton, M. C. 1986. Proposed mechanism for the nitrobenzene oxidation of lignin. *Holzforschung*. Vol. 40(2), pp. 93–97.

- Sell, J. and Feist, W. C. 1986. Role of density in the erosion of wood during weathering. *Forest Prod. J.* Vol. 36(3), pp. 57–60.
- Singh, A. P. and Dawson, B. S. W. 2003. The mechanism of failure of clear coated wooden boards as revealed by microscopy. *IAWA J.* Vol. 24(1), pp. 1–11.
- Spedding, D. J. 1970. Sorption of sulphur dioxide by indoor surfaces. II. *Wood. J. Appl. Chem.* Vol. 20(7), pp. 226–228.
- Stamm, A. J. 1959. Effect of polyethylene glycol on the dimensional stability of wood. *Forest Prod. J.* Vol. 9, pp. 375–381.
- Tarkow, H., Stamm, A. J., and Erickson, E. C. O. 1946. *Acetylated Wood*. Report 1593. U.S.D.A. Forest Service, Forest Products Laboratory.
- Torr, K. M., Dawson B. S. W., Ede, R. M., and Singh J. 1996. Surface changes on acetylation and exposure to ultraviolet radiation of *Pinus radiata* using x-ray photo-electron spectroscopy. *Holzforschung*. Vol. 50(5), pp. 449–456.
- Underhaug, A., Lund, T. J., and Kleive, K. 1983. Wood protection—The interaction between substrate and product and the influence on durability. *J. Oil & Col. Chem. Assoc.* Vol. 66(11), pp. 345–350.
- Usmanov, Kh. U. 1978. Degradation and stabilisation of cellulose acetates and some polymers based on vinyl fluoride. *Polym. Sci. Ser. A (USSR)*. Vol. 20(8), pp. 1683–90.
- Voulgaridis, E. V. and Banks, W. B. 1983. Laboratory evaluation of the performance of water repellants applied to long wood specimens. *Holzforschung*. Vol. 37(5), pp. 261–266.
- Wallace, J. M. and Hobbs, P. V. 1977. *Atmospheric Science: An Introductory Survey*. New York: Academic Press, p 328.
- Wengert, E. M. 1966. *Parameters for Predicting Maximum Surface Temperatures of Wood in Exterior Exposures*. Research Paper FPL 62. U.S.D.A. Forest Service, Forest Products Laboratory.
- Wiesner, J. 1864. The decomposition of wood in the atmosphere. *Sitzungsber. K. Akad. Wissenschaften Wien*. Vol. 49, pp. 61–94.
- Williams, R. S. 1987. Acid effects on accelerated wood weathering. *Forest Prod. J.* Vol. 37(2), pp. 37–38.
- Williams, R. S. 1983. Effect of grafted UV stabilizers on wood surface erosion and clear coating performance. *J. Appl. Polymer Sci.* Vol. 28(6), pp. 2,093–2,103.
- Williams, R. S. and Feist, W. C. 1988. Performance of finishes on wood modified with chromium nitrate versus chromic acid. *Forest Prod. J.* Vol. 38(11–12), pp. 32–35.
- Williams, R. S. and Feist, W. C. 1993a. Durability of paint or solid-color stain applied to preweathered wood. *Forest Prod. J.* Vol. 43(1), pp. 8–14.
- Williams, R. S. and Feist, W. C. 1993b. Finishing wood decks. *Wood Design Focus*, Fall, pp. 17–20.
- Williams, R. S., Knaebe, M. T., Sotos, P. G., and Feist, W. C. 2001a. Erosion rates of wood during natural weathering. Part I: Effects of grain angle and surface texture. *Wood Fibre Sci.* Vol. 33(1), pp. 31–42.
- Williams, R. S., Knaebe, M. T., and Feist, W. C. 2001b. Erosion rates of wood during natural weathering. Part II: Earlywood and latewood erosion rates. *Wood Fibre Sci.* Vol. 33(1), pp. 43–49.
- Williams, R. S., Plantinga, P. L., and W. C. Feist. 1990. Photodegradation of wood affects paint adhesion. *Forest Prod. J.* 40(1), pp. 45–49.
- Williams, R. S., Winandy, J. E., and Feist, W. C. 1987. Paint adhesion to weathered wood. *J. Coat. Tech.* Vol. 59(749), pp. 43–49.
- Yata, S. and Tamaru, T. 1995. Histological changes of softwood surfaces during outdoor weathering. *Mokuzai Gakkaishi*. Vol. 41(11), pp. 1,035–1,042.
- Yoshimoto, T., Minami, K., and Kondo, M. 1967. Photodegradation of wood. II. Imperfect hardening of cement caused with reducing substances produced in wooden molding board exposed to sunlight. *Mokuzai Gakkaishi*. Vol. 113(3), pp. 96–101.
- Zabel, R. A. and Morrell, J. J. 1992. *Wood Microbiology. Decay and Its Prevention*. San Diego: Academic Press.
- Zahora, A. R. 1992. A water repellent additive's influence on the field performance of southern yellow pine lumber. In *Proceedings of American Wood-Preservers Association*. Vol. 88, pp. 148–159.
- Zhang, X. 2003. *Photo-resistance of chemically treated wood*. M.Sc. Thesis, Department of Wood Science, University of British Columbia, Vancouver, BC, Canada.
- Zhang, J. and Kamden, D. P. 2000. Weathering of copper-amine treated wood. *Int. Res. Group on Wood Pres.* Document IRG/WP 40155.

CHAPTER 15

PROTECTION OF WOOD-BASED MATERIALS

Jeff Morrell

Department of Wood Science and Engineering, Oregon State University, Corvallis, Oregon

| | |
|--|-----|
| 15.1 INTRODUCTION | 299 |
| 15.2 ABIOTIC AGENTS | 299 |
| 15.3 BIOTIC AGENTS | 300 |
| 15.4 DECAY ORGANISMS | 301 |
| 15.5 INSECTS | 303 |
| 15.6 MAGNITUDE OF WOOD DETERIORATION LOSSES | 305 |
| 15.7 WOOD PROTECTION | 306 |

| | |
|------------------------------------|-----|
| 15.8 TREATMENT METHODS | 308 |
| 15.9 TREATMENT STANDARDS | 311 |
| 15.10 NEW TREATMENT PROCESSES | 311 |
| 15.11 ENVIRONMENTAL CONSIDERATIONS | 311 |
| 15.12 PRESERVATIVES | 312 |
| 15.13 REMEDIAL TREATMENTS | 315 |
| 15.14 NON-BIOCIDAL BARRIERS | 316 |
| 15.15 REFERENCES | 316 |

15.1 INTRODUCTION

The complex structure of wood makes it remarkably resistant to degradation by a variety of agents, but wood will degrade under the proper conditions. Wood degradation can be classified as damage caused by biotic (living) and abiotic (non-living) agents. In many instances, biotic and abiotic damage appear similar to the naked eye, but careful examination of the wood for biotic agents and careful attention to chemical changes associated with non-living agents of decay can be used to delineate the causal agent.

15.2 ABIOTIC AGENTS

Non-living or abiotic agents include weathering (Figure 15.1)(see Evans), mechanical wear, chemicals, and heat.

15.2.1 Mechanical Damage

Mechanical damage can occur from a variety of sources. For example, repeated abrasion can wear away the wood. This type of damage is most often seen on wood stairs, where the wood wears away on the most heavily traveled sections of the tread. Abrasion can be easily detected and repaired. Mechanical damage can also occur through repeated heavy loading of the wood (e.g., where heavy loads are repeat-

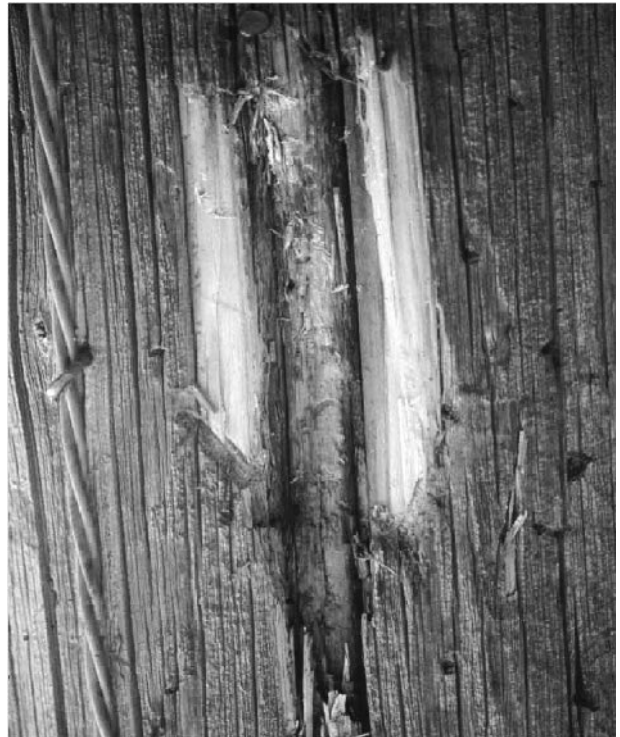


FIGURE 15.1 Weathering can turn light wood dark, but the damage is relatively shallow.

edly dropped on the wood). This loading can cause the annual rings to separate from one another, reducing material properties.

While wood is considered to be fairly resistant to attack by many chemicals, it will degrade upon prolonged exposure to strong acids or bases. Strong acids will tend to remove cellulose and hemicellulose, leaving the residual lignin behind. Acid-degraded wood looks like wood that has been attacked by brown rot fungi, but no fungi can be detected and the wood has a much lower pH than normal wood. The removal of the cellulose in acid-degraded wood sharply reduces its strength. This effect generally occurs so slowly that wood tanks are commonly used to store dilute acid solutions.

15.2.2 Strong Alkali or Bases

Strong alkali or bases tend to attack the hemicellulose and lignin, leaving the cellulose largely whole. Wood exposed to strong bases tends to be white and bleached, much like wood attacked by white rot fungi. This reaction is similar to the production of paper, wherein the lignin is removed, leaving cellulose-rich wood fibers behind. As with the strong acids, the absence of fungal hyphae and a very elevated pH are indicators of alkaline damage.

15.2.3 Salts and Heat

Salts can also damage the wood. Wood exposed to salt water tends to absorb the salty water. Repeated wetting and drying of wood fibers near the surface will result in a concentration of salt in the cell lumens. These cells can burst if they absorb too much salt. Although the overall effect on wood properties is minimal, the burst fibers can accumulate on the wood surface, creating a fuzzy appearance.

One well-known agent of degradation of wood is fire. Wood will combust when its temperature exceeds 275 °C. Exposure of wood to elevated temperatures below 275 °C can result in a gradual loss of material properties. The wood darkens and, as the damage proceeds, cross-breaks develop that resemble those associated with attack by brown rot fungi.

Hemicelluloses are generally most susceptible to heat damage, followed by cellulose and, finally, lignin. Damage can begin to occur as temperatures reach 100 °C, but the effects are very gradual at these lower temperatures. Hemicelluloses begin to decompose between 225–325 °C, while lignin is more temperature resistant, decomposing between 250–500 °C. Cellulose decomposes between 325–375 °C.

Heat-damaged wood in many ways resembles wood damaged by brown rot fungi, and the two were often considered to be caused by the same agents before people understood that fungi caused decay

15.3 BIOTIC AGENTS

From the time wood is formed in the living tree, it is susceptible to attack by a diverse array of organisms specialized for gaining access to energy rich polymers. Trees, however, are not defenseless against this onslaught. Living trees possess a variety of techniques for limiting attack, including the ability to produce copious amounts of resin or gums to wall off attacking agents. They also produce anti-fungal compounds that slow microbial attack and wall off or block fluid flow to infected areas. These activities cease once the tree dies and its resistance to degradation shifts to more passive approaches, including producing waxes that slow moisture uptake and heartwood extractives that limit attack, and ultimately, the intricately arranged lignocellulose matrix. The importance of the latter capability should not be overlooked. Many organisms are cellulolytic, but only a small percentage are capable of tapping the energy stored in wood because of the protection afforded by the lignin matrix.

Protecting wood from biological degradation requires understanding that nearly all wood-degrading organisms require water, oxygen, temperature and a food source (Figure 15.2). Most wood-degrading organisms are aerobic (require oxygen), but the oxygen levels required for decay by some fungi can be quite low (1–10 ppm). Air contains 19–20% oxygen, so this element is rarely limiting except in very wet

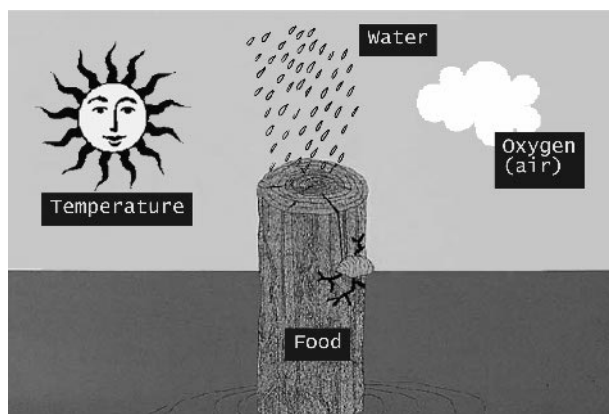


FIGURE 15.2 Most biological agents of deterioration have four basic requirements to cause damage.

environments where water completely fills the wood cell lumens to exclude air. While anaerobic bacteria can function in these environments, the rate of attack is slow and not a significant factor, except when wood is submerged for many decades.

Organisms that degrade wood have broad temperature tolerances. Many function at just about freezing, while others continue to damage wood at temperatures approaching 40 °C. Most wood-degrading organisms have temperature optima between 20–28 °C, but can survive prolonged exposures below 0 °C. Nearly all fungi can survive prolonged freezing, but most wood degrading organisms succumb to prolonged exposure above 45–50 °C, as these temperatures irreparably denature enzymes and other essential components of cellular machinery. Fungi are completely eliminated when the wood is heated above 67 °C for at least 75 minutes.

Water is perhaps the most critical microbial requirement. Water swells the wood, opening the polymers to allow penetration of enzymes; it allows for diffusion of enzymes to wood and breakdown products to the organisms; and, most importantly, it is a reactant. Many steps in the degradation of cellulose and hemicellulose require the addition of water by hydrolysis. For most organisms, the presence of free water is required before substantial degradation can occur. Although some insects can attack wood that is much drier, the point where free water is present (fiber saturation point) and most organisms can degrade wood, occurs between 27–30%, although this figure can vary. Moisture control plays a very important role in most approaches to limiting degradation of structures, and there are thousands of examples of well-designed and -maintained wood buildings that have stood for centuries. In the absence of moisture exclusion, the wood must be supplementally protected to provide acceptable service.

The food source for most wood-degrading organisms is the wood itself, although carpenter ants, carpenter bees, Pholads, and woodpeckers are all excellent examples of organisms that live in wood but do not use it as a food source. Most organisms, however, use the energy-rich polymers in wood as their primary food source, and have developed enzyme systems capable of unraveling the lignocellulose matrix to varying degrees. One approach to wood protection is to either alter the wood structure or poison it to make it toxic to attacking organisms. Our wood preservation industry focuses on this approach.

Preventing degradation generally involves removing or limiting one or more of the four basic requirements shown in Figure 15.2.

15.4 DECAY ORGANISMS

A range of organisms has evolved to either use wood as food source or live within its structure; these include bacteria, fungi, insects, marine borers, and woodpeckers. Each group has specific needs and has different effects on the wood.

15.4.1 Bacteria

Bacteria are single-cell prokaryotes that lack membrane-bound organelles; they reproduce by binary fission. While considered to be primitive organisms, bacteria have the ability to rapidly reproduce and occur in a variety of extreme environments. Bacteria that degrade wood tend to be relatively slow acting and limited in the types of damage they cause.

Logs that are stored in water for long periods can experience bacterial degradation of the pit membranes that connect individual cells. This increases the permeability of the wood and, once the log has absorbed enough water, it will sink to the bottom of the body of water. Bacterially-damaged logs also tend to wet more easily and will finish unevenly when painted.

Some bacteria are also capable of causing more substantial damage to the wood cell wall. Tunneling and cavitation bacteria produce tube- and diamond-like cavities within the wood cell walls in wood exposed in moist forest soil or immersed in water for long periods. Although this attack is largely confined to the wood surface, many of these bacteria are chemically tolerant and appear to be one of the first colonizers of preservative-treated wood in many environments. These bacteria do not cause substantial wood damage in most environments, but they can become important in submerged wood exposed for long periods.

15.4.2 Fungi

Fungi are filamentous, heterotrophic eukaryotes. While they are often compared with plants, they are not directly related to this group—they represent a completely separate order of organisms. Fungi that colonize wood-based materials can be characterized on the basis of the damage they cause to the wood, or the taxonomic origin of the particular fungal species. Wood damage is generally classified as mold, stain, brown rot, white rot, and soft rot. The wood-colonizing fungi include members of the *Ascomycetes*, *Fungi Imperfecti* and *Basidiomycetes*. In many cases, different fungi in the same taxonomic

group can cause different types of wood damage. For the purposes of this review, we will address fungal decay from the perspective of the damage caused to the wood.

15.4.2.1 Mold Fungi

Mold fungi are primarily *Ascomycetes* and *Fungi imperfecti* that use the sugars stored in the ray cells of the sapwood (Figure 15.3). The hyphae of these fungi are clear, but produce prodigious amounts of pigmented spores that discolor the wood surface. These spores can be removed by brushing the wood surface. Molds do not cause substantial damage to the wood they attack, although they can make the wood more permeable and therefore more easily wetted. This can increase the likelihood of decay. The spores of mold fungi can be allergens that aggravate asthma. Some mold fungi produce toxic compounds called mycotoxins. The most well-known example of a mycotoxin is aflatoxin, produced by *Aspergillus flavus* in peanuts. While these toxins can be important in some applications, there is no evidence that they are important in wood.

15.4.2.2 Stain Fungi

Stain fungi are *Ascomycetes* and *Fungi Imperfecti* that also utilize the stored sugars in the ray cells (Figure 15.4). The primary difference between these fungi and molds is that their hyphae eventually become pigmented a dark brown color, and this color gives the wood a bluish cast. Stain fungi cause permanent discoloration to the wood, reducing value where appearance is an issue. They also cause some reductions in toughness, which can limit uses where material properties are important.

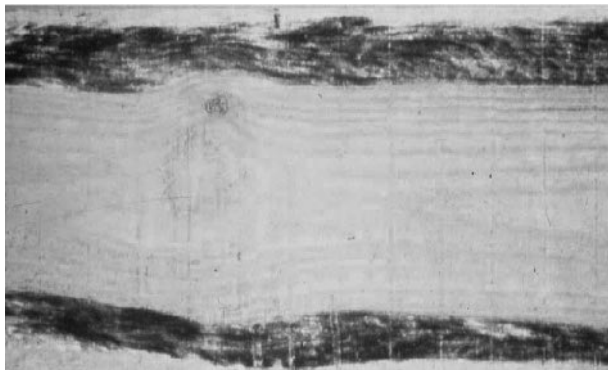


FIGURE 15.3 Mold fungi tend to grow on the sapwood of wet freshly sawn lumber.

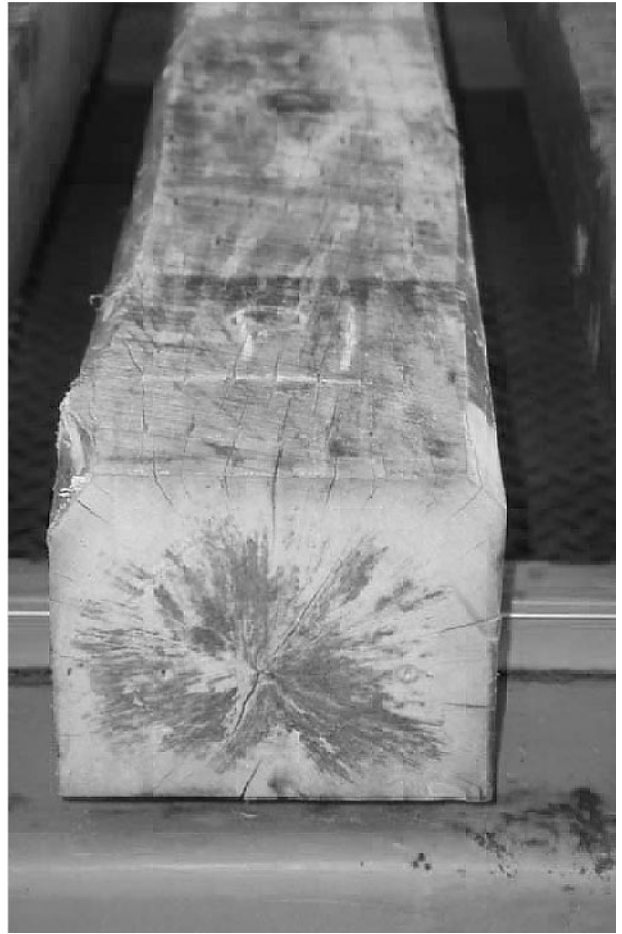


FIGURE 15.4 Sapstain fungi tend to cause damage more deeply in the wood, as shown by this railroad tie (sleeper).

15.4.2.3 Brown Rot and White Rot Fungi

Brown rot and white rot fungi are both primarily caused by *Basidiomycetes*, although some *Ascomycetes* also cause white rot attack (Figure 15.5). Brown rot fungi attack the stored sugars in the ray cells, but they also attack structural components in the wood cell wall. Brown rot fungi primarily attack cellulose and hemicellulose, leaving behind a modified lignin. The wood becomes brown (thus the name), and develops numerous cross-breaks as a result of the loss of integrity of the cellulose microfibrils. Brown rot fungi are important in wood structures because they tend to cause substantial losses in strength at very early stages of attack. As a result, wood that appears sound may fail suddenly. They are also important because these fungi tend to be more common on softwoods, and softwoods are the dominant building material in temperate climates.

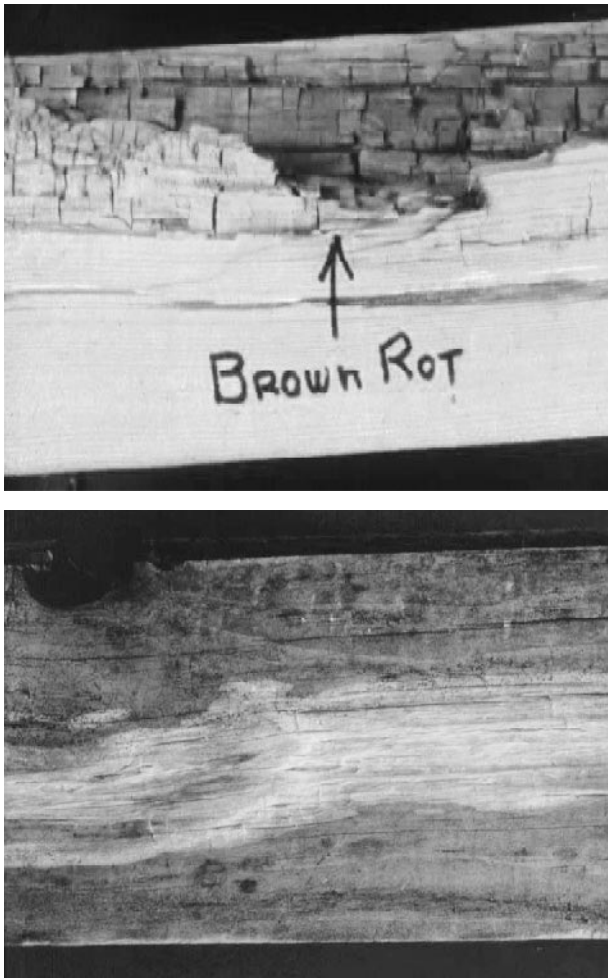


FIGURE 15.5 White and brown rot are distinguished by the patterns of damage as well as the color of the affected wood.

White rot fungi are believed to be more advanced because they have evolved the enzyme systems necessary to degrade all three wood polymers. In fact, some white rot fungi preferentially degrade lignin. White rot fungi tend to degrade wood at the same rate as the breakdown products are utilized. Thus, decay by these fungi is more gradual and the effects tend to become visible as the damage occurs. White rot fungi tend to be more prevalent on hardwoods.

15.4.2.4 Soft Rot Fungi

Soft rot fungi are found on wood in very wet environments, such as wood exposed in soils with high amounts of organic matter, or wood that is subjected to extreme changes in moisture content (such as the

above-ground parts of fences). Soft rot fungi were not fully described until the early part of the 20th century, although their damage was noted much earlier. There are two types of soft rot attack. Type 1 attack occurs when the fungal hyphae grow through the S-2 cell wall layer, producing a series of diamond-shaped cavities. Type 2 attack occurs when the fungi produce a gradual erosion of the S-2 cell wall layer from within the lumen. Both types of damage are primarily caused by *Ascomycetes* and *Fungi Imperfecti*. Some fungi can cause both types of damage, although Type 2 is the more prevalent attack mode. These fungi can become important because they attack the wood surface, gradually reducing the cross-sectional area until the wood fails. Soft rot attack is important in specialized environments, such as where wood is used in cooling towers or when poles are exposed in soils with a high nutrient level. These fungi appear to have adapted to thrive where more conventional brown and white rot fungi are less viable. In addition, many soft rot fungi are tolerant of preservatives, making them the first fungi to colonize preservative-treated wood.

15.5 INSECTS

A variety of insects have evolved the ability to use wood as either a food source or as a shelter in which to rear their young. While members of at least six insect orders attack wood, for practical purposes, only the *Isoptera*, *Coleoptera*, and *Hymenoptera* cause substantial economic damage to wood products. The characteristics of each will be addressed below.

The *Isoptera* (termites) are widely distributed around the world between 50 degrees north and south latitude. Termites are social insects with a highly organized caste system of workers and soldiers that revolves around providing for the queen. Termite workers avoid light and, therefore, are rarely seen outside the nest except when the winged reproductives swarm from the nest to start new colonies. Termites use wood as a food source, usually with the help of symbiotic protozoa in the mid-gut that help them to digest cellulose.

The groups of termites that attack wood can be broadly grouped into subterranean, dampwood, and drywood termites. Subterranean termites generally live in soil contact, although their connection to the soil can sometimes be remote. Some subterranean termites can attack wood well above the soil by constructing earthen tubes that allow them to carry moistened soil into a structure to wet the wood and allow it to be attacked. Colonies of subterranean ter-

mites can range from several hundred thousand to seven to eight million workers for species such as the Formosan termite.

Subterranean termite attack in wood structures can be addressed by using a combination of physical and chemical methods. First, structural contact with the soil is avoided. In addition, the soil beneath and surrounding the structure is either drenched with an insecticide, covered with a very fine-mesh stainless steel screen that prevents termites from moving upward, or covered with a fine granite or pumice gravel that limits termite tunneling. Finally, in areas with extreme termite attack, any wood in the structures is preservative-treated or is naturally termite resistant. Combinations of practices sharply reduces the risk of subterranean termite attack.

As the name implies, dampwood termites attack very wet wood which is not always in soil contact. These species are not widely distributed, but can be regionally important. They tend to live in smaller colonies (100,000 workers) and are more easily controlled by removing the source of moisture.

Drywood termites attack very dry wood that is usually above the ground, such as dead branches on trees (<13% moisture content). These termites are common in houses in desert areas, where they can cause extensive damage to roofs and trusses. The damage is often difficult to detect and even harder to control. Prevention is usually accomplished by screening vents to prevent termite entry. Once termites invade, fumigation is often the only solution to eliminating attack.

15.5.1 Coleoptera

Coleoptera (beetles) represent the largest order of insects, and a variety of beetle species have evolved to attack wood. Beetles can directly cause damage as they tunnel through the wood, or can vector fungi that subsequently stain or decay the wood (Figure 15.6). Many species of beetles lay their eggs on freshly fallen trees; the larvae then tunnel into the wood beneath, where they continue to damage the wood. Once the larvae have obtained a sufficient amount of nutrients, they pupate and then emerge as adults. The adults tunnel out of the wood and seek new host material. These beetles rarely re-infest the same piece of wood. Beetles that attack freshly fallen trees include bark beetles, ambrosia beetles, longhorn borers, and buprestids. Although all of these insects can cause wood damage, their impact can largely be controlled by timely processing of harvested timber. Their presence in finished prod-



FIGURE 15.6 Adult beetles, such as this golden buprestid beetle (*Buprestis aurulenta*), leave small exit holes on the wood surface, but can cause substantial internal damage.

ucts is an indication that materials may have been improperly stored.

Once wood has dried, it can sometimes be attacked by powderpost beetles. There are several groups of powderpost beetles, each with its own special range of wood species preferences and moisture content ranges. Powderpost beetles tend to attack the sapwood and prefer woods with larger pores. These beetles lay their eggs on the wood surface, then the emerging larvae tunnel into the wood, leaving little evidence of their presence on the wood surface. The damage is usually detected by the presence of small, round exit holes produced as the adults leave to seek new wood. Powderpost beetle prevention is relatively simple and can include coating the wood surface, application of insecticides, and regular inspection to detect infestations before they become widespread in a structure.

15.5.2 Hymenoptera

Hymenoptera include ants, bees, and wasps. While wood can be attacked by carpenter bees and *Sirex* wasps, by far the most damaging group of insects in this order are the carpenter ants. Carpenter ants are social insects with a structured caste system that includes major and minor workers who all serve the queen. Carpenter ants do not use wood as a food source, but instead tunnel through a log or timber, creating galleries in which to raise their larvae. The workers then leave the nest to forage for food to feed their young and support the queen. Carpenter ant colonies can range in size from several hundred to over a hundred thousand workers. Preventing carpenter ant damage can be challenging, since the workers do not eat the wood. The application of insecticidal barriers can help limit attack, but the primary focus on ant prevention is to remove woody debris from around a structure that might be suitable ant habitat.

15.5.3 Marine Borers

While the moisture contents of wood exposed in marine environments are too high to allow for attack by insects or most terrestrial fungi, several groups of marine organisms have evolved the ability to use wood for either shelter or as a food source. These organisms are extremely important recyclers of wood in marine environments, and, when wooden sailing ships ruled the seas, were the cause of many ship sinkings.

15.5.3.1 Shipworms

Shipworms are clam-like mollusks that begin life as free-swimming larvae. These larvae eventually settle on and bore into the wood. As they bore into the wood, their bodies become extended and worm-like, in some species reaching up to 1.5 m in length in as little as two years. These organisms are difficult to detect on the wood surface, although they may extensively damage the interior of the wood as they feed. Shipworm attack can be easily prevented by the use of wood treated with creosote or one of the inorganic arsenical-based preservatives.

15.5.3.2 Pholads

Pholads are also clam-like mollusks that begin life as free-swimming organisms that eventually settle on and bore into the wood. Pholads damage the

wood as their shells rub into the wood. This weakens the wood surface, which is then eroded away by wave action. Pholads are typically found in tropical and sub-tropical waters. Their attack can be easily limited by the use of creosoted wood.

15.5.3.3 Limnoria

Limnoria are mobile crustaceans that tunnel into and attack the wood surface, particularly around the tidal zone. Limnoria do not use wood as food source, and are primarily believed to use wood as shelter from predators. Although their tunnels are shallow and small, continued wave action wears away the wood weakened by these tunnels, forcing the limnoria to tunnel ever-deeper into the wood. This damage becomes particularly evident around tidal zones, where affected wood pilings will take on an hour-glass shape. Limnoria damage can be limited by the use of wood treated with creosote or the inorganic arsenicals. In some areas, *Limnoria tripunctata* is tolerant of creosote and the wood must be treated with the arsenicals. In extreme cases, dual treatments with both creosote and one of the arsenicals might be necessary.

While marine borers are often overlooked as wood destroyers, they cause an estimated \$500 million in damage per year in North America.

15.6 MAGNITUDE OF WOOD DETERIORATION LOSSES

Although there are no national data collection systems for quantifying wood losses caused by various agents of decay, it has been estimated that fully 10% of the timber cut each year is used to replace wood that has that has decayed in service. While this seems to be a staggering amount of wood, when one considers a few estimates for individual losses, the overall figure becomes more believable. For example, termites cause over \$1.5 billion in damage each year, primarily in the southeastern United States. Building decay has been estimated to cost \$364 million in the state of California; Since California represents about 10% of the U.S. economy, it could be inferred that, nationally, such losses might approach 10 times that amount. Compiling these estimates of losses caused by the various agents of wood decay-points to the staggering effects of biodeterioration in just one country. So what can be done to reduce this financial impact? In the next sections, we will dis-

cuss how to prevent wood deterioration, using our knowledge of what the various organisms require.

15.7 WOOD PROTECTION

Wood can be protected against biological degradation by limiting one or more of the four basic factors required for growth.

15.7.1 Limiting Oxygen for Limiting Degradation

It is generally not feasible to limit oxygen in wood structures, but there are phases in wood processing when it is, and there are some special applications where the exposure conditions are inherently oxygen-limiting.

Ponding or sprinkling logs with water has long been used to limit checking during log storage, but these practices also limit the potential for both insect and fungal attack. Soaking raises the wood moisture content to well over 100%, filling the lumens and excluding air. Prolonged water storage, however, can allow bacteria to proliferate. These bacteria degrade the pits that connect individual cells, making the wood more permeable. Excessive water sorption in these more permeable logs can lead to the logs sinking in the pond. A second problem with bacterial growth in long-term wet storage is a tendency to develop enzymatic stains that reduce lumber value. Careful inventory management to minimize storage is a simple method for reducing the risk of both sinkers and enzymatic stains.

Oxygen is also often limited when the wood is continuously exposed to water. Examples of such applications include foundation pilings, which are often driven into the water table; wood immersed in cooling towers; and the immersed portions of freshwater docks. The high moisture contents under these conditions generally limit oxygen availability, although care must be taken to ensure that the immersion is continuous, since repeated cycling between wet and dry conditions can allow decay fungi to begin to attack the wood.

15.7.2 Limiting Temperature

As with oxygen, there are relatively few applications where temperature can be controlled to the extent that microbial attack is limited, but temperature can be used effectively in other ways.

For example, for many years mills attempted to harvest logs during cooler times of the year, when insect and microbial activity was lowest. This is not feasible today because most mills run all year and must continually harvest materials.

Temperature can also be used as a wood sterilant. The two best examples of this approach are steaming for phytosanitation, and kiln drying. Generally, wood must be heated to 71 °C for a minimum of 75 minutes to eliminate fungi present. Insects succumb at much lower temperatures, so most sanitation guidelines assume that temperatures necessary to kill fungi are more than adequate for insects or other wood-inhabiting pests. Wood is an excellent insulator, so heating to the required temperature can take many hours, depending on the dimensions of the wood, the density, and the moisture content. Despite the time and associated energy costs, steaming is one of the processes recommended for disinfesting pallets and other wood products transported internationally. One disadvantage of steam heating is its temporary effect. Steam will kill nearly all life forms, but it does not provide lasting protection. As a result, steamed wood that remains wet can be colonized by a number of fungi and insects.

Kiln drying has the dual effect of using heat to kill any established organisms and lowering the wood moisture content to levels that limit renewed attack by most organisms. Kiln drying also stabilizes the wood. The disadvantages of kiln drying lumber are higher costs due to the energy required, and the introduction of some physical drying defects. In addition, kiln dried wood can still be attacked if it is rewetted, making it important to keep such lumber dry.

Heating either through steaming or kiln drying is clearly a temporary approach for protecting wood. There are also some novel approaches to alter the chemistry of wood to render it either less hygroscopic or susceptible to fungal attack. Heating at high temperatures in the absence of oxygen destroys hemicelluloses, and appears to permanently alter the ability of wood to sorb moisture. These technologies were developed several decades ago, but have recently emerged in Europe amid the search for non-chemical strategies for wood protection. Limited testing suggests that this thermally treated material is more durable than untreated wood, particularly if it is kept out of direct soil contact. However, these gains are offset by higher costs, substantial losses in material properties, and, with some heat treatment processes, a tendency to produce furans and other compounds that have environmental impact. Despite

these limitations, heat treatments are likely to receive continued interest to placate an increasingly chemophobic society.

15.7.3 Limiting Moisture

Because moisture is a major factor in wood deterioration, controlling moisture is, by far, the most common method for protecting wood. There are two types of moisture in wood: bound and free. Bound water is the water that sorbs to the wood structure. Free water is the water that is present in the cell lumens and other interstices. Free water generally occurs as the moisture content reaches 25–30% (weight basis), although it can vary by species. Although there are exceptions, most wood-inhabiting organisms require that free water be present before they can cause substantial damage to the wood.

Water plays a number of critical roles in the decay process. Water is a swelling agent in the wood, making the wood cell walls more accessible to microbial enzymes. Water is also a reactant in many degradation processes. Hydrolysis of cellulose and hemicelluloses through the addition of water to break the B 1-4 linkages is an important step in the degradation process. Water is also the medium of diffusion for the enzymes that move out of the fungi into the surrounding wood, as well as for the breakdown products as they diffuse back to the cells. The presence of free water is essential for all of these processes.

The knowledge that free water is necessary for attack can be exploited to create conditions that limit moisture. Builders have long known that moisture can be excluded in a number of ways, including the use of steep roofs that shed water, gutters and downspouts that route water away from the structure, roof overhangs that protect side walls from wetting, construction that avoids wood/soil contact, and the use of coatings to exclude moisture. While none of these approaches can completely exclude moisture, in combination with periodic maintenance they can all sharply reduce the risk of deterioration, as evidenced by the numbers of ancient wooden structures that exist in some countries.

15.7.4 Altering the Food Source

While moisture exclusion is the most common method for limiting biological degradation of wood, there are many applications where the wood is likely to be wet for some or all of its useful life. In these instances, the only practical method for preventing deterioration depends on the presence of compounds

that are toxic to the various agents of decay. These compounds can be naturally produced within the tree, or supplementally delivered to the finished product.

15.7.4.1 Natural Durability

The heartwood of some wood species has the ability to resist attack by one or more groups of the various agents of decay. As the sapwood in a standing tree dies, a series of complex chemical reactions convert the stored sugars into a range of toxic compounds that protect the inner heartwood of some species from attack (Figure 15.7). Humans have long exploited these materials for constructing durable structures. For example, the Phoenicians constructed their sailing vessels from durable cedars of Lebanon, and the Colonial navies used naturally durable live oak. While these materials can provide exceptional performance, not all species produce durable heartwoods; those that do cannot possibly provide all of the material needed. As an alternative, non-durable woods can be supplementally protected with chemicals, the approach taken by the various wood preservation industries.

Wood preservation has its origins in our earliest written history. Shipbuilders daubed various extracts on the surfaces of their boats in hopes of avoiding

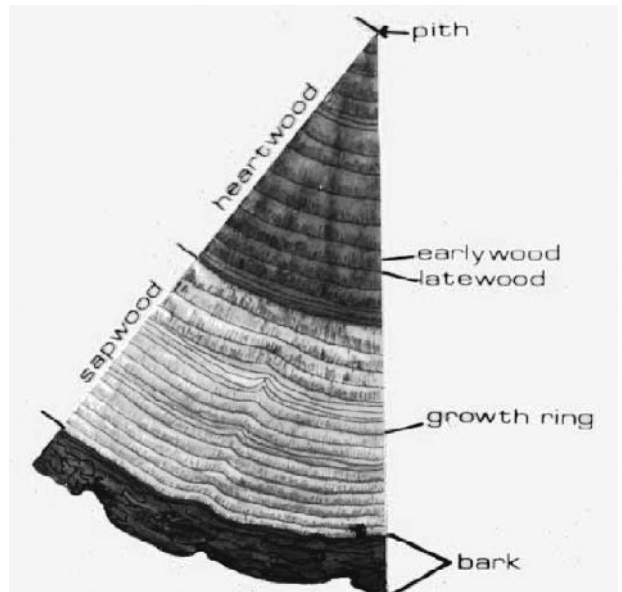


FIGURE 15.7 The outer living part of the tree (sapwood) tends to be non-durable, while the heartwood of some species exhibits resistance to attack by insects, fungi, or marine borers.

shipworm attack, but these efforts were largely ineffective. The so-called modern wood preservation industry can trace its origins to the desire by the British navy to protect its wooden vessels. That navy supported a series of efforts that lead to the nearly simultaneous development of creosote as a wood preservative, and the pressure-treating processes that force this material into the wood.

Wood treatment can be arbitrarily divided into short-term protection lasting less than six months, and longer-term protection that may need to last 50 or 100 years. Short-term protection is typically used to protect wood for limited periods of time when conditions will be suitable for decay. Such applications might include the protection of freshly sawn lumber, where the wood must be protected from stain and mold fungi for several days or months until it dries below the point where fungal attack can occur. The amount of chemical and the depth to which it must be applied to be effective will differ substantially from that needed to protect wood exposed in soil in a tropical environment for many years.

There are a variety of methods employed for moving chemicals into wood. In general, treatment involves introducing an adequate amount of chemical at a depth that will achieve the desired degree of protection. Thus, most treatment standards address *penetration* (the depth to which the chemical penetrates) and *retention* (the amount of chemical deposited in a specific area of the wood). Retention is usually expressed as weight of chemical per unit area of wood (pounds per cubic foot or kilograms per cubic meter).

15.8 TREATMENT METHODS

Treatment methods can vary with the application, the chemical, and the wood species. It is important to remember that what works well with one species or chemical may work poorly with a different combination. Prior testing or adherence to a known standard can reduce the risk of producing inferior treatments.

15.8.1 Brushing

Preservatives have been brushed on wood surfaces in hopes of extending surface life for as far back as history has been recorded (Figure 15.8). As one might expect, brushing provides a thin surface barrier against fungal or insect attack. The chemical



FIGURE 15.8 Brushing and soaking of wood in preservatives produce a relatively shallow zone of protection.

moves into the wood surface through capillary action, and the depth of penetration depends on the wood species and the chemical solvent. Brush treatments are usually applied by flooding the wood surface, allowing the chemical to stand for a few seconds, then brushing off the excess. These treatments can provide some protection when wood is exposed above the ground, especially if they are regularly reapplied, but are of little help in direct soil contact. The exception is with naturally durable wood species, where brush treatments have been shown to extend the life of species such as cedar or redwood. (Newbill and Morrell, 1990).

15.8.2 Dipping or Soaking

Dipping or soaking in preservative can provide slightly better protection than brushing, but once again, the movement of chemical is primarily through the capillary structure of the wood. The use

of longer soaking times can improve preservative penetration in the sapwood, but the depth of treatment will largely be limited by the heartwood. Treatment can also be improved by heating the solutions. Heating reduces the viscosity of the treatment solution, easing flow through the pits.

Dip or soak treatments are normally used where more sophisticated treatment methods are unavailable, but several industries rely heavily on dip treatments. In North America, nearly all of the wood used to produce exterior windows and doorframes is dip treated prior to use. Previous studies have shown that most windows decay at the joints along the end-grain. Since end-grain sorbs treatments more readily than the side grain and the species employed for these products are fairly permeable, dipping has long provided adequate protection for this exposure. Dipping is also used for treatment of building framing with boron compounds. In this case, the wood is treated shortly after cutting and the boron diffuses into the wet wood during a storage period prior to shipping. This process is also used to a limited extent for logs destined for log homes.

Dipping is also widely used for short-term protection of freshly sawn lumber against mold and stain fungi. The primary focus of these treatments is prophylactic, and short dips (30 seconds) provide a shallow barrier against fungal attack. These treatments provide three to six months of protection until the wood can be dried to levels where fungal attack is naturally limited.

15.8.3 Two-Stage Dip Diffusion

Two-stage dip diffusion treatments have also been employed in various part of the world. Originally developed using immersion in a copper compound followed by immersion in a chromium compound, these processes were developed for applications where access to more sophisticated equipment was lacking. In theory, the copper would diffuse into the wet wood, then the chromium would also diffuse inward. The hexavalent chromium would react with both the copper and wood to form an insoluble precipitate. Thus, the treatment becomes somewhat fixed to the wood. More recently, double diffusion treatments have been proposed, using sodium fluoride followed by copper sulfate. Double diffusion treatments were typically used for treatment of fence posts and other low cost materials in non-structural applications. Neither of these compounds is strongly fixed to the wood, making it less likely that this treatment will provide the long-term protection afforded by the copper/chromium combination.

15.8.4 Thermal Treatments

Thermal treatments are similar to soaking, but the process involves more heating and some pumping of fluids. In a thermal process, the treatment solution is added to a tank or vessel containing the wood, then the solution is heated for a period of eight to 16 hours. The solution is removed, then reintroduced into the vessel. This reduces the solution temperature slightly, and the cooler solution contacting the slightly hotter wood creates a partial vacuum that helps draw solution into the wood. The thermal process is used to treat wood species with relatively thin sapwood.

A variety of other treatment processes have been developed over the past century, but most of these have disappeared because they were too labor intensive, posed too much of a risk to workers, or were too expensive. One process that is periodically used is the *Boucherie* process. In this process, a cap is placed on a freshly cut cross-section of a tree. The cap has a hose which runs to a reservoir of treatment solution, which is elevated over the wood. The freshly cut tree is still capable of conducting fluids, and the slight downward pressure from the elevated solution combined with the conduction system of the wood serves to move the chemical upward into the tree. The result is a treated sapwood which, although not as well treated as might be possible using pressure treatment, can provide five to 10 times the service life of untreated wood. This process has been used in many tropical countries that lack pressure treatment facilities. It can also be accomplished by girdling the standing tree and placing a reservoir of chemical around the girdled area. The chemical solution is then drawn up the tree, preserving the sapwood.

15.8.5 Other Treatment Processes

The remaining treatment processes use combinations of vacuum and/or pressure to drive chemicals more deeply into the wood. All of these processes use enclosed treatment vessels that have the capacity to draw vacuum and apply pressure (Figure 15.9). They may also have the capability of applying steam, heating solutions, and condensing vapors that are emitted from the vessel. The basic treatment plant has changed little from that used in the late 1800s, with the exception that the plants have been redesigned to reduce the risk that chemicals will leave the treatment site. As a result, treating plants are generally covered and the ground surrounding the vessel is lined with a concrete drip pad. In addi-



FIGURE 15.9 Example of a pressure treatment cylinder.

tion, all pipes and tanks are above the ground so that leaks can be detected before they become a problem. Finally, some plants have air filtration systems to capture any organic vapors.

15.8.5.1 Vacuum Processes

In the vacuum process, the wood is placed in the treatment vessel, then a vacuum is drawn over the wood. The treatment solution is added to the vessel, then the vacuum is released. In some processes, this may be done a second time to enhance uptake. The vacuum process is usually used for treating windows and doorframes of easily treated species where the goal is primarily to achieve acceptable end penetration of a permeable wood.

15.8.5.2 Pressure Processes

There are three basic pressure processes, the full cell, and two variations of the empty cell process. All of these processes are primarily designed to treat the sapwood portion of the wood, although limited penetration of the heartwood may occur. As a result, pressure treatment produces an envelope of protection whose depth varies with wood species (Figure 15.10). The *full cell process* was patented by John Bethel in the 1830s; it involves placing the wood into the treating vessel, drawing a vacuum and adding the treatment solution (Figure 15.11). The vacuum is then released and the pressure is raised to the desired level and held until the proper amount of chemical solution has been injected. The pressure is then released and the solution is withdrawn. The pressure release causes some of the injected solution

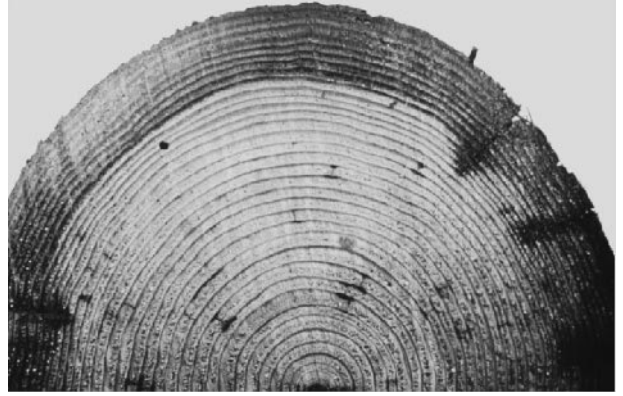


FIGURE 15.10 Preservative penetration in Douglas fir showing preservative treatment of the sapwood, but none in the heartwood.

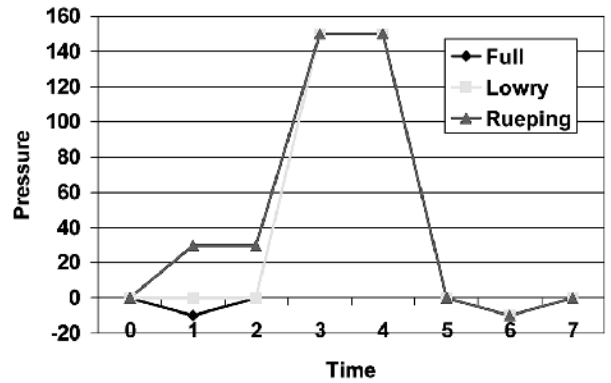


FIGURE 15.11 Schematic showing the pressure stages employed with the full (Bethel), Lowry, and Rueping cycles for pressure treatment of wood.

to be expelled from the wood in a process that is called kickback. The difference between the gross solution injected and the amount recovered from the kickback is called the net injection. This is the amount of chemical solution injected in the wood, as shown by the treating plant gages. The full cell (Bethel) process is generally used to treat wood with waterborne solutions, where the chemical concentration can be easily adjusted, or to treat wood with creosote to very high retentions.

Treatment by the full cell process using oil-based solutions generally produces excessively high loadings of oil that are not needed for adequate performance in terrestrial environments. For this reason, the *empty cell processes* were developed (Figure 15.11). These processes eliminate the vacuum, which results in a cylinder of air remaining in the wood at the start

of the pressure process. As the pressure is raised, this air is compressed in the wood. As the pressure is released at the end of the cycle, this air expands outward, carrying with it the preservative solution. As a result, the kickback is greater and the net injection is lower. There are two variations of the empty cell process. In the *Lowry process*, the treating solution is added and the pressure is raised and held until the desired gross injection occurs. In the *Rueping process*, the pressure is raised slightly (30–50 psi), then the treating solution is added and the pressure is raised to the target level. The additional air introduced into the wood prior to adding treating solution increases the amount of kickback produced at the end of the cycle, further reducing net injection.

15.9 TREATMENT STANDARDS

As might be expected, standards have evolved in each country or region to support treatment of the various commercial wood species. There are currently no international wood preservation standards, probably because of the array of chemical preferences, wood species employed, and regulatory issues regarding chemical usage. North America, which uses 60% of the world's treated wood production, uses voluntary consensus standards developed by the industry and wood users. The North American standards are results-oriented, in that they specify a certain target treatment level and leave the actual processes to the discretion of the treater. In other parts of the world, standards are developed by government entities and their use is mandatory in many applications. Most standards also determine the treatment level using a Hazard Class system, whereby treatment levels increase with increasing risk of damage. Thus, Hazard Class 1 is used to describe interior wood that will remain dry but might be subjected to insect attack, while Hazard Class 5 or 6 (depending on the country) might be wood exposed to marine borer attack.

15.10 NEW TREATMENT PROCESSES

The existing treatment technologies are clearly dated, but they have survived because they are inexpensive and largely effective for their intended purposes. These processes do have certain limitations. For example, pressure treatment of many composites with waterborne tends to induce permanent deformation in the products, reducing their value. In addition, pressure cannot completely overcome the

inherent resistance of many wood species to fluid ingress, resulting in incomplete treatment of many materials. These limitations have stimulated a diverse array of alternatives, but the two most feasible appear to be vapor phase treatments and supercritical fluid impregnation.

15.10.1 Vapor Phase Treatments

In vapor phase treatments, a compound with a high vapor pressure such as trimethyl borate is introduced into a vessel containing the wood under a vacuum. The chemical volatilizes the compound (in this case, the trimethyl borate), diffuses into the wood, and reacts with any moisture present to produce methanol. The reaction releases the borate, which is deposited into the wood. The vacuum is released, leaving some methanol and the borate in the wood. This process has been used to treat a number of composites, but its application is limited because the wood being treated cannot be too wet (i.e., moisture contents less than 6–8%), and the resulting treatment is not fixed. A similar process was studied with copper compounds, but it was never commercialized.

15.10.2 Supercritical Fluid Treatments

Supercritical fluid (SCF) treatments represent another possible treatment alternative. In these processes, a fluid (usually carbon dioxide) is heated and pressurized above the respective critical points. A SCF has properties that are intermediate between those of a gas and liquid. For example, the SCF may have diffusivities approaching those of a gas, meaning that it can easily move through wood that would resist liquid flow. In addition, some SCFs have solvating properties that approach those of a liquid, meaning that the fluid can carry sufficient amounts of biocide into the wood to afford protection against biodegradation. SCFs have been investigated on a number of materials and are currently being commercially applied in Denmark, but the process still needs considerably more research before it is more broadly commercially applicable.

15.11 ENVIRONMENTAL CONSIDERATIONS

Virtually all of the wood treating processes use some type of biocide to protect the wood. The riskiest part of the total life cycle of the product occurs during the treatment process. As a result, most regulations are

directed at the application stages of the life cycle. For example, in most countries, treatment plant workers must have some type of specialized training and must pass some type of written test showing that they know about pesticide handling and safety. In addition, plants are designed to minimize losses of chemicals to the surrounding environment. For example, the area around treating cylinders is generally a concrete pad designed to capture any drippage or leaks. Monitoring wells are placed at strategic locations around the plant to detect any groundwater contamination, and the drip pads are often covered to reduce the amount of rainfall striking the freshly treated wood and reduce the amount of runoff from the drip pad. These practices sharply reduce the risks associated with the manufacture of treated wood.

Recently, concerns about the use of treated wood have emerged regarding the potential for loss of preservative from the wood into the surrounding environment. There is no doubt that preservatives migrate from the wood into the surrounding environment, be it water or soil. The extent of movement is a function of the wood species, amount and type of chemical, the surrounding environment (soil type, rainfall, organic matter, etc.), and the treatment processes employed. For example, higher loadings in more permeable species are more likely to result in chemical migration than lower loadings in the same material. Treatment processes that fail to relieve internal pressure at the end of the process are more likely to lead to bleeding of oilborne preservatives once the wood is in service, and failure to properly condition wood treated with waterborne materials after treatment (usually by application of heat) can result in incomplete fixation, which will lead to excessive leaching. Some segments of the treating industry have responded to these issues by producing a series of Best Management Practices to improve treatment and reduce the risk of environmental contamination once the wood is in service. In addition, they have developed a series of models that allow users to predict the risk of using treated wood in aquatic environments under different flow conditions. These tools allow users of treated wood to minimize the environmental risks associated with these materials.

15.12 PRESERVATIVES

Preservatives can be classified in a number of ways, but the most common is by the solvent in which they are dissolved for wood impregnation. Oilborne preservatives include creosote, pentachlorophenol, copper naphthenate, and oxine copper, while waterborne

materials include many inorganic metal-based preservatives, as well as a number of organic biocides in emulsions that render them either water soluble or water miscible.

15.12.1 Oilborne Chemicals

Oil soluble preservatives are generally used where some resistance to moisture is desirable, and the wood will not be used in direct human contact.

15.12.1.1 Creosote

Creosote is the oldest of the currently used preservatives. First patented in the 1830s, creosote is a by-product of the coking of coal for steel production, and is produced by condensing a portion of the gases produced by the coking process. Creosote is actually a mixture of 200–400 compounds whose composition varies from batch to batch. The primary constituents are a group of polycyclic aromatic hydrocarbons (PAHs). Creosote is not an overly toxic preservative and it takes fairly high loadings (on the order of 20–25% by weight) to provide protection in terrestrial environments, and much more in marine exposures. However, this preservative provides excellent protection against a variety of organisms. The primary concerns with creosote are the toxicity and persistence of the PAHs, leading a number of countries to severely restrict the use of this system. Despite these restrictions, creosote is still used to treat about 25% of the treated wood produced in North America.

15.12.1.2 Pentachlorophenol

Pentachlorophenol was developed in the 1930s as one of the first synthetic organic wood preservatives. “Penta” is highly effective against fungi and insects, but not against marine borers. At one point, penta was the most widely used preservative, but concerns about the presence of dioxin contaminants resulted in a number of countries imposing restrictions on its use. The manufacturers responded by producing penta with less dioxin and have responded to many of the concerns raised by regulators. As a result, penta remains in use in a number of countries, but is primarily used where the risk of direct human contact with the treated wood is minimal.

15.12.1.3 Copper Naphthenate

Copper naphthenate was developed as wood preservative in the 1940s but saw little use because it was more costly than penta. The regulatory efforts to re-

strict or ban penta renewed interest in copper naphthenate in the early 1980s. Copper naphthenate is produced by reacting copper with naphthenic acid, which is produced as a byproduct of oil refining. Copper naphthenate is slightly less effective than penta but is about 10 times less toxic to humans than penta. Although the use levels remain small, interest in this preservative is growing.

15.12.1.4 Copper-8-quinolinolate

Copper-8-quinolinolate (oxine copper) was developed in the 1960s and is an excellent fungicide. However, its primary claim to fame is that wood treated with this chemical can be used for applications in direct contact with food. Unfortunately, oxine copper is rather expensive, so its uses have been limited to treatment of picnic tables, food crates, the truck beds for refrigerated trucks, and other specialized applications.

15.12.1.5 Other Oilborne Materials

It is obvious that the wood preservatives on which the industry depends have been around for many years. This long-term use attests to their efficacy but also suggests the need for renewed development of less broadly toxic systems for wood protection.

One other approach to dealing with the surface features of wood treated with oilborne systems has been to alter the solvent, usually by using more volatile solvents. Taken to the extreme, methylene chloride and liquified petroleum gas have both been used to treat poles with pentachlorophenol, although safety issues and performance concerns have led to the gradual decline in use of these treatments. The advantage of these treatments was that the solvent evaporated, leaving a clean, paintable surface. More recently, the use of pentachlorophenol and copper naphthenate in light organic solvent systems (LOSP) has gained favor in Australasia for the same reasons. The major concern with this type of treatment is the volatile organic compounds emitted following treatment.

15.12.2 Waterborne Chemicals

Water soluble preservatives are attractive because of their lower costs and because they enable the wood to be painted after treatment.

15.12.2.1 Chromated Copper Arsenate

Chromated copper arsenate (CCA) is the most commonly used waterborne wood preservative in the

world. First developed in the 1930s in India, CCA saw little use until the 1970s, when the demand for wood that was clean and paintable soared. CCA is a mixture of chromium trioxide, copper oxide, and arsenic pentaoxide. It is cheap, uses a number of components that are byproducts of other industrial processes, and, most importantly, reacts with the wood cell walls to become “fixed” to the wood. CCA is broadly effective against fungi, insects and marine borers and, at one point, it was used to treat 60% of the wood protected with preservatives. Environmental concerns, however, have recently emerged that caused the manufacturers of this preservative to withdraw it for residential applications in North America at the end of 2003. Many other countries have restricted CCA use in one way or another. The public concerns with CCA have revolved around the use of arsenic, even though the losses of arsenic from CCA-treated wood are minimal. Copper and chromium have also generated some concern because hexavalent chromium is a carcinogen, but CCA has been used for a long time because the fixation process converts the hexavalent chromium into the less toxic trivalent state. Most treating plants are required to hold treated wood for a certain period of time after treatment to allow these fixation reactions to proceed, to minimize the risk of exposure to hexavalent chromium by users of these products. Copper has also raised some concerns where treated wood is used in aquatic environments. However, data on copper migration from treated wood, and models developed to assess the risk of treated wood use in aquatic environments have shown that the use of treated wood poses little risk except in very slow moving waterways with minimal flushing. Despite its impending demise for residential use, CCA remains one of our most broadly effective wood preservatives.

15.12.2.2 Ammoniacal Copper Zinc Arsenate

Ammoniacal copper zinc arsenate (ACZA) is another water-based system, but this formulation uses ammonia instead of the acidic chromic acid to solubilize the copper. The ammonia in this system also tends to produce better preservative penetration (Figure 15.12). Once the ammonia evolves, the copper and zinc precipitate in the wood.

15.12.2.3 Acid Copper Chrome

Acid copper chrome (ACC) was developed in the 1940s and has primarily been used for the treatment of wood used in cooling towers. Like CCA, the

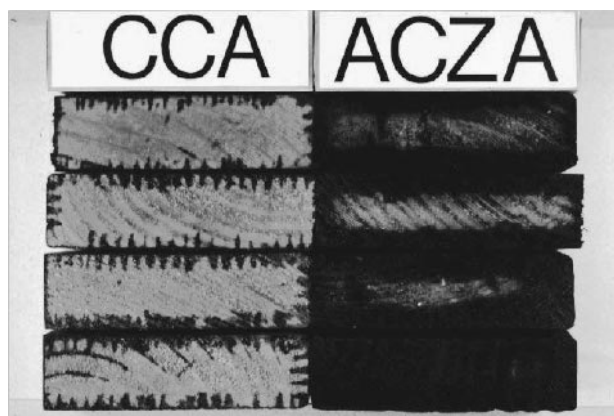


FIGURE 15.12 Examples of the differences in preservative treatment between chromated copper arsenate (CCA) and ammoniacal copper zinc arsenate (ACZA) on matched Sitka spruce lumber samples

chromium in ACC reacts with the wood to become fixed. There has been renewed interest in this system because of the pending loss of CCA for residential use.

15.12.2.4 Ammoniacal Copper Quat

Ammoniacal copper quat (ACQ) is a mixture of copper oxide and a quaternary ammonium compound. The copper is solubilized using ammonia or an amine, and the quat is added to provide supplemental protection against copper-tolerant fungi. This system has been available for approximately 12 years, but its use has only recently started to grow with the pending changes in the use of CCA. The primary advantage of ACQ is the absence of chromium and arsenic. Field tests indicate that this system performs nearly as well as CCA in terrestrial environments and slightly poorer than CCA in marine environments.

15.12.2.5 Copper Azole

Copper azole is another chromium- and arsenic-free preservative. This system is also formulated using either amine or ammonia to solubilize the copper, and has performed well in field tests. Like ACQ, copper azole is only just now beginning to see more widespread use in North America as CCA is phased out of the residential markets, but it has already been used for several years in Japan.

15.12.2.6 Copper HDO

Copper HDO is a newer preservative that is primarily used in Europe. This system contains copper hydroxide, Bis(N-cyclohexyldiazoniumdioxide) (HDO), and boron. It has many of the same advantages as ACQ and copper azole in that it lacks chromium or arsenic.

15.12.2.7 Boron and Fluoride

Two intriguing preservatives that have received some renewed interest are boron and fluoride. Both of these elements are toxic to a variety of organisms and both have the advantage of being capable of moving through wood with moisture. This allows either chemical to be applied by dipping wet or green wood in a concentrated treatment solution. The wood is then stored under non-drying conditions so that the chemical can diffuse through the wood. The disadvantage of either chemical is that there is no fixation, so the chemical can also leach from the wood. As a result, these treatments are really most useful where the wood is not likely to become wet. Boron has long been used to treat framing lumber in New Zealand to protect against powderpost beetles, and has recently been used in Hawaii to limit the potential for attack by Formosan termites. This chemical has exceptionally low toxicity to humans, making it especially attractive for treating wood framing in houses. Fluoride has been used to a limited extent in Europe, but its corrosivity limits its application

15.12.3 Future Wood Preservatives

Over time, the preservation industry is expected to move away from heavy metals for wood protection. This move is a reflection of the growing concerns about the effects of metals on the environment and the knowledge that some metal invariably moves from the treated wood into the surrounding environment. As a result, a number of organic molecules have emerged, including substituted isothiazolones and triazoles. Both of these groups have relatively low toxicity to non-target organisms (including humans). However, they are more costly and, because of their specificity, more likely to fail in severe exposures. In all likelihood, we will see a move to mixtures of organic biocides, most likely in water-based emulsion systems, but considerable regulatory change must occur before this shift can happen. In reality, this approach is similar to that taken with

CCA, which uses mixtures of metals with differing toxicity profiles to provide broader protection. At present, the alternative organic materials remain far too expensive to compete with metals for general commodity preservative treatments.

15.12.4 Wood Modification

An alternative to the use of toxic biocides is to modify one or more components of the wood so that it is resistant to biological attack, resists moisture uptake, or is chemically unrecognizable to the decay agent. Wood modification has been studied for over half a century, with mixed results. The two basic approaches are to either bulk the cell lumens to the point where moisture is excluded, or to add chemicals that react with the wood components. The primary bulking agents for wood modification have been the polyethylene glycols (PEGs). PEGs are available in a range of molecular weights, with the lower molecular weights penetrating the wood matrix more easily, but also being more liable to subsequent loss. PEG has primarily been used to stabilize degraded wood, such as that found in submerged shipwrecks. It has also been used as an additive in wood utility pole treatments in Canada, but its primary purpose is to soften the wood to facilitate climbing rather than have any impact on biological performance. In general, the long time periods required to achieve penetration and the oil-like texture of the treated wood make this process less feasible for most applications.

The other approach to bulking the wood is to impregnate the wood with monomers, such as resins, and then polymerize these materials *in situ*, using either heat or catalysts. This approach can work but the resulting products are extremely expensive. Marine-grade plywood, which contains up to 10% resin, is an excellent example of one such product.

The more commonly studied methods of wood modification involve treating the wood with reactive molecules that react with and alter the moisture holding capacity of the wood cell walls. One of the simplest of these is formaldehyde, which reacts with hydroxyl groups on the carbohydrates to reduce the hygroscopicity of the wood. Acetic anhydride and a host of other reactive compounds have also been employed. A number of studies have shown that chemical modification improves wood durability, but the primary drawback to these approaches has been cost. Typically, weight gains approaching 20–30% are necessary to protect the wood, making the

wood extremely expensive in comparison with conventional preservative treatments, where the amount of chemical added approaches 1.0–1.5% for most waterborne metal-based systems. In the absence of substantial regulatory changes, wood modification is likely to remain feasible only for specialty products whose price differential is not a problem.

15.13 REMEDIAL TREATMENTS

While we typically think of wood preservation from the standpoint of protecting freshly manufactured wood, there is also a considerable demand for supplemental protection of wood already in service. These treatments can be either external or internal.

External preservatives include most of the chemicals mentioned previously, but the systems may be formulated differently. For example, the below-ground portions of wood are often protected by application of preservative pastes that contain combinations of chemicals. Typically, these pastes contain both oilborne chemicals such as copper naphthenate or pentachlorophenol, that are intended to remain near the surface, and water soluble chemicals such as boron or fluoride, that are intended to move for some distance into the wood to control any established fungi. These treatments are normally applied at 10- to 15-year intervals.

Internal treatments can take a number of forms. At their simplest, holes are drilled into a void or other internal defect in the wood and preservative solution is pumped in under slight pressure. This approach works well with insect galleries but is less effective with decay, where the colonization patterns are more diffuse. The interior part of a larger timber or pole is likely to be liquid-impermeable heartwood, and chemicals added to the void are unlikely to move very far into this wood.

There are two alternatives to conventional preservatives for arresting decay in voids. The first uses either boron or fluoride compressed into rods. These rods are installed in holes drilled above and below the void. The rods are inserted and the holes are plugged. Moisture in the poles releases the chemicals, which slowly diffuse through the wood to arrest any fungal attack. The time required for this process depends on the wood species and moisture conditions, but it can take two to three years to reach protective levels. The advantage of these treatments is the relatively low toxicity of the chemicals. The disadvantage of the treatment is the time required for

the chemical to affect the established fungi. Over a two- to three-year period, the fungus will continue to degrade the wood.

The other internal treatment approach is to use chemicals that move through the wood as gases (fumigants). Fumigants were originally developed for sterilization of soil prior to planting. While fumigants are rapidly degraded in soils, some of these chemicals have substantial interactions with wood and remain detectable for two to up to 20 years after application. Like the boron/fluoride rods, fumigants are applied through holes drilled above and below the decayed area. The chemical is added and the holes are plugged. The chemical volatilizes and moves up and down from the hole. The advantage of fumigants is that they generally kill established fungi within one year of treatment, minimizing the risk of further damage to the wood. Four fumigants are used for wood treatment: chloropicrin (trichloronitromethane), metam sodium (32.1% sodium n-methyldithiocarbamate), methylisothiocyanate (MITC), and dazomet. Chloropicrin is, by far, the most effective fumigant, but it is also the most difficult to handle. As a result, its use is limited to wood located away from inhabited areas. Metam sodium is another liquid fumigant that is widely used for timbers and poles. This chemical is gradually being replaced by MITC and dazomet, both of which are solid at room temperature. MITC is usually applied in aluminum tubes and volatilizes to move into the wood. Dazomet is a crystalline powder that decomposes in the presence of water to produce MITC. All of these treatments rapidly eliminate fungi and remain effective for at least four to seven years after treatment. Chloropicrin provides up to 20 years of protection.

15.14 NON-BIOCIDAL BARRIERS

Along with chemicals, there may also be wood applications where physical barriers are adequate for protecting wood from deterioration. Ironically, physical barriers were an important tool for early shipbuilders, who sheathed the bottoms of their vessels in copper plate to limit marine borer attack. Two recent examples of barrier applications are the use of plastics for protecting marine pilings and utility poles. In the case of marine pilings, untreated wood coated with polyurethane provided excellent protection in southern California. In the case of the utility poles, the barrier was primarily applied to reduce the risk of chemical loss into the surrounding environment, but there is little doubt that it will also reduce the risk of

external decay. The absence of soil sharply reduces the microbial flora coming in contact with the wood. The primary drawback to these treatments is the initial costs, but there are clearly applications where the user is willing to pay the added cost to obtain other performance attributes.

15.15 REFERENCES

- Anonymous. 1998. All decked out. *Consumer Reports*. Vol. 63(6), pp. 32–34.
- Arnold, M., Feist, W. C., and Williams, R. S. 1992. Effect of weathering of new wood on the subsequent performance of semi-transparent stains. *Forest Products Journal*. Vol. 42(3), pp. 10–14.
- Banks, W. B. 1973. Water uptake by Scots pine sapwood and its restriction by the use of water repellents. *Wood Science and Technology*. Vol. 7, pp. 271–284.
- Banks, W. B. 1971. The role of water repellents in the protection of timber. In *Record of the Annual Convention British Wood Preserving Association*, pp. 129–147.
- Banks, W. B. and Voulgaridis, E. V. 1980. The performance of water repellents in the control of moisture absorption by wood exposed to the weather. In *Record of the Annual Convention British Wood Preserving Association*, pp. 43–52.
- Evans, P. D., Thay, P.D., and Schmalzl, K. J. 1996. Degradation of wood surfaces during natural weathering. Effects on lignin and cellulose and on the adhesion of latex primers. *Wood Science and Technology*. Vol. 30, pp. 411–422.
- Feist, W. C. 1990. Outdoor wood weathering and protection. In *Archaeological Wood: Properties, Chemistry, and Preservation*. R. M. Rowell and R. J. Barbour, Eds. Advances in Chemistry Series 225. Washington DC: American Chemical Society, pp. 263–298.
- Feist, W. C., Mraz, E. A., and Black, J. M. 1977. Durability of exterior wood stains. *Forest Products Journal*. Vol. 27(1), pp. 13–16.
- Grantham, J. B., Heebnik, T. B., Black, J. M., and Mraz, E. A. 1976. Natural exterior finishes for wood in the Pacific Northwest. *Forest Products Journal*. Vol. 26(8), pp. 21–27.
- Eaton, R. A. and Hale, M. D. C. 1993. *Wood: Decay, Pests, and Protection*. London: Chapman and Hall.
- Hilditch, E. A. and Crookes, J. V. 1981. Exterior wood stains, varieties performance and appearance. In *Record of the 1981 Annual Conventional British Wood Preserving Association*, pp. 59–63.
- Hill, R. R. 1973. Water repellent preservative finishes. *J. Oil Col. Chem Association*. Vol. 56, pp. 251–258.
- Hillis, W. E. 1987. *Heartwood and Tree Exudates*. Berlin: Springer-Verlag.
- Hunt, G. M. and Garratt, G. A. 1967. *Wood Preservation*. New York: McGraw-Hill.
- Kalnins, M. A. and Feist, W. C. 1993. Increase in wettability of wood with weathering. *Forest Products Journal*. Vol. 43(2), pp. 55–57.

- Mc Donald, K. A., Falk, R. H., Williams, R. S., and Winandy, J. E. 1996. *Wood Decks: Materials, Construction, and Finishing*. Madison, WI: Forest Products Society.
- MacLean, J. D. 1952. *Preservative Treatment of Wood by Pressure Methods*. Washington, DC: U.S. Department of Agriculture, Agricultural Handbook 40.
- Morrell, J. J., Schneider, P. F., and Williams, R. S. 2001. Protecting wood decks from biodegradation and weathering: Evaluation of deck finish systems. *Forest Products Journal*. Vol. 51(11/12), pp. 27–32.
- Scheffer, T. C. 1957. Decay resistance of western red cedar. *Journal of Forestry*. Vol. 55, pp. 434–442.
- Scheffer, T. C. 1971. A climate index for estimating potential for decay in wood structures above ground. *Forest Products Journal*. Vol. 21(10), pp. 25–31.
- Scheffer, T. C. and Cowling, E. B. 1966. Natural resistance of wood to microbial deterioration. *Annual Review of Phytopathology*. Vol. 4, pp.147–170.
- Valcke, A. and Stevens, M. 1988. Performance of wood preserving and wood finishing systems for external joinery exposed to natural weathering. In *Record of the Annual Convention British Wood Preserving Association*. pp. 39–50.
- Zabel, R. A. and Morrell, J. J. 1992. *Wood Microbiology: Decay and its Prevention*. San Diego: Academic Press.
- work groups/morrell/bjj/protection of woodbased materials.

SURFACE ENGINEERING

| | | |
|------------|--|-----|
| CHAPTER 16 | THE INTERSECTION OF DESIGN, MANUFACTURING, AND SURFACE ENGINEERING | 321 |
| CHAPTER 17 | PROTECTIVE COATINGS FOR ALUMINUM ALLOYS | 345 |
| CHAPTER 18 | CORROSION RESISTANT COATINGS AND PAINTS | 367 |
| CHAPTER 19 | PAINT WEATHERING TESTS | 387 |
| CHAPTER 20 | THERMAL SPRAY COATINGS | 405 |
| CHAPTER 21 | COATINGS FOR CONCRETE SURFACES: TESTING AND MODELING | 423 |
| CHAPTER 22 | THE ROLE OF INTRINSIC DEFECTS IN THE PROTECTIVE BEHAVIOR OF ORGANIC COATINGS | 449 |

CHAPTER 16

THE INTERSECTION OF DESIGN, MANUFACTURING, AND SURFACE ENGINEERING

Gary P. Halada
Clive R. Clayton

Department of Materials Science and Engineering, State University of New York, Stony Brook, New York

| | | | |
|--|-----|------------------------------------|-----|
| 16.1 INTRODUCTION | 321 | 16.5 THE ROLE OF COMPUTER MODELING | 337 |
| 16.2 SURFACE ENGINEERING DESIGN NEEDS | 322 | 16.6 SUMMARY | 339 |
| 16.3 SENSING OF DEGRADATION EFFECTS ON SURFACE CHEMISTRY | 326 | 16.7 REFERENCES | 340 |
| 16.4 TRADITIONAL AND EMERGING SURFACE ENGINEERING TECHNOLOGIES | 329 | | |

16.1 INTRODUCTION

When an engineered surface or coating is created, the designer or applications engineer is usually confronted with a few critical questions that will define success or failure. For example:

- What is the likelihood that a marine inhibitor application will limit pitting corrosion to an acceptable level for the design lifetime of a ship?
- If a composite paint coating is damaged, how quickly and easily (and cheaply) can the surface be repainted?
- What is really important when I have to choose a replacement for a well-established but poorly understood chemical pretreatment for an aircraft alloy?
- How can I prevent wear without changing the dimensions of my surface?

The common themes in all these questions are *functionality* and the related concept of *dependability*.

Surface engineering and coatings technologies focus on satisfying design needs for dependability and appearance, as well as serving various functional requirements (for example, creating adhesion layers in multi-component devices). By definition, dependability is a combination of *reliability* and *maintainability*.

More precisely, the component dependability ratio for a surface treatment would be the ratio of repair rate to failure rate. In other words, the more quickly a surface can be restored to functionality (repaired) or the lower the failure rate (and, hence the higher the reliability), the greater the dependability. In as much as any coating or surface treatment represents a component of an engineered system, the ideal dependable surface is functional (i.e., protective, the correct color, the correct texture, etc.) for as long as possible and will repair itself instantly if damaged under any of a number of conditions. Hence, the role of surface engineering is to develop just such a substrate/surface system. Although the best surface can wear (even one with a diamond-like coating) or corrode in an extreme environment, survivability can be tailored to individual design needs. Likewise, current research in “self-repairing” coatings promises tremendous advances in protection and maintenance of engineering materials, but these, too, must be chosen to match the operating environment and the nature of the substrate they protect.

Although an ideal surface might in practice be impossible, a number of technologies have been developed or are being developed to respond to the design needs of manufacturing. To try to address all these technologies, or even all the possible design needs, within the confines of this chapter would be equally impossible. Therefore, we will start with a broad look at a few areas of manufacturing needs, and then focus on categories of surface engineering technology that

have broad applicability, or that by their nature demonstrate how research and development is leading to advances toward an ideal surface treatment. Where possible, tables and graphics will be used to provide a focus for discussion and a summary of useful data for design engineer and researcher alike. The references at the end of the chapter provide a starting point for those interested in further research into a particular technology or application.

16.2 SURFACE ENGINEERING DESIGN NEEDS

In many industries, from gas and oil transmission to shipping to chemical processing, corrosion and its associated effects are leading causes of failure. Although corrosion can occur under a variety of environmental conditions and may involve numerous chemical mechanisms, two major categories commonly encountered are aqueous corrosion and microbially influenced corrosion (MIC).

16.2.1 Corrosion Resistance

16.2.1.1 Aqueous

Aqueous corrosion occurs due to electrochemical or galvanic processes at the surface of a metal, alloy, or composite (or even a ceramic in some cases) that is temporarily or permanently exposed to an aqueous environment containing charge carriers. The types of aqueous corrosion are summarized in Table 16.1 (after K. G. Budinski, *Engineering Materials*, 4th Ed., New York: Prentice-Hall, 1992.).

In the case of uniform corrosion, it is necessary to either remove the electrolyte itself or use a coating more resistant or noble in comparison to the substrate to prevent corrosion. Surface engineering technologies, such as chemical pretreatments con-

taining etchants, or laser or ion beam surface treatments, can also be used to affect the composition of the near surface region to provide a surface resistant to the expected engineering environment.

In order to develop a surface sufficiently resistant to localized corrosion (i.e., pitting), it is necessary to try to understand the underlying structure which influences the initiation of pitting. For example, the aerospace industry relies heavily on aluminum alloys for aircraft production. The commercial aluminum-copper alloy AA2024-T3, primarily used in aircraft in the form of sheet and fuselage and plate for the lower wing, contains several alloying elements that lead to the formation of a complex, multiphase structure (Figure 16.1). Cu, Mg, Mn, Si, and Fe are present in AA2024-T3 in appreciable amounts, and form Intermetallic Compounds (IMCs) of composition Al_2Cu , Al_2CuMg , Al_2Cu_2Fe , Al_7Cu_2Fe , $Al_{12}Si(FeMn)_3$, $Al_{20}Cu_2(MnFe)_3$, and $Al_{20}Cu_3Mn_3$. These secondary phase precipitates and intermetallic compounds enhance the mechanical strength of the alloy. However, these particles also enhance localized corrosion. Recent studies have shown that pitting corrosion tends to initiate at Cu-rich IMCs.¹ Al-Cu-Mn-Fe IMCs have also been found to be cathodic sites, strongly influencing corrosion, and pitting corrosion has been found to initiate at Al-Cu-Mg IMCs.² It has also been found that microcracks in the bulk material, presumably formed by hydrogen evolution, near IMCs can provide starting points for pitting.³ Other studies have found that pitting corrosion in 0.6M NaCl is related to Al_3Fe intermetallic inclusions in AA6061 alloy, which act as cathodic sites, leading to increased rates of dissolution around the particles.⁴

These alloys are protected through a series of surface modifications such as surface pretreatment, chromate conversion coating (CCC) followed by an optional application of a primer and a topcoat or a polymer based paint. Hence, CCCs are widely used

TABLE 16.1 Forms of Aqueous Corrosion Damage

| Type of Corrosion | Nature of Attack |
|---------------------------|--|
| Uniform | Uniform rusting or direct attack |
| Pitting | Localized, usually due to galvanic attack. Usually initiated at surface inclusions, defects or high energy point sites. |
| Crevice | Localized attack in metal-to-metal or metal-to-nonmetal crevices where corrodent is in the crevice |
| Galvanic | Where two dissimilar metals are in contact in an electrolyte |
| Stress corrosion cracking | Spontaneous corrosion-induced cracking of a material under applied or residual stress |
| Intergranular | Due to alloy segregation at grain boundaries |
| Dealloying | Due to preferential removal of one element or phase, leaving a susceptible microstructure |
| Erosion | Wear-based process |
| Filiform corrosion | Occurs under surface coatings; leaves distinctive "worm-like" trails |

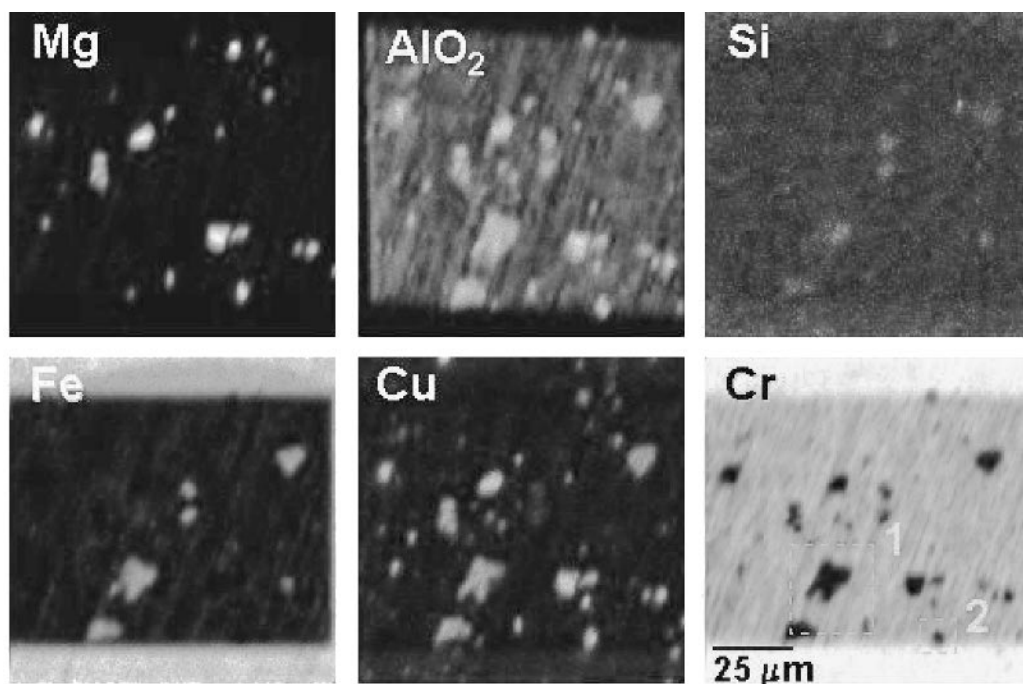


FIGURE 16.1 Secondary Ion Mass Spectroscopy chemical maps of aluminum alloy 2024-T3 with Alodine chromate conversion coating showing presence on intermetallic inclusions at the surface, following ion beam etch to remove approximately one-fifth of the average thickness of the coating. The chromate conversion coating layer on these particles (as shown by the Cr map) is significantly thinner than the surrounding metal matrix. (From Ref. 5).

in the aerospace industry. However, it has been shown that the presence of IMCs strongly affects both the thickness and the surface morphology of CCC formed on AA2024-T3.⁵ The application and corrosion-inhibiting mechanisms of these coatings will be discussed in some more detail in section 6.4 below.

16.2.1.2 Microbially Influenced Corrosion (MIC)

First recognized more than 60 years ago,⁶ microbiological corrosion was estimated in 1978 to cost U.S. industries more than \$16 billion.⁷ MIC is associated with the presence of a biofilm, which provides a microecology for aerobic and anaerobic bacteria. It is important to note that in nonsterile environments, biofilms are ubiquitous and are not necessarily associated with the cause of corrosion, but instead are simply attached to corrosion products and other rough topographies. The evolution of a biofilm has been illustrated in Figure 16.2, which has been adapted from the work of Shearer.⁸ In the first stage of biofilm formation, a conditioning film is first deposited on the substrate surface.

This foundation layer may be formed by the deposition of such organic molecules as lipids, humics, smaller chain organic acids, extracellular polysaccharides containing proteins, etc. The next stage is reversible association with planktonic species, followed by eventual irreversible binding of bacteria. The development of a mixed consortium of species leads to the formation of an ecologically balanced environment constituting a biofilm acting as an oxygen and pH barrier. Turbulent fluid flow and wet/dry cycles may lead to sloughing of the biofilm and the formation of pores and breaches in the film. Biocorrosion can be expected to result from such chemical systems as: oxygen differential cells, concentration polarization, crevice-like corrosion, and metabolic products which may induce pitting or chelation of components of passive films and salt films. The resulting surface chemical modification of the substrate material may be studied by surface analytical spectroscopy. Therefore, encouraged by the successful application of surface spectroscopy to the greater field of abiotic corrosion over the last 30 years, attempts have been made to develop surface analytical methods and practices to the study of this form of corrosion.^{9,10} As a result, for example, an improved

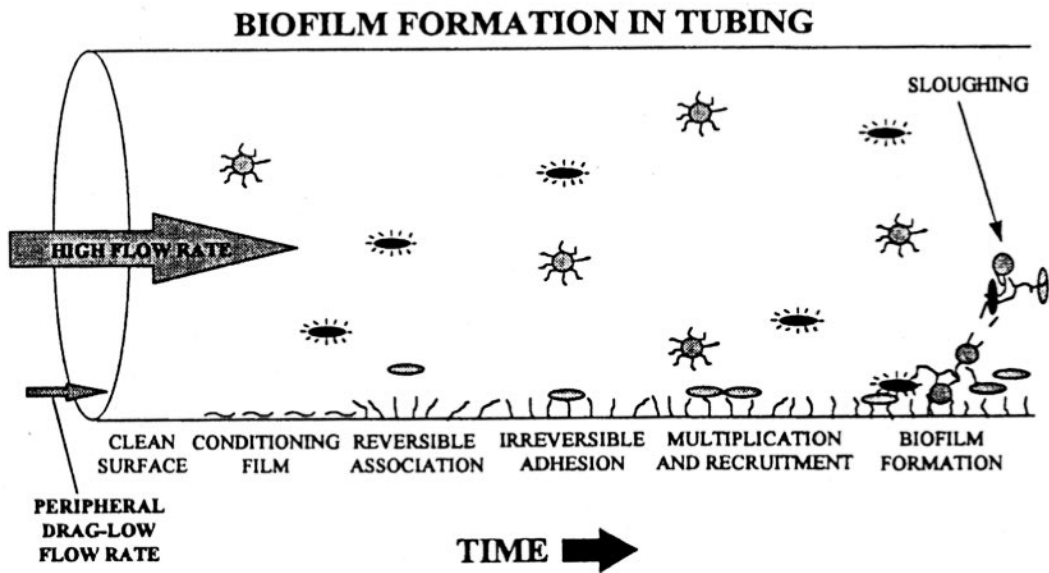


FIGURE 16.2 Biofilm formation in tubing (modified from Shearer⁸)

model has resulted which relates the effects of the microbial biofilm and microbial activity itself on the passive layer which is counted on to offer a kinetic and electrical barrier to the corrosion of stainless steels.

16.2.2 Tribological Damage

Another major area of degradation which is considered by designers of coatings is tribological damage or wear. Wear processes include abrasion, which can be further subdivided into low and high stress wear, gouging and damage from polishing; erosion including that resulting from impingement of solids or liquids (or combined as a slurry) and cavitation erosion; adhesion-based wear including that resulting from fretting, seizure and galling; and surface fatigue, which results in pitting, spalling, impact damage, and brinelling. A major engineering challenge is to produce surfaces with a greater toughness, which means that it is important to create a surface which can absorb or deflect the energetic processes which result in tribological damage. A sacrificial ablative coating, a coating with a high elastic modulus (but having good adhesion properties), or certain “self-healing” coatings would fit in this category. A soft electroplated coating such as Cd or Ag can “lubricate” the surface and prevent fretting erosion. A brittle surface coating would normally be a poor choice in designing to protect from wear if a high-stress working environment is expected.

Various “hard” coatings have also been developed which rely on attaining excellent adhesion to the substrate to ensure usefulness. For example, plasma sprayed ceramic coatings (which will be discussed in greater detail later) have relied on careful choice of powders and interfacial bond coats to promote adhesion to a substrate.

Anti-wear coatings and surface treatments protect through a combination of high surface hardness and self-lubricating properties. For example, a multi-functional coating has been developed using TiN and MoS_x to provide both hardness and a low coefficient of friction.¹¹ Moreover, damage from surface wear can often lead to corrosion of exposed underlying layers. For example, scratches through surface passive films can result in greatly increased rates of corrosion if mobile species are not freely available that can re-passivate these exposed surfaces. Recently, “self-repairing” coatings have been devised which can respond to such damage. For example, chromate conversion coatings contain a reservoir of labile chromate species which can migrate to scratches and help re-form the protective barrier (Figure 16.3).¹²

Some of the other types of coatings and treatments developed to limit tribological damage are described in Table 16.2.

16.2.3 Damage by UV/Humidity

UV/humidity effects are especially damaging to composite and polyurethane-based coatings systems. UV

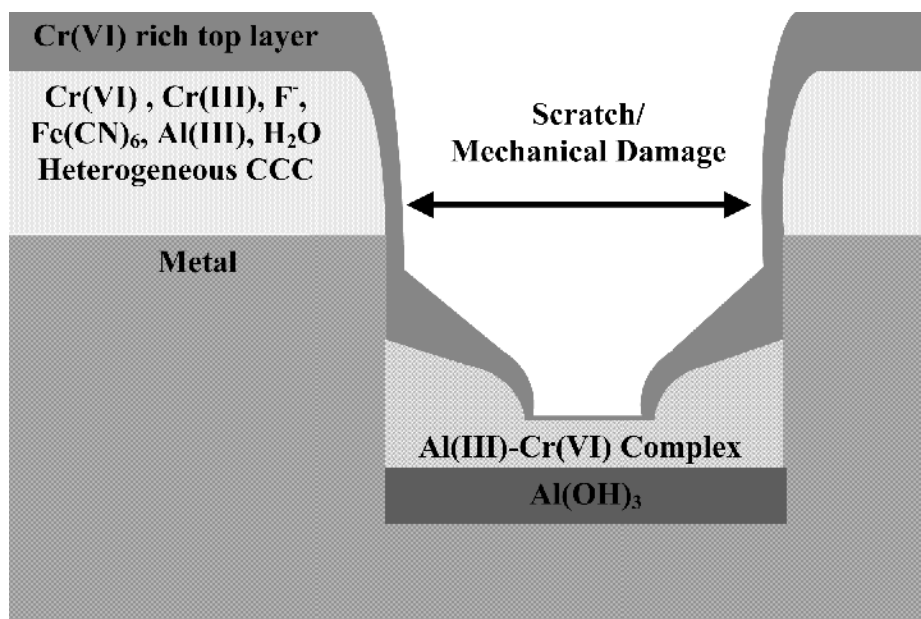


FIGURE 16.3 Model of repassivation of a deep scratch (which exposes the underlying metal) in a chromate conversion coating on aluminum-based aerospace alloys. (From Ref. 12).

TABLE 16.2 Coatings to Protect from Tribological Damage

| Treatment/Coating | Substrate(s) | Comments |
|---|------------------------------------|---|
| Electroplated soft coating | Metal | Protection from fretting |
| Surface nitriding | Metals, some composites | Formed by chemical treatment, ion implantation |
| Diamond-like carbon; includes diamond-like nanocomposites (DLN) | All | Formed by ion beam methods, chemical methods |
| Surface carbides | Metals | Formed by ion sputtering, chemical vapor deposition |
| High composites paint | Metals, composites, polymers | Usually multi-layer coatings involving surface pretreatment, a primer and a topcoat |
| Plasma sprayed ceramic coatings (including HVOF). | Metals, composites, some polymers | May use interfacial bond coat; can use for functionally graded coatings to improve adhesion and wear resistance |
| Multifunctional coatings | Depends on exact nature of coating | Combine hardness and low friction properties to resist galling |
| Nanocomposite coatings | Any; may be functionally graded | Cost may be an issue; may be optimized for improved adhesion |

impingement is of particular interest since any coating meant for service outdoors will be subject to near-continuous irradiation in the UV wavelength region. UV failures are generally due to the direct action of the UV light itself and are photochemical in nature.^{13–15} While the Earth’s atmosphere almost completely absorbs UV radiation below 280 nm as well as the bulk of UV from 300–380 nm, the small amount

that is able to penetrate the atmosphere to the surface of the Earth is, nevertheless, energetically sufficient to alter the organic chemical structure of many coating systems. This can lead to embrittlement of polymeric layers due to cross-linking, or chain scissioning, which can result in chalking or fading. This will be discussed in greater detail below, where we discuss polymeric/composite coatings.

16.2.4 Damage by Radioactivity

Under certain circumstances, engineering alloys and composites may be exposed to radioactivity for prolonged periods of time. In this case, we are not considering the unusual situation found in high-radiation environment of a nuclear reactor, but rather the long-term, low level radioactivity environment found, for example, in a spent fuel storage facility or a former military processing facility. Emission of gamma, beta, and alpha radiation by spent nuclear fuel and radioactive byproducts has been shown to result in radiolytic decomposition of water, forming a variety of oxidizing (H_2O_2 , and free radicals $\bullet\text{OH}$, $\text{HO}_2\bullet$, $\text{H}\bullet$) and reducing (H_2 , $\text{O}_2^{\bullet-}$, e^-) products, the concentration of which depends on the nature of the radioactivity and dosage.^{16,17} At temperatures below 1,000 °C, the oxidizing products are expected to predominate.¹⁸ In studies of an alpha-irradiated U(IV)/water interface, Sattonnay, et. al., found significant increases in U VI and H_2O_2 concentration and enhanced U dissolution, as well as a decrease in pH with increasing dosage.¹⁹ Scanning electron microscopy (SEM) of the irradiated interface shows grain-boundary attack, extensive transgranular boundary corrosion, and the presence of microcracks.

Radiolysis effects on engineering alloys has been indicated in a number of studies. In work at the Chalk River Nuclear laboratory, Urbanic et al. found that radiolysis in thick porous oxides formed on Zircaloy-2 reactor pressure tubes resulted in a highly localized altered water chemistry near the metal-oxide interface, independent of bulk water chemistry, causing accelerated oxidation kinetics.²⁰ Gamma radiolysis of water using radioactive waste has recently been tested by Sawasaki et al. for hydrogen production in the presence of high-Z metals.²¹ They also noted the resulting increase in surface oxidation of Ta, W and Pb. In studies by Min et.al., using a Co gamma source, the oxidative radiolysis products of simulated ground water at pH 7.2 increased the corrosion rate of Cu 1.5-fold, the corrosion rate of Al by a factor of 2.8, and that of Fe by a factor of 4.3.²² They also looked at several stainless steels and found a similar, if weaker, effect on overall oxidation.

Aside from the effects of oxidative radiolysis products on corrosion, other effects, whether directly or indirectly caused by radiolysis, may have an effect on the integrity and corrosion of materials, and, in particular, on waste container materials. This can include gas pressure generation (hydrogen, methane, nitrogen and nitrous oxide) from alpha or gamma exposure.²³ increases in glass decay,²⁴ hy-

drogen gas formation in cementitious matrix material,²⁵ and effect of radiolysis products on redox/corrosion models for stainless steel waste canister materials.²⁶

Overall, this indicates the need to consider carefully the environment of an engineered surface in order to provide sufficient protection from the effects of exposure.

16.3 SENSING OF DEGRADATION EFFECTS ON SURFACE CHEMISTRY

In the case of all degradation effects which will eventually result in a need for repair or re-coating (or in damage of the substrate surface itself), it is essential to employ sophisticated analytical techniques to elucidate the chemical and physical nature of the damage. A number of analytical techniques have found widespread use in the study of surface damage, including the effects of corrosion and wear. Optical microscopy (and its variants) is an obvious choice for initial analysis. In order to improve resolution beyond the "diffraction limit" imposed by the wavelength of light used, near field scanning optical microscopy uses a sub-wavelength light source (i.e., a small fiber optic probe) scanned a few nanometers over the surface of the sample.²⁷ Resolution is determined by diameter of the aperture at the tip of the probe, which must be kept close enough to the sample surface so that diffraction is not an issue. Transmitted or scattered light can be collected to construct an image of surface features down to about 50 nm.

Other types of microscopy can provide information on topographic or physical changes in a surface which has been exposed to a damaging environment. For example, atomic force microscopy (AFM) can provide information on surface changes on a relatively smooth substrate. AFM utilizes an atomically sharp tip (generally made of silicon nitride or silicon) which is brought into close contact with the sample under study and then rastered over the sample in order to produce a topographical map of the surface up to the atomic level (ten million times magnification).²⁸ The tip is mounted on the underside of a cantilever, the flexing of which is detected by the deflection of a laser beam. The advantage of using AFM over scanning electron microscopy (SEM) includes the ability to perform analysis in air, and without having to coat an insulating sample to make it conductive. Poorly conductive samples can be examined in some SEMs by using low current beams which limit sample charging. Environmental SEMs (ESEM) replace the vacuum with a gas,

sometimes water vapor, which amplifies backscattered electrons from the sample. ESEM can image hydrated or poorly conductive samples, but magnification above about 3,000 times is difficult. One drawback of AFM is the limited range of sample topography that can be safely imaged—in general, the maximum z-axis range of the scanner is about 0.2 microns.

Many samples, especially those of industrial interest, are too rough for most atomic force microscopy. Scanning optical microscopy does not require close contact, and determines depth changes through specimen movement (vertical resolution approximately 50 nm) and collection of multiple frames. Both images and three-dimensional height maps can be formed in this manner. By using laser scanning profilometry, a vertical resolution of about 5 nm can be attained (and a lateral resolution of around 2 microns). Without getting further into depth about traditional microscopic techniques of analysis, Table 16.3 provides a comparison of techniques and capabilities.

In many cases, it is essential to analyze surface chemistry as well as appearance or topography of

microscopic features. Over the past few decades, a number of surface analytical techniques have been developed to analyze surface chemistry and reactions, including the effects of degradation and corrosion. These include the high vacuum techniques, such as X-ray photoelectron spectroscopy (XPS), auger electron spectroscopy (AES), and static and dynamic secondary ion mass spectroscopy (SIMS). Other techniques that do not require a vacuum include synchrotron techniques (such as X-ray absorption methods), molecular spectroscopies such as Raman spectroscopy, and both laboratory- and synchrotron-based Fourier transform infrared spectroscopy (FTIR).

Although not usually recognized as such, FTIR can be a powerful tool for analyzing chemical bonds at surfaces. Various studies using mid- and far-IR ranges have proved the value of this technique for the analysis of adsorbed water on Pt surfaces,²⁹ in situ analysis of electrode interfaces during film growth,³⁰ and adsorption of thiocyanate on copper and gold electrodes.³¹ FTIR is a non-vacuum technique that can provide time-dependent imaging of chemical features associated with a variety of or-

TABLE 16.3 Comparison of Some Typical Microscopic Analysis Techniques

| Technique | Spatial (lateral) resolution | Depth of analysis | Advantages | Disadvantages |
|--|------------------------------|---|---|--|
| Optical microscopy | 1 μ | Surface focal point | Established technique Ease of operation | Optics to improve resolution, depth of field can be expensive Wavelength of light limits resolution |
| Near field scanning optical microscopy | 50 nm | Surface | Improved resolution beyond “diffraction limit” Variants such as shear-force NSOM can be used to map topography as well | Need vibration isolation, system for high precision movement to maintain required close working distance |
| Atomic force microscopy | 1.5–5 nm | 1 nm | Near-atomic resolution can measure elasticity, friction | Maximum z-range about 5 microns In contact mode, can alter or damage sample |
| Scanning tunneling microscopy | 0.1–1 nm | 4<1 nm as low as 0.01 nm vertical res. | Can provide surface potential mapping | High precision electro-mechanical system needed to maintain current, distance |
| Confocal microscopy/ profilometry | 1–2 μ | 5–50 nm | Provides topographic data Less affected by vibration and sample roughness as compared to standard optical microscopy | Lower lateral resolution than standard optical microscopy |
| Scanning electron microscopy | 2–3 nm | 1–5 μ | Environmental SEM in a gas is possible for volatile samples Semi-quantitative elemental analysis available through Energy Dispersive Analysis by X-Rays EDAX | Problems with non-conductive samples Fairly expensive system for high resolution work using high brightness electron source Vacuum technique |

ganic and many inorganic bonding states. Neufeld and Cole used FTIR (in reflection mode) to study the molecular chemistry of early stage corrosion film formation on a variety of metallic surfaces.³² Their data indicated that too thick a corrosion product resulted in loss of detail, presumably due to loss of signal through excessive IR absorption. A grazing angle configuration has been used to enhance the signal-to-noise ratio for IR analysis of lubricating oil thickness on magnetic disk media.³³ Data manipulation techniques can also be used to enhance the signal associated with the surface of a sample. For example, spectral subtraction (removing signal associated with the bulk) has been used to enhance surface sensitivity in FTIR analysis of thin layers of silane on mica.³⁴

Combining FTIR with other analytical techniques also provides a mechanism to identify vibrational features associated with the surface of a sample. Examples of this include combinations of FTIR with optical fluorescence in studies of polymer blends,³⁵ combinations of FTIR, X-ray Photoelectron Spectroscopy (XPS), and synchrotron X-ray absorption to study plasma-polymerized thin films,³⁶ and a combination of FTIR, XPS, and atomic force microscopy AFM, to analyze ion-beam modified polyimide layers.³⁷ Recently, scanning electron micro-

scopy/energy dispersive analysis by X-rays (SEM/EDAX), X-ray diffraction (XRD), and FTIR have been used together to identify corrosion products typical of atmospheric exposure of structural steel contaminated with uranium.³⁸ In recent work, Stoch et al. used a combination of FTIR and XPS to analyze the copper patina formed on roofs, finding contributions from atmospheric pollutants and deposits from windblown materials and birds.³⁹ In these cases, the combination of analytical techniques provided insight that individual techniques could not.

Table 16.4 provides a summary comparison of popular surface chemical analytical techniques.

FTIR, Raman spectroscopy, XPS, AES, and SIMS all possess advantages and disadvantages as surface analytical techniques (Table 16.4). Hence, it has been found to be valuable to combine these techniques, both with each other and with other analytical techniques, in order to develop a clear understanding of chemical processes at surfaces.⁴⁰

Recent development of FTIR microscopy has enabled chemical maps to be formed of bonding configurations associated with very small features, and thus has allowed the simultaneous optical and chemical exploration of degradation, corrosion and coatings on surfaces. For example, Maldener et al. ana-

TABLE 16.4 Comparison of FTIR, Raman, SIMS, XPS and AES for Surface Chemistry Analysis

| Technique | Advantages | Disadvantages |
|---|---|--|
| FTIR | Rapid data collection Non-vacuum technique Sub-micron surface sensitivity with ATR, glancing angle sampling Chemical mapping with microspectroscopy | Minimum spot size limited by wavelength and optics to approx. 10 microns Sensitivity limited to IR-absorbing bonds Interference from CO ₂ and water |
| Raman | Rapid data collection Non-vacuum technique Remote data collection with fiber optic probes Chemical mapping with microspectroscopy Limited interference from water | Minimum spot size limited by wavelength and optics to approx. 2 microns Sensitivity limited to Raman-active bonds |
| Secondary Ion Mass Spectroscopy SIMS. | ppb sensitivity Small spot (0.1 μ) chemical mapping Depth profiling with dynamic SIMS | UHV technique Problems with non-conductive samples |
| X-ray Photoelectron Spectroscopy (XPS). | Sub-monolayer surface sensitivity Detection of all elements (except H) Sensitive to speciation Non-destructive depth profiling through variable angle XPS | UHV technique Detection limit about 1–2 atomic % Possible photoreduction of high valent species (i.e., chromate). |
| Auger electron spectroscopy (AES) | Sub-monolayer sensitivity Small-spot imaging mode (<0.2 μ spot size) | UHV technique Detection limit about 1–2 atomic % Charging of non-conductive or poorly conductive samples disrupts data, images |

lyzed absorption of water and OH by single crystals of cassiterite.⁴¹ One study indicated that FTIR microspectroscopy provides a higher signal-to-noise ratio and overall more information than traditional bulk pelletization sampling techniques.⁴² The same study also used the interference fringes which sometimes occur in thin film studies using reflection FTIR microspectroscopy to determine sample thickness. Other applications for FTIR microspectroscopy have included aging studies of epoxide-impregnated polypropylene films,⁴³ micro-ATR spectroscopy of adhesion failure in polymers,⁴⁴ and studies of single pigment grains in ancient works of art.⁴⁵ Development of grazing incidence objectives and improved ATR accessories have led to enhanced surface sensitivity and expanded use of FTIR microspectroscopy as a surface analysis tool.⁴⁶ Figure 16.4 shows FTIR microspectroscopy chemical mapping performed on a polyurethane topcoat which is part of a composite polymeric coating system. While the complete mid-range infrared spectrum is collected at every point (spatial resolution of about 10×10 microns), individual peaks can be mapped on a thermal-type scale to indicate spatially distributed presence of different function groups or compounds. Using a synchrotron

IR source, greater resolution (down to 3–5 microns) and better signal to noise ratios can be attained.

16.3.1 Synchrotron-based Techniques

Although the availability of synchrotron light sources is limited, access can be obtained through outside user proposal processes, various participating group structures, or through another research institution with an established presence. When access is possible, additional analytical techniques can be employed which provide unique and valuable surface analytical tools. There is not sufficient space in this chapter to discuss the full extent of characterization technologies available or under development, but a brief summary is made in Table 16.5.

16.4 TRADITIONAL AND EMERGING SURFACE ENGINEERING TECHNOLOGIES

Obviously, far more types of protective coatings and surface treatments exist than can be discussed in this chapter. It would be instructive to examine a few sur-

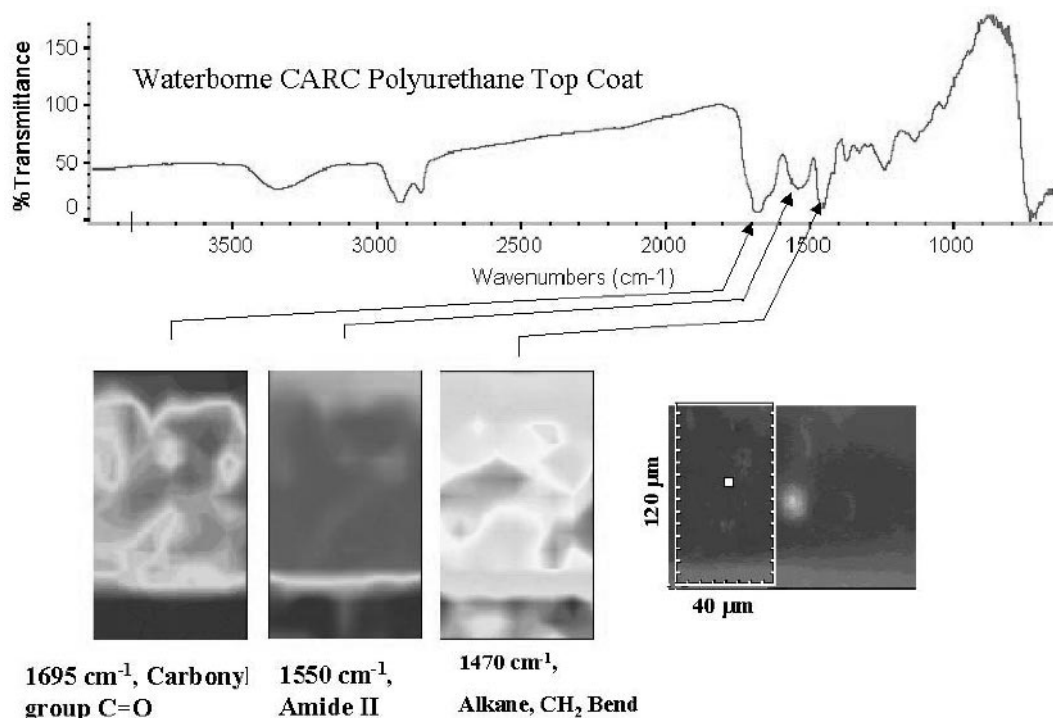


FIGURE 16.4 Spatial distribution of three selected peaks from a characteristic topcoat spectrum extracted from the center of the map (spatial location of spectrum indicated by white square in optical micrograph on right) using FTIR microspectroscopy. Lighter shade indicates greater peak intensity for indicated group. (From Ref. 1).

TABLE 16.5 Synchrotron-Based Analytical Techniques

| Synchrotron technique | Uses | Comments |
|---|--|---|
| X-ray fluorescence | Elemental analysis | XRF microscopy, resolution down to less than 0.2 micron |
| X-ray tomography | 3 dimensional structural imaging | Micron level resolution; useful for composites |
| X-ray near edge spectroscopy (XANES) | Oxidation state information | Small spot resolution down to microns; glancing angle mode to analyze surface species |
| Extended X-ray Absorption Fine Structure spectroscopy (EXAFS) | Bonding and structure information | Requires considerable data analysis; use of standards extremely helpful |
| Synchrotron Infrared spectroscopy (SIRS) | Bonding information; 'finger printing' analysis of many organic, some inorganic groups | Microspectroscopy with resolution better than that of laboratory-based FTIR Microspectroscopy (down to 3–5 microns), higher signal to noise ratio, more rapid data collection times |

face engineering technologies in more detail in order to understand how the choice and application of a suitable technology relates to design needs, environment and substrate.

16.4.1 Chromate Conversion Coatings

According to the Federation of Societies for Coatings Technology (Philadelphia), the term *conversion coating* refers to conversion of a metal's surface into a surface that will more easily accept applied coatings and/or provide for a more corrosion-resistant surface. It is been known for nearly a century that dichromate-based solutions can be used to produce a corrosion resistant film on metals, in general,^{47,48} and aluminum, specifically.^{49–55} In 1927, Evans suggested that the inhibitory action of chromates on iron could be due to its ability to repair the discontinuities in the oxide film on iron.⁵⁶ Later, Edeleanu and Evans proposed that aluminum metal, when exposed to chromate, reduces hexavalent chromium to trivalent chromium and gets oxidized to aluminum oxide during the process.⁵⁷ One of the first studies on the formation of chromate-based conversion coating on aluminum and aluminum alloy (aluminum-zinc) was conducted by Bauer, who later patented the process.⁵⁸ Chromates, even in very low concentrations, are known to increase the polarization resistance of aluminum alloys by a few orders of magnitude⁵⁹ and, hence, are considered to be efficient inhibitors. However, exact mechanisms for the inhibition are still unclear.

The industrial use of chromate conversion coatings was pioneered during the 1950s–1970s, which witnessed the exponential growth of the defense and

aerospace industries, the two major consumers of structural aluminum alloys. Newhard pioneered the development of accelerated conversion coating processes, resulting in the issue of several patents.^{60,61} Several other researchers also contributed to the development of the process.^{62,63} Currently, the Alodine 1200S[®] process is widely used to form CCCs on aluminum alloys. The process involves immersion of a previously deoxidized and desmuted sample in an Alodine bath at room temperature. The highly acidic bath has a pH ~1.5. Alodine 1200S[®] consists of CrO₃, KBF₄, K₃[Fe CN₆], K₂ZrF₆ and NaF⁶⁴ The exact composition of the Alodine 1200S[®] is proprietary information and, hence, is not known. Each chemical in Alodine[®] has an important role in the coating formation process. Chromate is the corrosion inhibiting species, fluoride activates the alloy surface by removing the oxide film,^{65–69} and ferricyanide accelerates the coating formation process.^{70–73}

16.4.2 Interaction of Chromates with Aluminum

Koudelkeva et al. studied the composition of the passive oxide films formed on aluminum exposed to chromate solution using XPS, and determined that the passive film was composed of Cr₂O₃, Al₂O₃, and hexavalent species.⁷⁴ Treverton and Davies studied the composition of CCCs formed on aluminum and found the presence of fluoride species in the coatings.⁶⁶ Later, the same group suggested, for the first time, that ferricyanide acted as accelerators in the formation of conversion coatings.⁷⁵ This was studied and verified by Xia and McCreery much later.⁷²

Abd-Rabbo et al. studied the development of a conversion coating on aluminum and suggested the mechanism of interaction of fluoride with the aluminum for the first time, and also observed the presence of Cr_2O_3 .⁷⁶ Katzman et al. indicated that HF or OH⁻ is necessary, along with hexavalent chromium, for the formation of corrosion protective coatings.⁶⁷ They proposed the coating to consist of a chromium oxide over a layer of mixed aluminum chromium oxide. Cr(VI) was found to be one-third of the total chromium. Yu et al. concluded that CCCs contain a significant amount of $\text{CrOOH}\cdot n\text{H}_2\text{O}$, and hexavalent chromium existed only in the outer layer of the coatings.⁷⁷ Rona et al. determined the storage conditions of CCC prior to painting to be nearly a year.⁷⁸ Using high resolution SEM, Treverton et al. observed that CCCs consisted of particles sized 10nm–60 nm, depending on the pretreatment.⁷⁹ Based on investigations performed on the mechanism of formation of CCCs on pure aluminum, Brown et al. concluded that reduction of dichromate tend to occur at flaws, which support electronic conduction.⁸⁰ Others also supported the theory.⁸¹

Waldrop and Kendig studied the nucleation of CCCs on the matrix of AA2024-T3 and two different IMCs (which are widely present in the alloy surface, as mentioned earlier). Their atomic force microscopy AFM. study showed that CCC formation on certain IMCs occurred at enhanced rates, while at some other IMCs like AlCuMg it was inhibited.⁸² These results were supported by earlier work from Halada, et al.⁸³ Later, a similar study on nucleation of CCCs was performed using AFM. by Brown and Kobayashi, who confirmed the earlier results.⁸⁴ Xia et al. studied the mechanism of protection offered by CCCs.⁸⁵ By monitoring the release of Cr(VI). from CCC, using UV-visible spectroscopy, it was suggested that Cr(VI) storage in a CCC involves the reversible formation of a Cr-VI-O-Cr-III mixed oxide. The “self-healing” properties of the conversion coatings have been associated with migration of the hexavalent chromates to actively corroding sites.^{86,87} (see Figure 16.3). Hence, the amount of hexavalent chromium in these coatings itself plays an important role in the protection offered to the substrates. It is considered that chromates can migrate from a reservoir somewhere in the conversion coating or primer to a distant active exposed site on the metal surface to inhibit the attack.

Wan et al. used XANES to determine the Cr(III)/Cr(VI) ratios before and after exposure to aggressive chloride solution.⁸⁸ Kendig et al. suggested that

unique corrosion-protective property of CCCs to be due to the availability of a source of the hexavalent chromium species that acts as an active inhibiting species.⁸⁹ They concluded that leached Cr(VI) might be providing protection to the aluminum. A similar study was conducted by Jeffcote, et al.⁹⁰ Illevbare et al. studied the oxygen reduction reaction (ORR) kinetics on several IMC.⁹¹ Their results indicated that Cr_2O_3 inhibits ORR kinetics and that CCC acted as a diffusive barrier to O_2 transport. Recently, Clark et al. studied the galvanic corrosion between copper and aluminum using a specially designed electrochemical cell.⁹² Cr(VI) was observed to act as a strong irreversible cathodic inhibitor on Cu and AA2024.

A working hypothesis for chromates being such effective inhibitors is that it is a very soluble, higher-valent cation of an element with a lower-valent ion Cr(III) that is very poorly soluble and forms a protective film. Oxidation of aluminum by chromates has been proposed in the early part of the 20th century as the reason for protection of the substrate.^{51,57} The oxidation leads to the formation of a passive oxide film. The oxide film was suggested to be Al_2O_3 . Later, studies showed the presence of trivalent chromium in the oxide film, and a mechanism for protection included the formation of a trivalent chromium oxyhydroxide containing barrier layer.^{66,93} Reduction of hexavalent chromium at the flaws or defects to trivalent state is one of the widely accepted mechanisms.^{89,94} Hence, the presence of excess mobile hexavalent chromium in the coatings lends the self-healing properties that were discussed earlier. Based on these studies, and combining other results, a few models for the structure composition and behavior of the coatings have been proposed. A model initially proposed by Hughes et al.⁷¹ was later modified by Kearns et al.⁹⁵ Recently, the model was further modified by Vasquez.⁹⁶ Using SIRMS, XPS, SIMS and XANES, the influence of microstructure on CCC formation and composition was studied. The study revealed Cu-rich regions at the outer layers of CCCs. Cu-rich IMCs were found to be surface depleted of Cr and enriched in CN. A Cu-CN complexing mechanism has been verified for the inhibition of formation of CCCs on Cu-rich IMCs.

16.4.3 Phosphate Treatments

Phosphate surface treatments are used to enhance paint adhesion and aid in corrosion protection, primarily on steel. Strong adhesion results from forma-

tion of P-O-C primary bonds at the polymer coating/phosphate interface and P=O/Fe complexes at phosphate/steel interfaces.⁹⁷ Corrosion protection is provided by the non-conductive, kinetic barrier provided by the phosphate layer (as well as the strong bonding with the protective paint coating).⁹⁸ Zinc phosphate coatings are widely used on steel, zinc, aluminum and sometimes cadmium, tin and magnesium surfaces. Based on the design need, phosphate treatments can provide corrosion protection in combination with bonding enhancement or even electrical insulation.⁹⁹

Phosphate coatings are mostly conversion coatings (similar to the chromate conversion coatings described above), requiring reaction of the bare metal surface in a solution containing soluble primary metal phosphates, phosphoric acid and various accelerators.¹⁰⁰ In the conversion mechanism, activated metal dissolution from the surface consumes protons from the conversion complex, resulting in an insoluble product which is deposited on the substrate surface. Hence various methods of activating the metal surface are used in practice to enhance the phosphating treatment.¹⁰¹

A number of modifications have recently been tested, both in formulation and in methodology, in order to enhance the protective or adhesion-promoting capabilities of the phosphate coatings.

16.4.4 Composite Paint Coatings

Although simple polymeric coatings have been used for various applications for some time (i.e. varnishes, urethanes), it is of greater general interest to the surface engineering industry to discuss multi-layer composite paint coatings that are used in many transportation and infrastructure applications. Many of these recent composite paint coatings have been developed to reduce the overall use of volatile organic compounds (VOCs) and, hence, reduce the associated toxicological hazards. VOCs have been incorporated as solvents in coating systems of all types, including those currently in use in such diverse applications as the automotive, decorative, and protective industries. One principle strategy of VOC reduction has been the introduction of coatings incorporating very high solids content by volume.

High-solids coatings, upon curing, are considered to be composite materials in that they are uniform coatings consisting of a continuous organic polymeric phase (amorphous or crystalline) in which a variety of inorganic pigments and fillers are hetero-

geneously dispersed. The polymeric phase is generally referred to as the binder, and acts as an encompassing medium that contains the inorganic additives. Of course, the binder exhibits mechanical properties independent of the inorganic additives embedded in it, and these mechanical properties play a dominant role in the mechanical behavior and performance of the coating system. These properties are functions of the chemical origins of the binder, as well as a variety of characteristics that arise during binder formation (referred to as "curing").

Two-component polyurethanes are one family of binders that has garnered increased popularity in the coatings industry. This is due to their broad spectrum of good mechanical/chemical behavior in service (excellent abrasion resistance, good chemical barrier properties and weathering resistance, and high hardness and heat resistance) as well as their increased pot/shelf life. Although initially created in 19th-century Germany, polyurethanes found little commercial use until the mid-1950s. Currently, they are manufactured at enormous industrial scales and can be found in coatings, foams, sealants, adhesives and other polymeric products.

All polyurethanes exhibit both urethane as well as urea functionality. Most commonly, they are the product of a reaction between an isocyanate-bearing species with a hydrogen donor species (typically a polyol). The two components are mixed in the presence of a solvent and applied to the surface for which the coating has been designed. The solvent is eliminated from the coating via evaporation (governed by its own volatility) resulting in (ideally) a completely cured, co-reacted solvent-free coating. Of course, in order to create a continuous polymeric binder phase, both the polyol as well as the isocyanate components must be at least difunctional. The degree of cross-linking can be directly controlled by introducing co-reactants exhibiting progressively greater functionality. This increases the likelihood of co-reacting functional groups encountering each other during curing and forming covalent primary valency bonds.

The degree of cross-linking can have a large impact on the mechanical properties and behavior of the binder. Generally speaking, as the cross-link density increases, the free volume of the binder decreases. This decrease in free volume is beneficial to the barrier properties of the film in that it is less likely to admit foreign chemical species, particularly those with bulky side groups.^{13,102} Furthermore, the tensile strength and hardness increases, albeit along with the

coatings' brittleness. This increase in brittleness can be detrimental in that it decreases the impact resistance and increases the likelihood of cracking and splitting, especially during foreign object impingement.^{102,103} The nature of the co-reactants can also play a large role in the service behavior of the coating. The choice of isocyanate-bearing species is generally limited to aromatic and aliphatic molecules. Aromatics exhibit excellent hardness and chemical resistance but, due to their heavily conjugated bonding structure, are extremely vulnerable to UV-induced free radical attack and alteration. To avoid this, aliphatic isocyanate-bearing compounds have been introduced. The aliphatics have very good UV durability and exhibit excellent barrier and mechanical properties as well. They are, however, more expensive. Furthermore, due to the toxicological hazard associated with the high vapor pressure of low molecular weight, isocyanate-bearing mer units such as Hexamethylene Diisocyanate (HDI), oligomeric biuret forms of polyfunctional isocyanates are now being used. While this generally increases the average molecular weight and should as a result require a stronger solvent system, it is necessary for the compliance with toxic hazard reduction mandates.

During service, the failure of high-solids coating systems can occur by a variety of physio-chemical mechanisms. These range from delamination of the coating from the substrate; interlayer delamination of the coating system itself; cracking and splitting; and osmotic blister formation leading to de-adhesion at the substrate/coating interface. Many of these failures are the result of a series of reactions/responses by the coating system to applied environmental stress, often initially instigated by chemical alterations and ultimately manifested as a stress response to the new state. For example, delamination at the coating/substrate interface or interlayer interface, for that matter, is the direct result of interfacial shear stresses rising to the point where they overcome the adhesion strength of the coating.^{13,104} These shear stresses can arise for a variety of reasons (thermal expansion mismatch between coating and substrate, coating swelling due to solvent/plasticizer infiltration, etc.).

UV impingement is of particular interest since, in certain circumstances, the UV energy is sufficient to rupture even covalent "backbone" bonds of the binder^{13,15} (-C-C-). More common, however, is a mechanism of electron excitation in some predisposed component of the system. Ignoring the particular vulnerability of aromatics to UV exposure (their

use in this regard has been almost completely phased out), the coating system designer must consider the interaction between the inorganic components of the coating (extenders, pigments, anti-corrosive additives, etc.), the UV impingement likely to be experienced in service, and the organic binder. Should any of these have an appreciable degree of photoactivity, their use in outdoor applications should be reconsidered. Semiconductor materials such as metal oxides are common choices when encountering these problems.

The white pigment TiO_2 is a semiconductive material with a band gap of sufficiently low energy that the small amount of UV present at sea level can be sufficient to eject electrons from the valence band to the conduction band. These electrons can initiate a free-radical chain reaction wherein the organic binder material is oxidized (the oxygen being supplied by the atmosphere) and a variety of functional groups can be formed. If carbonyl groups are not formed, contemporary models propose the formation of hydroperoxides¹⁵ (leading to possible secondary valency bonds between adjacent polymer chains and a net reduction in free volume as well as an increase in T_g and brittleness), and/or peroxide cross-links between adjacent chains. Increases in cross-link density over and above that originally designed for can cause a general increase in intrinsic stress in the coating.^{102,103,105,106} If this cross-linking should proceed to the point where the internal stress of the coating exceeds its own cohesive strength, cracking and splitting is usually the result. Of course, chain scission is another possible outcome, along with the side effects associated with it (chalking, increased porosity, decrease in T_g , etc.).

High-solids coatings usually employ some form of UV reflectance or absorbance via inorganic or organic additives.¹³ Typically, metal additives such as aluminum flakes are employed. They consist of plate-like grains of aluminum that are oriented parallel to the coating surface. Their intent is to shield the organic binder from direct UV impingement. An additional benefit is in the fact that due to their plate-like shape they cause any infiltrating species to follow a more circuitous route to the substrate interface, thereby delaying any possible failures as a result of such mechanisms. However, the plate-like shapes also exhibit sharp geometric asperities at the edges which may result in stress concentrations being set up in the organic matrix, particularly during high cyclic loading applications.

It becomes clear, then, that coating performance can be greatly enhanced by the use of a variety of solids at large volume content, while simultaneously satisfying the requirement for lower VOC usage. It is also apparent that as the number of components present in a particular composite coating system is increased, the possible failure modes can grow exponentially, so care must be taken in characterizing the failure mechanisms of such systems.

16.4.5 “Self-healing” Coatings

As mentioned in our definition of “dependability,” the speed of repair is an essential characteristic in development of a useful surface protection technology. The ideal coating or treatment would therefore be “self-repairable” at a near-instantaneous rate. Currently, a number of such “smart” coatings are under development. Basically, any scratch or damage would have to “re-coat” or protect itself in some way, due to reactions of the exposed substrate with the external environment. The chromate conversion coatings mentioned previously are a good example of a “self-healing” coating (see Figure 16.3).

16.4.6 Thermal Spray Methods

Air plasma spray (APS) is an efficient means of materials deposition and is primarily used in making protective coating on variety of metallic and ceramic substrates.^{107,108} In this deposition process, materials are injected into a high energy flame in the form of a powder. The powder particles melt and deposit on to a substrate. Upon deposition, the particles spread and solidify rapidly. The coating is built up by the successive deposition of many particles. Plasma spray ceramic coatings such as alumina and zircon, especially those using an interfacing bond coating, can provide excellent wear resistance.¹⁰⁹ Plasma spray is very useful in formation of nanocomposite metal-metal oxide ceramic coatings which can provide wear resistance and thermal barrier properties.¹¹⁰ High-velocity flame spray techniques can produce very dense, abrasion resistant coatings on metals. For example, optimized high velocity flame spray deposited WC-Co coatings resulted in resistance to abrasive-erosion which was 10–12 times better than that of uncoated steel.¹¹¹ A wide variety of refractory carbide based coatings are used in industrial components to lower friction and improve wear resistance. Traditional thermal sprayed hard coatings have deficiencies in these applications due to their high hardness, brittleness, and

inherent stresses. Functionally gradient material (FGM) concepts offer a means for optimizing tribological performance, for processing of thick layers, and for similarly meeting design requirements.¹¹² For example, damage resistant, functionally graded, carbide-based coatings (i.e., WC-Co/stainless steel) to improve wear resistance have been deposited through plasma spray and high-velocity oxy-fuel spray processes (HVOF).¹¹³

16.4.7 Ion Beam Treatment of Surfaces and Ion Beam Assisted Deposition (IBAD)

Ion beams have found multiple uses in doping of semiconductors, depth profiling in surface spectroscopies (including the electron and ion beam spectroscopies mentioned in this chapter), and for treating surfaces or depositing coatings on engineering materials to enhance resistance to corrosion and wear. For several decades, ion beam techniques have been used to increase wear and corrosion resistance of metallic and ceramic materials.^{114–17} For example, pulsed ion beams have been used to melt and rapidly resolidify stainless steel surfaces in order to remove inhomogeneities which play a role in enhancing localized corrosion.¹¹⁸ Surface implantation using carbon, boron and nitrogen ion beams has been used to enhance smoothness and improve hardness of polymers, including Mylar and Teflon.¹¹⁹ The passivity of Ta in NaCl solution has been markedly improved following ion implantation by 200 keV nitrogen and xenon ions.¹²⁰

Other ion beam treatment techniques include ion beam mixing and ion beam assisted deposition (IBAD). In ion beam mixing, a thin layer of surface material deposited previously is bombarded with energetic inert ions. Transfer of kinetic energy to the surface layer atoms results in penetration of those atoms into the underlying substrate, often resulting in a metastable or amorphous phase structure.¹²¹ One of the most valuable aspects of using ion implantation or ion beam mixing is in creating surface layers with improved wear or corrosion properties without significant changes in part dimensions. Creation of nitrides through nitrogen implantation, near-surface TiC through implantation of Ti followed by C, or ion beam mixing of thin RF-deposited surface layers of Al, Si, Mo and W into steel all resulted in geometry changes of less than 100 nm, but significant improvements in wear and friction tests.¹²² These authors noted that ion beam mixing had the advantages

over implantation alone of no limitation in impurity concentration and possible use of simple ion implanters without mass separation.

Environmental concerns regarding the disposal of toxic byproducts from the production of electroplated hard chromium (EHC), widely used as a wear- and corrosion-resistant tribological coating, have led many to consider ion beam assisted deposition (IBAD) and similar coating processes as potential replacements for electroplating technology. The ability of the IBAD process to carefully control coating properties like adhesion and stoichiometry allows production of coating systems that surpass the durability of EHC, with virtually no hazardous waste or chemical exposure during production. Specifically, IBAD chromium nitride (Cr_xN_y) is considered a candidate for EHC replacement because of its good corrosion resistance, high hardness, and overall similarity (in appearance and chemical compatibility) to EHC. Several studies have investigated the deposition of Cr_xN_y coatings using reactive ion plating,^{123,124,125,126} reactive sputtering,^{127,128} and IBAD,^{129,130} and have concluded that Cr_xN_y coatings can be formed with a hardness greater than that of ordinary $\text{Cr}^{123-126,129}$ and a wear rate an order of magnitude lower.¹²⁹

To be considered a useful replacement process, however, IBAD must overcome some difficulties inherent in most low temperature PVD processes e.g., high residual internal coating stresses which can lead to coating delamination. IBAD has also found value in improving the corrosion resistance of titanium foil windows used in the dry scrubbing of flue gasses—ion assisted deposition of palladium produced a 0.5-micron thick coating with adhesion properties superior to that produced by other ion beam techniques.¹³¹ IBAD has been used to deposit corrosion resistance metal nitride coatings¹³² and in formation of Si-containing diamond-like carbon (Si-DLC) coatings¹³³ for wear resistance.

Another recent innovation in ion beam techniques is the development of gas cluster ion beam (GCIB) Surface Processing. GCIB, due to a combination of high cluster mass, energy and momentum, produces effects very different from single ion-type techniques.^{134,135} Even though each cluster possesses a large amount of energy, the per-ion energy is low and the penetration depth is low. In addition, in GCIB many ions strike the surface in a very coherent beam and nearly simultaneously. GCIB has shown advantages in formation of high aspect ratio features and in surface planarization. Hence, it is

being studied for applications in the semiconductor and microelectromechanical engineering industries.

16.4.8 Chemical Vapor Deposition (CVD) and Physical Vapor Deposition (PVD)

In general, chemical vapor deposition (CVD) involves chemical reaction in gaseous compounds on or near a heated surface to create a coating. It can be used to create nanostructured and functionally-graded coatings (described in greater detail in section 16.4.10) and is capable of non-line-of-sight deposition. CVD has been used extensively in deposition of semiconductors in microelectronics, development of hard coatings (such as SiC, TiN, BN, Al_2O_3), metallic films for microelectronics and for protective coatings, and for fiber coating.¹³⁶ There are many variants in the classic methods of chemical vapor deposition which can be used to form surface protective coatings. Plasma-enhanced CVD uses plasma to ionize and dissociate gases; photo-assisted CVD uses light and lasers to locally heat the substrate; metalorganic CVD (MOCVD) uses metalorganic complexes as the precursor source, resulting in lower deposition temperature; flame-assisted CVD uses flame as a heating source; and so forth. As noted from this list, most variants involve other methods of heating the substrate or ionizing complexes, or different types of precursor materials. The criteria for selecting a process include the need not to inadvertently damage the substrate; choice of the type and thickness of coating; the size and shape of the substrate; equipment availability; and cost.

Physical vapor deposition (PVD) techniques are usually line-of-sight (i.e., evaporation and sputtering), and usually require a vacuum system and sintered or solid target sources. In many cases, only relatively small parts can be coated. Deposition temperatures vary, based upon the technique and the need to heat the substrate. A drawback to sputtering and ion beam techniques is the possible occurrence of preferential sputtering of one element over another from a multi-component target. This can be avoided using laser ablation as a deposition technique, as noted below.

16.4.9 Pulsed Laser Deposition

Pulsed laser deposition (PLD) involves using laser sources (from excimer to UV to Ti-Sapphire to Nd-YAG) at various pulse rates (from near continuous to femtosecond) and pulse energies to ablate material

from a target onto a substrate. As with other PVD techniques, it is primarily line-of-sight and may or may not require a vacuum or controlled environment, based on the reactivity of the species to be deposited. As noted above, this technique avoids the problem of preferential sputtering and, hence, is especially useful for rapid combinatorial chemical design of prototype coatings. A wide variety of protective coatings have been formed with PLD, including nanocrystalline Fe-Al and Ni-Al intermetallics for wear and corrosion resistance,¹³⁷ Hastelloy thin films deposited on carbon steel,¹³⁸ Nd-laser deposition in vacuum of vitreous lead-borate glasses resistant to annealing and corrosion,¹³⁹ deposition of TiC on bearing steels at room temperature,¹⁴⁰ and deposition of titanium oxide coatings onto iron and steel substrates for corrosion resistance.¹⁴¹ In all cases, coatings of metallic or intermetallic materials showed both homogeneity and uniformity of microstructure.

Pulsed laser ablation is a well-known technique used for thin film deposition of a variety of thin films for various applications. The diversity of thin films grown by this technique is extensive, though most of the films have been deposited using excimer lasers.^{142–145} However, a major disadvantage of the use of excimer lasers has been the deposition of irregular melted droplets on the deposited film. The source of these particulates has been attributed to heterogeneities of the target, fluctuations in the laser fluence, and other irregularities of the process. Most traditional laser processing is thermal-based, where surface temperatures rise to the melting and/or boiling point for material removal. Femtosecond laser ablation has emerged as a technique with distinct advantages over thermal laser-based coating deposition methods.

The extremely short pulse duration results in reduction or complete prevention of lateral thermal damage, as well as lower and more precise threshold fluences of ablation, quite unlike conventional nanosecond pulsed laser ablation. If the pulse duration is reduced to the pico- and femtosecond regime, the pulse intensity becomes high enough to initiate optical breakdown in the material, which results in non-thermal energy deposition and subsequent material removal. A review comparing femtosecond laser deposition and nanosecond pulse deposition of metals, polymers, semiconductors and ceramics is given by Shirk and Molian.¹⁴⁶ They concluded that the femtosecond pulses offer several advantages over longer pulses (nanosecond) in addition to negligible

thermal damage, including higher energy density, greater material removal and capability of processing any material. A number of other recent articles have noted these advantages for material ablation.^{147–151} Recently, femtosecond laser ablation has been utilized to produce a variety of thin films, including a-CN_x,¹⁵² ZnO films grown on Al₂O₃,¹⁵³ diamond-like carbon thin films,¹⁵⁴ thin gold films,¹⁵⁵ TiN films on silicon,¹⁵⁶ and SnO₂.¹⁵⁷

16.4.10 Functionalized Nanostructured Coatings Development

Functionalized nanostructures are currently being produced as coatings (including functionally graded coatings) using a number of the techniques described above, either individually or in combination. Nanoscale structure, whether referring to nanocrystallinity, nanoscale clusters, or supramolecular architecture represents the focus of much current research in development of functional engineering coatings. Roughly, these coatings may be divided into those which have unique properties (i.e., resistance to wear) based on the presence of nanoscale (10^{-9} to nearly 10^{-7} meters) crystals or particles, or those which are based on large molecules or complexes (e.g., supramolecules, crown ether structures), which by their chemical nature display new properties and performance. Though there is not room here to discuss many examples and the advantages or disadvantages of each, some of the examples cited previously do fall into one or the other of these categories. We have mentioned diamond-like nanocomposites and femtosecond laser deposited coatings, both of which represent functionalized nanostructured coatings. The composite paint coatings described earlier also contain nanoscale inorganic components that improve strength and performance.

Catledge et al. have recently used IBAD techniques to deposit a functionally-graded, nanocrystalline metalloceramic coating for Co-Cr-Mo alloys.¹⁵⁸ This coating is “functionally-graded” in that it is composed of metallic initial layers and a hard ceramic outer coating (Cr/CrTi/CrTiN). This type of grading results in improved strength, toughness and adhesion to the substrate. Functionally graded materials were first proposed to improve adhesion and minimize thermal stress in metal-ceramic composites used for rocket engines.¹⁵⁹ In the case of this coating, the inner metallic layers improve adhesion to the substrate and to the outer layer of the coating,

which is covalent in nature and provides wear and scratch resistance. The nanoscale nature of the grains of Cr formed at the metal interface improve both strength and toughness, and serves as a barrier to crack formation and propagation. Nanostructured mullite ($3\text{Al}_2\text{O}_3 \cdot \text{SiO}_2$) coatings have been found to have significantly higher hardness and Young's modulus as compared to a coating with micron sized grains.¹⁶⁰ Hard ceramic coatings, in general, show high plasticity,¹⁶¹ and the graded nature of this coating results in even greater toughness. Recently, a functionally graded coating with decreasing Si_3N_4 content from substrate to pure mullite outer layer has been developed to decrease sharp stress discontinuities at the substrate/coating interface.¹⁶² Other functionally graded coatings which have been reported on recently include TiC-TiN gradient coatings for wear resistance,¹⁶³ and a two-layer yttria stabilized zirconia YSZ /alumina coating deposited by HVOF plasma spray.¹⁶⁴ Nanoscale functional multi-layers have been used to reduce stress in hard coatings,¹⁶⁵ prevent crack tip propagation^{165,166} and increase volume energy by interaction of Fermi surfaces with additional Brillouin zones.^{167,168}

The second category of nanostructured coatings, based on the formation of coatings with unique supermolecular structure or containing large organic or inorganic complexes, can also be formed through various techniques, including variants of CVD and sol-gel processing, for example. In fact, many polymeric films may fall within this category. Hence, this is not always a new technology but rather a new approach to understanding, modeling and formulating protective coatings. In recent developments, a sol-gel method has been used to form a nanostructured polyurethane/oligosiloxane ceramer coating for aircraft.¹⁶⁹ The polyurethane provided the general mechanical properties and the polysiloxane functioned as an adhesion promoter and corrosion inhibitor. Certain conversion coatings made up of a complex molecular structure or self-healing coatings containing "reservoirs" of labile molecules may be considered nanostructured materials. The chromate conversion coatings, containing molecular complexes composed of mixed Al and Cr oxides as well as labile chromate species, could be considered nanostructural coatings.

As a candidate replacement technology for chromate conversion coatings on AA2024-T3, a new sol-gel technique using a preformed, self-assembled, nano-phase particle (SNAP) sol-gel system has been developed.¹⁷⁰ The SNAP coating was found to be

defect-free and interacted strongly with both the substrate and polymeric topcoat layers, hence fulfilling some of the requirements for a CCC-replacement technology. Recently, this hybrid nanocomposite coating's barrier performance has been improved by use of alumino-silane cross-linking.¹⁷¹

Table 16.6 provides a brief summary of the advantages and disadvantages of the coating and surface engineering technologies discussed.

16.5 THE ROLE OF COMPUTER MODELING

As computer programs and computer hardware have become both more sophisticated and more affordable, the role of numerical modeling in developing coatings and surface treatment technologies has come to the forefront of design and manufacturing. For the last 30 years, numerical modeling of processes at surfaces have suggested methods for optimization as well as innovations in surface modification. For example, numerical modeling has been used to model growth kinetics for a two-stage process for diffusion coating of Ni with Al.¹⁷² At elevated temperature, the aluminizing step was modeled as rapid parabolic growth of $\gamma\text{-Ni}_2\text{Al}_3$ at the interface, followed by homogenization. Computer modeling has been cited in the development and optimization of numerous plating and electrochemical surface finishing techniques.¹⁷³ The corrosion protective ability of paints on metal surfaces has been predicted using models which take into account changes in the ellipsometric parameter related to thickness alterations in the substrate oxide film.¹⁷⁴ Durability of coatings has been predicted by Cr solubility in Fe during a two-phase Cr coating process, showing good agreement with experiment.¹⁷⁵ Optical and topographic measurements have recently been combined in computer models to provide realistically rendered graphic images representing color and gloss standards for development of paint formulations.¹⁷⁶ Certainly, data handling and analytical techniques have provided a basis for accurate application of spectroscopic data to surface analysis, as noted in the examples described previously in this chapter.

Process engineering, especially, has benefited from the use of sophisticated numerical modeling. For example, computer modeling has played an important role in predicting the evaporation of solvents in coatings.¹⁷⁷ Computer modeling has provided a

TABLE 16.6 Advantages and Disadvantages of Some Surface Engineering Technologies

| Treatment technology | Advantages | Disadvantages |
|---|--|--|
| Chromate conversion coating (CCC) | “Self-healing” corrosion protection, especially for aluminum alloys Good adhesion for paint coatings | Contains carcinogenic hexavalent chromium |
| Phosphate treatments | Good for corrosion protection of steel Promotes paint adhesion | Non self-healing |
| Composite paint coatings | Proven technology; easy to apply Many formulations tailored to various design needs | Susceptibility to UV damage; pretreatment needed to promote adhesion |
| Thermal spray coatings | Non-vacuum technique Can coat large parts Can create free-standing coatings Good for a wide range of substrates Metallic, ceramic, polymer coatings possible | Line-of-sight coating technique Support structure needed for large-scale deposition Relatively thick coatings |
| Ion beam implantation | Good for forming wear, corrosion resistant surface regions on small areas; does not alter dimensions of part Ion beam mixing can be used for pre-deposited layers on surface | Possible radiation damage during process; vacuum technique Shallow penetration depth of ions |
| Ion beam assisted deposition | Good for functionally graded coatings, DLC | May need temperature control of substrate to improve coating formation, adhesion; vacuum technique |
| Laser ablation | Femtosecond, UV laser ablation results in little target or substrate heating Nanostructured coatings possible Can use pressed pellet targets No preferential sputtering | Excimer ablation can result in melting Vacuum necessary for reactive species |
| Chemical vapor deposition | Non-line-of-sight Variations enable lower substrate temperatures and control of coating thickness and morphology | Usually requires a heated substrate and a controlled-atmosphere chamber Can be low or high costs depending on variant chosen |
| Physical vapor deposition (PVD). | Most variants well understood Can control phases, morphology | Line-of-sight Usually requires a vacuum system Preferential sputtering from multi-element targets a problem Often expensive solid or sintered targets |
| Functionally-graded nanostructured coatings | A variety of coatings with tailorable performance characteristics may use various techniques (IBAD, thermal spray, PLD). Can be matched to substrate and design and environment conditions | Depends on techniques used |

way to combine multiple numerical analyses of substrate, coating method, and process in order to help understand current manufacturing processes and optimize them. Pranckh and Scriven have described a computer-aided method to simultaneously solve basic equations for fluid properties, including inertia, viscous forces, capillary forces, and elastic forces involved in blade coating of a deformable substrate,

which takes into account blade velocity and stiffness, coating thickness and geometry of the substrate.¹⁷⁸

Finite element computer programs have found important roles in numerous surface engineering technology development efforts, including prediction of skin thickness and distribution as a function of processing conditions and material properties in powder co-injection molding,¹⁷⁹ minimization of

potential energy at surface using finite elements in computer aided geometric design,¹⁸⁰ and boundary element modeling of a coating-substrate composite subjected to a stress field, taking into account the elastic moduli of both substrate and coating, as well as coating thickness.¹⁸¹ Finite element analysis has been used to study residual thermal stress in ceramic gradient wear-resistant coatings.¹⁸²

While these are just a few examples, many more exist that can be found in the examples provided by the manufacturers of many current finite element modeling packages. These methods are especially useful for examining the role of substrate surface energy, stress in coatings, and their influence on adhesion. It is clear that more sophisticated programs which are coming into common use will expand the role of computer modeling in this regard.

Currently, computer-based numerical methods are being tested and used that combine the prediction of single properties based on chemical formulation, with the type of interactive procedures mentioned above as in the case of finite element methods, used in prediction of substrate/coating properties such as adhesion and corrosion barrier properties. The optimization programs have been developed based on expert system interpretive databases, statistical analysis, and neural network principles. For example, a method based on spline interpolation has been developed by Guthrie and Lin¹⁸³ and has recently been applied to development of anti-corrosion coatings.¹⁸⁴ In this latter study, ratios of common paint pigments were combined with empirical data on hardness, flexibility, and adhesion of sample coatings, and a predictive model involving a spline interpolation fitting of data provided a reasonable prediction of optimum composition for corrosion protection. This was verified through salt-spray test results.

In addition to the predictive and analytical applications of computer modeling described above, use of modeling to describe microscopic surface features and even the molecular structure of surfaces and coatings can provide important insights for sur-

face engineering and coatings development. For example, modeling the micro-topography of a surface can provide important insight into adhesion of coatings by predicting interlocking sites on a substrate surface.¹⁸⁵ Molecular modeling is also being used to provide a better understanding of coating properties such as adhesion and surface coverage. Modeling of the interaction between methylbenzoyl propionic acid, the active ingredient in a waterborne corrosion inhibitor, and an iron oxyhydroxide surface indicated both the binding sites and packing efficiency with few gaps indicative of good adhesion.¹⁸⁶ The total interaction energy between surfaces and protein molecules has been used to help explain adhesion behavior based on local extremes in the calculated energies.¹⁸⁷ It is clear that sophisticated calculation of surface energies, topographies, and molecular interactions will lead to improved models of coating adhesion, surface protection, and other properties of interest to the surface engineering community. As these calculations are combined with statistical analysis and finite element methods, a more accurate, realistic and subsequently empirically useful data base will be developed.

16.6 SUMMARY

There is little doubt that extension of current performance requirements of engineered systems will continue and, along with them, the need to select or develop surface treatment or coating technologies that will optimize system performance. As can be seen from the examples presented here, there are three essential issues when considering how to develop a surface engineering process or system to meet design needs: (1) critical design knowledge, (2) critical system components, and (3) the critical actions which describe how the system will react or protect the substrate. Some of the elements corresponding to these different issues are summarized in Table 16.7.

TABLE 16.7 Critical issues in surface engineering selection and design

| Critical Knowledge | Critical Components | Critical Actions |
|---|---|--|
| Substrate composition Surface features, inclusions, defects Cleanliness Operating environment Engineering functions | Substrate Bare surface/treatment interface Pre-treatment Coating system Coating/environment interface | Environmental attack Direct energetic surface treatment Coating process Surface pre-treatment Cleaning/polishing |

For example, without the critical knowledge of surface composition, including inclusions or defects, choosing or developing an alternative coating system to deal with environmental attack would likely be unsuccessful.

Along with these critical issues, the surface engineer needs to consider the broad range of technologies available to help characterize and understand changes in surface chemistry and surface damage modes, and the need to understand both the value and the limitations of those technologies. Surface engineering will only advance as a field with the careful application of analysis, synthesis, and computational modeling—and, most importantly, recognition of the need to combine all three with a clear understanding of the manufacturing and design needs which drive development.

16.7 REFERENCES

- Keene, L., Clayton, C. R., Halada, G. P., McKnight, S. and Kosik, W. In *State-of-the-Art Application of Surface and Interface Analysis Methods to Environmental Material Interactions: In Honor of James E. Castle's 65th Year*, D. Baer, C. R. Clayton, G. Davis and G. Halada, Eds. *Proceedings of the Electrochemical Society*. Pennington, NJ: The Electrochemical Society, Vol. 2001–5, pp. 197–206, 2001.
- Leblanc, P., Frankel, G. S. *State-of-the-Art Application of Surface and Interface Analysis Methods to Environmental Material Interactions. Proceedings of the Electrochemical Society*. Vol. 2001–5, pp. 224–239, 2001.
- Suter, T., Alkire, R. C. *Journal of the Electrochemical Society*, Vol. 148(1), pp. B36–B42, 2001.
- Park, J. O., Paik, C. H., Huang, Y. H., Alkire, R. C. *Journal of the Electrochemical Society*, Vol. 146(2), pp. 517–523, 1999.
- Vasquez, M. J., Kearns, J. R., Halada, G. P., and Clayton, C. R. *Surface and Interface Analysis*, Vol. 33(10/11), pp. 796–806, 2002.
- Von Wolzogen, C. A. H. and van der Vlugt, L. S. *Water* The Hague, Vol. 18, p. 147, 1934.
- National Bureau of Standards. *Economic Effects of Metallic Corrosion in the United States*. NBS Special Publication 511-1. Washington, DC: National Bureau of Standards, 1978.
- Shearer, B. J. *Journal of the American Dental Association*, Vol 127, p. 181, 1996.
- Castle, J. E. In *Application of Surface Analysis Methods to Environmental/Materials Interactions*. D. R. Baer, C. R. Clayton and G. D. Davis, Eds. Pennington, NJ: Electrochemical Society, p. 1, 1991.
- Clayton, C. R. and Olefjord, I. In *Corrosion Mechanisms*. P. Marcus and J. Oudar, Eds. New York: Marcel Dekker, 1995.
- Cosemans, P., Zhu, X., Celis, J. P., Van Stappen, M. *Surface and Coatings Technology*, Vol. 174–175, pp. 416–420, 2003.
- Chidambaram, D., Vasquez, M. J., Halada, G. P. and Clayton, C. R. *Surface and Interface Analysis*, Vol. 35, pp. 226–230, 2003.
- Hare, C. H. *Protective Coatings: Fundamentals of Chemistry and Composition*, The Society for Protective Coatings, 1994.
- Irusta, L., Fernandez-Berridi, M. J. *Polymer Degradation and Stability*, Vol. 63, pp. 113–119, 1999.
- Wilhelm, C., Gaudette, J. *Polymer*, Vol. 33(16), pp. 4,019–4,031.
- Allen, A. O. *The Radiation Chemistry of Water and Aqueous Solutions*, Princeton: Van Nostrand, 1961.
- Spinks, J. W. T. and Woods, R. J. *An Introduction to Radiation Chemistry, 3rd Ed.* New York: Wiley-Interscience, 1990.
- Sunder, S. and Shoesmith, D.W. Report AECL-10395, Atomic Energy of Canada, Ltd., 1991.
- Sattonay, G., Ardois, C., Corbel, C., Lucchini, J. F., Barthe, M. F., Garrido, F., and Gosset, D. *Journal of Nuclear Materials*, Vol. 288, pp. 11–19, 2001.
- Urbanic, F. Cox, B. and Field, G. J. ASTM Special Technical Publication 939, pp. 189–205, 1987.
- Sawasaki, T., Tanabe, T., Yoshida, T. and Ishida, R. *Journal of Radioanalytical and Nuclear Chemistry*, Vol. 255(2), pp. 271–274, 2003.
- Maozhong Min, Weidong Zhong, Haosheng Jiang and Chemgyun Qi, *Yuanzining Kexue Jishu*, Vol. 27(5), pp. 458–463, 1993.
- Friedman, H. A., Dole, L. R., Gilliam, T. M. and Rogers, G. C. NTIS Report, ORNL/TM-9412, Energy Research Abstracts, Vol. 10 16, 1985.
- Wronkiewicz, D. J. *Mat. Res. Soc. Symp. Proc.*, Vol. 333 Scientific Basis for Nuclear Waste Management XVII, pp. 83–97, 1994.
- Kroth, K., Barnett, E., Bruecher, P. H., Lammertz, H. and Niephaus, D. *Waste Management '90*, Vol. 2, pp. 363–368, 1990.
- Macdonald, D. D. and Urquidi-Macdonald, M. *Corrosion*, Vol. 46(5), pp. 380–390, 1990.
- DeRose, P., Hwang, J., and Goldner, L. S., *Proc. SPIE, Laser Techniques for Surface Science III*, Vol. 3,272, pp. 93, 1998.
- Binnig, G., Quate, C.F., and Gerber, Ch., *Physical Review Letters*, Vol. 56(9), pp. 930–933, 1986.
- Melendres, C. A., Beden, B., Bowmaker, G., Liu, C. and VOL. Maroni, VOL. A. *Langmuir*, Vol. 9, p. 1, 1980, 1993.
- Melendres, C. A., Beden, B., and Bowmaker, G. *Journal of Electroanalytical Chemistry*, Vol. 383, p. 191, 1995.

31. Bron, M. and Holze, R. *Journal of Electroanalytical Chemistry*, Vol. 385, p. 105, 1995.
32. Neufeld, A. K. and Cole, I. S. Proceedings of the 13th Annual Corrosion Congress, paper 46, pp. 1–8, 1996.
33. Uno, M. *Oputoronikusu*, Vol. 122, pp. 87–92, 1992.
34. Vaagberg, L. *Kem. Tidskr.*, Vol. 101(10), pp. 45–52, 1989.
35. Dibbern-Brunelli, D., Atvars, T. D. Z., Joekes, I. and VOL.Barbosa, VOL. C. *Journal of Applied Polymer Science*, Vol. 69(4), pp. 645–655, 1998.
36. Retzko, I., Friedrich, J. F., Lippitz, A. and Unger, W. E. S. *Journal of Electron Spectroscopy and Related Phenomena*, Vol. 121, pp. 111–129, 2001.
37. Sahre, K., Eichhorn, K., Simon, F., Pleul, D., Janke, A. and Gerlach, G. *Surface and Coatings Technology*, Vol. 139(2–3), pp. 257–264, 2001.
38. Dodge, C. J., Francis, A. J., Gillow, J. B., Halada, G. P., Eng, C. W. and Clayton, C. R. *Environmental Science and Technology*, Vol. 36(16), pp. 3,504–3,511, 2002.
39. Stoch, A., J. Stoch, J. Gurbiel, M. Cichocinska, M. Mikolajczyk and M. Timler, *Journal of Molecular Structures*, Vol. 596, pp. 201–206, 2001.
40. Clayton, C. R. and G. P. Halada. *Zairyo-To-Kankyo (Corrosion Engineering)*, Vol. 50, pp. 364–372, 2001.
41. Maldener, J., F. Rauch, M. Gavranic and A. Beran, *Minerology and Petrology*, Vol. 71(1–2), pp. 21–29, 2001.
42. Ruau, O., P. Landais, and J. L. Gardette, *Fuel*, Vol. 76(7), pp. 645–653, 1997.
43. Gadoum, A., B. Gosse and J. P. Gosse, *Journal of Applied Polymer Science*, Vol. 62(10), pp. 1,679–1,692, 1996.
44. Buffeteau, T., B. Desbat, and D. Eyquem, *Vibrational Spectroscopy*, Vol. 11(1), pp. 29–36, 1996.
45. Bruni, S., F. Cariati, F. Casadio, and L. Toniolo, *Vibrational Spectroscopy*, Vol. 20(1), pp. 15–25, 1999.
46. Sweeney, M., F. Gaillard, I. Linossier, N. Boyer, and I. Stevenson, *Spectra Analysis*, Vol. 23(176), pp. 33–38, 1994.
47. Cushman, A. S. *Science*, Vol. 27, p. 666, 1908.
48. Cushman, A. S. *Engineering Record*, Vol. 57, p. 540, 1908.
49. Bauer, O. and O. Vogel, *Journal of the Society of Chemical Industry*, Vol. 35, p. 543, 1916.
50. Callendar, L. H. *Journal of the Institute of Metals*, advance proof 1925.
51. Callendar, L. H. *Engineering*, Vol. 120, p. 340, 1925.
52. Department of Science and Independent Research of Britain, Anodic oxidation of aluminum and its alloys as a protection against corrosion, 1926.
53. Edwards, J. D. and R. I. Wray, *Industrial and Engineering Chemistry Research*, Vol. 27, p. 1,145, 1935.
54. Herbig, W. *Aluminium*, Vol. 19, p. 371, 1937.
55. Rohrig, H. and K. Gaier, *Aluminium*, Vol. 19, p. 448, 1937.
56. Evans, U. R., *Journal of the Chemical Society*, Vol. 129, p. 1–20, 1927.
57. Edeleanu, C. and U. R. Evans, *Transactions of the Faraday Society*, Vol. 47, p. 1,121, 1951.
58. Bauer, O. and O. Vogel, GB Patent No. 226776, 1923.
59. Heine, M. A. and M. J. Pryor, *Journal of the Electrochemical Society*, Vol. 114, pp. 1001–1005, 1967.
60. Newhard, Jr., N. J., D. Y. Dollman, and L. Steinbrecher, Amchem Products, Inc. US Patent No. 2988465, 1961.
61. Newhard, Jr., N. J., Amchem Products, Inc. US Patent No. 3377212, 1968.
62. Russell, W. S. Hooker, Chemical Corp. US Patent No. 3385738, 1968.
63. Pearlstein, F. and L. Teitell, *Materials Performance*, 1974.
64. Materials Safety Data Sheet for Alodine 1200S, Parker-Amchem, Henkel Corporation Report, Parker-Amchem, Henkel Corporation.
65. Newhard, N. J., Jr., *Metal Finishing*, Vol. 70, p. 49, 1972.
66. Treverton, J. A. and N. C. Davies, *Metals Technology*, London, Vol. 4, p. 480, 1977.
67. Katzman, H. A., G. M. Malouf, R. Bauer, and G. W. Stupian, *Applied Surface Science*, Vol. 2, p. 416, 1979.
68. Hagans, P. and C. M. Haas, *Surface and Interface Analysis*, Vol. 21, p. 65, 1994.
69. Abbas, H. M., *Metal Finishing*, Vol. 93, p. 4, 1995.
70. Marikkannu, C., P. B. Srinivasan, S. Sathiyarayanan, and K. Balakrishnan, *Transactions of the Institute of Metal Finishing*, Vol. 73, p. 34, 1995.
71. Hughes, A. E., R. J. Taylor, and B. R. W. Hinton, *Surface Interface Analysis*, Vol. 25, p. 223, 1997.
72. Xia, L. and R. L. McCreery, *Journal of the Electrochemical Society*, Vol. 146, p. 3,696, 1999.
73. Juffs, L., A. E. Hughes, and P. J. K. Paterson, *Micron*, Vol. 32, p. 777, 2001.
74. Koudelkova, M., J. Augustynski, and H. Berthou, *Journal of the Electrochemical Society*, 1977.
75. Treverton, J. A. and N. C. Davies, *SIA, Surface and Interface Analysis*, 1981.
76. Abd Rabbo, M. F., J. A. Richardson, and G. C. Wood, *Corrosion Science*, Vol. 18, p. 117, 1978.
77. Yu, Zuzhan; Ni, Hongbin; Zang, Guansheng; Wang, Yamei; Dong, Shuzhong; Zhao, Guogin, *Applied Surface Science*, Vol. 62(4), pp. 217–221, 1992.
78. Rona, M. Z. Laszewska, and Y. A. E. Rafael, *Metal Finishing*, Vol. 86, p. 41, 1988.
79. Treverton, J. A. and M. Amor, *Journal of Material Science*, Vol. 23, p. 3706, 1988.
80. Brown, G. M. K. Shimizu, K. Kobayashi, G. E. Thompson, and G. C. Wood, *Corrosion Science*, Vol. 35, p. 253, 1993.
81. Breslin, C. B., G. Treacy, and W. M. Carroll, *Corrosion Science*, Vol. 36, p. 1,143, 1994.

82. Waldrop, J. R. and M. W. Kendig, *Journal of the Electrochemical Society*, Vol. 145, p. L11, 1998.
83. Halada, G. P., C. R. Clayton, M. J. Vasquez, J. R. Kearns, M. W. Kendig, S. L. Jeanjaquet, G. G. Peterson, G. S. McCarthy, and G. L. Carr, in *Critical Factors in Localized Corrosion III, A Symposium in Honor of the 70th Birthday of Jerome Kruger: 194th Meeting of the Electrochemical Society*, R. G. Kelly, P. M. Natishan, G. S. Frankel and R. C. Newman, Eds, 98-17, p. 139, The Electrochemical Society 1999.
84. Brown, G. M. and K. Kobayashi, *Journal of the Electrochemical Society*, Vol. 148, p. B457, 2001.
85. Xia, L., E. Akiyama, and G. Frankel, *Journal of the Electrochemical Society*, Vol. 147, p. 2,556, 2000.
86. Zhao, J., G. S. Frankel, and R. L. McCreery, *Journal of the Electrochemical Society*, Vol. 145, p. 2,258, 1998.
87. Ramsey, J. D. and R. L. McCreery, *Journal of the Electrochemical Society*, Vol. 146, p. 4,076, 1999.
88. Wan, J., G. E. Thompson, K. Lu, and C. J. E. Smith, *Physica B*, Vol. 209, p. 511, 1995.
89. Kendig, M. W., A. J. Davenport, and H. S. Isaacs, *Corrosion Science*, Vol. 34, p. 41, 1993.
90. Jeffcoate, C. S., H. S. Isaacs, A. J. Aldykiewicz, and M. P. Ryan, *Journal of the Electrochemical Society*, Vol. 147, p. 540, 2000.
91. Ilevbare, G. O. and J. R. Scully, *Journal of the Electrochemical Society*, Vol. 148, p. B196, 2001.
92. Clark, W. J., J. D. Ramsey, R. L. McCreery, and G. S. Frankel, *Journal of the Electrochemical Society*, Vol. 149, p. B179, 2002.
93. Sunderland, R. *Japanese Journal of Applied Physics*, Vol. 1, p. 347, 1974.
94. Lytle, F. W., R. B. Greeger, G. L. Bibbins, K. Y. Blohowiak, R. E. Smith, and G. D. Tuss, *Corrosion Science*, Vol. 37, p. 349, 1995.
95. Kearns, J. R. (1999).
96. Vasquez, M. J., G. P. Halada, C. R. Clayton, and J. P. Longtin, *Surface and Interface Analysis*, Vol. 33, p. 607, 2002.
97. Chhiu-Tsu Lin, Ping Lin and Faernando Quitian-Puello, "Interfacial Chemistry of a Single-Step Phosphate/Paint System," *Industrial and Engineering Chemical Research*, Vol. 32, pp. 818–825, 1993.
98. Leidheiser, Jr., H., "Electrical and Electrochemical Measurements as Predictors of Corrosion at the Metal Organic Interface," *Progress in Organic Coatings*, Vol. 7, p. 79, 1979.
99. Freeman, D.B. *Phosphating and Metal Pre-Treatment*. New York: Industrial Press. (1986).
100. Pearlstein, F. *Plating and Surface Finishing*, Vol. 22, no. 12, (1978).
101. Yang, J. K., J. G. Kim, J. S. Chun, *Thin Solid Films*, Vol. 10, p. 1, 1983.
102. Wicks Jr., Z. W., D. A. Wicks, J. W. Rosthauser, *Progress in Organic Coatings*, Vol. 44, 161–183, 2002.
103. Nichols, M. E., C. A. Darr, *Journal of Coatings Technology*, Vol. 70, No. 885, October 1998.
104. C. Boiziau, G. Lecayon, *Surface and Interface Analysis*, Vol. 12, pp. 475–485, 1988.
105. Nichols, M. E., J. L. Gerlock, C. A. Smith, C. A. Darr, *Progress in Organic Coatings*, Vol. 35, 153–159, 1999.
106. Abdelkader, A. F., J. R. White, *Progress in Organic Coatings*, Vol. 44, pp. 121–129, 2002.
107. Herman, H. *Scientific American*, Vol. 256, p. 112, 1988.
108. Herman, H. and S. Sampath, in *Metallurgical and Ceramic Protective Coatings*. K.H. Stern, Ed. London: Chapman and Hall, London, p. 261, 1996.
109. Das, S., Bandyopadhyay, P. P., Bandyopadhyay, T. K., Ghosh, S., Chattopadhyay, A. B. *Metallurgical and Materials Transactions A: Physical Metallurgy and Materials Science*, Vol. 34A 9, pp. 1,909–1,918, 2003.
110. Goswami, R., H. Herman, S. Sampath, X. Jiang, Y. Tian and G. Halada, *Surface and Coatings Technology*, Vol. 141, no. 2, pp. 220–226, 2001.
111. Arensburger, D. S., Sergei Yu. Zimakov and Priit A. Kulu, *Powder Metallurgy and Metal Ceramics*, Vol. 40, no. 3–4, pp. 127–134 2001.
112. Prchlik, L., Sampath, S., Gutleber, J., Bancke, G., Ruff, A. W., *Wear*, Vol. 249(12) pp. 1,103–1,115, 2001.
113. Prchlik, L., Vaidya, A., Sampath, S., *Ceramic Transactions*, Vol. 114 Functionally Graded Materials 2000, pp. 111–118, 2001.
114. Hartley, A. E. W. *Wear*, Vol. 34, p. 427, 1978.
115. Hirvonen, J. K. *Journal of Vacuum Science and Technology*, Vol. 15, p. 1,664, 1978.
116. Cuomo, J. J., J. M. E. Harper, C. R. Guarnieri, *Journal of Vacuum Science and Technology*, Vol. 20, p. 349, 1982.
117. Bull, S., *Materials World*, Vol. 1(6), pp. 340–342, 1993.
118. Buchheit, R. G., Maestas, L. M., McIntyre, D. C., Stinnett, R. W., Greenly, J. B., Sandia National Laboratories, Albuquerque, NM. Ed(s):. Srivatsa, Arun R., Clayton, Clive R., Hirvonen, James Karsten. *Advances in Coatings Technologies for Corrosion and Wear Resistant Coatings: Proceedings of a Symposium*, Las Vegas, NeVol., Feb. 12–16, 1995, pp. 163–72, 1995.
119. Lee, E. H., Lewis, M. B., Blau, P. J., Mansur, L. K., *Journal of Materials Research*, Vol. 6(3), pp. 610–28, 1991.
120. Huang, Ningkang, Feng, Zhirong, *Thin Solid Films*, Vol. 199(1), pp. 37–44, 1991.
121. Jagielski, J., A. Piatkowska, Z. Rymuza, Z. Kuszniere-wicz, D. Treheux, D. Boutard, L. Thome and G. Gawlik, *Wear*, Vol. 238, pp. 48–55, 2000.
122. Jagielski, J., A. Piatkowska, Z. Rymuza, Z. Kuszniere-wicz, D. Treheux, D. Boutard, L. Thome and G. Gawlik, *Wear*, Vol. 238, pp. 48–55, 2000.
123. Komiya, S., S. Ono, N. Umezue and T. Narusawa, *Thin Solid Films*, Vol. 45, p. 433, 1977.
124. Sato, T., M. Tada and Y. C. Huang, *Thin Solid Films*, Vol. 54, p. 61, 1978.

125. Wang, D. and T. Oki, *Thin Solid Films*, Vol. 185, p. 219, 1990.
126. Kashiwagi, K., K. Kobayashi, A. Masuyama and Y. Murayama, *Journal of Vacuum Science and Technology, A*, Vol. 4(2), p. 210, 1986.
127. Fabis, P. M., R. A. Cooke and S. McDonough, *Journal of Vacuum Science and Technology, A*, Vol. 8(5), p. 3,809, 1990.
128. Shih, K. K., D. B. Dove and J. R. Crowe, *Journal of Vacuum Science and Technology, A*, Vol. 4(3), p. 564, 1986.
129. Sugiyama, K., K. Hayashi, J. Sasaki, O. Ichiko and Y. Hashiguchi, *Surface and Coatings Technology*, Vol. 66, p. 505, 1994.
130. Ensinger, W., M. Kiuchi, Y. Horino, A. Chayahara, K. Fujii and M. Satou, *Nuclear Instrumentation and Methods, B*, Vol. 59/60, p. 259, 1991.
131. Barson, S. D., Skeldon, P., Thompson, G. E., Kolitsch, A., Richter, E., Wieser, X., Piekoszewski, J., Chmielewski, A. G., Werner, Z., Corrosion and Protection Centre, University of Manchester Institute of Science and Technology, Manchester, UK. *Surface and Coatings Technology*, Vol. 127(2–3), pp. 179–192, 2000.
132. Demaree, J. D., W. E. Kosik, C. R. Clayton and G. P. Halada, in *Surface Engineering in Materials Science I*, Proceedings of a Symposium during the TMS Annual Meeting, Nashville, Tennessee, March 12–16, 2000, pp. 335–345, 2000.
133. Clayton, C. R., M. E. Monserrat, G. P. Halada, C. G. Fountzoulas and J. K. Hirvonen, in *Ion Implantation Technology–98*, Proceedings of the XII International Conference on Ion Implantation Technology, Kyoto, Japan, 1998, J. Matsuo, G. Takaoka and I. Yamada, Eds. Piscataway, NJ: IEEE, pp. 885–888, 1999.
134. Yamada, I., J. Matsuo, Z. Insepov, D. Takeuchi, M. Akizuki and N. Toyoda, Surface Processing by Gas Cluster Ion Beams at the Atomic Molecular Level. *Journal Vacuum Science & Technology*, Vol. 14A, pp. 781–785, 1996.
135. Yamada, I. and J. Matsuo, Lateral Sputtering by Gas Cluster Ion Beams and Its Applications to Atomic Level Surface Modification. *Materials Research Society Symposium Proceedings*, Poker, Ila, Cheng, Harriott and Sigmon, Eds. Vol. 396, pp. 149–154, 1996.
136. Choy, K. L., *Progress in Materials Science*, Vol. 48(2), pp. 57–170, 2003.
137. Jozwiak, S., T. Durejko, Z. Bojar, D. Zasada and W. Mroz, *International Journal of Applied Mechanics and Engineering*, Vol. 7, pp. 323–327, 2002.
138. Vignolo, M. F., I. Avram, S. Duhalde, C. Morales, T. Perez, L. Cultrera, A., Perrone and A. Zocco, *Applied Surface Science*, Vol. 197/198, pp. 343–347, 2002.
139. Bychko, G. V., A. Grozhik and G. Yu Zonov, *Glass and Ceramics*, Vol. 56(3–4), pp. 123–126, 1999.
140. Radhakrishnan, G., P. M. Adams and D. M. Speckman, *Thin Solid Films*, Vol. 353(1,2), pp. 131–138, 2000.
141. Guidoni, A.G., V. Marotta, R. Teghil, T. M. Di Palma, A.M. Beccaria and L. Chiaruttini, *Surface and Coatings Technology*, Vol. 100–101(1–3), pp. 437–439, 1998.
142. Neifeld, R. A., S. Gunapala, C. Liang, S. A. Shaheen, M. Croft, J. Prince, D. Simons, H. T. Hill, *Applied Physics Letters*, Vol. 53, p. 703, 1988.
143. Yoshitake, T., T. Nishiyama, H. Aoki, K. Suizu, K. Takahashi, K. Nagayama, *Applied Surface Science*, Vol. 1,141 p. 129, 1999.
144. Yoshitake, T., T. Nagamoto, K. Nagayama, *Thin Solid Films*, Vol. 381, p. 236, 2001.
145. Willmott, P. R., J. R. Huber, ReVol. *Modern Phys.*, Vol. 72, p. 315, 2000.
146. Shirk, M. D., P. A. Molian, *Journal of Laser Applications*, Vol. 10, p. 18, 1998.
147. Perry, M. D., B. C. Stuart, P. S. Banks, M. D. Feit, VOL. Yanovsky and A. M. Rubenchik, Ultrashort-Pulse Laser Machining of Dielectric Materials, *Journal of Applied Physics*, Vol. 85, p. 6,803, 1999.
148. Mourou, G. The Ultrahigh-Peak-Power Laser: Present and Future, *Applied Physics B-Lasers and Optics*, Vol. 65, p. 205, 1997.
149. Longtin, J. P. Using Multiphoton Absorption With High-Intensity Lasers to Heat Transparent Liquids, *Chemical Engineering & Technology*, Vol. 22, p. 77, 1999.
150. Sparks, M., D. L. Mills, R. Warren, T. Holstein, A. A. Maradudin, L. J. Sham, E. Loh and D. F. King, *Physical Review B-Condensed Matter*, Vol. 24, p. 3,519, 1981.
151. Pronko, P. P., P. A. Vanrompay, C. Horvath, F. Loesel, T. Juhasz, X. Liu and G. Mourou, Avalanche Ionization and Dielectric Breakdown in Silicon With Ultrafast Laser Pulses, *Physical Review B-Condensed Matter*, Vol. 58, p. 2,387, 1998.
152. Szörenyi, T., E. Fogarassy, C. Fuchs, J. Hommet, F. Le Normand, *Applied Physics A*, Vol. 69, p. S941, 1999.
153. Perriere, J., E. Millon, W. Seiler, C. Boulmer-Leborgne, V. Craciun, O. Albert, J. C. Loulergue, J. Etchepare, *Journal of Applied Physics*, Vol. 91, p. 690, 2002.
154. Qian, F., V. Craciun, R. K. Singh, S. D. Dutta, P. P. Pronko, *Journal of Applied Physics*, Vol. 86, p. 2281, 1999.
155. Venkatakrisnan, K., B. Tan, B. K. A. Ngoi, *Optics and Laser Technology*, Vol. 34, pp. 199–204, 2002.
156. Bonse, J., M. Geuss, S. Baudach, H. Sturm, W. Kautek, *Applied Physics, A*, Vol. 69, p. S399, 1999.
157. Dominguez, J. E., X.Q. Pan, L. Fu, P. A. VanRompay, Z. Zhang, J. A. Nees, P. P. Pronko, *Journal of Applied Physics*, Vol. 91, pp. 1,060–1,066, 2002.
158. Catledge, S. A., Y. K. Vohra, S. Woodard and R. Venugopalan, *Applied Physics Letters*, Vol. 82(10), pp. 1,625–1,627, 2003.
159. Koizumi, M., M. Niino, *MRS Bulletin*, Vol. 20(1), pp. 19–23, 1995.
160. Sporn, D., Raether, F., Merklein, S., *Materials Science & Engineering, A: Structural Materials: Properties, Mi-*

- crostructure and Processing*, Vol. A168(2), pp. 205–208, 1993.
161. Voevodin, A. A., S.V. Prasad and J. S. Zabinski, *Journal of Applied Physics*, Vol. 82, pp. 855–890, 1997.
 162. M. Bartsch, B. Saruhan, M. Schmücker, H. Schneider, in *Proceedings of the FGM'98*, W. A. Kaysser Ed. Uetikon-Zurich: Trans Tech Publications, Inc., p. 250, 1999.
 163. Schulz, U., M. Peters, Fr. -W. Bach, G. Tegeder, *Materials Science and Engineering*, Vol. A362, pp. 61–80, 2003.
 164. Steffens, H. -D., J. Wilden, L. A. Josefiak, C. C. Berndt, T. Bernecki Eds. in *Proceedings of the UTSC'97*. Materials Park, OH: ASM International, p. 988, 1997.
 165. Holleck, H. and V. Schier, *Surface Coatings Technology*, Vol. 76/77, pp. 328–333, 1995.
 166. Subramanian, C. and K. N. Strafford, *Wear*, Vol. 165, pp. 85–92, 1993.
 167. Dunaev, N. M. and M. I. Zaharova, *Soviet Journal of Experimental Technology in Physics Letters*, Vol. 20, pp. 336–341, 1974.
 168. Tsakalakos, T. and J. E. Hilliard, *Journal of Applied Physics*, Vol. 54, pp. 734–740, 1983.
 169. Soucek, M. D.; Ni, Hai., *Journal of Coatings Technology*, Vol. 74(933), pp. 125–134, 2002.
 170. Vreugdenhil, A. J., Balbyshev, VOL. N., Donley, M. S., *Journal of Coatings Technology*, Vol. 73(915), 35–43, 2001.
 171. Khramov, A. N., Balbyshev, VOL. N., Voevodin, N. N., Donley, M. S., *Progress in Organic Coatings*, Vol. 47(3–4), pp. 207–213 2003.
 172. Hickl, Anthony J. and Richard W. Heckel, U.S. Nat. Technol. Inform. SerVol., AD Report No. 760365, 31 pp., 1973.
 173. Landolt, D., *Proceedings of the 11th World Congress on Metal Finishing*, pp. 1–10, 1984.
 174. Kruger, J., J. J. Carroll, A. J. Melmed, and J. J. Ritter, National Bureau of Standards, Report 10, Oredr No. AD-A112185, 48 pp., 1980.
 175. Shatinskii, V. F., A. I. Nesterenko, V. I. Korshun, and N. G. Nesterenko, *Fiziko-Khimichna Mekhanika Materialiv*, Vol. 19(6), pp. 30–33, 1983.
 176. Hunt, F.Y., E. Marx, G. W. Meyer, T.V. Vorburger, P. A. Walker and H. B. Westlund, *Service Life Prediction*, ACS Symposium Series 805, pp. 437–451, 2002.
 177. Lyons, D., *Journal of the Oil and Color Chemists Association*, Vol. 73(2), pp. 82–84, 1990.
 178. Pranchh, F. R. and L. E. Scriven, *Tappi Journal*, Vol. 73(1), pp. 163–173, 1990.
 179. Hanson, S., *Surface Engineering*, Vol. 15(2), pp 159–162, 1999.
 180. Herrmann, N., *Hungarian Journal of Industrial Chemistry*, Vol. 25(1), pp. 63–69, 1997.
 181. Njiwa, R. K., R. Consiglio and J. von Stebut, *Surface and Coatings Technology*, Vol. 102(1–2), pp. 138–147, 1998.
 182. Zeng, Qingdong; Xiao, Jinsheng; Qin, Feng; Liu, Chunxiao, *Wuhan Ligong Daxue Xuebao*, Vol. 25(1), pp. 34–36, 55, 2003.
 183. Guthrie, J. T., L. Lin and J. Mikac, *Journal of Surface Coatings International*, Vol. 75, p. 66, 1992.
 184. Lin, Long, J. T. Guthrie and Wei D. He, *Journal of Materials Science*, Vol. 38, pp. 1,097–1,104, 2003.
 185. Pogel, H., H. Weiss and D. Roth, *Surface Modification Technologies VIII: Proceedings of the 8th International Conference on Surface Modification Technologies*, Nice, Sept. 26–28, 1994, pp. 651–655, 1995.
 186. Frey, M., S. G. Harris, J. M. Holmes, D. A. Nation, S. Parker, P.A. Tasker, S. J. Teat and R. E. P. Winpenny, *Angewandte Chemie, International Edition*, Vol. 37(23), pp. 3,246–3,248, 1998.
 187. Ruggiero, C., M. Mantelli, A. Curtis, S. Zhang and P. Rolfe, *Medical and Biological Engineering and Computing*, Vol. 31(1), pp. 119–124, 1999.

CHAPTER 17

PROTECTIVE COATINGS FOR ALUMINUM ALLOYS

Thomas P. Schuman

Department of Chemistry, University of Missouri—Rolla, Rolla, Missouri

| | | | |
|---------------------------------|-----|------------------------|-----|
| 17.1 INTRODUCTION | 345 | 17.7 TOPCOATING | 361 |
| 17.2 SELECTING THE ALLOY | 345 | 17.8 UNICOATINGS | 363 |
| 17.3 COATING SYSTEM ENGINEERING | 348 | 17.9 SUMMARY | 363 |
| 17.4 METAL SURFACE PRETREATMENT | 348 | 17.10 ACKNOWLEDGEMENTS | 364 |
| 17.5 CONVERSION COATINGS | 352 | 17.11 REFERENCES | 364 |
| 17.6 PRIMERS | 358 | | |

17.1 INTRODUCTION

Aluminum is a light element of relatively low strength but good elasticity that is readily alloyed to improve its mechanical properties. As such, aluminum is rarely used in its pure form, except when used to conduct electricity where defect-free aluminum is necessary to avoid additional electrical resistance. Alloying with other metallic or semi-metallic elements creates defects or strains in the crystal lattice, or hard intermetallic precipitate particles, which strengthen the alloys' mechanical stress response at the expense of elastic strain.¹

Strain or elasticity is not the only tradeoff experienced in alloying. Electrical and thermal conductivity are sacrificed through creation of crystalline defect structures and semi-metallic compounds of lower conductance, as discussed above, where pure aluminum is necessary for efficient electrical conduction. Fatigue sensitivity is increased through reduced modes of deformation and propagation of crystal defects to create modes of crack failure. Metal homogeneity is reduced, potentially increasing the quantity of interstitial defects and permeability to atoms or small molecules. By far the greatest change in aluminum materials, next to those of mechanical properties, is corrosion resistance.²

Alloy selection is typically based on a material's properties—strength, flexibility, and resistance to fatigue—to accommodate an engineered design rather than corrosion resistance. Since fatigue resis-

tance is part of the design, then corrosion-related crevice corrosion and fatigue cracking are inherent in the design process. Since pitting can initiate crevice corrosion, pitting resistance should and does play a role in structural design. General corrosion is not as much designed for as managed through pretreatments. However, the alloy itself plays a large role in the ability to pretreat and protect the aluminum surface.

17.2 SELECTING THE ALLOY

Composition and processing of an alloy are responsible for the developed mechanical properties of the alloy. However, composition has the greatest effect on corrosion resistance of aluminum alloys with copper, a common alloying element, and iron, a common impurity, being the major culprits. Processing methods for wrought and cast alloys (i.e., mechanically (strain) hardened or tempered) vary with alloy composition. Composition and processing thus represent an engineering tradeoff in corrosion resistance with mechanical strength or toughness. Since the alloy compositions directly relate to the mechanism of hardening and strength development, particular classes of alloy composition tend to be more sensitive to corrosion. Copper concentrations and corrosion sensitivity are highest in the wrought 2XXX and 7XXX series, but also are present and similarly affect corrosion sensitivity in the cast al-

loys (e.g., the 380.0, 710.0, 295.0, 336.0, or 355.0 aluminum alloys).³

It is generally well known that different alloys have different susceptibility to corrosion and require different levels of corrosion protection. Not as well known is that even an identical alloy varies in inherent corrosion activity from lot to lot, where the most active lots may not be passivated, even by chromate pretreatment. Prescreening of alloys for corrosion activity prior to manufacture is thus suggested as part of a quality assurance program to avoid corrosion-sensitive lots.

Alloys based on AA2024 and AA7075, although the strongest of the aluminum alloys, tend to be the most corrosion sensitive. Figure 17.1 shows the electrochemical impedance spectroscopy (EIS) scans of AA7075 alloys from different manufacturer lots, immersed in a standard prohesion solution of aqueous 0.05% sodium chloride and 0.35% ammonium sulfate. Some material lots show higher impedance to corrosion than others. Impedance is an alternating current resistance, thus composed of real and imaginary vector components, which EIS measures of a corroding surface as a function of the alternating current frequency.

On a lot-to-lot basis, significant differences in the low frequency impedance can exist despite similar metal contents for each alloy and each being well within the AA7075-T6 specifications. Low frequency impedance of EIS measurement is equal to $R_{\Omega} + R_p$, where R_{Ω} is the solution interface resistance measured as the high frequency impedance, and R_p is the polarization resistance to corrosion.⁴ The inverse of R_p is proportional to the corrosion rate (i_{corr}). Since R_{Ω} are nearly equivalent, the measured R_p indicate the relative difference in corrosion rate between each alloy lot. A large difference in corrosion activity of the cleaned alloy surfaces can be readily discerned. It was found that alloys of higher surface copper content tended to be more corrosion active, while those of lower copper were less active. Corrosion activity has found to be related to, specifically, relative copper composition (also see Figs. 17.2 and 17.3).⁵

Manganese, silicon, and magnesium alloys are not sensitive to corrosion unless high concentrations of copper are also present. Therefore, the 1XXX (pure aluminum), 3XXX (manganese), 5XXX (magnesium), and 6XXX (silicon-magnesium) alloys are not generally sensitive to corrosion because the native

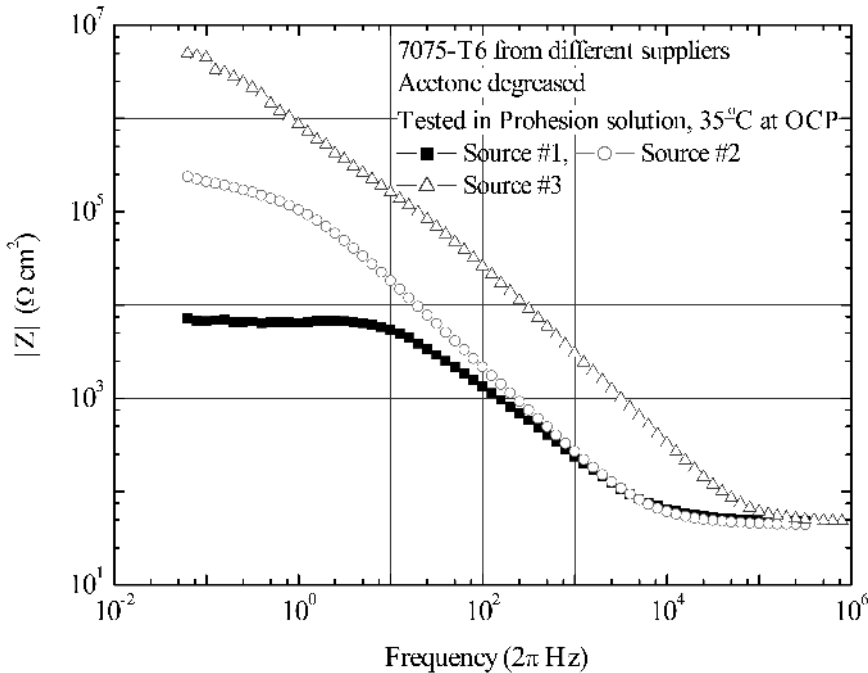


FIGURE 17.1 Bode plot of EIS measurements for taped 1 cm² area of aluminum alloy (AA) 7075-T6 panels from different suppliers immersed in 35 °C prohesion solution. The panels were acetone degreased only but show significant differences in low frequency polarization resistance as a function of the alloy source.⁵

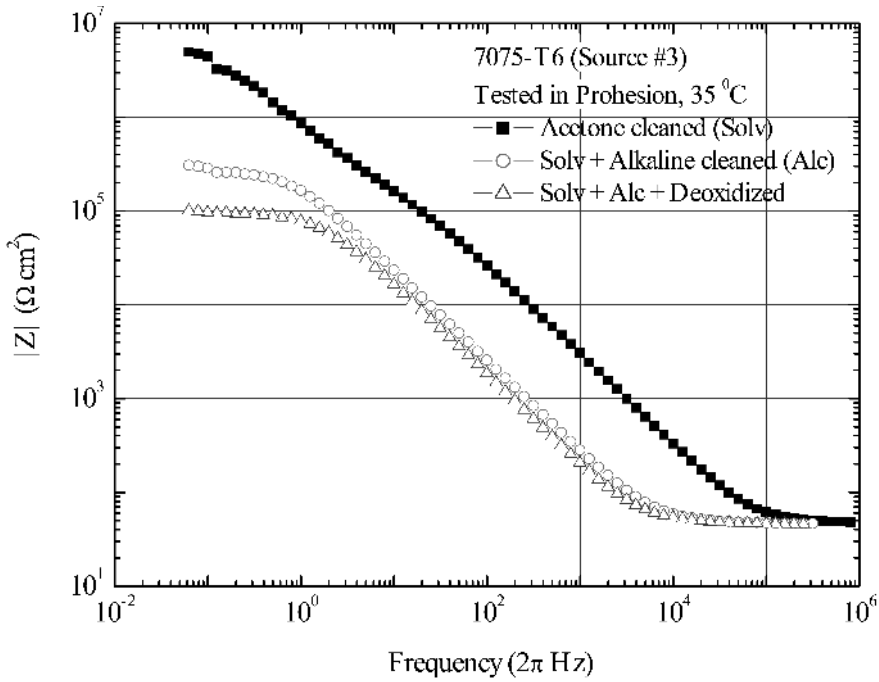


FIGURE 17.2 Bode plot of EIS measurements for taped 1 cm² area of AA7075-T6 panels from lot 3 immersed in 35 °C prohesion solution; acetone degreased, after alkaline cleaning, and after deoxidation. The panels were alkaline cleaned in Turko® 4215 NCLT (Henkel Surface Technologies) at 55 °C for 10 minutes and rinsed. Deoxidized panels were placed in Amchem 7-17 at room temperature for five minutes and rinsed with deionized water. The alloy shows differences in surface activity as a function of surface treatment.⁵

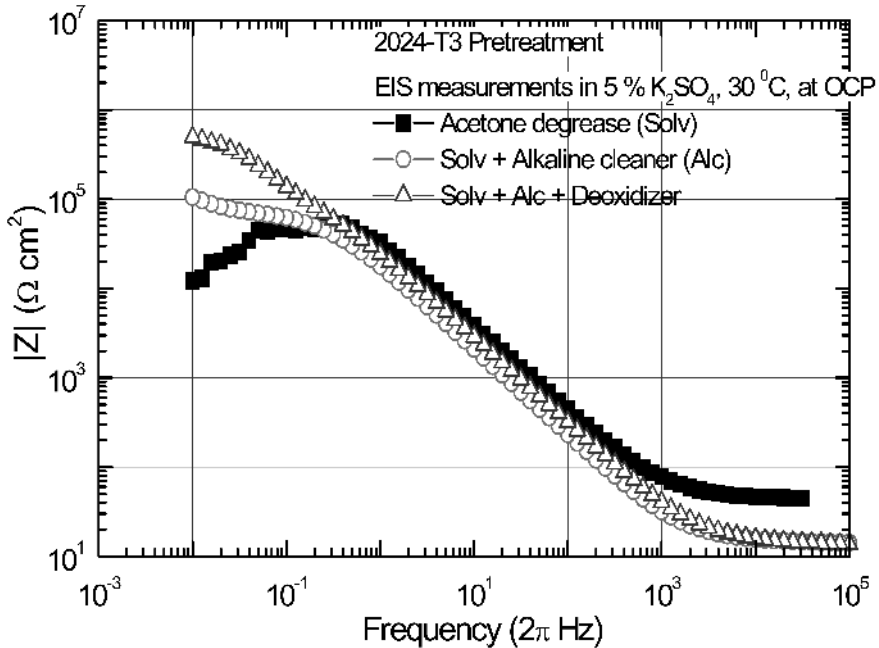


FIGURE 17.3 Bode plots of EIS measurements for AA2024-T3 alloy as a function of frequency and surface pretreatment. Small increases in R_p occurred with pretreatment order.⁵

oxide layer formed renders those surfaces passive to corrosion in most environmental conditions. Even the 7XXX alloys that do not contain copper provide “high” resistance to corrosion.³ Alloys that do not corrode, that generate durable oxide layers and self-passivate, may or may not require additional surface protection beyond the native oxide layer, depending on the use environment. Coatings, in general, provide surface protection for sensitive substrates.

17.3 COATING SYSTEM ENGINEERING

An infinite number of exposure conditions, and therefore approaches, are possible for the protection of substrates. Most approaches are readily discerned from others by the function that a coating will provide, based on the materials content and design compared to the required need for protection. A coating may be susceptible to identical conditions and not improve or protection of the substrate. For example, a typical latex polymer coating applied to a metal susceptible to corrosion in an exterior or marine environment will not provide an adequate moisture barrier, and will likely permit corrosion of the metal at a rate similar to the uncoated metal. The coating could even potentially worsen substrate degradation by changing the mechanism of degradation. For example, applying a coating that is more noble to the substrate metal may galvanically accelerate corrosion occurring in defect areas. A barrier coating can accentuate corrosion at a defect where, for a constant corrosion current, the rate of dissolution at the defect will appear enhanced. Still other surface coating approaches may be singled out based on appearance characteristics, including: spectral absorption or reflectance; material specifications including conductivity, strength, hardness, permeability, and flexibility; compatibility between coating systems or with the substrate material, including adhesion; and cost.

Organic primers and topcoatings, collectively called “over coatings,” are relatively thick coating layers that physically, as well as chemically, protect the substrate.⁶ Over coatings provide an enhanced physical surface protection and serve to shift the barrier interface farther from the metal surface to improve corrosion resistance. Over coating dry films are on the order of fractional- to multiple-mils thick.

However, organic primers and topcoatings typically neither adhere well to nor protect physically or chemically untreated aluminum, since the native aluminum oxide layer tends to be of poor mechanical structure. The aluminum oxide thus becomes a

polar, water-sensitive, weak boundary layer for the coating system. Therefore, organic over coatings are applied to pretreated aluminum where the aluminum surface has been “converted” to a different surface composition. Such pretreatments are thus commonly called “conversion coatings.” For this chapter, the term *coating* will apply to only the conversion coating layer, while *primer* or *over coatings* will describe primer layers applied to the converted surface. *Topcoating* will distinguish coatings applied atop the primer surface.

Coatings systems commonly used on aluminum structures include acid anodize-,^{7,8} phosphate-,⁹ lead-tin-,¹⁰ cobalt-,^{11,12} titanium-,¹³ zirconium-,¹⁴ manganate-,¹⁵ silicate-,^{16,17} chromate-,^{18–20} and rare earth-based^{21–23} systems. Each pretreatment type produces a surface coating that not only provides a first defense against corrosion, but also provides all-important adhesion that is needed for primer and topcoating performance. Pretreatment coatings can be used alone or in conjunction with over coatings, which add physical durability and generally improved corrosion protection. Conversion coatings serve to structurally and chemically stabilize and control the interfacial properties of the aluminum substrate to allow predictable, stable performance of the coated system.⁸

17.4 METAL SURFACE PRETREATMENT

Similar to conversion coatings providing stability and adhesion for over coatings, surface cleaning and pretreatments provide non-contaminated, uniform, controlled surface composition for application of a conversion coating for improved conversion coating performance. A review of cleaning and pretreatment for metals is given by Talbert.²⁴ Other summaries for cleaning and pretreatment processes may be found in military^{25,26} and professional society standard specifications.^{27,28}

17.4.1 Cleaning

Contaminants can prevent the assembly and adhesion of a uniform conversion coating, while a non-uniform coating can result in localized cathodic or anodic areas and enhanced corrosion sensitivity rather than protection. Cleaning and pretreatments can result in localized etching of sensitive alloy metal atoms and result in, for example, copper-enriched surfaces and enhanced corrosion activity (Figure 17.2), or compositionally neutral surfaces and improved corrosion activity shown by EIS as

high polarization resistance (Figure 17.3). Poor adhesion of surface coatings allows delamination of topcoatings at reduced peel strengths and promotes crevice and filiform corrosion at the weak interface. Cleaning processes are selected based on the surface composition to efficiently and effectively clean but avoid production of weak boundary layers and damage, such as surface enrichment of copper, in a permissible amount of time.²⁹

Surface compositions can be altered by the cleaning procedure through selective solvation of active surface atomic species of an alloy that, if redeposited, form smut on a surface to produce rather than remove contamination. The types of contaminants and surface content are specific to particular metals and their alloys, due to the specific manufacturing process. Cleaning process design must account for the variation in alloy composition, presence of a passive oxide layer, and contaminants, which can be significantly complex. Cleaner types are classified as alkaline, neutral, and acidic with better results typically achieved for alkaline baths. Common metal surfaces, their contaminating layers, and treatments to remove the contaminants are shown in Table 17.1.²⁴

17.4.2 Chemical Etch

Cleaning procedures are often complex and involve multi-step processes,^{9,26,30–35} which vary from alloy to alloy. A typical solvent wash will usually bulk degrease the part to be coated, using solvents to remove most, but perhaps not all, fabrication lubricants. Solvents can be recycled by filtration and/or distillation recovery. A second cleaning step uses an

TABLE 17.2 Selected Aluminum Finishing Specifications
Published by the Society of Automotive Engineers,
Warrendale, PA, 2003

| Specification | Title |
|---------------|--|
| SAE AMS2473G | Chemical Film Treatment for Aluminum Alloys, General Purpose Coating |
| SAE AMS2514A | Anodic Coating on Aluminum Alloys Sulfuric Acid Process, Resin-Sealed |
| SAE AMS2472E | Anodic Treatment of Aluminum Alloys, Sulfuric Acid Process, Dyed Coating |
| SAE AMS2470L | Anodic Treatment of Aluminum Alloys, Chromic Acid Process |
| SAE AMSC5541 | Chemical Conversion Coatings on Aluminum and Aluminum Alloys (see also reference 65) |
| SAE AMS1626B | Desmutter, Aluminum, Liquid |
| SAE AMS1625B | Desmutter, Aluminum, Powdered |
| SAE AMS2474C | Chemical Treatment for Aluminum Alloys, Low Electrical Resistance Coating |

alkaline solution treatment to remove any remaining grease contamination, with possible etching of the alloy surface depending on the alkalinity of the solution. The concentration of caustic controls the amount of surface etching, though many (or longer) time exposures to weaker alkalinity baths provide better and more consistent coating results.²⁴ Metasilicate dissolved in the alkaline solution is used to specifically inhibit etching and attack of the aluminum surface to prevent dulling but still provide bright, clean optical surfaces.³⁶ Therefore, metasilicate cleaners are usually specified as non-etching.

Etching cleaners are more active due to their higher alkalinity and are used purposefully to solu-

TABLE 17.1 Metal Cleaning Processes

| Metal | Probable Surface Contaminants | Typical Treatment Process |
|-------------------|--|---|
| Hot Rolled Steel | Mill scale, oxidation, carbon smut, grease, oil, dust and dirt | Blasting, alkaline cleaning, iron phosphate |
| Cold Rolled Steel | Rust inhibitors, oil, smut, dust and dirt | Alkaline cleaning, iron phosphate |
| Stainless Steel | Shop dirt, oils, passive oxide layer | Blast or acid etch to remove oxide layer, alkaline clean and rinse |
| Galvanized Steel | Shop dirt, oils from handling | Alkaline clean and iron or zinc phosphate |
| Extruded Aluminum | Oxide layer, shop dirt and oil | Alkaline clean and iron phosphate; from handling for added corrosion resistance, chromate treat |
| Cast Aluminum | Die release compounds, shop dirt and oil | Blast or polish to remove die release, alkaline clean and iron phosphate |
| Zinc | Die Cast Die release compounds, shop dirt and oil | Blast or polish to remove die release, alkaline clean and iron phosphate |

Source: Reprinted from Talbert, R., *The Powder Coater's Manual*, Vincentz Network, Hannover, Germany, 1998, used by permission.

bilize aluminum; however, alkaline etchants tend to remove more reactive species but leave the more noble metals (such as copper) in place, thus concentrating the copper or copper oxides at the surface. Enhanced surface copper concentrations lead to corrosion sensitivity for aluminum. Selectively reducing copper content is thus usually a goal of the pretreatment process to improve corrosion resistance. Some level of etching is required to remove topological defects such as scratches or surface contaminating coatings, when present.

Physical cleaning using blasting, abrasion, or polishing is commonly used for harder steel structures, but less commonly for the softer aluminum surface where less aggressive chemical cleaning with etching is preferred. Use of softer agricultural or polymer grits have better utility for aluminum. Physical cleaning may be required to remove hard, thick or scaly residues not reasonably accessible by cleaning baths. Profiling by grit blasting will require a thicker coating weight for proper coating thickness above the undulating surface. Smooth surfaces require less coating weight. For example, Boeing can use as little as 0.5mil ($\sim 12\mu\text{m}$) anticorrosion epoxy polyamide primer coating above a smooth, solution processed aircraft skin, which saves on production cost.

Solvent washing followed by alkaline cleaning alone was found effective at removing surface smut when employed with sonication, compared to more aggressive chemical cleaning methods for cleaning aluminum 6063 and 2219 alloys,³⁷ where temperature of the bath was important for proper wash solution etching activity. Rosenberg et al. noted that, although it was desirable, they found no universal cleaner that would, for instance, clean both aluminum and copper alloys effectively. Cleaning processes are thus specific to particular metals and alloys of metals even though these first two steps appear to be universal for most aluminum or aluminum alloy cleaning processes.

Cleaning efficiency can be rather simply assessed via a water break test, which tests the wettability of the surface by water. Application of water to a properly cleaned surface should form a smooth film rather than breaking. Breaking of the film indicates presence of hydrophobic, grease-like contaminants evidenced as a variation of the substrate surface tension.

17.4.3 De-smut/Deoxidation/Pickle

Once cleaned, the surface is then homogenized in terms of its surface composition, which can increase

or decrease local site activity to serve different purposes. For example, additional de-smutting of species generated or redeposited during cleaning may be removed. De-smutting, deoxidation, and pickling of a metal are synonymous processes that soften and/or completely remove contaminating surface oxides or other inorganic materials in order to expose a basis material surface. The generated surface may be used "as is" or as a preparation for further surface finishing.

In deoxidation, atomic concentration of surface species is remediated, such as reducing the amount of passive oxides, smut, and noble or active metal content. The end result of deoxidation is an oxide-free bare metal surface of controlled activity. *Smut* is a general term describing a surface residue that can be carbonaceous or, commonly, an intermetallic compound or metal oxide precipitate. Carbonaceous films tend to be inert and can require mechanical cleaning, such as grit blasting, surface abrasion, or ultrasound. Smut results from elements on an alloy, such as copper, silicone, or wax, which tend to leave insoluble films under the cleaning conditions employed.

Since the tendency and extent of smut formation varies alloy to alloy (but also lot to lot of the same alloy), deoxidation is often standard in many cleaning processes to generalize cleaning to all possible samples. The thickness and structure of the aluminum oxide, or non-aluminum metal oxide in the alloy, may be removed, reduced, or reconstructed to produce a durable boundary layer for proper adhesion of a coating. The reactivity of the surface may be altered so the conversion coating properly develops sufficient coating weight, uniformity and thickness.³⁶ Over-activation should be avoided, which can initiate or increase the alloy's tendency toward pitting corrosion.

The composition of a de-smut step is usually acidic, taking advantage of the solubility of metals, e.g., copper, and their oxides in acidic media, but could instead be strongly alkaline, e.g., using ammonia, in design. Acidic baths also serve to neutralize surface alkalinity residual from prior alkaline cleaning/etching. Because hydrochloric acid baths tend to be more aggressive than sulfuric acid, sulfuric acid can require higher temperatures or longer times to properly deoxidize.

Alternative deoxidizing bath compositions are based on nitric acid with added hydrofluoric acid. Hydrofluoric acids are especially used for silicon alloys to dissolve silicon deposits. For these baths, halogen concentration controls the surface reactivity

and etch rate. Nitric acid used in concentrations of 50–100% tends to likewise be less aggressive than halo acids, and forms thin but consistent oxide monolayers. For commercially pure aluminum or wrought aluminum-magnesium, 50% aqueous nitric acid is useful. Nitric or phosphoric acid baths tend to self-inhibit the dissolution process to prevent over etching. Phosphates may be added to other mineral acid baths to control their activity. Deoxidation baths may also be alkaline in composition, utilizing hydroxide or ammonia and facilitating hydroxide or ammonia and surfactants to dissolve the surface oxide layer and smut.

Since changes in surface reactivity of the deoxidation bath can be useful or harmful to the process, care must be exercised in employing inhibitors within the deoxidizing solutions to prevent over-activation but not preclude proper deoxidation/pickling. For baths that are too aggressive and overly etch or activate the alloy surface, an inhibitor is added to reduce the etch rate. Such additives are selected based on specificity; for example thiourea preferentially attaches to and passivates copper-rich sites. Zincate solutions (the zinc analogy to silicate) plated onto deoxidized aluminum retard excess surface dissolution or corrosion until a coating may be applied.

Metal ions can be added as accelerators to enhance the bath reactivity where the metal ions are noble to the substrate being deoxidized. Metal content in the bath can have dual accelerator/inhibitor functions. For example, chromate has been a typical bath inhibitor since the 1940s, and has both surface oxidative and corrosion inhibiting properties. Recent regulation^{38,39} of chromium (VI) as a hazardous waste has led to consideration and development of self-inhibiting, non-chromated alternatives such as ferric sulfate-, persulfate/bisulfate-, or boric-sulfuric-based deoxidizers and anodizing. However, non-chrome deoxidation technologies currently do not match the performance of chromate technology on all alloys.

Additional materials that are used in deoxidizer formulations include suspension agents. Surfactants, emulsifiers, flocculants and complexing agents prevent redeposition of stripped oxide layers, and aid removal of carbon or oily surface species. In addition, the surface-active agents lower the surface tension of the bath to provide enhanced wetting of the metal surface and improved surface access for the bath chemical agents. Flocculants or complexing agents aid precipitation of metals from the bath, as sludge or emulsified oils will tend to float on the bath surface.

Treatment baths lose activity over time as agents are transferred to rinse water or consumed by the dis-

solution of surface species; the bath loses activity to both the rinse water and to the metal part cleaning reactions. Alternatively, the bath gains metal content as surface elements are etched away. Each reduces the bath effectiveness over time, which may be assessed by supplier-provided titration analyses²⁵ as part of a quality assurance procedure. Depleted baths may be typically be regenerated by simply adding more of the proper reagent. Baths with excess metal content are either disposed of or remediated using selective precipitating agents, which are then sedimented, or filtered, and disposed. Bath renewal and disposal costs should be addressed in selecting a pretreatment system.

17.4.4 Rinsing

Rinsing between cleaning steps removes excess reagents from the surface and prevents cross-bath contamination and excess consumption of bath chemical agents. Two aqueous rinse steps are typically provided between alkaline cleaning and deoxidation to ensure complete removal of excess base, the first being a crude rinse and the second a final rinse. Likewise, after deoxidation, the acid treated surface is water rinsed only once prior to conversion coating or drying, since conversion baths tend to be acidic. Post-rinse steps after conversion coating neutralize surface acids or remove loosely attached coating or precipitated salts to promote over-coating or adhesive adhesion.

Rinsing steps raise the issues of bath longevity and remediation. When rinsing is part of an assembly, parts with residue transfer active bath agents to the rinse water. For toxic bath agents or strongly acidic or basic media, the rinse water must be remediated by disposal, which is most costly, by evaporation or neutralization/precipitation, which are time- or materials-intensive, respectively. Toxic solid waste sludge will require proper disposal.

17.4.5 Summary of Substrate and Cleaning Considerations

EIS measurements show differences in surface activity caused by pretreatment steps (Figures 17.1–17.4). Good substrates were defined as those showing high impedance upon immersion in a corrosion prohesion solution, while poor substrates had low impedance on the order of $10^4 \Omega\text{cm}^2$. On a “good” substrate, the impedance and polarization resistance to corrosion were decreased by the removal of passive aluminum oxide layers. On a “poor” substrate, pretreatment could increase, decrease, or not alter the im-

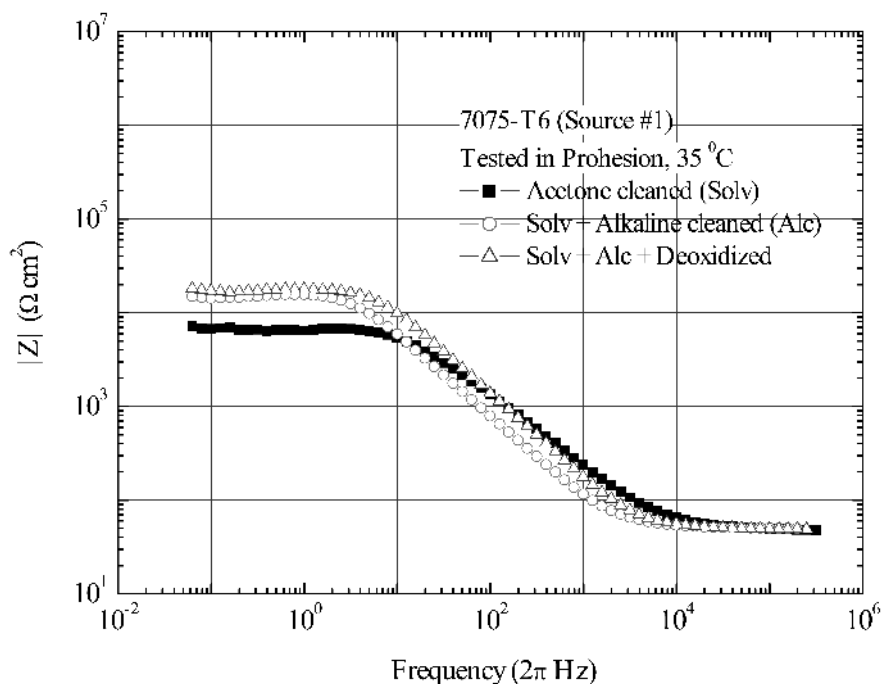


FIGURE 17.4 Bode plot of EIS measurements for taped 1 cm² area of AA7075-T6 panels from lot 1 immersed in 35 °C prohesion solution; acetone degreased, after alkaline cleaning, and after deoxidation. The panels were alkaline cleaned in Turko[®] 4215 NCLT (Henkel Surface Technologies) at 55 °C for 10 minutes and rinsed. Deoxidized panels were placed in Amchem 7-17 at room temperature for five minutes and rinsed with deionized water.⁵

pedance. Differences in activity were suspected to be caused by the content, distribution, or activity of (copper) intermetallic compounds, though the substrates differed in copper content by as little as tenths of a percent. However, the final impedance of a coated substrate was always higher for a “good” substrate, which in turn resulted in improved corrosion resistance, compared with performance of a “poor” substrate (see Section 17.5.4, Reprise: Alloy Considerations, below). Selection of good substrates through a valid, in our case, electrochemical Quality Control (QC) process using EIS would result in improved performance. Remediation of poor substrates by pretreatment, including conversion coating, as discussed below, may not be possible.

The goal of cleaning and pickling procedures is to synthesize a reproducible metal surface for the coating process which is commonly referred to as the *pretreatment*. Cleaning removes contaminants that hinder uniform pickling, and pickling or deoxidation provides a uniformly active surface through manipulation of surface composition. Activity of each step is controlled primarily by base or acid strength, but also by the use of inhibitors.

Longer bath times or multiple immersions provide better consistency and a more adherent, corrosion resistant surface than faster, higher strength

bath treatments. Poor outcomes can result from inadequate etch control to cause pitting initiation, enrichment of surface copper content, or incorporation of active ion species within the surface. Aluminum cleaning and pretreatment can be exceedingly complex, where experience is often the key to success in the coating of aluminum despite existence of standard, pre-established procedures.

17.5 CONVERSION COATINGS

Another coating design that can improve the quality of metal protection compared to the original oxide layer is a conversion coating. Conversion coating converts the natural oxide coating to that of a different metal oxide or to a metal salt composition. The new oxide or precipitated metal salt, as a surface coating layer, should form a consistent, dense film, and be structurally durable and more chemically resistant to dissolution by corrosive species, at extremes of pH, and at service temperatures.

17.5.1 Hard Anodizing^{35,40}

Anodize is a general term that may be applied to all conversion coatings. Anodizing is literally “oxidizing the surface metal,” (i.e., reacting the surface an-

odically, to generate a thick, dense, passive oxide on the metal surface). The anodizing process has been popular since the early 1960s but has been known since about 1930. Anodizing may be either electrochemically or chemically driven to cause formation of the oxide layer. Industrially, hard anodizing refers to the electrochemically driven surface treatment process. Standard anodize processes³⁵ are based on chromic,⁴¹ sulfuric,^{11,26,42-44} or phosphoric^{9,45-47} acid processes. Responding to the issue of chromate toxicity, other non-chromate processes have been developed based on lead-tin,¹⁰ cobalt,^{11,12} titanium,¹³ zirconium,¹³ manganate,¹⁵ and silicate^{16,17} systems.

Multivalent anions, such as borate,⁴² in the contacting solution during anodizing tend to allow formation of the oxide layer, while monovalent acid counterions tend to redissolve rather than build an oxide layer.⁴⁸ The anion of the anodizing acid is often found incorporated into the oxide layer, which can influence the corrosion performance. However, the retained presence of sulfate, in particular, has not been shown to influence corrosion, only the aluminum oxide structure,⁴⁹ which explains in part why sulfuric is commonly used for hard anodizing. A common misconception is that anodization adds a coating onto the surface. Rather, the anodization process converts the existing, reduced metal surface to its oxide, as a coating layer.

Regardless of the bath composition used to generate a hard anodize coating, the morphology for durable, unsealed coatings is similar (Figure 17.5).⁵⁰

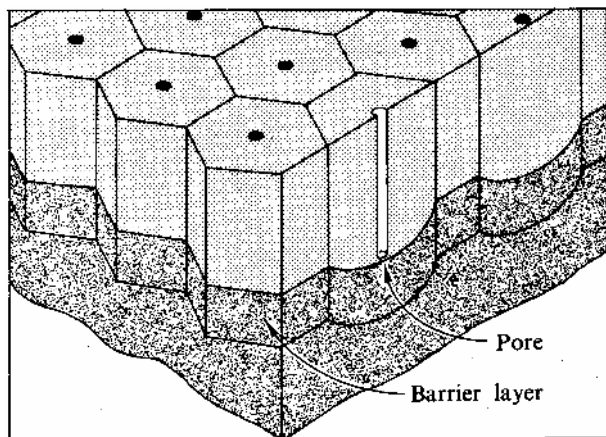


FIGURE 17.5 The formation of the anodized film progresses with the principal electrochemical action occurring in the area between the bottom of the pore and the aluminum substrate. The barrier layer beneath continues to reform as the oxide grows. [Source: Reprinted from Barkman, in *Anodizing Aluminium*. The Aluminium Federation, Eds. Portland House, Stag Place, London, 1967, p. 34, used by permission.]

The underlying or barrier layer, nearest the aluminum metal, is a rearranged aluminum oxide film, i.e., different than that present after cleaning and deoxidation, with nucleated anodes at the centers of hexagonal cells. The barrier layer migrates inward by continuous conversion to aluminum oxide driven by anodic current. The thickness of the barrier layer at each anode is proportional to the anodizing voltage.⁵⁰ The anodized coating thickness, equal to the barrier layer plus porous layer, is controlled by treatment time and current density of the applied voltage. The process can be conducted under either constant current or constant voltage control.⁴⁰

The initially deposited anodized surface, with the exception of the barrier layer, are porous in nature. Pores of near 250Å-diameter remain and are caused by transport of species away from the surface during the continuing anodic dissolution, the anodizing event. The path from the substrate may not be strictly linear, as impurities in the bath or substrate can alter the crystal structure around the pore and change its direction slightly. Generally, oxide growth is epitaxial but acute, not parallel, to the surface normal direction. Impurities that cause pore growth direction changes result from alloying elements that become dissolved into the bath, such as iron, copper, or magnesium.

The porous surface can be left as-is to provide an adhesive surface for an organic primer coating, dyed to fill the pores in creation of a decorative protective coating, or filled to create a self-sufficient protective coating to which over coatings can yet be applied with success. Filling of the pores is termed *sealing*. Dyes adsorb and complex into the oxide pores through a surface charge, or zeta, potential interaction.⁵¹ Treatment with metal cations of the dye are required prior to development with oxidizing or reducing species containing spectator cations. Adsorption first of dye cations avoids adsorption of the inactive, spectator cations, which preclude surface adsorption of the dye cations and intense color development. Sealing of the decorative, dyed surface occurs through pore occlusion by precipitating boehmites.

When used as a self-sufficient protective coating, a separate sealing step follows the anodizing reaction to fill in the remaining pores with inert or corrosion inhibiting salts.^{50,52} The filled pores then constitute part of the protective barrier. Common sealing treatments⁵² include coloration with dyes,⁵³ immersion in boiling water or steam,^{23,42,54,55} borate,^{7,47} nickel salts,^{42,54,56,57} phosphate or other anion salts, or may include inhibitors such as cobalt,¹¹ molybdate,⁵⁶⁻⁵⁸ lithium,⁵⁹ rare earths,^{42,60,61} or chromate.^{11,41,54,56,58,62-64} Sealing,

then, is a post-treatment of the porous anodize coating to improve performance.

Sealing is comprised of two chemical steps that concurrently compete—dissolution of the porous oxide layer and chemical conversion to inert surface salts results in pore filling. Since the sealing process is reactive and corrosive, dissolution of the oxide layer will occur and the rate of dissolution is controlled by temperature and pH. Higher temperature and extreme pHs aids dissolution.

Extremes of pH away from the isoelectric point of the aluminum oxide, from ~8–9 for gamma aluminum oxide to ~9.3 for boehmite, charge the aluminum surface through protonation/deprotonation of the surface oxide and aid dissolution of aluminum-oxo ions. The ionic content in solution controls the pH and can catalyze the ability to convert the aluminum oxide to a more stable salt, such as aluminum phosphate. Water sealing converts the surface to boehmite or aluminum hydrate.

Recall that in alloys that there are alloying elements present. These elements do not disappear but continue to affect the surface coating progress. There is an overall tendency for more active metals to be leached into solution while more noble elements, such as copper, remain or are redeposited from solution. Additives in coating baths seek to prevent selective removal of active elements or redeposition of copper.

Sealing processes may be delineated as cold (ambient) or hot (heated) processes. Cold processes have advantage over hot processes in complexity and cost, though hot processes appear to outperform cold treatments. Corrosion performance is directly related to the composition, thickness, density, and residual porosity of the anodize layer.

17.5.2 Chromate-based Conversion Coating

Current-driven processes are a mainstay of hard anodize coating systems, but suffer limitations in apparatus and electrical requirements. Chemically-driven coating systems are simpler in the application apparatus, but appear more difficult to design in theory and then in practice. For instance, chemical designs often present performance tradeoffs as a function of composition. The capacity to etch may be necessary as an anodic driving force in the conversion of aluminum metal to oxide, but can preclude film formation through the dissolution, or enrich copper through dissolution of more reactive metals. To further complicate matters, particular additives are commonly not understood in their mechanism of

action, making substitutions difficult or combinatorial. Hence, developing the chemical conversion coating can be as much or more of an art form than science.

Chromating has been the principal aluminum pretreatment since the 1940s. However, chromium and, in particular, soluble chromium (VI), is a reactive, toxic transition metal and subject to environmentally-based disposal restriction as a hazardous waste material or airborne contaminant.^{38,39} Chromium (III) oxide is not as significant a concern due to its low solubility and hindered bodily absorption. The reason for the longevity in usage of chromate, despite its toxicity and costs of disposal, is that the pretreatment processes utilizing chromate work well on most metals, and are consistent and generally forgiving of processing conditions. The converse is generally true as well, in that replacement technologies not based on chromium do not generally perform as well as chromate, especially in their ability to meet stringent U.S. military (MIL-) specifications⁶⁵ or commercial aircraft performance requirements,⁶⁶ and tend to be less consistent and forgiving. The reason for the success of chromate lies in its dual oxidation state and a smart-release transportability (Figure 17.6).⁶⁷

Until recently, even the mechanism of surface protection elicited by widely used chromate conversion coatings was not understood despite an estimated thousands of attempts to unravel its secret. Several recent experiments appear to have attained this goal.^{68–71} Chromate works as a team of cathodic inhibiting insoluble chromium (III) oxide and anodic inhibiting soluble, transportable chromium (VI) species. Chromium (III) oxide acts as a durable, relatively inert coating,⁷² which can include other multivalent cations that aid solubility control as introduced by the conversion coating process (see discussion of hard anodize ion content above). Upon damage to the coating, a pH-controlled transport mechanism is enabled by the local corrosion sites, cathodic and anodic.

Cathodic sites are basic in pH for a typical moist air exposure. Elevation in pH occurs due to an aerobic reduction of oxygen to hydroxide ion or through the anaerobic chemical reduction of H^+ from the interface. The pH of the interface can be locally quite different than the surrounding bulk, which may be observed through scanning reference electrode techniques (SRET) or scanning vibrating electrode techniques (SVET), which sense electrical fields or ion flux generated by surface-localized concentrations of ions (Figure 17.7).^{73,74}

Color shifts (Figure 17.8) toward white indicate higher anodic activity, while shifts toward purple-

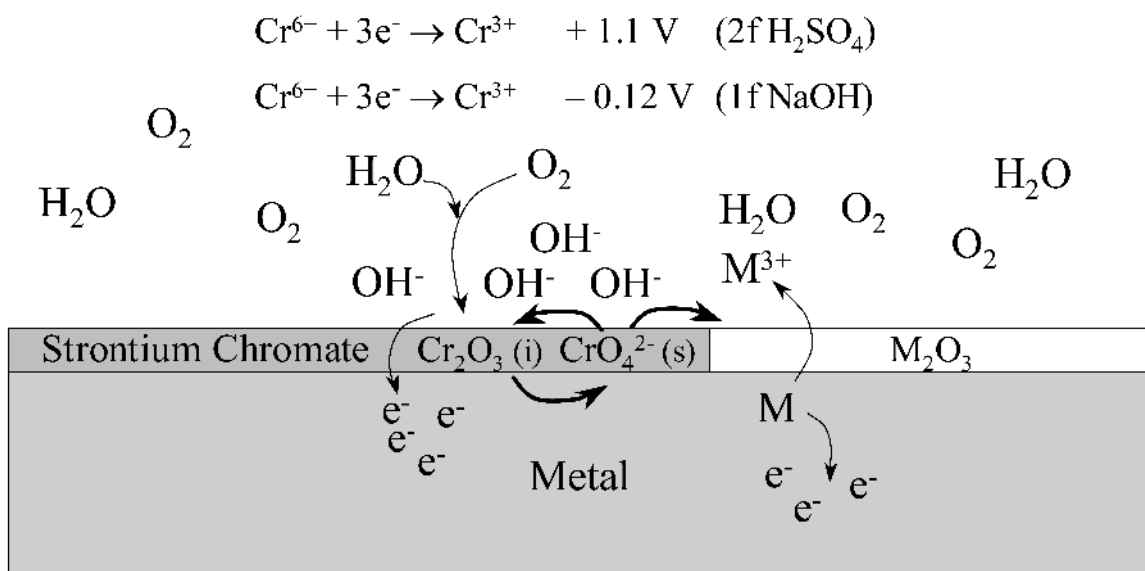


FIGURE 17.6 The corrosion protection, transport and feedback mechanism of chromate. The cycle is enabled by the electrochemical potential and solubility of chromium oxide as a function of valence state and pH.

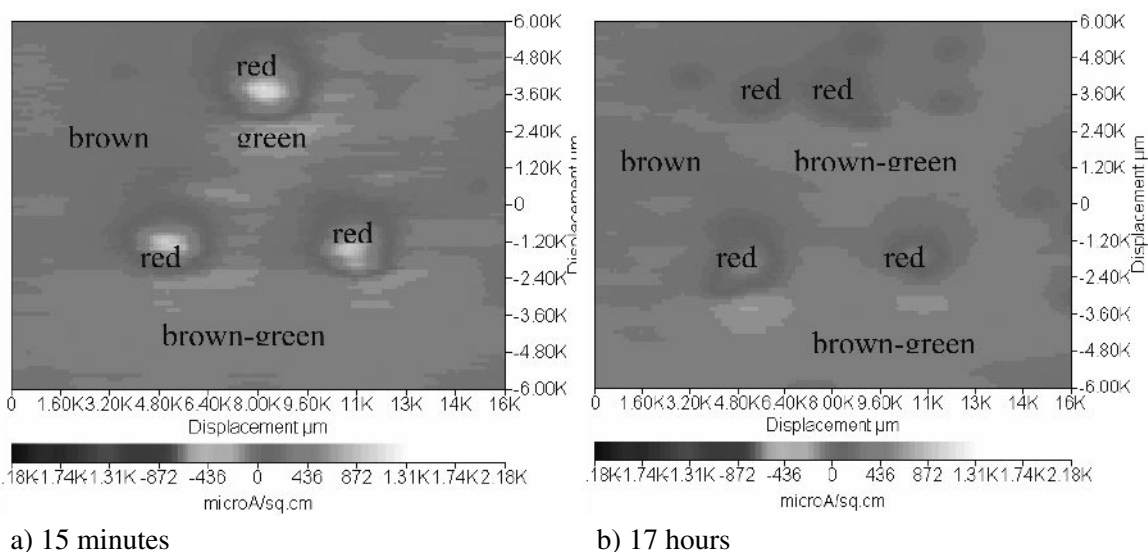


FIGURE 17.7 Scanning vibrating electrode technique (SVET) measurements of aluminum alloy AA7075-T6 immersed in 5mM aqueous NaCl are shown for (a) 15-minute and (b) 17-hour exposures. The coloration of the SVET scan shows localized anodes (red to white) and cathodes (green to purple) size and position as distributed over the alloy surface. Intensity and distribution change in response to a buildup of corrosion products and localized passivation. These scans show high SVET current density and corrosion activity.^{73,74}

black indicate higher cathodic activity. The corrosion rate scale shown is in microamperes per square centimeter, the current generated by the electrode motion through the electrical or ion field. The SVET figures shown in this chapter are obtained from substrates that have artificial defects (e.g., scratches, in the form of three drilled pits as an adaptation of drilled defects used in EIS measurements).⁷⁵ The

drilled defects simulate a mechanical defect and can demonstrate the potential to self-heal. Bare, degreased aluminum shows constant, strong activity that cycles somewhat due to the buildup and dissolution of corrosion products with time.

Chromate responds to local pH as a function of the corrosion site. For instance, anodes are generally acidic, either by consuming hydroxide through for-

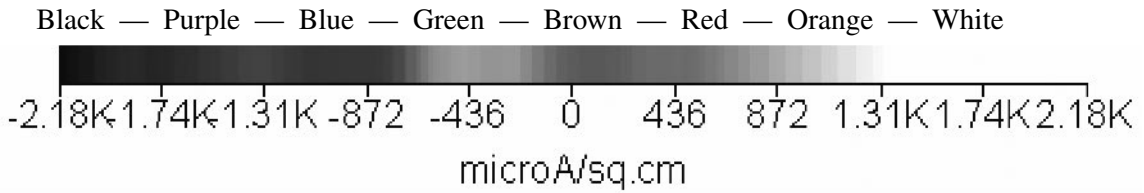


FIGURE 17.8 The SVET current scale shows the ion-induced SVET current, which is produced by the SVET probe moving in and out of the ion potential field. Both cathodic and anodic currents are shown through variation in color plot (not reproduced). The color scale above is labeled to show progression of current in the actual SVET plots to coincide with color labels below. Green-Blue-Purple-Black indicates increasing cathodic activity, while Red-Orange-White indicates increasing anodic surface activity. At “0” current, Red+Green yields a brown hue that indicates a passive surface.

mation of the metal (hydr)oxide or by generation of H^+ during hydrolysis of corrosion products. In acidic media, chromium (VI) becomes a strongly oxidizing species,^{67,76} easily capable of chemically anodizing the aluminum surface. Upon oxidizing the aluminum and forming aluminum oxide or hydroxide, the chromate can be reduced to insoluble chromium (III) and precipitates onto the newly formed oxide layer to heal the broken chromate surface.

In basic media, the half-cell corrosion potential for a chromium (III) ion is shifted toward spontaneous oxidation to chromium (VI),^{67,76} allowing the spontaneous formation of soluble chromium (VI) surface species. Electrochemical conversion to soluble species allows transport of once insoluble species to anodic sites. Once at the anodic site, the soluble species then respond to the local acidic environment.

As part of an entire chemical process (Figure 17.6), damage to a chromate conversion coated surface results in localized anodes on the exposed surface and nearby cathodes. Where cathodic areas develop on conversion coated areas, the conversion of chromium (III) into chromium (VI) is spontaneous and pH-mediated transport of chromium (VI) is allowed.^{68–71} Chromium (VI), on contacting the acidic anodic site, accelerates oxidation of (anodizes) the aluminum surface, reduces and becomes insoluble, self-healing the damaged chromate coating surface. The transport-precipitation process continues to shut down the electrochemical activity, ultimately producing a passive surface (Figure 17.9).^{73,74,77}

Chromate³⁵ can be applied in different forms originating as different bath compositions. The two most important of these are the chromium phos-

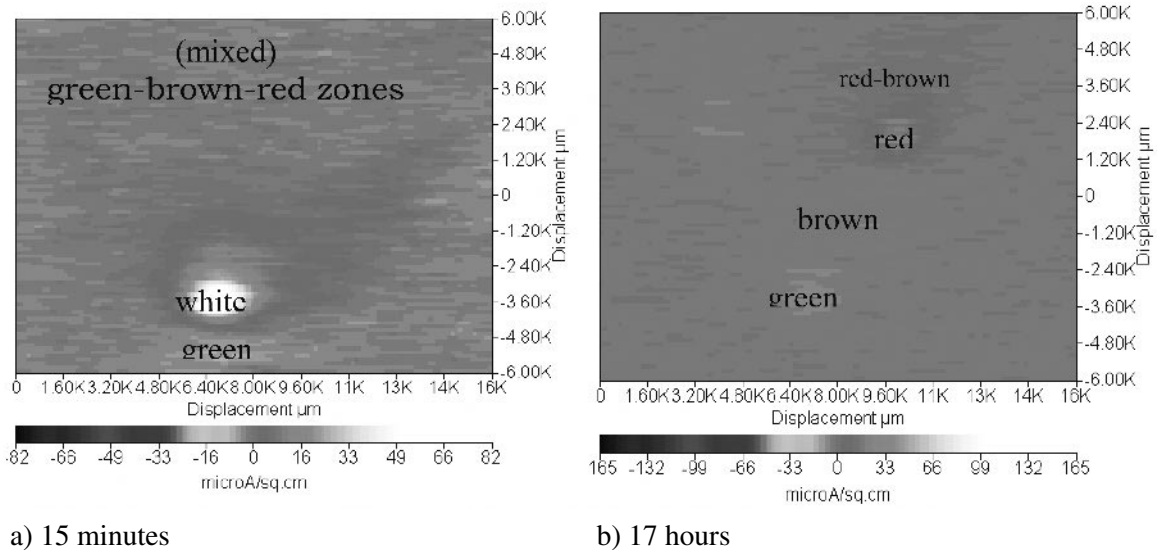


FIGURE 17.9 The SVET measurements of surface corrosion activity for a drilled chromate conversion coated AA7075-T6 panel after (a) 1-minute and (b) 30-minutes exposure to 5mM aqueous NaCl. Note low SVET current, the inversion of a localized anode into a weak cathode (Red/White to Green), and reduction in overall activity for both anodes and cathodes at prolonged exposure time.^{73,74}

phate, chromium chromate, and trivalent chromium⁶³ treatments. The chromium chromate treatment is yet higher in chromium concentration compared to a chromic acid anodize process, resulting in a durable chromium oxide surface layer of excellent adhesion and corrosion protection of the surface. Chromium phosphate, as a more stable salt species, is not as corrosion inhibiting as the chrome-concentrated chromium chromate coating. Chromium chromate passes the stringent military specification for corrosion resistance, 336 hours of neutral salt spray⁷⁸ exposure with no corrosion failure.

17.5.3 Cerium- and Rare Earth-based Conversion Coatings

Rare earth (lanthanide) elements are characterized by: large atomic radii; diverse allowable electronic configurations; formation of multiple oxidation states, typically +3 and +4 with occasional +2 valence state;⁷⁴ reactivity with water to form a neutral oxide; formation of stable, insoluble oxides of mixed valence states;⁷⁹ complex coordination chemistry;^{80–82} instability of lower valence salts in alkaline conditions, with a tendency to hydrolyze and precipitate as the hydrated oxide; and an extremely low reduction potential.^{76,83} An additional element that has been loosely grouped with the rare earths, though technically a *d*-transition element, is yttrium (Y) due to its large, negative reduction potential.

Essentially constant chemical properties across the lanthanide series dictate the corrosion inhibiting mechanisms and properties displayed by rare earth elements. Of the lanthanide series, lanthanum, cerium, praseodymium, and ytterbium have been most often examined as the most prevalent and inexpensive of the rare earth metals. Data for cerium are presented here, while the discussion regarding other rare earth elements will be analogous due to the similar properties across the chemical series.

Mixed valence oxides result due to the mismatch of the atomic radii of the rare earths with oxygen. Crystal lattice oxygen vacancies result and extra non-bonded electrons within cerium atoms of the crystal lattice, which are shared among neighboring cerium atoms. A localized, reduced valence on cerium is then observed. Therefore, lattice mismatch and crystal site vacancies result in locally reduced cerium formal valence throughout the crystal from +4 to +3, where the average valence is between +3 and +4. The partial valence states give the potential for unusual redox properties, oxygen transport as observed in fuel cell technology, and water and ion

complexation. Each of these contributes towards the cerium surface chemistry.

The general properties of cerium conversion coatings provide activity mainly as barrier coatings, providing suppression of the cathodic half-reaction.^{21,75,84–86} Cerium salts have been examined as solution inhibitors of aluminum corrosion and been found effective at cathodic reaction suppression.^{87,89–91} In addition, blends of rare earth compounds have been found to give synergistic protection when the nitrate salts were applied as a surface treatment.²²

A significant finding has been the demonstrated correlations between a convenient, short three-day soak EIS test and three-week salt fog performance for conversion coatings. Conversion coatings on a substrate that retain a final impedance higher than $10^5 \Omega\text{-cm}^2$ results (preferably over $10^6 \Omega\text{-cm}^2$) are most likely to pass MIL-C-5541 neutral salt fog testing.^{75,78} The procedure has been quite useful for screening chemistries as likely to pass a 336-hour neutral salt spray MIL-C-5541 specification.

In comparison with chromate treatments, rare earth elements do form durable aluminum alloy surface conversions but do not passivate anodic corrosion reactions.^{67,84} The chemistry of a rare earth conversion coating may be elucidated based on the electrochemistry and solubility of the species involved in corrosion inhibition (Fig. 17.10). Cerium (III/IV) redox potentials as a function of pH are similar to the chromium (III/VI) ion couple. However, cerium is insoluble in its higher oxidation state as the ceric/cerous mixed oxide but soluble in its lower valence state salt, such as cerous nitrate.

Soluble cerium can be synthesized at the acidic anode and insoluble ceric oxide at the alkaline cathode, analogous to that shown for chromate in Figure 17.6. While the oxide can inhibit oxygen reduction reactions as a barrier, as an insoluble coating it cannot be readily transported to an active anode. The stable rare earth oxide is not as strong an oxidant as the chromate anion and cannot effectively accelerate aluminum oxidation (i.e., quickly oxidize the aluminum surface to produce a passive layer). Even if ceric species near the anode can be transported in low concentration to the anode, the species become soluble cerous species at the anode only to be washed away by adventitious water and cannot precipitate at the anode as an insoluble salt to further passivate the corrosion site.

SVET measurements of cerium conversion coating corrosion activity in artificial drilled pits show a similar early distribution of anodes and cathodes as

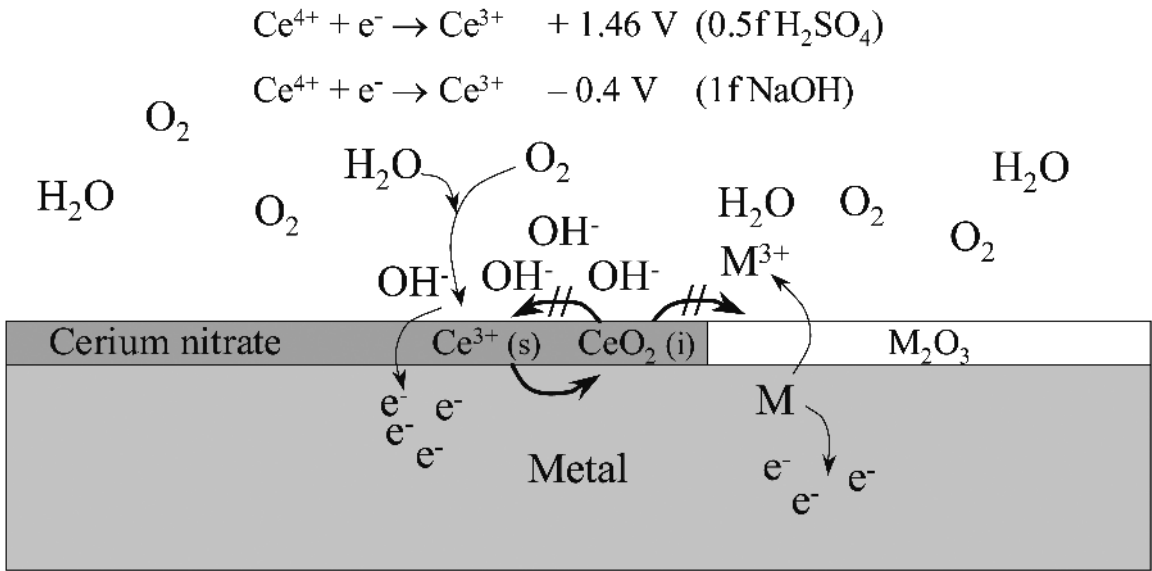


FIGURE 17.10 The corrosion protection, transport feedback mechanism of cerium is analogous to Figure 17.6 for chromate. While the electrochemical potentials are quite similar, perhaps even advantageous, to the chromate cycle, note the broken conversion cycle due to the poor solubility of the cerium (IV) oxide. For instance, the stable high valence oxide species is formed at high pH because it is stable but cannot transport well to anodes like soluble chromium (VI) oxide.

drilled chromate conversion coatings. However, usually only cathodic regions were observed to be affected by the cerium conversion coating (Figure 17.11), while anodic regions continued their activity unabated. The anode develops a more localized cathode to support continued corrosion activity. These combined data support the inhibition mechanism presented here and by others.^{56,77,84,92,93}

Thus, limitations inherent in the solubilities of rare earth species prevent full use of otherwise superb electrochemical properties. Typical electrochemical behaviors are similar to chromate, which result in reduced corrosion. Lacking anodic self-healing precipitation precludes a longevity similar to chromate coatings. The advantage for rare earths, if truly an advantage, is their very low toxicity. Rare earth technologies have demonstrated performance that is similar or superior to other non-chromium technologies.

17.5.4 Reprise: Alloy Considerations in Conversion Coating

Work by Yu⁵ has shown that despite conversion coating of a surface, based on chromate or cerate technologies, the obtained results were related to the initial corrosion sensitivity of the starting alloy. In

Figure 17.12 are shown DC polarization scans of conversion coated AA7075-T6 panels where the aluminum alloy was obtained from two different source lots. A DC polarization method measured the corrosion current density, equivalent to corrosion rate per surface area, as a function of the applied electrical potential in volts. The AA7075-T6 source lots were chromate and cerium conversion coated and tested for corrosion activity. Source 1 aluminum alloy after coating was observed to have a linear trend of higher corrosion current with increasingly anodic potential. Note that source 1 was initially (Figure 17.1) least corrosion resistant, showing lowest impedance. Source 1 alloy remained corrosion-sensitive even after conversion coating with chromate or cerium.

17.6 PRIMERS

The pretreatments and surface conversions described above are intended to produce surface coatings that provide not only a first defense against corrosion but also an adhesive surface. Adhesion is critical for primer and topcoating performance.⁶ While conversion coatings can be used alone, application of over coatings add barrier protection, phys-

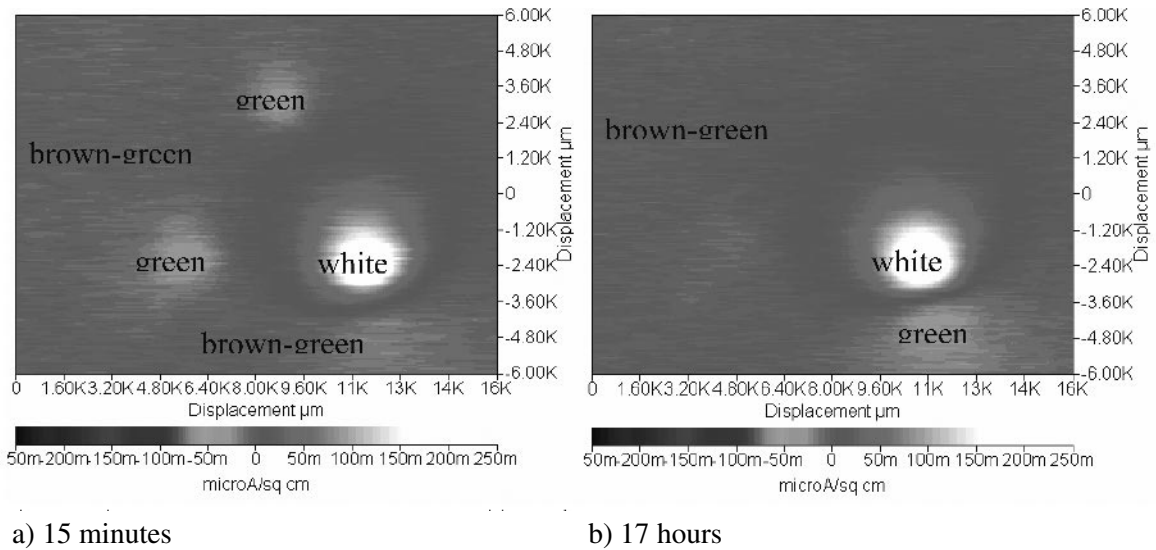


FIGURE 17.11 The SVET measurement of surface corrosion activity for a drilled cerium conversion coated AA7075-T6 panel after (a) 15-minutes and (b) 17-hours exposure to 5mM aqueous NaCl. In SVET analyses of the cerium conversion coating surface in the absence of co-inhibitors, the two cathodic (Green) regions were inhibited and passivated at prolonged exposure while the anodic (Red/White) region remained active. Also note the localized cathode adjacent to the active anode. Advancements have been made beyond this technological stage and are in applied patent.

ical durability and generally improved corrosion protection.

Conversion coatings serve to structurally and chemically stabilize and control the interfacial properties of the aluminum substrate to allow predictable, stable performance of the coated system. The surface conversion serves as the basis for over coating design, where the over coating chemistry should support that of the conversion coating, aiding pH control, self-healing properties, or supplementing a corrosion inhibiting mechanism. For instance, the most commonly used system for protection of aluminum alloy military and civilian aircraft from corrosion involves a chromium chromate or chromium-containing Alodine® surface treatment, followed by an epoxy polyamide primer containing strontium chromate, and an aesthetically-pigmented polyurethane top-coating. The polyurethane provides a light stable barrier protecting the underlying epoxy, the epoxy provides a store of chromate of controlled leach rate as the strontium salt, and the conversion coating anchors the system to the surface oxide of the aluminum alloy.

Adhesion to a surface is obtained through mechanical, chemical, electrostatic, and diffusive bonding. Mechanical bonding is the strongest because the fractal interface defies facile crack propagation, es-

pecially when supplemented by chemical bonding, but good mechanical bonding is not realized without good surface wetting. A liquid coating surface tension less than the surface energy provides spontaneous wetting of the surface by the coating. The larger the difference in surface tension between the coating and surface, the more pronounced the wetting and ability of the coating to penetrate into small surface pores. Upon hardening, good mechanical adhesion is obtained equal to the strength of the weakest component, the aluminum the oxide layer, the conversion coating, the interfacial regions, or within the primer matrix. Good mechanical adhesion improves surface durability as the properties of the coating, surface hardness and abrasion resistance, tensile and impact strength, and corrosion protection are directly related to the quality of surface adhesion.

Since solventborne primers typically have very low surface tensions, they provide good wetting and the ability to displace higher surface tension moisture from the surface. Since water is high in surface tension, poorer wetting would be obtained with waterborne coating technologies if not for the use of co-solvents and/or surfactants to reduce the surface tension and improve wetting. In addition, solventborne coatings can be more hydrophobic and have improved barrier properties compared to co-solvent-

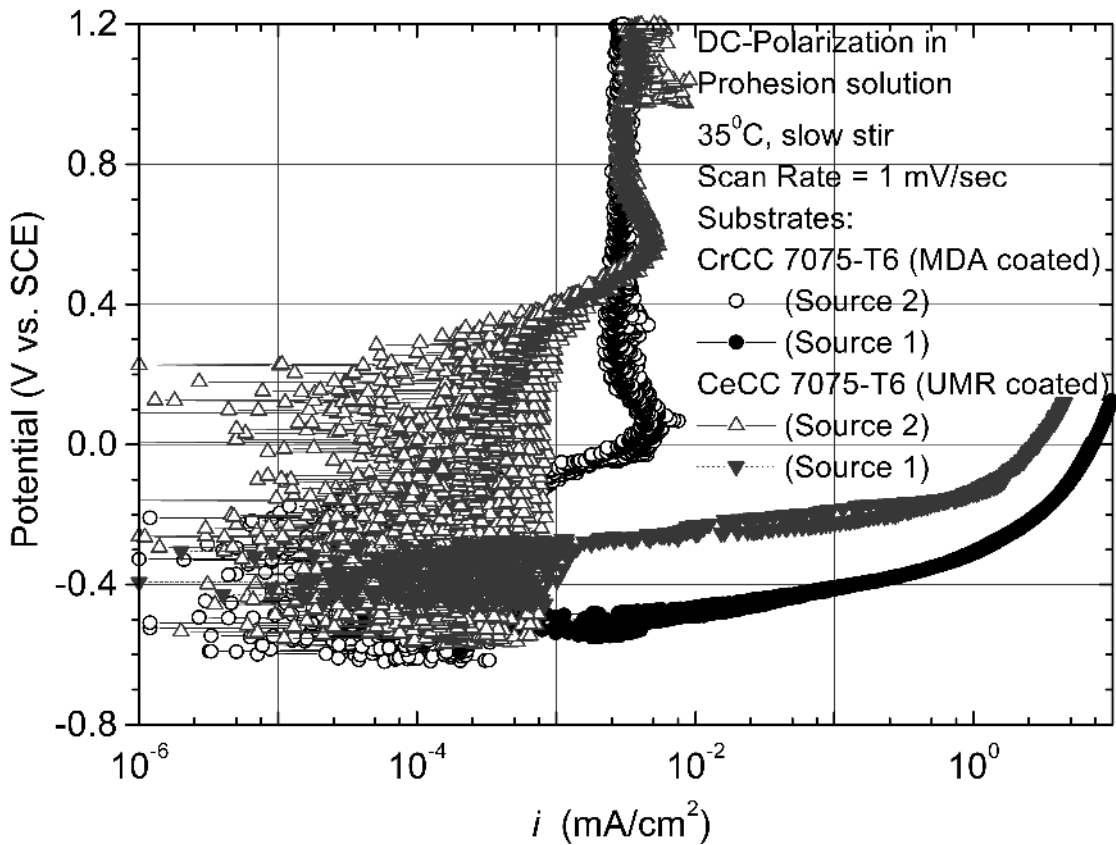


FIGURE 17.12 DC polarization measurements of chromate (CrCC) and cerium (CeCC) coated AA7075-T6 alloy, which shows the corrosion current density (i) as a function of potential for each aluminum source lot.⁵

and surfactant-laden waterborne coatings. Solvent-borne coatings also inherently contain more volatile organic content (VOC) pollutants.

Environmentally-friendly primer technologies include water-soluble and water dispersed coatings, powder coatings, and higher or 100% solids coatings. Viscosity is a limiting factor for any coating technology, controlling the surface application. Water dispersed technologies appear most advanced, with some⁸⁸ delivering the performance of low viscosity solventborne coatings at the expense of several percent of co-solvents.

The quality of adhesion is also related to formation of differential concentrations of water and oxygen, potentially forming galvanic cells or filiform corrosion. Poor adhesion observed as poor wetting provides a porous interface and a route for transport of moisture or air at the weak interface. These effects are often magnified by application of a barrier topcoating that further hinders transport of air or moisture through a film that otherwise could miti-

gate directional transport at an interfacial boundary. Filiform can be reduced by use of a more porous topcoating system to reduce localized water and/or air that result in galvanic corrosion elements. The more effective solution is a less porous interfacial region.

Although discussion of all coating property aspects is beyond the scope of this chapter (see references 4 and 5 for general texts), one other aspect that must be discussed is coating porosity and transport of corrosion inhibiting compounds (CICs). Epoxy polyamides are important for their flexibility through common, relatively inexpensive, and commercially available resins. The resins are flexible in molecular weight, stoichiometric equivalence, functional group contents, cure rate, and resulting physical properties including solubility. Mixing and matching of epoxy with polyamide resins allows fine-tuning of hydrophobicity and porosity, through composition and cross-link density, respectively, which control inhibitor migration and leach rates.

A localized, minimum active concentration of CIC species is required to prevent corrosion processes. Too little inhibitor can actually accelerate failures, while excess CIC is leached away and reduces available CIC and longevity. The job of selecting the inhibitor solubility, conversion coating, and primer layers is to match but not exceed the needed amount. For instance, strontium chromate has a low active solution concentration (0.01 mmol/L) necessary to give corrosion inhibition of AA7075-T6 in dilute salt solution and can obtain the near-ideal leach rate of 2.5×10^{-4} mmol/cm² hr from an epoxy polyamide primer.⁸⁹⁻⁹¹ Cerium inhibitors vary in leach rate (from epoxy polyamide) and protection afforded as a function of anion type. Cerium iodate in standard epoxy polyamide yields a release rate of 4.3×10^{-5} mmol/cm² hr.⁸⁹⁻⁹¹

Our recent studies into rare earth primer coatings have shown that the rare earth elements, particularly the +3 valence state salts, complex exothermically with the polyamide resin. Chromate salts show no such reactivity with the amide resin. Hence, the leach rate of even soluble salts are not what would be predicted based on solubility of the inhibitor alone.^{67,82}

Primer coatings are evaluated for corrosion performance by several means,⁹⁴ including wet adhesion, neutral salt fog exposure,⁷⁸ prohesion, EIS, artificial defect (drilled pit) DC polarization, open circuit potential, SVET, electrochemical noise, etc. While electrochemical test methods have made progress in recent years and salt fog studies have shown poor correlation to actual exterior, long-term exposures, neutral salt fog remains a standard accelerated test. Recently, correlations between cyclic prohesion/UV exposures with actual exterior weathering performance have been demonstrated.

Strontium chromate containing primer, applied over chromate conversion coated AA7075-T6 or AA2024-T3 and scribed through to a bare aluminum gouge, provides shiny scribe results after 2,000+ hours of ASTM B-117 neutral salt fog exposure (!). In comparison with carbon steel coated by a chromated primer at 2-mil thickness, 1,000 hours with rusted scribes of less than 1mm creepage from the scribe is a reasonable performance. Rare earth primers provide shiny scribe performance on AA7075-T6 or AA2024-T3 to about 800 hours neutral salt fog,⁷⁸ especially when enhanced with a co-inhibitor such as permanganate, chromate, technetate, molybdate, etc., that provide a transportable inhibitor, oxidative anodic acceleration, and an insoluble, precipitating oxide within locally acidic re-

gions analogous to chromate. These inhibitors convey a limited ability to passivate anodic regions and prevent corrosion, further optimizing rare earth system performance.

The performance of primer coated aluminum alloy is referenced in Figure 17.13, showing the stages of failure. Shiny scribes demonstrate the highest level of performance, followed by black spots within the scribed regions. Black corrosion products^{67,95} appear related to copper oxide residues. Black corrosion stains are followed by more extensive corrosion evidenced by fluffy, white salting and salt tailing. An alternative failure mode to salting is blistering.

Rare earth systems do match or exceed the performance of other non-chromate coating systems and, as such, are one of the few options for replacing toxic, chromium based paints. Cerium has been applied in electrodeposited coatings,⁹⁶ waterborne epoxy polyamide,^{67,97} and solventborne epoxy polyamide^{67,89-91} primer coatings. Complexation reactions between cerium and polyamide or amino resins have been observed for each of these systems, which resulted in reduced solubility of cerium salts and altered valence state.

17.7 TOPCOATING

The topcoating, like the primer, must adhere to its substrate. Since the topcoating is usually applied to a primer, often a recoat window is required to ensure good diffusive bonding between the underlying primer and topcoating. Diffusive bonding results from interaction and entanglement between polymer resins, and can include covalent reaction. The recoat window ensures the primer has sufficient resistance to avoid delamination but sufficiently low cross-link density and residual solvent sensitivity to allow polymer chain entanglement and functional group contact for covalent reaction.

Alternatively, primers are formulated at higher pigment volume concentrations (PVCs) and with silica pigments to provide a fractal surface upon drying for mechanical topcoating adhesion. While physically abrading the surface is likewise useful for creating mechanical adhesion, a physical abrasion method is often limited by time and labor requirements. Combined chemical and mechanical interactions ensure a durable, adhesive interface.

The job of the topcoating is to provide a functional appearance, added physical barrier protection, and filtration of high energy light in defense of the

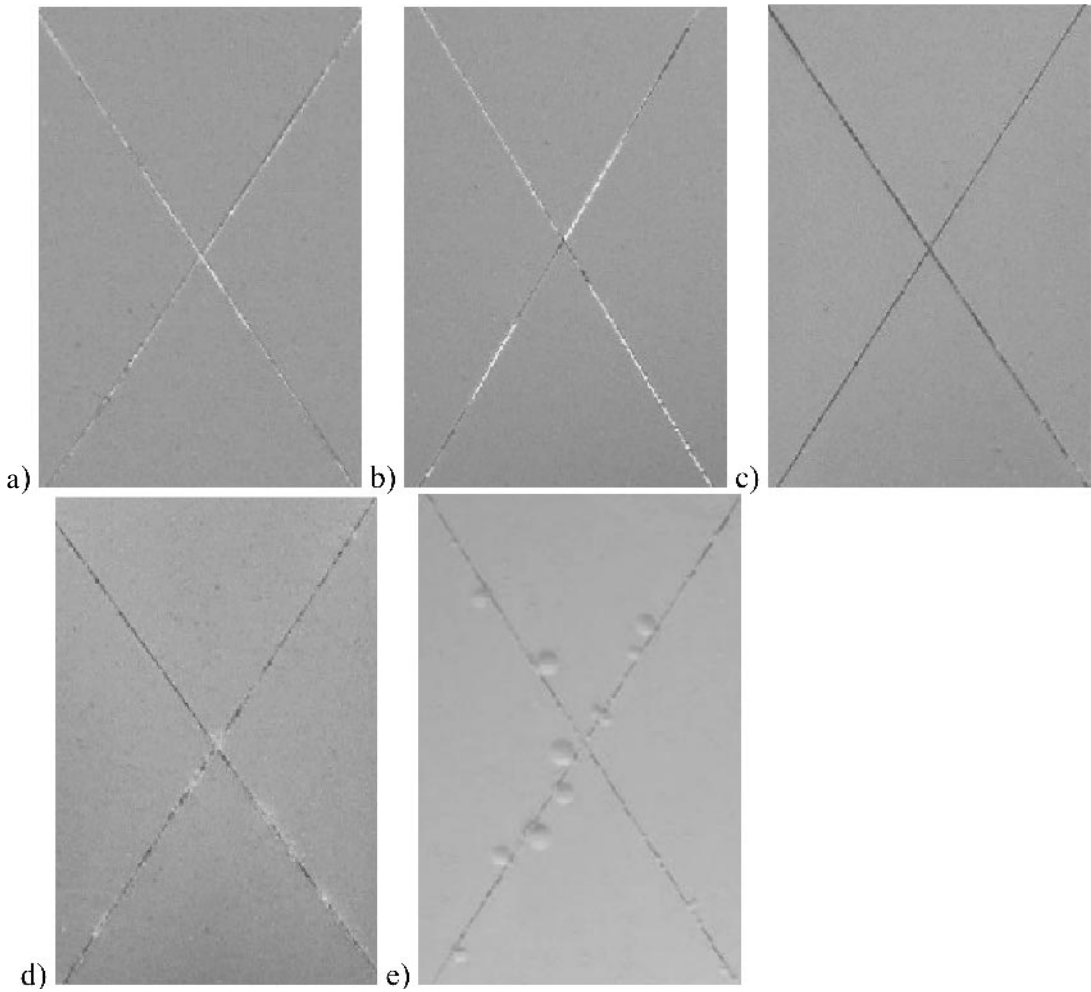


FIGURE 17.13 Performance of rare earth primer coated AA7075-T6 panels showing (a) shiny scribe, (b) shiny with black spots, (c) black scribe, (d) black scribe with white salt, and (e) salty scribe with blistering.

primer. Most of these properties are actually supplied by the pigmentation in the topcoating, while a light resistant resin binds the pigments into a film and to the primer. Additional primer layers also may be used to bolster the lower primer layers. For instance, the U.S. Navy uses an additional primer layer, non-chromated, followed by a weatherable topcoating on ships to maximize total weather and corrosion resistance. Aircraft, in contrast, utilize the thinnest layers possible to give complete surface coverage but minimize weight.

It is interesting to note that problems with military vehicle coatings often originate due to appearance rather than issues with functionality (e.g., corrosion resistance or radar absorption). Uninformed commanders often mistake outward appearance of

normal wear as a sign of poor maintenance, which can prompt hasty, ill-performed surface preparation in recoat operations for “lack of time” prior to inspection. Poor surface preparation to ensure adequate adhesion and coating thickness is tantamount to circumventing the very purpose of surface coating: protection. Complete surface refinishing to reduce a mottled but otherwise functional appearance can be both unwarranted and destructive.

Thermoset polyurethanes, which are generally physically and chemically weather-durable, have been the main topcoating resin system. These systems, despite being of good quality, still suffer color fade or haze. New technology, fluorocarbon topcoatings provide excellent UV light and fade resistance to allow coating design schedule, rather than ap-

pearance schedule, recoating⁹⁸ and therefore improved lifetime cost.

17.8 UNICOATINGS

Unicoatings are primer plus topcoating applied in a single layer. Unicoatings consistently have not performed equivalent to multilayer coating systems. However, appliqué versions of unicoatings have been of recent interest as a strategy to reduce recoat and routine maintenance issues.

17.9 SUMMARY

The corrosion protection of a surface can be thought of as converting the pre-existing surface to one less reactive and inert. The methodology for nearly all metals is similar but the compositions are necessarily different, because treatments that work on one metal as inhibitive may be a noble oxide, acting as cathode and accelerant of corrosion on another. The oxide layer of aluminum is its natural defense against corrosion and is particularly effective, e.g., the durable aluminum drink can.

The native aluminum oxide layer remains susceptible away from its isoelectric point where the metal ion or its oxo-anions are soluble and can be dissolved to expose bare aluminum, at acidic and extreme basic pHs. One way to shore up the performance is to thicken the oxide layer through anodizing. A second method employed during sealing of the anodized coating involves conversion of the oxide to a more pH stable salt, such as phosphate. A third method involves use of specific, metal oxide inhibitors to convert the surface into a more resistant surface oxide, i.e., conversion coating.

A durable surface conversion finish not only provides an unbroken barrier to corrosive species transport to/from the surface, but also mechanical strength in adhesion of over coatings. Inhibition of corrosion product species transport is equivalent to fixing the equilibrium of the corrosion process, which aids corrosion protection. Corrosive species and corrosion product transport are to be prohibited except where required to self-heal a damaged coating surface.

The pretreatment of the alloy is absolutely critical to obtaining adhesion and protection by the surface coating. Pretreatments include cleaning, deoxidation, and quality rinsing as part of the multi-step process. Cleaning removes contaminants that hinder

uniform pickling, and pickling or deoxidation provides a uniformly active surface through manipulation of surface composition. Anodizing or conversion coating pretreatment is a final step, conducted on freshly treated metal.

Chromates have been shown to work as conversion coatings on most metals to provide cathodic protection as an inert metal oxide (Cr_2O_3), while providing transport mechanisms (CrO_3 as CrO_4^{2-}) regulated by local pH conditions. The highly oxidizing chromate initiates formation of a native aluminum oxide and, with change in local pH, precipitates as an inert oxide onto the active anodic site. Self-healing is the ultimate factor in the success of chromate, which nearly all other inhibitors lack to some extent. If not for toxicity, it would remain the *modus operandi*. Rare earth technologies appear to be the most promising new technology, though advances in transport control are required to offer the performance of chromate conversion coatings.

Surface conversion coatings are chemically supported by primers, which are physically protected by topcoatings. Inhibitive pigments, such as chromate or molybdate, are added to provide additional ion support as transportable, precipitating species. Rate of transport is controlled by the permeability of the organic binder; it is desired to be slow but steady to maintain a long protective lifetime. Epoxy polyamides are the coating of choice, being chemically resistant to the localized pH extremes encountered in corrosion events and of controllable hydrophobicity and porosity.

A topcoating is necessary to protect the primer from light degradation, which is severe in the popular epoxy polyamide primer system, and provide an aesthetic, functional appearance. The topcoating itself must be opaque and resistant to high-energy light such as ultraviolet. Common systems employed are urethanes utilizing UV-resistant, acrylic polyols. Traditional systems have still been subject to relatively short-term color fading due to UV light. However, newer systems employing fluororesin technology have elicited long-term fade resistance and cost savings associated with downtime, surface preparation and application labor.

Selection of the alloy type and alloy quality drastically affects the resultant corrosion performance and, more importantly, the ability of the metal to be electrochemically passivated by coatings. The alloy type serves as the basis for selecting a particular surface treatment. High copper concentration alloys (e.g., the wrought 2000 series) tend to be more cor-

rosion active and least treatable, but may be necessary for their engineering properties. Development of improved alloys may, in the future relax the need for protective treatments.

17.10 ACKNOWLEDGEMENTS

The author thanks colleagues at the University of Missouri–Rolla for contributions of analytical data: Paul Yu, Shantanu Patwardhan, Ahmed Shahin, and Scott Hayes, without whom the utility of this chapter would have been reduced. The data contained herein is a review of public information assembled to aid development of new conversion coatings and organic primers for aluminum alloys. The author acknowledges startup support from the University of Missouri–Rolla Materials Research Center, Dr. James Stoffer, Director.

17.11 REFERENCES

1. Askeland, Donald R. *The Science and Engineering of Materials*. PWS-Kent, 1989, Chapter 13.
2. Davis, J. R., Ed. *Corrosion of Aluminum and Aluminum Alloys*, Materials Park, OH: ASM International, (1999).
3. Ghali, E. "Aluminum and Aluminum Alloys," In: *Uhlig's Corrosion Handbook*, R. Winston Revie, Ed. New York: John Wiley and Sons, Inc. (2000), Chapter 40.
4. Jones, D. A., *Principles and Prevention of Corrosion*, 2nd Ed. Upper Saddle River, NJ: Prentice Hall. (1996).
5. Yu, P. University of Missouri–Rolla, unpublished data, (2003).
6. Wicks, Z. W., Jones, F. N., and Pappas, S. P. *Organic Coatings: Science and Technology*. New York: John Wiley and Sons, Inc., (1992).
7. Thompson, G. E., Zhang, L., Smith, C. J. E., and Skeldon, P., *Corrosion*, 55(11), 1,052–1,061 (1999).
8. Indira, K. S., Subramanian, R., and Shenoi, B. A., *Metal Finishing*, 69(4), 53–8 (1971).
9. Miller, W. G. L., "Protection of Metal Surfaces," *British Patent # GB 1065825* (1967).
10. Lanier, V. I., *Elektrolit. Osazhdenie Spavlov*, 186–97 (1961).
11. Wanamaker, J. L., Weber, K. E., Hoch, G. M. "Corrosion-protected anodized aluminum surfaces," *U.S. Patent #3,790,453* (1974).
12. Alodine 2000 is a registered trademark of Henkel Surface Technologies.
13. Alodine 5200 is a registered trademark of Henkel Surface Technologies.
14. Alodine 4840 is a registered trademark of Henkel Surface Technologies.
15. Bibber, J. W., "Low temperature corrosion resistant aluminum and aluminum coating composition," *U.S. Patent # 5,707,465* (1998).
16. Stesikova, E., Metroke, T. L., Kachurina, O., Knobbe, E. T. *Proceedings of the 4th Conference on Aerospace Materials, Processes, and Environmental Technology* (2000), pp. 76–83.
17. McDonald, A. "Protective coating," *U.S. Patent 2,576,845* (1951).
18. Denault, G., "Anodizing aluminum or its alloys," *French Patent # FR 2058759* (1971).
19. Quattrone, C. "Aspects of electrolytic deposition on aluminum," *Galvanotecnica*, 11, 217–21 (1960).
20. Best, G. E., McGrew, J. W., "Inhibiting corrosion of steel, aluminum, and magnesium intermittently exposed to brines," *Corrosion*, 12, 286t–92t (1956).
21. Nelson, K. J. H., Taylor, R. J., Hughes, A. E., Hinton, B. R. W., Henderson, M. J., Wilson, L., Nugent, S. A., "Conversion coating and process and solution for its formation," *U.S. Patent 6,022,425*, February 8, 2000.
22. Lu, Y., Ives, M. B. "Method of increasing corrosion resistance of metals and alloys by treatment with rare earth elements," *U.S. Patent 6,068,711*, May 30, 2000.
23. Stoffer, J. O., O'Keefe, T. J., Lin, X., Morris, E.L., Yu, P., and Sitaram, S. P., "Electrodeposition of cerium-based coatings for corrosion protection of aluminum alloys," *U.S. Patent #5,932,083* (1999).
24. Talbert, R. *Powder Coater's Manual*. Hannover, Germany: Vincentz Network. (1998), Chapter II.
25. U.S. Army TACOM, MIL-HDBK-509(AT). (Washington, DC: U.S. GPO. (1998); see also reference 65.
26. Tharp, J. W. "Chemical filming of aluminum alloys for military applications," *Products Finishing*, 34(5), 64–8 (1970).
27. American Society for Testing and Materials (ASTM), West Conshohocken, PA; see also reference 94.
28. Society of Automotive Engineers (SAE), Warrendale, PA; see also Table 17.2 for pertinent SAE specifications for finishing aluminum surfaces.
29. Aluminum Association, *Care of Aluminum*. (Washington, DC: Aluminum Association. (1992).
30. Zippel, G. *Journal fuer Oberflaechentechnik*, 41(5), 60–61 (2001).
31. Kresse, J. and Nowak, A., "Alternatives to the chromating of aluminum alloys," *DFO/DGO-fagung*, Disseldorf, Germany, 14–15 February 1995.
32. Roland, W. A. and Droniou, P., *Metal Finishing*, 57 (1993).
33. Cole, H. G., "Corrosion and protection of aircraft," *1st International Congress on Metallic Corrosion*, London, 1961, pp. 642–5 (1962).
34. Raskin, M. "Electroplating on aluminum and its alloys," *Metal Finishing*, 44, 337–9 (1946).
35. Work, H. K. "Electroplating aluminum and its alloys," *Transactions of the American Electrochemical Society*, 53, 24 (1924).

36. Wernick, S., Pinner, R., Sheasby, P.G. *The Surface Treatment and Finishing of Aluminum and Its Alloys, 5th Ed.* (Materials Park, OH: ASM International. (1987), Volumes 1 and 2.
37. Rosenberg, R. A., McDowell, M. W., and Noonan, J. R., *Journal of Vacuum Science Technology, A: Vacuum, Surfaces, and Films*, 12(4, pt. 1), 1755–9 (1994).
38. Code of Federal Regulations, 40 CFR 261 (Washington, DC: U.S. GPO. (2002).
39. Code of Federal Regulations, a) 29 CFR 1910, b) 29 CFR 1915 (Washington, DC: U.S. GPO. (1996).
40. Brace, A., *Technology of Anodizing*. (Great Britain: Draper, Teddington. (1968).
41. Tharp, J. W., Tyminski, J. J. “Chromic and sulfuric acid anodizing of aluminum alloys for military applications,” *Plating*, 55(6), 580–3 (1968).
42. Mansfeld, F., Zhang, G. and Chen, C. “Evaluation of sealing methods for anodized aluminum alloys with electrochemical impedance spectroscopy,” *Plating and Surface Finishing*, 84(12), 72–81 (1997).
43. Moon, S., Sakairi, M., Takahashi, H., Shimamura, K. “Electroless Ni-P Deposition through Imperfections in Anodic Oxide Films on Aluminum and A15052 Alloy,” *Electrochemistry*, 71(4), 260–265 (2003).
44. Simmons, J. G. “Electrolyte for anodizing aluminum,” *GB Patent 1,070,782*, June 1, 1967.
45. Pires, I., Quintino, L., Rangel, C.M., Thompson, G. E., Skeldon, P., Zhou, X. “Influence of pre-treatments on the surface condition of 2024-T3 aluminium alloy,” *Transactions of the Institute of Metal Finishing*, 78(5), 179–185 (2000).
46. Keohan, F. L., Mitchell, A. J., Ragan, C. C., Bialic, L. J. “A new chromium free surface treatment for structural adhesive bonding of aluminum,” *International SAMPE Symposium and Exposition*, 38, 1,181–1,195 (1993).
47. Dasquet, J. -P., Caillard, D., Bonino, J. -P., Bes, R.S. “Characterization of the protective effect of aluminum surface treatments by d.c and a.c. measurements,” *Journal of Materials Science*, 36(14), 3,549–3,555 (2001).
48. Kissin, G. H., *Anodized Aluminum*, ASTM Technical Publication #388, West Conshohocken, PA: ASTM. (1965).
49. Murphy, J. F., “Chemical and Electrochemical Factors in the mechanism of formation and properties of anodic coatings,” in: *Symposium on Anodizing Aluminum*, London: The Aluminum Federation, Stag Place, April 1967, p. 3.
50. Barkman, E. F., “The structure, composition, and mechanism of formation of anodic oxides on aluminum,” in: *Symposium on Anodizing Aluminum*. London: The Aluminum Federation Stag Place, April 1967, p. 27.
51. Brace, A., *Technology of Anodizing* (Great Britain: Draper, Teddington. (1968), Chapter 12.
52. John, S. and Shenoi, B. A. “Sealing anodized aluminum. Review of theory and methods,” *Surface Finishing*, 74(7), 31–35 (1976).
53. John, S., Shenai, S.A. “Methods of color anodizing of aluminum and its alloys,” *Journal of the Color Society*, 23–24(4-1), 23–8 (1985).
54. Zuo, Y., Zhao, P -H. and Zhao, J -M, *Surface and Coatings Technology*, 166(2–3), 237–242 (2003).
55. Survila, E. and Andrews, D. P., *Transactions of the Institute of Metal Finishing*, 57(1), 15–37 (1979).
56. Baldwin, K. R., Lane, P. L. and Smith, C. J. E. “A chromate-free post-anodizing treatment for aluminum alloys using a double-immersion process,” *Interfinish* (2000), pp. 526–538.
57. Ventura, X. A., *Proceedings of the AESF SURF/FIN Annual International Technical Conference* (2002), pp. 434–451.
58. Kendig, M. and Thomas, C. *Journal of the Electrochemical Society*, 139(11), L103–L104 (1992).
59. Homma, N., Johnson, P. M., Carlson, L. R. “Process and composition for sealing porous coatings containing metal and oxygen atoms,” *U.S. Patent Appl. 0179189*, December 5, 2002.
60. Dull, D. L. and Mansfeld, F. B., “Rare-earth metal solutions for sealing of anodized aluminum alloys surface for corrosion resistance and paint adhesion,” *U.S. Patent #6,248,184* (2001).
61. Blohowiak, K. Y., Osborne, J. H., Anderson, R. A. and Cao, T. Q., “Method for promoting adhesion between a metal and an org. resin using silicon-yttrium sol film,” *U.S. Patent #5,958,578* (2003).
62. Kanagari, D. Mohan, S., Renganathan, N. G., Raj, V., Kumar, M. K. and Iyer, S. V., *Proceedings of the Electrochemical Society*, 2000-4, 305–316 (2000).
63. Pearlstein, F. and Agarwala, V. S. “Trivalent chromium solutions for applying chemical conversion coatings to aluminum alloys or for sealing anodized aluminum,” *Plating and Surface Finishing*, 81(7), 50–55 (1994).
64. Matzdorf, C. A., Kane, M. J. and Green, J. L., “Chromate post treatment of anodized aluminum to improve corrosion-resistance, abrasion and adhesion properties,” *U.S. Patent #6,511,532* (2003).
65. U.S. Military specification, MIL-C-5541E, (Washington, DC: U.S. GPO. (1990).
66. Boeing generally requires that coating systems on aluminum alloys provide a shiny, uncorroded scribe after 2,000 hours of ASTM B-117 neutral salt fog exposure, excellent intercoat adhesion, and an absence of filiform sensitivity. Chromate primer on chromate conversion coated AA7075-T6 or AA2024-T3 alloys, with or without polyurethane top-coating, meets or exceeds these requirements (see also MIL-C-5541).
67. Schuman, T., Shahin, A. and Stoffer, J. O., “Cerium Based Inhibitors of Aluminum Alloy Corrosion” *Proc. International Waterborne, High Solids, and Powder Coatings Symposium*, New Orleans, LA, February, (2002), p 371.
68. Zhao, J., Frankel, G., McCreery, R. L. “Corrosion Protection of Untreated AA2024-T3 in Chloride Solution by a Chromate Conversion Coating Monitored with Raman

- Spectroscopy," *Journal of the Electrochemical Society*, 145(7), 2,258–2,264 (1998).
69. Xia, L., McCreery, R. L. "Chemistry of a Chromate Conversion Coatings on Aluminum Alloy AA2024-T3 Probed by Vibrational Spectroscopy," *Journal of the Electrochemical Society*, 145(9), 3,083–3,089 (1998).
 70. Ramsey, J. D., McCreery, R. L. "In situ Raman Microscopy of Chromate Effects on Corrosion Pits in Aluminum Alloys," *Journal of the Electrochemical Society*, 146(11), 4,076–4,081 (1999).
 71. Xia, L., Akiyama, E., Frankel, G., McCreery, R. "Storage and Release of Soluble Hexavalent Chromium from Chromate Conversion Coatings," *Journal of the Electrochemical Society*, 147(7), 2,556–2,562 (2000).
 72. Katzman, H.A., Malouf, G.M., Bauer, R., Stupian, G.W. *Applied Surface Science*, 2, 416 (1979).
 73. Patwardhan, S. V. "SRET evaluation of conversion coatings on aluminum," M. S. thesis, University of Missouri–Rolla, June 2001.
 74. Schuman, T.P., Patwardhan, S. V., Hayes, S. A., Yu, P., Stoffer, J. O., O'Keefe, T. J. "The Practical Use of SRET in Surface Corrosion Assessments," *Proceedings of the Gateway Coatings Symposium*, St. Louis Society for Coatings Technology, St. Louis, MO, June 2001.
 75. Stoffer, J. O., O'Keefe, T. J., Morris, E., Hayes, S., Yu, P., Pittman, M. "Environmentally compliant aircraft coatings," *Polymeric Materials Science and Engineering*, 83, 311–312 (2000).
 76. Pourbaix, M. *Atlas of Electrochemical Equilibria in Aqueous Solutions*. Oxford, New York. (1966).
 77. Kendig, M. W., Davenport, A. J., Issacs, H. S. *Corrosion Science*, 34, 41 (1993).
 78. ASTM. Method ASTM B-117. (West Conshohocken, PA: American Society for Testing and Materials. (2003).
 79. Kulagin, N. A. "Mixed valency of the rare earth and actinium ions in solid states," *Journal of Alloys and Compounds*, 300-301, 348–352 (2000).
 80. Mehrotra, R. C., Kapoor, P. N., Batwara, J. M. "Coordination chemistry of lanthanides with emphasis on derivatives with lanthanide-oxygen-carbon bonds," *Coordination Chemistry Reviews*, 31(1), 67–91 (1980).
 81. Shore, S. G., Knoepfel, D. W., Deng, H., Liu, J., White, J. P., III, Chun, S. -H. "Coordination chemistry of lanthanides with transition metal anions," *Journal of Alloys and Compounds*, 249(1–2), 25–32 (1997).
 82. Schuman, T. P., Shahin, A. "XPS Characterization of Cerium (III-IV) Complexes," submitted: *Journal of Coordination Chemistry*, 2003.
 83. Hayes, S. A., Yu, P., O'Keefe, T. J., O'Keefe, M. J., Stoffer, J. O. "The Phase Stability of Cerium Species in Aqueous Systems," *Journal of the Electrochemical Society*, 149(12), C623–C630 (2002).
 84. Hinton, B. R. W., Arnott, D. R., and Ryan, N. E., *Metals Forum*, 7(4), 211 (1984).
 85. Arnott, D. R., Hinton, B. R. W., Ryan, N. E. "Cationic-film-forming inhibitors for the protection of the AA7075 aluminum alloy against corrosion in aqueous chloride solution," *Corrosion*, 45(1), 12–18 (1989).
 86. Hinton, B., Hughes, A., Taylor, R., Henderson, M., Nelson, K., Wilson, L. "The corrosion protection properties of a cerium oxide conversion coating on aluminum alloy AA2024," *Acta Technica Belgica Metallurgie*, 37, 165–168 (1997).
 87. Bhattamishra, A. K., Banerjee, M. K. "Study on corrosion behavior of aluminum-zinc-magnesium alloys in sodium chloride solution in presence of cerium salts," *Berg- und Huettenmaennische Monatshefte*, 137(11), 426–9 (1992).
 88. Albers, Richard A., "Water-reducible epoxy coating compositions," *U.S. Patent 4,501,832*, February 26, 1985.
 89. Smith, C. J. E., Baldwin, K. R., Garrett, S. A., Gibson, M. C., Hewins, M. A. H., Lane, P. L. "Development of chromate-free treatments for protection of aerospace aluminum alloys," *Acta Technica Belgica Metallurgie*, 37, 266–273 (1997).
 90. Smith, C. J. E., Hewins, M. A. H., Baldwin, K. R. "Corrosion inhibitors for advanced aerospace aluminum-lithium alloys," *8th European Symposium on Corrosion Inhibitors*, 10(2), 807–16 (1995).
 91. Smith, C. J. E., Baldwin, K. R., Hewins, M. A. H., Gibson, M. C. "A study into the corrosion inhibition of an aluminum alloy by cerium salts," In: *Progress in the Understanding and Prevention of Corrosion*. J. M. Costa, A. D. Mercer, Eds. London: Institute of Materials, (1993), pp. 1,652–1,663.
 92. Hughes, A. E., Taylor, R. J., Hinton, B. R. W., Wilson, L. "XPS and SEM characterization of hydrated cerium oxide conversion coatings," *Surface and Interface Analysis*, 23(7–8), 540–50 (1995).
 93. Wan, J., Thompson, G. E., Ng, T. K., Lu, K. Q., Smith, C. J. E. "XANES study of Ce- and Mo-containing conversion coatings on aluminum," *Journal de Physique IV*, 7(C2, X-Ray Absorption Fine Structure, Vol. 2), 1183–1184 (1997).
 94. Koleske, J.V., Ed. *Paint and Coating Testing Manual, 14th Ed.* West Conshohocken, PA: American Society for Testing and Materials. (1995).
 95. McCafferty, E., Trzaskoma-Palette, P. "Anodic dissolution and protection of AA7075 in hydroxide solutions," *Corrosion*, 53(3), 179–185 (1997).
 96. Morris, E. L., Stoffer, J. O., O'Keefe, T. J., Yu, P., Lin, X. *Polymer Materials Science and Engineering*, 78, 172 (1998).
 97. Vreugdenhil, A. J., Balbyshev, V.N., Donley, M. S. "Nanostructured Silicon Sol-Gel Surface Pretreatments for Al 2024-T3 Protection," *Journal of Coatings Technology*, 73, 35 (2001).
 98. Deft, Inc. in San Diego, CA supplies weather resistant primer and topcoating technologies to Boeing and the U.S. Air Force.

CHAPTER 18

CORROSION RESISTANT COATINGS AND PAINTS

R. G. Buchheit

Fontana Corrosion Center, Department of Materials Science and Engineering, The Ohio State University, Columbus, Ohio

- 18.1 SCOPE 367
- 18.2 CORROSION PROTECTION BY COATINGS AND PAINTS 367
- 18.3 ENGINEERING ALLOYS AND THEIR NEED FOR CORROSION RESISTANT COATINGS 371
- 18.4 CHARACTERISTICS AND USES OF CORROSION RESISTANT PAINT AND COATINGS 372
- 18.5 APPLICATION METHODS AND SURFACE PREPARATION 376
- 18.6 FACTORS AFFECTING COATING DEGRADATION 377
- 18.7 CORROSION UNDER COATINGS 377
- 18.8 COATING DEGRADATION AND EVALUATION METHODS 378
- 18.9 KEY APPLICATIONS 381
- 18.10 ENVIRONMENTAL HAZARDS 384
- 18.11 REFERENCES 384

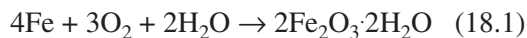
18.1 SCOPE

Most metallic alloys are susceptible to corrosion in their service environments. One of the most practical and cost-effective ways to slow or stop corrosion is by application of a protective coating or paint. Coatings and paints can be applied to large surface areas and are protective, even though they are relatively thin. They can be applied rapidly and the associated material and labor cost is usually much less than the cost (or value) of the object being protected. Over the past 150 years, corrosion resistant coating and paint technology has evolved steadily, resulting in a vast array of products for protecting many different substrates under many different conditions. Coating technology is certainly a mature discipline, but the field continues to evolve as new substrates are developed and made available for application and as new coatings and application methods are devised to meet emerging demands and constraints. Over the past 30 years, the desire to lower the toxic hazard and pollution has strongly influenced coating technology. This has resulted in the emergence of new coating systems and methods of application. This chapter focuses on issues related to protective coatings and paints used for structural metals and alloys used in high volume applications.

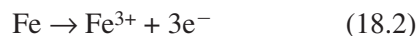
18.2 CORROSION PROTECTION BY COATINGS AND PAINTS

18.2.1 Corrosion Fundamentals

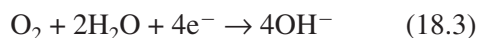
Paints provide corrosion protection of underlying metallic substrates by stopping one or more of the electrochemical or transport processes involved in substrate corrosion. To illustrate these elements, the corrosion of iron in oxygenated water is considered. The overall corrosion process is given by:



This reaction produces rust on steel during atmospheric exposure. The overall reaction consists of two partial reactions. An anodic, or oxidation, reaction results directly metal wastage:



A supporting cathodic, or reduction, reaction occurs to consume the electrons produced by the oxidation reaction:



Both reactions must proceed for corrosion to occur and all the electrons produced by oxidation must be consumed by reduction. These partial reactions may proceed at different physical locations on the metal surface. Electronic current must flow through the metal, and ionic current must flow through the environment between these regions for corrosion to proceed. Protective coatings and paints stop or slow one or both partial reactions, or ionic current flow between anodic and cathodic regions (Figure 18.1).

18.2.2 Barrier Protection

Perhaps the most evident form of corrosion protection is barrier protection. Some coatings and paints are impermeable by water. If moisture cannot contact the substrate, aqueous corrosion cannot occur. Electrochemical measurements, primarily those based on electrochemical impedance spectroscopy (EIS), show that many protective paints behave essentially as high resistivity dielectric layers that prevent current flow. Electrochemical activity associated with corrosion is absent [1]. Many polymers

and paints retain this dielectric behavior, even after exposure to bulk electrolytes for long periods of time. Their resistance to ionic current flow isolates anodic and cathodic sites from one another thereby slowing or stopping corrosion. Their inability to support electronic conduction prevents cathodic reactions from being supported on the coating.

Barrier protection is not always present in defect-free organic coatings. This point has been neatly illustrated by comparing the rates of oxygen and water consumption for unprotected steel with the rates at which these species can be transported through various resins and paints [2, 3]. In the cases examined, oxygen and water were transported through coatings faster than they would be consumed by corrosion process occurring on unprotected surfaces. Permeability, diffusion and solubility coefficients for selected polymers found in organic resins in paint support this general conclusion (Table 18.1) [4]. For example, diffusion coefficients for oxygen in many polymers are within an order of magnitude of the diffusion coefficient of oxygen dissolved in water (about $1 \times 10^{-5} \text{cm}^2/\text{s}$). Oxygen solubilities range from about 0.1 to over 1.0

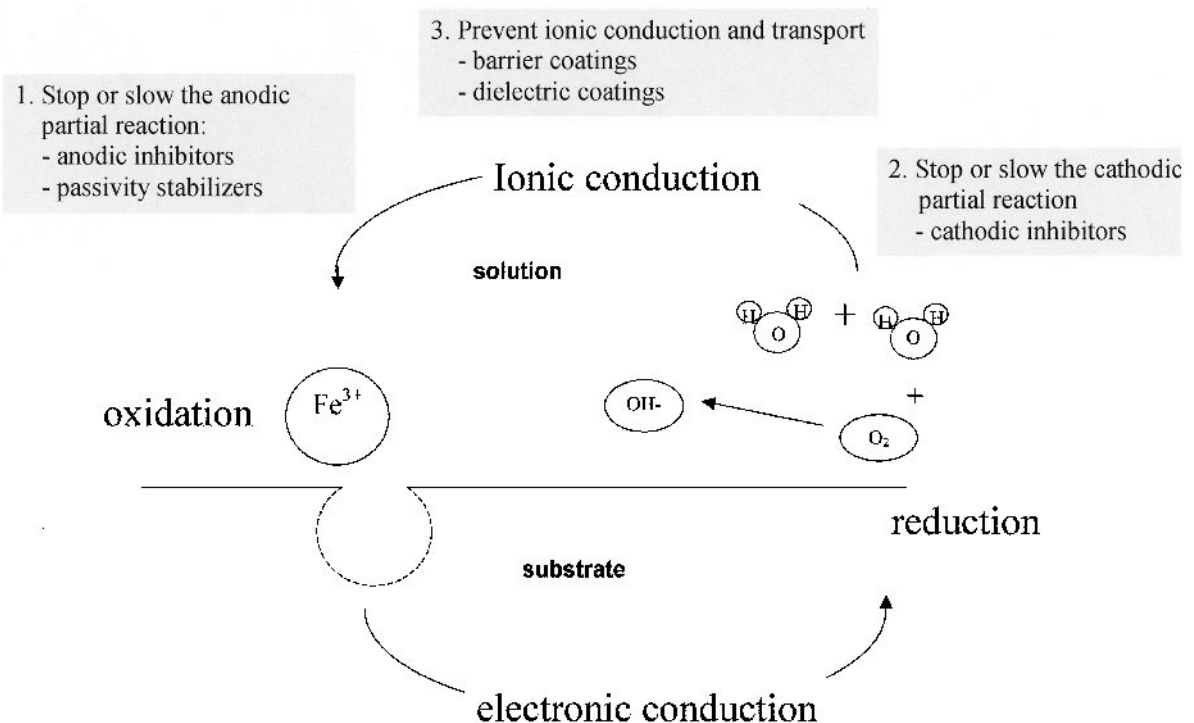


FIGURE 18.1 Three general strategies for slowing or stopping corrosion of metals used in protective paints and coatings.

TABLE 18.1 Permeability, Diffusion and Solubility Coefficients for Selected Polymers [4]

| Polymer | Permeability Coefficient $\frac{\text{cm}^3 (\text{STP}) \times \text{cm}}{\text{cm}^2 \times \text{s} \times \text{Pa}}$ | Diffusion Coefficient $10^6 \text{ cm}^2/\text{s}$ | Solubility Coefficient $\frac{10^6 \text{ cm}^2 (\text{STP})}{\text{cm}^3 \times \text{Pa}}$ | Temperature $^{\circ}\text{C}$ |
|---|--|---|---|-----------------------------------|
| Oxygen | | | | |
| Polystyrene | | 1.9 | | 25 |
| Polyvinylidene chloride | 0.00383 | | | 30 |
| Polyvinyl alcohol | 0.00665 | | | 25 |
| Polyethylene (high density, 0.964 g/cm ³) | 0.03 | 0.17 | 0.18 | 25 |
| Polyvinyl acetate | 0.136 | 0.0178 | 0.766 | 10 |
| Nitrocellulose | 1.46 | 0.15 | 0.975 | 25 |
| Polystyrene | 1.9 | | | 25 |
| Polyethylene (low density, 0.914 g/cm ³) | 2.2 | 0.46 | 0.472 | 25 |
| Polybutadiene | 14.3 | 1.5 | 0.957 | 25 |
| Natural Rubber | 17.6 | 1.73 | 1.02 | 25 |
| Chlorinated Rubber | 40.5 | | | 30 |
| Vulcanized Silicon Rubber | 367 | 12.0 | 3.06 | 0 |
| Water | | | | |
| Polyethylene (high density, 0.964 g/cm ³) | 9.0 | | | 25 |
| Polyvinylidene chloride | 7.0 | | | 25 |
| Polyethylene (low density, 0.914 g/cm ³) | 68 | | | 25 |
| Chlorinated Rubber | | 4,100 | | 25 |
| Polystyrene | 1,350 | | | 25 |
| Nitrocellulose | 4,720 | 0.0260 | 18,000 | 25 |

ppmw for the polymers listed in Table 18.1. This compares with a nominal saturation concentration of dissolved oxygen in seawater of about 8 ppm [5].

Defects can also compromise barrier protection. Holidays (pin holes that expose the substrate), density variation in the polymer, and interfaces associated with pigment particles are examples of defects that are regularly present in paints. All of these defects contribute to increased interaction between the substrate and the environment locally, leading to localized attack that can spread under the coating.

18.2.3 Anodic Protection and Active Corrosion Protection

Corrosion resistant paints and primers contain additions of sparingly- to slightly-soluble pigments that stabilize passivity of the underlying substrate, or that leach out to provide corrosion protection at macroscopic defects in the coating. Lead pigments in organic coatings such as red lead, Pb₃O₄, lead sulfate, PbSO₄, lead oxide, PbO, and lead suboxide, Pb₂O are passivity stabilizers for steel substrates. They are sparingly soluble and promote the development of

alkalinity in electrolytes taken up in a coating. The passive film on steel is stabilized under alkaline conditions. Additionally, dissolved lead reacts with free organic acids to form lead soaps with inhibitive properties. Dissolved lead is also mildly oxidizing with respect to steel. This also helps stabilize passivity of iron. It had been suggested that stabilization may even involve plating out of lead on the steel surface, forming local cathodic sites that ennoble the steel surface sufficiently to stabilize passivity. Active corrosion protection, or self-healing, refers to the ability of a coating to protect a scratch or defect in a coating by release of a soluble inhibitor. This property is most commonly associated with chromate-bearing coatings and makes them especially attractive corrosion resistant coatings. Chromate pigments such as calcium chromate, strontium chromate, zinc chromate, barium chromate, and lead chromate are potent inhibiting pigments that provide active corrosion protection. Dissolved hexavalent chromate is a strong oxidizer that inhibits anodic and cathodic reactions when it is reduced to its insoluble trivalent oxidation state on the metal surface. The family of chromate inhibitors exhibit a range of solubilities

TABLE 18.2 Saturation Concentrations for Chromate Compounds Used as Inhibiting Pigments [6]

| Inhibitor | $C_{\text{saturation}}$ (mmol/l) |
|----------------------------------|----------------------------------|
| BaCrO ₄ | 0.2 |
| SrCrO ₄ | 5 |
| CaCrO ₄ | 141 |
| Na ₂ CrO ₄ | 5.4×10^4 |

(Table 18.2). This allows coatings manufacturers to tailor chromate release for various applications. Too little chromate release leads to lack of corrosion protection. Too much release can trigger osmotic blistering [6].

18.2.4 Cathodic Protection

Cathodic protection involves polarization of a metal in the active direction (towards more reducing potentials). This has the effect of slowing or stopping metal oxidation. A familiar example of cathodic protection is found in galvanized steel. The galvanized layer is composed of Zn or a Zn-Al alloy. If the galvanized layer is breached, exposing the underlying steel substrate, the substrate is polarized by the layer and is protected against corrosion. The tradeoff is that the corrosion rate of the galvanized layer is increased. This tradeoff is acceptable because the presence of the layer is not essential for functional utility of the component. This form of cathodic protection is usually referred to as *sacrificial cathodic protection* because the galvanized layer corrodes to protect to underlying substrate. Sacrificial cathodic protection can be achieved in paints by using active metal pigment additions, such as zinc dust, to inorganic or organic coatings.

18.2.5 Zinc-rich Paints (ZRP) [7–10]

ZRPs deserve special attention here due to their unique mode of corrosion protection, which is essentially sacrificial cathodic protection. ZRPs consist of zinc or zinc oxide pigments mixed with inorganic or organic binder vehicles. These coatings are normally used for the protection of steel against atmospheric exposure and are applied in thicknesses ranging from 2–7 mils (50–175 μm). Organic topcoat protection is normally applied when these coatings are used in marine service. These paints contain high fractions of pigment, usually exceeding 92–95% of the dry film weight. This loading level is needed to effectively suppress rusting for useful periods of time. Pigments consist of a dispersion of spherical metallic 2–8 μm in

diameter [11], or a 4-to-1 mixture of metallic zinc particles and zinc oxide (ZnO) [9]. A dispersion in the pigment particle size ensures efficient pigment packing and electrical continuity throughout the coating. Too small an average pigment size can lead to excessive Zn dissolution and osmotic blistering. Too large an average size leads to inhomogeneous dispersion of pigment and formation of unprotected regions. ZnO itself is not an inhibitor, but can buffer acidic conditions in the coating and can release Zn cations which contribute to corrosion inhibition [9]. The zinc particles in the paint are in electrical contact with each other and with the underlying substrate, leading to sacrificial cathodic protection of steel. These paints are applied to steel surfaces by brushing or spraying, and are used in situations where galvanized coatings are impractical.

Inorganic ZRPs consist of zinc dust mixed with ethyl or alkyl silicates binder vehicles. After curing, these coatings are fully inorganic. Two-part ZRPs, consisting of the zinc pigment and the binder, are self-curing. Three-part ZRPs use an additional curing agent that is applied on top of the coating. These coatings are water-sensitive during curing, but less so thereafter. Inorganic ZRPs are conductive abrasion resistant and resistant to a range of atmospheric exposures, elevated temperatures, ultraviolet radiation, and natural and made-made chemicals and fluids [8]. Inorganic ZRPs are not suitable for constant immersion in aqueous electrolytes, and they are not resistant to strong acids (pH, 6.0) or alkalis (pH > 10.5) [8]. These coatings are not flexible and can easily crack and spall. Adhesion is critically dependent on scrupulous surface preparation. Normally, steel surfaces must be blasted clean immediately prior to coating application.

Organic ZRPs consist of zinc dust mixed with one of several organic binder vehicles. Suitable organic vehicles include chlorinated rubber, polystyrene, polyurethane, polyvinyl chloride, and epoxy, among others. These coatings provide corrosion protection in much the same way as inorganic ZRPs. However, due to the nature of the organic binders used, the coatings are much more flexible and surface preparation prior to application is less critical. These coatings are susceptible to blistering and have lower resistance to heat and ultraviolet radiation.

In recent years, waterborne paints have been introduced to reduce emission of volatile organic solvents during paint application. Metallic zinc pigments will dissolve with the production of hydrogen gas in such paints. Such reactions lead to dangerous pressure buildup in paint storage cans and degrade the pigment itself. Zinc pigments can be stabilized,

however, using a range of organic and inorganic inhibiting additives [12–14].

Other metallic pigments have been explored for use in cathodically protective paints. Manganese, which is an active metal whose ions also possess corrosion inhibiting properties, has been explored as a pigment in organic binders [15]. More recently, the use of aluminum-lithium alloy pigments has been demonstrated in both organic coatings and organic adhesives. Aluminum, stainless steel, nickel and bronze pigment additions are made to paints for decorative purposes. These pigments are not considered to confer corrosion inhibition [16].

18.2.6 Role of Adhesion

There is a great deal of practical experience to show that adhesion of a coating to the substrate is essential for the coating to provide corrosion protection. However, there is ongoing debate on the precise role of adhesion in coating failure and substrate corrosion. One school of thought, well supported by practice and experiment, is that adhesion plays the dominant role in determining the protectiveness of a coating [17]. Generally stated, the competing point of view is that coating breakdown allows interaction of the environment with the substrate, and coating separation follows substrate corrosion [18]. In any case, good adhesion is necessary to resist blistering, cathodic delamination, and filiform corrosion.

Factors that promote coating adhesion include surface cleanliness, surface roughness or etching, and the presence of oxide films that are artificially thickened or chemically modified by passivation, pickling, etching priming, and phosphating in the case of steels, and conversion coating or anodization in the case of aluminum and magnesium alloys. Chemical and mechanical adhesion are two components of that contribute to overall adhesion of a coating. Chemical adhesion, which is usually evident in the wettability of a surface by a paint, arises from chemical bonding between the coating and the substrate. Covalent chemical bonds lead to the greatest degree of coating adhesion. Metallic and ionic bonding are not important bonding types for organic coatings on metals. Other forms of bonding usually lead to weakly adherent coatings in the absence of mechanical bonding. Formation of covalent bonds between molecules in organic coatings and sites in oxide films is more readily achieved than direct bonding to metals. This is one reason why surface preparation involving film formation is often employed. Mechanical bonding relies on surface roughness and intimate contact of metal and coating

to generate a mechanical interlock that holds the coating to the metal. This leads to etching pretreatments that induce a fine amount of surface roughening to promote coating adhesion.

Once applied, mechanical properties of the coating become important to adhesion. Abrasion and impact resistance are important to resist local perforation or general thinning that might expose the substrate to the environment. Sufficient elasticity is necessary for the coating to expand and contract without leading to mechanical separation of the coating-metal interface due to thermal cycles.

18.3 ENGINEERING ALLOYS AND THEIR NEED FOR CORROSION RESISTANT COATINGS

18.3.1 Steel

Carbon and low alloy steels are not resistant to corrosion in natural environments [19]. All that is required for unprotected carbon steels to rust is moisture and oxygen. Some steels will rust quite rapidly in humid air even though condensation is not evident. As a result, corrosion resistant paints and coatings are necessary in almost all applications. A wide range of paints and coatings are available for steels, and the selection is based mainly on the expected service conditions. Generally, steels are cleaned to bare metal by abrasion, blasting, or chemical methods. They may be chemically passivated prior to painting. Chemical passivation helps to stabilize or reinforce the passive film on steel and clean the surface to make it receptive to the organic finish [20]. Any surface layers formed by passivation range from exceedingly thin (usually less than $0.1\mu\text{m}$, as occurs in pickling processes) to several micrometers in thickness when passivation by phosphate coating formation is carried out.

Alloy steels such as austenitic, ferritic, and martensitic grades are designed for increased corrosion resistance and are not normally painted for corrosion protection.

18.3.2 Aluminum

The corrosion resistance of aluminum to natural environments is excellent, due to the existence of a thin, but highly protective passive film that forms spontaneously when oxygen is present. However, to develop useful mechanical properties, Al is often alloyed with Cu, Zn, Mg, Si, Mn, and other transition metals in amounts up to 15% by weight [11]. These alloying additions almost always lower the corro-

sion resistance of the alloy, necessitating protective coatings for service in even mildly aggressive environments. Aluminum alloy surfaces are prepared for painting by chemically degreasing, deoxidizing, and conversion coating (or pretreating) the surface [21]. Degreasing involves the use of an alkaline solution that removes bulk and molecular organic contamination. Deoxidation is carried out using oxidizing acid solutions. Conversion coating is performed by contacting the surface with a solution that promotes the formation of a thickened oxide layer, which facilitates the adhesion of subsequently applied paint. This layer may have some intrinsic corrosion resistance. Chromate solutions have been used for many years to form chromate conversion coatings on Al alloys. These layers consist mainly of mixed chromium oxides and are 0.1–1.5 μm in thickness. Painting is normally carried out within 24 hours of conversion coating.

In some cases, Al alloys are anodized prior to painting. *Anodization* refers to electrolytic film formation. In this process, films are grown electrochemically by application of a current or voltage to the alloy's surface during immersion in an acidic bath that usually contains ingredients that promote formation of tightly adherent oxide films. Anodized coatings are on the order of 10–30 μm in thickness.

18.3.3 Magnesium

Magnesium and its alloys are very reactive in natural environments and corrosion resistant coatings are needed for long-term application of these materials. Magnesium alloys are prepared for painting in much the same manner as aluminum alloys. However, it is much more common for Mg alloys to be anodized prior to painting.

18.3.4 Galvanized Steel

Galvanized steels are quite corrosion resistant in natural atmospheric exposure, but they are often painted to suppress the formation of white rust and to slow consumption of the sacrificial galvanized layer itself.

18.4 CHARACTERISTICS AND USES OF CORROSION RESISTANT PAINT AND COATINGS [22–25]

18.4.1 Components of Corrosion Resistant Paint

The main ingredients in paints are an organic resin and pigment and particulate additives. All paints and coatings confer some degree of corrosion protection.

Paints designed especially for corrosion protection are no different other types of organic finishes, except that the resin is selected especially for its environmental resistance, and the pigment is selected for its corrosion inhibiting properties. For corrosion resistant coatings and paints, important resin systems include those based on epoxies, urethanes, alkyds, phenolics, vinyls, and acrylics. Some resins are formulated into liquids by dissolving in a suitable solvent, or by dispersing small resin particles in an emulsion. The resin forms a continuous coating and the liquid solvent or carrier evaporates. Other resins are liquids in which curing is induced by cross-linking polymer molecules. Cross-linking is induced by mixing the resin with a cross-linking agent, which is normally another low molecular weight polymer that becomes incorporated into the structure. Coatings of this type are “two part” coatings that require mixing prior to application in order to initiate the curing process

18.4.2 Corrosion Inhibiting Pigments

Corrosion inhibiting pigments are metal or metal oxide powders. Electrochemically active metals, mainly Zn, are added to organic resins to confer sacrificial cathodic protection for more noble substrates like steel. Zn-rich primers, discussed earlier, are the main example in this regard. The pigment volume concentration of the metallic pigment must be such that the particles are in physical and electrical contact with each other and with the substrate. Metal oxides used as pigments are usually sparingly soluble compounds [6]. When an electrolyte permeates the coating, the pigment dissolves, releasing anions and cations that slow the anodic or cathodic partial reactions. Some inhibitors also mediate solution pH. In the case of steel substrates, pigments that elevate the pH to 8 or greater are desirable because steel passivity is promoted under alkaline conditions. Careful attention must be paid to solubility. Too low a solubility leads to incomplete corrosion protection. Too high a solubility leads to osmotic blistering.

Chromate, phosphate, and silicate pigments are important classes of corrosion inhibiting pigments. Chromate pigments are slowly being phased out of paint formulations due to concerns over their toxic hazard.

18.4.3 Alkyd, Modified Alkyd, and Polyester Resins

Even though they are not the most protective of resins, oil-based alkyd coatings are perhaps the most widely used class of resins for protective paints



FIGURE 18.2 Alkyd coating (2–3 coats) on steel exposed to a marine environment. Increased corrosion damage near the water line illustrates the unsuitability of alkyd coatings for immersion service. [Source: E. D. D. During, *Corrosion Atlas*, 3rd Ed. New York: Elsevier, p. 293, 1997]

(Figure 18.2). They are commonly applied to steels for service in mildly aggressive environments. Alkyd and polyester resins are formed by the reaction of alcohol with acid. Alkyd resins consist of aromatic dibasic acid groups linked by polyols with fatty acid side groups, which are distributed along the polyol-aromatic acid chain. Unsaturated fatty acid side groups, typically derived from organic oil additions, are subject to oxidation in the presence of oxygen. This process, referred to as *auto-oxidation*, promotes cross-linking and curing of the resin. The type of oil used, the proportion of oil to resin (referred to as oil length), and the extent of the derived side group saturation strongly influences resin properties such as drying time, moisture sensitivity, hardness, and color. Long oil additions (> 65% by

weight) are used in primer coatings for painting pitted and rusted surfaces. Short oil additions (< 50%) are used to promote gloss, hardness, and to shorten drying time. Alkyd resin properties can be modified by additions of other resins. Silicone additions promote durability, gloss, and hardness. Phenolic resin additions reduce water uptake and promote resistance to alkaline environments. Vinyl additions render alkyd resins amenable to subsequent painting, making them excellent primers for a range of different topcoats.

Polyesters are alkyd-derived resins mixed with a reactive monomer such as styrene, diallyl phthalate, or vinyl toluene. Polyesters have relatively few unsaturated fatty acid side groups along the polyol-aromatic acid chain backbone, and do not cross-link and cure by auto-oxidation. Rather, they form by a copolymerization reaction catalyzed by oxidizers such as peroxide. Polyester coatings provide excellent chemical resistance, but derive adhesion from mechanical interlocking. As a result, they do not adhere well to smooth metal surfaces.

18.4.4 Epoxy Resins

As a class of coating resins, epoxies are widely used and extremely versatile, with high environmental resistance and good mechanical properties. Epoxy resins are long-chain compounds with epoxy groups located at chain ends. Using supplemental chemical curing agent additions, resins can be cross-linked through epoxy groups or inter-chain hydroxyl groups. Though epoxy resins can be used alone, many different cross-linking agents are known, leading to an ability to tailor formulations advantageously to achieve different combinations of properties. For corrosion resistant coatings, polyamine, polyamide, and phenol-formaldehyde curing agents additions are widely used. These are two-part coatings, in which the coating components are mixed prior to application. Once mixed, the pot life of the resin ranges from hours to a few days, depending on the coating type. Epoxy resins can also be esterified with fatty oils to produce epoxy esters. Such resins lead to coatings with properties that are somewhat better than alkyds.

Among the two-art epoxy resins, those cross-linked with polyamines are noteworthy. Polyamines are potent curing agents for epoxy-based resins. They are low molecular weight compounds that induce tight cross-linking and lead to excellent chemical resistance. Polyamine curing agents are added at rates ranging from 5–20% by weight. Diethylene triamine is perhaps the fastest curing agent among the

polyamines. Curing agents are effective at room temperature and ambient conditions. Coatings can be applied by spraying, brushing, and rolling.

Polyamides are also effective curing agents for epoxy resins. Polyamide resins are blended with epoxy at higher rates than polyamines (20–50%), leading to blended copolymer coatings with properties that depend on composition. Epoxy-polyamide coatings possess excellent flexibility and chemical resistance. They are somewhat less resistant to alkali and solvents than amine-cured epoxies.

Additions of coal tar pitch to epoxy resins results in a black coating with increased thermal and ultraviolet radiation resistance. Coal tar and epoxy are added in about equal quantities by weight. Curing agents are still present in the formulation. These coatings retain good environmental resistance and have a low moisture permeability due to the presence of coal tar. These gains in performance are made at the expense of coating brittleness, decrease in the ease of application, and lower adhesion of subsequently applied topcoats.

Yet another chemically resistant epoxy-based resin is the epoxy-polyester system. Epoxy-polyester resins are highly cross-linked when cured, leading to excellent chemical resistance. While the cohesive strength of polyester is high, polyester coatings do not adhere well to smooth metal surfaces. Blending with epoxy enables coatings with increased chemical resistance with adhesion and flexibility to be made. Epoxy-polyester coatings are used in applications where repetitive cleaning of the coating is needed, such as in food preparation areas, dairies, and pharmaceutical manufacturing and handling.

Like epoxy-polyesters, epoxy-phenolic coatings exhibit an attractive mix of high chemical resistance, mechanical flexibility, toughness, and adhesion. The one drawback of epoxy-phenolic coatings is the need for curing at elevated temperatures. Effective cross-linking occurs at temperatures ranging from 1,500–2,000 °C. Epoxies with high hydroxyl functionality facilitate cross-linking, resulting in an attractive mix of properties. In particular, epoxy-phenolic blends combine the acid resistance of phenolics with the alkali resistance of epoxies. For this reason, these coatings are often used as lining coatings for storage applications like rail tank cars and storage drums.

18.4.5 Vinyls

Useful levels of chemical resistance can be obtained from vinyl resins. Vinyl compounds most commonly used in coating applications are vinyl chloride, vinyl,

acetate, vinyl ether, vinyl butyral, or copolymer mixtures of these. These compounds are used in solutions, emulsions or dispersions, and coatings form by solvent evaporation-induced cross-linking at ambient or elevated temperatures. Vinyl dispersed in liquid plasticizers are referred to as *plastisols*. Vinyl dispersed in solvents are referred to as *organisols*. Plastisols are used in the application of coatings with high impact resistance, mechanical strength and flexibility are needed. Organisols are more easily pigmented and are easier to apply. Once cured, these coatings are resistant to aqueous solutions and many solvents. They are not resistant to the solvent in which the polymer was originally dispersed or dissolved. Vinyl butyral dosed with soluble chromate inhibitor is used as a wash primer, or *metal conditioner*. These coatings are very thin, on the order of several micrometers, but provide corrosion protection and make metal surfaces receptive to subsequently applied organic coatings. Overall, vinyl chloride coatings demonstrate the best chemical resistance. However, vinyl blends are frequently used because of the greater solubility of the other vinyl compounds and the desire to tailor properties such as chemical resistance to a specific environment.

18.4.6 Chlorinated Rubbers

Chlorinated rubber coatings form by solvent evaporation. Resins are fabricated by chlorination of natural rubber compounds. Resins are plasticized by additions of acrylic resins and can be stabilized by epoxy additions. Plasticizer additions affect water permeability and coating stiffness. Stabilizers mainly suppress unwanted gellation of the resin prior to application. Chlorinated rubber coatings are remarkably flexible and extendable, which contributes to overall durability. They are adherent to steel and concrete surfaces and have low water permeability. Chlorinated rubbers are resistant to many acids, alkalis and oxidizers. Notable exceptions include concentrated nitric acid, acetic acid, ammonium hydroxide, and sulfur dioxide solutions. Resistance to most organic solvents is poor. Chlorinated rubbers are degraded by ultraviolet radiation and heat. Stabilizing additions must be made to combat these forces. These coatings find application in marine service and as highway markings. However, these coatings are volatile organic solvent intensive and their use is subject to increasing restriction. As a result, the use of these coatings is diminishing, with acrylic coatings poised as performance-equivalent products with less of a pollution hazard.

18.4.7 Polyurethanes

Polyurethanes are a broad class of resins with wide-ranging properties. These resins are formed by reaction of a polyisocyanate with free hydroxyl groups in polyols such as acrylics, epoxies, polyesters, polyethers, and vinyls. As such, these coatings are two-part systems in which the isocyanate is mixed with the polyol just before application. Generally, polyurethanes combine good chemical and weathering resistance with high gloss and pigment color retention. They are not recommended for immersion service or exposure to strong acids or alkalis. Their resistance to chemical vapors and outdoor exposures of all types is good to excellent. For these reasons, polyurethanes are attractive candidates for applications where appearance and corrosion protection are required. Polyurethanes are often the coating of choice for topcoat applications. The precise mix of coating properties is strongly influenced by the nature of the polyol resin, although the nature of the isocyanate used is not unimportant. Pigments and other particulate additives impart color and mediate uncured resin viscosity, sag of the wet coating, and mechanical properties of the cured coating.

Both aromatic and aliphatic isocyanates are used in polyurethane resin formulation. Both types of resins demonstrate useful levels of chemical resistance and corrosion protection. Aromatic isocyanates result in higher rates of cross-linking and curing, but these resins are susceptible to yellowing and chalking due to sunlight exposure. Aliphatic isocyanates lead to lower rates of cross-linking and curing, and produce resins that exhibit better gloss, greater color retention, and better resistance to yellowing and chalking.

Polyurethanes for corrosion protection are based on acrylic, polyester, vinyl polyether, and alkyd polyols. Asphalts and coal tars are non-reactive constituents that add moisture and chemical resistance. Acrylic urethanes offer a good mix of aesthetics due to gloss retention and corrosion protection, particularly when aliphatic isocyanates are used. They are widely used for protection against outdoor weathering. Polyester urethanes are highly cross-linked resins when cured, though they are not suitable for immersion service. They also demonstrate a sensitivity to acids and alkalis. Polyether urethanes are noted for their elastomeric properties, but have a notable sensitivity to UV exposure. Vinyl urethanes exhibit abrasion resistance, toughness, and good chemical resistance. They are not as resistant to sol-

vents as acrylic and polyester urethanes. Epoxy urethanes tend to chalk and are not as chemically resistant as epoxy, amine-epoxy or polyamide epoxy resins. As a result, there is comparatively little impetus for their use in demanding applications.

The so-called "moisture cured" urethanes consist mainly of aromatic isocyanates. Polymerization of these urethanes is induced by water vapor present in humid air. These resins cure rapidly and at low temperatures to produce protective and durable coatings.

18.4.8 Acrylics

Acrylic coatings are yet another diverse class of organic coatings. Acrylic resins can be solvent deposited thermoplastics, cross-linked thermosets, or waterborne emulsions. Polyethyl acrylate and polymethyl methacrylate polymers and copolymer blends comprise this class of resins. As a class of resins, acrylics are fast-setting, easily pigmented coatings that exhibit high gloss, good color retention and UV resistance. They are resistant to weathering, but are not necessarily resistant to acids and alkalis. They are soluble in solvents such as ketones, aromatic hydrocarbons, aliphatic chlorinated hydrocarbons. Given these characteristics, acrylics are used mainly in coatings for protection against outdoor exposure.

Thermoplastic acrylics soften at low temperatures and allow for reflow and refinishing of defective, abraded or scuffed areas. Heat curing may be employed in coating applications, but this is done mainly to accelerate solvent evaporation. Thermoset coatings use a reactive polymer constituent to induce cross-linking. Epoxies, ureas, melamine-formaldehyde, and vinyl are used in this regard. It is usually the case that these cross-linking constituents are the majority component in the resin. The acrylic addition is used mainly to enhance gloss, color retention and UV stability.

18.4.9 Phenolic Resins

Phenolic resins are produced by thermally induced cross-linking of phenolformaldehyde. Thermal treatment, or heat curing, also drives off water, which is a byproduct of the cross-linking reaction. Phenol formaldehyde resins, which are produced by the reaction of phenol with formaldehyde, are normally dissolved in alcohol. The resin solution and additives can be applied to blasted or etched ferrous or non-ferrous substrates by spraying, brushing, or

slurry. Ten to twenty minutes are necessary for solvent evaporation and 20–30 minutes should be allotted for heat curing. Heat curing is carried out at temperatures ranging from 120–2,050 °C. Maximum coating thickness should not exceed 2–25 μm (0.75–1.0 mils). Thicker coatings must be built up using multiple applications. The resulting coatings are inert and non-toxic. They are suitable for linings in food processing and pharmaceutical equipment. Phenolic resins are not resistant to concentrated nitric acid, strong oxidizers including chlorine, or alkalis.

18.5 APPLICATION METHODS AND SURFACE PREPARATION

18.5.1 Coating Failure

Coating damage and substrate corrosion may manifest themselves in a range of different modes, but coating failure generally involves a serial sequence of events [26]:

1. Defect formation
2. Uptake of water ions and oxygen from the environment
3. Loss of adhesion, condensation of bulk electrolyte at the coating metal interface
4. Initiation and propagation of substrate corrosion

18.5.2 Defects

Defects may exist in the coating as a result of imperfections arising at the time of coating application (Figure 18.3). These defects may include entrained dust, dirt, moisture, oil or grease, lack of surface coverage, or lack of adhesion or the substrate. Mechanical defects may occur due to abrasion or impact. Chemical defects may arise by exposure to acids, or solvents. Defects may also arise due to elevated temperature exposure or exposure to light (UV damage). The defect structure in an organic coating system is important because it determines the course of subsequent corrosion damage.

18.5.3 Water Uptake [27, 28]

The second stage in the degradation process is water uptake and transport. Water uptake is aided by a molecular level defect specific to organic coatings commonly known as “pore space.” Pore space generally refers to open space between polymer chains or mol-

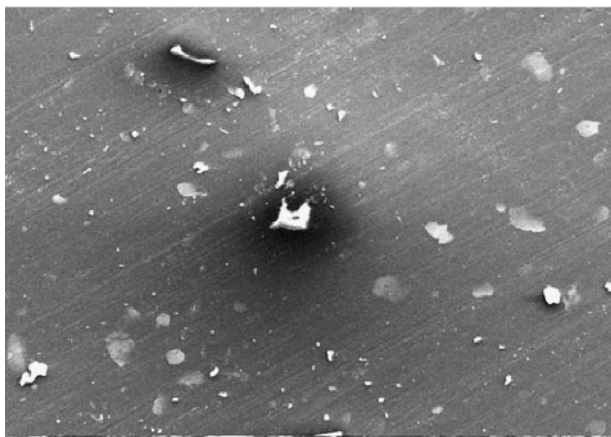


FIGURE 18.3 Scanning electron micrograph of metal flake paint for trucks showing entrained dirt, and intentionally added metal flakes.

ecules in the polymer film. In many coatings, this pore space allows uptake and transport of water and ions that leads to coating degradation and corrosion. Pore space is a natural consequence of polymer structure and is usually unavoidable, though some polymer coatings have very low water permeabilities (see Table 18.1). In aggressive environments, electrolytes may penetrate through defects, resulting in loss of adhesion.

18.5.4 Loss of Adhesion

Loss of adhesion may spread laterally from a defect site. Alternatively, loss of adhesion may occur under mechanically intact coatings when an electrolyte condenses at the metal–film interface to form a blister. Once an aggressive electrolyte has made contact with the metallic substrate, corrosion is likely.

18.5.5 Corrosion Initiation and Propagation

While corrosion is likely to initiate at defects and sites of decohesion, the propagation of corrosion is still strongly affected by the presence of the coating. The consequences of corrosion propagation range from one extreme to the other. Corrosion may be slowed significantly due to restricted mass transport of corrosion product, accumulation in defects, and strong coating-substrate adhesion. Conversely, it may be accelerated by formation and retention of aggressive local solution chemistries, softening of the

coating, and loss of coating-substrate adhesion. Common modes of corrosion damage accumulation are described below.

18.6 FACTORS AFFECTING COATING DEGRADATION

18.6.1 Light

Energetic photons at UV wavelengths (30–300 nm), a component of natural sunlight, can alter the structure and properties of polymer resins and protective coatings, in ways ranging from bond scission to photo-oxidation to molecular rearrangement [29]. Rearrangements at the molecular level lead to changes in properties important to protection such as permeability, mechanical properties, and polymer network shrinkage, which leads to cracking. UV exposure alone is sufficient to degrade many organic resins, causing them to lose protective abilities.

18.6.2 Temperature

Elevated temperature exposure can lead to unwanted softening and increased permeability, especially in thermoplastics. It may also lead to structural rearrangement of the polymer network that leads to cracking on cooling. Low temperatures can make coatings brittle and susceptible to impact damage. Temperature cycling can cause coating delamination due to differences in thermal expansion in the substrate and coating. Coatings with insufficient elasticity may crack upon thermal cycling.

18.6.3 Mechanical Action

Abrasion damage occurs due to dirt dust and particulates carried by moving air, rain, seawater, or other fluids. Over time, this can lead to local or general thinning of a protective coating.

18.6.4 Chemicals

Many resins can be attacked by solvents, and these incompatibilities are usually well known. However, certain liquids, which are not necessarily solvents, can permeate and swell certain resins and alter their mechanical properties, or dissolve solid additives. The most technologically important example of this phenomenon is the uptake of water by organic coatings, but other liquids are taken up by polymer resins as well. Chemical agents, both expected from service environments and unexpected from pollution,

and natural sources or accidents affect coating structure and chemistry in many diverse ways.

18.6.5 Weathering

When applied in the context of protective coatings, the term *weathering* is commonly used to account for the degradation of coatings due to the combined effect of the factors listed above during outdoor exposure. For the purposes of classification, weathering can be separated into physical and chemical subtypes. Physical weathering results in dimensional changes such as thinning without change to the coating chemistry or structure. Chemical weathering leads to changes in coating chemistry, structure, or both.

18.7 CORROSION UNDER COATINGS

18.7.1 Blistering

Corrosion under coatings takes on two general forms. The first is blistering. Blistering refers to local separation of the coating from the substrate (Figure 18.4). This local region swells as it fills with fluid or gas. The formation of fluid-filled blisters is attributed to osmotic pressure differences that drive water from the external environment into the blister

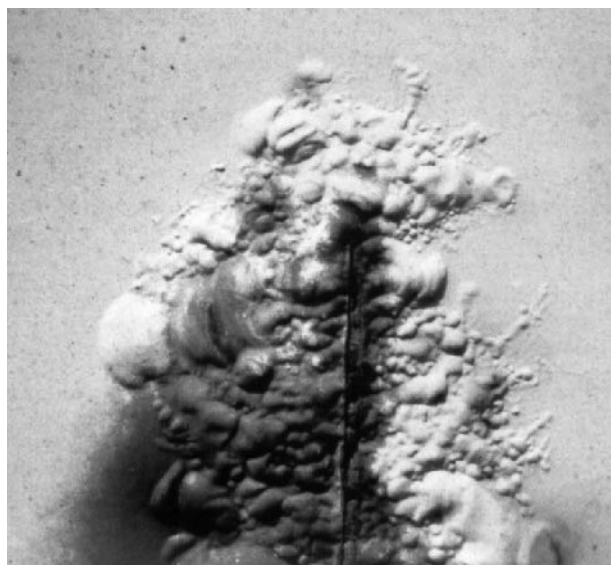


FIGURE 18.4 Well-developed undercoat blistering leading to corrosion of the substrate. [Source: E. D. D. During, *Corrosion Atlas*, 3rd Ed. New York: Elsevier, p. 297, 1997]

to reduce the gradient in the ionic strength across the coating [30]. In this case, the coating functions as a semi-permeable membrane that permits water transport, but restricts transport of large ions. Concentrated electrolytes can develop in blisters due to substrate corrosion, accumulation of soluble inhibitors and dissolution of surface contaminants. The latter two points illustrate the need for pigments with restricted solubility and proper surface cleaning prior to coating application. Gas-filled blisters develop when reduction reactions (such as hydrogen reduction) occur under the coating.

Blisters may evolve into anodic and cathodic forms [31]. In anodic blisters, the unprotected substrate corrodes with the formation of soluble and insoluble corrosion product. Cathodic blisters, the substrate appears to support cathodic reactions such as oxygen and hydrogen reduction. The underlying substrate may be unattacked or weakly attacked.

18.7.2 Filiform Corrosion

The second main mode of undercoating corrosion is *filiform corrosion*. Filiform corrosion occurs on metallic surfaces coated with organic films that are typically 0.1 mm (4 mils) thick. The pattern of attack is characterized by the appearance of fine filaments emanating in random directions from one or more initiation sites. Filaments may propagate in one direction over relatively long distances. The source of initiation is usually a defect or mechanical scratch in the coating. The filaments are fine tunnels composed of corrosion products underneath a bulged and cracked coating. Filiform tracks are visible at arm's length as small blemishes (Figure 18.5). Upon closer examination, they appear as fine striations shaped like tentacles or cobweb-like traces (Figure 18.6). Filiform corrosion is a variation of a differential aeration cell. A filiform track has an active head, which is deaerated and acidic, and a filamentous tail, which is aerated and alkaline. Separation of anode and cathode is essential for filiform corrosion to occur. As the filiform track proceeds, the coating and metal are disbonded and the coating is lifted. The precise mechanism by which disbondment and lifting happens has not been established, but some metal dissolution is involved. Filiform corrosion will occur in environments that contain species aggressive enough to cause corrosion attack of the substrate metal. The presence of oxygen is a requirement for filiform corrosion tracks to propagate. Oxygen is supplied to the cathodic regions behind the head of the track by diffusion through the corro-



FIGURE 18.5 Filiform corrosion on varnished steel subject to moist indoor atmospheres. [Source: E. D. D. During, *Corrosion Atlas*, 3rd Ed. New York: Elsevier, p. 285, 1997]

sion product in the tail, or by cracks in the coating uplifted by the passage of the head. Filiform corrosion does not directly affect the mechanical integrity of the structure. However, it is aesthetically unpleasing and causes progressive degradation of the protective organic coating, which may lead to the onset of more damaging forms of localized corrosion.

18.8 COATING DEGRADATION AND EVALUATION METHODS

18.8.1 Simulated Service Testing

Simulated service exposure testing replicates as closely as possible the expected service environment. Coated surfaces are prepared to closely replicate actual manufacturing, and such examples are expected to accumulate damage by the same mechanisms and at the same rate as components in actual service. Simulated service testing is not accelerated by increasing the aggressiveness of the exposure conditions. Rates of coating damage and substrate corrosion are usually slow, sometimes requiring years of exposure to develop meaningful results. Inspection is normally visual, though other more sophisticated forms of interrogation are not precluded, provided they are non-destructive and do not accelerate coating damage inadvertently. The type and mode of exposure conditions are highly specific and usually defined by vendor and customer. Broadly applicable standards for conducting such tests do not exist. Simulated service testing has the advantage of

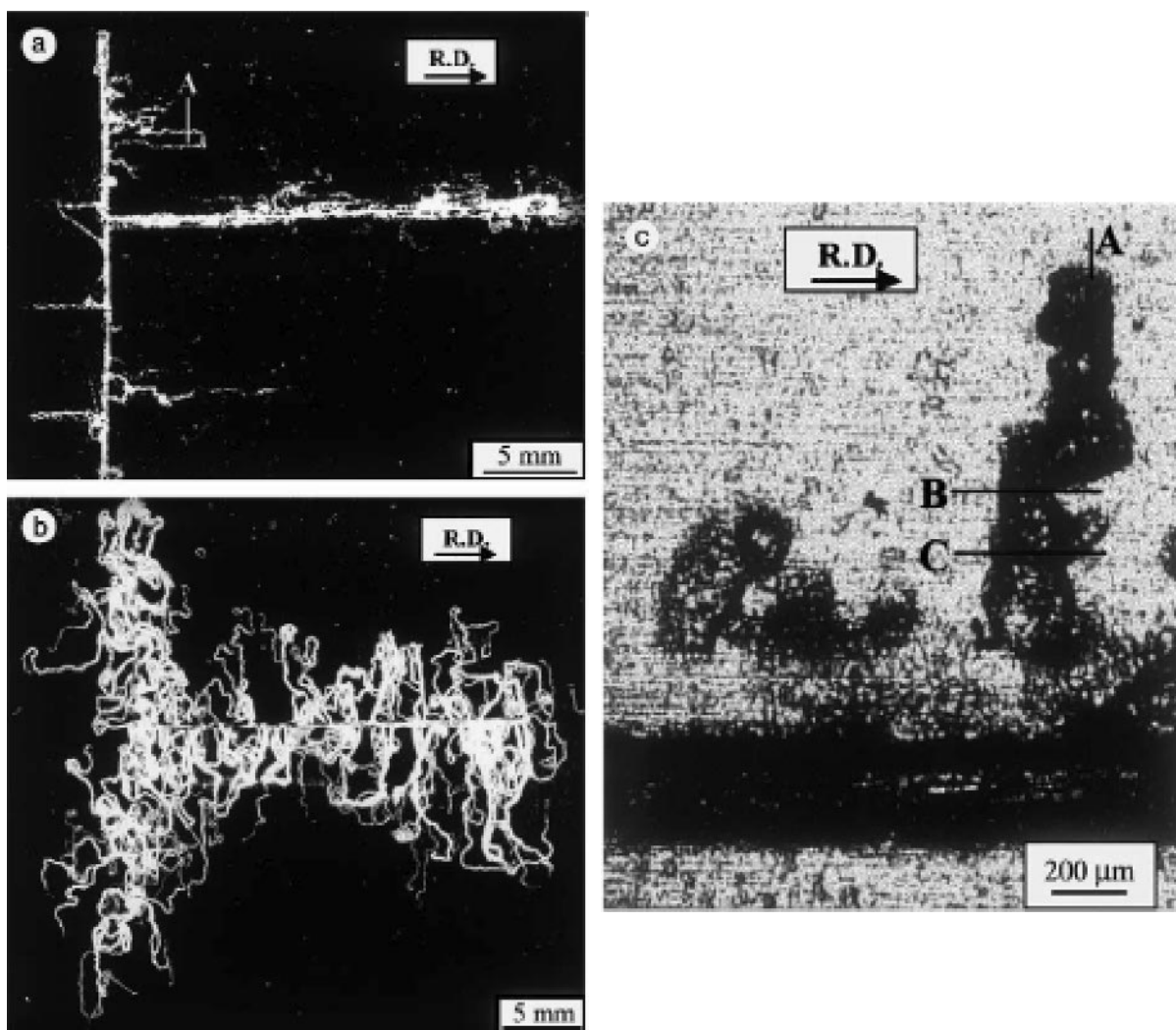


FIGURE 18.6 Filiform tracks on Al alloy 5005 (Al=0.89mg-0.17Fe) after constant humidity exposure (RH 65–75%) for 1,000 h at 400 °C. Substrates were clear coated with a 15–45- μm thick acrylic resin. [Source: X. Zhou, G. E. Thompson, G. M. Scamans, *Corrosion Science*, 45, 1,767, 2003]

bringing to bear all of the degradative forces on a coated metal surface in a manner that is realistic. The main disadvantage of this approach is that it is difficult to use such results to systematically explore and understand the influence of specific aggressive agents on damage processes.

18.8.2 Accelerated Exposure Testing [32–35]

Accelerated exposure testing of organic coatings is intended to determine coating protectiveness in a matter of weeks or months. It is normally intended

that the corrosion mechanisms operating in service are replicated in accelerated exposures. Widely used tests for organic coatings based on outdoor exposures include EMMAQUA, and Florida Exposure [35]. Cabinet tests include Neutral Salt Spray, QUV and Prohesion [36–38]. Table 18.3 lists several commonly used tests, and the exposure protocols.

Whether replication of mechanism is achieved is sometimes questioned. The question arises because to accelerate the accumulation of damage, the environment is often made more aggressive by increasing temperature, decreasing solution pH, increasing the concentration of attacking chemical agents, in-

TABLE 18.3 Accelerated Exposure Tests and Comments on Test Protocols

| Test Method | Comments |
|----------------------|--|
| Neutral Salt Spray | Exposure of samples to a 5% NaCl fog with a neutral pH at 950F. A very widely used test for assessing overall corrosion protection. Many different failure criteria exist, but the exposure protocol is specified in ASTM B117. |
| QUV | Artificial cabinet UV exposure. UV sources used include carbon arc lamps, xenon arc lamps and fluorescent tube lamps for creation of intense light in the 270–450-nm wavelength region. UV exposure is sometimes combined with humidity or cyclic exposures. See ASTM G53. |
| EMMAQUA | Equatorial Mounts with Mirrors for Acceleration plus a water spray cycle (“aqua”). Solar radiation reaching the samples is increased by about a factor of nine compared to natural exposures. Samples may heat, requiring active cooling |
| Florida Exposure | Natural outdoor exposure in southern Florida has become an accepted standard in several industries. High temperatures, intense sunlight, and high humidity represent accelerated exposure conditions compared to European environments. |
| Cathodic Disbondment | Tests coating disbondment under full immersion conditions. Cathodic polarization is often used to accelerated the rate of reduction reactions and develop local alkalinity that debonds and degrades organic coatings. Coating adhesion is then assessed by tape pulloff or a measurement of the delaminated area. See ASTM G80. |
| Prohesion | ASTM G 85-94 Annex A5 uses an aqueous solution containing 0.05% sodium chloride and 0.35% ammonium chloride. The test cycle consists of one-hour exposure to salt mist at ambient temperature followed by one-hour drying at 35°C. Results are thought to correlate better with performance in service than results from B117 salt spray. ASTM D 5894 uses a sequential prohesion/accelerated weathering test. Panels are exposed for one week according to ASTM G 85-94 Annex A5 followed by one week according to ASTM G 154, using UVA-340 lamps. |
| Immersion | Immersion of coated in deionized water leads to blistering in cases where soluble salts are present in on the substrate or in the coating. |
| Humidity | Testing is used to assess water uptake and corrosion protection at 100% relative humidity. Often used in conjunction with elevated temperature exposure or cyclic exposure. See ASTM G60. |
| Adhesion | Several types of tests exist, including adhesion during substrate bending and tape pulloff or scribed samples (e.g., ASTM D3359). |

creasing UV exposure, or deliberately inducing mechanical damage to the coating. Generally, the greater the degree of acceleration, the worse the correlation to natural damage accumulation. Nonetheless, rudimentary corrosion predictions have been formulated from empirical scaling rules derived from comparison of the performance of coatings in accelerated tests and performance in service. For example, exposure in Miami, Florida represents an acceleration of exposure in European climates by a factor of approximately four [35].

18.8.3 Proof Testing

Proof testing refers to rapid tests carried out on the production floor, or in a quality assurance laboratory to screen out defective coatings, to monitor the adequacy of coating operations, or to warrant acceptance of a production lot. The results of proof tests are also used as the response variable in process development projects, because the results are normally

available in a matter of minutes or hours, enabling rapid diagnosis of process variations. Coatings that perform well in certain types of proof tests may perform well in service. However, there are no general methods for using such data to predict service life. There are a wide range of proof tests for characterizing specific attributes of coating performance. These are described in a large number of standard procedures [39].

18.8.4 Electrochemical

Many electrochemical methods are of limited utility for studying the processes leading to organic coating degradation. In the early stages of coating breakdown, the interfacial impedance is exceedingly large and cannot be measured by a potentiostat. However, as the coating degradation process proceeds, the interfacial impedance falls to levels that can be effectively measured by electrochemical impedance spectroscopy (EIS) [1, 26, 40–44]. For this reason,

EIS has been particularly effective for quantitatively evaluating the progress of organic coating degradation and metallic corrosion that occurs as a result.

Direct current (DC) electrochemical methods are not well suited for characterizing breakdown of polymer coated metals for several reasons. First, coating breakdown is defect mediated, and results from measurement to measurement are usually quite irreproducible. Second, organic coatings are electrically resistive, and high potential drops develop across organic films when DC voltages are applied to the interface. This reduces the driving force for electrochemical reactions at the coating-metal interface. Often the extent of this potential drop is uncharacterized, which clouds interpretation of the resulting data. Third, as with all large signal DC measurements, application of a large polarization drives the electrode far from steady state, and far from the conditions under which corrosion naturally occurs. Additionally, application of high potentials may also lead to irreversible changes in the polymer structure, especially if dielectric breakdown is induced.

On the other hand, EIS is well-suited for the study of organic coating breakdown. It is sensitive to each of the four main stages of the coating breakdown process, and it can also be used in situ. Degradation of organic coatings occurs over the span of days and months (or longer), and is slow compared to the typical impedance spectrum collection times. As a result, EIS measurements can be used to measure changes in organic coating degradation in real time. Typically, the overall process of coating degradation and corrosion is analyzed using an equivalent circuit modeling approach [45]. Efforts have been aimed at understanding whether results from EIS testing can be used for making long-term predictions of coating life. Results suggest that this is possible [46].

18.9 KEY APPLICATIONS

18.9.1 Paints for Marine Service

Marine service includes exposure to oceans and the nearby atmospheric environment. The world's oceans contain about 3.5% NaCl by weight and lesser, but important amounts of the following ions: Mg^{2+} , Ca^{2+} , K^+ , SO_4^{2-} , HCO_3^- , Br^- . Marine organisms affect, and in some cases dominate, the corrosion behavior of metals. Coatings that retard the colonization of marine organisms are a significant component of corrosion protection in these environments. There are significant variations in the marine

environment due to location, local geography, and climate. Each of these factors must be carefully considered when evaluating coatings for marine service.

Within the marine environment there are several important subenvironments distinguished by different characteristics and aggressiveness [47]. The splash or spray zone is a well-aerated seawater environment where impinging seawater and entrained solids like sand may add a mechanical component to coating damage. In the tidal zone, coatings are subject to regular episodes of inundation and exposure. Macrofouling by various marine plants and animals is possible. Open ocean environments are usually well aerated at shallow depths. In these subenvironments, the micro- and macro-organisms are plentiful and may affect the protectiveness of coatings. The effect of aggressive pollutants is a concern, particularly in harbors. Deep ocean environments are also quite variable. The tendency for biofouling decreases with depth, due to the lack of sunlight. Temperature tends to decrease with depth, but dissolved oxygen, salinity, and pH vary irregularly. Marine atmospheres are characterized by high humidity and high levels of airborne chloride, both of which accelerate corrosion. Other variables that affect coating corrosion protection such as temperature, wind, sunlight, and pollution vary by location.

Epoxy coatings are workhorses for many marine service applications. They are durable and resistant to a range of exposure conditions, lasting for tens of years on offshore drilling platforms for example. They can be applied by brushing, rolling or spraying. Some can even be applied underwater. The class of epoxy coatings is chemically diverse, leading to the availability of coatings with a range of properties. Epoxies adhere well to substrates and are tolerant of imperfect surface preparation. For maximum corrosion resistance, epoxy coatings are applied over inhibiting coatings such as Zn-rich primers.

For immersion service conditions, inhibiting the growth of attached marine organisms is necessary [47]. Historically, cuprous oxide was added to coating formulations to impart resistance to marine life fouling. Due to environmental regulations, organotin compounds have largely replaced Cu compound additions in anti-fouling coatings, although these, too, are facing strict regulation. Organic anti-fouling compounds are known, but none appear to be as effective as metal- or metal oxide-based poisons. These compounds suppress growth by slowly dissolving into the surrounding water, achieving local concentrations that kill marine organisms. The effectiveness of anti-fouling agents is typically limited to

about a year, as the inhibiting agent is leached from the coating.

Alkyd, vinyl, and chlorinated rubber coatings all find application in marine service. Alkyd coatings are normally used in less severe environments. The oils in these coatings are subject to saponification by hydroxyl ions produced by the cathodic partial reaction of the corrosion process. Similarly, alkyd coatings are not suitable for use when cathodic protection is employed. Vinyl coatings are resistant to a wide range of water conditions. They are easily applied, adhere well, and are mechanically flexible. These coatings do not adhere well to previously corroded surfaces and must be applied in relatively thin coats (< 2 mils). Chlorinated rubber coatings have found application in marine service due to their tolerance of poor surface preparation and rapid drying characteristics, low water permeability, and UV resistance.

For applications involving cathodic protection, the use of saponification-resistant coatings is essential. Older coatings for such applications were based on phenolic and bituminous formulations. Higher performance epoxies, coal tar epoxies, vinyls, and chlorinated rubber coatings are now being used more regularly.

18.9.2 Paints for Automotive Service [48, 49]

Automotive coatings for exterior body panels are highly engineered to endure specific rigors of the road environment for years while maintaining a high degree of aesthetic appeal. Corrosion protection is imparted in many different parts of the coating system to resist the effects of road salts, pollution, acid rain, UV exposure, heat, and impingement of hard road debris.

Outer body panels on automobiles are Zn- or Zn-alloy-coated steels and plastics. Zinc coatings are applied to steel by hot dip processes and electrogalvanizing. Zn and Zn-Al layers are used. These layers provide barrier protection to the steel when they are unbreached and sacrificial cathodic protection if they are breached. In preparation for painting, Zn-coated steels are phosphate conversion coated to form a crystalline Fe-Zn phosphate layer. Conversion coatings are formed by immersion or spray after an aqueous degreasing operation. Conversion coated surfaces are primed with a cathodically electrodeposited inhibiting primer consisting of a high-build epoxy amine adduct resin and a corrosion inhibiting pigment like zinc chromate. Electrodeposited coatings are on the order of 30 μm thick, smooth and uni-

form, and largely free of pinholes and defects. A top coat is then applied to impart aesthetic appeal, barrier resistance to the environment, and mechanical resistance to impingement. The top coat normally consists of a 15- μm thick acrylic enamel color coat and a 40- μm thick clear acrylic top coat that provides luster, UV resistance, and color fading resistance. This layer also allows for polishing to remove fine dirt and debris.

18.9.3 Paints for Architectural Service [50, 51]

Protective paints on steel and aluminum structures must protect against natural outdoor exposures where the main aggressive agents are moisture, heat, sunlight, pollution, and mechanical damage. In some cases, maintenance of painted surfaces is impossible or economically impractical, and paints must provide protection for many years. In other cases, nearly continuous maintenance painting is essential for protection of the structure.

For steel structures, coating systems typically consist of a corrosion inhibiting primer coating and a topcoat for aesthetics and some barrier protection. As is normally the case, careful surface preparation involving degreasing, and mechanical abrasion or pickling is essential for maximum coating system protection. Zinc chromate or zinc-metal pigmented epoxies are common corrosion inhibiting primers. Synthetic resin topcoats have largely supplanted paints, based on natural resins such as linseed and tung oils. Alkyd and phenolic resins are used, but when alkaline conditions are expected, alkyds are to be avoided due to their tendency to saponify. Chemically cured resins provide excellent chemical resistance when needed. These include epoxies, polyurethanes, and polyesters.

An important application of epoxy resins is in the coating of rebar used in reinforced concrete [52–55]. Steel is normally passive in the alkaline cement paste of cured concrete. However, in service, chloride ingress and pH decreases due to cement carbonation can create an environment in which the rebar will corrode at unacceptable rates. Fusion-bonded epoxy coatings provide an added measure of corrosion protection under such conditions while sustaining the concrete-to-rebar bond necessary for mechanical reinforcement.

18.9.4 Paints for Aircraft [56, 57]

Aircraft are constructed mainly from aluminum alloys (> 75%). While steel tends to corrode uni-

formly, aluminum alloys corrode locally. When and where corrosion will occur is nearly impossible to predict. As a result, nearly all aluminum surfaces in aircraft are protected by coatings to minimize unpredictable localized corrosion.

Aircraft exterior environments are characterized by extreme variations in temperature (-50 to $+70^{\circ}\text{C}$), intense UV exposure at altitude, corrosive atmospheric environments that depend on where the aircraft is used, and exposure to various maintenance fluids and fuel. There are several characteristic internal environments. Transient condensate forms on the internal surfaces of airplanes in flight as the structure cools with increasing altitude. Around galleys and lavatories, spilled fluids migrate below deck and are trapped in various recesses and crevices. This can lead to local aggressive environments and severe corrosion.

Aircraft coating systems applied on exterior surfaces normally consist of a chromate conversion coating or anodized coating foundation layer, a corrosion inhibiting primer layer, and on exterior surfaces, a top coat. Coating systems on interior surfaces usually do not have a top coat applied. In this system, the foundation layer promotes adhesion of the organic layers to the substrate. Corrosion protection is derived mainly from the primer layer, which is typically a $25\text{-}\mu\text{m}$ thick epoxy-polyamide resin with sparingly soluble strontium chromate added as a pigment. The pigment volume content in these primers is on the order of 25%. The primer coating is quite permeable to water. However, when water penetrates the coating, the strontium chromate dissolves to form a corrosion inhibiting electrolyte that prevents corrosion of the substrate. The selection of SrCrO_4 as the inhibiting pigment is not incidental. The solubility of this compound is about 5 millimolar, which is sufficient to release enough chromate inhibitor to provide corrosion protection, but not so much as to induce osmotic blistering [6].

Exterior top coats mainly provide aesthetics, markings, and mediate visual and radar cross-sections in the case of military aircraft. These coatings may be minimal barriers to moisture so as to maximize other properties. Top coats must be UV resistant, tolerate extreme temperature variations, be impact resistant, and resistant to intermittent exposure to maintenance fluids (e.g., hydraulic fluid) and aircraft fuel. Isocyanate-cured polyester and acrylic resins containing pigments to impart necessary properties are most commonly used as topcoats. The weight of the paint on an aircraft is an important consideration that often limits the thickness of the

topcoat to $25\text{--}50\ \mu\text{m}$, bringing the total coating system thickness to $50\text{--}75\ \mu\text{m}$. Considering the excellent corrosion protection and limited thickness of these coatings, aircraft coating systems are one of the highest performance coating systems available.

18.9.5 Coatings for Buried Pipelines [58, 59]

Many transmission pipelines, including gas and oil transmission lines, are buried underground. Once buried, their surfaces are not easily accessed for maintenance. As a result, coating systems must be designed with long life and inaccessibility in mind. Coatings applied to pipelines are usually much thicker than paint-type coatings used in other applications. They are often used in conjunction with cathodic protection; their main functions are to provide a barrier to the external environment and to reduce cathodic protection requirements by limiting the exposed metallic surface area to that of defects and holidays.

Like many other environments, subsoil conditions vary and pose a range of aggressiveness that depends on variations in pH, free water, availability of oxygen, aggressive species concentration, and temperature. Coatings are subject to mechanical damage during transport and in-trench fitup. Once buried, the pressure of the soil and rocks may cause the coating to deform or break, exposing the underlying metal to the environment. When cathodic protection is employed, coatings must be resistant to alkaline attack and must not suffer disbonding or delamination.

Among the thinner coatings are fusion bonded epoxies, liquid epoxies and phenolics. Fusion bonded epoxy is electrostatically sprayed epoxy powder that is applied to surfaces that are preheated to $210\text{--}240^{\circ}\text{C}$. Upon application, the coating melts and flows to form a continuous and conformal coating up to $0.6\ \text{mm}$ in thickness. Liquid applied coatings based on polyurethane, epoxy and phenolic compounds also find application. Coal tar pitch is sometime added to polyamine-cured epoxy coatings. These coatings are noteworthy for their resistance to degradation under alkaline conditions, such as those produced during cathodic protection.

Notable among the thicker coatings used for pipeline protection are bituminous enamels, which are often used in conjunction with fiberglass tapes or felts for mechanical robustness, and asphalt mastics consisting of asphalt mixed with sand and limestone. Coatings of this type can be several to many mil-

limeters thick. They are excellent moisture barriers and can withstand very rough handling associated with emplacement of underground piping.

18.10 ENVIRONMENTAL HAZARDS

18.10.1 Lead

Lead pigmented paint is no longer marketed and newer, less hazardous alternatives have been successfully developed, but much lead paint remains in older homes where it is a toxic hazard to humans.[60] The main route of entry into the human body is by inhalation of dust from deteriorating painted surfaces. While the death rate due to lead poisoning has declined dramatically since the late 1970s, lead paint remains a public health concern [61].

18.10.2 Volatile Organic Coating (VOC) Emissions

VOC emissions pose acute hazards to workers and a long-term environmental pollution hazard. Most notable are ozone-depleting emissions such as chlorinated fluorocarbons. Reductions in VOC emissions have been achieved through the use of engineering controls on exhaust air, reduction in paint usage by high transfer efficiency application methods, and the development of new coating formulations [62]. New formulations include reduced VOC resins, the use of new solventless resins in applications where solvent-borne coatings were once standard, the emergence of high-performance waterborne coatings, and the use of heat-cured electrostatic powder coating.

18.10.3 Chromates [21]

Chromates are outstanding corrosion inhibitors for a wide range of metals. As a result, they are used widely in metal finishing for corrosion protection. Unfortunately, chromates are toxic in acute high level exposure and chronic low-level exposures. Hexavalent chromium is a proven cancer-causing agent. The regulations surrounding the use and disposal of chromates associated with painting is making them difficult and expensive to use. Ultimately, their use will be severely curtailed or eliminated as new environmentally friendly pigments and inhibitors are developed.

18.11 REFERENCES

1. J. Titz, G. H. Wagner, H. Spahn, M. Ebert, K. Juttner, W. J. Lorenz, *Corrosion. Sci.*, 46, 221 (1990).
2. J. E. O. Mayne, *The Mechanism of Protective Action of Paints*, p. 15:34 in *Corrosion*, Butterworths, London, 1976.
3. G. W. Walter, *Corrosion. Sci.*, 26, 27 (1986).
4. S. Pauly, *Permeability and Diffusion Data*, p. VI-435 in *Polymer Handbook*. New York: John Wiley & Sons, 1999.
5. R. H. Heidersbach, Marine Corrosion. In *Metals Handbook, 9th Ed.* Metals Park, OH, ASM International, p. 893, 1987.
6. J. Sinko, *Prog. Organic Coat.*, 42, 267 (2001).
7. A. Banov, *Paints & Coatings Handbook*. Farmington, MI: Structures Publishing Co., p. 29, 1973.
8. D. C. H. Nevison, Corrosion of Zn. In *Metals Handbook, Vol. 13*. Materials Park, OH: ASM International, p. 755, 1987.
9. H. F. Payne, *Organic Coating Technology*. New York: John Wiley & Sons, Inc., Vol. II, p. 1,293, 1961.
10. P. A. Schweitzer, *Corrosion-Resistant Linings and Coatings*. New York: Marcel Dekker, Inc., p. 309, 2001.
11. J. R. Vilche, E. C. Bucharsky, C. A. Giudice, *Corrosion. Sci.*, 44, 1,287 (2002).
12. B. Muller, I. Forster, W. Klager, *Prog. Org. Coat.*, 31, 229 (1997).
13. B. Muller, G. Kubitzki, G. Kinet, *Corrosion. Sci.*, 40, 1,496 (1998).
14. B. Muller, M. Shahid, G. Kinet, *Corrosion. Sci.*, 41, 1,323 (1999).
15. A. Z. Gomaa, M. A. Elghaffer, A. A. Salman, H. E. Nasr, *JOCCA-Surface Coatings International*, 74, 181 (1991).
16. J. Edwards, *Coating and Surface Treatment Systems for Metals: A Comprehensive Guide to Selection*. Materials Park, OH: ASM International, p. 367, 1997.
17. J. H. Osborne, K. Y. Blohowiak, S. R. Taylor, C. Hunter, G. P. Bierwagen, B. Carlson, D. Bernard, M. S. Donley, *Prog. Org. Coatings*, 41, 217-225 (2001).
18. E. P. M. VanWesting, G.M. Ferrari, J. H. DeWit, *Corrosion. Sci.*, 36, 979 (1994).
19. E. H. Phelps, *The Making, Shaping and Treating of Steel, 9th Ed.* Pittsburgh: Herbick and Held, p. 980, 1971.
20. K. Ogle, R.G. Buchheit, Conversion Coatings. In *Encyclopedia of Electrochemistry Vol. 4, Corrosion and Oxide Films*. Weinheim, Germany: Wiley-VCH, p. 460, 2003.
21. M. W. Kendig, R.G. Buchheit, *Corrosion. Sci.*, 59, 379 (2003).
22. A. Banov, *Paints & Coatings Handbook*. Farmington, MI: Structures Publishing Co., p. 15, 1973.
23. M. W. O'Reilly, J. T. Pringle, Paint Formulation. In *Corrosion, 2nd Ed.* London: Butterworths, p. 14:7, 1976.
24. H. F. Payne, *Organic Coating Technology, Vol. II*. New York: John Wiley & Sons, Inc., p. 1,266, 1961.

25. K. B. Tator, Organic Coatings and Linings. In *Metals Handbook, 9th Ed.* Metals Park, OH: ASM International, p. 399, 1987.
26. M. Kendig, J. Scully, *Corrosion*, 46, 22 (1990).
27. F. Bellucci, L. Nicodemo, *Corrosion*, 49, 235 (1993).
28. E. P. M. VanWesting, G. M. Ferrari, J. H. DeWit, *Corrosion. Sci.*, 36, 957 (1994).
29. N. S. Allen, *Engineering Plastics*, 8, 247 (1995).
30. T. Nguyen, J. B. Hubbard, J. M. Pommersheim, *J. Coat. Technol.*, 68, 45 (1996).
31. A. M. Mierisch, S. R. Taylor, *J. Electrochem. Soc.*, 150, B303 (2003).
32. B. R. Appleman, *J. Coat. Technol.*, 62, 57 (1990).
33. A. G. Forshee, *Metal Finishing*, 91, 35 (1993).
34. A. G. Forshee, *Metal Finishing*, 91, 50 (1993).
35. B. W. Johnson, R. McIntyre, *Prog. Org. Coat.*, 27, 95 (1996).
36. F. Altmayer, *Plating and Sur. Finish.*, 72, 36 (1985).
37. B. R. Appleman, P. G. Campbell, *J. Coat. Technol.*, 54, 17 (1982).
38. A. Forshee, *Metal Finishing*, 89, 45 (1991).
39. R. D. Granata, Nonmetallic Coatings. In *Corrosion Tests and Standards: Application and Interpretation*. Philadelphia: ASTM, p. 525, 1995.
40. M. W. Kendig, S. Jeanjaquet, J. Lumsden, Electrochemical Impedance of Coated Metal Undergoing Loss of Adhesion. In *Electrochemical Impedance: Analysis and Interpretation, ASTM STP 1188*. Philadelphia: ASTM, p. 407, 1993.
41. F. Mansfeld, M. W. Kendig, Electrochemical Impedance Tests for Protective Coatings. In *Laboratory Corrosion Tests and Standards*. Philadelphia: ASTM, p. 122, 1985.
42. F. Mansfeld, C. H. Tsai, *Corrosion*, 47, 958 (1991).
43. J. N. Murray, H. P. Hack, *Corrosion*, 48, 671 (1992).
44. C. H. Tsai, F. Mansfeld, *Corrosion*, 49, 726 (1993).
45. J. R. Macdonald, *Impedance Spectroscopy*. New York: John Wiley & Sons, Inc., p. 306, 1987.
46. R. G. Buchheit, M. Cunningham, H. Jensen, M. W. Kendig, M. A. Martinez, *Corrosion*, 54, (1998).
47. D. Aylor, Seawater. In *Corrosion Tests and Standards: Application and Interpretation*. Philadelphia: ASTM, p. 307, 1995.
48. Organic Coatings and Linings. In *Metals Handbook, 9th Ed.* Metals Park, OH: ASM International, p. 1,011, 1987.
49. G. P. A. Turner, Paint Finishes for Industrial Applications. In *Corrosion*. London: Butterworths, p. 14:59, 1976.
50. P. G. Gay, N. R. Whitehouse, Paint Finishes for Structural Steel. In *Corrosion*. London: Butterworths, p. 14:69, 1976.
51. J. E. Slater, Corrosion in Structures. In *Metals Handbook, 9th Ed.* Metals Park, OH: ASM International, p. 1,299, 1987.
52. A. B. Darwin, J. D. Scantlebury, *Cement & Concrete Composites*, 24, 73–78 (2002).
53. A. U. Malik, I. Andijani, S. Ahmed, F. Al-Muaili, *Desalination*, 150, 247–254 (2002).
54. Z. G. Matta, *Materials Performance*, 33, 52–55 (1994).
55. J. S. McHattie, I. L. Perez, J. A. Kehr, *Cement & Concrete Composites*, 18, 93–103 (1996).
56. M. L. Baucio, Corrosion in the Aircraft Industry. In *Metals Handbook, 9th Ed.* Metals Park, OH: ASM International, p. 1,019, 1987.
57. P. G. Gay, N. R. Whitehouse, Paint Finishes for Industrial Applications. In *Corrosion*. London: Butterworths, p. 14:53, 1976.
58. M. D. Allen, D. A. Lewis, Protective Coatings for Underground Use. In *Corrosion*. London: Butterworths, p. 14:89, 1976.
59. C. G. Siegfried, Corrosion of Pipelines. In *Metals Handbook, 9th Ed.* Metals Park, OH: ASM International, p. 1,288, 1987.
60. S. Bjerklie, *Modern Paint and Coatings*, 91, 12 (2001).
61. R. B. Kaufmann, T. D. Matte, C. J. Staes, *Environmental Research*, 91, 78 (2003).
62. K. L. Whittall, *Metal Finishing*, 96, 414 (1998).

CHAPTER 19

PAINT WEATHERING TESTS

Mark E. Nichols

Materials Research and Advanced Engineering, Ford Motor Company, Dearborn, Michigan

| | |
|--|-----|
| 19.1 INTRODUCTION | 387 |
| 19.2 DEGRADATION PROCESSES | 387 |
| 19.3 OUTDOOR EXPOSURE | 389 |
| 19.4 ARTIFICIALLY ACCELERATED WEATHERING TESTS | 393 |

| | |
|---|-----|
| 19.5 TEST CYCLES | 398 |
| 19.6 POST-EXPOSURE TESTING | 402 |
| 19.7 NON-TRADITIONAL MATERIAL EVALUATIONS | 402 |
| 19.8 FURTHER READING | 403 |
| 19.9 REFERENCES | 403 |

19.1 INTRODUCTION

Almost all manmade objects intended for service outside are painted. The function of the paint is multifold. Primarily, the paint serves a decorative function, in which its purpose is to enhance or change an object's appearance—to change its color or level of gloss, or to draw attention to some particular region on the object. However, just as importantly, objects are painted to protect them from the environment or to lengthen their lifetime. Coatings have long been recognized as protective prescriptions for items as diverse as airplanes, automobiles, bridges, houses, and machinery. Maximizing the life of a coating, and thereby the underlying object, has been a key goal of coatings scientists. In doing so, a variety of exposure methods and test protocols have been developed to anticipate the long-term weathering behavior of coatings.

19.2 DEGRADATION PROCESSES

Coatings, like all other materials, will begin to degrade when placed outside. Their degradation is due to the effect of various environmental pressures placed upon the coating. The weathering process is dominated by the effects of electromagnetic radiation (primarily ultraviolet radiation), heat, water (liquid and vapor), and atmospheric pollutants. Each of these plays a greater or lesser role, depending on

the coating and the specific geographic location in which a coating is exposed.

19.2.1 UV Radiation

The spectrum of radiation reaching the earth's surface at noon in Miami, FL is shown in Figure 19.1. Ozone in the earth's upper atmosphere prevents radiation of less than 295 nm wavelength from reaching the earth's surface. The intensity of radiation, of course, varies by season, time of day, and to a lesser extent, geographic location.

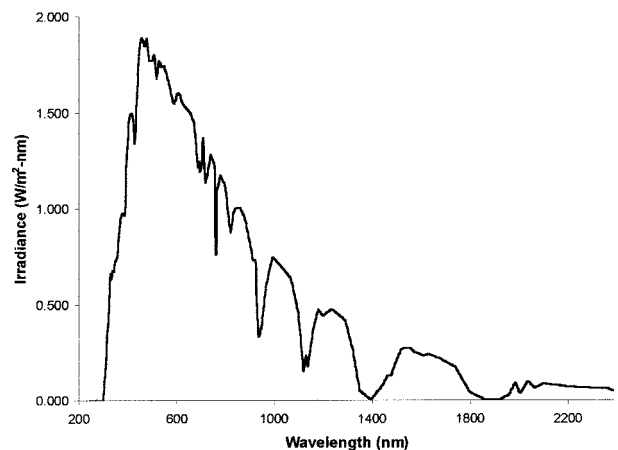


FIGURE 19.1 Spectrum of radiation reaching the earth's surface at noon in Miami, FL USA. [Data: Atlas Weathering Services Group]

For most coatings, radiation from the ultraviolet (UV) portion of the electromagnetic spectrum causes most of the damage during weathering. Thus, for coatings outdoors, radiation between 295–400 nm is the most damaging, as this radiation is most likely to initiate photo-oxidation. Photo-oxidation is the free radical process by which organic materials can degrade in the presence of light and oxygen. This process is shown schematically in Figure 19.2.¹ The initiation event can be due to absorption of UV light by any chromophore in the coating (i.e., polymer molecules, pigment particles, or even trace impurities in the resin such as end groups, additives, etc.). Each initiation event can lead to many tens of propagation events before the propagating radical chain is terminated. Additives can be added to coatings to retard the photo-oxidation process. Ultraviolet light absorber (UVA) can be added to prevent primary absorption, thereby reducing the rate of initiation. Hindered amine light stabilizer (HALS) can be added to scavenge radicals once they are produced, thereby prematurely terminating the radicals during the propagation stage. The use of these additives can significantly prolong the lifetime of organic coatings outdoors.

19.2.2 Water

Exposure to water has both a deleterious chemical and physical effect upon coatings. The organic binders in most coatings are subject to hydrolysis, that is, cleavage of the polymer chains in the presence of water molecules. This process occurs at all temperatures, but is especially prevalent at higher temperatures, such as those occurring during outdoor exposure. Melamine cross-linked coatings as well as polyesters are particularly susceptible to hy-

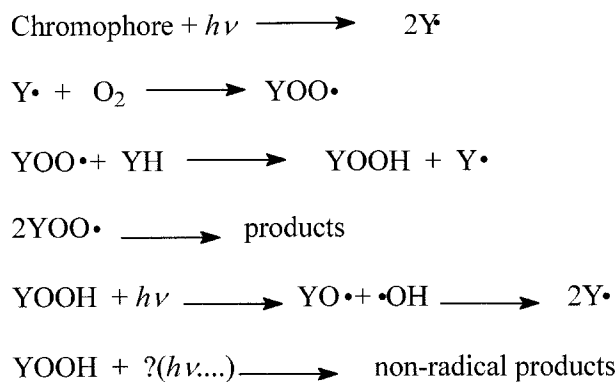


FIGURE 19.2 Schematic of photo-oxidation process. Y = polymer or organic component of a coating, including trace impurities.

drolisis, while urethanes are particularly resistant. One would expect that coatings exposed in Florida, where the average humidity is 84%, would hydrolyze faster than coatings exposed in Arizona, with an average humidity of 33%. However, recent data suggests that this is not true, and that only at unrealistically high dew points and temperatures is the rate of hydrolysis significantly different than the rates observed in Florida and Arizona.^{2,3}

Water can also act to physically degrade coatings. The washing action of liquid water on the surface of panels tends to extract small soluble molecules from the coatings, in addition to washing away surface debris. This can lead to a more rapid loss of gloss or chalking than would be observed without water washing. In addition, the swelling of the paint and substrate due to the absorption of water leads to repeated stress cycles on the coating. This is especially true of coatings on wood, where the anisotropic swelling of the wood can lead to cracking parallel to the grain direction.⁴ If small water soluble species are present in a coating, they can be extracted by liquid water. These aqueous solutions can set up significant osmotic pressure if small pores are present in the coating, which can then lead to blistering of the coating.⁵

19.2.3 Temperature

Elevated temperatures act to accelerate the deleterious effects of both radiation and water. Since the hydrolysis reactions and the propagation steps in photo-oxidation are both thermally activated, higher temperatures will lead to faster degradation rates and may even change the degradation pathway. This can be particularly important when comparing the weathering behavior of a series of coatings of different colors. Objects painted darker colors will typically be hotter than lighter objects. This temperature difference can lead a coating's degradation rate to be significantly color-dependant. As a guide, the temperature of a series of steel panels painted with different colors of automotive topcoats are shown in Figure 19.3. The actual temperature of a paint panel of any given color can be effected significantly by the choice of pigments used in the formulation, as some pigments absorb more strongly in the infrared region than others.

The temperature of a paint system also plays an important role from a mechanical stress standpoint. Each heating and cooling cycle, such as a diurnal cycle, induces a mechanical stress due to a mismatch in thermal expansion coefficients between the substrate and coating.⁶ The size of these stress cycles is

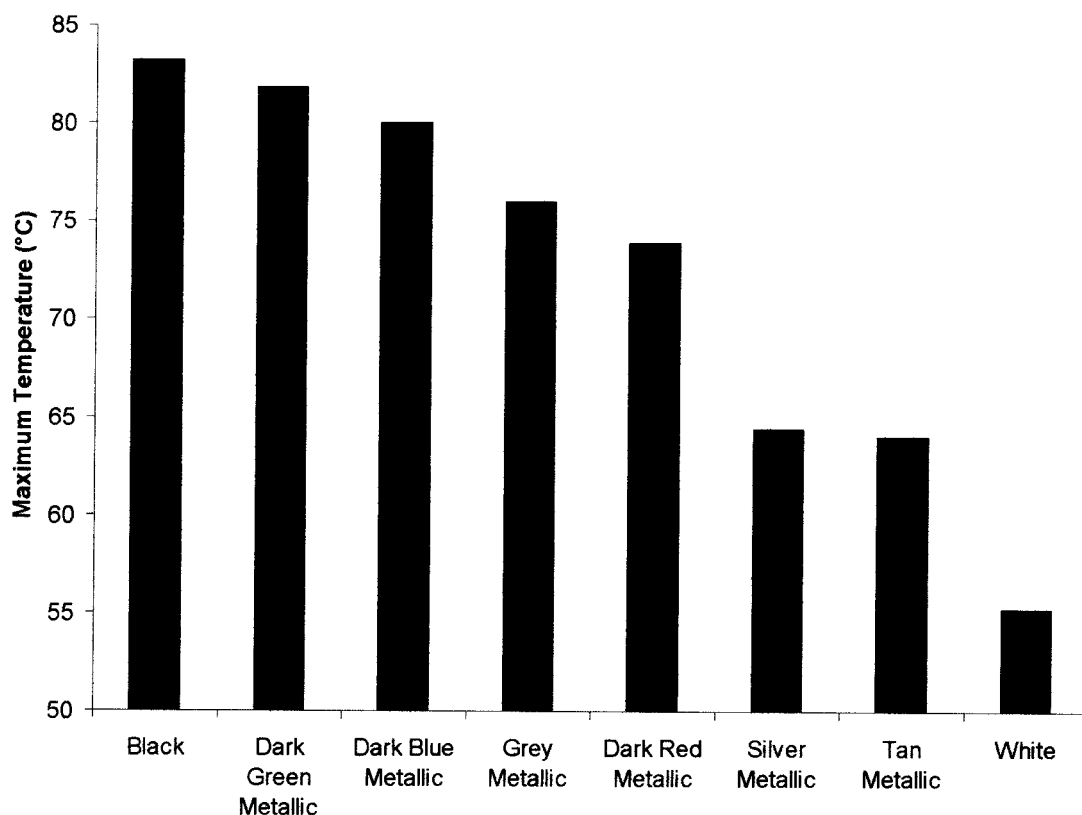


FIGURE 19.3 Maximum temperature of steel paint panels of various colors during Arizona exposure.

directly proportional to the temperature change. Thus, paint systems that are hotter will tend to be subjected to greater mechanical stresses than those that are exposed to lower temperature extremes, again favoring light colors over dark colors.

19.2.4 Other Exposure Variables

Although UV radiation, water, and temperature play the dominant roles in causing weathering-induced degradation of coatings, other factors can play a significant role in specific failure modes. Atmospheric pollution can lower the pH of rainfall, leading to acid etching of coatings. This is a widespread phenomenon with locally intense variations. Those areas downwind of significant industrial operations may experience significantly more acid etching than those areas isolated from the effects of industrial fallout. Attack by microorganisms can also lead to degradation of a coating. In particular, fungi can form on architectural and other paints, causing a black staining of the coatings. Biocides can be added to paint formulations to discourage attack by these organisms. Because of its lower energy, the effects of visible light on paint systems is thought to be less

significant than the effects of UV light. However, for pigmented systems, particularly organic pigments, the effects cannot be ignored.

19.3 OUTDOOR EXPOSURE

Outdoor exposure has long been the standard method of testing the long-term weatherability of coatings. However, this type of exposure provides no acceleration. Therefore, predicting the performance/appearance of a coating after 10 years of exposure requires 10 years of exposure. This time scale makes the use of outdoor weathering of little help to the coatings formulator, as it can only confirm the long-term performance of a coating. Unfortunately, the information obtained from a coating's performance during short-term outdoor exposures (one to two years) need not be indicative of the coating's long-term weathering performance, as many failures can appear suddenly, with little advance notice. Therefore, most coatings development relies on a combination of artificial accelerated weathering exposure to provide performance feedback quickly (see Section 19.4, Artificial Accelerated Weathering

Tests), outdoor exposure for confirmation, and the experience of paint chemists who are familiar with the history and effects of various formulation changes.

19.3.1 Climate

The advantage of outdoor exposure is that it is unambiguously representative of real-world performance (in that location). For years, exposure in southern Florida has been the standard geographic location for outdoor coatings exposure. This climate combines high sun load with high humidity and high time of wetness, making it one of the more harsh weathering climates on the planet. Other sites are slightly more harsh for given exposure conditions. Townsville, Australia, for example, is particularly harsh for humidity and biological attack. Exposure in the interior of the Arabian Peninsula has a higher sun load and temperature. However, these other areas are not as easily accessible, nor are they climates where large numbers of people live, so their testing popularity is not as great.

While Miami, Florida is typical of a subtropical climate, Phoenix, Arizona is a typical desert exposure site, where the UV dosage is slightly higher (~10%) than in southern Florida. The increased UV dosage is not due to latitude. Southern Florida is ac-

tually farther south than Phoenix, but the lack of cloud cover in Phoenix gives rise to less light scattering than in southern Florida. While the sun load and average temperatures are higher, Phoenix exposure is thought to be slightly less harsh than southern Florida exposure, due to Phoenix's low humidity and lack of rain.⁷ A comparison of the annual solar UV in both Miami and Phoenix is given in Figure 19.4. A comparison of other meteorologically significant data is given in Table 19.1.

When the effects of acid rain or industrial fallout are of concern, paint panels are typically exposed in Jacksonville, Florida. Here the "season" for acid rain occurs in May through August. The typical exposure time is 14 weeks. Acid etch conditions are high in the area due to the high heat and humidity of the environment, coupled with the proximity of several coal- and oil-fired power plants that produce significant emissions associated with acid rain production. However, year-to-year variation in the severity of the environment make this test somewhat more variable than standard outdoor exposure.

19.3.2 Exposure Conditions

At any given site, a variety of exposure conditions can be used. For automotive coatings, 5 degrees south-facing exposure is the standard. This exposure

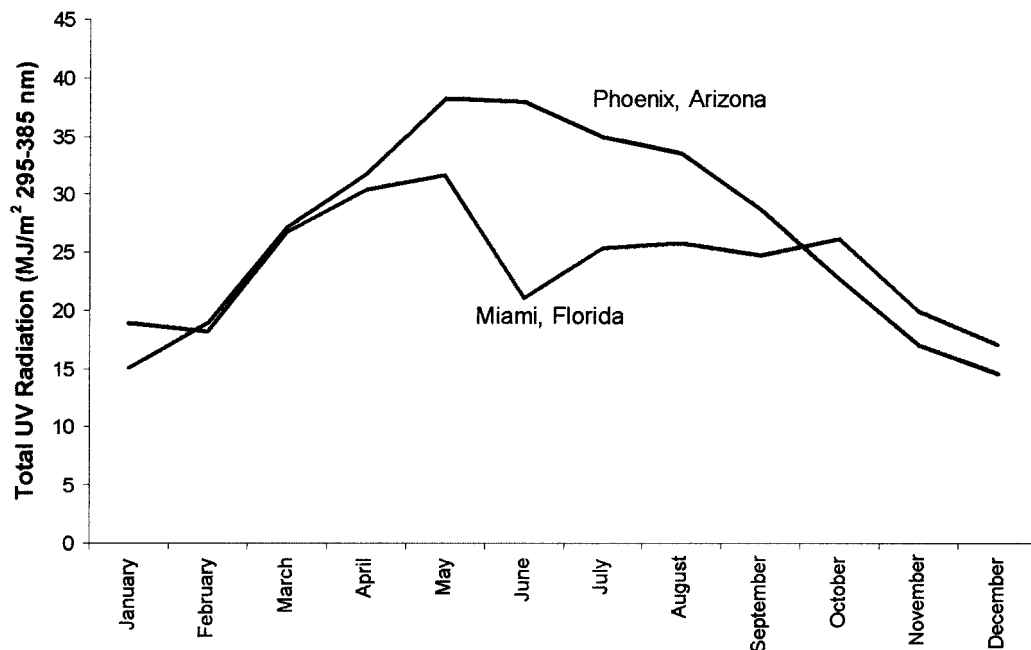


FIGURE 19.4 Total UV radiation in Miami, FL and Phoenix, AZ during 2002. [Data: Atlas Weathering Services Group]

TABLE 19.1 Climatic Data for Miami, FL and Phoenix, AZ

| Parameter | Miami, FL USA | Phoenix, AZ USA |
|---|---------------|-----------------|
| Total Solar UV (295–385 nm) 5 degrees south | 286.7 | 320.6 |
| Humidity (%)—Average, Maximum | 84, 98 | 29, 43 |
| Annual Rainfall (mm) | 1,481 | 102 |
| Time of Wetness 45-degree panel (hours) | 5,951 | 164 |
| Temperature (°C)—Average, Maximum | 24, 29 | 23, 30 |
| Black Panel Temperature (°C) 5 degrees south—Average, Maximum | 26, 46 | 25, 45 |

All data are for 2002 calendar year. Averages are yearly averages. Maximums are monthly maximum values. [Source: Atlas Weathering Services Group]

**FIGURE 19.5** Paint test panels exposed at 5 degrees facing south. [Picture courtesy of Q-Panel Company]

orients the sample facing south to increase exposure intensity and angles them 5 degrees up from horizontal to allow for rain shedding (see Figure 19.5). More intense exposure can be obtained by orienting samples south and holding them “at latitude” angle from the horizontal. For exposure in southern Florida, for example, the samples would be held at 26 degrees from the horizontal. The weatherability of architectural coatings is typically tested by weathering at 45 degrees from horizontal (Figure 19.6). Conversely, to test for mildew resistance in ar-

chitectural coatings, the sun load is minimized by exposing panels at 90 degrees, facing north (Figure 19.7).

To accelerate the effects of temperature, panels can be exposed “backed” or on a “black box,” where the panels are exposed on backing or black material to increase the exposure temperature and rate of degradation (Figure 19.8). To further accentuate the effects of temperature, specimens can be exposed under glass, where samples are placed under glass inside of a black box. This increases the heat and re-



FIGURE 19.6 Paint test panels exposed at 45 degrees facing south in Arizona. [Picture courtesy of Atlas Weathering Services Group]

moves liquid water from the degradation environment. This type of exposure is common for vehicle interiors (Figure 19.9).

19.3.3 Accelerated Outdoor Exposure

Acceleration of outdoor exposure has been accomplished by the use of arrays of mirrors (Fresnel reflectors) to concentrate the sun's light on paint panels. This testing, known by a variety of names such as Equatorial Mounted Mirrors for Acceleration (EMMA), (Equatorial Mounted Mirrors for Acceleration plus a water spray cycle ("aqua") (EMMAQUA), and others, uses machines outfitted with sensors that track the sun's position in the sky. By following the sun across the sky, the maximum irradiance can be achieved throughout the day. The machines are outfitted with blowers to keep the samples from overheating and water misting nozzles to apply liquid water at various times throughout the day

(Figure 19.10). Like standard outdoor testing, a variety of test protocols are possible, with daytime spray and night-time wetting being the most common. The advantages of this type of testing are the correctness of the light source and the additional speed it provides. Because the light used is reflected natural sunlight, no ambiguity is introduced by having unnatural wavelengths of light present (see Section 19.4, Artificial Accelerated Weathering Tests).

In addition, the use of mirrors allows for an acceleration factor of four to five, (averaged over one year) over standard Florida exposure. The exact acceleration factor depends on the time of year the samples are exposed. The acceleration factor in the winter is less than three and in the summer is greater than five. The disadvantages of solar reflector-type exposures are the cost, which is typically high and based on the linear inch of panel exposed, and the uncertainty surrounding the environmental stresses placed on the samples due to the lack of water in

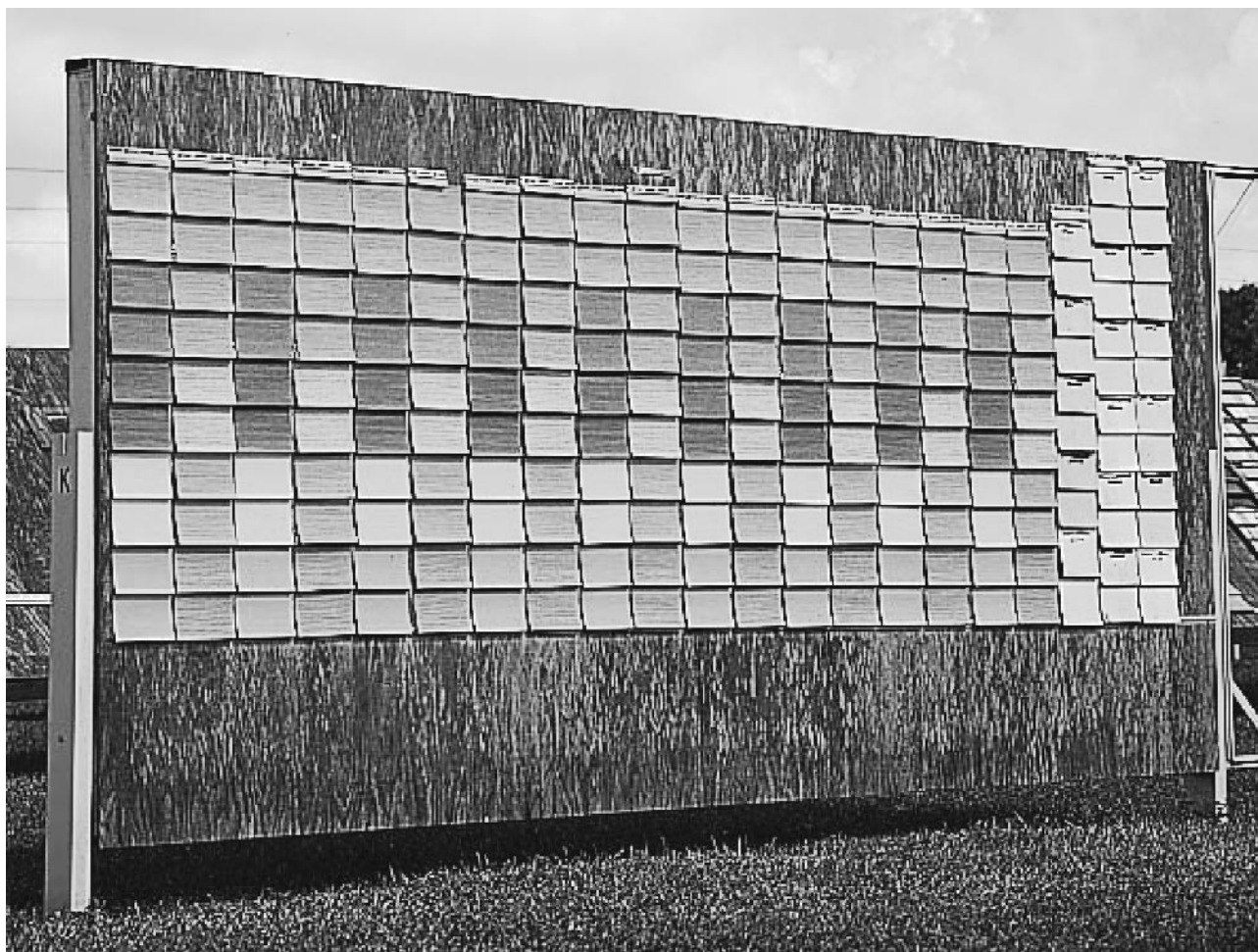


FIGURE 19.7 Architectural paint panels exposed at 90 degrees facing north. [Picture courtesy of Atlas Weathering Services Group]

the surroundings, even when the panels are sprayed regularly.

19.4 ARTIFICIALLY ACCELERATED WEATHERING TESTS

The goal of accelerated artificial weathering is to reproduce the important environmental conditions that exist in a given location outdoors in a well controlled device, while at the same time accelerating the degradation process. The desire for acceleration comes from the need to use weathering data to guide formulation and use/no use decisions, which cannot be practically guided by real-time outdoor exposure. The difficulty in accelerated testing, however, is in determining which conditions are important to re-

produce, how well they have to be reproduced, which outdoor environment to use as a standard, and to a lesser extent how to control the device. In recent years, the greatest effort has gone into trying to correctly reproduce the wavelength distribution of the light inside accelerated weathering chamber, as results have shown that this variable can have a dramatic effect on the trustworthiness of the test.

19.4.1 Spectral Power Distribution

Photochemical reactions drive most of the changes that occur in coatings during weathering exposure. These reactions occur when an organic material absorbs a light photon. Depending on the energy of the photon, the absorption can lead to the cleavage of a chemical bond and the production of a radical. These



FIGURE 19.8 Paint panels exposed under “black box” conditions. [Picture courtesy of Atlas Weathering Services Group]

radicals can then propagate throughout the material, leading to extensive chemical changes, as was shown in Figure 19.2. Only those photons absorbed by the material can cause chemical reactions. Thus, the effects of light on a material are dependant on the absorption spectrum of the material (including trace elements and impurities in the material) and the wavelength distribution of the incident radiation. For example, the absorption spectrum of a polyester urethane coating is shown in Figure 19.11. Radiation above 295 nm is only minimally absorbed by the coating and, therefore, causes few photochemical reactions. However, absorbance by the polymer increases at lower wavelengths, which can lead to significant chemical changes in the polymer. Light of these wavelengths is abundant in most accelerated tests, including borosilicate filtered xenon arc light (see Section 19.4.4, Xenon Arc Light Sources). However, there is little light below this wavelength

in sunlight. Therefore, this material undergoes little chemical degradation outdoors, but degrades rapidly in most accelerated tests. Even materials that do not absorb strongly at the wavelengths of irradiation can still undergo photochemistry due to the presence of impurities which do absorb and begin the photo-oxidation chain of reactions. Thus, the UV spectra of a material is only a starting point for understanding its photostability.

For terrestrial materials, the only light that is significant is that of wavelengths greater than 295 nm (refer to Figure 19.1), as the ozone layer in the stratosphere effectively absorbs radiation of lower wavelengths. Because different wavelengths of light can drive specific chemical reactions, accurately reproducing natural sunlight is the first step toward creating a reliable accelerated weathering test. Any differences between the light in an accelerated device and the light outdoors has the potential to lead to

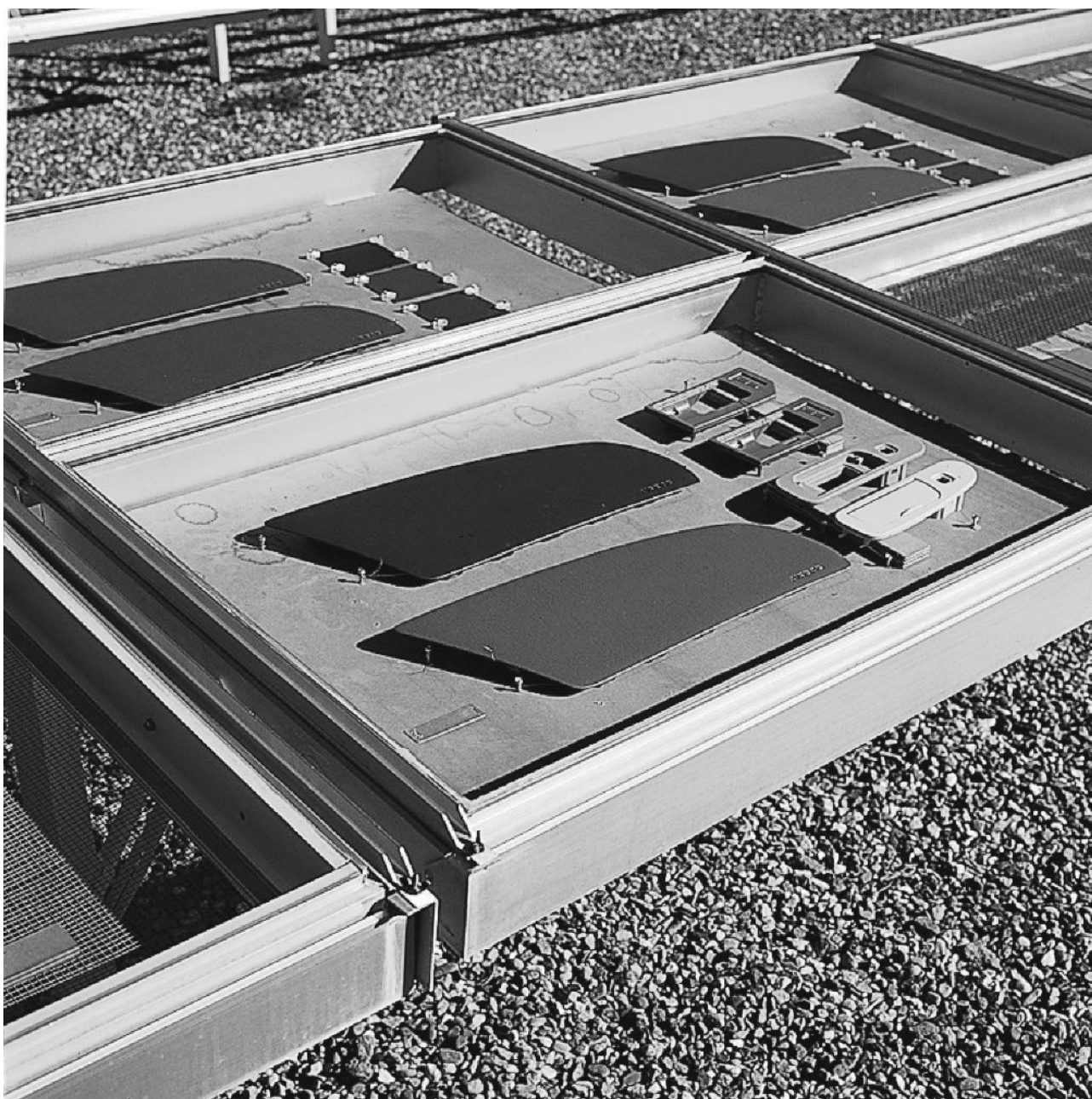


FIGURE 19.9 Automotive interior parts exposed “under glass.” [Picture courtesy of Atlas Weathering Services Group]

chemical reactions occurring in the accelerated tests that would not occur outdoors. Thus, the results from any artificial accelerated test that does not use a light source that accurately reproduces sunlight should be treated with caution (this includes all currently available tests!). Currently, no light source exactly matches sunlight over the entire UV and visible light range. Some match well in portions of the UV range and some are good matches in the visible

range. Work is still progressing on a better sources and filters to correctly reproduce sunlight.⁸

19.4.2 Fluorescent Light Sources

The least expensive accelerated weathering devices use fluorescent light bulbs as the light source. These bulbs have phosphor coatings on the inside of the bulbs to provide a specific wavelength distribution



FIGURE 19.10 Solar Fresnel mirror exposure apparatus in Arizona. [Picture courtesy of Atlas Weathering Services Group]

of light. The two most popular bulbs are those that have intensity maximums at 313 nm and 340 nm, respectively. The 313 bulbs are also known as UV-B bulbs or FS-40 bulbs. As can be seen in Figure 19.12, the 313 bulbs provide a poor match to wavelength distribution of sunlight, producing substantially more short-wavelength UV radiation than is present in sunlight. This excess short-wavelength light is particularly damaging due to its higher energy. Thus, the potential for unnatural chemical changes to occur during exposure with 313 bulbs is significant.⁹ While the 340 nm (UV-A) bulbs provide a substantially better match to sunlight in the short-UV wavelength region, the long wavelength and visible portion of the spectrum are poor matches to sunlight. Depending on the industry, a number of specifications exist detailing the operating conditions of the machines. While weathering specifica-

tions for use with these machines are well established, they are being phased out in favor of weathering chambers using higher intensity lights with better matches to natural sunlight.

19.4.3 Carbon Arc Light Sources

The spectral output of a carbon arc is dramatically different than that of terrestrial sunlight (Figure 19.13). These sources were originally developed to predict the fading of textiles. Weathering specifications based on carbon arc light sources have been out of favor in the coatings industry for some time. Two different sources have been used, the enclosed and the Sunshine Carbon Arc system, with the Sunshine Carbon Arc system more closely approximating natural sunlight. However, the use of these systems is not recommended.

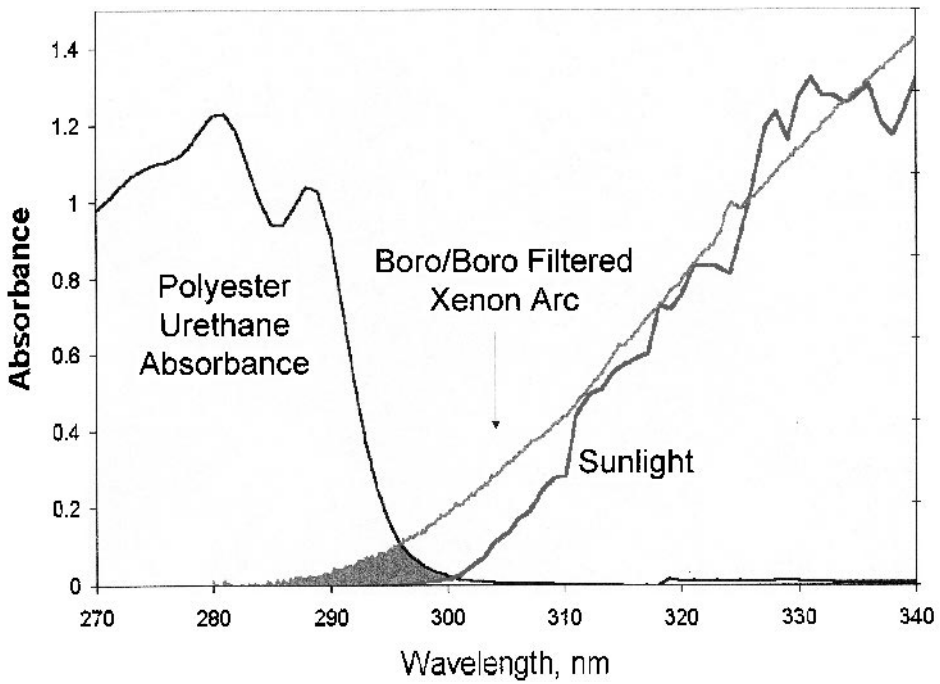


FIGURE 19.11 UV spectrum of a polyester urethane coating and spectrum of both terrestrial sunlight and borosilicate/borosilicate filtered xenon arc light. Note the overlap between boro/boro light and polyester urethane absorbance.

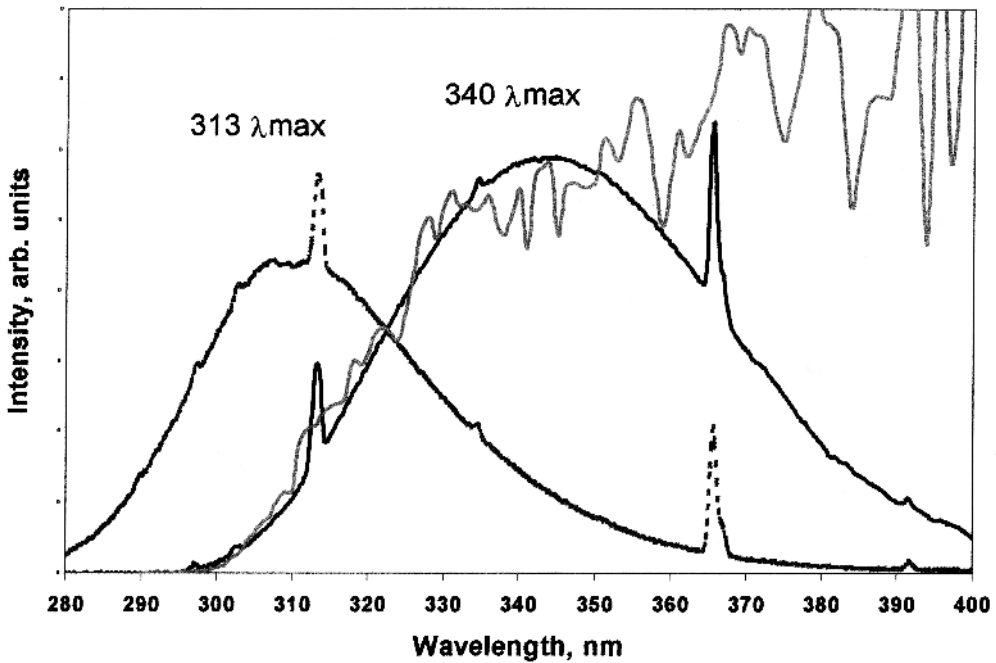


FIGURE 19.12 Spectral power distribution of fluorescent light bulbs used in accelerated weathering testing. Miami sunlight is shown for reference. [Data: Atlas Materials Testing Technology, LLC]

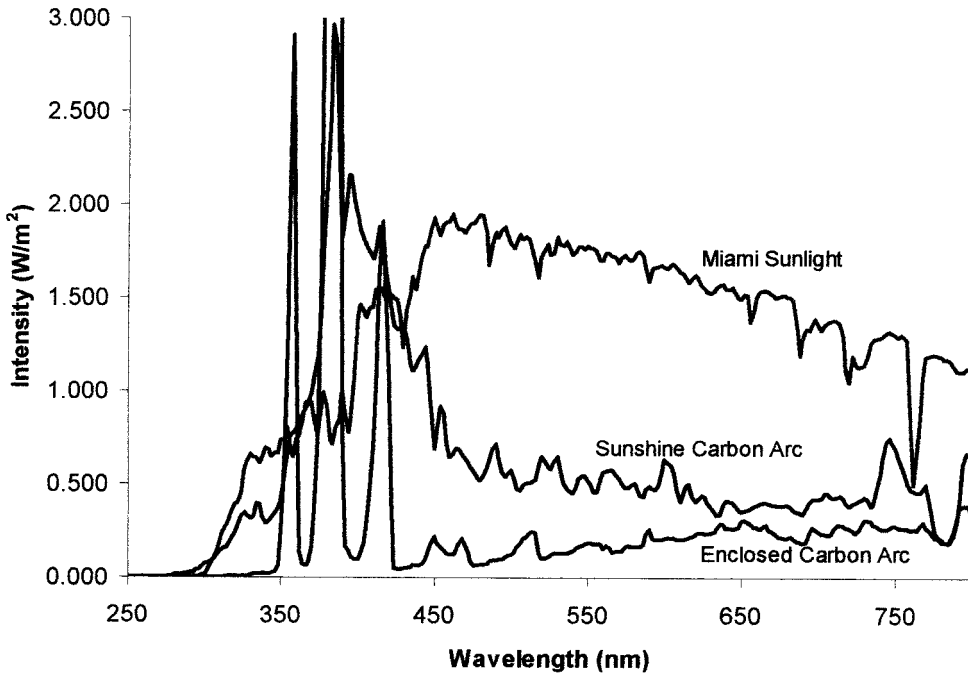


FIGURE 19.13 Spectral power distribution of carbon arc light sources. Miami sunlight is shown for reference. [Data: Atlas Materials Testing Technology, LLC]

19.4.4 Xenon Arc Light Sources

The adoption of filtered xenon arc light as a radiation source allows for a much more realistic approximation of sunlight. In practice, the xenon arc light is surrounded by a glass filter(s) to produce radiation with a specific wavelength distribution. The most popular filter combination is the so-called quartz/boro filter, which consists of a quartz inner filter and a borosilicate glass outer filter. In combination, these filters produce light with a wavelength distribution shown in Figure 19.14. While the approximation of sunlight is good above 310 nm, an abundance of unnaturally short wavelength UV light is present below 295 nm. This unnatural light can greatly distort the chemical changes that take place during accelerated weathering as compared to outdoor exposure. However, this filter combination remains popular in many industries.

A closer match to sunlight can be achieved by using borosilicate glass for both the inner and outer filters around a xenon arc light source (Figure 19.14). This filter combination eliminates much of the short-wavelength light present in quartz/boro filtered light. However, even this filter combination can allow shorter than natural wavelength light to strike samples, and even this small amount of excess light (below 295 nm) has been shown to give misleading

weathering results for some paint systems.⁸ Many specifications are slowly shifting from quartz/boro filtered xenon arc light to boro/boro filtered xenon arc light. The shift is occurring slowly, however, due to the lower acceleration factor when using boro/boro filters. Because the extra short-wavelength light in quartz/boro testing drives the chemistry faster (due to higher energies), a test run at the same irradiance, for example 0.55 W/m^2 @ 340 nm, with both quartz/boro and boro/boro filters will progress faster in the quartz/boro filtered test than in the boro/boro filtered test. However, the reliability of the test will be greater in the boro/boro test, due to the better match to sunlight. Even with the loss of speed, the boro/boro filters are recommended over the quartz/boro filters because false results obtained quickly are potentially very damaging.

19.5 TEST CYCLES

Once the light source is chosen, the next most important consideration for accelerated weathering is the choice of the test cycle. This brings into play the variables of temperature and water. To some extent, the choice of light source limits the choice of test cycles, as the fluorescent light sources are typically run in machines that allow for significantly less control

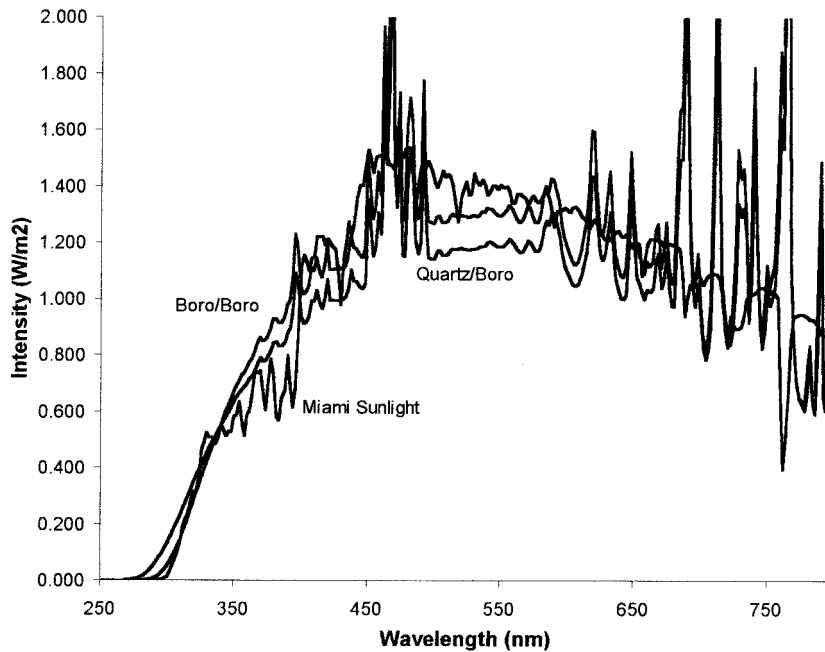


FIGURE 19.14 Spectral power distribution of filtered xenon arc light sources. Miami sunlight is shown for reference. [Data: Atlas Materials Testing Technology, LLC]

over the environmental parameters. Many of the most common cycles have been codified in specifications by various standards committees, such as ASTM, ISO, and SAE (see Table 19.2).

One of the most general accelerated weathering specifications is ASTM G26, which calls for the use of filtered xenon arc light. A typical xenon arc weathering machine of the type that can execute ASTM G26 is shown in Figure 19.15. G26 allows the user(s) to specify the duration of the light and dark cycles and the water spray and dry cycles. This differs from

the rigor of the SAE standards such as J1960, which specify all of the test conditions. SAE J1960 is the standard automotive accelerated weathering test protocol. It requires the use of quartz/boro filtered xenon arc light. The cycle is two hours of light followed by one hour of dark. Water is sprayed on the back of the panels during the dark cycle and on the front of the panels for 20 minutes of the light cycle. Irradiance is set at 0.55 W/m^2 @ 340 nm and the black panel temperature is 70°C during the light cycle.

Many applications still specify a test protocol using fluorescent light sources, the most popular of which is SAE J2020. This test procedure calls for cycles of eight hours of light at 0.43 W/m^2 @ 310 nm at 70°C , followed by four hours of dark with condensing humidity at 50°C . These tests are typically run with FS-40 (313 nm peak, also called UV-B) bulbs and less commonly, but preferably, with 340 nm peak irradiance (UV-A) bulbs. A typical machine that uses a fluorescent light source is shown in Figure 19.16.

Regardless of the type of exposure, the duration of exposure must be set such that the test time is representative of the time in service. Exact correlations, known as acceleration factors, are difficult to determine. Acceleration factors are the multiple over which the accelerated test weathers the sample com-

TABLE 19.2 Standard Weathering and Appearance Test Standards

| Test Method | Standard |
|--|-----------------------------|
| Static Outdoor Exposure | SAE J1976, ASTM D1014 |
| Accelerated Outdoor Exposure (Fresnel) | SAE J1961, ASTM G90 |
| Accelerated Xenon Arc Exposure | SAE J1960, ASTM G26 |
| Accelerated Fluorescent Exposure | SAE J2020, D4587, ISO 11507 |
| Paint Adhesion | ASTM D3359 |
| Paint Color Change | ASTM D2244 |
| Gloss | ASTM D523 |



FIGURE 19.15 Typical xenon arc type weathering chamber. (Picture courtesy of Atlas Materials Testing Technology LLC)

pared to a standard outdoor exposure. Part of the difficulty is that one material may have an acceleration factor of eight compared to Florida in a given test, while another may have an acceleration factor of 12. In addition, the acceleration factor may differ for a given material depending on the property being evaluated, such that one weathering protocol may give an acceleration factor of 10 for yellowing of a material, but an acceleration factor of 15 for gloss loss of

the same material. Thus, correlating a given amount of time in an accelerated weathering device to the time in, for example, Florida is risky.

This difficulty in correlating times between accelerated tests and outdoor exposure is fundamentally a problem of competing reactions that are accelerated at different rates. That is to say, the many different chemical reactions that take place during weathering all have different activation energies (temperature



FIGURE 19.16 Typical fluorescent lamp weathering chamber. (Picture Courtesy of Q-Panel Company)

sensitivity) and wavelength sensitivities. Because the conditions inside a weatherometer are different than in Florida, the balance of reactions is often different. The biggest difference is typically the mismatch between the wavelength distribution of natural sunlight and the light present inside a weathering chamber. If shorter-than-natural wavelength light is present in the accelerated weathering device, chemical changes can occur that will not occur during outdoor exposure. Some materials may be affected greatly by the presence of the short-wavelength light and some may be affected very little. Thus, the acceleration factors

for different materials can be distorted greatly by having a mismatch between natural sunlight and the light source in the weathering device.

Another complicating factor comes from choosing the environment one is trying to reproduce. The nominal goal is typically Florida, but not all failure modes are manifested most quickly during Florida exposure. In addition, Florida exposure is in itself non-reproducible, as annual fluctuations occur in all of the meteorological variables. Building this variability into accelerated testing will be challenging and is currently a topic of important research.¹⁰

19.6 POST-EXPOSURE TESTING

Exposure of test specimens is only the first step toward evaluating their weathering performance. The second step is to choose which properties to evaluate and how to evaluate them. For materials like coatings that serve a decorative function, the most important properties to evaluate are optical—gloss, distinctness of image (DOI), color, chalking, yellowing and others. Because these are the properties on which the customer or end user will judge the performance of the coating, the manner in which the characteristics change with weather exposure is important.

While a coating's main function is decorative, some of the most important failure modes are mechanical and occur with little warning. These failure modes can include cracking and delamination. To anticipate these failures, appearance tests alone will not suffice, and functional properties such as strength and adhesion must also be evaluated as a function of weather exposure. These properties are affected due to the chemical composition changes that occur in materials as they weather. Because only the exterior surface is exposed to all of the weathering elements, the properties of an exposed material can often be non-uniform. For example, a coating may embrittle and change color at the surface, but be close to pristine deeper into the coating layers. These gradients can have profound impacts on the mechanical performance of the coating.

19.6.1 Appearance Testing

A variety of tests exist to measure the appearance of coating, and this brief outline is not meant to be exhaustive. Complete details are collected in other works.¹¹

A change in the color of a coating is often caused by chemical composition changes of either a resin or pigment in the material formulation. These color shifts can be quite noticeable, especially if the color changes unevenly or if one component is next to another component with the same nominal color, for example, the fender and bumper of a vehicle. Color changes are typically measured with a colorimeter. The change in color ΔE^* can be measured using ASTM D2244. A person's eye is typically capable of discerning ΔE^* values greater than 0.5.

For most coatings, the change in surface roughness usually results in a change in gloss. Gloss is defined as the ratio of the intensity of a specular reflection to the intensity of the incident radiation. As the

surface of a coating becomes rougher, more of the light is reflected in off-specular directions, leading to a perceived dulling of the surface. This surface roughening is due to chemical degradation of the surface, followed by removal of the surface material by, for example, rain or washing. Thus, the presence of liquid water is important in the reduction of gloss. Panels weathered for equivalent times in Florida and Arizona typically show a much greater gloss loss in Florida due to the removal of the most heavily degraded surface material by rain. This degraded material stays on the surface in Arizona, leading to a smoother (but more chemically changed) surface.³

For coatings, adhesion to the substrate or underlying paint layers is one of the most important physical characteristics, and one of the properties most susceptible to deterioration by weathering. For this property, both the action of moisture and UV radiation are important. Unlike optical properties, adhesion cannot be tested non-destructively. The most common methods for adhesion measurements are through cross-hatching or scribing the sample and then using tape to remove poorly adhering material. Samples are often preconditioned in water or humidity after weathering and before adhesion testing to increase the severity of the test. This method is detailed in ASTM D3359.

Other optical properties can also be measured which can be important for a given application. These properties and the most relevant standards are given in Table 19.2.

19.7 NON-TRADITIONAL MATERIAL EVALUATIONS

While evaluation of easily observable appearance properties provides data regarding the performance of the material to-date in a weathering test, they provide little information about the future, as some weathering-induced failures can be quite sudden and occur with little prior warning. To anticipate these types of weathering-induced failures, new evaluation methods are being developed.

19.7.1 Chemical Metrics of Weatherability

Because the majority of the physical changes that a material undergoes during the weathering process are driven by chemical composition changes, following the chemical composition change of the material itself would intuitively seem like a logical method of quantifying the weatherability of a material. With re-

spect to Figure 19.2, the changes brought about by photo-oxidation should be measurable as an increase in the oxygen content of a material. While oxygen content itself is an imprecise measure of weatherability, the incorporation of oxygen into various functional groups in an organic material is readily measurable by infrared spectroscopy. These chemical composition changes typically progress monotonically during exposure and, thus, make reliable metrics for weatherability.¹²

Because one often wishes to compare the performance of different coatings or materials for the same application, any chemical composition change metric should be generic, such that it can be used to compare materials of disparate initial composition. One such technique uses Fourier Transform Infrared Spectroscopy (FTIR) to measure the concentration of –OH- and –NH-containing groups in a coating. The concentration of these function groups typically increases during weathering because they are products of the photo-oxidation process and, to a lesser extent, hydrolysis. Those coatings, whose concentration of –OH- and –NH-containing groups increase rapidly, typically weather poorly compared to those coatings that undergo slow chemical composition change.¹²

Another chemical metric of a coating's long-term weathering performance is the effectiveness and longevity of stabilizer additives in the coating. Many coatings contain a number of additives to help improve the coating's long-term weatherability. These additives include ultraviolet light absorbers (UVAs), hindered amine light stabilizers (HALS), and antioxidants. By measuring the concentration of these additives, insight can be gained into the long-term weathering performance. For example, if adequate weathering performance of a coating system is dependant on the presence of UVA in the topcoat, then the rate at which the UVA is depleted will have a direct impact on the long-term performance. Simple UV spectroscopy experiments can be used to measure the concentration of UVA in a coating as a function of weathering time.¹³

Additional weathering-related information can be obtained by determining not just the concentration and longevity of stabilizer additives, but also the physical distribution of those additives in a coating. Both UVAs and HALS can only protect a coating if they are present in the part of a coating that is being exposed. These additives typically get depleted at the surface of a coating, the very place they are needed most. Microtomy techniques can be used to measure the distribution of both UVAs and HALS in

a coating by successively slicing off thin layers of the coating, which can then be chemically analyzed for the presence of UVAs or HALS. The microtomed slices can be placed in a UV spectrometer for UVA analysis. By oxidizing the slices with peracid, the concentration of HALS can also be determined using electron spin resonance (ESR) spectroscopy. The infrared spectra of those same slices can be used to map the distribution of photo-oxidation (–OH- and –NH-containing groups) in the polymer, thus, providing a complete picture of degradation and additive longevity as a function of depth in a complete paint system.¹²

19.7.2 Mechanical Tests

In addition to the chemical means of anticipating long-term weathering performance, some specialized mechanical tests can be used to predict certain failure modes. For cracking failures, the use of fracture mechanics has proven to be useful in determining the propensity of a material (coating or plastic) to crack during weather exposure. This technique quantifies the brittleness of a material, termed the fracture energy, which can be measured as a function of weathering time.¹⁴ If the loads a material is subject to during weathering are known, then a time to failure can be estimated. This allows for the construction of failure envelopes that incorporate such parameters as coating thickness, process history, time, stresses, and weather exposure.

19.8 FURTHER READING

Interested readers are encouraged to read the articles cited in this chapter or a number of other quality texts which provide additional details on a variety of the topics mentioned in this chapter.^{11,15,5}

19.9 REFERENCES

1. Emanuel, N. M., Denisov, E. T., and Maizus, Z. K. *Liquid Phase Oxidation of Hydrocarbons*. New York: Plenum Press, 1967.
2. Nguyen, T., Martin, J., Byrd, E. and Embree, N. *J. Coat. Tech.*, 74, 65, (2002).
3. Nichols, M. E., and Gerlock, J. L., unpublished data.
4. Hill, L. W., *Mechanical Properties of Coatings*. Blue Bell, PA: Federation of Societies for Coatings Technology, 1984.
5. Schoff, C., *J. Coat. Tech* in press.
6. Nichols, M. E., and Darr, C. A., *J. Coat. Tech.*, 70, 141, (1998).

7. Bauer, D. R., *Polym. Deg. and Stab.*, 69, 297, (2000).
8. Gerlock, J. L., Peters, C. A., Kucherov, A. V., Misovski, T., Seubert, C. M., Carter III, R. O., and Nichols, M. E., *J. Coat. Tech.*, 75, 35, (2003).
9. Bauer, D. R., Gerlock, J. L., Mielewski, D. F., Paputa-Peck, M. C., and Carter III, R. O., *Polym. Deg. and Stab.*, 28, 39, (1990).
10. Martin, J. W. In *Service Life Prediction Methodology and Metrologies*. J. W. Martin and D. R. Bauer, Eds. Washington DC: American Chemical Society, 2001.
11. Koleske, J. V., Ed. *Paint and Coatings Testing Manual*. Philadelphia: ASTM, 1995.
12. Gerlock, J. L., Kucherov, A. V., and Nichols, M. E., *J. Coat. Tech.*, 73, 45, (2001).
13. Smith, C. A., Gerlock, J. L., and Carter, R.O. III, *Polym. Deg. and Stab.*, 72, 89, (2001).
14. Nichols, M. E., *J. Coat. Tech.*, 74, 39, (2002).
15. Wypych, G. *Handbook of Material Weathering*. Toronto: ChemTec, 1995.

Mitchell R. Dorfman

Global Turbine Sales Support, Sulzer Metco (US) Inc., Westbury, New York

| | | | |
|---|-----|---------------------------------|-----|
| 20.1 INTRODUCTION | 405 | 20.6 GENERAL APPLICATIONS | 416 |
| 20.2 THERMAL SPRAY BASICS AND PROCESSES | 406 | 20.7 MISCELLANEOUS APPLICATIONS | 421 |
| 20.3 MATERIALS CONSUMABLES | 410 | 20.8 COATING SELECTION | 421 |
| 20.4 MANUFACTURING PROCESSES | 411 | 20.9 SUMMARY | 421 |
| 20.5 THE FUNCTION OF A COATING AND ITS APPLICATIONS | 412 | 20.10 REFERENCES | 422 |

20.1 INTRODUCTION

Thermal spraying is an established industrial method for the surfacing and resurfacing of engineered components.¹⁻³ Metals, alloys, metal oxides, metal/ceramic blends, carbides, wires, rods and various composite materials can be deposited on a variety of substrate materials to form unique coating microstructures or near-net-shape components. Thermal spray coatings provide a functional surface to protect or modify the behavior of a substrate material and/or component. A substantial number of the world's industries utilize thermal spray for many critical appli-

cations.⁴ Key application functions include restoration and repair; corrosion protection; various forms of wear such as abrasion, erosion and scuff; heat insulation or conduction; oxidation and hot corrosion; electrical conductors or insulators; near-net-shape manufacturing; seals, engineered emissivity; abrasible coatings; decorative purposes; and more.

Thermal spray processes are easy to use, cost little to operate, and have attributes that are beneficial to applications in almost all industries. The benefits are typically lower cost, improved engineering performance and/or increased component life (Figure 20.1).

- Resist Wear
- Retard Corrosion
- Manage Thermal Efficiency
- Enhance Electrical Properties
- Control Dimensions & Clearances
- Salvage Worn Components



Reduce Cost Through

- *Better Performance*
- *Longer Component Life*
- *Decreased Maintenance*

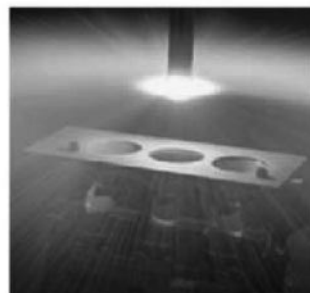


FIGURE 20.1 The benefits of thermal spray coatings.

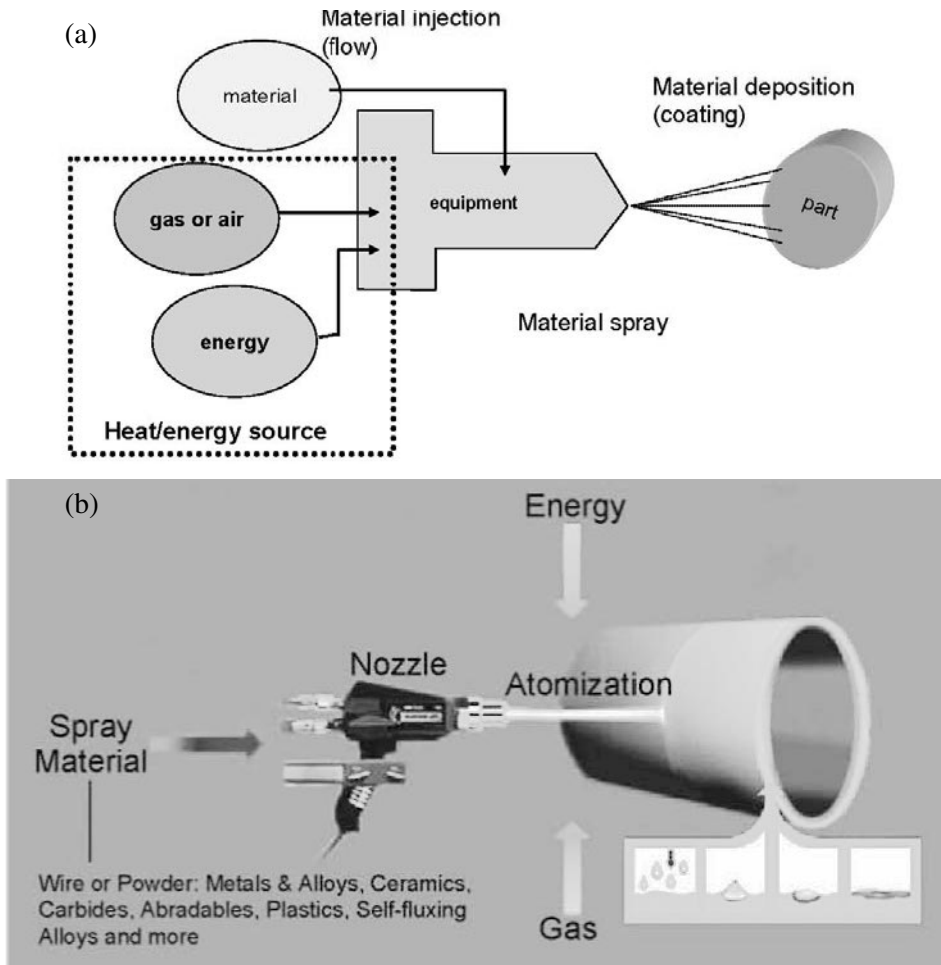


FIGURE 20.2 (a) Heat/energy source requirements. (b) Principle of thermal spray coatings.

20.2 THERMAL SPRAY BASICS AND PROCESSES

Figures 20.2(a) and 20.2(b) show the requirements for thermal spray—a heat/energy source and consumable materials.^{2,5} Gases, along with air in some cases, are needed to inject materials into the gun and to generate the necessary heat for melting. The high gas velocities associated with these processes cause material to be propelled as fine molten droplets which strike the part, solidify, and adhere. The mechanism of bonding is mostly mechanical, but in some cases is also metallurgical. The result is that each layer bonds tenaciously to the previous layer, forming a lamellar “pancake-like” splat structure. The properties of this coating are directly dependent on the combination of kinetic and thermal energy. Figures 20.3(a) and 20.3(b) show the various types of thermal spray processes in the marketplace today.

A summary of typical flame temperatures and particle velocities for the various processes are shown in Figure 20.4.

Five basic thermal spray processes are available commercially, and one new process is still in its infancy. Flame spray powder/wire, detonation, and High Velocity Oxygen Fuel (HVOF) are three of the basic processes associated with combustion. Plasma and wire arc are two other processes that utilize electric energy to help melt consumable materials. Of these five processes, HVOF and detonation spraying are two that result in high bond strength with extremely dense microstructures. Plasma coatings are also known to have high bond strength with relatively dense oxide-free microstructures when sprayed in either Low-Pressure Plasma Spray (LPPS) or Vacuum Plasma Spray (VPS) Systems.

Cold Spray is a new process that relies more on high velocity and kinetic energy and less on thermal

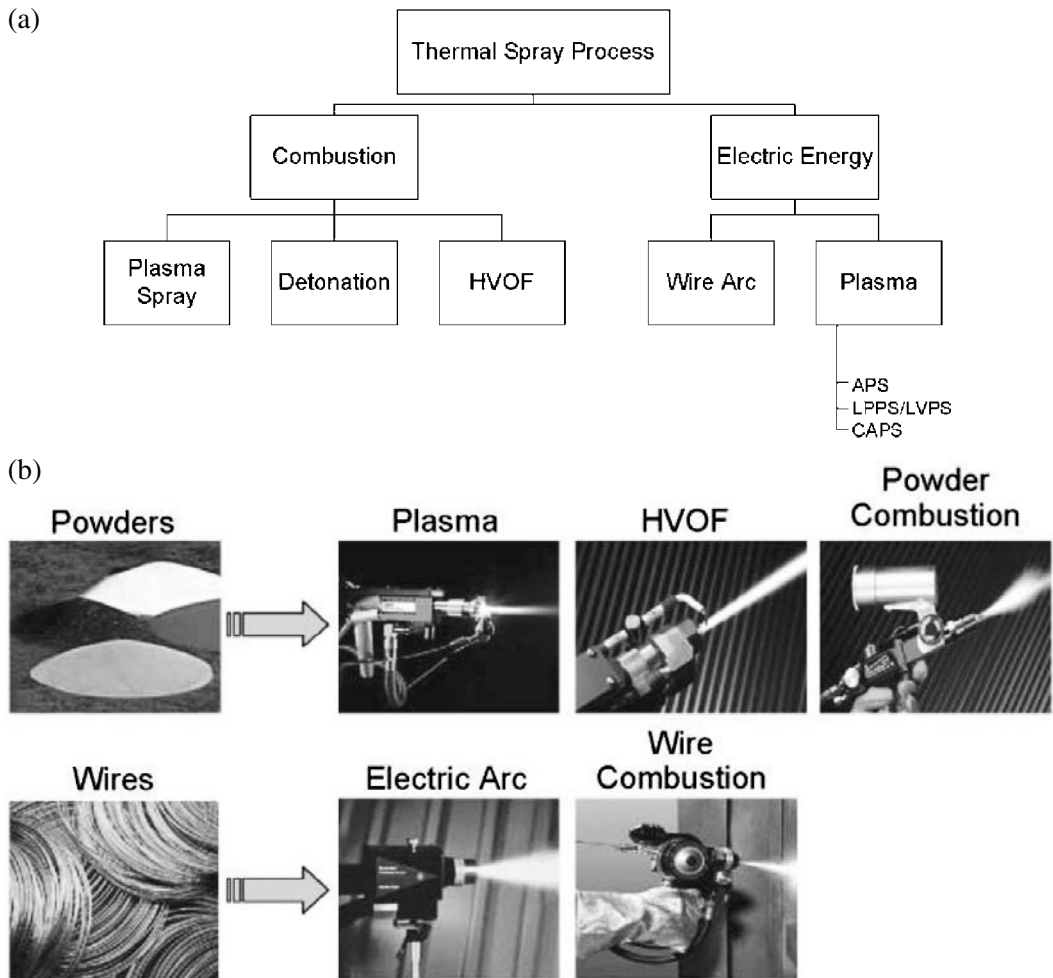


FIGURE 20.3 (a) Types of thermal spray processes. (b) Thermal spray materials and processes.

energy. Particle temperatures are lower than HVOF, but velocities are higher, enabling coating structures that resemble bulk wrought materials.

20.2.1 High Velocity Oxy-Fuel Processes

The newer HVOF guns generate an internal combustion jet with gas velocities that can exceed 2,100 m/sec (7,000 ft/sec), compared to older systems that approach 1,360 m/sec (4,500 ft/sec). The high gas velocities cause particle velocities of around 400–800 m/sec (1,320–2600 ft/sec), which is significantly higher than low velocity combustion processes. Combustion fuels include propylene, propane, natural gas, hydrogen, acetylene and kerosene.

The major advantage of this higher kinetic energy process is that coatings with greater density are possible. Other benefits include increased thickness ca-

pability, smoother surface finishes, lower oxide levels, and less effect on the environment (reduced decarbonization, oxidation and loss of key elements by vaporization). HVOF processes are suitable not only for applying Tungsten Carbide-Cobalt and Nickel Chromium-Chromium Carbide, but also for depositing wear and corrosion alloys such as Inconel (NiCrFe), Triballoy (CoMoCr) and Hastelloy (NiCrMo) materials. HVOF MCrAlY (M = Ni, Co or Fe) coatings are also replacing some LPPS coatings for high temperature oxidation, hot corrosion and thermal barrier bond coat applications for repair and restoration of existing components.

HVOF systems operate by injecting powder into a stream of burning gases. The material melts or softens and is propelled against the substrate. A characteristic of most HVOF guns is the multiple shock diamond pattern that is visible in the flame.

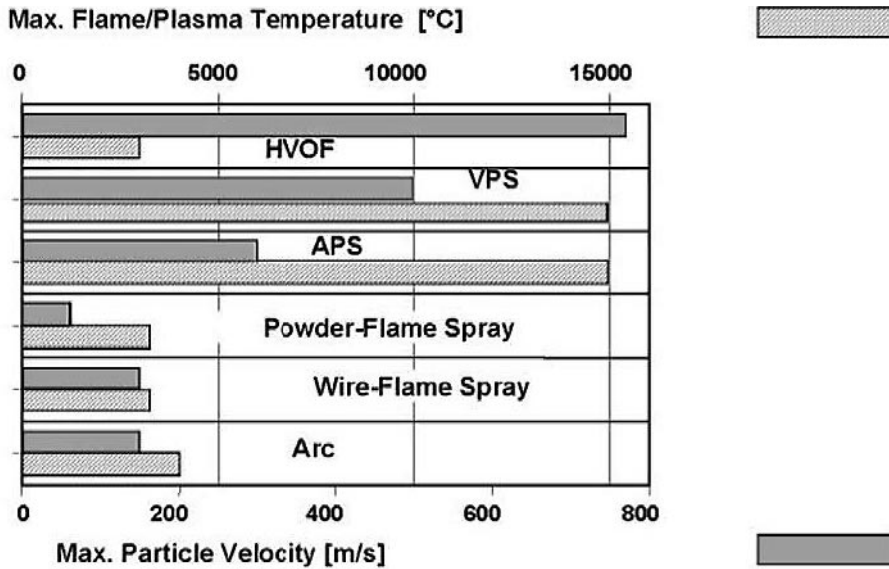


FIGURE 20.4 Thermal/kinetic energy comparison.

Upon exiting the nozzle, compressed flame gases undergo free expansion, thereby generating a supersonic jet.

Many HVOF devices are available. Although similar in design intent, gun design concepts are different. The designs vary by the type of gases, nozzle configuration, weight of the gun, particle injection method, and efficiency and type of cooling.

One type of gun design is the Diamond Jet Hybrid gun from Sulzer Metco, Inc. In this type of system, the oxygen fuel mixture consists of propylene, hydrogen, natural gas or propane. Fuel gases are mixed in a proprietary siphon system in the front portion of the gun. The mixed gases are injected from the nozzle and are ignited external to the gun. Ignited gases form a circular flame configuration, which surrounds the axially injected powder. The combustion gases, along with the heated powder, are accelerated further through the converging-diverging nozzle to hypersonic velocities.

20.2.2 Detonation Gun (D-Gun)

The D-Gun was developed in the 1960s at Union Carbide (Praxair Surface Technologies). The gun development was proprietary to Union Carbide, and coated parts and services were provided to many industrial segments and applications. One major benefit of the detonation process was that carbides could be applied to components with excellent bond strengths, hardness and density.

The detonation process is based on repetitive explosions or detonations of oxygen-fuel gas mixtures, rather than the continuous burning of a combustion flame, as in the HVOF process. Oxygen and acetylene are loaded into a long, water-cooled barrel with powder. The mixture is ignited and it explodes.

D-Gun coatings are applied in aerospace, industrial gas turbine (IGT) and a variety of industrial applications. Although D-Gun coatings have higher coating quality than slower velocity processes, HVOF processes have replaced the D-Gun for less stringent repair applications.⁶ In addition, the D-Gun is proprietary, and as a result, end users and designers need to send components out to have coatings applied. The result is longer production lead times when compared to in-house production capability.

20.2.3 Low Velocity Combustion

Both wire and powder flame spraying are based on the heat generated by the combustion of an oxygen fuel flame (oxy-acetylene, oxy-hydrogen or oxy-propane) to melt the spray materials. Combustion flame temperatures are around 3,000 °C (5,430 °F), but may vary somewhat depending on the specific gas and fuel ratios.

Particle velocities are low, typically around 40–100 m/sec, and vary with particle density, shape and surface texture. The low particle velocity results in coatings that generally have higher porosity levels and greater levels of oxides within their microstruc-

ture than other thermal spray processes. The slower particle velocity results in greater oxidation and decomposition of critical elements. In spite of these limitations, low velocity combustion processes have been successful in many applications.

An application in which combustion coatings are used is in clearance control coatings. In the case of abradable seal systems, the porosity helps to weaken the cohesive strength of the coating and allows for micro-rupture. Some customers recognize that low velocity combustion might not be the optimum choice of processes for an application, but may select combustion spray anyway because of the lower cost. Nickel-Graphite and Nickel Chromium Aluminum Bentonite coatings have been used for years in the aerospace industry. Today, more applications in the IGT sector are going to clearance control systems.

The combustion process involves either wire or powder. In the wire process, a flame gun pulls the wire into the combustion flame by means of an electric motor or a self-contained, variable-speed, air-driven turbine. A high-pressure air stream constricts the combustion flame and atomizes the molten tip of the wire, forming a metal spray stream.

The powder process is based on the same principles as the wire process, except that powder is the feedstock. In a powder flame spray gun, powder feedstock is fed into the combustion flame by a suction/gravity mechanism or a positive-pressure feeding system operated by a carrier gas. The combustion flame melts and propels the powder onto the substrate. One advantage of powder over wire is the wider range of materials in the market.

A typical gun used today in the thermal spray industry is the Metco 6P-II. The main function of this gun for turbine applications is abradable seal systems. Typical production times to spray seal segments may be over four hours and have 2–3 mm (0.08–0.12 in.) of coating. Typical spray rates are 4.5 kg/min (6–10 lb/h).

20.2.4 Twin Wire Arc Process

In the electric arc process, two electrically conductive wires are continuously brought into contact with each other at a predetermined angle. An arc is struck between the two wires when a voltage is applied. Temperatures approach 4,000 °C (7,230 °F) and particle velocities approach 50–150 m/s (140–540 ft/sec). The arc melts the tips of the wires and the molten metal is atomized by a continuous flow of air or a non-oxidizing gas (nitrogen, helium or argon).

Controlled feed rates of the wire ensure uniform melting.

Benefits of the arc process are that it is easy to use, simple to learn, portable and easy to maintain. The arc process also yields higher deposition rates and, in general, has higher bond strengths than low velocity combustion coatings. It also provides thicker coatings and lower operational costs than plasma. Other benefits are its ability to spray materials at high spray rates, relatively cool substrates and lower consumable costs than other processes.

One key application is in the aerospace industry.⁷ Here, Nickel Aluminum, Nickel-Chromium Aluminum, Inconel and Hastelloy wires are being used for dimensional restoration and repair of many different types of jet engine components. The Sulzer Metco SmartArc is just one example of electric arc equipment that is used for part restoration.

20.2.5 Plasma Deposition

In the plasma process, an electric arc is generated between a water-cooled tungsten electrode and an annular water-cooled copper anode. Plasma guns run on direct current; when an arc is struck between the electrode and the nozzle to complete the circuit, gases are typically dissociated and ionized, forming the plasma. A primary gas such as nitrogen or argon, in combination with a secondary gas such as hydrogen or helium, is heated and ionized to create the plasma “flame.” The energy is released when electrons drop to lower energy states and ions recombine. Although either nitrogen or argon can serve as the primary plasma gas, each has its own unique characteristics that may play a role in the success of the application.

Typical plasma gas temperatures range from 500–25,000 °C, depending on the gas mixtures, with particle velocities of 80–300 m/sec. Other key process variables that affect melting include nozzle diameter, powder port size and injection angle, gas velocity, feed rate and kW power settings (amperage and voltage). A secondary gas may be added to raise heat content and/or maintain constant voltage.

A benefit of the plasma process is its versatility in changing flame temperatures and particle velocities. This versatility enables a wider selection of material chemistries and particle size distributions. Furthermore, the high temperatures associated with plasma allow for the deposition of high melting point ceramics such as Yttria-stabilized Zirconia. These material systems are important in industrial gas turbine (IGT) components such as combustors and liners.⁸

Plasma guns seen in the thermal spray industry for spraying complex components include low and high power guns that can spray not only external surfaces, but internal surfaces as well. The correct equipment, along with proper robotic programming, is critical to the application success of thermal spray coatings.

20.2.6 Low Pressure Plasma Spraying (LPPs)

For more advanced applications in which plasma coating density needs to approach that of wrought alloys, LPPs and Vacuum Plasma Spray (VPS) systems are good choices. These systems represent a high capital expenditure, but the technical benefits, performance and cost per part for OEM components are excellent.

LPPs and VPS coatings typically have high bond strengths with very low levels of porosity and oxides. High quality coatings are achieved by placing a plasma gun in a reduced pressure between 50–200 mbar. Major applications for LPPs spraying are MCrAlY bond coats for thermal barriers, MCrAlY coatings for blades/vanes and buckets for oxidation and hot corrosion, and repair of superalloy components.

Typically, systems are highly integrated, fully automated and include preheating and cleaning of the component surface prior to coating deposition. When carried out in a vacuum, the parts can be processed in a stress-free condition without oxidation.

20.3 MATERIALS CONSUMABLES

The properties of a thermal spray coating are based on its microstructure characteristics, and these depend on both the material and the deposition method.⁹ Materials with identical chemistries may yield coatings with completely different properties. One of the main reasons for the number of different products with “similar chemistry” is the different design requirements imposed by the original equipment manufacturer (OEM).

Material properties can be affected by the manufacturing process, particle size, purity, crystallographic structure and particle shape. These differences can also influence application performance and final product price. For example, powders designed with narrow or very fine particle distributions are generally more expensive because manufacturing yields are typically lower. The user must determine

the characteristics most important for a particular application, and balance the commercial aspects of depositing a coating relative to its technical benefits. The result is that major manufacturers carry a wide selection of thermal spray materials in inventory.

Types of thermal spray materials include those for clearance control, thermal barrier coatings, wear resistance, and salvage and repair. Materials may be classified according to several characteristics, as described below.

20.3.1 Abradables

Abradables provide clearance control in high-speed applications in which near-zero clearance between moving parts is required. Types of abrasives include Aluminum Silicon-Polyester, Aluminum Silicon-Graphite, Nickel Graphite, Nickel Chromium Aluminum-Bentonite, Aluminum Bronze-Polyester, and MCrAlY-BN-Polyester.

20.3.2 Pure Metals, Alloys and Cermets

Pure metals, alloys, and cermets provide surface enhancement, corrosion, oxidation, abrasion resistance, electrical resistance and shielding. Types of materials include, but are not limited to, Copper, stainless steel, Molybdenum, Nickel-Aluminum, Inconel, MCrAlY, and blends of metal oxides such as Alumina and Nickel Chromium.

20.3.3 Carbides

Carbides improve surface hardness and add wear resistance. They include Tungsten Carbide-Cobalt, Tungsten Carbide-Cobalt Chromium, Nickel Chromium-Chromium Carbide, and blends of carbides and self-fluxing alloys.

20.3.4 Ceramics

Ceramics produce surfaces that either resist oxidation, abrasion, sliding wear, high-temperature corrosion, or that provide thermal insulation or electrical insulation. These include Aluminum Oxide, Chromium Oxide, Titania, Alumina-Titania, and Zirconium Oxide stabilized with either Calcia, Magnesia, Ytria or Ceria.

20.3.5 Self-Fluxing Alloys and Blends

Self-fluxing alloys and blends typically produce dense coatings that metallurgically bond with the substrate. They form non-porous protective finishes resistant to abrasion, cavitation, fretting particle ero-

sion and corrosion. Nickel Cobalt Chromium-Boron-Silicon-Carbon alloys and Carbide blends are examples of these types of material systems. Elements such as Silicon help to lower the melting point, while elements such as Carbon and Boron also act to change hardness.

20.3.6 Polymers

Polymers are specified by their chemistry, morphology, molecular weight, melt-flow index, particle size, and heating/cooling (melting) characteristics.¹⁰ Thermoplastics amenable to thermal spraying are polyethylene (PE), PE copolymers, polyesters, nylon, fluoropolymers, polymethyl methacrylate (PMMA), polyester etherketone (PEEK), and polyphenylene sulfide (PPS). Suitable application areas include low-friction applications, chemical resistance and sealing.

20.3.7 Thermal Spray Wires (arc and combustion)

Thermal spray wires (arc and combustion) are designed for general purpose dimensional restoration, cosmetic resurfacing, and anti-corrosion barriers. Types of materials include Zinc, Aluminum and Nickel-Aluminum.

20.4 MANUFACTURING PROCESSES

There are many methods for manufacturing thermal spray materials. Some of these methods combine two or more methods. The key is to develop a manufacturing method that allows materials to be deposited economically with performance consistency and reliability. Key methods include spray drying, cladding, sintering, fused and crushed, attrition milling, chemical methods, gas and water atomization, blends and plasma densification. A quick overview of some key manufacturing processes are listed below.

20.4.1 Spray Drying

A *Sol*, or slurry of one or several fine materials of similar size (1–10 μm) is atomized through a fine nozzle and sprayed into a heated (400 °C / 750 °F) chamber. The dried particles are *spherical and porous*, sized in the 5–250 μm range. Fine powders (1–10 μm) can be agglomerated by using a binder and spray drying. This creates a relatively inexpensive, free flowing, spherical composite particle. The spray dried powders are then classified by screening

and/or cyclonic separation. Figure 20.5 is a cross-section and SEM photomicrograph of a typical spray dried ceramic.

20.4.2 Plasma Densification

This is a process whereby an agglomerated powder is injected into high energy plasma and melted. The molten droplets are sprayed into a water-cooled chamber and collected for classification. Plasma densification alloys the agglomerated particles into a dense, homogenous powder. These densified powders produce premium coatings needed in the turbine industry. Hollow Oven Spherical Powder (HOSP) combines the flow ability benefits of spherical spray dried materials with the alloying advantage of fused materials.

20.4.3 Chemical and Mechanical Cladding

Mechanical clad processes use an organic binder to “glue” small particles to a larger core particle. A slurry of binder, core material, cladding component and water are mixed in a heated chamber. Chemical cladding is the reductions of salts or some other proprietary chemical reaction process to form a continuous layer of approximately 2–5 microns thickness on to a metallic or non-metallic core.

20.4.4 Sintering

A process where heat and pressure cause the particles to fuse to each other (typically WC-Co and metal oxides). The density and flow properties of the material will vary due to the time-temperature relationship during material processing.

20.4.5 Blending

Mechanical blending is a simple, low cost method used to produce multi-component powders.

20.4.6 Gas/Water Atomization

This method is used to produce various metallic thermal spray powders. Metals are combined and melted (e.g., in an induction furnace), fed through a nozzle into the atomization tank forming fine droplets, cooled by high pressure fluids (gasses or water) and collected in a water-cooled chamber. Gas-atomized materials are typically cleaner, spherical, and contain less oxygen. Water-atomized products are less expensive to manufacture and in some cases are more irregular in shape. There are typically more impurities with water-atomized products.

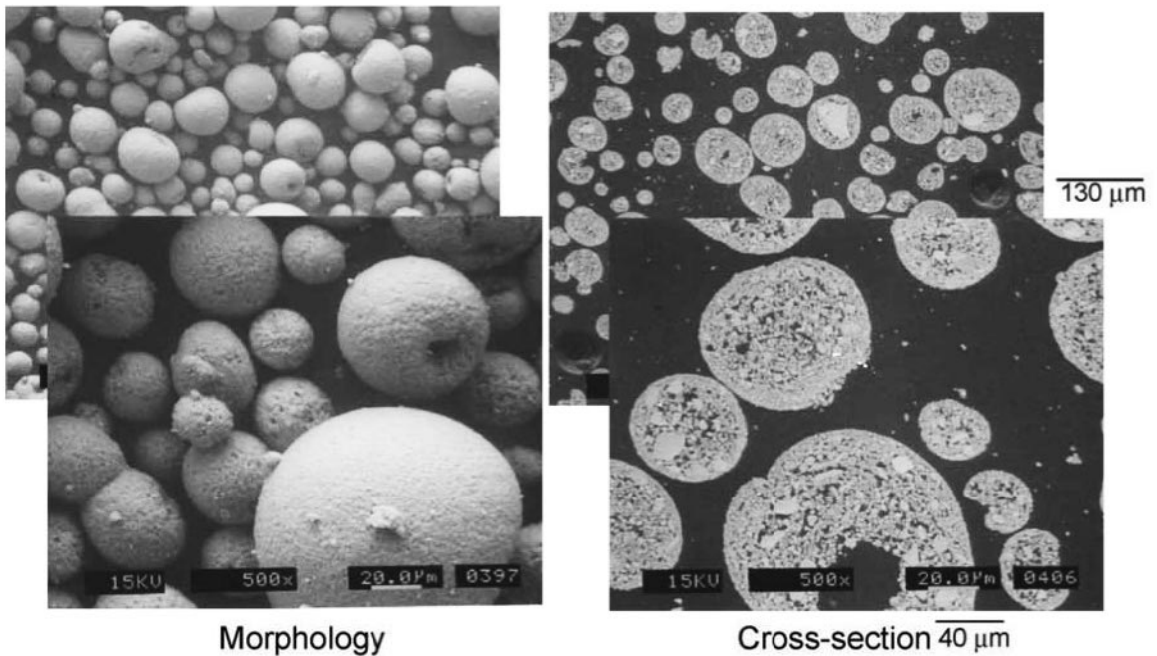


FIGURE 20.5 SEM and cross-sectional photomicrograph of YSZ powder.

20.4.7 Fused and Crushed

Ceramic materials are typically fused using an induction arc furnace. Crushing is possible and used primarily for ceramics and brittle metals. Large cast blocks or rods of raw material are crushed by mechanical force producing angular, irregular shaped particles. Crushed particles (10–44 (m) may be screened for use or milled to smaller sizes (<0.1 (m). Milling may be by either rod, ball or fluidized bed methods. When using rod or ball milling, care must be taken so that the grinding media does not contaminate the finished product. Examples include alumina and spinels.

20.4.8 Attrition Milling

This is similar to cladding, except that there is no organic binder. Mechanical energy causes fine raw materials to adhere to a larger core material. Typically, “balls” are used to cause the mechanical welding of the two materials.

20.5 THE FUNCTION OF A COATING AND ITS APPLICATIONS

Applications for thermal spray processes and materials have a broad range across all industrial sectors.^{11–15} Thermal spray processes are easy to use, cost little to operate, and have coating attributes that

are beneficial to applications in various industries. Applications include coatings for wear prevention, dimensional restoration, thermal insulation and control, corrosion resistance, oxidation resistance, lubrication films, abrasive actions, seals, biomedical environments, electromagnetic properties, etc., and the manufacturing of free-standing components, spray-formed parts and nanostructured materials. The following sections will discuss turbine and industrial applications.

20.5.1 Turbine Applications

Good examples of why coatings are used can be seen in the aerospace and IGT markets. In these markets, heat insulation, hot corrosion/oxidation resistance and abrasability are important. Today, engines require closer internal tolerances, higher rotational speeds and higher turbine inlet temperatures in order to improve engine efficiencies. In the past, overall IGT engine efficiency for simple cycle engines was approximately 35%. However, newer designs and the development of combined cycle engine concepts have increased efficiencies to 45–50%, with the future goal of approaching 60%. The ever-increasing requirements for more efficient turbines and reduced NO_x emissions have led to new materials, fabrication and process technologies, and surface modification techniques. However, advances in material and process technology such as directionally solidified

(DS) and single crystal (SC) alloys are currently operating near the strength limits, and material development is presently at a point of minimal return relative to the cost of research. Turbine entry temperatures and the temperature capabilities of high-temperature alloys have increased by about 745 °K and 440 °K, respectively, over the last four decades. Today, turbine blades and vanes are subjected to operating temperatures of 1,643 °K, which is why internal cooling schemes, new process technologies and coatings are important.

In the past, diffusion and overlay coatings were the two main types of coating systems used on IGT

components. These types of coatings were needed to enhance the life and performance of these engine components. Key coatings technology used over the years include slurry, pack cementation, galvanic, EB-PVD and thermal spray (air plasma, LPPS and HVOF). Figure 20.6 is a quick overview of various surface modification processes. The interaction of coating, substrate and environment is seen in Figure 20.7.

The objective of a coating is to protect the base material from oxidation, hot corrosion and wear. In addition, the application of heat-insulated resistant ceramics, typically called thermal barrier coatings

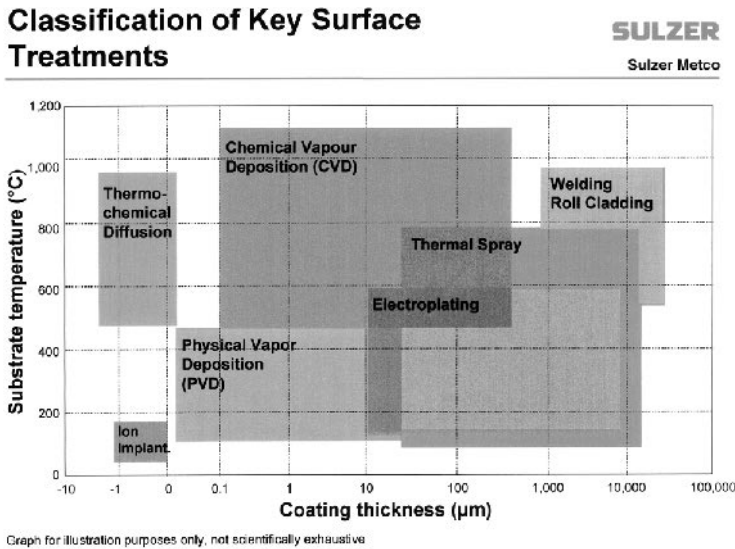


FIGURE 20.6 Classification of various surface treatments.

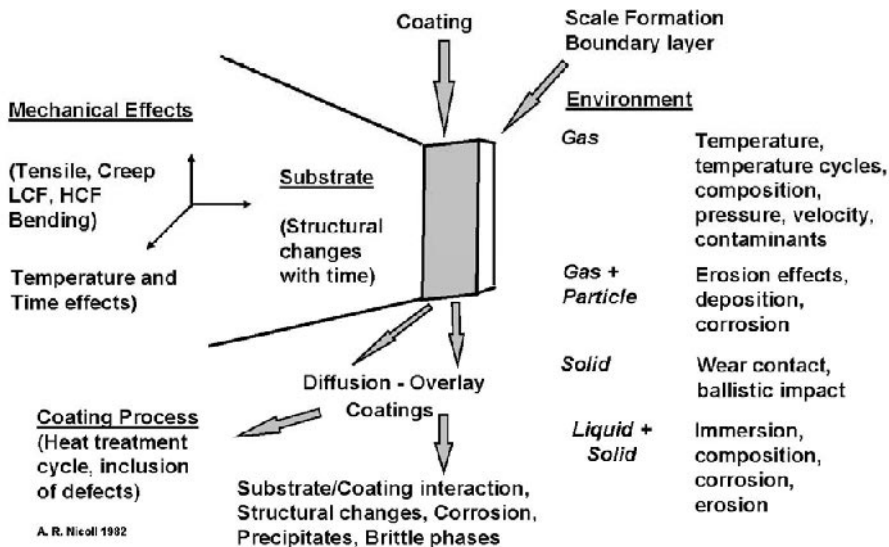


FIGURE 20.7 Interactions between the coating, substrate and environment.

(TBCs), on top of an oxidation resistant bond coat results in less heat effect on the base material. The benefits are improved mechanical properties and added life expectancy. The bond coat is typically an MCrAlY, where the M is a metal of either Nickel, Cobalt or a combination of both. Small changes in base metal temperature (100–300 °C) at these high temperatures and pressures can have a dramatic impact on a material's creep and high and low cycle fatigue resistance. Today, coatings are used in many hot section areas such as combustors, compressors and turbine sections of IGT engines. Types of components that use coatings are transition liners, combustor cans or heat shields, and various stationary and rotating blades. Future technology will incorporate the use of clearance control coatings to shroud segments. Carbide coatings are also being used as mating surfaces because of their excellent wear and fretting resistance.

The selection of coatings is based on several factors, these being service conditions that the coating needs to withstand, cost, and ease of application. Traditionally, coatings that are specified for a particular application are based on years of laboratory and field testing. Historically, the basic understanding of coatings comes from years of research and development in the aerospace industry. The aerospace industry has optimized many different types of coatings for various wear-fatigue of mid-span dampers on blades, oxidation of turbine blades, thermal barriers for combustion cans, abrasives for shroud segments, fretting materials for blade roots, and salvage and repair of bearings and shafts. Today, many of the same types of coating systems are used to improve the performance of IGT components even though some of the design conditions are different. Key differences are the size of the components, engine cycle time, chemistry of the fuel gas, material substrate chemistry, and weight limitations of the coating.

Key applications for thermal spray coatings in the aerospace and IGT segments can be seen below.

20.5.1.1 Clearance Control Coatings

Thermal sprayed abrasible seal coatings are used to control gas path clearance in gas turbine engines. The major benefits of clearance control coatings are increased engine efficiency and reduced fuel consumption. Although there are many types of coatings and methods to manufacture them, the operation of refurbishment of the seals must be simple, reliable and efficient. Thermal spray coatings meet these re-

quirements and are becoming the most popular choice for sealing. Thermal spray coatings are easily applied and can be removed by stripping, with comparable ease.

Abradable coatings must be readily abrasible (machinable) and yet resist impact erosion by ingested abrasive particles moving at high velocities. Other design criteria are thermal, chemical and microstructure stability. Coatings need to be compatible with various blading materials (Titanium, Steel, Inconel and CBN or SiC blade tips) at various incursion and rotational speeds. The majority of coatings today are used up to around 750 °C and generally use low velocity combustion or plasma as the thermal spray process of choice. However, as shown in Figure 20.8, thermal spray coatings are starting to see higher temperatures. Porous MCrAlYs, abrasibles and intermetallics are being used in the high temperature section of compressors, and ceramics are being designed in the turbine section, along with new blade tipping technology.

20.5.1.2 Heat Insulation

Thermal Barrier Coatings (TBCs) are being used to insulate gas turbine components that are subjected to excessive temperatures. Since low thermal conductivity allows these coatings to act as thermal barriers, the metal surface temperatures are decreased. Lower metal temperatures are given greater component durability by reducing creep stress and fatigue, while also reducing oxidation and corrosion rates. Large temperature drops allow engine manufactures to reduce cost by permitting the use of less exotic materials in the design of engine components, and/or to increase the fuel efficiency of the engine by operating at higher temperatures with reduced cooling flows.

Today, repeatable coating microstructures are being obtained with new powder development concepts, gun designs, controllers and work handling systems. The overall benefit is a wide range of unique TBC microstructures, and properties that are then tailored to meet the needs of specific applications in the aerospace and IGT markets.

Thermal barrier coatings consist of an oxidation resistant bond coat and a thermal insulating ceramic top coat; both applied using the plasma spray process. State of the art TBC systems consist of a dense, oxide-free MCrAlY bond coat (M consisting of Nickel and/or Cobalt) and a porous, finely micro-cracked 7–8wt% Ytria-stabilized Zirconia coating. Previous systems incorporated with NiAl or Nickel

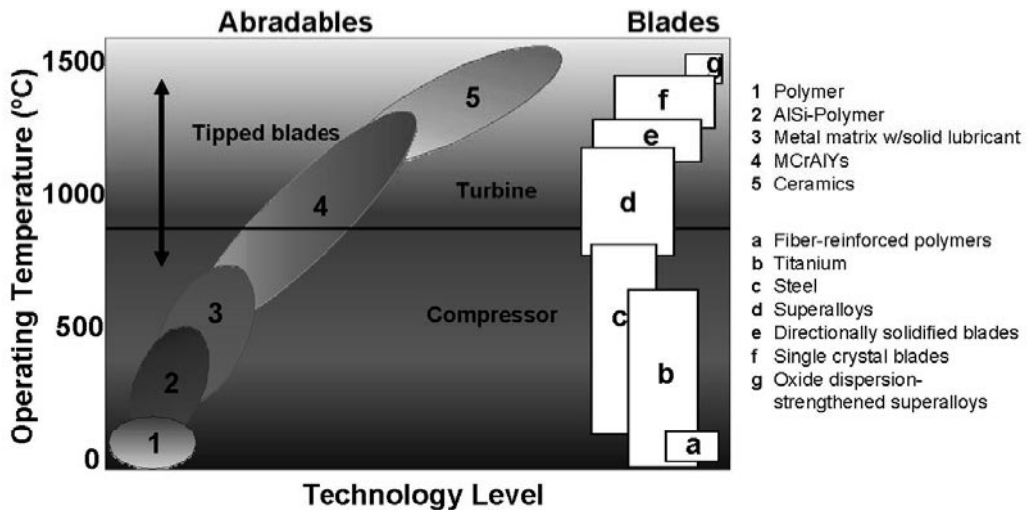


FIGURE 20.8 Concept of an abrasible family.

Chromium bond coats along with 24% Magnesia or 5wt% Calcia stabilized Zirconia. Materials that fill these bond coat requirements are generally NiCrAlY or CoNiCrAlY materials. Oxides such as Calcia, Magnesia and Ytria act to stabilize the crystallographic structure. This prevents large volume changes during heating and cooling of the coated component. The result is improved service life compared to Zirconia coatings that are not stabilized.

20.5.1.3 Oxidation Resistance

Oxidation is defined as a corrosion reaction in which the corroded metal forms an oxide. Usually, this reaction is with a gas containing oxygen, such as air. Metal systems need to form dense, well-adherent oxide films. The oxidation of steel does not form well-adherent oxide scales. This is why elements such as Chromium and Aluminum have been added to steel. Chromium forms chromium oxide scales, which are protective and make steel stainless in nature. For higher temperature applications, Nickel and Cobalt-based alloys have been utilized in the design of aerospace and industrial gas turbine components because of their mechanical and corrosion properties. However, increased concentrations of critical elements such as Aluminum, which form stable oxide scales of aluminum oxides, typically reduce the mechanical performance of the superalloys. It is for this reason that coatings are applied to critical airfoils and are used as bond coats for TBCs. Coatings can improve the corrosion/oxidation properties of these superalloys without undermining the

strength of the base material. Typical material systems are NiAl, NiCr, NiCrAl and MCrAlYs.

20.5.1.4 Hot Corrosion Resistance

Hot corrosion results from accelerated metal surface corrosion. This occurs from the combined effects of oxidation and reactions with contaminants, to form a molten salt on the metal that fluxes. This destroys or disrupts the normal protective oxide. Key contaminants are Sulfur, Sodium and Vanadium. Mechanisms of hot corrosion vary depending on temperature and environment, but coatings have been shown to improve the overall life of the component. Industrial gas turbine components have applied MCrAlYs with high concentrations of Chromium and Platinum Aluminide diffusion coatings to combat hot corrosion problems.

20.5.2 Coated Turbine Components

Examples of the types of IGT components and their function that are exposed to hot gases are as follows:

- **Combustors:** Compressed air mixes with the fuel gas and is ignited. Combustion continues until the flow of fuel is shut off. Due to the high temperatures (up to approximately 1,500 °C), combustion cans are typically thermally sprayed with plasma sprayed MCrAlYs and thermal barrier ceramics such as Ytria-stabilized Zirconia (Figure 20.9).
- **Transition Ducts:** The component ducts the hot gases from the combustor to the first row of sta-

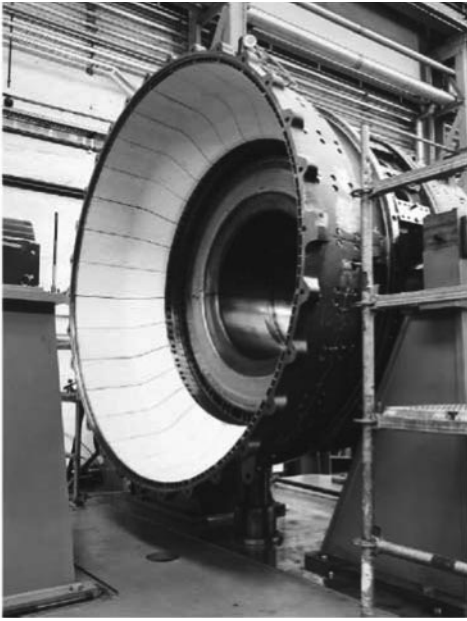


FIGURE 20.9 Combustion liner sprayed with thick YSZ plasma coating.

tionary airfoils. Specially designed internal diameter plasma guns and robotic programs are used to achieve uniform coating thickness. Parts are normally sprayed with air-sprayed MCrAlYs and YSZ top coats. Every OEM has their own coating specification standards on microstructure.

- **Stationary Airfoils:** Hot gases are taken from the combustor and turned so they reach the rotating blades at the optimum angle. The key properties are oxidation and hot corrosion. OEMs use LPPS, MCrAlYs, and plasma-applied YSZ ceramics. Repair applications use HVOF as alternatives to LPPS.
- **Rotating Airfoils:** These airfoils convert kinetic energy of the hot gases exiting the nozzle to shaft horsepower, which drives the compressor. Creep can be a problem on these blades. EB-PVD and LPPS are key processes for applying MCrAlYs.
- **Shroud Casings:** Tighter clearances in the compressor and turbine between the rotating blades and the shroud segments will result in improved engine performance. Types of material systems will be applied either using plasma or low velocity combustion. Porosity and/or dislocators are critical to the performance of abrasives. Turbine section coatings may see plasma-applied porous ceramics with specially designed blade systems, or in some cases “rub tolerant” MCrAlYs.

20.6 GENERAL APPLICATIONS

Other applications outside of the aerospace and industrial gas turbine segments can be seen in all stages of daily living. General applications for thermal spray coatings are corrosion, wear, and salvage and repair of worn or mismachined parts.

Today, significant financial losses may be incurred due to accelerated wear of reciprocating and rotating machinery, pump components, agricultural blades, mining equipment, valves in petrochemical environments, and cylinder liners and piston rings for automotive and heavy duty diesel applications. In order to minimize the effects of mechanical wear and extend product life, thermal spray coating solutions have been implemented in production and will be developed in the future for more demanding wear applications.

From Zinc and Aluminum that are used on bridges and water towers instead of paints, to metal oxide ceramics that are used in bath tubs and racing car engines, thermal spraying is truly a worldwide process. In fact, carbides are being used today on expensive golf clubs, and Titanium is being sprayed for biomedical applications. Automobiles are using thermal spray for piston ring and cylinder bore coatings. Other applications are seen in glass moulding, hard chrome plating, oil and gas, printing, and many other industries.

Key industrial and automotive applications include but are not limited to:

20.6.1 Corrosion Control

Thermal spray coatings are widely used in preventing corrosion of many materials with, very often, additional benefits of properties such as wear resistance. Thermal spray coatings for corrosion protection fall into three main groups: anodic coatings, cathodic coatings, and neutral coatings.

20.6.1.1 Anodic Coatings

Anodic coatings for the protection of iron and steel substrates are almost entirely limited to Zinc and Aluminum coatings or their alloys. Where coatings anodic to the substrate are applied, the corrosion protection is referred to as cathodic protection or sacrificial protection. The substrate is made to be the cathode and the coating is the sacrificial corroding anode. The metallizing process is an excellent means of protecting iron and steel from corrosion to almost any desired degree, from long-life coatings to inexpen-

sive coatings which are competitive with organic coatings such as paint. Heavy coatings of Zinc or Aluminum can be applied to meet the most severe corrosion conditions and give 15–50 years of life without any further maintenance. Aluminum has been found to be the most effective metal for protection of steel in offshore structures.

20.6.1.2 Cathodic Coatings

Cathodic coatings consist of a metal coating that is cathodic with respect to the substrate. A stainless steel or Nickel alloy coating would be cathodic to a steel base. Cathodic coatings can provide excellent corrosion protection. There is a very wide choice, particularly for steel base materials, ranging from stainless steel to more exotic materials like Tantalum to cater to the more extreme corrosive environments. However, a limitation of such coatings is that they must provide a complete barrier to the substrate from the environment. If the substrate is exposed to the corrosive environment, it will become the anode, and corrosion will be dramatically accelerated, resulting in spalling of the coating. Generally, sealing of these coatings is always recommended. Processes which provide the densest coatings are preferred (HVOF, plasma, and fused). Thick coatings will provide better protection than thin coatings.

20.6.1.3 Neutral Materials

Neutral coatings, such as Alumina or Chromium oxide ceramics, provide excellent corrosion resistance to most corrosive environments by exclusion of the environment from the substrate. Generally, a neutral material will not accelerate the corrosion of the substrate even if the coating is somewhat permeable, but any corrosion of the substrate interface with the coating should be avoided to prevent coating separation. Again, sealing of the coatings is recommended. The densest and thickest plasma-sprayed coatings are recommended. When stainless steel-type substrate materials are used where the exclusion of oxygen can cause crevice corrosion, Nickel Chromium bond coats are required.

20.6.2 Salvage and Repair

Thermal spray coatings are used to restore the dimensions of components that have been worn or corroded. Although the thermal spray coating does not add any strength to the component, it is a quick and economical way to restore the dimensions of parts. Subsequent grinding operations are often needed to

smooth the coatings surface and to bring the final dimensions to their appropriate tolerances. Thermal spray coatings for dimensional restorations are being used in every manufacturing industry.

Nickel 5wt% Aluminum powder is an example of a salvage and repair material. These powders are manufactured by a variety of different processes, and they may be mechanically clad, chemically clad, or gas- or water-atomized. The choice of process is based on the application. Key decisions to be made for salvage and repair materials are coating thickness, color match, surface profile after finishing, ease of finishing, bond strength, and application cost (deposition rate). Similar chemistries do not always guarantee equivalent performance. Nickel 5wt% Aluminum coatings with higher oxide levels are harder and more difficult to machine than coatings with lower oxide levels. Coatings with poor cohesive strength and unmelted particles will result in particle pull-out during finishing and result in a porous surface finish. Finally, a coating with unreacted aluminum within its microstructure may be a problem for parts exposed to caustic environments.

20.6.3 Wear Coatings

Wear is defined as the unwanted removal of material from a surface as a result of mechanical action. Mastering the wear process means controlling a complex set of system and process variables. This starts with a clear understanding of the component, its material history (alloy, chemistry, processing history, surface hardness, and grain size), the type of wear the component will see, and the type of environment (temperature and gas). Types of wear discussed below include sliding, abrasion, erosion, and fretting. For each type of wear, there is a specific characteristic for each mechanism. In more cases than not, wear has more than one mechanism associated with it. It is for these reasons field testing and product validation is critical before new components are put into service. Figure 20.10 shows the various mechanisms of wear.

20.6.3.1 Erosive Wear

Erosion occurs when solid particles impinge or impact on a surface resulting in eventual material removal. For solid impingement erosion at a shallow angle of attack, where the wear is similar to that of abrasion, high hardness coatings are required. For solid impingement angles near 90 degrees, coating toughness becomes more important. For cavitation and liquid impingement, generally, a coating with

WAYS MATERIALS WEAR

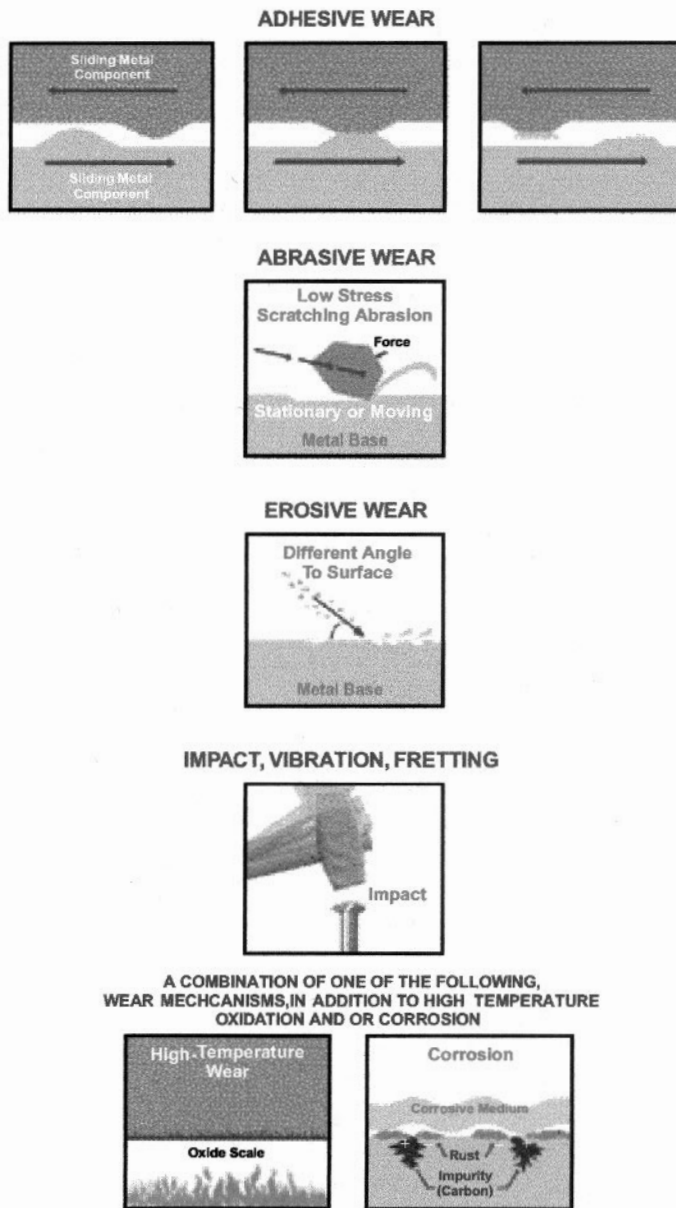


FIGURE 20.10 Various mechanisms of wear.

good surface fatigue resistance is needed. The mechanism of wear when engineering components see erosion is based on the angle of impact, the size of the particles, and the physical characteristics of the debris. The temperature and the environment can also play a role in wear. An example where solid particle erosion is important is on steam turbine blades. Typically, 400-series stainless steel blades are exposed to high temperatures of up to

540 °C (1,000 °F) and see fine particles of iron chromite. Historically, the cost to replace these blades have been significant, and researchers have therefore looked to coat these blades with proprietary material systems and processes. Overlay coatings of Nickel-Chromium/Chromium Carbide and FeCrAlY-Chrome Carbide are being used either by high-energy plasma, D-Gun or HVOF technology to solve these application problems, in addition to new

proprietary coating systems for repairing steam turbine blades.

Another area where high temperature erosion is a problem is in boiler tube applications in the paper and pulp industry. In these applications, boiler tubes are subjected to high temperature corrosion (sulfidation) and erosion. Typically in these black liquor recovery boilers, the combination of char (solid particles rich in sulfur) and the hot gas environment results in metal wastage of the tubes. In order to minimize this problem, Nickel-based alloys high in Chromium have been developed. Other material systems have investigated the benefits of Nickel Chrome/Chrome Carbide/self-fluxing alloy blends with HVOF technology.

Thermal spray coatings of Tungsten Carbide and Cobalt Chromium tungsten alloys have been used on slurry pumps, exhaust fans, and dust collectors to reduce erosion.

20.6.3.2 Fretting Wear

An excellent example of fretting wear is the vibration of fans and compressor blades in aerospace jet engine applications. This can be controlled by the use of mid-span dampers. A mid-span damper provides a contact point between blades to constrain motion, which would result in damaging blade vibration. In order to reduce wear, Tungsten-Carbide Cobalt coatings are applied. Failure of the coating typically occurs due to cracking and spallation from cyclic fatigue and impact. Based on this information, the material selection, spray and application process is critical to the success of the application. Today, HVOF Tungsten Carbide coatings are successfully being applied to replace D-Gun and high energy plasma systems. Controlling the compressive and residual stress within the coating system has been found to improve the cracking resistance.

Other examples where thermal sprayed coatings are used include dead centers, cam followers, and land-based turbine wear rings to prevent surface fatigue wear. Tungsten Carbide, Copper-Nickel-Indium, and Chrome Carbide coatings have been used for these applications

20.6.3.3 Adhesive / Sliding Wear

Sliding wear is defined according to the ASM/TSS Thermal Spray Terminology and Company *Origins* document as “[T]he motion of two (2) moving bodies in which these surface velocities, at the point of contact, are different with regard to magnitude and/or direction.” Key components of sliding wear

are mechanical loading, types of loads, chemical media, temperature, and type and amount of lubricant. Materials need to be tribologically compatible to each other. Examples of sliding wear are in reciprocating and rotating machinery. More specifically, sliding wear is common in automotive and heavy duty piston ring applications, synchronizer rings and transmission systems, automotive and large cylinder bores for gas transmission applications, hydraulic rods for earth-moving equipment, and landing gears for mainframe aerospace applications that replace hard chrome plating.

Historically, materials such as flame-sprayed Molybdenum and plasma-applied Molybdenum/self-fluxing alloys have been used in piston ring applications. Iron-Moly composite blends are being used in large cylinder applications. Other types of coating materials being investigated are carbide-containing coatings that are modified for sliding wear.

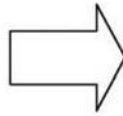
Today, a number of applications are replacing hard chrome plating with alternative materials and processes. HVOF technology is an excellent alternative due to environmental restrictions on chrome plating, ease of operation, quick turn around, wide material selection, and low cost. The U.S. Navy has approved HVOF coatings to replace hard chrome for hydraulic rods. Today, naval shipyards are spraying a tungsten carbide/cobalt-superalloy material in order to extend the life of these rods. Airframe manufacturers have also approved materials such as Cobalt Chromium-Tungsten Carbide for landing gear applications as shown in Figure 20.11. This HVOF material has been developed for the HVOF process, designed with the correct combination of wear, corrosion and fatigue resistance.

Thermal spray coatings for soft bearing surfaces allow the embedding of abrasive particles and permit deformation to accommodate some misalignment of the bearing surfaces. These surfaces require adequate lubrication and should be low in cost, as they wear in preference to the harder mating surface. Some of these coatings are quite porous, with the advantage that they act as reservoirs for lubricants. Thermal spray coatings for soft bearing surfaces commonly used include Aluminum Bronze, Phosphor Bronze, white metal or Babbitt, and Aluminum Bronze-polymer composites.

Thermal spray coatings for hard bearing surfaces are hard and have high wear resistance. Hard bearing materials are used where the embedding of abrasive particles and self-alignment are not required and where lubrication may be marginal. The inher-



Main piston
Cylinder & Axle
Bushings & Pins



4340 Steel
300M
Ti Alloy
Al 7075

FIGURE 20.11 Landing gear.

ent nature of thermal spray coatings seems to provide additional benefits over comparable wrought or cast materials due to the porosity acting as a lubricant reservoir, and the composite nature of included oxides and amorphous phases increasing wear resistance. Some coatings show relatively low macrohardness compared to wrought or cast materials, but very often show improved wear resistance. Thermal spray coatings used for hard bearing surfaces typically include cermet coatings like Tungsten Carbide-Cobalt and Chromium Carbide-Nickel Chromium, oxide ceramics like Chromium Oxide and Alumina, Molybdenum, and various hard alloys of Iron, Nickel, Chromium or Cobalt.

20.6.3.4 Abrasive Wear

Abrasive wear occurs with the removal of material by particles moving across a surface. The particles may be loose or part of another surface in contact with the surface being worn. Examples of abrasive wear applications are in the agriculture and glass industries. Cutting blades and glass mould plungers have Cobalt-Tungsten Carbide/self-fluxing alloys allied with either low- or high-velocity oxy-fuel gun processes. Tungsten Carbide, Alumina-Titania and steel coatings have been used for guide bars, pump seals and concrete mixer screws to reduce or eliminate abrasive wear.

As discussed earlier, the benefit of fusing the coating is to create a metallurgical bond between the substrate and coating, which improves the impact resistance. Important considerations for abrasive wear are the coating's matrix hardness and chemistry. Chromium and Molybdenum are added to improve Nickel, Cobalt or possibly Iron corrosion resistance. Boron and Carbon are added to increase coating hardness. Hardness and toughness typically run counter to each other and, therefore, the alloy design has to be optimized for the application.

The best coating system for abrasive wear is Tungsten Carbide-Cobalt. Typically, commercially available Tungsten Carbide-17wt% Cobalt is tougher than 12wt% Cobalt alloys. Key factors which affect the abrasive wear properties of Carbide coatings are carbide size, shape, powder manufacturing process and distribution. Volume percentage and type of carbide are also critical.

Plasma, HVOF, and D-Gun processes are used for less severe impact applications. Tungsten Carbide-Cobalt (Chromium) and Nickel Chromium-Chromium Carbide are the main carbides of choice in thermal spray industry. Tungsten Carbide-Cobalt is used for low temperature wear applications (400–500 °C), Cobalt-Chromium-Tungsten Carbide coatings for corrosive low temperature wear, and Nickel-Chromium-Chrome Carbides for high temperature wear (1,000 °C). Typically, carbide coat-

ings of Cobalt-Chrome have over four to six times the abrasive wear resistance of hard chrome plating and are approximately 30% better than Nickel Chrome-Chromium Carbide. Another interesting fact is that plasma-applied Chromium oxide typically has a coating harness around Rc 70, compared to Tungsten-Carbide-Cobalt coatings with a coating hardness around Rc 65–68. The abrasive wear of Chromium oxide coatings, however, is only 30–40% of Tungsten-Carbide Cobalt systems. The key point here is that material hardness is not the only factor in determining abrasive wear resistance between material systems.

As previously discussed, the majority of applications are based not on one mechanism, but many. A good example is a sucker rod coupling used in oil-field pumping machinery. Another example is in a pump volute used in the petroleum industry. A sucker rod sees abrasive, sliding, and corrosive wear. A volute pump sees abrasion, erosion, and corrosion. In the case of the sucker rod coupling, Nickel-based self-fluxing alloys are applied using low velocity combustion and then induction fused. Volute pumps have seen HVOF-applied Tungsten-Carbide 12% cobalt applied in order to extend the service life.

20.7 MISCELLANEOUS APPLICATIONS

20.7.1 Metal Workings

Tooling and die costs in metalworking operations contribute significantly to total production costs. Despite the high investment, wear leads to early failure of metalworking dies. Thermal spray deposition of wear resistant materials onto the parts of a die most prone to wear economically extends die life. An example is thermal spray deposition and high heat flux infrared post-treatment of Chrome Carbide coatings. Other coating materials that extend die life include: high temperature metallic materials that have known wear resistance and good fatigue life; oxidation resistant materials known for their extreme levels of wear resistance; and oxidation resistant materials that provide protection in thermal environments where wear and oxidation are limiting factors.

20.7.2 Traction

Traction coatings are used on rolls in the printing and papermaking industries to grab and feed paper. Because the traction of the coating depends substan-

tially on the degree of its surface roughness, nearly any material can be used to create a traction coating. However, in most applications where a traction coating is required, there is also a great amount of wear present and, therefore, the most common traction coating materials are carbides, stainless steels, and Nickel alloys.

20.7.3 Dielectric Coatings

The aerospace, automotive, and electronic packaging industries are the largest users of ceramic dielectric coatings. Dielectric coatings are either pure Aluminum oxide or a spinel. In either case, a very high density coating can be created that is capable of withstanding thousands of volts, depending on the coating thickness.

20.7.4 Release Coatings

Thermal-sprayed release coatings use a matrix, which is impregnated with a release agent of either Teflon or Silicone. Release coatings are used to provide a component with anti-stick characteristics as well as wear resistance. Components utilizing thermal-sprayed release coatings are typically used in the manufacturing of plastics, adhesives, rubber, and food products.

20.8 COATING SELECTION

The first step in selecting a thermal spray coating for a specific application is to define the coating function. For example, if a material is required for an automotive piston ring, then the key function that the coating needs to accomplish is to either improve or extend the life of a non-coated ring. Table 20.1 lists some of the most common wear functions for thermal spray coatings, the types of materials used, and application examples. In order to pinpoint the best material for a particular application, other factors need to be considered. Material cost, deposition rate, finishing requirements, coating thickness, part geometry, and equipment availability are all important items to consider.

20.9 SUMMARY

The design of the proper coating system is based on cost and technical considerations. Technical considerations are based on an understanding of the wear

TABLE 20.1 Material Selection

| Coating Function | Application | Materials |
|---------------------------------|----------------------------|---|
| Abrasive Wear | Cutting Blades | Tungsten Carbide-Cobalt |
| | Glass Mould Plungers | Nickel Chrome-Chrome Carbide |
| | Pump Volute | Cobalt-based Hardfacing Alloy |
| Sliding Wear | | Nickel/Cobalt Self-Fluxing Alloy |
| | Piston Rings | Cast Iron-Molybdenum |
| | Impeller Shafts | Molybdenum-based Self-Fluxing Alumina-Titania |
| | Cylinder Bores | Babbitt |
| Impact, Vibratory Fretting Wear | | Cobalt Chromium Molybdenum |
| | Mid-span Dampers | Tungsten Carbide Cobalt |
| Erosion/Cavitation Wear Chrome | Sucker Rods | |
| | Steam Turbine Blades (SPE) | Tungsten Carbide Cobalt |
| | Water Turbine Applications | Nickel Chrome-Chrome Carbide |

mechanism and environmental factors that the engineered parts are exposed to. Cost considerations include the materials used, the gun or process employed, consumables such as gas and electricity, labor costs, and the life of the component before it needs to be repaired.

Thermal spray processes are easy to use, cost little to operate, and have attributes that are beneficial to applications in almost all industries. The benefits are typically lower cost, improved engineering performance, and/or increased component life.

Thermal spray processes offer cost-effective manufacturing approaches which cut across all industrial sectors, solving many industrial problems and providing numerous applications. Thermal spray solutions are actively used in aerospace, agriculture, maritime, metal working, papermaking and printing, pumps/motors, electronics, computers, petrochemicals, geothermal, nuclear power, utilities involving power/water/sewage, golf, military, offshore oil platforms and submersed pipe lines, refineries, railroad, automotive, and diesel industries.

20.10 REFERENCES

1. H. Herman, S. Sampath and R. Mucune. Thermal Spray: Current Status and Future Trends. *Materials Research Society Bulletin*, July 2000, p. 17.
2. M. Dorfman. Thermal Spray Basics. *Advanced Materials & Processes*, July 2002 p. 47.
3. www.asminternational.org (Thermal spray Society)
4. M. Dorfman. Thermal Spray Applications. *Advanced Materials & Processes*, October 2002, p. 66.
5. M. Dorfman. Thermal Spray Processes. *Advanced Materials & Processes*, October 2002, p. 47.
6. R. Radmard, S. Strykewich, and L. Russo. Investigation of HVOF Carbides as D-Gun Coating Replacements in the Gas Turbine Industry. In *Proceedings of the United Thermal Spray Conference*, May 19, 1999, pp. 434–438.
7. P. Zajchowski and B. Crapo. The Evaluation of Three Dual-Wire Arc Sprayed Coatings. *Journal of Thermal Spray Technology*, Vol. 5(4), December 1996, pp. 457–462.
8. J. Wigren and L. Pejyd. Thermal Barrier Coatings—Why, How, Where and Where To.: In *Conference Proceedings of the 15th International Thermal Spray Conference*, Nice, France, May 25–29, 1998, pp. 1,531–1,547.
9. M. Dorfman. Thermal Spray Materials. *Advanced Materials and Processes*, September 2002, p. 46.
10. J. A. Brogan. Thermal Spraying of Polymers and Polymer Blends. *Materials Research Society Bulletin*, July 2000, p. 48.
11. J. Wigren and L. Pejyd. Tungsten Carbide Coatings on Jet Engine Components: Safe Aviation. *Sulzer Technical Review*, February 2000, p. 36.
12. M. R. Dorfman, U. Erning, and J. Mallon. Benefits of Clearance Control Thermal Spray Coatings: Sealing the Gap. *Sulzer Technical Review*, March 2001, p. 16.
13. G. Barbezat and R. Herber. Breakthrough in Improving Car Engine Performance through Coatings.: *Sulzer Technical Review*, February 2001, p. 8.
14. R. Pecoskie and D. Parker. Coatings Protect Severe Service Ball Valves. *Advanced Materials & Processes*, July 1993.
15. P. Meuter. Protecting Pumps Against Abrasive Wear.: *Sulzer Technical Review*, January 2001, p. 22.
16. P. Sahoo and G. W. Goward. On the Suitability and Application of MCrAlY Coatings Under Various Conditions. In *Proceedings of the National Thermal Spray Conference*, Houston, TX, September 11–15, 1995, pp. 539–544.

CHAPTER 21

COATINGS FOR CONCRETE SURFACES: TESTING AND MODELING

C. Vipulanandan

J. Liu

*Center for Innovative Grouting Materials and Technology (CIGMAT), Department of Civil and Environmental Engineering,
University of Houston, Houston, Texas*

| | |
|--|------------|
| 21.1 INTRODUCTION | 423 |
| 21.2 MATERIALS | 424 |
| 21.3 TESTING PROGRAMS AND RESULTS | 424 |
| 21.4 MODELING LIQUID TRANSPORT INTO COATED CONCRETE | 433 |

| | |
|-----------------------------|------------|
| 21.5 CONCLUSIONS | 446 |
| 21.6 ACKNOWLEDGEMENT | 446 |
| 21.7 REFERENCES | 446 |

21.1 INTRODUCTION

Cement concrete is a highly alkaline material that can easily deteriorate in acidic environments. Therefore, concrete structures in food factories, chemical plants and wastewater facilities are usually protected using various types of coating materials. In sewage facilities, sewer pipes and wastewater treatment plants are corroded by sulfuric acid from sulfuric-acid-producing bacteria (Soebbing, 1996 and Sand, 1994). The sulfuric-acid-producing bacteria found in sewer crowns thrive at low pH, which is inhibitory to most competitors. Islander (1991) reported that the concentration of sulfuric acid for the worst case in sewer environments was pH of 0.5 (close to the pH of a 3% sulfuric acid solution). Fattuhi and Hughes (1988) immersed concrete specimens in a channel containing an approximately 2% solution of continuously flowing sulfuric acid. Their results showed that after 48 days of exposure, the average mass change was 34.6%. Ehrich et al. (1999) studied biogenic and chemical sulfuric acid corrosion of mortars. For ordinary Portland cement mortar, the mass loss of the samples in the biogenic sulfuric acid environment was about 20% after 100 days, and the mass loss of the samples in the pH 2 chemical sulfuric acid environment was more than 15% after 25 renewals (every one to three days to renew the solution according to the pH of the solution).

A coating system that bonds to concrete and provides protection from microbial sulfuric acid attack

would have wide use in the wastewater industry (Redner et al., 1994). Redner et al. (1994) evaluated more than 20 different coating systems in an accelerated test program (in 10% sulfuric acid). Their test results showed that there were no fail-safe coatings. Even coatings that survived the accelerated test had failed in the field (Redner et al., 1994). Liu and Vipulanandan (1999) studied concrete specimens coated with an epoxy coating and immersed in 3% sulfuric acid. The results showed that for specimens without holidays in the coating film, the mass gain was only about 1% after three years, and the probability of failure increased with the increase in mass for coated concrete in 3% sulfuric acid. Hence, predicting the mass change in test specimens of coated concrete is very important in determining the service life of coated concrete and evaluating the effectiveness of coating materials.

When cement concrete was submerged in aggressive solutions, the mass change of the concrete was a key factor that indicated the degree of deterioration of concrete. Many researchers have developed models to predict the solution uptake of concrete. For example, Tang (1992) theoretically analyzed the fluid flow through hardened cement paste and derived the quantitative relationship between permeability and pore size distribution. Hinsenveld (1995) used the shrinking core model to predict the leaching process in cement-stabilized waste in acid. The relation between the amount of leached substances and exposure time was obtained. Mebarkia and Vipulanandan

(1995) developed a cylindrical model to predict mass increase of polymer concrete. Martys et al. (1997) analyzed sorption properties of mortars and concrete in water and suggested an empirical equation to predict water uptake in mortars and concrete. Gospodinove (1999) developed a model to numerically describe the concentration distribution of sulfate ion in concrete. Mainguy (2000) analyzed leaching of cement-based materials and modeled the process with the mass balance equation of calcium. In this study, the relationship between the effective diffusion coefficient and calcium concentration in solid/liquid phase was developed.

The penetrability of liquids through coating films was an important factor in protecting substrates from corrosion. Many studies on the transport of liquids in organic coatings were focused on water penetrating through free and applied coating films. Corti et al. (1982) studied the effect of steel and glass substrates on water absorption in epoxy-polyamide coating, and concluded that the free films showed a tendency toward greater water uptake. Thomas (1991) used Fick's first and second laws under the steady state condition, and studied water and gases penetrating through free coating films. Nguyen (1995) studied water diffusion in both free and applied (on metal and silicone) coating films based on Fick's second law under non-steady state conditions.

For concrete coatings, because of the porous nature of the substrate, the penetration of coatings into the concrete is a very important factor, and the interface properties may have affected the penetration of liquids. Therefore, it was necessary to incorporate the interface properties related to coating-concrete

in modeling the coated concrete behavior. In field applications, a coating system cannot be applied without holidays (pinholes) on concrete substrate and, hence, performance of the coated concrete should be evaluated with holidays. Liu and Vipulanandan (2003) developed models to predict the mass change of coated concrete. The pinhole effect has been considered in the models. This chapter presents a combination of test methods and models to predict mass change and pinhole effect for coated concrete. Test and analytical results for epoxy and polyurethane coatings are discussed.

21.2 MATERIALS

In this study, several commercially available polymer and cement-based coatings were used. Properties of some of the polymer based coatings are summarized in Table 21.1. It must be cautioned that the results from this study cannot be generalized to all coatings available in the market place.

21.3 TESTING PROGRAMS AND RESULTS

21.3.1 (a) Hydrostatic Test

In order to simulate hydrostatic pressure on concrete structures due to the ground water table, concentrically placed concrete pipes are used to develop the necessary full-scale testing conditions (Figure 21.1). This is achieved by using 900-mm (36-in.) inner pipes and 1,600-mm (64-in.) outer pipes with two concrete end plates. Based on the input from con-

TABLE 21.1 Properties of Coatings

| Coating | Material | Density kg/m ³ | Pulse Velocity (m/sec) | Hardness (Shore*) | Thickness mm** | Application Condition |
|----------------|----------------------------------|--|---------------------------|----------------------|------------------------------|--|
| Epoxy-1 | Pure epoxy | 1,190 | 2,512 | 70 | 2.0 | dry and wet surfaces |
| Epoxy-2 | Pure epoxy | 1,530 | 2,730 | 73 | 1.5 | dry and wet surfaces |
| Epoxy-3 | Pure epoxy | 1,200 | 2,532 | 71 | 2.0 | dry and wet surfaces |
| Epoxy-4 | Glass fiber reinforced Epoxy | 1,635 | 2,863 | 72 | 1.5 | dry and wet surfaces |
| Polyurethane-1 | Polyurethane | 1,130 | 2,283 | 67 | 1.1 | dry and wet surfaces |
| Polyurethane-2 | Polyurethane | 1,355 | 3,165 | 78 | 4.7 | dry and wet surfaces |
| Remarks | All are epoxy-based coatings. | Varied from 1,190 to 1,635 kg/m ³ | Increase with density | Similar hardness. | Varied from 1.5 to 2.0 mm | Physical properties of coatings are similar |

*Durometer Type D

**Ultrasonic Multi-Layer Coating Thickness Gage (PosiTector 100)

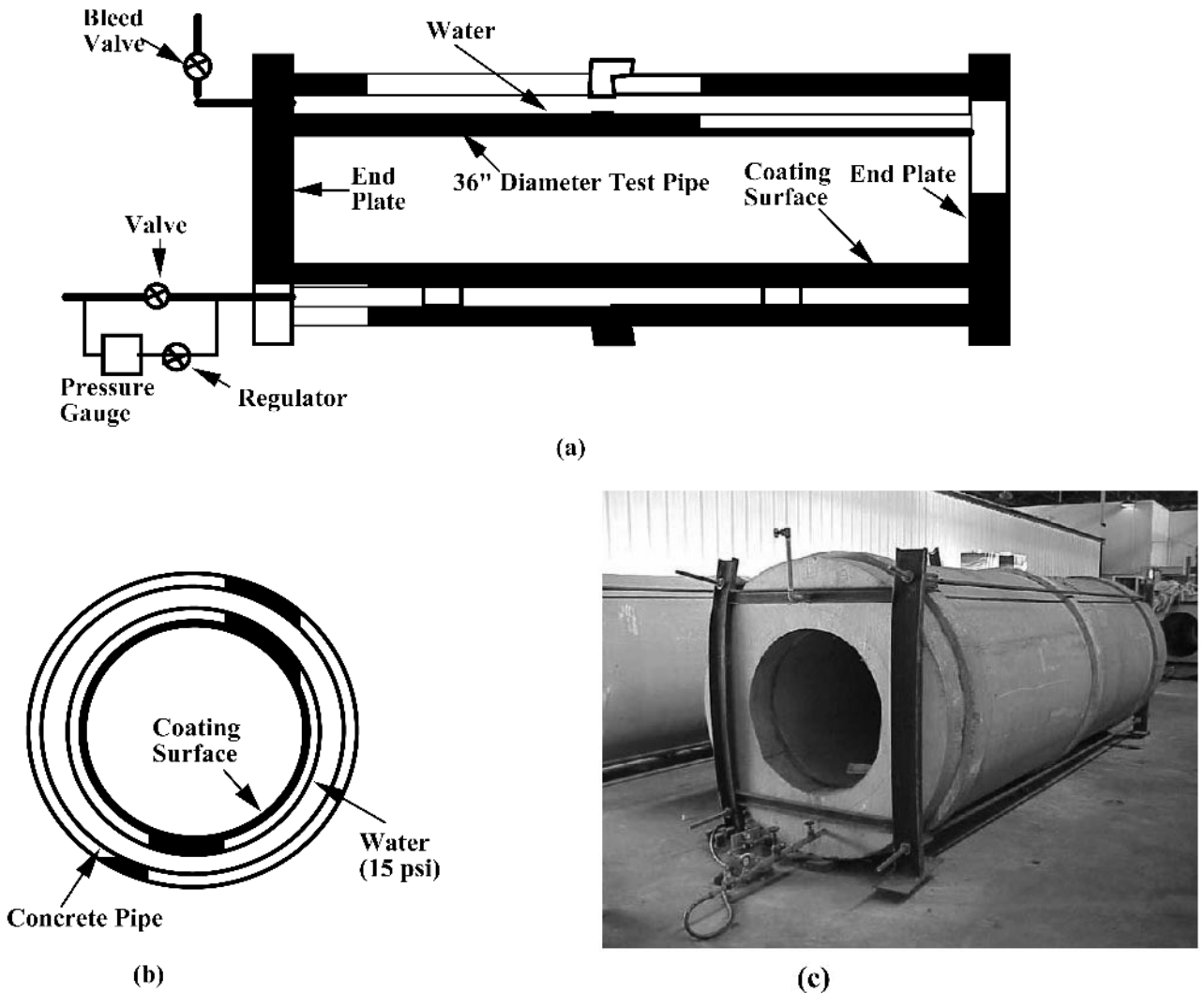


FIGURE 21.1 Hydrostatic test configuration: (a) elevation; (b) cross-section; (c) outside view.

tractors, 900-mm (36-in.) diameter pipe is the smallest man-entry pipe in which a coating applicator could operate with reasonable ease. Steel elements are used to support the entire setup. The inner concrete pipe surface represents a concrete surface under hydrostatic pressure, and coating a pipe surface (laid horizontally) represents most of the difficult conditions encountered in coating structures, such as in lift stations. The total area available for coating is 14 sq. m (150 sq. ft).

21.3.1.1 Dry Test

Coating was applied to new 900-mm (36-in.) diameter concrete pipes. The coated pipes were then placed in the pressure chamber for hydrostatic pressure testing.

21.3.1.2 Wet Test

The 900-mm (36-in.) concrete pipe was installed in the test chamber and pressurized at 105 kPa (32 feet of water head) for at least two weeks before applying the coating. The coatings were applied after water jet blasting or sand blasting the surface. The average application temperature was 650 °F. The moisture emission rate was 536 $\mu\text{g}/(\text{m}^2\cdot\text{sec})$ (9.49 lb/1,000 ft². 24 h, ASTM E 1907) on the concrete surface.

21.3.1.3 Measurements

Visual Inspection: The coated surfaces was visually inspected regularly and information on blistering, spalling, discoloring and cracking was noted and photographed.

In Situ Bonding Test (CIGMAT CT-2, Modified ASTM D 4541): In situ bonding tests on the coating materials were performed at the end of six months. A 51-mm (2-in.) diameter core drill was used to core into the concrete surface and isolate the test area, and a metal piece was glued to the coating with an epoxy (see Figure 21.2(a) and (b)). After 24 hours of curing, the test was performed, using a portable bonding strength tester (Figure 21.2 (c)).

The performance rating criteria were as follows: (i) Overall condition (appearance): good, satisfactory, bad; (ii) Surface texture: smooth, rough; (iii) Blistering: yes, no; (iv) Cracking: yes, no; (v) Change in color: yes, no; (vi) Overall finish (quality of the job): good, satisfactory, bad; (vii) Overall Rating: Pass, Satisfactory, Fail.

Over twenty different coatings have been evaluated and 90% of the coatings passed the test. The typical coating defects in the test included cracks on the coating surface, hard and soft blisters, and discolored spots (Figure 21.3).

21.3.2 (b) Bonding Test

In the bonding tests, CIGMAT CT-2 test (modified ASTM D 4541) and CIGMAT CT-3 test (modified ASTM C 321) were used to determine the bonding strength of coatings to concrete (Figure 21.2). Dry concrete specimens are stored in the room environment (temperature 23 ± 2 °C and humidity $50 \pm 5\%$), and wet concrete specimens were saturated in water at least seven days before coating.

21.3.2.1 CIGMAT CT-2 (Modified ASTM D 4541)

In this test, a 51-mm (2-in.) diameter circular area was used for testing (Figure 21.2(a)). In this case, the coatings were cured with one free surface. Dry and wet coated concrete blocks were cored using a diamond core drill to predetermined depth to isolate the coating. A metal fixture was then glued to the isolated coating section using a rapid-setting epoxy. Bonding strength was determined by pulling the metal fixture off the substrate.

21.3.2.2 CIGMAT CT-3 (Modified ASTM C 321)

In this test, the coating was sandwiched between a pair of rectangular concrete block specimens and then tested for bonding strength (Figure 21.2(b)). In

this case, the coatings were cured without free surfaces. Both dry and wet specimens were used to simulate the dry and wet coating conditions. The bonded specimens were cured under water up to the time of testing. Compared to CIGMAT CT-2 test, this was an easier test to perform, since no coring or gluing of metal fixture was required.

21.3.2.3 Failure Types

In order to understand the failure mechanism, the observed failure types in the CIGMAT CT-2 and CIGMAT CT-3 tests are defined and summarized in Table 21.2.

1. *Type B1 failure* is concrete failure. The failure occurred in concrete due to tension in the CIGMAT CT-2 test or bending in the CIGMAT CT-3 test. This type of failure is the most desired failure type because the bonding strength between coating and concrete is higher than the tensile strength or flexure strength of concrete.
2. *Type B2 failure* is coating failure, which is cohesive failure of coating. This type of failure indicates that the tensile strength of the coating is lower than the bonding strength and the tensile strength of concrete.
3. *Type B3 failure* is bonding failure where the failure occurs between coating and substrate. This type of failure indicates that the coating has poor bonding strength to concrete substrate.

The three failure types above are the most common observed failure types in the bonding tests. In addition to these three failure types, some other failure types can also occur in the tests.

1. *Type B4 failure* is a combined bonding and concrete failure, where the bonding strength of coating to concrete is close to the tensile/flexure strength of concrete.
2. *Type B5 failure* is a combined bonding and coating failure, where the bonding strength of coating to concrete is close to the tensile/flexure strength of coating.

The failure types observed in the bonding tests are shown in Figure 21.4. Through these bonding tests, the variation of the bonding strength of the coatings can be investigated. Typical variations of bonding strength with dry and wet concrete surfaces for some epoxy coatings are shown in Figs. 21.5 and 21.6.

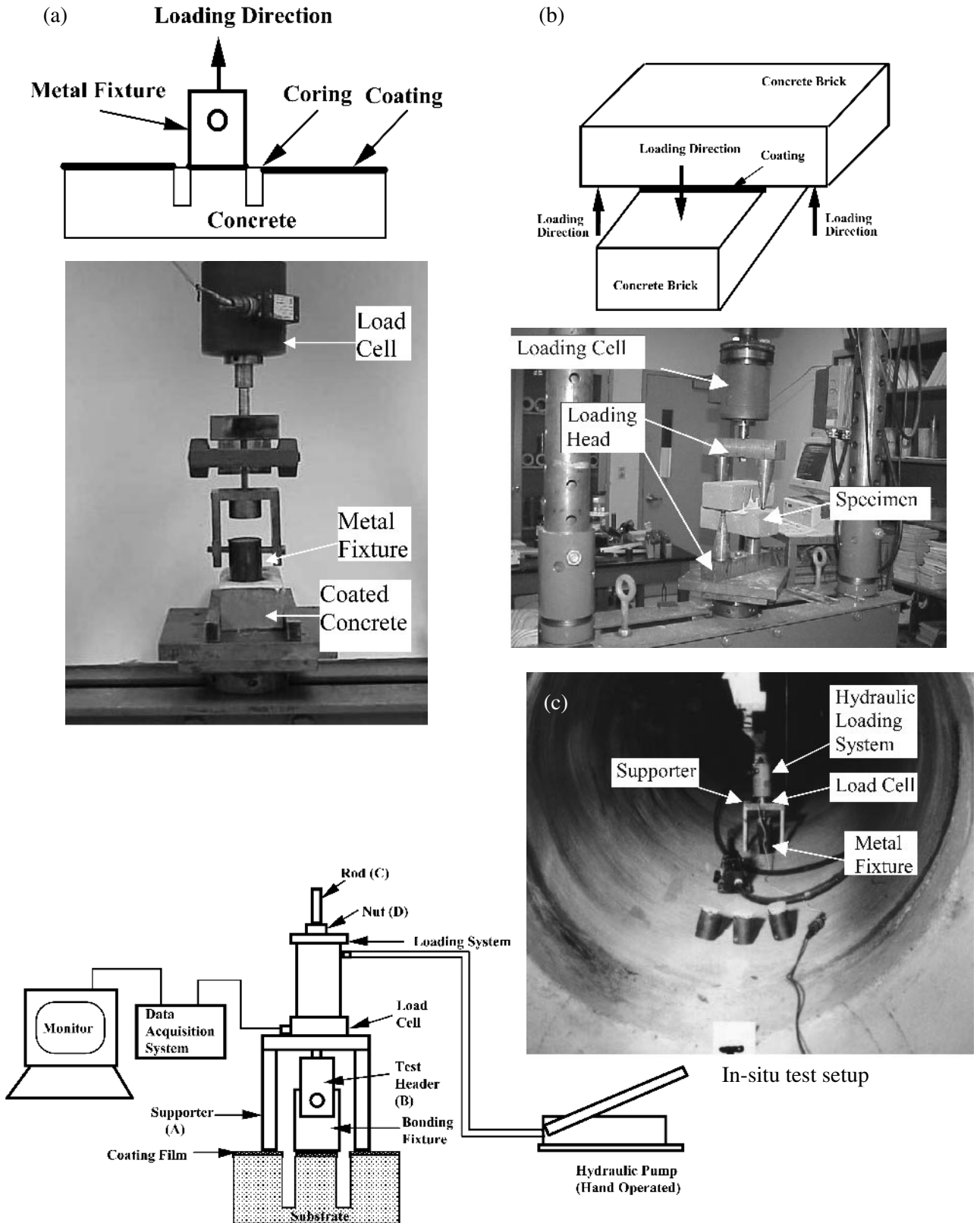


FIGURE 21.2 Defects observed in the hydrostatic test.

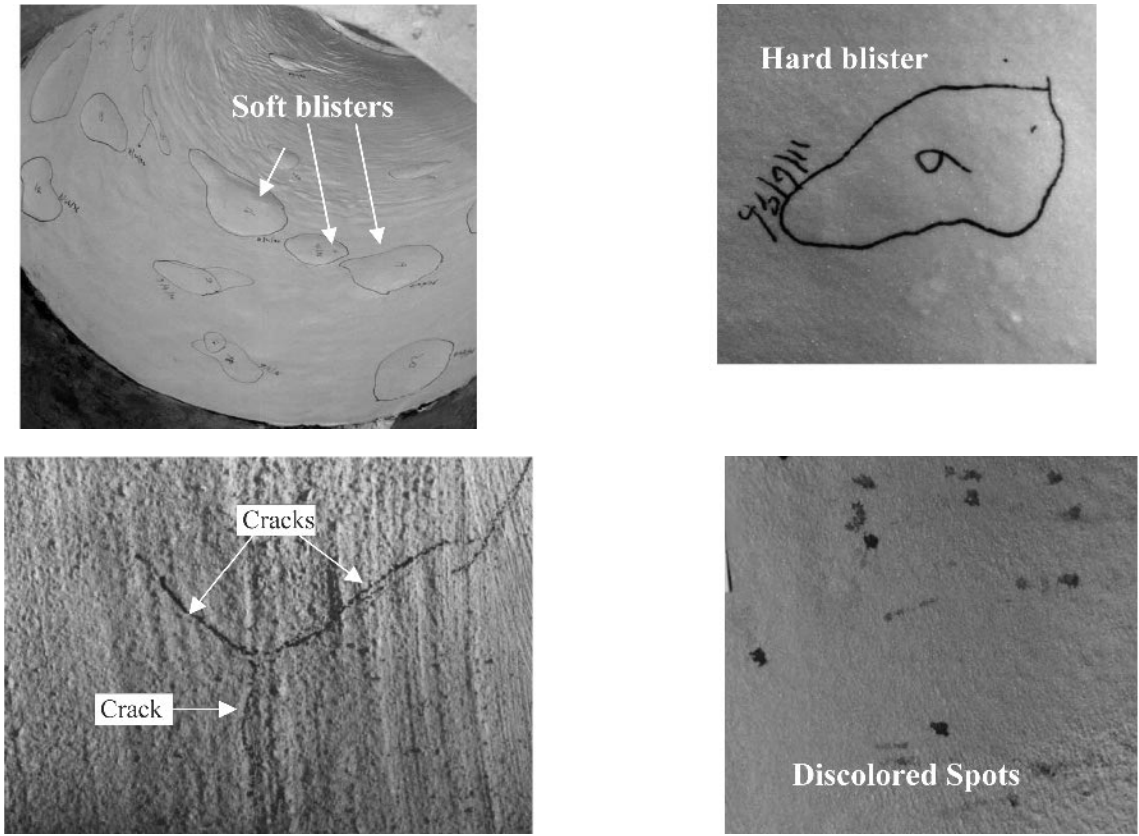


FIGURE 21.3 CIGMAT CT-2 and CIGMAT CT-3 test setups: (a) CIGMAT CT-2 test (modified ASTM D 4541 test); (b) CIGMAT CT-3 test (modified ASTM C 321 test); (c) CIGMAT CT-2 test (in situ bonding test).

21.3.3 (c) Pinhole Test—Chemical Resistance (CIGMAT CT-1, modified ASTM G 20)

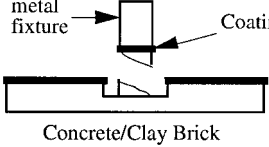
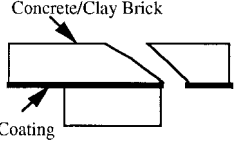
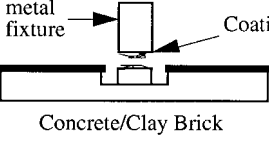
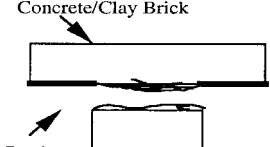
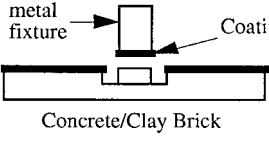
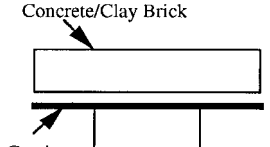
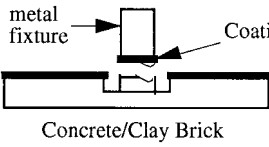
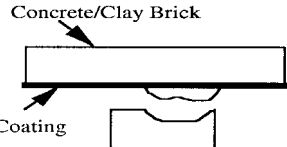
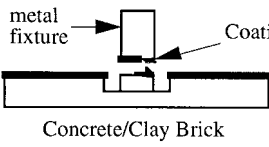
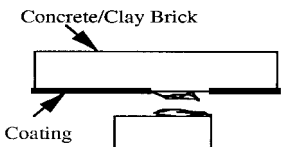
In order to study the chemical resistance of coated cement concrete, the ASTM G 20 test was modified to use with coated concrete. As shown in Figure 21.7, the specimens were immersed in a selected test reagent to half the specimen height in a closed bottle, so that the specimens are exposed to the liquid phase and vapor phase. (This method is intended for use as a relatively rapid test to evaluate the acidic resistance of coated specimens under anticipated service conditions.) Dry and wet (water saturated) cement concrete specimens were coated on all sides and tested. For the test, two radial holes were drilled into the coated specimen approximately 15 mm deep (considering the sizes of aggregates used in the concrete specimens). In this test, the changes in (1) weight of the specimen, and (2) appearance of the specimen were monitored at regular intervals. The two test reagents selected for this study were (1) deionized (DI) water (pH = 5 to 6),

and (2) 3% sulfuric acid solution (pH = 0.45, representing the worst reported condition in the wastewater system). Control tests were performed without pinholes.

The weight changes of uncoated dry and wet concrete (immersed in water for seven days) in DI water and 3% sulfuric acid are shown in Figure 21.8. Based on rate of weight change, the dry and wet concrete specimens became almost saturated in 84 days (12 weeks) in DI water. During this period, the weight increased for dry and wet concrete by 0.91% and 0.35%, respectively. The dry and wet concrete specimens in 3% sulfuric acid had a weight loss over 2% in seven days.

When coated concrete specimens are immersed in D.I. water and sulfuric acid solution, liquid will penetrate through the coating film, pinholes, and interface (exposed at the pinholes) into concrete. The mass increase for the coated concrete in the solutions may vary according to different coatings. The typical mass increase in coated concrete for some coatings are shown in Figs. 21.9 through 21.11. When sulfuric acid solution penetrates into concrete,

TABLE 21.2 Failure Types in CIGMAT CT-2 Test and CIGMAT CT-3 Test

| Failure Type | Description | CIGMAT CT-2 Test (Modified ASTM D4541 Test) | CIGMAT CT-3 Test (ASTM C321 Test) |
|--------------|-------------------------------|--|---|
| Type B1 | Substrate Failure |  |  |
| Type B2 | Coating Failure |  |  |
| Type B3 | Bonding Failure |  |  |
| Type B4 | Bonding and Substrate Failure |  |  |
| Type B5 | Bonding and Coating Failure |  |  |

acid will react with the $\text{Ca}(\text{OH})_2$ and other complexes in the cement. Based on the pH and sulfate concentration in the specimen, gypsum and/or ettringite are formed. Ettringite expands and causes coating cracking and blistering. Failure types observed when sulfuric acid attacked the coated concrete specimens included blistering at the pinhole, cracking of coating starting from the pinhole, or on the surface of the specimens.

21.3.4 Failure Criteria

In order to evaluate the performance of various coatings, the failure criteria for coated concrete are defined as follows:

- Criterion 1: When the diameter of the blister on the coating becomes larger than 25 mm (1 in.)
- Criterion 2: When the length of the crack on the coating is longer than 25 mm (1 in.)

- Criterion 3: Multiple blistering, multiple cracking on the coating surface which is not included in Criteria 1 and 2
- Criterion 4: Weight gain is more than 2%

21.3.5 Coating Concrete Failure Types

The coating failure types observed during the testing included cracking across the pinhole (mainly along the length of the cylindrical specimens), spalling, and blistering around the pinhole. The configurations of the failure types are shown in Figure 21.12.

21.3.5.1 Type C1 Failure

Major cracking across pinhole (Figure 21.12(a)). For coated specimens with pinholes, the concrete is directly in contact with sulfuric acid through the pinholes. Calcium hydroxide and other calcium complexes react with acid and forms gypsum and ettringite.

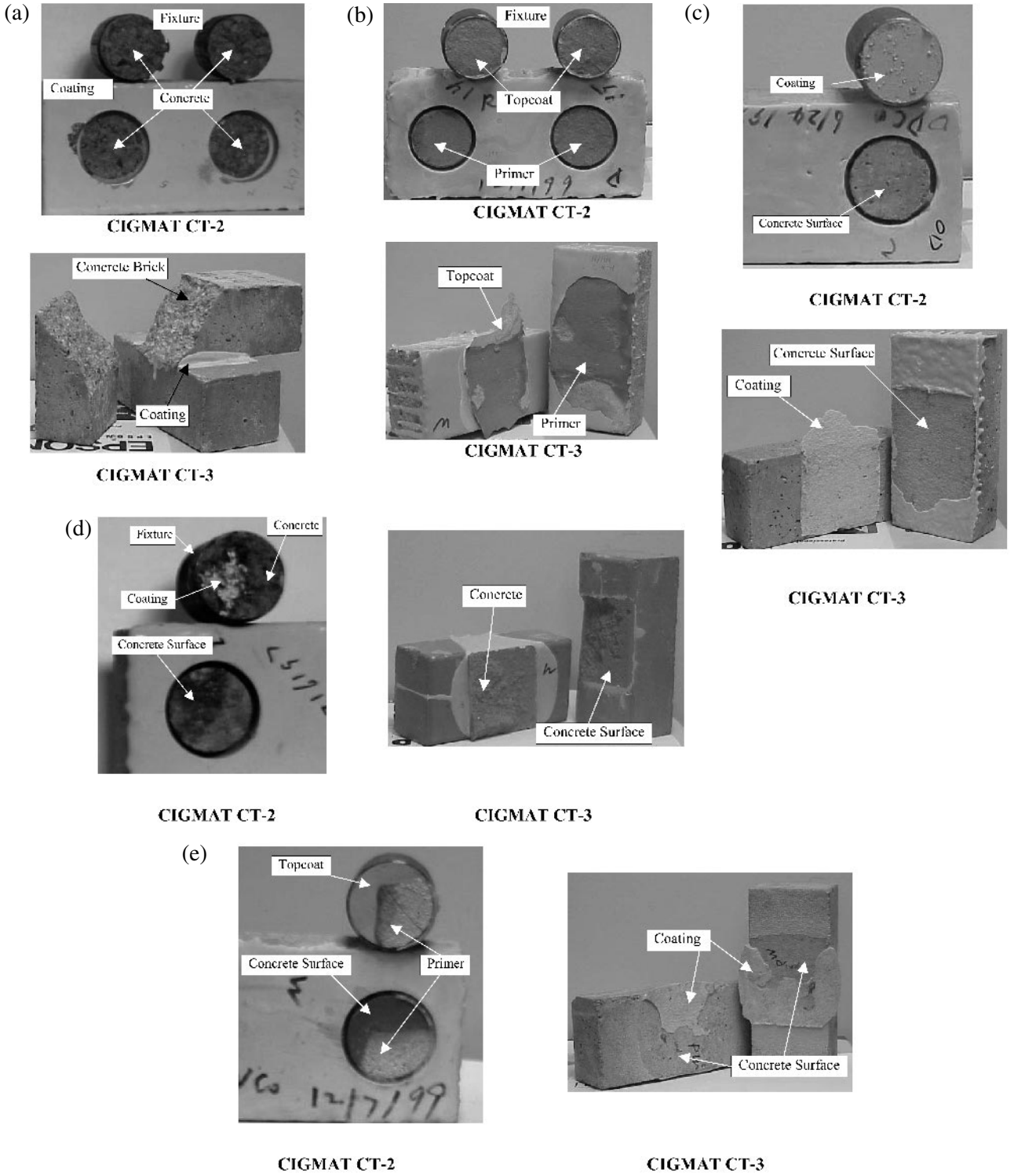
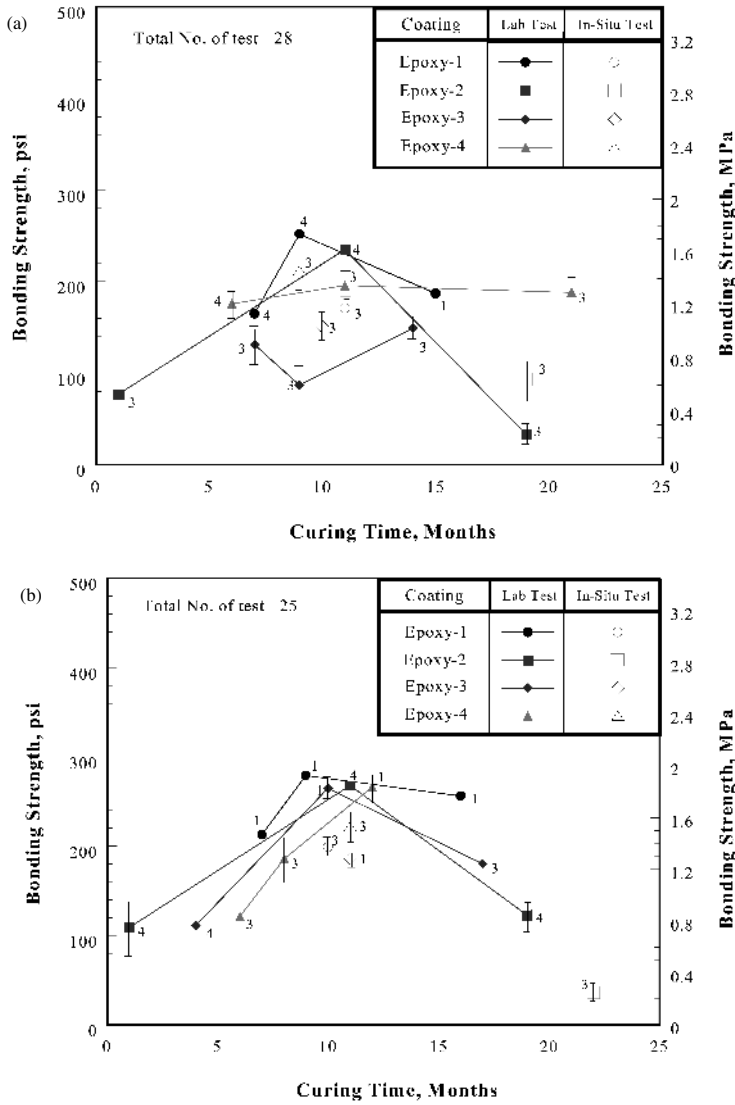


FIGURE 21.4 Bonding test failure types configured in Table 21.1: (a) Type B1 failure; (b) Type B2 failure; (c) Type B3 failure; (d) Type B4 failure; (e) Type B5 failure.



* Note: Numbers in the figures are failure types defined in Table 2.

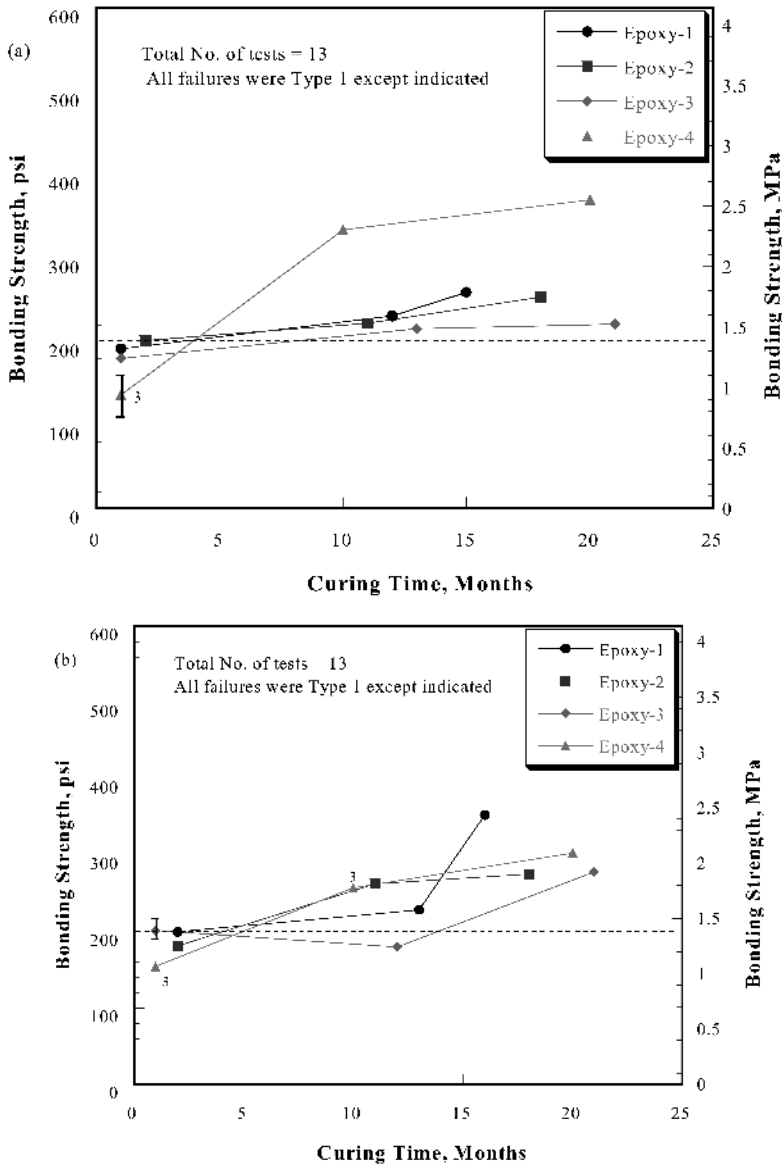
FIGURE 21.5 Test results from CIGMAT CT-2 (modified ASTM D 4541) tests. (a) For dry coated concrete. (b) For wet coated concrete.

ite at different pH levels. Expansion can be observed in the region, subjecting the coating to hoop tensile stresses and strains. Initially, small blisters are formed around the pinholes. The blisters continue to grow with the immersion time. Hence, the coating tends to confine the expansion of concrete, resulting in tensile stresses and strains in the coating. Pinholes further magnify the stresses in the coating. When tensile stress caused by concrete expansion exceeds the tensile strength of the coating, cracks occur in the direction of the length of the cylindrical speci-

men. Generally, coated concrete specimens that have larger pinholes cracked first.

21.3.5.2 Type C2 Failure

Random cracking of coating (Figure 21.12(b)). When sulfuric acid penetrates through the coating film and reacts with the concrete on the interface of the coating, and the concrete substrate reacts with the primer of the coating, random cracking may occur on the coating film. If the tensile strength of



* Note: Numbers in the figures are failure types defined in Table 2.

FIGURE 21.6 Test results from CIGMAT CT-3 (modified ASTM C 321) test. (a) For dry coated concrete. (b) For wet coated concrete.

the coating is low or the coating film is very thin (less than 1.5 mm), the coating film will crack at weak points due to concrete expansion. Cracks further develop and cause the coating film to peel off of the concrete substrate. In such cases, coatings fail faster than other failure types.

21.3.5.3 Type C3 Failure

Blistering around pinholes (Figure 21.12 (c)). When concrete expands, coatings deform without

cracking, and blisters mainly occur around the pinholes. This type of failure was observed in epoxy- and polyurethane-coated concrete specimens with pinholes in 3% sulfuric acid.

21.3.5.4 Type C4 Failure

Blistering on the coating surface (Figure 21.12(d)). In some cases, blisters are also observed on the coating film. Hard blisters on coating surface are caused by expansion of corroded concrete (or primer), while

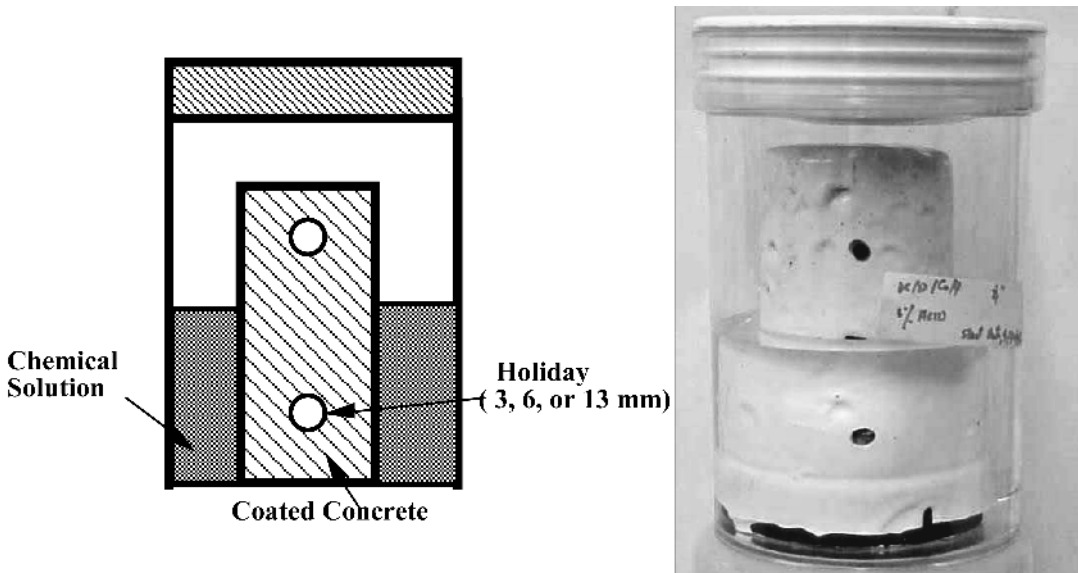


FIGURE 21.7 Chemical tests on coating materials for concrete (CIGMAT CT-1, modified ASTM G-20).

soft blisters on the coating surface are caused by osmotic pressure.

21.3.6 Time-to-failure Factor

For uncoated specimens in 3% sulfuric acid, failure was defined by 2% weight loss, and all specimens failed in seven days (t_0). In order to quantify the performance of coated concrete, the time-to-failure factor (K) is defined as the ratio of the failure time of the coated specimens to the failure time of the uncoated specimens in 3% sulfuric acid. (t) as follows:

$$K = \frac{t}{t_0} \tag{21.1}$$

As shown in Figure 21.13(a) and (b), the time-to-failure factors for Epoxy-1 are as follows.

For 100% passing:

Dry condition $K_{100} = \frac{t_{100}^D}{t_0} = \frac{200}{7} = 29,$

Wet condition $K_{100} = \frac{t_{100}^W}{t_0} = \frac{500}{7} = 71.$

For 50% pass:

Dry condition $K_{50} = \frac{t_{50}^D}{t_0} = \frac{300}{7} = 43,$

Wet condition $K_{50} = \frac{t_{50}^W}{t_0} = \frac{1100}{7} = 157.$

Where t_{100} = time for coated concrete 100% pass in acid.

t_{50} = time for coated concrete 50% pass in acid.

t_0 = time when uncoated concrete fails in acid.

D, W = dry and wet conditions, respectively

By comparing the time-to-failure factors for different coatings, the acid resistance of the coatings can clearly be classified. The higher the time-to-failure factors, the better the acid resistance of the coating.

21.4 MODELING LIQUID TRANSPORT INTO COATED CONCRETE

In order to better quantify the factors influencing the performance of coated concrete, models were developed based on a mass transfer concept.

21.4.1 (a) Physical Model

When coated concrete came into contact with liquid, liquid penetrated through the coating film into the concrete. Physical models for coated concrete when immersed in liquid can be divided into the following two categories, based on the reactivity of the liquids with the concrete substrate and coatings.

21.4.1.1 Category 1: No Chemical Reaction

If the liquid did not chemically damage either the coating film or the concrete, such as D. I. water in

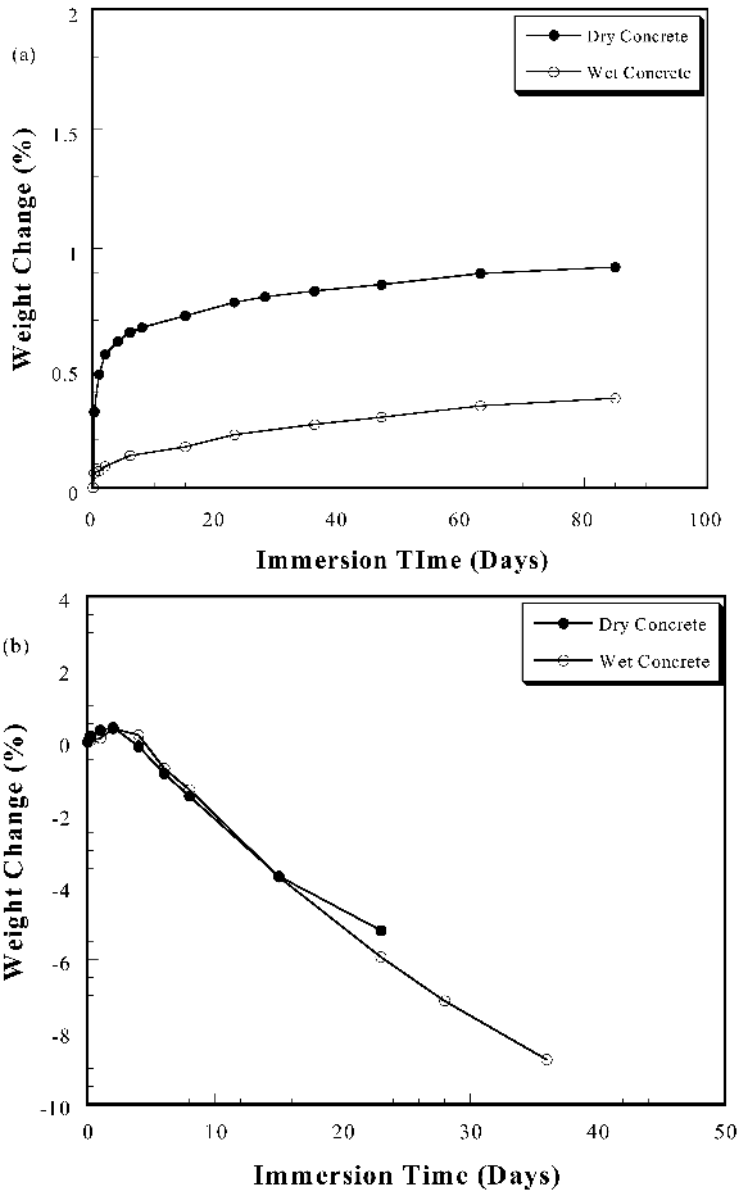


FIGURE 21.8 Weight change in uncoated concrete: (a) D.I. water; (b) 3% sulfuric acid.

the present study, the physical model of liquid penetrating into the coated concrete specimens can be represented as shown in Figure 21.14(a).

In this case, the liquid saturated the contact surface of the coating film. Due to the gradient of the degree of saturation in the coating film, the liquid penetrated through the coating film into the concrete substrate. It was assumed that there was no physical damage to either the coating film or the concrete.

21.4.1.2 Category 2: With Chemical Reaction

If the liquid, such as sulfuric acid solutions, reacts with the concrete substrate and damages the concrete matrix, the concrete will be attacked layer by layer, starting from the interface of the coating film and the concrete substrate. The physical model for this case can be represented as shown in Figure 21.14(b)

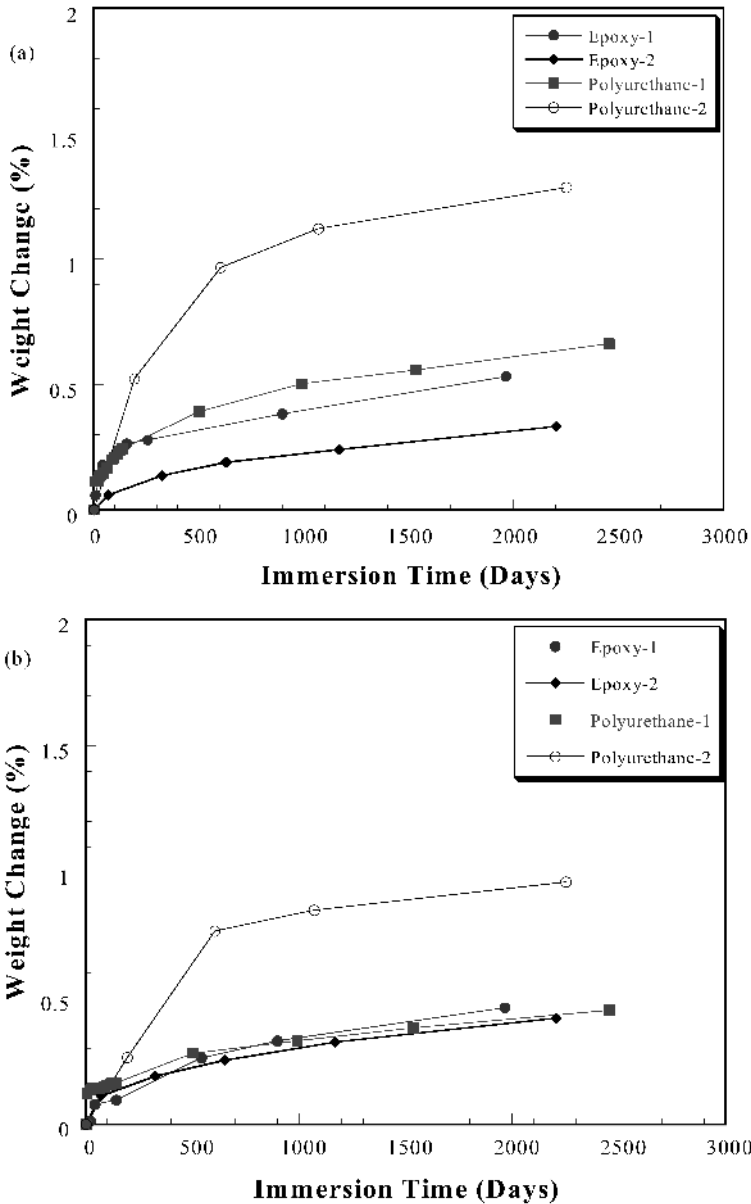


FIGURE 21.9 Weight change of coated concrete in D.I. water: (a) Dry concrete; (b) Wet concrete.

where there is a region of reacted concrete and the degree of saturation of the liquid in this concrete substrate is only in the reacted and affected zone.

21.4.1.3 Assumptions in Developing the Models

To simplify the process of liquid transport in coated concrete, some assumptions are made in developing

the models. According to the observed mechanisms, the assumptions for modeling the liquid uptake by coated concrete cylinders are as follows:

1. Degree of saturation of liquid (S) for coating and concrete is defined as follows:

$$\frac{\text{Mass of Liquid Absorbed}}{\text{Solid Volume}}$$

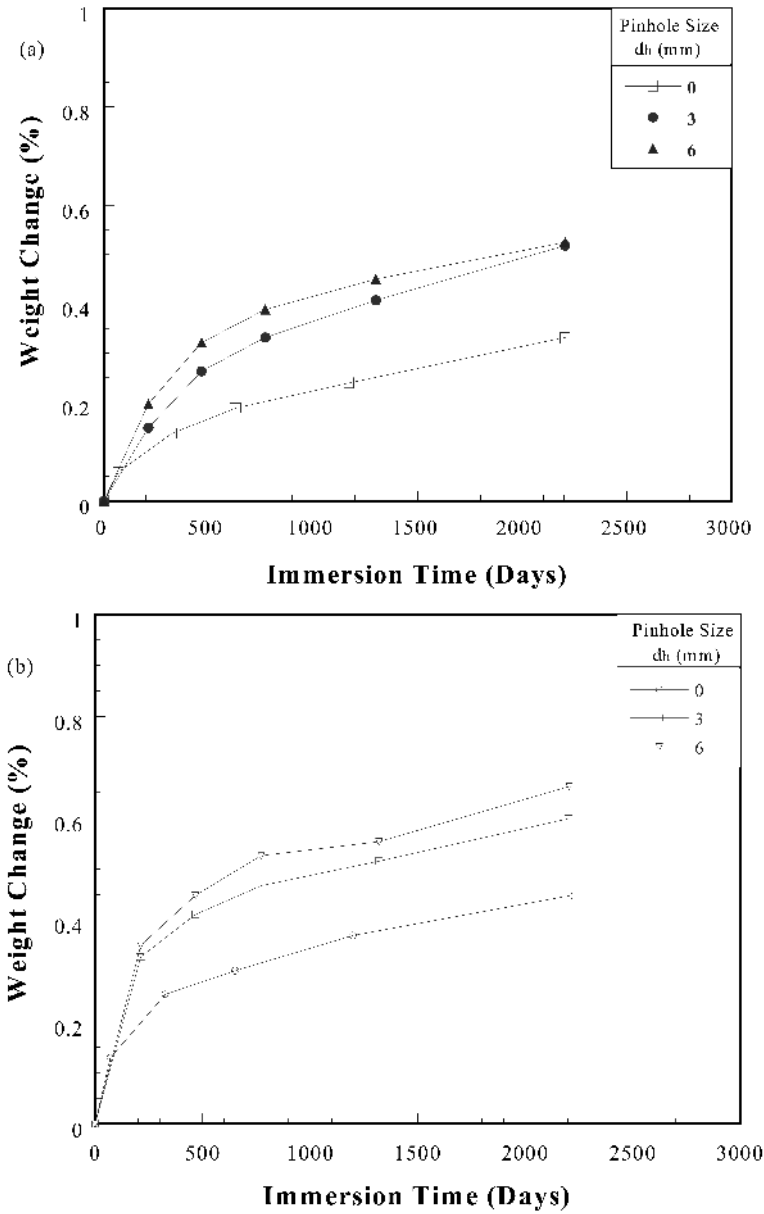


FIGURE 21.10 Pinhole effect on weight change of Epoxy-2 coated concrete in D.I. water: (a) Dry concrete; (b) Wet concrete.

- The process can be modeled by second-order differential equation (Crank, 1975)

$$\frac{\partial S}{\partial t} = D \left(\frac{\partial^2 S}{\partial x^2} + \frac{\partial^2 S}{\partial y^2} + \frac{\partial^2 S}{\partial z^2} \right); \quad (21.2)$$

where S is the degree of saturation of the coating or concrete

- The mass transfer coefficient is a constant in the coating film (D_{CT}), un-reacted concrete cylinder (D_{CO}), or reacted concrete region (D_{CO}^r)

- Coating surface in contact with the liquid is assumed to be saturated
- Coating film and concrete surface are in good contact, so there is no accumulation of liquid at the interface
- Coating film does not react with liquid

21.4.2 (b) Film Model (Model 1)

The coating thickness on the concrete cylinder was in the range of 1.5–2.0 mm for the two epoxy coat-

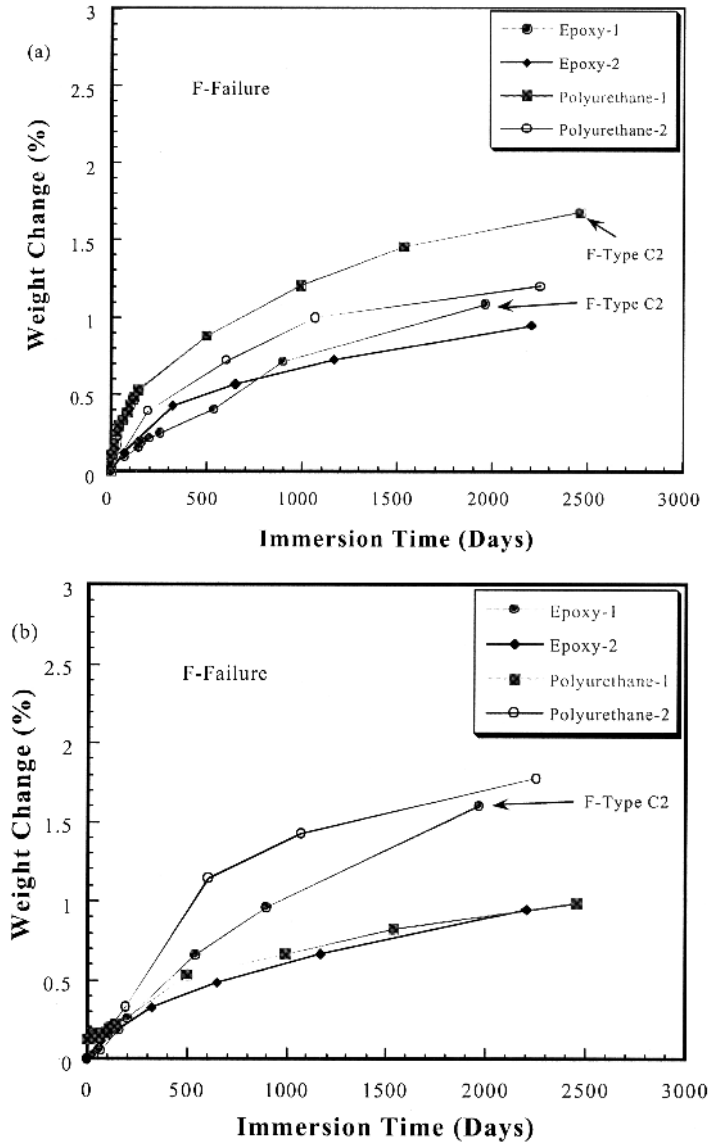


FIGURE 21.11 Weight change in coated concrete in 3% sulfuric acid: (a) Dry concrete; (b) Wet concrete.

ings; hence, it can be treated as a thin plane sheet. The degrees of saturation of the coating surface on the liquid side and the interface are S_0^{CT} and S_i^{CT} , respectively (Figure 21.14(a)).

The mass transport process in one dimension under non-steady state, if the transport parameter is D_{CT} , is given by (Crank, 1975)

$$\frac{\partial S}{\partial t} = D_{CT} \frac{\partial^2 S}{\partial x^2}, \quad (21.3)$$

where S = degree of saturation, g liquid/cm³ solid

T = time, sec
 x = dimension in the coating thickness direction, cm
 D_{CT} = mass transfer coefficient, cm²/sec

For a coating film on a porous substrate, the degree of saturation on the interface of the coating film and the substrate vary with time. If a small time interval t to $(t + dt)$ is considered, the process can be assumed to be a pseudo steady state. In this case, Eq. (21.3) in one dimension reduces to

$$\frac{d^2 S}{dx^2} = 0. \quad (21.4)$$

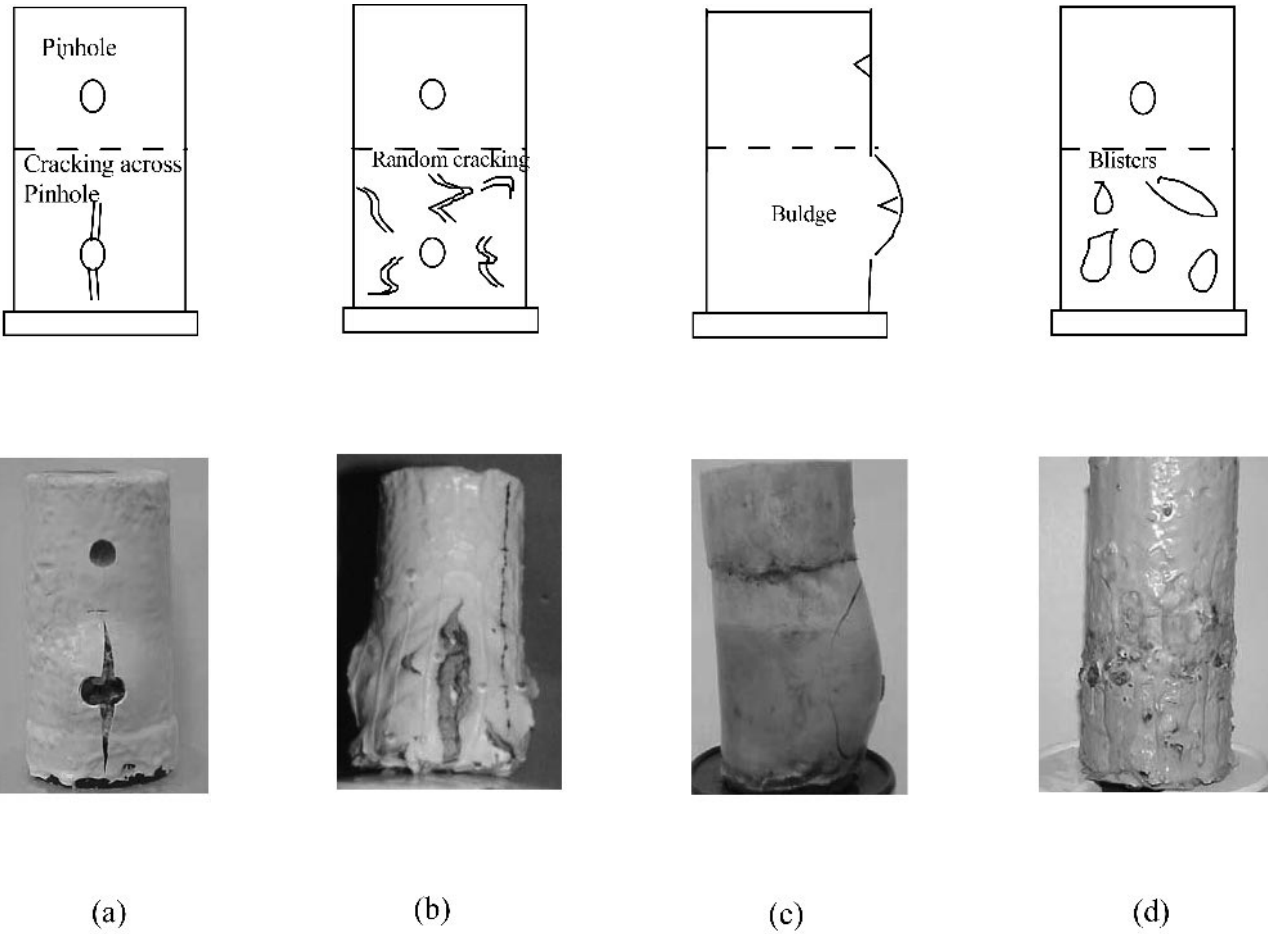


FIGURE 21.12 Failure types of coated concrete specimens.

Integrating Eq. (21.4) and applying the conditions at $x = 0, S = S_0^{CT}$ and $x = \ell, S = S_i^{CT}$, we have

$$\frac{S - S_0^{CT}}{S_i^{CT} - S_0^{CT}} = \frac{x}{\ell} \quad (21.5)$$

The rate of mass transfer F (g liquid/ cm^2 solid) through a plane sheet under steady state is given (Crank, 1975)

$$F = -D_{CT} \left(\frac{dS}{dx} \right), \quad (21.6)$$

Assuming that the degree of saturation on the interface (coating-concrete) varies with time t and can be represented by the following exponential function:

$$S_i^{CT} = S_0^{CT} (1 - e^{-\beta^{CT}t}), \quad (21.7)$$

where β^{CT} is a coating material parameter related to the rate of the coating film saturation. The lower the value of β^{CT} , the lower is the rate of saturation in the coating film. In selecting coatings for rehabilitation, low value of β^{CT} will be preferred.

Eq. (21.6) can be written as:

$$F_{(t)} = \frac{D_{CT}}{\ell} S_0^{CT} e^{-\beta^{CT}t}, \quad (21.8)$$

The amount of the substance transported through the coating film (in the present case around the cylindrical coated specimen) from time t to $(t + dt)$ is:

$$dW_t = 2\pi R h F_{(t)} dt \quad (21.9)$$

The accumulated amount of the substance transported through the coating film from time 0 to t is:

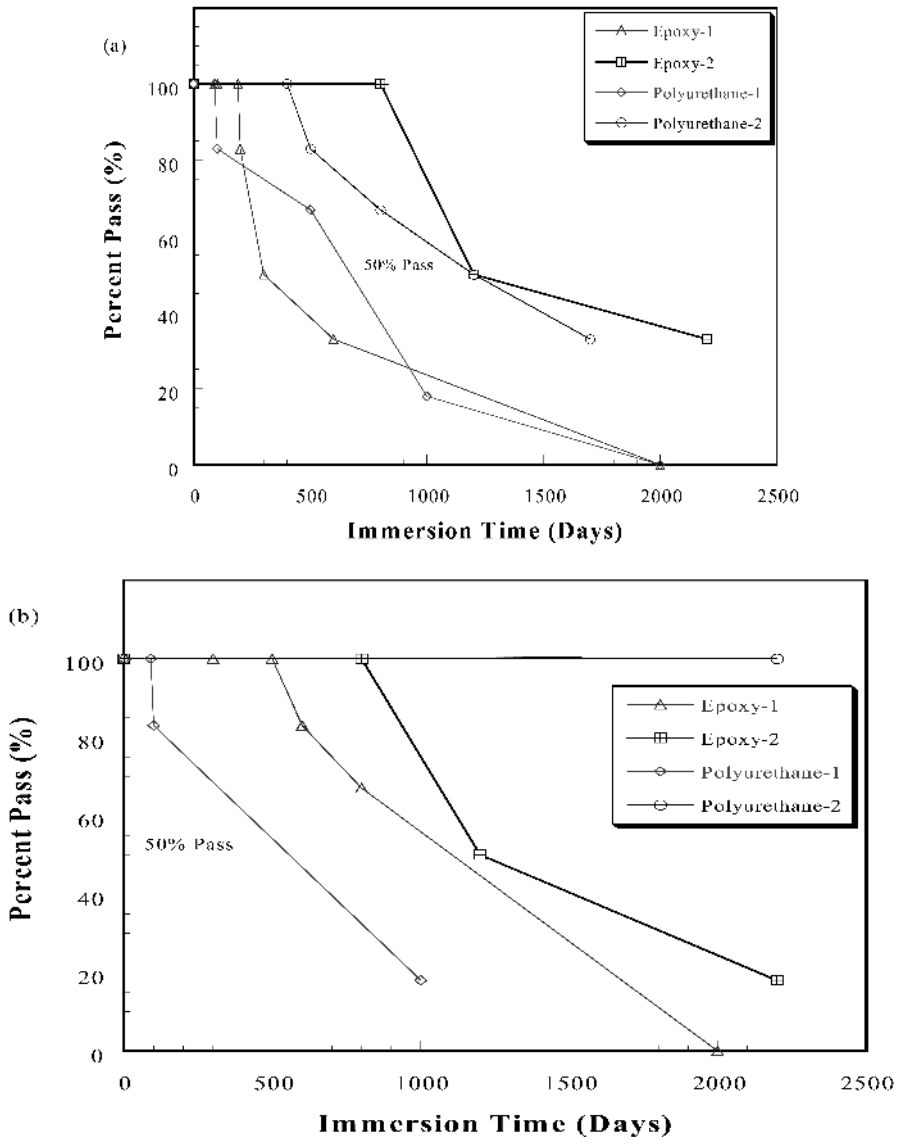


FIGURE 21.13 Percentage passing versus immersion time for dry and wet coated concrete in 3% sulfuric acid: (a) Dry coated concrete; (b) Wet coated concrete.

$$W_t = 2\pi Rh \int_0^t F_{(t)} dt, \quad (21.10)$$

$$W_t = \frac{2\pi Rh S_0^{CT} D_{CT}}{\beta^{CT} \ell} (1 - e^{-\beta^{CT} t}). \quad (21.12)$$

where R = radius of concrete specimen, cm
 h = height of specimen, cm

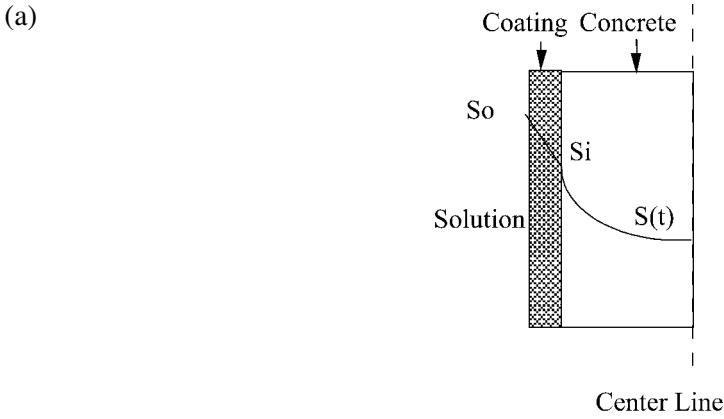
That is

$$W_t = 2\pi Rh \int_0^t \frac{D_{CT}}{\ell} S_0^{CT} e^{-\beta^{CT} t} dt, \quad (21.11)$$

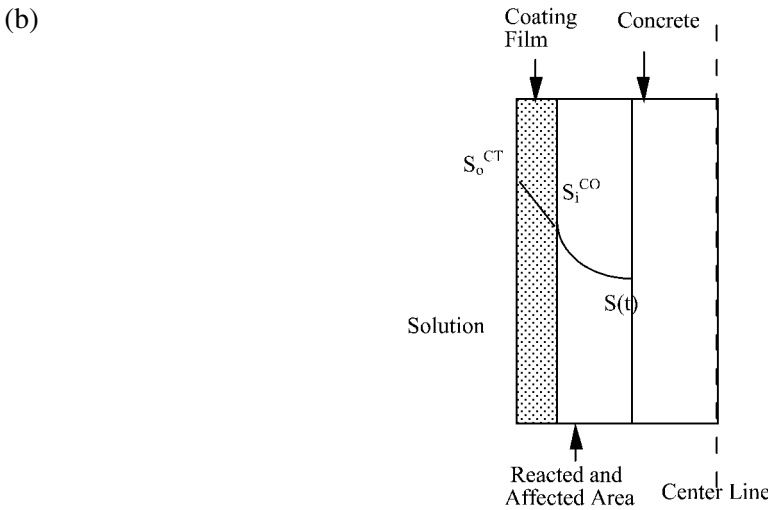
Finally, by integrating Eq. (21.11), the following relation is obtained:

Eq. (21.12) (Model 1) is the film model to predict the mass transfer through coating film on cylindrical concrete specimen which results in the measured mass change in the specimens.

The ultimate degree of saturation, S_0 , was obtained from the experiments on pure coating bulk materials. Relating Eq. (21.12) to the mass change-time relationship of coated concrete, the mass transfer coefficient and parameter β^{CT} for the two coatings can be obtained.



Where S_o ultimate degree of saturation in coating film;
 S_i degree of saturation at the interface of coating film-concrete substrate;
 $S(t)$ degree of saturation distribution of liquid inside concrete cylinder.



Where S_o^{CT} ultimate degree of saturation in coating film, g liquid/cm³ solid;
 S_i^{CO} degree of saturation on the interface of coating film and concrete substrate, g liquid/cm³ solid;
 $S(t)$ Degree of saturation distribution of liquid inside corroded zone of concrete cylinder, g liquid/cm³ solid.

FIGURE 21.14 Physical models of coated concrete in solution: (a) Film model; (b) Concrete model.

21.4.3 (c) Bulk Model (Based on Concrete)

21.4.3.1 Non-reactive Solution (Model 2)

For mass transport in cylindrical specimens, if the degree of saturation is a function of radius and time only, the second-order differential equation is:

$$\frac{\partial S}{\partial t} = \frac{1}{r} \frac{\partial}{\partial r} \left(r D_{CO} \frac{\partial S}{\partial r} \right), \quad (21.13)$$

where D_{CO} is the mass transfer coefficient of the substrate.

For liquid transport in a coated concrete cylinder without chemical reaction, the degree of saturation on the concrete surface changes with time. If the degree of saturation at the concrete surface is $\phi(t)$, the solution of the second-order differential Eq. (21.13) is given (Crank, 1975) by

$$S = \frac{2D_{CO}}{R} \sum_{n=1}^{\infty} \exp(-D_{CO}\alpha_n^2 t) \frac{\alpha_n J_0(r\alpha_n)}{J_1(R\alpha_n)} \int_0^t \exp(D_{CO}\alpha_n^2 t) \phi(t) dt, \quad (21.14)$$

where $J_0(R\alpha_n)$ is the Bessel function of the first order zero, $J_1(R\alpha_n)$ is the Bessel function of the first order, and s are the roots of $J_0(R\alpha_n)$.

Assuming $\phi(t) = S_0^{CO} \{1 - \exp(-\bar{\beta}t)\}$, representing the degree of saturation at concrete surface (coating-concrete interface) which approaches a limiting value S_0^{CO} , the sorption-time curve is given by Crank (1975):

$$\frac{W_t^{CO}}{\pi R^2 h S_0^{CO}} = 1 - \frac{2J_1\{(\bar{\beta}R^2/D_{CO})^{1/2}\} \exp(-\bar{\beta}t)}{(\bar{\beta}R^2/D_{CO})^{1/2} J_0\{(\bar{\beta}R^2/D_{CO})^{1/2}\}}$$

$$+ \frac{4}{R^2} \sum_{n=1}^{\infty} \frac{\exp(-D_{CO}\alpha_n^2 t)}{\alpha_n^2 \{ \alpha_n^2 / (\bar{\beta}/D_{CO}) - 1 \}}. \quad (21.15)$$

Figure 21.15 shows the liquid uptake curves for different values of parameter $\bar{\beta}R^2/D_{CO}(\lambda)$ (Crank 1975). /

From Figure 21.15, the solution uptake is determined by the parameter $\bar{\beta}R^2/D_{CO}$, which represents the effects of the coating material properties, and the parameter $(D_{CO}t/R^2)^{1/2}$ (x-axis), which represents the time effect.

Let

$$\lambda_{CO} = \bar{\beta}R^2/D_{CO}.$$

Approximating Eq. (21.14) and considering an exponential function of the form

$$\frac{W_t^{CO}}{\pi R^2 h S_0^{CO}} = \left\{ 1 - \exp \left[-\lambda_{CO} \left(\frac{D_{CO}t}{R^2} \right)^n \right] \right\}, \quad (21.16)$$

where n is a constant.

The Eq. (21.16) is best fitted to the standard curves in Figure 21.16 for different λ_{CO} values by using the least-square method. The parameter λ_{CO} and n with coefficient of correlation are summarized

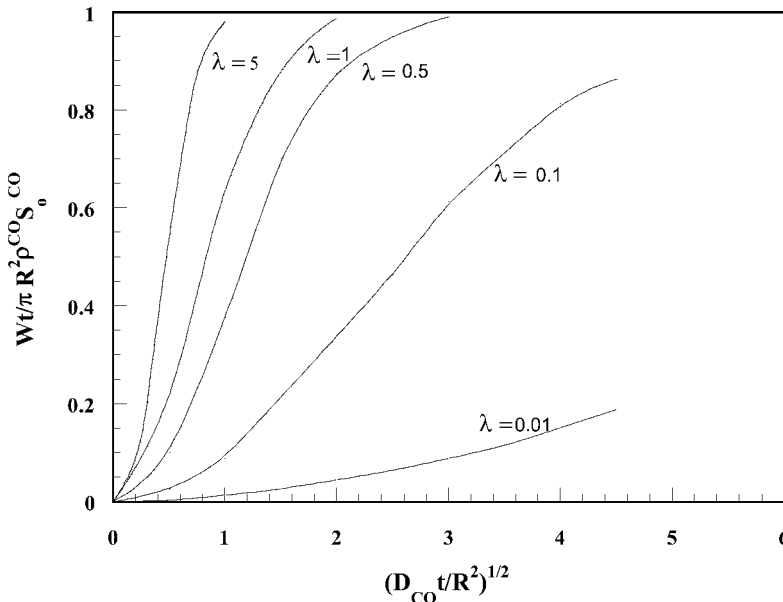


FIGURE 21.15 Calculated sorption curves for a surface degree of saturation given by $S_0^{CO} \{1 - \exp(-\bar{\beta}t)\}$ (Numbers on curves are values of $\bar{\beta}^2 / D_{CO}$) [Source: Crank, 1975]

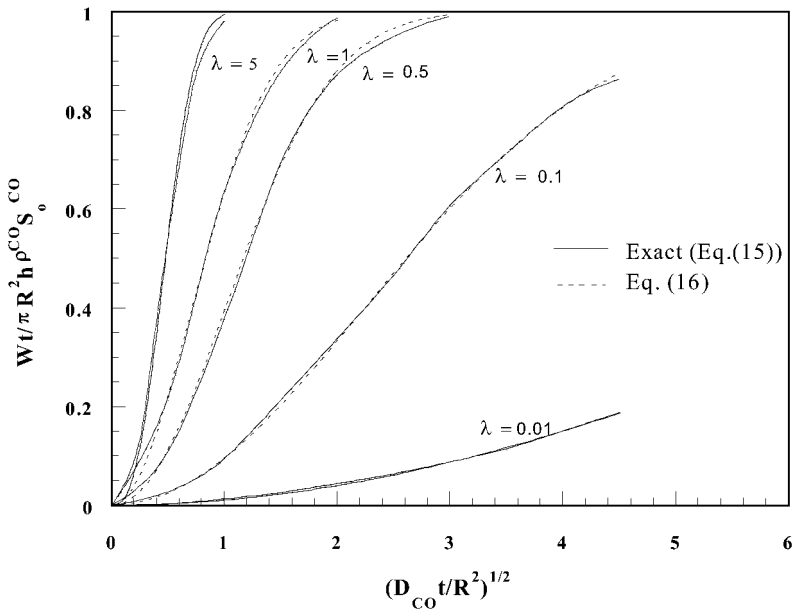


FIGURE 21.16 Comparing exact (solid line) solution to the approximate solutions for a surface degree of saturation given by: $S_0^{CO} \{1 - \exp(-\beta t)\}$ (Numbers on Curves Are Values of $\beta R^2 / D_{CO} (\lambda)$)

TABLE 21.3 Values of Parameter n from Curve Fitting

| λ_{CO} | n | Coefficient of Correlation |
|----------------|-------|----------------------------|
| 0.01 | 1.006 | 0.99 |
| 0.1 | 1.009 | 0.99 |
| 0.5 | 1.042 | 0.99 |
| 1 | 1.001 | 0.99 |
| 5 | 1.346 | 0.99 |

in Table 21.3. The value of n varied from 0.98 to 1.26 when the value of λ was in the range of 0.01 to 5.

The approximate solution for Eq. (21.16) is in good agreement with the solution suggested by Crank (1975) (Figure 21.16). The solid curves are the standard curves (Eq. (21.15)) as given by Crank (1975) while the dotted lines are the approximate solution from Eq. (21.16). The agreement of the fit indicates that the approximate solution can predict the mass increase in the specimens as the exact solution does Eq. (21.15) for the assumed degree of saturation ($\phi(t)$) at the concrete interface.

21.4.3.2 Reactive Solution (Model 3)

For liquid transport in concrete cylinders with chemical reaction, Eq. (21.13) can be modified as follows (Crank, 1975):

$$\frac{\partial S}{\partial t} = \frac{1}{r} \left\{ \frac{\partial}{\partial r} \left(r \frac{D_{CO}}{k + 1} \frac{\partial S}{\partial r} \right) \right\}, \quad (21.17)$$

where k is coefficient of chemical reaction. Eq. (21.17) can be solved analytically as Eq. (21.13). The mass transfer coefficient D_{CO} is replaced by D_{CO}^r where

$$D_{CO}^r = \frac{D_{CO}}{k + 1}.$$

So the solution for liquid transport in coated reactive cylinder substrate is as follows:

$$\frac{W_t^r}{\pi R^2 h S_0^r} = \left\{ 1 - \exp \left[-\lambda_{CO}^r \left(\frac{D_{CO}^r t}{R^2} \right)^n \right] \right\}, \quad (21.18)$$

where W_t^r is the mass change, is the ultimate degree of saturation in the reacted area, λ_{CO}^r is the mass transfer coefficient in reacted area, and is defined as before for the reacted region.

21.4.3.3 Effect of Holiday Sizes

It is difficult to apply coatings on a concrete surface uniformly without any defects. Holidays (pinholes) and other defects will develop during the coating process (Redner et al., 1994). Under service condi-

tions, the liquid will penetrate through the holidays on the coating surface into the concrete substrate and the interface. The holiday effect on liquid uptake can be clearly seen in Figure 21.17; hence, it is important to account for the holiday effect in the modeling.

The effect of holiday sizes on the liquid uptake of the coated substrate can be taken into account by introducing a parameter ξ which is a function of holiday sizes, to Eqs. (21.12), (21.16) and (21.18). Parameter ξ will be equal to 1 and assumed to reach the limiting value when the holiday size is large; hence parameter ξ is defined as

$$\xi = 1 + \frac{d_h}{k_1 + k_2 d_h}; \quad (21.19)$$

where d_h = holiday diameter, cm
 k_1, k_2 = parameters related to the coating

Introducing Eq. (21.19) to Eqs. (21.12), (21.16) and (21.18), the equations become

Model 1

$$W_t = \xi \frac{2\pi R h S_0^{CT}}{\beta^{CT}} \frac{D_{CT}}{\ell} (1 - e^{-\beta^{CT} t}), \quad (21.12a)$$

Model 2

$$\frac{W_t^{CO}}{\pi R^2 h S_0^{CO}} = \xi \left\{ 1 - \exp \left[-\lambda_{CO} \left(\frac{D_{CO} t}{R^2} \right)^n \right] \right\}, \quad (21.16a)$$

and

Model 3

$$\frac{W_t^r}{\pi R^2 h S_0^r} = \xi \left\{ 1 - \exp \left[-\lambda_{CO}^r \left(\frac{D_{CO}^r t}{R^2} \right)^n \right] \right\}. \quad (21.18a)$$

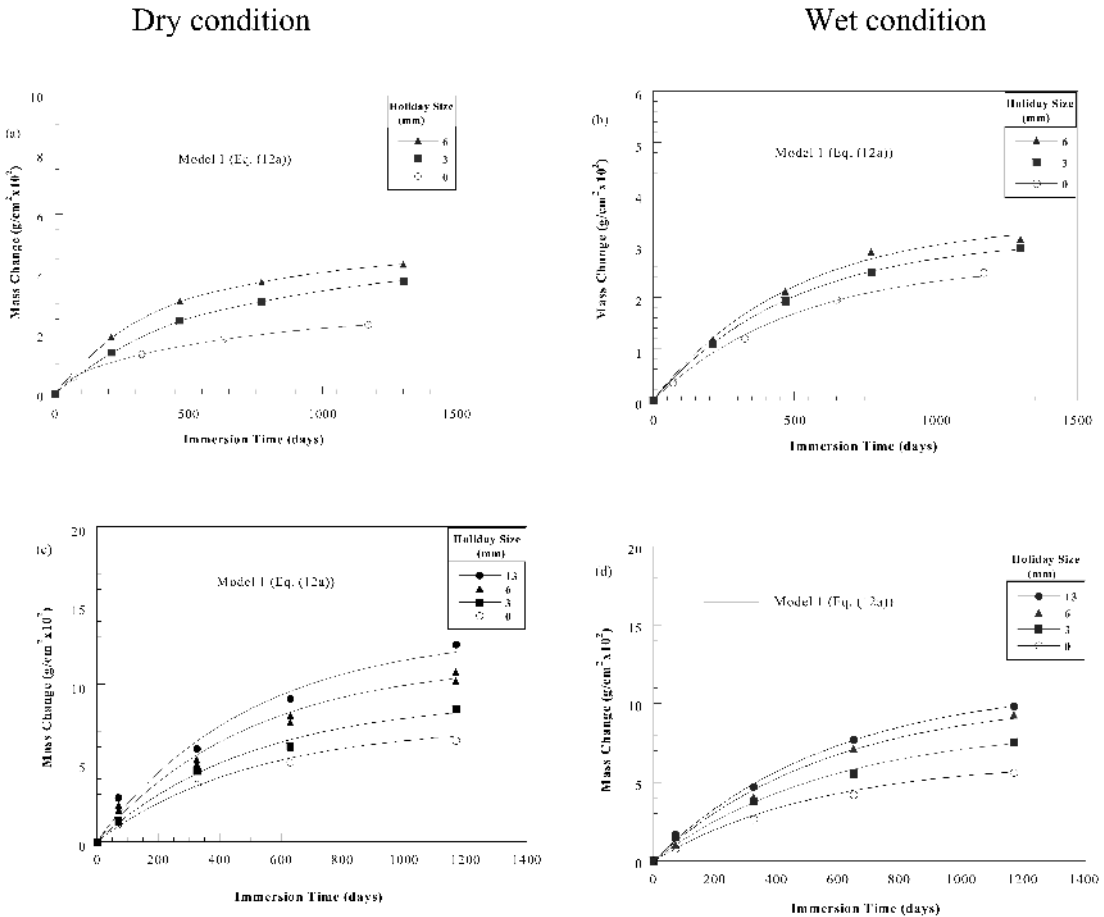


FIGURE 21.17 Comparison of the experimental data with Model 1 predictions in D.I. water and 3% sulfuric acid.

21.4.4 (d) Verifications of Models

21.4.4.1 Film Model (Model 1)

Using Eq. (21.12a), the mass change in the test specimens were predicted and compared to the experimental data in Figure 21.17. The ultimate degree of saturation of the coating (S_0^{CT}) was also determined from pure coating test data (Table 21.3). Based on the model predictions, the values of β^{CT} and D_{CT} for the two epoxy coatings in D.I. water and 3% sulfuric acid are summarized in Table 21.4 and Table 21.5.

The material parameter (β^{CT}) determines the rate of saturation on the coating-concrete interface, and parameters S_0^{CT} , β^{CT} and D_{CT} influence the total uptake of liquid. The material parameters (β^{CT}) for epoxy coatings varied from 0.0020–0.0035. The parameter β^{CT} for Epoxy 1 coating was not much affected by the liquid type and the conditions of concrete (dry or wet). This was not the case with Epoxy 2, where β^{CT} changed with liquid type and condition of concrete. The parameter (β^{CT}) almost tripled from dry concrete in D.I. water to wet condition in acid.

The mass transfer coefficient (D_{CT}) is proportional to the flux of the liquid. For Epoxy 1, the mass

transfer coefficients (D_{CT}) (Table 21.5) are very close in D.I. water and 3% sulfuric acid. The result indicated that solutions did not affect the performance of coating films, but the mass transfer coefficient of the Epoxy 2 coating film had substantially higher value in 3% sulfuric acid than that in D.I. water. Comparing the mass transfer coefficient (D_{CT}) from model 1 (Table 21.5) with the mass transfer coefficient (D) [from Mebarkia (1995)] (Table 21.3), the results indicate that the film mass transfer coefficients (D_{CT}) (Model 1) were lower than the bulk mass transfer coefficients (D) (Mebarkia 1995), except for Epoxy 2 in 3% sulfuric acid.

The comparison of model 1 and experiment data for Epoxy 1 is shown in Figure 21.17.

21.4.4.2 Bulk Models (Model 2 and Model 3)

The mass transfer coefficients of concrete in D.I. water (D_{CO}) and 3% sulfuric acid (D'_{CO}) can be obtained by fitting the cylindrical model (Mebarkia, 1995)] to experimental data of uncoated concrete specimens. The values of mass transfer coefficients were $2.55 \times 10^{-10} \text{ m}^2/\text{s}$ and $3.08 \times 10^{-10} \text{ m}^2/\text{s}$ in D.I. water and 3% sulfuric acid, respectively.

Using Eq. (21.16), Eq. (21.18), and experimental data, the parameters n , λ , and $\bar{\beta}$ can be obtained for different coatings. The values of n , λ , and $\bar{\beta}$ for different coating systems are shown in Table 21.4. The comparisons of model prediction (Eq. (21.16), Model 2 and Eq. (21.18), Model 3) to experiment data are shown in Figure 21.18.

The parameter $\bar{\beta}$ represents the saturation rate of the concrete surface. It can reflect the conditions of the interface between the coating and the concrete. Higher $\bar{\beta}$ value means that the coating may not form a good barrier on the concrete surface against solution penetration. From Table 21.6, the parameter $\bar{\beta}$ varied from 0.86×10^{-8} to 1.46×10^{-8} in D.I. Water, and from 2.20×10^{-8} to 4.71×10^{-8} in 3% sulfuric acid, respectively. The parameter n varied from 0.521 to 0.579 in D.I. Water, and from 0.493 to 0.761 in 3% sulfuric acid. The values of the parameter n for coated concrete are much less than the value of the parameter n from standard curves. This indicates that the process of liquid penetrating into coated concrete is not a pure diffusion process.

Relating Eqs. (21.16a) and (21.18a) to the experimental data under different holiday sizes, parameters k_l and k_2 can be obtained. The values of k_l and

TABLE 21.4 Values β^{CT} for Different Coatings (Model 1) (No Pinhole)

| Coating Material | Material Parameter β^{CT} | | | |
|------------------|---------------------------------|--------|------------------|--------|
| | D. I. water | | 3% Sulfuric acid | |
| | Dry | Wet | Dry | Wet |
| Epoxy-1 | 0.0023 | 0.0020 | 0.0020 | 0.0017 |
| Epoxy-2 | 0.0026 | 0.0035 | 0.0064 | 0.0070 |

TABLE 21.5 Values of Mass Transfer Coefficient (D_{CT}) for Different Coatings

| Coating Material | Mass Transfer Coefficient D_{CT} from Model 1 $10^{-13} \times \text{m}^2/\text{sec}$ ($10^{-12} \times \text{ft}^2/\text{sec}$) | | | |
|------------------|---|-------------|------------------|-------------|
| | D.I. water | | 3% Sulfuric acid | |
| | Dry | Wet | Dry | Wet |
| Epoxy-1 | 4.51 (4.86) | 3.94 (4.24) | 2.43 (2.62) | 1.97 (2.11) |
| Epoxy-2 | 4.86 (5.23) | 10.3 (11.1) | 27.8 (29.9) | 28.9 (31.1) |

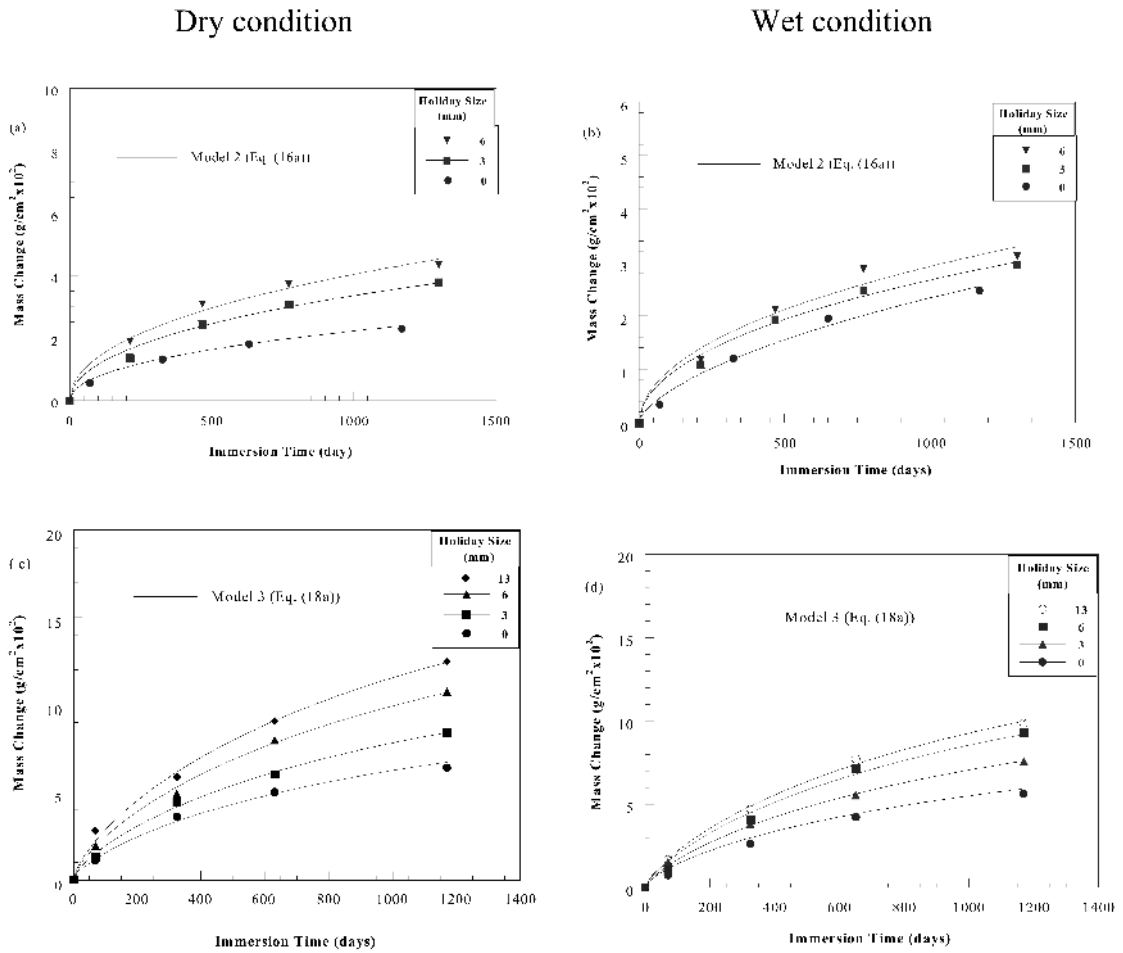


FIGURE 21.18 Comparison of the experimental data with Model 2 and Model 3 prediction in 3% sulfuric acid.

TABLE 21.6 Values of n and λ for Different Coating Coated Concrete

| Coating Material | Application Condition | n | | λ | | $\beta \times 10^{-8} \text{ s}^{-1}$ | |
|------------------|-----------------------|------------|------------------|------------|------------------|---------------------------------------|------------------|
| | | D.I. water | 3% Sulfuric Acid | D.I. water | 3% Sulfuric Acid | D.I. water | 3% Sulfuric Acid |
| Epoxy-1 | dry | 0.556 | 0.741 | 0.059 | 0.107 | 1.04 | 2.27 |
| | wet | 0.521 | 0.761 | 0.060 | 0.104 | 1.05 | 2.20 |
| Epoxy-2 | dry | 0.579 | 0.493 | 0.049 | 0.222 | 0.86 | 4.71 |
| | wet | 0.535 | 0.574 | 0.083 | 0.164 | 1.46 | 3.48 |

k_2 for different coatings in different solutions are summarized in Table 21.7.

The value of k_1 indicates the effect of holidays on liquid uptake of coated substrates. The smaller the value of k_1 , the more the effect of holidays on the liquid uptake of coated substrates. The value of k_2 indi-

cates the effect of holiday sizes on the liquid uptake of coated substrates. The smaller the value of k_2 , the more the effect of holiday sizes on the liquid uptake of coated substrates. The prediction of holiday size effect on mass change of Epoxy 1 coated concrete is shown in Figs. 21.17 and 21.18.

TABLE 21.7 Values of k_1 and k_2 for Different Coatings

| Coating Code | Coating Condition | D. I Water | | 3% Sulfuric Acid | |
|--------------|-------------------|------------|-------|------------------|-------|
| | | k_1 | k_2 | k_1 | k_2 |
| Epoxy-1 | Dry | 0.84 | 0.32 | 0.75 | 0.51 |
| | Wet | 1.79 | 0.20 | 0.85 | 1.58 |
| Epoxy-2 | Dry | 0.21 | 0.32 | 0.35 | 0.78 |
| | Wet | 0.30 | 0.50 | 0.55 | 1.07 |

21.5 CONCLUSIONS

A series of full-scale and laboratory tests were developed to evaluate the performance of coating materials for protecting dry and wet concrete substrates exposed to sulfuric acid environments. Commercially available polymer- and cement-based coatings were studied for a period of over five years. Analytical models were developed to predict mass change and holiday size effect on coated concrete. The performance of epoxy coated concrete in D.I. water and 3% sulfuric acid was investigated over three years. Based on the experimental results and analyses, the following observations are advanced:

1. The full-scale hydrostatic test was used to effectively evaluate the applicability of coatings onto concrete under hydrostatic back pressure up to 105 kPa (15 psi) with a moisture emission of 536 $\mu\text{g}/(\text{m}^2\cdot\text{sec})$ (9.49 lb/(1,000 $\text{ft}^2\cdot 24$ h)). Over 90% of the coatings tested passed this test.
2. Two bonding tests were modified, based on the ASTM standards. Based on the test results, five modes of failure have been identified. Bonding strength of the coatings varied from 0.25 MPa (36 psi) to 2.50 MPa (360 psi).
3. Chemical resistance tests can effectively evaluate the acid resistance of coated concrete. Test results showed that coatings substantially reduce solution penetration into coated concrete. The service life of coated concrete can be prolonged 14 to 114 times more than uncoated concrete in acid solutions.
4. The film model and concrete model developed in this study can be used to predict mass increase of coated concrete in reactive and non-reactive solutions. The model parameters were sensitive to the changes in coatings, solutions, and holiday sizes. Results showed that the models can better predict

the performance of coated substrate in long-term immersion conditions.

5. Bulk parameters obtained by testing coating materials alone may not represent the performance of coatings on concrete substrates.
6. Holidays can substantially increase the mass change in coated concrete. The test results and analyses showed that there is a limiting value for holiday size, beyond which the effect is minimal (depending on coatings and solutions).

21.6 ACKNOWLEDGEMENT

This project was supported by the Center for Innovative Grouting Materials and Technology (CIGMAT), under grants from the City of Houston, National Science Foundation (CMS-9526094, CMS-9634685), and various industries.

21.7 REFERENCES

1. Coti, H., Fernandez-Prini, R. and Gomez, D. 1982. Protective Organic Coatings: Membrane Properties and Performance. *Progress in Organic Coatings*, Vol. 10(1), 5–33.
2. Crank, J. *The Mathematics of Diffusion*, 2nd Ed. New York: Oxford University Press, 1975.
3. Ehrich, S., Helard, L., Letourneux, R., Willocq, J. and Bock, E. 1999. Biogenic and Chemical Sulfuric Acid Corrosion of Mortars. *Journal of Materials in Civil Engineering*, Vol. 11(4), 340–344.
4. Fattuhi, N. I. and Hughes, B. P. 1988. The Performance of Cement Paste and Concrete Subjected to Sulfuric Acid Attack. *Cement and Concrete Research*, Vol. 18(4), 545–553.
5. Gospodinove, P. N., Kazandjiev, R. F., Partalin, T. A. and Mironova, M. K. 1999. Diffusion of Sulfate Ions into Cement Stone Regarding Simultaneous Chemical Reactions and Resulting Effects. *Cement and Concrete Research*, Vol. 29(10), 1,591–1,596.
6. Hinsenveld, M. 1995. The Shrinking Core Model as a Representation of Leaching Processes in Cement Stabilized Waste. *Contaminated Soil* (Netherlands), 1,251–1,252.
7. Islander, R. L., Deviny, J. S., Mansfield, F., Postyn, A. and Shih, H. 1991. Microbial Ecology of Crown Corrosion in Sewers. *Journal of Environmental Engineering*, Vol. 117(6), 751–770.
8. Liu, J. and Vipulanandan, C. 1999. Testing Epoxy Coatings for Dry and Wet Concrete Wastewater Facilities. *Journal of Protective Coatings and Linings*, Vol. 16(12), 26–37.
9. Liu, J. and Vipulanandan, C. 2003. Modeling Water and Sulfuric Acid Transport through Coated Cement Concrete. *Journal of Engineering Mechanics*, Vol. 129(4), 426–437.

10. Mainguy, M. Tognazzi, C., Torrenti, J-M. and Adenot, F. 2000. Modeling of Leaching in Pure Cement Paste and Mortar. *Cement and Concrete Research*, Vol. 30(1), 83–90.
11. Martys, N. S. and Ferraris, C. F. 1997. Capillary Transport in Mortars and Concrete. *Cement and Concrete Research*, Vol. 27(5), 747–760.
12. Mebarkia, S. and Vipulanandan, C. 1995. Mechanical Properties and Water Diffusion in Polyester Polymer Concrete. *Journal of Engineering Mechanics*, Vol. 121(12), 1,359–1,365.
13. Nguyen, T., Bentz, D. and Byrd, E. 1995. Method for Measuring Water diffusion in a Coating Applied to a Substrate. *Journal of Coatings Technology*, Vol. 67(844), 37–46.
14. Redner, J. A., Hsi, R. P. and Esfandi, E. J. 1994. Evaluating Coatings for Concrete in Wastewater Facilities: An Update. *Journal of Protective Coatings and Linings*, Vol. 11(12), 50–61.
15. Sand, W., Dumas, T., Marcdargent, S., Pugliese, A. and Cabiron, J. 1994. Tests for Biogenic Sulfuric Acid Corrosion in a Simulation Chamber Confirms the On Site Performance of Calcium Aluminate-Based Concrete in Sewage Application. ASCE Material Engineering Conference, San Diego, CA, November 14–6,1994.
16. Soebbing, J. B., Skabo, R. R. and Michel, H. E. 1996. Rehabilitating Water and Wastewater Treatment Plants. *Journal of Protective Coatings and Linings*, Vol. 13(5), 54–64.
17. Tang, L. and Nilsson, L. 1992. A Study of The Quantitative Relationship between Permeability and Pore Size Distribution of Hardened Cement Pastes. *Cement and Concrete Research*, Vol. 22(4), 541–550
18. Thomas, N. L. 1991. The Barrier Properties of Paint Coatings. *Progress in Organic Coatings*, Vol. 19(2), 101–121.

CHAPTER 22

THE ROLE OF INTRINSIC DEFECTS IN THE PROTECTIVE BEHAVIOR OF ORGANIC COATINGS

S. Ray Taylor

Department of Biomaterials, School of Dentistry, University of Mississippi Medical Center, Jackson, Mississippi

22.1 INTRODUCTION 449

22.2 TYPES OF COATING DEFECTS 450

22.3 ELECTROCHEMICAL METHODS FOR THE LOCAL
CHARACTERIZATION OF COATINGS 451

22.4 FINDINGS THROUGH THE USE OF
LEIM AND LEIS 452

22.5 THE USE OF MOLECULAR PROBES 458

22.6 REFERENCES 460

22.1 INTRODUCTION

Organic coatings are a complex mixture of polymers, fluid carriers, pigments, corrosion inhibitors, and additives. They represent the oldest and most widely used method for protecting a metallic substrate from corrosion. While the presence of inhibitive pigments are an essential component of the corrosion protective qualities of some paint systems, the corrosion protection provided by an organic coating or coating system is typically considered to be a function of its barrier and adhesion properties. Most of the attention in the science of understanding and predicting the service life of organic coatings has been dedicated to an examination of the barrier properties of coatings and a determination of how, or if, the rate of ion ingress might be predictive of the corrosion protective properties of the coating.

Thus, one of the roles of an organic coating is to prevent ions from accessing the metallic substrate. Yet, we know that over time, water, ions, and some reducible species (typically oxygen) from the environment eventually penetrate the coating or coating system, and initiate electrochemical reactions (i.e., oxidation and reduction) at the metal interface. But why and how do water, ions, and gas enter the coating? If they enter the coating at some altered site or region, knowing the physical and chemical nature of this site (or region) and the means for eliminating them could form the basis for a new class of coatings with superior barrier coating properties.

Observationally, we know that the failure of an organic coated metal is initiated at some local site. Ignoring the obvious scenario of a physical breach (e.g., a pinhole), the question can be immediately raised as to whether this local corrosion event was: (i) the result of a local ionic pathway in the organic coating, a local substrate heterogeneity (e.g., an intermetallic particle) in the presence of a uniform diffusion front through the organic layer, or (ii) perhaps the juxtaposition of both a heterogeneity in the coating with a heterogeneity in the substrate. There is ample evidence that the micro-galvanic cells formed by intermetallic particles within an alloy facilitate localized corrosion. However, the mode by which ions and water penetrate a contiguous organic layer (i.e., the coating) has not been clearly delineated. The objective of this chapter is to address the question of whether ions and water penetrate the coating via discrete channels or as a uniform diffusion front, and to examine some of the new research tools that are being implemented to answer these questions.

In addition to the scientific quest of understanding the basis for transport of materials through a medium, there is also the technological motivation for the development of more perfect barriers. If it can be determined that a specific material defect due to a chemical heterogeneity or application procedure is the source for ionic ingress, then remedial measures can be taken so as to produce more impenetrable barriers. But the question regarding the mode of ion entry (i.e., whether ions enter through

discrete pathways or as a uniform front) must first be addressed.

22.2 TYPES OF COATING DEFECTS

Even for a coating made from a pure polymer (i.e., neat resin with no additives), multiple types of focal defects could act as local access sites for water and electrolyte entry. Some defects can be a result of manmade or external factors (i.e., *extrinsic* defects). Examples of this type of defect would include scratches, pinholes, thinned regions, bubbles produced by convection, and dust wicks. There are also defects which could arise as a result of the resin chemistry itself (i.e., *intrinsic* defects). It has been suggested that intrinsic ionic pathways might arise from poorly cross-linked areas, retained acid functionality in the resin, or other phenomena [1,2]. This chapter will not be concerned with extrinsic defects that are obvious sites for the initiation of corrosion failures. However, knowledge regarding the presence and prevalence of subtle forms of these types of defects should be determined and will hopefully fall out of any attempt to characterize intrinsic coating heterogeneities. This chapter will focus on the idea of whether water and ions move through contiguous organic coatings via intrinsic localized pathways. This is a much more difficult question, and one that requires new approaches to the local characterization of materials and electrochemical phenomena.

While bubbles and voids have been described above as being extrinsic-type defects (i.e., manmade), some could justifiably argue that they are, in many cases, intrinsic defects that are a result of the resin chemistry. Because of the numerous sources of bubbles, as well as the controversy which surrounds their source and importance to coating durability, it is worth discussing this type of defect in more detail.

Bubbles form in organic coatings through a variety of mechanisms [3]. They can arise from mechanical action of the resin, release of trapped gases from the substrate, evaporation of the solvent, or chemical reactions (e.g., the reaction between carbonate pigments and an acidic environment), or the reaction between the isocyanate group in a urethane binder with water to liberate carbon dioxide. The intrinsic reaction between the binder chemistry and water are what make bubbles an arguably intrinsic defect in these cases.

How bubbles and voids impact the protective qualities of the coating is controversial and may depend

on the origin and nature of the bubble. While a small number of bubbles are said to not fill with electrolyte and thus not affect the barrier properties of a coating [3], this may depend on the origin and nature of the bubble. Recent studies have shown that bubbles that form in a manner in which they are in contact with the substrate have a much more significant effect on the propensity for electrochemical processes to occur [4]. The fact that the presence of a void or bubble reduces the coating thickness at that point, coupled with the exposed substrate in the case of a contacting bubble, strongly implies that certain types of bubbles will reduce the service life of a coating. Significant bubbles in a coating will reduce coating strength (e.g., shear and compressive strength), and distort parameters such as dry film thickness and additive concentrations (e.g., anti-foulants) [3].

But what if there are no apparent defects in the coating? How then does electrolyte penetrate the polymer? This forms the basis of studies directed at the identification of intrinsic defects. Evidence that supports the notion of heterogeneous transport through coatings has come in many forms. Initial investigations of the origins of coating failure focused on electrical and electrochemical characterizations of dissected patches (1 cm²) of coatings [1,2]. These investigations determined the existence of two general types of behavior in epoxy materials (D- and I-type behavior) and that eventual coating breakdown was associated with specific regions of the coating whose conductivity changed proportionally with the conductivity of the electrolyte (D-type areas). These D-type regions were proposed to provide the eventual locus of failure and have been attributed to factors such as retained solvent, high acid functionality, poor cross-linking, and physical channels. In retrospect, these experiments were confounded by the fact that the coatings were analyzed following corrosion blister formation. The low pH beneath corrosion blisters could itself potentially alter the coating permeability [5].

Subsequent to the experiments above, two divergent theories have evolved for ionic transport through contiguous organic films [6]. One theory proposes that the flux of ions across the film is established by small imperfections or pores, which extend through the thickness of the coating and have cross-sections that are larger than the free space typically present between the molecular chains of the matrix [7–9]. An alternate theory proposes that the ions pass through the bulk matrix of the polymer film [10], but that there are regional differences within a single coating with regards to ion selectiv-

ity [11]. The latter theory is more in alignment with the D- and I-type behavior discussed above.

Evidence for local breakdown is also seen at early stages of coating exposure when using traditional electrochemical measurement methods. An examination of the time trajectory of certain electrochemical parameters, such as the open circuit potential and the pore resistance (a measure of the barrier properties), obtained during global (surface averaged) electrochemical impedance measurements, reveals the presence of metastable events. For example, the pore resistance unexpectedly decreases several orders of magnitude for a short period of time and then recovers within minutes or hours to the original value (or higher). This has been interpreted as the formation and healing of a local intrinsic defect. These metastable breakdown events may be one of the sources of error when using traditional barrier property measurements as a metric for the prediction of long-term coating behavior. If a global electrochemical impedance spectroscopy (EIS) measurement is made on an immersed coating at an instant in time in which one of these metastable breakdown events occurs, the results may not be reflective of the long-term behavior of the coating. This would lead to a skewed interpretation of the projected properties of the test sample.

In addition, the converse may occur. A coating which demonstrates an excellent time trajectory of barrier properties could suddenly develop a fatal flaw (or ionic pathway) soon after it is given a bill of good health. It is possible that the stochastic development of intrinsic defects has been responsible for the discrepancy between barrier property measurements and the prediction of service life. Information about intrinsic defects could provide the needed link between short-term and long-term behavior.

The thought that ions penetrate through local pathways also stems from the now standard terminology of *pore resistance* used to describe the breakdown of barrier properties. The need to insert another resistance into equivalent circuit analogues used to describe the EIS results of immersed coatings was recognized from a modeling standpoint [8]. This was later conceptualized from a phenomenological standpoint [7]. But the idea of coating porosity may stem from the early recognition that some coatings form structures that intrinsically possess pores [12].

The local chemical and electrochemical conditions that control these discrete and transient events are not well understood. From a mechanistic standpoint, further understanding of the nature and origin

of organic coating failure will require the use of localized electrochemical and chemical methods. A local electrochemical probe and mapping method that can systematically detect, locate, and characterize these defects will allow a more detailed analysis of the factors that control these metastable events that, in turn, ultimately control the function and service life of organic coatings.

22.3 ELECTROCHEMICAL METHODS FOR THE LOCAL CHARACTERIZATION OF COATINGS

Coating degradation and the establishment of underfilm corrosion requires ion transport and electrochemical reactions (i.e., oxidation and reduction) at the metal interface. Thus, it has been logical to approach the investigation and quantification of coating degradation with electrical and electrochemical methods. From the standpoint of global (i.e., surface averaged) measurements, the AC-based method Electrochemical Impedance Spectroscopy (EIS) has proven to be an extremely valuable test method for the characterization of organic coating degradation in aqueous media [7,13–20]. As discussed, while a global approach to the electrochemical assessment of coatings has proven to be successful in the delineation of general degradation kinetics, mechanistic and technical questions remain as to where, why, or how the coating has failed. One means of overcoming the limitations of global electrochemical measurements is to characterize the interface with localized methods.

A variety of DC and AC methods have been developed in various fields of science for the *in situ* examination of local electrochemical events. Some of these methods include: scanning reference electrode techniques [21–23], scanning vibrating probes [24–26], Kelvin probes [27–29], electrochemical microscopy [30–32], among other methods [33]. Each of these methods is useful, depending on the interface under study, the type of information desired, and the measurement resolution required. There are also topographic methods, such as atomic force microscopy, that can be used to investigate the surface morphology as opposed to electrochemical information (i.e., voltage and current). This method has been applied to bare electrodes in solution [34], as well as to the surfaces of organic coatings [35–37].

When considering the characterization of local electrochemical events on coated metal substrates, local electrochemical impedance techniques have

been a logical option based upon: (i) the ability of an AC-based method to lower the impedance of a dielectric-type interface (e.g., organically coated metal) by the use of higher frequencies of excitation; and (ii) the ability to more fully characterize a specific site by the application of a range of excitation frequencies to develop a local impedance spectra (LEIS—local electrochemical impedance spectroscopy). Local electrochemical impedance measurements have been made extensively on uncoated (i.e., bare) metal substrates [38–41]. However, it has only been recently that this method has been applied to coated metals [42–44].

22.4 FINDINGS THROUGH THE USE OF LEIM AND LEIS

22.4.1 LEIM and LEIS Methodology

Local electrochemical impedance measurements have been made using a variety of approaches [39–46], but all have employed the basic idea of comparing the voltage excitation to the current response on a local basis. One method that has been used to help characterize local film breakdown phenomenon employs a five-electrode arrangement (shown in Figure 22.1), which is composed of a typical three-electrode arrangement (working electrode, counter electrode, and reference electrode) used to control the DC potential and excite the interface potentiostatically with an AC signal, while two micro-reference electrodes are used to detect the local potential gradient in solution above the sample surface. This design differs from the methods used by others [45,46] in which a vibrating platinum electrode is used to acquire the local potential and current data. The vibrating platinum electrode approach may have advantages from the standpoint of spatial resolution and minimum corruption by frequency dispersion effects [46]. However, this approach has several drawbacks. It has a limitation of the excitation frequency imposed by the electrode vibration (or sampling) frequency selected. It suffers from the inherent instability of a non-reference electrode material (i.e., platinum), and it introduces solution convection by the vibration of the electrode. The five-electrode arrangement described utilizes real micro-reference electrodes, compares the local current to a local voltage, and has thus not shown frequency dispersion effects. It has a higher frequency capability, which is excellent for the characterization of coated metals, and does not stir the electrolyte when at site.

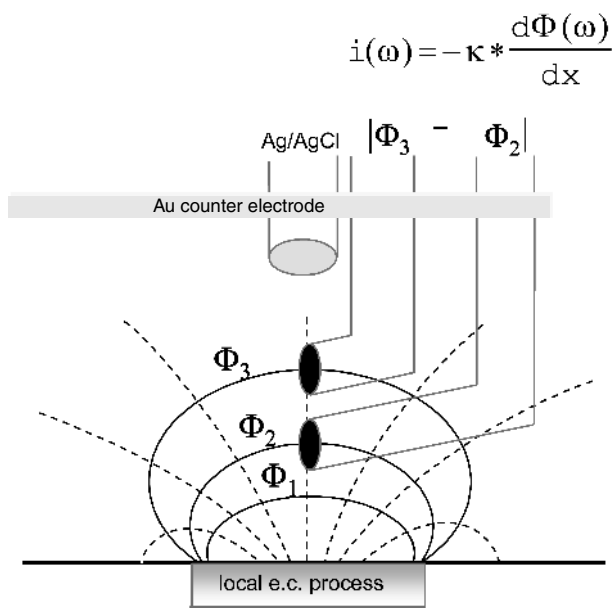


FIGURE 22.1 Schematic of five-electrode system used to measure the local electrochemical impedance. The two micro-reference electrodes assess the local potential gradient in solution above the surface. This potential is used to determine the local current density, which is then compared to the voltage excitation to determine the local impedance.

A local electrochemical impedance map (LEIM) can be obtained by holding the excitation frequency to a fixed value and then rastering the probe over the surface to determine the local impedance at discrete sites. The admittance magnitude (reciprocal of the impedance magnitude) is typically plotted so that areas of low impedance can be visualized as a peak rather than a trough. Local electrochemical impedance spectra (LEIS) can be obtained by holding the probe at a fixed site so that the excitation frequency can be swept over a range to determine the local impedance spectra at that site. The reader is directed to the literature for further details on this method [47].

22.4.2 Information Attained through the Use of LEIM and LEIS

22.4.2.1 Applications to Sources of Manufacturing Defects

One important example of how LEIM can provide insight into the complex interactions between the substrate, the coating, and the environment was seen in the study of a coil-coated aluminum product [48]. Aluminum beverage can lids were examined via

LEIM and shown to possess specific regions of corrosion activity (increased admittance), and specific regions of low activity. These regions occurred in bands across the surface of the can lid. Following the removal of the coating, microscopic examination of the substrate surface revealed the presence of small divots in the substrate surface. These divots existed in bands having dimensions similar to the bands observed via LEIM. The LEIM results and scanning electron micrographs of the surface are shown in Figs. 22.2 and 22.3.

The LEIM results informed the lid manufacturer that there may be the potential for corrosion problems at a time when no problems in the field had been reported. Further investigation into the source of these divots determined that the manufacturing procedure had been changed recently to increase the production speed. The means for increasing the rate of product feed through the stamping machines (i.e., roughening the feed-rollers) was also responsible for the production of the substrate divots. The small amount of plastic deformation caused by feed rollers was sufficient to alter the local interaction of the coating and substrate, and was sufficient to be de-

tected by LEIM. It was determined subsequent to these laboratory tests that these products began to fail in the field and that the small surface divots were the source of product failure.

22.4.2.2 Different Types of Failure Sites are Observed

It is of interest to understand the corrosion initiation and growth process on coated aerospace alloys. A typical aerospace alloy is the aluminum-copper-magnesium system AA2024-T3. This alloy forms intermetallics, which are good for mechanical reasons, but introduces significant corrosion susceptibility.

When this alloy is coated with epoxy resin (representative of an aerospace primer material) or other resin systems (e.g., polyurethane, vinyl, etc.) and subjected to a sodium chloride-containing solution (0.6 M NaCl), several types of corrosion sites can be observed [5]. These sites differ in local electrochemical behavior and in physical attributes.

In late stages, these local defects differ in their visual color. One type of defect was black in color, round in shape, with a diameter of 1–2 mm attained in two to seven days of exposure. Another type of defect was red in color, irregular in shape, and attained a size of 1–7 mm in one to two days of exposure.

LEIM of coated surfaces at very early times of exposure and prior to the appearance of any visible defect, revealed local sites in which high local admittance values were prevalent. In other sites, admittance peaks were observed, but the peaks were significantly smaller in value. A high admittance peak is indicative of greater ease for charge flow, while the lower admittance peak indicates charge flow greater than the surrounding bulk, but less than the high peak areas. This behavior was further confirmed with local electrochemical impedance spectroscopy. Both the LEIM and LEIS results are shown in Figs. 22.4 and 22.5, respectively.

Of relevance is the fact that the high admittance regions eventually formed the red-colored blister, and the regions where lower magnitude peaks were observed formed black-colored blisters. Subsequent chemical analysis of these blisters indicated that the pH within the red blisters was low (pH = 3–5), while the pH inside of the black blisters was significantly higher (pH = 8–11). Analysis of the ionic content of red blisters revealed significant amounts of Cu^{2+} , Al^{3+} , Mg^{2+} , and Cl^- , as well as acetate and formate in the case of polyurethane coatings [5]. Thus, early LEIM and LEIS results are predictive of the type of

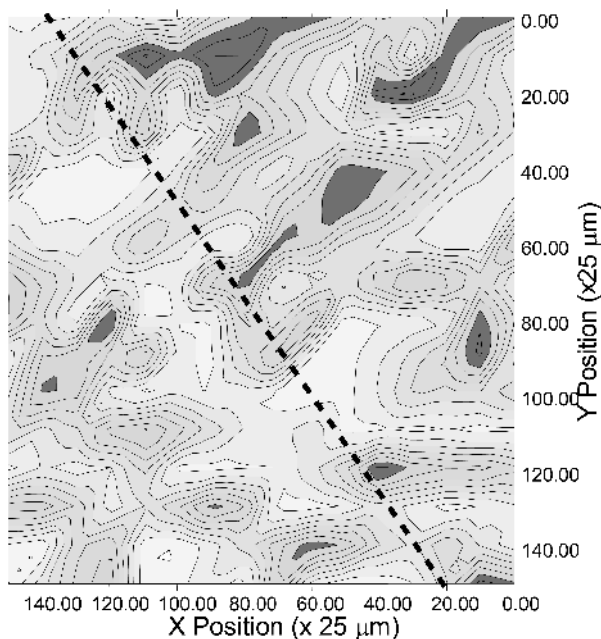


FIGURE 22.2 Local electrochemical impedance contour plot of a coil-coated aluminum beverage can lid in 0.6M NaCl. The dark regions are areas of increased electrochemical activity. The dashed diagonal line demarks a band of increased electrochemical activity (right of line) from a band of lower activity (left of line).

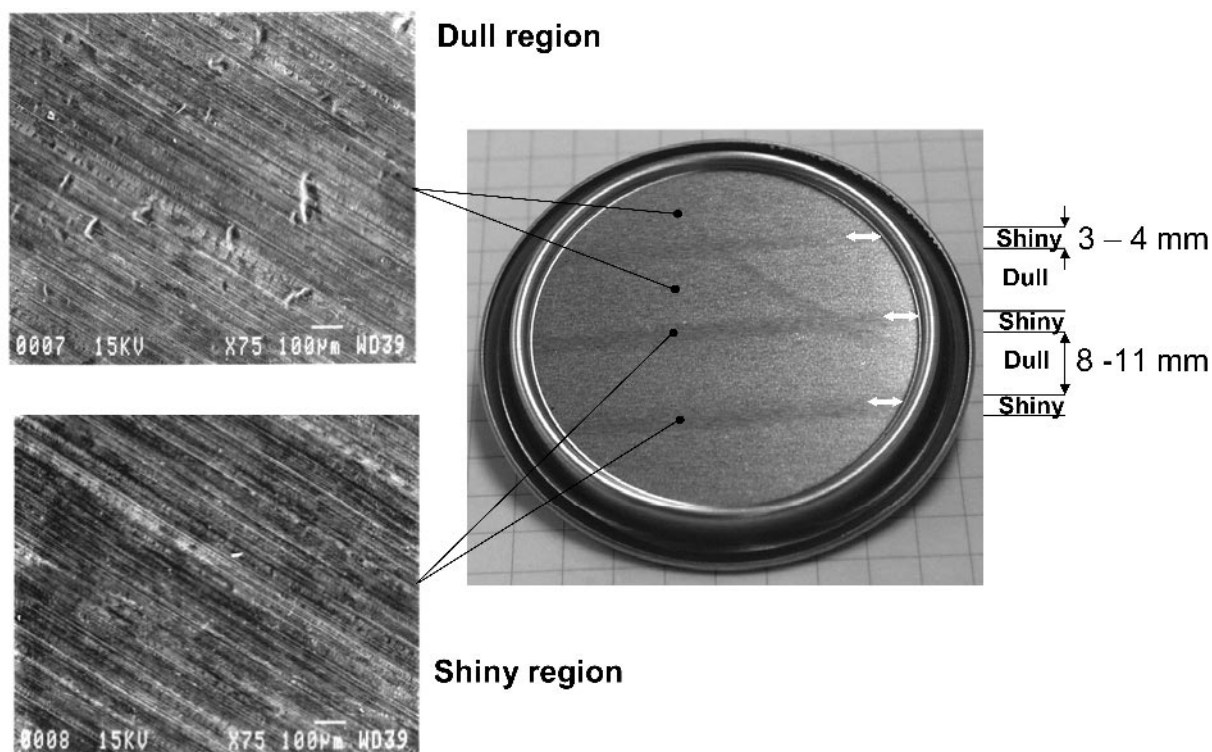


FIGURE 22.3 Optical (right) and scanning electron micrographs (left) of coil-coated aluminum beverage can lid (coating removed). Note the dull and shiny bands in optical image (right). The dull bands are a result of divots (top left) created by feed rollers, which in turn, facilitate the localized underfilm corrosion process described in Figure 22.2.

defect site that eventually forms on the coated aluminum surface, and high admittance peaks predict a more active corrosion site that is confirmed by the low pH, high chloride content, high cation content, and the evidence of resin hydrolysis (acetate from hydrolysis of polyurethane). The presence of possible coating hydrolysis caused by the underfilm solution raises the possibility of a feedback mechanism for coating degradation. The low pH created by the electrochemistry at the interface causes coating degradation, which allows further ingress of aggressive ions (chloride), etc. It is also possible that the initial ionic channel (if it exists) has an ion selective nature that allows significant chlorides to enter and elicit corrosion.

Because the experiments described above used an engineering alloy that contains many types of intermetallic particles, these results do not exclude the possibility that the localized electrochemical activity may have resulted from the heterogeneities (i.e., intermetallic particles) at the substrate surface. The presence of Cu^{2+} , Al^{3+} , and Mg^{2+} ions in the blister solution, suggest the involvement of the S-phase, an intermetallic known to initiate corrosion in this alloy

system [49]. Thus, the LEIM results suggest the presence of local ion channels within the coating, but are not conclusive. There is some role of substrate heterogeneities in the local degradation of this system.

22.4.2.3 Different Regions of Activity within a Single Defect

Continuous observation of a single red blister using LEIM revealed that one or more lobes grew from the original blister over time. These secondary lobes appeared to have a darker color than the initiation site. An LEIM map and corresponding optical image of a multi-lobed blister is shown in Figure 22.6. The initial blister contained a high-admittance site within it, possibly representing the site of initial electrolyte ingress. The secondary lobes had a much lower admittance, and were thus less active. Local open circuit potential values acquired by the use of micro-reference electrodes inserted beneath the coating revealed that the initial lobe had a more active potential ($-0.66 V_{\text{SCE}}$) than the secondary lobes ($-0.58 V_{\text{SCE}}$). Subsequent autopsy of the sample, shown in Figure 22.7, revealed that significant pitting occurred

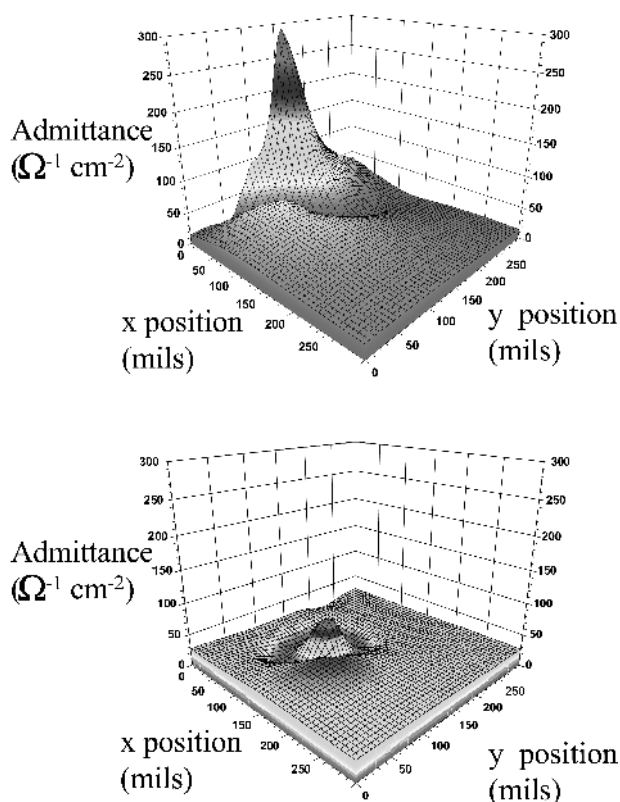


FIGURE 22.4 Local electrochemical impedance map (LEIM) at an early stage of immersion of an epoxy coating on AA2024-T3 (aluminum aerospace alloy) showing the increased admittance of a region that eventually forms a red-colored blister (top) and a black-colored blister (bottom).

beneath the initial lobe (higher admittance—more active). Again, the LEIM system was able to document unique electrochemical characteristics of the coating breakdown process and, again, there is evidence of a local pathway for ionic ingress. But, as before, the evidence is not conclusive. It is possible that the increased corrosion activity produced an increased electric field above this region, which then yielded the observed increased admittance.

22.4.2.4 Confirmation of a Growth/Death Cycle

In addition to locating defects in early stages of development and identifying different types of defects, LEIM has been used to monitor the time evolution of an intrinsic defect in a 50/50 polyether/polyester polyurethane-coated AA2024-T3 sample. Figure 22.8 shows the time course of a blister on poly-

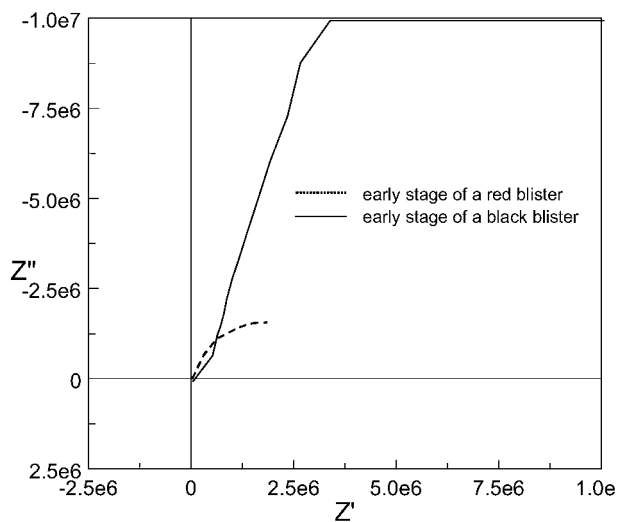


FIGURE 22.5 Complex plane plot (real, Z' versus imaginary, Z'') of local electrochemical impedance spectroscopy (LEIS) data from the defect areas described in Figure 22.4. The region that shows an increased admittance in Figure 22.4 (red, top) also shows a reduced impedance arc above. The region that shows a reduced admittance in Figure 22.4 (bottom, black) also shows an increased impedance arc in the LEIS spectra.

urethane-coated AA2024-T3 from an early non-visible stage (24 hours) to later stages of active corrosion. Several interesting features are observed: (1) the initial *decrease* in admittance in the earliest stage of observation (to 24 hours); (2) a decrease in admittance of the blister seen by the lower peak at 48 hours; and (3) the rapid rise in peak height at 52 hours. These features provide insight into the evolution of underfilm corrosion events, assuming that the data is not corrupted by artifact (e.g., instability of the micro-reference electrodes, or sampling errors caused by discrete sampling of the electric field). Other than possibly the “troughing” around the base of the large admittance peaks, artifactual sources of the observed LEIM behavior can be ruled out [50,51]. Hence, the observed changes in the LEIM data are to be interpreted as changes that result from changes in the materials and interface, and not to measurement artifact.

The changes in peak height are not a result of the biphasic nature of water uptake in polymer films. This is evidenced by the long-term nature of the observed peak height changes, where changes in water uptake occur within the first several hours of immersion. It is believed that the changes in peak height

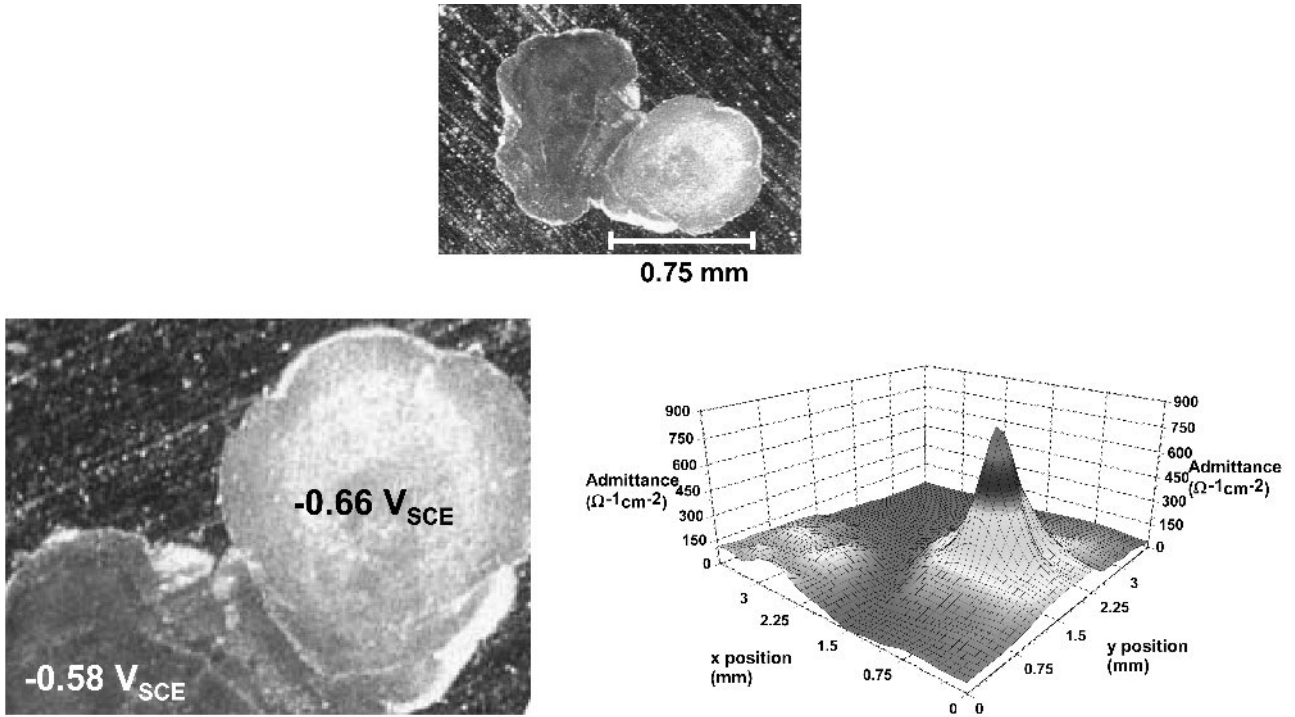


FIGURE 22.6 LEIM (bottom right) of a multi-lobed red-type defect. Note the increased admittance (increased electrochemical activity) of the right lobe. The right lobe also has a lower open circuit potential ($-0.66 V_{SCE}$).

are a result of metastable electrochemical events associated with the blister defect.

The admittance dip upon initial observation, a phenomenon observed in numerous experiments, was unexpected since the ingress of water and ions would be predicted to cause the admittance to increase. Since we can now assume that the observed LEIM behavior is real and reflective of the materials and interface, three possible explanations for the admittance dip can be proposed [52]. First, it is possible that a high impedance heterogeneity in the coating could be a site where corrosion initiates. However, this idea is not considered plausible because the dip is preceded by flat (uneventful) admittance behavior. An admittance dip due to an extrinsic coating heterogeneity resulting from application or handling would likely be present from the onset of LEIM measurements. Second, another possible source for the admittance dip is the nucleation of water on the substrate surface. Impedance values for two different scenarios were calculated and shown to be a possible cause for such an impedance (admittance) change [52]. Third, it is also possible that the accumulation of corrosion product is the origin of the decreased admittance. At this time, the accu-

mulation of a resistive corrosion product is considered the most plausible explanation of the admittance dips.

22.4.2.5 Origins of Ionic Ingress through the Coating

It was initially considered that the presence of admittance peaks in the early stages of chloride exposure were proof positive that ionic pores existed in the coating. However, more recent experiments using various combinations of coating materials (epoxy, vinyl, and polyurethane) on a variety of high-purity substrate metals (Au, Pt, Al, Cu) indicate that an alternate explanation for these admittance peaks is plausible. These experiments have indicated that an LEIM admittance peak observed on a coated alloy could result from a substrate site of low interfacial impedance covered by a coating whose general barrier properties are also intrinsically and uniformly low, but may have been further reduced by uniform water and ion ingress. For example, the low interfacial impedance of the substrate could arise from an intermetallic (e.g., Al_2CuMg) or actively corroding site. In the presence of a low impedance coating (i.e., uni-

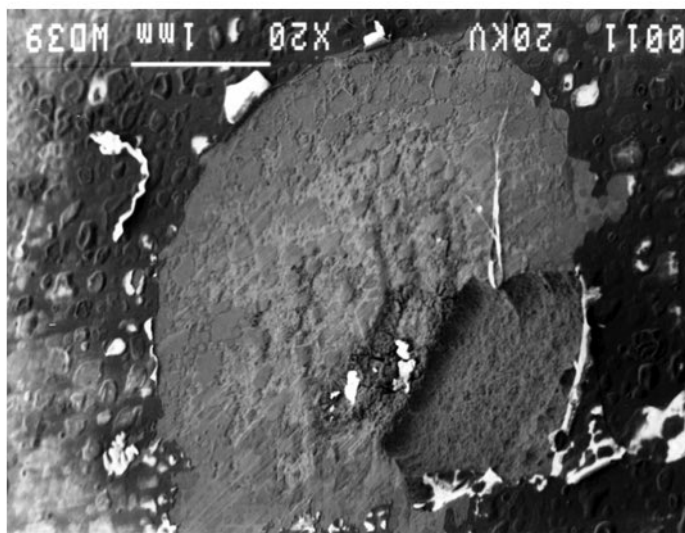
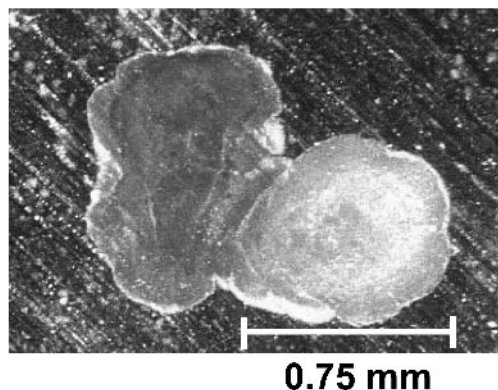


FIGURE 22.7 Scanning electron micrograph of autopsied red blister from polyurethane-coated AA2024-T3. Note the increased corrosion in the portion of the lobe that also showed an increased admittance peak in Figure 22.6.

formly hydrated, low barrier properties), the high activity of the substrate region is seen as an admittance peak. Thus, the definitive linkage of an LEIM admittance peak to a coating pore that allows water and ion ingress has not been conclusively established by these experiments.

22.4.2.6 Summary of Local Electrochemical Measurements on Coated Substrates

The ability to observe local electrochemical breakdown events of a coated metallic material can be beneficial from both a technological and mechanistic standpoint. LEIM has provided a preview to production-induced defects that would not otherwise have been visualized. This method has also allowed insight into the evolution of the coating breakdown

process. It has confirmed the metastable nature of breakdown events. Local electrochemical measurements have also shown that multiple types of corrosion defect sites can emerge, possibly as a result of different types of coating heterogeneities.

But these methods have also introduced additional questions. For example, why is the first appearance of a local electrochemical event seen as a reduced admittance (increased admittance)? More importantly, the idea that polymeric films possess local ionic paths requires further proof. The confounding that results from electrochemical experimentation on coated, heterogeneous, engineering alloys has not been offset by the scant amount of information from coated pure metals. In addition, there is always the possibility that a small imperfection in the “monolithic” substrate or a very subtle extrinsic defect in the coating is the source for ion

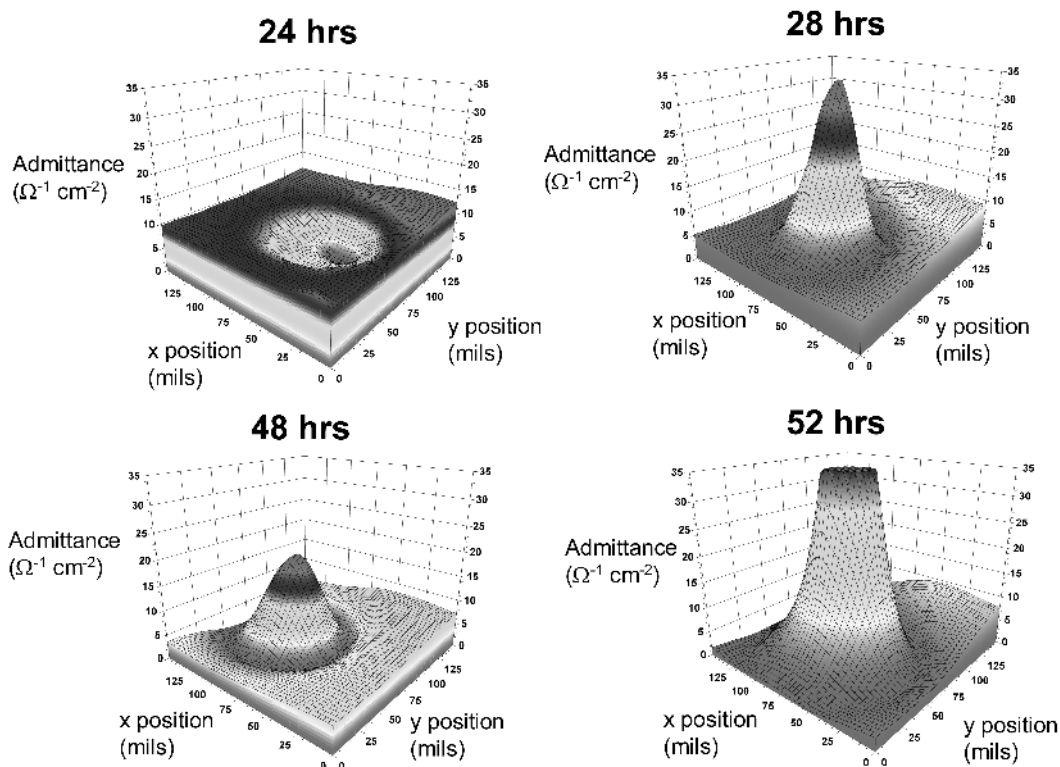


FIGURE 22.8 LEIM of polurethane-coated AA2024-T3 showing time evolution of underfilm electrochemical event (defect). Note the initial stage appears as a reduced admittance (increased impedance) and that the final stage is a very increased admittance. There are also defects in which the admittance decreases in the final stages.

ingress. To resolve the question of the existence of ionic pathways or “pores,” a more definitive experimental approach is required.

22.5 THE USE OF MOLECULAR PROBES

The definitive linkage of an LEIM admittance peak to a coating pore that allows water and ion ingress, thus acting as a locus of underfilm corrosion, has not been conclusively made. Perhaps a more definitive method for the identification of these ionic pathways is through the use of methods that have been employed in the medical and biological sciences to characterize the ultrastructure of cells and cell membranes [53,54].

Moiety or ion specific chromophores have been recently employed to help in the identification of ionic pathways within organic materials [55]. These chromophores are materials that have an altered fluorescence upon excitation when bound to a chemical species of interest. Initial experimentation has examined epoxy coating materials on glass slides. Glass slides have been employed as a substrate to eliminate

the confounding that occurs from the use of heterogeneous metallic substrates, as discussed previously. Initial experiments using molecular probes have exposed epoxy coatings on glass to sodium chloride solutions, and utilized chloride-specific molecular probes (e.g., MEQ, 6-methoxy-N-ethylquinolinium iodide). MEQ is a fluorescing molecule with a molecular weight of 315.15 g/M. It has absorption and emission wavelengths of 344 and 440 nm, respectively, and is also sensitive to Br^- , I^- , and SCN^- , but insensitive to NO_3^- , SO_4^{2-} , cations and pH [56].

Steady-state fluorescence microscopy has been used to visualize MEQ-tagged chloride ions within and on the surface of the coating. Both bright field and fluorescent field images are typically collected, where the fluorescent field must utilize the appropriate filters for the excitation light and emitted light.

Results from these initial experiments showed that the exposure of epoxy coatings to chloride and then to MEQ did indeed result in localized fluorescence. Figure 22.9 shows the bright field and fluorescent field micrographs of epoxy after one and three days of exposure to 0.1M NaCl solution at pH 2.5. Control experiments did not reveal these local-

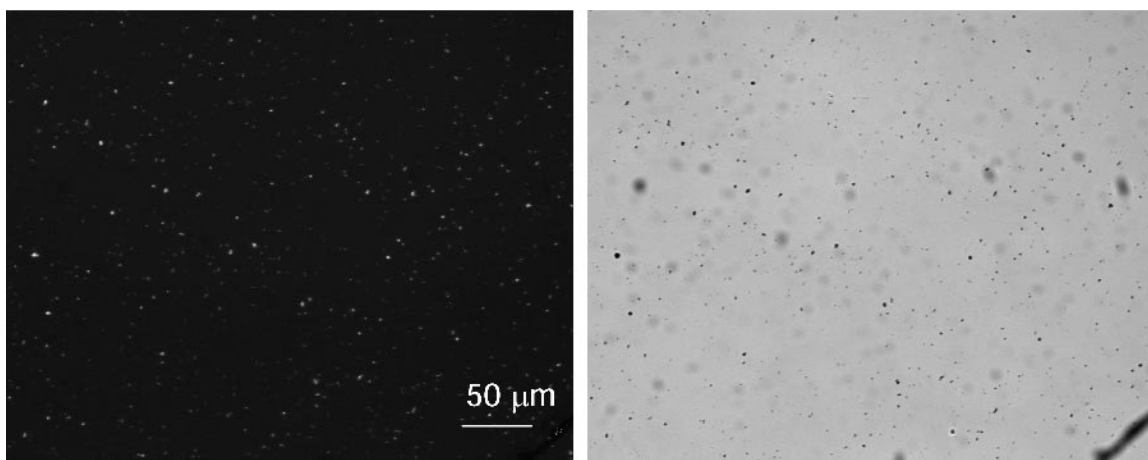


FIGURE 22.9 Fluorescent field (left) and bright field (right) of 10- μm -thick epoxy coating (on glass) following exposure to 0.1M NaCl and MEQ, a chloride-specific fluorescent probe.

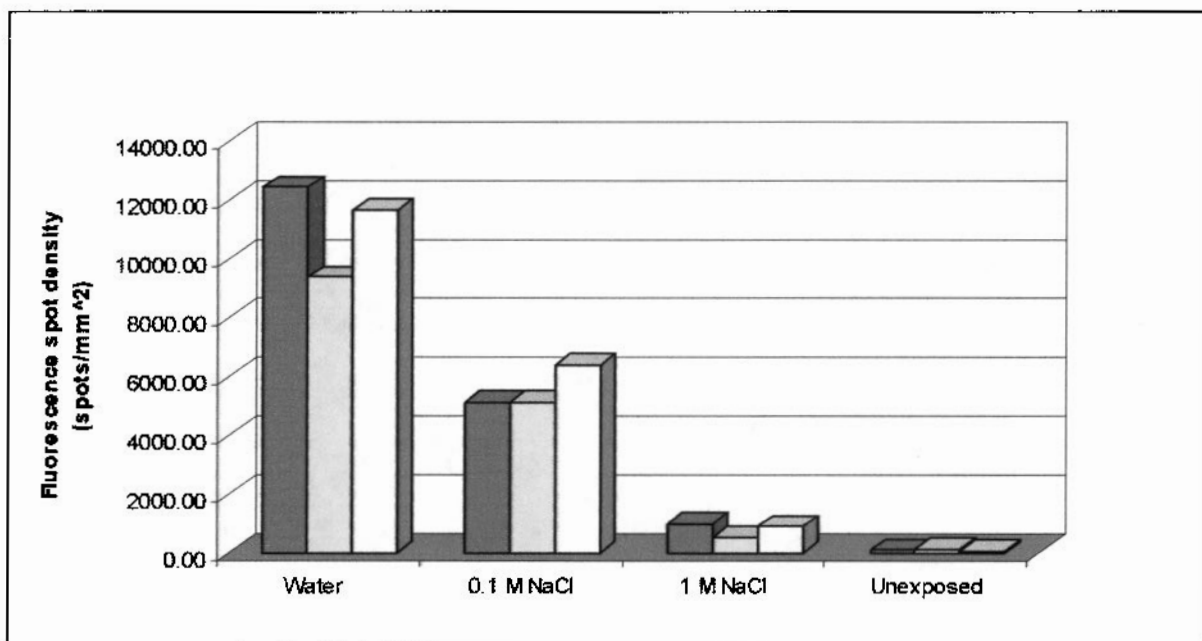


FIGURE 22.10 A chart summarizing the density of fluorescence sites observed on unexposed coatings, coatings exposed to water, 0.1 M NaCl and 1 M NaCl

ized sites, and thus it was concluded that the existence of local ionic channels in polymeric coatings, or at least the initial access to the material via adsorption at local sites, had been proven. But an examination of how halide-specific probes actually function would reopen the question regarding the nature of these sites.

Halide-specific probes such as MEQ actually quench fluorescence upon collision with halide ions. Therefore, MEQ would actually become dark when

bound to chloride, not bright as originally interpreted. The fluorescing sites observed in these initial experiments described above do not indicate the presence of chloride ions, but do indicate a material change of some type that occurs only when the coating is exposed to some environment.

It has been recently determined that the phenomenon of auto-fluorescence is responsible for the observed local fluorescence in epoxy coating materials following exposure to aqueous environments. These

auto-fluorescing spots can be observed after several months of desiccation. Since neither the epoxy, NaCl, or water are, by themselves, fluorescent materials, the auto-fluorescence is a result of some interaction of these materials. It is possible that hydration has either facilitated the rearrangement of the polymer chains, or has facilitated an interaction between water and epoxy such that the electronic structure of the local molecules in the epoxy have an enhanced fluorescence. The auto-fluorescence is indeed a result of exposure to water, as shown by the increase in spot density as a function of water activity. This is shown in Figure 22.10.

The experiments described reveal that water starts to influence the polymer in localized regions. This is suggestive of ionic pores. However, more conclusive experiments are underway. Since halide-specific probes have a quench-when-bound character, experiments are underway which utilize cationic probes. Preliminary evidence for local uptake of ions has been positive, with the use of these probe materials and three-dimensional sectioning using scanning laser confocal microscopy.

The use of molecular probe techniques is viewed as a method that will not only provide insight into the initiation sites for coating failure, but also as a method that could provide a promising technique for the quantitative laboratory characterization of the quality of a coating material. These methods lend themselves to the comparison of the barrier properties of polymers as a function of polymer chemistry, exposure environment (temperature, pH, UV, ion type, ion concentration, etc.), and time.

22.6 REFERENCES

1. D. J. Mills and J. E. O. Mayne. In *Corrosion Control by Organic Coatings*, H. Leidheiser Jr., Ed. Houston: NACE, 1981, pp.12–17.
2. J. E. O. Mayne, J. D. Scantlebury, *Br. Polym. J.*, 2(5): 240, 1970.
3. G. D. Mills, *Materials Performance*, March 2001: 50–53.
4. M. W. Wittmann, R. B. Leggat, and S. R. Taylor, *J. Electrochem. Soc.*, 146(11): 4,071–4,075, 1999.
5. A. M. Mierisch, J. Yuan, R. G. Kelly, and S. R. Taylor, *J. Electrochem. Soc.*, 146(12): 4,449–4,454, 1999.
6. D. Greenfield and J. D. Scantlebury, *J. Corr. Sci. Engr. 3* (Paper 5), 2000. <http://www.cp.umist.ac.uk/JCSE/>, ISSN.
7. M. W. Kendig and H. Leidheiser, Jr., *J. Electrochem. Soc.*, 123(7): 982–989, 1976.
8. L. Beaunier, I. Epelboin, J. -C. Lestrade, and H. Takenouti, *Surface Technol.*, 4: 237, 1976.
9. H. Corti, R. Fernandez-Prini, and D. Gomez, *Prog. Org. Coat.*, 10: 5–33, 1982.
10. J. E. O. Mayne, *Official Digest*. 1952 pp. 127–136.
11. E. M. Kinsella and J. E. O. Mayne. In *Proceedings of the 3rd International Congress on Metallic Corrosion*, Moscow, 1966, pp. 117–120.
12. A. A. Pollitt. *The Causes and Prevention of Corrosion*, London: Ernst Benn Ltd., 1923, p. 160.
13. L. M. Callow and J. D. Scantlebury, *J. Oil. Colour Chem. Assoc.*, 64(2): 83, 1981.
14. M. Piens and R. Verbist. In *Corrosion Control by Organic Coatings*, H. Leidheiser, Jr., Ed. Houston: NACE, 1981, pp. 103–110.
15. T. Szauer, *Prog. Org. Coat.*, 10: 171, 1982.
16. J. Hubrecht and J. Vereeken, *J. Electrochem. Soc.*, 132(2): 2,886, 1985.
17. M. W. Kendig, F. Mansfeld and S. Tsai, *Corr. Sci.*, 23(4): 317, 1983.
18. S. R. Taylor, *IEEE Trans. Electronic Insul.*, 24: 787, 1989.
19. F. Mansfeld and C. H. Tsai, *Corrosion*, 47: 958, 1991.
20. R. Hirayama and S. Haruyama, *Corrosion*, 47: 953, 1991.
21. H. S. Isaacs and B. Vyas. In *Electrochemical Corrosion Testing, ASTP STP 727*, F. Mansfeld and E. Bertocci, Eds., Philadelphia: ASTM, 1981, pp. 3–33.
22. S. J. Bates, S. R. Gsoden, and D. A. Sargent, *Mater. Sci. Technol.*, 5: 356, 1989.
23. V. S. Voruganti, H. B. Luft, D. Degeer, and S. A. Bradford, *Corrosion*, 47: 343, 1991.
24. H. S. Isaacs, *Corrosion*, 43: 594, 1987.
25. H. S. Isaacs, *Corr. Sci.*, 28: 547, 1988.
26. L. F. Jaffe and R. Nuccitelli, *J. Cell Biol.*, 64: 614, 1974.
27. M. Stratmann and H. Streckel, *Corr. Sci.*, 30: 681, 1990.
28. M. Stratmann and H. Streckel, *Corr. Sci.*, 30: 697, 1990.
29. M. Stratmann and H. Streckel, *Corr. Sci.*, 30: 715, 1990.
30. A. J. Bard, F. R. Fan, J. Kwak, and O. Lev, *Anal. Chem.*, 61: 132, 1989.
31. J. Kwak and A. J. Bard, *Anal. Chem.*, 61: 1,794, 1989.
32. M. V. Mirkin, *Anal. Chem. News Feat.*, A177, 1996.
33. S. R. Taylor, A. C. Hillier, and M. Seo, Eds. *Localized In-Situ Methods for Investigating Electrochemical Interfaces*. In *ECS Proceedings PV99-28*. Pennington, NJ: The Electrochemical Society, 2000.
34. H. J. Butt, M. Jaschke, and W. Ducker, *Bioelectrochem. Bioenergy*, 38: 191, 1995.
35. T. Gesang, R. Hoper, S. Diekoff, V. Schlett, W. Possart, and O. D. Hennemann, *Thin Solid Films*, 264: 194, 1995.
36. J. Frommer, *Angew Chem. Int. Ed. Engl.*, 3: 1,298, 1992.
37. G. P. Bierwagen, R. Twite, G. Chen, and D. E. Tallman, *Prog. Org. Coat.*, 32: 25, 1997.
38. H. S. Isaacs and M. W. Kendig, *Corrosion*, 36: 269, 1980.
39. R. S. Lillard, P. J. Moran, and H. S. Isaacs, *J. Electrochem. Soc.*, 139: 1,007, 1992.

40. F. Zhou, D. Thierry, and H. S. D. Isaacs, *J. Electrochem. Soc.*, 144: 1,208, 1997.
41. I. Annergren, D. Thierry, and F. Zhou, *J. Electrochem. Soc.* 144: 1,957, 1997.
42. R. Lillard, J. Kruger, W. S. Tait, and P. J. Moran, *Corrosion*, 51: 251, 1995.
43. M. W. Wittmann and S. R. Taylor. Advances in Corrosion Protection by Organic Coatings II. In *ECS Proceedings PV95-13*. J. D. Scantlebury and M. W. Kendig, Eds. Pennington, NJ: The Electrochemical Society, 1995, p.158.
44. M. W. Wittmann, R. B. Leggat, and S. R. Taylor, *J. Electrochem. Soc.*, 146(11): 4,076, 1999.
45. E. Bayet, F. Huet, M. Keddam, K. Ogle, and H. Takenouti, *J. Electrochem. Soc.*, 144: L87, 1997.
46. E. Bayet, Garrigues, F. Huet, M. Keddam, K. Ogle, N. Stein, and H. Takenouti. Localized In-Situ Methods for Investigating Electrochemical Interfaces. In *ECS Proceedings PV99-28*. S. R. Taylor, A. C. Hillier, and M. Seo, Eds. Pennington, NJ: The Electrochemical Society, 2000, pp. 200–211.
47. S. R. Taylor, *Prog. Org. Coat.*, 43: 141, 2001.
48. R. B. Leggat and S. R. Taylor, *Corrosion*, 55(10): 984, 1999.
49. R. G. Buchheit, R. P. Grant, P. F. Hlava, B. McKenzie, and G. L. Zender, *J. Electrochem. Soc.*, 144: 2,621, 1997.
50. A. M. Miersich and S. R. Taylor, *J. Electrochem. Soc.*, 150(7): B303, 2003.
51. A. M. Miersich and S. R. Taylor, *J. Electrochem. Soc.*, 150(7): B309, 2003.
52. A. M. Miersich and S. R. Taylor. Localized In-Situ Methods for Investigating Electrochemical Interfaces. In *ECS Proceedings PV99-28*. S. R. Taylor, A. C. Hillier, and M. Seo, Eds. Pennington, NJ: The Electrochemical Society, 2000, pp. 229.
53. R. P. Hangland and I. D. Johnson. In *Fluorescent and Luminescent Probes for Biological Activity, 2nd Edition*. W. T. Mason, Ed. Academic Press, NY, pp. 40–45, 1999.
54. A. Takahashi, P. Camacho, J. D. Lechleiter, and B. Herman, *Physiol. Rev.*, 79: 1,088–1,125, 1999.
55. P. Moongkhamklang and S. R. Taylor, *Prog. Org. Coat.*, 46: 259–265, 2003.
56. J. Birwersi and A. S. Verkman, *Biochemistry*, 30: 7,879–7,883, 1991.

INDUSTRIAL APPLICATIONS

CHAPTER 23 DEGRADATION OF SPACECRAFT MATERIALS 465

CHAPTER 24 CATHODIC PROTECTION OF PIPELINES 503

CHAPTER 25 TANKER CORROSION 523

CHAPTER 26 BARRIER PACKAGING MATERIALS 547

CHAPTER 27 CORROSION PREVENTION AND CONTROL OF CHEMICAL PROCESSING EQUIPMENT 565

Joyce Dever
Bruce Banks
Kim de Groh
Sharon Miller

NASA Glenn Research Center, Cleveland, Ohio

| | |
|---|------------|
| 23.1 INTRODUCTION | 465 |
| 23.2 ATOMIC OXYGEN EFFECTS | 466 |
| 23.3 CONTAMINATION EFFECTS | 477 |
| 23.4 SPACE RADIATION EFFECTS | 479 |
| 23.5 THERMAL AND THERMAL CYCLING EFFECTS | 487 |

| | |
|---|------------|
| 23.6 MICROMETEOROID AND ORBITAL DEBRIS EFFECTS | 491 |
| 23.7 CONCLUDING REMARKS | 494 |
| 23.8 REFERENCES | 496 |

23.1 INTRODUCTION

Materials used on exterior spacecraft surfaces are subjected to many environmental threats which can cause degradation. These threats include photon radiation, charged particle radiation, temperature effects and thermal cycling, impacts from micrometeoroids and debris, contamination, and low Earth orbit atomic oxygen. Space environmental threats to materials vary greatly, based on both the material and its environment. Environmental variables include orbital parameters for the mission, mission duration, the solar cycle and solar events, view angle of spacecraft surfaces to the Sun, and orientation of spacecraft surfaces with respect to the spacecraft velocity vector in low Earth orbit. It is evident that each mission has its own unique set of environmental exposure conditions that must be well understood for purposes of selecting durable spacecraft materials and interpreting observed degradation.

Fundamentally important properties for exterior spacecraft surfaces include structural integrity and thermo-optical properties. Problems occur when spacecraft materials become too thin or brittle to support a required load, or when protective thermal insulation film layers crack and peel away from the spacecraft. Operating temperatures of spacecraft systems rely on exterior surfaces possessing the required solar absorptance and thermal emittance values. Solar absorptance, α_s , is the fraction of incident solar energy that is absorbed by a surface. Thermal

emittance, ϵ , is the ratio of radiated energy emitted from a surface to that which would be emitted from a perfect (black body) emitting surface. Degradation of these thermo-optical properties can cause an undesirable change in temperature of the spacecraft or its components. Loss of transmittance through solar cell coverglass materials, such as by contamination, can result in decreased output of solar arrays, and, therefore, a reduction in overall spacecraft power. For electrical wiring and cables exterior to the spacecraft, polymer insulation can become degraded upon space radiation exposure.

Understanding the degradation of spacecraft materials can be determined through actual space-exposures and ground laboratory studies. Each has advantages and disadvantages. Opportunities for examining space flown materials, through retrieved flight hardware or dedicated experiments, are rare. Dedicated space flight experiments are expensive and require long lead times from planning to flight. Differences between the experiment environment, the intended mission environment, and synergistic environmental effects require cautious interpretation of results. Where it is not possible to retrieve spacecraft hardware, data available from satellite operations, such as power output and spacecraft surface temperatures, can also be used to assess material performance to some extent. Where severe degradation is evident, however, it is often not possible to conclusively identify the cause or mechanism of degradation, since comprehensive analysis of mate-

rials is not possible. Ground laboratory studies can be used to examine individual environmental effects or a combination of environmental effects. Laboratory tests can be conducted in a timely manner using accelerated levels for some environmental effects, but, due to the difficulties in exactly simulating the space effects, complex calibrations and cautious interpretation of the results are required. A combination of space exposures, ground laboratory studies and computational modeling is most useful for assuring durability of spacecraft materials.

This chapter includes descriptions of specific space environmental threats to exterior spacecraft materials. The scope will be confined to effects on exterior spacecraft surfaces, and will not, therefore, address environmental effects on interior spacecraft systems, such as electronics. Space exposure studies and laboratory simulations of individual and combined space environmental threats will be summarized. A significant emphasis is placed on effects of Earth orbit environments, because the majority of space missions have been flown in Earth orbits which have provided a significant amount of data on materials effects. Issues associated with interpreting materials degradation results will be discussed, and deficiencies of ground testing will be identified. Recommendations are provided on reducing or pre-

venting space environmental degradation through appropriate materials selection.

23.2 ATOMIC OXYGEN EFFECTS

23.2.1 Environment Description

Atomic oxygen is formed in the low Earth orbital environment (LEO) by photo dissociation of diatomic oxygen. Short wavelength (< 243 nm) solar radiation has sufficient energy to break the 5.12 eV O_2 diatomic bond [1] in an environment where the mean free path is sufficiently long ($\sim 10^8$ meters) that the probability of reassociation or the formation of ozone (O_3) is small. As a consequence, between the altitudes of 180–650 km, atomic oxygen is the most abundant species (Figure 23.1) [2]. Although excited states of atomic oxygen can be formed, their lifetimes are sufficiently short that the 3P ground state dominates the LEO atomic oxygen formation and is dependent upon the diatomic oxygen density and solar UV flux. Solar heating of the Earth's atmosphere causes an increase in the number density of atoms at a given altitude as the Earth rotates from sunrise toward solar noon. Because the atmosphere co-rotates with the Earth, the solar heated bulge in the atmosphere is pushed forward such that the peak

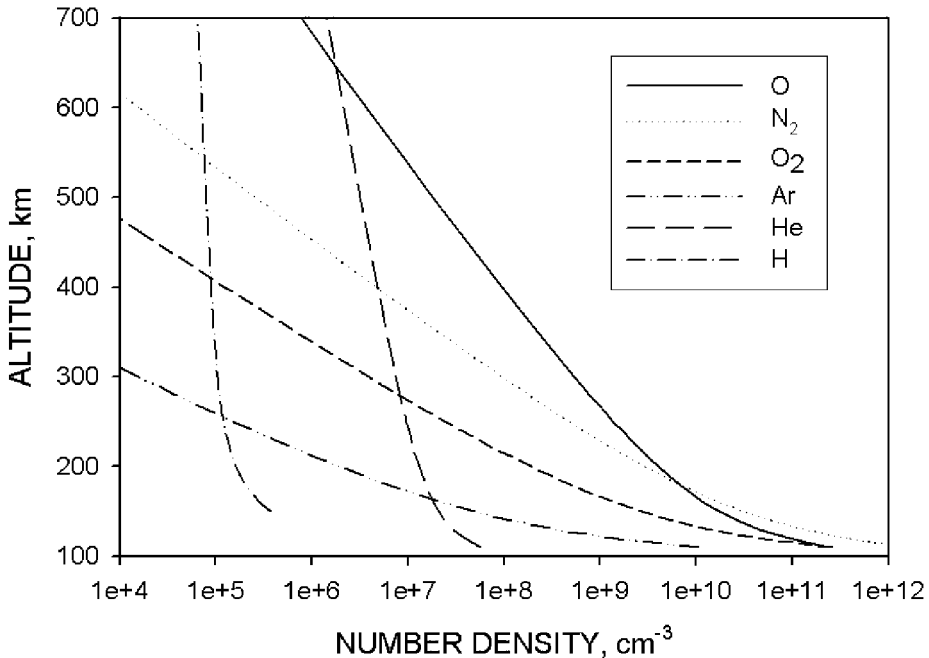


FIGURE 23.1 Density of atmospheric species as a function of altitude.

of the atomic oxygen density occurs at approximately 3 P.M. rather than solar noon. As a consequence, anti-solar facing surfaces, such as the back side of solar arrays, receive 25% more atomic oxygen fluence than the solar facing surfaces as the spacecraft orbits the Earth [3].

Solar-caused variations in the ultraviolet radiation impinging upon the LEO atmosphere can greatly change the atomic oxygen production rate (and, therefore, the arriving flux on spacecraft surfaces). Periods of high and low solar activity can change the arriving flux by a factor of up to 500, depending on altitude (Figure 23.2 [2]). Thus, the atomic oxygen flux cannot be accurately predicted due to uncertainty in the solar activity. The average atomic oxygen fluence per year varies as a result of the solar activity consistent with the 11-year sun spot cycle, as shown in Figure 23.3, for which data were calculated using the MSIS-86 atmospheric model [4]. Atomic oxygen can also be produced in other planetary environments where oxygen is present.

As a spacecraft orbits the Earth at velocities on the order of 7.7 km/sec, it runs into the atomic oxygen (hence the term “ram” atomic oxygen). If the spacecraft is in an orbit that has zero inclination then the average angle of attack of the atomic oxygen is

perpendicular to surfaces whose surface normal points in the direction of travel. However, most spacecraft have orbits which are inclined with respect to the Earth’s equatorial plane. This causes the average angle of attack of the arriving atomic oxygen to sinusoidally vary around the orbit as a result of the vectoral addition of the orbital spacecraft velocity vector and the atmosphere’s co-rotation velocity vector [5]. In addition, atomic oxygen atoms have thermal velocities associated with their Maxwell-Boltzman velocity distribution at the high temperatures of LEO which are typically $\sim 1,000$ °K [2]. The high velocity tail of the Maxwell-Boltzman distribution actually allows some atomic oxygen atoms to catch up with the trailing surfaces of a LEO spacecraft to produce a small flux which is orders of magnitude lower than the ram flux. Thus, the thermal velocities of the atomic oxygen associated with their Maxwell-Boltzman velocity distribution contributes as an additional component to the overall impact velocity of the atomic oxygen. If one adds the three vectoral components and averages over a typical 400-km orbit at 28.5 degrees inclination, then angular distribution of arriving atoms is as shown in Figure 23.4, where the arrival distribution in the horizontal plane is shown as a function of

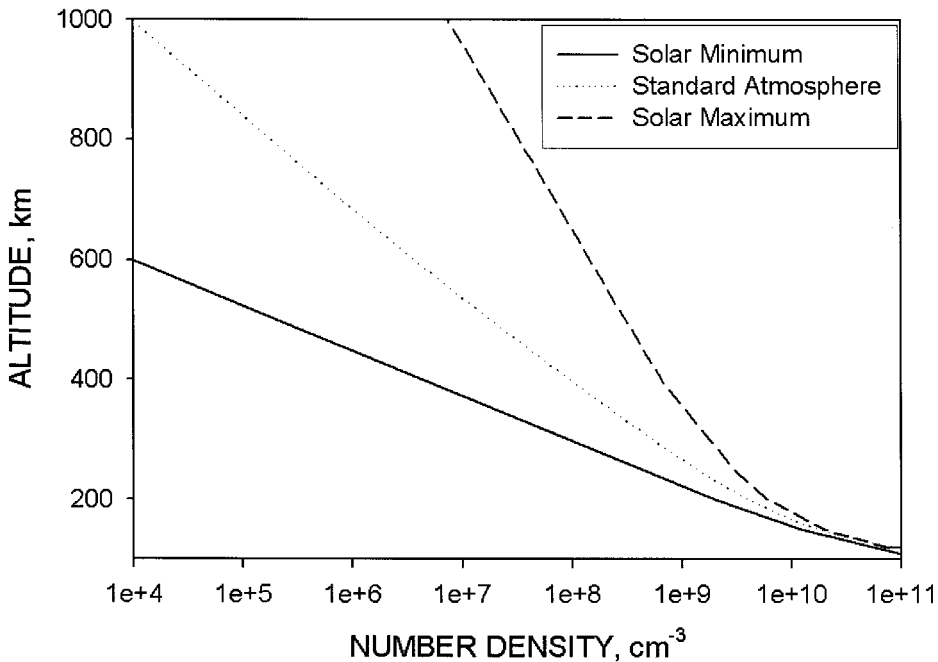


FIGURE 23.2 Atomic oxygen flux versus altitude for solar minimum, nominal (standard atmosphere), and solar maximum conditions.

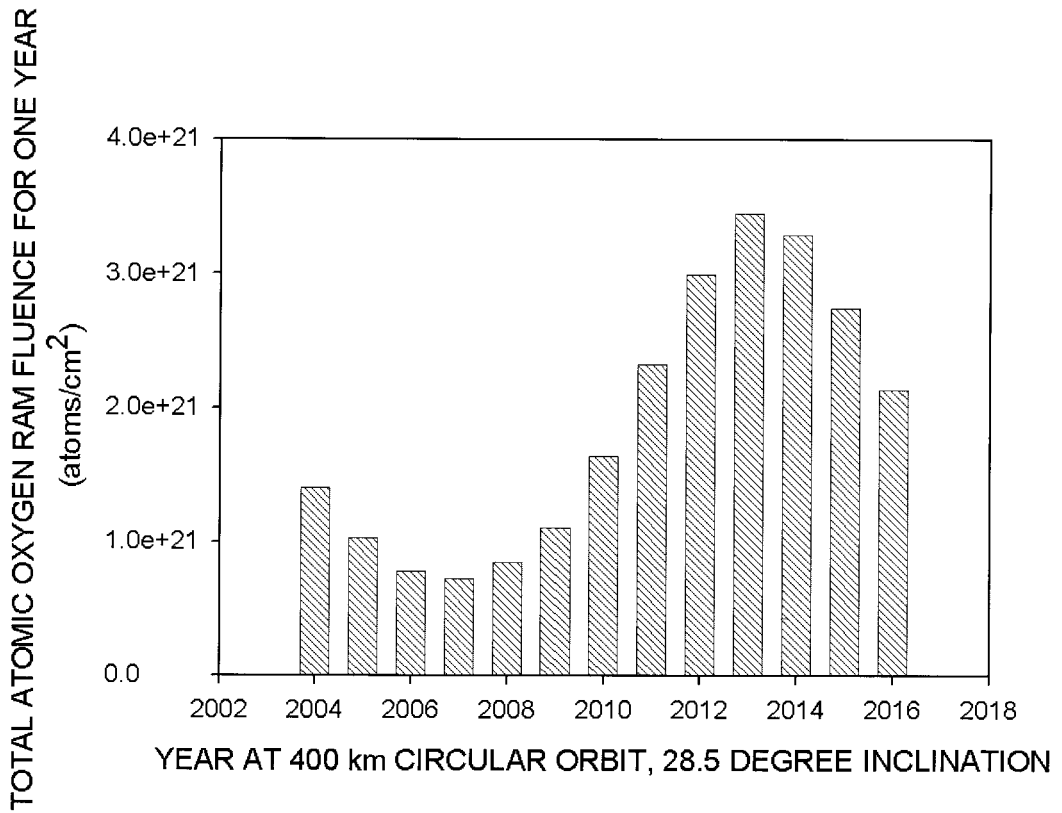


FIGURE 23.3 Atomic oxygen fluence per year during a solar cycle, based on MSIS-86 atmospheric model [4].

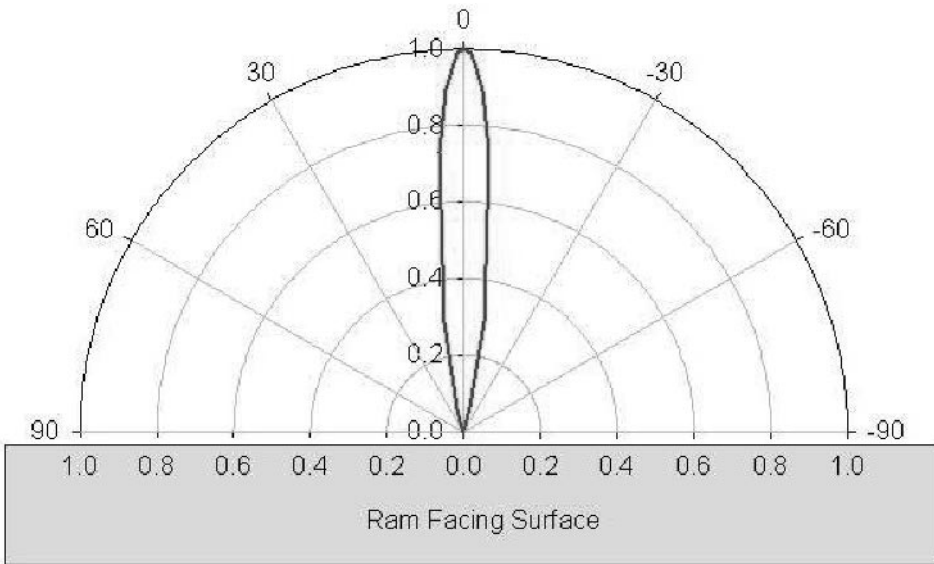


FIGURE 23.4 Atomic oxygen arrival flux relative to the ram direction for a 400-km orbit at 28.5 degrees inclination and 1,000 °K thermosphere.

incidence angle for surfaces normal to the ram direction [6].

Atomic oxygen can arrive at angles beyond 90 degrees from the orbital direction. For example, Figure 23.5 shows that a surface whose normal is 90 degrees with respect to the ram direction receives approximately 4% of the flux that occurs for a surface whose normal is parallel to the ram direction.

The impact energy of arriving atomic oxygen atoms also is dependent upon the following three contributions to the resulting velocity vectors: the orbital spacecraft velocity, the Earth's atmosphere co-rotation velocity, and atomic oxygen thermal velocity. Figure 23.6 is a plot of the energy distribution of atomic oxygen atoms as a function of altitude for a circular orbit with 28.5 degrees inclination and 1,000 °K thermosphere [7]. As can be seen, the average impact energy is $4.5 \text{ eV} \pm 1 \text{ eV}$ for a 400-km

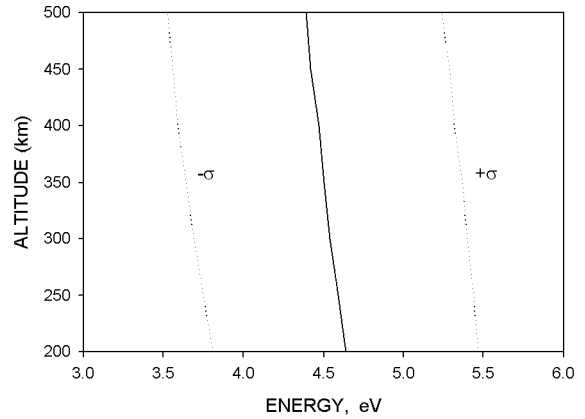


FIGURE 23.6 Energy distribution of atomic oxygen atoms as a function of altitude for a circular orbit at 28.5 degrees inclination and 1,000 °K thermosphere.

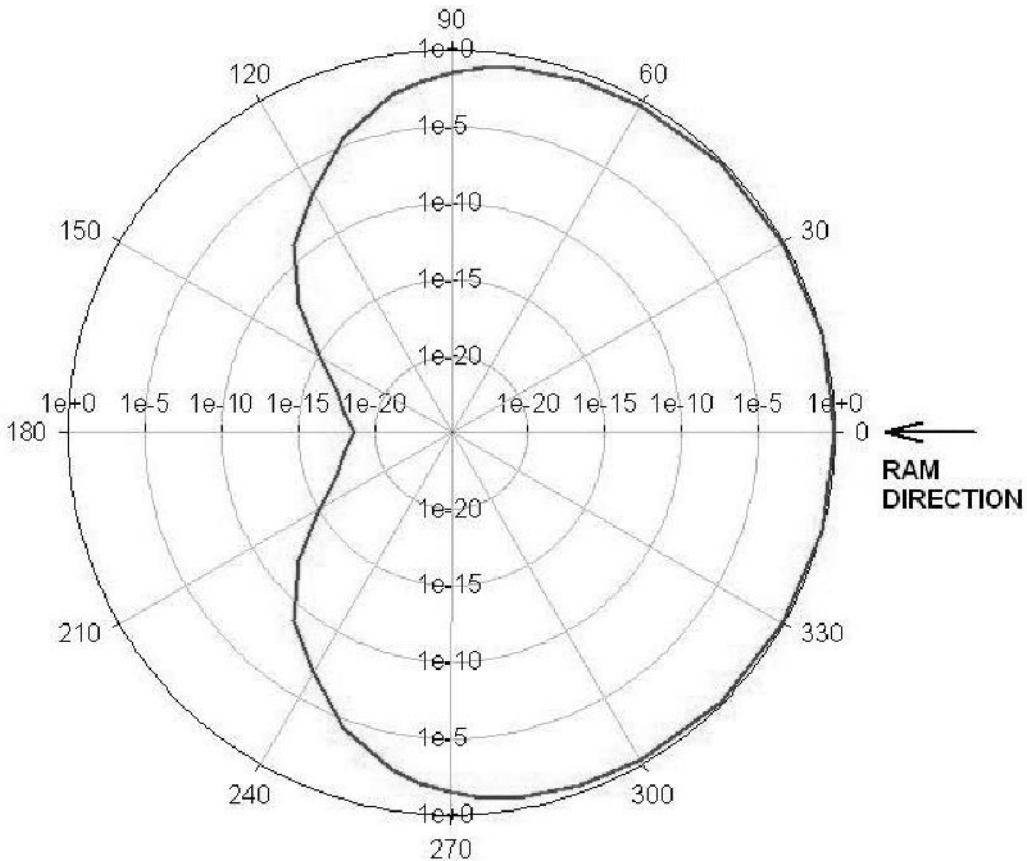


FIGURE 23.5 Polar plot of relative atomic oxygen flux as a function of the angle between the ram direction and the normal of the arrival surface for a LEO spacecraft in a 400-km orbit at 28.5 degrees inclination and 1,000 °K thermosphere.

orbit and the impact energy decreases with altitude. For highly elliptical orbits, the perigee ram impact energy can be significantly higher than for circular LEO orbits. Such elliptical orbits can also produce high fluxes near perigee due to the low altitudes involved. If a spacecraft is spinning with its axis of rotation perpendicular to the Earth then the average flux to any surface is simply $1/\pi$ of that of the ram direction.

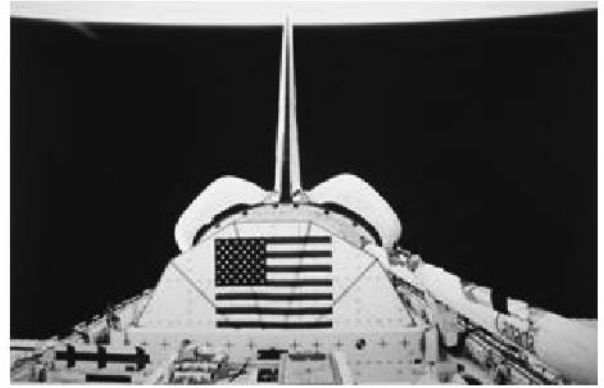
23.2.2 Interaction with Materials

Although LEO atomic oxygen possesses sufficient energy to break most organic polymer bonds and sufficient flux to cause oxidative erosion of polymers, there was little known or interest in atomic oxygen interaction with materials until the start of Space Shuttle missions. This is primarily because most prior missions occupied high altitude orbits where atomic oxygen densities are rather inconsequential.

One evidence of LEO environmental interaction with materials is the glow phenomena that occurs when atomic oxygen and other LEO atmospheric species impact spacecraft surfaces causing the creation of short-lived excited state species that emit visible radiation near the surfaces of spacecraft as shown in Figure 23.7, where Figure 23.7(a) was taken during the daylight and Figure 23.7(b) was taken as a time exposure at night [8–10].

The reaction of atomic oxygen with spacecraft materials has been a significant problem to LEO spacecraft designers. Atomic oxygen can react with polymers, carbon and many metals to form oxygen bonds with atoms on the surface being exposed. For most polymers hydrogen abstraction, oxygen addition or oxygen insertion can occur (Figure 23.8). With continued atomic oxygen exposure, all oxygen interaction pathways for hydrocarbons eventually lead to volatile oxidation products accompanied by the gradual erosion of hydrocarbon materials. Surfaces of polymers exposed to atomic oxygen also develop an increase in oxygen content as shown in Figure 23.9 [11].

The sensitivity of hydrocarbon materials to reaction with atomic oxygen is quantified by the atomic oxygen erosion yield of the material. The atomic oxygen erosion yield is the volume of a material that is removed (through oxidation) per incident oxygen atom. The most well-characterized atomic oxygen erosion yield is that of polyimide Kapton® H, which has an erosion yield of 3.0×10^{-24} cm³/atom for LEO 4.5 eV atomic oxygen [12,13]. Table 23.1 (14,15,16) lists the atomic oxygen erosion yields of



A.

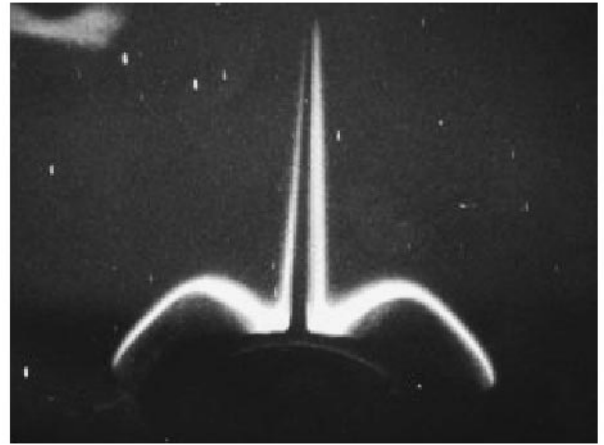


FIGURE 23.7 Low Earth orbital glow phenomena: (a) Photograph of the Space Shuttle tail during daylight; (b) Photograph of the Space Shuttle tail at night.

a wide variety of polymers, where many of the values were measured from space experiments and others are predicted values. The predicted erosion yield values (γ' mod-Correlation and $1/\text{Oxygen Index (OI)}$ Correlation [16]) listed in Table 23.1 were made based on predictive models, developed for the interaction of polymers with the LEO environment, and using information about the chemical composition, structure, and densities, as well as experimental data for OI [17].

The most common technique for determining the erosion yield of flight samples is through mass loss measurements. These measurements are made by obtaining mass measurements of the sample before and after flight. The erosion yield of the sample, E_S , is calculated through the following equation:

$$E_S = \frac{\Delta M_S}{(A_S \rho_S F)}, \quad (23.1)$$

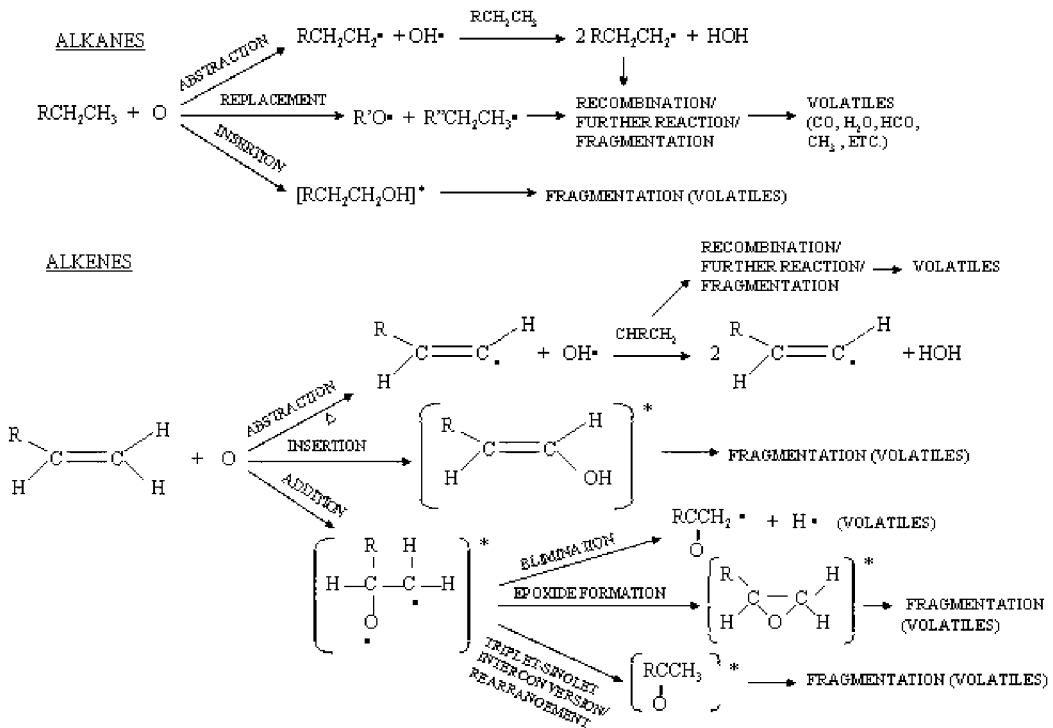


FIGURE 23.8 Atomic oxygen reaction pathways with polymers.

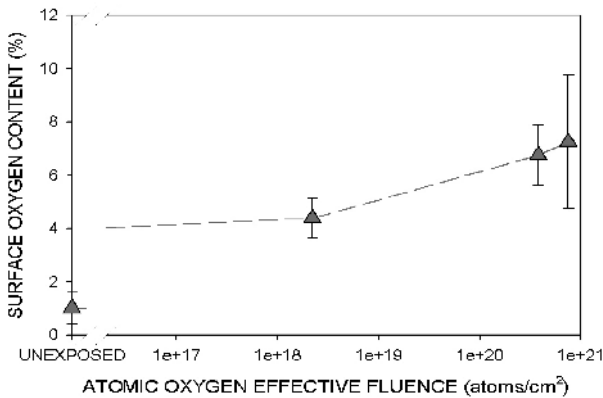


FIGURE 23.9 Surface oxygen content (measured using XPS) for chlorotrifluoroethylene as a function of atomic oxygen exposure level, where exposures were conducted in ground facility RF air plasma.

where E_S = erosion yield of flight sample (cm³/atom)

ΔM_S = mass loss of the flight sample (g)

A_S = surface area of the flight sample exposed to atomic oxygen attack (cm²)

ρ_S = density of sample (g/cm³)

F = fluence of atomic oxygen (atoms/cm²)

The atomic oxygen fluence, F , can be determined through the mass loss of a Kapton[®] witness sample because Kapton[®] has a well-characterized erosion yield in the LEO environment. Therefore, the atomic oxygen fluence can be calculated using the following equation:

$$F = \frac{\Delta M_K}{(A_K \rho_K E_K)} \quad (23.2)$$

where ΔM_K = mass loss of Kapton[®] witness sample (g)

A_K = surface area of Kapton[®] witness sample exposed to atomic oxygen (cm²)

ρ_K = density of Kapton[®] witness sample (1.42 g/cm³)

E_K = erosion yield of Kapton[®] witness sample (3.0×10^{-24} cm³/atom).

Thus:

$$E_S = E_K \frac{\Delta M_S A_K \rho_K}{\Delta M_K A_S \rho_S} \quad (23.3)$$

One of the critical issues with obtaining accurate erosion yield data from mass loss measurements is

TABLE 23.1 Atomic Oxygen Erosion Yields of Various Materials and Polymers

| Material | Abbrev. | Trade Names | Predicted Erosion Yield in LEO by Different Correlations Re^{LEO} (Ref. 16) ($\times 10^{-24}$ cm ³ /atom) | | Erosion Yield in LEO ($\times 10^{-24}$ cm ³ /atom) and references |
|--|--------------|---------------------------------|--|------------------|--|
| | | | γ' mod-Correlation | I/OI Correlation | |
| Acrylonitrile butadiene styrene | ABS | Cycolac; Lustran | 2.3 | 3.1 | |
| Carbon | | | | | 0.9–1.7 (Ref. 14) |
| Carbon (highly oriented py- rolytic graphite) | HOPG | Graphite | 1.0 | 1.3 | 1.04–1.2 (Ref. 15); 1.2–1.7 (Ref. 16); 1.2 (Ref. 14) |
| Carbon (pyrolytic polycrys- talline) | PG | Graphite | | | 0.61–1.2 (Ref. 15); 1.2 (Ref. 14) |
| Carbon (single crystal natural Class IIA diamond) | | Diamond | | | 0.0000 \pm 0.000023 (Ref. 15); 0.021 (Ref. 14) |
| Cellulose acetate | CA | Cellidor; Tenite Acetate | 6.8 | 3.2 (5.2) | |
| Cellulose nitrate | CN | Celluloid; Xylonite | 13.1 | | |
| Crystalline polyvinylfluoride w/white pigment | PVF | White Tedlar | 3.4 | 3.0 | 0.29 (Ref. 15); 3.2 (Ref. 16) |
| Diallyl diglycol and triallyl cyanurate | ADC | CR-39 | 6.1 | 4.6 | 6.1 (Ref. 16) |
| Epoxide or epoxy | EP | Epoxy resin | 2.9 | 2.3 | 2.7 (Ref. 16) Epoxy Resin 5208; 1.7 (Ref. 14) |
| Ethylene vinyl acetate copoly- mer | EVAC | Elvax | 3.9 | 3.5 | |
| Ethylene vinyl alcohol copoly- mer | EVAL (EVOH) | Eval | 3.5 | 3.0 | |
| Ethylene/propylene/diene | EPTR (EPDM) | Nordel; Keltan | 2.9 | 3.0 | |
| Fluorinated ethylene propylene | FEP | Teflon® FEP | 0.0 | n/a | 0.337 \pm 0.005* (Ref. 15); 0.35 (Ref. 15); 0.03–0.05 (Ref. 16); 0.037 (Ref. 15); 0.0 \rightarrow 0.05 (Ref. 14) |
| Halar ethylene-chlorotrifluo- roethylene | ECTFE | Halar | 2.0 | n/a | 2.0–2.1 (Ref. 15); 1.9 (Ref. 16) |
| Melamine formaldehyde resin | MF | Melmex; Melopas | 3.4 | | |
| Phenol formaldehyde resin | PF | Bakelite; Plenco; Durex | 2.3 | 2.5 | |
| Poly-(p-phenylene terephthala- mide) | PPD-T (PPTA) | Kevlar 29 | 2.5 | 2.9 | 1.5 \pm 0.5 Kevlar 29 (Ref. 15); 2.1–4.1 Kevlar 29 (Ref. 16); 4.0 \pm 0.5 Kevlar 49 (Ref. 15); 2.1–4.1 Kevlar 49 (Ref. 16) |
| Polyacrylonitrile | PAN | Acrilan; Barex; Orlon | 2.5 | 4.5 | |
| Polyamide 6 or nylon 6 | PA 6 | Caprolan; Akulon K; Ultramid | 3.7 | 3.6 | 2.8 \pm 0.2 (Ref. 15); 4.2 (Ref. 16) |
| Polyamide 66 or nylon 66 | PA 66 | Maranyl; Zytel; Durethane | 3.7 | 3.6 | 2.8 \pm 0.2 (Ref. 15) |
| Polybenzimidazole | PBI | Celazole | 1.9 | 1.8 | 1.5 (Ref. 16); 1.5 (Ref. 14) |
| Polycarbonate | PC | Lexan; Makrolon | 2.9 | 3.2 | 2.9 (Ref. 16); 6.0 (Ref. 14) |
| Polychlorotrifluoroethylene | PCTFE | Kel-F; Aclar | 1.0 | n/a | 1.97 \pm 0.12* (Ref. 15); 0.9 (Ref. 16) |
| Polyetheretherkeytone | PEEK | Victrex PEEK; Hostatec | 2.3 | 2.1 | 3.7 \pm 1.0 (Ref. 15); 2.3 (Ref. 15); 3.2–4.5 (Ref. 16) |
| Polyethylene | PE | Alathon; Lupolen; Hostalen | 3.0 | 4.2 | 3.97 \pm 0.23 (Ref. 15); 3.2–4.5 (Ref. 16); 3.3 (Ref. 14); 3.7 (Ref. 14) |
| Polyethylene oxide | PEO | Alkox; Polyox | 7.1 | 5.8 | |
| Polyethylene terephthalate | PET | Mylar; Tenite | 3.5 | 3.1 | 3.4–3.6 Mylar A (Ref. 15); 3.4–3.7 Mylar A (Ref. 14); 3.0 Mylar D (Ref. 15); 2.9–3.0 Mylar D (Ref. 14); 3.4–3.9 (Ref. 16); 1.5–3.9 (Ref. 14) |

TABLE 23.1 (Continued)

| Material | Abbrev. | Trade Names | Predicted Erosion Yield in LEO by Different Correlations Re^{LEO} (Ref. 16) ($\times 10^{-24}$ cm ³ /atom) | | Erosion Yield in LEO ($\times 10^{-24}$ cm ³ /atom) and references |
|---|---------|--------------------------------|--|------------------|--|
| | | | γ mod-Correlation | 1/OI Correlation | |
| Polyimide (PMDA) | PI | Kapton® HN | 2.9 | 2.0 | 3.0 (Ref. 16); 3.0 (Ref. 14) |
| Polyimide (PMDA) | PI | Kapton® H | 2.9 | 2.0 | 3.0 (Ref. 15); 2.89 ± 0.6 (Ref. 15); 3.0 (Ref. 16); 3.0 (Ref. 14) |
| Polyimide (PMDA) | PI | Black Kapton | | | 1.5–3.1 (Ref. 14) |
| Polymethyl methacrylate | PMMA | Plexiglas; Lucite | 5.1 | 4.5 | 6.3 ± 0.3 (Ref. 15); 3.9–4.8 (Ref. 16); 3.1 (Ref. 14) |
| Polyoxymethylene; acetal; polyformaldehyde | POM | Delrin; Celcon; Acetal | 8.0–12.0 | 5.0 | |
| Polyphenylene | PPH | | 1.8 | | |
| Polyphenylene isophthalate | PPPA | Nomex | 2.5 | 2.9 | |
| Polypropylene | PP | Profax; Propathene | 2.9 | 4.1 | 4.4 (Ref. 15) |
| Polystyrene | PS | Lustrex; Polystyrol; Styron | 2.1 | 6.0 | 4.17 ± 0.17 (Ref. 15); 1.8 (Ref. 16) |
| Polysulphone (Polysulfone) | PSU | Udel; Ultrason/S | 2.5 | 2.4–3.0 | 2.3 (Ref. 15); 2.1 (Ref. 16); 2.4 (Ref. 14) |
| Polytetrafluoroethylene | PTFE | Fluon; Teflon; Halon | 0.0 | n/a | 0.20 (Ref. 15); 0.37 ± 0.06 (Ref. 15); 0.03–0.05 (Ref. 16); 0.0–0.2 (Ref. 14) |
| Polyvinyl acetate | PVA | Elvacet | 6.2 | | |
| Polyvinyl alcohol | PVA(L) | Elvanol | 7.1 | 4.1 | |
| Polyvinyl fluoride | PVF | Tedlar | | | 3.8 clear (Ref. 15); 1.3–3.2 clear (Ref. 14); 0.05–0.6 white (Ref. 14) |
| Polyvinylidene chloride co- polymers | PVDC | Saran | 5.1 | n/a | |
| Polyvinylidene fluoride | PVDF | Kynar | 1.1 | n/a | 0.9–1.1 (Ref. 16); 0.6 (Ref. 14) |
| Polyxylylene | PX | Parilene; Parylene | 2.1 | | |
| Pyrone | PR | Pyrone | 2.4 | | 2.3 (Ref. 16); 2.5 (Ref. 14) |
| Tetrafluoroethylene-ethylene copolymer | ETFE | Tefzel ZM | 1.1 | n/a | 1.2 (Ref. 16) |
| Urea formaldehyde | UF | Beetle; Avisco | 5.1 | 3.0 | |

* Corrected for LDEF ram fluence of 9.09×10^{21} atoms/cm²

making sure that dehydrated mass measurements are taken. Many polymer materials, such as Kapton®, are very hygroscopic (absorbing up to 2% of their weight in moisture) and can fluctuate in mass significantly with humidity and temperature. Therefore, for accurate mass loss measurements to be obtained, it is necessary that the samples be fully dehydrated (e.g., in a vacuum desiccator) prior to measuring the mass, both pre-flight and post-flight.

There is a large variation in the erosion yield values for the space data provided in Table 23.1. This is because some flight experiments were exposed to low atomic oxygen fluences on-orbit, such as during a Shuttle flight experiment. Variations in much of the early LEO space data also occurred because some erosion yield data were not determined based on dehydrated mass measurements, introducing large

error for hygroscopic materials, especially for low fluence exposures or low erosion yield samples. The erosion yield values listed in Table 23.1 from Refs. 15 and 16 represent more recent erosion yield values.

A LEO environment experiment called the MISSE (Materials International Space Station Experiment) PEACE (Polymers Erosion And Contamination Experiment) Polymers contains 41 different polymers for long-term atomic oxygen erosion determination [18]. The MISSE PEACE Polymers samples were placed on the outside the ISS Quest Airlock in August, 2001 during shuttle mission STS-105. The experiment is scheduled to be retrieved during STS-114, more than three years after its installation on International Space Station (ISS). The erosion yield data (to be obtained using dehydrated pre- and post-mass measurements) from this long-

term ISS experiment will be directly compared with the predictions provided in Table 23.1.

Atomic oxygen can also oxidize the surfaces of metals to produce nonvolatile metal oxides. However, for most metals, the oxides tend to shield the underlying metal from oxidation. Silver is one exception, because silver oxide tends to spall from the underlying metal, thus allowing continued oxidation. Such effects caused silver solar cell interconnects to fail in LEO [13]. Atomic oxygen interaction with silicones causes oxidation and removal of methyl groups, and gradual conversion of the surface of silicones to silica [19–21]. This frequently results in shrinkage and crack formation in the exposed silicones (Figures 23.10 and 23.11) as they are transformed from low modulus polymers into the higher modulus silica.

Surfaces of materials with volatile oxidation products (such as hydrocarbon polymers) that are oriented in a fixed position with respect to the ram direction gradually develop left-standing cones, which point in the direction of arriving atomic oxygen. Thus, the microscopic roughness of the surfaces increases with time. Because the predominant erosion of one location is independent of any other location and atomic oxygen arrives randomly, the development of surface roughness obeys Poisson statistics. This causes the surface roughness to increase as the square root of the atomic oxygen fluence [22]. Figure

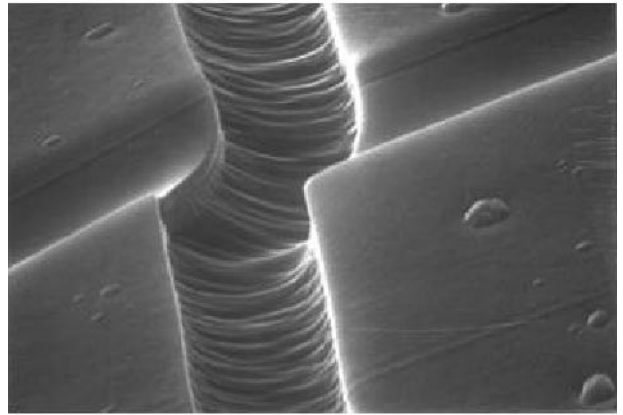
10 μm 

FIGURE 23.11 Scanning electron microscope photograph of DC 93-500 silicone showing cracking and subsequent branch cracking after atomic oxygen exposure to an effective fluence of 2.6×10^{21} atoms/cm² in a plasma asher facility.

23.12 shows typical atomic oxygen textured surfaces of Kapton[®] H polyimide, fluorinated ethylene propylene and chlorotrifluoroethylene after fixed-orientation exposure to atomic oxygen in LEO [23,24]. In addition to polymer thickness loss, such texturing causes an increase in diffuse reflectance and a de-

0.2 mm

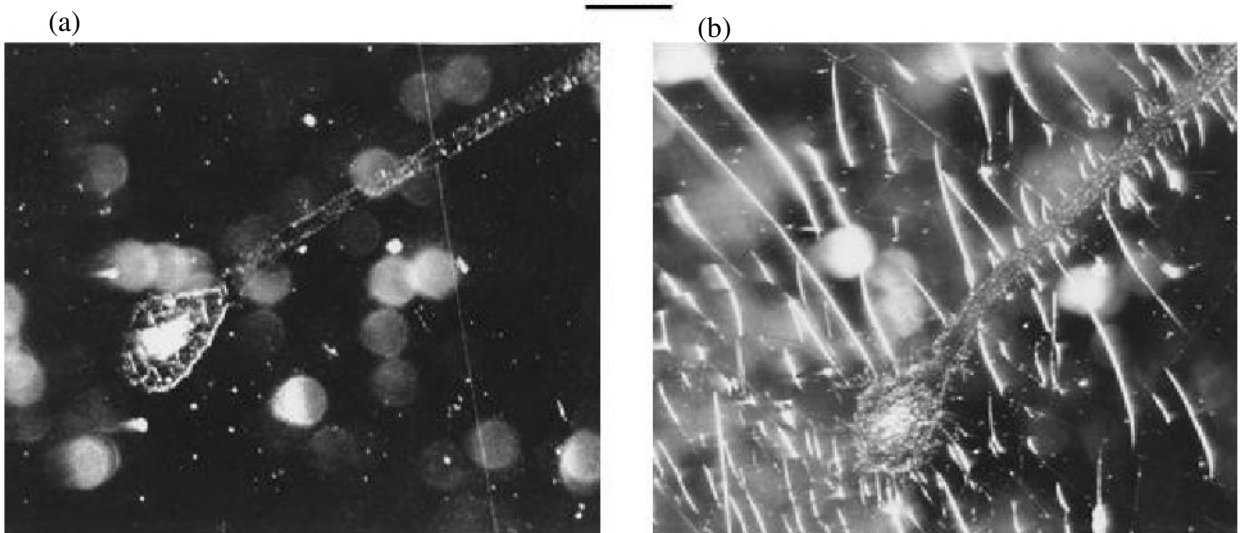


FIGURE 23.10 Effect of LEO atomic oxygen exposure (fluence of 2.3×10^{20} atoms/cm², Shuttle flight STS-46) on DC 93-500 silicone: (a) Photograph of unexposed DC 93-500 silicone, and (b) photograph of the same surface following exposure.

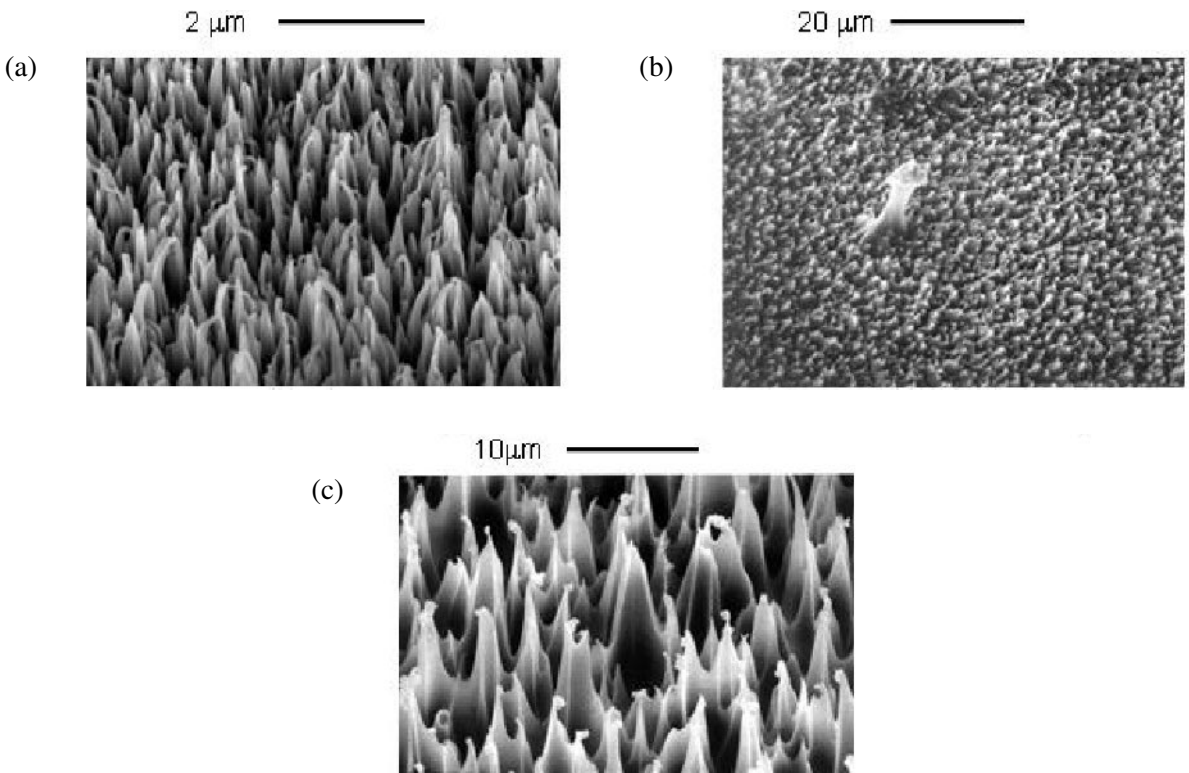


FIGURE 23.12 Scanning electron microscope photographs of LEO atomic oxygen textured polymers: (a) Kapton® H polyimide (atomic oxygen fluence = 2.3×10^{20} atoms/cm²); (b) Fluorinated ethylene propylene (FEP) Teflon® (atomic oxygen fluence = 7.78×10^{21} atoms/cm²); and (c) Chlorotrifluoroethylene (atomic oxygen fluence = 8.99×10^{21} atoms/cm²).

crease in specular transmittance of polymers [25]. Atomic oxygen exposure of hydrocarbon or halocarbon polymers that are pigmented or filled with metal oxide particles results in erosion of the polymeric content, resulting in gradual exposure of an increasing surface population of metal oxide particles that are poorly attached to each other [26]. The metal oxide particles, which become loosely attached, remain in contact and gradually shield the underlying polymer content from atomic oxygen erosion. Thus, the erosion yield can gradually decrease with atomic oxygen fluence.

23.2.3 Mitigation Techniques

Atomic oxygen erosion of thin polymers in LEO has represented a challenging spacecraft performance and durability problem for many years. Three approaches have been taken in efforts to reduce or eliminate atomic oxygen erosion of polymers. The three approaches to achieve polymer durability to atomic oxygen consist of: (1) the application of thin

film protective coatings made of atomic oxygen durable materials; (2) the modification of the surface of the polymers to make them more durable to atomic oxygen; and (3) the use of alternative polymers that contain metal atoms which develop a protective coating with atomic oxygen exposure.

The first and most widely used mitigation approach is the application of thin film metal, metal oxide or fluoropolymer-filled metal oxide protective coatings to polymers [27–31]. Thin film coatings of SiO₂, Al₂O₃, Indium Tin Oxide, Ge, Si, Al, and Au with thickness ranging from a few hundred to more than 100 nm are typically applied by sputter deposition or vapor deposition. For example, the SiO₂ coatings on Kapton® H polyimide for the solar array blankets on the International Space Station are 130 nm thick and applied by magnetron sputter deposition [32]. Although metal oxide coatings as thin as ~5.0 nm can provide atomic oxygen protection on ultra smooth surfaces, usually thicknesses of ~100 nm are used to ensure complete coverage over irregularities of debris, pits and rills on polymer surfaces. Coatings

which are factors thicker than 100 nm can more easily crack or spall due to either their intrinsic stress or inability to conform with flexure compression or expansion at their polymer substrates. The addition of fluoropolymer content to metal-oxide coatings allows factors greater strain-to-failure in the coatings. Such coatings can be deposited by co-sputter deposition of metal oxide and polytetrafluoroethylene Teflon® [25,27)].

The atomic oxygen durability of polymers that are protected by thin film coatings made of materials (which are themselves atomic oxygen durable) is largely dependent upon the number and size of pinwindow and scratch defects in the protective coatings (Figure 23.13). The application of 130-nm SiO₂ protective coatings on Kapton® polyimide can frequently reduce the rate of weight loss due to atomic oxygen erosion of Kapton® to less than 1% of that of unprotected Kapton® [32]. Atomic oxygen undercutting oxidation at sites of pin window and scratch defects can ultimately lead to mechanical failure of the polymer when a sufficient number of undercut cavities connect [29]. The growth of undercut cavities has been studied for polymer films coated on one side or both sides through the use of Monte Carlo computational modeling [7,33–36].

One approach to reducing the number of pinwindow and scratch defects in atomic oxygen protective coatings is to apply a surface tension leveling coating to the material prior to applying the protective coating. Studies have found the use of leveling coatings successful for increasing the atomic oxygen durability of protective coatings on composite materials based on decreasing defect densities [37,38].

For example, in one study a low viscosity epoxy was applied to the surface of several composite coupons. A protective layer of 1,000 Å of SiO₂ was deposited on top of the leveling coating, and the coupons were exposed to an atomic oxygen environment in a plasma asher. Pinhole populations per unit area were estimated by counting the number of undercut sites observed by scanning electron microscopy. Defect density values of 180,000 defects/cm² were reduced to about 1,000 defects/cm² as a result of the applied leveling coating [37]. Leveling coatings have also been found to improve the optical performance of composite concentrator surfaces by improving the specular reflectance [37,38].

The mitigation approach involving modification to the surface of polymers to make them more durable to atomic oxygen has primarily involved either implantation of metal atoms into the surface of the polymer [39] or chemical modification of the surface of the polymer to incorporate silicon atoms into the surface and near the surface. In both surface modification approaches, the degree to which the atomic oxygen erosion yield is reduced is dependent upon the aerial density of metal atoms that can be placed into the polymer surface.

The formation of alternative polymers that contain inorganic atoms has been approached through a variety of chemical formulations including the use of silicone co-polymers [40], polysilsesquioxane [41], cage coordination compound incorporation of metal atoms [42], and phosphorous-containing polymers [43]. As with the surface alteration approach, the durability of the alternative polymer is dependent upon the aerial density of inorganic atoms that

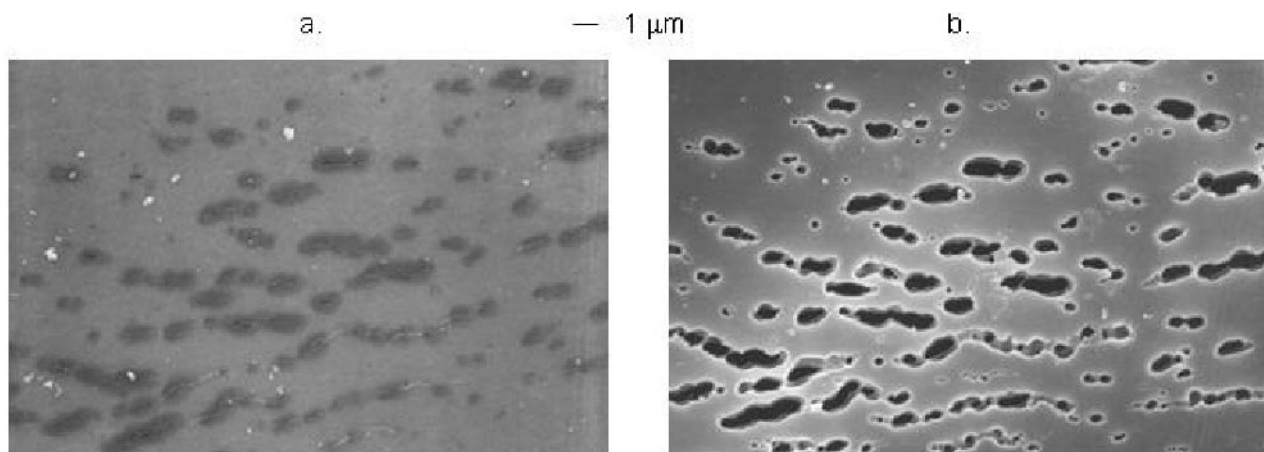


FIGURE 23.13 Scanning electron microscope photographs of LEO atomic oxygen exposed Kapton® from LDEF at sites of pinwindow and crack defects in a vacuum deposited aluminum protective coating: (a) Prior to removal of aluminumized coating; (b) After chemical removal of protective coating.

can be achieved. In addition, the alternative polymers must achieve the durability to other space environmental threats, such as UV radiation and ionizing radiation, to be considered suitable. Other properties, such as low solar absorptance, may be required, depending on the application. A benefit of some of the alternative polymers is lower solar absorptance than Kapton[®] [43].

23.3 CONTAMINATION EFFECTS

23.3.1 Sources and Transport of Spacecraft Contamination

Spacecraft contamination can be defined as molecular or particulate matter on or near a spacecraft surface that is foreign to that surface. Sources of spacecraft contamination can include thruster propellants and burn residue, outgassing of spacecraft materials, vented gases from spacecraft systems, fluids released from the spacecraft by dumping or leakage, micrometeoroids and orbital debris, and particles generated or redistributed during spacecraft mechanical operations or astronaut extravehicular activity (EVA) operations [44]. Comprehensive data on outgassing of spacecraft materials is found in Ref. 45. Space environment interactions with materials can also produce contaminants, such as volatile products of atomic oxygen reactions and ultraviolet-induced or radiation-induced chain scission products in polymer materials and residual non-oxidative films left free-standing due to atomic oxygen erosion of underlying material. Space environment effects, such as atomic oxygen, ultraviolet, and radiation interactions, can further modify contaminant species.

Spacecraft contaminants can either deposit onto spacecraft surfaces or remain in the vicinity of the spacecraft. Molecular contaminants can transport from surface-to-surface through various mechanisms, including line-of-sight transport, non-line-of-sight transport through reflection or scattering, and attraction of positively ionized contaminants to a negatively charged, sunlit spacecraft surface [46]. These transport mechanisms can put critical spacecraft surfaces at risk for contamination effects.

23.3.2 Contamination Effects on Spacecraft Surfaces

Buildup of molecular or particulate spacecraft contamination can cause degradation in transmittance, reflectance, solar absorptance, and thermal emit-

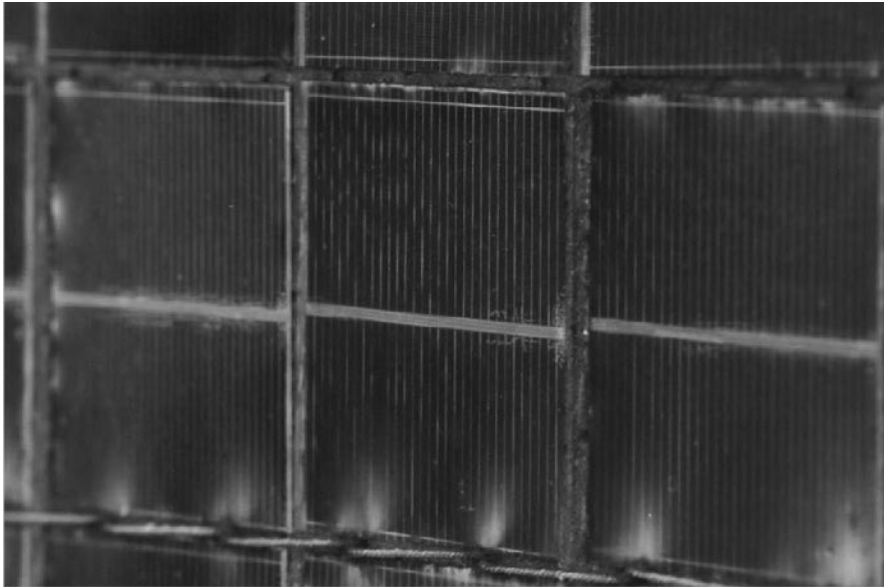
tance of surfaces. The impacts of this degradation include reduced performance of solar arrays, radiators, instrument optics, sensors, and other systems [44].

Some particularly detrimental cases of space environment interactions with spacecraft contamination include atomic oxygen oxidation of outgassed silicones to produce a non-eroding silica-based layer, and ultraviolet or ionizing radiation interactions with contaminants to produce a contaminant film. Examples of these cases will be discussed below.

23.3.2.1 Atomic Oxygen Interaction with Silicones

Almost all spacecraft have silicones on board in the form of adhesives, potting compounds and lubricants used in materials processing. Although most LEO spacecraft designers make efforts to use only silicones that are vacuum stripped to eliminate or reduce the amount of volatile short-chain content, silicone fragments are often evolved in the vacuum environment in LEO, with the process being further enhanced with atomic oxygen and/or radiation-induced bond breaking. The resulting silicone fragments can deposit on surfaces that are exposed to atomic oxygen. If the surfaces are not receiving atomic oxygen, then simple re-evaporation of the silicone can occur, providing that the surfaces are the same temperature or hotter than the source of the silicone. Or, UV may interact with the silicone fragments causing a polymerized contaminant layer to build up, as will be discussed in Section 23.3.2.2. With atomic oxygen arrival, oxidation reactions cause the silicones to lose hydrocarbon content and convert to a silica-based surface layer that is resistant to atomic oxygen erosion. Such processes occurred on the MIR Space Station, resulting in the accumulation (over a ten-year duration) of a microscopically rough coating on the solar array (Figure 23.14) which was up to 4.6 μm thick [19]. Such coatings tend to be rather transparent. However, if the silicone deposition is also accompanied by hydrocarbon deposition, a much more optically absorbing coating can result [47]. Figure 23.15 is a photograph of the anti-solar side of one of the MIR solar array solar cells. The contamination is much more absorbing. It appears as a tan-colored silica deposit formed by atomic oxygen reaction of silicones that were arriving at the same time hydrocarbons arrived from a polymer mesh behind the array. This contaminant layer was $\sim 1.24 \mu\text{m}$ thick.

(a)



(b)

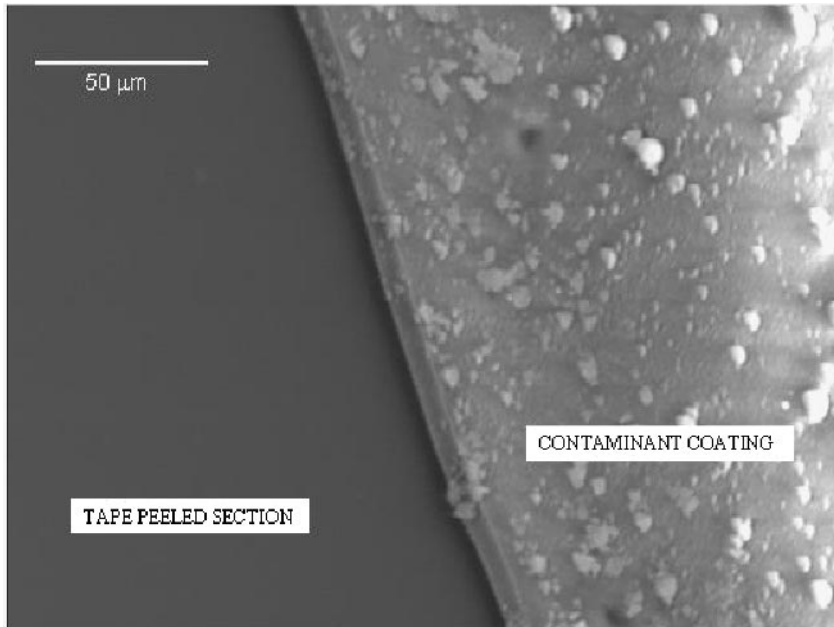


FIGURE 23.14 MIR solar array sun facing surface after 10 years in LEO: (a) Photograph showing silica contamination as a diffuse white deposit on the front surface of the solar cells; (b) Scanning electron microscope photograph of oxidized silicone contamination layer.

23.3.2.2 Photochemical Deposition of Contaminants

In the presence of UV light, contaminants can form a polymerized film on a spacecraft surface [46]. It has also been stated that charged particles might play a role in this polymerization process, either separately or synergistically [44]. Even though outgassing rates decrease with time, subsequent con-

taminant deposition rates do not decrease at the same rate. This is because photochemical contamination processes have been found to continue even when outgassing has subsided [44]. This can be a significant concern on long-duration missions.

The Long Duration Exposure Facility (LDEF) satellite, which was exposed for 69 months in the LEO environment, provided an interesting study of contamination processes as the leading edge re-

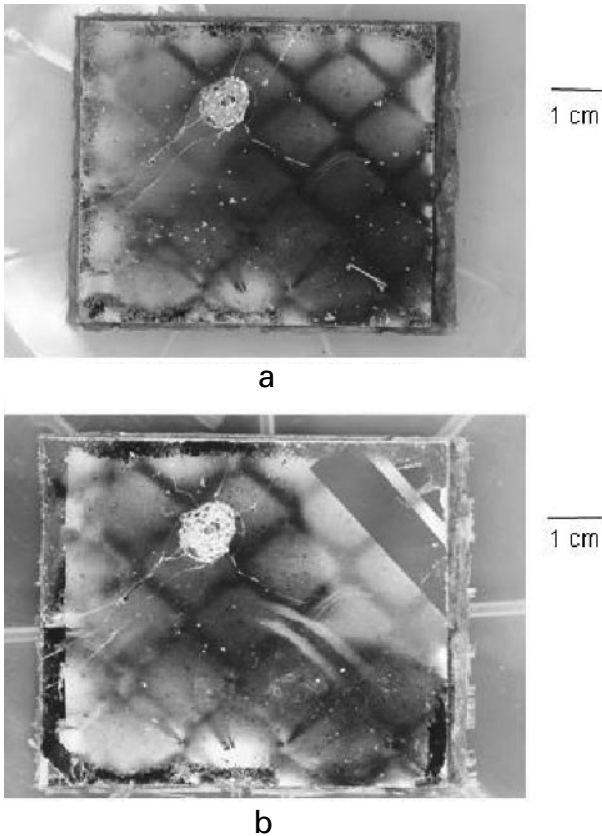


FIGURE 23.15 Back surface of MIR solar cell after 10 years in LEO: (a) photograph of contamination on solar cell back surface prior to “tape peel cleaning;” and (b) photograph of the same solar cell back surface after “tape peel cleaning” of the upper right corner to show a comparison of the contaminated and cleaned areas.

ceived a high fluence of directed ram atomic oxygen along with solar exposure, and the trailing edge received very little atomic oxygen along with similar solar exposure. Molecular contamination processes on LDEF surfaces varied from the leading edge to the trailing edge. Surfaces on the leading edge experienced removal of hydrocarbon-based contaminants and oxidation of silicone fragments leading to silica-rich, hydrocarbon-poor contaminant films. Surfaces on the trailing edge experienced the buildup of hydrocarbon contaminants and silicone fragments which became UV-darkened hydrocarbon-rich, silicone contaminant films.

23.3.3 Mitigation of Contamination Effects

Mitigation of spacecraft contamination effects is achieved through careful selection of materials (par-

ticularly low outgassing materials), a spacecraft design which minimizes contamination risk for critical components, and taking precautions for spacecraft cleanliness during ground assembly and on-orbit operations. Spacecraft materials outgassing data is found in Ref. 45, and detailed guidelines for spacecraft contamination control can be found in Ref. 48.

23.4 SPACE RADIATION EFFECTS

23.4.1 Solar Ultraviolet Radiation

23.4.1.1 Environment Description

Earth’s atmosphere absorbs all ultraviolet radiation from the Sun that is less than 0.3 microns in wavelength [46]; however, spacecraft outside of the Earth’s atmosphere and with a view of the Sun are subject to the full solar spectrum. Additionally, spacecraft surfaces without a direct view of the Sun, but with a view of Earth, may still experience solar ultraviolet effects due to Earth albedo, which is the Sun’s energy (~31%) reflected back to space by the Earth’s atmosphere [46]. The solar spectrum outside the Earth’s atmosphere at one astronomical unit from the Sun is referred to as the air mass zero (AM0) solar spectrum. Figure 23.16(a) shows the AMO solar spectrum in the wavelength range up to 250 nm and 23.16(b) shows the UV region of the AMO solar spectrum [49]. In general, the ultraviolet range is defined as the portion of the electromagnetic spectrum including wavelengths between 4–400 nm [50]. However, relevant to materials degradation in space, it is convenient to examine only those wavelengths which are significant in the AM0 solar spectrum. Integrated solar irradiance in various wavelength ranges are shown in Table 23.2 [49] along with the portion of the solar constant represented by each wavelength range. It is evident that wavelengths shorter than approximately 120 nm represent a negligible portion of the solar spectrum. Relevant to the study of space environment effects on materials, the ultraviolet range of wavelengths can be conveniently divided into two bands: Near UV (NUV) as the 200–400 nm range and vacuum UV (VUV) as the 100–200 nm range.

23.4.1.2 Effects on Materials

Polymers are particularly susceptible to ultraviolet radiation degradation, because many types of bonds in organic polymers are capable of absorbing UV light, which can lead to photochemical reactions

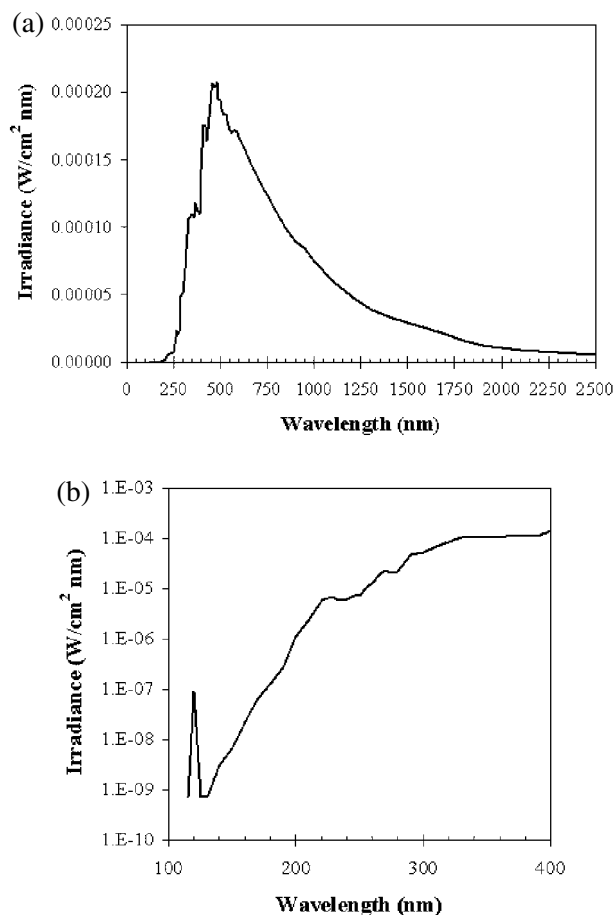


FIGURE 23.16 The air mass zero (AM0) solar spectrum: (a) the wavelength range up to 2,500 nm; (b) the UV portion of the AM0 solar spectrum from 100–400 nm.

TABLE 23.2 Air Mass Zero Integrated Solar Irradiance [49]

| Wavelength Range | Integrated solar irradiance in wavelength range (W/m ²) | Percent of Solar Constant within wavelength range |
|---------------------------------|---|---|
| $\lambda \leq 1000 \mu\text{m}$ | 1,366.1 | 100 |
| $\lambda \leq 400 \text{ nm}$ | 106.6 | 7.8 |
| $\lambda \leq 200 \text{ nm}$ | 0.10 | 0.007 |
| $\lambda \leq 120.5 \text{ nm}$ | 3.12×10^{-4} | 2.28×10^{-5} |

[46,51]. Additionally, impurities that are usually contained in synthetic polymers are often more likely to absorb UV light than the polymer itself, and can be significant contributors to the photochemical reactions within the polymer material [51]. Photochemical reactions within organic molecules may result in

effects such as discoloration of the material (increase in solar absorptance) or loss of mechanical properties due to chemical changes in the material. Important considerations for polymer UV durability in space are the wavelengths required to cause degradation, the depth of degradation, and synergistic effects with other environmental factors. It is generally thought that most polymers absorb approximately 95% of incident radiation below 250 nm within 0.3 μm from the surface [52]. However, based on the data shown in Figure 23.17, Teflon[®] FEP is an exception, as it transmits a significant amount of ultraviolet radiation through tens of micrometers in depth [53].

For polymer films whose thickness is significantly greater than the UV attenuation depth (the depth within which the majority of UV light is absorbed), the undegraded portion of the polymer thickness provides support to a degraded surface. However, for applications using polymer films whose thickness is on the order of the UV attenuation depth, the potential for UV degradation resulting in cracking of the full film thickness is significant.

Glass and ceramic materials have been observed to undergo ultraviolet radiation-induced darkening [50,54], also referred to as *solarization*. UV light interactions in glass and ceramic materials can cause formation of electrons or holes that are trapped in various defects. Some of these trapped species absorb light in specific wavelength ranges and are referred to as color centers [54]. UV-darkening can be affected by purity of the material, particle shape and size, surface chemistry and thermal history [55]. UV-darkening can be detrimental to spacecraft materials such as white paint coatings and solar cell cover glass.

In order to understand effects of space ultraviolet radiation on materials, it is useful to examine results of laboratory testing reported in the literature. However, results should be cautiously interpreted, because there are a multitude of variables associated with ultraviolet testing that make it difficult to compare results directly from one test to another. These variables include: wavelength range, spectral shape and intensity of the UV source, and the nature of the exposure environment (air, purge gas, or vacuum). It is important to note that UV-induced degradation reactions in polymers are also influenced by oxygen, where the quantum yield (i.e., number of scission products per incident photon) is often greater for reactions in the presence of oxygen [51,56]. Even vacuum systems contain some amount of oxygen from residual air in the system. For some materials, especially semiconductor pigmented paints, post-

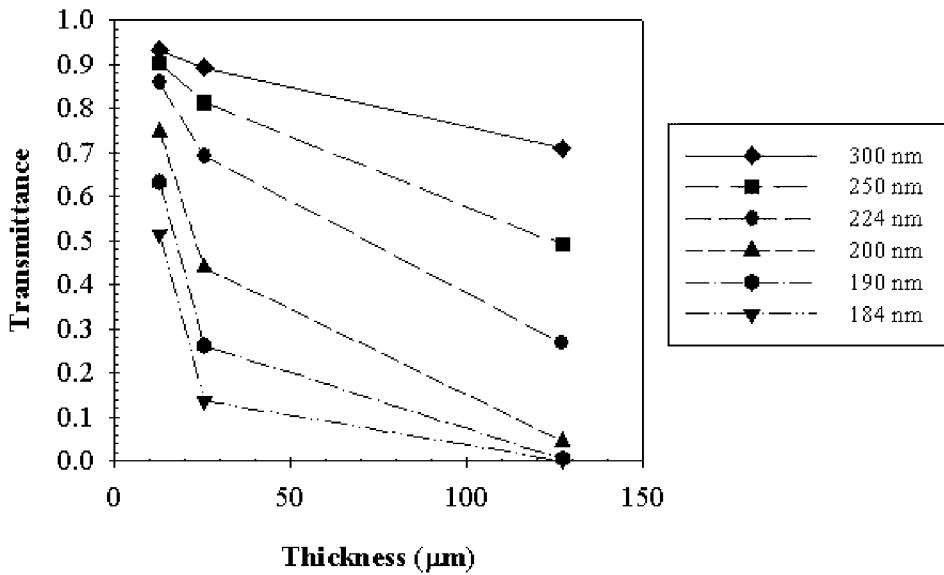


FIGURE 23.17 Transmittance as a function of FEP thickness.

irradiation exposure to air (as is often required for post-exposure analysis) can cause reversal of the UV-induced damage, sometimes referred to as “air bleaching,” creating an additional complication for interpreting test results [55].

23.4.1.2.1 Effects on Fluoropolymers. UV interactions with fluoropolymers have been found to cause loss of mechanical properties and loss of optical properties. Erosion, mass loss, and surface roughness increases have been observed for Teflon® fluorinated ethylene propylene (FEP) upon exposure to a broad spectrum (> 115 nm) VUV deuterium lamp providing wavelengths greater than 115 nm in vacuum [57,58]. Erosion of FEP was also observed upon exposure to monochromatic light of 147 nm [58]. Broad spectrum VUV (> 115 nm) also caused mechanical properties degradation for FEP [58]. One study [59] examined effects of broad spectrum VUV light on FEP using windows to produce lower cut-off wavelengths of 115 nm, 140 nm, and 155 nm. All wavelength ranges were found to produce degradation in the strength and elongation-to-failure of FEP, indicating that wavelengths greater than 155 nm are capable of degrading FEP. In another study, surface hardness of FEP was found to increase as a function of increasing exposure to broad spectrum VUV (> 115 nm), where surface hardness was used as a measure of surface embrittlement. In this test, surface hardness was analyzed using

atomic force microscopy (AFM) techniques [60]. Teflon® polytetrafluoroethylene (PTFE) was found to be more susceptible to UV damage than FEP [58].

Various synergistic effects were observed for fluoropolymers exposed to ultraviolet radiation during heating or thermal cycling. Tensile strength and elongation-to-failure were found to decrease for PTFE polymers upon UV exposure in the 185–369-nm wavelength range in vacuum or nitrogen at temperatures of 21–315 °C, suggesting that chain scission occurs in PTFE polymers [61]. UV exposure of FEP resulted in chain scission at ambient or slightly higher temperatures, and cross-linking above 80 °C [61]. VUV exposure (147-nm light) at temperatures of 120 °C and 150 °C resulted in a significant decrease in tensile strength and elongation compared to the negligible change observed for VUV alone [58]. Compared to VUV irradiation with steady-state heating at 100 °C, creep deformation increased for VUV irradiation with thermal cycling, which was attributed to FEP traversing between phases during thermal cycling [62].

Tedlar® (polyvinyl fluoride) is found to undergo loss of strength and elongation due to ultraviolet exposure as reported in the literature for terrestrial uses of Tedlar® [63]. Regarding testing for aerospace applications, Tedlar® materials were exposed to at least 2,500 equivalent sun hours in a facility that provided VUV (> 115 nm) and NUV (~200–400 nm) to sim-

ulate LEO and GEO solar conditions [64]. Results from this test showed that solar absorptance for an uncoated cloud white Tedlar[®] increased. Use of an Optical Coating Laboratory, Inc. (OCLI) multi-layer coating prevented a significant change in solar absorptance. The OCLI coating was thus found to perform well as a UV protective coating for white Tedlar[®]. However, another investigation showed that an OCLI coating did not adhere well to FEP [60], which will be described in Section 23.5.2.3.

Whereas VUV radiation from a deuterium lamp ($\lambda > 115$ nm) was found to cause mass loss of FEP, no mass loss was observed for unpigmented Tedlar[®] [65]. Lack of mass loss for Tedlar[®] was attributed to the fact that, unlike FEP, Tedlar[®] contains CH bonds. It was proposed that Tedlar[®] undergoes cross-linking that modifies the surface layer.

As illustrated through the examples above, ultraviolet radiation and synergistic effects with heating or thermal cycling are well known to cause degradation of mechanical properties and optical properties of fluoropolymers. The degree to which degradation occurs depends upon irradiation wavelengths, exposure temperatures, and the chemical nature of the fluoropolymer.

It is important to note that the spectral mismatch between the VUV deuterium lamp and the AM0 Sun may produce degradation mechanisms that are different between space and laboratory exposures. For example, the lamp's peak at around 160 nm coincides with a peak of Teflon[®] UV absorption [66]. There is no such peak in the solar spectrum. The VUV lamp peak may result in enhanced surface reactions for Teflon[®] which would not occur to as great an extent in space.

23.4.1.2.2 Effects on Polyimide Kapton[®]. Polyimide Kapton[®] shows minor changes in properties upon VUV exposure. In one study [67], a sample of 25.4- μ m Kapton[®] HN exposed to 1,100 equivalent VUV sun hours (115–200 nm VUV) did not experience any statistically significant changes in elongation or ultimate tensile strength. Minor changes in the reflectance spectrum in the ultraviolet-visible wavelengths due to this exposure may be indicative of some changes in surface chemistry, however. A minor increase in solar absorptance due to this VUV exposure, from approximately 0.23 to approximately 0.24, was also observed.

23.4.1.2.3 Effects on Epoxy Composites and Adhesives. In one study, it was found that UV exposure (220–300 nm wavelength range) of epoxy

resin caused degradation within the top 0.5–1.0 μ m layer) for exposure as little as 30 minutes of exposure [68]. Weight loss of epoxy composite materials was observed and was found to increase with increased UV irradiation time for a test conducted using an accelerated weathering tester consisting of medium-wave UV (200–300 nm) lamps in a system controlled at 50 °C [69]. Another test found that UV irradiation from medium-wave (200–300 nm) UV lamps initiated microcracks in graphite epoxy and glass epoxy composites, which then propagated upon thermal shock testing between 121 °C and liquid nitrogen temperature (–196 °C) [69]. On the Long Duration Exposure Facility (LDEF), which exposed materials to the space environment for 69 months, Hysol 934 epoxy adhesive was found to discolor and Hysol EA 9628 was found to have a decreased shear strength following flight. These effects were attributed to UV degradation [70].

23.4.1.2.4 Effects on White Paint Coatings. Space-stable coatings with low solar absorptance and high thermal emittance are important to spacecraft thermal control. Z93 and YB-71 paints, with zinc oxide and zinc orthotitanate pigments, respectively, in potassium silicate binders, have proven to maintain their thermo-optical properties in the space environment [55]. A paint formulation with zinc oxide pigment in a methyl silicone binder, designated as S13G/LO, provides a more flexible option for the white paint coating [55]. Development of these three types of paints originated based on the UV stability of the ZnO and Zn₂TiO₄ pigments. Other pigments examined were found to undergo significant UV degradation, including, zirconia, alumina, and silica pigments [55]. Although Z93, YB-71 and S13G/LO paints have shown appropriate space stability, the S13G/LO material degrades in UV somewhat faster than YB-71 or Z93, and, therefore, its use is limited to shorter duration missions. For example, for 5,000 equivalent sun hours of UV exposure, solar absorptance increases of \approx 0.02, 0.03, and 0.06 were observed for YB-71, Z93, and S13G/LO, respectively [55].

23.4.2 Ionizing Radiation

The ionizing radiation environment of space includes energetic charged species such as electrons and protons, and energetic photons such as x-rays and gamma rays. These energetic particles and photons are considered ionizing radiation because they ionize atoms as they move through a material. The

extent of high energy particle interactions with materials depends upon the type of radiation, its energy and the material. Details on the interactions of radiation with matter are comprehensively addressed elsewhere [71,72]. Materials degradation due to ionizing radiation can occur based on accumulation of absorbed energy in the material, referred to as total ionizing dose. Additionally, the rate at which the energy is deposited, referred to as dose rate, may also influence materials degradation. Radiation dose, referred to in SI units of grays (Gy), is the amount of radiation that deposits 1 J of energy per 1 kg mass of material. Another commonly used unit is the rad, which is 0.01 Gy. Sources of ionizing radiation within the space environment are described below.

23.4.2.1 Solar Flare X-ray Radiation Environment

Solar flares are releases of intense energy from the Sun occurring over a short duration (minutes to hours), observed as sudden brightening of the chromosphere of the Sun and producing energy throughout the electromagnetic spectrum from radio waves to gamma rays [46,73]. During the approximately 11-year solar cycle, periods of high solar activity are correlated with enhanced X-ray emission [46].

For spacecraft in Earth orbits, surfaces with a view of the Sun during periods of solar flares will be exposed to a significant flux of X-rays. The Geosynchronous Operational Environmental Satellites (GOES) have been monitoring the space solar X-ray environment since 1986, from their location in geosynchronous orbit at an altitude of approximately 35,800 km. GOES solar X-ray flux data, available through the National Oceanic and Atmospheric Administration (NOAA) National Geophysical Data Center (NGDC) [74] were used to estimate the solar flare X-ray environment in wavelength regions of 0.1–0.8 nm, 0.05–0.4 nm, 0.0124–0.05 nm, and 0.0124–0.05 nm for the Hubble Space Telescope (HST) mission in LEO [75]. These X-ray fluences and estimated dose depth profiles for FEP are shown in Figure 23.18(a).

23.4.2.2 Charged Particle Radiation Environment

The three main sources of charged particle radiation naturally occurring in space are galactic cosmic rays, solar proton events, and the trapped radiation belts. Galactic cosmic rays (GCRs) consist of low

flux ionized nuclei, mostly protons, generally providing a very low radiation dose rate, which is highest at solar minimum [46]. GCR radiation consists of ions of all elements of the periodic table and is composed of approximately 83% protons, 13% alpha particles (^4He ions), 3% electrons, and 1% of heavier nuclei [76]. Energies of GCR particles range from about 10^8 – 10^{19} eV [46]. Low altitude/inclination orbits are protected from some of the GCRs, because when a GCR approaches Earth in the plane of the equator, Earth's magnetic field bends the particle back to space or to the polar regions, depending on its initial direction and energy [46].

Solar proton events (SPEs) result from coronal mass ejections producing significant proton flux over short duration periods of, on average, one to five days [46]. Some SPEs are heavy-ion-rich with energies ranging from tens of MeV/per nucleon to hundreds of GeV/per nucleon [76]. Spacecraft in low Earth orbits, such as the Hubble Space Telescope, are generally protected by the magnetosphere from the majority of SPE proton flux, but SPEs are hazardous to spacecraft in high inclination orbits and geosynchronous orbit [75]. In the trapped radiation belts, also called the Van Allen belts, energetic electrons and protons are confined to gyrate around Earth's magnetic field lines. Trapped electrons have energies up to tens of MeV and trapped protons and heavier ions have energies up to hundreds of MeV [76]. Fluxes of protons and electrons in the trapped radiation belts are a function of particle energy, altitude, inclination, and solar activity and can increase during solar storms [46,76]. Peak fluxes of both electrons and protons occur at around 3,000 km and a second peak of electron flux occurs at around 25,000 km altitude [46]. Additional variables affecting trapped radiation flux include effects of Earth's poles and the South Atlantic Anomaly. Spacecraft in polar orbits experience greater charged particle dose rates than spacecraft in equatorial orbits due to Earth's magnetic field funneling charged particles into the polar regions [46]. An asymmetry in Earth's magnetic field lines causes charged particles to reach lower altitudes (< 1000 km) in the South Atlantic, so that spacecraft experience higher dose rates during passage over this region [46,76].

Estimates of the trapped proton and electron fluences have been obtained using NASA's proton (AP-8) and electron (AE-8) models [77,78]. The trapped electrons and protons are considered to be omnidirectional by the AP-8 and AE-8 models, although some degree of east-west asymmetry has been observed by spacecraft measurements in the time

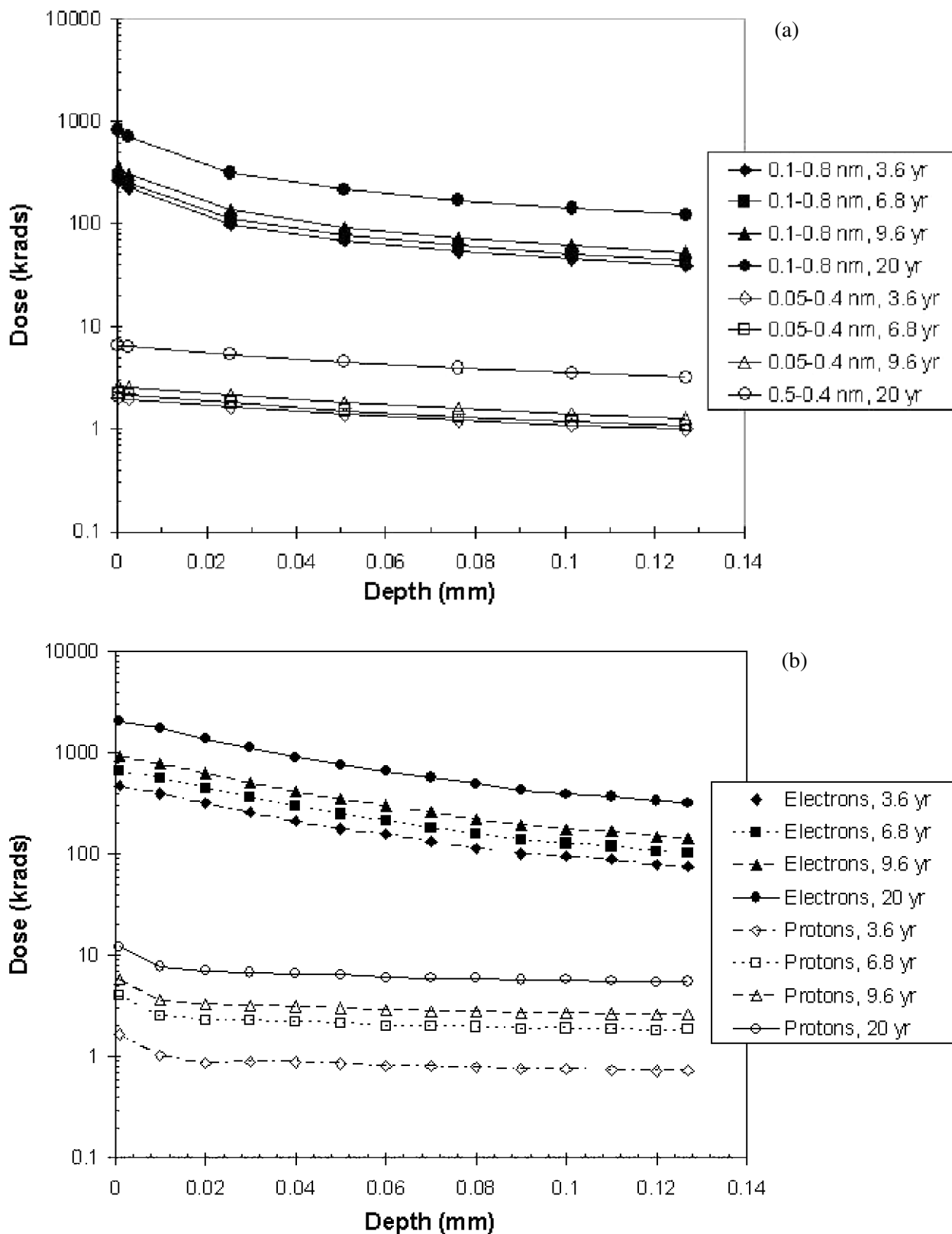


FIGURE 23.18 Dose-depth profiles for ionizing radiation in FEP for (a) solar flare x-ray exposure, and (b) trapped electron and proton radiation exposure for the Hubble Space Telescope environment.

since these models were developed [77]. Because of the approximately omni-directional nature of the trapped radiation, all exterior spacecraft surfaces are exposed to this radiation.

23.4.2.3 Space Ionizing Radiation Effects on Materials

23.4.2.3.1 Polymers. Ionizing radiation interacts with atomic nuclei and their surrounding electron clouds without specificity to particular chemical bonds, unlike ultraviolet radiation that is absorbed by particular chemical bonds [79]. Polymers can become degraded in physical and mechanical properties due to accumulated total dose of ionizing radiation, which includes electrons, protons and X-rays and GCRs.

Polymer films, such as FEP and Kapton[®], are commonly used on exterior spacecraft surfaces for thermal control blankets and adhesively bonded radiator surfaces, and, therefore, receive an unshielded dose of space radiation. Embrittlement and loss of strength are not significant concerns for radiator surfaces rigidly adhered to metal structures. However, for polymer films that are not rigidly supported, such as in multilayer insulation applications, degradation in mechanical properties can result in cracking of the exterior polymer film layers. Cracking in thermal blanket layers can compromise the thermal protection of underlying equipment and may pose a contamination risk if pieces of the cracked film become dislodged. In addition to thermal insulation blankets, other uses of polymers on spacecraft exterior surfaces include structural composites, adhesives, potting materials, and wiring/cable insulation.

As a guide to effects of radiation on spacecraft polymers, Table 23.3 shows the ionizing radiation

doses that have been found to produce mild to moderate and moderate to severe polymer degradation [80].

Relative degradation data such as in Table 23.3, which are found commonly in radiation effects references and which vary slightly among references (see also Refs. 46 and 81) can be used as a screening tool for materials selection, but it is important to consider that many other factors may play a role in overall materials degradation in a space radiation environment. For example, the uniquely low solar absorptance and high thermal emittance of FEP have led to its wide use for spacecraft thermal control, despite its susceptibility to radiation degradation.

Whereas the data in Table 23.3 are for polymers exposed to gamma radiation in air, it is generally found that irradiation in oxygen or air produces more severe degradation of polymers than irradiation in vacuum. For example, air or oxygen is known to significantly affect the radiation-induced degradation of PTFE, which undergoes scission at a much higher yield in air than in vacuum [79]. A similar finding was reported for x-ray irradiated Teflon[®] FEP, which experienced an increase in the degradation of mechanical properties after air exposure [82]. Also, many polymers which predominantly cross-link when irradiated in vacuum will undergo main chain scission when irradiated in air, indicating that not just the extent of degradation is affected by the exposure environment, but the mechanism of degradation as well [79].

Table 23.3 does not account for dose rate effects or synergistic effects of radiation and temperature. One report summarized that long-duration low dose rate exposures produced greater degradation of FEP than short duration high dose rate exposure, indicative of a possible dose rate effect. However, this ap-

TABLE 23.3 Effect of Gamma Radiation Dose on Some Common Spacecraft Polymers [80]

| Material | Gamma Radiation Dose (rad) | |
|--|----------------------------|---------------------------|
| | Mild to Moderate Damage | Moderate to Severe Damage |
| Teflon [®] fluorinated ethylene propylene (FEP) | 1E6-8E6 | 8E6-2E7 |
| Teflon [®] polytetrafluoroethylene (PTFE) | 2E4-1E5 | 1E5-2E6 |
| Kapton [®] , polyimide | 1E8-1E10 | 1E10-1E11 |
| Mylar, polyethylene terephthalate (PET) | 4E6-1E8 | 1E8-1E9 |
| Polyethylene | 1E7-8E7 | 8E7-2E8 |
| Polyurethane | 1E9-5E9 | 5E9-2E10 |
| Silicone | 1E8-1E9 | 1E9-5E9 |
| Epoxy | 2E8-8E8 | 8E8-5E9 |
| Nylon, polyamide | 3E5-2E6 | 2E6-2E7 |
| Polyvinyl chloride (PVC) | 1E7-7E7 | 7E7-2E8 |

parent dose rate effect was attributed to time spent at elevated temperatures rather than to dose rate alone [61]. This report stated that accelerated ground testing for ionizing radiation degradation to FEP may underpredict in-space damage by factors of three to 10, as a crude guideline. Further synergistic considerations for radiation and temperature are discussed in Section 23.5.2.3.

Newer applications for polymer films on spacecraft require large, lightweight, deployable and/or inflatable spacecraft structures, requiring significantly thinner materials than used in thermal blanket applications. Decreasing the thickness of a polymer increases the risk for radiation damage effects. This is because space ionizing radiation deposits a decreasing dose at increasing depths within a material, so that the greatest damage to a polymer film is at the surface and the damage decreases with increasing depth. An example of dose versus depth in FEP, a widely used and radiation-vulnerable material is shown in Figure 23.18 for solar flare x-rays and trapped electron and proton radiation on HST [75]. When ionizing radiation degradation is combined with ultraviolet degradation (another effect that diminishes with increased polymer thickness), it is evident that ultra-thin polymer films, such as gossamer structures, are at great risk of radiation-induced degradation. Because of the greater radiation sensitivity for thinner polymer films, accurate modeling of the space environment and associated dose-depth profiles for polymer films is critically important to predicting the durability of thin polymer films for use on large spacecraft structures for long-duration missions. Methods of modeling the space environment are described in Refs. 80 and 81, and methods for developing appropriate dose-depth profiles and space radiation simulation tests are described in Ref. 81.

Some newer polymer film materials have been studied for radiation durability applicable to use in deployable and inflatable spacecraft structures. Two studies [83,84] examined effects of electron and proton radiation, in some cases with ultraviolet radiation as well, on aromatic polyimide films to simulate exposure near the Earth-Sun Lagrangian points 1 and 2. Films tested included Kapton[®] HN, Kapton[®] E, Upilex[®] S, CP-1, CP-2 and either TOR-RC [83] or TOR-LM [84]. All materials were found to undergo increased solar absorptance due to the radiation exposure.

In addition to polymer mechanical degradation, electrical properties of polymers may also be compromised due to radiation. This is a particularly im-

portant effect for polymers used for electrical insulation, such as wiring or cable insulation. Ionizing radiation has been found to induce conductivity in polymer films [85]. This induced conductivity has been found to be material-dependent and dose rate-dependent, but independent of the type of ionizing radiation [85]. One study examined radiation-induced conductivity in various polymers upon exposure to gamma rays up to 10^6 Gy [86]. This study found increases in conductivity for polyethylene and polystyrene of two to three orders of magnitude, less than an order of magnitude increase for Teflon[®], and negligible increases in conductivity for nylon, epoxy, and polyvinyl chloride. This induced conductivity has been found to be temporary, however. Once the radiation exposure was discontinued, those materials which experienced radiation-induced conductivity recovered to near-initial conductivity within seconds to hours [86].

One complication of accelerated rate charged particle radiation testing of polymer materials is the possibility for charging of insulating polymer surfaces. PTFE, for example, is an excellent electrical insulator. On-orbit, the low current and dose rates permit continuous discharge of exposed PTFE materials. However, in ground laboratory accelerated tests, electrostatic charging of the PTFE target in high current/dose-rate laboratory electron beams can lead to deceleration and deflection of the incident electron beam, especially for lower energy electrons [87]. This effect needs to be considered when evaluating accelerated rate space simulation test results for insulating materials.

23.4.2.3.2 White Paint Thermal Control Coatings. Many satellite systems have used white paint thermal control coatings Z-93, YB-71, and S13GLO-1. As a result of a change in manufacturer of the potassium silicate binder/encapsulant material used in all three paints, extensive requalification testing examined radiation stability of the newly reformulated versions of these paints, Z-93P, YB-71P, and S13GPLO-1, along with comparison to their predecessors [55,88]. In one of the tests [88], samples were exposed to approximately 2,600 equivalent UV sun hours along with 40 keV electrons at a flux of 6×10^9 electrons/m²s for a total fluence of 3×10^{16} electrons/m². Table 23.4 shows solar absorptance changes for original and reformulated white paints due to this testing.

This study proved a very important point regarding spacecraft materials degradation. Even seemingly minor changes in a material can produce

TABLE 23.4 Solar Absorptance of Original and Reformulated White Paints Before and After Exposure to 2,600 Equivalent Sun Hours UV and 3×10^{16} electrons/m² at 40 keV Energy (Calculated from Original Data in Ref. 88)

| White Paint Type | Number of Samples | Avg. Solar Absorptance (pristine) | Avg. Solar Absorptance (post-test) | Avg. Solar Absorptance Increase |
|------------------|-------------------|-----------------------------------|------------------------------------|---------------------------------|
| Z-93 | 6 | 0.118 ± 0.014 | 0.155 ± 0.013 | 0.037 |
| Z-93P | 6 | 0.109 ± 0.001 | 0.152 ± 0.019 | 0.043 |
| S13GLO-1 | 6 | 0.166 ± 0.010 | 0.287 ± 0.014 | 0.121 |
| S13GPLO-1 | 7 | 0.150 ± 0.009 | 0.377 ± 0.087 | 0.227 |
| YB-71 | 7 | 0.103 ± 0.021 | 0.238 ± 0.054 | 0.135 |
| YB-71P | 9 | 0.091 ± 0.013 | 0.345 ± 0.037 | 0.254 |

significantly different vulnerability to radiation degradation. Radiation degradation of the white paint materials is very sensitive to impurity levels and processing conditions, so that even an “equivalent” chemical substitute for the potassium silicate binder did not produce a material with equivalent radiation durability. In fact, the YB-71P was found to be inadequately radiation stable to be space qualified, whereas Z-93P, using the same binder, was found to have adequate radiation stability to be considered space qualified [88].

23.4.3 Mitigation of Radiation Degradation

In general, mitigation of radiation degradation of spacecraft external materials is accomplished through careful material selection based on understanding radiation conditions for the mission and space ultraviolet and ionizing radiation durability of materials being considered. Where UV-vulnerable materials are necessary, some materials may be able to be protected through the use of protective coatings, such as the OCLI coating used on Tedlar[®] described in Section 23.4.1.2.1. Although the OCLI coating was successfully used on Tedlar[®], adhesion issues were observed when an OCLI coating was used on FEP, which will be described in Section 23.5.2.3, so protection for one material may not be a guarantee of successful protection application for another. Metallic coatings, such as vapor deposited aluminum (VDA), can generally protect vulnerable polymers from ultraviolet degradation, but processing defects, especially scratches or other types of line-shaped defects, may lead to local UV degradation. Additionally, metallic coatings and oxide coatings cannot provide significant protection from high energy ionizing radiation. In most cases, vulnerable materials, even with protective coatings, should be tested to the

most conservative conditions to estimate their lifetime at mission conditions. It must be considered that radiation effects are often synergistic with thermal effects, which will be described in Section 23.5, and ground laboratory evaluations should consider all aspects of the space environment together.

23.5 THERMAL AND THERMAL CYCLING EFFECTS

23.5.1 Environment Description

Earth orbital environments are capable of producing significant temperature variations as the spacecraft passes from sunlight to shadow. The number of thermal cycles expected for a mission depends upon the orbit. For example, spacecraft in LEO complete one orbit approximately every 90 minutes and spacecraft in geosynchronous orbit complete one orbit each Earth day (24 hours). The range of temperature which a material experiences during thermal cycling depends upon its thermo-optical properties (solar absorptance and thermal emittance), its view of the Sun, its view of the Earth, its view of other surfaces of the spacecraft, durations of time in sun and in shadow, and the influence of equipment or components that produce heat.

23.5.2 Effects on Materials

On-orbit temperatures and thermal cycling pose a threat to materials durability for various reasons. First, for inhomogeneous materials in intimate contact with one another, such as in composites or coated materials, a mismatch in coefficients of thermal expansion may lead to cracking or delamination when the material experiences significant temperature excursions. Second, mechanical properties of polymer materials can be a strong function of tem-

perature [89]. Therefore, during the course of on-orbit thermal cycling, a polymer may experience temperatures at which it has decreased strength or ductility, making it more vulnerable to damage. Because radiation damage is generally more concentrated at the exposed surface of a material and diminishes through the thickness, one can consider that a radiation-damaged polymer no longer has homogenous properties through its thickness, making it vulnerable to effects of a mismatch in coefficient of thermal expansion (CTE).

23.5.2.1 Effects on Composites

One report described results of an in-depth study of the effects of thermal cycling on composites for space applications including a carbon fiber-reinforced epoxy (ERL1962) and carbon fiber-reinforced cyanate ester (RS3) [90]. Variables in the study included thermal cycling temperature range, composite layer thickness, matrix type, and fiber type. It was found that cyanate ester matrix composites are more resistant to thermal cycling-induced microcracking than epoxy matrix composites. For carbon fiber epoxy matrix composites, the number of microcracks induced by thermal cycling reaches a saturation level as early as several hundred cycles, with many microcracks being observed after only a few thermal cycles. However, cyanate ester matrix composites show a threshold effect such that for less severe temperatures, thermal cycling does not cause any significant microcracking, and, for temperature ranges that do cause microcracking, a saturation level may be in the thousands of cycles. Also, composites with thinner laminate layers (50.8 μm) were found to be more susceptible to microcracking than composites with thicker layers (127 μm).

The Long Duration Exposure Facility provided opportunities to examine materials degradation due to space exposure in low Earth orbit for 69 months. Figure 23.19 shows an example of an apparent space thermal cycling-induced crack in an aluminum-chromium coating on a graphite epoxy panel that was located on the leading edge of LDEF [91]. Atomic oxygen erosion of the graphite epoxy is also evident in the cracked area.

23.5.2.2 Effects on Spacecraft Paint Coatings

Z-93, a zinc oxide pigment/potassium silicate binder white paint applied to aluminum substrates, has been

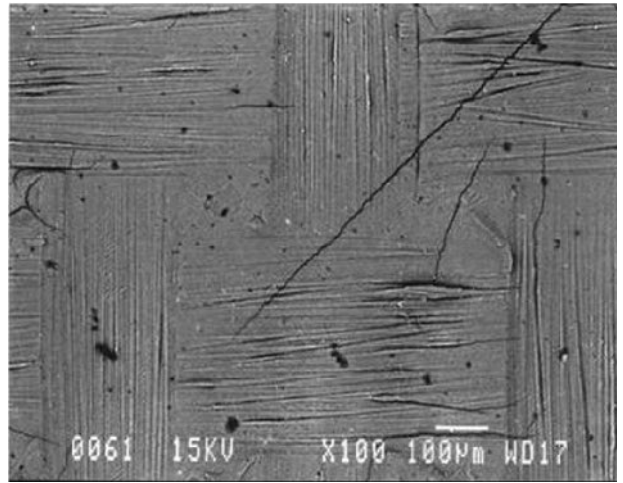


FIGURE 23.19 Backscattered electron micrograph showing thermal cycle-induced microcracks in an Al/Cr coated graphite epoxy sample that was located on the leading edge of LDEF.

observed to microcrack upon thermal cycling [92]. This is an expected result of the CTE mismatch between the coating and the substrate. However, with proper substrate surface preparations, delamination and spalling are prevented, so, despite a “mud-tiled” appearance due to microcracking, the painted surfaces exhibit durability to orbital thermal cycling. Anodized aluminum substrates can provide a less severe CTE mismatch for Z-93 and minimize the degree of microcracking [92].

23.5.2.3 Synergistic Thermal, Thermal Cycling and Radiation Effects on Uncoated and Coated Teflon® FEP

Z93 white paint, applied to aluminum substrates, has been observed to microcrack upon thermal cycling [92]. In one test, thermal cycling was found to cause delamination and spalling of protective oxide coatings on FEP [60]. In this study, coatings examined included SiO_x (where $x \sim 2$) and a coating consisting of alternating layers of SiO_2 , TiO_2 , and Ta_2O_3 developed by OCLI. Samples were exposed to 5 kGy of 1 MeV electron radiation followed by thermal cycling, nominally from -115°C to $+90^\circ\text{C}$. Whereas some OCLI-coated samples that were unexposed to radiation and thermal cycling showed signs of minor coating adhesion problems, such as cracking and loss of coating in bent areas, spalling and delamina-

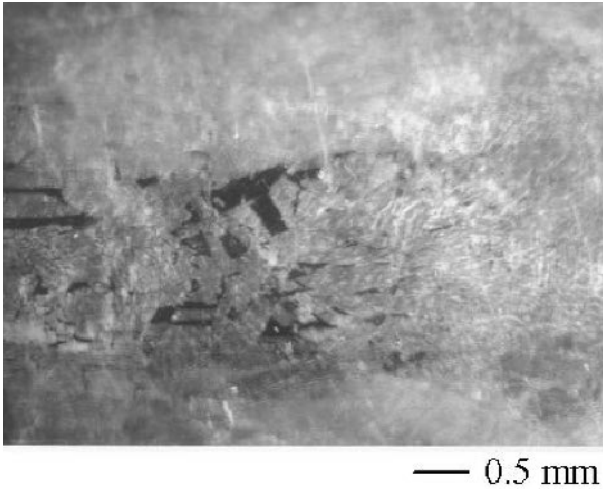


FIGURE 23.20 Sample of 2-mil-thick FEP with OCLI oxide coating (total coating thickness in range of 700–1,400 nm) following electron radiation exposure and thermal cycling. Dark regions indicate areas where coating is missing.

tion were observed only for samples which had been exposed to thermal cycling following radiation. An example of the effects of electron radiation and thermal cycling on the OCLI/FEP is shown in Figure 23.20. Severity of delamination and spalling was found to be worse for thicker coatings.

The VDA-coated 127- μm -thick FEP outermost layer of the multilayer insulation blankets on the Hubble Space Telescope has become embrittled, resulting in severe on-orbit cracking as shown in Figure 23.21. A sample of FEP retrieved during the second servicing mission (SM2), after 6.8 years in space, was significantly more embrittled than the same thickness FEP retrieved during the third servicing mission (SM3A), after 9.7 years in space. One of the differences in the environmental exposures between these samples was the maximum temperature exposure during thermal cycling. The retrieved SM2 insulation section curled after cracking, exposing the lower emittance back-surface aluminum to space. It was estimated that this extremely embrittled piece of insulation reached approximately 200 °C on-orbit, 150 °C higher than the nominal temperature extreme (–100 °C to +50 °C for solar facing FEP on HST). A review board that investigated the severe FEP degradation on HST concluded that electron and proton radiation combined with on-orbit thermal cycling was necessary to cause



FIGURE 23.21 Large cracks in outer layer of solar facing MLI on HST as observed during SM2, after 6.8 years in space.

the observed cracking of FEP on HST at areas of stress concentrations [93]. Several studies have been conducted to investigate the space environmental factors responsible for the degradation of FEP on the HST, including examinations of the combined effects of radiation and temperature or temperature cycling.

One study examined the differences in degradation produced by the space environment and ground testing intended to replicate exposure conditions for FEP on the Hubble Space Telescope [94]. Samples of 127- μm FEP film were exposed to 0.5 MeV electrons and 1 MeV protons to provide fluences equivalent to those of various HST exposure durations up to 20 years. This radiation exposure was followed by thermal cycling in the temperature range of –100 °C to +50 °C, the nominal range for the FEP exterior layer of thermal insulation on HST. Thermal cycling was conducted in a nitrogen purged chamber at a nominal rate of four cycles per minute. Effects of these exposures compared to HST exposures on

strength and elongation of FEP are shown in Figure 23.22. It is evident that laboratory testing severely underpredicted the on-orbit degradation caused by HST exposure of FEP for even 3.6 years, where laboratory exposures equivalent to 20–40 years in space were required for similar degradation. The data point for SM2 (6.8 yr) in Figure 23.22, near zero elongation, is shown for reference; however, as described above, this FEP sample was exposed to an upper temperature limit of ~ 200 °C, much higher than the nominal FEP materials on HST, which reach 50 °C.

Research has been conducted to determine the effects of heating on irradiated FEP in order to better

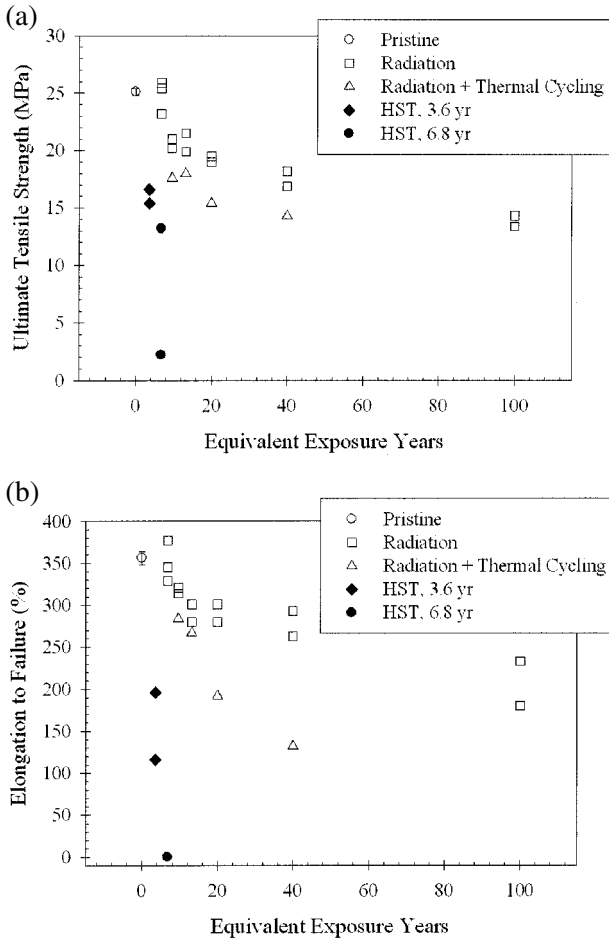


FIGURE 23.22 Charged particle radiation and radiation with sequential thermal cycling effects on mechanical properties of 5-mil Teflon® FEP with comparison to FEP retrieved from HST during SM1 (3.6 years in space) and during SM2 (6.8 years in space): (a) ultimate tensile strength, and (b) elongation at failure.

understand the effect of temperature on the rate of degradation, and on the mechanism of degradation of FEP insulation in the LEO environment. In one study, samples of pristine FEP, x-ray irradiated FEP, and FEP retrieved from HST were heated from 50 °C to 200 °C at 25 °C intervals in a high vacuum furnace and evaluated for changes in tensile properties and density [95]. Even though the ground laboratory x-ray exposure (conducted at room temperature) provided an areal dose (D, the total energy absorbed per unit area integrated through the full thickness in FEP) that was orders of magnitude higher than the HST on-orbit areal dose, it did not produce the extent of damage observed for the HST-exposed FEP. However, the laboratory exposure provided sufficient degradation to show the effects of subsequent heating on irradiated FEP. This study found that heating did not embrittle non-irradiated FEP Teflon®; however, there was a significant dependence of the embrittlement of irradiated FEP on heating temperature, with near complete loss of elongation at failure at 100 °C and higher. These results are shown in Figure 23.23.

This and other studies [96] support the conclusion that radiation (solar, x-ray, particle radiation) induced chain scission is the primary mechanism of embrittlement of FEP on HST, and indicate the significant impact of the on-orbit temperature of FEP with respect to its degradation in the space environment.

One study examined candidate materials to replace the degrading outer layer of aluminized FEP on HST. Candidate materials that were considered are indicated in Table 23.5. Various sets of these

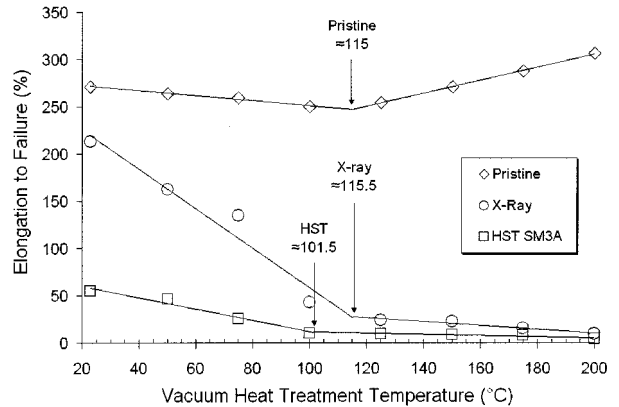


FIGURE 23.23 Percent elongation at failure of pristine, ground laboratory x-ray exposed and retrieved HST FEP as a function of vacuum heat treatment temperature.

TABLE 23.5 HST Thermal Control Candidate Replacement Materials

| Material | Sample Id. | Candidate Material |
|----------|---------------|--|
| 1 | B1.1 and M2.1 | 10 mil FEP/Ag/Inconel/adhesive/Nomex [®] (polyphenylene isophthalate) scrim |
| 2 | B1.2 and M2.2 | 5 mil FEP/Ag/Inconel/adhesive/fiberglass scrim/adhesive/2 mil Kapton [®] |
| 3 | B1.3 and M2.3 | 10 mil FEP/Al/adhesive/Nomex [®] scrim |
| 4 | B1.4 and M2.4 | 5 mil FEP/Al/adhesive/fiberglass scrim/adhesive/2 mil Kapton [®] |
| 5 | B1.5 and M2.5 | 5 mil FEP/Ag/Inconel/adhesive/Nomex [®] scrim |
| 6 | B1.6 and M2.6 | 5 mil FEP/Al/adhesive/Nomex [®] scrim |
| 7 | B1.7 and M2.7 | OCLI multi-layer oxide UV blocker/2 mil white Tedlar [®] |
| 8 | B1.8 and M2.8 | 5 mil FEP/Al (current HST material) |
| 9 | B1.9 and M2.9 | SiO ₂ /Al ₂ O ₃ /Ag/Al ₂ O ₃ /4 mil stainless steel |
| 10 | B1.0 and M2.0 | Proprietary Teflon [®] FEP/AZ93 White Paint/Kapton [®] |

candidate replacement materials were exposed to combinations of electron/proton radiation, atomic oxygen, soft x-rays, thermal cycling and near-ultraviolet radiation at various facilities in order to evaluate their HST on-orbit durability [97,98]. Two sets of samples (B1 and M2) previously exposed to charged particle radiation were exposed to soft x-rays, and one sample set (B1) was also thermal cycled under load. Thermal cycling temperatures ranged between $-100\text{ }^{\circ}\text{C}$ to $+50\text{ }^{\circ}\text{C}$ and spring loading provided stress on each sample of approximately 12.4 MPa. Samples received 1,000 thermal cycles. Thermal cycled samples are shown in Figure 23.24. Metallized 5-mil-thick FEP samples B1.2 and B1.4, shown in Figure 23.24(a), with fiberglass scrims and Kapton[®] substrates, tore in half during thermal cycling under load [97]. This may be attributed to the low tear resistance of Kapton[®]. These samples performed worse than Sample B1.8, shown in Figure 23.24(b), the current HST MLI material (5-mil-thick aluminized-FEP), which tore about 90% of the width during thermal cycling. Tear propagation of the B1 samples was attributed to thermal cycling under a high load. The prior radiation exposures did not appear to have an additional effect on tearing, and no tearing occurred due to mechanical load cycling. Following the evaluation of all test results, 5-mil FEP/Al/adhesive/Nomex[®] scrim was recommended as replacement material for the outer thermal blanket layer for HST [98].

Ground-based environmental durability tests, such as that discussed in Ref. 94, indicate that exposing materials in accelerated tests to environmental models predicted spacecraft mission exposures of UV and/or ionizing radiation sources does not simulate the extent of damage that occurs in the space en-

vironment. One approach to overcoming the difficulties in simulating the space environment using ground-based testing is to calibrate the facility using data from actual space-exposed materials to determine exposure levels required to replicate degraded properties observed in space. Reference 99 describes a ground-to-space correlation method that uses a multiple-step process to determine the durability of expanded-polytetrafluoroethylene (ePTFE) for International Space Station (ISS) applications, based on ground-based x-ray irradiation and heating exposure that simulates bulk embrittlement as occurs in fluorinated ethylene propylene (FEP) thermal insulation covering the Hubble Space Telescope. This method was designed to damage the back-surface of equivalent thickness ePTFE to the same amount of scission damage as occurred in HST FEP (based on elongation data), and then correct for differences in ground test ionizing radiation versus space radiation effects, temperature variations, space ionizing radiation environment variations (spacecraft altitude, inclination and duration), and thickness variations.

23.6 MICROMETEOROID AND ORBITAL DEBRIS EFFECTS

23.6.1 Environment Description

Micrometeoroids are of extraterrestrial origin and, as such, will have a flux which is reasonably constant with time. Their velocity is typically in the 4–51 km/sec range [100,101], with an average velocity near 20 km/sec. As shown in Figure 23.25, as micrometeoroid particle size decreases, the flux of

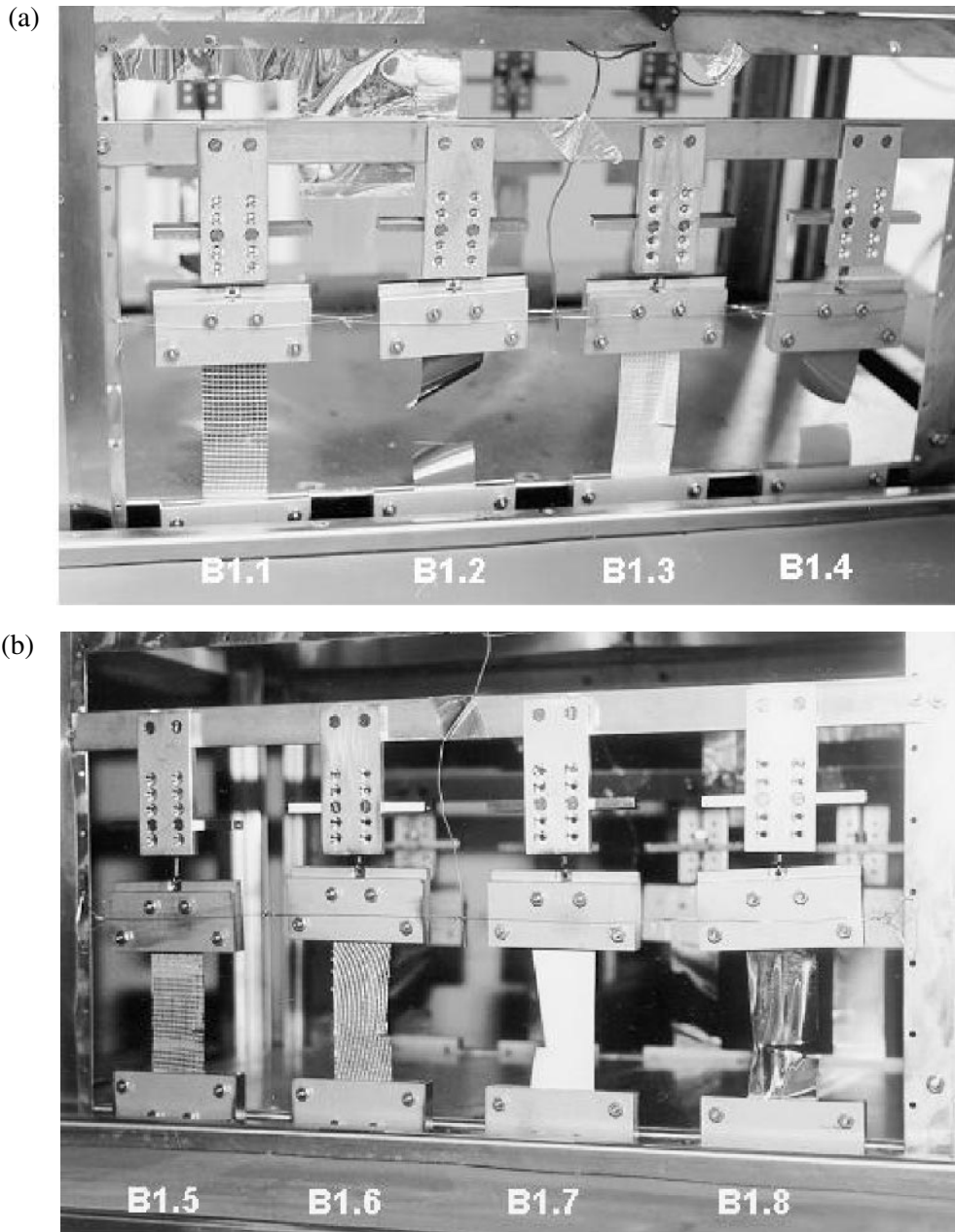


FIGURE 23.24 Candidate Hubble Space Telescope MLI under tension in the Rapid Thermal Cycling Facility after 1,000 thermal cycles. (a) samples B1.1 - B1.4 and (b) samples B1.5-B1.8.

particles increases. Orbital debris is of man-made origin as a result of spent solid rocket booster exhaust, satellite breakups or other man-caused origins. Orbital debris has an average velocity of 8.7 km/sec [102]. Because of the man-made origin and atmospheric drag, orbital debris flux is highly dependent upon the world's spacecraft launch frequency and oc-

currences of orbital breakups. The orbital debris size distribution can also be seen in Figure 23.25. The Micrometeoroid Flux Model shown in Figure 23.25 was developed based on the Cour-Palais model [103], and the Debris Flux Model was developed based on the Kessler model [104]. For a spacecraft with a fixed orientation relative to the ram velocity direction, the

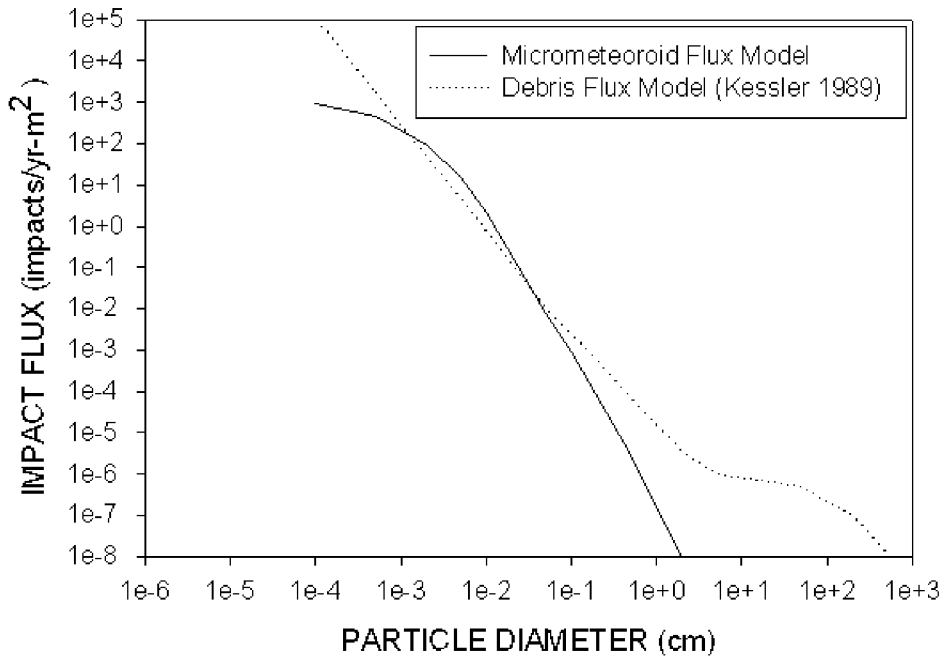


FIGURE 23.25 Micrometeoroid and debris particle flux, versus diameter for low Earth orbit (500 km).

combined occurrence of micrometeoroid and orbital debris impacts is non-uniform around the spacecraft. This is the case for LDEF, which was in LEO for 69 months. Figure 23.26 shows a polar plot of the number of impacts around LDEF [105]. Row 9 was facing the ram direction (the leading edge), and row 3 was the trailing edge.

23.6.2 Interactions with Materials

The impact of micrometeoroid or orbital debris with spacecraft materials is usually sufficiently energetic to cause vaporization of the impacting particle, as well as produce an impact crater of volume an order of magnitude greater than the impacting particle. For example, the kinetic energy of an aluminum particle traveling at 6 km/sec is sufficient to vaporize aluminum to form a crater that is roughly five times the diameter of the incoming particle [106]. Figure 23.27 shows scanning electron microscope photographs of typical hypervelocity impact craters in aluminum and fluorinated ethylene propylene (FEP) Teflon[®] from the LDEF spacecraft [107]. The violence of the microscopic explosive vaporization can cause delamination in layered materials as shown in Figure 23.28, which shows a layered structure of FEP, silver, and Z306 black paint flown on LDEF

that was delaminated over a diameter an order of magnitude greater than the impacting particle, followed by subsequent atomic oxygen oxidation of the underlying silver [108]. The ejection of impact crater material can be a source of spacecraft self-contamination. Large particle impacts, although rare in occurrence, have the potential to penetrate pressure vessels or cause structural damage. The largest impact crater on the LDEF spacecraft was 5.7 mm in diameter [109].

23.6.3 Mitigation Techniques

Localized damage caused by micrometeoroid or orbital debris impacts on spacecraft surfaces can be mission-threatening if the impact occurs on electrical wires, power cables or pressure vessels. Reduction in the probability of catastrophic loss in an electrical power conductor can be achieved through use of a ladder-configured conductor rather than a single conductor. The concept is that one would divide the current into two smaller conductors that are separated with occasional rung conductors that could carry current back and forth across the two main long conductors in case one conductor was severed by hypervelocity impact. Only a short length of single conductor between the rungs on either side of

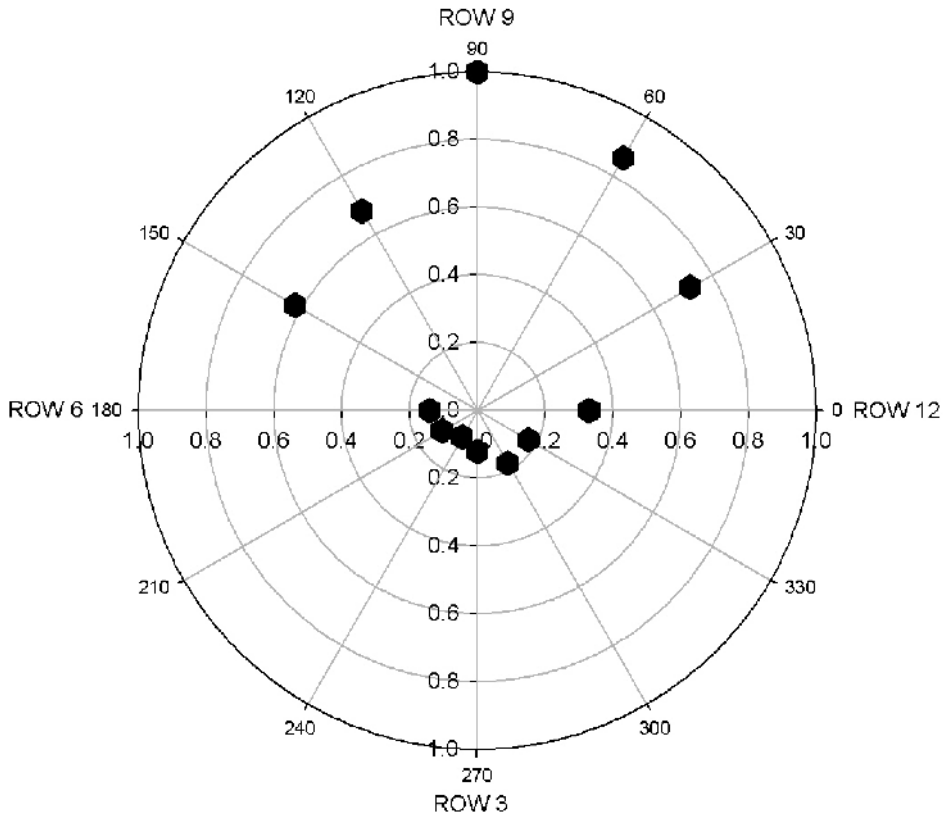


FIGURE 23.26 Angular dependence of impacts around the LDEF spacecraft.

impact breakage site would have to carry twice the normal current.

Mitigation techniques for power cables can simply be the use of redundant separated cables so that the probability of all cables failing is acceptably small. The same technique is applicable to electrical signal conductors. Such techniques are simple to accomplish in flat ribbon conductors that are laminated with polymer insulation.

Because one micrometeoroid or debris impact can cause total loss in pressure of a tank or container that can fail a mission or cause loss of life for manned missions, mitigation techniques are important. The technique used to prevent penetration of pressure vessels has been to add an outer thin wall, often called a "Whipple shield," to cause the impacting particle to break up upon impact [110,111]. The debris from the impact then spreads over a large area on the surface of the pressure vessel, which is spaced concentrically inside the shield material. Because the debris is spread over a large area, its ability to penetrate the inner critical chamber is greatly reduced. Variants of this concept for structured projec-

tion of tubular structures include filling the space between two sides of a tubular structure with low density ceramic fiber fill, which also acts to absorb the energy of the broken up primary impact debris [111]. Damage to the back wall of the structure is prevented by the energy-absorbing fill material.

23.7 CONCLUDING REMARKS

Spacecraft materials exposed to low Earth orbit environments have been found to undergo degradation or damage due to environmental threats including atomic oxygen, contamination, radiation, temperature effects and temperature cycling, and micrometeoroids and orbital debris. The degree to which the space environment degrades or damages materials depends upon the unique conditions of an individual spacecraft environment and the susceptibility of the material to being altered by these environmental exposures. As has been shown in this chapter, space environment interactions with materials are complex, often producing combined or synergistic effects. Ac-

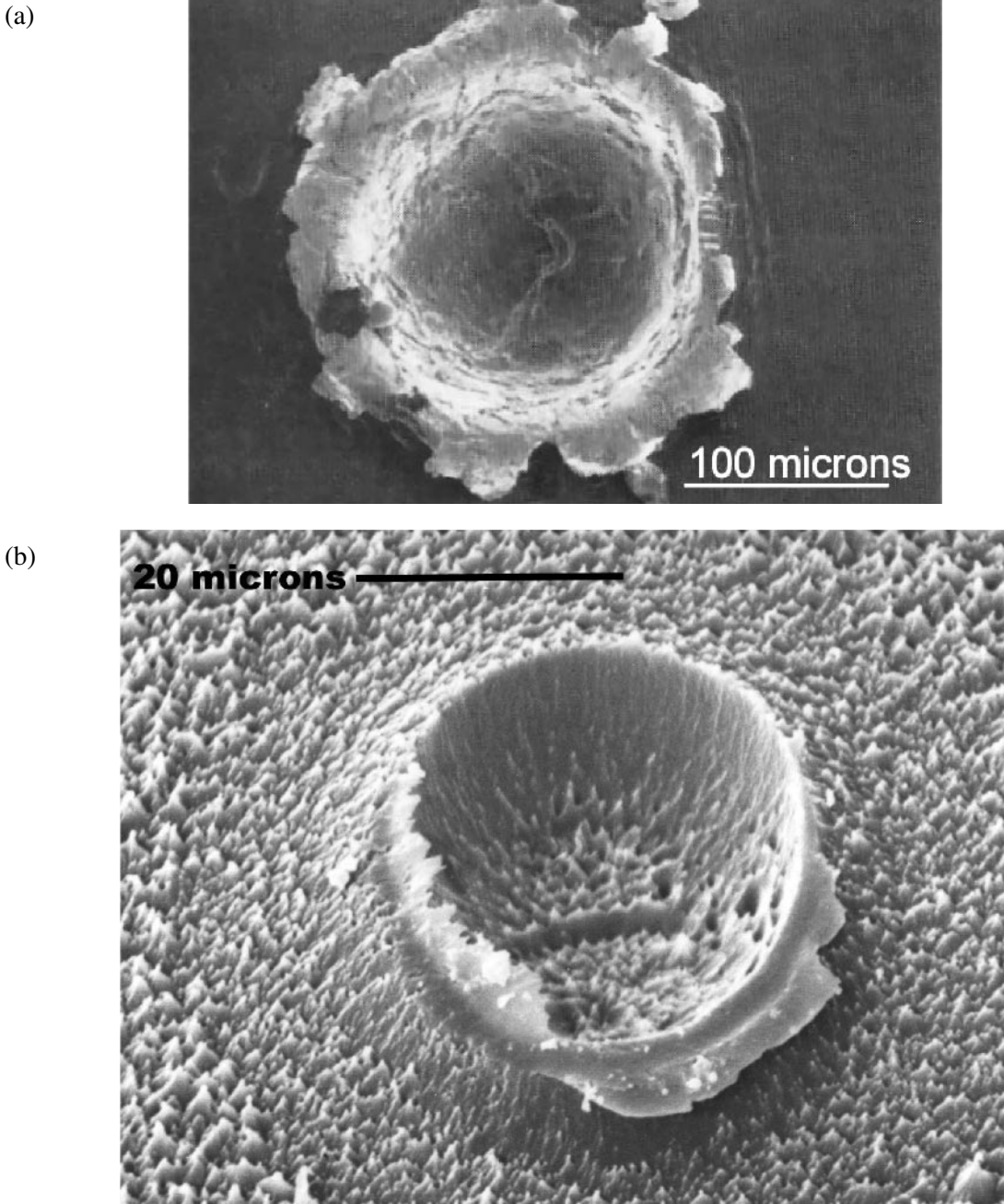


FIGURE 23.27 Scanning electron microscope photographs of impact craters on the LDEF spacecraft: (a) In aluminum; (b) In fluorinated ethylene propylene (FEP) Teflon.

curately predicting the behavior of materials in these complex space environments is important to the success of space missions, yet can be difficult to accomplish.

Since the first Space Shuttle flights, significant advancements have been made in understanding

atomic oxygen effects on materials, namely: (1) in quantifying atomic oxygen degradation for many polymers; (2) in development of coatings to prevent atomic oxygen degradation; (3) in development of calibrated laboratory simulation methods; and (4) in development of modeling tools to predict in-space

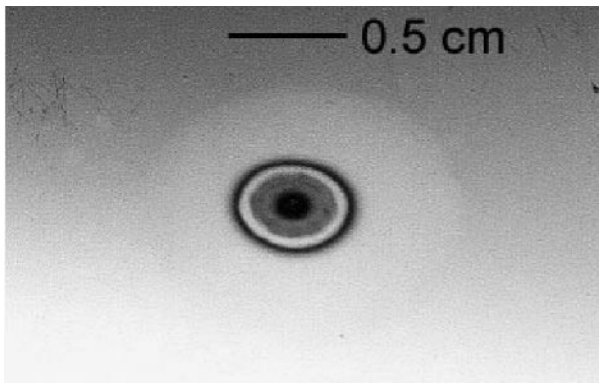


FIGURE 23.28 Photograph of impact site on Fluorinated ethylene propylene (FEP) Teflon[®] that was backed with silver and Z 306 paint.

degradation. However, for radiation effects and synergistic effects with temperature, accelerated testing in the laboratory using individual or combined environments to estimated mission exposure fluences or doses has been generally unable to accurately replicate damage observed in space. Furthermore, complex differences between the space and laboratory environments require cautious interpretation of results. These complications of predicting durability of spacecraft materials have led to efforts in developing ground-to-space correlation methods for radiation durability testing (for example, exposing Teflon[®] materials to exposures based on the dose of radiation that produces reduction in FEP mechanical properties equivalent to that observed in space, rather than to actual mission fluence exposures).

As space missions are becoming longer in duration and require lighter-weight materials with specially tailored properties, it is critical that advancements continue in understanding material degradation mechanisms and in the development of simulation laboratory durability testing and modeling capabilities. This is crucially dependent on the retrieval and subsequent testing of long duration space-exposed materials, such as the MISSE flight experiment. These advancements will ensure accuracy in predicting long-term material durability in the space environment for future missions.

23.8 REFERENCES

- Dickerson, R. E., Gray, H. B., and Haight, G. P. *Chemical Principles, 3rd Ed.* Menlo Park, CA: Benjamin Cummings Publishing Co. Inc. 1979, p. 457.
- N.O.A.A., N.A.S.A. and U.S.A.F. *U.S. Standard Atmosphere, 1976.* NASA Tech. Memo TMX-74335, 1976.
- Banks, B. A., Rutledge, S. K., de Groh, K. K. Low Earth Orbital Atomic Oxygen, Micrometeoroid, and Debris Interactions with Photovoltaic Arrays. Presented at the 11th Space Photovoltaic Research and Technical Conference (SPRAT XI), NASA Lewis Research Center, Cleveland, OH, May 7–9, 1991.
- Hedin, A.E. MSIS-86 Thermospheric Model. *Journal of Geophysical Research*, Vol. 92, 1987, p. 4,649.
- de Groh, K. K. and Banks, B. A. Atomic Oxygen Undercutting of Long Duration Exposure Facility Aluminized-Kapton Multilayer Insulation. *Journal of Spacecraft and Rockets.* (AIAA), Vol. 31(4), July–August 1994, pp. 656–664.
- Banks, B. A., de Groh, K. K., Rutledge, S. K., and DiFilippo, F. J. Prediction of In-Space Durability of Protected Polymers Based on Ground Laboratory Thermal Energy Atomic Oxygen. In *Protection of Materials and Structures from the Low Earth Orbit Space Environment.* J. I. Kleiman and R. C. Tennyson, Eds. The Netherlands: Kluwer Academic Publishers, 1999, pp. 89–100.
- Banks, B. A., Rutledge, S. K., Auer, B. M. and DiFilippo, F. J. Atomic Oxygen Undercutting of Defects on SiO₂ Protected Polyimide Solar Array Blankets. In *Materials Degradation in Low Earth Orbit.* V. Srinivasan and B. Banks, Eds. TMS, 1990, pp. 15–33.
- Mende, S. B., Swenson, G. R., and Clifton, K.S. *Science*, Vol. 225:191, 1984.
- Rice, C. J., Russell, R. W. Infrared Spectral Measurement of Space Shuttle Glow. *Geophysical Research Letters*, 19(10), 22 May, 1992, pp. 989–992.
- Caledonia, G.E. Laboratory Simulations of Energetic Atom Interactions Occurring in Low Earth Orbit. In *Rarefied Gas Dynamics: Space Related Studies.* E. O. Munts, D. P. Weaver, and D. H. Campbell, Eds. Vol. 116, *Progress in Astronautics and Aeronautics*, AIAA, 1989, pp. 129–142.
- Mata, A., Su, X., Fleischman, A., Banks, B., Miller, S., and Midura, R. Osteoblast Attachment to a Textured Surface in the Absence of Exogenous Adhesion Proteins. In *IEEE Transactions on Nanobioscience*, Vol. 2(4), December 2003.
- Banks, B. A., Rutledge S. K. Low Earth Orbital Atomic Oxygen Simulation for Materials Durability Evaluation. In *Proceedings of the 4th European Symposium on Spacecraft Materials in Space Environment*, Toulouse, France, 6–9, September, 1988, pp. 372–392.
- Leger L. J. *Oxygen Atom Reaction With Shuttle Materials at Orbital Altitudes—Data and Experiment Status.* AIAA-83-0073, January, 1983.
- Banks, B. A., S. K. Rutledge, P. E. Paulsen and T. J. Steuber. *Simulation of the Low Earth Orbital Atomic Oxygen Interaction With Materials by Means of an Oxygen Ion Beam.* Presented at the 18th Annual Symposium on Ap-

- plied Vacuum Science and Technology, Clearwater Beach, FL, February 6–8, 1989; NASA TM 101971, 1989.
15. Banks, B. A. The Use of Fluoropolymers in Space Applications. In *Modern Fluoropolymers*. J. Scheirs, Ed. New York: John Wiley & Sons, Ltd., 1997, pp. 103–113.
 16. Integrity Testing Laboratory, Inc. *Prediction of Erosion of Polymer-Based Materials by Atomic Oxygen in LEO*. Final Report, GRC Contract #C-72917-G, 1998.
 17. Kleiman, J., Iskanderova, Z., Banks, B. A., de Groh, K. K., and Sechkar, E. A. In *Proceedings of the 8th International Symposium on Materials in a Space Environment*, Arcachon, France, June 5–9, 2000.
 18. de Groh, K. K., B. A. Banks, A. M. Hammerstrom, E. E. Youngstrom, C. Kaminski, L. M. Marx, E. S. Fine, J. D. Gummow, and D. Wright. MISSE PEACE Polymers: An International Space Station Environmental Exposure Experiment. In *Proceedings of the Conference on ISS Utilization—2001*, October 15–18, 2001, Cape Canaveral, FL. AIAA #2001-4923; also NASA TM-2001-211311, November 2001.
 19. Banks, B. A., de Groh, K. K., Rutledge, S. K., and Haytas, C. A. *Consequences of Atomic Oxygen Interaction with Silicone and Silicone Contamination on Surfaces in Low Earth Orbit*. 44th Annual Meeting, sponsored by the International Society for Optical Engineering, Denver, CO, July 21, 1999; NASA TM-1999-209179.
 20. de Groh K. and McCollum T. Low Earth Orbital Durability of Protected Silicones for Refractive Photovoltaic Concentrator Arrays. *Journal of Spacecraft and Rockets*. Vol. 32:1, Jan.–Feb., 1995.
 21. Banks, B. A., de Groh, K., Rutledge, S., and DiFilippo, F. *Prediction of In-Space Durability of Protected Polymers Based on Ground Laboratory Thermal Energy Atomic Oxygen*. Presented at the 3rd International Conference for Protection of Materials and Structures from Low Earth Orbit Space Environment, University of Toronto Institute for Aerospace Studies, Toronto, Canada, April 25–26, 1996; NASA TM-107209.
 22. Banks, B., Miller, S., de Groh, K., Chan, A., and Sahota, M. *The Development of Surface Roughness and Implications for Cellular Attachment in Biomedical Applications*. Materials Research Society 2001 Fall Meeting, Boston, MA, November 26–0, 2001; NASA TM-2001-211288.
 23. de Groh, K. K., Banks, B. A. and Smith, D. C. *Environmental Durability Issues for Solar Power Systems in Low Earth Orbit*. *Solar Engineering 1995*, Vol. 2, pp. 939–950; NASA TM 106775, March 1995.
 24. Banks, B. A., Rutledge, S. K., de Groh, K. K., Mirtich, M. M., Gebauer, L., Olle, R., and Hill, C. *The Implications of the LDEF Results on Space Station Freedom Power System Materials*. 5th International Symposium on Materials in a Space Environment, Cannes-Mandelieu, France, September 16–0, 1991.
 25. Banks, B. A., Mirtich, M. J., Rutledge, S. K., Swec, D. M. and Nahra, H.K. *Ion Beam Sputter-Deposited Coatings for Protection of Spacecraft Polymers in Low Earth Orbit*. 23rd Aerospace Sciences Meeting (AIAA), Reno, NV, January 14–17, 1985; NASA TM-87051.
 26. Silverman, E. M. *Space Environmental Effects on Spacecraft: LEO Materials Selection Guide*. NASA Contractor Report 4661, Part 2, August, 1995, Section 10-38.
 27. Banks, B. A., Mirtich M. J., Rutledge, S. K., and Swec, D.M. *Sputtered Coatings for Protection of Spacecraft Polymers*. 11th International Conference on Metallurgical Coatings (AVS), San Diego, CA, April 9–13, 1984; NASA TM-83706.
 28. Dever, J. A., Rutledge, S. K., Hambourger, P. D., Bruckner, E., Ferrante, R., Pal A.M., Mayer, K., and Pietromica, A. J. *Indium Tin Oxide-Magnesium Fluoride Co-Deposited Films for Spacecraft Applications*. International Conference on Metallurgical Coatings (AVS), San Diego, CA, April 24–26, 1996; NASA TM-1988-208499.
 29. Banks, B. A., Snyder, A., Miller, S. K., Demko, R. *Issues and Consequences of Atomic Oxygen Undercutting of Protected Polymers in Low Earth Orbit*. 6th International Conference on Protection of Materials and Structures from Space Environment, Toronto, Canada, May 1–3, 2002; NASA TM-2002-211577.
 30. Rutledge, S. K., Mihelcic, J. A. The Effect of Atomic Oxygen on Altered and Coated Kapton Surfaces for Spacecraft Applications in Low Earth Orbit. In *Materials Degradation in Low Earth Orbit*. V. Srinivasan and B. Banks, Eds. TMS, 1990, pp. 35–48.
 31. Goode, D. C., Williams, A. W., Wood, N. J., and Binzarkaria, A. Photothermal Imaging of Gold and Vermiculite Coated Kapton Exposed to Atomic Oxygen. In *ESA Proceedings of the 6th International Symposium on Materials in a Space Environment*, Nov. 1994, SEE N95-27568 09-23, pp. 201–206.
 32. Rutledge, S. K., Olle, R. M. Space Station Freedom Solar Array Blanket Coverlay Atomic Oxygen Durability Testing Results. In *Proceedings of the 38th International SAMPE Symposium*, May 10–13, 1993, pp. 679–693.
 33. Banks, B., Stueber, T., and Norris, M. *Monte Carlo Computational Modeling of the Energy Dependence of Atomic Oxygen Undercutting of Protected Polymers*. 4th International Space Conference ICPMSE-4, Toronto, Canada, April 23–24, 1998; NASA TM-1998-207423.
 34. Banks, B. A., Auer, B. M., Rutledge, S. K., Gebauer, L. and Sechkar, E. A. Monte Carlo Modeling of Atomic Oxygen Interaction with Protected Polymers for Projection of Materials Durability in Low Earth Orbit. In *Proceedings of the MRS 1992 Spring Meeting*, San Francisco, CA, April 27–May 1, 1992.
 35. Banks, B. A. and Stueber, T. J. Monte Carlo Computational Techniques for Prediction of Atomic Oxygen Erosion of Materials. In *Proceedings of the NATO Advanced Research Workshop on Computer Modeling of Electronic and Atomic Processes in Solids*. R. C. Tennyson and A. E. Kiv, Eds. Wroclaw, Poland, May 20–23, 1996. The Netherlands: Kluwer Academic Publishing, 1997.

36. Banks, B. A., Miller, S. K. R., de Groh, K. K., and Demko, R. Scattered Atomic Oxygen Effects on Spacecraft Materials. In *Proceedings of the 9th International Symposium on Materials in a Space Environment*, Noordwijk, The Netherlands, June 16-20, 2003, ESA SP-540, pp. 145–152.
37. Jaworske, D. A., K. K. de Groh, G. Podojil, T. McCollum and J. Anzic. Leveling Coatings for Reducing the Atomic Oxygen Defect Density in Protected Graphite Fiber Epoxy Composites. *Journal of the IES* (Institute of Environmental Sciences), May/June 1994, Vol. XXXVII(3), pp. 26–31.
38. de Groh, K. K., T. M. Dever, and W. F. Quinn. *The Effect of Leveling Coatings on the Atomic Oxygen Durability of Solar Concentrator Surfaces*. NASA TM 102557, April 1990.
39. Iskanderova, Z. A., Kleiman, J. I., Gedimenko, Y., Morrison, W. D., and Tennyson, R. C. Surface Modification of Polymer-Based Materials by Ion Implantation—A New Approach for Protection in LEO. In *Protection of Materials and Structures for the Low Earth Orbit Space Environment*. J. I. Kleiman and R. C. Tennyson, Eds. The Netherlands: Kluwer Academic Publishers, 1999, pp. 225–234.
40. Rutledge, S. K., Cooper, J. M., and Olle, R. M. The Effect of Atomic Oxygen on Polysiloxane-Polyimide for Spacecraft Applications in Low Earth Orbit. In *Proceedings of the 4th Annual Workshop on Space Operations Applications and Research (SOAR '90)*. Albuquerque, NM, June 26–28, 1990; NASA CP 3103 Vol. II, pp. 755–762.
41. Gonzalez, R. I., Tomczak, S. J., Minton, T. K., Brunsvold, A. L., and Hoflund, G. B. Synthesis and Atomic Oxygen Erosion Testing of Space-Survivable POSS (Polyhedral Oligomeric Silsesquioxane) Polyimides. In *Proceedings of the 9th International Symposium on Materials in a Space Environment*. Noordwijk, The Netherlands, June 16–20, 2003. ESA SP-540, pp. 113–120.
42. Illingsworth, M. L., Betancourt, L., He, L., Chen, Y., Terschak, J. A., Banks, B. A., Rutledge, S. K., and Cales, M. *Zr-Containing 4,4'-ODA/PMDA Polyimide Composites*. NASA TM-2001-211099, 2001.
43. Shepp, A., Haghghat, R., Lennhoff, J., Schuler, P., Connell, J., St. Clair, T., Vaughn, J., and Swiener J. TOR and COR AO-VUV Resistant Polymers for Space. In *Protection of Materials and Structures for the Low Earth Orbit Space Environment*. J. I. Kleiman and R. C. Tennyson, Eds. The Netherlands: Kluwer Academic Publishers, 1999, pp. 235–254.
44. Chen, P. T. *Contamination Effects due to Space Environmental Interactions*. American Institute of Aeronautics and Astronautics, AIAA Paper 2001-0095, January 2001.
45. Walter, N. A. and Scialdone, J. J. *Outgassing Data for Selecting Spacecraft Materials*. National Aeronautics and Space Administration, NASA Reference Publication 1124, Rev. 4, June 1997.
46. Tribble, A. C. *The Space Environment: Implications for Spacecraft Design*. Princeton, NJ: Princeton University Press, 1995.
47. Noter, Y., Grossman, E., Genkin, L., Haruvy, Y., Murat, M., Ross, I., Vered, R., Lifshitz, Y., Efraty, Y., Granot, H., Halbersberg, A., Luria, H., and Stoler, A. *Variations in the Telemetry of an Offeq Satellite's Sun Sensors*. Presented at the 3rd International Space Forum on Protection of Materials and Structures from Low Earth Orbit Space Environment, University of Toronto Institute for Aerospace Studies, Toronto, Canada, April 25–26, 1996.
48. Tribble, A. C., Boyadjian, B., Davis, J., Haffner, J., and McCullough, E. *Contamination Control Engineering Design Guidelines for the Aerospace Community*. National Aeronautics and Space Administration, NASA Contractor Report 4740, May 1996.
49. American Society for Testing and Materials. *Solar Constant and Air Mass Zero Solar Spectral Irradiance Tables*. ASTM-E 490-73a (Reapproved 1992).
50. Koller, L. R. *Ultraviolet Radiation*. New York: John Wiley & Sons, Inc., 1965.
51. Schnabel, W. *Polymer Degradation: Principles and Practical Applications*. New York: Macmillan Publishing Co., Inc., 1981, Chapter 4.
52. Adams, M. R. *The Degradation of Polymeric Spacecraft Materials by Far-UV Radiation and Atomic Oxygen*. UMI Dissertation Services, Ann Arbor, MI, 1993, p. 138.
53. Dever, J. A., Pietromica, A. J., Stueber, T. J., Sechkar, E. A., and Messer, R. K. *Simulated Space Vacuum Ultraviolet (VUV) Exposure Testing for Polymer Films*. AIAA Paper 2001-1054, American Institute of Aeronautics and Astronautics, January 2001.
54. Gatto, A., Escoubas, L., Roche, P., and Comandré, M. Simulation of the Degradation of Optical Glass Substrates Caused by UV Irradiation While Coating. *Optics Communications* 148, 1998, pp. 347–354.
55. Harada, Y. and Deshpande, M. *Requalification of White Thermal Control Coatings*. Wright Laboratory Report WL-TR-94-4126, October 1994.
56. McKellar, J. F. and Allen, N. S. *Photochemistry of Man-made Polymers*. London: Applied Science Publishers, Ltd., 1979, p. 31.
57. Grossman, E., Noter, Y., and Lifshitz, Y. Oxygen and VUV Irradiation of Polymers: Atomic Force Microscopy (AFM) and Complimentary Studies. In *Proceedings of the 7th International Symposium on Materials in Space Environment*, Toulouse, France, June 16-20, 1997. Published by ESA, Noordwijk, Netherlands, pp. 217–222.
58. Skurat, V. E., Barbashev, E. A., Budashov, I. A., Dorofeev, Yu. I., Nikiforov, A. P., Ternovoy, A. I., Van Eesbeek, M., and Levadou, F. The Separate and Combined Effects of VUV Radiation and Fast Atomic Oxygen on Teflon FEP and Silicon Carbide. In *Proceedings of the 7th International Symposium on Materials in Space Environment*, Toulouse, France, June 16-20, 1997. Published by ESA, Noordwijk, Netherlands, 1997, pp. 267–279.

59. Dever, J. A., and McCracken, C. A. Effects of Various Wavelength Ranges of Vacuum Ultraviolet Radiation on Teflon FEP Film. In *Proceedings of the 9th International Symposium on Materials in a Space Environment*, European Space Agency, ESA SP-540, September 2003, pp. 367–373.
60. Dever, J. and de Groh, K. *Vacuum Ultraviolet Radiation and Atomic Oxygen Durability Evaluation of HST Bi-Stem Thermal Shield Materials*. NASA/TM-2002-211364, February 2002.
61. Jukeikis, H. S. *Space Radiation Effects on Teflon Films*. Report SAMSO-TR-79-070, The Aerospace Corporation, September 1979.
62. Toupikov, V. I., Khatipov, S. A., Charniavsky, A. I., and Stepanov, V. F. Degradation of Mechanical and Electro-physical Properties of Teflon FEP Films Under Combined Action of Far Ultraviolet and Thermal Cycling. In *Proceedings of the 7th International Symposium on Materials in Space Environment*, Toulouse, France, June 16–20, 1997. Published by ESA, Noordwijk, Netherlands, 1997, pp. 77–85.
63. DuPont, Technical Information on Tedlar (Polyvinyl fluoride film), <http://www.dupont.com/tedlar/>, 2003.
64. Stuckey, W. K. and Meshishnek, M. J. *Space Environmental Stability of Tedlar with Multi-Layer Coatings: Space Simulation Testing Results*. Aerospace Corp., Report AD-A387139; TR-2000(85665)-8; SMC-TR-00-03 under Contract F04701-93-C-0094, El Segundo, CA., Aug. 20, 2000.
65. Grossman, E., Noter, Y. and Lifshitz, Y. Oxygen and VUV Irradiation of Polymers—Atomic Force Microscopy (AFM) and Complementary Studies. In *Proceedings of the 7th International Symposium on Materials in Space Environment*, Toulouse, France, June 16–20, 1997. Published by ESA, Noordwijk, Netherlands, 1997, p. 217–223.
66. Seki, K., Tanaka, H., and Ohta, T. Electronic Structure of Poly(tetrafluoroethylene) Studied by UPS, VUV Absorption, and Band Calculations. *Physica Scripta*, Vol. 41, 1990, pp. 167–171.
67. Dever, J. A., Messer, R., Powers, C., Townsend, J., and Wooldridge, E. Effects of Vacuum Ultraviolet Radiation on Thin Polyimide Films. *High Performance Polymers*, Vol. 13(3), September 2001, pp. S391–399.
68. Luoma, G. A. and Rowland, R. D. *The Effects of Sunlight and Humidity on CF-188 Composite Resin*. Defence Research Establishment Pacific Technical Memorandum 89-07, April 1989.
69. Liao, W. B. and Tseng, F. P. Effect of Long-Term Ultraviolet Light Irradiation on Polymer Matrix Composites. *Polymer Composites*, Vol. 19(4), pp. 440–445, 1998.
70. Silverman, E. M. *Space Environmental Effects on Spacecraft: LEO Materials Selection Guide*. Prepared for Langley Research Center under Contract NAS1-19291, NASA Contractor Report 4661 Part 1, August 1995.
71. Holmes-Siedle, A. and Adams, L. *Handbook of Radiation Effects*. New York: Oxford University Press, 2002.
72. Hastings, D. and Garrett, H. *Spacecraft-Environment Interactions*, New York: Cambridge University Press, 1996.
73. Website of the National Oceanic and Atmospheric Administration's Space Environment Center, Primer on Space Weather, <http://www.sec.noaa.gov/primer/primer.html>.
74. Website of the National Oceanic and Atmospheric Administration's National Geophysical Data Center, Space Physics Interactive Data Resource, <http://spidr.ngdc.noaa.gov/spidr>.
75. Dever, J. A., de Groh, K. K., Banks, B. A., Townsend, J. A., Barth J., L., Thomson, S., Gregory, T., and Savage, W. Environmental Exposure Conditions for Teflon FEP on the Hubble Space Telescope. *High Performance Polymers*, 12(1), March 2000, pp. 125–139.
76. Barth, J. L. Space and Atmospheric Environments: From Low Earth Orbits to Deep Space. In *Proceedings of the 9th International Symposium on Materials in a Space Environment*, European Space Agency, ESA SP-540, September 2003, pp. 17–30.
77. Sawyer, D. M., Vette, J. I. *AP-8 Trapped Proton Environment for Solar Maximum and Solar Minimum*. NSSDC/WDC-A-R&S, 76-06. Greenbelt, MD: NASA/Goddard Space Flight Center, December 1976.
78. Vette, J. I. *The AE-8 Trapped Electron Model Environment*. NSSDC/WDC-A-R&S 91-24. Greenbelt, MD: NASA/Goddard Space Flight Center, November 1991.
79. Schnabel, W. *Polymer Degradation: Principles and Practical Applications*. New York: Macmillan Publishing Co., Inc., 1981, Chapter 5.
80. Holmes-Siedle, A. and Adams, L. *Handbook of Radiation Effects*. New York: Oxford University Press, 2002, pp. 568–570.
81. Stuckey, W. K. and Meshishnek, M. J. Solar Ultraviolet and Space Radiation Effects on Inflatable Materials. In *Gossamer Spacecraft: Membrane and Inflatable Structures Technology for Space Applications*. C. H. M. Jenkins, Ed. Progress in Astronautics and Astronautics, Volume 191. Reston, VA: American Institute of Aeronautics and Astronautics, 2001, pp. 303–320.
82. de Groh, K. K. and Gummow, J. D. Effect of Air and Vacuum on the Tensile Properties of X-ray Exposed Aluminized-FEP. *HPP*, Vol. 13(3), September 2001, pp. S421–S431.
83. Russell, D. A., Connell, J. W., and Fogdall, L. B. Electron, Proton, and Ultraviolet Radiation Effects on Thermophysical Properties of Polymeric Films. *Journal of Spacecraft and Rockets*, Vol. 39(6), Nov.-Dec. 2002, pp. 833–838.
84. Dever, J., Semmel, C., Edwards, D., Messer, R., Peters, W., Carter, A. and Puckett, D. *Radiation Durability of Candidate Polymer Films for the Next Generation Space Telescope Sunshield*. AIAA 2002-1564, April 2002.
85. Laghari, J. R. and Hammoud, A. N. A Brief Survey of Radiation Effects on Polymer Dielectrics. *IEEE Transactions on Nuclear Science*, Vol. 37(2), April 1990, pp. 1,076–1,083.

86. Harrison, S. E. *A Study of Gamma Ray Photoconductivity in Organic Dielectric Materials*. Sandia Corporation, Report SCDC-2580, 1962.
87. Koontz, S. L., Golden, J. L., Lorenz, M. J., and Pedley, M. D. Ionizing Radiation Effects on ISS ePTFE Jacketed Cable Assembly. In *Proceedings of the 9th International Symposium on Materials in a Space Environment*, Noordwijk, The Netherlands, June 16–20, 2003. ESA SP-540, September 2003, pp. 297–301.
88. Meshishnek, M. J., Hemminger, C. S., and Gyetvay, S. R. *Space Environmental Exposure of IITRI White Thermal Control Paints*. Aerospace Corporation, Report TR-95(5904)-2, April 27, 1995.
89. Reed, R. P., Schramm, R. E., and Clark, A. F. Mechanical, Thermal, and Electrical Properties of Selected Polymers. *Cryogenics*, Vol. 13, February 1973, pp. 67–82.
90. Brown, T. L. Microcracking of Materials for Space. Ph.D. Dissertation, Virginia Polytechnic Institute and State University, October 1998. Also, Final Report for Grant NAG-1-1912, NASA Langley Research Center, October 1998.
91. de Groh, K. K., Banks, B. A. and Smith, D. C. Environmental Durability Issues for Solar Power Systems in Low Earth Orbit. *Solar Engineering 1995*, Vol. 2, pp. 939–950; also NASA TM 106775, March 1995.
92. Daneman, S. A., Babel, H. W., and Hasegawa, M. M. *Selection Rationale, Application, Optical Properties, and Life Verification of Z-93 for the Space Station*. McDonnell Douglas Aerospace, Report 94H0632, August 1994.
93. Townsend, J. A., Hansen, P. A., Dever, J. A., de Groh, K. K., Banks, B. A., Wang, L., and He, C. Hubble Space Telescope Metallized Teflon FEP Thermal Control Materials: On-orbit Degradation and Post-retrieval Analysis. *High Performance Polymers*, 11(1), March 1999, pp. 81–100.
94. Townsend, J., Powers, C., Viens, M., Ayres-Treusdell, M., and Munoz, B. Degradation of Teflon FEP Following Charged Particle Radiation and Rapid Thermal Cycling. In *Proceedings of the 20th Space Simulation Conference: The Changing Testing Paradigm*, National Aeronautics and Space Administration, CR-1998-208598, October 1998, pp. 201–209.
95. de Groh, K. K. and Martin, M. *The Effect of Heating on the Degradation of Ground Laboratory and Space Irradiated Teflon FEP*. National Aeronautics and Space Administration, TM-2002-211704, July 2002.
96. de Groh, K. K., Dever, J. A., Sutter, J. K., Gaijer, J. R., Gummow, J., D., Scheiman, D. A. and He, C. Thermal Contributions to the Degradation of Teflon FEP on the Hubble Space Telescope. In *Proceedings of the 46th International SAMPE Symposium and Exhibition, Book 2*. Long Beach, CA, May 6–10, 2001. Covina, CA: Society for the Advancement of Material and Process Engineering (Science of Advanced Materials and Process Engineering Series), Vol. 46, 2001, pp. 1,826–1,840.
97. de Groh, K. K., Banks, B. A., Sechkar, E. A. and Scheiman, D. A. *Simulated Solar Flare X-Ray and Thermal Cycling Durability Evaluation of Hubble Space Telescope Thermal Control Candidate Replacement Materials*. Presented at the 4th ICPMSE Conference, Toronto, Canada, April 23–24, 1998; NASA TM-1998-207426, December 1998.
98. Townsend, J. A., Hansen, P. A., McClendon, M. W., de Groh, K. K. and Banks, B. A. Ground-Based Testing of Replacement Thermal Control Materials for the Hubble Space Telescope, Special Issue: *High Performance Polymers*. Vol.11, 1999, pp. 63–79.
99. de Groh, K. K., Banks, B. A., Dever, J. A. and Hodermarsky, J. C. Use of Hubble Space Telescope Degradation Data For Ground-Based Durability Projection of ePTFE on ISS. In *Proceedings of the 9th International Symposium on Materials in a Space Environment*, Noordwijk, The Netherlands, June 16–20, 2003. ESA SP-540, September 2003, pp. 281–290.
100. Kinard, W. H. and Martin, G. D. Long Duration Exposure Facility (LDEF) Space Environments Overview. In *Proceedings of the LDEF—69 Months in Space First Post-Retrieval Symposium*, Kissimmee, FL, June 2–8, 1991, NASA CP-3134 Part 1, pp. 49–60.
101. Zook, H.A. Deriving the Velocity Distribution of Meteoroids from the Measured Meteoroid Impact Directionality on the Various LDEF Surfaces. In *Proceedings of the LDEF—69 Months in Space First Post-Retrieval Symposium*, Kissimmee, FL, June 2–8, 1991, NASA CP-3134 Part 1, pp. 569–579.
102. Shipman, J. and Williamson, J. AIAA Survivability Technical Committee Draft. *Aerospace America*, December 1997.
103. Cour-Palais, B.G. et al. *Meteoroid Environment Model—1969 (Near Earth to Lunar Surface)*. NASA SP-8013, 1969.
104. Kessler, D. J., Reynolds, R. C., Anz-Meador, P. D. *Orbital Debris Environment for Spacecraft Designed to Operate in Low Earth Orbit*. NASA TM-100471, 1988.
105. See, T. H., Mack, K. S., Warren, J. L., Zolensky, M. E., and Zook, H. A. Continued Investigation of LDEF's Structural Frame and Thermal Blankets by the Meteoroid and Debris Special Investigation Group. In *Proceedings of the LDEF—69 Months in Space Second Post-Retrieval Symposium*, San Diego, CA, June 1–5, 1992. NASA CP-3194 Part 2, pp. 313–324.
106. Mandeville, J-C. Micrometeoroids and Debris on LDEF. In *Proceedings of the LDEF—69 Months in Space Second Post-Retrieval Symposium*, San Diego, CA, June 1–5, 1992. NASA CP-3194 Part 2, pp. 303–312.
107. Bunch, T. E., diBrozolo, F. R., Fleming, R. H., Harris, D. W., Brownlee, D., and Reilly, T. W. LDEF Impact Craters Formed by Carbon-Rich Impactors: A Preliminary Report. In *Proceedings of the LDEF—69 Months in Space First Post-Retrieval Symposium*, Kissimmee, FL, June 2–8, 1991. NASA CP-3134 Part 1, pp. 549–564.
108. Stein, B. A., Pippin H. G. Preliminary Findings of the LDEF Materials Special Investigation Group. In *Proceed-*

- ings of the LDEF—69 Months in Space First Post-Retrieval Symposium*, Kissimmee, FL, June 2–8, 1991. NASA CP-3134 Part 2, pp. 617–641.
109. Zolensky, M. E., Zook, H. A., Horz, F., Atkinson, D. R., Coombs, C. R., Watts, A. J., Dardano, C. B., See, T. H., Simon, C. G., and Kinard W.H. Interim Report of the Meteoroid and Debris Special Investigation Group. In *Proceedings of the LDEF—69 Months in Space Second Post-Retrieval Symposium*, San Diego, CA, June 1–5, 1992. NASA CP-3194 Part 2, pp. 277–302.
110. Schwinghamer, R. J. and Whitaker, A. *Shield Design for Protection Against Hypervelocity Particles*. NASA Tech Briefs , ISSN 0145-319X/ December 1, 1993, p. 76.
111. Christiansen, E. L. *Meteoroid/Debris Shielding*. NASA TP-2003-210788, August, 2003.

Branko N. Popov**Swaminatha P. Kumaraguru***Center for Electrochemical Engineering, Department of Chemical Engineering, University of South Carolina, Columbia, South Carolina*

| | |
|---|------------|
| 24.1 FUNDAMENTALS | 503 |
| 24.2 CATHODIC PROTECTION CRITERIA | 507 |
| 24.3 FIELD DATA AND DESIGN ASPECTS | 508 |
| 24.4 MONITORING METHODS | 511 |

| | |
|--|------------|
| 24.5 DESIGN OF CATHODIC PROTECTION SYSTEMS | 512 |
| 24.6 COMPUTER-AIDED DESIGN OF CATHODIC PROTECTION | 517 |
| 24.7 REFERENCES | 518 |

24.1 FUNDAMENTALS

24.1.1 Principle

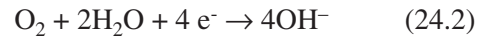
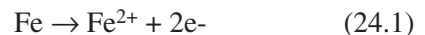
Pipelines are exposed to aggressive soil, varying climatic conditions, microorganism and stray currents that initiate corrosion processes. The research carried out in the last several decades indicated that cathodic protection is the most promising method for protecting pipelines.¹⁻³ Basic information on cathodic protection is well-documented in several textbooks and handbooks.⁴⁻¹⁰

Sir Humphrey Davy¹¹ reported in 1824 that copper could be successfully protected against corrosion by coupling it to iron or zinc. In the 1920s, cathodic protection was used for the first time to protect buried pipelines carrying oil and gases. In the successive decades, there were immense developments in cathodic protection systems. Since the beginning of this century, thousands of miles of buried pipelines and cables have been effectively protected by cathodic protection. Cathodic protection is also applied to storage tanks, ships, offshore drilling structures, condensers and concrete bridges.

Cathodic protection is defined as reduction or elimination of corrosion by making the metal a cathode by means of an impressed current or attachment to a sacrificial anode (usually magnesium, aluminum or zinc).¹² This is an electrochemical method that uses cathodic polarization to control the kinetics of the electrode processes occurring on the metal/

electrolyte interface. The principle of cathodic protection can be explained by the Wagner Traud mixed potential theory.^{6,13}

For iron corroding in an aerated neutral electrolyte, the following reactions take place:



According to mixed potential theory, any electrochemical or corrosion process can be divided into two or more oxidation [(Eq. (24.1))] and reduction [(Eq. (24.2))] partial reactions with no net accumulation of electric charge during the process. The corrosion will start only when both the cathodic reaction and the anodic reaction occur simultaneously. The total rate of oxidation must equal to the total rate of reduction. The relationship between the anodic and cathodic partial currents for the above system is presented in Figure 24.1. In this figure, the mixed potential theory and kinetic equations were used to explain the corrosion of iron. Iron interfaced with electrolyte starts to dissolve (anodic reaction) with the reduction of oxygen to form OH⁻ ions. As a result of corrosion, an equilibrium state is established. Under equilibrium conditions, the rate of the reduction reaction (cathodic) equals the rate of the oxidation (anodic) reaction. The only point in the system (Figure 24.1) where the total rates of oxidation and reduction are equal is at the intersection represented

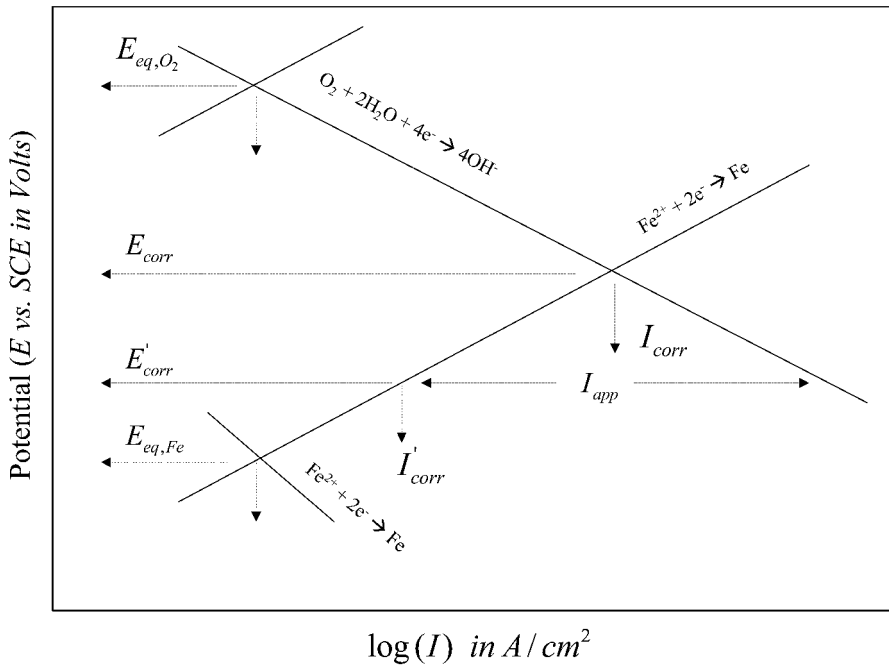


FIGURE 24.1 Evans Diagram—principle of cathodic protection.

as a mixed or corrosion potential, (E_{corr}). The current density corresponding to the corrosion potential is called corrosion current density (i_{corr}). At E_{corr} the rate of iron dissolution is equal to the rate of oxygen reduction. Four electrons are provided by the anodic reaction [(Eq. 24.1)] to reduce one oxygen molecule to four hydroxide anions. The difference between the corrosion potential (E_{corr}) and the reversible potential ($E_{eq,Fe}$) of the corroding metal is the driving force for the corrosion processes. Thus, if the slopes of both polarization curves and the exchange current densities are known, it is possible to predict the corrosion rate of iron from electrochemical data. As illustrated in Figure 24.1, by cathodically polarizing the cathode in a negative direction from the corrosion potential, the corrosion rate decreases. By polarizing the system from E_{corr} to E'_{corr} with a known applied current (I_{app}), the corrosion current decreases from I_{corr} to I'_{corr} . For a complete inhibition of the corrosion processes, it is necessary, as shown in Figure 24.2, to polarize the metal to its reversible potential $E^{Fe/Fe^{2+}}$. The applied current at this point is known as a protection current $i_{protection}$.

24.1.2 Types of Cathodic Protection (CP)

Based on the type of the polarization used to protect the structure, CP systems are divided into sacrificial anode or impressed current systems.

24.1.2.1 Sacrificial Anode Cathodic Protection

In this system, the corrosion protection is accomplished by coupling a less noble (i.e., more electronegative) metal in the Galvanic Series with the pipeline. A schematic of sacrificial CPs is given in Figure 24.3.⁸ The more noble pipeline in this galvanic couple is cathodically polarized, while the less noble metal is anodically dissolved. Sacrificial anodes serve as a source of electrical energy. High purity anodes (zinc, aluminum or magnesium) are required to avoid significant anode polarization and accumulation of insulating reaction products.

The anode is packaged in a backfill consisting of 75% gypsum, 20% betonite and 5% sodium sulfate. The purpose of the backfill is to absorb corrosion products and water from the soil to keep the anodes active. The sacrificial anodes are coupled to the pipeline at regular intervals, based on the current requirements needed to protect the pipeline.

Sacrificial anodes do not require an outside power source; rather, they provide their own power and need minimum maintenance. Sacrificial coatings are recommended for use with a well-coated structure with minimum chance of being damaged during its useful life. Requirements for a “good sacrificial anode” are as follows:

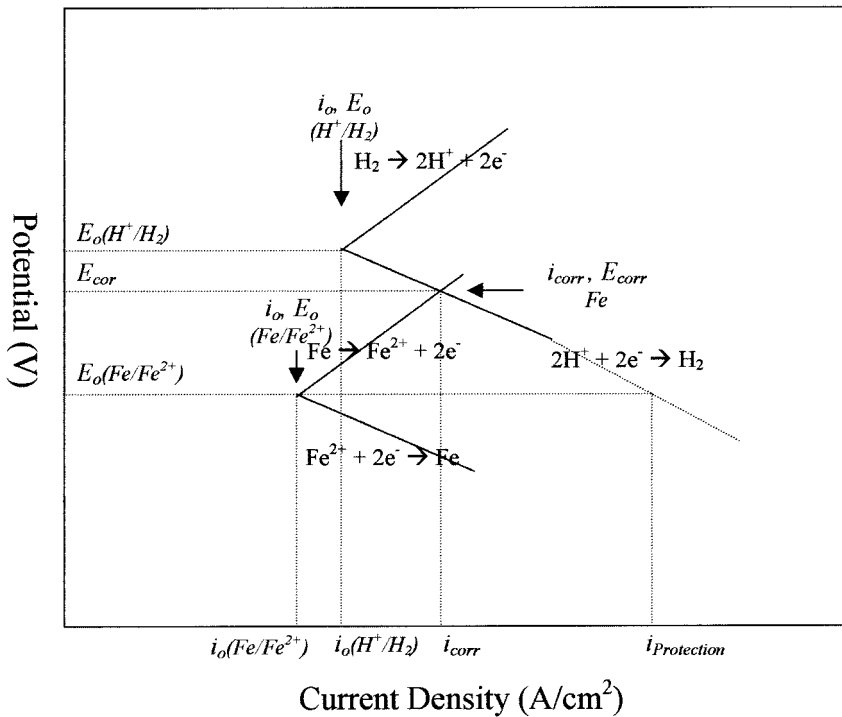


FIGURE 24.2 Evans Diagram showing the protection current for a corroding Fe system in acidic environment.

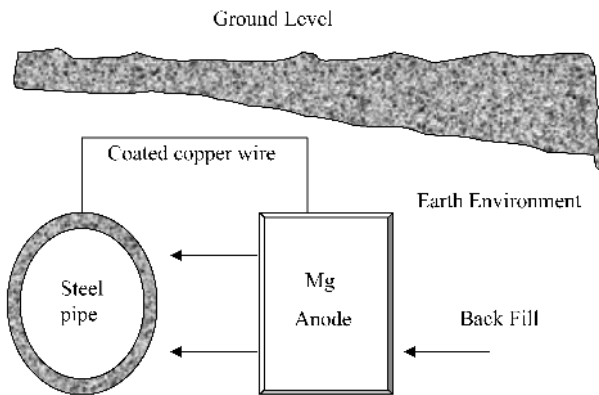


FIGURE 24.3 Protection of an underground pipeline with a magnesium anode.

Magnesium and zinc are the most often used galvanic anodes for the cathodic protection of pipelines.¹⁴⁻¹⁶ The corrosion potential difference of magnesium with respect to steel is 1 V, which limits the length of the pipeline that can be protected by one anode. Economic considerations have led to the use of aluminum and its alloys. However, aluminum passivates easily, thus decreasing the current output. To avoid the passivation process, aluminum is alloyed with tin, indium, mercury or gallium. The electrochemical properties of these alloys, such as the theoretical and the actual output, the consumption rate, efficiency, and the open circuit (corrosion) potential, are given in Table 24.1.¹⁷

24.1.2.2 Impressed Current CP

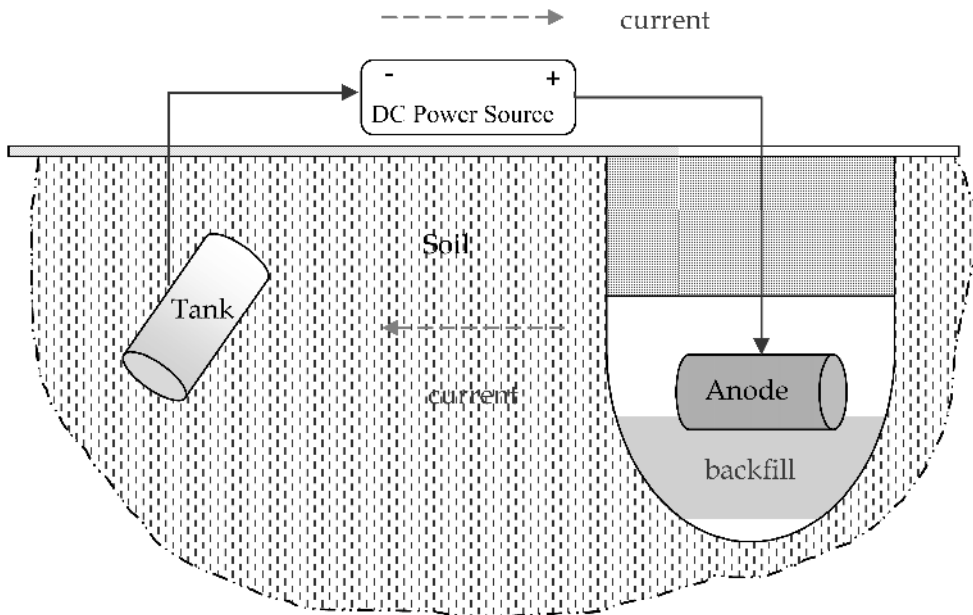
As shown in Figure 24.4,⁸ in this system the external DC current is supplied from a power source such as rectifier. The external DC current is used cathodically to polarize the pipeline. Impressed current systems can be used to protect bare and poorly coated pipelines because of high current capacity. The anodes are made of durable materials that resist wear or dissolution. Iron with 14% silicon, carbon and graphite are some of commonly used anodes for protection of pipelines.¹⁸⁻²⁰ All impressed current CPs

1. The potential between the anode and the corroding structure must be large to overcome the formation of anode cathode cells on the corroding structure.
2. When drawing current, the anode should not be polarized to a large extent.
3. The anode must have high anode efficiency (i.e., the current produced by the metal dissolution must be readily available for cathodic protection).

TABLE 24.1 Galvanic Anode Characteristics

| Material | Theoretical Output (A-h/kg) | Actual Output (A-h/kg) | Eff. | Consumption | |
|--------------------------|--------------------------------|---------------------------|--------|------------------|-------------------------------|
| | | | | Rate (kg/A-year) | Potential to CSE ^b |
| Zinc Type I | 860 | 781 | 90% | 11 | 1.06 |
| Zinc Type II | 816 | 739 | 90% | 12 | 1.10 |
| Magnesium H-1 alloy | 2,205 | 551–1,279 | 25–58% | 6.8–16 | 1.40–1.60 |
| Magnesium High Potential | 2,205 | 992–1,191 | 45–54% | 7.3–8.6 | 1.70–1.80 |
| Al/Zn/Hg | 2,977 | 2,822 | 95% | 3.1 | 1.06 |
| Al/Zn/In | 2,977 | 2,591 | 87% | 3.3 | 1.11 |

[Source: From J. H. Fitzgerald, III, *Uhlig's Corrosion Handbook*, R. Winston Revie, Ed. Reprinted by permission, John Wiley & Sons, Inc.]

**FIGURE 24.4** Schematic of cathodic protection system using impressed current.

require routine maintenance because they involve a power supply and more electrical connections than sacrificial systems.

24.1.3 Selection of CPs

When selecting the type of cathodic protection system, the designer should consider the size of the structure to be protected and past project experience in operating and maintaining both types of systems.

24.1.3.1 Basis for Selecting a Sacrificial Anode System

Advantages:

1. External power source is not required
2. Installation is less complex

3. Uniform distribution of current
4. Minimum maintenance
5. Minimum cathodic interference

Limitations:

1. Current output is limited. It has limited driving potential, therefore the protection for the bare steel area is limited for each anode.
2. Poorly coated structures need more anodes
3. Ineffectiveness in high resistive environments

24.1.3.2 Basis for Selecting an Impressed Current System

Advantages:

1. Applicable for wider range of voltage and current requirements

2. High current can be impressed with a single ground bed
3. Single installation can protect larger surface of the metallic structure
4. Uncoated and poorly coated structures can be effectively protected
5. Voltage and current can be varied to meet the pipeline changing conditions with time

Limitations:

1. Overprotection leads to coating damage and hydrogen embrittlement
2. The system is affected by interference problems
3. External power is necessary, thus the system is vulnerable to power failure

24.2 CATHODIC PROTECTION CRITERIA

24.2.1 Potential Criteria

R. J. Kuhn first postulated in 1933 that the potential needed to stop corrosion is probably in the neighborhood of -0.85 V versus Cu/CuSO_4 .²¹⁻²³ Over the years, after extensive study on cathodic protection,²⁴⁻²⁹ the criteria for cathodic protection has been documented by National Association of Corrosion Engineers (NACE).³⁰ NACE RP-01-69 specifies: "A negative (cathodic) potential of at least 850 mV versus Cu/CuSO_4 should be applied to protect the structure."^{30,31} However, in the presence of sulfides, bacteria, elevated temperatures, acid environments and dissimilar metals, the criteria of -850 mV may not be sufficient.³²⁻³⁵ According to NACE, one should also take into account the IR drop at the metal/soil interface, which is included in most prac-

tical measurements; it is of uncertain value, depending on the electrolyte (soil) resistance.

For other metals such as aluminum and copper piping, NACE RP-01-69 suggests a minimum of 100 mV cathodic polarization between the structure surface and a stable reference electrolyte contacting the electrolyte. Some of the other criteria suggested by NACE RP-01-69 and Gummow²² are summarized in Table 24.2.⁶

24.2.2 IR Drop Considerations

The IR drop is caused by the current flow through the soil, the pipe coating, and the metallic path.³⁶ All cathodic protection potential measurements contain an IR drop component when a CP current or interference current is present.³⁷ The measured potential (E_m) is the sum of the polarized potential (E_p) measured near the cathode electrolyte interface and the IR drop along the path. On a new pipeline that has a high performance coating, a large IR drop is produced due to extremely high dielectric resistance of the coating. When the current direction is toward the structure, the polarity of the IR drop is additive and, hence, the measured potential (E_m) is greater than E_p . This contributes to the structure appearing to be better protected than it really is. When the current direction is opposite (away) from the structure, as in the case of stray current, the IR drop subtracts from the E_p and makes the structure appear to be less protected than it really is. When the IR drop is high, both effects could be detrimental. Measuring the IR drop is crucial in evaluating the correct polarized potential. Gummow summarizes several methods that have been developed to measure the IR drop,³⁸ namely:

TABLE 24.2 Criteria for Cathodic Protection

| Criterion | Measurement Condition | Comments |
|--|---|--|
| 1. Potential less than -0.85 V versus Cu-saturated CuO_4 for steel | Current on (IR_Ω present) | Meaningful in some environments Uncertain due to IR_Ω |
| 2. Cathodic polarization more than 300 mV active to corrosion potential of structure | Current on (IR_Ω present) | Uncertain due to interferences from IR_Ω |
| 3. Cathodic polarization more than 100 mV active to corrosion potential of structure | Current interrupted (IR_Ω absent) | Interruption techniques difficult to implement |
| 4. Cathodic polarization to a potential where Tafel behavior achieved | Current variable (IR_Ω present) | Difficult to determine in presence of IR_Ω |
| 5. Net protective current flows from electrolyte into the structure surface | Unspecified | Correct in theory Difficult to determine in practice |

[Source: From D. A. Jones, *Principles and Prevention of Corrosion*. Reprinted by permission, Prentice Hall]

1. Extrapolation of potential measurements taken with the reference electrode placed at increasing distances from the pipe
2. Extrapolation using a stepwise current reduction technique
3. Interruption of the current with the measurement of an "instant off" potential

Current interruption is considered to be the best IR drop correction technique. However, current interruption technique is very difficult to conduct for large structures such as pipelines, and that is why use of the IR coupons technique (see Section 24.4.1.3) to estimate the IR drop has been implemented worldwide.

24.2.3 Electrochemical Basis for CP Criteria

At the reversible potential/half cell potential, the rate of anodic reaction ($\text{Fe} \rightarrow \text{Fe}^{2+} + 2\text{e}^-$) is equal to the rate of cathodic reaction while the net current flow is zero.^{39,40} Thus, when polarized to the reversible potential, the corrosion rate of the metal is equal to zero. The reversible potential of the system can be calculated from the Nernst equation,⁴¹ as follows:

$$E_{\text{Fe}/\text{Fe}^{2+}} = -0.44 + \frac{0.059}{2} \log(\text{Fe}^{2+}) \quad (24.3)$$

The activity of Fe^{2+} in equilibrium is determined by the solubility of the covering layer of $\text{Fe}(\text{OH})_2$.

$$a_{\text{Fe}^{2+}} = \text{solubility product} / (\text{OH}^-)^2 \quad (24.4)$$

The concentration of (OH^-) can be estimated, assuming that its concentration at equilibrium is twice that of (Fe^{2+}) according to $\text{Fe}(\text{OH})_2 = \text{Fe}^{2+} + 2\text{OH}^-$. The calculated potential is -0.59 V versus SHE, (-0.91 V versus Cu/CuSO_4 reference electrode). The value of this potential is in agreement with the empirical value of -0.85 V versus Cu/CuSO_4 discussed earlier.

24.3 FIELD DATA AND DESIGN ASPECTS

Successful application of cathodic protection depends upon the selection, design, installation and maintenance of the system. Before designing cathodic protection, adequate field data must be collected, analyzed and evaluated. The nature and

conditions of the soil are reflected by field measurements like soil resistance, hydrogen ion activity (pH) and the redox potential. To understand the nature of the pipeline, potential measurements, coating resistance and meaningful design current requirement tests must be conducted.

24.3.1 Soil Resistance

The soil resistance is one of the most important factors in selecting a ground bed location. The type of anode and the number of anodes required,⁴² the length and diameter of the backfill column, the voltage rating of the rectifier, and power cost are all influenced by the soil resistance.⁴³ Marshy soils have low resistance, while rocky soils may have resistance of several thousands of ohms.⁴⁴ The corrosion activity is always an inverse function of the soil resistance. The current drastically increases in low resistive soils, which contributes the dissolution of the anode to increase.⁴⁵ The corrosion activity of steel exposed to soils of varying activity is given in Table 24.3.⁴⁵ The soil resistance can be estimated by using the methods described below.

24.3.1.1 Wenner Four Pin Method

This is the most commonly used method for measuring soil resistance. In this method, as shown in Figure 24.5, four pins are placed at equal distances, a . A current is then sent through the two outer pins (C_1 and C_2).^{46,47} By measuring the voltage across the two inner pins, the soil resistance can be calculated using Ohm's Law ($V=IR$). Soil resistance (ρ) can be determined using the equation:

$$\rho = 191.5 \times R \times L \quad \Omega \text{ cm.} \quad (24.5)$$

TABLE 24.3 Classification of Soil Corrosivity Based on Soil Resistivity

| Resistivity Range Ωcm | Corrosivity |
|-------------------------------------|-------------|
| 0–1,000 | Very severe |
| 1,001–2,000 | Severe |
| 2,001–5,000 | Moderate |
| 5,001–10,000 | Mild |
| 10,001 + | Very mild |

[Source: Adapted from J. D. Palmer, *Materials Performance*, 13(1), 41, 1974]

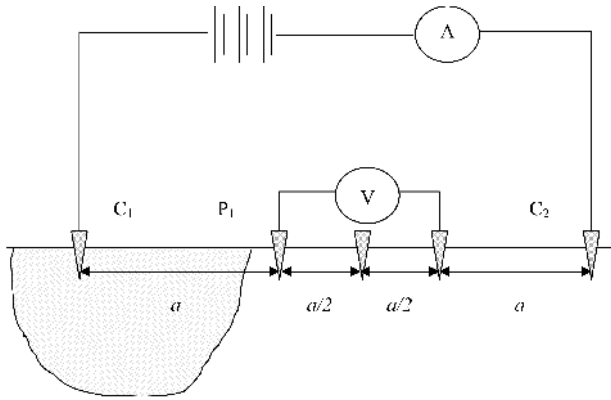


FIGURE 24.5 Wenner four pin method for measuring soil resistance.

where R is resistance in ohms and L is the length of the pin spacing. This method gives an average in situ resistance at a depth equal to the pin spacing. Foreign buried structures may interfere with the measurements when using the Wenner method. Therefore, it is important to position the pins perpendicular to the underground pipeline.⁴⁸ Placing the pins parallel to the pipeline results in resistance values that would be lower than the actual resistance. If the specific soil resistance varies vertically with the depth t , an apparent specific resistance can be obtained from a combination of the resistances of the upper and lower layers. It is recognized that the influence of the lower soil layer is only significant when $a > t$.⁴⁹

24.3.1.2 Soil Box Method

This method is based on the same principle as the Wenner four pin test method. There are four points of electrical contact with the soil; the current is driven through the two outer points and the voltage drop is measured across the two inner points. In the soil box, however, the outer points are the metal end plates of the box, rather than pins. The inner points are pins, just as in the Wenner four pin method. The resistance is calculated by using Ohm's Law. The resistance (ρ) is given by

$$\rho = R \frac{WD}{L}, \quad (24.6)$$

where W , D and L are the soil box dimensions. The soil box method gives very accurate results for fluids. However, the value measured for soil samples

may differ from those measured at actual sites due to variations of natural conditions including moisture, compaction, void ratio, particle size, etc. If the soil resistance varies with depth, the samples must be taken from an accurate map of soil resistance in the area. This method is more time-consuming than the Wenner four pin method.

24.3.2 Hydrogen Ion Activity (pH)

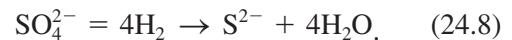
The soil pH is a measure of the hydrogen ion activity:

$$pH = -\log_{10} [a_{H^+}], \quad (24.7)$$

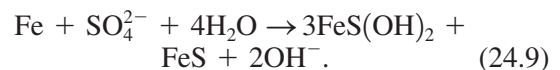
where a_{H^+} corresponds to the activity of hydrogen ions. pH of soils may vary in range between 3.5–10. The metal corrosion rates increase with a decrease of the soil pH. It is well known that iron passivates at pH higher than 9.⁸ The soil pH can be determined by testing the underground water in the area of interest. In the absence of any underground water, the pH can be measured by mixing one volume of soil with one volume of distilled water. Antimony and copper/copper sulfate electrodes can be used to obtain in situ soil pH values.

24.3.3 Microbiological Activity and Redox Potential

Soils may become more aggressive in the presence of microbiological activity. Commonly observed bacteria present in the soils are the sulfate-reducing type (*Desulpho Vibrio desulpharicans*). This bacterium consumes hydrogen and reduces sulfates to sulfide.^{50–52}



The product formed is hydrogen sulfide, which reacts with steel and produces black FeS. Under anaerobic conditions the reaction is:



It is explicit that hydrogen is consumed and H_2S is formed. The corrosion acceleration by bacteria is two-fold. The hydrogen consumption accelerates corrosion by decreasing the cathodic polarization. Also, iron sulfide formation increases the corrosion rate by forming a galvanic couple with the bare steel.^{53,54} Bacteria survive by consuming certain

types of adhesives. The conditions favorable for prompting bacteriological activity include a temperature range of about 35–400 °C and a pH range between 5.5–8.5.

The presence of bacterial activity can be qualitatively established by placing a few drops of hydrochloric acid on the corrosion products. The evolution of H₂S indicates the existence of anaerobic bacteriological activity. Bacteriological existence can be also established by measuring the redox potential. This can be done by placing a redox probe into freshly dug soil at the pipeline depth. The potential is measured between a clean platinum surface and a saturated calomel reference electrode.^{55–58} The redox potential measurement data and the tentative anticipated bacteriological activity are shown in Table 24.4.⁵⁹

Besides sulfate-reducing bacteria, sulfur-oxidizing bacteria (*Thiobacillus*, thioxidants) can also exist in aerated environments. During their metabolic activity, these bacteria consume oxygen and oxidate sulfides to sulfuric acid (H₂SO₄). They can produce sulfuric acids with concentrations as high as 10% (i.e., pH 0.5).⁶⁰ In general, microbiological activity can increase the corrosion rate by:

1. Depolarizing the cathodes
2. Creating corrosion products that can be effective cathodes
3. Causing damage to coatings and exposing structure to environments

24.3.4 Coating Resistance

Cathodic protection is always applied as a complementary protection to the coating. The coating reduces the amount of current necessary to be impressed for cathodic protection. Current requirements or current density measurements are related to

TABLE 24.4 Classification of Soil Resistance Based on Oxidation-Reduction Potential

| Redox potential volts versus SCE | Anaerobic condition |
|----------------------------------|---------------------|
| Below 0.100 | Severe |
| 0.100 to 0.200 | Moderate |
| 0.200 to 0.400 | Slight |
| Over 0.400 | None |

[Source: Adapted from R. L. Starkey and K. M. Wight. *Anaerobic Corrosion of Iron in Soil*. American Gas Association Monograph, New York, 1945]

the coating conductance/resistance.^{61,62} The coatings that are used to protect pipelines include: (i) coal tar and asphalt enamels, (ii) mastics, (iii) waxes, (iv) poly vinyl chloride, (v) polyethylene tapes, (vi) thermosetting epoxy resins, and (vii) epoxy coatings. A perfect coating has a coating resistance in the order of 10¹⁰ Ω cm². Unfortunately, the coatings are not perfect; they develop holidays and deteriorate with time. Coating damages are caused by chemicals present in soil, bacteriological activity, penetration by tree roots, and thermal and mechanical stress.^{63,64}

24.3.4.1 Determination of Coating Resistance

Effective coating resistance can be determined at any section of the pipeline by applying a cathodic current.^{59,62} The temporary current should be interrupted at defined time intervals (40 seconds, with 20 seconds off). The current-induced difference may be found out at two different locations of the pipeline. Once the difference in pipeline current $I = (I_{\text{on}} - I_{\text{off}})$ and the difference in potential $[E = E_{\text{on}} - E_{\text{off}}]$ are known at two locations, the coating resistance can be estimated by using the expression:

$$R_c = E_1 + \frac{E_2}{2(I_1 - I_2)}, \quad (24.10)$$

where E_1 and E_2 are the differences in the remote electrode potential in volts, and I_1 and I_2 are the differences in pipeline current in amperes. The effective coating resistance can be estimated by multiplying with the surface area (Ω cm²).

24.3.5 Required Current Density

A critical part of design calculations for cathodic protection systems is the amount of current density (protection current) required to change the structure's potential to -0.85 V versus Cu/CuSO₄. The current density required for complete protection depends on the metal that is protected and on the environment. This current can be estimated from the Evans plots that are shown in Figs. 24.1 and 24.2. However, since these measurements are based on theoretical values and laboratory experiments, when applied to pipelines they might result in significant errors. To estimate the current necessary to protect the pipeline in service, one should perform a field test. The field test is performed by applying a test

current to the structure; the resultant change of the structure to soil potential is measured. From these data, the current requirement can be estimated.⁶²⁻⁶⁵ For a new pipeline installation, the current density requirements are usually estimated from the previous estimates, such as those presented in Table 24.5.⁶⁶ For coated pipelines, the amount of the exposed steel depends on the quality of the coating. An arbitrary coating efficiency of 90–95% (10–5% bare steel) is assumed in current requirement calculations. Current density requirements for soils, seawater and a variety of other aqueous environments are available.⁶⁷⁻⁷⁰

The total current requirements (I_c) in mA is thus the total area A_c in m^2 of the pipe multiplied by the percent of bare metal and the current density required (I_{req}), or:

$$I_c = A_c \cdot f_c \cdot i_c I_{req}, \quad (24.11)$$

where I_c is the total current requirements in milliamperes (mA), A_c is the total area of the pipeline in square meters (m^2), and f_c is the fraction of the external pipe surface exposed at coating defects and bare metal areas.

24.4 MONITORING METHODS

The effectiveness of the cathodic protection can be determined by monitoring the pipeline potential using the Close Interval Potential Survey (CIPS) method, or by using Direct Current Voltage Gradient (DCVG) or IR coupons techniques. Also, physical and electrochemical methods can be used to estimate the corrosion rates of cathodically protected systems.

TABLE 24.5 Current Requirements for Cathodic Protection of Bare Steel

| Environment | mA/m ² |
|---|-------------------|
| Neutral soil | 4.5–16.0 |
| Well aerated neutral soil | 21.5–32.0 |
| Highly acid soil | 32.0–160.0 |
| Soil supporting sulfate-reducing bacteria | 65.0–450.0 |
| Heated soil | 32.0–270.0 |
| Stationary fresh water | 11.0–65.0 |
| Moving, oxygenated fresh water | 54.0–160.0 |
| Seawater | 32.0–110.0 |

[Source: From U.S. Air Force Manual 88-9, *Corrosion Control*, p. 203]

24.4.1 Potential Surveys

Measuring the pipeline potential with reference to a non-polarized reference electrode (e.g., Cu/CuSO₄) is one of the most commonly used methods for potential surveys of pipelines. This method is based on the potential criteria listed in the previous section. Presently, inexpensive battery-operated light (50 MOhm or higher) internal resistance voltmeters with a resolution of 1mV are widely available. Also, micro-processor digital recorders (called data loggers) are more frequently used for monitoring pipeline potential.

24.4.1.1 CIPS Technique

The CIPS method is based on connecting a thin, strong cable to a monitored pipeline and performing frequent potential readings along the route.⁷¹ The operator carries a battery-operated portable computer in a field backup, while walking the line. Wire connected to a terminal point is reeled out through a distance counter. The potential of the buried surface is measured through a walking stick reference electrode thrust in to the earth at about 1-m intervals. Potential versus distance readings are automatically logged into the computer. Special software is used for processing the data.⁷²

24.4.1.2 DCVG Method

The DCVG method technique provides evaluation of CP effectiveness and detection of defects in insulation by determining the zones of inflow or outflow of polarizing current.⁷³⁻⁷⁶ When the impressed cathodic protection current reaches the insulation defects, it causes a drop of voltage in the soil. This potential difference can be detected between the two electrodes placed on the ground, using a sensitive mV meter. The center point of the defect area can be located by means of two perpendicular measurements series. The size of the insulation defect is characterized by a relative number, the so-called % IR number obtained from the potential gradient graphs and soil resistance measurements. A distinctive feature of this technique is that even small defects can be located accurately, with a claimed accuracy of about 10 cm. With the DCVG method, parallel pipelines can be inspected at the same time. It does not require extra current input. Noises from other current sources can be eliminated easily. This method is also effective in the case of pipelines without cathodic protection, by using temporary anodes

and CP stations. In recent years, there have been improvements in this method contributing to more precise monitoring of pipelines.⁷⁷

Combined methods are also used to monitor the cathodic protection efficiency. In the intensive measurement described by Wessling,⁷⁸ both CIPS and DCVG methods are used. The worker walks along the pipeline route and records the distance and the “switch on” and “switch off” potential changes versus the portable reference electrode, at small intervals. The measurements are supplemented with ON/OFF potential gradients in one or two directions perpendicular to the pipeline. The measured (real) values serve as the basis for calculation of the insulation defects (% IR). Other technique such as the Intensive Holiday Detection (IHD) method can be used to detect the coating defects in pipelines. Implementation of the above methods has led to a considerable decrease in the number of breakdowns of underground pipelines.

24.4.1.3 IR Coupons/ Simulation Probes

Coupons have been used extensively for years in the laboratory and in field environments to determine the corrosion rate of metals under various conditions.⁷⁹ They were used specifically to test the effectiveness of the -850 mV (versus Cu/CuSO₄ electrode) and the -100 mV polarization potential shift cathodic protection criteria.

Coupons have been used to monitor cathodic protection systems in Europe since 1960.⁸⁰ Most of these coupons have been installed since 1975. Coupons are used in the form of steel electrodes of a strictly determined shape and surface area, protected by cathodic protection together with the structure. A schematic of the coupon installation on a pipeline is shown in the Figure 24.6.⁸¹ Disconnecting the coupon momentarily from the pipe interrupts the coupon current and provides an opportunity to measure the “instant off” potential. Further remnants of IR drop can be eliminated by fixing the reference electrode near the coupon or by using an electrolytic bridge.^{82,83} Using these coupons, the IR free potential can be measured without interrupting the cathodic protection to the pipeline.⁸¹ A distinctive feature of the use of coupons is that the effects of steady-state and DC transit stray currents^{84–86} can be measured accurately.

In 1994, B. A. Martin reported on the use of coupons to monitor the impressed current cathodic protection system at river crossings on a pipeline in Papua, New Guinea.⁸⁷ More than 400 probes have

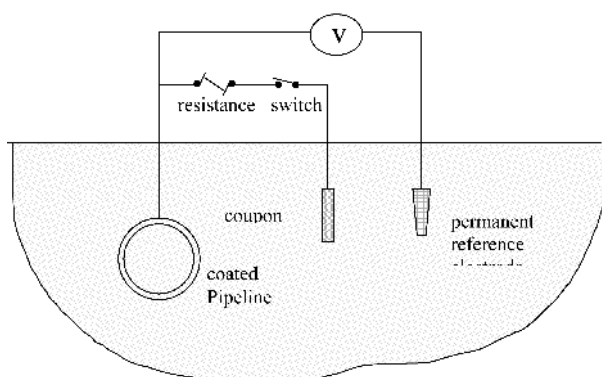


FIGURE 24.6 Coupon simulator circuit to determine IR drop.

been installed on the Trans-Alaska pipeline system since 1994.⁸⁸ Use of coupons has proven to be very effective for measuring the level of cathodic polarization and for detection of holidays.

24.4.2 Corrosion Rate Measurements

The most widely used potential monitoring measurements are based on the protection potential criteria. Despite the improvements in these methods, they only indicate if the pipeline is protected, underprotected or overprotected. These methods are not capable of estimating the corrosion rates or predicting the life expectancy of the system. A more advantageous solution would be introduction of a kinetic CP criterion that would allow maintaining the metal structure corrosion rate at a given level depending on actual requirements.

Several electrochemical and physical methods can be used to measure the corrosion rate of the system. Some of the commonly used methods are listed in Table 24.6. The use of these electrochemical tools in monitoring the corrosion rate of cathodically protected structures was reviewed by several researchers.^{89–93} More information, and the scope of corrosion rate measurements of cathodically polarized metal structures by electrochemical techniques, can be obtained in the reviews by Janowski.^{94,95}

24.5 DESIGN OF CATHODIC PROTECTION SYSTEMS

The ideal design for a cathodic protection system is one which will provide the desired degree of protection at the minimum total annual cost over the pro-

TABLE 24.6 Physical and Electrochemical Methods for Corrosion Rate Measurements

| Physical Methods | Electrochemical Methods |
|-----------------------|--|
| Gravimetry | Tafel polarization |
| Electrical resistance | Linear polarization |
| Radiography | Electrochemical impedance spectroscopy |
| Ultrasonic | Harmonic synthesis |
| Eddy currents | Electrochemical noise |

jected life of the structure. Design of cathodic protection systems for pipelines has been extensively researched and several standards have evolved over the decades of its application.^{62,96–113} A detailed description has been illustrated in the work of A. W. Peabody and others.⁶² The basic procedure involved in the design of cathodic protection is summarized below.

24.5.1 Choice of the CP System

It is essential to make an important decision on the selection of the CP system to be installed. The choice of the CP system is based on the environment in which the pipeline is operated, with the merits of each system as illustrated in Section 24.1.3. Sacrificial protection is generally employed in environments with low soil resistance (10,000 Ωcm) with a relatively low protective current requirement because of the low driving voltage. Well-coated and isolated pipelines favor the installation of a sacrificial system in highly resistive soils. On the other hand, impressed current systems are usually installed in conditions where the current requirements are higher, and for pipelines which are bare or poorly coated. In all cases, the final decision is based on the total installation and annual maintenance costs of the systems.

24.5.2 Design of Sacrificial Protection Systems

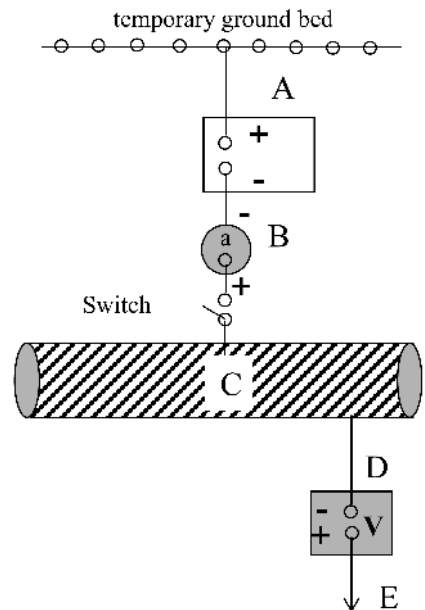
The basic design of sacrificial CP system includes calculation of cathodic protection circuit resistance, potential difference between the anode and the structure, anode output, number of anodes, and the anode life expectancy. A schematic of the cathodic protection test is given in Figure 24.7. To estimate current requirements, a test is needed to determine the cur-

rent (i_c) needed to provide adequate protection for the pipeline. This can be done by applying current using a temporary test setup as shown in Figure 24.7, and adjusting the current from the rectifier until the cathodic protection criteria are reached.

24.5.2.1 Cathodic Protection Circuit Resistance

The cathodic protection circuit resistance includes the anode to soil resistance, resistance of the wire/cable, and the structure to soil resistance.

24.5.2.1.1 Anode Resistance. The anode resistance has a significant role in determining the amount of the anode material to be used.⁹⁶ The anodes used in the sacrificial cathodic protection system are of three types, namely, vertical anodes, horizontal anodes, and grouped anodes. Typical graphite anode-vertical and horizontal installation is shown in Figs. 24.8 and 24.9, respectively. The re-



- A - DC power source
- B - Ammeter
- C - Buried structure
- D - High resistance voltmeter
- E - Remote CuSO₄ reference electrode

FIGURE 24.7 Cathodic protection requirement test: (a) DC power source; (b) ammeter; (c) buried structure; (d) high resistance voltmeter; (e) remote CuSO₄ reference electrode.

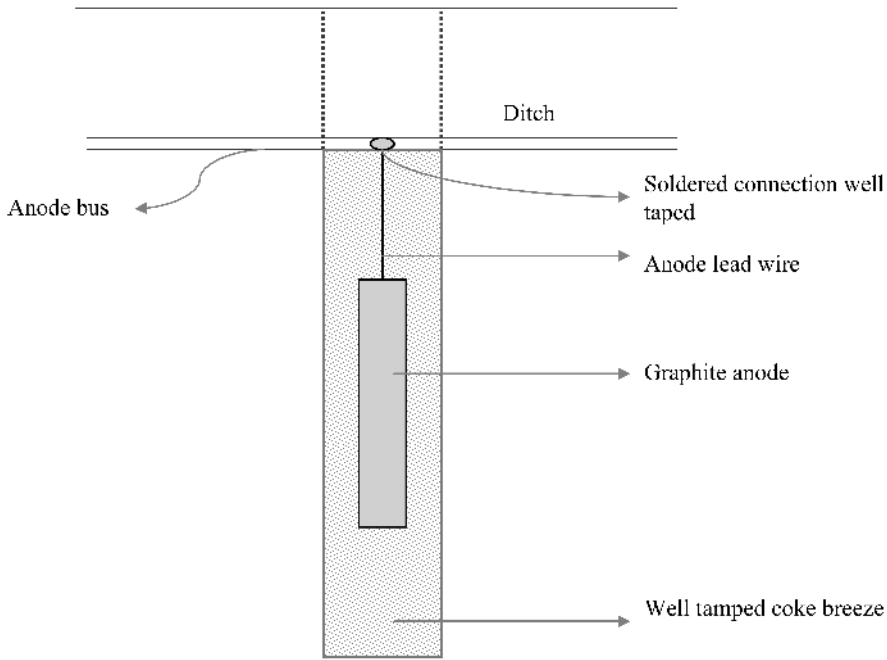


FIGURE 24.8 Typical graphite anode—vertical installation.

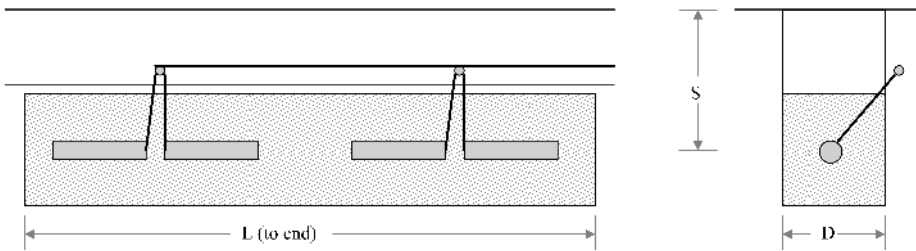


FIGURE 24.9 Typical graphite anode—horizontal installation.

sistance of the vertical anode to earth is calculated using the Dwight formula⁹⁷:

$$R_v = \frac{\rho}{2\pi L} \left(\ln \frac{8L}{d} - 1 \right), \quad (24.12)$$

where R_v is the resistance to earth in ohms (Ω), ρ is the soil resistance in ohm centimeters (Ωcm), L is the anode length in centimeters, and d is the anode diameter in centimeters.

If horizontal anodes are used, the resistance to earth (s) given by a modified Dwight formula^{101,102}:

$$R_h = \frac{\rho}{2\pi L} \left(\ln \left[\frac{4L^2 + \sqrt{(2h)^2 + L^2}}{2dh} \right] + \frac{2h}{d} - \frac{\sqrt{(2h)^2 + L^2}}{L} - 1 \right), \quad (24.13)$$

where R_h is the resistance of anode to earth in ohms (Ω), L is the anode length in centimeters, d is the anode diameter in centimeters, and h is depth below the surface to the center of the anode, in centimeters.

In case of grouped anodes, the resistance to earth is given by the Sunde equation^{62,103}:

$$R_n = \frac{\rho}{2pNL} \left(\ln \frac{8L}{d} - 1 + \frac{2L}{S} \ln 0.656N \right), \quad (24.14)$$

where R_n is the resistance of anodes to earth in ohms, L is the anode length in centimeters, d is the anode diameter in centimeters, N is number of anodes, and S is center-to-center spacing of anodes, in centimeters.

24.5.2.2 Cable Resistance. The anode and the structure are interconnected by copper cables. The copper cables have an inherent resistance (R_w) to

current flow. Table 24.7 presents the resistance of copper cable data.¹⁰⁷

24.5.2.3 Structure to Electrolyte Resistance.

The structure to electrolyte resistance is not very significant. Detailed information on calculating structure to electrolyte resistance can be obtained in the work of A. W. Peabody.

24.5.2.4 Total Circuit Resistance. The total cathodic protection circuit resistance, R_t (W), is given by:

$$R_t = R_a + R_w + R_{soil}, \quad (24.15)$$

where R_a is the anode resistance, R_w is wire resistance, and R_{soil} represents the soil resistance.

24.5.2.5 Anode Output. The anode output depends on the anode circuit resistance and potential difference between the anode and the pipeline. The anode output is directly proportional to the potential difference between the open circuit potential of the anode (ϕ_a) and the cathodically polarized potential of the pipeline (E_p). The current output, I_a in milliamperes, is then calculated from Ohm's Law:

$$I_a = \frac{(E_p - \phi_a)}{R_a} 1000. \quad (24.16)$$

TABLE 24.7 Resistance and Current Capacity Data for Copper Cable

| Size AWG | Dc Resistance 20°C, W/meter | Max dc. Current Capacity (A) |
|----------|-----------------------------|------------------------------|
| 14 | 8.4650 | 15 |
| 12 | 5.3152 | 20 |
| 10 | 3.3466 | 30 |
| 8 | 2.0998 | 45 |
| 6 | 1.3222 | 65 |
| 4 | 0.8334 | 85 |
| 3 | 0.6595 | 100 |
| 2 | 0.5217 | 115 |
| 1 | 0.4134 | 130 |
| 1/0 | 0.3281 | 150 |
| 2/0 | 0.2608 | 175 |
| 3/0 | 0.2070 | 200 |
| 4/0 | 0.1641 | 230 |
| 250 MCM | 0.1388 | 255 |

[Source: From J .H. Fitzgerald, III, *Uhlig's Corrosion Handbook*, R. Winston Revie, Ed. Reprinted by permission, John Wiley & Sons, Inc.]

24.5.2.6 Number of Anodes and Anode Life.

The number of anodes is calculated from the anode output and the current density requirements. The number of anodes (N) required is given by:

$$N = \frac{i_c A_c}{I_a}, \quad (24.17)$$

where A_c is the area of structure to be protected and i_c is the cathodic current density required for protection.

The life of the anode is given by the formula¹¹⁰:

$$L = \frac{Th.W.E.UF}{h.I_a}, \quad (24.18)$$

where L is life in years, Th is the theoretical A-h/kg output (Table 24.1), W is the anode weight in kilograms, E is current efficiency (Table 24.2), UF is the utilization factor, h is hours per year (8,766), and I_a is the anode output in amperes. The utilization factor is usually chosen as 0.85 (85%). This means that once the anode is 85 % consumed its resistance to earth begins to increase to the point where its output is reduced significantly.

24.5.3 Design of Impressed Current Systems

Design of impressed current systems primary involves the anode selection, rectifier selection, ground-bed selection and calculation of the I-ground-bed resistance and other main parameters.

24.5.3.1 Current and Potential Distributions of the Protected Structure

An analytical approach to determine the current and potential distribution as a function of distance x along a coated pipeline of infinite length are given by these attenuation equations¹¹¹:

$$\left. \begin{aligned} E_x &= E_o \exp(-\alpha x) \\ i_x &= i_o \exp(-\alpha x) \end{aligned} \right\} \quad (24.19)$$

where E_o and i_o are the potential and current at the point of connection to the anode (also known as the drainage point), and α is the attenuation coefficient.

$$\alpha = \frac{R_s}{R_k} \quad (24.20)$$

R_s is the longitudinal resistance pipe resistance per unit length and $R_k = (R_s R_L)^{1/2}$, and

$$R_L = (E_x - E_0)/(I_x - I_0), \quad (24.21)$$

where R_L is defined as the leakage resistance of the pipeline, and $E_x - E_0$ is the ohmic potential drop along the coating. The attenuation equations between two drainage points separated by a distance $2d$ are:

$$\left. \begin{aligned} E_x &= \frac{E_o \cosh \alpha(d - x)}{\cosh \alpha d} \\ i_x &= \frac{i_o \sinh \alpha(d - x)}{\sinh \alpha d} \end{aligned} \right\} \quad (24.22)$$

The variation of potential with distance, along with the cathodic protection criteria, is given in Figure 24.10. Attenuation curves with driving potential (ΔE) and polarization potential (ΔE_p) are given in Figure 24.11. Driving potential is defined as a difference between the “on” potential and “off” potential, while polarization potential is defined as the difference between the “off” potential and the open circuit potential at each point.

24.5.3.2 Anode Selection

Selection of the anode in the case of an impressed current CP system is primarily based on the dissipation rate of the anode. Low resistance to current

flow, low dissipation rate, physical robustness, fabricability, and minimal cost are the desirable properties of candidate anode materials. High silicon, chromium-bearing cast iron has a low dissipation rate. Dissipation rate varies with the environment; however, 0.5 kg/A-year is a typical requirement for the impressed current CP of pipelines.

24.5.3.3 Anode Requirements

In this case of a cathodic protection system, the weight and number of anodes to be used is calculated from the desired life of the system. Prolonged life of the anode is essential to decrease the maintenance cost of the impressed current cathodic protection system. Dissipation rate of the anode is a measure of the life of the anode. For a high silicon, chromium-bearing cast iron, the dissipation rate is 0.5 kg/A-year. The weight of the anode is given by:

$$W_i = D_r \cdot I_c \cdot L, \quad (24.23)$$

where D_r is the dissipation rate in kg-A/year, I_c is the current required in amperes, L is the desired life in years, and W_i is the total weight of the anode in kilograms. The number of anodes required is given by the ratio of total weight to individual anode weight.

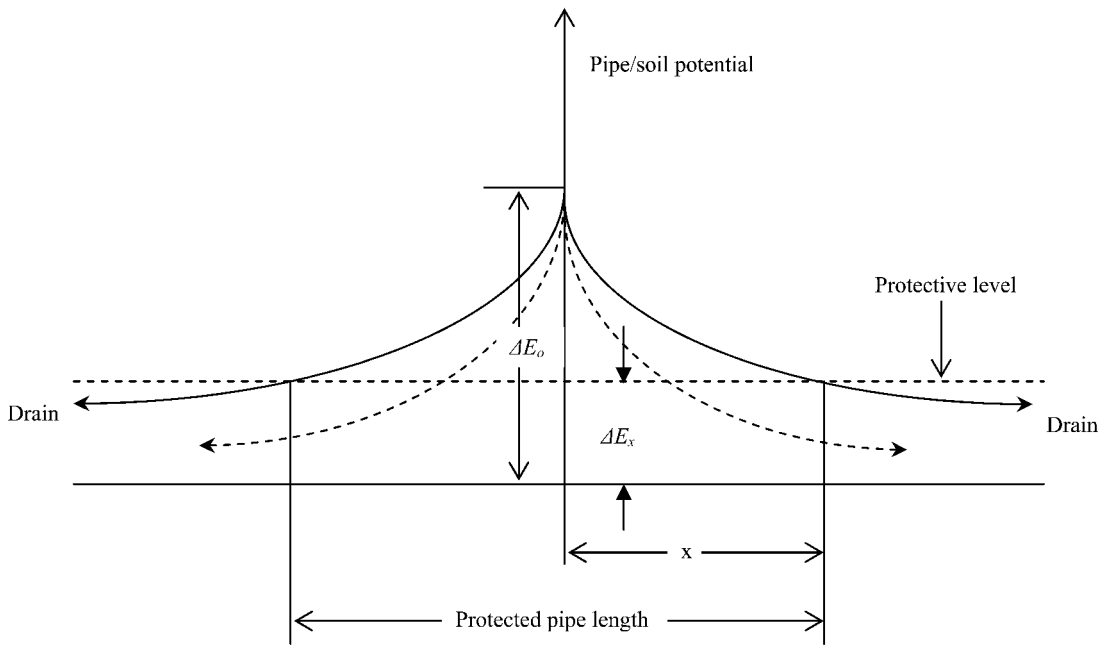


FIGURE 24.10 Theoretical attenuation of potential between two drainage points on a pipeline.

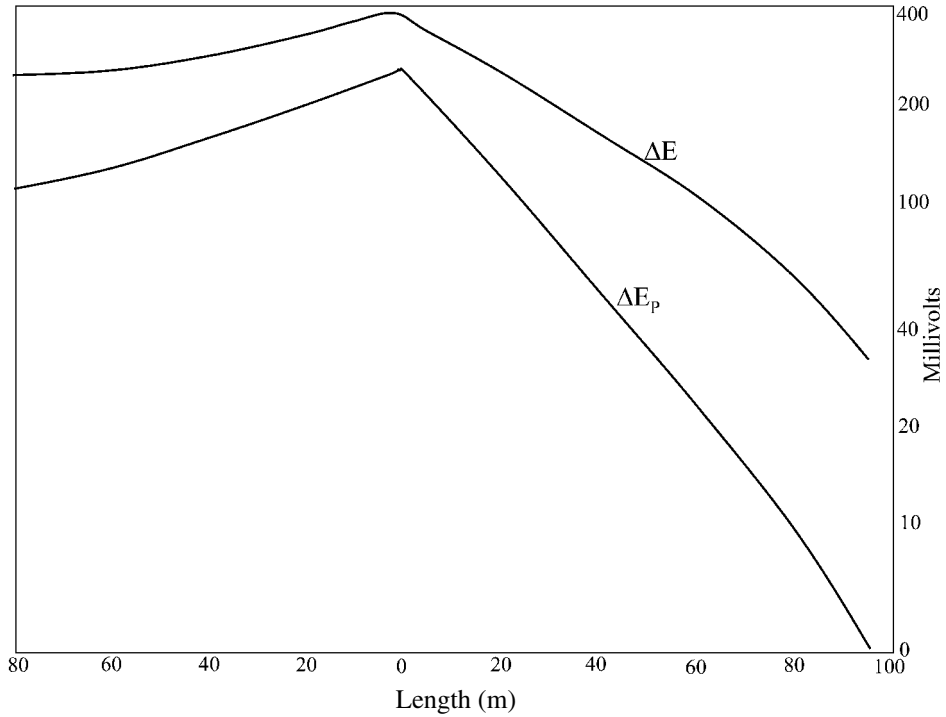


FIGURE 24.11 Attenuation Curves: Driving Voltage (ΔE) and Polarization Potential (ΔE_p) as a function of distance along the line.

24.5.3.4 Ground Bed Resistance

The ground bed resistance is similar to that of the total circuit resistance calculated for the design of sacrificial system (Section 5.2.1). In this case, multiple anodes are used and the resistance of anode to ground is calculated from the Sunde equation.¹⁰³

24.5.3.5 Rectifier Selection

Over the years, the quality of the coating decreases, leading to exposure of the bare steel. The current requirements increase with time for accomplishing a complete cathodic protection. Hence, the required driving voltage determined by Ohm’s Law is scaled up by 1.5 times to that required normally for a newer pipeline.

$$E = \frac{I_{req}}{R_t} \times 1.5 \quad (24.24)$$

24.5.3.6 Ground Bed Selection

The anodes are usually arranged horizontally or vertically, depending on the nature of the soil and the proximity of nearby structures. Deep vertical ground

beds six to 12 inches in diameter and up to 100 meters deep are used for pipelines, where the surface soil is dry and non-conductive and long distances must be protected.¹⁰⁸ Other instances where deep ground beds are necessary include sites where the right-of-way for surface ground beds cannot be obtained. Figure 24.12 shows a deep anode bed. Deep ground beds are conventionally backfilled with coke breeze for improved electrical contact to the soil, or with lubricated fluidizable coke, which can be pumped out later when the anode needs replacement.¹¹⁰

24.6 COMPUTER-AIDED DESIGN OF CATHODIC PROTECTION

The last decade has seen immense development in the use of computer modeling techniques for the design of cathodic protection. Large pipelines of complex design are being installed on land and in offshore environments, all of which require cathodic protection for corrosion prevention. Modeling CP systems has been useful for troubleshooting existing structures, design analysis of sacrificial and

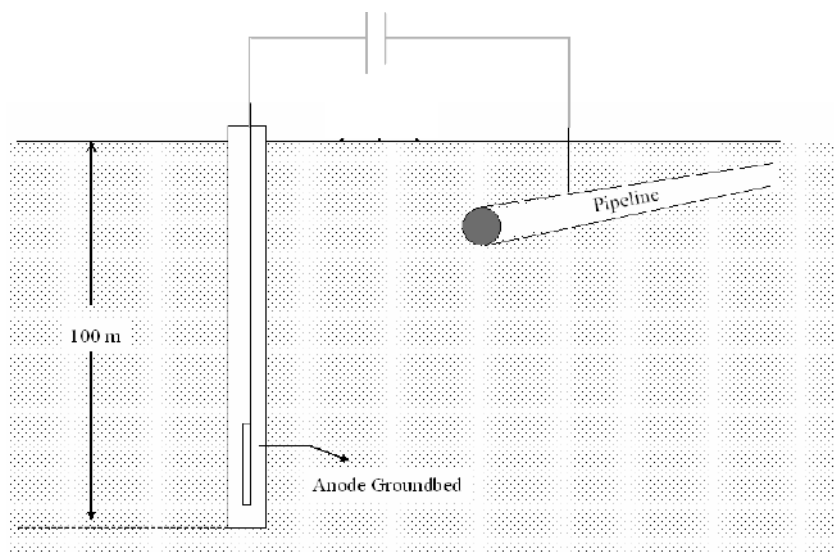


FIGURE 24.12 Impressed current cathodic protection using a deep anode ground bed.

impressed current systems, checking for interference effects, attenuation, and prediction of life of the systems.^{12–118} Several numerical methods are used for the modeling of the CP systems, including: (i) the boundary element method, (ii) the finite difference method, (iii) the finite element method, and (iv) the integral equation method.^{119,120} All of these methods involve the numerical solution of the Laplace equation:

$$\nabla^2 E = 0. \quad (24.25)$$

The above equation is derived from the electroneutrality law for homogenous environments and is the governing equation to be solved for determining the potential distribution. To solve this equation, appropriate boundary conditions need to be specified. Finite element methods divide the three-dimensional electrolyte volume into a network of finite “nodes” whose electrical properties are connected to one another by linear equations. Finite element methods yield potential and current distributions within the electrolyte volume. Incorporation of the polarization at the anode and cathode surfaces is difficult at volume boundaries. The Boundary Element Method (BEM) has shown considerable promise in addressing this problem. The electrode surface is divided into discrete boundary elements, which are solved numerically. Unlike the finite difference methods, in the BEM only the electrode surfaces are divided into

discrete elements, not the entire volume; this leads to decreased computation power.

With steady development in the modeling methods and computational techniques, this approach is expected to rule the future of cathodic protection design. Development of models has led to a widespread increase in the theoretical understanding of these systems. In the future, it is expected to play a wide role in the development of new designs with out wasting money on field experimental projects.

24.7 REFERENCES

1. T. Anderson and A. Misund. *J. Pet. Technology*, April, 709, 1983.
2. J. S. Mandke. *Oil and Gas Journal*, October 29, 40, 1990.
3. *Improving the Safety of Marine Pipelines*. Washington, DC: Committee on the Safety of Marine Pipelines, Marine Board, National Research Council, 1994.
4. W. Beckmann, W. Schwenk, W. Prinz. *Handbook of Cathodic Corrosion Protection: Theory and Practice of Electrochemical Protection Processes*. Houston: Gulf, 1997.
5. J. Morgan. *Cathodic Protection*, 2nd Ed. Houston: NACE, 1987.
6. D. A. Jones. *Principles and Prevention of Corrosion*. Upper Saddle River, NJ: Prentice Hall, 1996.
7. R. Juchniewicz, J. Jankowski, K. Darowicki. *Cathodic and Anodic Protection in Corrosion and Environment Degradation*. M. Schutzee, Ed. 1,383, Weinheim: Wiley-VCH, 2000.

8. Herbert H. Uhlig and R. Winston Revie. *Corrosion and Corrosion Control*, 3rd Ed. New York: John Wiley & Sons, Inc., 1985.
9. Wilson Lynes, *J. Electrochem. Soc.*, 98, 120, 1951.
10. R. Burns and W. Bradley. *Protective Coatings for Metals*, 3rd Ed. Columbus, OH: American Chemical Society, 1, 104, 1967.
11. H. Davy. *Philos. Trans. Roy. Soc.*, 114, 151, 1824.
12. *Corrosion Basics*. NACE, 1984.
13. C. Wagner, W. Traud. *Z. Elektrochem.*, 44, 391, 1938.
14. P. F. George, J. J. Newport, and J. L. Nichols. *Corrosion*, 12, 627, 1956.
15. G. W. Kurr. *Materials Performance*, 19(4), 34, 1979.
16. G. Doremus and J. G. Davis. *Materials Performance*, 6(1), 301, 1967.
17. C. F. Schreiber, V. Ashworth and C. J. L. Booker, Eds. *Cathodic Protection Theory and Practice*. Chichester, West Sussex, England: Wiley Horwood, 1, 94, 1986.
18. J. A. Jakobs. *Materials Performance*, 20(5), 17, 1981.
19. NACE. *Corrosion*, 16, 65, 1960.
20. W. T. Bryan. *Materials Performance*, 9, 25, 1970.
21. R. J. Kuhn. *API Proc.* 14, 157, 1933.
22. R. A. Gummow. *Materials Performance*, 25, 9, 1986.
23. W. J. Schwerdtfeger and O. N. Madorman. *Corrosion*, 8, 391, 1952.
24. L. P. Sudrabin, and F. W. Ringer. *Corrosion*, 12(5), 351, 1957.
25. S. P. Ewing. *Corrosion*, 13, 767, 1957.
26. M. Romanoff. *Underground Corrosion*. Houston: NACE, 1989.
27. *Cathodic Protection Criteria—A Literature Survey*. Houston: NACE, 1989.
28. T. J. Barlo and W. E. Berry. *Material Performance*, 23, 9, 1984.
29. K. G. Compton. *Materials Protection*, 4(8), 93, 1965.
30. *Control of External Corrosion on Underground or Submerged Metallic Piping*, NACE Standard RP-01-69-96 Item 21001. Houston: NACE.
31. R. Heidersbach. *Metals Handbook-Corrosion*, 9th Ed. Metals Park, OH: ASM International, Vol. 13, 470, 1987.
32. T. J. Barlo and W. E. Berry. *Materials Performance*, 23, 9, 1984.
33. L. P. Sudrabin and F. W. Ringer. *Corrosion*, 13, 351, 1957.
34. K. Fischer. *Materials Performance*, 20, 41, 1981.
35. T. Kobayashi. Effect of Environmental Factors on the Protective Potential of Steel. In *Proceedings of the 5th International Congress on Metallic Corrosion*. Houston: NACE, 627, 1974.
36. D. A. Jones. *Principles and Prevention of Corrosion*, 2nd Ed., Upper Saddle River, NJ: Prentice Hall, 1996.
37. Jeff Didas. *Material Performance*, 39(4), 26, 2000.
38. R. A. Gummow. *Material Performance*, 37(8), 24, 1998.
39. D. Jones. Electrochemical Fundamentals of Cathodic Protection. *CORROSION/87*, Paper 317. Houston: NACE, 1987.
40. R. B. Mears and R. H. Brown. *Trans. Electrochem. Soc.*, 74, 519 1938.
41. Allen J. Bard, Larry R. Faulkner. *Electrochemical Methods—Fundamentals and Applications*, 2nd Ed. New York: John Wiley & Sons, Inc., 2001.
42. A. W. Peabody. Use of Magnesium for Cathodic Protection of Pipelines in High Soil Resistive Environments. Ebasco Services Inc., NY. *Corrosion*, 15, 497t, 1959.
43. H. C. Van Nouhuys. Cathodic protection and High Soil Resistivity Soil. Southeastern Pipeline Co., Atlanta, GA. *Corrosion*, 9, 448, 1953.
44. J. D. Palmer. Soil Resistivity—Measurement and Analysis. *Materials Performance*, 13(1), 41, 1974.
45. Marshall E. Parker. *Pipeline Corrosion and Cathodic Protection*, Houston, TX: Gulf Publishing.
46. F. Wenner. "A Method of Measuring Earth Resistivity," Report No. 258, Bulletin of Bureau of Standards, 12, No. 3, October 11, 1915.
47. J. Ufermann and K. Jahn. *BBC-Nachrichten*, 49, 132, 1967 (in German).
48. *Field Measurement of Soil Resistivity Using the Wenner Four-Electrode Method*, ASTM Standard G57-95a, West Conshohocken, PA: ASTM International.
49. H. Thiele. *Die Wsserereerschliebung*. Essen: Vulkan-Verlag, 1952.
50. C. A. H. von Wolzogen Kuhr and L. W. van der Vlugt. *Water* 18, 147, 1934.
51. L. L. Varton, Ed. *Sulfate Reducing Bacteria*. New York: Plenum, 1995.
52. J. A. Hardy. *British Corrosion Journal*, 18, 190 1983.
53. R. G. Worthingham, T. R. Jack, and V. Ward. *Biologically Induced Corrosion* (S.C. Dexter Ed.), Houston, TX: NACE 330–339, 1986.
54. R. A. King and J. D. A. Miller. *Nature* (London), 233, 491, 1971.
55. R. L. Starkey and K. M. Wight. *Final Report of the American Gas Association Iron Corrosion Research Fellowships*. New York: American Gas Association, 1945.
56. F. Kajiyama. Apparatus for Measuring the Corrosivity of the Soil. Japanese Patent Application 58-208654, 1982.
57. C. G. Deuber and G. B. Deuber. *Development of Redox Probe*. Final Report to American Gas Association, Research Project PM-20, 1956.
58. F. E. Costanzo and R. E. McVey. Development of the Redox Probe Field Technique. *Corrosion*, 14, 268T, 1958.
59. R. L. Starkey and K. M. Wight. *Anaerobic Corrosion of Iron in Soil*. Monograph. New York: American Gas Association, 1945.
60. D. H. Popo, T. P. Zintel, A. K. Kurivilla and O. W. Silbert. *Corrosion*, 88, 79, 1988.

61. J. L. Banach. *Pipeline Industry*, March, 62, 1998.
62. A. W. Peabody. *Control of Pipeline Corrosion*. Houston: NACE, 1967.
63. D. C. Tracy. *Pipeline Gas Ind.*, 80(2), 27, 1997.
64. A. C. Coates. *Pipeline Digest*, April, 11, 1991.
65. R. Heidersbach. *Metals Handbook-Corrosion*, 9th edition, Metals Park, OH: ASM International Metals Park, OH, 13, 475, 1987.
66. A. Kumar et al. *Impressed Current Cathodic Protection Systems Utilizing Ceramic Anodes*. Champaign, IN: U.S. Army Corps of Engineers Construction Engineering Research Laboratories, 1990, Table A-1.
67. F. W. Hewes. *Cathodic Protection Theory and Practice*. V. Ashworth and C. J. L. Booker, Eds. Chichester, West Sussex, England: Wiley (Horwood), 1, 226, 1986.
68. B. S. Wyatt. *Cathodic Protection Theory and Practice*. V. Ashworth and C. J. L. Booker, Eds. Chichester, West Sussex, England: Wiley Horwood, 1, 143, 1986.
69. J. S. Gerrard. "Practical Applications of Cathodic Protection, *Corrosion*, Vol. 2. (L. L. Shreir, Ed.) London: Newnes-Butterworths, 57, 11, 1976.
70. Foster, T. and Moores, V. G. *Cathodic Protection Current Demand of Various Alloys in Sea Water*. Paper 254 presented at CORROSION/86, March, 1984.
71. J. M. Leeds. *Pipeline Corrosion Conference*, Houston, TX: Gulf Publishing Co, p. 6, 1995.
72. J. Suprock and T.R. Wilken. *Cathodic Protection Theory and Practice*. V. Ashworth and C. J. L. Booker, Eds. Chichester, West Sussex, England: Wiley (Horwood), 1, 249, 1986.
73. J. M. Leeds and J. Grapiglia. *Corrosion Prevention and Control*, 42(4), 77, 1995.
74. C. Ringas, J. M. Leeds and P. Oosthuizen. *The Application of DC Voltage-Gradient Technology to Accurately Determine Buried Pipeline Rehabilitation Requirements* Pipeline Risk Assessment, Rehabilitation and Repair Conference, Houston, TX, September 12–15, 1994. Organized by Pipeline Industry and Pipes & Pipelines International.
75. Z. Masilela and J. Pereira. Using the DCVG Technology as a Quality Control Tool During Construction of New Pipelines. *Engineering Failure Analysis*, 5(2), 99, 1998
76. N. G. Thompson. Paper 588 at CORROSION/93 Houston: NACE, 1993.
77. Janusz Winski. *Corrosion Technology*, 84(6), 120, 2001.
78. D. Wessling. *Capabilities and Limitations of Techniques for Assessing Coating Quality and Cathodic Protection of Buried Pipelines*. Cathodic Protection Theory and Practice Conference, Sopot, 2002.
79. *The State-of-the-Art of Using Buried Coupons in Cathodic Protection*. GERG PC-2 Transport and Storage Cathodic Protection Joint Research Team, 1991.
80. T. Kasahara, K., Sato, T., and Adachi, H. *Materials Performance*, March, 1979.
81. R. A. Gummow. Using Coupons and Probes to Determine Cathodic Protection Levels. *Materials Performance*, 37(8), 24, 1998.
82. J. Didas. Practical Applications and Limitations of Buried Coupons Utilized for ITDrop Measurements.
83. K. Kasahara, T. Sato, H. Adachi. *Materials Performance*, 3, 1979.
84. R. Kennelley, R. Degerstedt, M. Orazem, M. Esteban. *Full Scale Laboratory Evaluation of Parallel Anode CP System for Coated Pipelines with Comparison to 2D and 3D Models*. Paper 528 at CORROSION/95. Houston: NACE, 1995.
85. W. H. Seagers. *Adverse Telluric Effects on Northern Pipelines*. Society of Petroleum Engineers, SPE 22178, 1991.
86. R. Greenwood. *The Effects of Transient Stray Current on Cathodically Protected Pipelines*. British Gas Engineering Research Report, R. 3495.
87. B. A. Martin. *Materials Performance*, March, 1994.
88. D. Stears, R. Degerstedt, O. Moghissi, L. Bone, Paper 564 at CORROSION/97.7, 1997.
89. N. G. Thompson, B. C. Syrett. Paper 429 at CORROSION/93. 13, 1993.
90. R. Juchniewicz, J. Janowski. Application of Impedance Spectroscopy to the Assessment of Cathodic Protection Effectiveness. In *Progress in Understanding and Prevention of Cathodic Protection Ineffectiveness*. J. M. Costa and A. D. Mercer, Eds. London: EFC, 2, 1,401, 1993.
91. L. G. Cooper. Sensing Probes and Instruments for Electrochemical and Electrical Resistance Corrosion Monitoring. In *Corrosion Monitoring in Industrial Plants Using Nondestructive Testing and Electrochemical Methods*. G. C. Moran and P. Labin, Eds. Philadelphia: ASTM, STO 908, 237, 1986.
92. J. Janowski. A New Approach to Harmonic Analysis. In *Proceedings of EUROCORR'98*, Utrecht, 1998.
93. J. Janowski. Application of AC Electrochemical Techniques for Corrosion Rate Monitoring in Cathodically Protected Systems. In *Proceedings of EUROCORR'99*, Aachen, 1999.
94. J. Janowski. *Corrosion Reviews*, 20, 159 2002.
95. J. Janowski, *Corrosion Reviews*, 20, 179 2002.
96. *Anode Resistance Fundamentals and Applications—Classic Papers and Reviews*. Houston: NACE, 1986.
97. *Pipeline Cathodic Protection—Part 2: Cathodic Protection of Offshore Pipelines*. Working Document ISO/TC 67/SC2 NP 14489, International Standards Organization, May 1, 1999.
98. Freiman, L. I. *Protection of Metals*. Translation of Zashchita Metallov. 38(3), 277, 2002.
99. Russell, W. B. Cathodic Isolation/Protection Technologies Applied to Underground Metallic Structures. In *Proceedings of the Appalachian Underground Corrosion Short*

- Course 117*. The Rustrol Group of Companies, Burlington, ON, Canada, 2001.
100. Carlson, L. E., Fritzgerald, J. H., III, Webster, F. R. D.. *Materials Performance*. 40(8), 28, 2001.
 101. H. B.Dwight. *Electrical Engineering*, 55(12), 1,319 1936.
 102. A. Kumar et al. Cathodic Protection, Impressed Current Systems Utilizing Ceramic Anodes.
 103. E. D.Sunde. *Earth Conduction Effects in Transmission Systems*. New York: D.Van Nostrand, 1949.
 104. Capper, H. W. *Experience of Cathodic Protection for Structures and Pipelines*. Croydon, UK: Walton Int. Ltd., I Mech E Conference Publications (7), 27, 1979.
 105. Jenkins, J. *Cathodic Protection System Design 3. Sacrificial Anode System Design Principles for Underground Structures*. Naval Fac. Eng. Serv. Cent., Port Hueneme, CA. Avail. NTIS. Report 1995.
 106. William H. Hartt. *Retrofit Cathodic Protection of Marine Pipelines Associated With Petroleum Production*. Mineral Management Services, VA, 2001.
 107. Advanced Course Text, Chapter 5, Appalachian Underground Corrosion Short Course, West Virginia University, Morgantown, WV, 1993.
 108. T. H. Lewis. *Deep Anode System*. Hattiesburg, MS: Loresco International, 1997.
 109. Baboian, R., P. F. Drew, and K. Kawate. *Materials Performance*, 23(9), 31, 1984.
 110. L. L. Shrier and P. C. S. Hayfield. *Cathodic Protection Theory and Practice*. V. Ahsworth and C. J. L Booker, Eds. Chichester, West Sussex, England: Wiley Horwood, 1, 94, 1986.
 111. H. H. Uhlig and R. W. Revie. *Corrosion and Corrosion Control*. New York: John Wiley & Sons, Inc., p.223, 1985.
 112. Cochran, J. and Mayes, F. Paper 333 at CORROSION/84, New Orleans, April 2, 1984.
 113. Bethune, K. and Hartt, W. H. *Corrosion*, 57(1), 78, 2001.
 114. Orazem, M. E., Esteban, J. M., Kennelley, K. J., Degerstedt, R. M. *Corrosion*, 53(6), 427, 1997.
 115. Pierson, P., Bethune, K. P., Hartt, W. H., Anathakrishnan, P. *Corrosion*, 56(4), 350, 2000.
 116. Lee, Sang-Heog and Han, Jeong-Seb. *Corrosion*, 25(3), 340, 1996.
 117. Degerstedt, Ross M., Kennelley, Kevin J., Orazem, Mark E., Esteban, J. M. *Materials Performance*, 35(6), 16, 1996.
 118. Juchniewicz, R., Walaszkowski, J., Widuchowski, A. Stankiewicz, E. *Pol.Ochrona przed Korozja*, 27(10), 257, 1984.
 119. C. S. Chapra and Canale, R. P. *Numerical Methods for Engineers*, 2nd Ed. New York: McGraw-Hill, p. 734, 1988.
 120. C. A. Brebbia and S. Walker. *Boundary Element Techniques in Engineering*. London: Newness-Butterworth, 1980.

CHAPTER 25

TANKER CORROSION

Ge Wang

John S. Spencer

American Bureau of Shipping, Houston, Texas

Sittha Saidarasamoot

Swieng Thuanboon

Royal Thai Navy

| | |
|--|-----|
| 25.1 INTRODUCTION | 523 |
| 25.2 TANKER STRUCTURES | 527 |
| 25.3 CORROSION MECHANISMS IN TANKERS | 529 |
| 25.4 CORROSION STATISTICS | 534 |
| 25.5 CORROSION RISK TO STRUCTURAL INTEGRITY | 536 |

David L. Olson

Brajendra Mishra

Colorado School of Mines, Golden, Colorado

| | |
|---|-----|
| 25.6 MEASUREMENT AND MONITORING OF CORROSION DEGRADATION | 538 |
| 25.7 PREVENTION AND MITIGATION | 538 |
| 25.8 RELATED REQUIREMENTS IN MARINE INDUSTRY | 540 |
| 25.9 REFERENCES | 544 |

25.1 INTRODUCTION

The transportation of fuel and liquid chemicals is of strategic importance to international commerce. The energy and manufacturing sectors of modern civilization rely on the uninterrupted flow of these commodities. The result of expanding economies in both the developed and developing worlds and the uniform global distribution of fuel and chemical production sites have encouraged the use of extremely large tankers and has demanded an extended service life for many tankers.

As of October, 2003 there were approximately 3,578 oil tankers in service, totaling about 301,400,000 dwt [1]. Roughly 58% of them are double-hulled tankers. Tankers are commonly categorized based on their sizes as: Handy size (10,000–60,000 dwt), Panamax size (60,000–80,000 dwt), Aframax (80,000–120,000 dwt), Suezmax (120,000–200,000 dwt), and Very Large Crude Oil Carriers or VLCC (200,000 dwt and above). Figure 25.1 shows an oil tanker in service.

25.1.1 An Example of a Marine Incident Caused by Corrosion

On passage in the western Mediterranean with a full load of gasoline, the 30,577 dwt (deadweight tone) tanker, *M. V. Castor* encountered deteriorating weather conditions on December 26, 2000. During the night of December 30, the officer of the watch



FIGURE 25.1 An oil tanker.

reported a strong smell of gasoline. Daybreak confirmed that the vessel had suffered severe structural damage to the deck plating. When the weather abated, a close-up visual inspection was made during daylight hours on December 31, which confirmed that a series of cracks in the deck plating at the forward end of the three No. 4 tanks had spread an estimated 22 meters in length, which was almost the entire breadth of the vessel. The vessel's course was altered to bring the vessel to a port of refuge. It arrived at the port of Nador, Morocco on January 1, 2001.

The American Bureau of Shipping, which issued the safety certificates to the vessel following inter-

national regulations and design and inspection standards, released a technical report on this incident [2], and concluded that the near-disaster was largely attributable to severe corrosion in the deck area. The deck plates and the supporting members, deck longitudinals and deck girders suffered various degrees of corrosion. In some locations, the web plate of some deck longitudinals was totally wasted away. This situation caused loss of support of deck plates from deck longitudinals. The unsupported span of the deck plate increased, with a corresponding decrease in buckling strength. In heavy seas, buckling repeatedly occurred under the action of the cyclic

wave loads. Plastic deformation accumulated and eventually cracks appeared.

Figure 25.2 shows schematic of the *M. V. Castor* and damage location. Figure 25.3 shows the damage deck of the *M. V. Castor*. Clearly, the damage is accompanied by heavy corrosion and severe buckling deformation. Figure 25.4 shows the heavily corroded under-deck area. The structures internal to the tanks suffered a variety of corrosion wastage, which triggered the structural failure of the deck.

The severe loss of thickness of many structural members in not very accessible areas, due to aggressive corrosion, was the primary cause of the failure

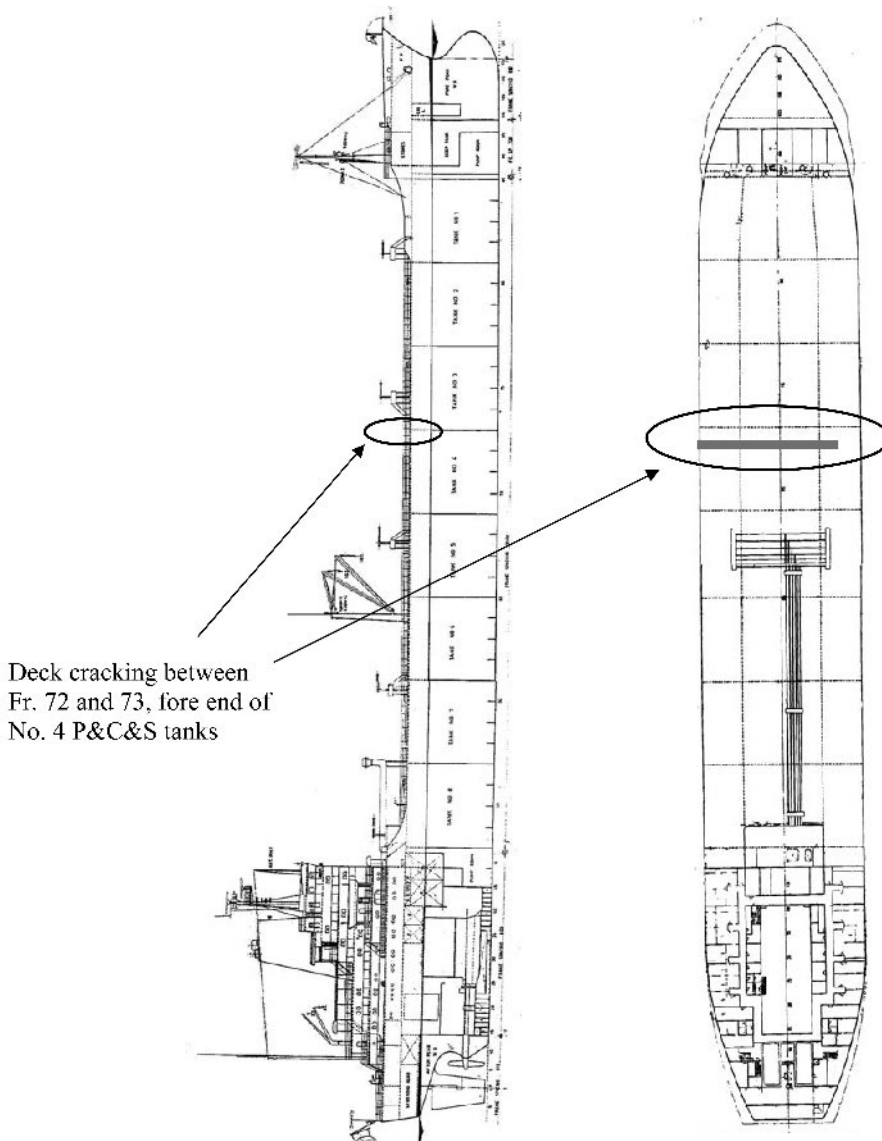


FIGURE 25.2 Schematic of *M. V. Castor* and location of damage [2].



FIGURE 25.3 Cracked deck of M. V. Castor [2].



FIGURE 25.4 Heavily corroded under-deck area of M. V. Castor [2].

of the *M. V. Castor* [2]. Heavy corrosion was associated with the breakdown of protective coatings of many interior parts of the tanks, especially the under-deck portion. After the coating breakdown, a combination of several factors, such as dynamic loading and cyclic stresses, repeatedly spalled the protective rust layer of the steel surface, resulting in a faster corrosion rate than that found in static structures where the products of corrosion are allowed to accumulate. Corrosion continued to compromise the thickness of the structural members, leading to initiation of the structural flexing. At this point, when flexing caused frequent spalling of the rust layer, the corrosion rate would accelerate and approach a value corresponding to that of free steel surface. The loss of thickness resulted in a loss of stiffness, and up to an extreme condition, a loss in load-bearing capacity. Eventually, this situation led to crack initiating and propagating across the deck at mid-section due to high stress-low cycle fatigue.

After the incident, the *M. V. Castor* was deemed totaled, and eventually scrapped. Repair of the ves-

sel having this extent of damage was not considered economically feasible, and even if repaired, it would be risky to use it again.

Transportation of oil using tankers is a business having very high liability. The *M. V. Castor* and *M. V. Nakhodka* incidents directly demonstrate the severe threat of corrosion to safety and the sea environment.

25.1.2 Economic Considerations

The primary cost of corrosion protection in tankers can be divided into two major categories [1,3]:

1. *The cost as part of the new construction of the ships.* These costs include corrosion-resistant materials, coatings, and cathodic protection systems installed during construction.
2. *The cost of repairs and maintenance.* These costs include the replacement of ship hull plates, the removal and reapplication of coatings, and the cost of the additional cathodic protection application. The downtime cost due to corrosion maintenance is included according to the revenue lost due to the ship being out of service while repairs and maintenance are being performed.

The majority of the corrosion prevention costs on new ship construction results from the application of coatings to the hulls, decks, and, most importantly, the ballast and storage tanks. The actual cost of applying a coating is relatively more than the cost of the coating materials themselves. The biggest portion of the cost of coating application comes from the surface preparation needed to prepare for coating. Most modern coatings require extensive surface grit blasting to remove all of the corrosion, scale, and other products on the steel. Without the proper surface preparation, the coating will not properly adhere to the steel surface and corrosion problems will be much more likely. Another large portion of the application cost of a coating is in the labor needed to properly apply the coating. The coating must be hand-applied to corners and other areas to ensure coverage of the edges when the coating shrinks while drying.

It has been estimated that for most ships, the cost of applying the coatings to a ship is 7% of the total building cost. While the cost of applying a proper coating is high, it was four to 14 times more expensive to replace corroded steel than to apply a coating during construction and then maintain that coating [4]. The cost for the coatings applied for oil carriers is slightly higher, at 10% of a ship's construction

cost. Oil tankers require better coatings than most of the industry due to the corrosive nature of the chemicals transported, such as the hydrogen sulfide present in crude oils. The cost of coatings for cruise ships is also approximately 10%. Some of this expense for cruise ships results from the need for better coatings for tanks that hold the wastewater. An estimate was made that cathodic protection systems and corrosion-resistant materials add an additional 3% to the building cost. For most classes of ships, the total cost of corrosion protection for a new construction can be estimated at 10% of the total construction cost, with oil tankers and cruise ships having slightly higher corrosion protection expenditures, 13%. The exception to this general range of numbers is the class of chemical tankers, because the storage tanks in these ships are made of stainless steel in order to be resistant to the chemicals that they transport. Because of this need, the literature estimates that the cost of corrosion protection for a chemical tanker is 30% of the new build cost.

To estimate the total cost of corrosion for new ship construction, data on the number of ships in the world were combined with an estimate of the average cost of a vessel for each type of ship and the percentage of the construction cost attributable to corrosion protection. This information is reported in Table 25.1. To calculate an average cost per year, the number of ships was multiplied by the estimated vessel cost and the percentage of the vessel cost attributable to corrosion. The sale prices of several new and used vessels of various ages were used to estimate the average cost for each class of ship. This resulting value was then divided by 25 years, which is the average life of ships, to obtain an average cost

per year. As indicated in the table, the world cost of corrosion from new ship construction is approximately \$7.5 billion per year. If 15% of the world cost is attributable to the United States, the annual cost of corrosion from new ship construction in the United States is estimated at \$1.12 billion.

The second portion of the cost of corrosion in the shipping industry is the cost of corrosion repairs and maintenance, as well as the downtime needed to perform these repairs. Table 25.2, based on literature and discussions with industry experts, shows the average estimated cost of annual repairs for each class of ship, including the cost of downtime associated with the cost of the repairs. To calculate the total costs, the number of ships of each type was multiplied by the repair and downtime estimates. The total cost for repairs for the world shipping sector was calculated at \$5.4 billion per year, while the cost of downtime was estimated at \$5.2 billion per year. The U.S. portion of these annual costs would be estimated at \$810 million for repairs and \$785 million for downtime.

From the cost estimates of new construction and repair maintenance, the total cost of corrosion in the shipping industry can be estimated. The yearly cost of increased corrosion resistance in new ship construction in the United States was estimated at \$1.12 billion, and the cost of repairs and maintenance was estimated at \$810 million, with the cost of downtime at \$785 million. Therefore, the total cost of corrosion for the U.S. shipping industry is estimated at \$2.7 billion per year. Such costs warrant the exploration of advanced nondestructive methods for the detection and measurement of corrosion and wastage associated with ships.

TABLE 25.1 Average Corrosion Cost per Year Due to New Construction for Each of the Major Types of Ships [3]

| Type of Ship | Number of Investigated Ships | % Cost of Construction Due to Corrosion | Average Cost per Vessel (\$x million) | Average Corrosion Cost per Year (\$x million) |
|--------------------|------------------------------|---|---------------------------------------|---|
| Oil tankers | 6,920 | 13 | 50 | 1,799 |
| Chemical tankers | 2,471 | 30 | 50 | 1,483 |
| Bulk dry | 6,252 | 10 | 20 | 500 |
| Cargo/Roll on-off | 18,611 | 10 | 15 | 1,117 |
| Fishing | 23,711 | 10 | 5 | 474 |
| Supply/Tugs | 12,954 | 10 | 11 | 570 |
| Refrigerated cargo | 1,441 | 10 | 6 | 35 |
| Cruise | 337 | 13 | 20 | 350 |
| Passenger/Ferry | 5,386 | 10 | 24 | 517 |
| Others | 7,724 | 10 | 20 | 618 |
| | | | World Total | \$7,463 |

TABLE 25.2 Estimated Average Corrosion Cost per Year Due to Maintenance, Repairs, and Downtime for Each of the Major Types of Ships [3]

| Type of Ship | Number of Investigated Ships | Average Corrosion Repair Cost per Ship (\$x thousand) | Total Yearly Repair Cost (\$x million) | Average Corrosion Downtime Cost per Ship (\$x thousand) | Total Yearly Downtime Cost (\$x million) |
|--------------------|------------------------------|---|--|---|--|
| Oil tankers | 6,920 | 200 | 1,384 | 140 | 969 |
| Chemical tankers | 2,471 | 300 | 741 | 140 | 346 |
| Bulk dry | 6,252 | 50 | 313 | 56 | 350 |
| Cargo/Roll on-off | 18,611 | 50 | 931 | 73 | 1,303 |
| Fishing | 23,711 | 25 | 593 | 20 | 474 |
| Supply/Tugs | 12,954 | 50 | 648 | 50 | 648 |
| Refrigerated cargo | 1,441 | 50 | 72 | 50 | 72 |
| Cruise | 337 | 200 | 67 | 1,000 | 337 |
| Passenger/Ferry | 5,386 | 50 | 269 | 56 | 302 |
| Others | 7,724 | 50 | 386 | 56 | 433 |
| | | World Total | \$5,404 | World Total | \$5,234 |

25.2 TANKER STRUCTURES

The structure of tankers is complex. The hull structures are designed to have adequate strength against failures of yielding, buckling and fatigue. Corrosion has always been identified as being important both for the integrity and economic concern for commercial tankers. Corrosion can cause wastage of the hull plates, reducing load-bearing capacity of structural members. Even though there are numerous methods for corrosion mitigation and protection which include coatings, cathodic protection, and use of corrosion resistance materials, there is always the continuous loss of materials, demanding steel replacement under some circumstances.

25.2.1 Double-Hull Tankers

The majority of tankers are single-hulled, where there is only one layer of steel separating the carried oil and sea water. The schematics of a single-hull tanker are shown in Figure 25.5.

On March 24, 1989, the *Exxon Valdez* ran aground in Prince William Sound, Alaska, causing 42 million liters (11 million gallons) of crude oil to be spilled. The clean-up cost was in billions of dollars. To avoid similar accidents in the future, the U.S. Congress passed the Oil Pollution Act in 1990 (OPA90). This law required all new tankers operating in the United States to be built with a double hull. OPA90 is followed by the International Maritime Organization (IMO), a United Nations organization that is devoted to safety at sea. Now all oil carriers are built with a double hull [6].

A double-hulled ship is built with an additional inner hull. The space between the inner and outer hulls is not used for cargo, but can be used for ballast, so if the outer hull is penetrated, the cargo would still be protected within the inner hull, avoiding pollution from spilled cargo oil. A schematic of double-hulled ship structure is illustrated in Figure 25.6.

Though all new construction of tankers are double hulls, single-hull tankers are the dominant vessels transporting oil around the world. The latest tanker accidents, such as *M. V. Castor* and *M. V. Erika*, have caused heightened concerns over the safety of tankers, and more and more countries are moving forward to accelerate the phasing-out of single-hull tankers.

The experience with double-hulled tankers is limited. Most double-hulled tankers were built in the 1990s and have had less than 10 years of service. Some double-hulled tankers have experienced corrosion much earlier than would be expected from single hulls. Causes are being investigated, but are not fully understood.

The additional layer of steel of the double-hulled increases the size, weight, and amount of steel needed to build a ship that will carry the same amount of oil. Because of the increased volume and weight, naval architects often decided to use more high-tensile strength (HT) steel in the design of new double-hulled tankers. By using HT steel, thinner steel plates can be used, while still satisfying the scantling requirements of the various classification societies. The combined effect of double-hull design and increased use of HT steel results in a reduction

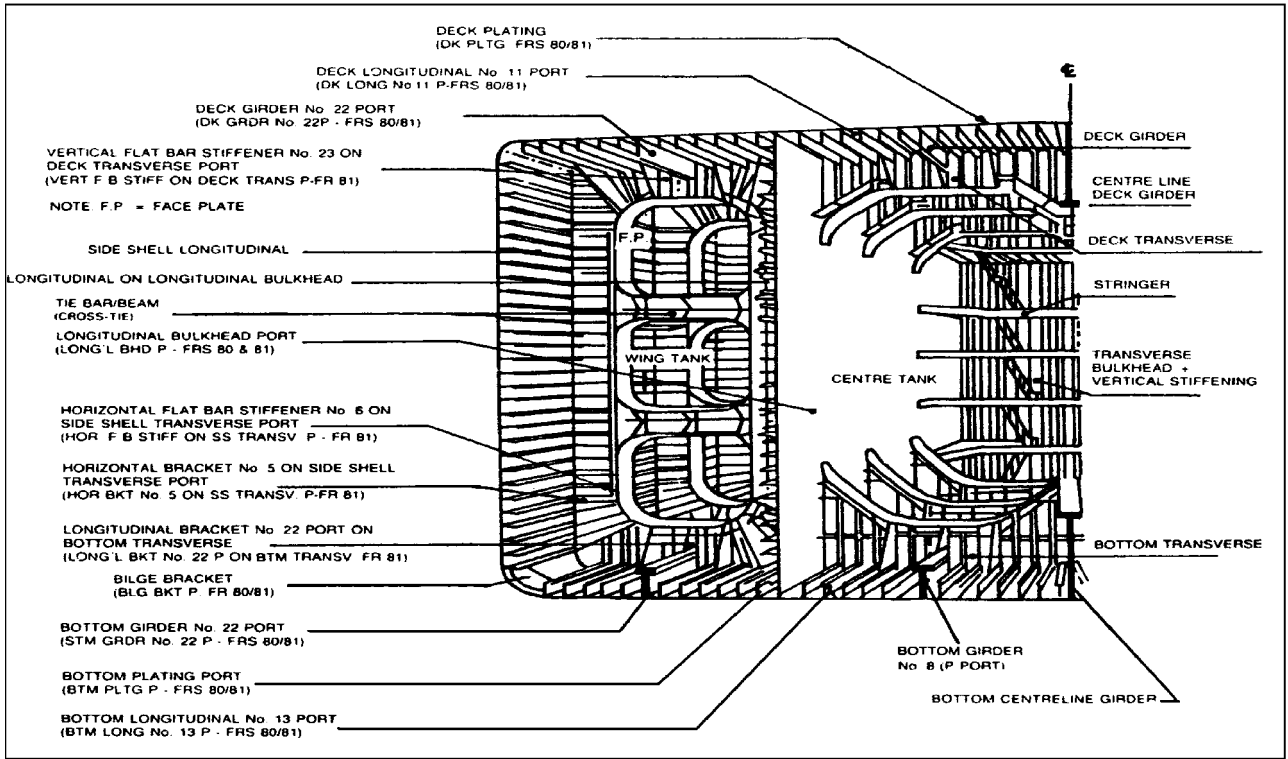


FIGURE 25.5 Illustration of the complex internal structures of a single-hull tanker [5].

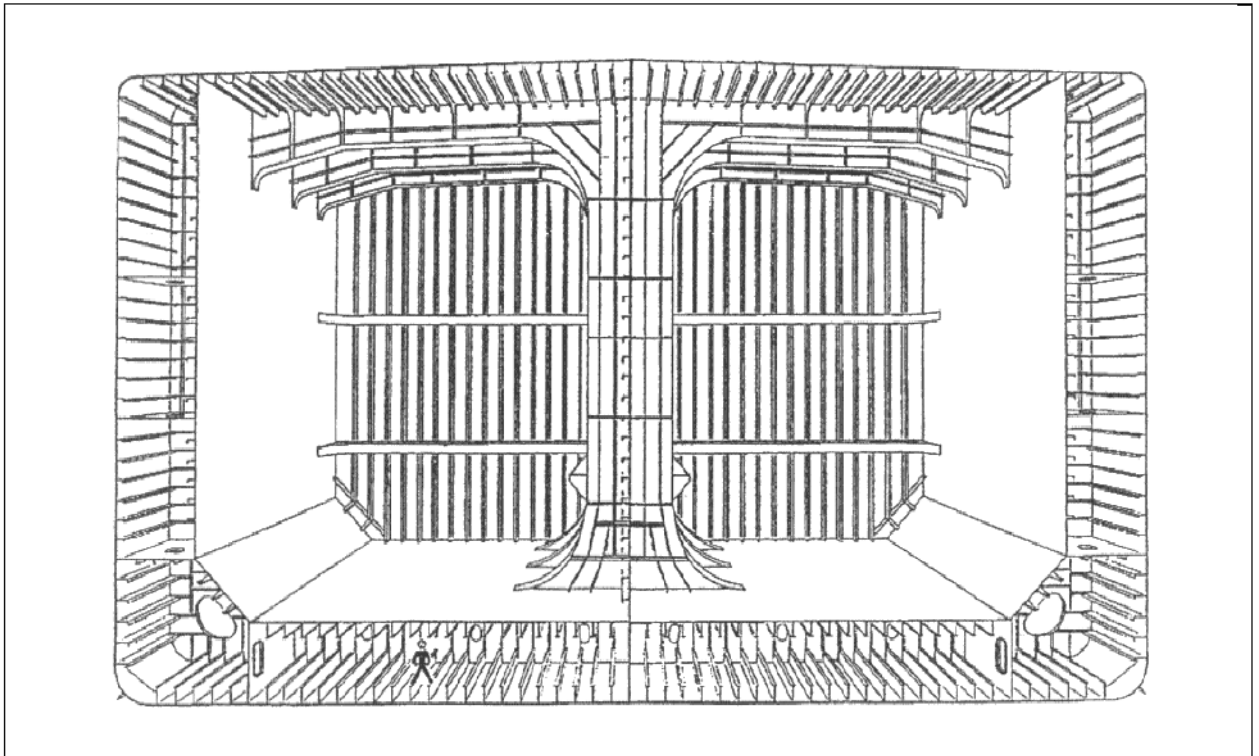


FIGURE 25.6 Schematic of double-hull ship structure [5].

of about 20% in plating thickness in certain areas (for example, see the statistics of structural scantlings of oil tankers by Wang and Spong [7]). Therefore, the hull will flex more with wave motion and movement of the cargo within the tanks. Areas such as the deck, inner skin, inner bottom, and bottom shell may be subject to increased deflections. This movement could particularly accelerate corrosion on under-deck surfaces, thereby loosening scale and rust and exposing a new layer of steel to corrosion environment. This greater flexing of the thinner scantling can be considered the “dynamic accelerator” in the corrosion process.

Beyond the dimensional differences between single and double-hulled tankers, differences between the environments in the cargo tanks have also been found. The cargo tanks in double-hulled tankers are usually warmer due to the thermos effect. When the oil is loaded into a tanker, it generally cools down to the temperature of the surrounding water within a couple of days for a single-hulled tanker. However, for double-hulled tanker, it may take much longer to reach sea temperature because the outer hull creates an interspace which acts as an insulator. The temperature may never reach sea temperature on short voyages. Following an Arrhenius behavior, the corrosion rate doubles for every 10 °C increase in temperature; therefore, if the average temperature of the tank is 20 °C warmer, then the average corrosion rate is quadrupled. Furthermore, many of the coatings, particularly tar epoxies, do not handle high temperatures well and will degrade more rapidly.

25.2.2 Floating Production, Storage, and Offloading (FPSO) Vessels

Because of the length of time and high cost of transporting oil and gas from reservoir to production facilities on land, oil and gas industries try to minimize these costs by using facility platforms and Floating Production, Storage and Offloading (FPSO) systems. A FPSO system is an offshore production facility that is typically ship-shaped and stores crude oil in tanks. The crude oil is periodically offloaded to shuttle tankers for transport to shore. FPSOs may be used as production facilities to develop marginal oil fields or fields in deep-water areas remote from the existing OCS pipeline infrastructure. Additional information about FPSOs can be found in references 8, 9, and 10. There are approximately 85 FPSOs currently operating around the world. There are approximately 10 FPSO units coming on line per year worldwide, and 80 or more FPSOs are planned or

under study for future field developments [11]. Of this fleet of FPSOs, approximately 65% are converted from trading tankers, primarily older vintage single-hull tankers. Figure 25.7 shows the *Terra Nova* FPSO and Figure 25.8 illustrates the schematic of an FPSO with upper deck modules.

Compared to the trading tankers, FPSOs have very limited corrosion experience, with an estimated total cumulative operating experience in the range of only 500–600 years [7]. This experience is compared to other offshore installations such as fixed platforms, which have well over 100,000 combined operating years of experience, with many platforms still in operation 10–20 years after their 20-year designed life. In comparison, FPSO installations tend to be in their infancy, with only 15% of the fleet having been in operation for more than 10 years. Because of this situation, there is a lack of systematic experience-based data for conceptual and preliminary design, or for the evaluation of the long-term performance specific to ship-shaped FPSOs. At the same time, there is an increasing interest in their application, and the number of FPSOs is growing. This combination makes the development of relevant design data both necessary and very useful. Because of the obvious similarity between tankers and FPSOs, the tankers experiences are heavily relied upon. Almost all the design and inspection standards for FPSOs are based on those standards for tankers.

25.3 CORROSION MECHANISMS IN TANKERS

25.3.1 Types of Corrosion in Tankers

Three types of corrosion have been found to commonly exist within ships [13,14]: general, pitting and grooving corrosion.

25.3.1.1 General Corrosion

General corrosion is the most common type of corrosion in ship structures. The corrosion product appears as a non-protective rust which can uniformly occur on uncoated internal surfaces of a ship. The rust scale continually breaks off and exposes fresh metal to the corrosive environment. The rust scale also appears to have a constant thickness and similar consistency over the surface. The mechanism of general corrosion is demonstrated in Figure 25.9.

There are micro-cathodic and anodic areas caused by variations in grain structure, impurities in the



FIGURE 25.7 Photograph of Floating Production, Storage and Offloading (FPSO) vessel [12].

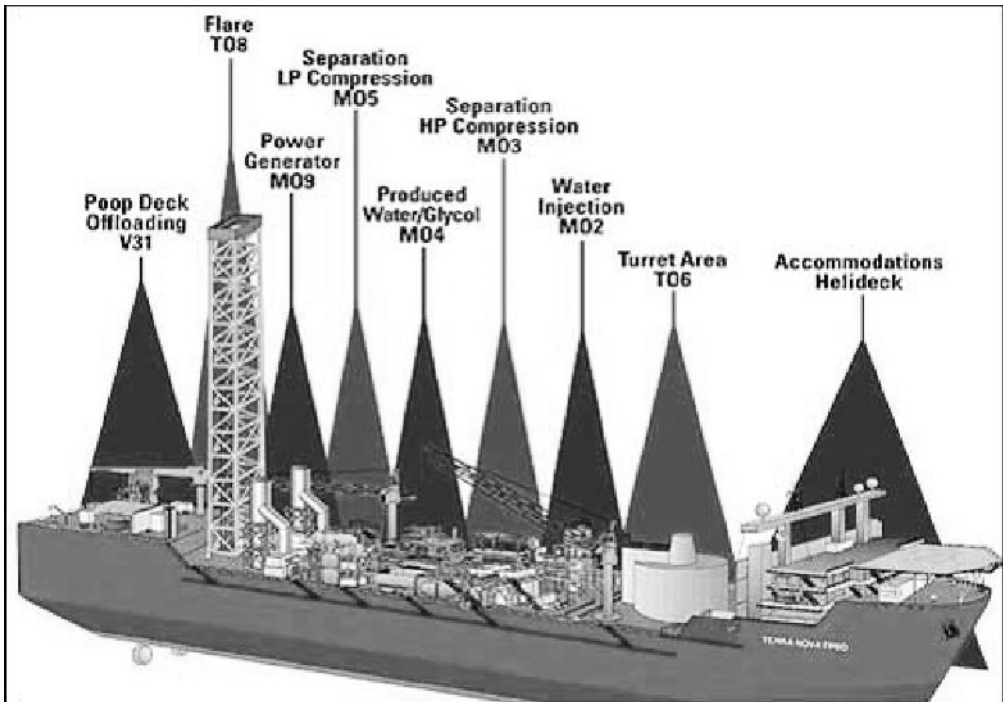


FIGURE 25.8 Schematic of Floating Production, Storage and Offloading (FPSO) Vessel [12].

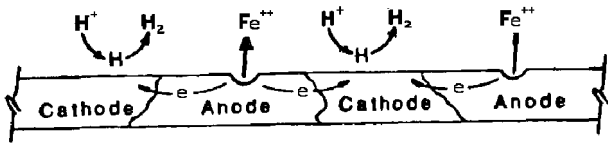


FIGURE 25.9 General corrosion [14].

metal, alloying elements, and other inhomogeneities. For general corrosion, the cathodic and anodic areas constantly switch back and forth due to a difference in potential or degree of polarization, thus accounting for the uniform corrosion of the surface.

25.3.1.2 Pitting Corrosion

Pitting corrosion is a localized corrosion that occurs on bottom plating, other horizontal surfaces, and at structural details that trap water. This damage is a very serious type of corrosion—the attack produces deep and relatively small-diameter pits that can lead to hull penetration in isolated random places with the consequent pollution risk. Pitting is often described as cavities whose sites of corrosive attack are relatively small compared to the overall exposed surface. It is a localized form of corrosion and usually grows in the direction of gravity. It is also self-generating (i.e., autocatalytic), starting from impurities in the metal, scale or other deposits, or some inhomogeneity in the metal. Figure 25.10 illustrates the progressive pit being formed. Pitting requires the breakdown of the protective film.

25.3.1.3 Grooving Corrosion

Grooving corrosion is a specialized form of erosion corrosion which also occurs frequently within ships. This corrosion, sometimes referred to as “in-line pit-

ting attack,” is a linear corrosion occurring at structural intersections where water collects or flows. Grooving can also occur on vertical members and flush sides of bulkheads.

All metals, even stainless steel, may incur corrosion from microbiologically-influenced corrosion (MIC). Corrosive bacteria thrive in low oxygen or oxygen-free environments and require some type of food source. Most of these types of bacteria convert sulfur to H_2S , which is an active reagent to promote an acid corrosive environment. In an ideal environment, microbes might double their mass every 20 minutes [15], but such condition rarely exist on board vessels. On board ships, microbes can thrive in the water layer at the bottom of oil cargo tanks and in the sediment in ballast tanks. Once bacteria become established, they become difficult to control and may corrode steel up to 1.6–3.2 mm per year.

25.3.2 Major Corrosion Mechanisms in Different Locations

Generally stated, marine corrosion of structural steel will occur wherever salt water is present. However, corrosion also occurs in areas of the ship that are not directly exposed to salt water. Many factors, associated with the cargo as well as ship operations, often combine to create corrosive environments within ships.

All cargo ships experience corrosion; the extent and severity depend on such factors as cargo, temperature, humidity, and protection system. Ballast tanks in all ships will have similar corrosive patterns but dry cargo compartments will not suffer the same amount of corrosion wastage as liquid cargo compartments. The majority of internal structures within a ship usually experience corrosion to a certain extent. Horizontal structural members encounter the

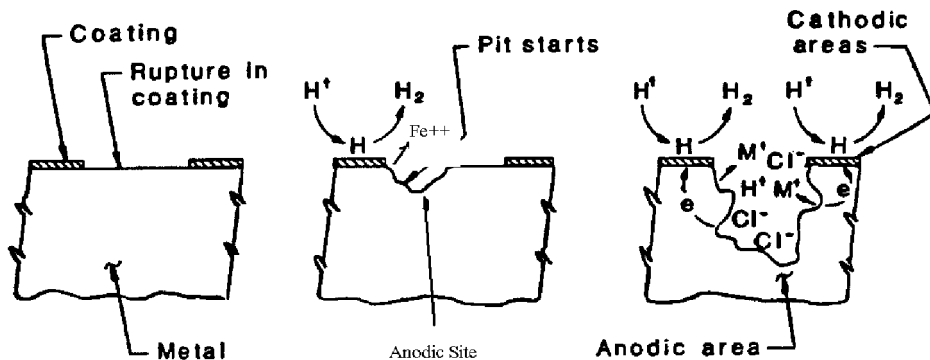


FIGURE 25.10 Pitting corrosion [14].

greatest corrosive attack, simply because they collect and trap water, which facilitates pit growth.

Locations where corrosion will most likely affect structural integrity are described in the following sections.

25.3.2.1 Bottom Plating

The bottom plating within a ship typically experiences the greatest amount of corrosion wastage due to collection of water on the bottom plate, resulting in pitting, grooving, and general wastage. For coated plating, wastage will take the form of localized pitting and grooving by way of coating failure. For inorganic zinc coatings, the wastage will tend to be patches of scaly areas with only minimal thickness loss. For coal tar epoxy-coated plating, wastage will tend to be deep pits of limited area that present a definite risk of bottom penetration if not repaired.

For uncoated tanks, bottom wastage is more general; the higher velocity flow paths of the drainage patterns are affected to a greater extent than stagnant areas. Thus, wastage is highest by way of cutouts in transverse web frames and bottom longitudinals, and lowest just forward and aft of web frames outside the line of the cutouts. Figure 25.11 illustrates an example of this loss pattern. Bottom wastage gen-

erally increases from forward to aft, most likely due to water wedges caused by the normal trim patterns by the stern, both in full load and ballast. However, this characteristic can be reversed on some ships where the tendency is to trim slightly by the bow in the full load condition. The water wedges are a combination of unstrippable ballast water and water settling out from cargo within certain compartments. Thus, aft bays of liquid cargo and ballast tanks can experience corrosion almost continuously. Grooving of the welds of bilge longitudinals as well as thinning and cracking at the toes of longitudinal girder brackets also occur on bottom plating and often on other typical areas of bottom structure.

The bottom structure is an important area to survey because it is where corrosion is most prevalent and it is a location critical to structural integrity.

25.3.2.2 Side Shell and Bulkhead Stiffeners

Wastage patterns on the side shell and the stiffened sides of bulkheads are usually limited to the horizontal webs of the stiffening. In coated tanks, wastage occurs by way of coating failures which generally start at welds, cutouts and sharp edges. In uncoated tanks, wastage is more general and usually increases toward the bottom of the tank. Deep pitting

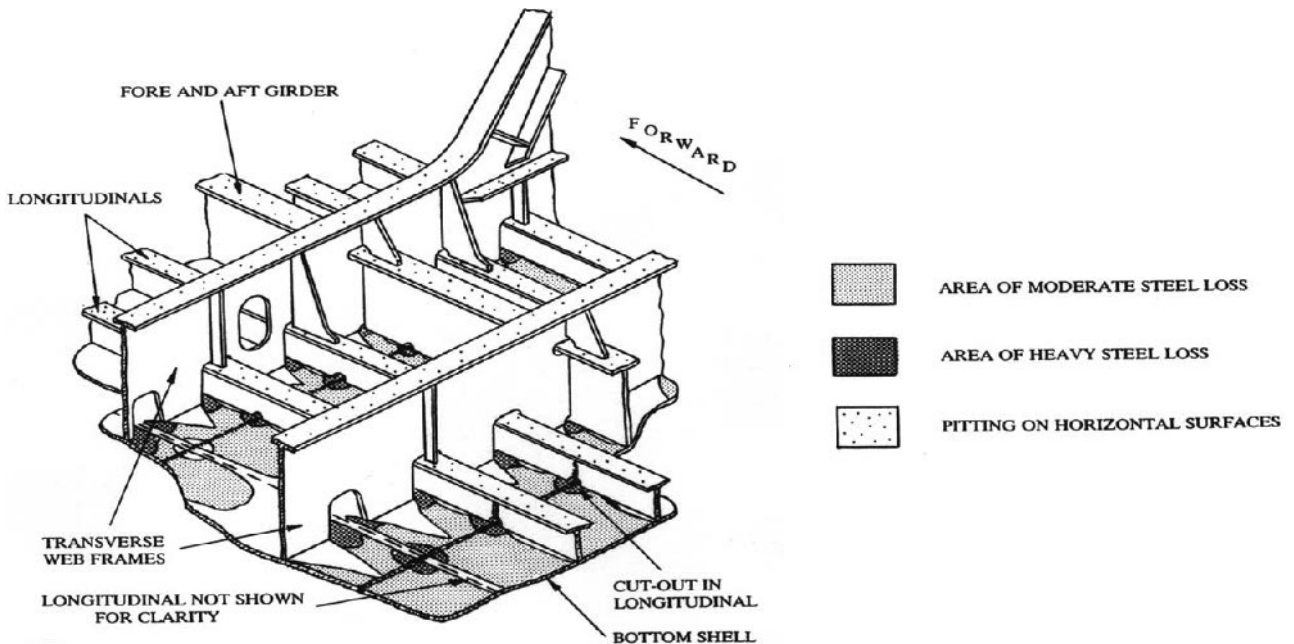


FIGURE 25.11 Schematic of steel degradation in ship bottom plate [14].

is often found on lower stiffening, usually near web frames. On ships with fabricated longitudinals where the flat face extends above the web, wastage can be rather severe due to the trapping of water on the web.

25.3.2.3 Under Deck Areas

Corrosion wastage may occur at connections of deck longitudinals to deck plating by way of coating failure. Uncoated compartments suffer more uniform corrosion both when empty and when full of either liquid cargo or ballast. When the compartment is empty, the area is subject to a highly corrosive, moist, salt-laden atmosphere. Oxygen is readily available high in the compartment from hatches, vents and deck openings, and contributes greatly to the uniform corrosion process. When a compartment is full of ballast or liquid cargo, general wastage results from the same causes in this ullage space area because the deckhead is not protected by an oil film. Deck platings are important structural locations to survey because these structural members are the most critical to the structural integrity of the hull as a whole.

25.3.2.4 Special Locations

There are other special locations that should be surveyed where local corrosion is prevalent. Wastage can occur in high stress areas where coatings break down and corrosion attack begins. These locations include longitudinal cutouts in frames. The plating under bellmouths is vulnerable to general wastage in both coated and uncoated tanks due to the added effects of high velocity during ballast discharge. Other special locations should be surveyed where structural integrity is reduced or in areas where watertight integrity is reduced.

25.3.3 Corrosive Environments in Tankers

Different ship types have different corrosion mechanisms. Various corrosion mechanisms can exist in any particular location. For example, the under-deck area is subjected to “sweet” CO_2 corrosion and “sour” H_2S or sulfur corrosion.

There are many factors that influence corrosion. These factors may include [16–19]:

- Coating: Coating type and longevity, surface preparation and coating application, coating breakdown

- Cathodic protection
- Corrosion environment: Composition and properties of cargo, humidity, temperature, acidity, salinity, presence of oxygen
- Operation: Time in ballast, trading route, tank washings, inert gas
- Microbial-induced corrosion
- Structural designs

These factors make up only a partial list. Many factors interact with others, complicating the problem further. The itemized factors discussed hereafter pertain mostly to the mechanisms of corrosion in marine structures and tankers [21].

25.3.3.1 Diffusion

Corrosion rates are controlled by diffusion of reactants to and from the metal surface. Exposed bare steel surfaces will corrode at a greater rate than those surfaces covered with a coating or a compact layer of rust. The corrosion is also controlled by the diffusion of oxygen through the water to the surface. High flow areas such as in the vicinity of bellmouths will corrode at high rates because of the increase in oxygen concentration. Areas covered by a thin, conducting, moisture film such as in a ballast tank or the ullage space at the top of the tank (where air is trapped) tend to corrode the steel faster than the submerged areas where there is a lower oxygen level.

25.3.3.2 Temperature

As corrosion rates are controlled by the diffusion of reagent and chemical reactions, both chemical reactions and diffusion are a strong function of temperature. The higher the temperature, the faster the corrosion rate will be obtained. The corrosion will be more complex in double-hulled tankers due to the difference of inner and outer shell and heat transfer concerns.

25.3.3.3 Conductivity

The corrosion rates will increase as the conductivity of the medium increases due to the presence of more ions in the solution. Aqueous corrosion requires an electrical circuit between anodic and cathodic surfaces within an electrolyte. The corrosion rate of steel reaches maximum at close to the normal ionic content of sea water (approximately 3 mol.pct).

25.3.3.4 Type of Ions

There are some types of ions in sea water or in cargoes that affect corrosion. For example, chloride ions are the most destructive, while sulphate and other sulfur-containing ions also represent a major problem.

25.3.3.5 Acidity and Alkalinity (pH)

The corrosion rate varies due to changes in the cathodic reduction reaction. In the intermediate pH of 4–10 range, the corrosion rate is nearly constant where a passive oxide or hydroxide film is stable. Many of the common constructional metals, such as copper, iron and nickel, have increased corrosion in low pH solutions due to the higher availability of oxidizing H^+ and solubility of oxides.

25.4 CORROSION STATISTICS

Statistics reveal that corrosion is the number one cause of marine casualties in old ships [22]. Damage

to ships due to corrosion is very likely, and the likelihood increases with the aging of ships.

25.4.1 Collective Data

The Tanker Structure Co-operative Forum (TSCF) publications [19] are widely referred to and generally regarded as the best source of information on corrosion in tankers. The information is based on the inputs from the TSCF members, including the major oil companies and leading classification societies. The collective data of TSCF has influenced the design, maintenance and inspection of tankers since its inception. In addition to TSCF, there have been some other similar studies in the last 10 years (e.g., Paik et al., 2003 [17], Wang et al., 2003 [21], Harada et al., 2001 [22]).

The common finding from the review of corrosion measurement data has been that ballast tanks experience the highest corrosion rate, as seen in Table 25.3. This finding is due to the greater exposure of metal to salt water, increasing the corrosion rate. However, a recent statistical study [18,23]

TABLE 25.3 Corrosion Rate for Various Structural Members [19,23]

| Structure | Tank | Wang et al. (2003) | | | TSCF (1992) |
|---------------|-----------|--------------------|-----------|---------|-------------|
| | | Mean | Deviation | Maximum | Range |
| Dk pl | Cargo | 0.066 | 0.069 | 0.580 | 0.03–0.10 |
| | Ballast | 0.055 | 0.042 | 0.277 | 0.10–0.50 |
| Dk long web | Cargo | 0.055 | 0.055 | 0.807 | 0.03–0.10 |
| | Ballast | 0.047 | 0.051 | 0.444 | 0.25–1.00 |
| Dk long fl | Cargo | 0.037 | 0.030 | 0.243 | — |
| | Ballast | 0.044 | 0.041 | 0.175 | — |
| Side shell | Cargo | 0.044 | 0.046 | 0.547 | 0.03 |
| | Ballast | 0.043 | 0.038 | 0.573 | 0.06–0.10 |
| Side long web | Cargo | 0.040 | 0.034 | 0.567 | 0.03 |
| | Ballast | 0.042 | 0.042 | 0.800 | 0.10–0.25 |
| Side long fl | Cargo | 0.033 | 0.021 | 0.171 | — |
| | Ballast | 0.032 | 0.030 | 0.482 | — |
| Btm shell | Cargo | 0.085 | 0.076 | 0.690 | 0.04–0.30 |
| | Ballast | 0.049 | 0.051 | 0.320 | 0.04–0.10 |
| Btm long web | Cargo | 0.032 | 0.022 | 0.207 | 0.03 |
| | Ballast | 0.027 | 0.020 | 0.117 | — |
| Btm long fl | Cargo | 0.047 | 0.062 | 0.730 | — |
| | Ballast | 0.045 | 0.066 | 0.700 | — |
| Long bhd pl | Btw cargo | 0.049 | 0.059 | 0.654 | 0.03 |
| | Others | 0.051 | 0.046 | 0.470 | 0.10–0.30 |
| Bhd long web | Cargo | 0.038 | 0.031 | 0.411 | 0.03 |
| | Ballast | — | — | — | 0.20–1.20 |
| Bhd long fl | Cargo | 0.045 | 0.044 | 0.782 | — |
| | Ballast | — | — | — | 0.20–0.60 |

[Unit: mm/year] Abbreviations: btw = between, bhd = bulkhead, dk = deck, fl = flange, long = longitudinal, pl = plate.

shows a different trend: Corrosion wastage in cargo oil tanks is found to be much more severe than that of ballast tanks. This trend may be attributed to the fact that ballast tanks are now coated while cargo oil tanks are not required to be coated.

25.4.2 Corrosion Rate Studies

Figure 25.12 shows schematically the available models for corrosion wastage published to date. These models are used for assessing structural conditions resulting from corrosion and to clarify the nature of corrosion behavior. They do not address the mechanics of corrosion.

Typically, it is assumed that corrosion does not take place when a coated structure is first placed in service. Usually, this service experience is the period before the coating breaks down and loses its effectiveness in protecting the steel. After that, corrosion begins and wastage increases over time.

For the second stage of corrosion, there are three types of models for corrosion progress:

- *Corrosion wastage linearly increases with time (line a).* This behavior is perhaps the most common and most widely used assumption in structural strength analyses. It assumes that the corrosion is a general attack and that the resulting corrosion product does not serve as protecting barrier for the corrosive reagents. It suggests that the chemical reaction at the interface between the metal and the corrosive media is the rate-controlling mechanism. This mechanism of corrosion is activation-controlled. Examples are TSCF [19] and Paik et al., 2003 [17].

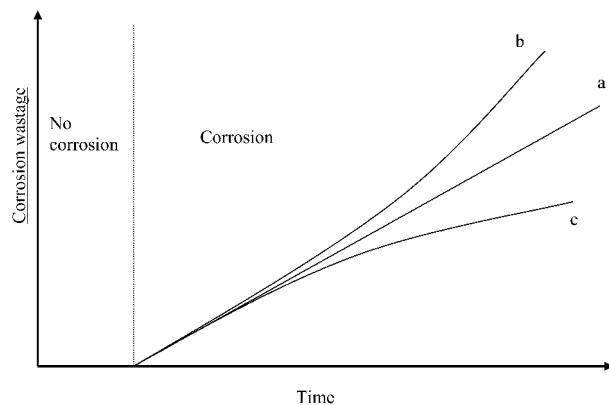


FIGURE 25.12 Existing models for corrosion progress.

- *Corrosion increases and accelerates over time (line b).* This behavior occurs when rust buildup is disturbed as a structure flexes under the wave action [19,24]. This behavior causes the degradation of the protective coating. When the coating is no longer a barrier, then the rate potentially achieves the high and fairly constant value of the chemical attack on a free metal surface.
- *The rate of corrosion wastage slows down with time (line c).* This occurs when the steel is gradually covered by scale and rust, preventing further exposure of new steel to corrosive environment. This scale indicates some degree of hindrance to the transport of corrosive reagent through the scale. As the scale grows, the rate parabolically reduces in time. This mechanism of corrosion is diffusion-controlled. Sometimes a paralinear behavior is achieved where both the interfaces (metal-scale and scale-corrosive fluid) exhibit loss behavior. Here the corrosion rate starts out parabolically with time and changes to a linear rate. An example may be found in Yamamoto and Ikegami 1998 [25].
- As a variation of line c, corrosion wastage eventually approaches a constant linear rate (paralinear behavior). Paralinear behavior suggests two moving boundaries. The metal is corroding at the metal/scale interface and the thick scale is exfoliating at the scale/liquid interface. An example may be found in Guedes Soares and Garbatov 1996 [26].

The corrosion rate is the slope of the lines in Figure 25.12. Obviously, the corrosion rate in existing models can be linear, parabolic and paralinear. These models offer some interpretation to the corrosion attack. They may be useful for some situations, but not all situations. The nature of a marine environment, with its continuously varying parameters, makes developing mechanistic modeling difficult. Statistical analysis with a parabolistic interpretation offers the best predictions. Such analysis requires a larger data set of corrosion measurements.

25.4.3 High Corrosion Rates for Flexing Structural Members

The corrosion rate of steel in sea water in terms of exposure time is illustrated in Figure 25.13. It can be seen that the initial corrosion rate is very high for carbon steel in sea water. As the ship ages and thins in many different areas, some of which are hard to coat and difficult to monitor, the thinner members

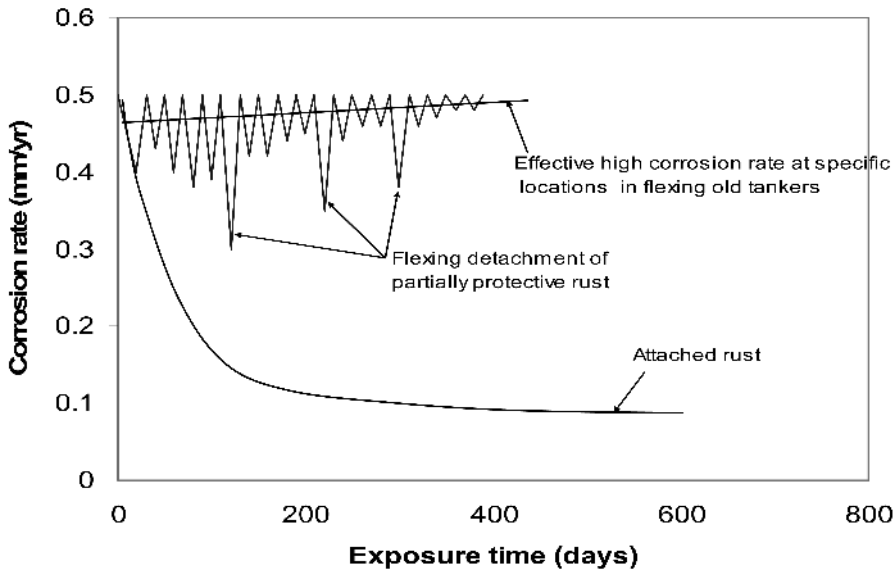


FIGURE 25.13 Corrosion rate prediction of ship steel in sea water with and without flexing [24].

are more prone to flexing in heavy seas. During regular sea conditions, corrosion of steel members will have formed a partial protective barrier of rust. This rust layer is the reason why laboratory corrosion coupon tests in stationary sea water report a reducing corrosion rate with exposure time. But during heavy sea conditions, the flexing of these members will detach the rust barrier, allowing accelerated corrosion of unprotected steel. Older ships, which have often gone without significant maintenance or replacement of corroded structural sections, sometimes exhibit the extremely high corrosion rates, as suggested in Figure 25.13. The flexing initiates the detachment of coatings that subsequently leads to accelerated corrosion of bare steel.

25.5 CORROSION RISK TO STRUCTURAL INTEGRITY

Corrosion is a major cause of marine structural failures. Corrosion results in a loss of structural strength at local and global levels, and leads to fatigue failure and stress corrosion cracking. Some recent marine incidents with tankers have been directly linked to accelerated corrosion.

The risks of corrosion wastage to aging ships' structural integrity have been assessed using the observations of the corrosion wastage database [17,18, 26,27]. The investigated risks are loss of local struc-

tural member's strength, loss of global hull girder strength, and shortened maintenance intervals.

25.5.1 Corrosion Causes Loss of Strength of Individual Structural Members

Some recent oil tanker incidents took place when ships were loaded in a sagging condition. Deck plates were under compression and, as a result, buckling and ultimate strength were reduced due to reduced plate thickness, which led to catastrophic failure.

Table 25.4 shows the loss of buckling strength of deck plates assuming that they are 20 years old and have different levels of corrosion wastage. The plates are compressed at the shorter edges from lon-

TABLE 25.4 Buckling Strength of Deck Plates for Different Levels of Corrosion Wastage [18]

| Ship | Corrosion | Thick (mm) | Buckling/yield |
|------|-----------|------------|----------------|
| SHT | As-built | 24.0 | 0.832 |
| | Slight | 23.4 | 0.824 |
| | Moderate | 22.9 | 0.816 |
| | Severe | 20.5 | 0.770 |
| DHT | As-built | 19.0 | 0.788 |
| | Slight | 18.4 | 0.774 |
| | Moderate | 17.9 | 0.761 |
| | Severe | 15.5 | 0.677 |

gitudinal bending of the hull girder. The slight, moderate and severe corrosion levels are corresponding to the 50th, 75th and 95th percentiles of collective databases of corrosion measurements. They may be regarded as the results of different maintenance practices, though other factors such as coating condition may also play a role.

In the case of severe corrosion, the buckling strength of a deck plate is reduced by about 7% for the single-hull tanker (SHT), and by 14% for the double-hulled tanker (DHT). Combined with the reduced hull girder strength, the deck plates may buckle under heavy seas.

25.5.2 Corrosion Causes Loss of Hull Girder Strength

Hull girder section modulus is a well-accepted parameter measuring the longitudinal bending strength of ships. This modulus is perhaps the single most important design parameter describing hull girder strength. Hull girder section modulus to the deck often determines the bending strength of the entire hull girder.

Table 25.5 shows the loss of hull girder section modulus to deck as a result of different levels of corrosion wastage. When every structural member is severely corroded, the single-hull tanker (SHT) has an 11.5% reduction in hull girder strength, and the double-hulled tanker (DHT) has a 12.7% reduction [18].

TABLE 25.5 Hull Girder Section Strength for Different Levels of Corrosion Wastage for both Single Hull Tankers (SHT) and Double-Hulled Tankers (DHT) [18]

| Ship | SHT | DHT |
|----------|--------|--------|
| As-built | 100.0% | 100.0% |
| Slight | 97.0% | 96.7% |
| Moderate | 94.5% | 94.0% |
| Severe | 88.5% | 87.3% |

25.5.3 Severe Corrosion Requires More Frequent Inspection or Maintenance

Figure 25.14 is the estimated time-dependent annual reliability index of a stiffened plane at the bottom of a cargo hold of a single-hull tanker 232 meters in length. This bottom panel is acted upon by in-plane compression due to longitudinal bending, and by lateral loads due to water pressure. The ultimate strength of the panel is calculated and compared with the external loads. It is assumed that plates are replaced at special surveys when wasted by 20%. If corrosion remains slight, inspections at five-year intervals will be sufficient, and no plate renewals are needed for more than 30 years. When experiencing a moderate level of corrosion, inspections at five-year intervals seem sufficient for maintaining the reliability index at reasonable levels, though plate renewals are expected after 30 years in service. When experi-

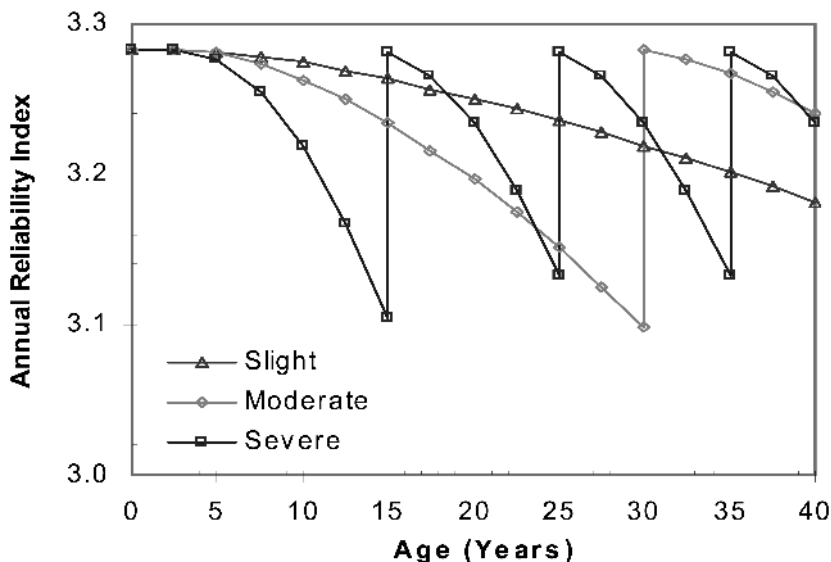


FIGURE 25.14 Annual reliability index of a stiffened panel at a tanker's bottom for different corrosion levels [18].

encing a severe level of corrosion, inspections at five-year intervals cannot prevent the reliability index from becoming too low.

25.6 MEASUREMENT AND MONITORING OF CORROSION DEGRADATION

Visual methods for ship inspection have been accepted for a long time. Different devices and techniques have been developed. Charge-coupled devices are relatively inexpensive, using optical scanning devices to record the images and then process them by computer. This technique can scan large areas such as ships but is limited to exposed surfaces only [28].

Ultrasonic thickness measurement is the primary means of detecting the remaining thickness of structural members. Ultrasonic waves have been used for the detection of a variety of material defects. By sending ultrasonic waves through substrates and measuring reflection and transmission amplitudes, traveling time, and attenuation, the discontinuities or internal defects can be detected and the plate thickness can be calculated. Time consumed to thoroughly test a large structure is the major disadvantage of ultrasonic measurement because of the need for point-by-point examination [29].

Furthermore, preparation of the surface and coupling media are required. For large area inspection, ultrasonic guided waves have been used. Now, ultrasonic thickness measurements are being used and accepted by many organizations and societies. The average plate thickness of a ship's hull can be determined. The new trends of measurement are concentrated on the measure of the thickness or corrosion wastage of the area or structure that affects the strength of the entire structure, or the area that has more risk of corrosion than the entire area of the vessel. The advantage of guided waves is the ability to travel along the surface and make measurements faster than with the use of bulk waves [30–32].

Marine structures are particularly challenging to assess for corrosion. Further investigation into this area is important because the corrosion damage is costly. Many new nondestructive evaluation techniques are being developed [24,33]. There are two categories of nondestructive methodologies that can be used to evaluate corrosion wastage in marine structures:

Active sensors: The sensors that are used to measure the corrosion features and location by way of active inspection are active sensors. The active

measurement should provide accurate data, clearly demonstrate characteristics of damage, and take a short time, appropriate to a limited maintenance time interval.

Passive methods: Passive methods include the sensors that have been set up to monitor the in situ condition of the inspected structure or provide continuous measurements. Passive sensors are often used for early warning, and active measurement is used after early warning or during the maintenance intervals.

Active and passive corrosion sensing and monitoring have been developed in several applications such as in aircraft, vessels, pipelines and offshore platforms. Varieties of techniques are used. The marine industry will experience more technical transfer of these advanced methods to improve its ability to predict time and location for plate replacement and repair.

25.7 PREVENTION AND MITIGATION

There are several ways to protect marine structures from corrosion damages, such as coatings, cathodic protection, or using corrosion resistant materials. Steel is often coated with paint, and sacrificial anodes are fitted at some locations. These practices serve to reduce and, in some instances, effectively deter corrosion and mitigate corrosion consequences.

25.7.1 Coatings

Coating is the most commonly used method for combating corrosion and is the best protective device for marine structures, whether high above water, at the splash line, or in immersed areas. It works on the principle of completely separating the metal from the corrodent or slowing down the reaction that may occur between the metal to be protected and the corrodent. Detection of coating degradation and damages are indications of corrosion-damaged sites. A summary of paint and coating is provided by the guidance notes on the application and maintenance of marine coating systems [15].

Paint can be described as a liquid material capable of being applied or spread over a solid surface on which it subsequently dries or hardens to form a continuous, adherent film. Paints basically consist of three major components and many additives, which are included in minor quantities. The major components are:

- Binder (also called vehicle, medium, resin, film, or polymer)

- Pigment and extender
- Solvent

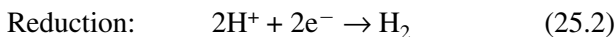
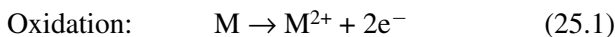
Of these components, only the first two components are in the final dry paint film. Solvent is used to dissolve and transport the other components to form the initial film, but inevitably, some solvent is always retained in practice, depending upon the level of ventilation. The paint is meant to make the path for the corrosive environment highly resistive and tortuous.

Surface preparation is the most important of the coating practices. The optimum performance of the best coating materials cannot be obtained over a poorly prepared surface. If contaminants such as grease, oil, salt and dirt are not removed, adhesion will be compromised and osmotic blistering may occur. Loose rust left on the surface will cause loosening of the coating. The standard of surface preparation may include nonabrasive and abrasive blast cleaning. Further details can be obtained from references 15 and 19.

25.7.2 Cathodic Protection

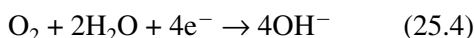
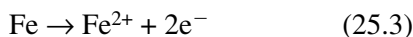
Cathodic protection is one of the most reliable methods that are currently used in marine application. By using this method, corrosion can be reduced to virtually zero [34].

Considering the electrochemical reactions between a metal and an acid, two kinds of electrochemical half-cell reactions occur:



The metal loses its own electrons as it oxidizes, and is thus corroded. On the other hand, H^{+} from the acid will receive electrons from the metal and is discharged as hydrogen gas.

With cathodic protection, the metal structure to be protected will be connected to a more anodic metal, a sacrificial anode, as shown in Figure 25.15. In the tanker, the reaction between ferrous alloys and water is:



Cathodic protection can reduce corrosion rates by using a sacrificial anode such as zinc to connect with

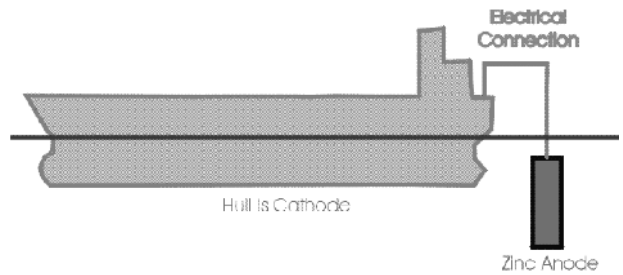


FIGURE 25.15 Schematic of cathodic protection in ship [21].

ferrous alloys. Electrons flow from a sacrificial anode to cathode (ferrous alloys). These electrons not only reduce the rate of half cell reaction [Eq. (25.3)] but also increase the rate of oxygen reduction [Eq. (25.4)]. Therefore ferrous alloys will be protected from corrosion. Also, cathodic protection will increase pH at the surface of ferrous alloys because it generates alkaline hydroxyl ions (OH^{-}) during the reaction. When OH^{-} reacts with calcium and magnesium in seawater, it will generate calcareous deposition, as seen in Figure 25.16.

These calcareous depositions can help to decrease current, which is why they are used in cathodic pro-

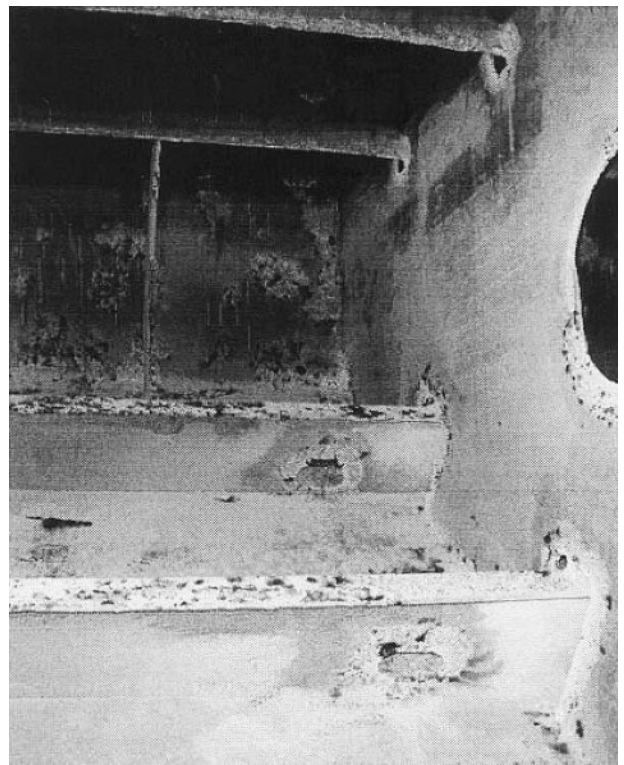


FIGURE 25.16 Calcareous deposits in tanker [21].

tection and keep the steel surface passive. Therefore, the surface of ferrous alloys is protected even if their coatings are destroyed. Also, with the help of this residual passive film, tankers will be protected from dampness when they are empty because cathodic protection cannot work at those times. Consequently, the efficiency of cathodic protection can be evaluated by considering the condition of the anode and the quantity of calcareous deposits which cover the tankers.

The Galvanic Series in Table 25.6 is a list of corrosion potentials. To select a metal to be a sacrificial anode, one considers the more active metals. The examples of sacrificial anodes are magnesium, zinc, and aluminum. Generally, zinc and aluminum are selected for high-efficiency sacrificial anodes in seawater applications, as they produce electron potentials of less than -1,000 mV. Also, magnesium anodes, being the most aggressive anodic material, are

not recommended for ballast tanks because hydrogen generated from the magnesium can destroy the coating of ballast tanks.

25.8 RELATED REQUIREMENTS IN MARINE INDUSTRIES

Shipping is perhaps the most international of all the world's great industries and one of the most dangerous. It has always been recognized that the best way of improving safety at sea is by developing general requirements that everyone will follow.

25.8.1 Classification Societies and IACS

Classification societies were established to act as neutral third parties, undertaking ship surveys in support of insurers [35]. The standards applied did not stem from governmental authorities but, rather, were established by the industry itself. The process that emerged has long served as a model of self-regulation.

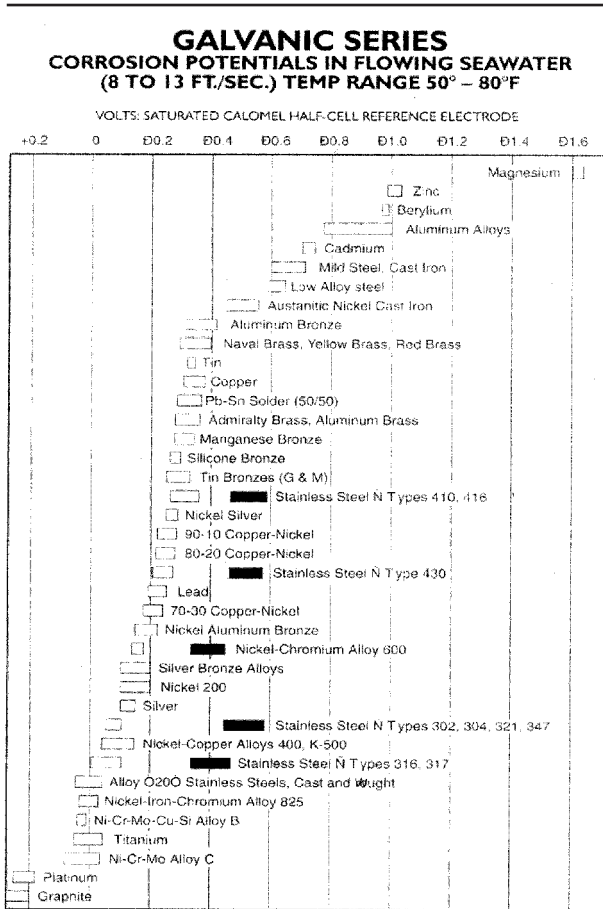
Classification societies are the primary means by which the shipping industry regulates itself and verifies the maintenance of ship safety. Classification societies establish standards, usually called classification rules, regulating design and maintenance of ships, and conduct periodic surveys to implement these standards.

In addition to the classification rules, governmental administrations codify safety standards for ships on the basis of international conventions or laws enacted on their own authority. The classification societies undertake statutory surveys on behalf of flag administrations because they are usually the only organizations with the technical capability and expertise to do so. Classification societies, however, are private entities, and class surveyors are not a substitute for governmental officials who have enforcement powers.

The International Society of Classification Societies (IACS) [35] was formed by seven leading societies on September 11, 1968. With 90% of world cargo-carrying tonnage covered by the rules of IACS members, IACS plays a vital role in improving the standards of the maritime industry.

The value of their combined and unique level of knowledge and experience was quickly recognized. In 1969, IACS was given consultative status with the International Maritime Organization (IMO) [36], with the first Permanent Representative appointed in 1976. It remains the only non-governmental organization with Observer status which is able to develop and apply rules.

TABLE 25.6 The Galvanic Series of Metals [34]



Alloys are listed in the order of the potential they exhibit in flowing seawater. Certain alloys indicated by the symbol: ■ in low-velocity or poorly aerated water, and at shielded areas, may become active and exhibit a potential near 0.5 volts.

25.8.2 International Maritime Organization (IMO)

Because of the international nature of the shipping industry, it has long been recognized that action to improve safety in maritime operations would be more effective if carried out at an international level rather than by individual countries acting unilaterally and without coordination with others. Although a number of important international agreements had already been adopted, many nations believed that there was a need for a permanent body which would be able to coordinate and promote additional measures on a more regular basis.

It was against this background that a conference held by the United Nations in 1948 adopted a convention establishing the International Maritime Organization (IMO) as the first-ever international body devoted exclusively to maritime matters [36].

The purposes of the organization, as summarized by Article 1(a) of the Convention, are “to provide machinery for cooperation among governments in the field of governmental regulation and practices relating to technical matters of all kinds affecting shipping engaged in international trade; to encourage and facilitate the general adoption of the highest practicable standards in matters concerning maritime safety, efficiency of navigation and prevention and control of marine pollution from ships.” The organization is also empowered to deal with administrative and legal matters related to these purposes. IMO is the United Nations’ specialized agency responsible for improving maritime safety and preventing pollution from ships.

IMO is a technical organization and most of its work is carried out in a number of committees and subcommittees. IMO has promoted the adoption of some 40 conventions and protocols and adopted well over 800 codes and recommendations concerning maritime safety, the prevention of pollution and related matters.

Measures introduced by IMO have helped ensure that the majority of oil tankers are safely built and operated and are constructed to reduce the amount of oil spilled in the event of an accident. Operational pollution, such as from routine tank cleaning operations, has also been cut.

The most important regulations for preventing pollution by oil from ships are contained in Annex I of the International Convention for the Prevention of Pollution from Ships, 1973, as modified by the Protocol of 1978 relating thereto (MARPOL 73/78). The International Convention for the Safety of Life at Sea (SOLAS), 1974, also includes special requirements for tankers.

25.8.3 Consideration of Corrosion in Design and Maintenance

Classification societies have set safety standards requiring that structural scantlings of ships be designed with a certain allowance for corrosion wastage. This design allowance is normally known as “corrosion addition” (Figure 25.17). Generally, an additional thickness is added to the nominal plate thickness that is determined according to the expected loads and permissible resultant stresses. Corrosion additions provide a safety margin for avoiding an undue increase of working stresses, and a means for avoiding unnecessary frequent steel renewals.

Ships in service are periodically surveyed and inspected. While deemed necessary according to defined criteria (i.e., the wastage allowances shown in Figure 25.17), wasted plates are recommended for replacement. Corrosion wastage allowances for individual structural members have been generally given as percentages of as-built scantlings. Currently, IACS is trying to establish a direct relationship between the corrosion additions and corrosion wastage allowances [38,39]. Classification societies advise their surveyors and vessel owners of maximum corrosion wastage allowances. Under some circumstances, the hull girder strength has to be assessed before steel renewals are requested. Criteria pertaining to whether a structure has to be replaced or may remain in place are established based on judgments about possible consequences of failures, the materials, corrosion types (pitting or general corrosion), and many other factors.

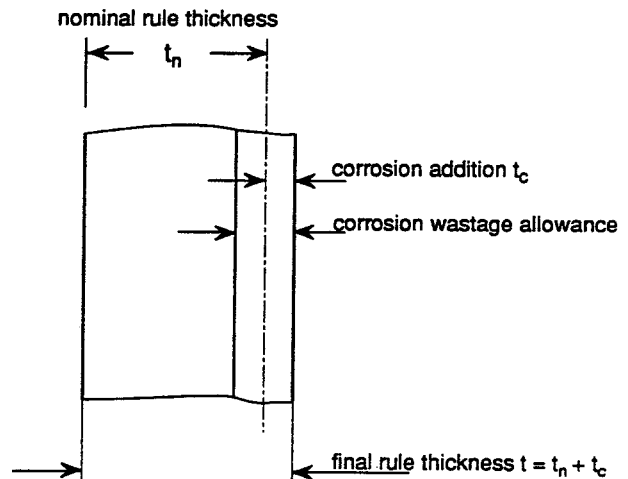


FIGURE 25.17 Schematic of corrosion addition and corrosion wastage allowance [19].

25.8.4 Surveys

Classification societies' surveys confirm the condition of a vessel through a process of overall examinations, close-up examinations, and thickness measurements. Surveys are typically of the following types, according to the Steel Vessel Rules of American Bureau of Shipping [37]:

1. *Annual Surveys* are carried out each year to ensure that the hull structure and piping are maintained in satisfactory condition. An annual survey typically takes one to two days. Usually, the survey includes the externally accessible hull and piping surfaces.
2. *Intermediate Surveys* are carried out at the midpoint of the five-year special survey/certificate cycle, and consists of the same inspection of external hull and piping surfaces as the annual surveys plus an examination of ballast tanks and cargo tanks. The aim of the intermediate surveys is to verify that conditions have not deteriorated at a rate greater than that assumed during the preceding special survey. For vessels that are older than 10 years, the extent of survey is increased. Thickness measurements may be required. Intermediate surveys take about three to four days to complete.
3. *Special Surveys* are carried out every five years in order to provide an in-depth examination of the structural condition of the vessel. All compartments are subjected to survey and the vessel is dry-docked. Special surveys take about one to two weeks, and their extent increases with the age of the ship.

As part of the Special Survey, an overall examination is carried out in all cargo tanks, ballast tanks, pump rooms, pipe tunnels, cofferdams and void spaces. This examination is supplemented by thickness measurements and testing as deemed necessary, to ensure that the structural integrity remains effective. The examination is structured to be sufficient to discover substantial corrosion, significant deformation, fractures, damages or other structural deterioration. For tankers and bulk carriers aged 15 years and older, the Intermediate Survey has been enhanced to the scope of a Special Survey.

In addition to overall examination, close-up examination is carried out on representative structural members, with requirements based on age and type of vessel. Tanks and structural members are selected for close-up examination that will provide the best representative samplings of areas likely to be most exposed to the effects of corrosion, sloshing and stress concentration.

The hull classification surveys consist of overall surveys supplemented by a sampling process of close-up examinations and thickness measurements. The specified examinations are based on age and type of vessel. Sampling locations are chosen by the Surveyor to be representative of areas likely to be most exposed to corrosion effects. The locations selected for sampling are based on the conditions found at time of that survey as well as conditions documented in past surveys, particularly the previous Special Survey.

25.8.5 Thickness Measurement Requirements and Procedures

The purpose of thickness measurements by classification societies is to establish, in conjunction with a visual examination, that the condition of the existing structure is fit for continued service during the subsequent survey interval, assuming that the vessel is properly operated and maintained [2,37]. Thickness measurements are used as a criterion to assess a ship structure, not a standalone method of inspection. Thickness measurements are a confirmation of conditions cited by the Surveyor.

The thickness measurement requirements and locations for Annual and Intermediate Surveys are based on the conditions found at the time of that survey as well as conditions documented at the previous Special Survey. The specified thickness measurements for a Special Survey are based on age and type of vessel.

The transverse sections of thickness measurements are usually where the greatest reductions are suspected to occur. The Surveyor will indicate the locations to be measured, preferably after carrying out an overall examination of all tanks. The Surveyor will specify additional thickness measurements in areas of known or suspected wastage. During the thickness measurement process, the Surveyor will also advise if any additional readings are to be taken to confirm questionable readings or marginal conditions.

In summary, the thickness measurement process is a sampling process used by the Surveyor to assess the ship structure. It is not a standalone inspection technique. Thickness measurement locations should be chosen from areas likely to be most exposed to corrosion effects. The process requires the Surveyor to monitor the thickness measurement results to increase density of thickness measurement readings to confirm questionable readings or marginal conditions in order to ascertain corrosion patterns.

25.8.6 Wastage Allowance

Individual plates or structural members that are wasted in excess of allowable limits are to be cropped

and renewed. The primary concerns in assessing overall wastage are the hull girder strength and the local buckling strength. The wastage allowance established by classification societies consists of three limits:

1. Maximum permissible wastage of individual plates, usually expressed as a percentage of the as-built scantling
2. Buckling limits to individual plates, usually expressed as the limits to the ratio of width over

TABLE 25.7 Individual Wastage Allowances, Conventional Vessels 90 M and Over, Built to ABS Class
(See Notes 11, 12 and 13) [37]

| Ordinary and High Strength Steel | BUILT 1962 OR LATER | Long'yly framed vessels built prior to 1962. Transv'yly framed vessels of all ages (See Note 9). Dry cargo barges 90 meters and over. Tank barges 90–122 meters (295–400 ft) (See Note 10). |
|--|-----------------------------|---|
| | Single Bottom Tankers | Bulkers, OBOs, Double Bottom Tankers, and Containerships |
| Strength Deck Plating | 20% | 20% |
| Continuous Long'l Hatch Coamings and Above Deck Box-Girders | — | 20% |
| Deck Plates within Line of Hatches and at Ends. | 30% | 30% |
| Forecastle, Poop and Bridge Deck Plates; Superstructure End Bulkheads | 30% | 30% |
| Tween Deck Plates | — | 30% |
| Sheer Strake Plates | 20% | 20% |
| Side Shell Plates | 25% | 25% |
| Bilge Strake Plates | 20% | 25% |
| Bottom Plates | 20% | 25% |
| Keel Plates (See Note 4) | | |
| Outermost Strake of Inner Bottom (See Note 5) | — | 20% |
| Other Plates of Inner Bottom (See Note 5) | — | 25% |
| Top Strake of Longitudinal Bulkheads and Top Strake of Topside Tank Sloping Plating | 20% | 20% |
| Bottom Strake of Longitudinal Bulkheads | 20% | 25% |
| Other Plates of Longitudinal Bulkheads, Topside Tank Sloping Plating, Hopper Tank Sloping Plating and Transverse Bulkheads (See Notes 6 and 7) | 25% | 25% |
| Internals including Longitudinals, Girders, Transverses, Struts, Bulkhead Webs and Stringers, Brackets and Hatch Side Girders | 25% | 25% |
| Plates in way of Top of Tanks | 30% | 30% |
| Underdeck Box Girders (Long'l or Transverse) | — | 20% |
| Hatch Covers (See Note 8). Hatch coamings and brackets | 30% | 30% |

- Notes:*
1. Internals included in longitudinal strength must be continuous or be effectively developed at ends, throughout amidships 0.4L.
 2. Structure must meet individual member thickness and average wastage requirements.
 3. If design was originally approved on basis of engineering analysis (such as car carriers and other specialized vessels), or if owner specially requests, the wastage may be assessed on engineering basis (i.e., acceptable stress levels and structural stability).
 4. Keel plates are to be renewed when they reach the minimum allowed thickness for adjacent bottom plating.
 5. 30% for bulk carriers and OBOs.
 6. Bulk Carriers for which IACS UR S19 applies: the corrugated transverse watertight bulkhead between cargo holds 1 and 2 are to be assessed in accordance with S19 for initial compliance and subsequent continued compliance at each Intermediate Survey and Special Periodic Survey–Hull.
 7. Bulk carriers for which UR S18 applies: the corrugated transverse W.T. bulkheads are to comply with the steel renewal provisions of S18.
 8. The hatch covers of bulk carriers to which IACS UR S21 applies are to comply with the steel renewal provisions of S21.
 9. Wastage allowances in column 2 (Bulkers, OBOs, etc.) apply to vessels with a combination of transverse and longitudinal framing.
 10. Wastage allowances in column 1 or 2, depending on the barge's construction, apply to tank barges over 122 m (400 ft) in length.
 11. The individual wastage allowances are acceptable provided the SM is not less than 90% of the greater SM required: (a) at the time of new construction, or (b) by 3-2-1/3.7.1(b).
 12. For tankers 130 m in length and above and over 10 years of age, sectional area calculations are to be carried out by a Technical Officer.
 13. For vessels built to other society rules, the Technical Office carrying out the initial plan review is to be contacted for wastage allowances.

thickness for plates, depending on the location in the structure

3. Minimum acceptable global hull girder strength, usually expressed as the percentage of as-built section modulus of the hull girder, or approximately measured as a minimum allowable areas of deck or bottom sectional areas.

25.9 REFERENCES

1. *Oil & Tankers Trades Outlook*. London: The Clarkson Research Studies, November, 2003.
2. *ABS 2001*. Technical report of investigation into the damage sustained by the M. V. Castor on December 30, 2000. Houston: American Bureau of Shipping. www.eagle.org.
3. Johnson, J. T. 2002. CC Technologies Laboratories, Inc., Dublin, OH.
4. Weber, P. F. 1984. *Structural Surveys of Oil Tankers*. Transactions IME.
5. *Guidance Manual for Tanker Structures*. Tanker Structure Co-operative Forum in Cooperation with IACS, 1997, London: Witherby & Co., Ltd. 1997.
6. Towers, R. 2000. Accelerated Corrosion in Cargo Tanks of Large, Double-Hull ships: Causes and Countermeasures. *Journal of Protective Coating and Linings*, Vol. 17(3), pp. 30–38, 41–42.
7. Wang G., Spong, R. 2003. *Experience-Based Data for FPSOs Structural Design*. Offshore Technology Conference, May 5–8, 2003, Houston, TX. (Available from OTC 15068).
8. www.gomr.mms.gov
9. 2001 Worldwide Survey of Floating Production, Storage and Offloading (FPSO) Units. *Offshore Magazine*, August 2001.
10. SBM IMODCO. *The FPSO Contractor Solution*. FPSO Global Workshop, September 24–25, 2002.
11. IMA. 2001., *Floating Production Systems—Assessment of the Outlook for FPSO Vessels, Production Semis, TLPs and Spars*. Washington, DC.: International Maritime Association, Inc., 2001.
12. www.terranovaproject.com
13. Titcomb, A. N. 1982. *Evaluation of Internal Tank Corrosion and Corrosion Control Alternatives*. 14th Annual OTC, Houston, TX May 3–6, 1982.
14. Stambaugh, K. A., Knecht, J. C. 1988. *Corrosion Experience Data Requirements (SSC-348)*. Annapolis, MD: Giannotti & Associates, Inc.
15. American Bureau of Shipping (ABS). 1998. *Guidance Notes on the Application and Maintenance of Marine Coating Systems, 2nd Ed*. Houston: ABS.
16. Melchers, R. E. 2001. “*Probabilistic Models of Corrosion for Reliability Assessment and Maintenance Planning*.” 20th International Conference on Offshore Mechanics and Arctic Engineering, Rio de Janeiro, Brazil, June 3–8, 2001.
17. Paik, J. K., Wang G., Thayamballi, A. K., Lee, J. M. 2003. *Time-Variant Risk Assessment of Aging Ships Accounting for General/Pit Corrosion, Fatigue Cracking and Local Dent Damage*. World Maritime Technology Conference, October 17–20, 2003, San Francisco, CA.
18. Wang, G., Spencer, J., Sun, H. H. 2003. *Assessment of Corrosion Risks to Aging Ships Using an Experience Database*. OMAE 2003, June 8–13, 2003, Cancun, Mexico. (Available from ASME, NY)
19. TSCF (Tanker Structure Co-operative Forum). 1992. *Condition Evaluation and Maintenance of Tanker Structures*. London: Witherby & Co., Ltd.
20. Japan Ministry of Transport. 1997. Report on the investigation of causes of the casualty of Nakhodka. The committee for the investigation on causes of the casualty of Nakhodka.
21. Contraros, P. D., Callow, L., Lomas, J. and Hinchley, J. 2002. *Corrosion Prevention—Marine Coatings, Inspection, Maintenance and Application of Coatings in Ballast and Cargo Tanks and Holds*. American Bureau of Shipping Technical Report PID: N9746701.
22. Harada, S., Yamamoto, N., Magaino, A., Sone, H. 2001. *Corrosion Analysis and Determination of Corrosion Margin, Part 1 and 2*. IACS discussion paper.
23. Wang, G., Spencer, J., Elsayed, T. 2003. *Estimation of Corrosion Rates of Structural Members in Oil Tankers*. OMAE 2003, June 8–13, 2003, Cancun, Mexico. (Available from ASME, NY)
24. Saidarasamoot, S., Olson, D. L., Mishra, B., Spencer, J. S. and Wang, G. 2003. *Assessment of the Emerging Technologies for the Detection and Measurement of Corrosion Wastage of Coated Marine Structures*. OMAE 2003, June 8–13, 2003, Cancun, Mexico. (Available from ASME, NY)
25. Yamamoto, N., Ikegami, K. 1998. A Study on the Degradation of Coating and Corrosion of Ship’s Hull based on the Probabilistic Approach.” *Journal of Offshore Mechanics and Arctic Engineering*. 120, 121–128.
26. Guedes Soares, C. and Garbatov, Y. 1996. Reliability of Maintained Ship Hulls Subjected to Corrosion. *Journal of Ship Research*, 40(3), 235–243.
27. Guedes Soares, C. and Ivanov, L. D. 1989. Time Dependent Reliability of the Primary Ship Structure. *Reliability Engineering and System Safety*, 26, 59–71.
28. Agarwala, V. S. and Ahmad, S. 2000. *Corrosion Detection and Monitoring—A Review*. Paper 271 at CORROSION/2000. NACE International.
29. Bray, D. E. and Stanley, R. K. 1997. *Nondestructive Evaluation: A Tool in Design, Manufacturing, and Service*. New York: CRC Press.
30. Rose, J. L. 2002. Standing on the Shoulders of Giants: An Example of Guided Wave Inspection. *Materials Evaluation*, Vol. 21(1), pp. 53–59.
31. Zhu, W., Rose, L., Barshinger, J. N., Agarwala, V. S. 1998. Ultrasonic Guided Waves NDT for Hidden Corrosion. *Res Nondestr Eval*, 1998, Vol. 10, pp. 205–225.

32. Song, W. J., Rose, J. L., and Whitesel, H. 2003. An Ultrasonic Guided Wave Technique for Damage Testing in a Ship Hull. *Materials Evaluation*, Vol. 22(1), pp. 94–98.
33. ABS. 2003. Technical Report of Assessing in Promising Nondestructive Methods for Detection and Measurement of Corrosion Wastage. Houston: American Bureau of Shipping. www.eagle.org.
34. Jones, D. A. 1996. *Principles and Prevention of Corrosion 2nd Ed.* Upper Saddle River, NJ: Prentice Hall.
35. International Association of Classification Societies (IACS). 2003. <http://www.iacs.org.uk>.
36. International Maritime Organization (IMO). 2003. www.imo.org.
37. ABS. 2003. *Steel Vessel Rules*. Houston: American Bureau of Shipping.
38. www.jtprules.com
39. www.jbprules.com

CHAPTER 26

BARRIER PACKAGING MATERIALS

Mikael S. Hedenqvist

Department of Fibre and Polymer Technology, Royal Institute of Technology, Stockholm, Sweden

26.1 INTRODUCTION 547
26.2 FACTORS DETERMINING THE BARRIER PROPERTIES
OF POLYMERS 547

26.3 FOOD PACKAGING 560
26.4 ACKNOWLEDGMENTS 562
26.5 REFERENCES 562

26.1 INTRODUCTION

Plastic packaging materials offer toughness, lighter weight and a level of design flexibility that glass and metal cannot meet. On the other hand, they are permeable to gases, vapors and liquids and this limits their use to products that do not require the highest barrier protection. There are, however, ways to improve their barrier properties and to make them competitive with glass and metal. No other material group offers the same huge range in permeability as polymers do. The oxygen permeability of poly(trimethyl silyl propyne) is 10 million times higher than for a typical liquid crystalline polymer. The success in obtaining a packaging material with optimal barrier properties requires knowledge on all levels, from atomistic details to converting and handling properties (Figure 26.1). It is important to understand how the introduction of new molecular groups affects the molecular rigidity, the material crystallinity, the interlayer adhesion and the folding/sealing properties. All these parameters have an impact on the final packaging barrier properties. The important factors that determine and enhance the barrier properties are described below, with practical examples in packaging. The focus is on gas, vapor and liquid barrier properties, but UV protection will also be addressed. In the last part of this chapter, the problems associated with selecting packaging materials for food, one of the largest packaging areas, are discussed.

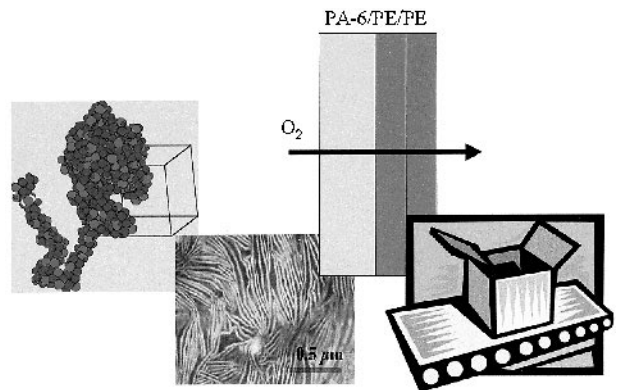


FIGURE 26.1 From molecular details to converting behavior, know-how on all levels is a prerequisite for optimal barrier performance. From left to right: an atomistic model of poly(vinyl alcohol) chain; the semi-crystalline structure of polyethylene as revealed by transmission electron microscopy; oxygen diffusion in a polymer laminate film and a converted package.

26.2 FACTORS DETERMINING THE BARRIER PROPERTIES OF POLYMERS

Figure 26.2 illustrates an attempt to generalize and categorize the factors that influence the barrier properties. It should be mentioned that the factors are often linked together (e.g., the generation of a more

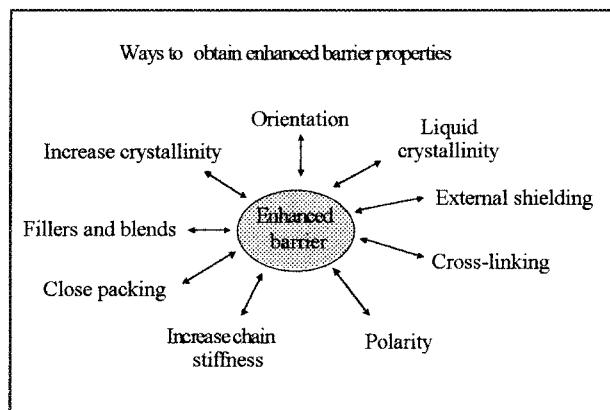


FIGURE 26.2 A chart categorizing the factors that affect the barrier performance.

closely packed molecular system often triggers an increase in crystallinity). Nevertheless, by experimenting with these factors in a controlled and systematic way, the engineer should be able to meet specific packaging requirements. In the following sections, the different factors will be discussed and illustrated.

26.2.1 Polarity

Hydrogen or dipolar bonds lower the mobility of the polymer chains. Hydrogen bonds between neighboring chains increase the energy associated with their separation. Consequently, hydrogen or dipolar bonds make it more difficult for the solute molecule to penetrate the polymer network (Figure 26.3).

The most popular barrier polymer today is poly(ethylene-co-vinyl alcohol). It is preferentially made from poly(ethylene-co-vinyl acetate) (EVAc) through a saponification procedure [1]. First, the vinyl acetate monomer is blended in an autoclave

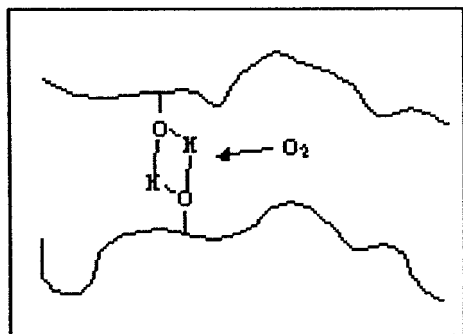


FIGURE 26.3 The blocking of a diffusing oxygen molecule caused by hydrogen bonds.

with a solvent (e.g., a dialkyl sulfoxide, DMSO) and a radical initiator (e.g., 2,2'-Azobisisobutyronitrile AIBN). The autoclave is then pressurized with ethylene gas at 60 °C and the polymerization is initiated. EVAc polymer is obtained after precipitation in water. The washed EVAc is subsequently dissolved in methanol and saponification is initiated by adding sodium hydroxide at 60 °C. After the precipitation, dehydration, purification, drying and pulverisation steps, the final EVOH polymer is obtained. Depending on the requirements, it is possible to vary the ethylene content in EVOH. Typical contents are 25–45 mol% ethylene [1]. A high ethylene content makes EVOH less moisture sensitive. In fact, EVOH may be used without external protection if the ethylene content is high (as in the case of a EVOH/HDPE laminate bottle for mustard). A high ethylene content reduces the amount of hydrogen bonds and the degree of crystallinity, both leading to lower gas barrier properties. Thus, when hydrogen bonds are the main barrier mechanism, a compromise has to be made between moisture sensitivity and gas barrier properties.

To illustrate the effect of hydrogen bond content and moisture sensitivity, we measured the oxygen permeability of LDPE/EVOH/LDPE laminates in our own laboratory. In dry conditions the permeability was reduced by almost eight times by reducing the ethylene content in EVOH from 44 mol% to 32 mol%. At 50–75 % relative humidity (RH), the improvement was only by a factor of four, due to larger reduction in gas barrier properties at moist conditions of the 32 mol% ethylene material. A problem which must be considered when retorting packagings is that the polar and hydrogen-bonding barrier polymers lose many of their protective properties at elevated temperature and humidity. Since they are normally layered between less hygroscopic layers, it might take a long time before they regain their original barrier properties. For example, PP/EVOH/PP and PP/PA6/PP films showed oxygen permeabilities three days after retorting which were, respectively, 50–100 times and two to four times higher than those of the original films [2]. The high gas barrier properties of poly(ethylene-co-vinyl alcohol), poly(vinyl alcohol), polyketone and poly(acrylonitrile) are due mainly to their hydrogen bonds (Figure 26.3, Table 26.1). Poly(acrylonitrile) is known as Barex and is used for its good barrier properties in, for example, toothpaste [3] and fruit juice [4] packagings.

In a system of polyvinyl alcohol and water, it has been recently shown that the hydrogen bonds between neighbouring chains are more effective in re-

TABLE 26.1 Oxygen Diffusivity and Permeability of Several Polymers at 25 °C

| Polymer | D (cm ² /s) | P (cm ³ cm/ cm ² s Pa) |
|--|--------------------------|---|
| PVOH (23 °C) ^a | | 0.00005·10 ⁻¹³ |
| PAN ^a | | 0.00015·10 ⁻¹³ |
| PA6 (30 °C) ^a | | 0.0285·10 ⁻¹³ |
| Polyaminoether ^b | | 0.00032·10 ⁻¹³ |
| Poly(acrylonitrile-co-acrylate) ^b | | 0.012·10 ⁻¹³ |
| Polyketone ^c | | 0.0054·10 ⁻¹³ |
| Natural rubber ^a | 1.73·10 ⁻⁶ | 17.6·10 ⁻¹³ |
| LDPE ^a | 4.6·10 ⁻⁷ | 2.2·10 ⁻¹³ |
| HDPE ^a | 1.7·10 ⁻⁷ | 0.3·10 ⁻¹³ |
| Vectra A950 ^d | 1.2·10 ⁻⁹ | 0.00023·10 ⁻¹³ |
| Vectra RD501 ^d | 7.3·10 ⁻¹⁰ | 0.00016·10 ⁻¹³ |
| PETP (amorphous) ^a | 4.5·10 ⁻⁹ | 0.04·10 ⁻¹³ |
| PEN, oriented ^c | | 0.008·10 ⁻¹³ |
| Butyl rubber ^a | 8.1·10 ⁻⁸ | 0.977·10 ⁻¹³ |
| Poly(vinylidene chloride) ^a | | 0.004·10 ⁻¹³ |
| Polyimide ^f | | 1 (a.u.) |
| Polyimide-7.5% Montmorillonite ^f | | <0.2 (relative to pure polyimide) |
| Oriented PETP ^g | 3.1·10 ⁻¹⁰ | 0.037·10 ⁻¹³ |

Notes: (a) [42]; (b) [8]; (c) [43]; (d) [44,45]; (e) [46] based on 4.9 times lower permeability than PETP at 30 °C; (f) [47]; (g) [48]



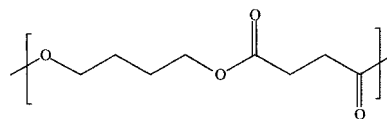
FIGURE 26.4 Coffee bags made of oriented PP and co-extruded PE/EVOH/PE (Sengewald Verpackungen). [Source: Photo reprinted by permission of *Packaging World*, Summit Publishing Co.]

ducing solute motion than the hydrogen bonds that are formed between the polymer and the polar solute (water) [5]. However, as the concentration of the polar solute increases, more and more polymer-polymer hydrogen bonds are broken. This leads to a plasticized polymer with inferior barrier properties. Table 26.2 shows that the polar or hydrogen bonding

TABLE 26.2 Water Vapor Permeability of Some Selected Biodegradable Polymers and Polyethylenes

| Material | WVTR (23 °C 100%RH) | WVTR (38 °C 100%RH) |
|---|------------------------|------------------------|
| | gmm/m ² day | gmm/m ² day |
| Bioplast GF 102 (starch and polycaprolactone) | 69 | 60 |
| Skygreen (Aliphatic polyester) | 108 | 300 |
| Bionolle 1001 (Aliphatic homopolyester) | 58 | 161 |
| Bionolle 3001 (Aliphatic copolyester) | 98 | 248 |
| HDPE | 0.06 | 0.16 |
| LDPE | 0.14 | 0.41 |
| VLDPE | 0.27 | 0.78 |

[Source: These are unpublished data from our lab.]



Poly(butylene succinate) (Bionolle 1001)

polymers are significantly more permeable to water than unpolar polyethylene.

Renewable polymeric gas barriers are usually rich in polar and/or hydrogen bonding groups. Those include starch-based and protein based materials, including polylactic acid and corn zein. Polylactic acid is a good aroma barrier most suitable for retail containers (Figure 26.5). This, plus its better oxygen barrier properties compared to polyethylene, are due to its content of polar groups [6]. The fact that the polymer can be used in contact with relatively moist



FIGURE 26.5 Deli foods in NatureWorks™ PLA from Cargill Dow, LLC. [Source: Photo reprinted by permission of *Packaging World*, Summit Publishing Co.]

food without deteriorating is probably due to the fact that its crystallinity is enhanced through biaxial orientation [7]. Poly(acrylonitrile-co-acrylate) (Figure 26.6), poly(glutarimide-co-methacrylate), poly(xylene adipamide) and poly(hexamethylene terephthalamide) are other examples of barrier polymers where the hydrogen bonds play important roles.

A particularly interesting new group of polymers with excellent barrier properties are the thermoplastic epoxies, phenoxies, and among these, especially the poly(amino ethers) are desirable because of their low price [8]. The poly(amino ether) in Figure 26.7 has one of the lowest oxygen permeabilities reported for a 100% amorphous polymer. Its oxygen permeability is at least 125 times lower than that of PETP (see Table 26.1). It is interesting to note that the

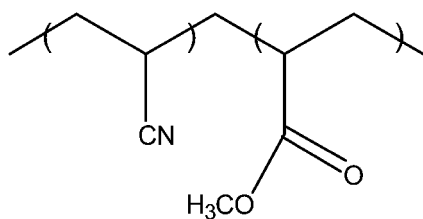


FIGURE 26.6 Poly(acrylonitrile-co-acrylate).

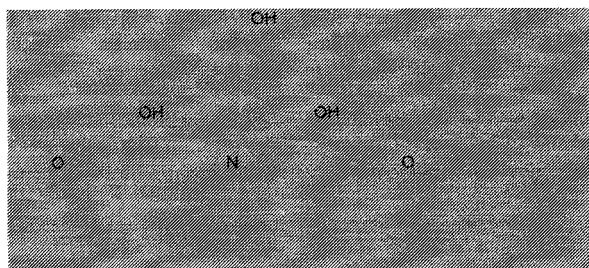


FIGURE 26.7 A poly(amino ether) based on ethanolamine.

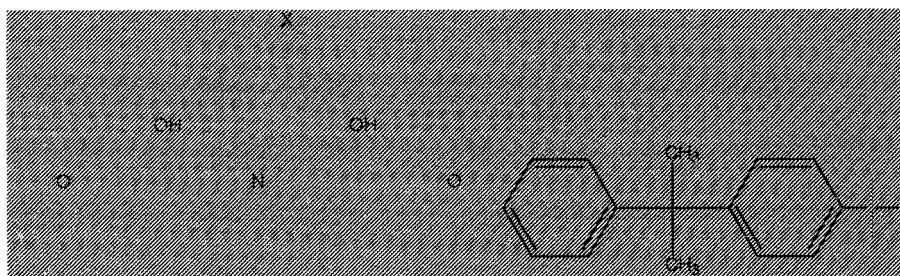


FIGURE 26.8 Pendant functionality ($-X$) on a polyaminoether.

combination of hydrogen bonds and a stiff moiety (benzene ring) is especially effective in enhancing the gas barrier properties. An excellent example is the aromatic polyamide MXD6. Both chain stiffness and MXD6 will be discussed in a later section.

Apart from being excellent barrier materials, they offer high clarity, good mechanical properties and they are easy to process. They exist as either semi-crystalline or amorphous materials. They can be compression- and injection-molded, co-extruded, thermoformed and blow molded. In contrast to most other polar polymers, the phenoxies do not lose their barrier properties in humid environments [8]. In fact, some of these polymers improve their barrier properties in moist conditions. It is suggested, based on density and positron annihilation measurements, that water occupies free volume and also increases the interchain hydrogen bond strength.

The effect of pendant functionality on the oxygen permeability is illustrated for the poly(amino ether) in Figure 26.8. By replacing $-X$ from $-OH$ to $-CH_3$ or $-O-CH_3$, the oxygen permeability increases almost one order of magnitude, whereas it is unchanged if $-X$ is $-NH-CO-CH_3$ [8]. Within the same "group" of polymers, there is normally a clear correlation between the barrier properties and the glass transition temperature. Enhanced intermolecular bond strength and chain stiffness yield high glass transition temperature and good barrier properties. In the same way as hydrogen bonds provide gas barrier properties, the absence of these and other polar interactions provides good barrier properties toward polar vapors and liquids. Therefore, polyolefins and fluoropolymers are normally excellent moisture barriers.

26.2.2 Crystallinity

Polymer crystals are impenetrable to most solutes. Consequently, the solute solubility, diffusivity and

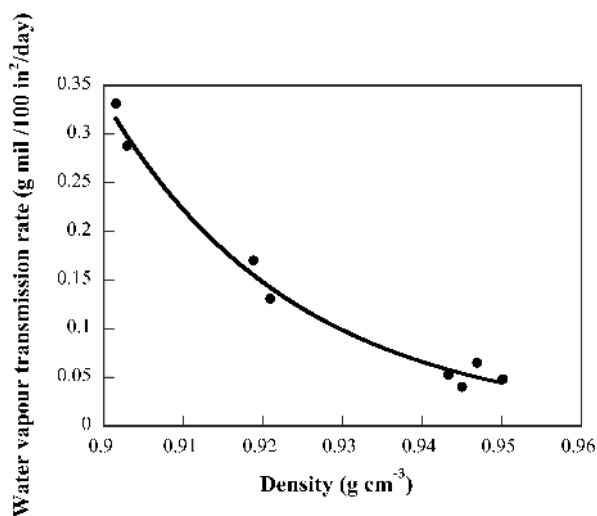


FIGURE 26.9 Water vapor transmission rate as a function of polyethylene density. [Source: Drawn after data of Shah et al. [53].]

permeability decrease with increasing crystallinity (see Figure 26.9 and compare natural rubber, LDPE and HDPE in Table 26.1). The best polymeric barrier material is a 100% crystalline polymer. Paraffins (i.e., polyethylene of very low molar mass) have a crystallinity close to 100%. Unfortunately, in this case, the high crystallinity is accompanied by extreme brittleness.

Even though the polymer contains dipoles, a high crystallinity can prevent moisture sensitivity. Examples are poly(vinylidene chloride) (PVDC) and polychlorotrifluoroethylene (PCTFE) with the tradenames Saran[®] and Aclar[®], which are used, for example, as blister materials (Figure 26.10). Aclar films have a water vapor transmission rate that is more than 10 times less than that of PVC [9]. PVDC has a water vapor transmission rate that is 10–100 times lower than that of PVC [10].

26.2.3 Liquid Crystallinity

Polymers possessing liquid crystalline molecular order (i.e., liquid crystalline polymers (LCPs as shown in Table 26.1) are today the best polymer barrier materials, especially in humid conditions (Figure 26.11). The liquid crystalline state, characterized by a relatively mobile close-packed molecular structure, is obtained by using rod-like chains. These are obtained by polymerizing with one or several types of aromatic monomers (Figure 26.12).

The advantage of these polymers compared to 100% crystalline polymers is that the former do not



FIGURE 26.10 PVDC are often used in blisters. The blister packaging above is not necessarily of PVDC, it merely serves as an illustration of a blister.

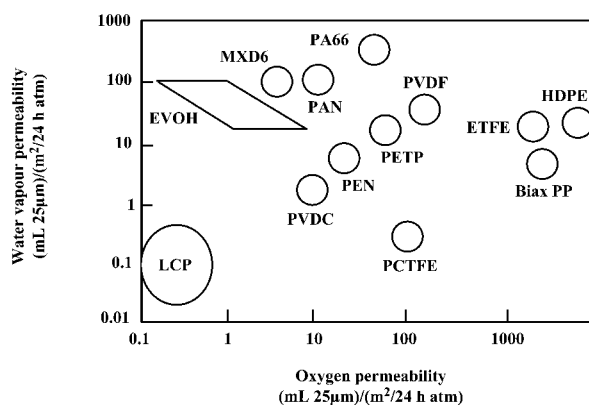


FIGURE 26.11 A map of oxygen and water vapor permeability for several polymers. [Source: Courtesy of Superex, Inc. and drawn from Ref. [54]. Copyright ©2004, Wiley Interscience. Reprinted by permission of John Wiley & Sons, Inc.]

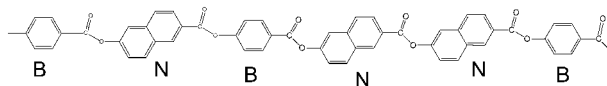


FIGURE 26.12 Typical structure of the random liquid crystalline co-polyester, Vectra[®]. B and N correspond, respectively, to the monomers: p-Hydroxy benzoic acid (HBA) and 2-Hydroxy-6-naphthoic acid (HNA). [Courtesy of Göran Flodberg, STFI-Packforsk]

lose their mechanical properties even at 100% liquid crystallinity. The general picture is that the stiff polymer chains are ordered locally in domains. The degree of molecular packing within each domain is high and it is believed that the domains are impenetrable to most chemically inert solutes. At domain

boundaries the degree of molecular order and, consequently, the degree of packing is low. It is believed that solute molecules penetrate the material through these boundaries (disclinations) (Figure 26.13). Hence, if the number of disclinations is lowered, the barrier properties of the liquid crystalline polymers are improved and the permeability should approach that of a 100% crystalline polymer. The number of disclinations can be reduced by annealing at high temperature or by orienting the material. The absence or limited use of these polymers as barrier materials today is due to their high price and the fact that they are difficult to process; these factors might possibly be overcome in the near future. For example, LCP is believed to replace polyimide in micro-electronic equipment where moisture absorption must be minimized [11].

26.2.4 Stiff Molecules

The energy required to separate chain segments in a polymer increases with the stiffness of the polymer. The effect of placing the stiff terephthalic unit on a flexible chain is illustrated by comparing the oxygen permeability of PETP and natural rubber. The PETP oxygen permeability is 440 times lower than that of natural rubber (Table 26.1). Replacing the benzene ring with a naphthoic unit (Figure 26.14), lowers the oxygen permeability a further five times (compare PETP and PEN in Table 26.1).

An example where chain stiffness, in combination with non-polarity, provides excellent moisture resistance is the cyclo-olefin co-polymer family (COC). These co-polymers can be formed by first reacting ethylene with cyclopentadiene to form 2-norbornene. This is subsequently co-polymerized with

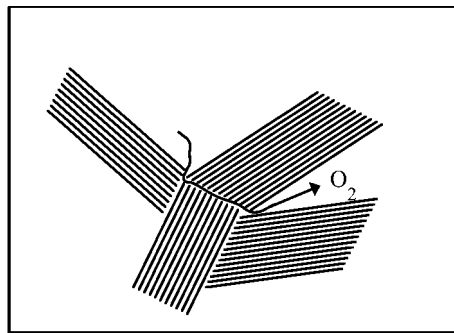
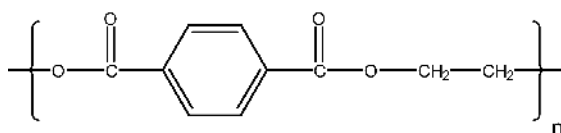
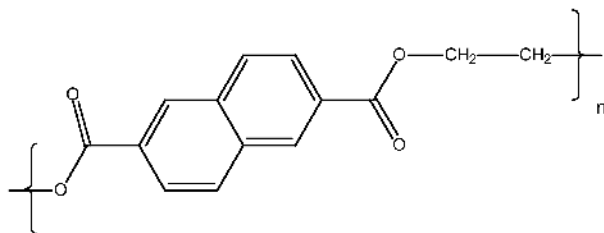


FIGURE 26.13 An oxygen molecule diffusing through the disclinations of a liquid crystalline polymer.



PET



PEN



Monolayer PEN

FIGURE 26.14 The molecular structures of PETP and PEN together with PEN bottles [12]. [Source: Photo reprinted with permission of Gardner Publications, Inc.]

ethylene using a metallocene catalyst to yield the COC (Figure 26.15). The copolymerization with 2-norbornene leads to a state where crystallinity is suppressed and chain stiffness enhanced. The loss in crystallinity (which provides good clarity) is thus compensated for by the enhanced chain stiffness, leading to unchanged or enhanced barrier properties.

The clarity, high moisture resistance and inertness make the COCs suitable as blister materials, high-resolution CD-ROMs and flexible packagings [12, 13]. For example, the Topas[®] COC polymer is currently used in laminates with polyolefins in blister

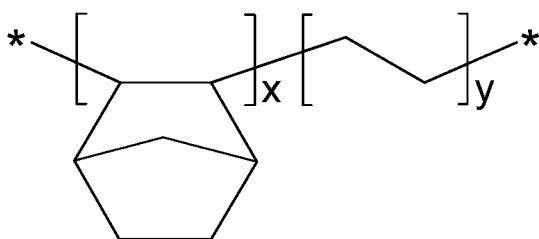


FIGURE 26.15 The molecular structure of the norbornene- (x) ethylene (y) copolymer (COC).

packagings for aspirin tablets [12]. Interestingly, the oxygen permeability is less than a factor of two times higher than high density polyethylene for a COC which has a glass transition as high as 140 °C, corresponding to a norbornene content of 51 mol% [14]. Polystyrene ($T_g = 105$ °C) has a six times higher oxygen permeability compared to high density polyethylene. The relatively low oxygen permeability of COC is due to its low oxygen diffusivity as compared to both polyethylene and polystyrene, which in turn must be due to its high chain rigidity (compare the T_g s of polystyrene and COC). The effect of the presence of 2-norbornene is obvious. The oxygen diffusivity of the COC with 52 mol% 2-norbornene is two orders of magnitude lower ($D = 1 \cdot 10^{-8}$ cm²/s) than that of the analogue with only ethylene units (“amorphous polyethylene”), taken here as natural rubber (see Table 26.1).

26.2.5 Close packing

Molecular close packing leads to high intermolecular friction and a decrease in segmental mobility. Stereoregular molecular architecture favors close packing. Butyl rubber is unique with respect to its high barrier and high damping properties (Table 26.1 and Figure 26.16). The symmetrically placed methyl groups on the isobutylene monomer, shown within brackets in the butyl rubber chain in Figure 26.17, provide a high degree of chain packing and a large intermolecular contact area.

Physical aging and antiplasticization lead to enhanced molecular packing and, thus, better barrier properties. On the contrary, plasticizing solutes lowers the barrier efficiency. The solute molecules force the polymer chains apart, leading to smaller interactions between the polymer chains and, thus, an overall higher mobility and free volume of the system. Hydrophilic polymers, including polyamides, poly-



FIGURE 26.16 Butyl rubber gloves. [Source: Photo reprinted by permission of CitizenSafe.]

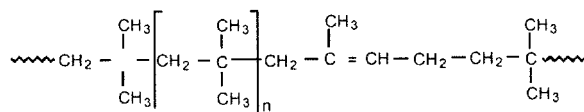


FIGURE 26.17 Butyl rubber molecule.

saccharides, proteins and poly(vinyl alcohol), lose, to various degrees, their barrier efficiency in polar environments (e.g., water, ethanol). In a similar way, hydrophobic polymers, including polyethylene, polypropylene and poly(tetrafluoroethylene), lose their barrier efficiency in non-polar media (e.g., fats and oils). The oxygen permeability of HDPE films increases more than 30% when exposed to fermented milk (1.5% fat), and the oxygen permeability of PVOH increases 2,500 times when the relative humidity goes from 0% RH to 100% RH [15].

26.2.6 Chemical Cross-links

Chemical cross-links shorten the “flexible” length of a polymer molecule. Thus, the molecular mobility of the polymer chain segments is reduced and the mobility of the diffusing solute molecule will therefore also be reduced. Ebonite (highly cross-linked natural rubber) is a better barrier compared to “normal” loosely cross-linked natural rubber. Cross-linked polyethylene is a better barrier than uncross-linked polyethylene of similar crystallinity (Table 26.3). The effect of cross-linking is greater for larger solutes, since they require the redistribution of larger

TABLE 26.3 The Effects of γ -ray Cross-linking on the Gas Permeabilities in Polyethylene [49]

| Molecule | $P^* \cdot 10^{10}$ (35 °C) ^a | | % change in P |
|-------------------------------|--|---------|---------------|
| | 0 Mrad | 50 Mrad | |
| He | 9.4 | 8.8 | 6.4 |
| N ₂ | 1.95 | 1.45 | 25.6 |
| CH ₄ | 5.1 | 3.7 | 27.4 |
| C ₂ H ₆ | 8.7 | 6.25 | 28.2 |
| C ₂ H ₈ | 14.5 | 8.6 | 40.7 |

a) in $\text{cm}^3(\text{STP}) \text{ cm} (\text{torr s cm}^2)^{-1}$

polymer segments in order to jump into new positions, as compared to smaller solutes. The PPG Industries, Inc. has developed a methodology whereby PET bottles are coated with cross-linked epoxy-amine-based coatings (Bairocade[®], Figures 26.18 and 26.19) [16]. The shelf life is increased approximately 10 times when the PET bottles are coated (Figure 26.19).

The epoxy-amines are made from diglycidyl ethers from, respectively, 2,2'-bis(4-hydroxyphenyl) propane (bisfenol A), bis(4-hydroxyphenyl) methane (bisfenol F) and butanediol, which are reacted with an amine (triethylene tetramine or tetraethylene pentamine) (Figure 26.20) [17,18]. The diglycidyl ethers are referred to as, respectively, DGEBA (or BADGE), DGEBF and DGEBD. The best barrier properties are obtained if an excess of the amine is used. Furthermore, a large number of hydrogen bonds (hydroxyl and amine groups) and a low content of pendant methyl groups favors good gas barrier properties [18]. The barrier coatings, in the form of either solvent or aqueous solutions, are applied,



FIGURE 26.18 Bairocade coated PET bottles. [Source: Photo reprinted with permission of PPG Industries, Inc. and Gardner Publications, Inc.]

O₂ Barrier Performance on Beer Bottles (.5L)

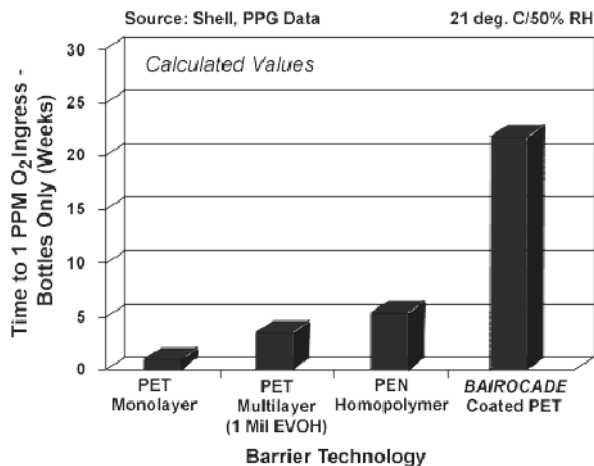


FIGURE 26.19 Performance of PEN and uncoated, laminated and Bairocade coated PET bottles. [Source: Photo reprinted by permission of PPG Industries, Inc.]

preferably by spraying or rolling techniques. Dipping and brushing are other possible techniques [17].

26.2.7 Fillers and Blends

Fillers that are impenetrable to solute molecules serve as obstacles and decrease the permeability of the polymer. This effect is enhanced if the fillers are flake-like and if the flakes are oriented in the plane of the film. The flake-like fillers are usually of inorganic origin but they can also consist of, for example, a high barrier polymer. Flake-like fillers with a high surface area combined with proper surface coating are favorable in terms of obtaining high barrier properties. By bonding to the surrounding polymer matrix, the particles will not only act as physical obstacles, they will lower the flexibility of the adjacent polymer chains and, thus, enhance the polymer matrix barrier properties in the region close to the particles (Figure 26.21). These phenomena, provided the particles are dispersed evenly, lead to only a small amount of filler, typically less than 5 w%, being needed to obtain enhanced strength, stiffness and barrier properties. The small amount and the small particle thicknesses (on the orders of nanometers) ensure that the toughness and transparency are not severely altered in the presence of the particles. Flake-like fillers with nanometer thicknesses include silicates, e.g., montmorillonite [19]. Montmorillonite clay particles have a thickness of 1 nm and a width of several microns (Figure 26.22).

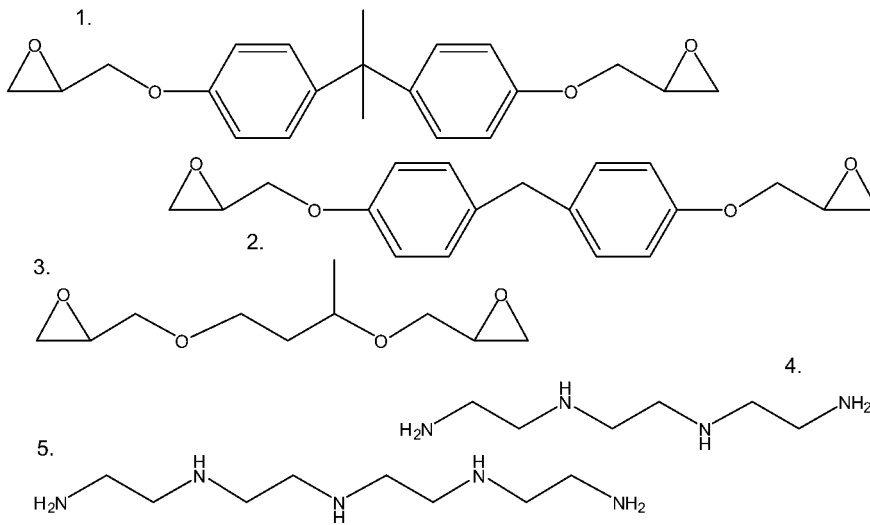


FIGURE 26.20 The molecular structure of (1) DGEBA, (2) DGEBF, (3) DGEBD, (4) triethylene tetramine, and (5) tetraethylene pentamine.

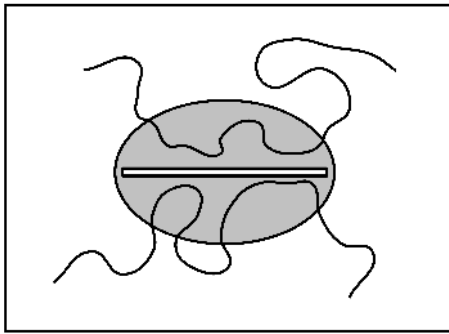


FIGURE 26.21 The polymer matrix region (grey area) bonded to a montmorillonite particle.

By injection or stretch-blow molding, it is possible to “flatten” out droplets of a dispersed high barrier polymer in a host polymer matrix. Provided the inter-component adhesion is good, the barrier properties of the laminate are significantly improved. Figure 26.23 shows stretched out LCP particles in an LCP/polyethylene injection molded blend. Figure 26.24 shows the decrease in oxygen permeability for the same blend as a function of LCP-content. To illustrate the similarity between the effects of incorporating inorganic flake fillers and having polymer flake particles present, the decrease in oxygen permeability for an injection molded montmorillonite/BAK system is also shown.

Honeywell, Inc. produces polyamide-6 montmorillonite nanocomposites (Aegis[®]) which, in combination with an oxygen scavenger, is used in a three-layer PET-bottle for beer by Anchor Brewing in San

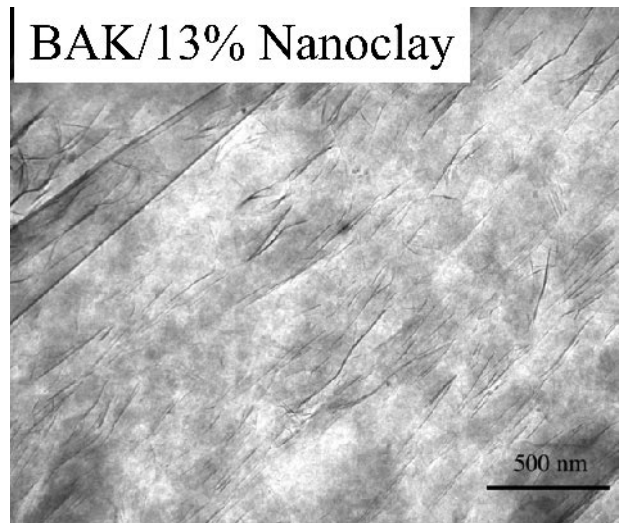


FIGURE 26.22 13% montmorillonite particles (black) dispersed in a polyester (BAK[®]) matrix [19]. The scale bar corresponds to 500 nm. [Source: Reprinted with permission of Society of Plastics Engineers, Inc.]

Francisco [16]. The nanocomposites are preferably made in situ during polyamide polymerization to ensure proper filler exfoliation. At 3.5% of bottle weight, the nanocomposite extends the shelf life from nine to 16 weeks. The power of the nanocomposite is due to the combined effect of the 2% montmorillonite fillers and the oxygen scavenger. Compared to pure polyamide, the fillers lower the oxygen and the carbon-dioxide permeabilities by, respectively, four and three times, and the oxygen scav-

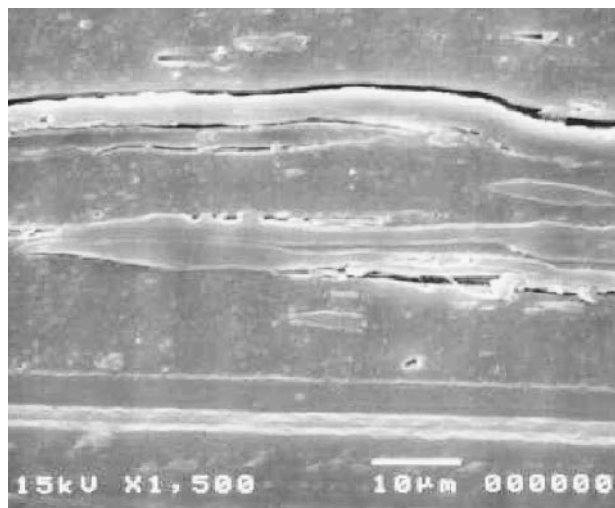


FIGURE 26.23 Scanning electron micrograph of a freeze-polished 9 vol.% LCP (Vectra RD501)/polyethylene blend taken 30 mm from the center of the injection molded disc. The stretched-out LCP particles (9 vol%) lie in the direction perpendicular to the disc thickness [55]. [Source: Reprinted with permission of Society of Plastics Engineers, Inc.]

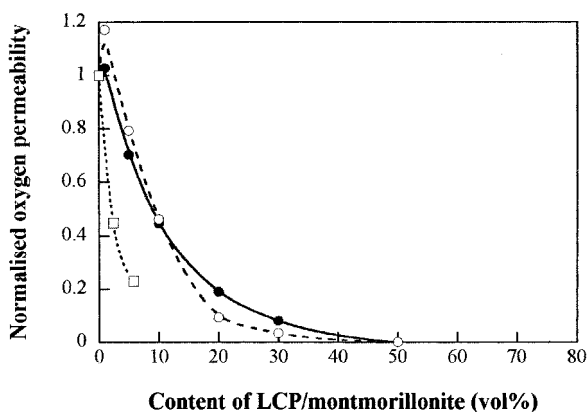


FIGURE 26.24 The oxygen permeability relative to the value of the permeable matrix for an injection molded Montmorillonite/BAK blend (○) (unpublished data obtained in our lab) and LCP/polyethylene blends (A950 (λ) and RD501 (μ)) [55].

enger provides a 100-times-better oxygen barrier during a limited time period [20].

Examples of commercially available polymer blends for packaging include PET/PEN, PA6/PA-MDX6 and PE/COC. Although these blends are not perfectly miscible, they do not form the typical filler-matrix morphology shown for LCP/PE above.

Aran (Scotland) has introduced small single serve injection/stretch-blow molded light-weight jam jars



FIGURE 26.25 Single-serve Aran jars made by a 60/40 PET/PEN blend. [Source: Photo reprinted by permission of BP Chemicals.]

made of PET/PEN blends, rather than PET, in order to be able to hot fill jam at 85 °C (Figure 26.25) [21,22]. The blend components are immiscible, but transesterification reactions during mixing enhances miscibility and yields a system that is clear and has a single glass transition. T_g is higher than for PET; 90–95 °C for a 60/40 PET/PEN blend. It is observed that the oxygen permeability is lower for the mixture than predicted by the simple rule of mixing.

Blending techniques have also been developed to lower the gas permeability of polyamide-6, especially at moist conditions. For example, PA6 is blended with the polyarylamide PA-MDX6 (Figure 26.26), a product of the polymerization of adipinic acid and m-xylylene diamine. Figure 26.27 shows that the oxygen transmission rate decreases non-linearly with the content of PA-MDX6. The film stiffness and the hot tack strength of polyethylene is improved by blending it with a COC polymer [12]. This will allow for a downgauging of packaging thickness and better economy.

26.2.8 Orientation

Molecular orientation reduces the polymer fractional free volume and the molecular mobility, and induces crystallinity. This leads to low solute permeability. Consequently, biaxially and uniaxially stretched films of polypropylene, polyamide and

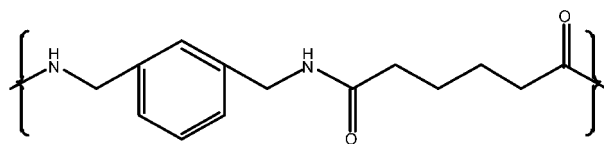


FIGURE 26.26 Polyamide-MDX6.

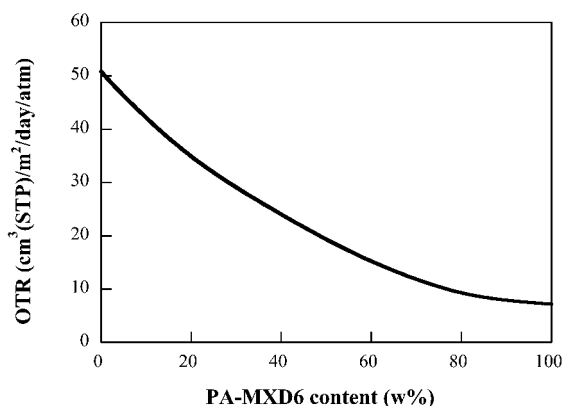


FIGURE 26.27 Oxygen transmission rate at 60% RH and 23°C for polyamide-6/polyamide MXD6 blends. [Source: Redrawn from [56].]

PET are popular in barrier applications. Oriented PET has at least one order of magnitude lower oxygen diffusivity than the corresponding unoriented film (Table 26.1). A polyamide-6 film stretched biaxially two times its original length at 100 °C, corresponding to a 76% molecular orientation, experienced a tripled enhancement in oxygen barrier [23]. Interestingly, its fracture strain was reduced by the same factor (~3). The yield strength increased moderately (~1.5 times).

Oriented PP is used for water resistant labels on bottles [24] and as food wraps [25]. Figure 26.28 shows candy pops wrapped with a biaxially oriented polypropylene (BOPP) film coated on one side with an acrylic that provides an aroma barrier and a glossy appearance to improve product presentation.

Uni-axial orientation may sometimes yield sufficient film properties. Figure 26.29 shows how the



FIGURE 26.28 Candy pops wrapped by an acrylic coated BOPP film [25]. [Source: Photo reprinted by permission of *Packaging World*, Summit Publishing Co.]

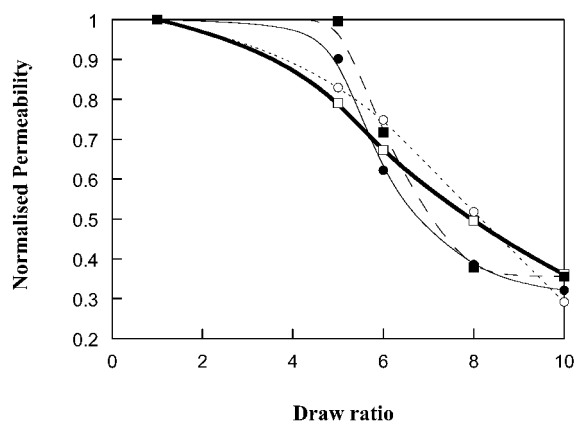


FIGURE 26.29 Permeability to O₂ (0% RH) (●), O₂ (50% RH) (■), CO₂ (0% RH) (○) and H₂O (85% RH) (□), normalized with respect to the value for the undrawn specimen, as a function of draw ratio. [Source: Drawn from Ref. [57]. Copyright©2004, Wiley Periodicals, Inc. Reprinted by permission of John Wiley & Sons, Inc.]

permeabilities of some gases and water decrease with increasing degree of orientation for uni-axially oriented polyketone.

26.2.9 External Shielding and Lamination (Including UV-protection)

In many applications, it has turned out that the best combination of packaging properties, including barrier protection, is obtained by using laminated structures. It is not uncommon that packaging films are made up of more than five layers. The Heinz condiment pouches in Figure 26.30 are made up of an eight-layer structure with, from the outside to the inside, lacquer/print/PVDC/PET/Aluminum/PVDC/adhesive/LDPE [26]. The lacquer protects the print and the adhesive joins LDPE to the rest of the film. The vacuum-deposited aluminum layer provides excellent oxygen and moisture barrier properties and light protection. The PVDC copolymer provides extra oxygen and moisture protection, and LDPE serves as a fat and moisture barrier. PET provides mechanical integrity and flex crack resistance. The LDPE and PVDC layers provide sealability.

There are different reasons for lamination. As shown above, the hygroscopic barrier materials usually need to be protected from the surrounding moisture. Figure 26.31 shows an early (1974) Japanese ketchup bottle that illustrates this [27]. PP and EVAc limits the ingress of moisture to the EVOH barrier. The external PC layer was added to provide a dust-



FIGURE 26.30 The Heinz condiment pouches. A 2-mil structure of: lacquer/print/Mylar[®] MC2 PET/adhesive/LDPE [26]. The Mylar[®] MC2 PET layer consists of a laminate of PVDC/Clear PET/Aluminum/PVDC. [Source: With permission of Dupont.]

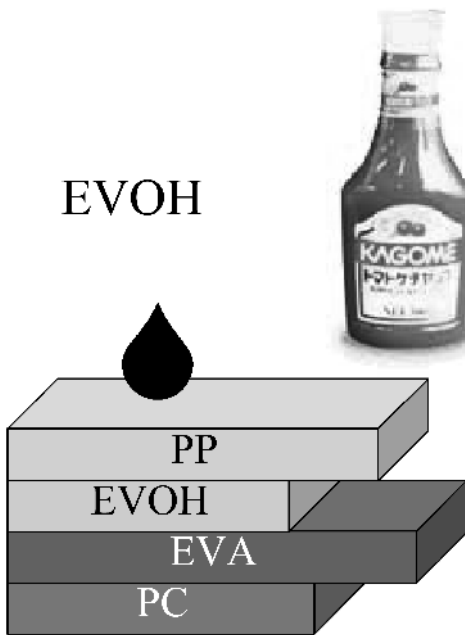


FIGURE 26.31 The packaging structure of the ketchup bottle from 1974 [27]. [Source: The bottle is reprinted with permission from Reed Business.]

free glossy look. In later versions of the ketchup bottle, EVOH is still protected with PP (MPP) and the adhesion is obtained by the use of maleated PP. For enhanced efficiency, a regrind layer is included (Figure 26.32).

PP/Regrind/mPP/EVOH/mPP/PP
inner: 10/45/2.5/5/2.5/35 (%)

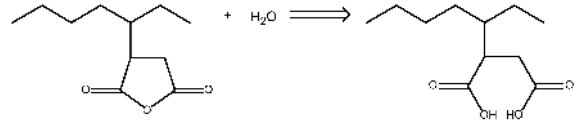


FIGURE 26.32 The layer structure in the modern ketchup bottle (within the frame) and the reaction of maleated PP with water at higher temperature to yield polar hydroxyl groups that enhances compatibility with the EVOH component.

SiO_x plasma deposition has become an attractive alternative to aluminium as a barrier component. It offers gas barrier protection and transparency. However, it needs a support and it is scratch sensitive and brittle [28]. Scratch sensitivity can be overcome by coating bottles on the inside (Figure 26.33) [29]. The thickness of the glass layer, typically around 10–100 nm, is chosen based on the combination of barrier efficiency and toughness [30]. Both brittleness and barrier efficiency increase with increasing glass thickness. The quality of the SiO_x coating is usually better when deposited on stiffer polymers (e.g., PET) rather than on softer ones (e.g., LDPE)

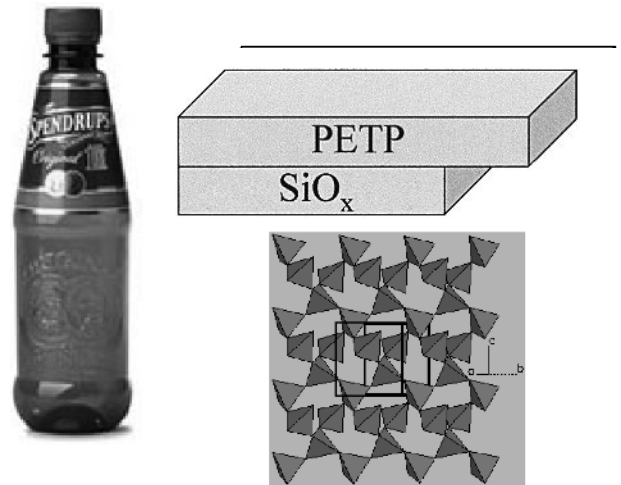


FIGURE 26.33 Swedish beer in a Glaskin[™] PET bottle. The SiO_x coating is located on the inside of the bottle wall and consists of an imperfect silicon tetrahedral three-dimensional structure (shown next the the bottle). [Source: The bottle is reprinted with permission of Spondrups.]

[28]. Improvements in gas barrier protection by a factor of 100 is not unrealistic when using the SiO_x deposition.

Other ceramic or similar options that are available as barrier coatings are “amorphous carbon” and Al_2O_3 . In 2000, Kronenbourg beer introduced their PET beer bottles that were coated on the inside with amorphous carbon using the Sidels Actis™ concept [31]. This coating is obtained through the generation of a cold plasma of acetylene gas. The amorphous carbon coating, with a thickness of typically 150 nm, lowers the oxygen and carbon dioxide permeability by, respectively, 30 and seven times [31,32].

The good properties, in combination with a lower price than SiO_x , makes Al_2O_3 an interesting choice [33]. Besides having enhanced gas and water vapor barrier properties, aluminium oxide-coated polyesters are thermally stable, possess excellent clarity, can be combined with any sealant and, in some cases, are even autoclavable. Other examples of ceramic coatings that have been considered for barrier improvement of plastics include SiN and ZnO [30].

Where transparency and microwavability are not critical, aluminium-based barriers are probably the ultimate choice for long shelf life (Figure 26.34).



FIGURE 26.34 A polypropylene bag metallized on the inside with a 30-nm-thick aluminium layer.

Aluminium can be incorporated as a foil, which is laminated with the adjacent materials, or it can be applied as a metallized layer. Foil thicknesses normally range between 6–200 μm [34]. It is easy to understand that with a thickness of 6 μm the weight of aluminium in, for example, an aseptic one-litre milk carton is only 1.5 g. Foils are laminated by various lamination techniques, including “hot melt” and “heat and pressure” lamination onto, for example, paper, paperboard, PETP, LDPE, LLDPE and HDPE [35].

Metallizing involves evaporation of aluminium at 1,400 °C onto a plastic film in vacuum. Typical thicknesses are on the order of less than 15 nm [30] to a few tenths of a nanometer (Figure 26.34). At these thicknesses, pinholes may be critical and metallized films are therefore normally laminated further to protect the metal layer. Although the improvement could be as high as 100 times, the metallized films are not as tight as the thicker foils, which may show, at a thickness of 25 μm , undetectably small values.

So far, we have dealt exclusively with protection against gases, vapors and liquids. However, for completeness, UV-barrier properties will now be addressed. A major cause of photo-oxidation of photo-sensitive products (including fats, beer, juice, and milk) is near-ultraviolet light (300–400 nm) [36]. The problem is that common transparent plastics are poor UV-barriers. PETP transmits light above 310 nm [36]. There are, however, ways to improve the UV-barrier efficiency. Black ink [37] and carbon black [38] are efficient but they also reduce the transmission of visible light. Organic UV absorbers (e.g., benzotriazole) or modified polymers can be used. However, these may cause problems in terms of cost, recyclability and safety [36]. By reducing the size of inorganic particles (e.g., TiO_2 and ZnO) to levels below where visible light is not scattered, it is possible to maintain polymer clarity. It is important here that the particles do not form aggregates. To further extend the UV absorption capability, the inorganic particles can be doped with iron ions. Elemental silicon, aluminium, chromium, nickel and copper are all efficient UV blockers [39]. These may be layered on plastics by the use of sputtering or various vapor deposition techniques, including anodic arc evaporative and plasma vapor deposition. These typically 50-nm-thick layers should be protected by the use of some top-coating. A patent describes the dipping of a Si-layered PETP-bottle in an aqueous low-molar mass carboxy-methyl cellulose solution to obtain the top coating [39].

26.3 FOOD PACKAGING

26.3.1 Introduction

Food products are usually complex systems that require a complex type of protection for prolonged shelf life. Living food-stuff that produce CO_2 (e.g., fermented milk) require a packaging which is permeable to CO_2 [40]. At the same time, water loss must be kept low, which in turn requires a high water barrier. The product also needs to be protected from oxygen and light that will eventually oxidize the fat.

The shelf life of a food product is dependent on time, temperature, moisture, light, gases, pressure, and types of biochemical and microbiological systems present. In the following section, some of these factors will be discussed, and it will conclude with a brief summary of polymers used in packaging. The topic is important since the packaging industry is the major consumer of plastics (37% by weight) [41].

26.3.2 Effects of Temperature and Time

Temperature control is one of the most important parameters to limit growth of micro-organisms. Bacterial growth at freezing temperatures is prohibited and growth increases drastically above 20–35 °C. At higher temperatures bacterial growth is slowed down again and bacteria may be completely destroyed. Pasteurization occurs at approximately 80 °C and sterilization is obtained at approximately 120 °C. After preservation, the time until renewed bacterial growth occurs depends on the heat sensitivity of the various bacteria.

26.3.3 Effects of Moisture

An important function for food packaging materials is to delay the water vapor transport into or out of the food. Meats and milks must not lose too much water. Fresh vegetables lose their texture if water activity is too low. To keep the activity of microorganisms to a minimum in dry foods, it is important to minimize the inflow of water. Note that because even dry foods (e.g., dried meals and soups) contain water (30–40%RH), little additional water would therefore be needed to raise the moisture content to hazardous values. Figure 26.35 shows the relative humidity region where the different microorganisms grow. Above 80% RH, food-stuff is considered to be microbiologically active. Drying is the cheapest way of preserving food for a six-month period (i.e., without the onset of mold growth).

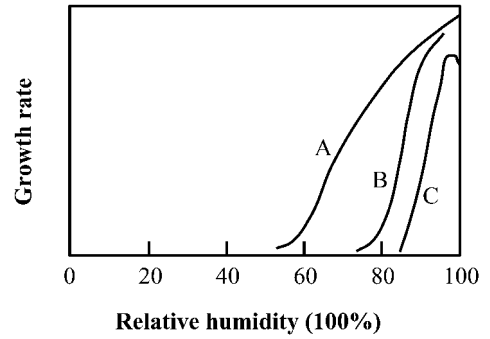


FIGURE 26.35 Effect of moisture on the growth of A, mold; B, yeast; and C, bacteria. [Source: Redrawn from ref. [50]. With kind permission of Kluwer Academic Publishers.]

To select a packaging material for a food product, it is important to know the range in water activity (a_w) or moisture content that is necessary to preserve the food quality. Figure 26.36 shows the acceptable ranges for some selected food-stuff. Above or below these values, the food-stuff is spoiled.

Interestingly, it has been shown that many food products are spoiled when the food moisture content is above the Brunauer-Emmett-Teller (BET) moisture level, which corresponds to a monolayer of water molecules ($a_w = 0.2$ – 0.3). Moreover, the rate of chemical and enzyme reactions that leads to deterioration increases drastically for every 0.1 a_w increase above the BET value.

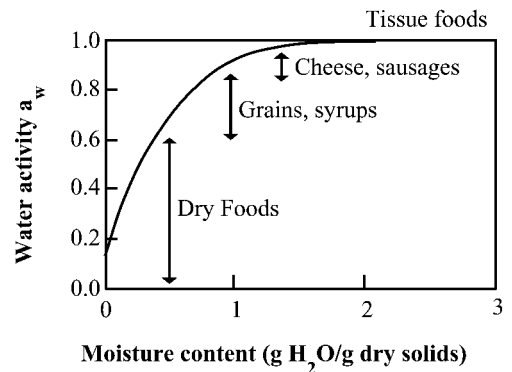


FIGURE 26.36 Water activity and moisture content for some foods. [Source: Redrawn from ref. [50]. With kind permission of Kluwer Academic Publishers.]

26.3.4 Effects of Oxygen

Fresh vegetables are usually picked before they ripen fully. During storage they are therefore in need of oxygen to respire. A packaging material with moderate oxygen permeability is suitable here. Vegetable and animal fats react with oxygen in the presence of light. Aldehydes are formed that make the fat rancid, leading to bad taste and flavor. This is especially critical for moist oil. These substances require a high-oxygen and light-barrier packaging material.

The fat in both fresh and cured meat is susceptible to oxidation in the presence of air. It is, however, not a good solution in the short term to avoid oxygen, since anaerobic microbes may then grow on the fresh meat. It is also important, for aesthetic reasons, that fresh meat is red while displayed on the shelf in the store. Fresh cut meat is purple due to myoglobin. It becomes red when the meat is exposed to oxygen, because myoglobin turns into oxymyoglobin. Oxymyoglobin is not stable and turns into metmyoglobin that yields a brown color. Thus, if the oxygen source is cut off the meat turns brown.

Modified atmosphere packagings (MAP) are used for several food-stuffs, including fresh meat, bacon, sausages, liver, and salads; it has been shown that MAP can extend the shelf life for several days for a fresh product (e.g., for fresh meat, an atmosphere of

20% CO₂ and 80% oxygen is used). The basic idea of many MAP packaging for fresh produce is to have an atmosphere that reduces the respiration rate of the food stuff and thereby prolongs its freshness.

26.3.5 Specific Requirements for Food and Material Selection

It is complicated to estimate the maximum tolerated uptake of different gases and vapors before the food product is spoiled. The reason is that many food products consist of several different food components. An empirical and general guideline is, however, given in Table 26.4 for some food products.

TABLE 26.5 Calculated Upper Limits of Oxygen Permeabilities Needed for Preserving the Food Quality during One Year and One Week

| | Permeability O ₂ (Barrer) | Maximum O ₂ Perm (Barrer) | |
|--|---|---|----------|
| | | 1 Year | 1 Week |
| FOOD OR BEVERAGE | | | |
| Canned milk, meats | | 0.0004–0.002 | 0.02–0.1 |
| Baby food | | | |
| Beer, ale, wine | | | |
| Instant coffee | | | |
| Canned vegetables, Soups, spaghetti | | | |
| Canned fruits | | 0.002–0.006 | 0.1–0.3 |
| Nuts, snacks | | | |
| Dried foods | | | |
| Fruit juices, drinks | | 0.004–0.016 | 0.2–0.8 |
| Carbonated soft drinks | | | |
| Oils, shortenings | | 0.021–0.084 | 1.1–4.4 |
| Salad dressings | | | |
| Jams, pickles, Vinegars | | | |
| Liquors | | | |
| Peanut butter | | | |
| POLYMERS | | | |
| LDPE | 2.9 ^a | | |
| HDPE | 0.4 ^a | | |
| APET | 0.06 ^a | | |
| Poly(lactic acid) | 0.6 ^b | | |
| Polyesteramide | 0.3 ^c | | |
| Poly-ε-caprolac- tone | 0.5 ^d | | |
| PA-6 | 0.018 ^a | | |
| Nitrile barrier resin | 0.0055 ^a | | |
| PVdC | 0.00034–0.0010 ^a | | |
| EVOH | 0.00014 ^a | | |

TABLE 26.4 Requirements for Preserving the Food Quality During a Year (25 °C)^a

| Food or beverage | Maximum estimated acceptable oxygen gain (ppm) | Maximum acceptable water gain or loss (%) |
|--------------------------------|--|---|
| Canned milk, meats and fish | 1–5 | 3, loss |
| Poultry | | |
| Canned vegetables | | |
| Soups | | |
| Sauces | | |
| Canned fruits | 5–15 | 3, loss |
| Nuts, snacks | | 5, gain |
| Dried foods | | 1, gain |
| Fruit juices, soft drinks | 10–40 | 3, loss |
| Carbonated soft drinks | | |
| Oils, fats, shorten- ings | 50–200 | 10, gain |
| Salad dressings | | |
| Pickles | | 3, loss |
| Preserves | | |

(a) From ref. [50]

Notes: (a) [42]; (b) [51], co-polymer; (c) [19]; (d) [52]

From Table 26.4 it is possible to calculate the upper limit of acceptable permeability. This is possible by assuming that there is a steady-state gas flow into or out of the product and packaging during the entire shelf life. It is also possible to calculate the upper limit of acceptable permeability if the product is to be stored for only a week, for example. Here it is assumed that the same oxygen uptake or water gain/loss limits hold also for shorter shelf lives. The calculated oxygen permeabilities are given in Table 26.5, together with oxygen permeabilities for a few selected polymers.

As observed in Table 26.5, the demands are high for most oxygen sensitive products, and not many polymers can meet the requirements for a one year shelf life. EVOH is, of course, a good candidate and is also frequently used in food packaging applications.

26.4 ACKNOWLEDGEMENTS

Inger Lord at my department is gratefully acknowledged for assisting with the copyright work.

26.5 REFERENCES

1. Takanori, K., Akimasa, A., Fumio, N., Katsumi, S., Hisamichi, Y., Takeshi, M. In *Patent, esp@cenet* (Kuraray Co., Japan, 1992).
2. Axelsson-Larsson, L. In *Foods and Packaging Materials—Chemical Interactions*. P. Ackermann, M. Jägerstad and T. Ohlsson, Eds. Cambridge: The Royal Society of Chemistry, 1995, 129.
3. www.flexipack.co.id.
4. www.bppetrochemicals.com. BP Petrochemicals, Naperville, 2000.
5. Karlsson, G. E., Johansson, T. S., Gedde, U. W., Hedenqvist, M. S. *J Macromol Sci-Phys.* 2002; B41:185.
6. Selin, J. -F. Report 13. *Tekes*. Helsinki, 1997.
7. Cargill Dow, LLC. Datasheet 2003.
8. Silvis, H. C. *Trends Polym Sci.* 1997, 5:75.
9. www.sepha.com.
10. www.hgc.hydro.com.
11. www.reed-electronics.com.
12. Ticona. Technology Info on Topas® 2001.
13. Lamonte, R. R., McNally, D. *Advanced Materials and Processes*. March, 2001.
14. Poulsen, L., Zebger, I., Klinger, M., Eldrup, M., Sommer-Larsen, P., Ogilby, P.-R. *Macromolecules*. 2003, 36:7,189.
15. Jansson, S. E. A., Gallet, G., Hefti, T., Karlsson, S., Gedde, U. W., Hedenqvist, M. S. *Packag Techn Sci.* 2002, 15:287.
16. Leaversuch, R. In *Plastics Technology*. Online article, 2003.
17. Nugent, R. M. J., Niederst, K. W., Seiner, J. A. *United States Patent* (PPG Industries, Inc., U.S.A., 1994).
18. Lange, J., Nicolas, B., Galy, J., Gerard, J.-F. *Polymer*. 2002, 43(22):5,985.
19. Krook, M., Albertsson, A. -C., Gedde, U. W., Hedenqvist, M. S. *Polym Eng Sci.* 2002, 42:1,238.
20. Socci, E. P., Akkapeddi, M. K., Worley, D. C. In *ANTEC* 476, 2001.
21. www.bpchemicals.com. Naphthalates.
22. Reynolds, P. *Packaging World Magazine*, www.packworld.com, 1996, 34.
23. Worley, D. C. I., Akkapeddi, M. K., Socci, E. P. Honeywell—Plastics, technical papers, 2003.
24. ExxonMobil Chemical Co. *Packaging World Magazine*. www.packworld.com 2001, May, 10.
25. UCB Films, Inc. *Packaging World Magazine*. www.packworld.com, 2002, March.
26. www.dupont.com/packaging.
27. Louis, P. J. *Packaging Digest*. 1999, December, 48.
28. Hedenqvist, M. S., Johansson, K.S. *Surface Coat Techn.* 2003, 172, 172.
29. TetraPak. *Plast Net*. 2000, January.
30. Chatham, H. *Surface Coat Techn.* 1996, 78:1.
31. Guillet, B. In *Drinktec 2001*. Stand 521/539, Munich, 2001.
32. www.actis-tm.com. SIDEL, 2003.
33. Berger, K., Doudrill, D. *Medical Device and Diagnostic Industry*. 2001, August.
34. Labberton, M. G. *European Aluminium Association*. Report. Brussels, 1997.
35. www.saarcnet.org.
36. Shirakura, A., Takeda, A., Kaito, C. In *Proceedings of the Worldpak 2002 Conference*. 2002, 1:417.
37. Soichi, A., Yoshiaki, O. Patent. esp@cenet 2003.
38. Klint, L., Bergholtz, L. Patent, esp@cenet 1999.
39. Rule, M., Ehrich, H., Shi, Y. Patent, esp@cenet 2002.
40. Jansson, S. A. E., Edsman, C. J., Gedde, U. W., Hedenqvist, M. S. *Packag Techn Sci.* 2001, 15:119.
41. Maxwell, J. *Plastics, The Layman's Guide*. Cambridge: The University Press, 1999.
42. Pauly, S. In *Polymer Handbook*. J. Brandrup, E. H. Immergut, and E. A. Grulke, Eds. New York: John Wiley & Sons, Inc., 1999.
43. Marklund, E., Gedde, U. W., Hedenqvist, M. S., Wiberg, G. *Polymer*. 2001, 3,153-3,160.
44. Flodberg, G., Hellman, A., Hedenqvist, M., Sadiku, E. R., Gedde, U. W. *Polym Eng Sci.* 2000, 40:1,969.
45. Flodberg, G., Höjvall, L., Hedenqvist, M., Sadiku, E. R., Gedde, U. W. *Intern J Polym Mater*. 2000.
46. McGonigle, E. -A., Liggat, J. J., Pethrick, R. A., Jenkins, S. D., Daly, J. H., Hayward, D. *Polymer*. 2001, 42:2,413.
47. Lau, T., Kaviratna, P. D., Pinnavaia, T. J. *Chem Mater*. 1994, 6:573.

48. Hedenqvist, M., Gedde, U. W. *Packag Techn Sci.* 1999, 12:131.
49. MacDonald, R. W., Huang, R. Y. M. *J Appl Polym Sci.* 1981, 26:2,239.
50. Ashley, R. J. *Permeability and Plastics Packaging.* J. Comyn, Ed. London: Elsevier, 1985.
51. CPLA. Technical data sheet from DIC 1997.
52. Hedenqvist, M. S., Ohrlander, M., Palmgren, R., Albertsson, A. -C. *Polym Eng Sci.* 1998, 38:1,313.
53. Shah, K., Ling, M. T. K., Woo, L., Nebgen, G., Edwards, S., Zakarija, L. *Medical Plastics and Biomaterials Magazine.* 1998, September:52.
54. Luise, R. R. In *Wiley Encyclopedia of Packaging Technology.* A. R. Brody and K. S. Marsch, Eds. New York: John Wiley & Sons, Inc., 1997.
55. Flodberg, G., Hedenqvist, M., Gedde, U. W. *Polym Eng Sci.* 2003, 43:1,044.
56. Mitsubishi Gas Chemical Company I. MX Nylon Web Catalog 2003.
57. Backman, A., Lange, J., Hedenqvist, M. S. *Journal of Polymer Science, Part B: Polymer Physics.* 2003.

CHAPTER 27

CORROSION PREVENTION AND CONTROL OF CHEMICAL PROCESSING EQUIPMENT

William Stephen Tait

Pair O Docs Professionals L.L.C., Madison, Wisconsin

| | | | |
|--|-----|---|-----|
| 27.1 INTRODUCTION | 565 | 27.5 CORROSION PREVENTION AND CONTROL THROUGH CORROSION TESTING | 577 |
| 27.2 DIFFERENT TYPES OF CORROSION | 565 | 27.6 CHAPTER SUMMARY | 580 |
| 27.3 PREVENTING AND CONTROLLING CORROSION | 567 | 27.7 SOURCES OF FURTHER INFORMATION | 580 |
| 27.4 SELECTING CORROSION RESISTANT MATERIALS FOR CHEMICAL PROCESSING EQUIPMENT | 575 | 27.8 REFERENCES | 580 |

27.1 INTRODUCTION

A typical chemical process can include many different types of equipment. For example, a chemical process could include one or more:

- Reaction vessels
- Mixing vessels
- Heat exchangers
- Storage tanks
- Pumps
- Valves
- Transfer pipelines

One can imagine that numerous different metals and alloys are used to fabricate the different types of equipment that are part of a chemical process. Indeed, the number of different metals and alloys available for the chemical process industry is extensive, and often mind-boggling, particularly when one is responsible for specifying the most corrosion resistant materials for each type of equipment, while trying to minimize the total cost of the equipment for the chemical process.

Almost all metals are oxides in their natural state, and considerable energy is required to transform these oxides into metals. Unfortunately, metals and their alloys have a very strong tendency to corrode and thus return to their stable oxide form. Indeed, metal alloys often have an even stronger tendency to

corrode than their constituent metal components. For example, in certain situations pure iron is significantly more resistant to corrosion than low carbon steel.

This chapter will focus on the major methods for preventing or controlling chemical process equipment corrosion. I will not be so brash as to claim that reading this chapter will transform the reader into an expert on corrosion prevention and control. Such a claim is irresponsible. However, this chapter will provide the reader with a background on:

- How to identify the more common forms of chemical processing equipment corrosion
- The different ways that chemical processing equipment corrosion can be prevented or controlled
- How to effectively communicate with corrosion professionals in those instances when a consultant is needed to help solve a processing equipment (or system) corrosion problem

27.2 DIFFERENT TYPES OF CORROSION

Many different types of corrosion could shorten processing equipment service lifetime. One important method for preventing and controlling corrosion is being able to identify the type of corrosion that is degrading your processing equipment. As you can imagine, there are many different types of corrosion.

Some types of corrosion are typically a nuisance, such as uniform rusting, and some types of corrosion, such as pitting and stress corrosion cracking, can lead to catastrophic equipment failure or failure of the entire chemical process.

Each type of corrosion is initiated in a different way, and the methods for preventing and controlling each type of corrosion can be significantly different. Corrosion types can be broadly categorized as:

1. Uniform or general corrosion
2. Localized corrosion

The basics of corrosion engineering and science are discussed in another chapter in this handbook, so let us briefly review how general and localized corrosion are different, and how you can recognize each type.

27.2.1 Uniform or General Corrosion

Uniform or general corrosion occurs over most (if not all) of a piece of chemical processing equipment, hence the name *uniform* or *general corrosion*. Figure 27.1 is a photograph of general corrosion on the gate from a gate valve used in a chemical transfer pipeline.

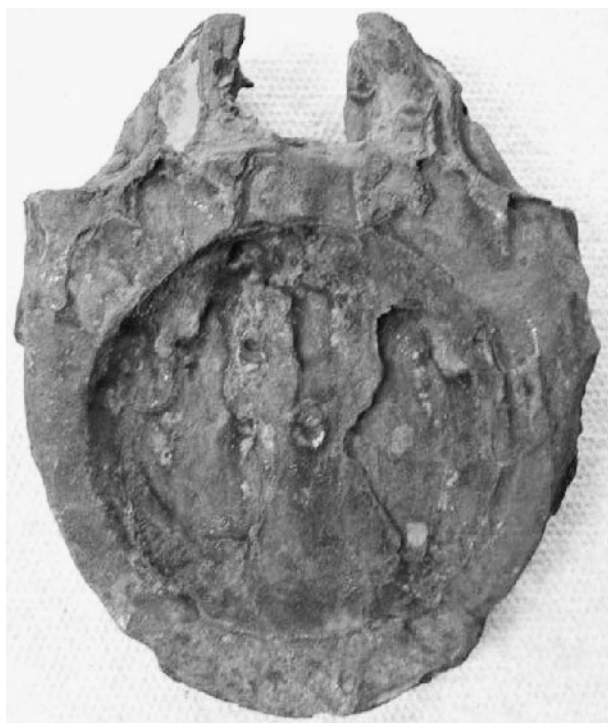


FIGURE 27.1 General (uniform) corrosion on a low carbon steel gate valve.

The solution being transferred through the valve was an aqueous solution that caused extensive uniform corrosion. The corrosion also reduced the thickness of the pin that attached the gate to the valve shaft so that the pin was too thin to support the gate's weight and it fell into the bottom of the valve body.

Even though general corrosion is often referred to as uniform corrosion, the depth of corrosion on the metal surface is actually not totally uniform, as can be seen in Figure 27.1. Indeed, there are typically peaks and valleys over the metal surface when general corrosion attacks a metal. However, corrosion is considered to be general when there are no *small deep* corroded areas on the metal.

27.2.2 Localized Corrosion

Localized corrosion (in contrast to general corrosion) is observed in small *local* areas on chemical processing equipment. Figure 27.2 contains an example of pitting corrosion in a chemical transfer pipeline. Localized corrosion, such as that shown in Figure 27.2, penetrates the metal very rapidly. Indeed, localized corrosion rates are often several orders of magnitude greater than the corrosion rates for general corrosion.

27.2.3 Estimating Processing Equipment Service Lifetime from Corrosion Rate Data

Corrosion rates are typically recorded in mils per year (1 mil = 0.001 inches). The service lifetime of

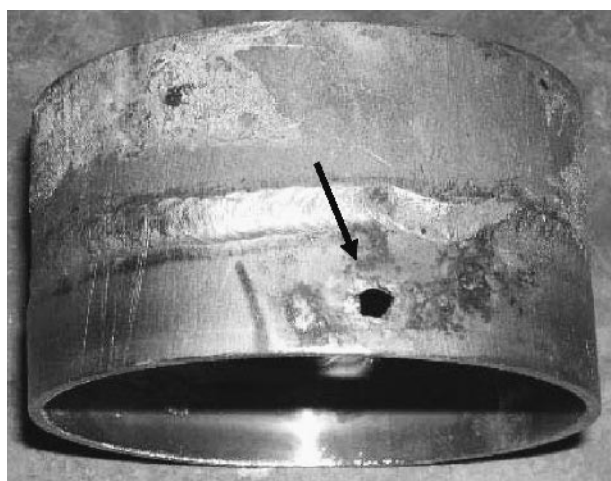


FIGURE 27.2 Pitting corrosion perforated this section of a stainless steel chemical transfer pipeline. The perforation is well outside of the weld heat affected zone, so the pitting corrosion was not caused by weld sensitization.

chemical equipment can be estimated by dividing the corrosion rate into the wall thickness of the equipment:

$$\text{Estimated service lifetime} = \frac{\text{equipment wall thickness}}{\text{Corrosion rate}} \quad (27.1)$$

For example, if the corrosion rate is 5 mils per year (5 mpy) and the processing equipment has a 1/8-inch-thick wall (125 mils), then the estimated service lifetime is:

$$\begin{aligned} \text{Estimated Service Lifetime} &= \frac{125 \text{ mils}}{5 \text{ mpy}} \\ &= 25 \text{ years} \end{aligned}$$

One should keep in mind that equipment which is bearing a load or under pressure needs a minimum wall thickness to prevent equipment failure. Thus, Eq.(27. 1) could be modified for load-bearing or pressurized equipment as follows:

$$\text{Estimated Service Lifetime} = \frac{\text{minimum equipment wall thickness}}{\text{Corrosion rate}} \quad (27.2)$$

The corrosion rates used with Eqs. (27.1) and (27.2) could be either the general or localized corrosion rates. I recommend that both rates be used with Eqs. (27.1) and (27.2) because the service lifetime for general corrosion is most often significantly longer than the service lifetime for localized corrosion rates.

27.3 PREVENTING AND CONTROLLING CORROSION

There are a number of ways to prevent and control corrosion, and the diagram in Figure 27.3 summarizes the important elements of a comprehensive corrosion prevention and control program. Let us briefly discuss each element in Figure 27.3.

27.3.1 Experience and Knowledge

How do we know which corrosion prevention and control program to use for new chemicals, chemical streams or new chemical processes? The obvious answer is through experience and knowledge. But how is that experience and knowledge acquired? Experts in the field of Continuing Professional Education refer to *knowing-in-action* (experience) and *reflec-*

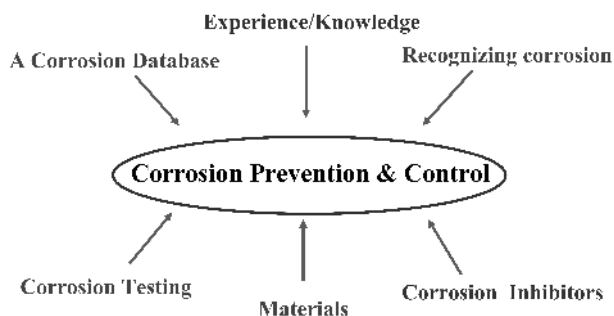


FIGURE 27.3 The important elements in a comprehensive corrosion prevention and control program.

tion-in-action (knowledge) as the ways that professionals perform professional practice, such as selecting and implementing a program for preventing and controlling chemical processing equipment corrosion.

Professionals analyze and codify expert practices, in particular, knowledge gained from experience, examples, observations, corrosion problems, descriptions, experiments and networking [1]. This practical knowledge (i.e., experience) must be integrated into a framework that includes pertinent explanatory theories and applied theories (i.e., knowledge).

Knowledge without practical experience, or experience without theoretical frameworks, are incomplete and will not result in useful, predictive professional practice. In other words, experience and knowledge are complementary. Thus, using specialized corrosion knowledge (e.g., from published or company corrosion databases) and everyday experience (e.g., talking with experienced personnel about your corrosion problem) yields useful and actionable corrosion prevention and control measures for chemical processing equipment.

Experience combined with knowledge allows one to avoid repeating past mistakes and, thus, projects are completed more efficiently. For example, one would not use UNS Type S30400 stainless steel to construct a pipeline for transferring hydrochloric acid based on the experience of others, the specifications for this type of stainless steel, and published corrosion rate information for stainless steel in hydrochloric acid.

Technical associations have knowledge bases that are available to members and can be purchased. For example, the National Association of Engineers (NACE) (www.nace.org) publishes the corrosion rates for numerous metals and alloys in a wide range

of chemical streams [2]. ASM International (www.asm-intl.org) also publishes numerous books on a variety of materials used to fabricate chemical process equipment.

27.3.2 Recognizing the Different Types of Corrosion that Can Degrade Process Equipment Performance and Equipment Service Lifetime

The types of corrosion are so numerous that they cannot be completely covered in a single chapter, or even a single book. For, example, The Nalco Chemical Company publishes a book that is devoted to only identifying corrosion failures of the boiler equipment used to provide steam to chemical processing plants [3].

However, this section provides a brief overview of the more common types of chemical processing equipment corrosion so that the reader can visually identify corrosion. Identifying the type of corrosion is the first step toward preventing and controlling the corrosion of your chemical process equipment.

27.3.2.1 Recognizing Chemical Processing Equipment General (Uniform) Corrosion

This section discusses three types of general (uniform) corrosion:

1. Surface corrosion
2. Cavitation corrosion
3. Erosion corrosion

Surface Corrosion. Figure 27.4 contains a photograph of a stainless steel component removed from equipment used to process food. Notice the extensive general (uniform) corrosion on the face of the C-shaped portion of the component.

Maintenance personnel cleaned the food processing equipment between production runs with steel wool. Steel is softer than stainless steel and will smear, contaminating the stainless steel surface with iron. The iron contamination rapidly corrodes, as seen in Figure 27.4.

A stainless steel wire brush should be used to clean stainless steel if abrading is the cleaning method of choice. Soap solutions could also be used to clean stainless steel parts. Stainless steel can also be cleaned with acid solutions. The National Association of Corrosion Engineers TM0169-76 standard



FIGURE 27.4 The surface of this stainless steel part was cleaned with steel wool. The resulting contaminated surface rusted while the part was in use.

test method contains a table of acid solutions for cleaning various metal alloys [4].

Cavitation Corrosion. Cavitation occurs in pumps when the inlet of the pump does not supply the pump with fluid fast enough to match the amount of fluid that is discharged from the pump outlet. Gas bubbles form inside the pump under these conditions and subsequently collapse under pressure. High-speed fluid strikes the metal when the bubbles collapse at the metal surface. Cavitation and corrosion work to cause more rapid equipment degradation than would occur with either corrosion or cavitation alone because:

- Metal corrosion forms metal oxides and metal hydroxides on the metal surface
- The high-speed fluid (caused by cavitation) impinges on the metal and removes the metal oxides and metal hydroxides, exposing fresh metal
- The fresh metal corrodes

The above cycle repeats until the metal component fails.

Strictly speaking, the sample shown in Figure 27.5 is not from a chemical process. However, this example is one of the most pronounced examples of cavitation corrosion that I have seen, so I included it as an example in this chapter. Propellers with similar shapes to that in Figure 27.5 are also used in chemical mixing kettles. Notice the grooves in the metal in Figure 27.5. Cavitation can be avoided by proper design of the piping system, proper sizing of



FIGURE 27.5 Cavitation corrosion of a stainless steel propeller.

fluid pumps, and proper design of the propellers used in mixing kettles.

Erosion Corrosion. Erosion corrosion is similar to cavitation corrosion in that fluid movement removes corrosion from the metal surface, thus exposing fresh metal for further corrosion. The difference between cavitation corrosion and erosion corrosion is that fluid movement over the corroded metal surface enhances corrosion instead of high-speed fluid impinging on the metal surface. Erosion corrosion follows a basic pattern of:

- Metal corrosion forms metal oxides and metal hydroxides on the metal surface
- Fluid moving over the metal removes the oxides and hydroxides, exposing fresh metal
- The fresh metal corrodes

This process continues to cycle from beginning to end until the metal component fails.

Figure 27.6 contains a photograph of an impeller removed from a failed brass water pump, and a close-up photograph of one of the corroded impeller blades. The erosion-corrosion process continued until the pump no longer pumped water. A chemical corrosion inhibitor or selection of a more corrosion resistant brass would have prevented this failure.

27.3.2.2 Recognizing Localized Corrosion

This section discusses seven types of localized corrosion:



FIGURE 27.6 Erosion corrosion of a brass water pump. (Top) Photograph showing all of the corroded pump impellers. (Bottom) Close-up of the erosion corrosion on one of the pump impellers.

1. Pitting corrosion under deposits
2. Pitting corrosion in crevices
3. Stress corrosion cracking
4. Microbial-induced corrosion
5. Galvanic corrosion
6. Tuberculation corrosion
7. Exfoliation corrosion

Pitting Corrosion under Deposits. Several alloys, such as stainless steels and nickel alloys, form thin transparent passive oxide layers on their surfaces. This passive layer is usually a protective barrier between the base metal and the chemical stream. However, the chemical stream could interact with the passive layer. The layer would be degraded by

the chemical stream and the layer would quickly reform with oxygen or other oxidizing chemicals dissolved in the chemical stream.

Non-porous deposits on metal surfaces can restrict or even prevent oxygen (or other oxidizing chemicals) from reaching the metal surface, and thus prevent reforming of the passive oxide layer. This type of situation could produce pitting corrosion under the deposit.

Figure 27.7 contains a photograph of a section of stainless steel pipe that was used to transfer a viscous liquid from a mixing kettle to equipment that filled the liquid into plastic bottles. The pipeline was traced with electrical heating tape to maintain the temperature so that the liquid viscosity was low enough to be able to pump the liquid from the kettle to the filling equipment. The section of pipeline in Figure 27.7 was located in an area of the factory that was difficult to access. Thus, the contractor attached the heating tape linearly across the pipe (the dashed lines in Figure 27.7) instead of spirally winding the tape around the pipe.

Notice the three elliptical rings above the arrows in Figure 27.7. These rings are the remnants of dark brown deposits that formed under the heat tape inside the pipe. The pipeline perforated under these deposits, as can be seen in the close-up photograph in Figure 27.8.

Investigation of the deposits revealed that they were formed when the material in the pipeline was charred at hot spots under the heat tape. Charring occurred during processing downtimes when the pipeline was full. The charred material formed non-porous deposits on the pipe wall that deprived the stainless steel of oxygen (to replenish its passive layer) and caused rapid pitting corrosion.



FIGURE 27.8 The deposits baked on by hot spots on the pipe surface created corrosion and perforation under the deposits. This photograph is an enlargement for one of the deposits seen in Figure 27.7.

This pipeline failure could have been avoided by spirally winding the heat tape around the pipeline to provide more uniform heating. Temperature probes could also have been installed at various locations along the pipeline so that the amount of heat could have been reduced during downtimes, and thus avoided baking deposits on the pipe surface.

Pitting Corrosion in Crevices. Crevices are very small gaps between two surfaces. Crevices are formed when two layers of materials overlap, or

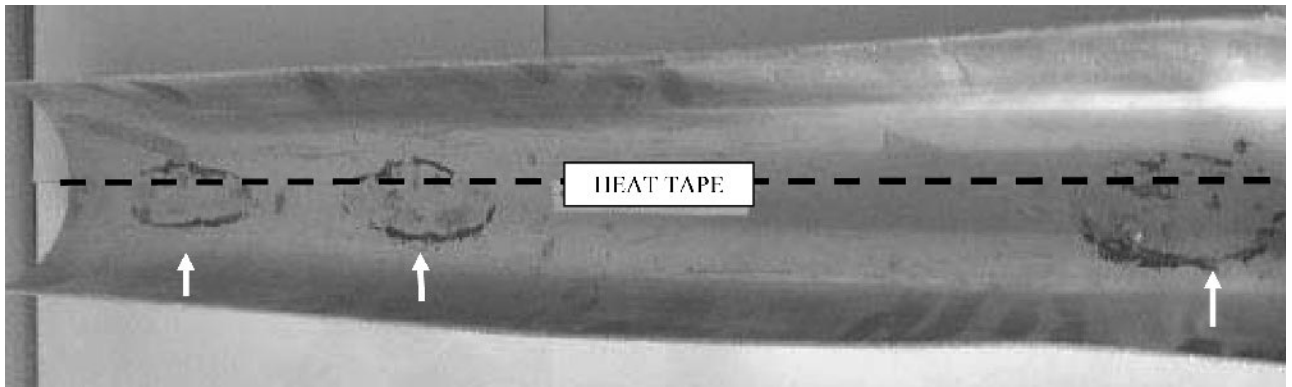


FIGURE 27.7 The heat tape was attached along length instead of wound around the pipe.

where fasteners are used to join two components. The movement of the chemical stream into and out of crevices is restricted, creating an extremely corrosive micro-environment inside of the crevice. Crevice corrosion is characterized by very rapid general corrosion in conjunction with pitting corrosion inside of the crevice.

Figure 27.9 contains a photograph of a section of sanitary pipe that was removed from the bottom of a stainless steel storage tank. The arrows indicate the locations of extensive crevice corrosion along the edge of the piece. Overtightening of the gasket distorted it and raised the gasket away from the flange face to form crevices between the gasket and the metal at several areas along the flange face. The chemical stream diffused into the crevices and caused the severe crevice corrosion seen in Figure 27.9. Proper tightening of the gasket would have avoided creating crevices between the gasket and the flange face, and thus avoided the severe crevice corrosion.

Stress Corrosion Cracking. Pitting corrosion can also lead to cracking of the metal. Residual stresses or stresses created by thermal loads, external mechanical loads, or internal pressure create a very high stress at the bottom of the pit that can lead to metal cracking.

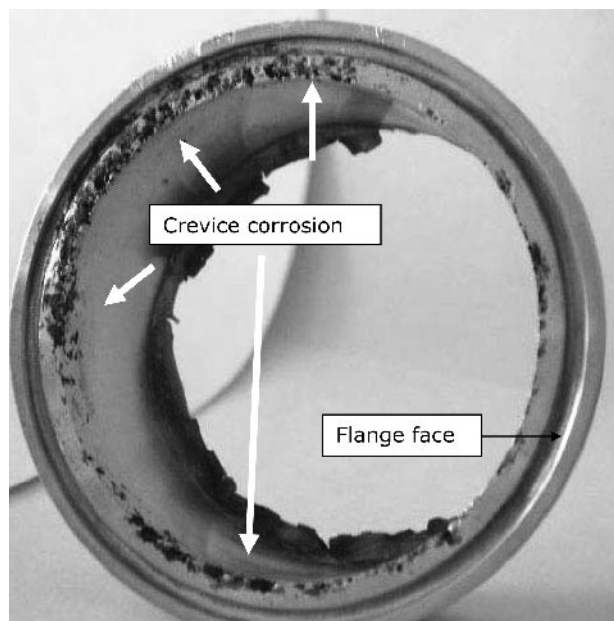


FIGURE 27.9 Crevices created under the gasket for this sanitary pipe caused severe crevice corrosion in the form of deep pits under the gasket.

Figure 27.10 contains photographs of two stainless steel tubes that were removed from a shell-and-tube heat exchanger. The top tube is the water side of the tube, and the bottom tube is a cross-section of the product side of the heat exchanger tube. The two arrows on the bottom tube locate a crack in the tube. This crack penetrated through the tube in several places along the crack length, allowing water to spray into the hot product stream.

Notice the hard water deposits on the top tube in Figure 27.10. The heat exchanger was not sized properly, so water at the heat exchanger outlet was hotter than the inlet water, causing calcium and magnesium compounds to precipitate on the tube surfaces next to the exchanger outlet. Pitting corrosion initiated under these deposits (or precipitates), and chloride ions migrated into the pits, producing the appropriate chemistry to cause cracking.

This problem could have been avoided in several ways:

- The heat exchanger could have been specified to prevent calcium and magnesium precipitates from depositing on the tube surfaces
- Softened, deionized, or deionized-reverse osmosis water could have been used instead of tap water to avoid precipitating calcium and magnesium
- Scale-preventing chemicals and corrosion inhibitors could have been added to the cooling water

Microbial-Induced Corrosion. Figure 27.11 contains an example of microbial-induced corrosion on stainless steel. This section of pipe is a sanitary pipe elbow that was removed from the bottom of a mixing kettle. Notice the *water-staining* on the pipe at the top of the photograph in Figure 27.11 (inside the dashed lines). Notice also the clusters of large pits at the bottom of the photograph (indicated by the multiple dark arrows), next to the area where the gasket seals against the pipe flange.

The elbow in Figure 27.11 was overtightened (like the sanitary pipe in Figure 27.9), causing the gasket to extrude above the flange into the interior of the elbow. The extruded gasket formed a wall that produced a small reservoir of product when the kettle was drained. The dashed lines in Figure 27.11 indicate the approximate boundary of the fluid reservoir, and the two arrows inside the dashed lines locate the water-staining. Bacteria grew in this reservoir, nourished by the residual product. Bacteria ex-

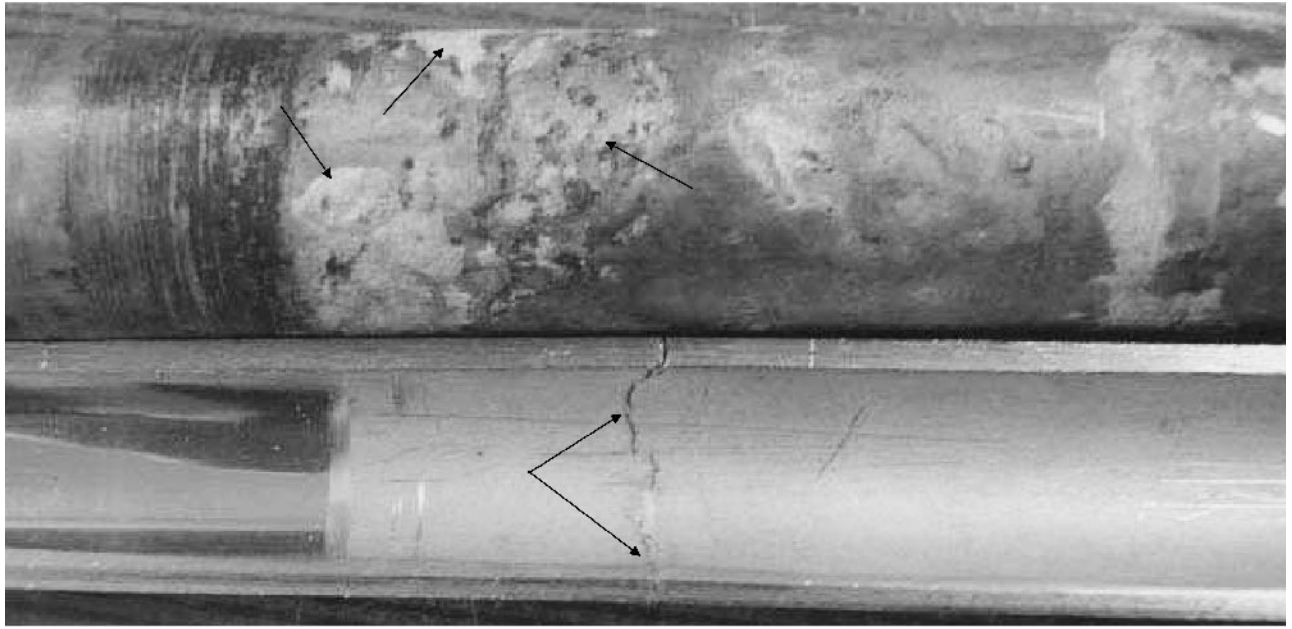


FIGURE 27.10 Stress corrosion cracking of a stainless steel heat exchanger.

crete organic acids as they grow and multiply, so the fluid under the bacteria colonies had a low pH, plus oxygen was restricted from reaching the metal under the colonies. The low pH and restricted oxygen access produced the pitting corrosion under the bacteria colonies.

The localized corrosion in Figure 27.11 was almost halfway through the pipe wall after a few days. This elbow would have quickly perforated had it not been removed for a routine maintenance. This corrosion could have been avoided by: (a) not overtightening the gasket, and (b) thoroughly rinsing the kettle with water after it was drained.

Galvanic Corrosion. Metals develop measurable electrical potentials (or a potential difference between the metal and a reference electrode) when submerged in a solution. These potentials are referred to as open circuit potentials or corrosion potentials [5].

The composition of the chemical stream determines the open circuit potential of a given metal or alloy. For example, steel has one open circuit potential in tap water, and an entirely different open circuit potential in hydrochloric acid. Thus, metal and alloy open circuit potentials are a reaction of the metal or alloy to its environment and are not an intrinsic property of the metal or alloy.

A large potential difference between two different metals can cause galvanic corrosion between the two metals. The metal with the smallest open circuit potential will corrode and is referred to as the anode. The metal with the largest open circuit potential will not corrode and is referred to as the cathode.

There are three conditions needed for galvanic corrosion to occur between two different metals:

1. The two metals have significantly different open circuit potentials
2. The two metals are in electrical contact with each other (e.g., they are directly touching each other)
3. There is an electrolyte covering the contact area between the two metals

The magnitude of galvanic current is determined in part by the ratio of the cathode and anode areas [6].

$$\text{Galvanic rate} = \left(\frac{\text{Anode base corrosion rate}}{1 + \left| \frac{\text{cathode area}}{\text{anode area}} \right|} \right) \quad (27.3)$$

The galvanic corrosion rate in Eq. (27.3) increases as the area of the anode (the metal with the smaller open circuit potential) becomes smaller. Let us look at two examples of galvanic corrosion.

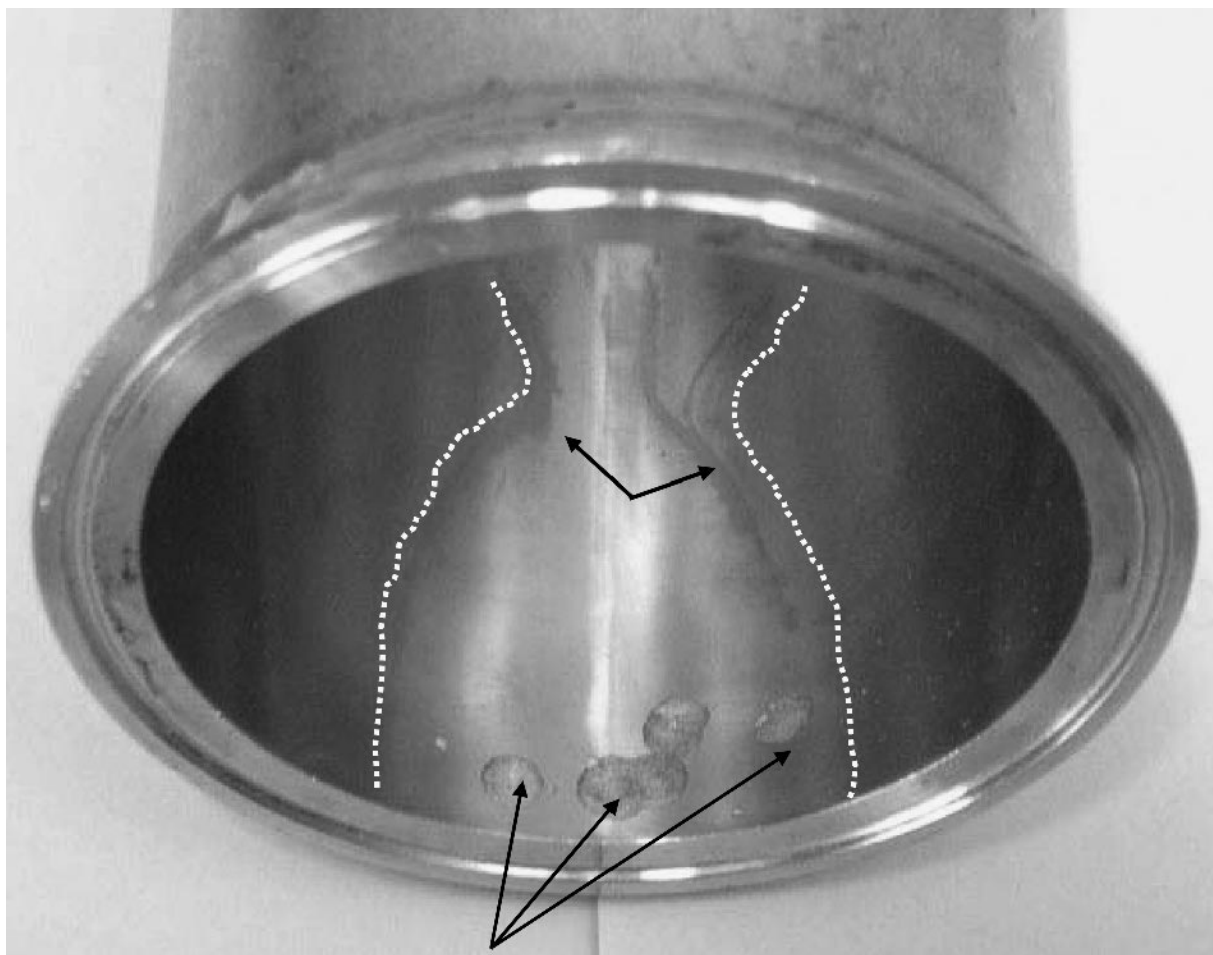


FIGURE 27.11 The gasket on this section of sanitary pipe created a fluid reservoir. Water and residual product created conditions for growth of bacterial colonies and subsequent microbial-induced corrosion. This section of sanitary pipe was located at the bottom of a large mixing kettle.

Large anode in contact with a small cathode. The photograph in Figure 27.12 shows a small cathode (a zinc-coated steel sheet metal screw) in contact with a large anode, UNS Type A1100 aluminum sheet metal. Notice that the aluminum is black and the steel screw is only slightly white. The white material on the screw and the white halo around the screw is most likely zinc oxide, so the aluminum sheet metal is essentially protecting the steel from corroding. Indeed, the screw would be completely covered with rust if it was not in (electrical) contact with the aluminum sheet metal.

Small anode in contact with a large cathode. The photograph in Figure 27.13 contains a small anode (a zinc-coated steel screw) in contact with a large cathode, a piece of UNS Type S30400 stainless steel

sheet metal. Notice that the screw is severely corroded in this case. Indeed, the fluid contained by the sheet metal leaked around the screw shaft. The small rust-halo around the screw is steel corrosion from the screw that precipitated from solution onto the stainless steel. Galvanic corrosion between the stainless steel and the screw accelerated the corrosion of the zinc-coated screw.

Fastening together or overlapping two different metals should be avoided whenever possible. However, if you cannot avoid fastening together or overlapping two different metals, then select the two metals such that you have a large anode in contact with a small cathode.

Tuberculation in a hot water pipeline. Figure 27.14 contains an example of a section of UNS Type



FIGURE 27.12 Galvanic corrosion where a large anode area is in contact with a small cathode area.

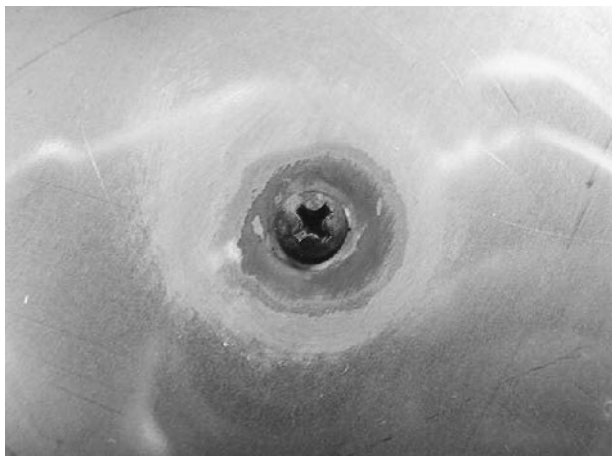


FIGURE 27.13 Galvanic corrosion where a small anode area is in contact with a large cathode area.

S31600 stainless steel pipe removed from a hot water transfer pipeline. Notice the dark brown nodules that look somewhat like tubercles found on structures and boats exposed to sea water. Deep pits are under with each tubercle, and these pits caused perforation and cracking (at the pits) of the hot water pipeline.

This type of problem can be avoided by adding chemical corrosion inhibitors to the hot water stream to prevent formation of tubercles. Choosing a more corrosion resistant metal alloy for the transfer piping could also have prevented this problem from occurring. Periodic pigging of the pipeline might also



FIGURE 27.14 Tuberculation corrosion inside of a stainless steel pipeline used to transfer 180 °F hot water for heating mixing vessels.

have stopped pitting and cracking by removing the tubercles. However, periodic pigging is not as effective in preventing and controlling tuberculation corrosion as is the other two methods.

Exfoliation corrosion. Aluminum components are often extruded into shape instead of being cast or forged. Extruding metals can, in some instances cause it to form a laminated microstructure. Corrosion between the laminate layers produces flakes of metals. The corroded metal in this case often has the appearance of a pile of leaves, hence the name exfoliation corrosion. Figure 27.15 contains an example of exfoliation of an aluminum component from equipment used to produce medical saline solutions. An alternate material of construction was chosen to replace the extruded aluminum components in this case.

27.3.3 Corrosion Inhibitors

Corrosion inhibitors are chemicals that are added to a chemical stream to prevent corrosion, or lower the rate of corrosion so that the processing equipment will have a suitable service lifetime. Corrosion inhibitors are often the most costeffective way to prevent or control corrosion because they allow one to use less expensive metals for a corrosive environment.

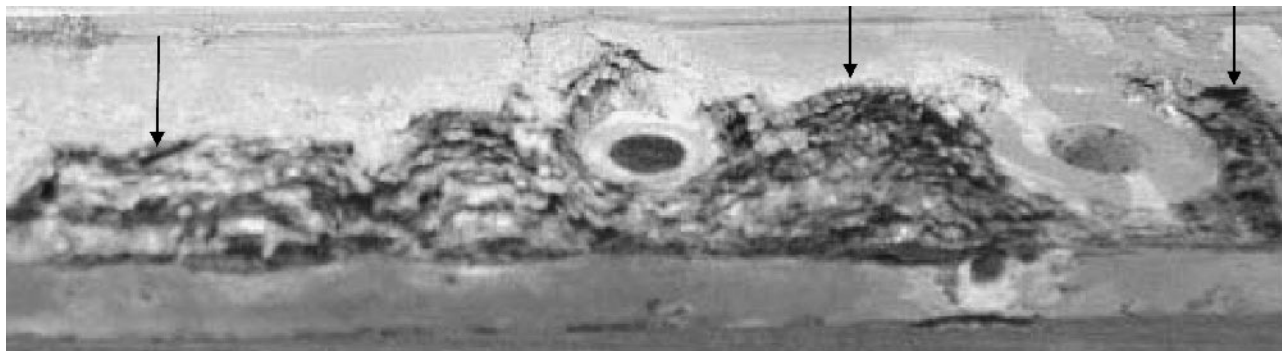


FIGURE 27.15 Exfoliation corrosion of an extruded aluminum part removed from medical saline solution manufacturing equipment.

There are literally thousands of corrosion inhibitors [7]. Consequently, the process of selecting a corrosion inhibitor is often overwhelming, particularly when one is assigned to select a corrosion inhibitor for the first time. The process of selecting a corrosion inhibitor can be made less daunting by:

- Engaging a consultant who is NACE-certified in the use of corrosion inhibitor development. See www.nace.org/nace/content/education/certification/CertSearch.asp
- Reading one or more of the books that discuss the fundamentals of corrosion inhibition. See www.nace.org/nacestore/deptnpage.asp?Cat%5FID=17608web%5Fname=Books (Enter *inhibitors* or *corrosion inhibitors* in the search box on this page and you will obtain a list of numerous publications on corrosion inhibitors.) See also www.Snyapseinfo.com
- Searching patents for corrosion inhibitors

Please remember that the corrosion inhibitors listed in patents are protected by patent laws, and using patented inhibitors without the inventor's permission could result in costly litigation.

Results from corrosion inhibitor research (that is not patented or proprietary) is published in corrosion journals, such as:

- *Corrosion* (www.nace.org)
- *Journal of the Electrochemical Society* (www.electrochem.org)
- *Corrosion Engineering and Science* (published by www.maney.co.uk)

27.4 SELECTING CORROSION RESISTANT MATERIALS FOR CHEMICAL PROCESSING EQUIPMENT

Corrosion can also be prevented or controlled by selecting metal alloys that are corrosion resistant. I avoid using the term corrosion proof because there is always a chemical stream that will cause a given alloy to corrode. For example, gold is resistant to a very wide variety of corrosive liquids, but will corrode rapidly in hydrogen cyanide. Silver is also a very corrosion resistant material that corrodes in chemical streams containing sulfurous chemicals.

27.4.1 Low Carbon Steels

Low carbon steels are suitable for use with anhydrous liquids, such as hydrocarbon solvents, or chemical streams that have a low amount of water (e.g., on the order of 1 ppm or less). Low carbon steels are typically unsuitable for use with aqueous chemical streams unless a corrosion inhibitor is incorporated in the stream. There are also situations where suitable service lifetimes are obtained with low carbon steels in aqueous streams by increasing the equipment wall thickness (not this author's first choice, however).

Consulting a table of corrosion resistances [2] or conducting corrosion testing is always recommended when considering the use of low carbon steels with a chemical stream that contains, or could be contaminated with, water.

27.4.2 Stainless Steels

There are numerous types of stainless steels, and one should keep in mind that a given type of stainless steel was originally formulated to provide corrosion resistance for a specific environment. For example, UNS Type S20910 stainless steel was originally formulated to resist corrosion by sulfuric acid. While this stainless steel has been successfully used for many other applications, it has also failed when used with low pH, high chloride chemical streams.

Specifications for each type of stainless steel are available from the supplier, and these specifications often list chemicals and chemical streams for which the type of stainless steel is resistant to corrosion. I strongly recommend conducting corrosion tests when considering using any type of stainless steel for a chemical or a chemical stream that is not listed in its specifications.

27.4.3 Copper and its Alloys

Copper and brass (i.e., copper alloys) are often used for water service. However, variations in water chemistry could cause pitting corrosion and failure of copper and alloys (e.g., brass). Unfortunately, the data on how various water chemistries lead to corrosion of copper and its alloys is dispersed throughout numerous technical journals and books, or in proprietary company data bases.

Thus, it is strongly recommended that one either conduct an extensive search of the technical literature, or conduct corrosion testing when considering the use of a new copper alloy for water service. Leidheiser's book [8] contains a good review of copper alloy corrosion for those interested in gaining more knowledge about the corrosion behavior of these materials.

27.4.4 Nickel Alloys

Nickel alloys such as Hastelloys (e.g., UNS N10276), and Incolloys (e.g., UNS N08800)—often referred to as super-alloys—are often used for very corrosive environments and high temperature corrosive environments. The companies that supply these materials often provide tables that list the corrosion resistance of the material for a number of different environments. The International Nickel Association (http://www.nidi.org/index.cfm/ci_id/11930.htm) also has an extensive database on the corrosion resistance of various nickel alloys in a variety of chemical streams.

Please keep in mind that these materials will also corrode in certain chemical process streams. For example, I once observed a sample of Hastelloy C-276 (UNS N10276) rapidly corrode (very deep pits within one month) in a hair conditioner that never went to market because of its corrosivity.

One should always conduct corrosion tests when the chemical stream is not listed by the supplier as being one for which the nickel alloy is corrosion resistant.

27.4.5 Titanium

Titanium alloys are light-weight and very corrosion resistant for environments containing large amounts of chlorides (e.g., sea water). However, titanium often rapidly corrodes in high pH aqueous chemical streams. Suppliers of titanium alloys often provide corrosion resistance tables, and corrosion testing is recommended for chemicals and chemical streams that are not listed in these tables.

27.4.6 Aluminum Alloys

Aluminum alloys are corrosion resistant in atmosphere, but often have poor corrosion resistance when submerged in aqueous environments. Aluminum corrosion resistance is also often only high in a restricted range of pH. For example, data has been published [6] that shows aluminum corrosion rates are very low when the chemical stream pH is between approximately 4 and 7, but the corrosion rates are very high when the pH is either below 4 or above 7.

Aluminum suppliers also provide corrosion resistance tables, and corrosion testing is strongly recommended when your chemicals and chemical streams are not listed in these tables.

27.4.7 Coatings for Preventing and Controlling Corrosion

Coating metals is another means of protecting metal equipment from corrosion. Coating inexpensive metals, such as low carbon steels, often allows these metals to be used for corrosive environments. Coatings can be:

- Latex and acrylic paints
- High temperature cured acrylic or epoxy coatings
- Electrodeposited metal coatings
- Metal clad coatings

- Glass linings
- High temperature Teflon®

Corrosion testing of these materials should be conducted with your chemical stream, unless there is extensive corrosion data on the coated metal and your chemical stream.

27.5 CORROSION PREVENTION AND CONTROL THROUGH CORROSION TESTING

Corrosion testing is an important element of a comprehensive corrosion prevention and control program. Corrosion testing is used to:

- Determine if a metal or a coated metal will corrode in a given chemical stream
- Select corrosion resistant metals and alloys for a given chemical
- Select chemical corrosion inhibitors so that less expensive materials can be used with a corrosive chemical stream
- Select coatings to protect your chemical process equipment from corrosion

There are many different types of corrosion tests, and corrosion testing is discussed more completely in another chapter of this handbook. However, two types of electrochemical tests, (1) direct current polarization methods, and (2) electrochemical impedance spectroscopy, merit a brief discussion in this chapter because they provide reliable corrosion data in a short time-frame. A book written by this author is listed in the Reference section of this chapter for those who would like a more in-depth discussion on electrochemical corrosion test methods.

27.5.1 Direct Current Polarization Methods

Samples of the metal or the alloy being considered for the equipment, or several samples of metals and alloys, are placed in a test cell such as the GEN4 Multi-Cell shown in Figure 27.16. Figure 27.17 shows a sample of welded UNS S31600 stainless steel used with the GEN4 Multi-Cell. The dotted white circle in the middle of the sample shows the approximate area that is exposed to the environment.

Samples of various alloys being considered for your processing equipment are sealed under the test

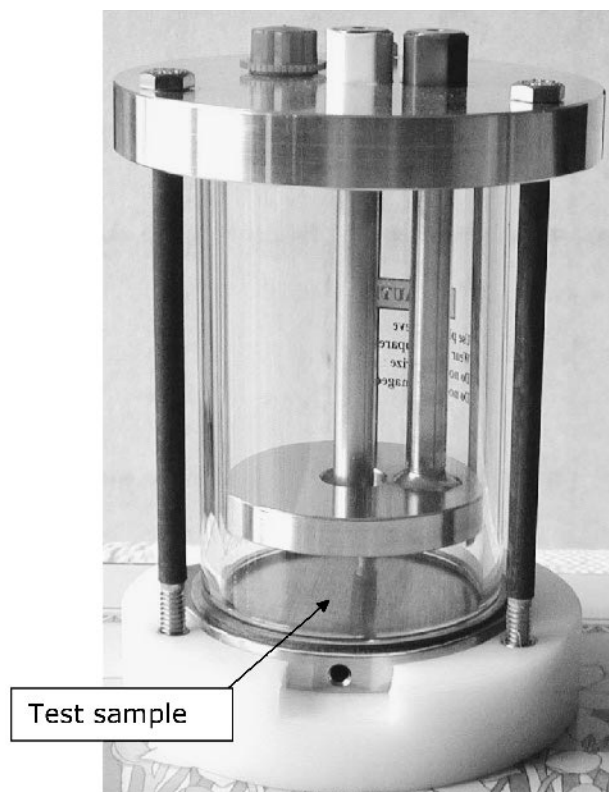


FIGURE 27.16 The GEN4 Multi-Cell for electrochemical corrosion testing. [Source: Photograph provided by Greatglas, Inc. (www.greatglas.com).]

cell glass body with a gasket, and the cell is partially filled with the chemical stream in question. The test samples are equilibrated, and then the test cell is connected to electrochemical test equipment.

Figure 27.18 contains an example of cyclic polarization data collected on a metal sample, such as that in Figure 27.17. The applied potential is plotted on the Y-axis in Figure 27.18, and the current is plotted on the X-axis as the absolute log values of the current. A portion of the curve in Figure 27.18 is due entirely to localized corrosion on the sample. Figure 27.19 provides two examples of samples that had curves like that in Figure 27.18. Notice in both samples that the localized corrosion, be it pitting or crevicing, is extensive and deep. Thus, the type of curve in Figure 27.18 is indicative of metal equipment that will prematurely fail from localized corrosion.

The cyclic polarization method is useful for determining:

- What materials will resist crevice and pitting corrosion

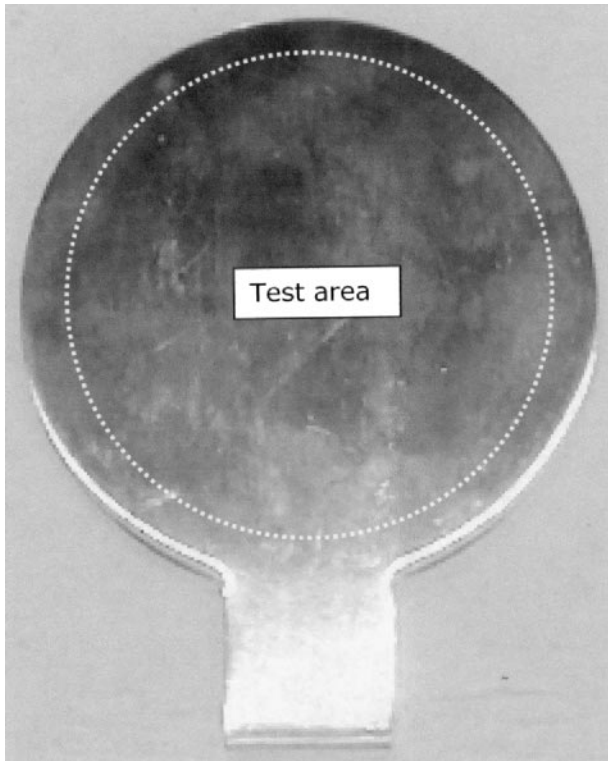


FIGURE 27.17 A welded stainless steel sample used for corrosion testing with the GEN4 Multi-Cell in Figure 27.16.

- What corrosion inhibitors will prevent pitting corrosion
- Pitting corrosion rates for estimating equipment service lifetime using Eqs. (27.1) and (27.2)

Direct current polarization methods are not useful for samples that have a high electrical resistance, such as coated metals, or for chemical streams

that have low electrical solution conductivity (i.e., low ionic conductivity), such as solvents contaminated with low amounts of water. Electrochemical impedance spectroscopy is used for these types of situations.

27.5.2 Electrochemical Impedance Spectroscopy

Electrochemical impedance spectroscopy uses the same type of test cell that is shown in Figure 27.16. A sample of the coated metal is cut into a shape similar to that shown in Figure 27.17 and placed under the glass body of the test cell. Figure 27.20 contains an example of EIS data collected on a corroding coated metal. Electrochemical impedance spectroscopy method is useful for determining:

- What coating will protect the equipment from corrosion
- What is the coated metal service lifetime

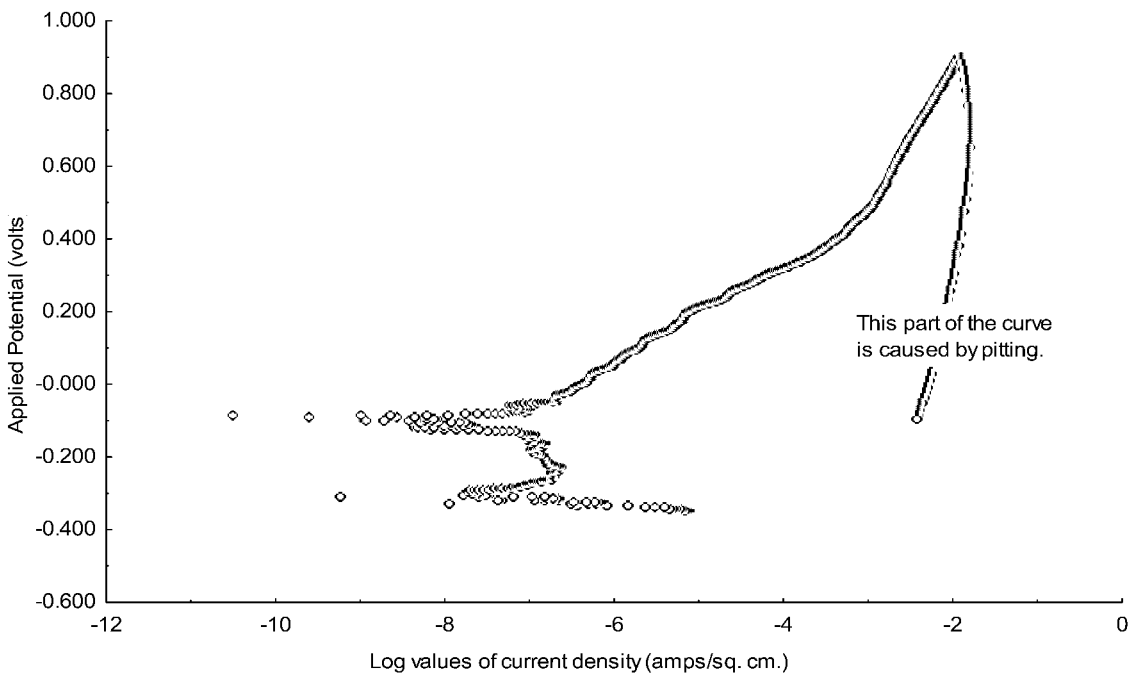


FIGURE 27.18 Cyclic polarization data with extensive positive hysteresis.

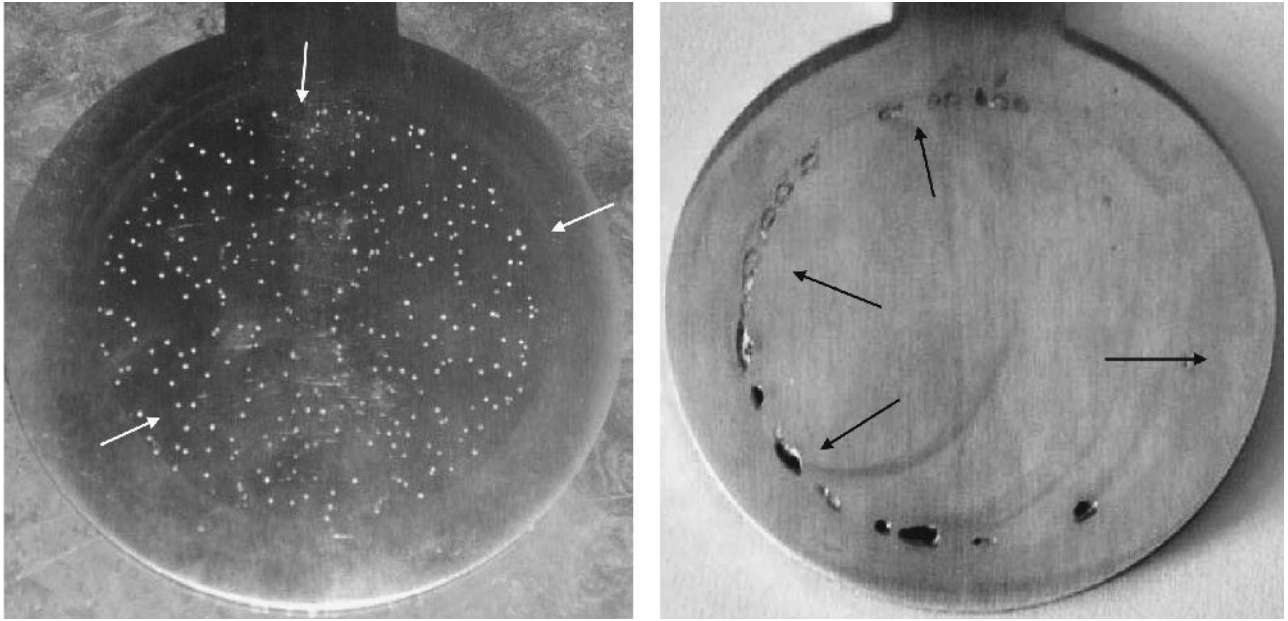


FIGURE 27.19 Two types of localized corrosion that produce positive hysteresis in cyclic polarization data. (*Left*) Extensive pitting corrosion (the pits appear to be white spots in this photograph). (*Right*) Extensive crevice corrosion under the test cell gasket.

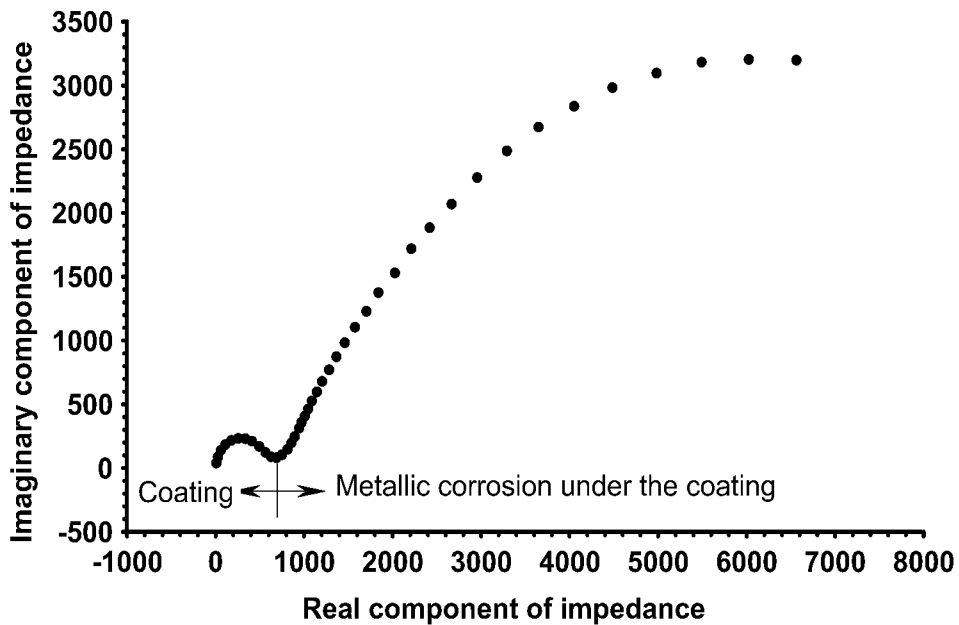


FIGURE 27.20 Electrochemical impedance spectroscopy data for a corroding coated metal.

27.5.3 Databases for Controlling and Preventing Chemical Process Equipment Corrosion

Experience becomes knowledge when it is reproducible, verifiable, and recorded. Databases take on a wide variety of formats and contain numerical and descriptive information, referred to as metafiles. Metafiles give the numbers in the data base meaning and thus make the numbers useful. A database could consist of the following:

- The rate of corrosion (number)
- The ultimate equipment service lifetime (number)
- The type of metal used to fabricate the processing equipment (metafile)
- A diagram or a description of the process (metafile)
- The chemical composition of the process stream (metafile)

Databases allow experience to become knowledge and provide this knowledge in an accessible format for future applications. Building and using a database is perhaps one of the most efficient ways to prevent and control processing equipment corrosion.

27.6 CHAPTER SUMMARY

There are numerous ways to prevent and control processing equipment corrosion:

- Accurately *identify the type of corrosion* so that an appropriate corrosion prevention and control measure can be selected, or so that future corrosion problems can be avoided
- Use *corrosion testing* with your specific chemicals and chemical streams to select *corrosion resistant metals and alloys* for your chemical processing equipment
- Use *corrosion testing* with your specific chemicals and chemical streams to select *coatings* to prevent and control chemical process equipment
- Select a chemical *corrosion inhibitor* to prevent and control processing equipment corrosion
- Use the *experience* in your company to help avoid corrosion problems and to find effective ways to prevent and control corrosion
- Use the *knowledge* in public domain *databases* to guide the selection of the metals and alloys for fabricating your chemical processing equipment

- Build, maintain and use a *company corrosion data-base* to guide the design and development of future chemical processing equipment and processes

In closing, I would like to thank Dr. Susan Whitworth-Tait for her extensive help in writing Section 27.3.1 on experience and knowledge.

27.7 SOURCES OF FURTHER INFORMATION

This chapter in the *Handbook of Environmental Degradation of Materials* is intended to provide information to those accountable for preventing and controlling chemical processing equipment corrosion. Normally I would provide an extensive list of references for this type of chapter. However, I am deviating from my normal practice and providing a few references plus a list of books that contain information and data that will assist the reader with preventing and controlling corrosion of metals used to fabricate chemical processing equipment.

27.8 REFERENCES

1. L. Curry, J. F. Wergin and Assoc., *Educating Professionals: Responding to New Expectations for Competence and Accountability*. San Francisco: Jossey-Bass Publishers, 1993.
2. R. D. Port and H. M. Herro. *The Nalco Guide to Boiler Failure Analysis*. New York: McGraw-Hill, Inc., 1991.
3. NACE. *Corrosion Data Survey—Metals Section, 6th Ed.* Houston: National Association of Corrosion Engineers, 1985.
4. NACE. *Book of Standards, 1990 Ed.* Standard Test Method TM0169-76. , Houston: National Association of Corrosion Engineers, 1990, p.8.
5. A. J. Bard, R. Parsons, J. Jordan, Eds. *Standard Potentials in Aqueous Solutions*. New York: Marcel Dekker, Inc., 1985.
6. H. H. Uhlig and R. W. Revie. *Corrosion and Corrosion Control, 3rd Ed.* New York: John Wiley & Sons, 1985, p. 346.
7. R. H. Hausler, Ed. Corrosion Inhibition. In *Proceedings of the International Conference on Corrosion Inhibition*. Houston: National Association of Corrosion Engineers, 1988.
8. H. Leidheiser, Jr. *The Corrosion of Copper, Tin, and their Alloys*. Huntington, NY: Robert E. Krieger Publishing Company, 1979.
9. W. S. Tait. *An Introduction to Electrochemical Corrosion Testing for Practicing Engineers and Scientists*. Madison, WI: Pair O Docs Professionals, L.L.C., 1994.

10. SAE and ASTM. *Metals and Alloys in the Unified Numbering System*. SAE HS-1086 FEB93 and ASTM DS-56 E, 6th Ed. A joint publication of the Society of Automotive Engineers (SAE), Inc. and the American Society for Testing and Materials. Warrendale, PA, 1993.
11. ISO. *Standard 9223, Corrosion of Metals and Alloys—Classification of Corrosivity of Atmospheres*. International Organization for Standardization, Geneva, 1992.

Index

Index Terms

Links

A

| | | | | | | |
|---|---------|-----|-----|-----|-----|-----|
| AAC (alkylammonium compound) | 290 | | | | | |
| Abiotic agents, wood degradation and | 299 | | | | | |
| Abradables | 410 | | | | | |
| Abrasive wear | | | | | | |
| coating degradation and | 377 | | | | | |
| thermal spray coatings and | 418 | 420 | | | | |
| ACC (acid copper chrome) | 313 | | | | | |
| Accelerated testing | | | | | | |
| artificial, for paint weathering | 393 | 394 | 395 | 396 | 397 | 398 |
| CFRP composites, methodology for | 67 | | | | | |
| for organic coatings exposure | 379 | | | | | |
| traditional protocol, plastics and | 66 | | | | | |
| Acid copper chrome (ACC) | 313 | | | | | |
| Acidic chloride salts, failure analysis and | 43 | 44 | 45 | | | |
| Acidic gases, laboratory tests and | 49 | | | | | |
| Acoustic Emission Technique (AET) | 110 | | | | | |
| ACQ (ammoniacal copper quat) | 290 | 314 | | | | |
| Acrylic coatings | 375 | | | | | |
| Acrylonitrile, migration of | 76 | | | | | |
| Activation energy | 110 | 112 | 115 | 116 | 117 | |
| Active corrosion protection | 334 | 369 | | | | |
| ACZA (ammoniacal copper zinc arsenate) | 313 | | | | | |
| Adhesion | | | | | | |
| corrosion-resistant coatings and | 371 | | | | | |
| loss of | 376 | | | | | |
| Adhesive fatigue/failure | 75 | | | | | |
| Adhesive wear, thermal spray coatings and | 418 | 419 | | | | |
| Adhesives | | | | | | |
| release coatings and | 421 | | | | | |
| ultraviolet radiation and | 482 | | | | | |
| Aerobic microorganisms | 186 | 187 | 190 | | | |
| Aerospace industry | | | | | | |
| advanced composite systems, physical aging and | 160 | | | | | |
| aircraft power plants, high-temperature corrosion and | 150 | | | | | |
| aluminum-copper-magnesium alloy and | 453 | | | | | |
| coatings and | 382 | | | | | |
| cost of corrosion and | 12 | 14 | 18 | | | |
| polymeric composite materials and | 193 | | | | | |
| spacecraft materials degradation and | 465-501 | | | | | |
| surface treatments and | 359 | | | | | |
| thermal spray coatings and | 419 | 421 | | | | |

Index Terms

Links

| | | | | | | |
|---|---------|-----|-----|-----|-----|-----|
| thermal spraying and | 414 | | | | | |
| AES (Auger Electron Spectroscopy) | 110 | 115 | 327 | | | |
| AET (Acoustic Emission Technique) | 110 | | | | | |
| AFM (atomic force microscopy) | 326 | | | | | |
| Agricultural production, cost of corrosion and | 16 | 18 | | | | |
| Air plasma spray (APS) | 334 | | | | | |
| Alcohol distillery failure analysis case study | 42 | | | | | |
| Alcohol vapor | 39 | 40 | 41 | 42 | | |
| Alkalis, wood degradation and | 300 | | | | | |
| Alkyd resins | 372 | | | | | |
| Alkylammonium compound (AAC) | 290 | | | | | |
| Alloy oxidation | 122 | 123 | 124 | 125 | 126 | 127 |
| | 128 | 129 | 130 | 131 | 132 | |
| commercial alloys and | 128 | 129 | 130 | 131 | 132 | |
| multi-component alloys and | 125 | 126 | 127 | 128 | | |
| Alloys | | | | | | |
| chemical process equipment corrosion and | 565 | 567 | 568 | 569 | | |
| | 574 | 575 | 576 | 577 | | |
| corrosion-resistant | 8 | 575 | | | | |
| corrosion-resistant coatings/paints for | 367 | 371 | | | | |
| scaling of in sulfur dioxide-containing atmospheres | 138 | 139 | 140 | 141 | | |
| thermal spraying and | 410 | | | | | |
| Alodine® surface treatment | 330 | 359 | | | | |
| Aluminum | | | | | | |
| as alloying element | 122 | 124 | | | | |
| exfoliation corrosion and | 574 | | | | | |
| interaction with chromates | 330 | | | | | |
| packagings and | 559 | | | | | |
| Aluminum alloys | | | | | | |
| corrosion-resistant coatings and | 371 | | | | | |
| protective coatings for | 345-366 | | | | | |
| surface pretreatment and | 348 | 349 | 350 | 351 | 352 | |
| Ammoniacal copper quat (ACQ) | 290 | 314 | | | | |
| Ammoniacal copper zinc arsenate (ACZA) | 313 | | | | | |
| Anaerobic microorganisms | 187 | 188 | 190 | | | |
| Analyses | 29 | | | | | |
| at low conversion | 73 | | | | | |
| See also Testing | | | | | | |
| Anode materials, impressed cathodic protection and | 237 | | | | | |
| Anodic protection | | | | | | |
| corrosion costs and | 9 | | | | | |
| thermal spray coatings corrosion control and | 416 | | | | | |
| Anodic reaction | 85 | | | | | |
| Anodizing | 352 | 353 | 354 | 372 | | |
| Ants, wood degradation and | 305 | | | | | |
| Appearance testing, for coatings | 402 | | | | | |
| Appliances (home appliances), cost of corrosion and | 17 | 18 | | | | |

Index Terms

Links

| | | | | | | |
|---|-----|-----|-----|-----|-----|-----|
| APS (air plasma spray) | 334 | | | | | |
| Aqueous corrosion | 322 | | | | | |
| Aramids fibers, thermal protective clothing and | 262 | | | | | |
| Architectural structures, coatings and | 382 | | | | | |
| Arrhenius analysis | 69 | 71 | | | | |
| ASM International, chemical process equipment and | 568 | | | | | |
| ASTM standards | | | | | | |
| cabinet tests and | 54 | | | | | |
| concrete coating bonding tests and | 426 | 428 | | | | |
| concrete coating pinhole tests and | 428 | 433 | | | | |
| electrochemical tests and | 57 | | | | | |
| immersion tests and | 50 | | | | | |
| laboratory testing and | 49 | 50 | 51 | 52 | | |
| weathering/appearance tests and | 399 | | | | | |
| Atomic force microscopy (AFM) | 326 | | | | | |
| Atomic oxygen | 466 | 467 | 468 | 469 | 470 | 471 |
| | 472 | 473 | 474 | 475 | 476 | 477 |
| Attrition milling (thermal spraying) | 412 | | | | | |
| Auger Electron Spectroscopy (AES) | 110 | 115 | 327 | | | |
| Austenitic stainless steels | 32 | 129 | | | | |
| CSCC and | 42 | | | | | |
| Auto-oxidation | 373 | | | | | |
| Automotive industry, coatings and | 382 | 421 | | | | |

B

| | | | | | | |
|---|---------|-----|--|--|--|--|
| Bacteria | 53 | | | | | |
| biofouling and | 179-206 | | | | | |
| chemotaxis of | 180 | | | | | |
| failure analysis and | 39 | | | | | |
| sulfate-reducing | 509 | | | | | |
| sulfur-oxidizing | 510 | | | | | |
| wood degradation and | 301 | | | | | |
| Bairocade® coating | 554 | | | | | |
| Ballast tanks, corrosion rates and | 534 | | | | | |
| Barrier materials, for packagings | 547-563 | | | | | |
| Barrier protection | 368 | | | | | |
| Bases, wood degradation and | 300 | | | | | |
| BC (bob and cup) testing geometry | 69 | | | | | |
| BCB (benzocyclobutenes), physical aging and | 161 | | | | | |
| BEA (Bureau of Economic Analysis) industry categories | 5 | | | | | |
| Bees, wood degradation and | 305 | | | | | |
| Beetles, wood degradation and | 304 | | | | | |
| BEM (Boundary Element Method) | 518 | | | | | |
| Benzocyclobutenes (BCB), physical aging and | 161 | | | | | |
| Biocides | 311 | 389 | | | | |
| Biofilms | 179-196 | 323 | | | | |
| Biofouling | 179-206 | | | | | |

Index Terms

Links

| | | | | | | |
|--|-----|-----|-----|-----|-----|-----|
| Biotic agents, wood degradation and | 300 | | | | | |
| Bismaleimides (BMI)-based composites, physical aging and | 160 | | | | | |
| Bisphenol A diglycidyl ether | 72 | 73 | | | | |
| Bisphenol A epoxy, physical aging and | 160 | | | | | |
| Bisphenol A polycarbonate, physical aging and | 158 | | | | | |
| Blending (thermal spraying) | 411 | | | | | |
| Blends, polymers and | 554 | 555 | 556 | | | |
| Blistering | 377 | | | | | |
| coated concrete and | 425 | 429 | 430 | 431 | 432 | 433 |
| BMI (bismaleimides)-based composites, physical aging and | 160 | | | | | |
| Bob and cup (BC) testing geometry | 69 | | | | | |
| Bonding tests, for coated concrete | 426 | | | | | |
| Boron | 314 | 315 | | | | |
| Bottom plating, corrosion and | 531 | 532 | | | | |
| Boucherie process (wood protection) | 309 | | | | | |
| Boundary Element Method (BEM) | 518 | | | | | |
| BPA-PC | 71 | | | | | |
| Bridges, cost of corrosion and | 11 | 18 | | | | |
| Brittle failure, of plastics | 73 | | | | | |
| Brominated flame retardants | 244 | 246 | | | | |
| Brown rot fungi, wood degradation and | 302 | | | | | |
| Brushing (wood protection) | 308 | | | | | |
| Buckling deformation | 524 | 536 | 543 | | | |
| Bulkhead stiffeners, corrosion and | 532 | | | | | |
| Bureau of Economic Analysis (BEA) industry categories | 5 | | | | | |

C

| | | | | | | |
|---|-----|-----|----|--|--|--|
| C-276 (nickel-base alloy) | 38 | | | | | |
| Cabinet tests | 53 | 54 | 55 | | | |
| Cables, spacecraft and | 493 | | | | | |
| Cabrera-Mott model | 115 | 117 | | | | |
| Calorimeter-type sensors | 270 | | | | | |
| Carbides, thermal spraying and | 410 | | | | | |
| Carbon arc light sources, for artificial accelerated weathering tests | 396 | | | | | |
| Carbon fiber reinforced polymer (CFRP) composites | | | | | | |
| accelerating testing methodology for | 67 | | | | | |
| thermal cycling and | 488 | | | | | |
| thermogravimetric analysis and | 72 | | | | | |
| Carbon fiber, thermal protective clothing and | 262 | | | | | |
| Carbon nanotubes, aging and | 162 | | | | | |
| Carbon steel | 27 | | | | | |
| corrosion-resistant coatings and | 371 | | | | | |
| oxidation behaviors and | 128 | | | | | |
| in sea water, corrosion rates for | 535 | | | | | |
| Carbonation corrosion | 166 | | | | | |
| Cast iron, as anode material | 237 | 238 | | | | |

Index Terms

Links

| | | | | | | |
|---|---------|-----|-----|-----|-----|-----|
| Castor (M. V.), marine incident and | 523 | 524 | 525 | | | |
| Cathodic protection (CP) | 229-241 | 370 | | | | |
| coating resistance and | 510 | | | | | |
| concrete and | 171 | | | | | |
| corrosion costs and | 9 | | | | | |
| defined | 230 | 503 | | | | |
| field data and design for | 508 | 509 | 510 | 511 | 512 | 513 |
| | 514 | 515 | 516 | 517 | 518 | |
| internal surfaces and | 240 | | | | | |
| marine applications and | 539 | | | | | |
| monitoring methods for | 511 | | | | | |
| pipelines and | 503-521 | | | | | |
| thermal spray coatings corrosion control and | 417 | | | | | |
| types of | 504 | 505 | 506 | 507 | | |
| Cathodic reaction | 85 | | | | | |
| CCA (chromated copper arsenate) | 289 | 313 | 314 | | | |
| CCC (chromate conversion coatings) | 330 | 354 | 355 | 356 | 357 | |
| SNAP coatings and | 337 | | | | | |
| CE (counter electrode) | 56 | | | | | |
| Cellulose | | | | | | |
| photodegradation of | 279 | | | | | |
| physical aging and | 157 | | | | | |
| thermogravimetric analysis and | 72 | | | | | |
| Cement concrete, coatings for | 423-447 | | | | | |
| Ceramic fiber fill | 494 | | | | | |
| Ceramics | | | | | | |
| thermal spraying and | 410 | 413 | | | | |
| ultraviolet radiation and | 480 | | | | | |
| Cerium-based conversion coating | 357 | | | | | |
| Cermets | 410 | | | | | |
| CFD (Computational Fluid Dynamics) | 223 | | | | | |
| CFRP (carbon fiber reinforced polymer) composites | | | | | | |
| accelerating testing methodology for | 67 | | | | | |
| thermal cycling and | 488 | | | | | |
| thermogravimetric analysis and | 72 | | | | | |
| Charged particle radiation | 483 | | | | | |
| Chemical aging of plastics | 153 | | | | | |
| Chemical cladding (thermal spraying) | 411 | | | | | |
| Chemical cross-links | 553 | | | | | |
| Chemical etch | 349 | | | | | |
| Chemical industry | | | | | | |
| cost of corrosion and | 16 | 17 | 18 | 19 | | |
| oxidation and | 132 | | | | | |
| Chemical kinetics | 69 | 70 | 71 | | | |
| Chemical process equipment | | | | | | |
| corrosion prevention/control and | 565-581 | | | | | |
| corrosion-resistant materials and | 575 | 576 | 577 | | | |
| failure analysis in | 27-45 | | | | | |

Index Terms

Links

| | | | | | | |
|--|---------|-----|-----|-----|-----|-----|
| Chemical repellents | 183 | | | | | |
| Chemical tankers. See Tankers | | | | | | |
| Chemical vapor deposition (CVD) | 335 | | | | | |
| Chemicals | | | | | | |
| coating degradation and | 377 | | | | | |
| inorganic, wood protection and | 288 | | | | | |
| laboratory tests and | 49 | | | | | |
| Chemotaxis of bacteria | 180 | | | | | |
| Chloride diffusion coefficient, chloride ingress and | 172 | | | | | |
| Chloride ingress | | | | | | |
| chloride diffusion coefficient and | 172 | | | | | |
| into concrete | 165 | 166 | 167 | 168 | 169 | 170 |
| Chloride ions, tanker corrosion and | 534 | | | | | |
| Chloride stress corrosion cracking (CSCC) | 41 | | | | | |
| Chloride threshold values | 166 | | | | | |
| Chlorides, failure analysis and | 43 | 44 | 45 | | | |
| Chlorinated rubber coatings | 374 | | | | | |
| Chloropicrin | 316 | | | | | |
| Chromate conversion coatings (CCC) | 330 | 354 | 355 | 356 | 357 | |
| SNAP coatings and | 337 | | | | | |
| Chromated copper arsenate (CCA) | 289 | 313 | 314 | | | |
| Chromates | 384 | | | | | |
| interaction with aluminum | 330 | | | | | |
| Chromium | | | | | | |
| as alloying element | 122 | | | | | |
| chromated copper arsenate and | 313 | | | | | |
| oxidation and | 119 | | | | | |
| Chromium-bearing high silicon cast iron, as anode material | 238 | | | | | |
| Chromium trioxide, wood protection and | 288 | | | | | |
| Chromophores, organic coatings and | 458 | | | | | |
| CI (corrosion intensity) | 94 | 95 | 96 | | | |
| CICs (corrosion inhibiting compounds) | 360 | | | | | |
| CIGMAT CT-1 test, for concrete coating pinhole tests | 428 | 433 | | | | |
| CIGMAT CT-2/CIGMAT CT-3 tests, for coated concrete | | | | | | |
| bonding | 426 | 428 | | | | |
| CIPS (Close Interval Potential Survey) | 511 | | | | | |
| Classification societies | 540 | 541 | 542 | | | |
| Clearance control coatings | 414 | | | | | |
| Climate, coating degradation and | 390 | | | | | |
| Close Interval Potential Survey (CIPS) | 511 | | | | | |
| Close packing | 553 | | | | | |
| Clothing, thermal protection and | 261-275 | | | | | |
| Co-polymers | 552 | | | | | |
| Coal power plants, high-temperature corrosion and | | 149 | | | | |
| Coatings | | | | | | |
| for aluminum alloys | 345-366 | | | | | |
| anodic | 416 | | | | | |

Index Terms

Links

| | | | | | | |
|---|---------|-----|-----|-----|-----|-----|
| cathodic protection and. See Cathodic protection | | | | | | |
| composite paint | 332 | 333 | 334 | | | |
| for concrete | 423-447 | | | | | |
| conversion | 330 | 337 | 352 | 353 | 354 | 355 |
| | 356 | 357 | 358 | | | |
| corrosion costs and | 6 | | | | | |
| corrosion-resistant | 367-385 | | | | | |
| characteristics/uses of | 372 | 373 | 374 | 375 | 376 | |
| chemical process equipment and | 576 | | | | | |
| degradation of | 376 | 377 | 378 | 379 | 380 | 381 |
| industrial applications and | 381 | 382 | 383 | 384 | | |
| flame retardants in | 219 | | | | | |
| lot variations and | 346 | | | | | |
| microbial biofilms and | 194 | | | | | |
| neutral | 417 | | | | | |
| tanker protection and | 538 | | | | | |
| thermal spray | 405-422 | | | | | |
| weathering tests for | 387-404 | | | | | |
| for wood | 287 | 288 | 289 | 290 | 291 | 292 |
| | 293 | | | | | |
| Cobalt, oxidation and | 119 | | | | | |
| COCs (cyclo-olefin co-polymers) | 552 | | | | | |
| Coefficient of thermal expansion (CTE) | 488 | | | | | |
| Coke deposition | 35 | | | | | |
| Coleoptera (beetles), wood degradation and | 304 | | | | | |
| Combustion turbines, high-temperature corrosion and | 150 | | | | | |
| Combustion, heat release rates and | 222 | | | | | |
| Combustors, industrial gas turbines and | 415 | | | | | |
| Composite laminates, physical aging and | 160 | | | | | |
| Composite paint coatings | 332 | 333 | 334 | | | |
| Compression stress-relaxation (CSR) testing | 71 | | | | | |
| Computational Fluid Dynamics (CFD) | 223 | | | | | |
| Computer modeling | | | | | | |
| material flammability and | 223 | | | | | |
| pipeline cathodic protection and | 517 | | | | | |
| surface engineering and | 337 | 338 | 339 | | | |
| Concrete | | | | | | |
| coatings for | 423-447 | | | | | |
| failure of | 429-433 | 430 | 431 | 432 | 433 | |
| liquid transport into | 433-446 | | | | | |
| testing | 424-433 | | | | | |
| reinforced, environmental degradation of | 165-177 | | | | | |
| Conductivity, tanker corrosion rates and | 533 | | | | | |
| Constant strain rate (CSR), master curves and | 67 | | | | | |
| Conversion coatings | 330 | 337 | 352 | 353 | 354 | 355 |
| | 356 | 357 | 358 | | | |
| Copper | | | | | | |
| aluminum alloys and | 345 | | | | | |

Index Terms

Links

| | | | | | | |
|--|---------|-----|-----|-----|-----|-----|
| chromated copper arsenate and | 313 | | | | | |
| Copper azole | 290 | 314 | | | | |
| Copper HDO | 314 | | | | | |
| Copper monoethanolamine (Cu-MEA) | 290 | | | | | |
| Copper naphthenate | 312 | 313 | | | | |
| Copper-8-quinolinolate (oxine copper) | 313 | | | | | |
| Corrosion | | | | | | |
| chloride stress corrosion cracking and | 41 | | | | | |
| control methods/services and | 6 | 7 | 8 | 9 | 10 | |
| cost of | 3-24 | 47 | | | | |
| extrapolations and | 20 | | | | | |
| methodologies for determining | 4 | 5 | 6 | | | |
| microbial corrosion | 185 | | | | | |
| as percentage of GDP | 4 | 6 | | | | |
| steel in concrete | 165 | | | | | |
| defined | 47 | 229 | | | | |
| electrochemical | 81-103 | | | | | |
| forms of | 47 | | | | | |
| industry sector analysis and | 10 | 11 | 12 | 13 | 14 | 15 |
| | 16 | 17 | 18 | 19 | 20 | |
| initiation/propagation and | 376 | | | | | |
| microbial | 185 | 186 | 187 | 188 | 189 | 190 |
| | 191 | 192 | | | | |
| of metallic material in liquid | 81 | | | | | |
| prevention of. See Prevention | | | | | | |
| testing. See Testing | | | | | | |
| under deposit | 44 | 569 | | | | |
| See also Oxidation | | | | | | |
| Corrosion current (I _{corr}) | 97 | 98 | 99 | 100 | 101 | |
| Corrosion inhibiting compounds (CICs) | 360 | | | | | |
| Corrosion inhibiting pigments | 372 | | | | | |
| Corrosion inhibitors | | | | | | |
| chemical process equipment and | 575 | | | | | |
| concrete and | 170 | | | | | |
| corrosion costs and | 8 | | | | | |
| Corrosion intensity (CI) | 94 | 95 | 96 | | | |
| Corrosion penetration rate (CPR) | 94 | 96 | | | | |
| Corrosion rates | 47 | 48 | 49 | 50 | 55 | 56 |
| | 57 | 58 | 59 | 60 | | |
| chemical process equipment and | 566 | | | | | |
| equation for | 49 | 58 | | | | |
| hot corrosion and | 143 | | | | | |
| measuring | 512 | | | | | |
| tankers and | 533 | 535 | | | | |
| Corrosion-resistant alloys (CRAs) | | | | | | |
| chemical process equipment and | 575 | | | | | |
| corrosion costs and | 8 | | | | | |
| Corrosion-resistant coatings/paints | 367-385 | | | | | |

Index Terms**Links**

| | | | | | | |
|---|-----|-----|-----|--|--|--|
| chemical process equipment and degradation of industrial applications and | 576 | | | | | |
| Counter electrode (CE) | 56 | | | | | |
| Coupons | 511 | 512 | | | | |
| CP. See Cathodic protection | | | | | | |
| CPR (corrosion penetration rate) | 94 | 96 | | | | |
| Cracking | | | | | | |
| coated concrete and | 425 | 429 | 431 | | | |
| of plastics, mechanical testing and | 73 | | | | | |
| stress corrosion and | 47 | 571 | | | | |
| CRAs (corrosion-resistant alloys) | | | | | | |
| chemical process equipment and | 575 | | | | | |
| corrosion costs and | 8 | | | | | |
| Crazing | 154 | | | | | |
| Creep | 34 | 74 | | | | |
| adhesive failure and | 75 | | | | | |
| Creosote | 312 | | | | | |
| Crevice corrosion | 47 | 570 | | | | |
| Cross-linking | 553 | | | | | |
| Crushing (thermal spraying) | 412 | | | | | |
| Crystallinity, barrier properties and | 550 | 551 | 552 | | | |
| CSCC (chloride stress corrosion cracking) | 41 | | | | | |
| CSR (compression stress-relaxation) testing | 71 | | | | | |
| CSR (constant strain rate), master curves and | 67 | | | | | |
| CTE (coefficient of thermal expansion) | 488 | | | | | |
| Cu-MEA (copper monoethanolamine) | 290 | | | | | |
| Current density, cathodic protection and | 510 | | | | | |
| CVD (chemical vapor deposition) | 335 | | | | | |
| Cyclic-anodic-polarization behavior | 101 | | | | | |
| Cyclic oxidation tests | 110 | | | | | |
| Cyclic polarization | 59 | | | | | |
| Cyclo-olefin co-polymers (COCs) | 552 | | | | | |

D

| | | | | | | |
|---|-----|-----|-----|-----|-----|-----|
| Dazomet | 316 | | | | | |
| DBDPO (decabromodiphenyl oxide) | 246 | 247 | 248 | | | |
| DCVG (Direct Current Voltage Gradient) | 511 | | | | | |
| De-smutting | 350 | | | | | |
| Decabromodiphenyl oxide (DBDPO) | 246 | 247 | 248 | | | |
| Deck of ships, corrosion in areas beneath | 533 | | | | | |
| Defect structure, oxide scales and | 110 | 111 | 112 | | | |
| Degradation | | | | | | |
| analyzing | 326 | 327 | 328 | 329 | | |
| of coatings/paints | 376 | 377 | 378 | 379 | 380 | 381 |
| | 387 | 388 | 389 | 390 | 391 | 392 |
| | 393 | | | | | |

Index Terms

Links

| | | | | | | |
|---|---------|-----|-----|-----|-----|-----|
| of plastics | 153 | 154 | 155 | 156 | 157 | 158 |
| | 159 | 160 | 161 | 162 | 163 | |
| by radioactivity | 326 | | | | | |
| of spacecraft materials | 465-501 | | | | | |
| tribological | 324 | | | | | |
| types of | 79-225 | | | | | |
| UV/humidity | 324 | | | | | |
| Degradation of ortho-methyl phthalate ester (DMPE) | 195 | | | | | |
| Denture lining materials, testing of | 76 | | | | | |
| Deoxidation | 350 | | | | | |
| Department of Defense (DoD), cost of corrosion and | 17 | 18 | | | | |
| Department of Energy (DoE), cost of corrosion and | 17 | | | | | |
| Dependability | 321 | 334 | | | | |
| Deposit corrosion | 142 | 143 | 144 | 145 | | |
| testing methods for | 144 | | | | | |
| Design considerations | | | | | | |
| shipping industry and | 541 | | | | | |
| surface engineering and | 322 | 323 | 324 | 325 | 326 | 339 |
| Detonation thermal spraying | 406 | 408 | | | | |
| DHTs (double-hull tankers) | 527 | 528 | 529 | | | |
| structural integrity risk and | 537 | | | | | |
| Differential scanning calorimetry (DSC) | 75 | | | | | |
| Diffusion | | | | | | |
| determining mechanism of | 113 | | | | | |
| oxide scales and | 110 | 111 | 112 | | | |
| Diglycidyl ether of bisphenol A | 72 | 73 | | | | |
| Dioxins | 246 | 249 | 250 | 251 | 252 | 253 |
| | 254 | 255 | | | | |
| combustion/incineration and | 253 | | | | | |
| Dipping (wood protection) | 308 | | | | | |
| Direct current polarization methods | 577 | | | | | |
| Direct Current Voltage Gradient (DCVG) | 511 | | | | | |
| DMA (dynamic mechanical analysis) | 66 | | | | | |
| adhesive fatigue testing and | 75 | | | | | |
| DMPE (degradation of ortho-methyl phthalate ester) | 195 | | | | | |
| DoD (Department of Defense), cost of corrosion and | 17 | 18 | | | | |
| DoE (Department of Energy), cost of corrosion and | 17 | | | | | |
| Double-hull tankers (DHTs) | 527 | 528 | 529 | | | |
| structural integrity risk and | 537 | | | | | |
| Drainage current, impressed cathodic protection and | 240 | | | | | |
| Drinking water, cost of corrosion and | 13 | 18 | | | | |
| DSC (differential scanning calorimetry) | 75 | | | | | |
| Dynamic mechanical analysis (DMA) | 66 | | | | | |
| adhesive fatigue testing and | 75 | | | | | |
| E | | | | | | |
| EDAX (Energy Dispersive X-ray Analysis) | 110 | | | | | |

Index Terms

Links

| | | | | | | |
|--|--------|-----|-----|-----|-----|-----|
| Education and training, corrosion control and | 9 | | | | | |
| E-glass/vinyl ester composites, physical aging and | 159 | | | | | |
| EHC (electroplated hard chromium) | 335 | | | | | |
| EIS. See Electrochemical Impedance Spectroscopy | | | | | | |
| Elastomers, aging and | 162 | | | | | |
| Electrical utilities, cost of corrosion and | 13 | 18 | 19 | 20 | | |
| Electrical wires, spacecraft and | 493 | | | | | |
| Electrochemical cell | 82 | 83 | 84 | 85 | | |
| corrosion calculations and | 86 | | | | | |
| Electrochemical corrosion | 81-103 | | | | | |
| measurements and | 98 | 99 | 100 | 101 | 102 | |
| Electrochemical equilibrium | 87 | 88 | 89 | 90 | 91 | 92 |
| Electrochemical Impedance Spectroscopy (EIS) | 60 | | | | | |
| chemical process equipment testing and | 578 | | | | | |
| corrosion-resistant paints and | 368 | | | | | |
| organic coating degradation and | 381 | 451 | | | | |
| Electrochemical kinetics | 92 | 93 | 94 | 95 | 96 | 97 |
| Electrochemical noise (EN) measurements | 61 | | | | | |
| Electrochemical tests | 55 | 56 | 57 | 58 | 59 | 60 |
| | 61 | 62 | 577 | 578 | 579 | |
| for coatings | 380 | | | | | |
| for organic coatings | 451 | 452 | 453 | 454 | 455 | 456 |
| | 457 | 458 | | | | |
| Electrochemical thermodynamics | 81 | 82 | 83 | 84 | 85 | 86 |
| | 87 | 88 | 89 | 90 | 91 | 92 |
| Electron Spectroscopy for Chemical Analysis (ESCA) | 110 | | | | | |
| Electron spin resonance (ESR) | 115 | 403 | | | | |
| Electron tunneling | 117 | | | | | |
| Electronic insulating materials, biodeterioration of | 192 | | | | | |
| Electronic packagings, thermal spray coatings and | 421 | | | | | |
| Electronics, cost of corrosion and | 16 | 18 | | | | |
| Electroplated hard chromium (EHC) | 335 | | | | | |
| Ellingham diagrams | 106 | | | | | |
| Embedded thermocouple sensor | 270 | | | | | |
| EMMA test | 392 | | | | | |
| EMMAQUA test | 392 | | | | | |
| Empty cell process (wood protection) | 310 | | | | | |
| EN (electrochemical noise) measurements | 61 | | | | | |
| Energy Dispersive X-ray Analysis (EDAX) | 110 | | | | | |
| Engineering alloys, corrosion-resistant coatings and | 371 | | | | | |
| Environment | | | | | | |
| coatings and | 384 | | | | | |
| flame retardants and | 244 | 245 | 246 | 247 | 248 | 249 |
| | 250 | 251 | 252 | 253 | 254 | 255 |
| | 256 | 257 | | | | |
| metallic materials failure analysis and | 27-45 | | | | | |
| wood treatments and | 311 | | | | | |
| See also Pollution | | | | | | |

Index Terms

Links

| | | | | | | |
|---|-------|-----|-----|-----|-----|-----|
| Environmental SEMs (ESEM) | 326 | | | | | |
| Environmental stress cracking (ESC) | 154 | | | | | |
| Environmentally assisted cracking | 47 | 48 | 49 | 51 | | |
| EPDM (ethylene-propylenediene monomer) | 71 | | | | | |
| Epoxy composites, ultraviolet radiation and | 482 | | | | | |
| Epoxy formulations, physical aging and | 159 | | | | | |
| Epoxy resins | 373 | | | | | |
| Equatorial Mounted Mirrors for Acceleration tests | 392 | | | | | |
| Equilibrium half-cell potentials | 83 | 86 | 89 | 91 | | |
| Erosive wear, thermal spray coatings and | 417 | | | | | |
| ESC (environmental stress cracking) | 154 | | | | | |
| ESCA (Electron Spectroscopy for Chemical Analysis) | 110 | | | | | |
| ESEM (Environmental SEMs) | 326 | | | | | |
| ESR (electron spin resonance) | 115 | 403 | | | | |
| Etching | 349 | | | | | |
| Ethylene-propylenediene monomer (EPDM) | 71 | | | | | |
| Evaluating | | | | | | |
| coating degradation | 378 | 379 | 380 | 381 | | |
| primer performance | 361 | | | | | |
| skin burns | 271 | | | | | |
| See also Testing | | | | | | |
| EVOH polymer | 548 | 557 | 562 | | | |
| Exfoliation corrosion | 47 | 574 | | | | |
| Experience, chemical process equipment corrosion prevention/ control and | 567 | | | | | |
| Experiments. See Testing | | | | | | |
| Exposure conditions, coating degradation and | 390 | | | | | |
| Exxon Valdez | 527 | | | | | |
| F | | | | | | |
| Factor-jump thermogravimetry | 73 | | | | | |
| Failure analysis | | | | | | |
| of metallic materials | 27-45 | | | | | |
| reports and | 29 | | | | | |
| Faraday's law | 94 | 95 | 96 | | | |
| Farming, production, cost of corrosion and | 16 | 18 | | | | |
| Feed preheater, failure analysis case study and | 29 | 30 | 31 | 32 | | |
| FEP (fluorinated ethylene propylene) | 480 | 481 | 482 | 483 | 484 | 485 |
| thermal and radiation effects on | 486 | 487 | 488 | 489 | 490 | 491 |
| Fertilizer plant failure analysis case studies | 488 | 489 | 490 | 491 | | |
| | 29 | 30 | 31 | 32 | 33 | 34 |
| | 35 | | | | | |
| FGM (functionally gradient material) | 334 | | | | | |
| Fiber-reinforced polymeric composite materials (FRPCMs), biodeterioration of | 193 | | | | | |
| Filiform corrosion | 378 | | | | | |
| Fillers, polymers and | 554 | 555 | 556 | | | |

Index Terms

Links

| | | | | | | |
|--|---------|-----|-----|-----|-----|-----|
| Film-forming finishes, for wood | 287 | | | | | |
| Fire. See Material flammability | | | | | | |
| First-order reactions | 69 | 70 | | | | |
| Flame retardants | 217 | 218 | 219 | | | |
| defined | 243 | | | | | |
| exposure levels and | 255 | | | | | |
| for clothing | 261 | | | | | |
| how they work | 243 | 244 | 245 | 246 | | |
| polymeric | 243-259 | | | | | |
| regulatory controls and | 256 | | | | | |
| Flame spray powder/wire thermal spraying | 406 | 408 | | | | |
| Flame spread | 220 | | | | | |
| Floating Production, Storage and Offloading (FPSO) systems | 529 | | | | | |
| Flow rate, laboratory tests and | 49 | | | | | |
| Fluid flow, effect on corrosion | 62 | | | | | |
| Fluorescent light sources, for artificial accelerated weathering tests | 395 | | | | | |
| Fluoride | 314 | 315 | | | | |
| Fluorinated ethylene propylene (FEP) | 480 | 481 | 482 | 483 | 484 | 485 |
| | 486 | 487 | 488 | 489 | 490 | 491 |
| thermal and radiation effects on | 488 | 489 | 490 | 491 | | |
| Fluoropolymers, ultraviolet radiation and | 481 | | | | | |
| Food | | | | | | |
| packaging materials and | 560 | 561 | 562 | | | |
| processing, cost of corrosion and | 16 | 18 | | | | |
| storage, acrylonitrile/styrene migration and | 76 | | | | | |
| Food products, release coatings and | 421 | | | | | |
| Force measurements | 71 | | | | | |
| Fourier transform infrared spectroscopy (FTIR) | 327 | 328 | 329 | | | |
| coating weatherability testing and | 403 | | | | | |
| FPSO (Floating Production, Storage and Offloading) systems | 529 | | | | | |
| Freezing, wood weathering and | 280 | | | | | |
| Fretting wear, thermal spray coatings and | 418 | 419 | | | | |
| FRPCMs (fiber-reinforced polymeric composite materials) | | | | | | |
| biodegradation of | 193 | | | | | |
| FTIR (Fourier transform infrared spectroscopy) | 327 | 328 | 329 | | | |
| coating weatherability testing and | 403 | | | | | |
| Full cell process (wood protection) | 310 | | | | | |
| Fumigants, wood protection and | 316 | | | | | |
| Functionality | 321 | | | | | |
| Functionalized nanostructures coatings | 336 | | | | | |
| Functionally gradient material (FGM) | 334 | | | | | |
| Fungi, wood degradation and | | 301 | | | | |
| Fusing (thermal spraying) | 412 | | | | | |

Index Terms

Links

G

| | | | | | | |
|--|-----|-----|-----|-----|-----|-----|
| Galactic cosmic rays (GCRs) | 483 | | | | | |
| Galvanic cathodic protection | 230 | 231 | 232 | 233 | 234 | 235 |
| | 236 | 237 | | | | |
| Galvanic corrosion | 572 | | | | | |
| Galvanic Series | 540 | | | | | |
| Galvanized steels, corrosion-resistant coatings and | 372 | | | | | |
| Galvanizing, corrosion costs and | 7 | | | | | |
| Galvanodynamic polarization | 59 | | | | | |
| Galvanostatic polarization | 59 | | | | | |
| Garment flammability | 261 | | | | | |
| Gas cluster ion beam (GCIB) | 335 | | | | | |
| Gas environments, oxidation in mixed environments and | 132 | 133 | 134 | 135 | 136 | 137 |
| Gas industry, cost of corrosion and | 12 | 17 | 18 | 19 | 20 | |
| Gas phase corrosion | 151 | | | | | |
| Gas pipelines, cost of corrosion and | 11 | 18 | | | | |
| Gas turbines | 412 | 413 | 414 | 415 | 416 | |
| superalloys and | 131 | | | | | |
| ternary alloy oxidation and | 141 | | | | | |
| Gas/water atomization (thermal spraying) | 411 | | | | | |
| Gasification property, heat release rates and | 222 | | | | | |
| GCIB (gas cluster ion beam) | 335 | | | | | |
| GCRs (galactic cosmic rays) | 483 | | | | | |
| GDP (gross domestic product) | | | | | | |
| BEA industry categories and | 5 | | | | | |
| corrosion costs as percentage of | 4 | 6 | | | | |
| cost of corrosion and | 17 | 18 | | | | |
| Generalized electrochemical cell reaction | 83 | 84 | 85 | | | |
| Gibb's free energy | 82 | 83 | 84 | 85 | | |
| Glass | | | | | | |
| thermal protective clothing and | 262 | | | | | |
| ultraviolet radiation and | 480 | | | | | |
| Glass fiber epoxy composites, physical aging and | 160 | | | | | |
| Glass fiber-reinforced polyester (GRP), heat release | | | | | | |
| rates and | 221 | | | | | |
| Government agencies, cost of corrosion and | 17 | 18 | | | | |
| Graphite, as anode material | 237 | | | | | |
| Gravimetric method | 109 | | | | | |
| Grooving corrosion, ships and | 531 | | | | | |
| Gross domestic product. See GDP | | | | 507 | 515 | |
| Ground bed | 229 | 233 | 234 | 235 | 236 | 237 |
| | 238 | 239 | 240 | 241 | | |
| GRP (glass fiber-reinforced polyester), heat release rates and | 221 | | | | | |

H

| | | | | | | |
|------------------------|--|-----|-----|--|--|--|
| Hafnium, oxidation and | | 118 | 119 | | | |
|------------------------|--|-----|-----|--|--|--|

Index Terms**Links**

| | | | | | | |
|---|-----|-----|-----|-----|----|----|
| Half-cell potentials | 82 | 83 | 84 | 85 | 86 | 87 |
| | 88 | 89 | 91 | | | |
| Halide concentration testing | 49 | | | | | |
| Halide-specific probes, organic coatings and | 459 | | | | | |
| Halogen-containing flame-retardants | 219 | 243 | | | | |
| Halogenated dibenzo-p-dioxins. See Dioxins | | | | | | |
| HALS (hindered amine light stabilizers) | | | | | | |
| coating degradation and | 388 | 403 | | | | |
| wood protection and | 292 | | | | | |
| Hard anodizing | 352 | 353 | 354 | | | |
| Hazardous materials storage, cost of corrosion and | 12 | 18 | | | | |
| Hazardous materials transport, cost of corrosion and | 15 | 18 | | | | |
| HBCD (hexabromocyclododecane) | 249 | | | | | |
| Heartwood, durability of | 307 | | | | | |
| Heat exchanger tubes, failure analysis and | 39 | 40 | 41 | 42 | | |
| Heat insulation, thermal spraying applications and | 414 | | | | | |
| Heat release rates | 220 | 221 | 222 | 223 | | |
| Heat, wood degradation and | 280 | 300 | | | | |
| Hemicelluloses | 286 | | | | | |
| heat damage and | 300 | | | | | |
| Henriques Damage Integral burn model | 271 | | | | | |
| Hexabromocyclododecane (HBCD) | 249 | | | | | |
| High-alloy stainless steel tubes, failure analysis case study and | 32 | 33 | 34 | 35 | | |
| High-nickel alloys, failure analysis case study and | 35 | 36 | 37 | 38 | | |
| High-temperature oxidation. See Oxidation | | | | | | |
| High-tensile strength (HT) steel, tankers and | 527 | | | | | |
| High-velocity oxygen fuel (HVOF) thermal spraying | 406 | 407 | 408 | 334 | | |
| Highways, cost of corrosion and | 11 | 18 | | | | |
| Hindered amine light stabilizers (HALS) | | | | | | |
| coating degradation and | 388 | 403 | | | | |
| wood protection and | 292 | | | | | |
| Hindered phenolic antioxidants | 292 | | | | | |
| Holidays. See Pinholes | | | | | | |
| Home appliances, cost of corrosion and | 17 | 18 | | | | |
| Hot corrosion | 142 | 143 | 144 | 145 | | |
| testing methods for | 144 | | | | | |
| thermal spraying applications and | 415 | | | | | |
| Hot-dip galvanizing, corrosion costs and | | 7 | | | | |
| HST (Hubble Space Telescope) | 483 | | | | | |
| FEP degradation and | 489 | 490 | 491 | | | |
| HT (high-tensile strength) steel, tankers and | | 527 | | | | |
| Hubble Space Telescope (HST) | 483 | | | | | |
| FEP degradation and | 489 | 490 | 491 | | | |
| Hull girder strength, corrosion and | 537 | 541 | 543 | | | |
| HVOF (high-velocity oxygen fuel) thermal spraying | 334 | 406 | 407 | 408 | | |
| Hydrogen embrittlement | 47 | | | | | |
| Hydrogen-induced cracking | 47 | | | | | |
| Hydrogen ion activity | 509 | | | | | |

Index Terms

Links

| | | | | | | |
|--|-----|-----|-----|-----|-----|-----|
| Hydrostatic testing, coated concrete and | 424 | 425 | 426 | | | |
| Hymenoptera, wood degradation and | 305 | | | | | |
| I | | | | | | |
| IACS (International Society of Classification Societies) | 540 | | | | | |
| IBAD (ion beam assisted deposition) | 334 | | | | | |
| Icorr (corrosion current) | 97 | 98 | 99 | 100 | 101 | |
| Ignition properties | 219 | | | | | |
| IGTs (industrial gas turbines) | 412 | 413 | 414 | 415 | 416 | |
| superalloys and | 131 | | | | | |
| ternary alloy oxidation and | 141 | | | | | |
| IHD (Intensive Holiday Detection) | 512 | | | | | |
| Immersion tests | 48 | 49 | 50 | 51 | 52 | 53 |
| IMO (International Maritime Organization) | 541 | | | | | |
| Impressed current cathodic protection | 237 | 505 | | | | |
| choosing | 513 | | | | | |
| designing | 515 | 516 | 517 | | | |
| Impurities, in oxides | 111 | | | | | |
| Incinerators, high-temperature corrosion and | 150 | | | | | |
| Industrial gas turbines (IGTs) | 412 | 413 | 414 | 415 | 416 | |
| superalloys and | 131 | | | | | |
| ternary alloy oxidation and | 141 | | | | | |
| Industry sectors, corrosion costs and | 5 | 10 | 11 | 12 | 13 | 14 |
| | 15 | 16 | 17 | 18 | 19 | 20 |
| Infrared (IR) | 115 | | | | | |
| Infrastructure, cost of corrosion and | 11 | 18 | | | | |
| Initial oxidation | 115 | 116 | 117 | 118 | | |
| Inorganic additives, in paints | 332 | 336 | | | | |
| Inorganic compounds, wood protection and | 289 | | | | | |
| Inorganic hydroxides | 219 | | | | | |
| Insects, wood degradation and | 303 | 304 | 305 | | | |
| Intensive Holiday Detection (IHD) | 512 | | | | | |
| Intergranular corrosion | 47 | | | | | |
| Internal resistance | 233 | 235 | | | | |
| International Convention for the Prevention of Pollution | | | | | | |
| from Ships | 541 | | | | | |
| International Convention for the Safety of Life at Sea (SOLAS) | 541 | | | | | |
| International Maritime Organization (IMO) | 541 | | | | | |
| International Society of Classification Societies (IACS) | 540 | | | | | |
| Interstitials, in oxides | 111 | | | | | |
| Invertebrate settlement | 181 | 182 | 183 | 184 | 185 | |
| Ion beam treatment techniques | 334 | | | | | |
| Ion ingress | 449 | 456 | | | | |
| Ionizing radiation, spacecraft materials degradation and | 482 | 483 | 484 | 485 | 486 | 487 |
| IR (infrared) | 115 | | | | | |
| IR coupons | 511 | 512 | | | | |
| IR drop, cathodic protection and | 507 | | | | | |

Index Terms

Links

| | | | | | | |
|--|-----|-----|-----|-----|-----|-----|
| Iron | | | | | | |
| aluminum alloys and | 345 | | | | | |
| oxidation and | 119 | | | | | |
| ISO standards, weathering/appearance tests and | 399 | | | | | |
| Isoconversional diagnostic plots | 73 | | | | | |
| Isoptera (termites), wood degradation and | 303 | | | | | |
| Isothermal oxidation | 110 | | | | | |
| K | | | | | | |
| Kamal method | 73 | | | | | |
| Kapton® | 470 | 471 | 472 | 473 | 474 | 475 |
| | 476 | 477 | 485 | | | |
| Kevlar® | 261 | 262 | | | | |
| chemical aging and | 153 | | | | | |
| Kinetics | | | | | | |
| chemical | 69 | 70 | 71 | | | |
| galvanic systems and | 232 | 233 | 234 | | | |
| oxidation and | 106 | 107 | 108 | 109 | | |
| Kissinger method | 72 | 73 | | | | |
| Knowledge, chemical process equipment corrosion prevention/ control and | 567 | | | | | |
| L | | | | | | |
| Lamination, packaging and | 557 | 558 | 559 | | | |
| Lanthanides | 357 | | | | | |
| Laser ablation | 335 | | | | | |
| Lattice defects | 112 | | | | | |
| LDEF (Long Duration Exposure Facility) satellite | | | | | | |
| contamination processes and | 478 | | | | | |
| epoxy adhesives and | 482 | | | | | |
| impact craters and | 493 | | | | | |
| Lead paint | 384 | | | | | |
| Lectins | 181 | 182 | 183 | | | |
| LEED | 115 | | | | | |
| LEIM (local electrochemical impedance map) | 452 | 453 | 454 | 455 | 456 | 457 |
| | 458 | | | | | |
| LEIS (local electrochemical impedance spectra) | 452 | 453 | 454 | 455 | 456 | 457 |
| | 458 | | | | | |
| LEO atomic oxygen | 466 | 467 | 468 | 469 | 470 | 471 |
| | 472 | 473 | 474 | 475 | 476 | 477 |
| Life-cycle modeling, concrete and | 171 | 173 | | | | |
| Light | | | | | | |
| coating degradation and | 377 | 389 | | | | |
| wood weathering and | 277 | 278 | 279 | 280 | 281 | |
| Light organic solvent systems (LOSP) | 313 | | | | | |
| Limnoria, wood degradation and | 305 | | | | | |

Index Terms

Links

| | | | | | | |
|--|-----|-----|-----|-----|-----|-----|
| Linear polarization resistance (LPR) | 58 | | | | | |
| Linear rate law | 108 | | | | | |
| Liquid crystallinity | 551 | | | | | |
| Liquid hydrochloric acid, nickel-based alloys and | 37 | | | | | |
| Liquid transmission pipelines, cost of corrosion and | 11 | 18 | | | | |
| Local electrochemical impedance map (LEIM) | 452 | 453 | 454 | 455 | 456 | 457 |
| | 458 | | | | | |
| Local electrochemical impedance spectra (LEIS) | 452 | 453 | 454 | 455 | 456 | 457 |
| | 458 | | | | | |
| Localized corrosion | 47 | 48 | 49 | 50 | 51 | 52 |
| | 53 | 54 | 57 | 58 | 59 | 60 |
| chemical process equipment and | 566 | 469 | 570 | 571 | 572 | 573 |
| | 574 | | | | | |
| cyclic-anodic-polarization behavior and | 101 | | | | | |
| Logarithmic Law, Mott theory of | 117 | | | | | |
| Logarithmic oxidation | 106 | 107 | 108 | | | |
| Long Duration Exposure Facility (LDEF) satellite | | | | | | |
| contamination processes and | 478 | | | | | |
| epoxy adhesives and | 482 | | | | | |
| impact craters and | 493 | | | | | |
| LOSP (light organic solvent systems) | 313 | | | | | |
| Low-alloy ferritic steels, oxidation behaviors and | 128 | | | | | |
| Low-alloy steel pipes, failure analysis case study and | 29 | 30 | 31 | 32 | | |
| Low permeability concrete | 169 | | | | | |
| Low-pressure plasma spraying (LPPS) | 410 | | | | | |
| Low-temperature oxidation | 115 | | | | | |
| Lowry process (wood protection) | 311 | | | | | |
| LPPS (low-pressure plasma spraying) | 410 | | | | | |
| LPR (linear polarization resistance) | 58 | | | | | |

M

| | | | | | | |
|--|-----|-----|-----|--|--|--|
| M. V. Castor, marine incident and | 523 | 524 | 525 | | | |
| M. V. Nakhodka, marine incident and | 525 | | | | | |
| Macrofouling | 179 | | | | | |
| Magnesium alloys, corrosion-resistant coatings and | 372 | | | | | |
| Magnesium anodes, vs. zinc anodes | 235 | | | | | |
| Magnesium, aluminum alloys and | 346 | | | | | |
| Maintainability | 321 | | | | | |
| Manganese | | | | | | |
| aluminum alloys and | 346 | | | | | |
| improved alloy mechanical properties and | 128 | | | | | |
| Manufacturing, cost of corrosion and | 15 | 18 | 20 | | | |
| MAP (modified atmosphere packagings) | 561 | | | | | |
| Marine corrosion | 531 | 532 | 533 | | | |
| Marine industry, coatings and | 381 | | | | | |
| Marine organisms | 381 | | | | | |
| wood degradation and | 305 | | | | | |

Index Terms

Links

| | | | | | | |
|---|---------|-----|-----|-----|-----|-----|
| Marker technique | 113 | | | | | |
| Mass balance test | 114 | | | | | |
| Master curves | 66 | 67 | 68 | 69 | | |
| Material flammability | 207-225 | | | | | |
| flame retardants and | 217 | 218 | 219 | | | |
| flammability properties and | 219 | 220 | 221 | 222 | 223 | |
| tests and | 210 | 211 | 212 | 213 | 214 | |
| | 215 | 216 | 217 | | | |
| Mechanical cladding (thermal spraying) | 411 | | | | | |
| Mechanical testing | | | | | | |
| of coatings/paints | 403 | | | | | |
| of plastics | 73 | 74 | 75 | | | |
| Mell and Lawson burn model | 274 | | | | | |
| Membranes, for concrete | 169 | | | | | |
| Mercury/saturated-mercurous-chloride half-cell | 83 | | | | | |
| Metal conditioner, vinyl butyral as | 374 | | | | | |
| Metal dusting | 148 | | | | | |
| Metallic coatings | | | | | | |
| corrosion costs and | 6 | | | | | |
| polymer protection and | 487 | | | | | |
| Metallic materials | | | | | | |
| atomic oxygen and | 474 | | | | | |
| chemical process equipment corrosion and | 565-581 | | | | | |
| corrosion costs and | 3-24 | | | | | |
| corrosion equation for | 55 | | | | | |
| corrosion of. See Oxidation | | | | | | |
| corrosion-resistant coatings/paints for | 367-385 | | | | | |
| failure analysis of | 27-45 | | | | | |
| Pourbaix diagrams and | 87 | 88 | 89 | 90 | 91 | 92 |
| | 230 | | | | | |
| surface pretreatment and | 348 | 349 | 350 | 351 | 352 | |
| testing, vs. plastics | 65 | | | | | |
| thermal spray coatings and | 405-422 | | | | | |
| Metalorganic CVD (MOCVD) | 335 | | | | | |
| Metalworking industry, thermal spray coatings and | 421 | | | | | |
| Metam sodium | 316 | | | | | |
| Methylisothiocyanate (MITC) | 316 | | | 323 | | |
| Microbial-induced corrosion (MIC) | 53 | 185 | 186 | 187 | 188 | 189 |
| | 190 | 191 | 192 | | | |
| ships and | 531 | | | | | |
| chemical process equipment and | 571 | | | | | |
| Microbiological activity, pipelines and | 509 | | | | | |
| Microfouling | 179 | | | | | |
| Micrometeoroids | 491 | 492 | 493 | 494 | | |
| Microorganisms | 53 | 323 | | | | |
| biofouling and | 179-206 | | | | | |
| coating degradation and | 389 | | | | | |
| failure analysis and | 39 | | | | | |

Index Terms

Links

| | | | | | | |
|--|-----|-----|-----|-----|-----|-----|
| ships and | 531 | | | | | |
| wood weathering and | 277 | 281 | | | | |
| Microscopy techniques | 326 | | | | | |
| Migration of acrylonitrile and styrene | 76 | | | | | |
| Military aircraft, coatings and | 383 | | | | | |
| Military vehicles, coatings and | 362 | | | | | |
| Mining, cost of corrosion and | 16 | 18 | | | | |
| MISSE PEACE polymers experiment | 473 | | | | | |
| MITC (methylothiocyanate) | 316 | | | | | |
| Mixed gas environments, oxidation and | 132 | 133 | 134 | 135 | 136 | 137 |
| MOCVD (metalorganic CVD) | 335 | | | | | |
| Modified atmosphere packagings (MAP) | 561 | | | | | |
| Modulus | 66 | 67 | 68 | | | |
| Moisture. See Water | | | | | | |
| Mold fungi, wood degradation and | 302 | | | | | |
| Molecular probes, organic coatings and | 458 | 459 | 460 | | | |
| Molecular spectroscopies | 327 | | | | | |
| Motor vehicles, cost of corrosion and | 13 | 18 | | | | |
| Mott Theory of Direct Logarithmic Law | 117 | | | | | |
| Municipal incinerators, high-temperature corrosion and | 150 | | | | | |

N

| | | | | | | |
|---|-----|-----|-----|----|--|--|
| n-type oxides | 112 | | | | | |
| NACE (National Association of Engineers) | | | | | | |
| cathodic protection criteria and | 507 | | | | | |
| corrosion rates and | 567 | | | | | |
| NACE International | 5 | | | | | |
| corrosion control services and | 9 | | | | | |
| Nakhodka (M. V.), marine incident and | 525 | | | | | |
| Nanostructured coatings | 336 | | | | | |
| Nanotubes, aging and | 162 | | | | | |
| National Association of Engineers. See NACE | | | | | | |
| Natural gas (NG), failure analysis case study | 29 | 30 | 31 | 32 | | |
| Near UV (NUV) | 479 | 481 | | | | |
| Negative chemotaxis | 181 | | | | | |
| Nernst equation | 86 | 230 | 241 | | | |
| Neutral coatings | 417 | | | | | |
| NG (natural gas), failure analysis case study | 29 | 30 | 31 | 32 | | |
| Nickel | | | | | | |
| as alloying element | 122 | | | | | |
| oxidation and | 118 | | | | | |
| Nickel-based alloys | 27 | 124 | 129 | | | |
| corrosion-resistant alloys and | 8 | | | | | |
| failure analysis case study and | 38 | | | | | |
| Niobium, oxidation and | 119 | | | | | |
| Noble metals | | | | | | |
| cathodic protection and | 231 | 504 | | | | |

Index Terms

Links

| | | | | | |
|---|---------|-----|-----|-----|---------|
| chemical etch and | 350 | | | | |
| oxidation and | 118 | 119 | 120 | 121 | 122 |
| thermal spraying and | 410 | | | | |
| Nomex® | 261 | | | | |
| nth-order reactions | 69 | 70 | | | |
| Nuclear waste storage, cost of corrosion and | 17 | 18 | | | |
| NUV (near UV) | 479 | 481 | | | |
| Nylon 11, physical aging and | 158 | | | | |
| Nylon 1212, thermogravimetric analysis and | 72 | | | | |
| Nylon 66, physical aging and | 158 | | | | |
| O | | | | | |
| OBDDPO (octabromodiphenyl oxide) | 248 | | | | |
| OCLI coating | 482 | 487 | 489 | | |
| Octabromodiphenyl oxide (OBDDPO) | 248 | | | | |
| ODS (oxide dispersion-strengthened) alloys | 132 | | | | |
| Oil exploration/production, cost of corrosion and | 15 | 18 | | | |
| Oil Pollution Act of 1990 | 527 | | | | |
| Oil tankers. See Tankers | | | | | |
| Oilborne preservatives | 312 | | | | |
| Optical sensors | 270 | | | | |
| Orbital debris | 491 | 492 | 493 | 494 | |
| Organic chloride | 35 | 36 | 37 | 38 | |
| Organic coatings | 374 | 375 | 376 | 377 | 378 379 |
| | 380 | 381 | | | |
| corrosion costs and | 6 | | | | |
| extrinsic defects in | 450 | | | | |
| intrinsic defects in | 449 | 450 | 451 | 452 | 453 454 |
| | 455 | 456 | 457 | 458 | 459 460 |
| | 461 | | | | |
| growth/death cycle of | 455 | | | | |
| Organic flame retardants | 244 | | | | |
| Organic primers | 348 | | | | |
| Organisols | 374 | | | | |
| Orientation, barrier properties and | 556 | | | | |
| Outdoor exposure, of coatings/paints | 389 | 390 | 391 | 392 | 393 |
| Over coatings | 348 | 358 | | | |
| Overprotection | 241 | | | | |
| Oxidation | 105-152 | 229 | | | |
| alloys and | 122 | 123 | 124 | 125 | 126 127 |
| | 128 | 129 | 130 | 131 | 132 |
| commercial alloys | 128 | 129 | 130 | 131 | 132 |
| multi-component alloys | 125 | 126 | 127 | 128 | |
| criteria of | 106 | | | | |
| industrial examples of | 148 | 149 | 150 | 151 | |
| initial | 115 | 116 | 117 | 118 | |
| isothermal | 110 | | | | |

Index Terms

Links

| | | | | | | |
|---|-----|-----|-----|-----|-----|-----|
| logarithmic | 106 | 107 | 108 | | | |
| low-temperature | 115 | | | | | |
| measurement techniques for | 108 | 109 | 110 | | | |
| microbial | 185 | 186 | 187 | 188 | 189 | 190 |
| | 191 | 192 | | | | |
| parabolic | 108 | | | | | |
| pure metals and | 118 | 119 | 120 | 121 | 122 | |
| vs. sulfidation | 134 | 135 | 136 | | | |
| thick layer | 117 | | | | | |
| thin layer | 106 | 108 | 115 | 116 | 117 | 118 |
| See also Corrosion | | | | | | |
| Oxidation kinetics | 106 | 107 | 108 | 109 | | |
| Oxidation resistance, thermal spraying applications and | 415 | | | | | |
| Oxide dispersion-strengthened (ODS) alloys | 132 | | | | | |
| Oxide scale spallation | 145 | | | | | |
| Oxides | | | | | | |
| chemical process equipment corrosion and | 565 | | | | | |
| n-type | 112 | | | | | |
| p-type | 112 | | | | | |
| Oxine copper (copper-8-quinolinolate) | 313 | | | | | |
| Oxygen | | | | | | |
| food packagings and | 561 | | | | | |
| with sulfur dioxide, ternary alloy oxidation and | 141 | | | | | |
| wood protection and | 306 | | | | | |
| Oxygen tracer technique | 113 | | | | | |
| Ozawa-Flynn-Wall method | 72 | 73 | | | | |

P

| | | | | | | |
|--|---------|-----|-----|-----|-----|-----|
| p-type oxides | 112 | | | | | |
| Package boiler tubes, failure analysis and | 42 | | | | | |
| Packaging, barrier materials for | 547-563 | | | | | |
| Paints | 387-404 | | | | | |
| composite | 332 | 333 | 334 | | | |
| corrosion-resistant | 367-385 | | | | | |
| characteristics/uses of | 372 | 373 | 374 | 375 | 376 | |
| chemical process equipment and | 576 | | | | | |
| degradation of | 376 | 377 | 378 | 379 | 380 | 381 |
| industrial applications and | 381 | 382 | 383 | 384 | | |
| tanker protection and | 538 | | | | | |
| weathering tests for | 387 | 388 | 389 | 390 | 391 | 392 |
| | 393 | 394 | 395 | 396 | 397 | 398 |
| | 399 | 400 | 401 | 402 | 403 | 404 |
| white thermal control | 482 | 486 | 488 | | | |
| See also Coatings | | | | | | |
| Paper industry | | | | | | |
| cost of corrosion and | 16 | 17 | 18 | 19 | 20 | |
| thermal spray coatings and | 421 | | | | | |

Index Terms

Links

| | | | | | | |
|--|-----|-----|-----|-----|-----|----|
| Paper, physical aging and | 157 | | | | | |
| Parabolic oxidation | 108 | | | | | |
| Passivation | 90 | 91 | 92 | | | |
| Passive corrosion rates | 58 | | | | | |
| PBBEs (polybrominated biphenyl ethers) | 245 | | | | | |
| PBBs (polybrominated biphenyls) | 244 | 245 | 246 | 247 | | |
| regulatory controls and | 257 | | | | | |
| PBDDs (polybrominated dibenzodioxins) | 244 | | | | | |
| PBDFs (polybrominated dibenzofurans) | 244 | | | | | |
| PBDPO flame retardants | 245 | 246 | 247 | 248 | 249 | |
| PBI (polybenzimidazole) | 261 | 263 | | | | |
| PBO (polyphenylene-benzobisoxazole) | 263 | | | | | |
| PBR (Pilling Bedworth Ratio) | 145 | | | | | |
| PCBs (polychlorinated biphenyls) | 246 | 247 | 248 | | | |
| PE (polyethylene) | | | | | | |
| biodeterioration of packaging materials and | 193 | | | | | |
| cross-linked | 553 | | | | | |
| PeBDPO (pentabromodiphenyl oxide) | 248 | | | | | |
| PEGs (polyethylene glycols) | 315 | | | | | |
| PEI (polyether imide) | 72 | | | | | |
| PEN bottles | 552 | 554 | 556 | | | |
| Penetrating finishes for wood | 287 | | | | | |
| Penetration, wood protection and | | 308 | | | | |
| Pennes burn model | 272 | | | | | |
| Pentabromodiphenyl oxide (PeBDPO) | 248 | | | | | |
| Pentachlorophenol | 312 | 313 | | | | |
| PET bottles | 554 | 555 | 556 | 557 | | |
| Petrochemical industry | 152 | | | | | |
| cost of corrosion and | 16 | 17 | 18 | 19 | | |
| oxidation and | 132 | | | | | |
| Petrochemical plant failure analysis case studies | 35 | 36 | 37 | 38 | 39 | 40 |
| | 41 | 42 | | | | |
| Petroleum refining | 152 | | | | | |
| cost of corrosion and | 16 | 18 | | | | |
| pH | | | | | | |
| of concrete | 165 | | | | | |
| laboratory tests and | 49 | | | | | |
| of soil | 509 | | | | | |
| tanker corrosion and | 534 | | | | | |
| Pharmaceutical industry | | | | | | |
| cost of corrosion and | 16 | 17 | 18 | 19 | | |
| oxidation and | 132 | | | | | |
| Phase stability diagrams | 137 | | | | | |
| PHE (plate-type heat exchanger), failure analysis case study and | 38 | | | | | |
| Phenolic resins | 375 | | | | | |
| Pholads, wood degradation and | | 305 | | | | |
| Phosphate surface treatments | 331 | | | | | |
| Phosphorous-containing flame retardants | 219 | | | | | |

Index Terms

Links

| | | | | | | |
|---|---------|-----|-----|-----|-----|-----|
| Photodegradation | 65 | | | | | |
| Photothermodegradation | 65 | | | | | |
| Phthalate acids | 195 | | | | | |
| Phthalate esters | 195 | | | | | |
| Physical aging of plastics | 154 | 155 | 156 | 157 | 158 | 159 |
| role of water in | 160 | 161 | 162 | | | |
| role of water in | 161 | | | | | |
| Physical vapor deposition (PVD) | 335 | | | | | |
| PI (polyimide) | 263 | | | | | |
| Pickling | 350 | | | | | |
| Pigments, in coatings/paints | 369 | | | | | |
| corrosion inhibiting | 372 | | | | | |
| Pilling Bedworth Ratio (PBR) | 145 | | | | | |
| Pinholes | 171 | 369 | | | | |
| concrete coatings and | 424 | 428 | | | | |
| Pipelines | | | | | | |
| buried, coatings and | 383 | | | | | |
| cathodic protection of | 503-521 | | | | | |
| impressed cathodic protection and | 237 | | | | | |
| monitoring methods for | 511 | | | | | |
| ground bed spacing and | 238 | 239 | 240 | 241 | | |
| hot water, tuberculation in | 573 | | | | | |
| microbial corrosion and | 185 | 186 | 187 | 188 | 189 | 190 |
| protection of, soil resistance and | 191 | 192 | | | | |
| stray current corrosion and | 509 | | | | | |
| stray current corrosion and | 508 | | | | | |
| stray current corrosion and | 241 | | | | | |
| Pitting corrosion | 42 | 47 | | | | |
| chemical process equipment and | 569 | 570 | 571 | | | |
| concrete and | 167 | 168 | 169 | 170 | | |
| cyclic-anodic polarization behavior and | 101 | | | | | |
| tankers and | 531 | | | | | |
| Plasma densification (thermal spraying) | 411 | | | | | |
| Plasma thermal spraying | 334 | 406 | 410 | | | |
| Plastic deformation | 34 | | | | | |
| Plasticizers, biodeterioration and | 195 | | | | | |
| Plastics | 65 | | | | | |
| chemical/physical aging of | 153 | 154 | 155 | 156 | 157 | 158 |
| corrosion costs and | 159 | 160 | 161 | 162 | 163 | |
| lifetime predictions of | 8 | | | | | |
| lifetime predictions of | 65 | 66 | 67 | 68 | 69 | 70 |
| lifetime predictions of | 71 | 72 | 73 | 74 | 75 | 76 |
| lifetime predictions of | 77 | | | | | |
| packaging materials and | 547-563 | | | | | |
| release coatings and | 421 | | | | | |
| as waste material, degrading | 65 | | | | | |
| Plastisols | 374 | | | | | |
| Plate-plate (PP) testing geometry | 69 | | | | | |

Index Terms

Links

| | | | | | | |
|--|---------|-----|-----|-----|-----|----|
| Plate-type heat exchanger (PHE), failure analysis case study and | 38 | | | | | |
| PLC (polymer liquid crystal), creep behavior and | 74 | | | | | |
| PLD (pulsed laser deposition) | 335 | | | | | |
| Polarity, barrier properties and | 548 | 549 | 550 | | | |
| Polarization | 59 | 89 | 90 | 91 | 92 | 93 |
| | 94 | 95 | 96 | 97 | 98 | 99 |
| | 100 | 101 | 102 | | | |
| polarization curves and | 96 | 97 | 98 | 99 | | |
| Pollution | | | | | | |
| coating degradation and | 389 | | | | | |
| ships/tanks and | 527 | 541 | | | | |
| wood weathering and | 281 | | | | | |
| See also Environment | | | | | | |
| Poly(ethyl acrylates), physical aging and | 157 | | | | | |
| Poly(ethyl methacrylates), physical aging and | 157 | | | | | |
| Polyamide 11, physical aging and | 158 | | | | | |
| Polybenzimidazole (PBI) | 261 | 263 | | | | |
| Polybrominated biphenyl ethers (PBBEs) | 245 | | | | | |
| Polybrominated biphenyls (PBBs) | 244 | 245 | 246 | 247 | 248 | |
| regulatory controls and | 257 | | | | | |
| Polybrominated dibenzodioxins (PBDDs) | 244 | | | | | |
| Polybrominated dibenzofurans (PBDFs) | 244 | | | | | |
| Polychlorinated biphenyls (PCBs) | 246 | 247 | 248 | | | |
| Polyester resins | 372 | | | | | |
| Polyether imide (PEI) | 72 | | | | | |
| Polyethylene (PE) | | | | | | |
| biodegradation of packaging materials and | 193 | | | | | |
| cross-linked | 553 | | | | | |
| Polyethylene glycols (PEGs) | 315 | | | | | |
| Polyimide (PI) | 263 | | | | | |
| Polyimide gas separation membranes, physical aging and | 159 | | | | | |
| Polyimide Kapton® | 470 | 482 | | | | |
| Polyimides, biodegradation of | 192 | 193 | 194 | 195 | | |
| Polyisocyanurate foam, physical aging and | 158 | | | | | |
| Polymer liquid crystal (PLC), creep behavior and | 74 | | | | | |
| Polymer-modified asphalt, master curves and | 68 | | | | | |
| Polymeric wastes, nonisothermal kinetic testing and | 72 | | | | | |
| Polymers | | | | | | |
| atomic oxygen exposure and | 470 | | | | | |
| mitigation techniques for | 475 | 476 | 477 | | | |
| barrier packaging materials and | 547-563 | | | | | |
| biodegradation of | 192 | 193 | 194 | 195 | | |
| concrete coatings and | 424 | | | | | |
| corrosion costs and | 8 | | | | | |
| fillers/blends and | 554 | 555 | 556 | | | |
| flame retardancy and | 243-259 | | | | | |
| ionizing radiation and | 485 | | | | | |

Index Terms

Links

| | | | | | | |
|--|---------|---------|---------|-----|-----|----|
| material flammability and | 207-225 | | | | | |
| MISSE PEACE experiment and | 473 | | | | | |
| space radiation and, mitigation techniques for | 487 | | | | | |
| thermal decomposition of | 208 | | | | | |
| thermal spraying and | 411 | | | | | |
| thermal variations and | 487 | | | | | |
| ultraviolet radiation and | 479 | | | | | |
| Polyolefins, environmental stress cracking and | 154 | | | | | |
| Polyphenylene ether (PPE) composites, physical aging and | 157 | | | | | |
| Polyphenylene sulfide (PPS) | 263 | | | | | |
| thermal decomposition testing and | 73 | | | | | |
| Polyphenylene-benzobisoxazole (PBO) | 263 | | | | | |
| Polypropylene, thermogravimetric analysis and | 72 | | | | | |
| Polystyrene, physical aging and | 157 | | | | | |
| Polysulfone, mechanical testing and | 74 | | | | | |
| Polytetrafluoroethylene (PTFE) | 263 | 486 | | | | |
| Polyurethane foam, physical aging and | 158 | | | | | |
| Polyurethanes | 375 | | | | | |
| Polyvinyl chloride (PVC), physical aging and | 155 | | | | | |
| Polyvinylidene fluoride (PVDF), physical aging and | 156 | | | | | |
| Polyvinylpyrrolidone (PVP), physical aging and | 158 | | | | | |
| Pore space | 376 | | | | | |
| Ports, cost of corrosion and | 12 | 18 | | | | |
| Potential criteria, cathodic protection and | 507 | | | | | |
| Potential surveys, for pipelines | 511 | | | | | |
| Potentiodynamic polarization | 59 | | | | | |
| Potentiostatic polarization | 58 | | | | | |
| Potentiostats | 56 | | | | | |
| Pourbaix diagrams | 87 | 88 | 89 | 90 | 91 | 92 |
| cathodic protection and | 230 | | | | | |
| Powder coatings | 360 | | | | | |
| Powder thermal spraying | 406 | 408 | | | | |
| Power cables, spacecraft and | 493 | | | | | |
| Power plants, oxidation and | 132 | 149 | | | | |
| PP (plate-plate) testing geometry | 69 | | | | | |
| PPE (polyphenylene ether) composites, physical aging and | 157 | | | | | |
| PPS (polyphenylene sulfide) | 263 | | | | | |
| thermal decomposition testing and | 73 | | | | | |
| Premature failures | 27 | | | | | |
| Preservatives, wood treatments and | 311 | 312 | 313 | 314 | 315 | |
| Pressure processes (wood protection) | 310 | | | | | |
| Pressure vessels | 493 | | | | | |
| Pressure, laboratory tests and | 49 | | | | | |
| Prevention | 21 | 227-317 | 565-581 | | | |
| See also Coatings | | | | | | |
| Primers | 358 | 359 | 360 | 361 | | |
| evaluating performance of | 361 | | | | | |
| Printing industry, thermal spray coatings and | 421 | | | | | |

Index Terms

Links

| | | | | | |
|--|---------|---------|-----|-----|---------|
| Production, cost of corrosion and | 15 | 18 | 20 | | |
| Proof testing, for coatings | 380 | | | | |
| Protective coatings. See Coatings | | | | | |
| Protective measures | 227-317 | 565-581 | | | |
| <i>See also</i> Coatings | | | | | |
| PTFE (polytetrafluoroethylene) | 263 | 486 | | | |
| Pulp industry, cost of corrosion and | 16 | 17 | 18 | 19 | 20 |
| Pulsed laser deposition (PLD) | 335 | | | | |
| Pure metals. See Noble metals | | | | | |
| PVC (polyvinyl chloride), physical aging and | 155 | | | | |
| PVD (physical vapor deposition) | 335 | | | | |
| PVDF (polyvinylidene fluoride), physical aging and | 156 | | | | |
| PVP (polyvinylpyrrolidone), physical aging and | 158 | | | | |
| Pyrocal sensor | 269 | | | | |
| Pyrolysis | | | | | |
| computer modeling and | 223 | | | | |
| flame retardants and | 244 | | | | |
| Pyroman System | 267 | | | | |
| R | | | | | |
| Radiant coils, failure analysis case study and | 35 | 36 | 37 | 38 | |
| Radiant Panel System | 267 | | | | |
| Radiant Protective Performance (RPP) | 266 | | | | |
| Radioactivity damage | 326 | | | | |
| Radiolysis | 326 | | | | |
| Railroads, cost of corrosion and | 12 | 14 | 18 | | |
| Ram atomic oxygen | 467 | 479 | | | |
| Raman spectroscopy | 327 | | | | |
| Rare earth-based conversion coating | 357 | | | | |
| Rare earth elements, improved oxidation behavior and | 128 | | | | |
| RE (reference electrode) | 56 | | | | |
| Reaction order | 69 | | | | |
| Reaction to fire. See Material flammability | | | | | |
| Rebar coatings, concrete and | 171 | | | | |
| Red cedar, heat release rates and | 221 | | | | |
| Redox potential, pipelines and | 509 | | | | |
| Reference electrode (RE) | 56 | | | | |
| Reformer tubes, failure analysis case study | 32 | 33 | 34 | 35 | |
| Regulatory controls | | | | | |
| fire safety code testing | 210 | 211 | 212 | 213 | 214 |
| flame retardants and | 256 | | | | |
| <i>See also</i> Standards | | | | | |
| Reinforced concrete | | | | | |
| chloride ingress and | 165 | 166 | 167 | 168 | 169 170 |
| environmental degradation of | 165 | 166 | 167 | 168 | 169 170 |
| | 171 | 172 | 173 | 174 | 175 176 |
| | 177 | | | | |

Index Terms

Links

| | | | | |
|--|-----|-----|-----|-----|
| protection systems for | 169 | 170 | 171 | 172 |
| Release coatings | 421 | | | |
| Reliability | 321 | | | |
| Research and development | 9 | | | |
| material flammability testing and | 214 | 215 | 216 | 217 |
| thermal protective clothing and | 261 | | | |
| Resins | 372 | 373 | 374 | 375 |
| Resistance calculations, galvanic cathodic protection and | 234 | | | |
| Restoration, thermal spray coatings and | 417 | | | |
| Retention, wood protection and | 308 | | | |
| Reversible electrical work | 82 | | | |
| Rigid thermoplastic polyurethane (RTPU) materials, environmental | | | | |
| stress cracking and | 154 | | | |
| Rinsing, metal surface pretreatment and | 351 | | | |
| Rotating airfoils, industrial gas turbines and | 416 | | | |
| RPP (Radiant Protective Performance) | 266 | | | |
| RTPU (rigid thermoplastic polyurethane) materials, environmental | | | | |
| stress cracking and | 154 | | | |
| Rubber | | | | |
| aging and | 162 | | | |
| release coatings and | 421 | | | |
| Rueping process (wood protection) | 311 | | | |
| Rutile | 120 | | | |

S

| | | | | |
|--|-----|-----|-----|-----|
| S13G/LO paint | 482 | 486 | | |
| Sacrificial anodes, corrosion costs and | 9 | | | |
| Sacrificial cathodic protection | 370 | 504 | | |
| choosing/designing | 513 | 514 | 515 | |
| SAE standards | | | | |
| metal alloy decontamination and | 349 | | | |
| weathering/appearance tests and | 399 | | | |
| Salt, wood degradation and | 300 | | | |
| SAMPE (Society for the Advancement of Material and Process Engineering) | 76 | | | |
| Saturated calomel electrode (SCE) | 56 | 83 | 101 | |
| Scale spallation | 145 | | | |
| Scales | 110 | 111 | 112 | |
| multi-component alloys and | 125 | 126 | 127 | 128 |
| Scanning electron microscopy (SEM) | 110 | 326 | | |
| Scanning electron microscopy/energy dispersive analysis by X-rays (SEM/EDAX) | 328 | | | |
| Scanning optical microscopy | 326 | | | |
| Scanning reference electrode techniques (SRET) | 354 | | | |
| Scanning vibrating electrode techniques (SVET) | 354 | | | |
| SCE (saturated calomel electrode) | 56 | 83 | 101 | |

Index Terms

Links

| | | | |
|--|-----|-----|-----|
| SCF (supercritical fluid) treatments, for wood | 311 | | |
| Scrap steel, as anode material | 237 | | |
| Sealers, for concrete | 169 | | |
| Sealing | 354 | | |
| Second-order reactions | 69 | 70 | |
| Secondary Ion Mass Spectrometry (SIMS) | 110 | 113 | 327 |
| Self-assembled, nano-phase particle (SNAP) coatings | 337 | | |
| Self-fluxing alloys/blends | 410 | | |
| Self-healing coatings | 334 | 369 | |
| SEM (scanning electron microscopy) | 110 | 326 | |
| SEM/EDAX (scanning electron microscopy/energy dispersive analysis by X-rays) | 328 | | |
| Sensing devices, skin burns and | | 268 | |
| SET (stored energy test) | 267 | | |
| Sewer systems, cost of corrosion and | | 13 | 18 |
| Shawbury-Wallace relaxometer | 71 | | |
| SHE (standard hydrogen electrode) | 83 | | |
| Shipping industry | | | |
| cost of corrosion and | 14 | 18 | |
| standards and | 540 | | |
| Ships | | | |
| beneath deck corrosion and | 533 | | |
| grooving corrosion and | 531 | | |
| microbial-induced corrosion and | 531 | | |
| wood protection and | 307 | 316 | |
| Shipworms, wood degradation and | 305 | | |
| Shroud casings, IGTs and | 416 | | |
| SHTs (single-hull tankers) | 527 | 528 | 529 |
| structural integrity risk and | 537 | | |
| Side shell, corrosion and | 532 | | |
| Silicon | | | |
| as alloying element | 122 | 125 | |
| aluminum alloys and | 346 | | |
| Silicones, atomic oxygen and | 474 | 477 | |
| Silver corrosion | 87 | | |
| Silver-silver chloride electrode (SSE) | 56 | | |
| SIMS (Secondary Ion Mass Spectrometry) | 110 | 113 | 327 |
| Simulated service exposure testing, for coatings | 378 | | |
| Single-hull tankers (SHTs) | 527 | 528 | 529 |
| structural integrity risk and | 537 | | |
| Sintering (thermal spraying) | 411 | | |
| SiO _x coating | 488 | | |
| Site visits | 28 | | |
| Skin burns | | | |
| evaluating | 271 | | |
| sensing devices and | 268 | | |
| Sliding wear, thermal spray coatings and | 419 | | |
| Smoke, material flammability and | 207 | 213 | 222 |

Index Terms

Links

| | | | | | | |
|---|---------|-----|-----|-----|-----|-----|
| Smut | 350 | | | | | |
| SNAP (self-assembled, nano-phase particle) coatings | 337 | | | | | |
| Soaking (wood protection) | 308 | | | | | |
| Society for the Advancement of Material and Process Engineering (SAMPE) | 76 | | | | | |
| Soft rot fungi, wood degradation and | 303 | | | | | |
| Soil box method, for soil resistance measurement | 508 | | | | | |
| Soil pH | 509 | | | | | |
| Soil resistance | 233 | 235 | | | | |
| cathodic protection and | 508 | | | | | |
| Solar flare x-ray radiation | 483 | | | | | |
| Solar proton events (SPEs) | 483 | | | | | |
| Solar radiation | | | | | | |
| wood coatings and | 287 | | | | | |
| wood weathering and | 277 | | | | | |
| Solar ultraviolet radiation, spacecraft materials degradation and | 479 | 480 | 481 | 482 | | |
| Solarization | 480 | | | | | |
| SOLAS (International Convention for the Safety of Life at Sea) | 541 | | | | | |
| Solvent washing | 349 | | | | | |
| Solventborne primers | 359 | | | | | |
| Spacecraft materials, degradation of | 465-501 | | | | | |
| interactions with atomic oxygen | 470 | 471 | 472 | 473 | 474 | 475 |
| space radiation and | 479 | 480 | 481 | 482 | 483 | 484 |
| spacecraft contamination and | 477 | 478 | 479 | | | |
| Specific Technology Groups (STGs) | 5 | | | | | |
| Spectral power distribution | 393 | 394 | 395 | | | |
| SPEs (solar proton events) | 483 | | | | | |
| Spray drying (thermal spraying) | 411 | | | | | |
| SRET (scanning reference electrode techniques) | 354 | | | | | |
| SSE (silver-silver chloride electrode) | 56 | | | | | |
| Stain fungi, wood degradation and | 302 | | | | | |
| Stainless steel | 27 | | | | | |
| concrete and | 171 | | | | | |
| corrosion-resistant alloys and | 8 | | | | | |
| failure analysis and | 39 | 40 | 41 | 42 | | |
| immersion tests and | 49 | | | | | |
| oxidation resistance of | 129 | | | | | |
| Standard hydrogen electrode (SHE) | 83 | | | | | |
| Standards | | | | | | |
| cabinet tests and | 54 | | | | | |
| concrete coating bonding tests and | 426 | 428 | | | | |
| concrete coating pinhole tests and | 428 | 433 | | | | |
| electrochemical tests and | 57 | | | | | |
| immersion tests and | 50 | | | | | |
| laboratory testing and | 49 | 50 | 51 | 52 | | |
| metal alloy decontamination and | 349 | | | | | |
| shipping industry and | 540 | | | | | |

Index Terms

Links

| | | | | | | |
|--|-----|-----|-----|-----|-----|-----|
| weathering/appearance tests and | 399 | | | | | |
| wood protection and | 311 | | | | | |
| Stationary airfoils, IGTs and | 416 | | | | | |
| Stern-Geary method | 100 | | | | | |
| STGs (Specific Technology Groups) | 5 | | | | | |
| Stiff molecules, barrier properties and | 552 | | | | | |
| Stiffeners of bulkheads, corrosion and | 532 | | | | | |
| Stoll Curve burn model | 271 | | | | | |
| Stored energy test (SET) | 267 | | | | | |
| Strain, measuring in plastics | 66 | | | | | |
| Stray current corrosion | 241 | | | | | |
| Stress | | | | | | |
| measuring in plastics | 66 | | | | | |
| thermal cycling and | 145 | 146 | 147 | 148 | | |
| Stress corrosion cracking | 47 | 571 | | | | |
| Styrene, migration of | 76 | | | | | |
| Sulfate-reducing bacteria | 509 | | | | | |
| Sulfidation | | | | | | |
| of alloys | 136 | | | | | |
| high-temperature | 31 | | | | | |
| vs. oxidation | 134 | 135 | 136 | | | |
| Sulfur dioxide, ternary alloy oxidation and | 141 | | | | | |
| Sulfur dioxide-containing atmospheres, scaling of alloys and | 138 | 139 | 140 | 141 | | |
| Sulfur-oxidizing bacteria, pipelines and | 510 | | | | | |
| Sulfur, metal dusting and | 149 | | | | | |
| Sulfuric acid plant case study | 38 | | | | | |
| Superalloys | 131 | | | | | |
| Supercritical fluid (SCF) treatments, for wood | 311 | | | | | |
| Surface engineering | | | | | | |
| design considerations and | 322 | 323 | 324 | 325 | 326 | 339 |
| technologies for | 329 | 330 | 331 | 332 | 333 | 334 |
| | 335 | 336 | 337 | | | |
| advantages/disadvantages of | 338 | | | | | |
| See <i>also</i> Coatings; Protective measures | | | | | | |
| SVET (scanning vibrating electrode techniques) | 354 | | | | | |
| Synchrotron techniques | 327 | 329 | | | | |

T

| | | | | | | |
|-----------------------------|---------|-----|-----|-----|--|--|
| Tafel extrapolation | 99 | | | | | |
| Tafel polarization behavior | 93 | 94 | 98 | | | |
| Tankers, corrosion and | 523-545 | | | | | |
| measuring/monitoring | 538 | 542 | | | | |
| preventing/mitigating | 538 | 539 | 540 | 541 | | |
| protection costs and | 525 | 526 | 527 | | | |
| structural integrity risk | 536 | 537 | 538 | | | |
| types of corrosion | 529 | 530 | 531 | | | |
| Tantalum, oxidation and | 118 | 119 | | | | |

Index Terms

Links

| | | | | | | |
|---|---------|---------|-----|-----|-----|-----|
| TB (torsion bar) testing geometry | 69 | | | | | |
| TBCs (thermal barrier coatings) | 413 | | | | | |
| Technora® | 263 | | | | | |
| Tedlar®, ultraviolet radiation and | 481 | | | | | |
| TEF (toxicity equivalence factor) | 250 | 252 | | | | |
| Teflon® | 263 | 486 | | | | |
| Teflon® FEP | | | | | | |
| impact craters and | 493 | | | | | |
| thermal and radiation effects on | 488 | 489 | 490 | 491 | | |
| ultraviolet radiation and | 480 | 481 | | | | |
| Telecommunications, cost of corrosion and | 13 | 18 | | | | |
| Temperature | | | | | | |
| coating degradation and | 377 | 388 | | | | |
| food packagings and | 560 | | | | | |
| laboratory tests and | 49 | | | | | |
| spacecraft materials degradation and | 487 | 488 | 489 | 490 | 491 | |
| tanker degradation and | 533 | | | | | |
| wood protection and | 306 | | | | | |
| TEQs (Toxicity Equivalents) | 253 | 254 | 255 | 256 | | |
| Termites, wood degradation and | 303 | | | | | |
| Test cycles, for accelerated weathering | 398 | 399 | 400 | 401 | | |
| Testing | 47-63 | 387-404 | | | | |
| cabinet | 53 | 54 | 55 | | | |
| chemical process equipment and | 577 | 578 | 579 | 580 | | |
| coatings | 387-404 | | | | | |
| concrete coatings | 424 | 425 | 426 | 427 | 428 | 429 |
| | 430 | 431 | 432 | 433 | | |
| electrochemical | 55 | 56 | 57 | 58 | 59 | 60 |
| | 61 | 62 | | | | |
| failure analysis and | 29 | | | | | |
| hot corrosion and | 144 | | | | | |
| immersion | 48 | 49 | 50 | 51 | 52 | 53 |
| material flammability and | 210 | 211 | 212 | 213 | 214 | 215 |
| | 216 | 217 | | | | |
| fire safety code testing | 210 | 211 | 212 | 213 | 214 | |
| research and development testing | 214 | 215 | 216 | 217 | | |
| plastics | 65 | 66 | 67 | 68 | 69 | 70 |
| | 71 | 72 | 73 | 74 | 75 | 76 |
| post-exposure, for coatings | 402 | | | | | |
| thermal protective clothing | 265 | 266 | 267 | 268 | | |
| See also Evaluating | | | | | | |
| Testing geometries | 68 | | | | | |
| Textile products, thermal protection and | 261 | 262 | 263 | 264 | 265 | 266 |
| | 267 | 268 | 269 | 270 | 271 | 272 |
| | 273 | 274 | 275 | | | |
| Thermal barrier coatings (TBCs) | 413 | | | | | |
| Thermal cycling | | | | | | |
| spacecraft materials degradation and | 487 | 488 | 489 | 490 | 491 | |

Index Terms

Links

| | | | | | | |
|---|-----|---------|-----|-----|-----|-----|
| stresses and | 145 | 146 | 147 | 148 | | |
| Thermal decomposition testing | 71 | 72 | 73 | | | |
| Thermal protective clothing (TPC) | 261 | 262 | 263 | 264 | 265 | 266 |
| | 267 | 268 | 269 | 270 | 271 | 272 |
| | 273 | 274 | 275 | | | |
| Thermal Protective Performance (TPP) | 265 | 269 | | | | |
| Thermal spray coatings | 334 | 405-422 | | | | |
| selection considerations and | 421 | | | | | |
| Thermal spray wires | 411 | | | | | |
| Thermal spraying, industrial applications and | 412 | 413 | 414 | 415 | 416 | 417 |
| | 418 | 419 | 420 | 421 | | |
| Thermal treatments, for wood | 309 | | | | | |
| Thermobalance | 110 | | | | | |
| Thermochemical stability diagrams | 137 | | | | | |
| Thermocouple-type sensors | 270 | | | | | |
| Thermogage™ | 270 | | | | | |
| Thermogravimetric analysis | 72 | 109 | | | | |
| Thermoset polyurethanes | 362 | | | | | |
| Thick layer oxidation | 117 | | | | | |
| Thin layer oxidation | 106 | 108 | 15 | 116 | 117 | 118 |
| Throwing power | 240 | | | | | |
| Time-temperature superimposition (TTS) | 66 | | | | | |
| Titanium alloys, corrosion-resistant alloys and | 8 | | | | | |
| Titanium, oxidation and | 118 | 119 | 120 | | | |
| Topcoatings | 348 | 361 | 362 | 363 | | |
| Torsion bar (TB) testing geometry | 69 | | | | | |
| Torvi burn model | 273 | | | | | |
| Toxic products | | | | | | |
| chromates and | 384 | | | | | |
| dioxins and | 246 | 249 | 250 | 251 | 252 | 253 |
| | 254 | 255 | | | | |
| material flammability and | 207 | 213 | 222 | | | |
| organic flame retardants and | 244 | | | | | |
| PBDPO flame retardants and | 246 | 247 | 248 | 249 | | |
| VOC emissions and | 332 | 370 | 384 | | | |
| Toxicity equivalence factor (TEF) | 250 | 252 | | | | |
| Toxicity Equivalents (TEQs) | 253 | 254 | 255 | 256 | | |
| TPC (thermal protective clothing) | 261 | 262 | 263 | 264 | 265 | 266 |
| | 267 | 268 | 269 | 270 | 271 | 272 |
| | 273 | 274 | 275 | | | |
| TPP (Thermal Protective Performance) | 265 | 269 | | | | |
| Traction coatings | 421 | | | | | |
| Transition ducts, industrial gas turbines and | 415 | | | | | |
| Transportation, cost of corrosion and | 13 | 18 | | | | |
| Trapped radiation belts | 483 | | | | | |
| Tribological damage | 324 | | | | | |
| TTS (time-temperature superimposition) | 66 | | | | | |
| Tuberculation, in hot water pipelines | 573 | | | | | |

Index Terms**Links**

| | | | | | |
|--|-----|-----|-----|-----|-----|
| Two-stage dip diffusion (wood protection) | 309 | | | | |
| U | | | | | |
| Uhlig report/method | 3 | 6 | | | |
| Ultraviolet light. See UV light | | | | | |
| Under deposit corrosion | 44 | | | | |
| Under-film corrosion | 451 | | | | |
| Undercoating corrosion | 377 | | | | |
| Unicoatings | 363 | | | | |
| UNS N08811 (high-nickel alloy) | 35 | 36 | 37 | | |
| UNS N10276 (nickel-base alloy) | 38 | | | | |
| Utilities, cost of corrosion and | 12 | 18 | | | |
| UV absorbers (UVAs) | | | | | |
| barrier packaging materials and | 559 | | | | |
| coating degradation and | 388 | | | | |
| coating weatherability and | 403 | | | | |
| wood protection and | 292 | | | | |
| UV/humidity damage | 324 | | | | |
| UV impingement, composite paint coatings and | 333 | | | | |
| UV light | | | | | |
| barrier packaging materials and | 559 | | | | |
| coating degradation and | 387 | | | | |
| spacecraft materials degradation and | 478 | 479 | 480 | 481 | 482 |
| wood weathering and | 278 | 279 | 280 | 281 | |
| UVAs. See UV absorbers | | | | | |
| V | | | | | |
| Vacancies, in oxides | 111 | | | | |
| Vacuum plasma spray (VPS) | 410 | | | | |
| Vacuum processes (wood protection) | 310 | | | | |
| Vacuum UV (VUV) | 479 | 481 | | | |
| Vapor deposited aluminum (VDA) | 487 | | | | |
| Vapor phase treatments, for wood | 311 | | | | |
| Varied heating rate | 73 | | | | |
| VDA (vapor deposited aluminum) | 487 | | | | |
| Vickers micro-indentation | 75 | | | | |
| Vinyl butyral | 374 | | | | |
| Vinyl resins | 374 | | | | |
| Volatile organic compounds (VOCs) | 384 | | | | |
| composite paint coatings and | 332 | | | | |
| waterborne paints and | 370 | | | | |
| Volume defects | 111 | 112 | | | |
| VPS (vacuum plasma spray) | 410 | | | | |
| VUV (vacuum UV) | 479 | 481 | | | |

Index Terms

Links

W

| | | | | | | |
|---|---------|-----|-----|-----|-----|-----|
| Wagner Hauffe rules | 112 | | | | | |
| Wagner's theory of thick layer oxidation | 117 | | | | | |
| Wash primer, vinyl butyral as | 374 | | | | | |
| Wasps, wood degradation and | 305 | | | | | |
| Wastage allowances | 541 | 542 | 543 | 544 | | |
| Wastewater industry, concrete coatings and | 423 | | | | | |
| Water | | | | | | |
| coating degradation and | 388 | | | | | |
| food packagings and | 560 | | | | | |
| ingress of into coatings | 449 | 456 | | | | |
| plastics aging and | 161 | | | | | |
| potable, cost of corrosion and | 13 | 18 | | | | |
| wood protection and | 307 | | | | | |
| wood weathering and | 280 | | | | | |
| Water-cooled thermal sensors | 270 | | | | | |
| Water dispersed coatings | 360 | | | | | |
| Water-soluble primers | 360 | | | | | |
| Water uptake | 376 | | | | | |
| Waterborne preservatives | 313 | | | | | |
| Waterways, cost of corrosion and | 12 | 18 | | | | |
| WE (working electrode) | 56 | | | | | |
| Wear, thermal spray coatings and | 417 | 418 | 419 | 420 | 421 | 422 |
| Weathering | 277 | | | | | |
| coatings/paints and | 377 | 387 | 388 | 389 | 390 | 391 |
| | 392 | 393 | 394 | 395 | 396 | 397 |
| | 397 | 398 | 399 | 400 | 401 | 402 |
| | 403 | 404 | | | | |
| wood and | 277 | 278 | 279 | 280 | 281 | 282 |
| | 283 | 284 | 285 | 286 | 287 | |
| Wenner four pin method, for soil resistance measurement | 508 | | | | | |
| Whipple shield | 494 | | | | | |
| White paint thermal control coatings | 482 | 486 | 488 | | | |
| White rot fungi, wood degradation and | 302 | | | | | |
| Wire arc thermal spraying | 406 | 410 | | | | |
| Wire thermal spraying | 406 | 408 | | | | |
| Wood | 277-317 | | | | | |
| charring of, computer modeling and | 223 | | | | | |
| degradation of | 299 | 300 | 301 | 302 | 303 | 304 |
| | 305 | | | | | |
| costs and | 305 | | | | | |
| heartwood durability and | 307 | | | | | |
| modifying | 315 | | | | | |
| protection of | 287-317 | | | | | |
| against biological degradation | 306 | 307 | 308 | | | |
| future trends in | 293 | | | | | |
| photoprotection methods | 287 | 288 | 289 | 290 | 291 | 292 |

Index Terms

Links

| | | | | | | |
|--|-----|-----|-----|-----|-----|-----|
| short-term/long-term treatment methods | 308 | | | | | |
| | 308 | 309 | 310 | 311 | 312 | 313 |
| | 314 | 315 | 316 | | | |
| weathering of | 277 | 278 | 279 | 280 | 281 | 282 |
| | 283 | 284 | 285 | 286 | 287 | |
| painting/finishing and | 286 | | | | | |
| Wood cell lumen fill treatments | 291 | | | | | |
| Wood-plastic composites (WPCs), wood protection and | 292 | | | | | |
| Working electrode (WE) | 56 | | | | | |
| WPCs (wood-plastic composites), wood protection and | 292 | | | | | |
| X | | | | | | |
| X-ray Photoelectron Spectroscopy (XPS) | 115 | 327 | | | | |
| Xenon arc light sources, for artificial accelerated weathering tests | 398 | | | | | |
| XPS (X-ray Photoelectron Spectroscopy) | 115 | 327 | | | | |
| X-ray diffraction (XRD) | 328 | | | | | |
| Y | | | | | | |
| YB-71 paint | 482 | 486 | | | | |
| Z | | | | | | |
| Z-93 paint | 482 | 486 | | | | |
| thermal cycling and | 488 | | | | | |
| Zebra mussels | 184 | | | | | |
| Zero-order reactions | 69 | | | | | |
| Zinc anodes, vs. magnesium anodes | 235 | | | | | |
| Zinc-rich paints (ZRPs) | 370 | | | | | |
| Zirconium, oxidation and | 118 | 119 | | | | |
| Zone models | 223 | | | | | |
| ZRPs (zinc-rich paints) | 370 | | | | | |